FACULTAD DE INGENIERIA U.N.A.M.
DIVISION DE EDUCACION CONTINUA

A LOS ASISTENTES A LOS CURSOS

Las autoridades de la Facultad de Ingeniería, por conducto del jefe de la División de Educación Continua, otorgan una constancia de asistencia a quienes cumplan con los requisitos establecidos para cada curso.

El control de asistencia se llevará a cabo a través de la persona que le entregó las notas. Las inasistencias serán computadas por las autoridades de la División, con el fin de entregarle constancia solamente a los alumnos que tengan un mínimo de 80% de asistencias.

Pedimos a los asistentes recoger su constancia el día de la clausura. Estas se retendrán por el periodo de un año, pasado este tiempo la DECFI no se hará responsable de este documento.

Se recomienda a los asistentes participar activamente con sus ideas y experiencias, pues los cursos que ofrece la División están planeados para que los profesores expongan una tesis, pero sobre todo, para que coordinen las opiniones de todos los interesados, constituyendo verdaderos seminarios.

Es muy importante que todos los asistentes llenen y entreguen su hoja de inscripción al inicio del curso, información que servirá para integrar un directorio de asistentes, que se entregará oportunamente.

Con el objeto de mejorar los servicios que la División de Educación Continua ofrece, al final del curso deberán entregar la evaluación a través de un cuestionario diseñado para emitir juicios anónimos.

Se recomienda llenar dicha evaluación conforme los profesores impartan sus clases, a efecto de no llenar en la última sesión las evaluaciones y con esto sean más fehacientes sus apreciaciones.

Atentamente

División de Educación Continua.

Palacio de Minería Calle de Tacuba 5 Primer piso Deleg. Cuauhtémoc 06000 México, D.F. APDO. Postal M-2285
Teléfonos: 512-8955 512-5121 521-7335 521-1987 Fax 510-0573 521-4020 AL 26

PALACIO DE MINERIA

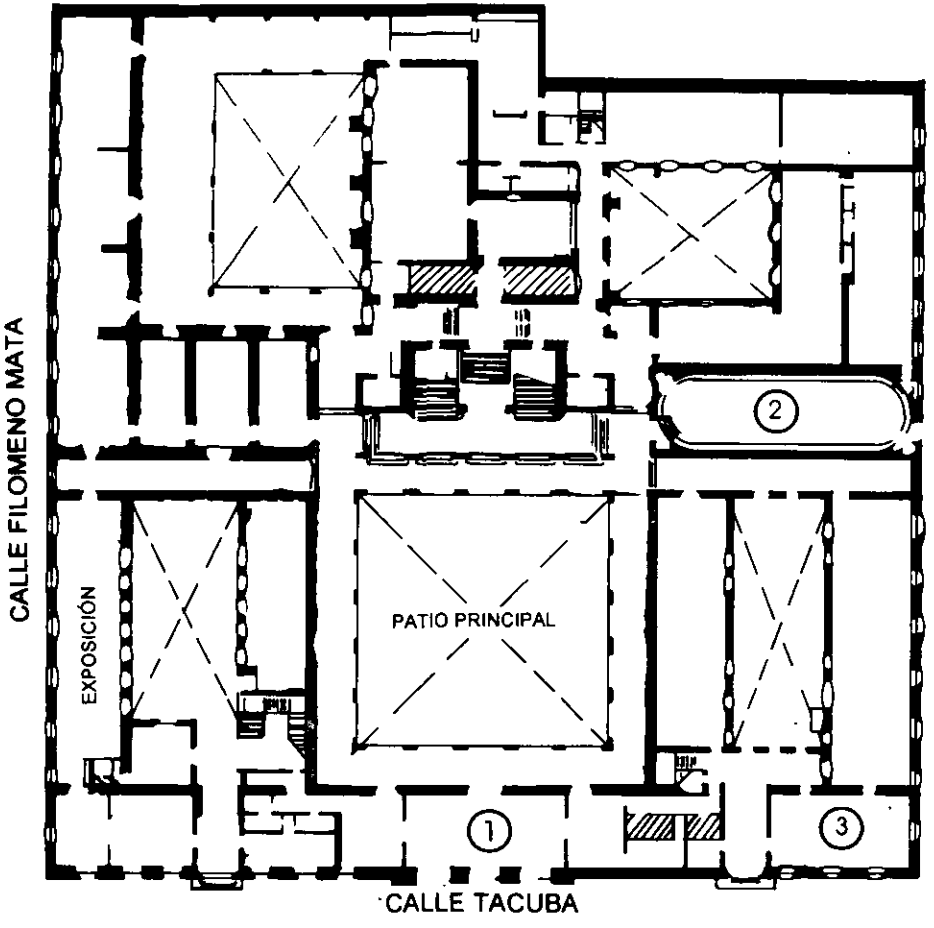

PLANTA BAJA

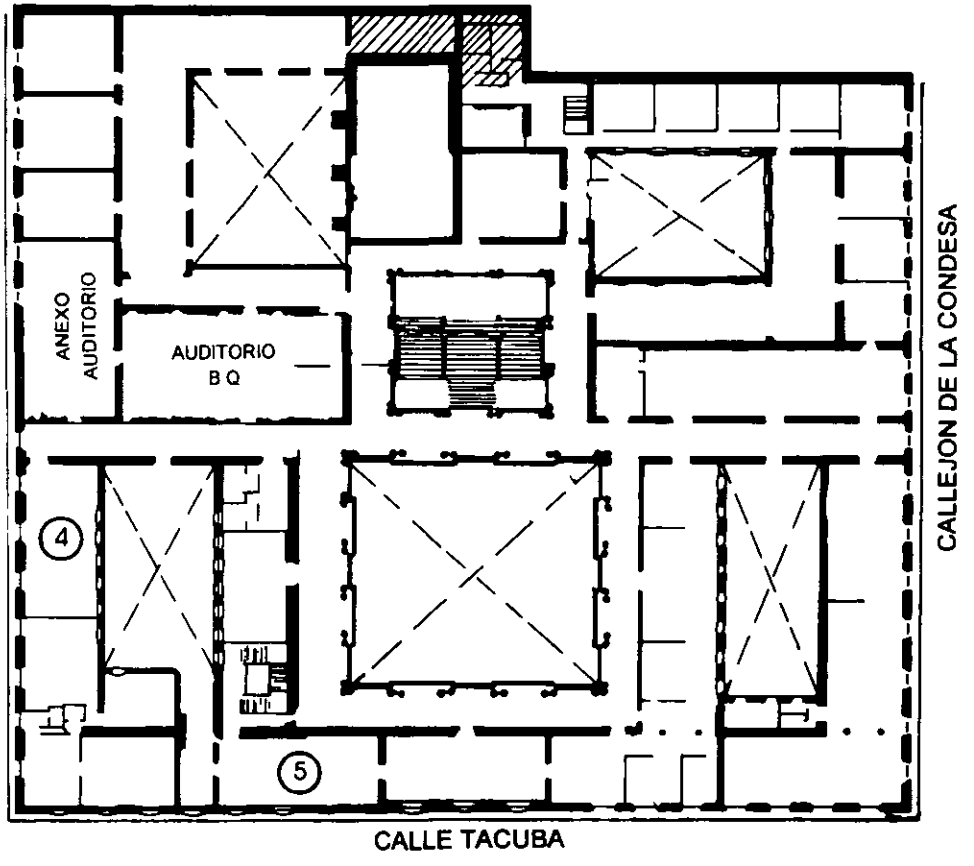

MEZZANINNE

PALACIO DE MINERIA

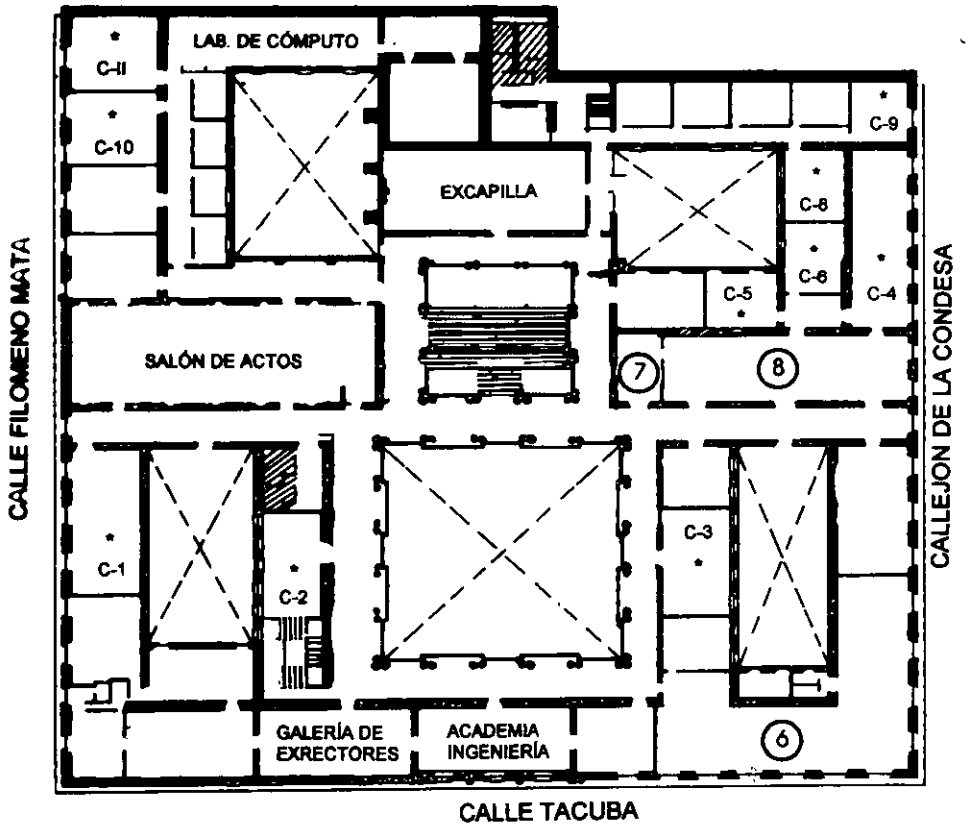

1er. PISO

GUÍA DE LOCALIZACIÓN

1. ACCESO
2. BIBLIOTECA HISTÓRICA
3. LIBRERÍA UNAM
4. CENTRO DE INFORMACIÓN Y DOCUMENTACIÓN "ING. BRUNO MASCANZONI"
5. PROGRAMA DE APOYO A LA TITULACIÓN
6. OFICINAS GENERALES
7. ENTREGA DE MATERIAL Y CONTROL DE ASISTENCIA
8. SALA DE DESCANSO

SANITARIOS

* AULAS

DIVISIÓN DE EDUCACIÓN CONTINUA
FACULTAD DE INGENIERÍA U.N.A.M.
CURSOS ABIERTOS

DIVISIÓN DE EDUCACIÓN CONTINUA
DEC

XII CURSO INTERNACIONAL DE CONTAMINACION DE ACUIFEROS
MODULO 3.- MODELOS MATEMATICOS EN GEOHIDROLOGIA
Y CONTAMINACION DE ACUIFEROS

2 AL 6 DE OCTUBRE DEL 2000

DIA	HORA	TEMA	PROFESOR
LUNES 2	9:00 A 11:00	INTRODUCCION	DR. ADOLFO CHAVEZ
	11:00 A 14:00	PRINCIPIOS DE LOS MODELOS	DR. ADOLFO CHAVEZ
	16:00 A 19:00	INTRODUCCION AL VMODFLOW	DR. ADOLFO CHAVEZ
MARTES 3	9:00 A 14:00	INTRODUCCION AL VMODFLOW	DR. ADOLFO CHAVEZ
	16:00 A 19:00	MODELO DE ZONAS DE PROTECCION	ING. OSCAR ESCOLERO
MIERCOLES 4	9:00 A 14:00 Y 16:00 A 19:00	MODELOS DE TRANSPORTE	M. EN C. FERNANDO LARA
JUEVES 5	9:00 A 14:00 Y 16:00 A 19:00	MODELOS EN GEOHIDROLOGIA GEOQUIMICA Y PRUEBAS DE BOMBEO	M. EN C. LUIS LESSER
VIERNES 6	9:00 A 14:00	MODELOS EN GEOHIDROLOGIA	ING. JUAN MANUEL LESSER
	16:00 A 19:00	MESA REDONDA	ING. JUAN MANUEL LESSER

DIVISION DE EDUCACION CONTINUA
FACULTAD DE INGENIERIA, UNAM
CURSOS ABIERTOS

DIVISIÓN DE EDUCACIÓN CONTINUA

CURSO: XII CURSO INTERNACIONAL DE CONTAMINACIÓN DE ACUIFEROS
MODULO III: MODELOS MATEMÁTICOS EN GEOHIDROLOGIA Y CONTAMINACION DE ACUIFEROS
FECHA: Del 02 AL 06 de octubre del 2000 CA 097

EVALUACIÓN DEL PERSONAL DOCENTE

(ESCALA DE EVALUACIÓN: 1 A 10)

CONFERENCISTA	DOMINIO DEL TEMA	USO DE AYUDAS AUDIOVISUALES	COMUNICACIÓN CON EL ASISTENTE	PUNTUALIDAD
Dr. Adolfo Chávez Rodríguez				
Ing. Oscar Escolero Fuentes				
M. en C. Fernando Lara Guerrero				
Ing. Juan Manuel Lesser Illades				
M. en C. Luis Lesser				

Promedio _____

EVALUACIÓN DE LA ENSEÑANZA

CONCEPTO	CALIF.
ORGANIZACION Y DESARROLLO DEL CURSO	
GRADO DE PROFUNDIDAD DEL CURSO	
ACTUALIZACION DEL CURSO	
APLICACION PRACTICA DEL CURSO	

Promedio _____

EVALUACIÓN DEL CURSO

CONCEPTO	CALIF
CUMPLIMIENTO DE LOS OBJETIVOS DEL CURSO	
CONTINUIDAD EN LOS TEMAS	
CALIDAD DEL MATERIAL DIDÁCTICO UTILIZADO	

Promedio _____

Evaluación total del curso_____

Continúa...2

1. ¿Le agradó su estancia en la División de Educación Continua?

SI ☐ NO ☐

Si indica que "NO" diga porqué: _____

2. Medio a través del cual se enteró del curso:

Periódico *La Jornada*	
Folleto anual	
Folleto del curso	
Gaceta UNAM	
Revistas técnicas	
Otro medio (Indique cuál)	

3. ¿Qué cambios sugeriría al curso para mejorarlo?

_____

_____

_____

_____

_____

_____

4. ¿Recomendaría el curso a otra(s) persona(s) ?

SI ☐ NO ☐

5. ¿Qué cursos sugiere que imparta la División de Educación Continua?

_____

_____

_____

_____

_____

_____

6. Otras sugerencias

_____

_____

_____

_____

_____

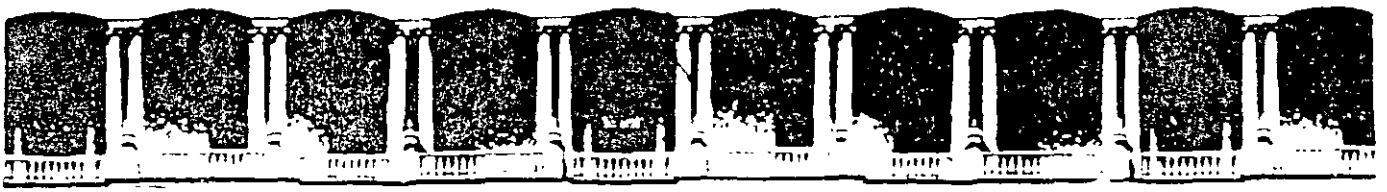

FACULTAD DE INGENIERIA U.N.A.M.
DIVISION DE EDUCACION CONTINUA
CURSOS ABIERTOS

XII CURSO INTERNACIONAL DE CONTAMINACIÓN DE ACUÍFEROS

MODULO III: MODELOS MATEMÁTICOS EN GEOHIDROLOGIA Y CONTAMINACIÓN DE ACUIFEROS

TEMA

MANUAL PARA LA UTILIZACIÓN DEL VISUAL MODFLOW

EXPOSITOR: M. EN C. LUIS ERNESTO LESSER CARRILLO
PALACIO DE MINERIA
OCTUBRE DEL 2000

1. ABRIR UN ARCHIVO O CREAR UNO NUEVO

1. En *file* se utiliza *open* para abrir un modelo ya extistente.
2. En *file* se utliza *new* para crear un modelo nuevo.
3. Al crear un modelo nuevo se pide el nombre y el subdirectorio donde se va a almacenar. Es recomendable tener un subdirectorio especifico para cada modelo.
4. A continuación se piden las unidades en que se trabajara a lo largo del modelo.
5. En este momento se pregunta si se desea tener como base algun dibujo (generalmente hecho en autocad). El archivo tiene que estar en formato *dxf*. en autocad se teclea *dxfout* para crear un archivo en este formato.
6. A continuacion se dan las caracteristicas de la malla de discretización. Se piden la coordenada mínima y máxima en *X*. asi como el número de columnas deseadas en el modelo. De esta manera el modelo calcula el tamaño de cada columna.
7. Los mismos datos se requieren para el eje *Y* (renglones) y el eje *Z* (capas). Esta malla podra despues ser modificada. Nótese que si se tomo como base un dibujo *dxf*. las coordenadas máximas y mínimas son tomadas de este dibujo. aunque si se desea se pueden modificar.
8. A continuación se muestra la zona discretizada y el plano base. En el menú principal se escoge *input* para alimentar el modelo con los datos.

2. ALIMENTACION DE LOS DATOS DEL MODELO

- En el menú que aparece del lado izquierdo existen 3 opciones para visualizar las columnas, renglones o capas del modelo.
- En *goto previous* o *next* se puede visualizar la capa anterior o. la siguiente. Tambien se pude visualizar la columna o renglón siguiente o anterior, si estas se están visualizando.
- Del menu que se encuentra en la porción baja de la pantalla:

  F1 - *(help)* Ayuda.

  F2 - Después de presionarlo podemos obtener las coordenadas de cualquier punto del modelo.

  F3 - *(save)* Para salvar.

  F4 - *(map)* Para introducir otro dibujo o plano base al modelo. Se pueden añadir el número de dibujos o planos base que se deseé.

  F5 - *(zoom in)* Para tener un acercamiento de alguna porción del modelo.

  F6 - *(zoom out)* Para tener una visualización completa de la zona del modelo.

  F7 - *(pan)* Para desplazarse por el modelo al estar en acercamiento.

  F8 - *(vert exag)* Para determinar la exageración vertical que se utilizará para poder visualizar mejor las secciones.

  F9 - *(overlay)* Esta opción se utiliza para "apagar" o "prender" las capas de dibujos. Es decir para poder visualizar o no ciertos dibujos que se hayen importado en *F4*, o la distribución de las diferentes características del modelo como los pozos, recarga, conductividad hidráulica, etc.

  F10 - *(main menu)* Para regresar al menú principal.

1. Modificación de la malla y delimitación de celdas activas e inactivas

- En el menú superior se selecciona *grid*.
- Con las opciones *add column*, *delete column* y *add row*, *delete row* se pueden agregar o borrar columnas o renglones del modelo.

- Lo mismo se puede hacer con las capas cuando se visualiza una sección. Nótese que ésta es una discretización matemática, y no forzosamente se necesita discretizar en el mismo número de estratos geológicos. Es decir, un estrato geológico puede subdividirse para efectos de discretización, teniendo las mismas características todas las subcapas creadas para éste estrato.
- Para importar la superficie del terreno o la base de alguna capa, se utiliza la opción *import surface* Con esto en vez de que el modelo sea un cubo perfecto, se podran tener en cuenta las irregularidades del terreno, o de las capas geologicas.
- Las superficies se pueden importar en archivos en formato *ASCII*. Los archivos deben ser una lista de tres columnas de las coordenadas en X,Y,Z de varios puntos, o se puede importar un archivo creado en SURFER (*grd*).
- Las celdas inactivas son zonas donde el modelo no interviene. Para delimitarlas se utiliza la opción *inactive cells*. Se puede trazar un polígono para marcarlo como inactivo. Para revertir la elección se puede tambien marcar, un polígono activo.
- Esta delimitación se realiza en una sola capa. Es importante copiar esta información a las capas que lo requieran, usando el comando *copy polygon*.

2. Asignación de valores de conductividad hidráulica y almacenamiento

- En el menú superior se selecciona *properties* y ya sea *conductivity* o *storage*.
- A continuación se asignan los valores de conductividad hidráulica, almacenamiento y porosidad que por default asignara el modelo a todos los nodos.
- Posteriormente se zonifica la malla con las opciones del menú izquierdo *assign single*, *polygon* o *window*.
- Después de seleccionar una zona se puede elegir entre darle un valor nuevo *(new)* o de asignarle algún valor que haye sido designado con anterioridad.
- Dependiendo si se escoje *conductivity* o *storage* en la opción de *properties*, se podrá zonificar la conductividad hidráulica o el almacenamiento y la porosidad.
- Es importante copiar las propiedades necesarias a las capas que lo requieran utilizando la opción *copy layer* del menu izquierdo.

- **Nota:** A cada nueva propiedad se le asigna un color distinto para ser distinguido en el modelo. El color blanco representa el valor que se dió como defalut.

3. Asignación de fronteras

- En *boundaries* se encuentran las diferentes opciones de frontera. Se pueden asignar como línea, polígono o ventana por medio del menú de la izquierda.
- En la opción de *recharge* se agrega la regarga en mm/año. Nótese que no solo la recarga por lluvia puede ser representada de esta manera, tan solo se necesitan respetar las unidades en que esta recarga se asigna.

4. Alimentacion de la información de los pozos

- En la opción de pozos *(wells)* se pueden añadir, borrar, copiar o editar pozos por medio del menú izquierdo.
- Al seleccionar *add well* se localiza el punto donde se localiza el pozo. En la ventana que aparece a continuación se agregan los datos del pozo como el nombre, el intervalo en que el pozo se encuentra ranurado y el historial de bombeo del pozo.

NOTAS:

a) No se puede nombrar un pozo como otro anterior.

b) Las unidades de bombeo son m^3/día.

c) Si el pozo es de recarga las unidades de bombeo se denotan con signo positivo.

d) Si el pozo es de bombeo las unidades de bombeo se denotan con signo negativo.

e) El modelo no tiene una escala de tiempo real, así que es necesario tomar la fecha en que se inicia la simulación como día cero dentro del modelo. De esta manera las fechas del historial del pozo, así como el resto de los datos del modelo que tienen variación con el tiempo, deben de ser asignados en número de días a partir de la fecha que se tomó como día cero.

3. PARA CORRER EL MODELO

- En el menú principal se escoge *run.*
- Se escoge si la simulación es en estado transitorio *(transient)* o estacionario *(steady-state).*
- Se selecciona *run*, y se selecciona *modflow.*
- Si se desea correr el *modptah*, zona de balance *(zone budget)* o *MT3D* también se seleccionan.

---

4. PARA VISUALIZAR LOS RESULTADOS

- En el menú principal se selecciona *output.*
- Si el modelo fué corrido en estado transitorio, en *time* se puede escoger el momento en el tiempo en que se desea visualizar la configuración de la superficie piezométrica.
- En *goto* se puede visualizar la configuración de la superficie piezométrica en las diferentes capas.
- En *options* se puede modificar el intervalo utilizado para configurar y el valor del contorno máximo y mínimo.
- En el menú superior, en *velocities* se obtienen vectores del flujo del agua en donde se aprecia la dirección del movimiento del agua subterránea. En *options* se puede escoger el tamaño relativo de estos vectores y su densidad por área. **Estos vectores no son propiamente líneas de flujo, ya que estas, por definición no se cruzan entre si.**

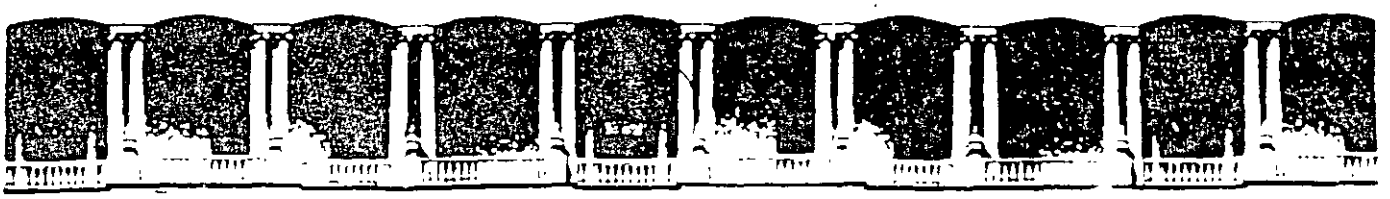

FACULTAD DE INGENIERIA U.N.A.M.
DIVISION DE EDUCACION CONTINUA

CURSOS ABIERTOS

XII CURSO INTERNACIONAL DE CONTAMINACIÓN DE ACUÍFEROS

MODULO III: MODELOS MATEMÁTICOS EN GEOHIDROLOGIA Y CONTAMINACIÓN DE ACUIFEROS

TEMA

EJEMPLO DEL VISUAL MODFLOW

EXPOSITOR: M. EN C. LUIS ERNESTO LESSER CARRILLO

PALACIO DE MINERIA
OCTUBRE DEL 2000

1. DESCRIPCION DEL PROBLEMA

Este ejemplo está basado en el flujo del agua subterránea en un sistema formado por un acuífero libre en la porción superior, un acuitardo en la porción media, y un acuífero confinado en la porción inferior, como se muestra en la figura 1.

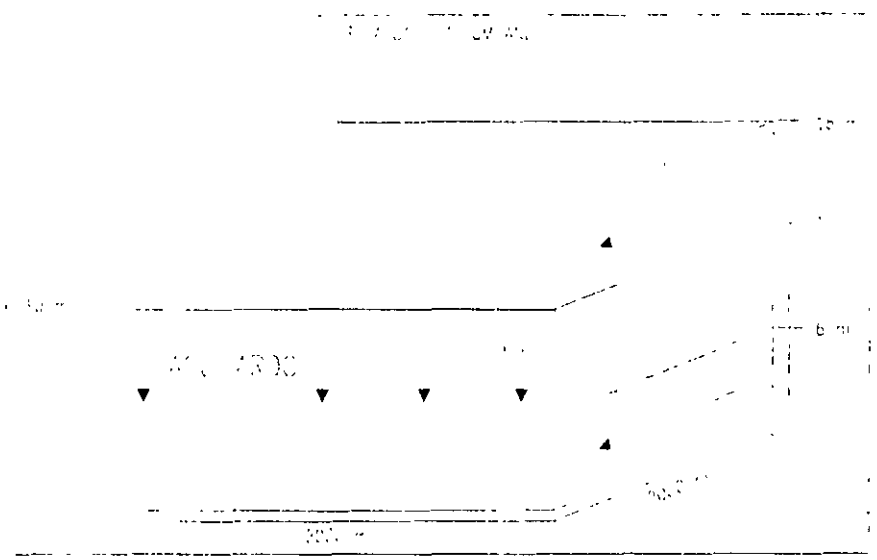

Figura 1. Dimensiones del acuifero

Notas:

- Este ejemplo está tomado del manual de Visual Modflow por Waterloo Hydrogeologic Inc.
- El simbolo ↵ significa enter.
- El simbolo ↖ significa presionar el botón izquierdo del mouse.

2. CREACION DE UN NUEVO MODELO

Estando en el sistema operativo teclear

VMODFLOW ↵

Esto nos lleva a la pantalla de Visual Modflow

O.K.

FILE

NEW

Aparecerá una ventana preguntando por el nombre del nuevo modelo.

Teclear el nombre del nuevo modelo:

VMEJEM ↵

(Visual Modflow asigna automáticamente la terminación .vmf)

Aparecerá una ventana para escoger las unidades deseadas (figura 2). Las unidades se seleccionan utilizando el mouse.

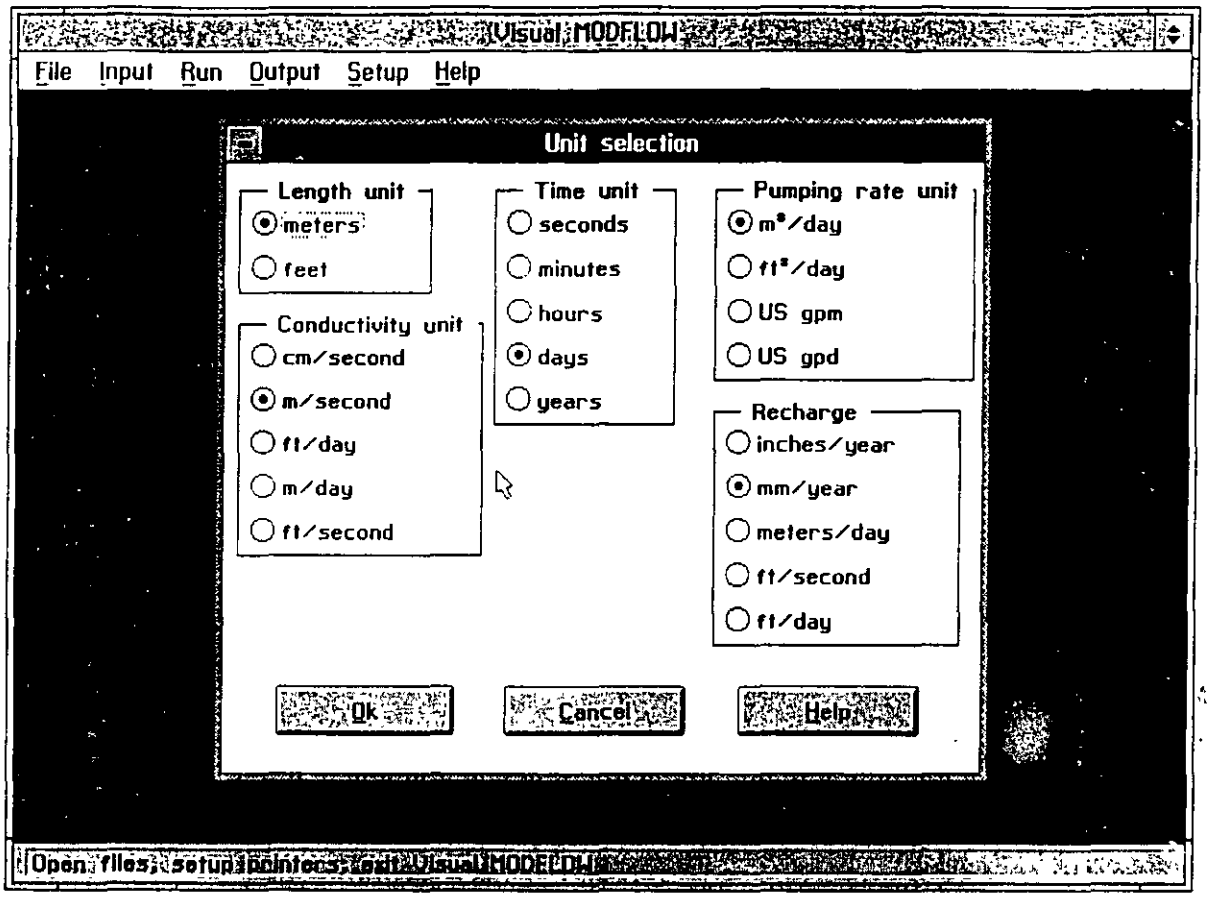

Figura 2. Ventana de selección de unidades

- **meters**
- **m/sec**
- **days**
- **m^3/day**
- **mm/year**

- O.K.

3. DISEÑO DE LA MALLA

La siguiente ventana preguntará si se desean importar las coordenadas de un mapa en formato *dxf*.

- YES
- VMEXAMP.DXF

En el caso en que se ha escogido un mapa, Visual Modflow leerá las coordenadas máximas y mínimas del mapa y las sugerirá como las dimensiones del modelo. Aparecerá una ventana para definir las dimensiones y características de la malla (figura 3) solo se requiere teclear sobre los espacios o sobre los valores sugeridos para modificarlos.

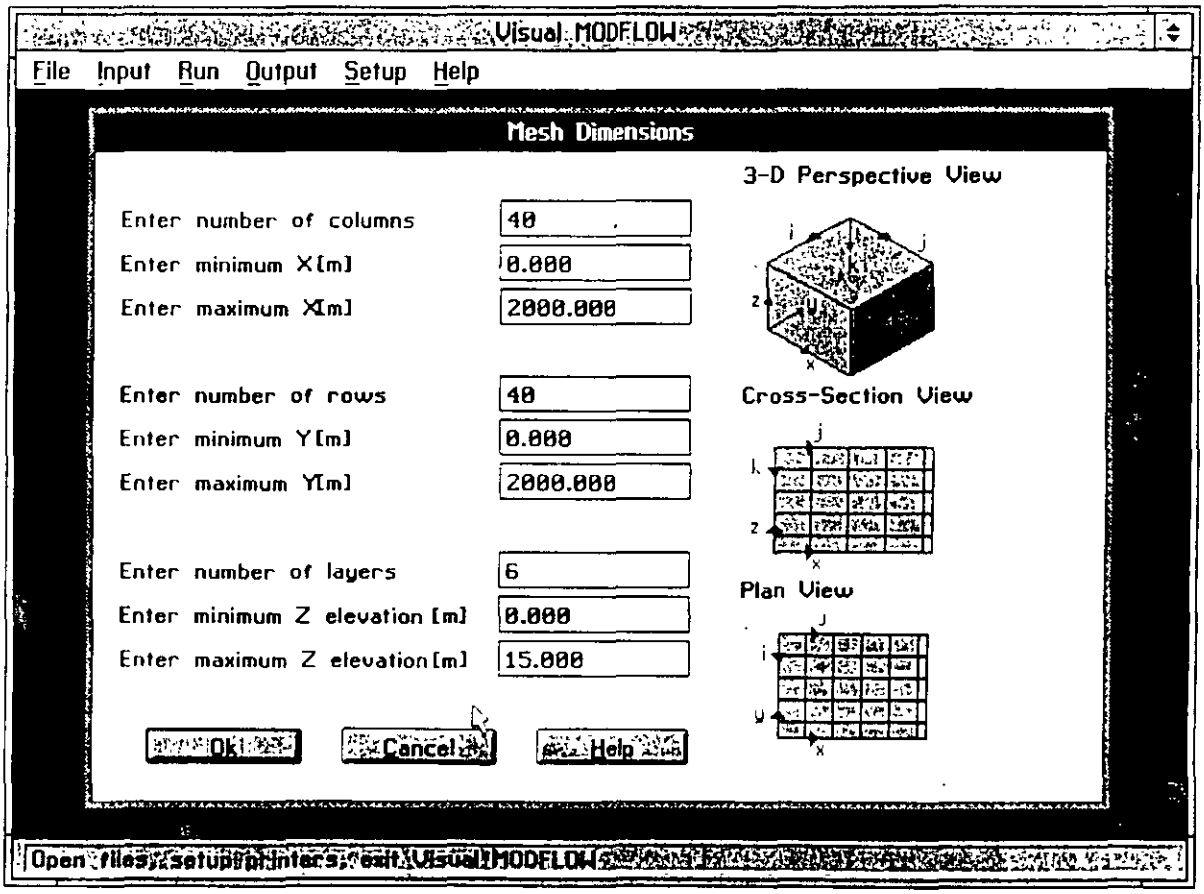

Figura 3. Ventana de diseño de la malla

Enter number of columns **40** ↵
Enter Minimum X (m) **0** ↵
Enter Maximum X (m) **2000** ↵

Enter number of rows **40** ↵
Enter Minimum Y (m) **0** ↵
Enter Maximum Y (m) **2000** ↵

Enter number of layers **6** ↵
Enter Minimum Z (m) **0** ↵
Enter Maximum Z (m) **15** ↵
O.K.

Una malla de 40 x 40 y el plano base aparecerán en la pantalla (figura 4).

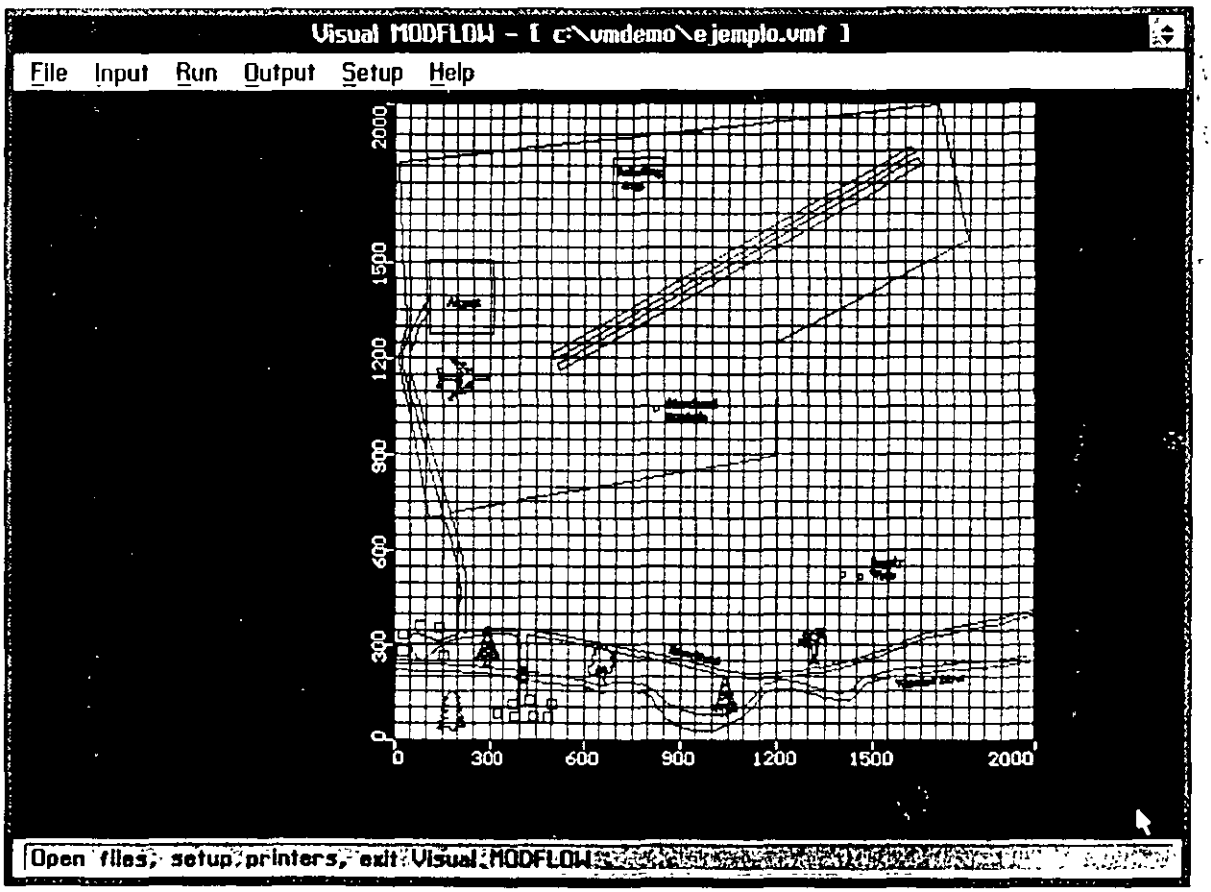

Figura 4. Archivo importado en formato *dxf*

4. REFINAMIENTO DE LA MALLA

Se necesita refinar la malla alrededor de los pozos de abastecimiento de agua *(supply wells)* y de la perforación abandonada *(abandoned borehole)*. El tamaño de la celda representa el tamaño del pozo, por lo tanto una malla mas discretizada simulará el pozo de una manera mas realística. Además del tamaño del pozo, si existe abatimiento alrededor del pozo, una discretización mayor producirá pendientes menos abruptas del nivel estático en zonas de abatimiento.

- en INPUT
- en ADD COLUMN

Mover el mouse a cualquier lugar en la malla y el BOTON DERECHO DEL MOUSE. Haciendo esto se puede definir los lugares exactos para definir la discretización de la malla Aparecerá una ventana para la información de la malla (figura 5).

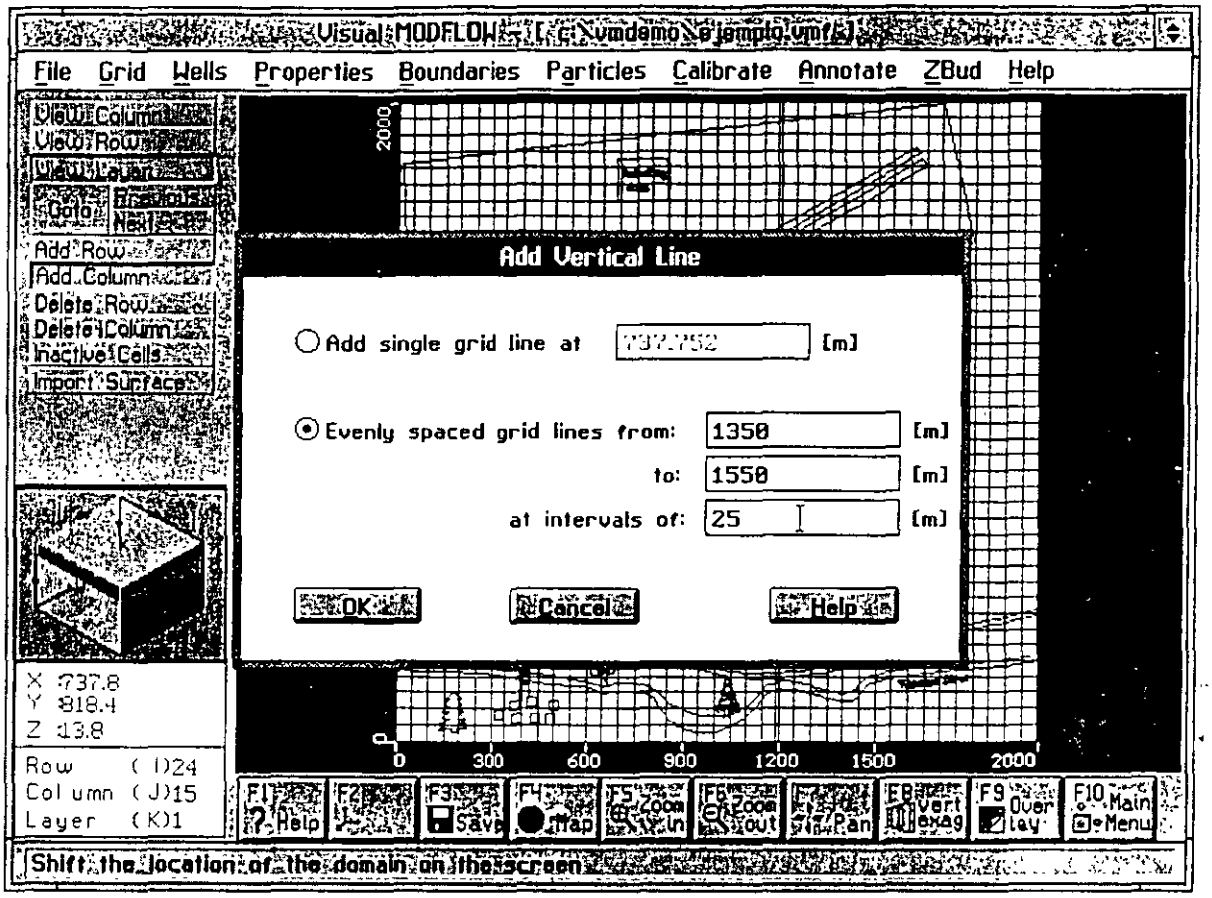

Figura 5. Ventana de refinamiento de la malla

Escoger **EVENLY SPACED GRID LINES FROM:** (líneas igualmente espaciadas desde:) en el círculo vacío.

En las ventanas asignar los siguientes valores:

from **1350**
to **1550**
at intervals of **25**
en O.K

en ADD ROW

Mover el mouse a cualquier lugar en la malla y el BOTON DERECHO DEL MOUSE.

Aparecerá una ventana para la información de la malla.

Escoger **EVENLY SPACED GRID LINES FROM:** (líneas igualmente espaciadas desde:) en el círculo vacío.

En las ventanas asignar los siguientes valores:

from **450** ↵
to **600** ↵
at intervals of **25** ↵
🖱 en O.K.

Esto a refinado la malla alrededor de los pozos de abastecimiento de agua *(supply wells).*

Ahora lo haremos alrededor de la perforación abandonada *(abandoned borehole)*

🖱 en ADD COLUMN

Mover el mouse a cualquier lugar en la malla y 🖱 el BOTON DERECHO DEL MOUSE.

Aparecerá una ventana para la información de la malla.

Escoger **EVENLY SPACED GRID LINES FROM:** (líneas igualmente espaciadas desde:) 🖱 en el círculo vacío.

En las ventanas asignar los siguientes valores:

from **795** ↵
to **900** ↵
at intervals of **10** ↵
🖱 en O.K.

🖱 en ADD ROW

Mover el mouse a cualquier lugar en la malla y 🖱 el BOTON DERECHO DEL MOUSE.

Aparecerá una ventana para la información de la malla.

Escoger **EVENLY SPACED GRID LINES FROM:** (líneas igualmente espaciadas desde:) 🖱 en el círculo vacío

En las ventanas asignar los siguientes valores:

from **950** ↵
to **1100** ↵
at intervals of **10** ↵
🖱 en O.K

Ahora vamos a determinar la exageración vertical.

🖱 VIEW ROW

Mover el cursor a cualquier lugar en la malla. Al mover el cursor de arriba hacia abajo de la malla el renglón ocupado cambia a color rojo. en cualquier renglón. Ahora ha sido transferido de una vista aérea a una vista de sección. En este momento el modelo no tiene exageración vertical. Para poder visualizar la sección mejor:

F8 (Del menú de la parte inferior de la pantalla)

Aparece una ventana, escribir:

25

O.K.

Ahora se visualizan las 6 capas en la pantalla.

5. PARA IMPORTAR UNA SUPERFICIE

VIEW COLUMN

Mover el mouse a la malla y en cualquier columna.

IMPORT SURFACE

Aparecerá una ventana como la de la figura 6.

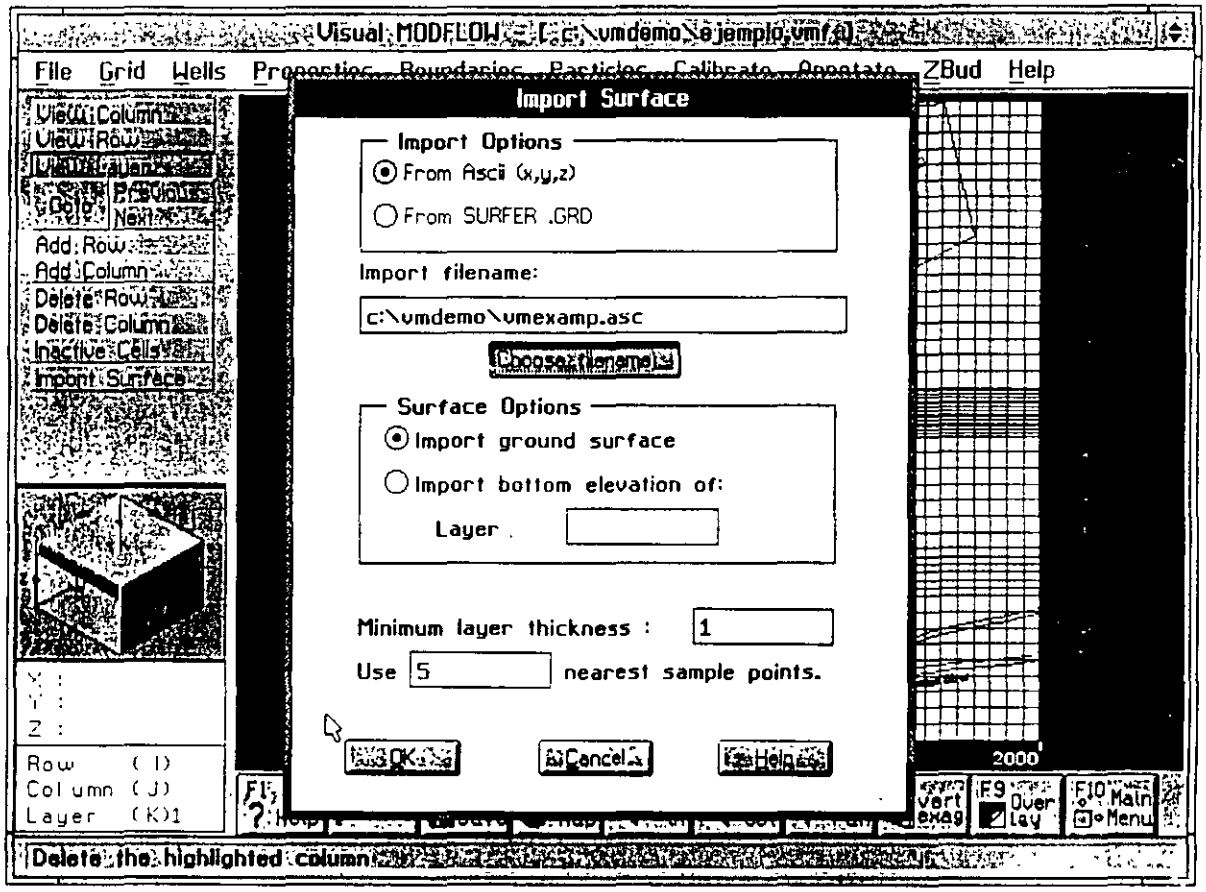

Figura 6. Menu para importar superficies

en CHOOSE FILENAME

Para escoger el archivo conteniendo la superficie.

VMEXAMP ASC

- O.K.
- O.K.

Esto importará una superficie con una pendiente que va de 18 metros al norte hasta 15 metros al sur (figura 7).

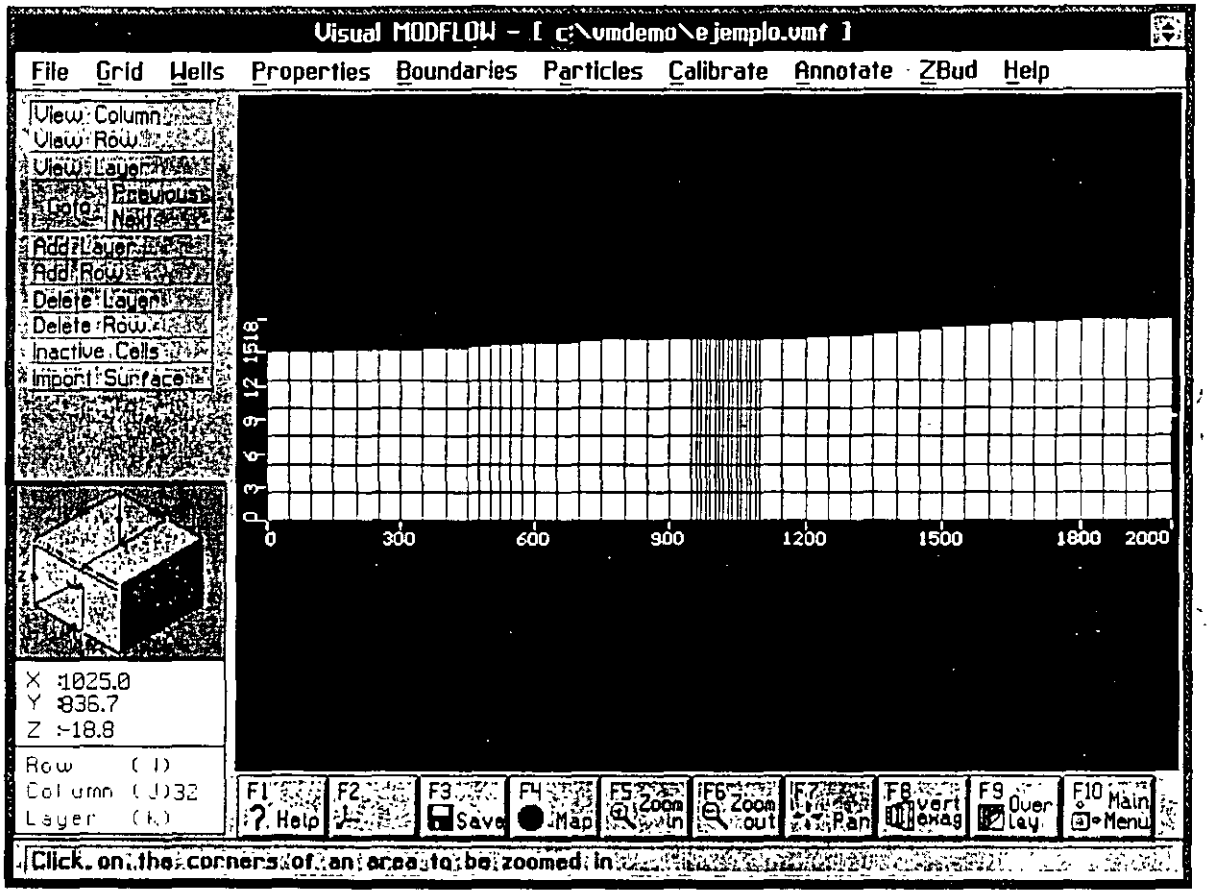

Figura 7. Superficie topográfica importada

6. ASIGNACION DE LOS VALORES DE CONDUCTIVIDAD HIDRAULICA, ALMACENAMIENTO Y RECARGA

- VIEW LAYER

Seleccionar la capa superior y . Esto deberá de crear una vista aérea del lugar.

- PROPERTIES (en el menú superior)
- CONDUCTIVITY

En este momento el modelo preguntará si se desea salvar la información de la malla.

- en YES

Hay que asegurarse de estar viendo la capa superior (capa 1). Esto se puede ver en el cubo que se encuentra en la parte inferior izquierda.

A continuación una ventana pide los valores que se asignarán como default a todas las celdas. Después se podrán modificar los valores a cada celda.

Conductividad hidráulica en X y Y (Kx y Ky) en m/s:	**2e-4**
Conductividad hidráulica en Z (Kz) en m/s:	**2e-4**
Coeficiente de almacenamiento(Ss) en 1/m:	**1e-4**
Rendimiento específico (Sy):	**0.2**
Porosidad (Por):	**0.35**

- O.K.

Ahora se asignará el valor de conductividad hidráulica del acuitardo (capas 3 y 4).

- GO TO (en el menú de la izquierda)

Aparecerá una ventana, escribir:

3

- O.K.
- ASSIGN WINDOW

Mover el mouse a la celda de la esquina superior izquierda y en el centro de la celda. Después mover el mouse a la esquina inferior derecha y en el centro de la celda. Esto creará una ventana que cubrirá toda la capa. Aparecerá una ventana para asignar la conductividad.

NEW

Toda la malla cambiará a color azul. Asignar los valores de conductividad hidráulica del acuitardo:

Kx (m/s) = **1e-10**

(El valor de Ky será asignado automáticamente)

Kz (m/s) = **1e-10**

O.K.

COPY LAYER (del menú izquierdo)

Aparecerá una venatana, escoger:

COPY ALL PROPERTIES (seleccionando el recuadro)

LAYER 4 (le dará un color verdoso a la capa)

O.K.

Ahora se asignarán los valores de almacenamiento al acuitardo.

PROPERTIES (en el menú superior)

STORAGE

ASSIGN WINDOW

Mover el mouse a la celda de la esquina superior izquierda y en el centro de la celda. Después mover el mouse a la esquina inferior derecha y en el centro de la celda. Esto creará una ventana que cubrirá toda la capa. Aparecerá una ventana para asignar el almacenamiento.

NEW (toda la malla cambiará a color azul)

Asignar los valores de almacenamiento y porosidad:

Ss (1/m): **1e-2** ↵

Sy: **0.003** ↵

Por: **0.65** ↵

- O.K.
- COPY LAYER (del menú izquierdo)

Aparecerá una ventana, escoger:

- COPY ALL PROPERTIES (seleccionando el recuadro)
- LAYER 4 (le dará un color verdoso a la capa)
- O.K.

Para comprobar los valores tanto de conductividad como de almacenamiento mediante en EDIT SINGLE, del menú izquierdo. Esto creará una ventana mostrando los valores de conductividad hidráulica y el almacenamiento para cada celda mediante un en ella.

Ahora se simulará el efecto de la perforación abandonada para ver el efecto en transporte.

- PROPERTIES
- CONDUCTIVITIES
- GO TO (Dar un valor de 1 para ir a la capa 1)
- O.K.
- ZOOM IN (Del menú inferior)

Hacer una ventana cerca de la perforación abandonada *(abandoned borehole)*

- ASSIGN SINGLE (Esto es para asignar propiedades a una sola celda)

Aparecerá una ventana de asignación (figura 8).

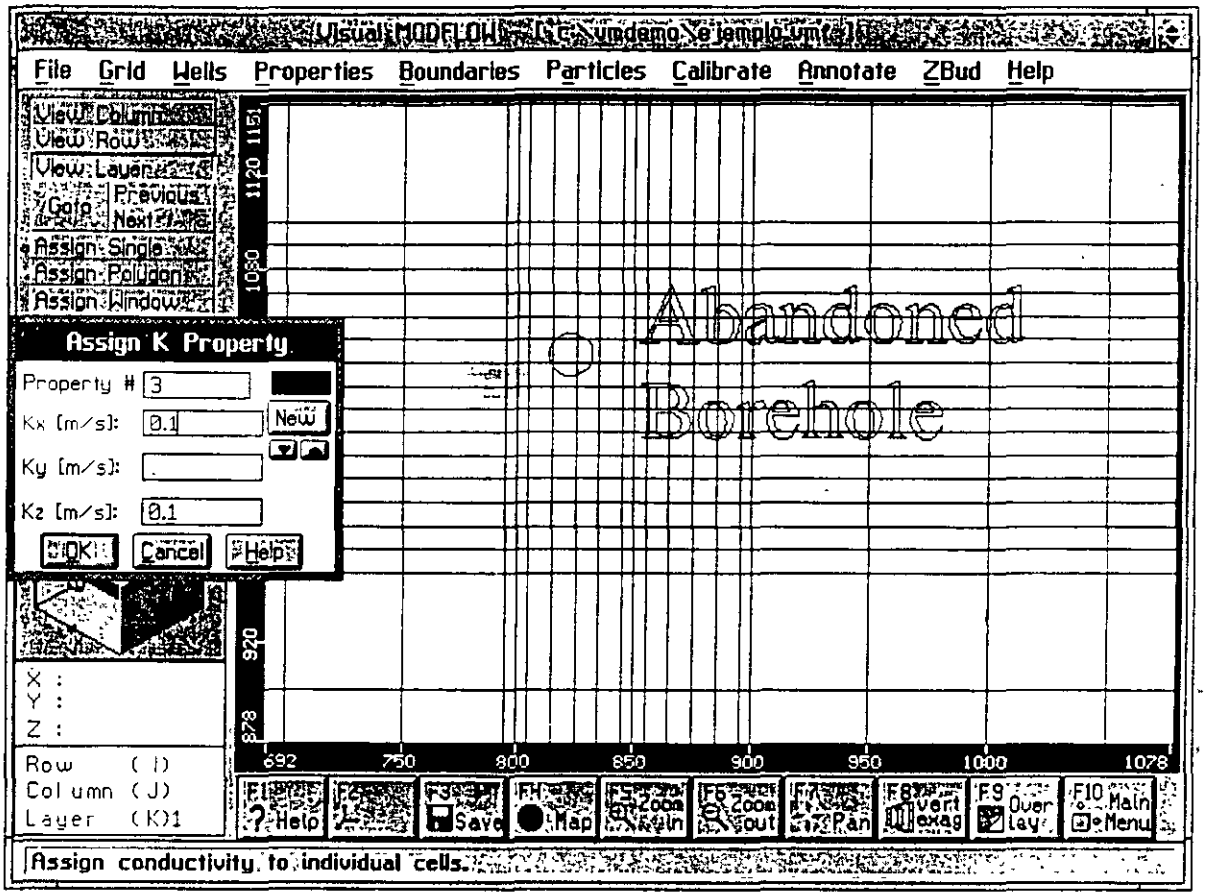

Figura 8. Asignando las propiedades a la perforación abandonada.

NEW (Dará un color verde)

Asignar los siguientes valores:

Kx (m/s) = **1e-1**

(El valor de Ky será asignado automáticamente)

Kz (m/s) = **1e-1**

En el centro de la perforación abandonada (definida por el círculo) para designar la celda a la que se le asignarán las propiedades.

O.K.

COPY LAYER (del menú izquierdo)

Aparecerá una ventana, escoger:

COPY ONLY PROPERTY #

Escribir:

3

SELECT ALL

Todas las capas cambiarán de color (figura 9).

O.K.

ZOOM OUT

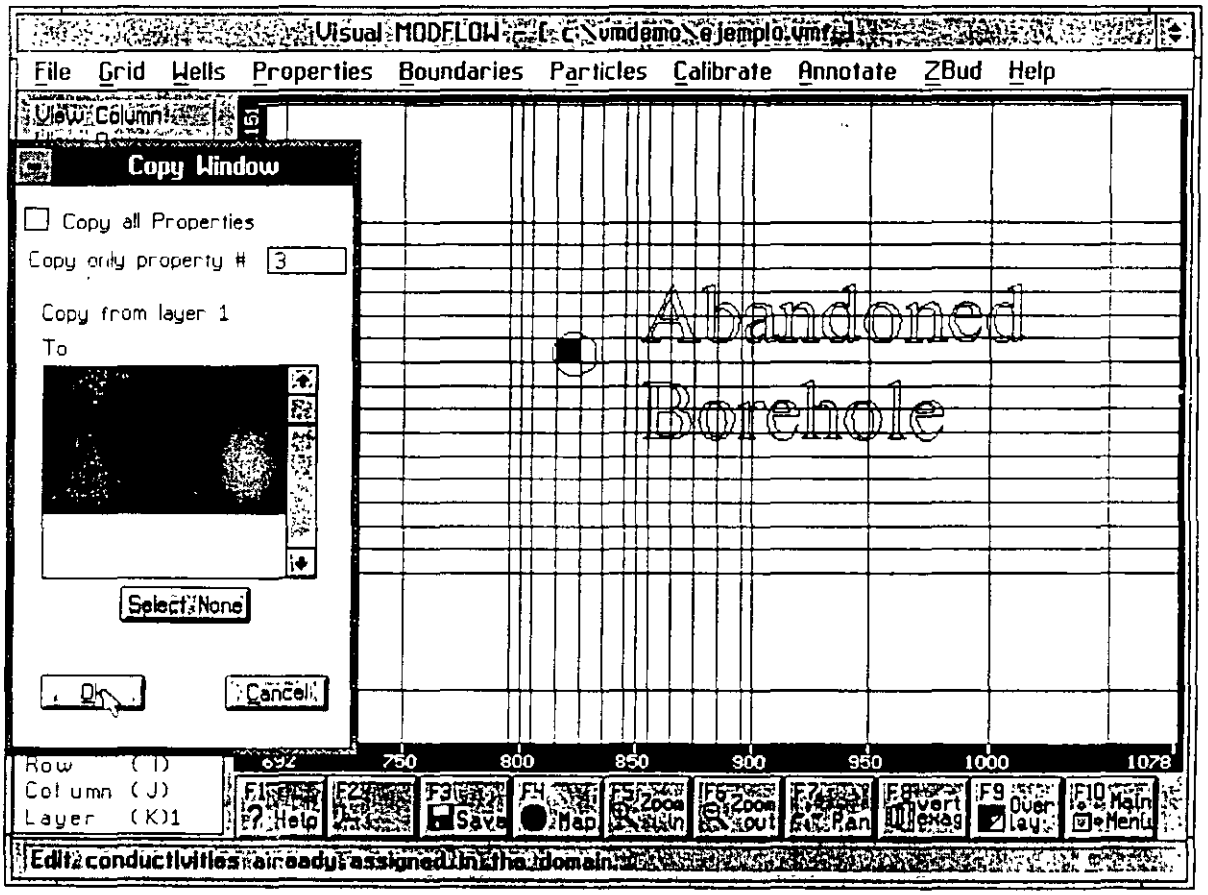

Figura 9. Copiando las propiedades de la perforación abandonada.

Ahora se le dará a la capa superior la recarga.

PROPERTIES

RECHARGE

NOTA: En la nueva versión de Visual Modflow, tanto la recarga como la evapotranspiración, se encuentran en el menú de fronteras (*BOUNDARIES)* y no en el de propiedades.

Aparecerá una ventana para asignar el valor de recarga por default. Escribir:

100 ↵

O.K.

Visual Modflow asigna automáticamente la recarga a la capa superior del modelo.

7. DELIMITACION DE LAS FRONTERAS DE FLUJO

- BOUNDARIES
- CONSTANT HEAD

Aparecerá una ventana preguntando si se desea salvar la información.

- YES
- ASSIGN LINE (del menú izquierdo)

Mover el mouse a la celda de la esquina superior izquierda y en el centro de la celda. Después mover el mouse a la esquina **superior** derecha y **con el botón derecho** en el centro de la celda. Una línea horizontal de celdas cambiará a color rosa y aparecerá una ventana para asignar los valores de carga constante (figura 10). Asignar los siguientes valores:

Code # : **1**
en el cuadro de STOP TIME
Stop time: **3650**
Start point. **18**
End Point. **18**
O.K.
La línea rosa cambiará a color rojo indicando que la carga constante ha sido asignada.

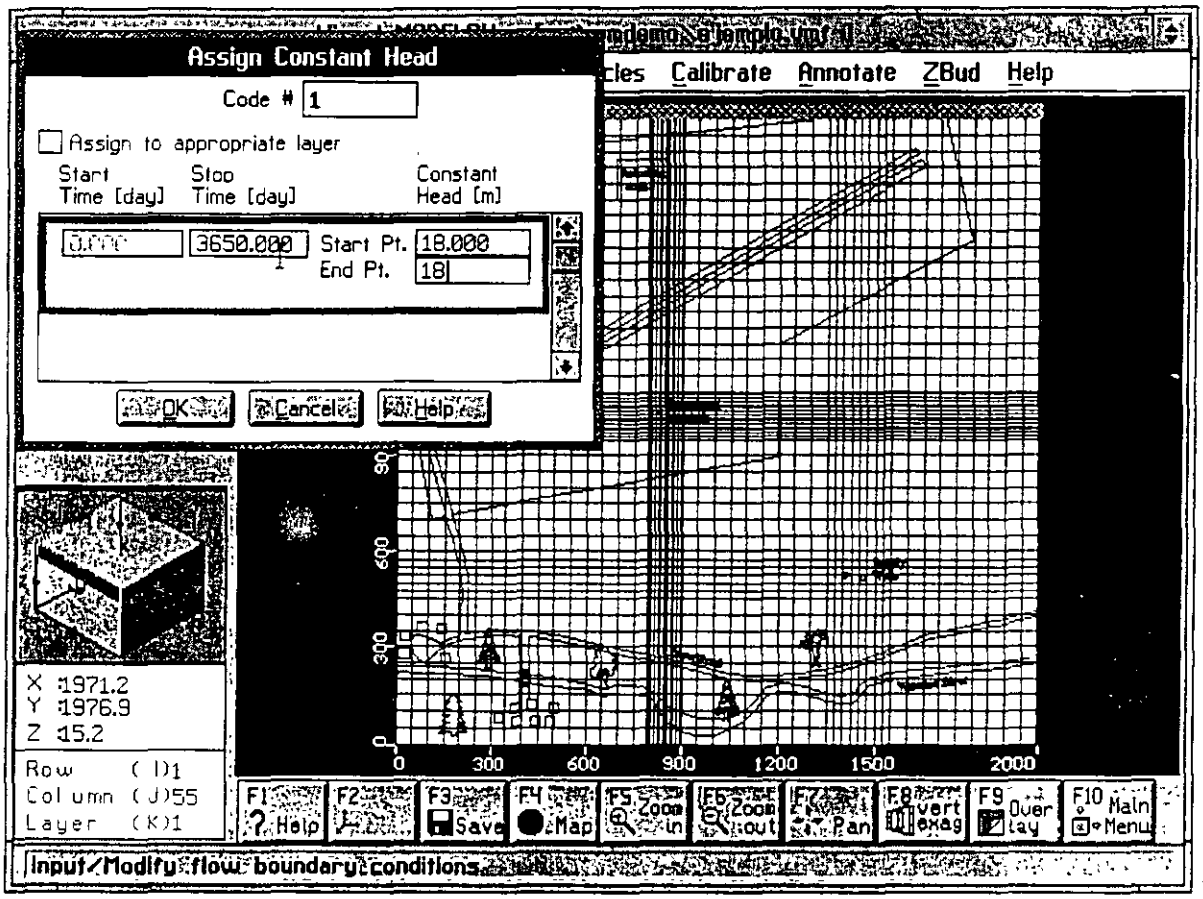

Figura 10. Menú para la asignación de la carga constante

- COPY LAYER

Aparecerá la ventana para copiar propiedades. En el cuadro COPY ONLY CODE # ya tendrá el número 1.

- LAYER 2 (esto hará cambiar de color la capa 2)
- O.K.

Ahora asignaremos los valores de carga constante del acuífero inferior.

- GO TO (en el menú de la izquierda)

Escoger:

5 ↵

- O.K.

ASSIGN LINE

Mover el mouse a la celda de la esquina superior izquierda y en el centro de la celda. Después mover el mouse a la esquina **superior** derecha y **con el botón derecho** en el centro de la celda. Una línea horizontal de celdas cambiará a color rosa y aparecerá una ventana para asignar los valores de carga constante. Asignar los siguientes valores:

Code # **2**
en el cuadro de STOP TIME
Stop time: **3650**
Start point: **16.5**
End Point: **16.5**
O.K.
La línea rosa cambiará a color rojo indicando que la carga constante ha sido asignada

COPY LAYER

Aparecerá la ventana para copiar propiedades. En el cuadro COPY ONLY CODE # reemplazar el valor tecleando el número **2**.

LAYER 6 (esto hará cambiar de color la capa 6)

O.K.

ASSIGN LINE

Mover el mouse a la celda de la esquina **inferior** izquierda y en el centro de la celda. Después mover el mouse a la esquina **inferior** derecha y **con el botón derecho** en el centro de la celda. Una línea horizontal de celdas cambiará a color rosa y aparecerá una ventana para asignar los valores de carga constante. Asignar los siguientes valores:

Code # **3**
en el cuadro de STOP TIME
Stop time: **3650**
Start point: **14.5**
End Point: **14.5**
O.K.
La línea rosa cambiará a color rojo indicando que la carga constante ha sido asignada.

COPY LAYER

Aparecerá la ventana para copiar propiedades. En el cuadro COPY ONLY CODE # reemplazar el valor tecleando el número 3.

- LAYER 6 (esto hará cambiar de color la capa 6)
- O.K.

Después de asignar los valores de carga constante:

- VIEW COLUMN
- en cualquier columna para ver una sección del modelo (figura 11).

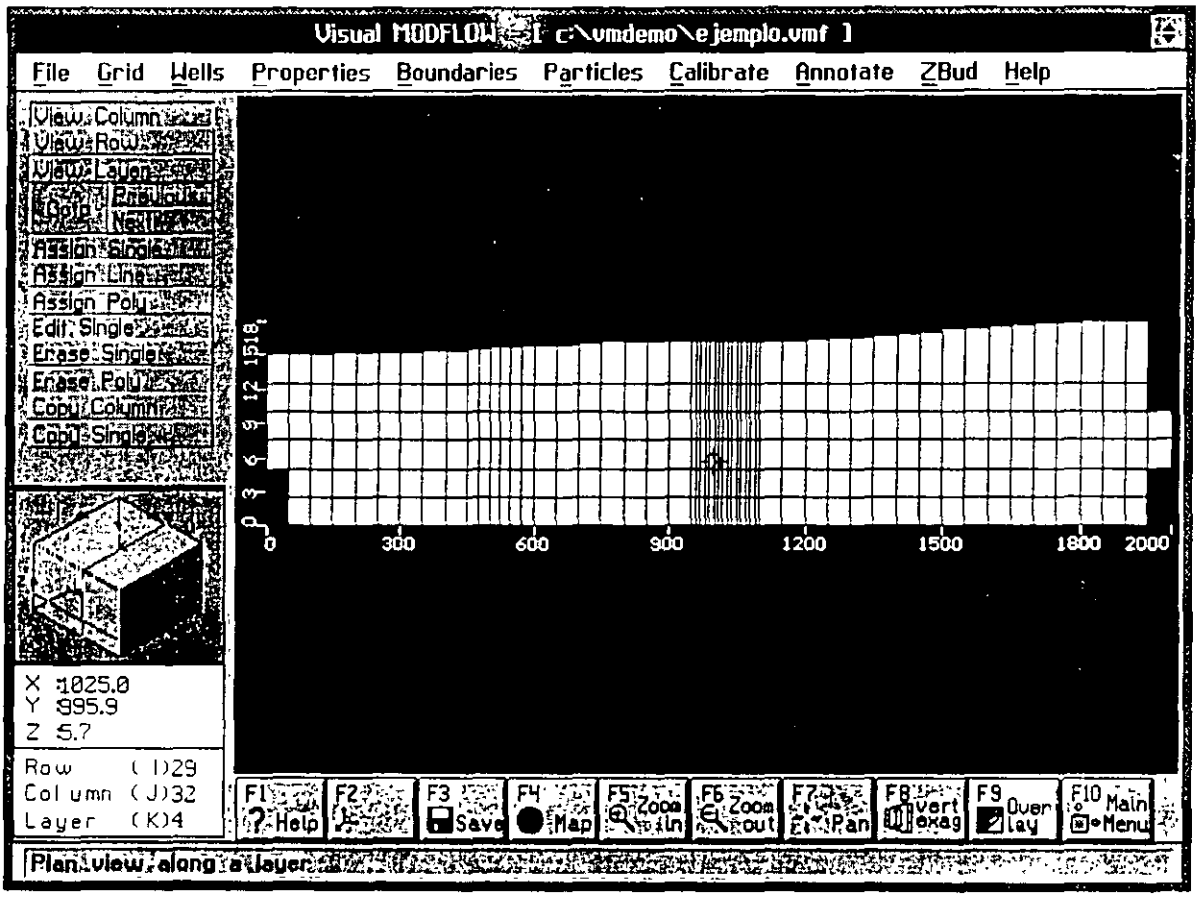

Figure 11. Fronteras de carga constante

Ahora asignaremos la frontera del río al sur de la zona.

- VIEW LAYER
- en la capa superior del modelo (capa 1)
- BOUNDARIES
- RIVERS

ASSIGN LINE

Utilizando el plano base como guía se hay que digitalizar el río mediante comenzando desde el margen inferior izquierdo y tratando de seguir su contorno. Cuando se ha llegado al final (al margen inferior derecho) hay que **en el botón derecho.** Aparecerá una ventana para pedir la información del río (figura 12).

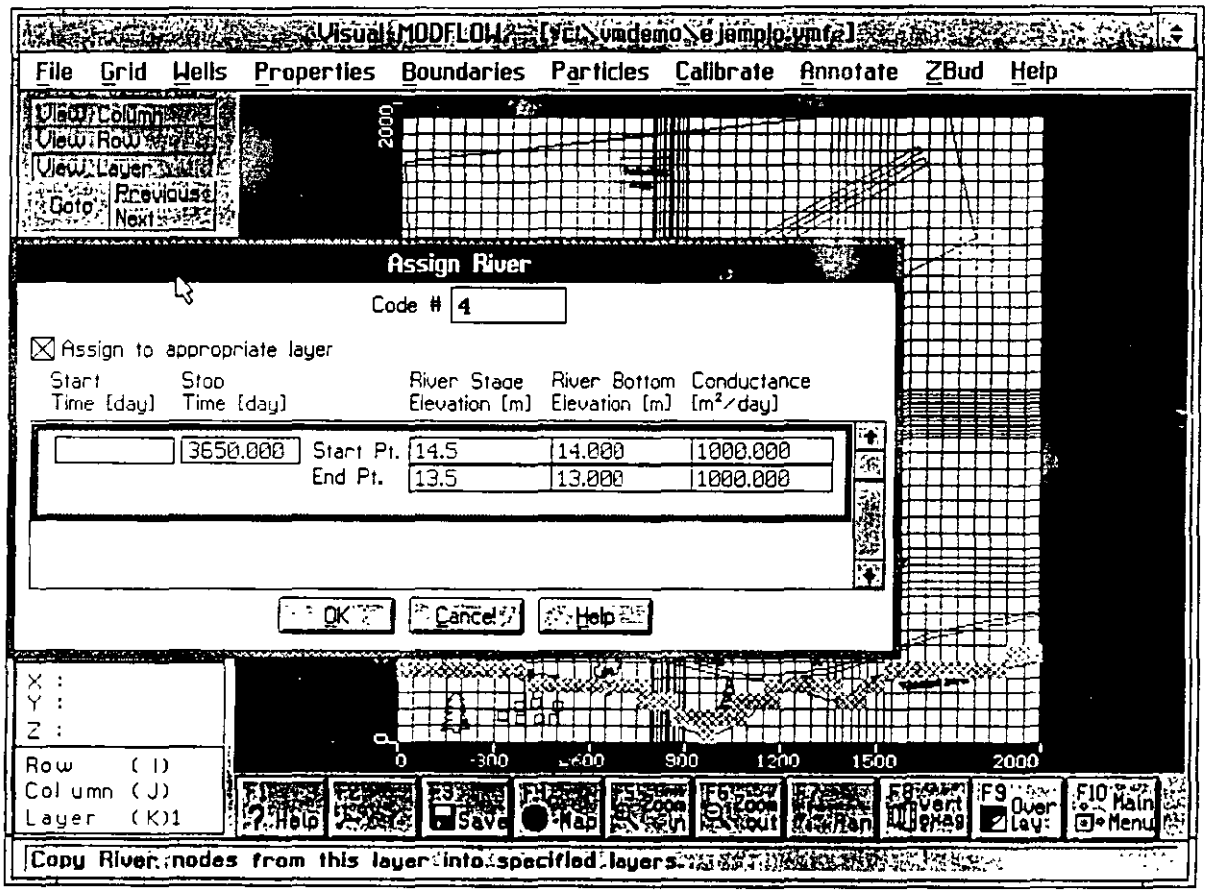

Figura 12. Ventana de información del río.

Asignar los siguientes valores:

Code # **4**

en el cuadro de STOP TIME

Stop time: **3650**

Start Point River Stage: **14.5**

Start Point River Bottom: **14.0**

Conductance: **1000**
End Point River Stage: **13.5**
End Point River Bottom: **13.0**
Conductance: **1000**
O.K.

Después de que el río ha sido definido, una línea azul delimitará su extensión.

8. ASIGNACION DE PARTICULAS

Ahora asignaremos algunas partículas que emanen de la zona de tanques *(refueling area)* para delimitar el area de influencia que tienen estos tanques. Las partículas pueden ser de 2 tipos: *backward*, para delimitar el area de donde las partículas provienen; y *forward*, para delimitar el area hacia donde van las partículas.

NOTA: Esta manera de simular el movimiento de las partículas se realiza tomando en cuenta UNICAMENTE el flujo del agua subterránea. En la nueva versión del Visual Modflow se encuentra un paquete de simulación de movimiento de contaminantes mucho mas completo, llamado MT3D.

- PARTICLES
- YES (Para salvar la información de las fronteras)
- ADD CIRCLE
- En el centro del area de tanques *(refueling area)* que se encuentra en la porción centro-superior de la zona. Expander el círculo que se forma hasta que cubra el recuadro del area de tanques y . Aparecerá una ventana (figura 13) seleccionar:
- FORWARD
- O.K.

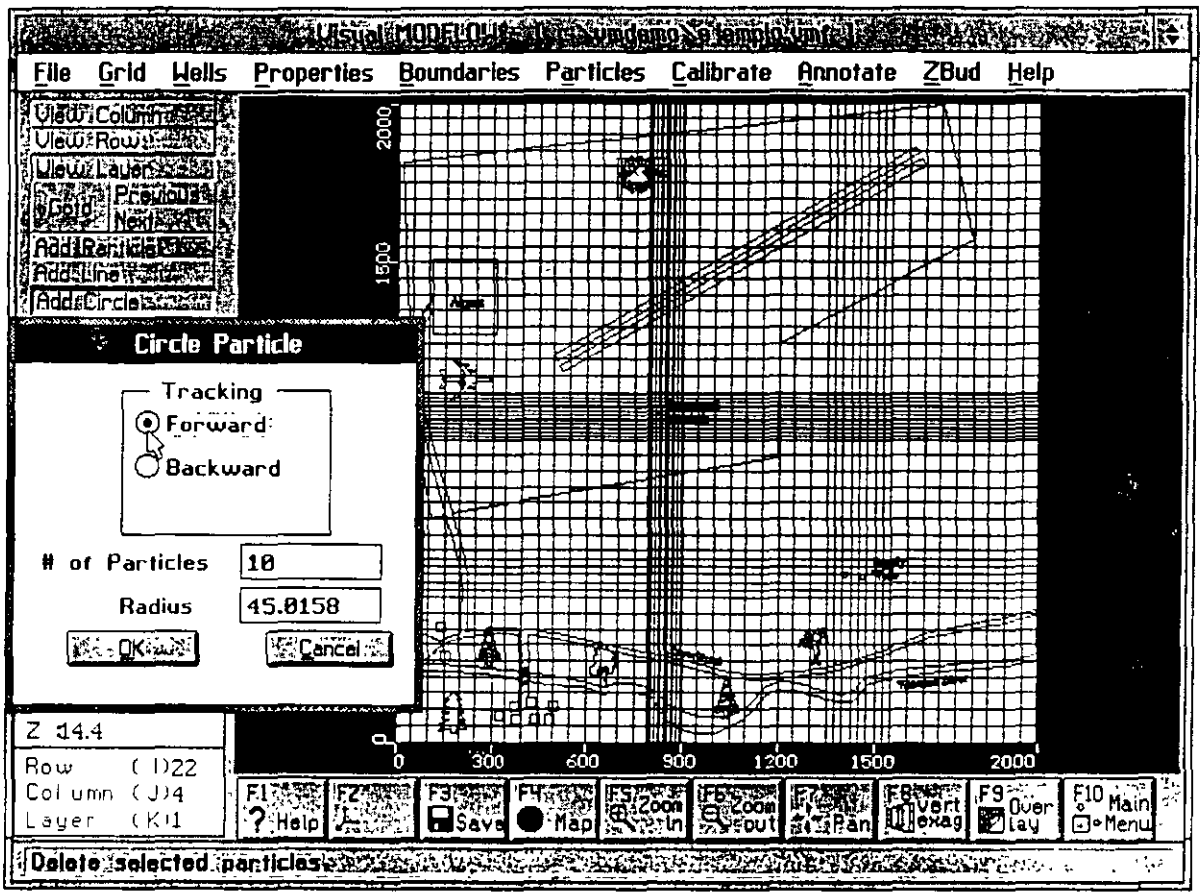

Figura 13. Agregando partículas

9. AGREGANDO POZOS

- WELLS
- YES (Para salvar la información de las partículas)
- ZOOM IN (F5)
- cerca de los pozos de abastecimiento de agua *(supply wells)* y hacer una ventana que los abarque volviendo a para conseguir un acercamiento de la zona.
- ADD WELL

Mover el cursor al centro del pozo de la izquierda y en él. Aparecerá una ventana con la información del pozo (figura 14).

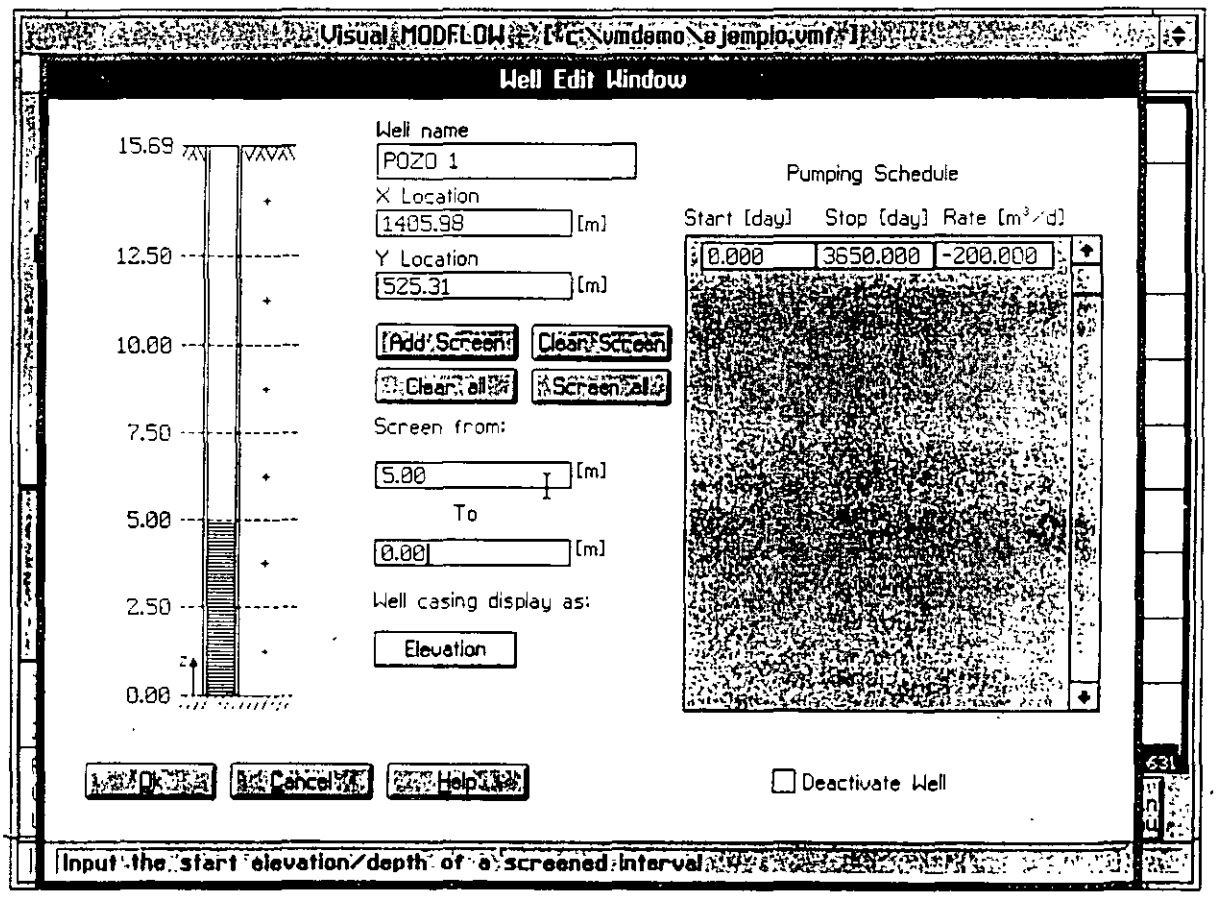

Figura 14. Información del pozo

Agregar la siguiente información:

Well Name: **POZO 1**
Stop Day: **3650**
Rate: **-200**

NOTA: El bombeo del pozo debe de ser de **negativo**. Si el pozo es de inyección el signo debe ser **positivo.**

- ADD SCREEN

Estos pozos deberán estar ranurados solo en el acuífero inferior, que son los últimos 5 metros del modelo. dentro del pozo a una elevación aproximada de 5 metros, y hay que mover la barra roja hasta la base del pozo y otra vez. Los últimos 5 metros del pozo deben de haber cambiado de color representando el intervalo ranurado.

- O.K.
- COPY WELL

Mover el cursor hasta que esté posicionado sobre el pozo izquierdo y , después mover el cursor al pozo de la derecha y en él para copiar el pozo.

- EDIT WELL
- El pozo de la derecha

Cuando aparezca el menú cambiar el nombre del pozo por **POZO 2** y en O.K.

- MAIN MENU (F10) (Del menú inferior)
- YES (para salvar la información de los pozos)

10. PARA CORRER VISUAL MODFLOW

- RUN
- O.K. (para aceptar el estado estacionario)
- RUN MODEL

NOTA: La versión de Visual Modflow que se les ha entregado es un DEMO de práctica que no tiene la capacidad de correr el modelo.

Aparece una ventana para definir que es lo que se va a correr (figura 15).

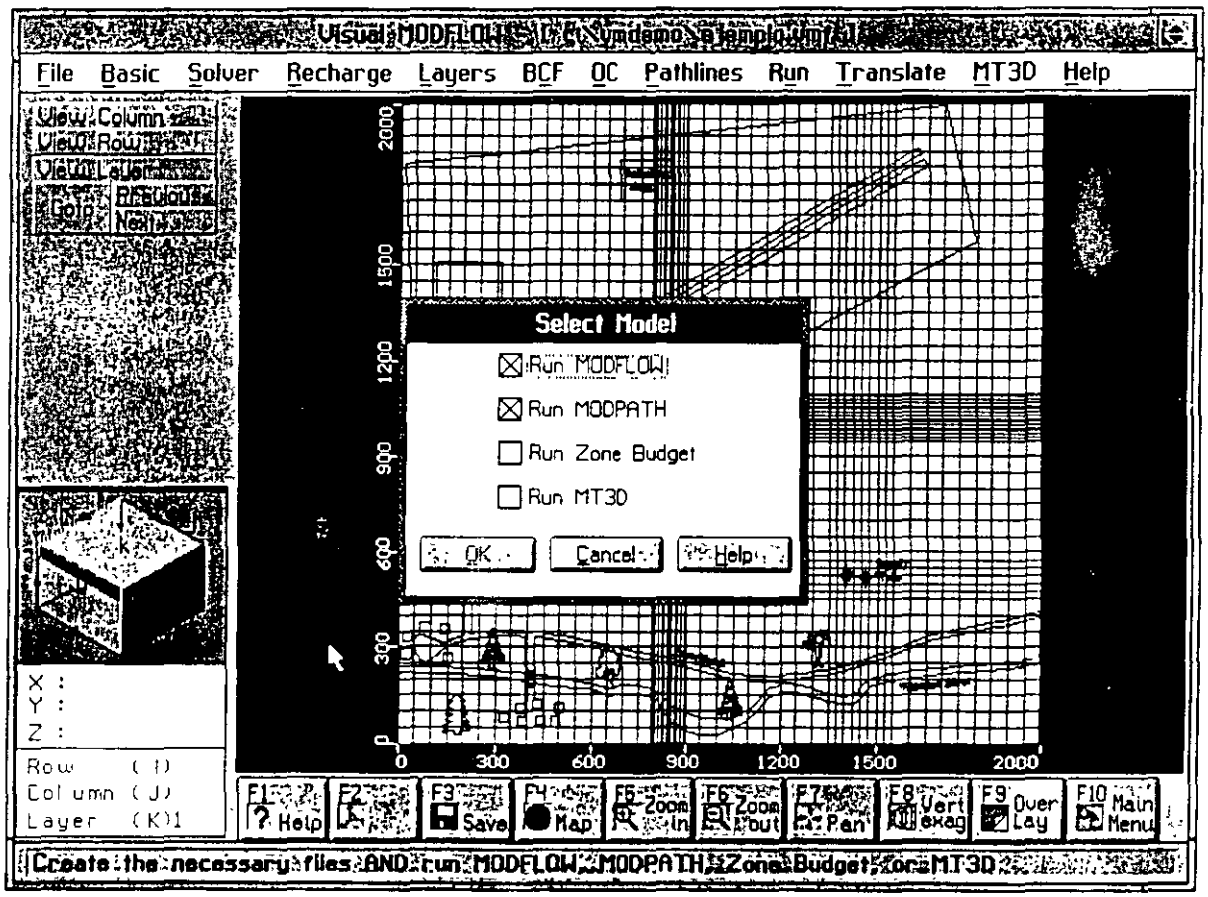

Figura 15. Corriendo el Visual Modflow

- en el recuadro de MODFLOW
- en el recuadro de MODPATH
- O.K.

11. VISUALIZACION DE LOS RESULTADOS

OUTPUT

Esto nos permite ver los niveles piezométricos calculados para el acuífero superior (figura 16).

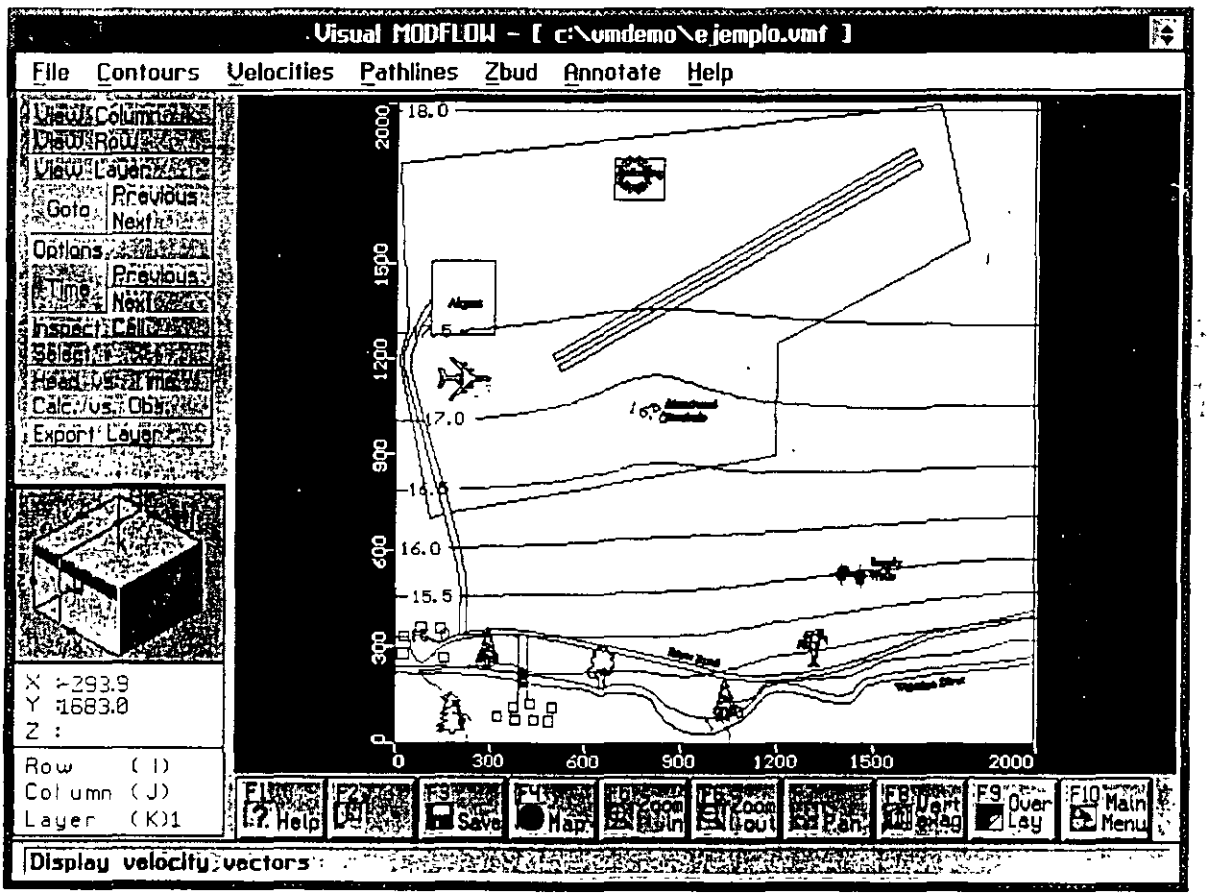

Figura 16. Niveles piezométricos

PATHLINES (del menú superior)

Esto nos permite ver el movimiento de las partículas (figura 17).

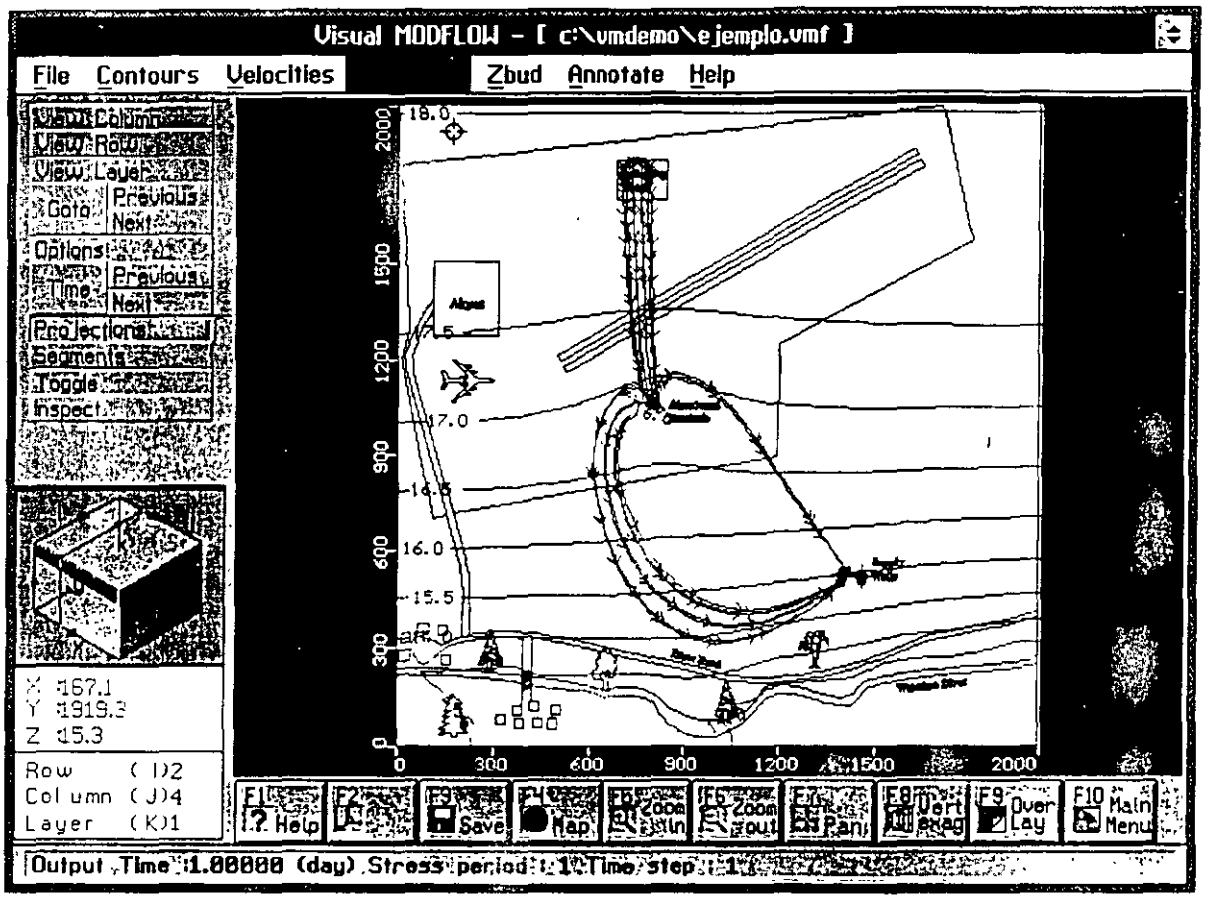

Figura 17. Movimiento de las partículas

VIEW COLUMN

Mover el cursor hacia alguna columna cerca de la perforación abandonada y . Esto nos dará una visión de la sección del modelo (figura 18).

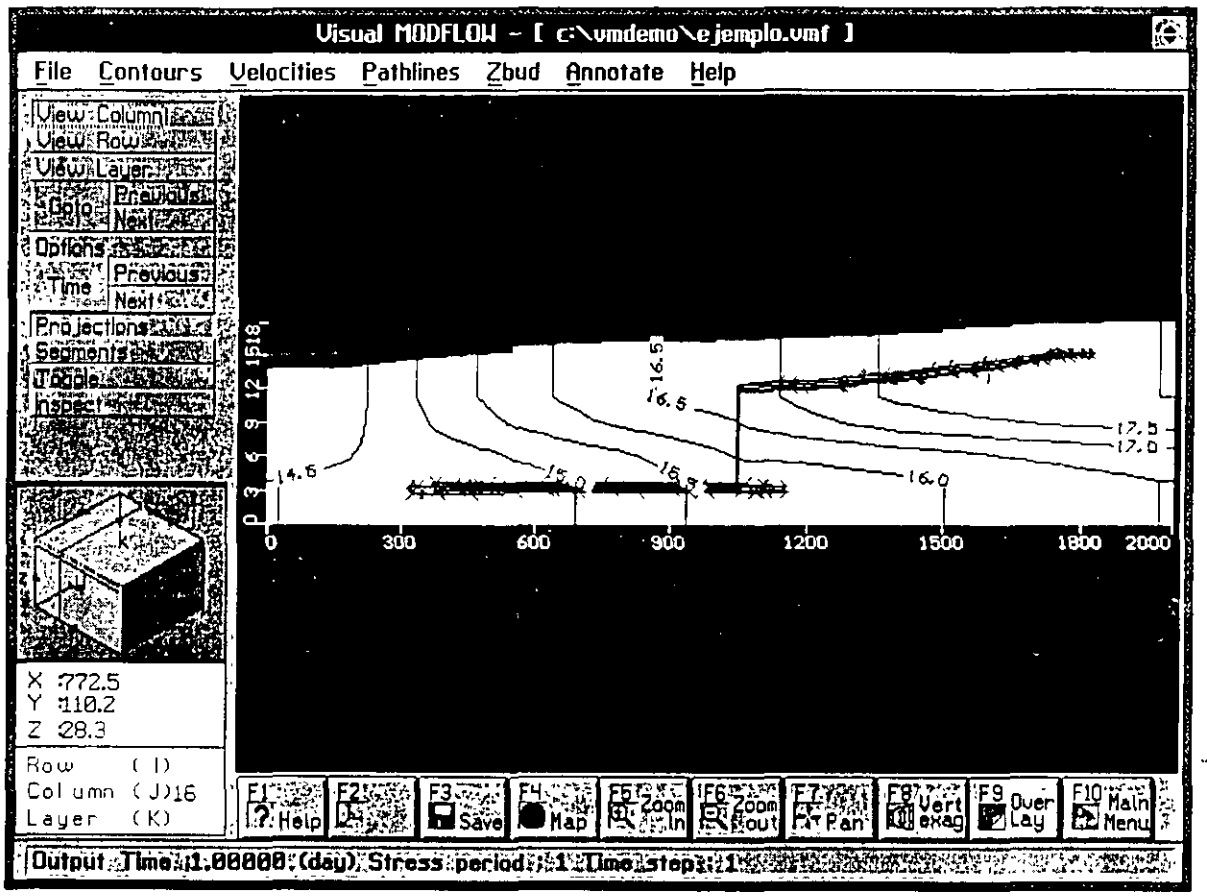

Figura 18. Movimiento de las partículas en sección

La figura 19 muestra en un acercamiento del movimiento de las partículas, y se aprecia como es que la contaminación del acuífero superior puede llegar a los pozos de abastecimiento que bombean del acuífero inferior por medio de la perforación abandonada.

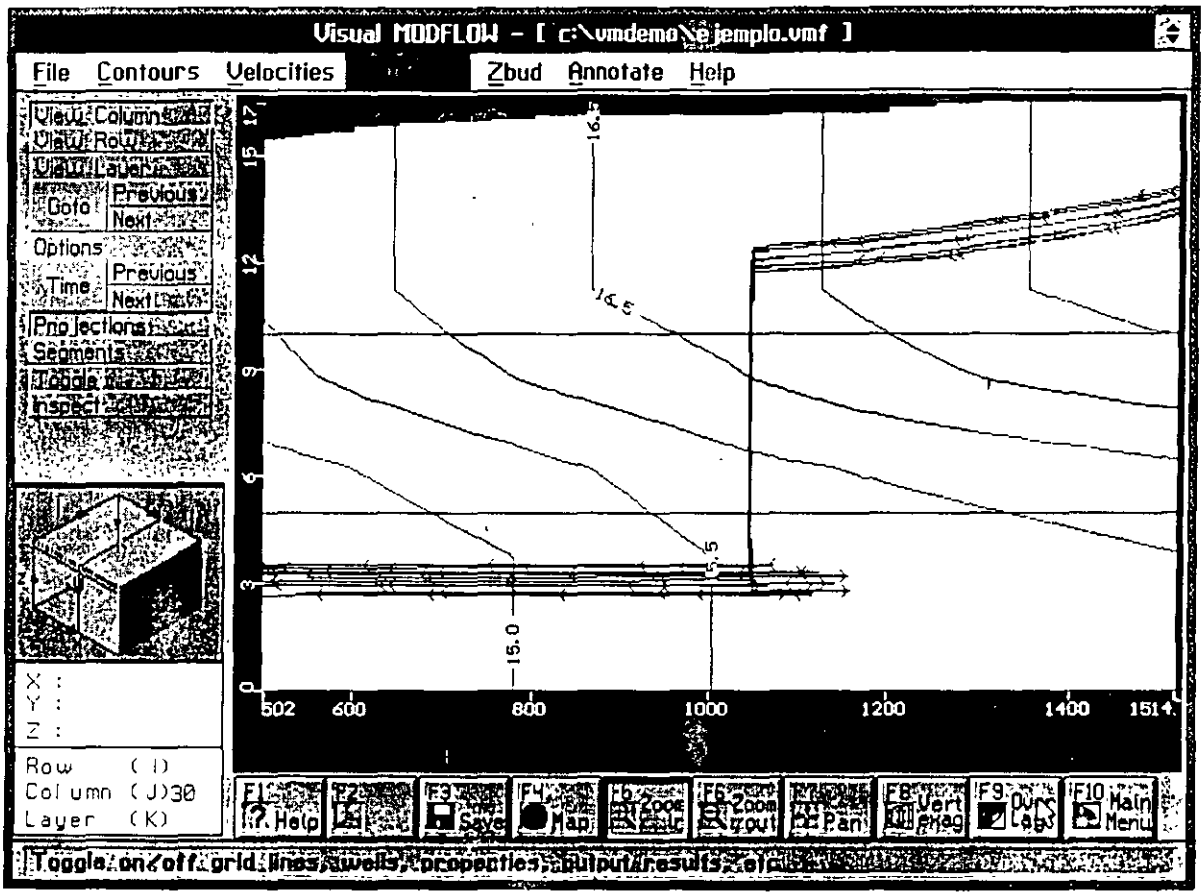

Figura 19. Movimiento de las partículas a través de la perforación abandonada.

Las figuras 20 y 21 muestran el resultado si la conductividad hidráulica que simula la perforación abandonada no hubiera sido tomada en cuenta. Este resultado predeciría que la contaminación permanecería en el acuífero superior sin infiltrarse por la perforación abandonada. De esta manera se predeciría erroneamente que los pozos de abastecimiento no se contaminarían.

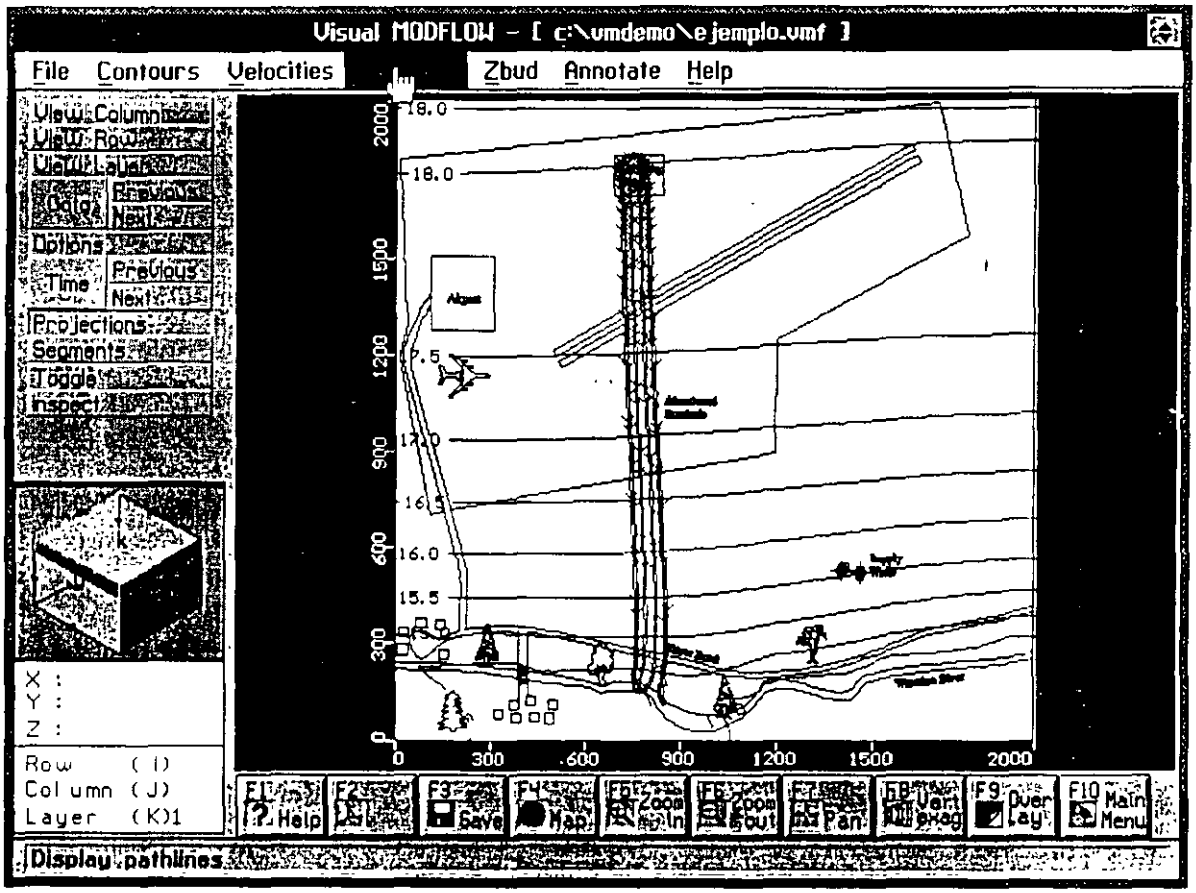

Figura 20. Movimiento de partículas cuando no se toma en cuenta la perforación abandonada.

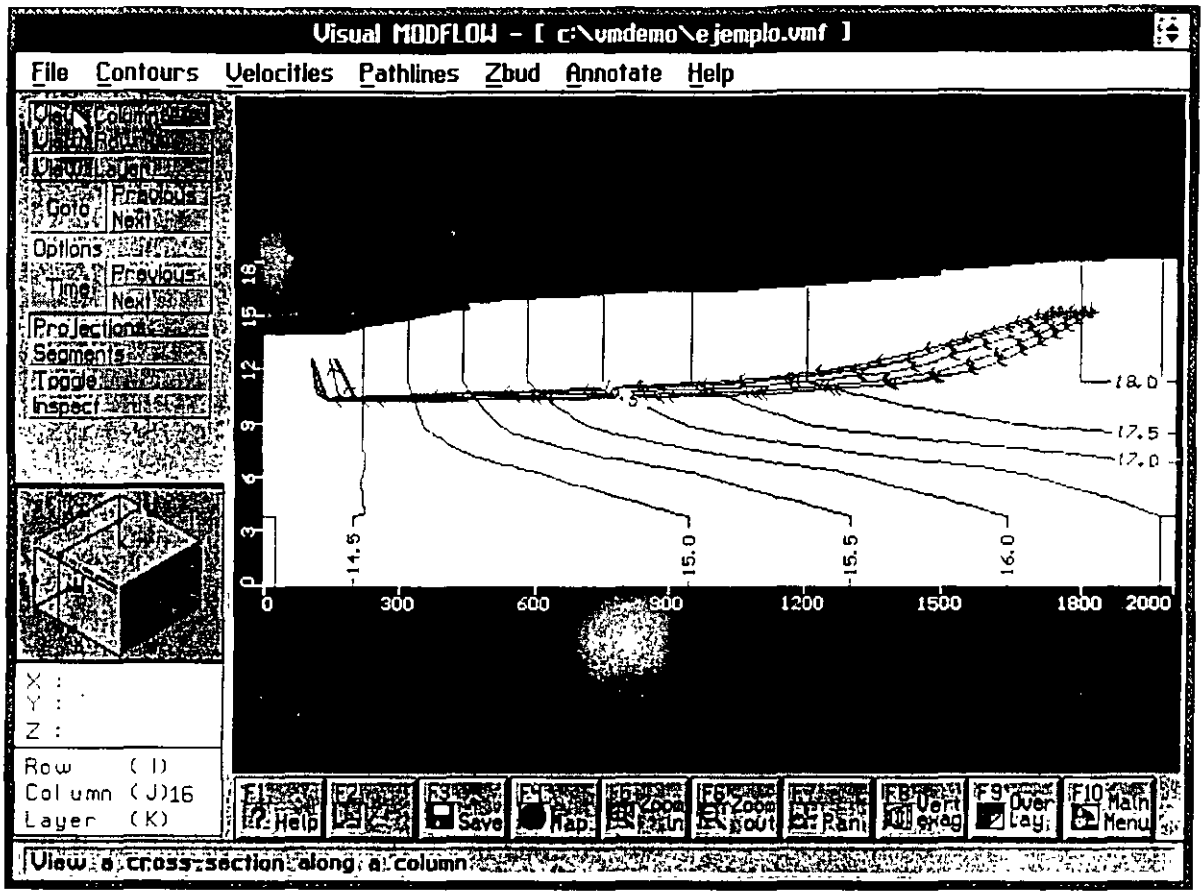

Figura 21. Sección mostrando que el movimiento de las partículas está restringido al acuífero superior, cuando no se toma en cuenta la infiltración por medio de la perforación abandonada.

- MAIN MENU (del menú superior)
- FILE
- EXIT

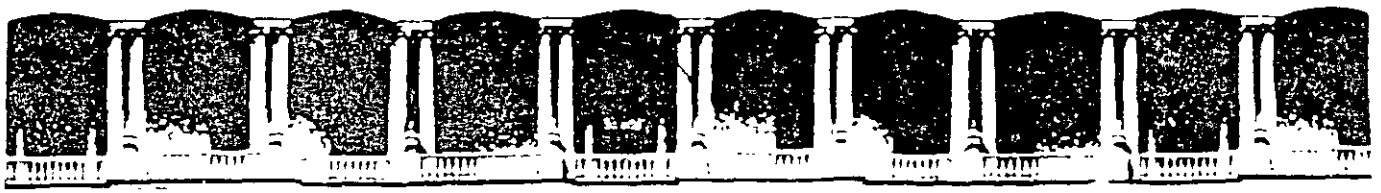

FACULTAD DE INGENIERIA U.N.A.M.
DIVISION DE EDUCACION CONTINUA

CURSOS ABIERTOS

XII CURSO INTERNACIONAL DE CONTAMINACIÓN DE ACUÍFEROS

MODULO III: MODELOS MATEMÁTICOS EN GEOHIDROLOGIA Y CONTAMINACIÓN DE ACUIFEROS

TEMA

MODELOS DE TRANSPORTE

EXPOSITOR: M. EN C. FERNANDO LARA GUERRERO
PALACIO DE MINERIA
OCTUBRE DEL 2000

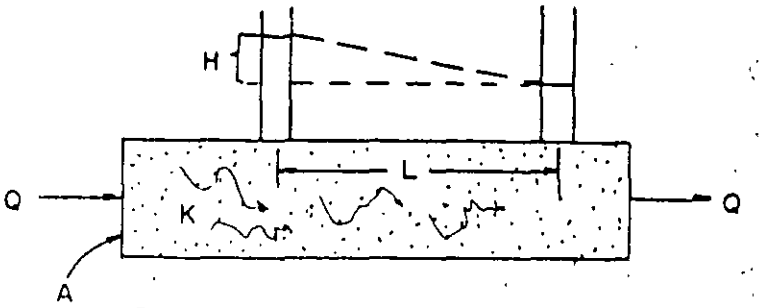

Gradiente = H/ L = I, la energía requerida para mover el agua L.
Q = Flujo (gpd).
A = Area transversal (ft^2)
K = Conductividad hidráulica = gpd ft

Tubo vertical con flujo ascendente

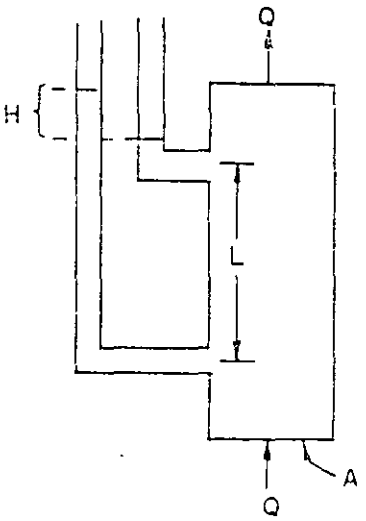

Tubo vertical con flujo descendente

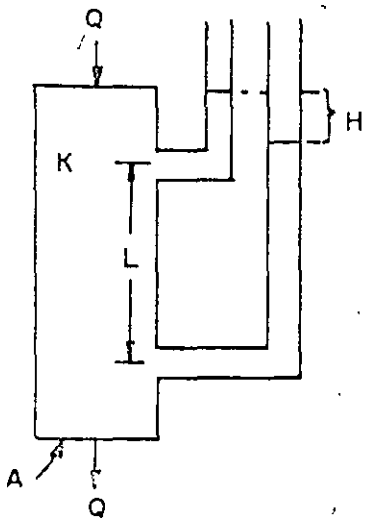

Condiciones de campo

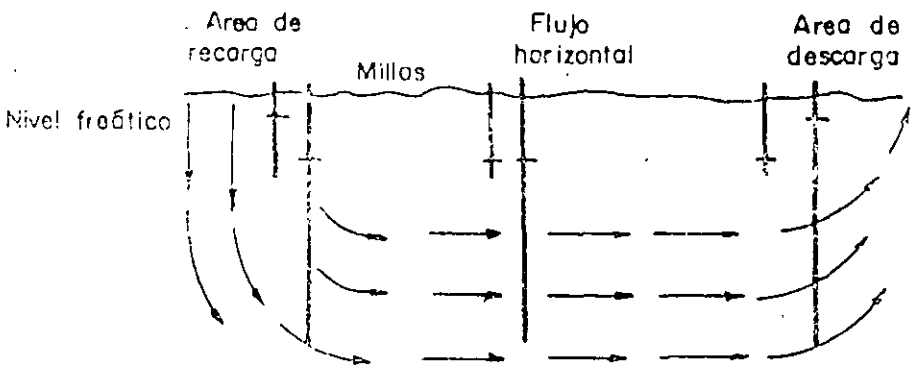

Explicación gráfica de la ley de Darcy.

Modelación Numérica del Flujo y Transporte de Contaminantes

Ing. Fernando Lara
Instituto Mexicano de Tecnología del Agua

Problemas Asociados a la Contaminación de Acuíferos

En general, se deben responder tres preguntas básicas relacionadas con los contaminantes en el subsuelo:

En qué dirección se mueven ?

Con qué velocidad se mueven ?

Cuál será su concentración en el tiempo y el espacio?

Objetivos de la Modelación de Transporte de Contaminantes

- Análisis de la trayectoria y tiempo de arribo de los contaminantes
- Evaluación de la pluma contaminante en el espacio y el tiempo
- Estimación de la concentración y curvas de concentración
- Evaluación del riesgo a la contaminación
- Evaluación de medidas de saneamiento y protección de acuíferos

Transporte de Solutos en un Sistema de Flujo Subterráneo

Transporte de masa

- Advección
- Dispersión
- Difusión

Transferencia de masa

- Filtración
- Adsorción-absorción
- Intercambio iónico
- Precipitación
- Biodegradación

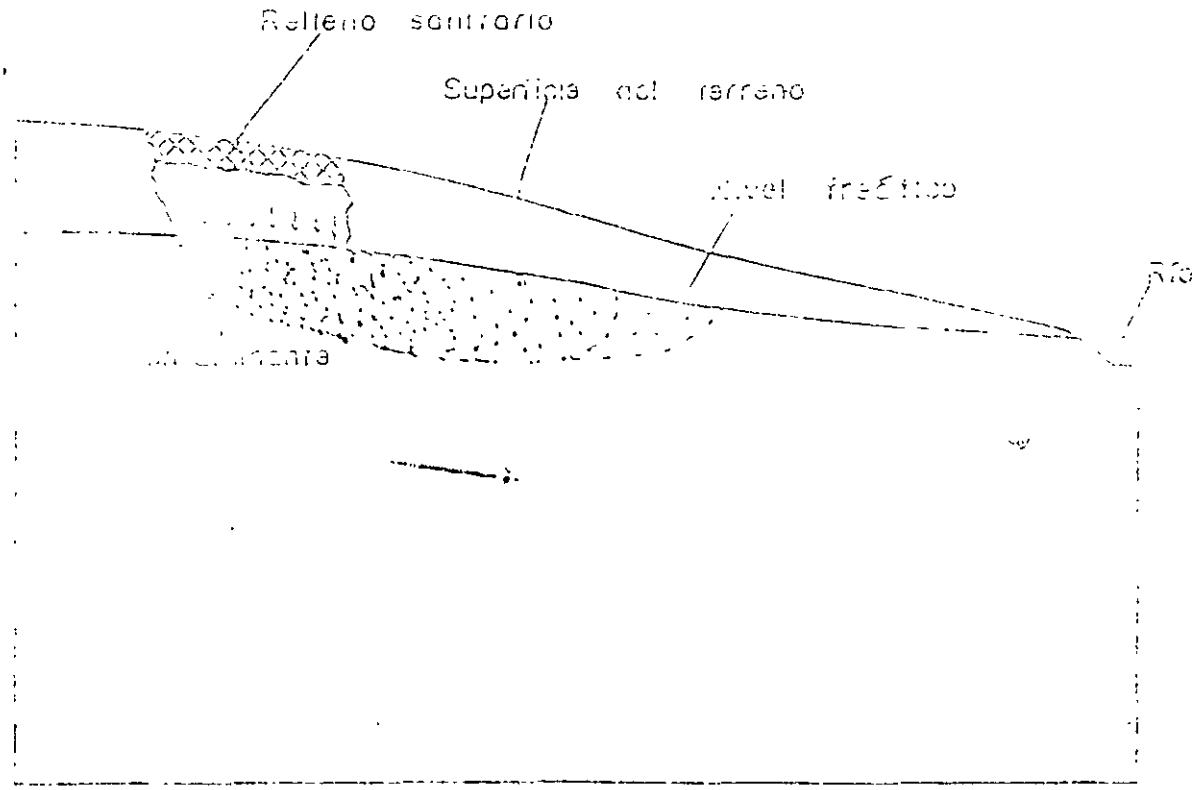

Representación esquemática de la contaminación del agua subterránea en una sección transversal de un sistema acuífero. Fetter y Lehr, 9.

ADVECTION AND DISPERSION OF A CONTAMINANT SLUG

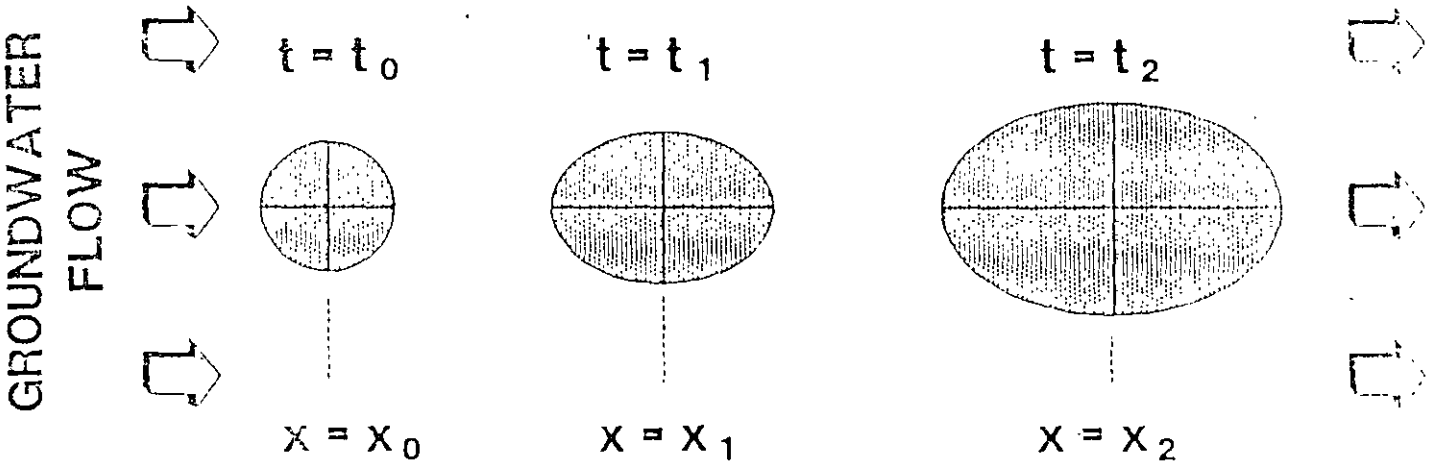

igure 11 Transport of a contaminant slug through a porous aquifer.

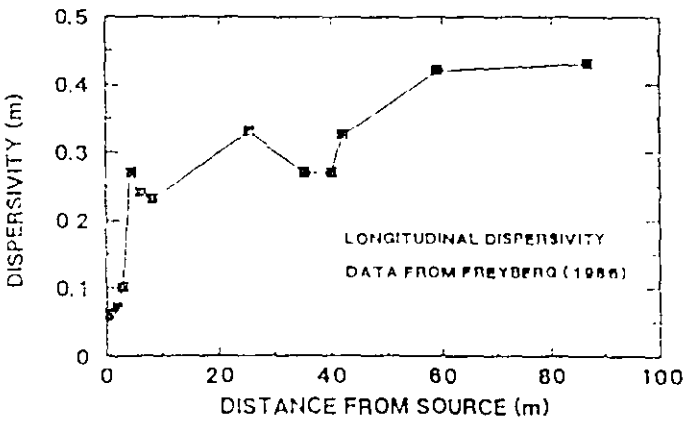

Figure 12. Increase in longitudinal dispersivity with transport distance

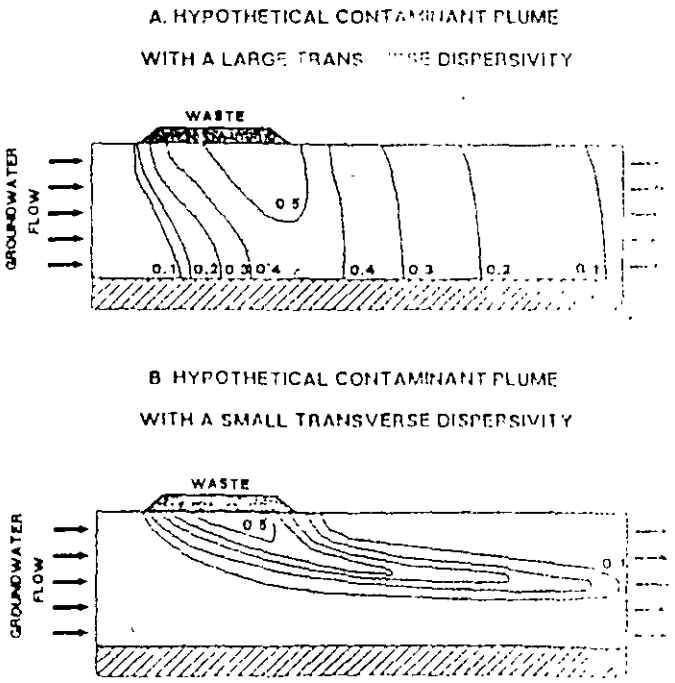

Figure 13 Hypothetical contaminant plumes for large (A) and small (B) dispersivities

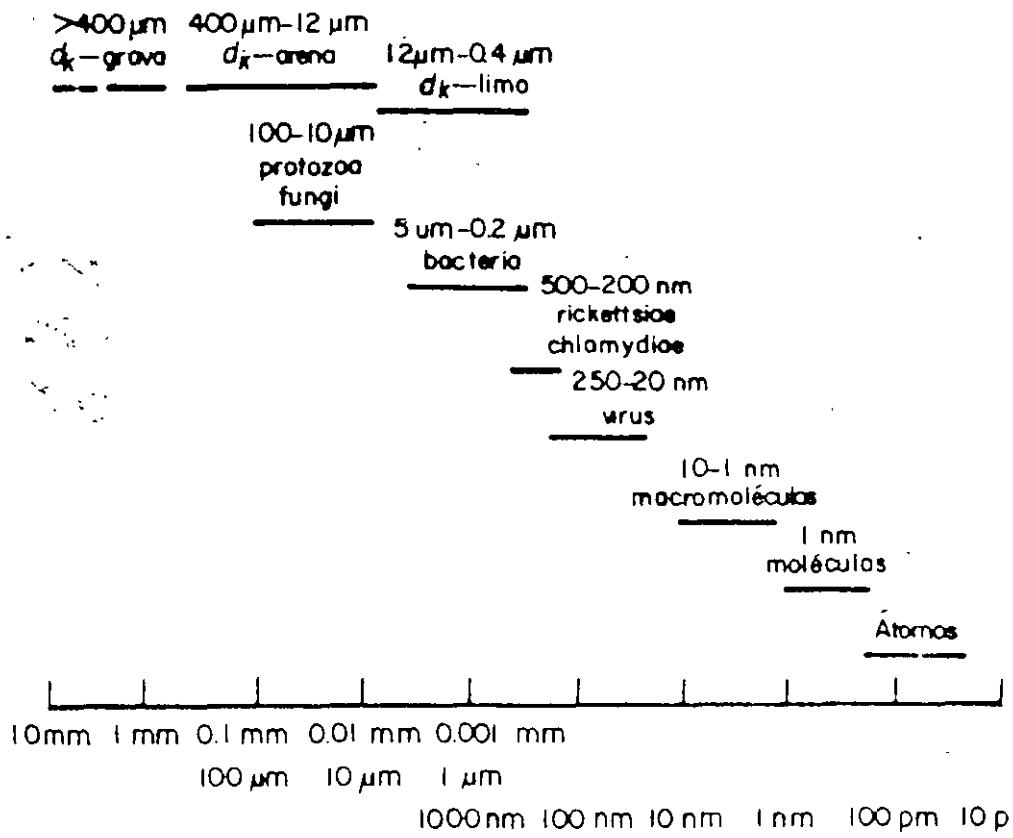

Comparación de los tamaños de los microorganismos con respecto al tamaño de los granos de sedimento, moléculas y átomos *(Modificado de Matthess y Pekdeger, 1985)*.

Constante de eliminación del 99.9% de algunas bacterias y virus en el agua subterránea.

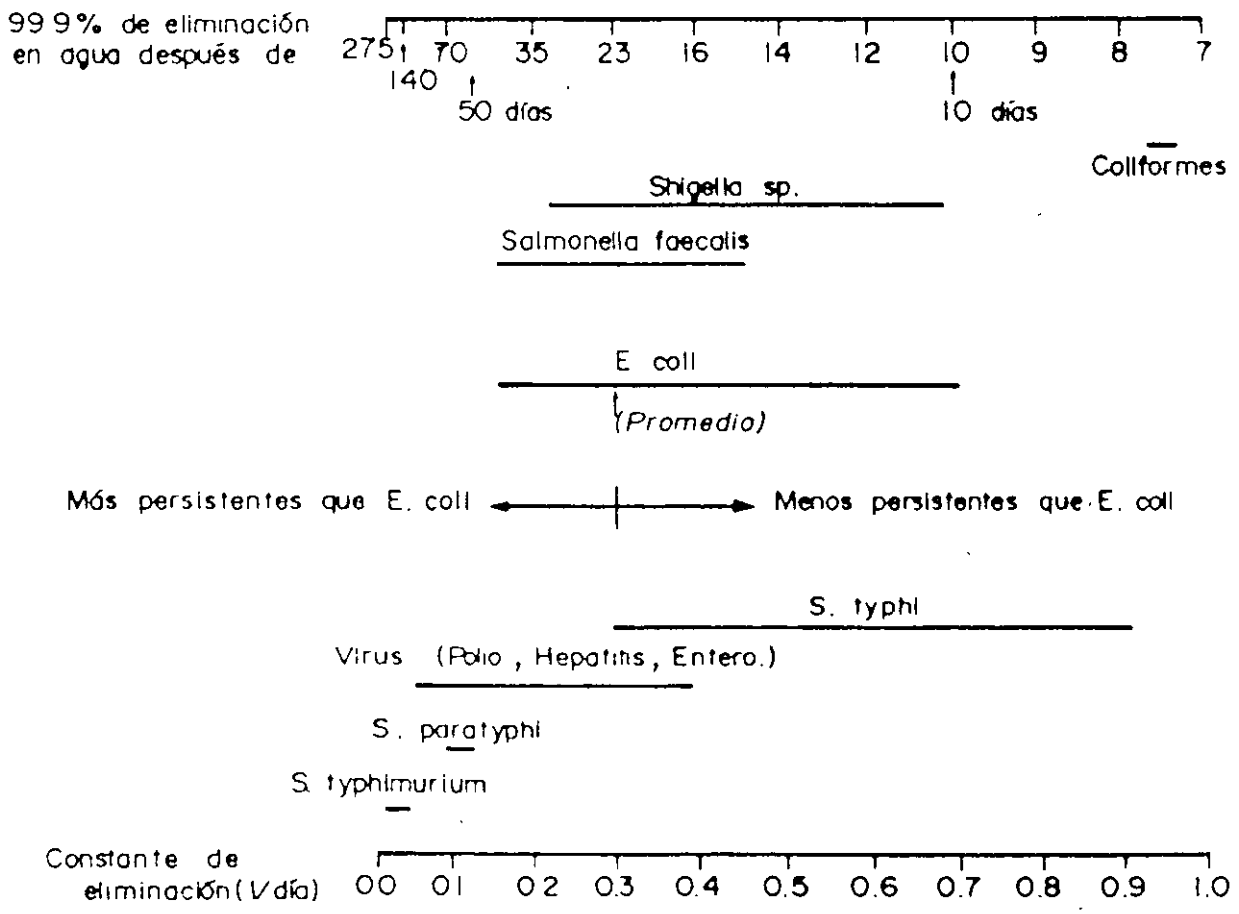

Referencia Matthess et al 1985

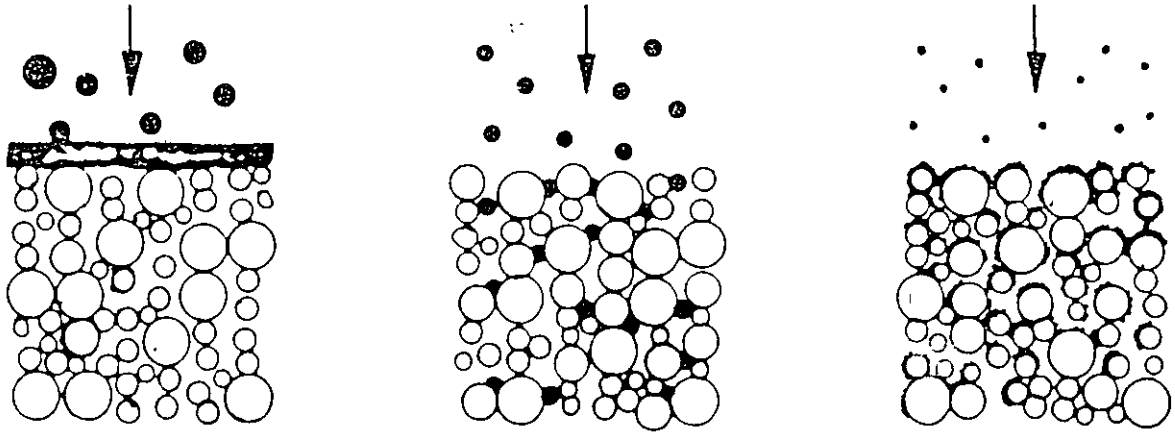

Mecanismos de filtración que limitan el movimiento de partículas a través del medio poroso *(Mc Cowell – Boyer et al., 1986)*

Procesos que controlan el transporte de masa

Proceso	*Definición*	*Impacto en el transporte*
Advección	Movimiento de masa como resultado del flujo subterráneo	Uno de los procesos más importantes de transporte.
Dispersión	Mezcla de fluidos debido al efecto de la heterogeneidad en el subsuelo.	Mecanismo de atenuación. Reduce y dispersa la concentración del contaminante.
Difusión	Movimiento de concentración en respuesta a un gradiente de concentración	Mecanismo de atenuación. Reduce la concentración

(Adaptado de NCR, 1991)

ESCALAS DE HETEROGENEIDAD EN LOS ACUÍFERO

(ADAPTADO DE SPITZ Y MORENO, 1996)

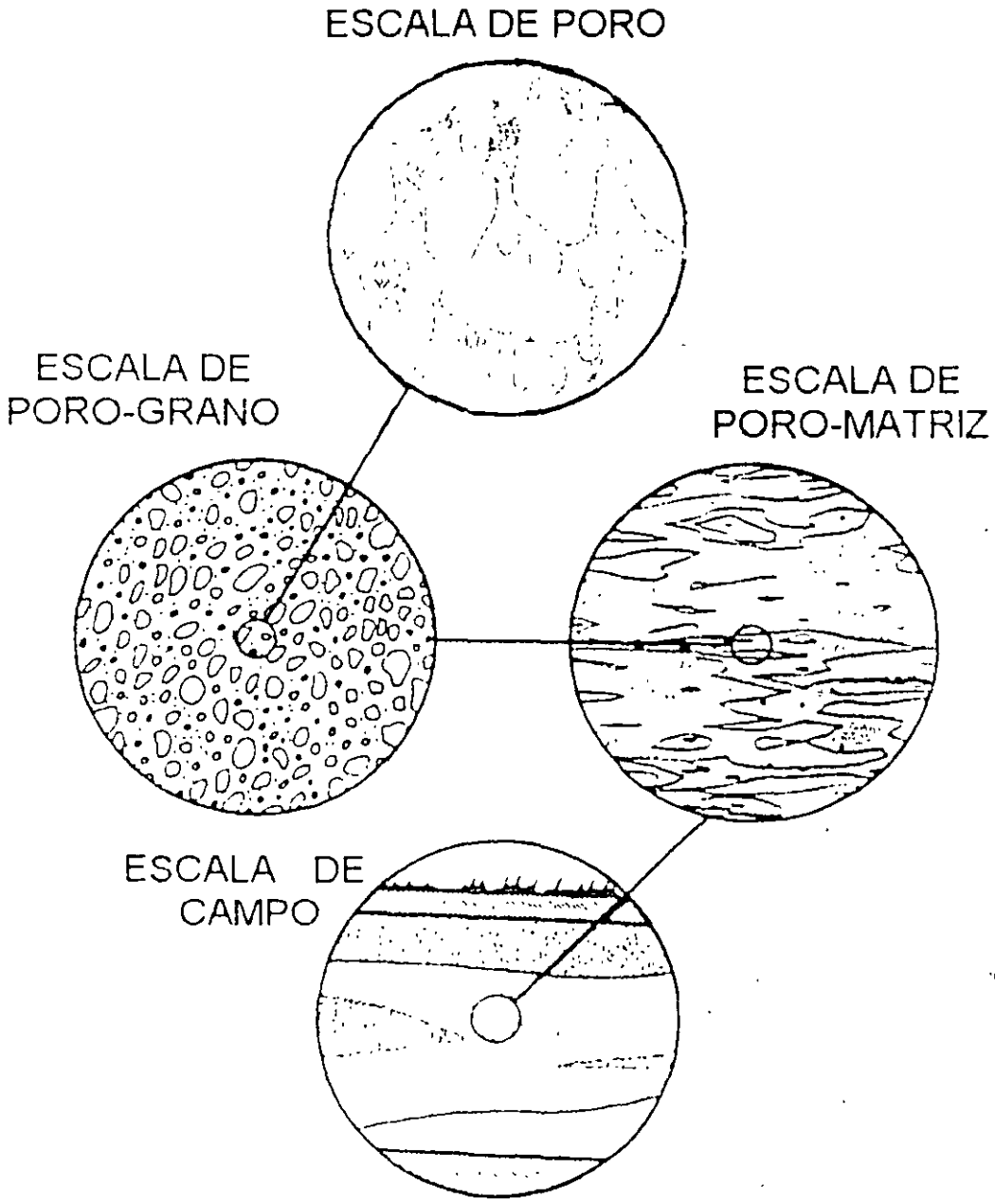

Introducción

Los modelos de computo son herramientas esenciales para analizar problemas complejos de flujo y transporte en el subsuelo.

Los modelos se refieren a la aplicación de programas de computo que resuelven un conjunto de ecuaciones, que representan el modelo matemático de un proceso físico o químico que ocurre en el subsuelo

Su aplicación permite estimar la respuesta de la carga hidráulica y la concentración cuando hay variaciones en las propiedades hidráulicas y en la recarga o extracción de un acuífero.

Ecuación de flujo en tres dimensiones:

$$K_x \frac{\partial^2 h}{\partial x^2} + K_y \frac{\partial^2 h}{\partial y^2} + K_z \frac{\partial^2 h}{\partial z^2} = S_s \frac{\partial h}{\partial t} - R$$

Cloruro,
(Advección y dispersión)

1 día 85 días 462 día 647 días

Tetraclo,
(Advección, dispersión y sorpción)

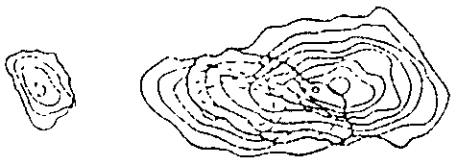

16 días 380 días 633 días

Tetracloroetileno,
(Advección, dispersión y sorpción)

16 días 350 días 633 días

Tolueno
(Advección, dispersión, sorpción y biodegradación)

3 53 108 días

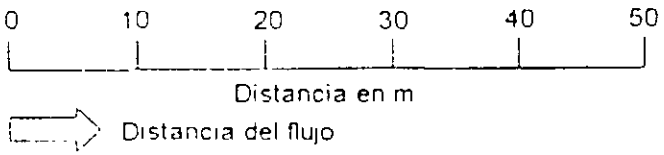

EFECTO COMBINADO DE LOS FENÓMENOS DE ADVECCIÓN, DISPERSIÓN, SORPCIÓN Y BIODEGRADACIÓN EN UN ACUIFERO DE ARENA EN BORDER, ONTARIO. (ADAPTADO DE SPITZ Y MORENO, 1996)

Características de los Modelos de Transporte de Contaminantes

- Los modelos de transporte son una valiosa herramienta para el análisis y la solución de problemas de contaminación en el subsuelo.

- Su aplicación más útil radica en simular escenarios y evaluar métodos para el saneamiento de los acuíferos.

- Es poco probable que las capacidades predictivas de los modelos mejoren en el futuro. El desarrollo de los modelos se dirige a modelos de tipo éstocastico.

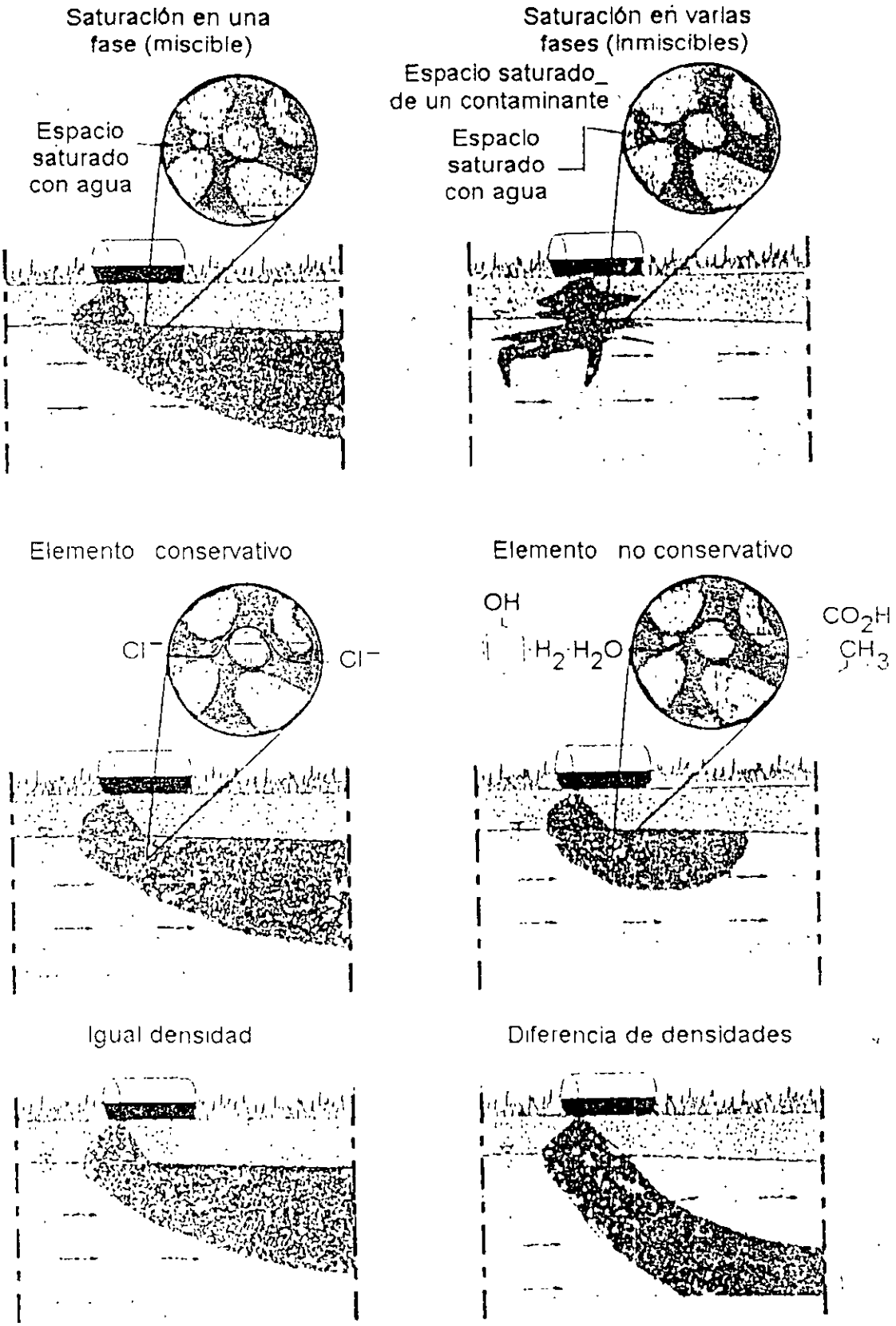

TIPOS DE CONTAMINANTES Y SU EFECTO SOBRE EL FLUJO Y TRANSPORTE EN EL SUBSUELO

(ADAPTADO DE SPITZ Y MORENO, 1996)

Características de los Modelos de Transporte de Contaminantes.

- En un modelo de transporte existe una gran diferencia si los solutos están presentes en una capa de baja o alta velocidad.

- Una parte fundamental del modelo de transporte de contaminantes es la construcción del modelo de flujo. Este debe satisfacer un alto grado de exactitud.

- Los modelos de transporte poseen menor poder predictivo que los modelos de flujo.

Modelo Físico

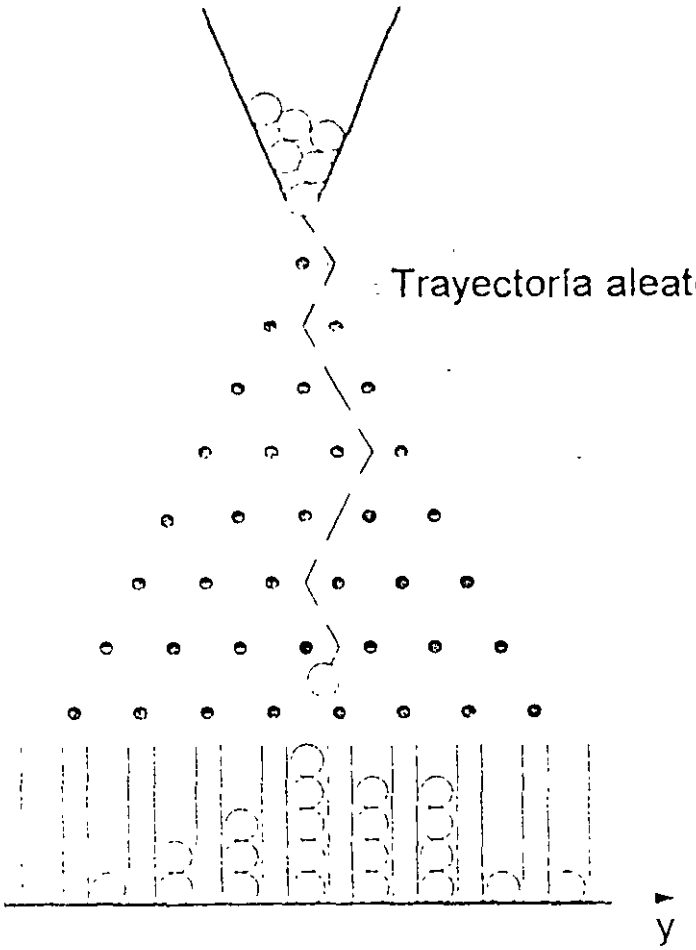

Aproximación analítica

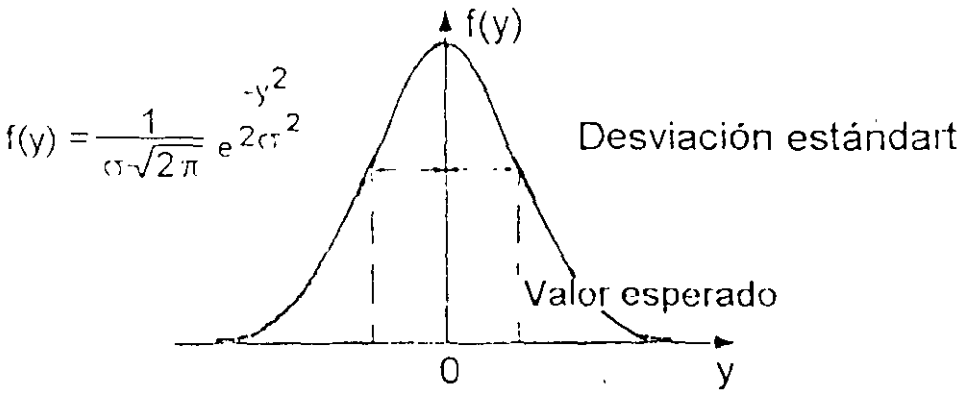

ILUSTRACIÓN DEL FENÓMENO DE DISPERSIÓN LATERAL

(ADAPTADO DE SPITZ Y MORENO, 1996)

DIFERENCIAS FINITAS

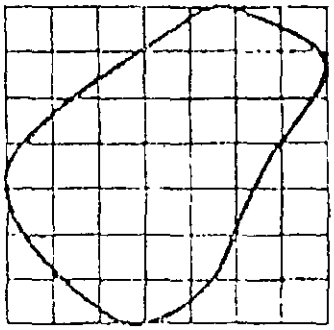

ELEMENTOS FINITOS

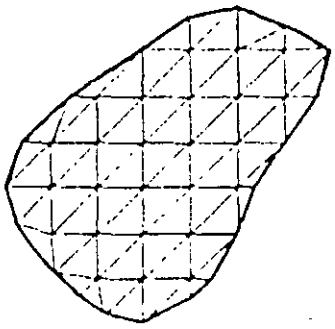

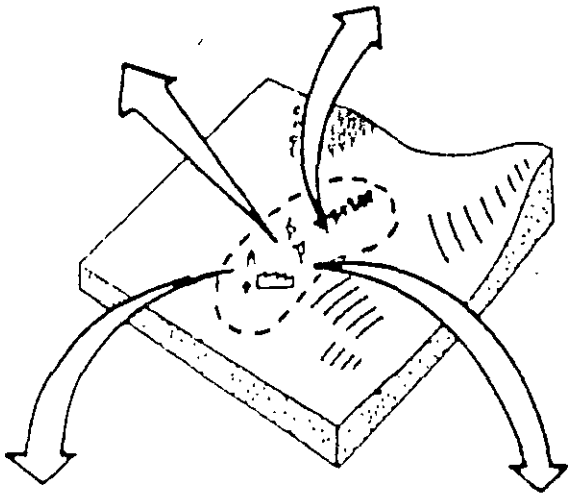

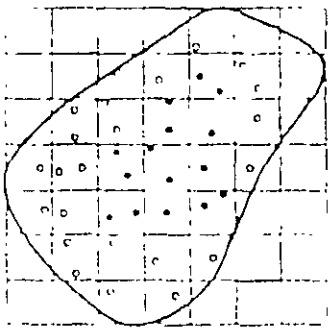

METODO DE LAS
CARACTERISTICAS

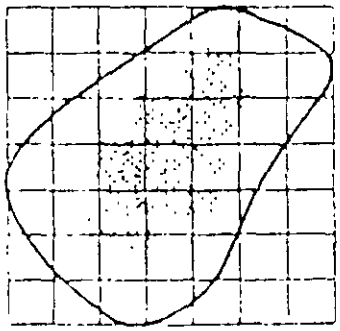

TRAYECTORIA ALEATORIA
("RANDOM WALK")

TIPOS DE MODELOS DE TRANSPORTE

La ecuación de transporte en una dimensión en un medio poroso homogéneo e isótropo que incluye sorpción y decaimiento, se puede expresar como (Fetter, 1990):

$$\frac{\partial C}{\partial t} = D_L \frac{\partial^2 C}{\partial x^2} - v_x \frac{\partial C}{\partial x} - \frac{B_d}{\phi} \frac{\partial C}{\partial t} + \left(\frac{\partial C}{\partial t}\right)_{rxn}$$

dispersión advección sorpción reacción

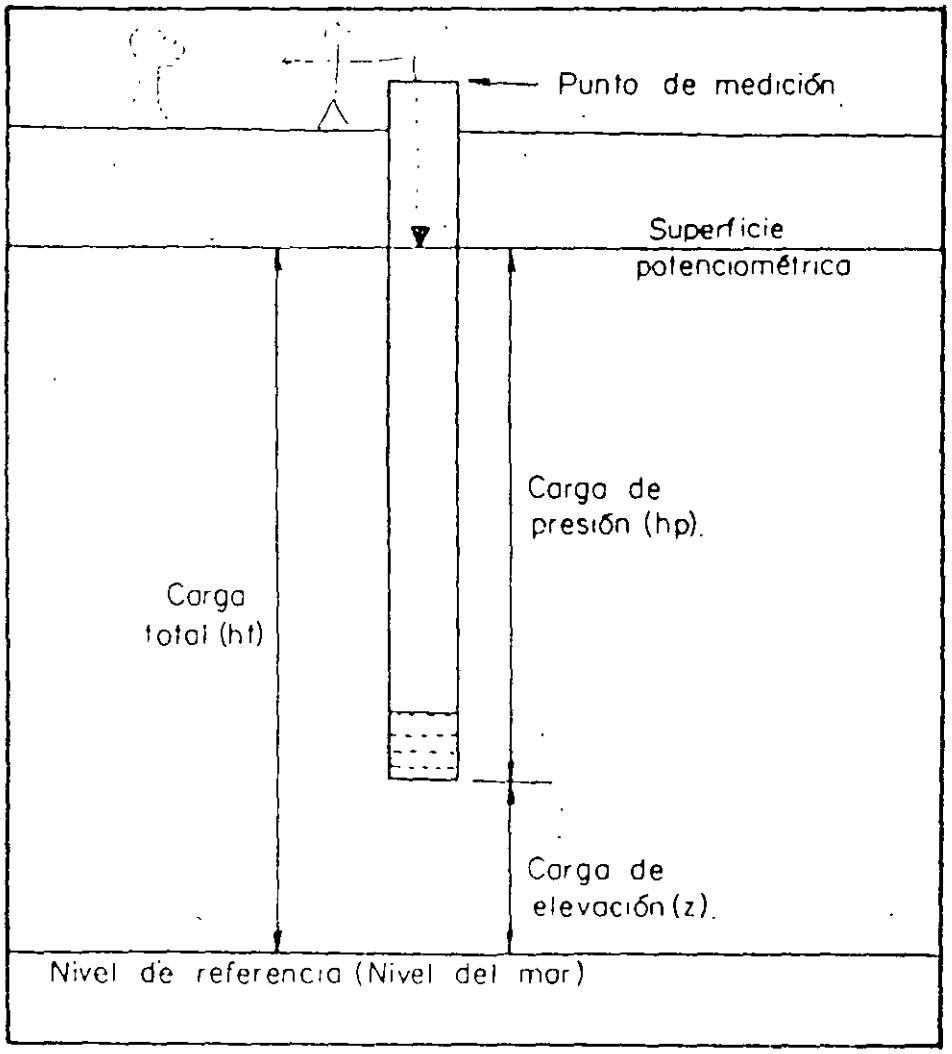

Relación entre carga hidráulica total, carga de presión y carga de elevación.

Tipos de Modelos Numéricos

(Anderson,MP. Prickett, T.,A,1994)

Familias de Programas

Flujo subterráneo	PLASM		MODFLOW	AQUIFEM
Transporte		RNDWALK	MT3D	
Trayectoria de particulas	FLOWPATH		PATH3D	MODPATH

Flujo saturado variable	FEMWATER	VS2D
Transporte saturado variable	FEMWASTE	VS2DT

Programas únicos

Flujo subterráneo	AQUIFEM-1
Transporte	BIO1D,USGS MOC, SWIFT/389
Flujo saturado variable	UNSAT2
Transporte en un medio variable saturado	SUTRA

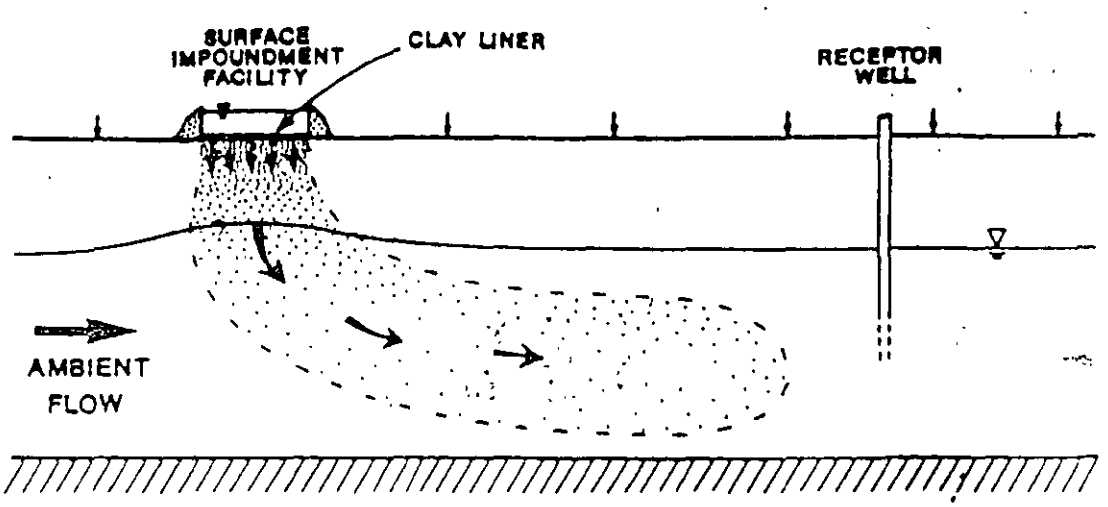
SURFACE IMPOUNDMENT FACILITY
CLAY LINER
RECEPTOR WELL
AMBIENT FLOW

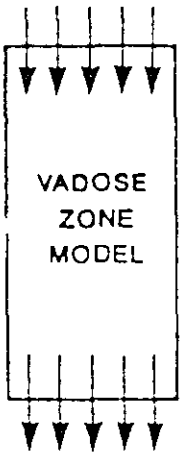
VADOSE ZONE MODEL

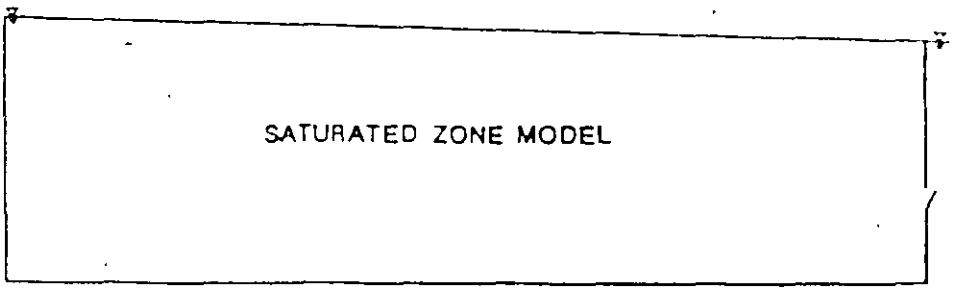
SATURATED ZONE MODEL

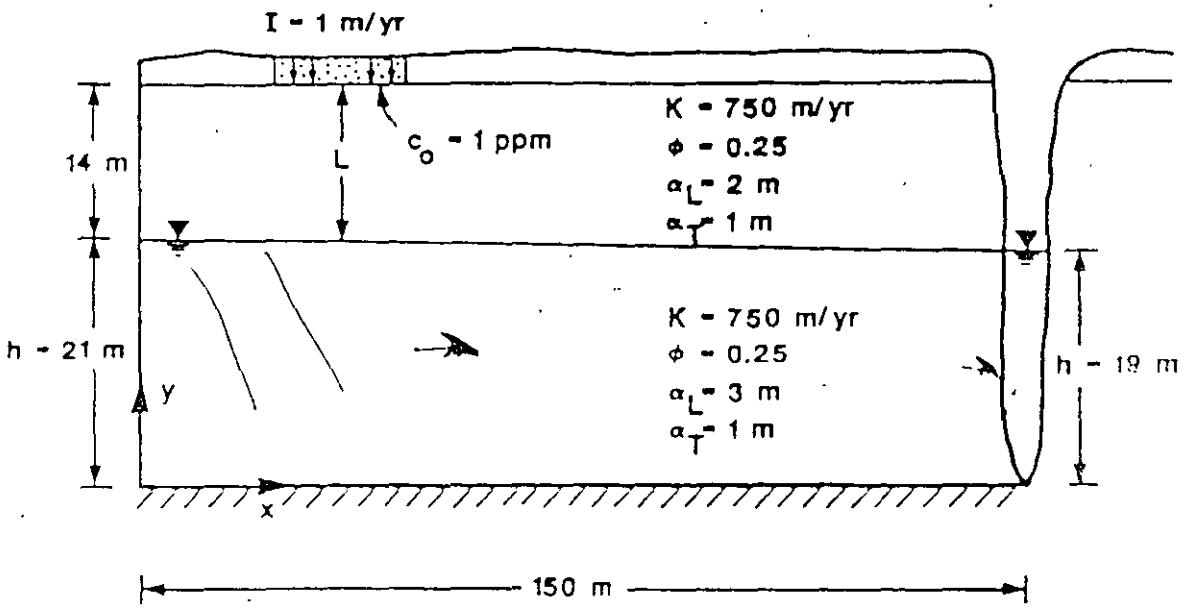
I = 1 m/yr
14 m
L
c_o = 1 ppm
K = 750 m/yr
ϕ = 0.25
α_L = 2 m
α_T = 1 m
h = 21 m
y
K = 750 m/yr
ϕ = 0.25
α_L = 3 m
α_T = 1 m
h = 19 m
x
150 m

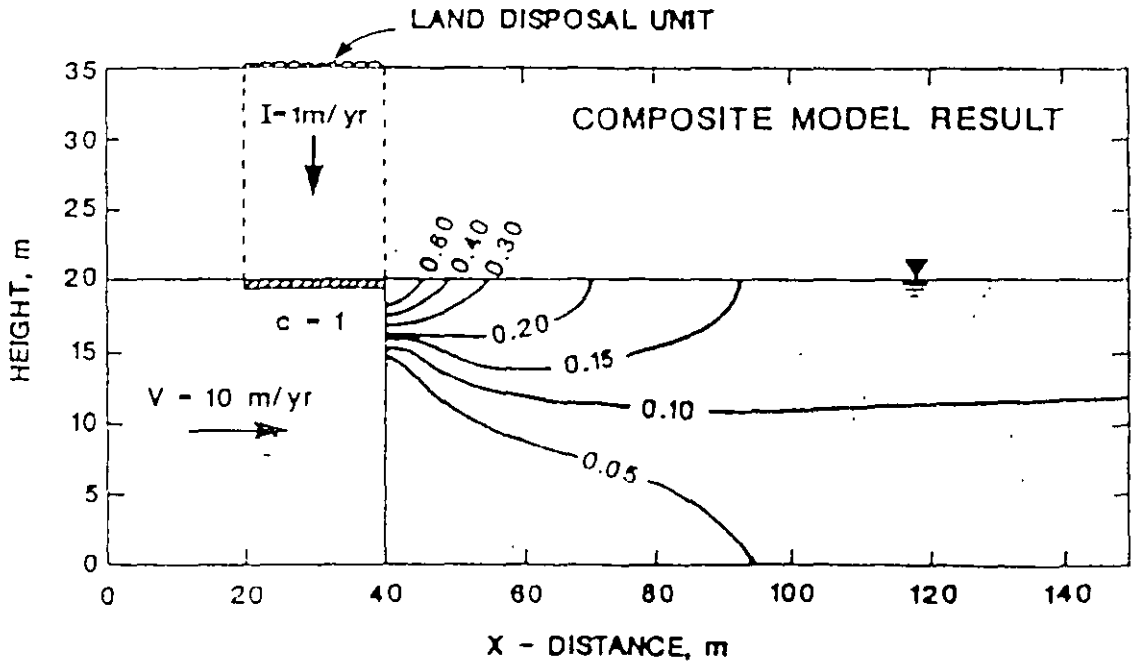
LAND DISPOSAL UNIT
I = 1m/yr
COMPOSITE MODEL RESULT
0.80
0.40
0.30
0.20
0.15
0.10
0.05
c = 1
V = 10 m/yr
HEIGHT, m
X - DISTANCE, m
0
5
10
15
20
25
30
35
0
20
40
60
80
100
120
140

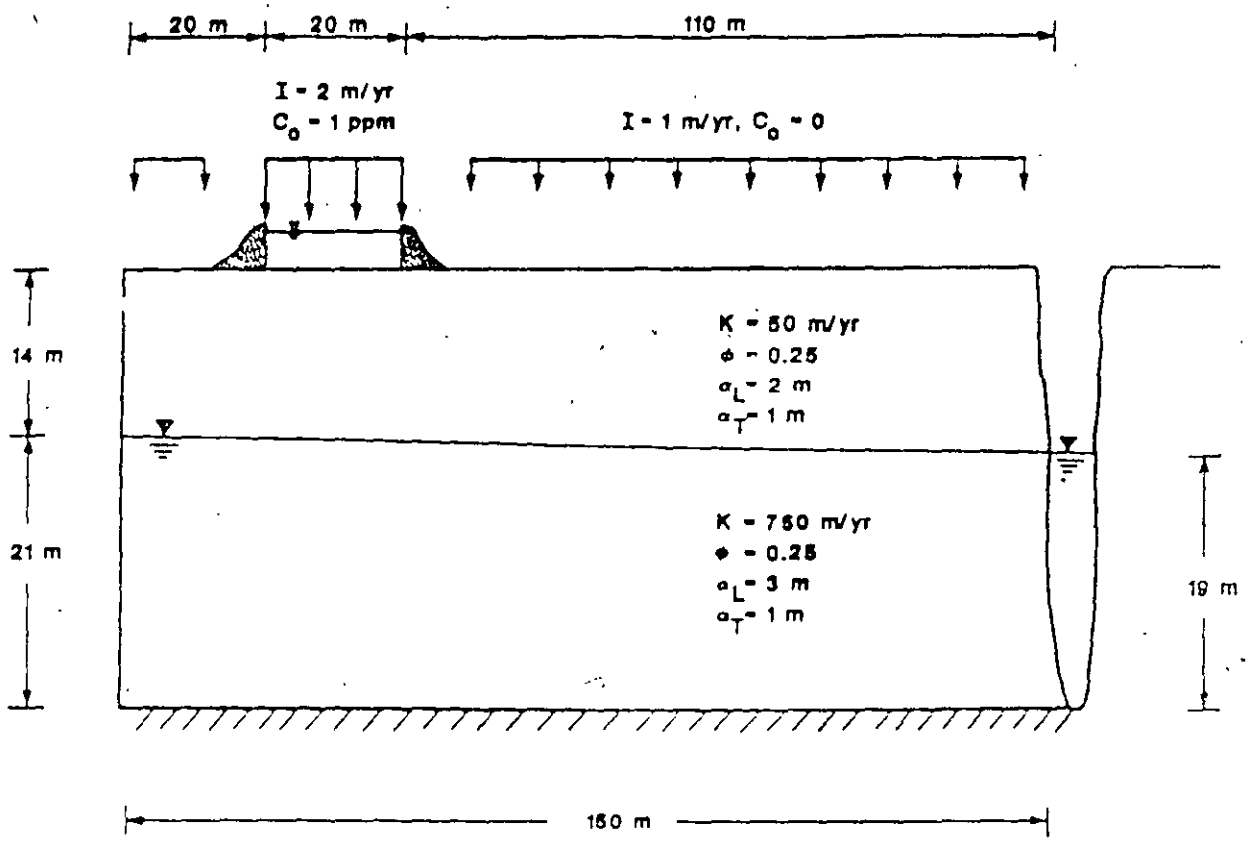
20 m
20 m
110 m
I = 2 m/yr
C_o = 1 ppm
I = 1 m/yr, C_o = 0
14 m
21 m
K = 50 m/yr
ϕ = 0.25
α_L = 2 m
α_T = 1 m
K = 750 m/yr
ϕ = 0.25
α_L = 3 m
α_T = 1 m
19 m
150 m

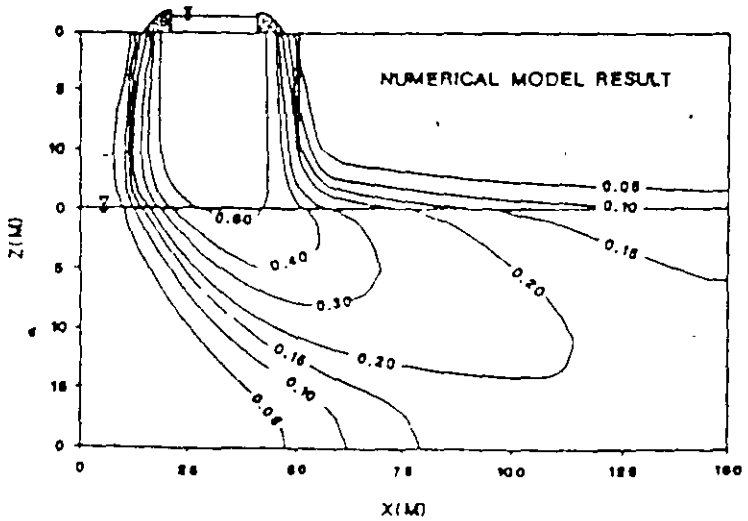
NUMERICAL MODEL RESULT
0.60
0.40
0.30
0.20
0.16
0.10
0.06
0.20
0.16
0.10
0.06
Z(M)
X(M)

Modelos de Trayectoria de Partículas

Los programas que simulan el movimiento de los solutos únicamente por advección se conocen como modelos de trayectoria de partículas ("Particle traking"). No calculan la concentración de solutos.

Debido a su facíl aplicación son más populares que los programas de transporte de solutos. Las simulaciones permiten calcular la trayectoria de las partículas y el tiempo de transito.

Los modelos de trayectoria de partículas son una alternativa para simular el transporte de solutos cuando el grado de incertidumbre, asociado con los parámetros de dispersión y de retardación es muy grande.

Área de protección de fuentes subterráneas de abastecimiento de agua potable.

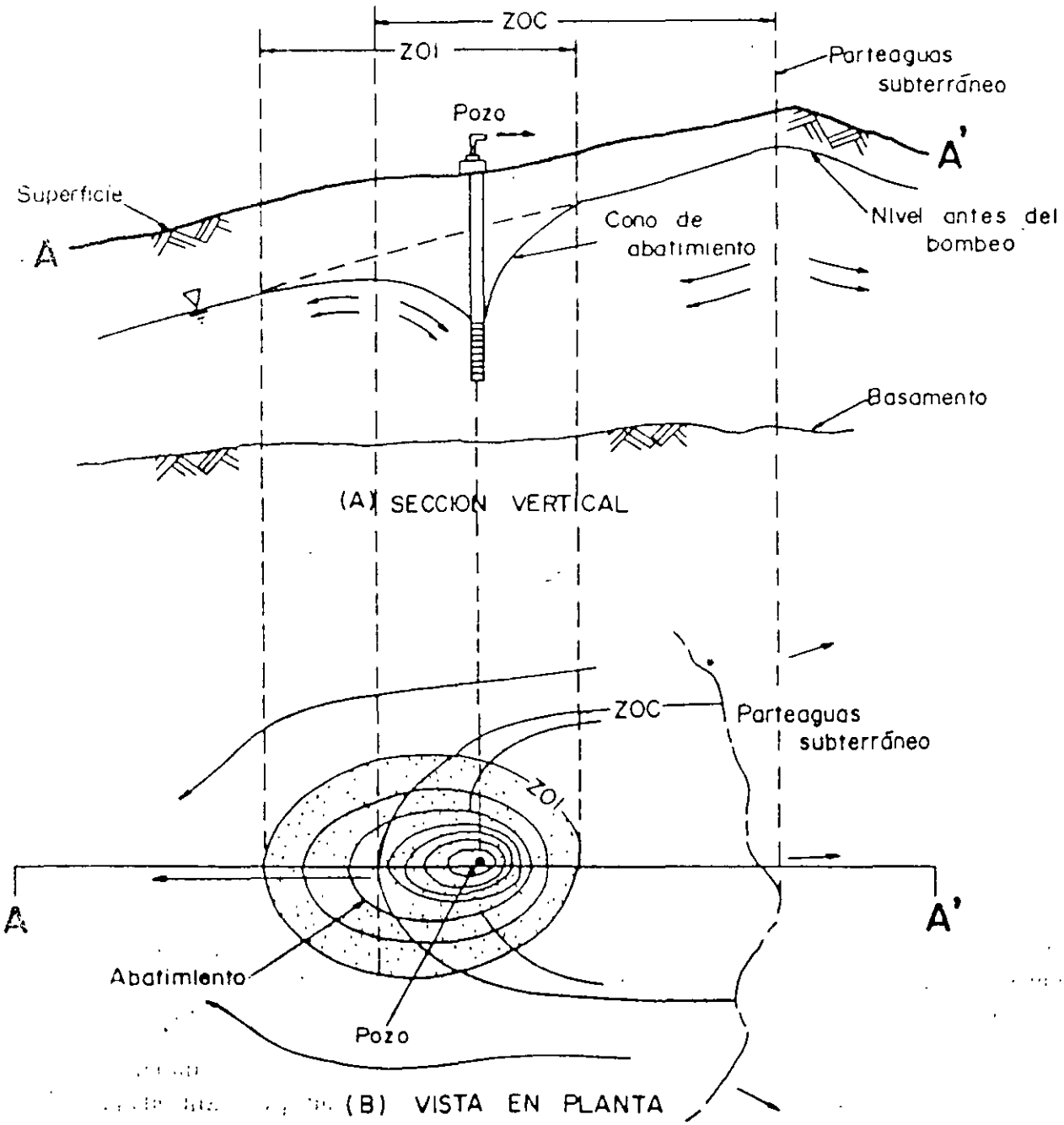

SIMBOLOGIA

- Nivel estático
- Dirección de flujo
- Pozo de bombeo
- ZOI Zona de influencia
- ZOC Zona de contribución

Datos Requeridos por un Modelo de Transporte

1. Modelo de Flujo

   - Mapa hidrogeológico
   - Continuidad y espesor de capas permeables y confinantes
   - Distribución de T y S
   - Mapa de elevación del nivel estático y sus variaciones en el tiempo
   - Distribución del bombeo en el tiempo y el espacio
   - Estimación y distribución de la recarga
   - Interacción agua superficial y agua subterránea

2. Modelo de Transporte de Solutos

   - Distribución de las cargas hidráulicas calculadas en el modelo de flujo
   - Estimación de parámetros: coef. de dispersión (long. y trans).; porosidad efectiva : factores de retardación
   - Concentración de la calidad natural del agua
   - Tipo y distribución del contaminante en el tiempo y el espacio

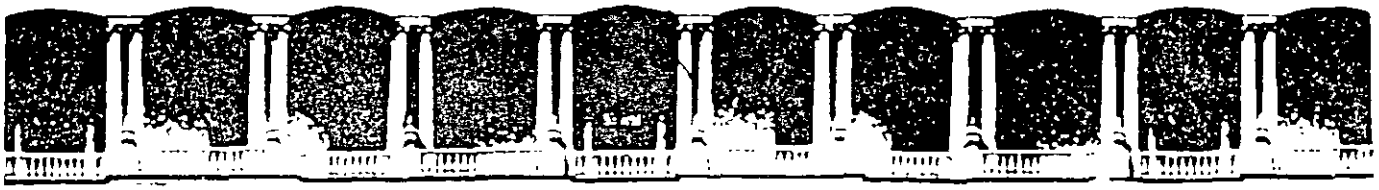

FACULTAD DE INGENIERIA U.N.A.M.
DIVISION DE EDUCACION CONTINUA

CURSOS ABIERTOS

XII CURSO INTERNACIONAL DE CONTAMINACIÓN DE ACUÍFEROS

MODULO III: MODELOS MATEMÁTICOS EN GEOHIDROLOGIA Y CONTAMINACIÓN DE ACUIFEROS

TEMA

PREDICTION OF REGIONAL GROUND WATER FLOW TO STREAMS

EXPOSITOR: DR. ADOLFO CHAVEZ RODRIGUEZ

PALACIO DE MINERIA
OCTUBRE DEL 2000

Prediction of Regional Ground Water Flow to Streams

by S. Christensen[a], K.R. Rasmussen[a], and K. Møller[a]

Abstract

Database information on geology, hydrology, and hydrometeorology may form an excellent basis for studying ground water flow and seepage to surface water in a catchment. In a field case study of a 114 km^2 catchment, geological database information was used to determine layer thicknesses and boundary conditions as well as to parameterize a ground water flow model. Hydraulic head and stream flow data were used to estimate the model parameters by nonlinear regression. The uncertainty of the estimated parameters and of the predicted stream flow gains was quantified by individual likelihood method confidence intervals. During four stages of calibration, ranging from using only head data to also using an extensive set of measured stream flow gains, no parameter estimates changed significantly, but the number of parameters was increased from 12 to 14 in order to fit local stream flow gains. This indicates that the geology-based parameterization is firm.

Adding stream flows to the calibration data reduced the uncertainty of the estimated parameters significantly. However, the uncertainty of some of the parameters was significant even when an extensive set of measured stream flow gains and hydraulic heads was used to calibrate the model. Parameter uncertainty is reflected in the uncertainty of the predicted stream flow gains. When an extensive set of stream flow data was used during calibration, the prediction uncertainty is up to ±25% in large streams, and up to ±60% in smaller streams. The confidence intervals in general are skewed, and they are very skewed in the case where no stream flow measurements were used to calibrate the model.

The case study shows that even when relatively extensive geological information and calibration data are available, there may be significant uncertainty connected with the prediction of local discharge of ground water to streams. Reducing uncertainty in such cases will require extensive field investigations in order to improve the definition of recharge areas and to describe the local fluxes and flow patterns in the aquifers.

Introduction

Predicting regional ground water seepage to streams is important in a variety of environmental management and engineering problems. Thus the background for the present paper is a study of whether and where nutrients in seeping ground water can be reduced through recreation of wetlands along streams. This involves a number of basic questions: where does ground water seepage occur, and is it from near-surface aquifers or from deep aquifers? Answers will typically be assessed by using a catchment scale ground water model, but to what extent are such model predictions reliable?

Based on a case study of Danish catchments we discuss how well ground water seepage can be predicted by using a ground water model, given that the model is (typically) conceptualized from qualitative geological information available in databases, and calibrated to fit (1) hydraulic head data measured throughout the catchment; and (2) stream flow measured in a few main tributaries.

It is commonly accepted that the efflux of ground water from deep aquifers varies very little during the year, or even from year to year, while the discharge from near-surface aquifers can vary almost instantaneously due to variations in precipitation (Bear 1979; Freeze and Cherry 1979; Christensen 1994). However, after long dry periods drain and overland flow becomes insignificant, and the discharge from near-surface aquifers tends to stabilize at a low to moderate level or, in areas where such aquifers are shallow, almost vanish. It is in this baseflow situation when ground water discharge is quasi-stationary that we can actually estimate it from synchronously, closely spaced, stream flow measurements.

In the first section of the paper we describe the studied area using available database information. We describe the geology in as great detail as we think possible on a catchment scale. In the next section the geological model is used to conceptualize and parameterize a ground water model. Thereafter, the model is calibrated by nonlinear regression using MODFLOWP (Hill 1992). This method has at least two important advantages for this study: (1) it is efficient and objective when the model parameters are predefined and the accuracy of the data are known; and (2) it makes it possible to analyze and compare calibration results using statistical methods. The calibration of the model is based on fitting to synchronously measured sets of hydraulic head data, and to more or less extensive data sets of stream flow, and thus illustrates how stream flow data influence parameter estimates and uncertainties. Then the variously calibrated models are used to predict the stream flow at a number of measuring stations throughout the catchment. Finally, predicted and measured values are compared and the prediction uncertainty is quantified by individual likelihood method prediction and confidence intervals.

[a]Department of Earth Sciences, University of Aarhus, Ny Munkegade bygn. 520, DX 8000 Aarhus C., Denmark. E-mail: steenchr@geoserver1.aau.dk (first author); geolkrr@aau.dk (second author).

Received February 1997, accepted September 1997.

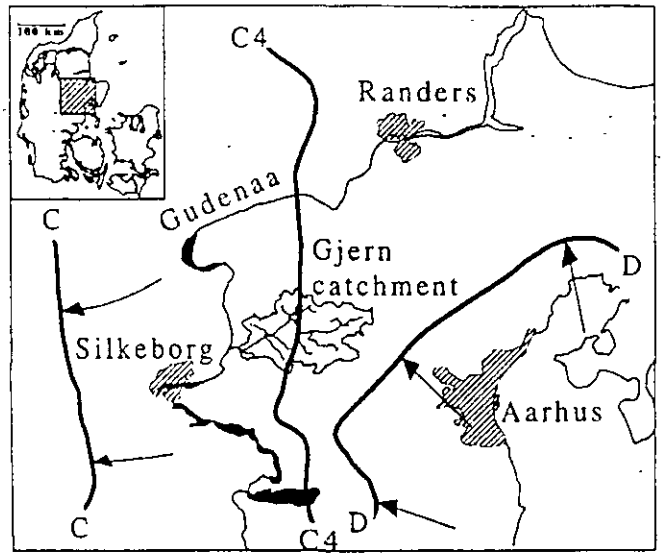

Figure 1. The Gjern catchment in eastern Jutland with position of ice borders and directions of ice advance (Larsen and Kronborg 1994). (C) main Weichselian ice border; (D) east Jutland Weichselian ice-border; (C_4) temporary position of the ice border during the retreat of the Weichselian ice.

The Gjern Field Area

The investigations presented in this paper were carried out in the Gjern catchment in eastern Jutland, Denmark (Figure 1).

Topography and Land Use

In Figure 2a we have plotted the topographic divide from 1:25,000 maps with 2.5 m contours, whereas the digital elevation model (Figure 2a) is based on digitized 5 m contour lines. The highest parts of the catchment along the southern and eastern drainage divides have elevations more than 100 m above datum, while at the main runoff gauging station at Smingevad the elevation is only 19 m. The catchment area for this station is 114 km^2. The land use is 77% cultivated, 14% forest, 4.5% wetland and riparian meadows, and 3% urban areas and roads, (Hoffman et al. 1997). Lakes amount to approximately 0.5%, Soebygaard soe (0.4 km^2) being the largest. The riparian zones of the catchment are influenced very little by reclamation in comparison with many other Danish catchments, and wetlands are well represented along the various stream courses.

Hydrometeorology and Hydrology

Precipitation is measured daily at several stations within the catchment by the Danish Meteorological Institute (DMI). For the period 1961–90, the annual precipitation was estimated as 730 mm when applying corrections for loss due to evaporation and aerodynamic effects (Allerup and Madsen 1979), and there are no important spatial variations within the catchment. The regional potential evapotranspiration for the period 1981–94 is 560 mm/y.

Gjern aa, the main stream, flows approximately northeast-southwest in the deeply incised Gjern valley. Daily records of runoff have been collected at the main station (Smingevad) since 1972, and the average is 193 mm/y for the period 1974–1992 (Clausen 1995). The main tributaries are Gjel back and Voldby back (Figure 2a), both with several automatic gauging stations, and during low flows single measurements of discharge were obtained synchronously at 19 stations (Figure 2b).

The total ground water abstraction is about 1 million m^3/year and corresponds to 10 mm/year, or just over 1% of the annual precipitation.

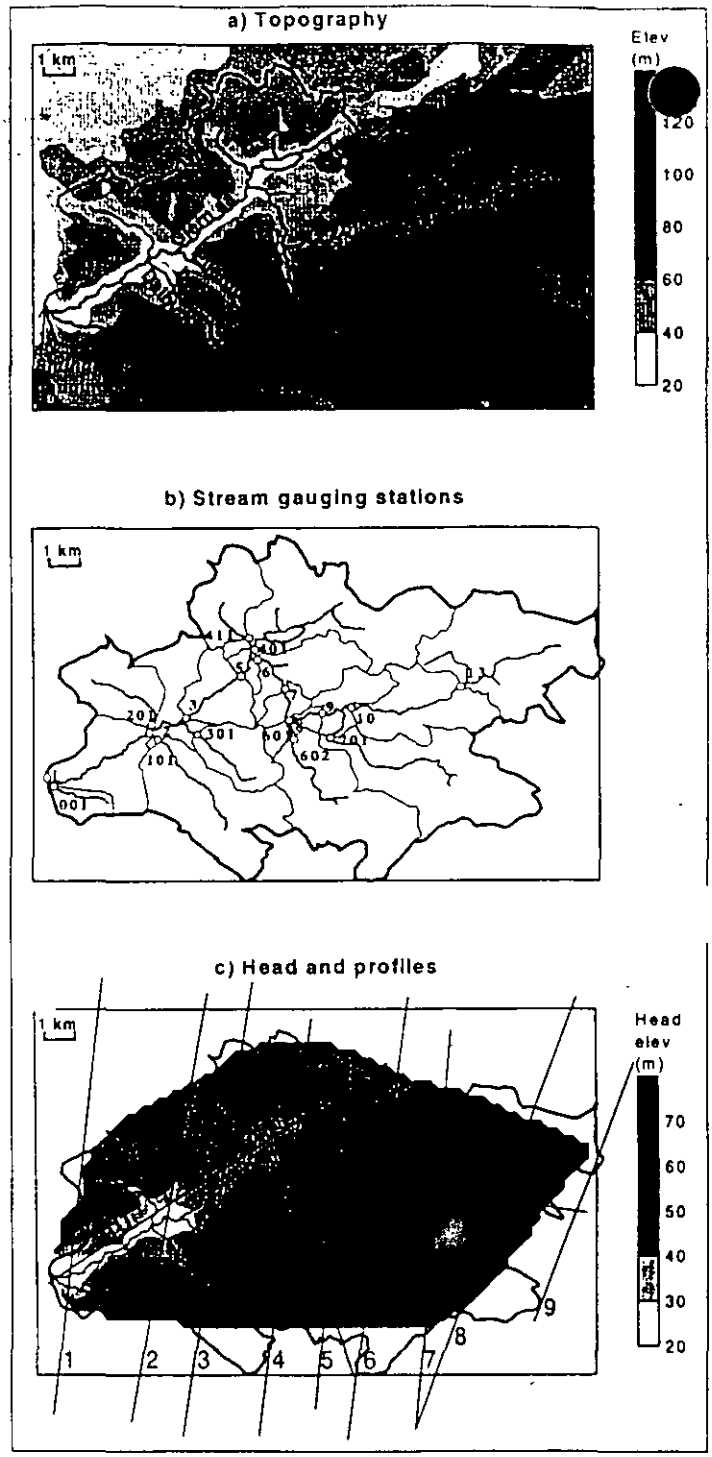

Figure 2. (a): Catchment topography; (b) Discharge stations with topographical catchments; (c) Hydraulic head of the primary aquifer; 1 to 13 mark positions of geological profiles.

Geology

During the late Oligocene and early Miocene eras, a shallow marine silt and clay facies was deposited (Ziegler 1990). Within the Gjern catchment the clay deposits form relatively thick beds (Rasmussen 1961) which presumably form the lower impern boundary for the circulating fresh water.

In the middle Miocene era, a marine regression followed and limnic micaceous sand was deposited, interbedded with quartz sand/gravel, micaceous clay and silt, and thin coal beds (Rasmussen 1961). Generally, the coarse sediments were deposited by large river systems and have a large areal extent. Silts and clays were deposited

in lakes and abandoned river branches, and the horizontal extent of the fine sediments is therefore less than that of the coarse sediments.

During the Pleistocene era, the area was glaciated at least four times. Glacial activity modified the older deposits and left capping layers of till and melt water sediments, often with complex interbedded structures. Of special relevance for this study is that during the Weichselian glaciation the main ice border (C, Figure 1) and the east Jutland ice border (D) were formed west and east of the Gjern catchment while a third ice border (C_4, from the retreat of the main ice) crossed the catchment in the north-south direction (Larsen and Kronborg 1994).

We have used the information in the PC well database (PC-ZEUS) of the Geological Survey of Denmark and Greenland (GEUS) to set up our detailed geological model. We selected the lithological information from all wells in the area which are deeper than 30 m (149) and used this to construct 13 geological cross-sections (Figure 2c) across the catchment. Figure 3 shows two examples.

There are 65 wells which are believed to reach the marine clay or end shortly above, but only for a few of these is the geological record unambiguous. At the ice border C_4, just south of Soebygaard where the main streams join, well data are sparse and 95 transient electromagnetic soundings were made (Møller 1994) in order to estimate the depth to the well-conducting marine clay (Figure 4a). It should be noted that the Gjern valley, which runs almost straight northeast-southwest, cuts deeply into the pre-quaternary surface. However, we find no evidence in either the well records or the transient electromagnetic soundings to suggest that the Gjel back or Voldby back can also be detected in the pre-quaternary surface.

Generally the well logs indicate that in the Gjern valley and the tributaries the valley infill is mostly sandy. Semi-permeable beds that inhibit the exchange between the ground water and the streams are mostly missing in the Gjern valley but are commonly found in the tributary valleys.

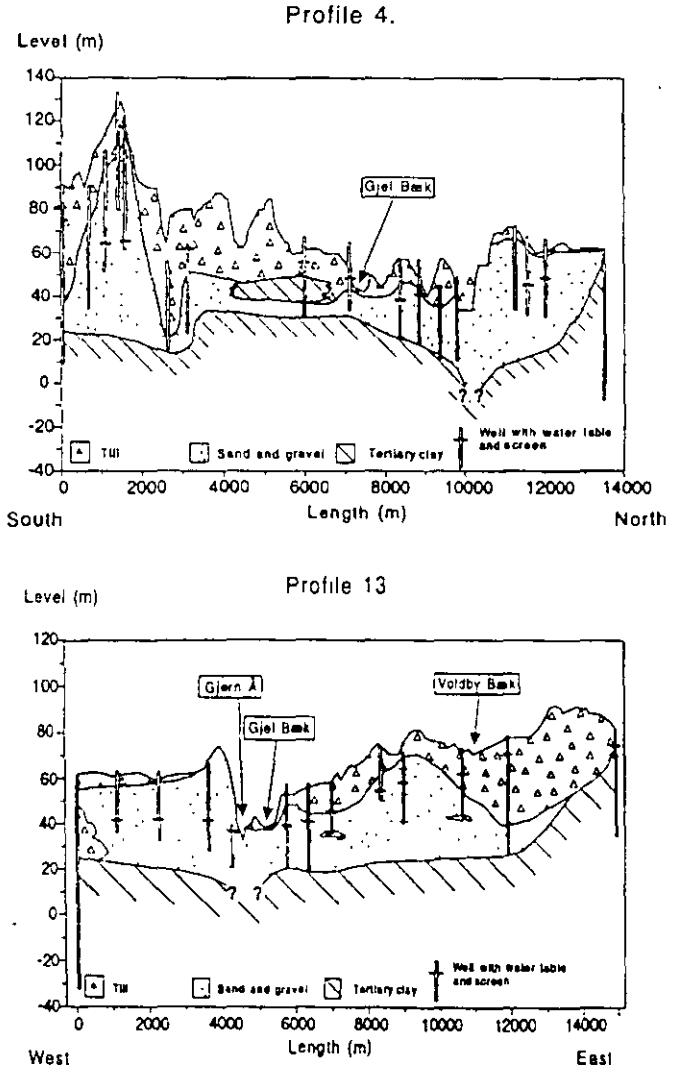

Figure 3. Geological profiles from the Gjern catchment: north-south cross section (4); east-west cross section (13).

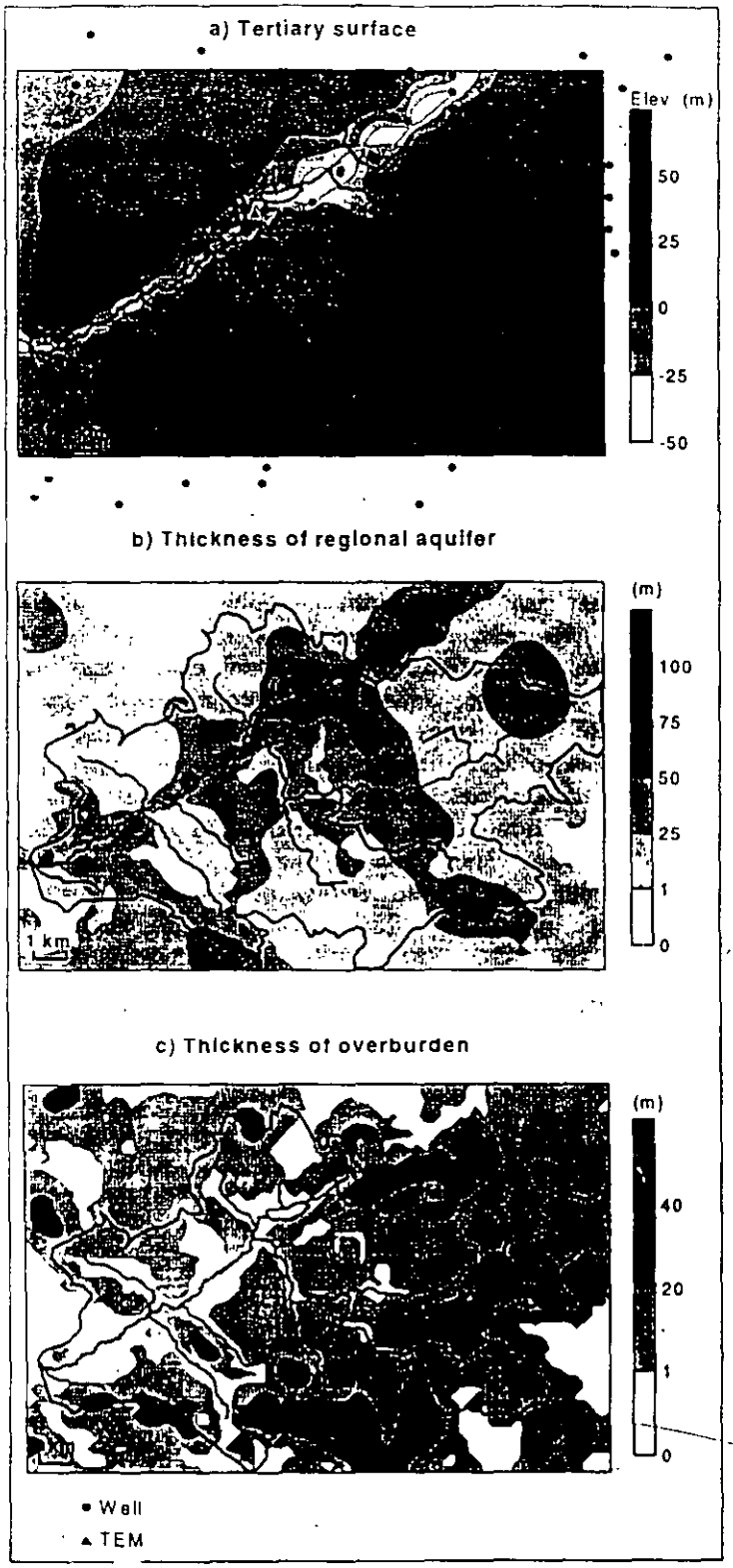

Figure 4. (a) contour map of the impermeable base; (b) isopach map of the regional aquifer; (c) isopach map of aquitard (white areas also indicate areas where the recharge is directly to the regional aquifer).

aquitard/secondary aquifer. Here permeable refers to gravel or sand, and also areas with a thin clay cap at the surface which is assumed to be permeable due to fractures down to a depth of 5 m. Below this depth clay is assumed to be semi-permeable. We have used 178 well lithology logs to locate the areas with leakage and recharge, respectively (indicated in Figure 4c as areas with and without overburden, respectively). We make the rough assumption that the water table in the aquitard is 3 m below the surface.

The recharge depends on precipitation, evapotranspiration and land use, and it can be estimated directly from actual data using root zone modeling. However, land use data are not currently available from a database, and therefore we treat recharge as a parameter of the ground water model and subsequently estimate it by calibration.

The magnitude and the direction of leakage depends on the thickness and vertical hydraulic conductivity of the aquitard, and on the vertical hydraulic gradient between the aquitard and the regional aquifer. In the present case the bottom surface of the aquitard was interpolated from the lithology logs of 178 boreholes, and its top surface estimated to be 5 m below ground level. The resulting aquitard thicknesses are shown in Figure 4c. The vertical hydraulic conductivity of the aquitard is estimated by calibrating the ground water model.

Aquifer Transmissivity

The deposits of the primary aquifer can consist of glaciofluvial sand and gravel, Tertiary quartz sand and gravel, and Tertiary micaceous sand. The aquifer transmissivity (T) has only been estimated from pumping tests of two wells, but the lack of good quality data on the transmissivity field is probably typical for most Danish catchments. It is not economically feasible (Christensen 1997) to acquire data on the entire transmissivity field of a regional aquifer from pumping tests. Information on the transmissivity field must therefore be based on alternative methods. We are reluctant to use specific capacity as an estimator for T, mainly because the available information on T in wells is often too sparse to form a reliable regression, and secondly because this method in some cases gives poor estimates (Christensen 1995). We therefore assume that the hydraulic conductivity K is constant within each lithologically defined zone (Figure 5), and estimate K by ground water model calibration. Since we have calculated the aquifer thickness (Figure 4b) using the well log information we can also estimate T.

The Efflux from the Aquifer

The efflux from the aquifer is partly due to abstraction and partly due to ground water seepage to streams. The abstractions were measured whereas the seepages were estimated as follows. The minimum stream flow (MSF) is normally recorded during long dry spells in late summer when the only contribution to stream flow is ground water seepage. Therefore we use the median MSF as a measure of the average seepage flow from the primary and the secondary aquifers. Given the zonation of the hydraulic conductivity of the aquifer we divided the stream system into segments between the gauging stations in Figure 2b. This allowed us to analyze and compare the interaction of ground water and stream flow for zones and segments along the stream.

The interaction between stream flow and ground water seepage is governed by the hydraulic conductance of the stream bed and of the difference between the stream water level and the hydraulic head in the aquifer. The conductance is a function of the length and width of the stream, and of the thickness and hydraulic conductivity of the stream bed. Here the length and width of stream reaches and the stream water levels were roughly estimated from 1:25,000 topographical maps. The location and thickness of the stream b were estimated from the geologic cross sections and shallow a holes along the streams, whereas the stream bed conductivity is estimated by calibration of the ground water model.

Ground Water Model

In order to simulate the (quasi) steady-state flow of ground water to the streams within the catchment we use the numerical ground water modeling code MODFLOWP (Hill 1992), which is a nonlinear regression version of the USGS finite-difference modeling code MODFLOW (McDonald and Harbaugh 1988).

The model is set up with two layers, and both are simulated as being confined even though they are both unconfined within parts of the catchment. This approximation is made in order to stabilize the calculation of heads as well as to stabilize the regression.

The upper layer of the model represents the area with a secondary aquifer, and the areas with a water table in till above an aquitard. In the secondary aquifer, in part of zone 6, ground water can flow horizontally. The transmissivity function of this aquifer is approximated by a constant value, which is calibrated, and the hydraulic head is a dependent variable calculated by the model. Everywhere else in the upper layer we assume that horizontal flow (in the till) is negligible during steady-state flow, and that the water level (and thus the hydraulic head) is fixed at 3 m below ground level.

The lower model layer represents the regional aquifer, and the hydraulic head in the entire layer is a dependent variable calcul by the model. The saturated aquifer thickness function of the lo layer was approximated in the following way: in areas where the aquifer is confined, we used the contoured values in Figure 4b; in areas with a free water table, the thickness was calculated as the difference between the interpolated water table and the bottom of the aquifer contoured in Figure 4a. The resulting thicknesses are held constant during the calibration. The hydraulic conductivity function of the lower aquifer is approximated by a constant value within each of the seven lithology zones (Figure 5). To better fit the calibration data, zone 8 was added during the calibration. These eight conductivities are estimated by calibration.

The interaction between the two model layers represents the leakage between the regional aquifer and the upper secondary aquifer or the water table in the till. In areas with no aquitard, the secondary and regional aquifers are lumped together in the lower model layer and the upper layer is deactivated. There is no geological evidence for assuming a variable conductivity of the aquitard within the catchment, so we assume one constant value which is estimated by calibration.

The influx is modeled in one of three ways: (1) as recharge directly to the lower model layer in areas with no aquitard; (2) as recharge to the upper model layer in areas with a secondary aquifer above the aquitard; or (3) as leakage from the upper to the lower layer in areas with an aquitard but no secondary aquifer. The recharge to each of the two layers (aquifers) is assumed spatially constant and estimated by calibration.

The efflux is modeled as abstractions or as as leakage from the aquifers to the streams. The leakage depends on the stream bed conductance, and on the difference between the (given) water level of the stream and the (calculated) hydraulic head in the aquifer. The stream bed conductance function was initially approximated by a constant hydraulic conductivity times a spatially variable factor depending on length, width and stream bed thickness. During cal-

ibration a separate hydraulic conductivity for one of the tributaries was added as a parameter.

The horizontal boundary conditions are no-flux boundaries coinciding with the ground-water divide shown on Figure 2b, which partly coincides with geological boundaries of low-permeable clay or till.

The model thus has (up to) 14 parameters estimated by calibration: eight hydraulic conductivities in the lower regional aquifer (K_1-K_8); one transmissivity for the upper aquifer in zone 6 (T_u); one vertical hydraulic conductivity for the confining layer (KV); two recharge values, i.e., one for the lower aquifer (RCH_1) and one for the upper aquifer (RCH_2); and two stream bed conductivities, i.e., KST_1 for the stream system in general and KST_2 for the upper part of Ellerup back. For K_1-K_8, T_u, KV, KST_1, and KST_2 we use log-transformed values during the estimation.

The finite-difference grid is homogeneous with 250 m grid spacing in both directions. No grid refinement is made near the streams because these take several directions within the catchment. The number of active flow cells in the upper model layer is 1118, and the number of constant head cells is 2050. There are 3870 active flow cells in the lower model layer. The interaction between aquifers and streams was simulated using the MODFLOW stream package (Prudic 1989).

Methods of Calibration and Uncertainty Analysis

Calibration is done by nonlinear regression to make the model fit hydraulic head as well as stream flow data. The function minimized during the regression is (Hill 1992):

$$S(b) = [h^* - h(b)]^T V_h^{-1} [h^* - h(b)] + [\Delta q^* - \Delta q(b)]^T V_{\Delta q}^{-1} [\Delta q^* - \Delta q(b)] \quad (1)$$

where

- b is the vector of parameters to be estimated
- h^* is the vector of measured hydraulic heads
- h(b) is the corresponding vector of predicted (modeled) heads at the measured wells using the parameters b
- V_h is the covariance matrix of errors of the heads
- Δq^* is the vector of measured gains in stream flow along stream courses
- $\Delta q(b)$ is the corresponding vector of calculated flow gains using the parameters b
- $V_{\Delta q}$ is the covariance matrix of the errors in stream flow gains

It is assumed that the head errors are independent and therefore V_h is a diagonal matrix. Stream flow gains calculated from measurements are known to be correlated, and we therefore modified MODFLOWP to allow $V_{\Delta q}$ to be a full covariance matrix. These covariances are calculated by Equation A1 derived in Appendix A.

The uncertainty of a calibrated parameter can be illustrated by its individual confidence interval, which is commonly calculated using linear approximations (e.g., Seber and Wild 1989). However, synthetic case studies (Cooley and Vecchia 1987; Vecchia and Cooley 1987; Hill 1989, Cooley 1993a,1993b) and a field case study (Christensen and Cooley 1996) show that the confidence intervals for the parameters of ground water models, as well as the predictions made by such models, are often nonlinear. In such cases linear approximations should not be used to calculate confidence intervals. We have therefore adopted the likelihood method (Donaldson and Schnabel 1987), which can be used to calculate confidence intervals on the estimated parameters as well as on the output from a nonlinear regression model with normally distributed residuals (Vecchia and Cooley 1987, Clarke 1987). The upper and lower limits of the confidence interval for a function $g(\beta)$, where β is the true set of parameters, are calculated as the maximum and minimum value of $g(b)$, respectively, under the constraint that:

$$\frac{(n-p)}{p} \frac{S(\beta) - S(\hat{b})}{S(\hat{b})} \le d^2_{1-\alpha} \quad (2)$$

where n is the number of calibration data, p is the number of estimated parameters, $\hat{b}$ is the optimum parameters found by minimizing Equation 1, and $d^2_{1-\alpha}$ is a problem-dependent statistic. Notice that $g(\beta)$ can be any function of the parameters: e.g., it can be a parameter of the ground water model, or it can be a stream flow gain calculated by the model. Vecchia and Cooley (1987) showed that the same computer program can be used to both estimate the parameters by nonlinear regression and to calculate the confidence limits of the desired confidence intervals. We have thus implemented the likelihood method in the nonlinear regression code.

For an individual $(1-\alpha)$% confidence interval

$$d_{1-\alpha} = \frac{t_{1-\alpha/2}(n-p)}{\sqrt{p}} \quad (3)$$

where $t_{1-\alpha/2}(n-p)$ is the student t-distribution with (n-p) degrees of freedom. Donaldson and Schnabel (1987) argue that individual likelihood method confidence intervals should be nearly exact for models with little intrinsic nonlinearity, whereas they may not be accurate for models with large intrinsic nonlinearity. In some of the following cases the local intrinsic nonlinearity of the model, as measured by Linssen's modified Beale's measure (Linssen 1975), is within the roughly linear range, and the corresponding confidence intervals calculated by the likelihood method may therefore be too small. To partly compensate for the intrinsic nonlinearity we have increased the used t-statistic as suggested by Beale (1960, Equation 2.21).

Calibration Data

The hydraulic head is known at 64 positions within the model area, but the quality of these data varies. At 31 wells the well elevation (WE) was measured with GPS, while in 25 wells it was estimated from 1:25,000 scale maps, and in 23 of the latter wells gaugings were asynchroneous. Finally, the head in the secondary aquifer was estimated at eight positions where the well elevations were also estimated from a map. Calibration and residual analyses (Cooley and Naff 1990) showed that the variance of the residuals between the measured and the simulated heads were higher than explained by the uncertainties on the measurement above. This is probably due to the model error introduced by the approximations made in the parameterization of the model, where we neglect heterogeneity at scales smaller than the zones, partial penetration of wells, etc. In the regression we therefore increased the variances of the head measurements by an equal amount (near 10 m^2) for all the wells.

Measurements of stream baseflow were available from 19 gauging stations (Figure 2b). We judged the standard deviations of these data to be from 5% at stations with a flow higher than 50 L/s, to 25% at stations with flows at 5-10 L/s. At station 411 (Figure 2b), with a flow of only 1 L/s the standard deviation was set to 200%. The measured flows were used to calculate the gain in stream flow along the 19 courses (between the gauging stations in Figure 2b), and the corresponding covariance matrix ($V_{\Delta q}$, Equation 1) of the flow gains were calculated from the measured flow uncertain-

tainty is between ±5% and ±60% for the courses with smaller gains.

Discussion and Conclusions

The study showed that the geological information in the GEUS database is useful to interpolate layer thicknesses as well as to define the parameters of a regional-scale ground water model. From the geological data alone we defined 12 parameters that were estimated by model calibration. During our four stages of calibration, where we went from using only data on hydraulic heads to also using an extensive set of stream flow gains, none of the estimates of these 12 parameters changed significantly. Addition of flow-gain data to the calibration record only changed (i.e., reduced) the uncertainty of the estimates.

The GEUS information on hydraulic head in the aquifers was collected over more than 50 years and is obviously of questionable quality. We therefore collected as many accurate head data as possible. However, analyses of the data showed that in this case the small-scale variations in head (due to heterogeneity, partial penetration of the wells, etc.) dominated over the measurement error that we found in the GEUS data. It is therefore likely that using the GEUS head data for model calibration would not have affected our results significantly.

Synchronous measurements of the spatial distribution of low flow in catchments was introduced more than 20 years ago in Denmark. At least one set will now be available for many larger catchments; in the Gjern catchment, for instance, data from 1976 and 1990 were available. During the project we have acquired several more sets, mostly for the purpose of testing the stability in our estimation procedure of the median annual minimum discharge, but also to supplement with data from the smallest stream courses.

Going through four stages of calibration we have demonstrated the importance of using efflux data together with hydraulic head data when calibrating a ground water model—primarily because the uncertainty of the estimates will be significantly reduced. Take for example the estimated recharge to the lower regional aquifer: in the case where we only used head data, the 95% confidence interval for the recharge estimate ranged from 40 mm/y to 1432 mm/y, whereas the interval was an order of magnitude smaller (from 139 mm/y to 292 mm/y) when we also used all the available information about stream flow to calibrate the model. However, the uncertainty of the estimated recharge and of other estimated parameters was significant even when we used the entire set of measured stream flow gains and hydraulic heads to calibrate the model.

Uncertainty in the estimated parameters is naturally reflected in the uncertainty of the gains in stream flow predicted by the ground water model. The confidence intervals of the predicted flows are very wide in the case where no stream flow data were used for calibration, whereas they narrow more and more as increasing amounts of flow data were used. However, the uncertainty is still significant for some of the predicted flows even when we used the entire set of stream flows: in large streams the uncertainty is up to ±25%, in smaller streams up to ±60%.

Nonlinear regression using MODFLOWP (Hill 1992) was very efficient for calibrating the model. We implemented Vecchia and Cooley's (1987) version of the likelihood method in our regression code in order to calculate nonlinear individual confidence and prediction intervals. In most cases these calculations were also efficient. It has not yet been proven that individual intervals calculated by the likelihood method are exact, but on the other hand there is no evidence that they would not be (Donaldson and Schnabel 1987; Cooley 1997; Cooley 1996). At the least, other studies we have cited show evidence for concluding that these nonlinear individual intervals are significantly better approximations than the traditionally used linearized intervals. It is mentioned that for our case study the calculated nonlinear confidence intervals are skewed and wider (in some cases very skewed and much wider) than the corresponding linearized intervals. Therefore, if we had based our analysis on linearized instead of nonlinear confidence intervals, the conclusions regarding the uncertainty of predicted stream flow gains would have been less pessimistic. Further, if we had compared measured stream flow gains with linearized (instead of likelihood) prediction intervals, an unlikely large number of measurements would fall outside their respective prediction interval, and this would lead to the wrong conclusion that there is a significant disagreement between the model predictions and the measurements.

The overall conclusion of this study is that many relevant data for ground water and surface water modeling studies are easily available from databases. This information is useful and in some cases, where the information is dense and of reasonable quality, it may be a sufficient base for an entire study of the regional ground water and surface water flow. However, even in a case like the one studied here, with a fairly dense geological data set and an extensive set of high quality calibration data, there still may be significant uncertainty connected with the prediction of local seepage of ground water to the streams. In such cases more detailed—but presumably more expensive to acquire—hydrogeological information will be needed to improve the definition of recharge areas and to describe the local fluxes in the aquifers. Hydraulic head data are not sufficient for the calibration of a regional-scale ground water flow model. The model uncertainty is reduced significantly (in our case, by an order of magnitude) if measured discharges at a few key points in the stream system are included in the calibration data. Using a spatially dense, instead of a sparse, set of measured stream flows for the calibration will only cause a modest reduction of uncertainty. On the other hand, dense stream flow measurements may reveal model error (in our case, inaccuracies in the geological model) which, when corrected, may cause simulations to change significantly.

Acknowledgments

We wish to thank R.L. Cooley for very useful discussions and comments on this paper in general and on the calculation of confidence intervals in particular. We also thank the County of Aarhus for supplying digital topographical data. This study was funded by the Danish Environmental Research Program 1992-1996 and by the Danish Natural Sciences Research Council.

Appendix A: Derivation of Covariance of Stream Flow Gains

A generalized expression from which the stream flow gain along a stream course (with index I) can be calculated from the measured stream flows, Q_i, is:

$$\Delta Q_I = \sum_i l_{I,i} Q_i$$

I_i is 1 for Q_i at the downstream station of the course; -1 for Q_i at the upstream stations along the course; and 0 for Q_i at stations not located along the course. Thus, for instance, if Q_{10} and Q_{13} are the measured flows at stations 10 and 13 (Figure 2b), respectively, the gain along the corresponding stream course is:

$$\Delta Q = Q_{10} - Q_{13}$$

If there are tributaries to the stream course we can have more than one upstream station. In Figure 2b the gain along the course from the two upstream stations 8 and 602 to the downstream station 7 can be calculated as:

$$\Delta Q = Q_7 - Q_8 - Q_{602}$$

More than one downstream station may also occur if the stream branches into two or more runs. The covariance between the gain along two stream courses is

$$\mathrm{Cov}(\Delta Q_i, \Delta Q_j) = E\{(\sum_i I_i Q_i)\cdot(\sum_j I_j Q_j)\} - E\{\sum_i I_i Q_i\}\cdot E\{\sum_j I_j Q_j\}$$

or

$$\mathrm{Cov}(\Delta Q_i, \Delta Q_j) = \sum_i \sum_j I_i I_j \{E\{Q_i Q_j\} - E\{Q_i\}\, E\{Q_j\}\}.$$

If the flow measurements are independent, then:

$$E\{Q_i Q_j\} - E\{Q_i\}\, E\{Q_j\} = 0, \qquad i \neq j$$

and

$$E\{Q_i Q_j\} - E\{Q_i\}\, E\{Q_j\} = \sigma_i^2, \qquad i = j$$

where σ_i^2 is the variance of Q_i. This means that only measurements that are shared between the two calculated gains contribute to the covariance.

For courses that are not overlapping, one measurement is shared if the two courses are connected, namely the measurement at the connecting point. This point is obviously at the downstream end of the one course and at the upstream end of the other. The covariance is therefore.

$$\mathrm{Cov}(\Delta Q_i, \Delta Q_j) = -\sigma_c^2 \qquad \text{(A1)}$$

where σ_c^2 is the variance of the flow measured at the connecting point

References

Allerup, P., and H. Madsen. 1979. Accuracy of Point Precipitation Measurements. Climatological papers, No. 5. Copenhagen: Danish Meteorological Institute.

Beale, E.M.L. 1960. Confidence regions in non-linear estimation. *Journal of the Royal Statistical Society, Series B* 22, no. 1: 41-76.

Bear, J. 1979. *Hydraulics of groundwater.* New York: McGraw-Hill Inc.

Christensen, S. 1994. Hydrological model for the Tude aa catchment. *Nordic Hydrology* 25, no. 3. 145-166.

Christensen, S. 1995. Prediction of log-transmissivity—1. Using specific capacity. *Nordic Hydrology* 26, no. 1. 1-20.

Christensen, S. 1997. On the strategy of estimating regional-scale transmissivity fields. *Ground Water* 35, no. 1: 131-139.

Christensen, S., and R.L. Cooley. 1996. Simultaneous confidence intervals for a steady-state leaky aquifer groundwater flow model. In *Calibration and Reliability in Groundwater Modelling*, ed. K. Kovar and P. van der Heijde. IAHS publ. no. 237, 561-569. Wallingford, United Kingdom: IAHS Press, Institute of Hydrology.

Clausen, B. 1995. Discharge data collection and analysis strategies in low flow studies. *Nordic Hydrology* 26, no. 3: 191-204.

Clarke, G.P.Y. 1987. Approximate confidence limits for a parameter function in nonlinear regression. *Journal of the American Statistical Association* 82, no. 397: 221-230.

Cooley, R.L. 1993a. Exact Scheffé-type confidence intervals for output from groundwater flow models, 1. Use of hydrogeologic information. *Water Resources Research* 29, no. 1: 17-33.

Cooley, R.L. 1993b. Exact Scheffé-type confidence intervals for output from groundwater flow models, 2. Combined use of hydrogeologic information and calibration data. *Water Resources Research* 29, no. 1: 35-50.

Cooley, R.L. 1996. Interview by author, Spring 1996, Denver, Colorado.

Cooley, R.L. 1997. Confidence intervals for ground water models using linearization, likelihood, and bootstrap methods. *Ground Water* 35, no. 5: 869-880.

Cooley, R.L., and R.L. Naff. 1990. Regression modelling of groundwater flow. U.S. Geological Survey Techniques of Water-Resources Investigations, Book 3, Chapter B4.

Cooley, R.L., and A.V. Vecchia. 1987. Calculation of nonlinear confidence and prediction intervals for ground-water flow models. *Water Resources Bulletin* 23, no. 4: 581-599.

Donaldson, J.R., and R.B. Schnabel. 1987. Computational experience with confidence regions and confidence intervals for nonlinear least squares. *Technometrics* 29, no. 1: 67-82.

Freeze, R.A., and J.A. Cherry. 1979. *Groundwater.* New Jersey: Prentice-Hall, Inc.

Hill, M.C. 1989. Analysis of accuracy of approximate, simultaneous, nonlinear confidence intervals on hydraulic heads in analytical and numerical test cases. *Water Resources Research* 25, no. 21: 177-190.

Hill, M.C. 1992. A computer program (MODFLOWP) for estimating parameters of a transient, three-dimensional ground-water flow model using nonlinear regression. U.S. Geological Survey Open-File Report 91-484.

Hoffmann, C.C., M. Mbai, and G. Blicher-Mathiesen. 1997. Studies of hydrological and biological processes in a freshwater wetland. In prep.

Larsen, G., and C. Kronborg. 1994. Geologically speaking: The Middle Jutland (In Danish: *Geologisk set: Det mellemste Jylland*). Brenderup:Geografforlaget.

Linssen, H.N. 1975. Nonlinearity measures: A case study. *Statistica Neerlandica* 29, 93-99.

McDonald, M.G., and A.W. Harbaugh. 1988. A modular three-dimensional finite-difference ground-water flow model. U.S. Geological Survey Techniques of Water-Resources Investigations, Book 6, Chapter A1.

Møller, K. 1994. Hydrogeological investigations in the Gjern aa Catchment (In Danish: *Hydrogeologiske undersoegelser i Gjern aaens opland*) M.S. thesis, Department of Earth Sciences, Aarhus University, Denmark.

Prudic, D.E. 1989. Documentation of a computer program to simulate stream-aquifer relations using a modular, finite-difference, groundwater flow model. U.S. Geological Survey Open File Report 88-729.

Rasmussen, L.B. 1961. The Miocene formations in Denmark (In Danish: *De miocaene formationer i Danmark*). The Geological Survey of Denmark, IV Raekke, vol. 4, no. 5. Copenhagen: Geological Survey of Denmark.

Seber, G.A.F., and C.J. Wild. 1989. *Nonlinear regression.* New York: John Wiley and Sons.

Vecchia, A.V., and R.L. Cooley. 1987. Simultaneous confidence and prediction intervals for nonlinear regression models with application to a groundwater flow model. *Water Resources Research* 23, no. 7: 1237-1250.

Ziegler, P.A. 1990. *Geological Atlas of Western and Central Europe: 1. Europe Geology,* 2nd ed. Maatschappij: Shell B.V.

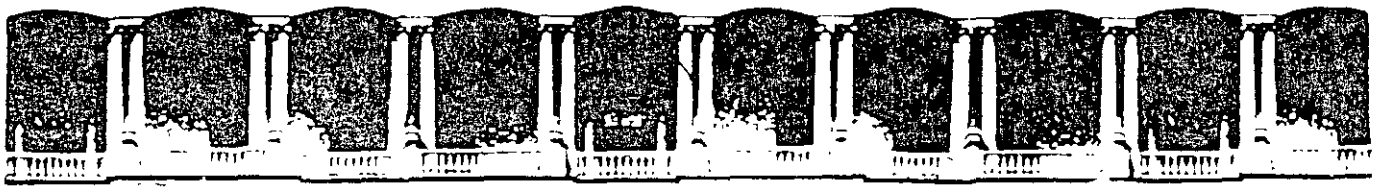

FACULTAD DE INGENIERIA U.N.A.M.
DIVISION DE EDUCACION CONTINUA

CURSOS ABIERTOS

XII CURSO INTERNACIONAL DE CONTAMINACIÓN DE ACUÍFEROS

MODULO III: MODELOS MATEMÁTICOS EN GEOHIDROLOGIA Y CONTAMINACIÓN DE ACUIFEROS

TEMA

THE DIFFERENT CHARACTERISTICS OF AQUIFER PARAMETERS AND THEIR IMPLICATIONS ON PUMPING – TEST ANALYSIS

EXPOSITOR: DR. ADOLFO CHAVEZ RODRIGUEZ

PALACIO DE MINERIA
OCTUBRE DEL 2000

The Different Characteristics of Aquifer Parameters and Their Implications on Pumping-Test Analysis

by J. J. Jiao and C. Zheng[a]

Abstract

The concepts of two-way coordinates and one-way coordinates are used to describe the different characteristics of two key aquifer parameters, transmissivity and storativity, under constant-rate pumping conditions. A two-way coordinate is such that the conditions at a given location are influenced by changes in conditions on either side of that location; a one-way coordinate is such that the conditions at a given location are influenced by changes in conditions on only one side of that location. Results from sensitivity analysis indicate that storativity has the characteristics of two-way coordinates, but transmissivity has the characteristics of one-way coordinates, i.e., its information can be transferred mainly from upstream to downstream. An upstream observation well can produce information on storativity both upstream and downstream, but it can produce little information on transmissivity downstream.

These characteristics of the aquifer parameters have important implications on pumping-test designs and interpretation. For example, to estimate the parameters of an anomalous zone in an aquifer, an observation well should be located downstream but near the zone. It should not be placed upstream if the parameters downstream are to be estimated. An observation well which can provide adequate information for estimating storativity may not provide adequate information for estimating transmissivity, and vice versa. The aquifer area represented by estimated storativity may be different from that represented by estimated transmissivity.

Introduction

The influence of heterogeneities on aquifer parameter estimation based on pumping tests has received much attention for years. A sensitivity analysis is used as an important approach to understand the behavior of hydraulic parameters in an aquifer with zones which have parameters significantly different from those of the background aquifer (e.g., McElwee, 1982; Butler, 1988; Butler and McElwee, 1990; Jiao, 1995). The findings about the features of these anomalous zones in the context of pumping-test analyses can be summarized as the following: (1) A parameter can be best estimated from drawdown-time data when the sensitivity of the parameter is not only large but also changing significantly with time; (2) The influence of anomalous zones on drawdown during a pumping test lasts only a limited time; (3) The influence of a zone less permeable than the background aquifer material is much larger than that of a zone more permeable; and (4) It is easier to estimate transmissivity than storativity because transmissivity sensitivity is usually much larger than storativity sensitivity.

It has been demonstrated that the area represented by the estimated parameters is much smaller than that covered by the cone of depression (Jiao, 1993). Therefore, after parameters are estimated, it may be of interest to know what portion of the aquifer is primarily represented by the estimated parameters. Before a pumping test, it may also be necessary to design the location of an observation well in such a way that the information on a particular portion of the aquifer can be best obtained. This requires an understanding of the relationships among the characteristics of aquifer parameters, flow field, and the spatial coordinates.

While most studies are concerned with the general features of the properties of anomalous zones, Oliver (1993) seems to be the first to concentrate specifically on the different characteristics of transmissivity and storativity in response to pumping. He concluded, based on a particular case study, that the influence of storativity is nearly radially symmetric so that the effect of a low-storativity region is essentially the same in any direction, but the influence of transmissivity on drawdown at observation wells is not spatially uniform within that area. This suggests that storativity and transmissivity have different characteristics related to spatial coordinates.

An attempt is made in this paper to examine the different characteristics of transmissivity and storativity under constant-rate pumping conditions using numerical simulations. Two concepts, two-way coordinates and one-way coordinates, which were first used in numerical heat transfer and fluid flow (Patankar, 1980), are introduced to understand the characteristics of these two parameters. A two-way coordinate is such that the conditions at a given location are influenced by changes in conditions on either side of that location; a one-way coordinate is such that the conditions at a given location are influenced by changes in conditions on only one side of that location. For example, the flow field between two rivers provides an example of two-way coordinates. The head at any given point in the flow field is influenced by changing the head of either river. Another example is solute transport. For dispersion-dominated problems, space coordinates are two-way coordinates. But a space coordinate can very nearly become one-way under advection. If there is a strong unidirectional flow in the coordinate direction, significant influence travels only from upstream to downstream. Conditions at a point are then affected largely by the upstream conditions and very little by the downstream ones. Advection is a

[a]Department of Geology, University of Alabama, P. O. Box 870338, Tuscaloosa, Alabama 35487.

Received April 1995, revised October 1995, accepted November 1995.

one-way process, but dispersion has two-way influence. For advection-dispersion problems the properties of space coordinates have the dual properties of one-way and two-way coordinates. When the velocity is large, advection dominates over dispersion and thus makes the space coordinate nearly one-way. It becomes necessary to use special numerical methods such as upstream-weighted methods and characteristics methods to account for one-way properties of spatial coordinates in advection-dominated problems (Jiao and Chen, 1987; Zheng and Bennett, 1995).

In this paper, the sensitivity features of drawdown to aquifer parameters under constant-rate pumping conditions in one-dimensional flow systems are first examined to investigate the different characteristics of transmissivity and storativity. The influence of the location of an anomalous zone on drawdown in an observation well is further studied by analyzing the sensitivity features of aquifer parameters in radial one-dimensional flow systems. Finally, the impact of the characteristics of transmissivity and storativity on their estimation is demonstrated using a hypothetical example.

Sensitivity Analysis

A sensitivity analysis is the study of a system's response to various disturbances. The response of the aquifer system may be expressed in terms of drawdown or hydraulic head. Because pumping-test analysis is of particular concern, drawdown, s, is used. Mathematically, the sensivitity is the partial derivative of drawdown with respect to a model parameter. For example, the sensitivity of drawdown to transmissivity, T, can be defined as:

$$U_T = \frac{\partial s}{\partial T} \tag{1}$$

A disadvantage of the sensitivity defined by equation (1) is that the magnitude depends on the dimension and unit of the particular parameter. A normalized sensitivity can be defined as (e.g., McElwee, 1987):

$$U'_T = T\frac{\partial s}{\partial T} = \frac{\partial s}{\partial T/T} \tag{2}$$

The normalized sensitivity describes the influence of ratio change in a parameter. Thus, normalized sensitivities can be readily plotted together and compared. The storativity sensitivity U_S or normalized storativity sensitivity U'_S can be defined in the same way. In terms of parameter estimation, the absolute magnitude of a sensitivity, not its signed value, is of importance. In the following discussion, when the word "sensitivity" is used, the absolute magnitude of sensitivity is implied.

There are three methods for determining sensitivity coefficients of aquifer parameters: (1) analytical expressions; (2) numerical solution of a partial differential equation; and (3) finite-difference approximations (Beck and Arnold, 1977) For simple ground-water problems, there are analytical expressions for parameter sensitivity. When analytical solutions are not available, numerical solutions can be used to determine sensitivity. Sensitivity equations can be easily derived from flow equations and solved by conventional numerical approaches used for flow modeling. For instance, sensitivity equations were solved by Sykes et al. (1985) using the Galerkin finite-element method to assess the uncertainty of prospective radioactive waste repositories. Jiao (1993) solved sensitivity equations modified from a

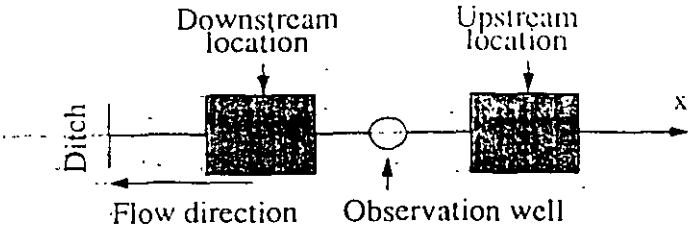

Fig. 1. Schematic representation of an observation well, and the upstream and downstream locations of an anomalous zone in one-dimensional flow field. (Background aquifer parameters $T' = 60\ m^2/d$, $S' = 6 \times 10^{-3}$; zone parameters $T' = 6\ m^2/d$, $S' = 6 \times 10^{-4}$).

radial numerical flow model by Rushton and Chan (1976) to understand the sensitivity features of pumping-test drawdown to aquifer parameters. However, the easiest and most straightforward method is the finite-difference approximation. For example, by running the flow model twice with two slightly different values of a parameter, say T, the sensitivity is simply given by:

$$U_T \approx \Delta s/\Delta T = \frac{s(T + \Delta T) - s(T)}{\Delta T} \tag{3}$$

The approximation becomes increasingly accurate as ΔT approaches zero. Jiao (1993) demonstrated that, for radial flow, the sensitivities evaluated from the above approximation are virtually identical to those using a numerical solution to the corresponding partial differential sensitivity equations.

In this paper, for sensitivity analysis in simple one-dimensional flow, the finite-difference approximation is used. For sensitivity analysis in radial one-dimensional flow, the sensitivity equation modified from a radial numerical flow model (Jiao, 1993) is used. The details on how sensitivity equations are derived from flow equations and then solved numerically can be found elsewhere (e.g., McElwee, 1987; Jiao, 1993).

Characteristics of Aquifer Parameters in One-Dimensional Flow

Consider a semi-infinite aquifer (Figure 1). The left boundary is a fully penetrating ditch. The parameters of the aquifer are $T' = 60\ m^2/d$, $S' = 6 \times 10^{-3}$. After time $t > 0$, water is pumped out from the ditch at a constant rate $q = 0.025\ m^2/d$. A simple finite-difference model with space increment $\Delta x = 100$ m is used to simulate the drawdown in the aquifer. The right boundary is chosen to be at 1000 km so that no drawdown is observed at the boundary during the pumping period of 100 days. An observation well is located at $x = 900$ m. Assume that there is an anomalous zone of 200 m long which has parameter $T = 6\ m^2/d$, $S = 6 \times 10^{-4}$, and is 300 m from the observation well. The different influence of this zone on drawdown at the observation well when the zone is located downstream and upstream of the well will be investigated.

Figure 2a shows how the normalized sensitivity of dimensionless drawdown $[(2(\pi)^{1/2}T's)/(q\Delta x)]$ to downstream zone storativity (S_d) and upstream zone storativity (S_u) changes with dimensionless pumping time $[T't/S'(\Delta x)^2]$. Although the downstream storativity is always more sensitive than the upstream storativity, the difference becomes small as pumping continues.

Figure 2b shows how the normalized sensitivity of dimensionless drawdown to downstream zone transmissivity (T_d) and

Table 1
Data Sets Used for Calibration

A.	Hydraulic head data
B.	Hydraulic head data, and stream flow at main station (1)
C.	Hydraulic head data, and stream flow at main station (1) and two main tributaries (stations 6 and 401)
D.	Hydraulic head data, and 18 stream flow gains

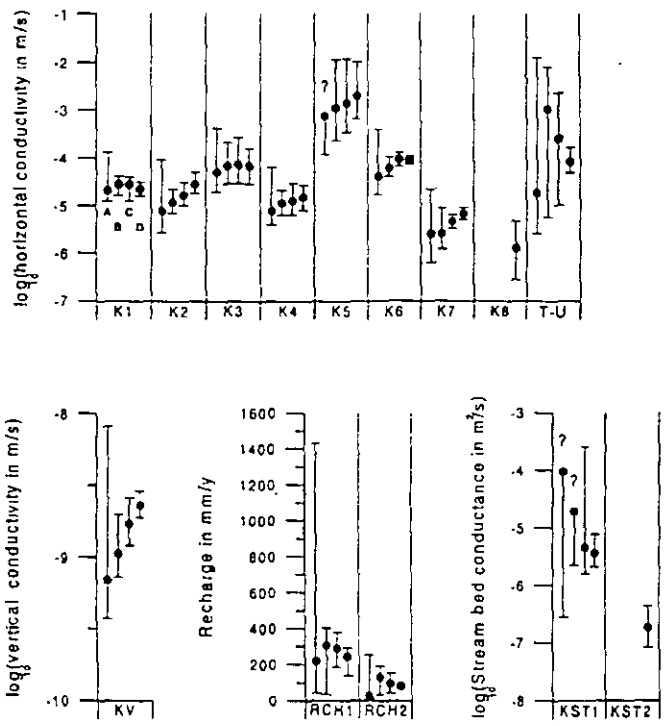

Figure 6. Parameter estimates and their 95% confidence intervals (case A-D).

ties. Calibration and residual analyses (Cooley and Naff 1990) indicated that this covariance matrix gives reasonable weight to the flow-gain data. To illustrate the importance of the stream flow data, we calibrated the model to fit the four data sets (A-D) listed in Table 1.

Calibration Results

For the data in Table 1, the estimated parameters and their calculated confidence intervals are shown in Figure 6. Residual analyses (Cooley and Naff 1990) showed that there is no significant bias in the calibrated models, and a hypothesis that the residuals are normally distributed cannot be rejected.

In case A we used only hydraulic head data to calibrate the 12 parameters that we initially identified from our geological and hydrogeological models, i.e., the $\log_{10}$-values of K_1-K_7, T_u, KV, and KST_1, and the untransformed values of RCH_1 and RCH_2. At this stage we had not recognized zone 8 (Figure 5) as a separate conductivity zone for the lower aquifer, and it is therefore contained in zone 2. Similarly, from our initial geological information we did not expect the upper part of Ellerup baek to have different stream bed conductance from that of the other stream courses, so KST_1 was assumed to be effective for all streams.

All 12 parameters could be estimated by nonlinear regression, whereas there were convergence problems with calculating most of the confidence limits. To make these calculations converge we had to manually adjust two parameters (KST_1, and RCH_2 - T_u, which are correlated) and let the algorithm estimate the other 10 parameter values. It is therefore likely that the calculated confidence intervals are too small. Despite all efforts with manual parameter adjustment, we could not calculate the upper confidence limits for K_5 and KST_1.

In case A, all the estimates fall within expected ranges except RCH_2, which seems to be too small (26 mm/y). However, the confidence interval for RCH_2 is so wide that the parameter estimate cannot be postulated to be significantly different from that of RCH_1. The confidence interval for RCH_1 spans from 40 mm/y to 1432 mm/y, i.e., from a lower value corresponding to the leakage rate through till in a similar area (e.g., Christensen 1994) to an upper value about twice as large as the annual precipitation, which is unrealistic. Nevertheless this case shows how well (or badly) the recharge can be estimated from head data alone. Similarly, Figure 6 shows that the estimated conductivity of the confining layer is very uncertain.

The estimated $\log_{10}$ conductivities of the lower aquifer generally show higher values for zones with Quaternary melt water deposits (K_3, K_5, and K_6) and lower values for the zones with Tertiary limnic deposits (K_1, K_4, and K_7). However, it was expected that the conductivity of zone 2, which contains layers of clean quartz sand, should be higher than the other zones with Tertiary limnic deposits. Due to the large uncertainty in the estimated recharge and leakage, the uncertainty of the estimated conductivities as well as of the transmissivity in the upper aquifer and of the stream bed conductance is considerable.

In case B the measured stream flow at the downstream gauging station was added to the calibration record. As in case A, all 12 parameters could be estimated, but fewer of the confidence interval calculations had convergence problems. This was avoided by manually adjusting one parameter, KST_1, and calculating the others with the algorithm (as in case A, the intervals calculated partly by manual iteration may be too small). For the calculation of the upper confidence limit of KST_1 convergence could not be achieved.

The changes in the estimates from case A to case B (Figure 6) are not significant if you take the confidence intervals from case A into consideration, and the ordering of estimated conductivities and of estimated recharge remains the same.

The parameter uncertainties are reduced somewhat by also using information about the efflux from the catchment to calibrate the model. However, the uncertainties of estimated recharge and confining layer conductivity (and other parameters) are still large. This indicates that even though the calibrated model fits the overall flux within the catchment, the prediction of local fluxes is uncertain.

In case C we increased the number of measured stream flow gains from one to three in the calibration record. The stream flow gains are: Gjel baek with tributaries upstream of gauging station 6 (Figure 2b); Gjern aa with tributaries upstream of station 401; and Gjern aa with tributaries downstream of stations 6 and 401 (the gains were calculated from the measured stream flows at stations 1, 6, and 401).

The calculations converged for the parameter estimation as well as for the calculations of confidence limits. It did not change the estimates significantly, whereas the uncertainty of several of the parameters was reduced. This is also the case for the confining layer conductivity, KV, and for the estimated recharge rates, RCH_1 and RCH_2. The two estimated recharge rates are each within the expected ranges and they are significantly different: the rate to the lower aquifer, RCH_1, is 289 mm/y; and the rate through till to the upper aquifer, RCH_2, is 99 mm/y (3×10^{-9} m/s) which is not sig-

nificantly different from the estimated conductivity of the confining till layer (1.7×10^{-9} m/s). The uncertainty of some of the estimated hydraulic conductivities is also reduced significantly. Increasing the number of measured stream flow gains thus improves the model's ability to calculate the local fluxes.

In case D the number of stream flow gains used to calibrate the model was increased to 18; i.e., we used the measured gains between all the gauging stations (Figure 2b) except at station 411 where the baseflow <1 L/s. Initially we estimated the same 12 parameters as in the previous cases. All calculations of estimates and confidence limits converged. However, the estimated recharge to the lower aquifer decreased by more than 100 mm/y compared to case C, and the calibrated model still had problems with reproducing the measured flow in two minor tributaries: at gauging station 001 the calculated flow was 5 L/s against a measured flow of 16 L/s; and at station 301 the calculated flow was 13 L/s against a measured value of 8 L/s. Analyses of the results showed that during the regression the recharge was forced down to an unexpected low level to compensate for problems with matching the measured low flow at station 301 (Ellerup baek). This low flow could be reproduced only if the stream bed conductance upstream of station 301 was lower than for the rest of the stream system. Finally, the relatively high flow measured at station 001 could not be reproduced by the initial zonation of lower aquifer conductivities.

Additional drilling to the 1.5 m depth in the bottom of Ellerup baek revealed that the stream bed consists of gravel deposits at the gauging station (301), but 200 m upstream it is low-permeable peat, and 400 m upstream it is till. This indicated that the stream bed in the upper part of this tributary is indeed low-permeable. Further, a re-evaluation of our geological profiles between stream gauging stations 1 and 2 indicated that the lower aquifer could be missing or at least be very thin south of this part of Gjern aa. If this observation was implemented in the model, we expect it would increase the seepage of ground water upstream of station 001.

At this stage, we decided to modify the parameterization of the model so that a separate hydraulic conductivity for zone 8 (Figure 5) and a separate stream bed conductivity for the upper part of Ellerup baek could be estimated. The total number of parameters estimated in case D thus increased to 14, i.e., the $\log_{10}$ values of K_1-K_8, T, KV, KST_1, and KST_2, and the untransformed values of RC and RCH2. Analyses of residuals and likelihoods showed that the parameterization produces a better fit to the data than the initial one. The estimates and their ordering are not significantly different from the previous cases (Figure 6), but the width of most confidence intervals is considerably reduced. However, the recharge to the lower aquifer, RCH_1, is still uncertain with a confidence interval ranging from 139 mm/y to 292 mm/y. We therefore believe that even though the uncertainties of the local fluxes are reduced as compared to the previous model calculations, they may still be significant.

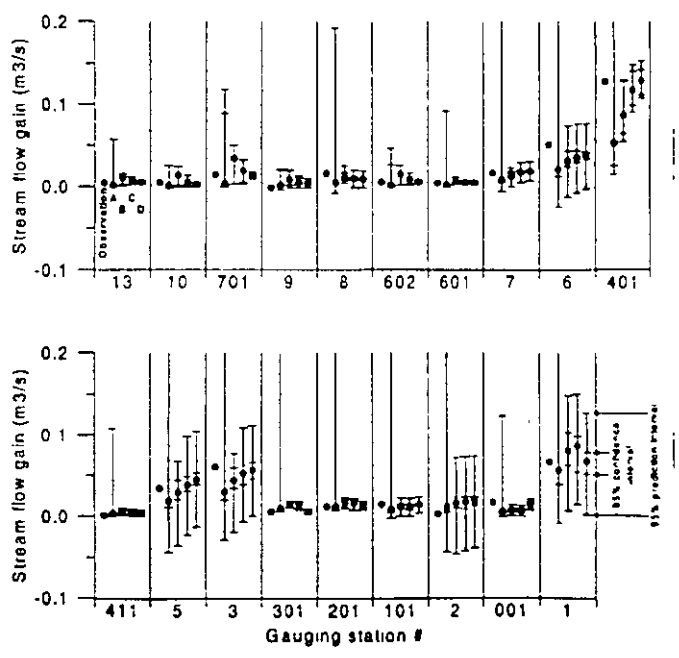

Figure 7. Observed and predicted (case A-D) stream flow gains. In some cases the confidence limits can barely be distinguished from the prediction limits.

Prediction of Stream Flow Gains

Each of the calibrated models (A-D) were used to predict the 19 stream flow gains between the gauging stations. The limits of the confidence intervals for the predictions were calculated in the same way as for the parameter intervals, i.e., by using Equation 2 as the constraint. The limits of the corresponding prediction intervals were calculated similarly by using the constraint

$$\frac{(n-p)}{p}\,\frac{S(\beta)-S(\hat{b})+e_k^2/v_k}{S(b)} \le d^2_{1-\alpha} \qquad (4)$$

instead of Equation 2. In Equation 4, e_k is the error of the measured flow, v_k is the variance of e_k, and, for individual intervals, the previously mentioned statistic corrected for intrinsic non-

The predicted flows and their 95% individual confidence prediction intervals are shown in Figure 7. As for the parameter intervals, in case A and B, and also in a few cases for case C and D, KST had to be manually adjusted to make the calculations of the interval limits converge. The corresponding intervals may therefore too small.

In case A, all the measured flows fall within the prediction intervals of the predicted flows. The prediction intervals as well as confidence intervals are very wide, again a consequence of the high uncertainty related to the estimated recharge and confining layer conductivity. Even though several of the upper interval limits fall outside the range of Figure 7, they are finite and their calculations converge and fulfill the above constraints.

In case B, one measured flow gain (301) is outside the corresponding 95% prediction interval. However, it is expected that one out of 19 measurements will fall outside this interval. Figure 7 also shows that the use of the overall efflux to calibrate the model narrows the confidence intervals significantly, but several of them are still very wide.

In case C, two measurements (301 and 001) fall outside the corresponding 95% prediction intervals. This is not unlikely as the probability that more than one of 19 measurements will fall outside a 95% prediction interval is 24% (test in the binomial distribution). Figure 7 shows that adding the three stream flow gains to the calibration record narrows several of the confidence intervals.

In case D, with 14 estimated parameters, all measured gains fall within the prediction intervals. The confidence intervals are narrower than in the previous cases, but in several cases the uncertainty is significant: for the stream courses with high measured gains (cases 5, 3, and 1) the uncertainty of the predicted gain (measured/predicted, or relative difference between the confidence interval limit and the predicted value) is in the range from ±10% to ±25%, whereas the

upstream zone transmissivity (T_u) changes with dimensionless pumping time. The T_d sensitivity increases to a maximum and then gradually decreases with time, but T_u sensitivity increases with time during the whole pumping period. The T_u sensitivity is generally much larger than T_d sensitivity except at the very beginning of pumping when the aquifer near the upstream zone is not yet disturbed.

Comparison of Figures 2a with 2b shows that the difference between S_d and S_u is generally much smaller than that between T_d and T_u. As time increases, the former decreases significantly and the latter increases. In terms of storativity, the influence of the upstream and downstream zones on the drawdown in the observation well is of the same order of magnitude, but, in terms of transmissivity, the influence of the upstream zone is much more significant. This indicates that transmissivity has the characteristics of one-way coordinates and storativity has the characteristics of two-way coordinates. These characteristics become more obvious as pumping continues.

The different magnitudes of the sensitivity values shown in Figure 2 have important implication in parameter estimation. It is much easier to estimate transmissivity of the zone than storativity because transmissivity sensitivity is much larger than storativity sensitivity; it is much easier to estimate the upstream transmissivity of the zone than to estimate the downstream transmissivity because T_u is much larger than T_d. When the sensitivity of zone storativity approaches a constant as shown in Figure 2a, essentially no information can be gained about the storage properties of the zone from the drawdown data. The same is true for the transmissivity of the downstream zone. More detailed discussion about these general sensitivity features of anomalous zones can be found in Butler and McElwee (1990), Butler and Liu (1993), and Jiao (1993).

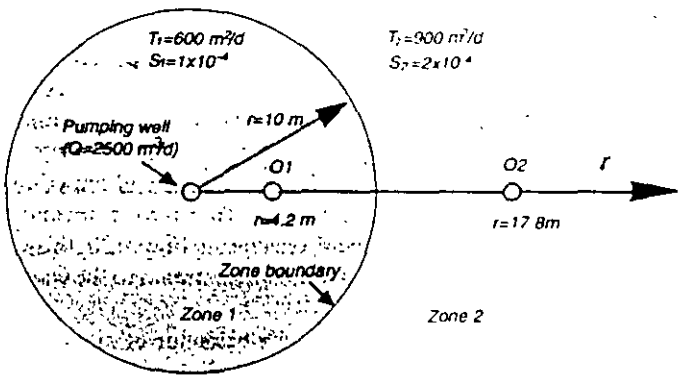

Fig. 3. Schematic representation of two-zone aquifer in a radially symmetric system.

Characteristics of Aquifer Parameters in Radially One-Dimensional Flow Field

Consider a radially symmetric aquifer of two zones. The aquifer configuration, well locations, pumping rate, and parameters are shown in Figure 3. The aquifer is assumed to be confined and extended to infinity.

Figure 4 shows how the normalized sensitivities of dimensionless drawdown $[(4\pi T_2 s)/Q]$ to S_1 and T_1 change with dimensionless time $(T_2 t/S_2 l^2)$, where l is the radius of inner zone. The general sensitivity features shown in Figure 4 have been discussed in detail (Jiao, 1993). What is of interest here is the different characteristics between transmissivity and storativity. Figure 4a shows that the maximum storativity sensitivity for the well at 17.8 m is about 17% of that at 4.2 m. However, Figure 4b shows that the maximum transmissivity sensitivity at 17.8 m is only about 3% of that at 4.2 m. This indicates that an upstream

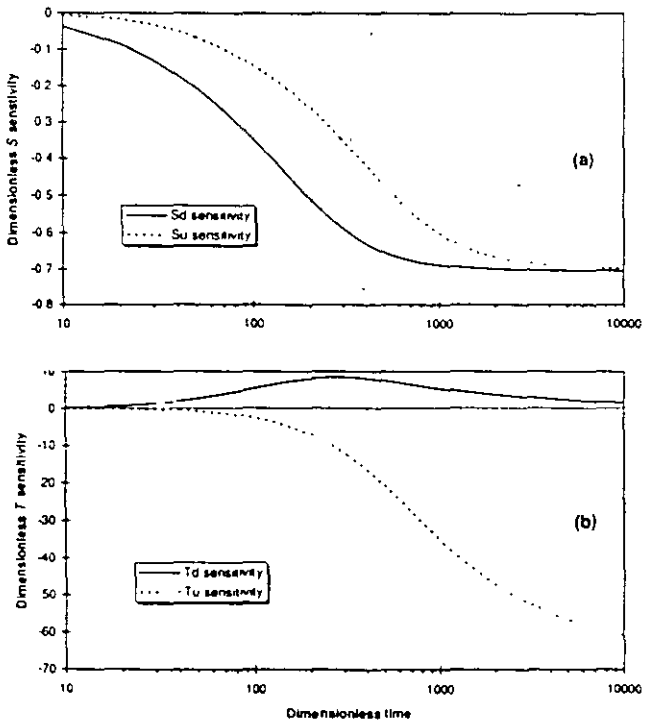

Fig. 2. Change of normalized sensitivities of dimensionless drawdowns $[(2(\pi)^{1/2}T's)/(q\Delta x)]$ to (a) storativity and (b) transmissivity of downstream and upstream zones with dimensionless time $[T't/S'(\Delta x)^2]$.

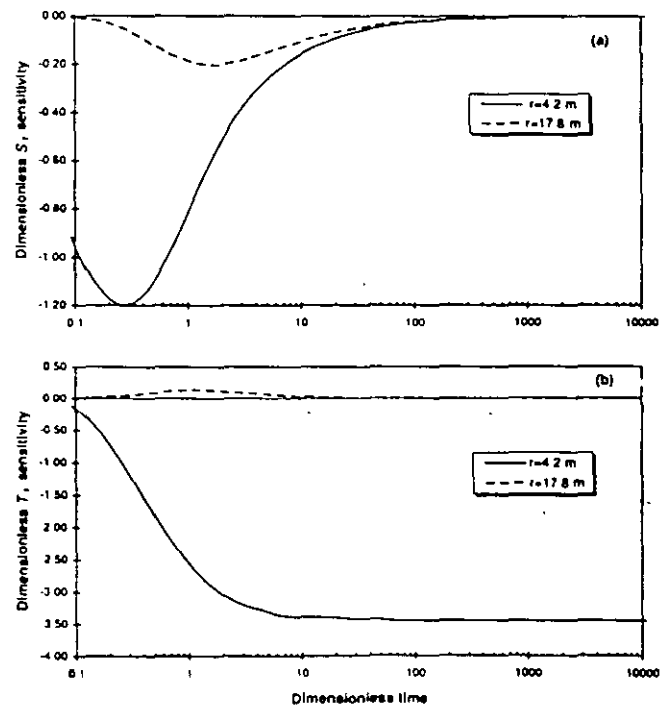

Fig. 4. Change of normalized sensitivities of dimensionless drawdowns $[(4\pi T_2 s)/Q]$ in inner and outer zones to (a) storativity, and (b) transmissivity of inner zone with dimensionless time $(T_2 t/S_2 l^2)$. ($T_1 = 600$ m²/d, $S_1 = 1 \times 10^{-4}$, $T_2 = 900$ m²/d, $S_2 = 2 \times 10^{-4}$).

estimate downstream transmissivity. Storativity reflects the aquifer's ability to release water, it has the characteristics of two-way coordinates. It depends on both the upstream and downstream portions of the location where it is "sampled" and can be estimated by drawdowns both upstream and downstream. The estimate of S_1 from the drawdown in Zone 2 is erroneous because, in the radial flow model, the sensitivity of drawdown in Zone 2 to storativity is very small due to the distance from O2 to Zone 1. However, the reason for the erroneously estimated T_1 by drawdown in Zone 2 seems deeply rooted in the characteristics of the parameter. Transmissivity reflects the aquifer's ability to transmit water; it has the property of one-way coordinates. Information on transmissivity can be transferred mainly from upstream to downstream. The information on the transmissivity of the downstream portion of an aquifer cannot be well reflected by the drawdown in the upstream portion aquifer.

This example also shows that parameters estimated from an observation well very near the pumping well can represent the flow properties of both the aquifer portion near the pumping well and the portion in the distance. Parameters estimated from an observation well at distance will, however, represent mainly the flow property of the aquifer between the location of the observation well and the distant portion of the aquifer which is influenced by the pumping. Similar conclusions were also reached by Butler and Liu (1993).

Summary and Discussion

The different characteristics of transmissivity and storativity under constant-rate pumping conditions have been examined and the influence of these characteristics on parameter estimation investigated using a hypothetical example. The results show that transmissivity has the characteristics of one-way coordinates and storativity has the characteristics of two-way coordinates. Information on transmissivity is transferred mainly from upstream to downstream. More specific conclusions can be presented as: (1) Sensitivity behavior of storativity is significantly influenced by local flow properties, but that of transmissivity is controlled mainly by the general flow properties of the flow field; (2) Drawdown in an observation well is more sensitive to the storativity of a downstream zone than that of an upstream zone, but the difference is not significant; (3) Drawdown in an observation well is more sensitive to the transmissivity of an upstream zone than that of a downstream zone and the difference is very significant. The sensitivity of drawdown to transmissivity of a downstream zone is characterized by a small positive value over a limited time period.

The above conclusions have implications in pumping-test design and parameter estimation in nonuniform aquifers. In order to estimate the parameters of a zone and the background aquifer, an observation well should be located downstream but near to the zone. It should not be placed upstream if the parameters downstream are to be estimated. An upstream well can produce information of storativity of both upstream and downstream, but it cannot produce much information about the transmissivity downstream. Because of the different characteristics between transmissivity and storativity of a nonuniform aquifer, a well may provide adequate information for storativity estimation, but may not provide adequate information for transmissivity estimation. The aquifer area represented by estimated storativity may be different from that represented by estimated transmissivity even when both are estimated from the same data. Estimated storativity may reflect the features of the aquifer downstream more than that of the aquifer upstream, but the estimated transmissivity may represent mainly the features of the aquifer upstream.

In this paper, examples are limited to confined aquifers, but the general conclusions may be true for unconfined aquifers with thickness significantly larger than drawdown. The discussion on the characteristics of aquifer parameters is based on constant-rate pumping conditions in one-dimensional flow systems. The characteristics of aquifer parameters under more general conditions, such as regional two-dimensional flow fields, may be different and is a topic for further investigation.

Acknowledgment

The authors would also like to thank A.L.H. Gameson for his review and constructive criticism of the earlier draft of this paper and the three anonymous reviewers for their many valuable comments. This work is supported in part by a grant from the School of Mines and Energy Department (SOMED) at the University of Alabama.

References

Beck, J. V. and K. J. Arnold. 1977. Parameter Estimation in Engineering and Science. John Wiley, New York.

Butler, J. J. 1988. Pumping tests in nonuniform aquifers: The radially symmetric case. J. Hydrol. v. 101, no. 1/4, pp. 15-30.

Butler, J. J. and W. Liu. 1993. Pumping tests in nonuniform aquifer: The radially asymmetric case. Water Resour. Res. v. 29, no. 2 pp. 259-269.

Butler, J. J. and C. D. McElwee. 1990. Variable-rate pumping tests fo radially symmetric nonuniform aquifers. Water Resour. Res. v. 26, no. 2, pp. 291-306.

Jiao, J. J. 1993. Sensitivity features of aquifer parameters and their implications on parameter estimation. Ph D. thesis, School of Civil Engineering, Birmingham Univ., UK.

Jiao, J. J. 1995. Sensitivity analysis of pumping tests in non-uniform aquifers. Hydrological Sciences Journal. v. 40, no. 6 (in press).

Jiao, J. J. and Z. Chen. 1987. An improved characteristic-rectangular finite element method in the solution of two-dimensional water-quality model transport problems. Selected Papers of Hydrogeology and Engineering Geology. no. 6 (in Chinese), pp. 13-24.

Knopman, D. S. and C. I. Voss. 1987. Behavior of sensitivities in the one-dimensional advection-dispersion equation: implications for parameter estimation and sampling design. Water Resour. Res. v. 23, no. 2, pp. 253-272.

McElwee, C. D. 1982. Sensitivity analysis and the ground-water inverse problem. Ground Water. v. 20, no. 6, pp. 723-735.

McElwee, C. D. 1987. Sensitivity analysis of groundwater models. In: Advances in Transport Phenomena in Porous Media, ed. by J. Bear and M. Y. Corapcioglu. NATO Adv. Study Inst. Ser. Ser. E, v. 128, pp. 751-817.

Oliver, D. S. 1993. The influence of nonuniform transmissivity and storativity on drawdown. Water Resour. Res. v. 29, no. 1, pp. 169-178.

Patankar, S. V. 1980. Numerical Heat Transfer and Fluid Flow. McGraw-Hill.

Rushton, K. R. and Y. K. Chan. 1976. A numerical model for pumping test analysis. Proc. Instn. Civ. Engrs. Part 2, v. 61, pp. 281-296.

Sykes, J. F., J. L. Wilson, and R. W. Andrews. 1985. Sensitivity analysis for steady-state groundwater flow using adjoin operators. Water Resour. Res. v. 21, no. 3, pp. 359-371.

Yeh, W.W-G. and N. Z. Sun. 1985. An extended identifiability in aquifer parameter identification and optimal pumping test design. Water Resour. Res. v. 20, no. 12, pp. 1837-1847.

Zheng, C. and G. D. Bennett. 1995. Applied Contaminant Transport Modeling: Theory and Practice. Van Nostrand Reinhold, New York. 440 pp.

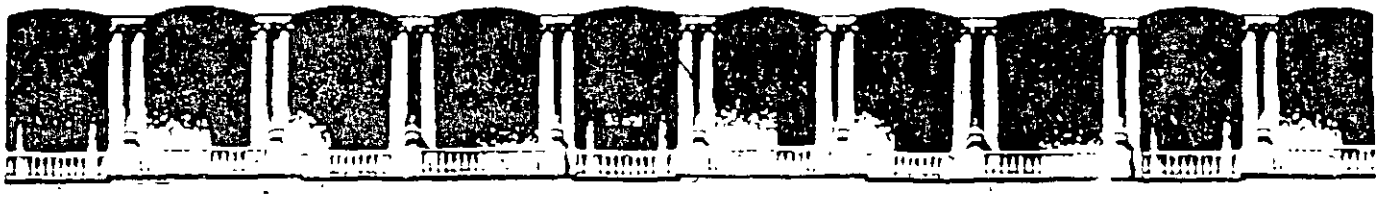

FACULTAD DE INGENIERIA U.N.A.M.
DIVISION DE EDUCACION CONTINUA
CURSOS ABIERTOS

XII CURSO INTERNACIONAL DE CONTAMINACIÓN DE ACUÍFEROS

MODULO III: MODELOS MATEMÁTICOS EN GEOHIDROLOGIA Y CONTAMINACIÓN DE ACUIFEROS

TEMA

SALTER WATER INTRUSION IN THE COSTA DE HERMOSILLO, MÉXICO: A NUMERICAL ANALYSIS OF WATER MANAGEMENT PROPOSALS

EXPOSITOR: DR. ADOLFO CHAVEZ RODRIGUEZ

PALACIO DE MINERIA
OCTUBRE DEL 2000

Salt-Water Intrusion in the Costa de Hermosillo, Mexico: A Numerical Analysis of Water Management Proposals

by Robert W. Andrews[a]

ABSTRACT

As a result of anthropogenic discharges of ground water far exceeding natural recharge, the Costa de Hermosillo aquifer is being actively intruded by salt water. Because this aquifer is utilized as the sole source of irrigation water for one of Mexico's principal agricultural districts, the application of any future management scheme to control this intrusion must be closely evaluated prior to implementation. A hydrologic and water quality simulation model is applied to the Costa de Hermosillo aquifer to assess the areal and temporal variations in head, velocity, and concentration as a result of changes in the present discharge distribution. The known hydrologic conditions are reproduced as a means of calibrating the model. Only qualitative statements on the future behavior of the aquifer are possible due to the uncertainty of the magnitude of various aquifer parameters and initial conditions. The model employed in this study is found to be a useful technique for the analysis of the effects of the proposed pumping stresses.

INTRODUCTION

Salt-water intrusion into coastal aquifers has been the focus of a considerable research effort. The interest in and study of this problem has been necessitated by the increased demands placed on subsurface-water supplies in large metropolitan areas and irrigation projects which border many of the coastal regions around the world. If the water resources within these coastal areas are to be adequately managed, it is necessary to be able to predict the salinity changes to be expected within the aquifer given any proposed discharge scheme. Reviews of salt-water intrusion occurrences and the effectiveness of current control efforts are given by Newport (1975) and Kashef (1977).

Means of quantifying salt-water intrusion have been undertaken by numerous researchers. Early studies generally assumed that a discrete interface separated the two immiscible fluids. Analytical expressions of this interface, such as the Ghyben-Herzberg relationship, were utilized to define the position of this boundary. Bear (1979) summarizes the existing analytical methods used to assess steady state and transient sharp interface locations within the vertical plane. Subsequent investigators, however, have described the existence of a dispersion zone in which the salt water mixes with fresh water. A steady-state solution of the concentration distribution in the vertical plane incorporating the effects of dispersion is discussed by Henry (1960).

Several numerical solution schemes have been applied to the evaluation of salt transport in coastal aquifers. The models generated for application to salt-water intrusion may be classified according to whether a sharp or dispersed interface is assumed, an areal or vertical cross-sectional plane through the aquifer is considered, transient or steady-state equations are used to describe the fluid flow and mass transport, and finite elements or finite differences are employed in the spatial discretizations.

Numerical approximations of dispersed intrusion zones have most commonly been conducted within the vertical plane. Using the method of characteristics, Pinder and Cooper (1970) solved for the transient position of the

[a]Department of Geology and Geophysics, University of Connecticut, Storrs, Connecticut 06268 (currently with INTERA Environmental Consultants, Inc., 11999 Katy Freeway, Houston, Texas 77079).

Discussion open until May 1, 1982.

salt-water front, including the effects of dispersion. Lee and Cheng (1974) employed the finite element method to evaluate the steady-state chloride distribution in coastal aquifers. Transient simulations of the dispersion zone using the finite element method are presented by Segol and Pinder (1976).

A considerable amount of work has been undertaken recently to evaluate the areal intrusion of salt water. Without exception, the techniques employed have assumed the dispersive effects to be negligible. VandenBerg (1974) approximated the position of the interface by displacing a set of traveling points located on the interface. Several investigators have determined the sharp interface position within the areal plane by solving the vertically integrated areal flow equations in both the fresh-water and salt-water regions, using the constraint that the fluid pressures across the interface are equal. This has been accomplished using finite differences (Bonnet and Sauty, 1975; Mercer *et al.*, 1980) and finite elements (Pinder and Page, 1977; Sa da Costa and Wilson, 1979).

The justification each of the above researchers employ for the assumption of a sharp interface is that the transition zone between the fresh water and salt water is narrow in comparison to the extent of the ground-water system. Although this assumption certainly eases the numerical difficulties inherent in solving the mass transport equation and is indeed appropriate for many field occurrences of salt-water intrusion, it does not hold in all cases. If the dispersion zone is extensive, as it is in the case of the Biscayne aquifer of southeastern Florida (Kohout, 1964), then it is necessary to take into account the dispersion process in the analysis of salt-water intrusion.

Numerous codes have the capability of solving the areal flow and transport equations, incorporating the effects of dispersion, for evaluating salt-water intrusion (including, but not limited to, Segol *et al.*, 1975; INTERCOMP, 1976; and Konikow and Bredehoeft, 1978). An examination of the literature to date reveals, however, that none of these solution routines have been utilized for the specific problem of assessing areal salt transport in coastal aquifers subject to ground-water pumpage. As discussed above, only flow and transport in the vertical plane adjacent to coasts have been simulated. This is unfortunate in light of the fact that in most occurrences of salt-water intrusion it is the areal extent of intrusion which is of greatest interest to the planner charged with protecting the ground-water resource. It is the areal distribution of wells and the influence these discharge areas have on the areal salt distribution which must be considered.

Therefore, a need exists for a model which can be utilized to solve the areal flow and transport equations in order to assess areal salt intrusion into coastal aquifers subject to ground-water withdrawals. It is this type of model which is developed in the present investigation and applied to simulate the salt-water intrusion within the Costa de Hermosillo aquifer in Sonora, Mexico. While perhaps not suitable for all field areas and more prone to numerical instabilities, it is felt that such a model can be of use in the study of areal intrusion when the dispersion zone cannot be ignored.

RELEVANT EQUATIONS/SOLUTION ROUTINE

As the development of the appropriate partial differential equations describing unconfined ground-water flow and the transport of conservative chemical species in porous media have been reported thoroughly in the literature (see Bear, 1979; Konikow and Grove, 1977; among others), their generation will not be reiterated. The relevant equations for areal flow of ground water and mass transport are respectively

$$S_y \frac{\partial h}{\partial t} + \frac{\partial \bar{q}_\alpha}{\partial x} + W = 0 \qquad (1)$$

and

$$\frac{\partial}{\partial x_\alpha}\left[\Theta D_{\alpha\beta}\, \ell(h) \frac{\partial C}{\partial x_\beta}\right] - \bar{q}_\alpha \frac{\partial C}{\partial x_\alpha} - \ell(h) \frac{\partial (\Theta C)}{\partial t} = 0 \qquad (2)$$

where

S_y specific yield, dimensionless;

h hydraulic head, m;

$\bar{q}_\alpha$ specific discharge through the entire saturated thickness of the aquifer, m^2/s;

W rate of recharge or discharge, m/s;

Θ porosity, dimensionless;

$D_{\alpha\beta}$ macroscopic hydrodynamic dispersion coefficient, m^2/s;

$\ell(h)$ saturated thickness of the aquifer, m;

C concentration of conservative ion, mg/l;

α, β indices describing spatial directions.

It should be noted that the above form of the mass transport equation assumes the concentration of the source/sink fluid is the same as the average concentration of the fluid within the aquifer at the

recharge/discharge point. If this were not the case a source term would be required in the ...ulation. In the present study the specific yield and porosity are assumed to be equivalent.

The decoupled form of the flow and transport equations is utilized in this study. This is a consequence of the fact that all parameters are averaged over the vertical dimension and the Dupuit approximation is assumed to be applicable. This allows the utilization of the hydraulic head form of the flow equation rather than the fluid pressure form. Density dependent flows due to concentration gradients, which are important in many simulations conducted in the vertical plane, are not significant when considering areal transport.

The specific discharge vector is related to the hydraulic head by the Dupuit approximation of Darcy's law

$$\bar{q}_\alpha = \Theta v_\alpha \ell(h) = -K_{\alpha\beta}\ell(h)\frac{\partial h}{\partial x_\beta} \qquad (3)$$

where v_α is the seepage velocity (m/s), and $K_{\alpha\beta}$ is the hydraulic conductivity tensor (m/s).

Assuming the molecular diffusion is negligible, ... macroscopic dispersion tensor for isotropic ...rous media may be represented

$$D_{\alpha\beta} = a_T |v| \delta_{\alpha\beta} + (a_L - a_T) v_\alpha v_\beta / |v| \qquad (4)$$

where $|v| = (v_\alpha^2 + v_\beta^2)^{1/2}$, the average seepage velocity; $\delta_{\alpha\beta}$ is the Kronecker delta; and a_L and a_T are the longitudinal and transverse dispersivities (m), respectively (Bear, 1979, p. 234).

The numerical method chosen to generate approximating equations to the ground-water flow and mass transport equations is that of the Galerkin weighted-residual finite element technique. Because detailed descriptions of this method and its application to the above equations are available in numerous manuscripts (see Connor and Brebbia, 1976; Pinder and Gray, 1977; Grove, 1977), only the final matrix equations are presented below. The systems of equations to be solved are

$$[A]\left\{\frac{\partial h}{\partial t}\right\} + [B]\{h\} = \{F\} \qquad (5)$$

and

$$[M]\left\{\frac{\partial C}{\partial t}\right\} + [N]\{C\} = \{R\} \qquad (6)$$

where the components in the coefficient matrices are

$$a_{ij} = \int\int S_y N_i N_j \, dA \qquad (5a)$$

$$b_{ij} = \int\int K_{\alpha\beta}\ell(h)\frac{\partial N_i}{\partial x_\alpha}\frac{\partial N_j}{\partial x_\beta} dA \qquad (5b)$$

$$f_i = -\int\int W N_i \, dA + \int N_i K_{\alpha\beta}\ell(h)\frac{\partial h}{\partial n} dS \qquad (5c)$$

and

$$m_{ij} = \int\int \Theta\ell(h) N_i N_j \, dA \qquad (6a)$$

$$n_{ij} = \int\int \left[\Theta D_{\alpha\beta}\ell(h)\frac{\partial N_i}{\partial x_\alpha}\frac{\partial N_j}{\partial x_\beta} + q_\alpha N_i \frac{\partial N_j}{\partial x_\beta}\right] dA \qquad (6b)$$

$$r_i = \int N_i \Theta D_{\alpha\beta}\ell(h)\frac{\partial C}{\partial n} dS \qquad (6c)$$

where N_i and N_j are the coordinate or basis functions. The surface integrals of equations (5c) and (6c) result from application of Green's theorem to the terms containing second order derivatives. They correspond to specified fluid flow and mass flux, respectively, across the aquifer boundaries. These integrals need be evaluated only if Neumann boundary conditions are specified. After application of the boundary conditions and incorporation of an implicit finite difference approximation for the temporal derivative, the resultant linear systems of equations are solved by a Gausslan elimination routine.

NUMERICAL INSTABILITIES

Numerical solutions of the convective-dispersive equation commonly exhibit instabilities. These instabilities are characterized by either oscillations in the concentration distribution as a sharp front is approached or numerical dispersion which tends to smear the concentration front. The difficulties are intensified when convective transport dominates over dispersive transport. Additionally, when a discrete model is utilized to approximate any transport system, the velocity distribution will not be continuous. In finite element discretizations this results from the fact that velocities are generated for each element separately, causing interelement values at the same node to be nonuniform.

Numerical instabilities were not foreign to the present investigation, particularly oscillations in the vicinity of the front, and various techniques were employed to minimize these difficulties. These methods are summarized below. This discussion by no means covers all possible means suggested to reduce numerical errors, as a considerable volume of research has been conducted in this field, but it does seek to enumerate those utilized at one time or another during the present study.

Several techniques have been suggested to minimize discontinuous velocities. Segol *et al.* (1975) solved the flow equation for the areal components of the velocity vector simultaneously with the head, although at the expense of increased computational storage requirements and costs. Utilizing the equivalence between the discontinuous velocities generated in flow problems and discontinuous stresses common in elasticity problems, local or global least squares smoothing routines similar to those used by Hinton and Campbell (1974) or Hinton *et al.* (1975) also may be employed to reduce these errors. Although these methods were applied to the present simulation, they did not reduce the numerical oscillations present in the solution.

Varied efforts have been proposed to reduce the effects of numerical oscillations and dispersion generated in simulating the transport equation. It is apparent that any reduction in mesh size (whether spatial or temporal) should improve the solution, although the increased costs of such alterations often prohibit as fine a discretization as is necessary (or desirable) for the problem at hand. Several methods are based on improved approximations of the temporal derivative such as using an arbitrary time increment or higher order finite difference approximations. Once again, these did not dampen the oscillations observed in the present study.

A technique which effectively reduces the oscillations generated when simulating convective dominant transport is to employ upwind weighting functions in the weighted residual formulation (Heinrich *et al.*, 1977). This technique has its roots in the backward (upwind or upstream) difference approximations of the convective terms utilized in finite difference approximations (Spalding, 1972). Recent extensions of the original steady-state upwind weighting scheme to transient problems have been discussed by Huyakorn and Nilkuha (1979), Gureghian *et al.* (1980), and Yeh and Ward (1981). Although this method appears to offer some advantages over conventional Galerkin weighting functions for convective dominant transport simulations, it was found to be ineffective in eliminating the oscillations which were prevalent in the current application.

In an attempt to eliminate numerical oscillations contributed by the temporal derivative, several investigators have suggested the diagonalization of the time matrix in the finite element approximation ([M] in equation 6). Instead of integrating the consistent time matrix by Gaussian quadrature yielding a symmetric banded matrix, this approach evaluates the integrals at the nodes themselves resulting in the diagonal time matrix. Such a diagonalization procedure when applied to linear elements is easily incorporated into the computer code by replacing the consistent time matrix with a lumped matrix, where the coefficients of the lumped matrix are evaluated by placing the sum of the columns of the consistent matrix along the diagonal and setting all off-diagonal terms to zero. Discussions of this method may be found in Hinton *et al.* (1976) and Neuman and Narasimhan (1977). In order to obtain stable results in the simulation of salt transport in the Costa de Hermosillo aquifer, the time matrix had to be diagonalized. This technique effectively eliminated the undershoot problem (large negative concentrations adjacent to the coast) which existed when the consistent time matrix was employed.

Although application of lumped time matrices to the finite element solution of the transport equation have been successfully performed by Gureghian *et al.* (1980) and Yeh and Ward (1981), some controversy exists surrounding the utilization of this method. Several authors have suggested (Gresho *et al.*, 1978; Huyakorn and Nilkuha, 1979) that lumping the mass matrix actually degrades the accuracy of the numerical method by generating excessive numerical dispersion. In order to ascertain whether the concerns expressed by the above researchers would be detrimental in the current simulation, several one-dimensional transport simulations were conducted. Using similar Courant ($v\,\delta t/\delta x$) and Peclet numbers ($v\,\delta x/D$) as employed in the field problem (approximately 0.03 and 20, respectively), it was found that the only way to successfully eliminate the large oscillations downgradient from the intruding front was to lump the time matrix (Andrews, 1979). Although a slight increase in numerical dispersion was observed when using the lumped time matrix, this increase was determined to be acceptable given the goal to eliminate the oscillations.

In summary, a considerable amount of controversy exists as to the effectiveness of upwind weighting functions and/or diagonalization of the time matrix as means to reduce numerical instabilities inherent in solving convective dominant mass transport using the finite element method. It appears that both methods introduce some numerical dispersion into the solution while decreasing the oscillations. The evidence for or against each method is not compelling enough at this point to warrant complete acceptance or rejection of either solution scheme. More work

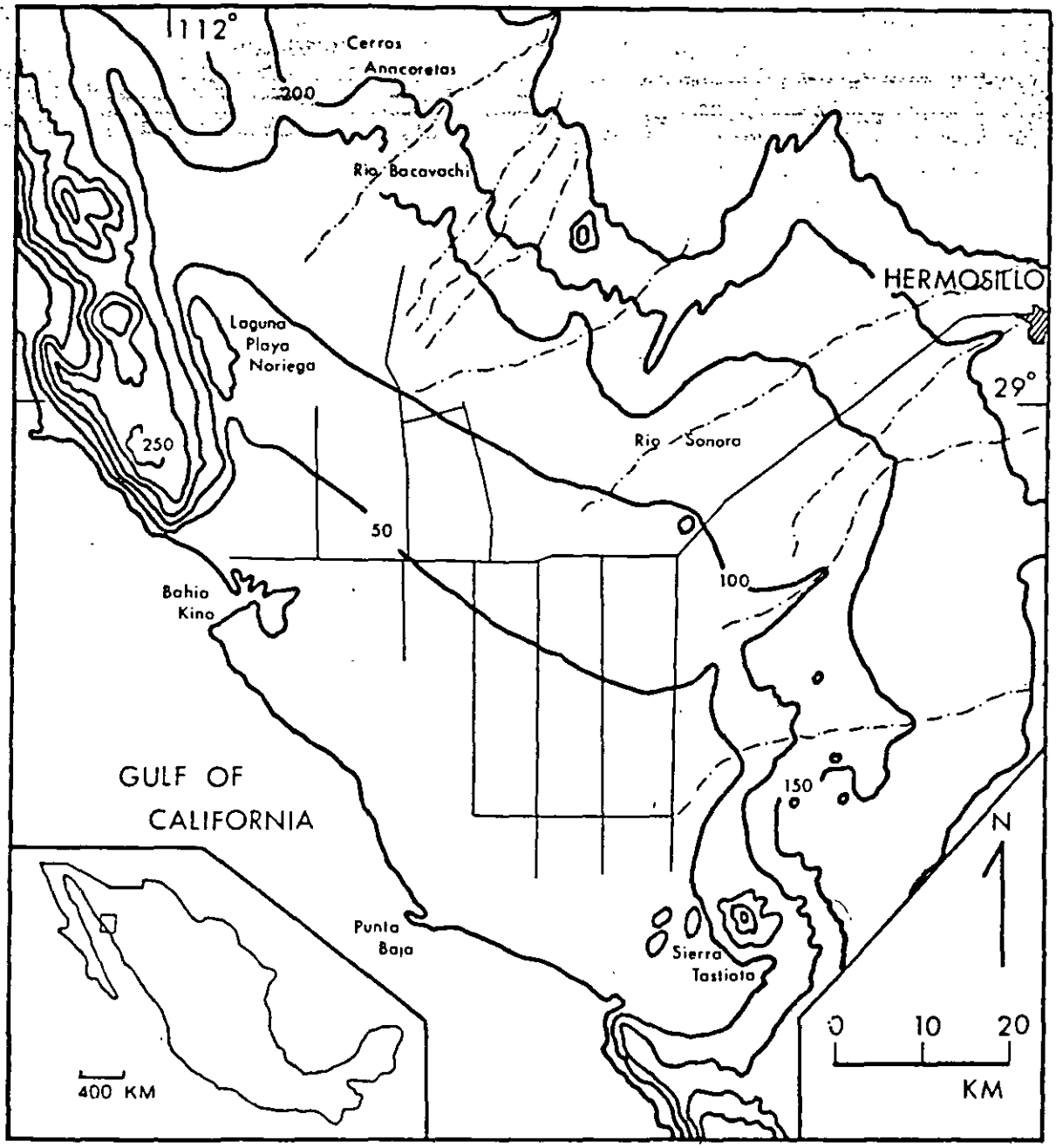

Fig. 1. Location and physiography of the Costa de Hermosillo, Sonora. Elevations in meters above mean sea level. Contour interval is 50 meters.

is needed to delineate when the application of each method is the most beneficial. It is not the purpose of this paper to offer a definitive comparison between the two methods. Suffice it to say that both were employed in the present study, and although diagonalization of the time matrix was necessary to eliminate the large oscillations in the chloride distribution observed in the present problem (manifesting itself with large negative concentrations adjacent to the coast), both should be investigated for subsequent applications.

FIELD AREA

The area chosen for this study on the use of numerical modeling to analyze various management proposals applied to a coastal aquifer is the Costa de Hermosillo irrigation district (Figure 1). The district lies adjacent to the Gulf of California in the State of Sonora, Mexico. The entire district comprises an area of approximately 7500 square kilometers of which about 1200 square kilometers are presently being cultivated.

The geology of the Hermosillo area consists of

Late Mesozoic fine-grained clastics and interbedded volcanics cut by Early Tertiary granitic to granodioritic intrusives and overlain by rhyolite flows, pyroclastics, and ignimbrites. This basement complex is blanketed by a thick sequence of interbedded silts, sands, and gravels ranging in age from Miocene to Recent which were generally deposited as coalescing alluvial fans along numerous northwest-southeast-trending normal faults. It is this deposit of granular material which constitutes the unconfined Hermosillo aquifer. Underlying the coarser material, at depths ranging from 150 to 300 m, is a thick marine clay (Jimenez, 1965) which is assumed to behave as an aquiclude.

Considering the paucity of rainfall (averaging 20 cm per year), and the lack of adequate surface-water supplies in the Costa de Hermosillo, it has been necessary to rely exclusively on the availability of ground water for the extensive irrigation needs of the district. The total discharge from the aquifer increased steadily following the emplacement of the first wells in 1945, and for the past 25 years has varied between 760×10^6 and 1140×10^6 m^3/yr from about 484 production wells.

Annual recharge to the Hermosillo aquifer is estimated to range from 250×10^6 to 350×10^6 m^3 (Matlock *et al.*, 1966). This recharge is divided about evenly between precipitation, irrigation return flows, and underflows from the Rios Sonora and Bacavachi. This is based on the assumption that approximately 10% of the applied water from irrigation and rainfall recharges the aquifer, the rest being lost to evaporation and transpiration. Recharge is incorporated in the present model by applying the annual contribution due to areal precipitation and irrigation return flows to appropriate interior nodes while specifying a constant recharge at boundary nodes adjacent to the Rios Sonora and Bacavachi.

The excess withdrawals over recharge have created overdrafts from the Hermosillo aquifer ranging from 450×10^6 to 900×10^6 m^3/yr since 1954. As a result, water-table declines of up to 40 m were generated in interior regions of the district by 1973 (Cummings, 1974). Observed piezometric surfaces during the early phases of ground-water development (1954) and after 16 years of intense discharge (1970) are illustrated in Figures 2 and 3, respectively.

By lowering the piezometric surface below sea level, the natural hydraulic gradient towards the coast has been reversed in the Hermosillo area. This reversal has enhanced the landward migration of salt, as is seen in the temporal variation of the

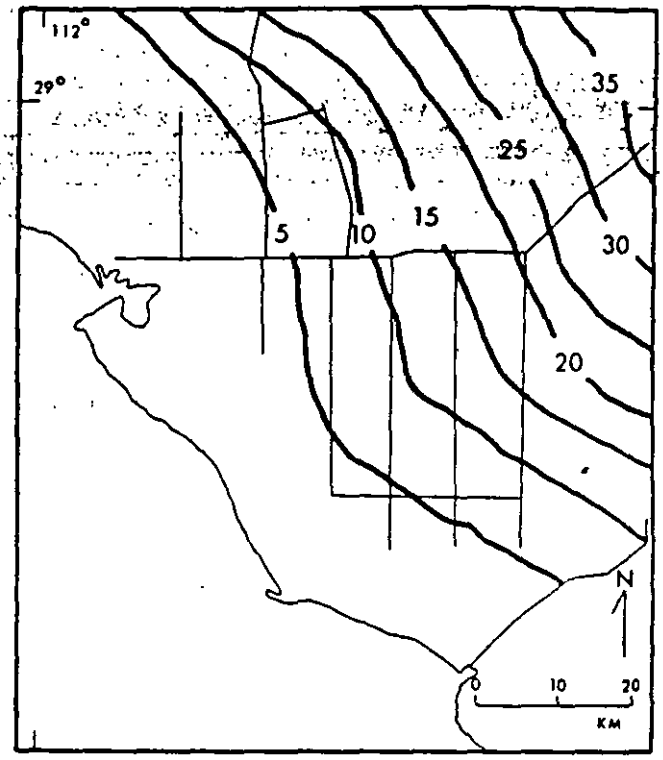

Fig. 2. Observed 1954 potentiometric surface. Elevations in meters above mean sea level.

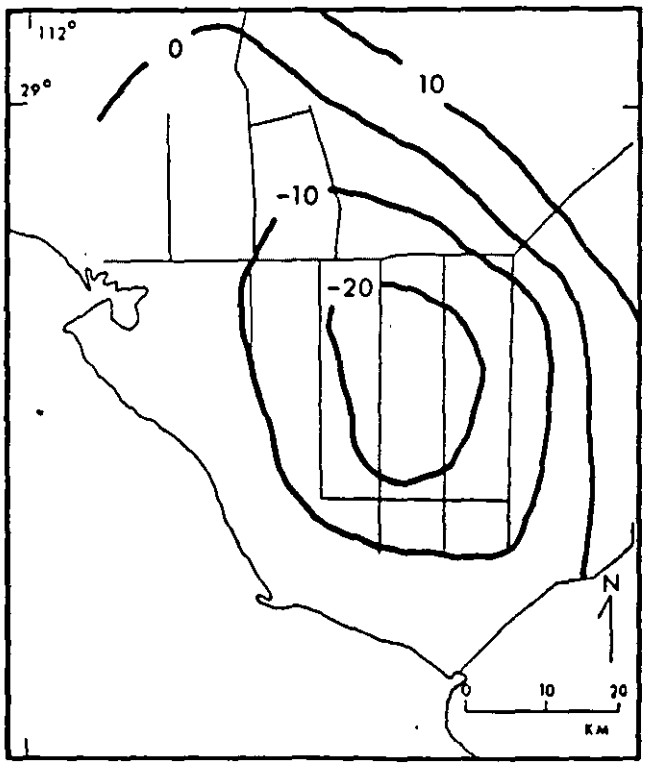

Fig. 3. Observed 1970 potentiometric surface. Elevations in meters above mean sea level.

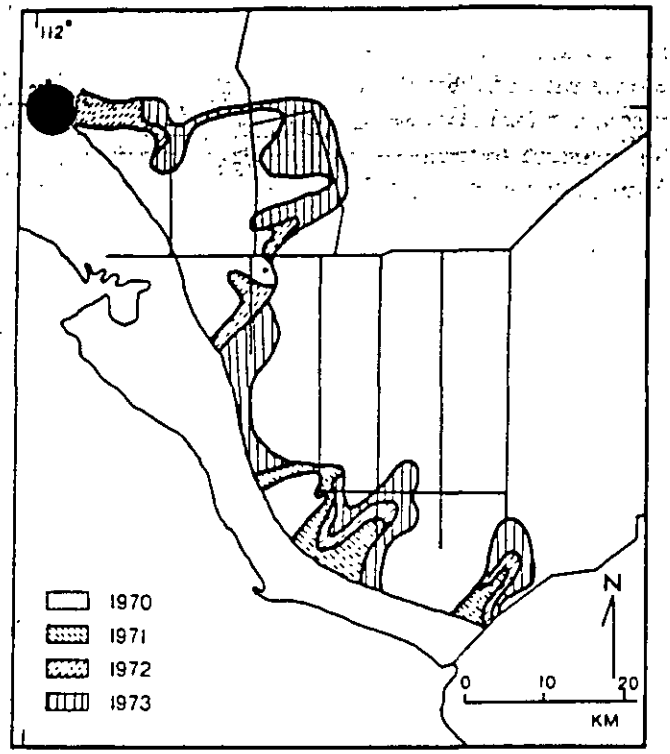

Fig. 4. Total dissolved solids for the years 1970 through 1973. Areas with greater than 525 mg/l total dissolved solids are depicted.

t. .issolved solids from 1970 to 1973 (Figure 4). It is generally believed that the two major intrusion zones within the aquifer represent buried alluvial channels which act as conduits for the intruding salt water (Domenico *et al.*, 1974). Although no wells exist within 10 kilometers of the coast, total dissolved solids concentrations in excess of 1200 mg/l and chloride concentrations greater than 400 mg/l have been observed in several wells within the major intrusion zones. These wells fully penetrate the aquifer and are well mixed, thus giving an average concentration at the point of extraction. The background chloride concentration in this area is about 20 mg/l.

Prior to applying the numerical procedure discussed above to the Costa de Hermosillo aquifer it is necessary to first define the relevant aquifer properties as well as the initial and boundary conditions. Based on a number of studies conducted by the Secretaria de Recursos Hidraulicos (SRH) and others, a considerable amount is known about the nature and extent of the Hermosillo aquifer. Th· ·itial saturated thickness of the aquifer a s approximately 150 m. Based on aquifer tests performed by the SRH, the transmissivity was found to vary between 0.05 and 0.12 m^2/s (Cruickshank and Chavez-Guillen, 1969). In the present study the initial (pre-pumping) transmissivity was assumed to be 0.1 m^2/s within the interior regions. The areas encompassed by the buried alluvial valleys were assigned transmissivities of 0.12 m^2/s, while a value of 0.06 m^2/s was applied to the finer-grained sediments in the coastal zones. The aquifer was assumed to be isotropic. Specific yield values ranging from 0.08 (Cruickshank and Chavez-Guillen, 1969) to 0.1 (Matlock *et al.*, 1966) to 0.15 (Domenico *et al.*, 1974) have been proposed for the Hermosillo aquifer. In the present study the specific yield and porosity were assumed to be equivalent and equal to 0.15, except in the major intrusion zones where they were reduced to 0.06 in order to successfully recapitulate the observed chloride distributions. Longitudinal and transverse dispersivities of 100 meters and 30 meters respectively were utilized in the transport simulation. Varying the dispersivity did not affect the simulated results to any significant degree (Andrews, 1979).

All boundaries of the Costa de Hermosillo aquifer were treated as either constant potential (Dirichlet) or constant flux (Neumann) type boundaries. The coastal boundary nodes in the simulation of the head distribution were assigned a constant head of 0.0 m, while all other boundary nodes were treated as Neumann type ($\partial h/\partial n = 0$). Although the latter no-flow boundary may not be strictly correct, except to the south where the study area is bounded by intrusive rock units, it was felt to be adequate as these boundaries are well removed from the central discharge region, and hence do not affect the solution in this region. For the solution of the mass transport equation a constant chloride concentration of 19,000 mg/l, the chloride concentration of sea water, was assumed to be applicable along the coast. All other boundaries are represented by Neumann no-flow conditions ($\partial C/\partial n = 0$) which are appropriate as long as the flow is parallel to the boundary or the boundary is far enough removed from the area encompassed by the intruding salt.

Although recorded water-table elevations were available from data compiled by SRH (Figure 2), the lack of data available within approximately 10 km of the coast and the temporal lag prior to the collection of concentration data (which commenced in 1964) precluded the existence of information regarding the initial areal extent of salt in the Costa de Hermosillo aquifer. Several methods were considered in the current study for the determination of the initial chloride distribution. One possibility was to model the steady-state chloride

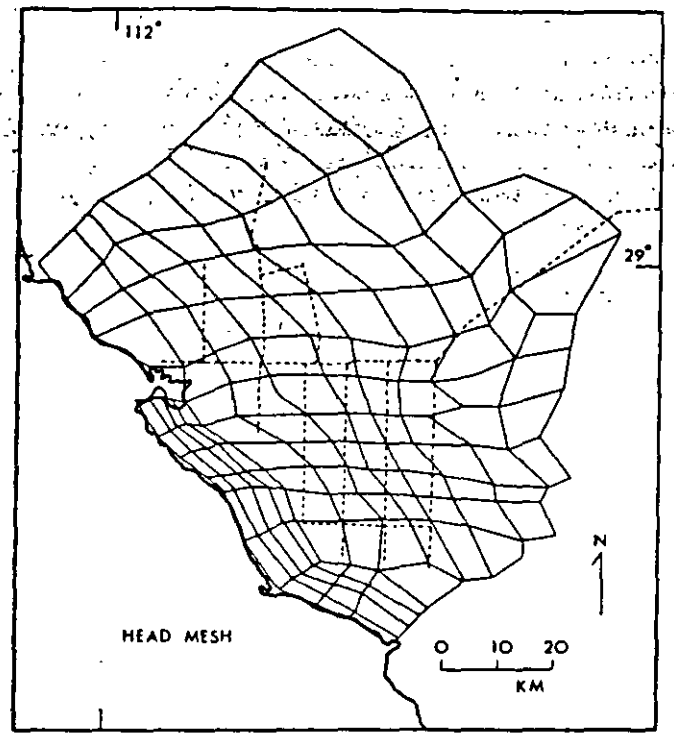

Fig. 5. Finite element mesh used in head simulations.

distribution in the vertical plane (see Segol and Pinder, 1976) and to subsequently average the concentration over the depth. Stable results were not attainable using this method due to the large aspect ratio required for the simulations in the vertical plane and the extremely low hydraulic gradients within the Hermosillo aquifer. Another possible means of calculating the steady-state areal or vertical concentration distribution is to assume hydrostatic conditions and employ the Ghyben-Herzberg relationship. Assuming no diffusion zone and a salt-water density of 1.025 gm/cm^3, the use of the Ghyben-Herzberg formula would place the pre-pumping interface further inland than the observed data warrant. A third method is to evaluate the depth to the stationary interface as a parabolic function of distance inland from the coast (Glover, 1959; Bear, 1979, pp. 393-396). This means of determining the steady-state concentration distribution is appealing because it resembles several observed steady interfaces as well as some numerical approximations to interface problems (e.g., Sa da Costa and Wilson, 1979, p. 159). This latter method was employed in the present study by first defining the position of the steady-state sharp interface and then averaging the chloride concentration over the depth by determining the relative percent of the saturated aquifer containing salt and fresh water. Although this technique may not yield the exact initial chloride distribution in the Hermosillo aquifer, it is felt to be a reasonable approximation.

The finite element discretizations applied to the Costa de Hermosillo aquifer are shown in Figures 5 and 6 for the head and concentration simulations, respectfully. A much finer mesh is utilized in the concentration simulations in order to reduce the numerical instabilities generated in solving the convective-dispersive equation. Heads generated in the flow simulations are extrapolated to the finer concentration mesh prior to the solution of the nodal specific discharge vectors. It

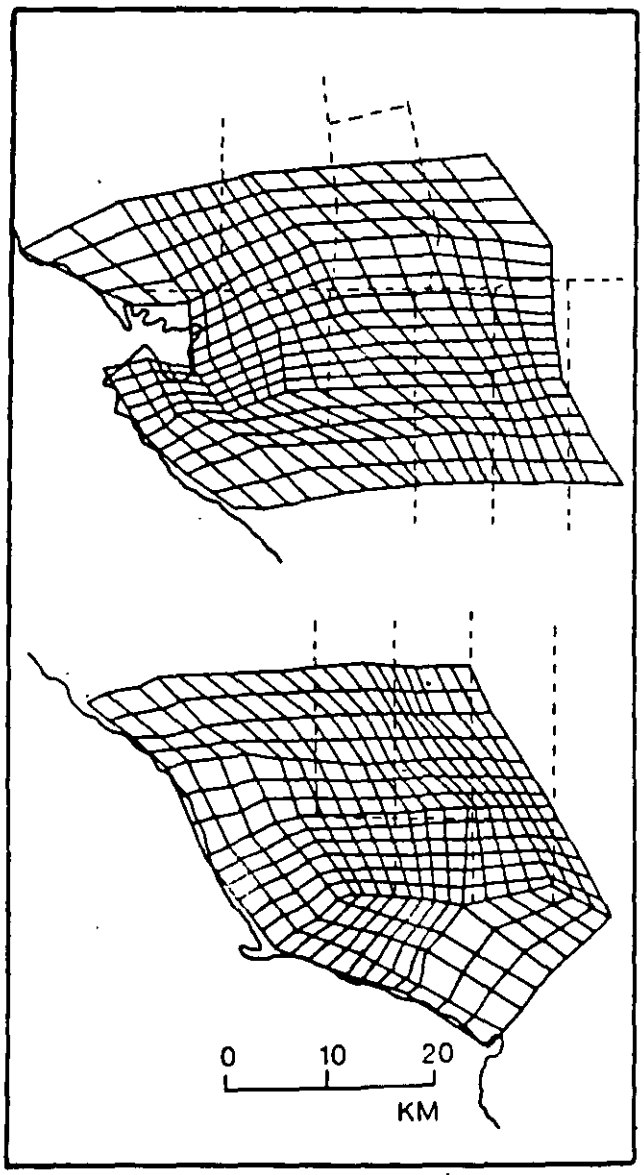

Fig. 6. Finite element meshes used in concentration simulations.

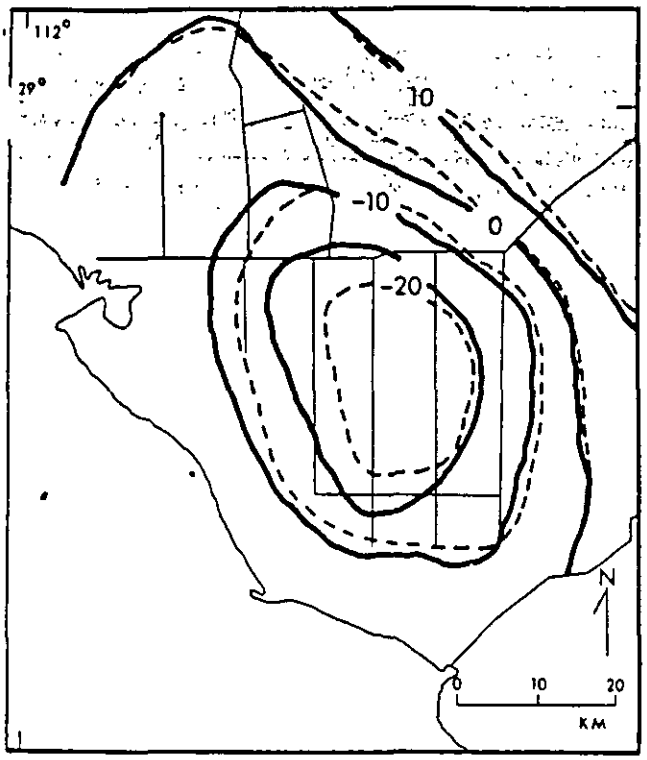

Fig. 7. Observed (dashed) and simulated (solid) 1970 potentiometric surface. Elevations in meters above mean sea level.

should be noted that the concentration mesh refinement does not generate a more exact velocity distribution, but decreases the errors associated with trying to fit a relatively sharp interface through widely-spaced nodal points. The use of two separate meshes in the concentration simulations was for purposes of convenience. A total of 167 nodes are used in the head simulations, while 358 nodes are utilized in the northern concentration mesh and 326 nodes are employed in the southern concentration mesh.

Recapitulation of the observed head and concentration distributions over a period of known ground-water discharges is a prerequisite to any model which is to be used for the evaluation of future discharge schemes. Starting with the known initial piezometric surface (Figure 2) and the pumping rates from 1954 to 1970, the model discussed above is seen to generate a head distribution which closely approximates the observed 1970 piezometric surface (Figure 7). At no node is there a greater than 5 m difference between the simulated and observed heads. Although the simulated match on the western fringe of the central discharge region could have been improved by increasing the specific yield in this area, this modification would not have allowed a successful recapitulation of the concentration distribution.

Recapitulation of the known concentration distribution posed several problems. The lack of any recorded "initial" concentration distribution, the paucity of data available within about 10 km of the coast, and the temporal variability in the chloride concentrations observed at many of the wells all contributed to the uncertainty involved in the recapitulation of the chloride distribution. In spite of these limitations, it was possible to generate a chloride distribution which closely approximated the 1970 observed distribution (Figure 8). In so doing, a low porosity and specific yield (averaging 0.06) had to be incorporated in the major intrusion zones. The high chloride concentrations observed in the northern fringe of the study area were not reproducible in any of the concentration recapitulations. Examining the head distribution in this area it is apparent that the hydraulic gradients and hence convective fluxes are small in comparison with the rest of the region. The poor quality water in this area appears to be not the result of salt-water intrusion, but instead is probably due to high chloride indigenous ground waters which may be the result of a buried Plio-Pleistocene playa deposit.

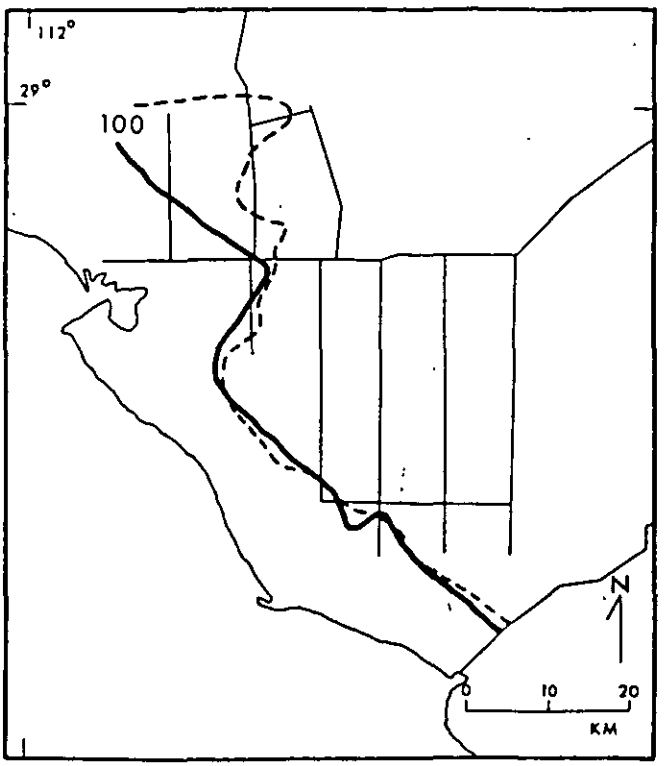

Fig. 8. Observed (dashed) and simulated (solid) 1970 chloride distributions. Contours represent the 100 mg/l isochlor.

EVALUATION OF MANAGEMENT PROPOSALS

Several options for controlling the rate and extent of intruding salt water into coastal aquifers have been proposed (Newport, 1975). Among the alternatives which have been suggested as being potentially applicable to the Costa de Hermosillo irrigation district are

1. Relocating the wells by either moving the wells inland or dispersing the wells to eliminate areas of concentrated discharge, and

2. Reducing the amount of water pumped from the aquifer by improving the irrigation efficiency (Domenico *et al.*, 1974).

These proposals certainly do not exhaust the possible discharge schemes which may be applied to the Hermosillo aquifer, some of which have been investigated by the author (Andrews, 1979). They are meant to be illustrative of results obtainable utilizing the developed areal model to assess the impact of various management stresses. The discussion which follows will focus on the effects these proposed management schemes would produce on the head and chloride distributions were they to be applied to the Costa de Hermosillo irrigation district. In these simulations it is assumed that the recapitulated head and concentration distributions previously generated provide suitable initial conditions. Each simulation is conducted over a 34-year time span using a one-half year time step.

It must be stressed that the results contained herein should not be interpreted as absolute estimates of future head and chloride distributions. The uncertainties discussed require not only a degree of subjectivity on the part of the modeler, but more importantly the realization that only qualitative statements on the future behavior of the aquifer system are possible. Thus it is impossible to predict with any degree of certainty what the chloride concentration will be at a given point in space and time. What can be garnered from the simulations are the general trends in the head and chloride distributions and the relative impacts to be expected given various applied stresses.

One means suggested of reducing the lateral intrusion of salt water caused by excessive pumping is to simply move the wells further inland. The essential aim is not only to relocate those wells which are being threatened by the intruding salt water, but also to reduce the inward convective transport of salt so that more interior wells may be preserved. In applying this management scheme to the Costa de Hermosillo irrigation district, 92 wells with a total withdrawal of 162×10^6 m^3/yr (which represents 18% of the basinwide totals) were removed from the area adjacent to the coast and installed in zones in the northern and eastern sectors of the district. The head distribution obtained after 34 years of simulation using this management policy appears in Figure 9. As expected, the maximum drawdown region has shifted about 10 km inland as a result of the discharge relocation. In addition, there is a sharp increase in the hydraulic gradients in the region between the maximum drawdown region and the coastal region from which the pumpage was eliminated. Although not depicted on the Figure, at early times subsequent to the application of this pumping policy, the rate of head decline in the coastal region (up to 15 km away from the coast) was sharply reduced due to the cessation of ground-water withdrawal from this area. The simulated chloride distribution under this management policy is depicted in Figure 10. It is clear that a sizable portion of the pumping capacity of the aquifer would be affected by the intruding salt if this discharge policy were employed.

With the realization that it is the volume of

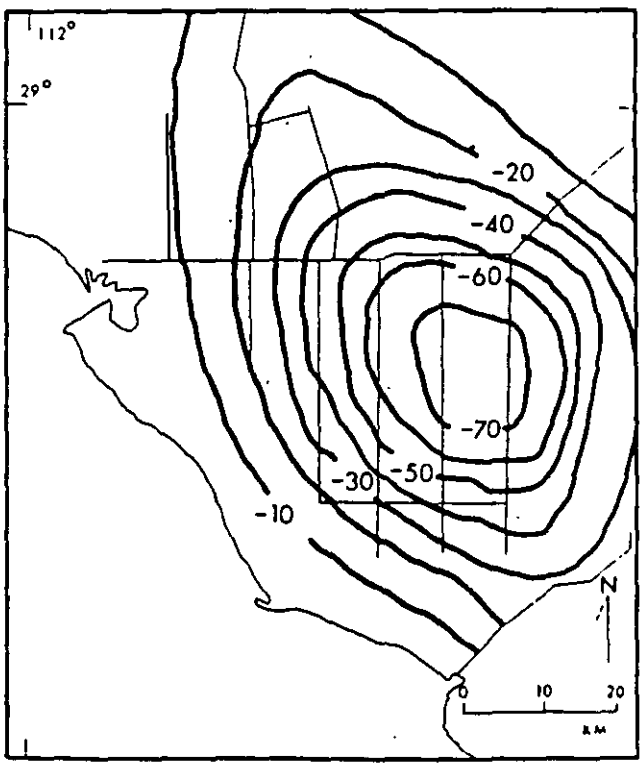

Fig. 9. Simulated potentiometric surface after 34 years using the management proposal to relocate the coastal discharge. Elevations in meters above mean sea level.

water discharged from a coastal aquifer and the ltant head decline and hydraulic gradient sal which eventually lead to the intrusion of salt water, an apparent means of controlling the influx of salt water is to simply reduce the amount of water pumped from the aquifer. Busch *et al.* (1966) have estimated that a potential reduction in total discharge of 20% is possible in the Hermosillo aquifer by improving the present irrigation efficiency. Experiments conducted in northern Mexico indicate that water requirements can be decreased by about 15% while at the same time increasing yields approximately 25% when irrigation improvements are employed (Domenico *et al.*, 1974). It is thus possible to significantly reduce the water needs in the Hermosillo area while still obtaining benefits that compare favorably with those currently earned in the district.

The discharge distribution used in the proposal to minimize water withdrawals assumes a 20% discharge reduction at all wells for the first five years, 27% for the second five years, and 33% for the third five years, after which 64 coastal wells are removed yielding a total discharge reduction of 42%. The simulated head distribution after 34 years using this management proposal is depicted in Figure 11. The decreased discharge in this management plan has significantly reduced the drawdowns in the central portion of the district compared to those generated in the well relocation scheme. Although the cessation of pumpage from the coastal wells has increased the hydraulic gradients between the coastal and maximum drawdown regions, the effect is not as noticeable as in the previous management scheme. This is due to the smaller number of wells involved and the temporal delay before the wells are removed from production.

The simulated chloride distribution after 34 years using the discharge minimization policy is shown in Figure 10 for comparison to the well relocation management scheme. The extent of intrusion in the minimized pumpage scheme is generally less than when the previous pumping policy is used. This is a result of the reduced drawdowns and hence reduced gradients when the total discharge is minimized.

The fact that the coastal wells continue to pump for the first 15 years of the discharge

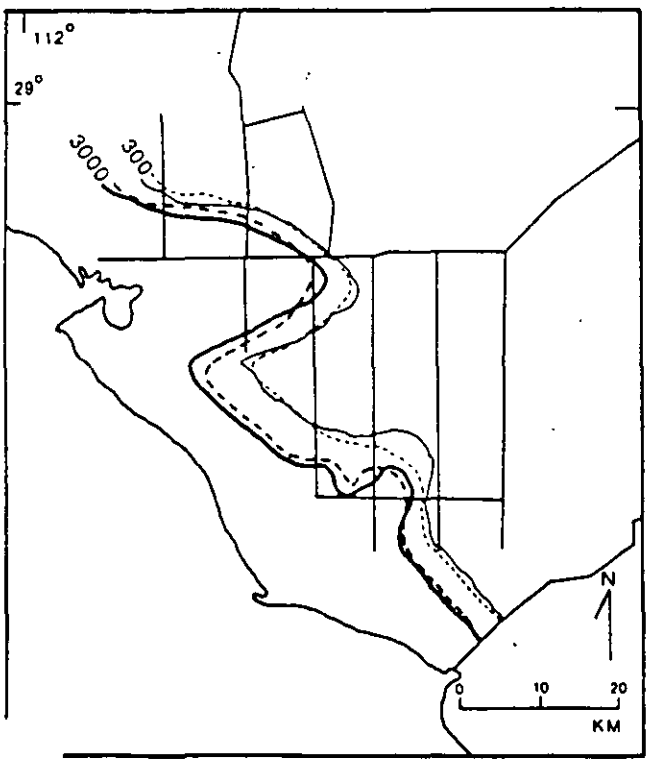

Fig. 10. Simulated chloride distributions after 34 years using the management proposals to relocate the coastal discharge (solid) and minimize water withdrawals (dashed). Contours represent the 300 mg/l and 3000 mg/l isochlors.

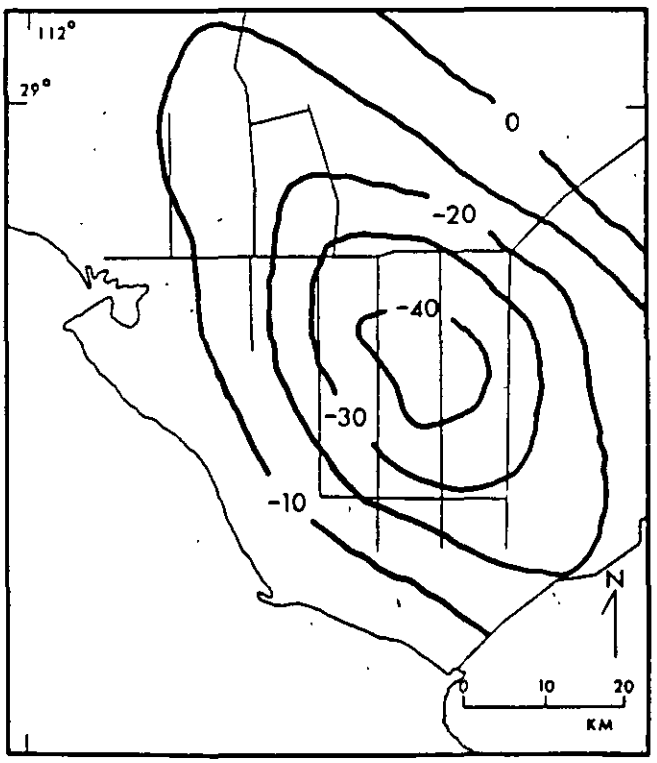

Fig. 11. Simulated potentiometric surface after 34 years using the management proposal to minimize water withdrawals. Elevations in meters above mean sea level.

minimization plan, albeit at decreased rates, does not allow as great a reduction in hydraulic gradients in the coastal region as was realized in the well relocation scheme. Hence for early times, when the intruding salt water is confined within this coastal zone, the relocation scheme provides reduced rates of transport. This is compounded by the lower hydraulic conductivities in the zone between the buried alluvial channels. This reduction is manifested in Figure 10 by the inland extent of the 3000 mg/l isochlor. Once the salt water enters the enhanced hydraulic gradient region between the coastal area and the central pumping region, however, the transport inland is increased.

CONCLUSIONS

Successful water management in an area irrigated with ground water, such as the Hermosillo irrigation district, is greatly enhanced by the ability to predict and evaluate the impact of any proposed modifications in irrigation practices or withdrawal distributions on both the quantity and quality of the ground water. Hence, an accurate hydrologic and water quality simulation model is a desirable management tool for predicting responses and affording a rational basis for the development and use of the ground-water resource. Various management schemes proposed for the Hermosillo irrigation district have been investigated to ascertain the effect each would impose on the transient areal distributions of head and chloride concentration within the aquifer.

In comparing the results generated by applying the various discharge distributions to the Costa de Hermosillo aquifer, several significant features are observed. For the hydrogeologic conditions of the Costa de Hermosillo, the salt intrusion is essentially irreversible. It is impossible to reverse the inland transport of salt due to the magnitude of the drawdowns and hydraulic gradients within the interior regions of the district by the time any management plan is initiated. In addition, once the salt water is inland its movement is independent of what happens along the coast. The management schemes that attempt to restore coastal hydraulic heads, and in so doing reduce the hydraulic gradients and transport of salt inland, are of little benefit in reducing the long-term intrusion.

It is worthwhile to stress the preliminary and qualitative nature of the results simulated using the various management alternatives proposed for the Costa de Hermosillo irrigation district. These limitations are necessary because of the uncertainty and variability inherent in the parameter identification and simulation process. The vast areal extent of the aquifer makes it virtually impossible to obtain the desired spatial frequency of data and also required a nodal spacing of several kilometers, inducing a certain amount of numerical instability in the finite element simulation. Although only qualitative statements of the relative impact each management scheme would impose on the aquifer system are possible, it is felt that the simulation technique employed in this study provides a rational basis for analyzing the effect future proposals would have on the areal and temporal distribution of salt within the aquifer. Although areal sharp interface intrusion models would eliminate the numerical oscillation and dispersion problems, because only the flow equations are solved, they would not be appropriate in the present case due to the extensive dispersion zone.

ACKNOWLEDGMENTS

The work upon which the above discussion is based comprised a portion of the author's Ph.D. research at the University of Illinois at Urbana-Champaign (Andrews, 1979). The major advisor for this study was Pat Domenico, whose support and encouragement are gratefully acknowledged. Computational support was provided by the University of Illinois Research Board.

REFERENCES

Andrews, R. W. 1979. The digital simulation of areal salt transport to evaluate water management proposals in a coastal aquifer. Ph.D. dissertation. Univ. of Illinois, Urbana, Ill. 216 pp.

Bear, J. 1979. Hydraulics of Groundwater. McGraw-Hill, New York, NY. 567 pp.

Bonnet, M., and J. P. Sauty. 1975. Un modele simplifie pour la simulation des nappes avec intrusion saline. A.I.H.S. Symposium Application of Mathematical Models in Hydrology and Water Resources Systems, Bratislava. AIHS Publ. No. 115, pp. 45-56.

Busch, C. D., W. G. Matlock, and M. M. Fogel. 1966. Utilization of water resources in a coastal groundwater basin, Part I: Evaluation of irrigation efficiency. J. Soil and Water Conser. v. 21, no. 5, pp. 163-166.

Connor, J. J., and C. A. Brebbia. 1976. Finite Element Techniques for Fluid Flow. Butterworth, Woburn, Mass. 310 pp.

Cruickshank, C., and R. Chavez-Guillen. 1969. Modelo matematico "DAS" para el estudia del comportamiento de acuiferos. Ingen. Hidraulica en Mex. v. 23, no. 1, pp. 31-42.

Cummings, R. G. 1974. Interbasin water transfers: a case study in Mexico. Resources for the Future, Johns Hopkins Press, Washington, D.C. 114 pp.

Domenico, P. A., F. J. Tapia Garcia, and L. Uribe. 1974.

Alternative policies for water management in the Costa de Hermosillo. Unpublished study conducted for Plan Nacional Hidraulicos under the auspices of the World Bank.

over, R. E. 1959. The pattern of fresh-water flow in a coastal aquifer. J. Geophys. Res. v. 64, pp. 457-459.

Gresho, P. M., R. L. Lee, and R. L. Sani. 1978. Advection-dominated flows, with emphasis on the consequences of mass lumping. Gallagher, R. H., *et al.*, eds. Finite Elements in Fluids. v. 3, pp. 335-350.

Grove, D. B. 1977. The use of Galerkin finite element methods to solve mass-transport equations. U.S. Geol. Survey Water Resour. Invest. 77-49, 61 pp.

Gureghian, A. B., D. S. Ward, and R. W. Cleary. 1980. A finite element model for the migration of leachate from a sanitary landfill in Long Island, New York — Part I: Theory. Water Resour. Bull. v. 16, no. 5, pp. 900-906.

Heinrich, J. C., P. S. Huyakorn, O. C. Zienkiewicz, and A. R. Mitchell. 1977. An "upwind" finite element scheme for two-dimensional convective transport equation. Int. J. Numer. Methods Eng. v. 11, pp. 131-143.

Henry, H. R. 1960. Salt intrusion into coastal aquifers. Int. Assoc. Sci. Hydrol. Publ. 52, pp. 478-487.

Hinton, E., and J. S. Campbell. 1974. Local and global smoothing of discontinuous finite element functions using a least squares method. Int. J. Numer. Methods Eng. v. 8, pp. 461-480.

Hinton, E., F. C. Scott, and R. E. Ricketts. 1975. Local least squares stress smoothing for parabolic isoparametric elements. Int. J. Numer. Methods Eng. v. 9, pp. 235-238.

Hinton, E., T. Rock, and O. C. Zienkiewicz. 1976. A note on mass lumping and related process in the finite element method. Earthquake Eng. and Struc. Dynamics. v. 4, pp. 245-249.

Huyakorn, P. S., and K. Nilkuha. 1979. Solution of transient transport equation using an upstream finite element scheme. Appl. Math. Model. v. 3, pp. 7-17.

INTERCOMP. 1976. A model for calculating effects of liquid waste disposal in deep saline aquifers. U.S. Geol. Survey Water Resour. Invest. 76-61, 263 pp.

Jimenez Villalobos, A. 1965. Condiciones de las aguas subterraneas en el Distrito de Riego Numero 51. Costa de Hermosillo, Son., Ing. Hidraulica en Mex. v. 19, no. 3, pp. 65-79.

Kashef, A. I. 1977. Management and control of salt-water intrusion in coastal aquifers. CRC Crit. Rev. Environ. Control. v. 7, pp. 217-275.

Kohout, F. A. 1964. The flow of fresh water and salt water in the Biscayne aquifer of the Miami area, Florida. Sea Water in Coastal Aquifers. U.S. Geol. Survey Water-Supply Paper 1613-C, pp. 12-32.

Konikow, L. F., and J. D. Bredehoeft. 1978. Computer model of two-dimensional solute transport and dispersion in groundwater. U.S. Geol. Survey Techniques of Water Resour. Inv. Bk. 7, Ch. C2, 90 pp.

nikow, L. F., and D. B. Grove. 1977. Derivation of equations describing solute transport in ground water. U.S. Geol. Survey Water Resour. Inv. 77-19, 34 pp.

Lee, C. H., and T. S. Cheng. 1974. On seawater encroachment in coastal aquifers. Water Resour. Res. v. 10, no. 5, pp. 1039-1043.

Matlock, W. G., M. M. Fogel, and C. D. Busch. 1966. Utilization of water resources in a coastal groundwater basin, Part II: Groundwater supply and incipient saltwater intrusion. J. Soil and Water Conserv. v. 21, no. 5, pp. 166-169.

Mercer, J. W., S. P. Larson, and C. R. Faust. 1980. Simulation of salt-water interface motion. Ground Water. v. 18, no. 4, pp. 374-385.

Neuman, S. P., and T. N. Narasimhan. 1977. Mixed explicit-implicit iterative finite element scheme for diffusion type problems: I. Theory. Int. J. Numer. Methods Eng. v. 11, pp. 309-323.

Newport, R. D. 1975. Salt water intrusion in the United States. R. S. Kerr Environmental Research Laboratory. Ada, Oklahoma. 31 pp.

Pinder, G. F., and H. H. Cooper. 1970. A numerical technique for calculating the transient position of the saltwater front. Water Resour. Res. v. 6, no. 3, pp. 875-882.

Pinder, G. F., and W. G. Gray. 1977. Finite Elements in Surface and Subsurface Flow. Academic Press, New York. 295 pp.

Pinder, G. F., and R. H. Page. 1977. Finite element simulation of salt water intrusion on the South Fork of Long Island. Gray, W. G., G. F. Pinder, and C. A. Brebbia, eds. Finite Elements in Water Resources, Pentech Press, London. pp. 2.51-2.69.

Sa da Costa, A.A.G., and J. L. Wilson. 1979. A numerical model of sea water intrusion in aquifers. R. M. Parsons Lab. Rept. No. 247. MIT, Cambridge, Mass. 245 pp.

Segol, G., and G. F. Pinder. 1976. Transient simulation of saltwater intrusion in southeastern Florida. Water Resour. Res. v. 12, no. 1, pp. 65-70.

Segol, G., G. F. Pinder, and W. G. Gray. 1975. Numerical simulation of saltwater intrusion in coastal aquifers. Water Resources Program, Princeton Univ., Princeton, New Jersey.

Spalding, D. B. 1972. A novel finite difference formulation for differential expressions involving both first and second derivatives. Int. J. Numer. Methods Eng. v. 4, pp. 551-559.

VandenBerg, A. 1974. A digital simulation of horizontal salt-water encroachment induced by fresh water pumping. Environmental Canada Scientific Series No. 41, 27 pp.

Yeh, G. T., and D. S. Ward. 1981. FEMWASTE: A finite-element model of waste transport through porous saturated-unsaturated media. ORNL-5601. Oak Ridge National Laboratory, Oak Ridge, Tennessee. 137 pp.

• • • •

Robert W. Andrews holds his A.B. degree from Earlham College, Indiana, and the Ph.D. from the University of Illinois at Urbana. He is presently an Assistant Professor in the Geology and Geophysics Department at the University of Connecticut. Dr. Andrews' current research interests include the numerical modeling of flow and transport phenomena and the assessment of organic contaminant transport in porous media.

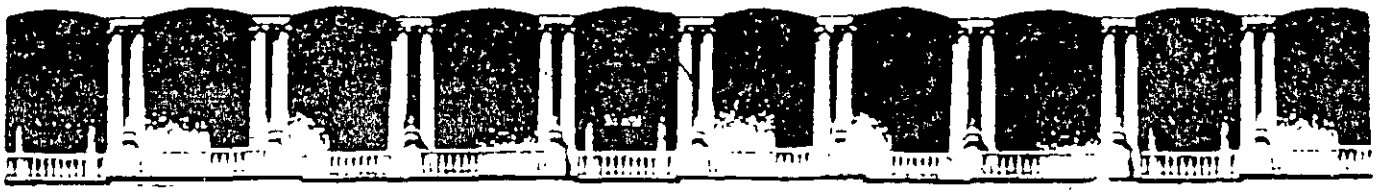

FACULTAD DE INGENIERIA U.N.A.M.
DIVISION DE EDUCACION CONTINUA

CURSOS ABIERTOS

XII CURSO INTERNACIONAL DE CONTAMINACIÓN DE ACUÍFEROS

MODULO III: MODELOS MATEMÁTICOS EN GEOHIDROLOGIA Y CONTAMINACIÓN DE ACUIFEROS

TEMA

ESTIMATION OF MOUNTAIN FRONT RECHARGE TO REGIONAL AQUIFERS

(II)

EXPOSITOR: DR ADOLFO CHAVEZ RODRIGUEZ

PALACIO DE MINERIA
OCTUBRE DEL 2000

WATER RESOURCES RESEARCH, VOL. 30, NO. 7, PAGES 2169–2181, JULY 1994

Estimation of mountain front recharge to regional aquifers 2. A maximum likelihood approach incorporating prior information

Adolfo Chavez

Facultad de Ingenieria, Universidad Autonoma de Chihuahua, Chihuahua, Mexico

Soroosh Sorooshian and Stanley N. Davis

Department of Hydrology and Water Resources, University of Arizona, Tucson

Abstract. In this two-part series a stochastic estimation procedure applicable to the analytic streamflow model derived in the companion is introduced. The parameter estimation problem is posed in the framework of maximum likelihood theory, where prior information about the model parameters and a suitable weighting scheme for the error terms in the estimation criterion are included. Various optimization methods are combined for parameter estimation. The issues of model and parameter identifiability, uniqueness, and stability are addressed, and strategies to mitigate identifiability problems in our modeling are discussed. The seasonal streamflow model is applied to a mountainous watershed in southern Arizona, and maximum likelihood estimates of mountain front recharge and other model and statistical parameters are obtained. The analysis of estimation errors is performed in both the eigenspace and the original space of the parameters.

Introduction

The analytical model of the seasonal streamflow developed in paper 1 [*Chavez et al.*, this issue] is conceptual and contains unknown parameters that need to be identified for a particular watershed. A parameter identification process (model calibration) is required to adjust the model parameters to satisfy some criterion (criteria) of minimization of the output errors. In general, some parameters may be directly identifiable from field measurements (e.g., watershed area), whereas others are estimated according to criteria of goodness of fit (e.g., effective initial abstraction).

In this paper we pose the parameter estimation problem in the framework of maximum likelihood theory as presented by *Sorooshian and Dracup* [1980]. We extend Sorooshian and Dracup's formulation by including prior information about the model parameters following the approach adopted by *Carrera and Neuman* [1986] in connection with the groundwater hydrology inverse problem. An "automatic" parameter estimation procedure is then employed to obtain the optimal parameter estimates of our seasonal streamflow model, in particular, long-term effective subsurface outflow from the watershed.

Maximum Likelihood Framework

Consider a sequence of n years where seasonal streamflow at the watershed outlet in year k is modeled by (25) in paper 1 [*Chavez et al.*, this issue] if applied in an entirely lumped manner or by a particular combination of equations of this form if the watershed were divided into m subareas. Incorporating the effect of errors, the seasonal streamflow is expressed as

$$Q_k^* = f(\mathbf{P}_k, \nu_k; \Theta) + \varepsilon_k, \qquad k = 1, \cdots, n \tag{1}$$

where $f(\ )$ represents the deterministic relationship between the input given by $\mathbf{P}_k$ and ν_k, which are the m-dimensional vectors of seasonal rainfall and number of rainstorms in the season, respectively, and the seasonal streamflow response, which is measured by Q_k^*. The stochastic error term ε_k is composed by the additive effect of streamflow measurement errors and errors resulting from imperfections associated with the model equation, as well as uncertainties in the measured inputs and the physical parameters Θ.

Assuming that the joint probability distribution of the errors is normal with zero mean and covariance matrix Ω_Q, the log likelihood function takes the form

$$S = S(\Theta, \Omega_Q) = -\tfrac{1}{2} n \ln (2\pi) - \tfrac{1}{2} \ln |\Omega_Q| - \tfrac{1}{2} [(\mathbf{Q} - \mathbf{Q}^*)^T \Omega_Q^{-1} (\mathbf{Q} - \mathbf{Q}^*)] \tag{2}$$

where $|\Omega_Q|$ and Ω_Q^{-1} are the determinant and the inverse of the covariance matrix Ω_Q, respectively; and $\mathbf{Q}^*$ and $\mathbf{Q}$ are the measured and the "true" streamflow values for a given parameter vector Θ, respectively. Minimization of the above log likelihood function with respect to the unknown parameters provides the model parameter values that maximize the probability of observing $\mathbf{Q}^*$.

If the errors are assumed to be heteroscedastic and uncorrelated, the maximum likelihood function (2) reduces to the following weighted least squares criterion:

$$\min_{(\Theta)} \mathrm{OF} = \sum_{k=1}^{n} w_k (Q_k - Q_k^*)^2 \tag{3}$$

Paper number 93WR03370.
0043-1397/94/93WR-03370$05.00

where $w_k = \sigma_k^{-2}$ are the weights equal to the inverse values of the variances of the error. This assumption is reasonable, due to the large time interval between measurement values and due to the typical high variability in annual runoff (especially characteristic of arid and semiarid regions).

The computation of the proper values of the weights has been a major problem in the calibration of rainfall-runoff models. The computation of the variance of the error from data is rarely possible, because no repeat of measurements is usually available at each level k. *Sorooshian and Dracup* [1980] proposed an alternative method based on stabilization of the variance through the use of the Box-Cox [*Box and Cox*, 1964] power transformation which relates the variance of each error to its associated output value. This leads to the following expression for the log likelihood objective function, which is optimized with respect to Θ, λ, and σ_Q^2:

$$S = n \ln (2\pi\sigma_Q^2) - \sum_{k=1}^{n} \ln w_k + \sigma_Q^{-2} \sum_{k=1}^{n} w_k (Q_k - Q_k^*)^2 \tag{4}$$

where w_k is the weight at year k that is computed by

$$w_k = f_k^{2(\lambda - 1)} \tag{5}$$

in which f_k is the expectation of Q_k, and λ is the unknown transformation parameter which stabilizes the variance to σ_Q^2. The value of λ is sought directly through satisfying the necessary condition for optimality when Θ is assumed known. That is,

$$\frac{\partial S}{\partial \lambda} = 0$$

yielding

$$\sum_{k=1}^{n} \ln Q_k^* - \sigma_Q^{-2} \sum_{k=1}^{n} w_k \ln Q_k^* (Q_k - Q_k^*)^2 = 0 \tag{6}$$

In this work, $f_k = Q_k^*$ was used in the computation of the weights (in the original work the authors used the computed flows). *Fulton* [1982] showed that this results in a more stable estimation scheme. Furthermore, this form leads to more tractable expressions for the first and second derivatives of the objective function with respect to the model parameters.

For the case of homoscedastic errors (independent of time and magnitude of the associated flows), the optimization procedure will automatically select the value of $\lambda \approx 1.0$. This results in $w_k = 1$ for all k, and the objective function is equivalent to the simple least squares criterion. If, however, the variance of the error is proportional to a power function of the magnitude of the flows, then the procedure will select a value of $\lambda \neq 1.0$. For the case where larger flows are associated with larger variances of the error, as illustrated by *Sorooshian and Dracup* [1980], the maximum likelihood (ML) estimate of λ will be less than unity, indicating that lower flows (which have smaller error variances) are weighted more heavily in the objective function.

Incorporation of Prior Information About the Parameters

In our parameter identification problem, improved estimates $\hat{\Theta}$ of the model parameters Θ are sought by relying on streamflow measurements Q^* at the watershed outlet. In theory, a parameter estimation problem is well posed if a unique and stable solution exists. In this work, however, we also strive for conceptually realistic parameter estimates.

Let us designate the "true" values of the model parameters by Θ and their prior estimates (or "measured" values) by Θ^*. Discrepancies between measured and true quantities, $Q^* - Q$ and $\Theta^* - \Theta$, will be referred to as "measurement errors." On the other hand, discrepancies between measured and computed quantities, $Q^* - \hat{Q}$ and $\Theta^* - \hat{\Theta}$, are called "residuals." Although, in theory, ML estimation is posed in terms of "prior errors" which are usually taken to be the measurement errors, in practice, estimation is performed by optimizing an objective function in terms of the residuals. The latter are a combination of measurement errors and errors arising from an inexact model structure. Consequently, the prior statistics entering into the objective function or estimation criterion should reflect both types of errors.

Discrepancies between measured and computed streamflow values are due to many factors, which include instrumental, methodological, personal, computational, and sampling [*Boyer*, 1964], not to mention imperfect model structure. Thus on the basis of the central limit theorem the combined error of these contributing factors may be assumed normally distributed with zero mean. Inasmuch as not all of these factors can be quantified statistically at the outset, we write, in the manner of *Neuman and Yakowitz* [1979], the covariance matrix of the prior streamflow errors as

$$\Omega_Q = \sigma_Q^2 \Lambda_Q \tag{7}$$

where σ_Q^2 is the stabilized variance and Λ_Q is a symmetric positive definite matrix, diagonal in our case, of which the diagonal elements are $(Q_k^*)^{2(1-\lambda)}$. The statistical parameters σ_Q^2 and λ may be estimated jointly with the model parameters Θ through the stagewise optimization procedure outlined in the next section.

Prior errors in the model parameters are also due to many factors. Thus in the spirit of *Carrera and Neuman* [1986] we hypothesize that if these parameters undergo suitable transformations (for example, a logarithmic transformation), their prior errors can be considered normally distributed with zero mean. However, because some of the factors contributing to those errors cannot be quantified statistically, we write the covariance matrix Ω_p of the prior errors associated with parameter type Θ_p (p is initial abstraction, recharge), or its transform, as

$$\Omega_p = \sigma_p^2 \Lambda_p \tag{8}$$

where σ_p^2 is either a known or an unknown positive scalar and Λ_p is a known symmetric positive definite matrix.

For the initial abstractions, (8) is rewritten as

$$\Omega_h = \sigma_h^2 \Lambda_h \tag{9}$$

and for recharge, (8) reduces to

$$\Omega_\gamma = \sigma_\gamma^2 \tag{10}$$

In this work the prior estimation variance of the long-term effective seasonal subsurface outflow, or mountain front recharge, σ_γ^2 is assumed to be completely known.

It depends on the method employed to obtain that prior estimate and on the specific hydrogeologic conditions. A value for it can be provided if the accuracy of the method under given conditions is known. Otherwise, that variance can be obtained from the range of variation of the parameter, its lower limit being zero and letting its upper limit be assumed. In this regard, we find it convenient to enable the modeler to enrich the calibration process with qualitative information derived from experience.

Following *Carrera and Neuman*'s [1986] approach, we assume, for operational reasons and without loss of generality, that the prior estimates of the different parameter types are mutually uncorrelated. The global covariance matrix of the model parameters, Ω_Θ, is thus block diagonal, its diagonal components being Ω_p. We also assume that prior streamflow errors and prior parameter estimation errors lack cross correlation, and therefore streamflow values used for parameter estimation must not be used to derive prior parameter estimates.

With regard to obtaining prior information about the model parameters, in paper 1 we introduced a procedure to estimate initial abstraction without relying on streamflow data, whereas later in this paper we will mention methods to provide a prior estimate of long-term effective subsurface outflow, which are independent of streamflow measurements as well.

Now, let $z^* = (Q^*, \Theta^*)^T$ be a vector incorporating the available streamflow and model parameter data, and let $\pi = (\sigma_Q^2, \sigma_h^2, \lambda, \cdots)$ be a vector of all the unknown statistical parameters characterizing the prior errors. If $\beta = (\Theta, \pi)^T$ is the vector of all the unknown parameters, then the likelihood $L(\beta|z^*)$ of a hypothesis regarding the value of β given z^* and a specific model structure (mathematical model, parameterization, error structure, etc.) is proportional to $f(z^*|\beta)$, the probability density of observing z^* if β was true. Inasmuch as $L(\beta|z^*)$ is a function of the parameters, it is called the likelihood function.

Once the data have been properly transformed to yield normal distributions of the prior errors, and in view of our assumptions concerning the lack of correlation between prior estimates of different parameter types and the lack of cross correlation between prior streamflow errors and prior parameter estimation errors, the likelihood function takes the form

$$L(\beta|z^*) = f(z^*|\beta) = (2\pi)^{-N/2}|\Omega_z|^{-1/2} \cdot \exp\left[-\tfrac{1}{2}(z^* - z)^T\Omega_z^{-1}(z^* - z)\right] \quad (11)$$

Here N is the total number of prior data, and Ω_z is the covariance matrix of the prior errors:

$$\Omega_z = \begin{vmatrix} \Omega_Q & 0 \\ 0 & \Omega_\Theta \end{vmatrix} \quad (12)$$

where Ω_Q and Ω_Θ are the covariance matrices of the prior streamflow errors and model parameters errors given by (7) and (8), respectively. Recall that Ω_Θ is block diagonal, with diagonal components Ω_p.

In practice, ML estimates are generally obtained by minimizing the log likelihood function:

$$S = -2 \ln [L(\beta|z^*)] \quad (13)$$

As pointed out by *Carrera and Neuman* [1986], this criterion makes it relatively easy to introduce prior information about the parameters into the estimation scheme. This is because of the property that the log likelihood of a hypothesis, given all the data, is the sum of the log likelihoods of the same hypothesis, given each separate set of data.

Including prior information about the model parameters in criterion (4) according to (11) yields

$$S_1 = n \ln (2\pi\sigma_Q^2) - \sum_{k=1}^{n} \ln w_k + \frac{1}{\sigma_Q^2}\sum_{k=1}^{n} w_k(Q_k - Q_k^*)^2 + \frac{1}{\sigma_h^2}\sum_{l=1}^{n_h}\frac{(h_l - h_l^*)^2}{\sigma_{h_l}^2} + n_h \ln \sigma_h^2 + \frac{1}{\sigma_\gamma^2}(\gamma - \gamma^*)^2 \quad (14)$$

where n is the number of streamflow data, n_h is the number of initial abstractions (subareas) with prior information, $\sigma_{h_l}^2$ is the "relative" variance of the prior estimation of initial abstraction h_l, where l is the subarea index, and γ and γ^* are long-term effective subsurface outflow from the entire watershed (or a transformation of it) and its prior estimate, respectively. The variance of the prior estimation of γ, σ_γ^2, is assumed to be known.

In the special case when the statistical parameters (σ_Q^2, σ_h^2, and λ) are fixed, the first, second, and fifth terms of (14) are known, and the minimization of S_1 is then equivalent to the minimization of

$$S_2 = \sum_{k=1}^{n} w_k(Q_k - Q_k^*)^2 + \varphi_h \sum_{l=1}^{n_h}\frac{(h_l - h_l^*)^2}{\sigma_{h_l}^2} + \frac{\sigma_Q^2}{\sigma_\gamma^2}(\gamma - \gamma^*)^2 \quad (15)$$

where

$$\varphi_h = \frac{\sigma_Q^2}{\sigma_h^2} \quad (16)$$

The first and second derivatives of S_2 with respect to the model parameters can be expressed in closed form, thus suggesting the use of the Newton method, or a modification of it, for the minimization of S_2. We achieved fairly fast convergence rates by combining Newton's method with Armijo's rule, while setting the prior estimates as initial parameter values.

In turn, the ML estimation of λ can be sought from (6). Inasmuch as λ cannot be expressed explicitly in terms of the remaining terms, it has to be estimated iteratively. As recommended by *Sorooshian and Dracup* [1980], the method of false position is used to accomplish this estimation.

The ML estimation of σ_Q^2 and σ_h^2 when φ_h is given can be obtained by applying the method of Lagrange multipliers in a derivation similar to that presented by *Carrera and Neuman* [1986] to yield

$$\sigma_Q^2 = \frac{1}{n + n_h}(S_Q + \varphi_h S_h) \quad (17)$$

where

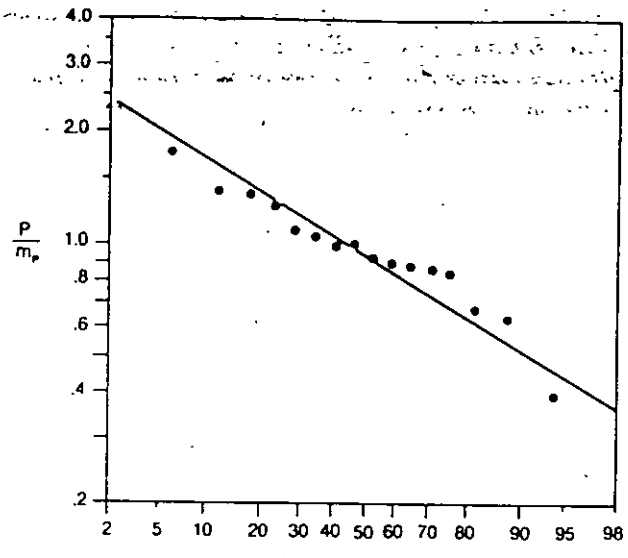

Figure 1. Frequency of summer precipitation at Sabino Canyon station.

$$S_Q = \sum_{k=1}^{n} w_k (Q_k - Q_k^*)^2 \tag{18}$$

$$S_h = \sum_{l=1}^{n_h} \frac{(h_l - h_l^*)^2}{\sigma_{h_l}^2} \tag{19}$$

$$\sigma_h^2 = \frac{\sigma_Q^2}{\varphi_h} \tag{20}$$

Finally, convergence to the optimum φ_h can be achieved by a golden section search.

ESTIMA Procedure

A stagewise optimization procedure (entitled ESTIMA) for the joint estimation of model and statistical parameters is outlined as follows:

1. Set $\sigma_Q^2 = 1.0$ and $\lambda = 1.0$ as initial estimates of the variance of the transformed streamflows and the transformation parameter. Use the golden section method to minimize S_1, equation (14), with respect to the weighting parameter φ_h.
2. For the first iteration, select a reasonable set of values for the model parameters Θ, and in subsequent iterations, use the previously converged Θ values. Use the Newton method, or a modification of it, to minimize S_2, equation (15), with respect to Θ.
3. Compute the streamflow values for the converged Θ vector of step 2. Then, using the false position method, compute the optimal value of λ from (6).
4. Return to step 2 and repeat the optimization process. The new weights w_k are computed using the optimal value of λ from step 3. Repeat steps 2 and 3 until the absolute difference between consecutive evaluations of S_1 is within a prespecified tolerance.
5. Use the converged values of Θ and λ to compute σ_Q^2 from (17). Repeat steps 2–5 until the absolute difference in consecutive values of σ_Q^2 is within a prespecified tolerance.
6. Let the golden section search for optimum φ_h continue, returning to step 2 after each iteration. The search should continue until convergence is obtained within a prespecified tolerance.

Application to Sabino Creek Watershed in Southern Arizona

The ESTIMA procedure was applied to estimate mountain front recharge jointly with other model and statistical parameters from Sabino Creek watershed in southern Arizona. This estimation was done for the summer rainy season only. This is because snowfall is significant at the higher elevations of the mountains during the winter period, and our analytical modeling of the seasonal streamflow does not consider the contribution from snowmelt to surface runoff.

Hydrogeology of the Mountain Front

The Basin and Range Province of southern Arizona is characterized by north-northwest trending mountain ranges isolated by alluvial basins. The Sabino Canyon watershed drains a portion of the Santa Catalina Mountains, which are composed of layered gneiss that is folded in a complex of anticlines and synclines and contains water along fractures only [*Davidson*, 1973]. The location of the study area is shown in paper 1 [*Chavez et al.*, this issue, Figure 9). The Catalina fault separates the gneissic mountain mass from the alluvium of the Tucson Basin. The elevation of the mountains extends from about 3000 to 9000 ft (914 to 2743 m).

The average annual precipitation in the basin is 11 in (27.9 cm) and is about 30 in (76.2 cm) in the highest portions of the Santa Catalina Mountains. Precipitation is distributed almost equally between the summer and the winter. Most of the summer precipitation occurs during July through September and is mainly convective, while most of the winter precipitation occurs from December through March and is frontal in nature.

Mountain front recharge to the basin includes groundwater flow through fractures and underflow through the sedi-

Table 1. Summer Streamflow and Precipitation Data at the Sabino Watershed

		Subarea L		Subarea U	
Year	Q, cm	P_L, cm	$\bar{h}_L$, cm	P_U, cm	$\bar{h}_U$, cm
1950	1.47	18.49	0.69	27.69	0.97
1951	2.40	20.28	0.85	33.80	1.45
1952	0 90	20.04	0.67	32.27	0.93
1953	1.88	16.56	1.01	27.11	1.61
1954	6.28	35.33	1.03	52.28	1.49
1959	3.92	28.46	1.31	40.15	2.30
1960	0.20	9.91	0.75	10.63	1.10
1961	2.01	16.82	0.67	26.34	1.13
1965	0.34	13.63	0.61	19.92	0.84
1967	2.40	21.96	0.81	28.50	1.13
1968	1.28	13.70	0.58	18.35	0.83
1969	1.25	20.12	0.70	30.18	0.98
1971	3.98	31.93	1.03	38.95	1.26
1972	0.32	21.41	0.89	24.47	0.96
1973	1.22	16.72	0.73	25.40	1.19
1974	1.24	25.13	0.65	39.11	0.96

Summer refers to July, August, and September. Average storm depth is represented by $\bar{h}$.

Table 2. Prior Estimates for Sabino Watershed (Summer)

Combination	g	$h_{r,L}$, cm	$h_{r,U}$, cm	σ_g^2	$\sigma_{h_{r,L}}^2$*	$\sigma_{h_{r,U}}^2$*
1	−1.1	1.70	2.78	0.20	1.00	1.00
2	−1.1	1.70	3.14	0.20	1.00	1.00
3	−1.1	1.70	3.67	0.20	1.00	1.00
4	−1.1	1.95	2.78	0.20	1.00	1.00
5	−1.1	1.95	3.14	0.20	1.00	1.00
6	−1.1	1.95	3.67	0.20	1.00	1.00
7	−1.1	2.29	2.78	0.20	1.00	1.00
8	−1.1	2.29	3.14	0.20	1.00	1.00
9	−1.1	2.29	3.67	0.20	1.00	1.00

*Relative variances.

ments of the drainage channels. Stable isotope studies [*Simpson et al.*, 1970; *Gallaher*, 1979] provided evidence that recharge along the mountain front is higher during the winter than during the summer.

Mifflin [1968] suggested that topography may affect recharge. Deep canyons tend to develop along zones of greater structural weakness associated with fracture zones. The discharge of groundwater in the mountain fracture system to the streams in the canyons favors mountain front recharge to occur as underflow through the sediments of the drainage channels rather than as deep circulation through fractures.

Summer Streamflow Model

Like in many other mountainous watersheds in arid and semiarid regions, the lower slopes of the Sabino Creek watershed are characterized by xerophytic vegetation, whereas the tops of the mountains are characterized by evergreen woodlands and coniferous forests. In addition, differences in relief exist between the lower slopes and the more inclined tops of the mountains. These differences in vegetation type and slope should determine a difference in initial abstraction between both mountainous subareas; hence a modeling strategy of dividing the watershed into those two subareas should help mitigate the identifiability problems arising from the application of the model in an entirely lumped manner. Consequently, for the modeling of summer streamflow from the Sabino Canyon watershed, we proceed as follows:

First, *Chavez et al.* [this issue] developed an analytical model of seasonal streamflow. This model is written here as

$$Q_k = R_k - G \tag{21}$$

where Q_k and R_k are the seasonal streamflow and surface runoff in year k, respectively, and G is the long-term effective groundwater runoff or mountain front recharge.

Then, the watershed was divided into the two major subareas, namely, the lower slopes (L) and the tops of the mountains (U), of which the extension is shown in Figure 10 in paper 1. By assuming that surface runoff from subarea U to subarea L occurs exclusively as channel flow and by neglecting evaporation losses along the streams, we express surface runoff from the entire watershed as

$$R_k = R_{L,k} + R_{U,k} \tag{22}$$

Here $R_{L,k}$ is surface runoff from subarea L, which by (23) in paper 1 is

$$R_{L,k} = 2(h_{r,L}/\bar{h}_{L,k})^{1/2} K_1[2(h_{r,L}/\bar{h}_{L,k})^{1/2}] P_{L,k} \tag{23}$$

and $R_{U,k}$ is surface runoff from subarea U, given by

$$R_{U,k} = 2(h_{r,U}/\bar{h}_{U,k})^{1/2} K_1[2(h_{r,U}/\bar{h}_{U,k})^{1/2}] P_{U,k} \tag{24}$$

where $h_{r,L}$ and $h_{r,U}$ are the initial abstractions in subareas L and U, respectively, $P_{L,k}$ and $P_{U,k}$ are total precipitation, and $\bar{h}_{L,k}$ and $\bar{h}_{U,k}$ are the average storm depths in the same subareas.

Thus the summer streamflow is modeled by (21), where the surface runoff is given by (22), (23), and (24). The model parameters to be estimated are the initial abstractions of rainfall at subarea L and subarea U, $h_{r,L}$, and $h_{r,U}$, respectively, and the long-term effective subsurface outflow from the entire watershed, G.

Prior Information About Mountain Front Recharge

Total summer precipitation in the Tucson Basin can be approximately fitted by a lognormal distribution (Figure 1), and we will assume here that the seasonal mountain front recharge is to be lognormally distributed as well.

Mountain front recharge is usually estimated for a particular year. For the Tucson area, *Belan* [1972] and *Olson* [1982] evaluated recharge from the Santa Catalina and the Tanque Verde mountains, respectively, through a flow net analysis where the water table map was based on data from one water year only. In turn, *Merz* [1985] evaluated recharge from the Santa Rita Mountains through a water balance analysis based on data from a single water year.

Note that, under the ML criterion, model parameters are viewed as fixed but uncertain quantities and, consequently, the discrepancy between the seasonal recharge in a particular year and its long-term effective value is regarded as a prior estimation error. In the ML estimation criterion (11), prior estimation errors were assumed to be jointly normally distributed. Consequently, if one of the above estimates of mountain front recharge, proportioned for the season of interest according to some selected criterion, is to be taken as a prior estimate of the long-term effective mountain front recharge G and because of the assumption that seasonal recharge is lognormally distributed, we must work with the parameter $g = \log G$, for which the prior estimation error is normally distributed. (Note that besides the natural variation

Table 3. ML Estimates of Model and Statistical Parameters for Sabino Watershed (Summer)

	Model Parameters			Statistical Parameters				Prior Estimation Variance		
Combination	g	$h_{r,L}$, cm	$h_{r,U}$, cm	σ_Q^2	λ	φ_h	σ_h^2	σ_g^2	$\sigma_{h_{r,L}}^2$	$\sigma_{h_{r,U}}^2$
1	−0.780	3.05	3.80	0.359	0.580	0.253	1.419	0.20	1.419	1.419
2	−0.751	2.68	3.88	0.383	0.628	0 507	0.755	0.20	0.755	0.755
4	−0.738	3.03	3.74	0.359	0.584	0.341	1.053	0.20	1.053	1.053
7	−0.586	3.02	3.59	0.350	0.573	0.589	0.594	0.20	0.594	0.594

Table 4. Covariance and Correlation Matrices of Estimation Errors for Sabino Watershed (Summer)

	Combination 2			Combination 7		
	g	$h_{r,L}$, cm	$h_{r,U}$, cm	g	$h_{r,L}$, cm	$h_{r,U}$, cm
g	0.1410	−0.2270	−0.3110	0.0974	−0.2070	−0.5210
$h_{r,L}$	−0.0604	0.5042	−0.6490	−0.0448	0.4819	−0.4790
$h_{r,U}$	−0.0632	−0.2493	0.2928	−0.0735	−0.1501	0.2041

Upper triangle is correlation matrix; lower triangle and main diagonal are covariance matrix.

of the seasonal recharge from year to year, there is an additional source of uncertainty due to estimation error. We will assume here that the combination of these two types of "errors" is lognormally distributed.) Expressed in terms of g, our seasonal streamflow model (equation (21)) becomes

$$Q_k = R_k - 10^g \tag{25}$$

Although this assumption introduces some extra nonlinearity into the model, the convergence properties of the optimization algorithm under this reparameterization were found to be much better, this is due to the scaling effect introduced by the logarithm, which reduces the condition number of the Hessian matrix of the estimation criterion.

Concerning the uncertainty in the prior estimation of recharge, *Belan and Matlock* [1973] assessed mountain front recharge along the eastern Santa Catalina Mountains by flow net analysis of the 1930 water level contour map and postulated that their estimation error may be as large as an order of magnitude. Other estimations or other approaches could be more accurate than Belan and Matlock's. However, when we add the estimation uncertainty to the natural year-to-year variation of the seasonal recharge, we postulate that 1 order of magnitude is a reasonable uncertainty for the prior estimation of the long-term effective mountain front recharge in a more general case, that is, an uncertainty of 1 in log recharge, provided that the estimation is based on data from one particular year or season.

Results and Discussion

The Sabino Creek gaging station is located near the base of the Santa Catalina Mountains, and streamflow data were obtained from U.S. Geological Survey summaries for the period 1951–1974. Precipitation data were obtained from climatological summaries of the National Weather Service at Sabino Canyon station (32°18', 110°49', 2640 ft (805 m)), located near the streamflow gaging station, for the period 1951–1974 and at the high-altitude stations of Mount Lemmon Inn (32°27', 110°45', 7780 ft (2371 m)), for the period 1951–1962, and Palisade Ranger (32°25', 110°43', 7945 ft (2422 m)), for the period 1965–1974. Discontinuities appear in the records, particularly at the high-altitude stations.

The lower slopes (subarea L) of the watershed extend over an area of 8600 acres (3480 ha), and the tops of the mountains (subarea U) occupy 13,160 acres (5326 ha). The increase with elevation of the expected amount of precipitation per season on the Santa Catalina Mountains is approximately linear [*Duckstein et al.*, 1973] Based on this fact, we divided the entire watershed into elevation zones and assigned a precipitation depth value to each of these zones by linear interpolation between the values at Sabino Creek and at the high-altitude stations. Total precipitation values for subareas L and U were obtained by multiplying the depths in each of the elevation zones by its respective area and by summing over the number of elevation zones in the subarea.

Data departing more than two standard deviations from the regression line between seasonal streamflow and precipitation in the entire watershed were regarded as outliers and were not included in the computations. Streamflow and precipitation data for Sabino watershed are listed in Table 1.

Using groundwater data and through a flow net analysis, *Mohrbacher* [1983] estimated mountain front recharge from Sabino watershed and adjacent areas to be about 50 ac ft yr^{-1} per mile of mountain front (mmf) (38,335 m^3 yr^{-1} per kilometer of mountain front). However, streamflow statistics [*Anderson and White*, 1979] show that the contribution of the summer flow to the total average annual flow at Sabino Creek gaging station is 27%. By assuming the same proportion for mountain front recharge, we come up with a value of 13.5 ac ft per mmf (10,350 m^3 yr^{-1} per kilometer of mountain front) for the summer period. Then, for the 6 mi (9.6 km) of mountain front along which Sabino watershed and adjacent

Table 5. Eigenvalues and Eigenvectors of Estimation Covariance Matrix for Sabino Watershed (Summer)

Component	Combination 2 Eigenvectors			Combination 7 Eigenvectors		
	Vector 1	Vector 2	Vector 3	Vector 1	Vector 2	Vector 3
g	0.6801	−0.7325	0.0300	0.7973	−0.5902	0.1262
$h_{r,L}$	0.4188	0.3545	−0.8360	0.3237	0.5948	0.7358
$h_{r,U}$	0.6018	0.5811	0 5479	0.5093	0.5458	−0 6653

The eigenvalues for combination 2 are 0.0479, 0.2204, and 0.6697 for vectors 1, 2, and 3, respectively. The eigenvalues for combination 7 are 0.0268, 0 1847, and 0.3070 for vectors 1, 2, and 3, respectively

Table 6. Prior and ML Estimates for Sabino Watershed (Summer) With $\sigma_g^2 = 0.20$

	Model Parameters			Statistical Parameters				Prior Estimation Variance		
	g	$h_{r,L}$, cm	$h_{r,U}$, cm	σ_Q^2	λ	φ_h	σ_h^2	σ_g^2	$\sigma_{h_{r,L}}^2$	$\sigma_{h_{r,U}}^2$
Prior	−1.100	2.29	2.78	...	...	...	...	(0.20)	0.50*	1.00*
ML	−0.534	2.71	3.63	0.366	0.601	0.675	0.542	...	0.271	0.542

Value in parentheses is assumed to be known.
*Relative variance.

areas are contributing [see *Chavez et al.*, this issue, Figure 10], 81 ac ft (99,992 m^3) are being recharged during the summer rainy season. Finally, by assuming a uniform contribution in recharge depth across Sabino watershed and adjacent areas, we divide 81 ac ft by 31,424 acres (12,717 ha) (total contributing area) to obtain 0.00258 ft or 0.079 cm of mountain front recharge during the summer period.

Prior information about the space and time long-term effective initial abstraction of rainfall in subwatershed L, $h_{r,L}$, and subwatershed U, $h_{r,U}$, was obtained through the application of the VEHBAL procedure [*Chavez et al.*, this issue]. Note that the VEHBAL procedure does not involve the use of observed streamflows and therefore the assumption of lack of cross correlation between prior parameter estimation errors and streamflow measurement errors is satisfied.

Surface runoff and hence h_r showed a rather high sensitivity to the plant coefficient k_v. Because this vegetation property cannot be determined with high accuracy, the nine combinations of the $h_{r,L}$ and $h_{r,U}$ values obtained through the VEHBAL procedure were introduced as prior information in the ESTIMA procedure. The next step involved the determination of the "best" combination (among the nine) in terms of their relative consistency with the rest of the prior data and using the analysis of the stochastic properties of the ML estimators.

Mohrbacher [1983] calculated mountain front recharge using groundwater data from 1970 to 1979, which partly overlaps the time period considered here. Proportioned for the summer season, his estimate is 0.079 cm, of which the logarithm is −1.10. However, in most of the cases, mountain front recharge is estimated with data from 1 water year only. Thus for a more general discussion we will regard Mohrbacher's estimate as representative of only 1 year and assign an uncertainty of about 1 order of magnitude to it ($\sigma_g^2 = 0.20$). Afterward, a final estimate of recharge will be produced by assigning a smaller (more reasonable for this case) variance to that prior estimation ($\sigma_g^2 = 0.10$).

The nine combinations of $h_{r,L}$ and $h_{r,U}$ taken as prior information about initial abstraction are listed in Table 2, and the results of the application of the ESTIMA procedure appear in Table 3. The procedure was unable to identify an optimum for combinations 3, 5, 6, 8, and 9. This is indicative of incompatibility among prior data. Combination 7 showed the smallest prior estimation variance of the initial abstractions, $\sigma_h^2 = 0.594$, and the smallest variance of the transformed flows, $\sigma_Q^2 = 0.350$. We conclude that combination 7 is the one most consistent with measured flows, being followed by combination 2.

Nonuniqueness in the solution was not an issue in any of the cases. Approximately the same parameter estimates were obtained starting from different sets of initial parameter values.

Covariance and correlation matrices of estimation for the model parameters are shown in Table 4 for combinations 2 and 7. Smaller diagonal terms in the estimation covariance matrix were obtained for combination 7, and parameter correlation is not high for any combination.

Eigenvalues and eigenvectors of the estimation covariance matrix are listed in Table 5. As expected, the smaller eigenvalues correspond to combination 7. We also notice from this table that, in both cases, the component of g in the eigenvector corresponding to the largest eigenvalue is small, indicating that the highest parameter interaction occurs between the initial abstractions. This result is expected because of the high correlation between seasonal precipitations in subareas L and U.

In the VEHBAL procedure it was assumed that the change in soil moisture storage between the beginning and the end of the summer rainy season is negligible. That assumption is more closely satisfied under the low precipitation–high potential evaporation conditions at subarea L than under the higher precipitation–lower potential evaporation conditions at subarea U. We will account for this fact by associating a smaller variance to the prior estimation of $h_{r,L}$ relative to the prior estimation of $h_{r,U}$.

The ESTIMA procedure is then applied to combination 7 using 0.50 and 1.00 as the relative values of the prior

Table 7. Covariance and Correlation Matrices of Estimation Errors for Sabino Watershed (Summer) at Parameter Vector (−0.534, 2.71, 3.63)

	g	$h_{r,L}$	$h_{r,U}$
g	0.0863	−0.2070	−0.5690
$h_{r,L}$	−0.0294	0.2344	−0.3990
$h_{r,U}$	−0.0744	−0.0859	0.1979

Upper triangle is correlation matrix; lower triangle and main diagonal are covariance matrix.

Table 8. Eigenvalues and Eigenvectors of Estimation Covariance Matrix for Sabino Watershed (Summer) at Parameter Vector (−0.534, 2.71, 3.63)

Components	Eigenvectors		
	Vector 1	Vector 2	Vector 3
g	0.7973	−0.5902	0.1262
$h_{r,L}$	0.3237	0.5948	0.7358
$h_{r,U}$	0.5093	0.5458	−0.6653

The eigenvalues are 0.0268, 0.1847, and 0.3070 for vectors 1, 2, and 3, respectively.

Table 9. Structural Identifiability Matrix and Sensitivity Ratios for Sabino Watershed (Summer) at Parameter Vector (−0.534, 2.71, 3.63)

	g	$h_{r,L}$	$h_{r,U}$
g	14.51	7.31	12.97
$h_{r,L}$	7.31	4.70	8.16
$h_{r,U}$	12.97	8.16	14.73

The sensitivity ratios are 2.20, 5.24, and 5.28 for g, $h_{r,L}$, and $h_{r,U}$, respectively.

estimation variances of $h_{r,L}$ and $h_{r,U}$, respectively. Results are listed in Tables 6, 7, and 8, where the estimation variance of all the model parameters is smaller than their prior estimation variance. In particular, for g and $h_{r,U}$, the estimation variance reduced by over a half. Notice also that the condition number CN, defined as the ratio of the largest to the smallest eigenvalue, is 11.5.

The stability of the solution can be assessed qualitatively in terms of convergence characteristics and the condition number of the estimation covariance matrix. Convergence was fast and smooth in all the cases tested and, as expected, the number of iterations was dependent on the initial parameter values. In turn, the condition number decreased from 18.2 to 11.5 by changing the relative variance of $h_{r,L}$ from 1.0 to 0.5, indicating that instability is reduced when prior $h_{r,L}$ is estimated with a higher precision than prior $h_{r,U}$. An explanation for this is to be sought in the smaller sensitivities of the computed flows to $h_{r,L}$ as compared to $h_{r,U}$.

The structural identifiability matrix (see the appendix) $\nabla^2_\Theta SI(\Theta)$, which is based purely on model properties and is independent of the stochastic nature of the output observation errors, is evaluated at (−.534, 2.71, 3.63), and the results are listed in Table 9. This matrix is positive definite; consequently, the model structure is locally identifiable. However, its condition number is fairly high (CN = 235), indicating that the model structure is poorly identifiable. The

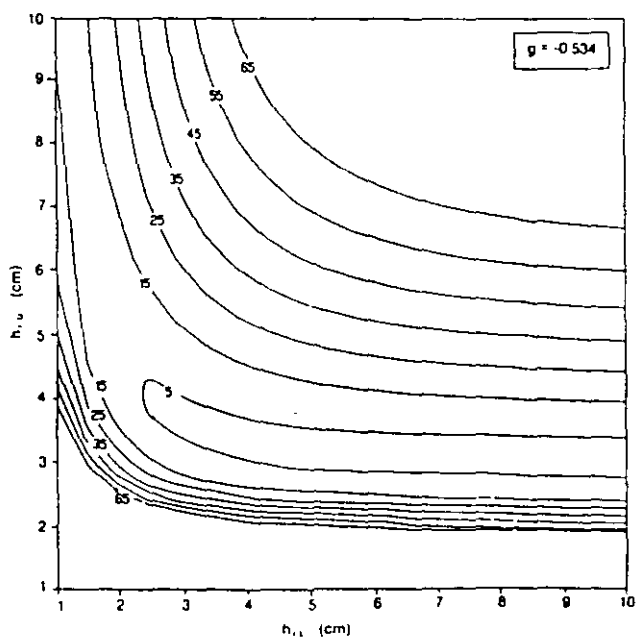

Figure 2. ML criterion contour map for $h_{r,U}$ versus $h_{r,L}$ with no prior information about the model parameters.

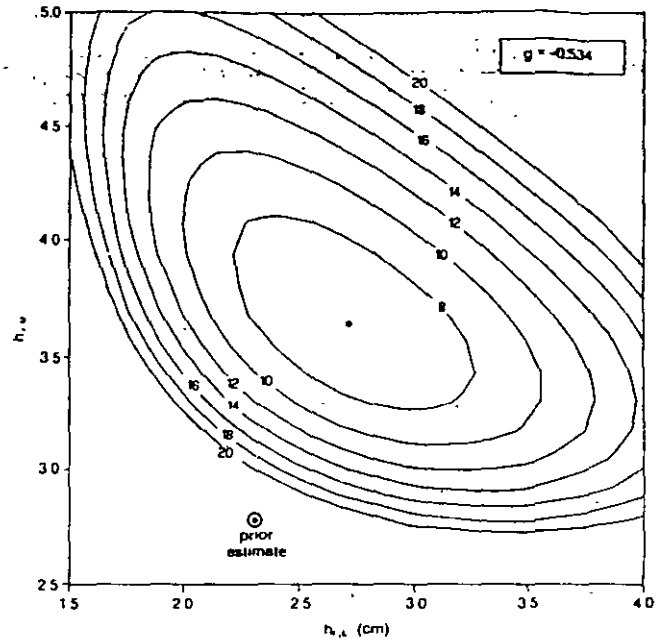

Figure 3. ML criterion contour map for $h_{r,U}$ versus $h_{r,L}$ with prior information about the model parameters.

smallest diagonal element is $\nabla^2 SI_{22}$, confirming the smaller structural sensitivity to parameter $h_{r,L}$ as compared to $h_{r,U}$. Parameter $h_{r,L}$ is less activated than $h_{r,U}$ because of the lower seasonal precipitation in subwatershed L. In turn, the sensitivity ratio (η) indicates that the main parameter interaction occurs between $h_{r,L}$ and $h_{r,U}$. This results from the

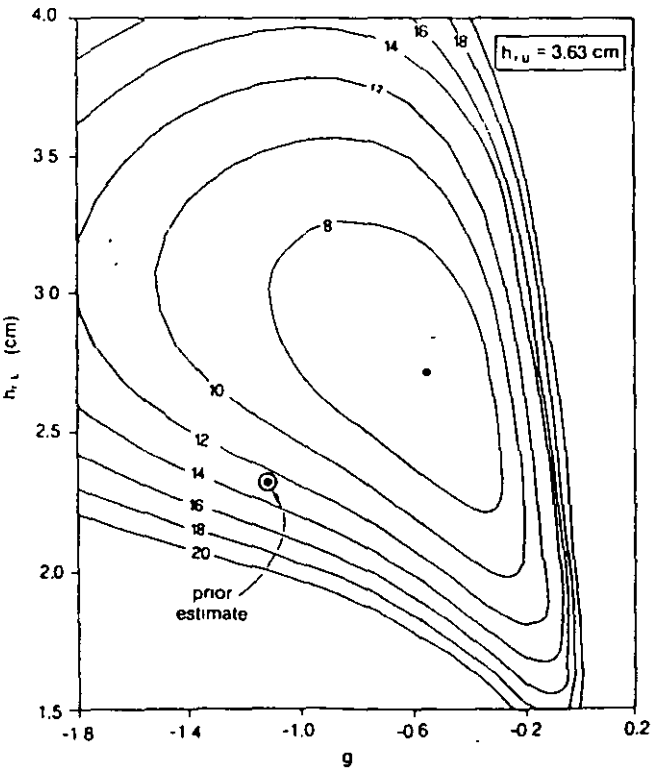

Figure 4. ML criterion contour map for $h_{r,L}$ versus g with prior information about the model parameters.

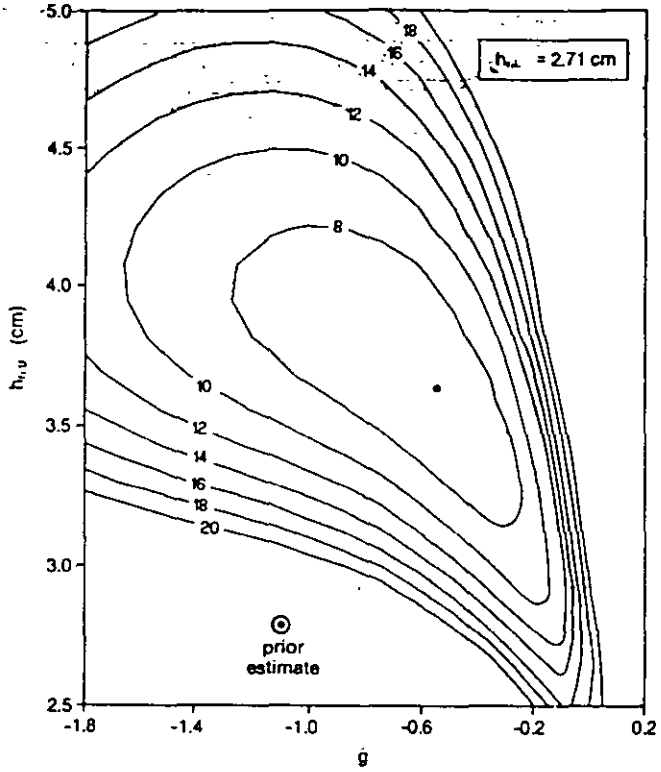

Figure 5. ML criterion contour map for $h_{r,U}$ versus g with prior information about the model parameters.

high correlation between seasonal precipitation at subarea L and subarea U.

Once the measurement noise is introduced, the situation worsens. Figure 2 shows the contours of the log likelihood criterion (equation (14)) when no prior information about the parameters is included. The optimum $h_{r,L}$ occurs at the unrealistic value of $+\infty$. In fact, no realistic solution to this problem can be obtained without including prior information about the parameters.

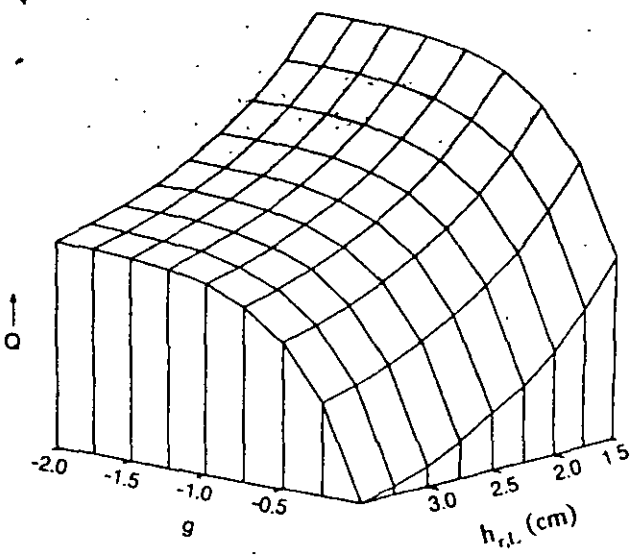

Figure 7. Sensitivity of computed streamflow to g and $h_{r,L}$.

Figures 3, 4, and 5 show the contours of the log likelihood criterion (equation (14)) when prior information about the parameters is included. A unique and realistic solution is now apparent.

The sensitivity of the computed flow to the model parameters is shown in Figures 6, 7, and 8. In Figure 6 we notice that the computed flow is more sensitive to $h_{r,U}$ than to $h_{r,L}$. The higher seasonal precipitation in subwatershed U determines that a larger runoff be generated when $h_{r,U}$ tends to zero than when $h_{r,L}$ does. The larger area of subwatershed U also contributes to this effect. Figures 7 and 8 show that the sensitivity of the computed flows to g increases as this parameter does. On the other hand, the scattergram of computed and measured streamflows is shown in Figure 9.

As Mohrbacher's recharge estimation is based on groundwater data from 1970 to 1979, overlapping partly the time period considered here, his estimate may be considered

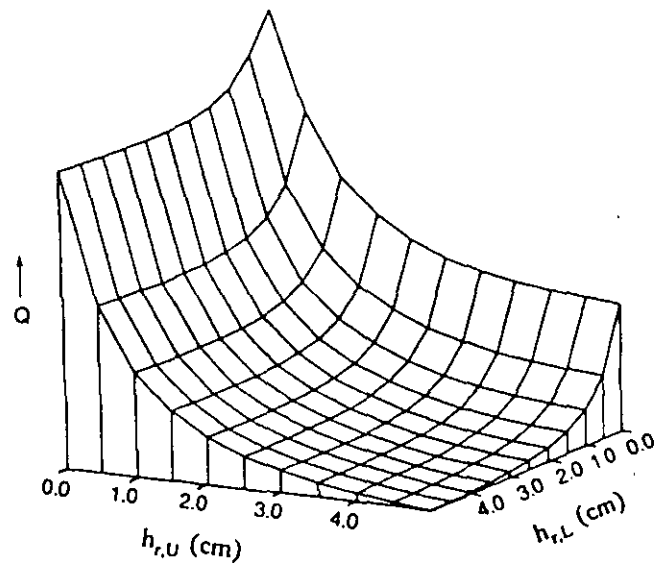

Figure 6. Sensitivity of computed streamflow to $h_{r,L}$ and $h_{r,U}$.

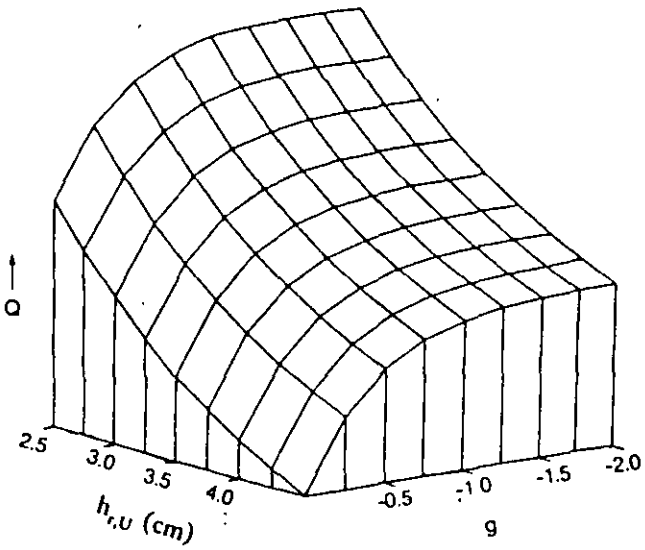

Figure 8. Sensitivity of computed streamflow to g and $h_{r,U}$.

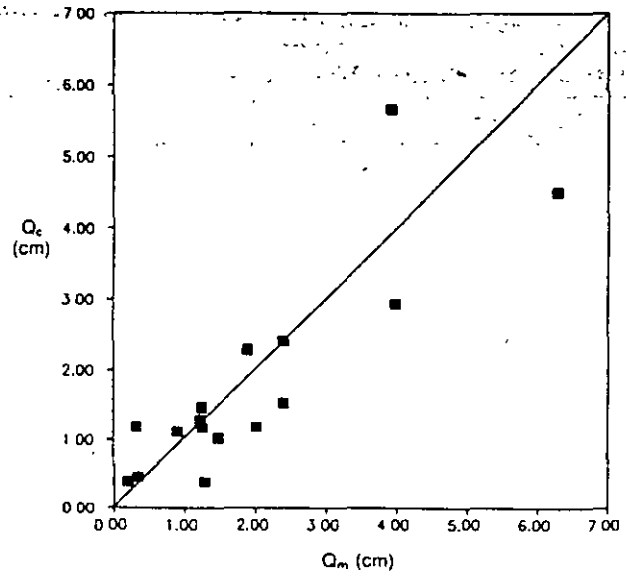

Figure 9. Scattergram of computed and measured summer streamflows at Sabino Creek gaging station.

more reliable than one representing a single year or season. Consequently, we will seek a final estimation of mountain front recharge for the summer period by reducing the prior estimation variance of log recharge from 0.20 to 0.10. Results are shown in Tables 10, 11, and 12. Our final estimate of log recharge is −.977, or 0.11 cm, or 18.8 ac ft yr^{-1} per mmf (14,414 m^3 yr^{-1} per kilometer of mountain front).

In those tables we particularly notice that the ML estimate of log recharge is now closer to its prior estimate and that its reduction in variance is marginal. A better prior estimation of the initial abstractions could contribute to further reduce the log recharge estimation variance. However, this and the previous results suggest that the improvement provided by our procedure is marginal when the prior estimates of log recharge are relatively reliable and that the procedure is particularly suitable to improve less reliable recharge estimates, that is, those whose uncertainty is about 1 order of magnitude or greater. Estimates with this uncertainty are common in practice.

On the other hand, we also notice from Table 2 that the condition number of the estimation covariance matrix has reduced to 8.3, illustrating the beneficial effect on stability of providing a more reliable prior estimate of log recharge.

Table 11. Covariance and Correlation Matrices of Estimation Errors for Sabino Watershed (Summer) at Parameter Vector (−0.977, 2.84, 3.86)

	g	$h_{r,L}$	$h_{r,U}$
g	0.0931	−0.0730	−0.2230
$h_{r,L}$	−0.0133	0.3620	−0.655
$h_{r,U}$	−0.0314	−0.1821	0.2133

Upper triangle is correlation matrix; lower triangle and main diagonal are covariance matrix.

Conclusions

The following conclusions can be drawn from paper 2 of this two-part series:

1. Our model of the seasonal streamflow fit the observations for the mountainous watershed of Sabino Canyon in the Tucson Basin reasonably well. However, in view of the nature of its derivation, this model is expected to underestimate large flows in many instances. The effect of this underestimation on the parameter estimates is minimized through the weighting scheme adopted. That is, errors associated with larger flows, which are less reliable, are less heavily weighted in the estimation criterion. A larger reduction in their weights is achieved by expressing the weighting factor in terms of the measured flows rather than in terms of the computed ones.

2. The weighting scheme adopted enabled the estimation of the most likely weights for the error terms in the estimation criterion. This scheme proved to be quite appropriate in our modeling because of the adequate response of the statistical parameters associated with it to account for the changing variance of the streamflow errors, which were qualitatively verified through the scattergram.

3. We have illustrated the beneficial effect of the inclusion of prior information about the model parameters in the estimation criterion. Prior information increases the chances for a unique, stable, and realistic solution to a parameter estimation problem. Improved estimates of the model parameters were achieved whenever the optimization procedure converged. Lack of convergence was attributed to incompatibility among prior data and model inadequacies.

4. No nonuniqueness problems were detected, and convergence to the optimum was fast and smooth whenever a solution existed. These convergence properties hold for the model reparameterized in terms of log recharge. Difficulties in convergence were encountered with the original model.

5. Instability in the solution, as qualitatively measured by the condition number of the estimation covariance matrix, was found to be small or moderate for the cases tested.

Table 10. Prior and ML Estimates for Sabino Watershed (Summer) With $\sigma_g^2 = 0.10$

	Model Parameters			Statistical Parameters				Prior Estimation Variance		
	g	$h_{r,L}$, cm	$h_{r,U}$, cm	σ_Q^2	λ	φ_h	σ_h^2	σ_g^2	$\sigma_{h_{r,L}}^2$	$\sigma_{h_{r,U}}^2$
Prior	−1.100	2.29	2.78	...	...	...	...	(0.10)	0.50*	1.00*
ML	−0.977	2.84	3.86	0.395	0.647	0.442	0.894	...	0.447	0.894

Value in parenthesis is assumed to be known.
*Relative variance.

Table 12. Eigenvalues and Eigenvectors of Estimation Covariance Matrix for Sabino Watershed (Summer) at Parameter Vector (−0.977, 2.84, 3.86)

Components	Eigenvectors		
	Vector 1	Vector 2	Vector 3
g	0.6962	−0.7177	−0.0166
$h_{r,L}$	0.3915	0.3990	−0.8292
$h_{r,U}$	0.6017	0.5707	0.5588

The eigenvalues are 0.0585, 0.1255, and 0.4845 for vectors 1, 2, and 3, respectively.

Log recharge should be the parameter less affected by instability in view of its minimal interaction with other parameters.

6. The measures of model structural and parameter identifiability adopted proved to be useful tools to ascertain the relative sensitivity of the streamflows to the model parameters and for isolating those parameters that are highly interacting and poorly identifiable.

7. The analysis of the estimation errors, performed in the original space of the parameters, showed no high correlations among the model parameters and a large reduction in the estimation variance of the parameters when the prior estimation error of recharge was assumed to be about 1 order of magnitude. Only a marginal improvement, however, was achieved when that prior estimate was considered to be more reliable. This suggests that our procedure is particularly useful when uncertainties of about 1 order of magnitude or larger are associated with the prior estimate of mountain front recharge. Uncertainties of this magnitude are common in practice.

8. The analysis performed in the eigenspace of the parameters showed that, in all the cases, the estimates of combinations of initial abstractions are much less reliable than combinations which include log recharge. Therefore we conclude that parameter estimation was successful, in general, and that our approach is particularly suitable for the estimation of mountain front recharge.

9. As our parameter estimation approach requires prior information about the long-term effective mountain front recharge on a seasonal basis and because the variance of that prior information must be provided, we encourage hydrologists involved in the assessment of mountain front recharge to look closely into the uncertain aspects of their estimations and to reckon, at least qualitatively, the reliability of their particular estimates under specific hydrogeologic conditions.

10. Likewise, we encourage hydrologists to look into the seasonal and year-to-year variations of that recharge whenever data are available, as well as to evaluate separately, whenever possible, the contributions from the two sources of lateral recharge, namely, the contribution originated in the mountain mass and the contribution originated along the stream channels between the base of the mountain and the regional aquifer boundary.

Appendix: Structural and Parameter Identifiability Measures

Sorooshian and Gupta [1985] developed a measure of structural identifiability in the region local to Θ in terms of what they called the "structural identifiability matrix" $\nabla^2_\Theta SI(\Theta)$. This matrix is written as

$$\nabla^2_\Theta SI(\Theta) = 2\nabla_\Theta Q(\Theta)^T \nabla_\Theta Q(\Theta) \tag{A1}$$

or equivalently

$$\nabla^2 SI_{ij} = 2\sum_{k=1}^{n}\left\{\frac{\partial Q_k(\Theta)}{\partial \Theta_i}\frac{\partial Q_k(\Theta)}{\partial \Theta_j}\right\} \tag{A2}$$

The structural identifiability matrix can be either positive definite or positive semidefinite. The diagonal elements of $\nabla^2_\Theta SI(\Theta)$ are all nonnegative. If the matrix is positive definite, then the model structure is locally identifiable.

A measure of parameter identifiability called the "sensitivity ratio" provides useful information about interactions among many parameters simultaneously in the multiparameter space. It is useful specifically for isolating those parameters that are highly compensating and poorly identifiable. The sensitivity ratio η_i of parameter Θ_i is defined as

$$\eta_i = \frac{\mathrm{PS}_i(\Theta)}{\mathrm{CPS}_i(\Theta)} = \left[\frac{s_{ii}}{s_{ii} - g_i^T G_i^{-1} g_i}\right]^{1/2} \tag{A3}$$

where $\mathrm{PS}_i(\Theta)$ is called "parameter sensitivity index," $\mathrm{CPS}_i(\Theta)$ is "conditional parameter sensitivity" (see Figure A1), G_i is the $(p-1)\times(p-1)$ submatrix of $\nabla^2_\Theta SI(\Theta)$ obtained by deleting the ith row and column, g_i is the $(p-1)\times 1$ vector equivalent to the ith column of $\nabla^2_\Theta SI(\Theta)$ with the ith element deleted, and s_{ij} is the ijth element of $\nabla^2_\Theta SI(\Theta)$.

When $\eta_i = 1$ there is no compensation for the effects of parameter Θ_i on the model output by the other parameters. As η_i gets larger, this indicates poorer and poorer identifiability of parameter Θ_i in relation to other parameters.

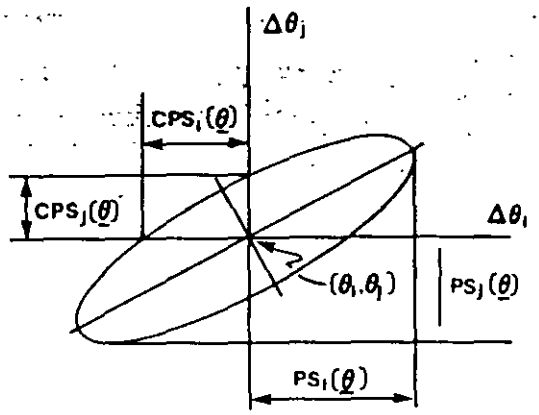

Figure A1. Two parameter examples of an indifference region.

Notation

CN condition number.
CPS conditional parameter sensitivity.
f_k expectation of Q_k.
$f(\ )$ response of the selected watershed model.
$f(\ ,\ ,\cdot)$ probability density function.
g decimal logarithm of G.

g_i ith column of $\nabla^2_{\theta} SI(\ )$ with ith element deleted.

G long-term effective seasonal mountain front recharge.

G_i submatrix of $\nabla^2_{\theta} SI(\ )$ deleting ith row and column.

h_l effective initial abstraction in subarea l.

h_l^* prior estimate of h_l.

h_r space and time effective initial abstraction.

$h_{r,L}$ effective initial abstraction in subarea L.

$h_{r,U}$ effective initial abstraction in subarea U.

$\bar{h}_{L,k}$ average storm depth in subarea L.

$\bar{h}_{U,k}$ average storm depth in subarea U.

k index for the year.

l index for subareas in a watershed.

ln ( ) natural logarithm of ( ).

log ( ) decimal logarithm of ( ).

$L(\ )$ likelihood function.

m number of subareas in a watershed.

ML maximum likelihood criterion.

n number of years of streamflow record.

n_h number of subareas with prior data about initial abstraction.

N total number of prior data.

OF objective function.

p index for parameter type.

$\mathbf{P}_k$ vector of m seasonal precipitation values.

$P_{L,k}$ seasonal precipitation in subarea L.

$P_{U,k}$ seasonal precipitation in subarea U.

PS parameter sensitivity index.

$\mathbf{Q}$ vector of n "true" seasonal streamflow values.

$\mathbf{Q}^*$ vector of n measured seasonal streamflows.

Q_k kth element of $\mathbf{Q}$.

Q_k^* kth element of $\mathbf{Q}^*$.

R_k seasonal surface runoff.

$R_{L,k}$ seasonal surface runoff from subarea L.

$R_{U,k}$ seasonal surface runoff from subarea U.

s_{ij} ijth element of $\nabla^2_{\theta} SI(\ )$.

S log likelihood function.

S_1 log likelihood function with prior data about model parameters.

S_2 equivalent form to S_1 obtained by fixing the statistical parameters.

S_Q weighted sum of squared seasonal streamflow errors.

S_h weighted sum of squared initial abstraction errors.

SLS simple least squares criterion.

T transpose.

w_k kth weight used in the objective function.

$\mathbf{z}$ vector of "true" streamflow and model parameter values.

$\mathbf{z}^*$ vector of available streamflow and model parameter data.

β vector of unknown model and statistical parameters.

γ long-term effective seasonal mountain front recharge (or a transformation of it).

γ^* prior estimate of γ.

ε_k stochastic error term.

η sensitivity ratio.

λ transformation parameter of flows.

Λ_p relative covariance matrix of prior errors of parameter type p.

Λ_h relative covariance matrix of prior initial abstraction errors.

Λ_Q relative covariance matrix of prior streamflow errors.

ν_k vector of m seasonal number-of-storm values.

π vector of unknown statistical parameters.

σ_g^2 prior estimation variance of log recharge.

σ_h^2 multiplicative factor for the relative covariance matrix of prior initial abstraction errors.

$\sigma_{h_l}^2$ relative variance of the prior error of h_l.

σ_p^2 multiplicative factor for the relative covariance matrix of prior errors associated with parameters type p.

σ_k^2 error variance of the kth streamflow.

σ_Q^2 stabilized variance of the transformed flows.

σ_γ^2 prior estimation variance of γ.

Θ vector of the "true" model parameters.

Θ^* vector of prior estimates of model parameters.

$\hat{\Theta}$ vector of maximum likelihood estimates of model parameters.

Θ_p vector of model parameters type p.

φ_h weighting parameter for the initial abstractions.

Ω_h covariance matrix of prior initial abstraction errors.

Ω_p covariance matrix of prior errors associated with model parameters type p.

Ω covariance matrix of prior streamflow errors.

Ω_z covariance matrix of prior errors associated with model and statistical parameters.

Ω_Θ global covariance matrix of prior errors of model parameters.

$\nabla^2_{\theta} SI(\ )$ structural identifiability matrix.

$K_1[\ ]$ Bessel function of order one.

Acknowledgments. The authors gratefully acknowledge the constructive comments and recommendations provided by Paul Hsieh of the U.S. Geological Survey, and Amado Guzman, Vijai Gupta, and Jene Michaud of the University of Arizona. Partial support was provided by the National Science Foundation under grants ECE-86105487 and BSC-8920851.

References

Anderson, T. W., and N. D. White, Statistical summaries of Arizona streamflow data, *U.S. Geol. Surv. Water Resour. Invest.*, 79-5, 1979.

Belan, R. A., Hydrogeology of a portion of the Santa Catalina Mountains, M.S. thesis, Dep. of Hydrol. and Water Resour., Univ. of Ariz., Tucson, 1972.

Belan, R. A., and W. G. Matlock, Groundwater recharge from a portion of the Santa Catalina Mountains, paper presented at Hydrology and Water Resources in Arizona and the Southwest, 1973 Meetings, Ariz. Sect., Am. Water Resour. Assoc. and Hydrol. Sect., Ariz.-Nev. Acad. of Sci., Tucson, Ariz., 1973.

Boyer, M. B., Streamflow measurement, in *Handbook of Applied Hydrology*, Sec. 15, edited by V. T. Chow, McGraw-Hill, New York, 1964.

Box, G. E. P., and O. R. Cox, The analysis of transformations, *J. R. Stat. Soc., Ser. B*, 26(2), 211–252, 1964.

Carrera, J., and S. P. Neuman, Estimation of aquifer parameters under transient and steady state conditions, 1, Maximum likelihood method incorporating prior information, *Water Resour. Res.*, 22(2), 199–210, 1986.

Chavez, A., S. N. Davis, and S. Sorooshian, Estimation of mountain front recharge to regional aquifers; 1, Development of an analytical hydroclimate model, *Water Resour. Res.*, this issue.

Davidson, E. S., Geohydrology and water resources of the Tucson Basin, Arizona, *U.S. Geol. Surv. Water Supply Pap., 1939-E*, 1973.

Duckstein, L., M. M. Fogel, and J. L. Thames, Elevation effects on rainfall: A stochastic model, *J. Hydrol., 18*, 21–35, 1973.

Fulton, J. L., Discussion, modification, and extension of some maximum likelihood techniques for model calibration with application to rainfall-runoff models, report, Syst. Eng. Dep., Case West. Reserve Univ., Cleveland, Ohio, Aug. 1982.

Gallaher, B. M., Recharge properties of the Tucson Basin aquifer as reflected by the distribution of a stable isotope, M.S. thesis, Dep. of Hydrol. and Water Resour., Univ. of Ariz., Tucson, 1979.

Merz, A., Mountain-front recharge from the Santa Rita Mountains to the Tucson Basin, M.S. thesis, Dep. of Hydrol. and Water Resour., Univ. of Ariz., Tucson, 1985.

Mifflin, M. D., Delineation of ground-water flow systems in Nevada, *Tech. Rep. Ser. H-W, Hydrol. Water Resour. Publ. 4*, Desert Res. Inst., Univ. of Nev., Reno, 1968.

Mohrbacher, C. J., Mountain-front recharge to the Tucson Basin from the Santa Catalina Mountains, Arizona, M.S. thesis, Dep. of Hydrol. and Water Resour., Univ. of Ariz., Tucson, 1983.

Neuman, S. P., and S. Yakowitz, A statistical approach to the inverse problem of aquifer hydrology, 1, Theory, *Water Resour. Res., 15*(4), 845–860, 1979.

Olson, M. C., Mountain-front recharge to the Tucson Basin from Tanque Verde Canyon, Arizona, M.S. thesis, Dep. of Hydrol. and Water Resour., Univ. of Ariz., Tucson, 1982.

Simpson, E. S., D. Thourud, and I. Friedman, Distinguishing seasonal recharge to groundwater by deuterium analysis in southern Arizona, paper presented at World Water Balance, Reading Symposium, Int. Assoc. of Sci. Hydrol., Reading, England, July 1970.

Sorooshian, S., and J. A. Dracup, Stochastic parameter estimation procedures for hydrologic rainfall-runoff models: Correlated and heteroscedastic error cases, *Water Resour. Res., 16*(2), 430–442, 1980.

Sorooshian, S., and V. K. Gupta, The analysis of structural identifiability: Theory and application to conceptual rainfall-runoff models, *Water Resour. Res., 21*(4), 487–495, 1985

A. Chavez, Facultad de Ingenieria, Universidad Autonoma de Chihuahua, Apartado Postal 1528-C, Chihuahua, Chih. 31160, Mexico

S. N. Davis and S. Sorooshian, Department of Hydrology and Water Resources, University of Arizona, Tucson, AZ 85721.

(Received August 19, 1993; revised November 18, 1993, accepted November 29, 1993.)

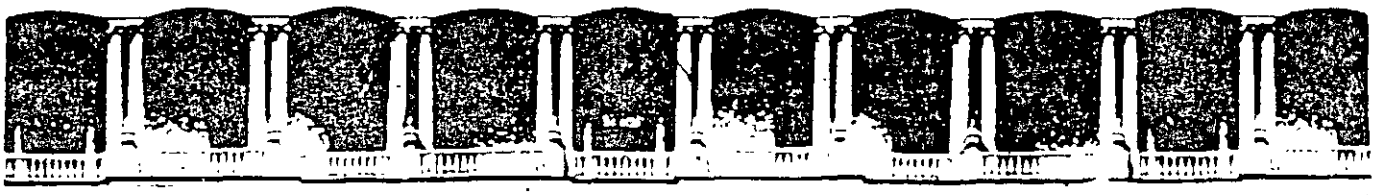

FACULTAD DE INGENIERIA U.N.A.M.
DIVISION DE EDUCACION CONTINUA

CURSOS ABIERTOS

XII CURSO INTERNACIONAL DE CONTAMINACIÓN DE ACUÍFEROS

MODULO III: MODELOS MATEMÁTICOS EN GEOHIDROLOGIA Y CONTAMINACIÓN DE ACUIFEROS

TEMA

OPTIMIZACION DEL BOMBEO EN EL ACUÍFERO DE VILLA DE REYES, SAN LUIS POTOSI

EXPOSITOR: DR. ADOLFO CHAVEZ RODRIGUEZ
PALACIO DE MINERIA
OCTUBRE DEL 2000

Optimización del bombeo en el acuífero de Villa de Reyes, San Luis Potosí

Adolfo Chávez Rodríguez

Facultad de Ingeniería, Universidad Autónoma de Chihuahua

Sergio Flores Castro

Departamento de Geohidrología, Comisión Federal de Electricidad

El acuífero de Villa de Reyes satisface la demanda de agua de una de las centrales termoeléctricas de la Comisión Federal de Electricidad y ha estado sujeto a sobreexplotación. En los últimos años se han incrementado sus ritmos de abatimiento, lo que ha impulsado el desarrollo de un modelo que permita diseñar una política de explotación óptima de este acuífero. Este modelo se formuló con un enfoque de ingeniería de sistemas donde se integra un modelo de simulación de flujo de agua subterránea con otro de decisión. Este está dado tanto como una función objetivo por optimizar, que en este caso significó la minimización de la suma de los abatimientos en zonas seleccionadas del acuífero, como por un conjunto de restricciones físicas y socioeconómicas que condicionan la explotación del agua subterránea. El acoplamiento de ambos modelos se efectuó mediante la técnica de funciones de respuesta. Se concluyó que un sistema de bombeo es óptimo cuando, al plantear la minimización de abatimientos, es el que ofrece mayores ventajas desde los puntos de vista hidrológico y socioeconómico.

En los últimos años el acuífero de Villa de Reyes, en el estado de San Luis Potosí, ha presentado un abatimiento continuo de los niveles estáticos, ocasionado por el bombeo en pozos someros de usos agrícola y doméstico y en pozos profundos de la Comisión Federal de Electricidad (CFE). Estos últimos satisfacen los caudales de agua requeridos para la operación de la Central Termoeléctrica San Luis Potosí.

Esta situación hidrogeológica hizo necesario el diseño e implementación de un esquema de bombeo encaminado a reducir al mínimo los efectos adversos de la sobreexplotación, como el incremento de los costos de bombeo, la inutilización de las obras de captación, y un posible deterioro de la calidad del agua subterránea. Al mismo tiempo, la implantación de este esquema de bombeo extendería la vida útil del sistema acuífero con sus consecuentes beneficios socioeconómicos en los niveles local y nacional.

El esquema de explotación óptima de un acuífero se puede diseñar mediante la técnica de funciones tecnológicas algebraicas, mejor conocidas como funciones de respuesta, la cual ha probado ser la más eficiente para este propósito. Las funciones de respuesta relacionan el bombeo en pozos con los abatimientos en los mismos, y en la práctica, se obtienen mediante un modelo digital de simulación de flujo de agua subterránea. El Departamento de Geohidrología de la Comisión Federal de Electricidad construyó un modelo de simulación del acuífero de Villa de Reyes, en colaboración con la Residencia de Estudios de Ingeniería Civil en Querétaro (Depto. de Geohidrología y Residencia de Estudios de Ingeniería Civil de Qro., 1989).

En este artículo se desarrolla un modelo de manejo del sistema acuífero de Villa de Reyes, donde se integra el modelo digital de simulación con otro de decisión mediante la técnica de fun-

ciones de respuesta. Este modelo de manejo constituye un problema de programación lineal, cuya solución proporciona los esquemas de bombeo óptimo dentro de las condicionantes del sistema. Como un antecedente a este trabajo se tiene el caso del acuífero de Samalayuca, Chihuahua, donde se adoptó un enfoque metodológico similar (Chávez *et al.*, 1989).

Hidrogeología del área de Villa de Reyes

El valle de Villa de Reyes se localiza en la zona semiárida del centro de México, y el área de estudio queda comprendida entre los 21° 40' y 21° 60' de latitud norte, y entre los 100° 60' y 101° 00' de longitud oeste. La central termoeléctrica se ubica cerca del poblado del mismo nombre, aproximadamente a 35 km al sur de la ciudad de San Luis Potosí (véase ilustración 1). La precipitación media anual en el área es de 427 mm, con una evaporación potencial superior a los 2 000 mm.

El valle es de origen tectónico, habiéndose formado por una fosa estructural que aloja principalmente material volcánico. Sus límites naturales son la sierra de San Miguelito por el noroeste y la de Santa María por el sureste. El sistema acuífero del valle es de tipo libre mixto, con un estrato superior formado por depósitos de relleno consistentes en material volcanoclástico intercalado con gravas, arenas y limos, que tiene un espesor promedio de 150 m. Subyaciendo a este estrato se halla una unidad volcánica constituida básicamente por ignimbritas y riolitas, cuyo espesor promedio es de 700 m. Esta unidad muestra porosidad y permeabilidad secundarias por fracturamiento. El flujo regional de agua subterránea guarda una dirección preferente SW–NE paralela a las sierras mencionadas (Flores *et al.*, 1990).

Hasta 1986 el sistema acuífero del valle se aprovechaba únicamente mediante pozos de uso agrícola y doméstico perforados en el relleno granular, con un bombeo conjunto de poco más de 20 000 m³/día que ocasionó un abatimiento promedio del nivel estático de 1.5 m/año. En ese año entraron en operación pozos profundos de la CFE que extrajeron en conjunto 11 500, 29 700 y 29 100 m³/día en 1986, 1987 y 1988, respectivamente, lo que provocó un abatimiento promedio de 3 m/año en el medio fracturado e incrementó a 2 m/año el abatimiento promedio en el medio granular.

Los pozos de la CFE están agrupados en tres baterías, a la número I corresponden los pozos 5,

1. Localización del valle de Villa de Reyes, SLP

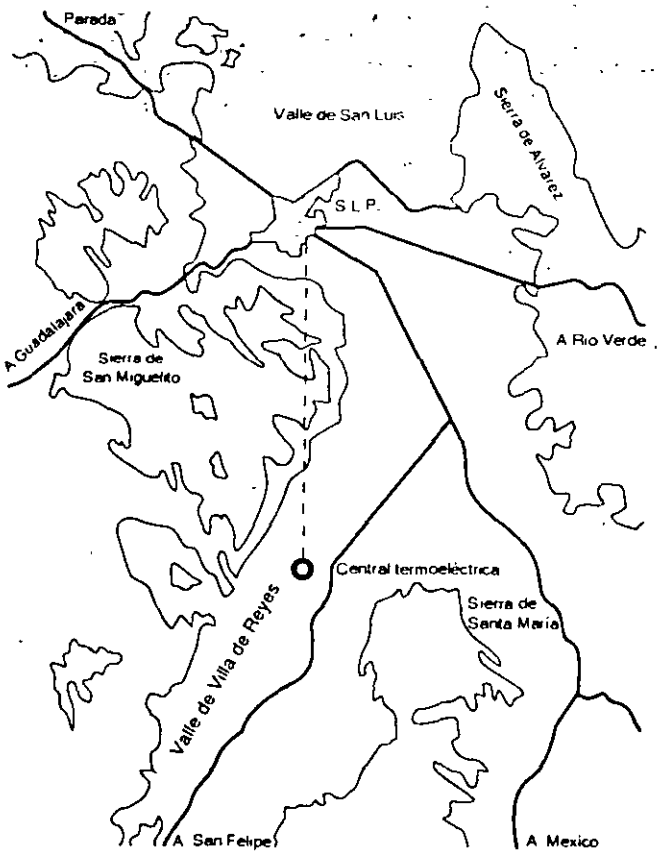

7, 8, 9, 12, 16 y 21; a la II, los pozos 13 y 14; y a la III, los pozos 2, 3, 4, 11, 17, 18, 19 y 20.

La principal fuente de recarga en el área está representada por un flujo profundo ascendente hacia el medio fracturado en la zona de los pozos 7, 9 y 21 de la CFE, procedente de un sistema regional de fallas, que aporta un caudal aproximado de 26 500 m³/día (Depto. de Geohidrología y Residencia de Estudios de Ingeniería Civil en Querétaro, 1989).

Diseño de esquemas de explotación óptima

Los modelos de simulación de flujo se han empleado para predecir la respuesta hidráulica de los sistemas acuíferos ante diversas políticas de explotación. Empero, el número de posibles esquemas de bombeo es infinito en teoría y muy alto en la práctica, por lo que la búsqueda del esquema de explotación óptima por ensayo y error es lenta y costosa, a más de que este procedimiento no garantiza la obtención del óptimo. Sin embargo, con un enfoque de ingeniería de sistemas es posible diseñar tal esquema integrando el modelo digital de simulación con uno económico o de asignación

Un modelo de decisión es la expresión matemática de un criterio de preferencia acerca de los efectos hidrológicos o económicos de la explotación del acuífero; e incluye un conjunto de restricciones físicas y/o socioeconómicas asociadas a tal explotación

La integración del modelo de simulación de flujo con el de decisión constituye el modelo de manejo del sistema acuífero, cuya solución, que es el esquema de bombeo óptimo, se puede obtener mediante técnicas de optimización matemática.

Definición de la función de respuesta

Aunque existen varias técnicas para acoplar los modelos de flujo con los de decisión, la conocida como funciones de respuesta ha probado ser la más eficiente. Esta técnica implica la determinación de la relación funcional entre el bombeo en pozos a través del tiempo y el abatimiento en los mismos (Maddock, 1972).

En la práctica las funciones de respuesta se obtienen mediante un modelo digital de simulación, por lo que se expresará la relación entre bombeo y abatimiento en términos de celdas de bombeo y no de pozos. La forma general de esta relación es:

$$s(k,n) = \sum_{j=1}^{M} \sum_{i=1}^{n} B(k,j,n-i+1)\, Q(j,i) \qquad (1)$$

donde $s(k,n)$ es el abatimiento promedio en la celda k al final del n–ésimo lapso; M, el número de celdas de bombeo; $Q(j,i)$, el caudal de bombeo en la celda j durante el i–ésimo período, n, el número total de periodos, y $B(k,j,n-i+1)$ es el coeficiente de respuesta. Este coeficiente representa el abatimiento promedio en la celda de observación k al final del n–ésimo periodo, debido a un bombeo unitario en la j–ésima celda efectuado durante el i–ésimo lapso. El conjunto de coeficientes de respuesta constituye la función de respuesta, que normalmente se presenta en forma matricial.

Los coeficientes de respuesta se obtienen, por lo general, mediante un modelo digital de simulación de flujo, asignando un bombeo unitario a la primera celda de manejo durante el primer periodo y un bombeo nulo para el resto. Este procedimiento se repite para cada una de las celdas de interés Los abatimientos calculados al final de cada lapso son los coeficientes de respuesta.

Cálculo de la matriz de respuesta de los pozos CFE

Se construyó un modelo de simulación de flujo en diferencias finitas para el acuífero de Villa de Reyes con base en el código de computadora MODFLOW como un antecedente a este trabajo (Depto. de Geohidrología y Residencia de Estudios de Ingeniería Civil en Querétaro, 1989, Maddock y Harbaugh, 1984).

Este acuífero se encuentra en un régimen transitorio de flujo desde fecha indeterminada anterior a 1986, año en que entraron en operación los pozos de la CFE. El modelo de simulación se implementó a dos capas, donde la superior corresponde al medio granular y la inferior al fracturado. La calibración de este modelo se efectuó durante 1986 y 1987, y la verificación, en 1988, iniciando en el mes de enero en cada caso. Este modelo de simulación se empleó para obtener la matriz de respuesta. Las funciones de respuesta, al relacionar linealmente el bombeo con el abatimiento, exigen un comportamiento lineal o al menos cuasilineal del acuífero. El acuífero de Villa de Reyes es libre y, por tanto, intrínsecamente no lineal; sin embargo, su comportamiento será cuasilineal mientras los abatimientos del nivel freático sean pequeños comparados con el espesor saturado.

Como horizonte de manejo se seleccionó un periodo de 5 años, en el que se supone que cada pozo de la CFE bombeará a caudal constante, lo que en la práctica se podría considerar como la extracción promedio del pozo durante los 5 años, siempre que no hubiese periodos muy prolongados de operación a caudales muy por encima o muy por debajo de ese promedio. Cabe hacer notar que un horizonte de simulación superior a 5 años proporcionaría resultados muy inciertos, en vista de la longitud del periodo sobre el cual se calibró el modelo.

Para obtener la matriz de respuesta de los pozos de la CFE, únicos que fueron considerados susceptibles de manejo, se siguió el procedimiento descrito en la sección anterior, seleccionando para este fin un bombeo unitario de 10 000 m³/día, el cual en teoría se puede elegir de manera arbitraria, pero en la práctica debe ser lo suficientemente alto para reducir a un nivel aceptable el efecto relativo de los errores de discretización numérica. De acuerdo con esto, se aplicó un bombeo de 10 000 m³/día a la primera celda de manejo (pozo 2) durante 5 años, donde el abatimiento calculado en cada una de las 17 celdas de manejo al final de este periodo es la primera fila de la matriz

de respuesta. Este procedimiento se repitió en secuencia para el resto de las celdas de manejo hasta obtener la matriz completa. Esta resultó ser aproximadamente simétrica, lo que indica un comportamiento cuasilineal del acuífero durante el periodo señalado (véase cuadro 1).

La matriz de respuesta obtenida se presenta en el cuadro 2, donde se observa que los coeficientes más altos corresponden a aquellas celdas (pozos) situadas en la zona de mínima conexión hidráulica vertical entre los medios acuíferos, o sea, en la mitad suroeste del área de estudio.

Formulación del modelo de manejo

El modelo de manejo del sistema acuífero de Villa de Reyes está constituido por la integración del modelo de flujo con un modelo de decisión a través de la función de respuesta, como ya se mencionó. Este último incluye una función objetivo por optimizar, que en nuestro caso se ha planteado como la minimización de la suma de los abatimientos en zonas seleccionadas del acuífero, lo que refleja la intención de reducir a un mínimo los efectos adversos de la sobreexplotación y de maximizar la vida del acuífero.

La solución a este modelo de manejo es aquel esquema de bombeo que reduce al mínimo los abatimientos dentro de las restricciones físicas que condicionan la explotación del agua subterránea, al tiempo que se satisface la demanda de la central termoeléctrica. Desde el punto de vista de la optimización matemática se considera a la relación funcional entre el bombeo y el abatimiento, dada por la función de respuesta, como una de las restricciones del sistema.

1. Coeficiente de respuesta en las celdas de pozos someros para un periodo de 5 años con bombeo unitario de 10 000 m³/día en los pozos de la CFE

		Pozos someros																
		397 399	398	461	416	449	462	460	381	447 448	425	337	419	375	376	804	373	368
	2	0	1	7	0	0	0	7	5	1	4	9	0	5	6	5	5	5
	3	1	1	4	1	1	7	4	3	2	6	8	1	10	6	6	4	3
	4	1	2	4	1	1	6	3	2	2	6	6	1	8	5	5	3	3
P	5	1	2	4	1	1	5	3	2	2	6	5	1	7	4	4	3	2
O	7	1	1	4	1	1	5	3	2	2	5	4	2	6	4	4	2	2
Z	8	1	1	3	2	1	5	3	2	1	4	4	2	5	3	3	2	2
O	9	1	1	4	1	1	5	3	2	2	4	4	2	6	3	4	2	2
S	11	0	0	4	0	0	4	6	6	1	2	7	0	5	7	7	8	7
	12	1	1	4	2	1	5	3	2	1	4	4	2	5	3	3	2	2
	13	1	1	5	1	1	5	4	3	2	5	5	1	6	4	4	3	3
C	14	1	1	5	1	1	6	4	3	1	5	5	1	5	4	4	3	3
F	16	1	1	3	1	1	5	3	2	1	4	4	2	5	4	2	2	2
E	17	0	1	7	0	0	4	3	6	1	2	5	0	3	4	4	5	5
	18	0	1	5	0	0	4	8	6	0	2	7	0	4	5	5	6	6
	19	0	0	4	0	0	3	6	7	0	2	6	0	4	5	5	8	8
	20	0	0	5	0	0	3	7	8	0	2	5	0	4	5	5	7	7
	21	1	1	4	1	1	5	3	7	1	4	3	2	6	4	4	6	2

2. Matriz de respuesta en las celdas de los pozos de la CFE para un periodo de 5 años con bombeo unitario de 10000 m³/día

	2	3	4	5	7	8	9	11	12	13	14	16	17	18	19	20	21
2	15	6	5	4	4	4	4	5	4	4	5	4	6	7	5	5	4
3		17	9	8	6	6	6	5	6	6	7	6	4	4	4	4	6
4			21	13	10	9	9	3	9	9	9	9	3	3	3	3	9
5				29	16	15	15	3	15	14	13	15	3	3	3	3	16
7					30	26	27	3	26	20	17	26	3	3	3	3	26
8						37	28	3	33	20	17	31	3	3	3	3	24
9							32	3	28	20	18	29	3	3	3	3	26
11								12	3	3	3	3	5	6	7	6	3
12									38	20	17	32	3	3	3	3	24
13										35	25	20	4	3	3	3	20
14											34	17	4	4	4	4	17
16												35	3	3	3	3	25
17													13	7	6	6	3
18														11	7	7	3
19															10	8	3
20																10	2
21																	29

Ahora, considerado un horizonte de manejo de 5 años, a fin de obtener los caudales óptimos de operación de los pozos de la CFE para este periodo único, se omiten los índices relativos a los lapsos en la ecuación (1), y el modelo de manejo se formula de acuerdo con los siguientes planteamientos:

Esquema de bombeo óptimo A

Este diseño plantea la obtención de un esquema de bombeo óptimo de los pozos de la CFE donde se minimizan los abatimientos sólo en estos pozos, sin considerar los efectos sobre el medio granular, lo cual se expresa mediante la siguiente función objetivo.

$$\text{minimizar} \quad \sum_{k=1}^{n_f} s(k) \qquad (2)$$

donde $s(k)$ es el abatimiento en la celda k al final del período de 5 años, que es el horizonte de manejo, y n_f es el total de las celdas de bombeo (pozos de la CFE).

Las restricciones impuestas son las siguientes.

(i) $s(k) \leq s_{max}(k)$ para toda k

(ii) $Q(k) \leq Q_{max}(k)$ para toda k

(iii) $$\sum_{k=1}^{M} Q(k) \geq D$$

(iv) $$s(k) = \sum_{j=1}^{M} B(k,j)Q(j)$$ para toda k

donde $s(k)$ es el abatimiento al final del horizonte de manejo en la celda k; M, el número total de celdas de manejo, que en este caso es igual a n_f; $Q(j)$, el caudal de bombeo en la celda j; $B(k,j)$, el coeficiente de respuesta, que representa el abatimiento en la celda k al final del horizonte de manejo debido a un bombeo unitario en la celda j; $s_{max}(k)$, es el abatimiento máximo permisible al final del horizonte de manejo en la celda k; $Q_{max}(k)$, el caudal de bombeo máximo posible en la celda k; y D es la demanda de agua de la central termoeléctrica.

La restricción del tipo (i) condiciona al abatimiento en cada celda de los pozos de la CFE a no exceder un valor máximo permisible al final del horizonte de manejo; la segunda restricción (ii) establece que ningún pozo de la CFE puede ser bombeado por encima de su capacidad de diseño, o de un cierto caudal máximo posible; la tercera (iii) exige que la extracción conjunta de los pozos de la CFE satisfaga al menos la demanda de la central termoeléctrica; y la última (iv) expresa la relación funcional entre el bombeo y el abatimiento, y es a través de esta restricción como se establece el vínculo entre el modelo de simulación de flujo y el modelo de decisión. Este modelo de manejo, representado por la ecuación (2) y el conjunto de restricciones (i) a (iv), constituye un problema de programación lineal, el cual fue resuelto con el paquete de computadora LP88 versión 3.12 (Eastern Software Products, 1983).

El abatimiento máximo permisible del nivel estático en cada pozo de la CFE se estableció como la diferencia entre el nivel de la base de la cámara de bombeo y el nivel dinámico actual, a la que se restaron 20 m, con el fin de dar un margen de seguridad ante la previsible, aunque difícilmente cuantificable, acentuación de la diferencia entre el nivel estático y el dinámico al descender ambos.

El esquema de bombeo óptimo se diseñó para una demanda de la central termoeléctrica de 450 l/s (38 880 m³/día). En el cuadro 3 se enlistan las restricciones pertinentes, mientras que en el 4 se presenta la solución al modelo de manejo Esta solución es el esquema de bombeo que reduce a un mínimo la suma de los abatimientos en celdas de los pozos de la CFE dentro de las restricciones impuestas. Este conjunto de valores constituye el esquema de bombeo óptimo A.

Esquema de bombeo óptimo B

Se puede plantear un esquema alternativo de bombeo de los pozos de la CFE que sea óptimo al

3. Restricciones de abatimiento y bombeo de los pozos de la CFE

Pozo	Profundidad de la cámara de bombeo (metros)	Nivel dinámico (metros)	Abatimiento máximo permisible a 5 años (metros)	Caudal de bombeo máximo posible (l/s)
2	200	70	110	63
3	197	66	111	52
4	198	78	100	77
5	200	76	104	34
7	199	82	97	60
8	177	82	75	42
9	245	108	117	42
11	247	130	97	33
12	200	100	80	52
13	213	140	53	20
14	245	107	118	22
16	250	110	120	37
17	246	83	143	75
18	250	69	161	32
19	248	61	167	49
20	250	67	163	71
21	244	67	157	63

considerar el sistema acuífero completo, es decir, al buscar la minimización de abatimientos tanto en el medio fracturado como en el granular. En este caso la función objetivo toma la siguiente forma:

$$\text{minimizar} \quad \sum_{k=1}^{n_f} s(k) + \sum_{k'=1}^{n_g} s(k') \qquad (3)$$

donde n_g es el número de celdas de interés en el medio granular, y $s(k')$, el abatimiento en la celda k' de ese mismo medio.

En este caso, las restricciones impuestas son las siguientes:

(i) $s(k) \leq s_{max}(k)$ para toda k

$s(k') \leq s_{max}(k')$ para toda k'

(ii) $Q(k) \leq Q_{max}(k)$ para toda k

(iii) $\sum_{k=1}^{M} Q(k) \geq D$

(iv) $s(k) = \sum_{j=1}^{M} B(k,j)Q(j)$ para toda k

$s(k') = \sum_{j=1}^{M} B(k',j)Q(j)$ para toda k'

donde M es el número de celdas de manejo, que también en este caso es igual al número de pozos de la CFE, n_f. $B(k',j)$ es el coeficiente de respuesta que relaciona el bombeo en el j-ésimo pozo de la CFE con el abatimiento en la k'-ésima celda del medio granular.

Dado que se tienen 17 celdas de pozos profundos de la CFE, y con el fin de dar el mismo peso en la función objetivo (3) a ambos medios acuíferos, se seleccionaron las 17 celdas de pozos someros con mayor extracción entre las 23 existentes en el área. Cabe mencionar que en las 6 celdas excluidas los bombeos son muy reducidos. En el cuadro 4 se presentan los coeficientes de respuesta que relacionan el bombeo en los pozos de la CFE con el abatimiento en las celdas de los pozos someros que ahí se indican para el periodo de 5 años. La ubicación de los pozos someros considerados se muestra en la ilustración 2a.

El modelo de manejo representado por la función objetivo (3) y su conjunto de restricciones asociadas constituye también un problema de programación lineal, y su solución es el esquema de bombeo de los pozos de la CFE que minimiza la suma de los abatimientos en los dos medios acuíferos dentro de las restricciones impuestas. Para los pozos de la CFE estas restricciones fueron las mismas consideradas en el diseño del esquema óptimo A, mientras que para las celdas de los pozos someros se permitió un ambatimiento máximo de 20 m en el periodo de 5 años.

La solución al modelo de manejo de acuerdo con este diseño se muestra en el cuadro 4, y al comparar estos resultados con los obtenidos en el diseño previo se puede notar que la distribución del bombeo de los pozos de la CFE es marcadamente distinta; por ejemplo, los pozos 2, 3 y 18 operan en el esquema óptima A pero no en el B, mientras que los pozos 5, 8, 16 y 21 bombean en el esquema óptimo B pero no en el A.

Es importante destacar que se ensayó el diseño de ambos esquemas óptimos para demandas de agua mayores que 450 l/s, resultando que en el caso del esquema A no fue factible obtener una solución óptima con una demanda de 700 l/s, mientras que en el caso del esquema B, el método de optimización no convergió para una demanda de 550 l/s, lo cual significa que no es posible satisfacer estas demandas sin violar las restricciones físicas que condicionan la explotación del sistema acuífero.

4. Esquema de bombeo de los pozos de la CFE para una demanda de 450 l/s

Pozo	1989 ajustado	Optimo A	Optimo B
2	46	63	0
3	48	52	0
4	36	75	76
5	20	0	34
7	39	0	0
8	28	0	42
9	35	0	0
11	8	33	28
12	36	0	0
13	8	0	0
14	6	0	0
16	10	0	37
17	16	75	75
18	24	32	0
19	32	49	49
20	9	71	71
21	49	0	38

2. Predicción de abatimiento del nivel estático (en metros) con el esquema de bombeo de 1989 ajustado a 450 l/s en los pozos de la CFE; a) de enero de 1989 a enero de 1994 en el acuífero granular y b) a enero de 1994 en el acuífero fracturado

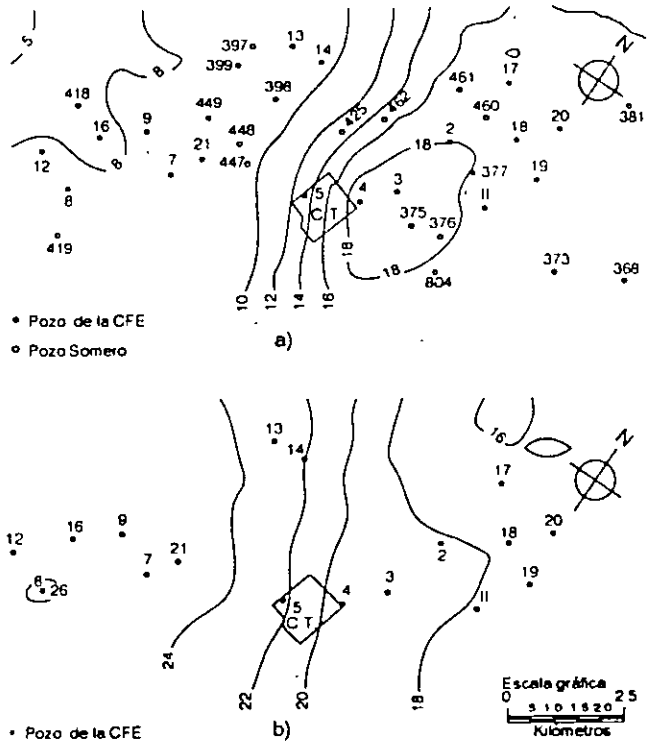

Predicción de la evolución del nivel estático

La evolución del nivel estático en ambos medios se predijo mediante el modelo digital de flujo para un horizonte de 5 años tomando como niveles iniciales los correspondientes a enero de 1989.

En ese año, que es el último con registro hidrométrico, el bombeo conjunto de los pozos de la CFE fue de 374 l/s (véase cuadro 5). Con el fin de comparar consistentemente la predicción bajo este esquema de bombeo con la que resulta de los esquemas óptimos A y B, se incrementaron los caudales de los pozos de la CFE del año de 1989 para bombear en conjunto 450 l/s, pero respetando la aportación relativa de cada pozo al

5. Bombeo promedio de los pozos de la CFE durante el año de 1989

Pozo	Caudal (l/s)	Porcentaje
Batería I		
5	16 8	4 5
7	32 6	8.7
8	23 7	6.3
9	29 0	7.7
12	29 8	8 0
16	8 1	2 2
21	40.7	10 9
Batería II		
13	6 8	1 8
14	4 8	1 3
Batería III		
2	38.5	10.3
3	40 1	10.7
4	29.4	7.9
11	6 7	1.8
17	13 5	3.6
18	20.0	5.4
19	26 4	7 1
20	7.2	1.9
Total:	374.1	100 0

total bombeado en ese año. Este esquema se llamará en lo sucesivo "esquema de bombeo de 1989 ajustado", y en el cuadro 4 se muestran los caudales por pozo que lo definen.

En las ilustraciones 2a y 2b se aprecia la predicción de abatimiento de nivel estático de enero de 1989 a enero de 1994 en los medios granular y fracturado, respectivamente, con el esquema de bombeo de 1989 ajustado. En la ilustración 2a se observa un abatimiento máximo de más de 18 m en el medio granular en la zona del pozo 3, que decrece hasta 6 m en la esquina poniente del área de estudio. En cuanto al medio fracturado, se observa en la ilustración 2b un abatimiento máximo de 26 m en la zona del pozo 8, y un mínimo de alrededor de 16 m en la porción noroeste del área.

Con respecto a la predicción bajo el esquema de bombeo óptimo A, donde se considera únicamente la minimización de abatimientos en el medio fracturado, los abatimientos predichos a enero de 1994 en los medios granular y fracturado se muestran en las ilustraciones 3a y 3b, respectivamente. En la 3a se observa que el abatimiento máximo predicho para el medio granular bajo este esquema de bombeo es de más de 23 m al noreste del área, y el mínimo es de 5 m hacia la esquina poniente. En la 3b, que corresponde al medio fracturado, se aprecia un abatimiento máximo de 24 m en la misma porción noreste, y una recuperación de niveles (signo negativo en la ilustración) en la mitad suroeste del área con un máximo de recuperación de 20 m en la zona del pozo 12.

La predicción de abatimiento del nivel estático en el periodo de enero de 1989 a enero de 1994 bajo el esquema de bombeo óptimo B se ejemplifica en las ilustraciones 4a y 4b para los medios granular y fracturado, respectivamente. Este esquema de bombeo fue diseñado planteando la minimización de abatimientos en el sistema global, dando la misma ponderación a los dos medios acuíferos. Como se puede observar en la ilustración 4a, el abatimiento máximo en el medio granular es de más de 20 m sobre la porción noreste del área, con un mínimo de 6 m en la esquina poniente. En la 4b se aprecia en el medio fracturado un abatimiento máximo de 21 m hacia el noreste en la zona de los pozos 19 y 20, y abatimientos entre 8 y 10 m en la porción suroeste del área.

Conclusiones y recomendaciones

De los resultados de la predicción bajo los tres esquemas de bombeo propuestos, se concluye que si bien el esquema de bombeo de 1989 ajustado conduce a los menores abatimientos en el medio

3. Predicción de abatimiento del nivel estático (en metros) de enero de 1989 a enero de 1994 con el esquema de bombeo óptimo A; a) en el acuífero granular y b) en el acuífero fracturado

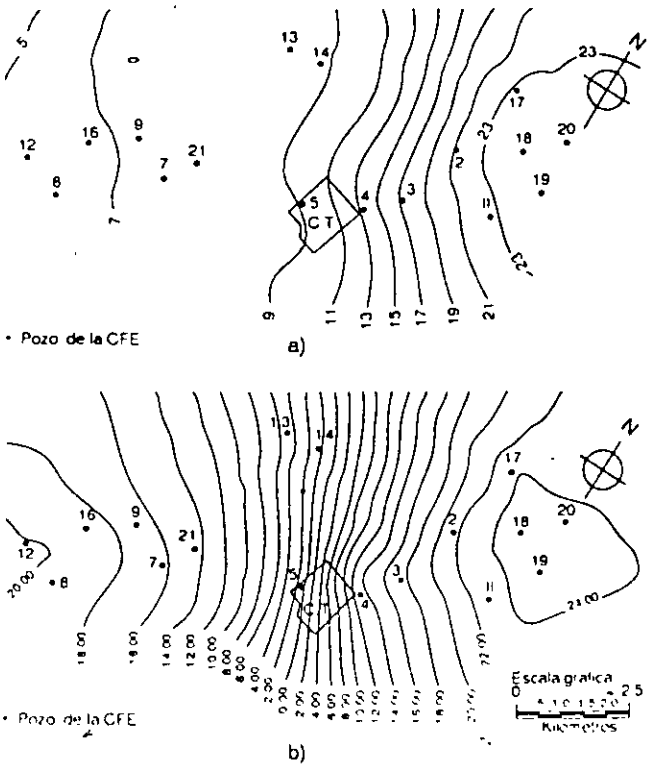

4. Predicción de abatimiento del nivel estático (en metros) de enero de 1989 a enero de 1994 con el esquema de bombeo óptimo B; a) en el acuífero granular y b) en el acuífero fracturado

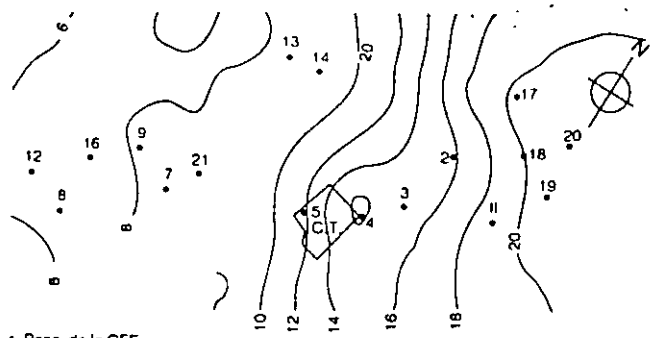

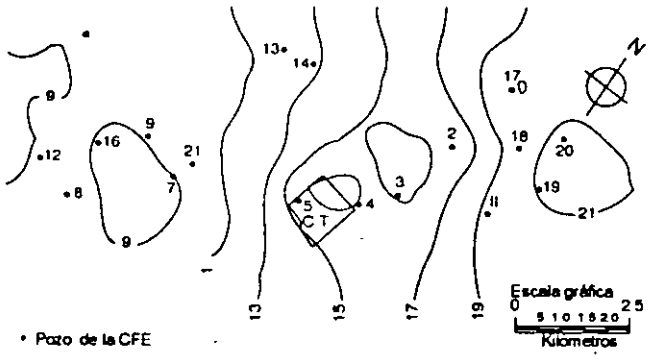

granular, es también el esquema que ocasiona los mayores abatimientos en el medio fracturado, con los inconvenientes del caso para la operación de los pozos de la CFE, en particular para los de la batería I.

Por otra parte, el esquema de bombeo óptimo A ofrece las mejores condiciones para la operación de los pozos de la CFE de las baterías I y II; sin embargo, provoca los mayores abatimientos en el medio granular.

En cuanto al esquema de bombeo óptimo B, se observa que ocasiona abatimientos relativamente pequeños en el medio fracturado en las zonas de las baterías I y II, y abatimientos menores a los que produce el esquema óptimo A en la zona de la batería III. Además, como es de esperarse, el esquema óptimo B induce abatimientos inferiores en el medio granular que los obtenidos con el esquema de bombeo óptimo A.

Comparando las predicciones del esquema óptimo B con las del esquema de bombeo de 1989 ajustado, se observa que aunque este último ocasiona menores abatimientos en la porción noreste del área, su efecto es fuerte sobre la mayor parte del medio fracturado, afectando considerablemente a la mayoría de los pozos de la CFE

De las comparaciones anteriores se puede concluir que el esquema de bombeo óptimo B ofrece ventajas de orden hidrogeológico y socioeconómico sobre los otros dos esquemas. Desde el punto de vista operacional, el cuadro 6 indica los volúmenes anuales de extracción recomendables. En este cuadro se aprecia que para la batería I sólo los pozos 5, 8, 16 y 21 deberán operar normalmente, quedando los pozos 7, 9 y 12 de respaldo. Es conveniente que los pozos 13 y 14 que conforman la batería II se utilicen de respaldo. En el caso de la batería III, la extracción se deberá efectuar en los pozos 4, 11, 17, 19 y 20, manteniendo los pozos 2, 3 y 18 de respaldo.

En todos los casos se recomienda atender a la hidrometría mensual de los pozos, procurando que sus volúmenes anuales de extracción se apeguen a los indicados en el cuadro 6. Los pozos de respaldo sólo deberán operar temporalmente en caso de fallas mecánicas en los otros.

6. Volumen de extracción anual recomendado en los pozos de la CFE para una demanda total promedio de 450 l/s

Pozo	Volumen (miles de m³)
Batería I	
5	1072
7	0
8	1325
9	0
12	0
16	1167
21	1198
Batería II	
13	0
14	0
Batería III	
2	0
3	0
4	2397
11	883
17	2365
18	0
19	1545
20	2239
Total	14191

Referencias

Chávez, A., M. Hernández, y S. Flores. "Modelación digital y optimación de acuíferos", *Ingeniería Hidráulica en México*, pp. 31–39, mayo–agosto de 1989.

Departamento de Geohidrología, y Residencia de Estudios de Ingeniería Civil de Querétaro. *Modelación del Comportamiento del Acuífero de Villa de Reyes, S. L. P. para el Estudio de disponibilidad de agua a la Central*

Termoeléctrica San Luis Potosí, Comisión Federal de Electricidad, octubre de 1989.

Eastern Software Products, Inc. *Linear programming for IBM personal computer*, v. 3 12, 1983

Flores, S., A Alcalá y M Hernández. *Características geohidrológicas en el área de la Central Termoeléctrica San Luis Potosí*, Pub. GH-5, Gerencia de Estudios de Ingeniería Civil, CFE, julio de 1990.

Maddock, T. III. "Algebraic technological function from a simulation model", *Water Resour. Res.*, B(1), 129-134, 1972.

McDonald, M. G., y A W. Harbaugh. "A modular threedimensional finite-difference ground-water flow model", *US Geological Survey*, Reston, VA, 528 p , 1984

FACULTAD DE INGENIERIA U.N.A.M.
DIVISION DE EDUCACION CONTINUA

CURSOS ABIERTOS

XII CURSO INTERNACIONAL DE CONTAMINACIÓN DE ACUÍFEROS

MODULO III: MODELOS MATEMÁTICOS EN GEOHIDROLOGIA Y CONTAMINACIÓN DE ACUIFEROS

TEMA

ESTIMATION OF MOUNTAIN FRONT RECHARGE TO REGIONAL AQUIFERS

EXPOSITOR: DR. ADOLFO CHAVEZ RODRIGUEZ
PALACIO DE MINERIA
OCTUBRE DEL 2000

WATER RESOURCES RESEARCH, VOL. 30, NO. 7, PAGES 2157–2167, JULY 1994

Estimation of mountain front recharge to regional aquifers 1. Development of an analytical hydroclimatic model

Adolfo Chavez
Facultad de Ingeniena, Universidad Autonoma de Chihuahua, Chihuahua, Mexico

Stanley N. Davis and Soroosh Sorooshian
Department of Hydrology and Water Resources, University of Arizona, Tucson

Abstract. This paper addresses the hydroclimatic modeling of mountain front recharge to regional aquifers. An analytical relationship between the mean seasonal precipitation and runoff is obtained based on a conceptualization of the hydrologic processes occurring in hard rock mountainous terrain and a derived-distribution approach where the input variables are considered to be stochastic and their probability distributions are transformed into the probability distribution of the output variable by using the deterministic physical process. In a first-order approximation a relationship between the seasonal values of precipitation and runoff is obtained. An analytical model of the seasonal streamflow is then developed where initial abstraction and the long-term effective subsurface outflow, or mountain front recharge, are viewed as unknown model parameters. In addition, a procedure that combines the water balance equation with a relationship provided by the so-called "vegetal equilibrium hypothesis," and which enables the estimation of effective soil-related parameters jointly with the mean seasonal evapotranspiration and surface runoff, is introduced. This procedure is applied to a mountainous watershed in southern Arizona.

Introduction

The two main mechanisms of natural recharge to regional aquifers in arid and semiarid areas are channel recharge and mountain front recharge. While mountain front recharge is a vital component of the groundwater system in many of these areas [*Feth*, 1964], it constitutes only a minor fraction of the total amount of water delivered to the area by precipitation and therefore cannot be estimated reliably by "gross" water balance calculations.

Estimates of mountain front recharge to regional aquifers are required for management purposes, particularly in order to determine the safe yield from wells in groundwater basins where overall recharge is small and development may readily lead to overdraft conditions. Such basins are common in arid and semiarid regions. Estimates of mountain front recharge also provide prescribed flux values for digital models of regional groundwater flow.

However, data on groundwater in the mountain and the mountain front region are ordinarily limited to a few widely spaced wells, springs, and base flow streams. This scarcity of data, along with uncertainties inherent in the data and calculations, may lead to errors of up to an order of magnitude in the estimation of mountain front recharge [*Belan and Matlock*, 1973].

With regard to the inverse problem in groundwater hydrology, also known as the groundwater parameter estimation problem, *Carrera and Neuman* [1986b] found that prescribed head conditions at the aquifer boundary resulted in smaller sensitivities than prescribed nonzero flux, hence this suggests that one should impose the latter condition whenever possible. *Carrera and Neuman* [1986a] posed the inverse problem in the framework of maximum likelihood estimation with prior information about the parameters. In their formulation the prior head errors and the prior parameter estimation errors were assumed to lack cross correlation, and for this reason, they cautioned that head values used for inverse modeling must not be used to derive prior parameter estimates. This rules out the use of flow net analysis to provide prior information about mountain front recharge for inverse modeling purposes, at least within the framework of Carrera and Neuman's approach.

Prior estimates of mountain front recharge can be obtained with the aid of environmental isotopes [*Simpson et al.*, 1970; *Gallaher*, 1979; *Olson*, 1982] and hydrochemical mass balance calculations [*Thorne*, 1982; *Adar*, 1984]. These methods are associated with large uncertainties; hence according to conclusions reached by *Carrera and Neuman* [1986b] regarding mathematical conditions for well-posedness, estimates based on them do little to reduce the degree of ill-posedness of the inverse problem.

An alternative approach to estimation of mountain front recharge is the use of hydroclimatic models. Such models are particularly useful in areas where reasonable records of rainfall and streamflow exist but where there is almost no data on groundwater.

In paper 1 of this two-part series we develop analytical models of the seasonal surface runoff and streamflow based on a conceptual model of hydrologic processes that should approximate some types of field conditions, in particular, hard rock mountainous watersheds where deep percolation occurs exclusively through fractures; these models (1) are formulated in terms of parameters with physical significance,

Paper number 93WR03369
0043-1397/94/93WR-03369$05.00

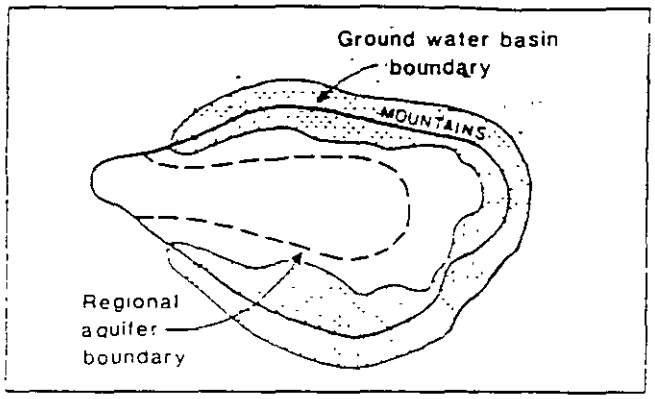

Figure 1a Groundwater basin and regional aquifer boundaries in plan

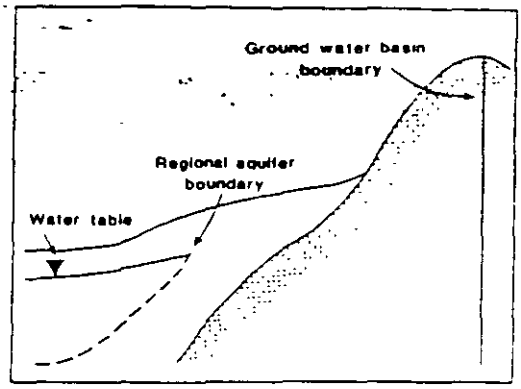

Figure 1b. Groundwater basin and regional aquifer in cross section.

thus facilitating the conceptual interpretation of these parameters and the development of criteria for regionalization, (2) make use of data ordinarily recorded at climatological and hydrometric stations, thus increasing model applicability, and (3) favor the inclusion of data obtained by remote-sensing techniques, such as satellite imagery and aerial photography, inasmuch as they can rapidly provide a low-cost characterization of drainage areas and aid in the assessment of some watershed parameters.

We also introduce a quantitative procedure that e ies the estimation of mean surface runoff and evapotranspiration jointly with effective soil-related parameters This procedure is developed through the combination of the water balance equation and a relationship provided by the so-called "vegetal equilibrium hypothesis" [*Eagleson*, 1978f] Initial abstractions obtained in this manner are to be used as prior estimates within a stochastic parameter estimation approach given by *Chavez et al* [this issue] (paper 2 of the series) which incorporates prior information about the model parameters This approach is applied to our seasonal streamflow model where the long-term effective groundwater runoff or mountain front recharge, is viewed as one of the model parameters

Conceptualization

To set up a conceptual framework for the development of analytical models of the seasonal surface runoff and streamflow and a procedure to estin mountain front recharge, the following definitions are introduced in agreement with *Wilson et al* [1980]: (1) a groundwater basin is an area within which groundwater flow paths are toward a regional aquifer, (2) a regional aquifer is the largest body of continuous saturation in a groundwater basin, (3) a local flow system is a small, saturated groundwater flow system that is isolated from the regional aquifer, and (4) a regional flow system is a saturated system that is connected to the regional aquifer.

In many areas the groundwater basin coincides with the watershed bounda *Wilson et al* [1980] emphasized the distinction between the regional aquifer boundary and the groundwater basin, as well as the difference between the regional aquifer boundary and the base of the mountain These differences are shown in Figures 1a and 1b, and both local and regional flow systems are illustrated in Figure 2

Mountain front recharge is defined by *Wilson et al* [1980] as recharge which occurs along the portion of the regional aquifer boundary that parallels a mountain area According to this definition the components of this type of recharge are (1) the infiltration of streamflow from the washes and rivulets between the bases of the mountains and the regional aquifer boundary and (2) the subsurface inflow from the mountain mass to the basin-fill sediments.

In mountainous terrain, the permeability of which is fracture controlled, subsurface inflow includes both groundwater flow through fractures and underflow through the sediments of the washes and canyons that drain the mountains In this paper we deal only with the estimation of subsurface inflow from the mountain mass to the basin-fill sediments, which, in terms of the mountainous watersheds, is the subsurface outflow. Here we will use this term and mountain front recharge interchangeably.

Our conceptualization of the hydrologic processes that occur in mountainous hard rock terrain, and that ultimately deter ine mountain front recharge, includes the following assumptions and simplifications: (1) no consideration is given to snow or ice, (2) soil cover is small or nonexistent, (3) permeability of the mountain mass is secondary and fracture controlled, (4) porosities and permeabilities may develop in the upper zone of the bedrock by surface disturbances such as small fractures, cracks, and weathering, (5) only vertical water flow occurs in the upper unsaturated

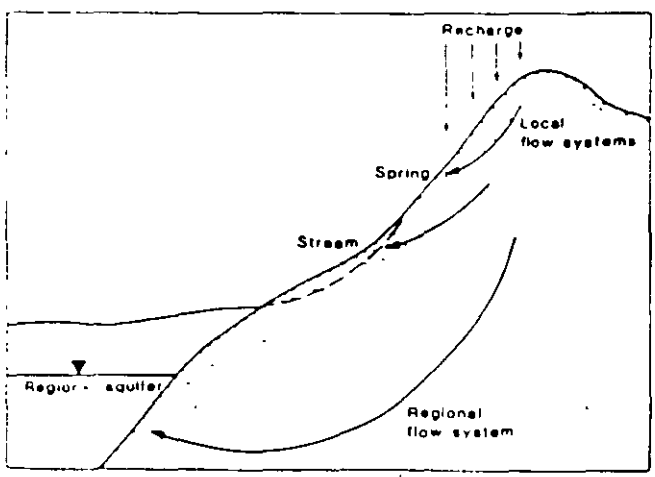

Figure 2. Local and regional flow systems in the mountains.

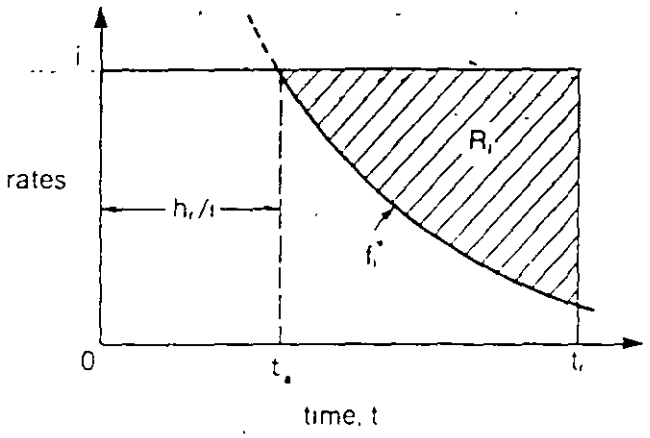

Figure 5. Generation of surface runoff R_j during a typical storm

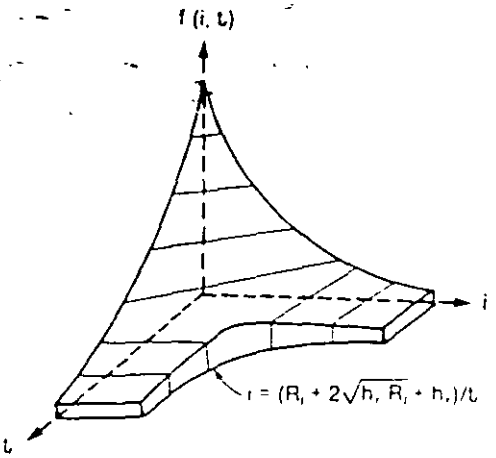

Figure 7. Calculation of surface runoff distribution.

equals the storm depth h_r. If $t_r > h_r/i$, as shown in Figure 5, initial abstraction is satisfied, and surface runoff is generated starting from time $t = h_r/i$ until time $t = t_r$.

Based on our assumption that areal infiltration does not contribute to deep percolation and because of the finite storage capacity of the upper zone of the bedrock, infiltration capacity must approach zero at large times. With no physical analogy to the matrix infiltration equation, we model infiltration capacity by

$$f_t^* = (h_r i)^{1/2} t^{-1/2} \tag{2}$$

where it is assumed that the infiltration rate is equal to infiltration capacity once initial abstraction is satisfied.

The cumulative distribution function of the storm surface runoff can be found according to

$$\text{Prob}\,[R_j < z] = F[R_j] = \iint_{R(z)} f(i, t_r, h_r)\, dR \tag{3}$$

where $f(i, t_r, h_r)$ is the joint probability function of storm intensity, storm duration, and initial abstraction, and $R(z)$ is the region of integration. In a zero-order approximation we will consider h_r to be a constant at its space and time effective value, thus forcing all variability to come from the storm parameters, and equation (3) becomes

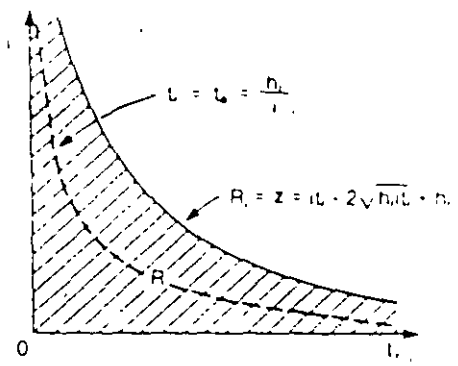

Figure 6. Integration region for probability of surface runoff.

$$F[R_j] = \iint_{R(z)} f(i, t_r|h_r)\, dR = \iint_{R(z)} f(i, t_r)\, dR \tag{4}$$

where the region of integration is illustrated in Figure 6.

The integration of the joint distribution $f(i, t_r)$ from the axes out to the dashed curve $t_a = t_r$ gives the probability that no surface runoff occurs. Integrating all the way out to the curve $R_j = z$ provides the probability that a particular storm will produce $R_j \le z$.

We will derive the probability distribution of surface runoff by integrating the difference between rainfall intensity and the infiltration equation over the duration of a rainstorm. Infiltration is assumed to occur uniformly over both the bare and the vegetated portions of the surface. Hence

$$R_j = \int_{h_r/i}^{t_r} (i - (h_r i)^{1/2} t^{-1/2})\, dt = it_r - 2(h_r it_r)^{1/2} + h_r \tag{5}$$

where R_j is surface runoff generated by the jth rainstorm.

Now, by assuming that storm intensity i and storm duration t_r are independent and exponentially distributed,

$$f(i, t_r) = \alpha\delta e^{-\alpha i - \delta t_r} \tag{6}$$

where α^{-1} is the mean storm intensity, δ^{-1} is the mean storm duration, and because of the independence assumption $\alpha^{-1}\delta^{-1}$ is the mean storm depth, equal to m_H. Using (6), we can prepare a three-dimensional view of the probability calculation of (4), as shown in Figure 7.

Substituting (6) into (4) and using (5) gives

$$\text{Prob}\,[R_j < z] = \alpha\delta \int_0^{h_r/z} e^{-\delta t_r}\, dt_r \int_0^{(z + 2(h_r z)^{1/2} + h_r)/i} e^{-\alpha i}\, di \tag{7}$$

or

$$\text{Prob}\,[R_j < z] = 1 - \delta \int_0^{h_r/z} \exp\,[-\delta t_r - (\alpha/t_r)(z + 2(h_r z)^{1/2} + h_r)]\, dt_r, \tag{8}$$

and finally

zone of the bedrock, (6) moisture storage capacity of the upper zone of the bedrock is not exceeded during a rainstorm event, (7) areal infiltration does not contribute to deep percolation, (8) deep percolation occurs only through fractures connected to a local flow system or to the regional flow system, (9) fractures where deep percolation occurs collect water from surface runoff (overland flow and/or channel flow), (10) water collected by these fractures is instantly drained and hence is not available for evaporation, (11) channel precipitation is negligible, (12) evaporative losses from surface runoff are negligible, (13) water infiltrated along the drainage channels is not available for evapotranspiration, (14) local flow systems which feed springs and drainage channels may be present in the mountain mass, (15) the regional aquifer may be replenished by groundwater flow through fractures and by underflow through the sediments of the drainage channels, and (16) the replenishment to the regional aquifer is stationary in the long term

Analytical Models of the Seasonal Surface Runoff and Streamflow

In this section an analytical model of the seasonal surface runoff is introduced, by virtue of our conceptualization of the hydrologic processes in the mountainous area, this is equal to water yield. A seasonal streamflow model is then derived on the basis of the definition of water yield. This model includes long-term effective subsurface outflow (mountain front recharge) as a model parameter

Modeling Approach

We adopt the approach that, in applied statistics, is referred to as one of "derived distributions." In this approach the input variables are considered to be stochastic, and their probability distributions are transformed into the probability distribution of the output variables by use of the deterministic model of the physical process. This approach is illustrated in Figure 3.

Precipitation is represented by a sequence of randomly sized and spaced rectangular pulses (Figure 4). This approach enables us to conveniently represent the distribution of two critical periods, the duration t_r of precipitation during which infiltration and or surface runoff occurs and the interval between storms, t_b, during which evapotranspiration occurs [*Eagleson*, 1978a, b]

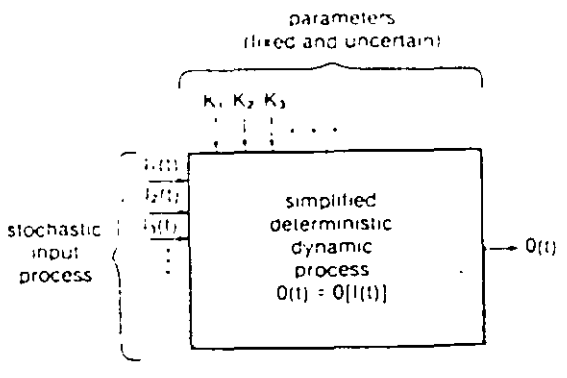

Figure 3. A simple statistical dynamic process

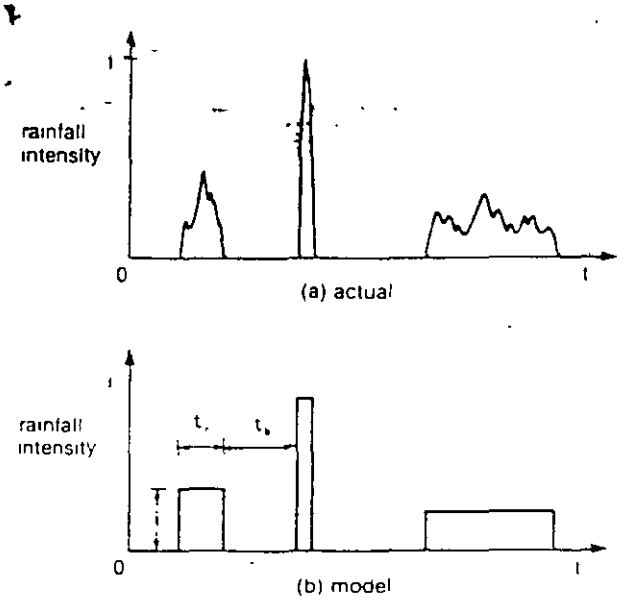

Figure 4. Model of precipitation event series

Surface Runoff

First, in the manner of *Eagleson* [1978c], we will derive the probability distribution of surface runoff on an event basis to establish a relationship between the expected values of seasonal runoff and rainfall. Then, in a first-order approximation, a relationship between the seasonal values of precipitation and runoff will be obtained.

In order to model surface runoff generation, a quantitative model of infiltration is required. Some authors [*Eagleson*, 1978c, *Clapp*, 1982; *Milly and Eagleson*, 1982; *Milly*, 1986] developed event-based simulation models of vertical water flow in the soil that were formulated in terms of basic soil hydraulics parameters and explicitly incorporate soil water dynamic processes. In particular, *Milly* [1986] used the hydrologic concept of time condensation and simplified soil moisture kinematics to allow closed-form solutions of the Richards equation to serve in continuous simulation of the vertical exfiltration and infiltration under randomly varying forcing

In this work we adopt a simpler and essentially conceptual approach to model infiltration into the upper zone of the bedrock which includes initial abstraction as the only soil-related parameter and facilitates the analytical derivation of the probability distribution of surface runoff. In this approach we assume that infiltration and surface runoff occur during a storm period, whereas evapotranspiration occurs during an interstorm period, exclusively

We represent rainstorms by a sequence of randomly sized and spaced rectangular pulses where, for any single storm,

$$i(t) = i = \text{constant}, \qquad 0 \le t \le t_r \tag{1}$$

where i is rainfall intensity (L/T) and t_r is storm duration. The generation of surface runoff during a rainstorm starting at $t = 0$ is represented in Figure 5. In this figure, t_a is time at which initial abstraction h_r is satisfied, and f_c^* is infiltration capacity.

In this model of surface runoff generation there is an initial withdrawal of rainfall to satisfy initial abstraction h_r. If $t_r \le h_r/i$, there is no surface runoff, and the rainfall withdrawal

$$\text{Prob}\,[R_j < z] = 1 - 2(\alpha\delta)^{1/2}(z^{1/2} + h_r^{1/2}) \cdot K_1[2(\alpha\delta)^{1/2}(z^{1/2} + h_r^{1/2})] \quad (9)$$

where $K_1[\ ]$ is the modified Bessel function of order one.

The probability of zero surface runoff is

$$\text{Prob}\,[R_j = 0] = 1 - 2(\alpha\delta h_r)^{1/2}K_1[2(\alpha\delta h_r)^{1/2}] \quad (10)$$

and hence the probability density function $f(R_j)$ must be a compound distribution having an impulse given by (10) at the origin with a continuous portion of area

$$\text{Prob}\,[R_j > 0] = 2(\alpha\delta h_r)^{1/2}K_1[2(\alpha\delta h_r)^{1/2}] \quad (11)$$

To obtain the probability density function of R_j, we first approximate (9) for large z, as follows:

$$\text{Prob}\,[R_j < z] = 1 - 2(\alpha\delta z)^{1/2}K_1[2(\alpha\delta z)^{1/2}] \quad (12)$$

and differentiating this equation we get, for large R_j,

$$f(R_j) = 2\alpha\delta K_0[2(\alpha\delta R_j)^{1/2}] \quad (13)$$

where $K_0[\ ]$ is the modified Bessel function of order zero.

From the above approximation the area of the continuous part of the density function is

$$\int_0^\infty f(R_j)\,dR_j = 1 \quad (14)$$

which is different by the factor

$$2(\alpha\delta h_r)^{1/2}K_1[2(\alpha\delta h_r)^{1/2}]$$

from the true value given by (11).

We now approximate the continuous portion of the probability density function of surface runoff over its full range by (13) rescaled through multiplication by the above factor in order to give it the proper area. That is,

$$f(R_j) = 4(\alpha\delta)^{1/2}(h_r)^{1/2}K_0[2(\alpha\delta R_j)^{1/2}]K_1[2(\alpha\delta h_r)^{1/2}]; \quad R_j > 0 \quad (15)$$

The mean value of the complete distribution is then

$$\text{Ev}\,[R_j] = \int_0^\infty f(R_j)\,dR_j = 2(h_r/\alpha\delta)^{1/2}K_1[2(\alpha\delta h_r)^{1/2}] \quad (16)$$

We now obtain an expression for the expected value of seasonal surface runoff. By the assumption of independent r and t_r, $\alpha\delta$ may be replaced by the reciprocal of the mean storm depth, m_H^{-1}, in (16), that is,

$$\text{Ev}\,[R_j] = 2(h_r m_H)^{1/2}K_1[2(h_r/m_H)^{1/2}] \quad (17)$$

Summing the random variable R_j over the random number of rainstorms per season, v, defines the seasonal surface runoff R_s:

$$R_s = \sum_{j=1}^{v} R_j \quad (18)$$

and its expected value, $\text{Ev}\,[R_s]$, is given by

$$\text{Ev}\,[R_s] = m_v\,\text{Ev}\,[R_j] \quad (19)$$

In the same manner we express the total rainfall per season in terms of the individual storm depths as

$$P_s = \sum_{j=1}^{v} h_j \quad (20)$$

of which the expected value $\text{Ev}\,[P_s]$ is given by

$$\text{Ev}\,[P_s] = m_{P_s} = m_v m_H \quad (21)$$

Finally, by using (17) and (21), we write (19) as

$$\text{Ev}\,[R_s] = 2(h_r m_v/m_{P_s})^{1/2}K_1[2(h_r m_v/m_{P_s})^{1/2}]m_{P_s} \quad (22)$$

Thus far, we have the relationship between the expected values of seasonal surface runoff and rainfall provided by (22). In the manner of *Eagleson* [1978g] the relationship between the seasonal values themselves is given in a first-order approximation as

$$R_s = 2(h_r/\bar{h}_s)^{1/2}K_1[2(h_r/\bar{h}_s)^{1/2}]P_s \quad (23)$$

The variation of the surface runoff function R_s/P_s with the initial abstraction h_r for selected values of the average storm depth in the season, $\bar{h}_s$, is illustrated in Figure 8.

Seasonal Streamflow

In our conceptual model of the hydrologic processes in mountainous areas, deep percolation occurs only through fractures which collect moisture from surface runoff, that is, from overland flow and/or channel flow. We also assume no evaporative losses from surface runoff. Therefore in this case, surface runoff is equal to water yield. Taking this fact into account, and by definition of water yield, the seasonal streamflow Q_s, as measured at the base of the mountain, is

$$Q_s = R_s - G_s \quad (24)$$

where R_s and G_s are the seasonal surface runoff and groundwater runoff, respectively.

By making the simplifying assumption that all variation in Q_s comes from variation in precipitation, we will consider G_s to be fixed at its long-term effective value G, and (24) becomes

$$Q_s = R_s - G \quad (25)$$

This equation, with R_s given by (23), provides an analytical model to estimate the seasonal streamflow in terms of the seasonal rainfall P_s, the average storm depth in the season, $\bar{h}_s$, and the unknown parameters of the hydrologic process, namely, the space and time effective initial abstraction h_r and the long-term effective seasonal groundwater runoff, or mountain front recharge, G.

Mean Seasonal Water Balance

The change in soil moisture storage is usually neglected in the mean annual water balance. If this change is considered small for a particular rainy season, it is assumed that the system is stationary in the mean, and because surface runoff is assumed equal to water yield in our case, the water balance is expressed as

$$\text{Ev}\,[P_s] = \text{Ev}\,[E_{T_s}] + \text{Ev}\,[R_s] \quad (26)$$

where

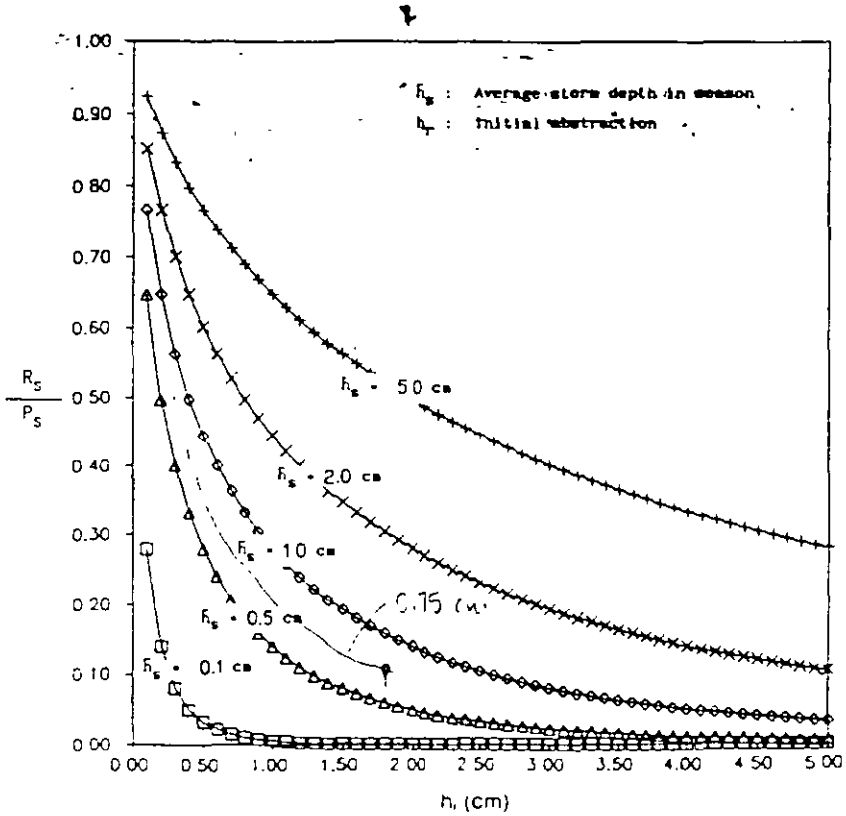

Figure 8. Plot of surface runoff function.

$E_V[\ ]$ expected value of $[\ ]$,
P_s seasonal precipitation,
E_s seasonal evapotranspiration,
R_s seasonal surface runoff.

The expected value of seasonal surface runoff can be calculated by (22). On the other hand, *Eagleson* [1978d] derived the expected value of seasonal evapotranspiration in terms of soil and vegetation properties, potential evapotranspiration, and the known distributions of storm depth and time between storms. In the appendix a modification of the Eagleson expression for the interstorm bare soil evaporation is presented (equations (A1)–(A3)), where in view of our conceptualization of the hydrologic processes in hard rock terrain, capillarity rise from the water table is neglected. The expected value of seasonal evapotranspiration can be computed by (A7).

Eagleson selected a gamma distribution for the storm depth in the derivation of the expected value of seasonal evapotranspiration. This distribution is inconsistent with the exponential distributions of storm intensity and storm duration that, for analytical tractability, were assumed to derive the relationship between mean seasonal surface runoff and rainfall (equation (22)). However, this inconsistency should be of minor practical relevance in the general case. Furthermore, it must be emphasized that (26) will be used in combination with a relationship provided by the "vegetal equilibrium hypothesis" in order to obtain an estimate of effective initial abstraction that is intended to serve only as prior information in the procedure for stochastic parameter estimation introduced in paper 2.

Vegetal Equilibrium Hypothesis

If the surface retention capacity and the climatic and vegetation parameters are known, the evaporation parameter E in (A7) remains to be determined. This parameter is also called the bare soil evaporation effectiveness and represents the relative importance of soil properties in the dynamics of exfiltration. Equation (22) involves the space- and time-effective initial abstraction h_r, a soil-related parameter which also remains to be evaluated. Consequently, the water balance equation (26) includes E and h_r as unknown parameters, and an additional relationship is necessary to solve for them. This relationship will be provided by the so-called "vegetal equilibrium hypothesis."

Although the dynamics of the climate-soil-vegetation system have been long recognized, the mechanism that drives the interaction among the components of the system has not been well understood. A remarkable contribution to bridge this conceptual gap was made by *Eagleson* [1978f] through the development of the vegetal equilibrium hypothesis. This hypothesis proposes that the natural vegetation density in a watershed will seek, through natural selection, an optimal "climax" value at which available soil moisture is a maximum. The hypothesis operates during the vegetal growing season and was reasonably verified by *Tellers and Eagleson* [1980] with data from 11 watersheds in humid and arid environments.

One practical implication of the vegetal equilibrium hypothesis is that it is possible, knowing the climate, to determine effective hydrologic properties of soils through

observations of the canopy cover density. This capability makes it useful in regional hydrologic studies.

The vegetal equilibrium hypothesis states that, in the short term, natural vegetation systems of a given plant coefficient k_{ϕ}, which is the ratio of potential rates of transpiration and soil surface evaporation, reach a "growth equilibrium" density $M = M_0$ at which the soil moisture is maximum because, at this state, stress is minimized. Maximum soil moisture is equivalent to minimum soil moisture loss by evapotranspiration. In practice, however, it is total evapotranspiration Ev $[E_T]$ that is minimized. Thus

$$\frac{\partial \text{ Ev } [E_T]}{\partial M} = 0 \qquad \text{at} \quad M = M_0 \tag{27}$$

VEHBAL Procedure

Modifying the computational procedure of *Tellers and Eagleson* [1980], the evaporation parameter E and the initial abstraction h_r are estimated through the water balance equation (equation (26)) and the relationship provided by the vegetal equilibrium hypothesis (equation (27)) in the following sequential process, which for future reference we will call VEHBAL:

1. Pick a value for the evaporation parameter E and use (A7) to calculate seasonal evapotranspiration Ev $[E_T]$ for different values of M until (27) is minimized. If the vegetation density obtained is not equal to the observed value M_0, E is incremented and a new M is found. Once the process converges, both E and Ev $[E_T]$ are determined.
2. Pick a value for the initial abstraction h_r and calculate seasonal precipitation P_s through (26) and (22), using the value of Ev $[E_T]$ previously determined. If P_s is not equal to the mean seasonal precipitation m_{P_s}, the value of h_r is changed and a new computed precipitation is obtained. Once this process converges, h_r is determined.

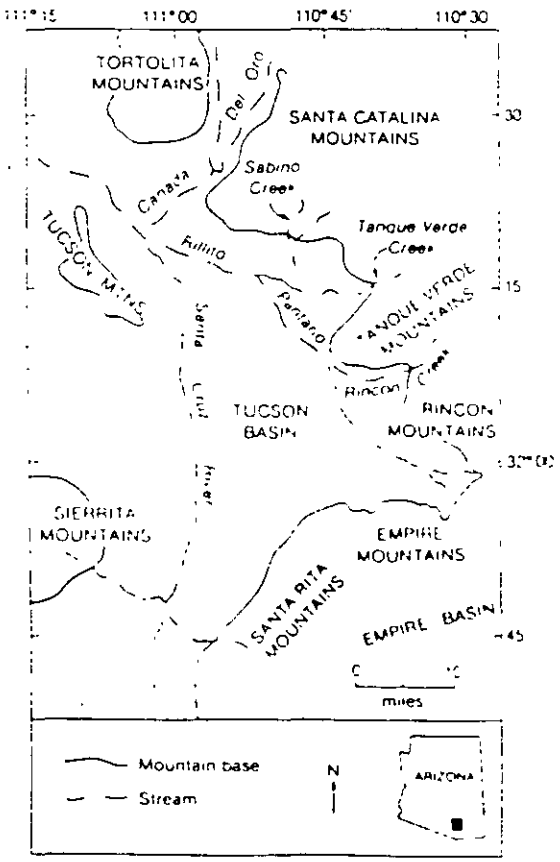

Figure 9. Location of study area

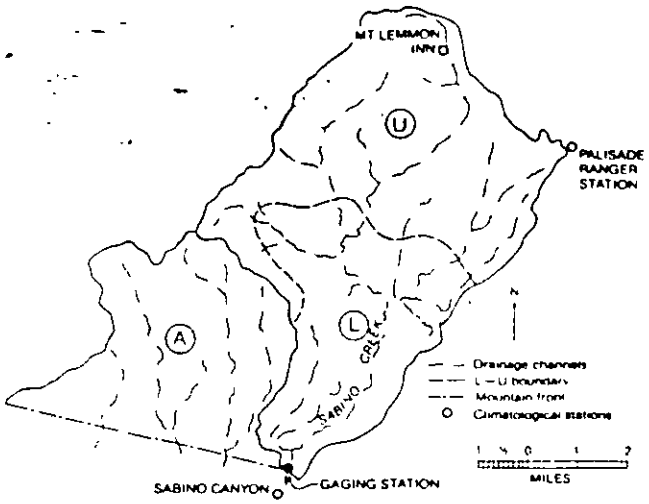

Figure 10. Lower slopes (L) and tops of the mountain (U) in Sabino Creek Watershed and its adjacent mountainous area (A).

Application to a Mountainous Watershed

Effective soil-related parameters are estimated jointly with mean seasonal evapotranspiration and surface runoff for the Sabino Creek watershed in southern Arizona. Inasmuch as the vegetal equilibrium hypothesis operates during the vegetal growing season, which for the perennial species of the mountainous areas in the Basin and Range Province of North America is the summer rainy season [*Shreve*, 1915], we restricted the estimation to this period, which in the study area extends over the months of July, August, and September. We also assumed that the change in soil moisture between the start and the end of this rainy season is negligible, so that (26) holds, and the VEHBAL procedure may be applied.

Sabino Creek drains a portion of the Santa Catalina Mountains (Figures 9 and 10), and its watershed extends from 2800 ft (853 m) at the outlet to over 9000 ft (2743 m) at the highest points. Two major subareas can be identified in this watershed, as well as in many other mountainous watersheds in the Basin and Range Province, namely, the lower slopes (L), characterized by relatively sparse xerophytic vegetation, and the tops of the mountain (U), characterized by evergreen woodlands and coniferous forests. The VEHBAL procedure was applied separately to each of these two major subareas.

The average rate of potential evapotranspiration was calculated for the period 1965–1974 using *Van Bavel*'s [1966] combination form of the *Penman* [1948] equation

$$\bar{e}_p = \frac{\bar{q}_i(1 - A) - \bar{q}_b + H}{\rho_w L_e (1 + \gamma/\Delta)} \tag{28}$$

in which

$\bar{q}_i$ average rate of insolation,
$\bar{q}_b$ average rate of net outgoing longwave radiation;

Table 1. Computation of Potential Evapotranspiration at Sabino Watershed (Summer Rainy Season)

Subarea	$\bar{T}_a$, °C	N	S	$\bar{q}_i$*	A	$\bar{q}_b$*	H*	$1 + \gamma/\Delta$	$\bar{e}_p$, cm d^{-1}
L	24 8	0.42	0 48	558	0.14	124	57	1.347	0.513
U	18 4	0 42	0 57	558	0 14	134	52	1.517	0 439

*Units are in calories per square centimeters per day

H average residual sensible heat flux,
A shortwave albedo of surface,
ρ_e mass density of liquid water, 1 g cm^{-3},
L_e latent heat of vaporization, 597 cal g^{-1},
γ/Δ atmospheric parameter, a function of atmospheric temperature.

The average rate of insolation was calculated from records at the University of Arizona in Tucson, compiled by *Hands and Durrenberger* [1976]. An albedo value of 0.14 was assigned to the rocky surface of the mountainous watershed [*Eagleson* 1970]. The net outgoing longwave radiation was estimated from *Eagleson* [1977] as

$$\bar{q}_b = (1 - 0.8N)(0.245 - 0.145 \cdot 10^{-10}\bar{T}_a^4) \text{ cal cm}^{-2} \text{ min}^{-1} \quad (29)$$

where N is seasonal fractional cloud cover, and $\bar{T}_a$ is the average seasonal atmospheric temperature in degrees kelvin. The average "drying power" H of the atmosphere was evaluated from *Eagleson* [1977]

$$H = \bar{q}_b/[0.25 + 1.01 - \bar{S})] \quad (30)$$

where $\bar{S}$ is the average fractional relative humidity.

In turn, the atmospheric parameter was calculated from *Eagleson* [1977]

$$\frac{1}{1 - \gamma/\Delta} = 0.42 + 0.013\bar{T}_a \quad (31)$$

with the average seasonal temperature in degrees Celsius.

The atmospheric temperature, cloud cover, and relative humidity were all obtained from National Weather Service (NWS) publications and averaged over the summer rainy season (July, August, and September). The climatological stations involved were Sabino Canyon, near the base of the mountain, and the high altitude station of Palisade Ranger (Figure 10). Representative values of temperature and relative humidity for subareas L and U were obtained by linear interpolation between both stations. Cloud cover observations were available at Sabino Canyon only, and the seasonal value at this station was assigned to both subwatersheds.

Precipitation at the same climatological stations was also obtained from NWS publications. *Duckstein et al.* [1973] reported an approximate linear increase of mean seasonal precipitation with elevation on the Santa Catalina Mountains, and linear interpolation was employed to assign representative values of mean total precipitation to subareas L and U. Data involved in the computation of mean potential evapotranspiration are listed in Table 1.

Likewise, statistical parameters in (A1) were estimated for subwatersheds L and U from linearly interpolated mean values of the storm-related variables. Following *Tellers and Eagleson* [1980], a value of 0.1 cm was assumed for the surface retention capacity in both subwatersheds.

Vegetation coverage was reported by *Whittaker et al.* [1968] to be around 30–50% in deserts of the lower slopes of the Santa Catalina Mountains and 60–80% in woodlands of higher elevations. In this work we selected canopy density values of 40 and 70% for subareas L and U, respectively. Climatic and vegetation parameters at Sabino Creek Watershed are listed in Table 2.

With respect to the plant coefficient k_v, information is not available for the individual subwatersheds L and U. Thus we will approximate its value with the following procedure. *Eagleson and Tellers* [1982] derived a theoretical relationship between average evapotranspiration efficiency β and equilibrium canopy density M_0. The former is defined as the ratio of the average annual evapotranspiration to the average potential bare soil evaporation. By superimposing theoretical curves to the observations of M_0 and β at 11 watersheds covering a wide range of the arid-humid climatic spectrum, they found that the observations lay from slightly below the theoretical curve for $k_v = 0.60$ to slightly above the curve for $k_v = 1.00$.

Inasmuch as the plant coefficient tends to be smaller for plants of the arid zone, we applied the VEHBAL procedure selecting the values 0.55, 0.56, and 0.57 for subarea L and, more arbitrarily, the values 0.69, 0.70, and 0.71 for subarea U. The sensitivities of the mean summer evapotranspiration to vegetal canopy density at subarea L ($k_v = 0.55$) and subarea U ($k_v = 0.69$) are shown in Figures 11 and 12, respectively.

Results from the VEHBAL procedure are listed in Table 3 where, in particular, we notice a rather high sensitivity of the computed initial abstractions to the plant coefficient k_v. In general, this coefficient is difficult to evaluate with a high accuracy for most of the individual watersheds or subwatersheds. The uncertainty of the initial abstraction can be assessed by specifying realistic upper and lower limits of k_v for each case under consideration.

In paper 2 a stochastic parameter estimation approach which relies on streamflow data and incorporates prior information about the model parameters will be introduced. This procedure will be applied to our model of seasonal streamflow (equation (25)) to obtain improved estimates of the initial abstractions $h_{v,L}$ and $h_{v,U}$ along with mountain front recharge G. These estimates can then be used to adjust

Table 2. Climatic and Vegetation Parameters at Sabino Watershed (Summer Rainy Season)

Subarea	$m_{p,v}$, cm	$\bar{h}_{i,v}$, cm	$\bar{e}_{p,v}$, cm d^{-1}	κ	β, d^{-1}	$m_{s,v}$, days	M_0
L	20 57	0.75	0 513	0 64	0 360	92	0 40
U	28 10	1.02	0.439	0 74	0 360	92	0 70

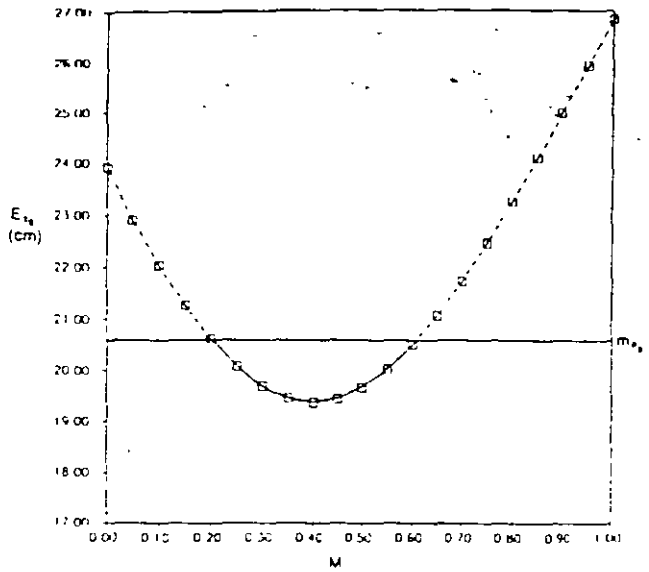

Figure 11. Sensitivity of mean summer evapotranspiration to vegetal canopy density at subwatershed L.

the mean seasonal values of the water balance components computed here. In the context of this stochastic approach for parameter estimation, the values of $h_{,L}$ and $h_{,U}$, obtained through the VEHBAL procedure, are regarded as prior estimates, the uncertainties of which are incorporated into the formulation. We will apply this approach by introducing each of the nine combinations of $h_{,L}$ and $h_{,U}$ values shown in Table 3 as prior information about the initial abstractions and selecting the "best" combination based on consistency with the rest of prior data and using the analysis of the stochastic properties of the estimators.

Conclusions

1. An analytical model of the mean seasonal surface runoff was developed through a derived-distribution approach where the input variables are considered to be stochastic and their probability distributions are transformed into the probability distribution of the output variable by using the deterministic physical process.

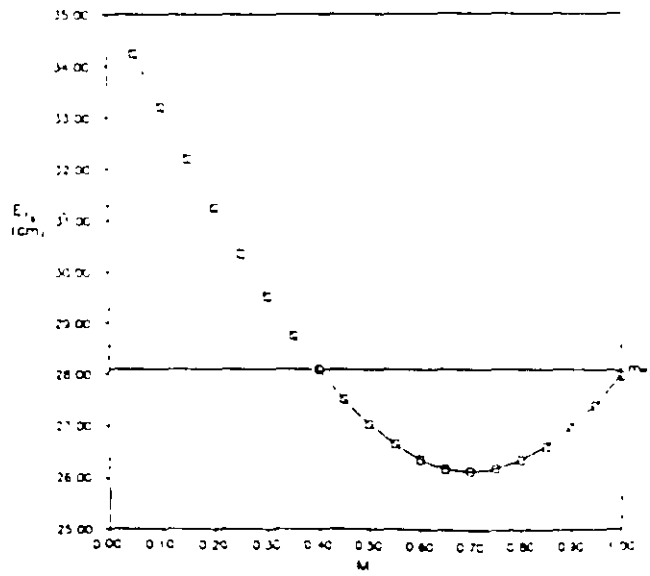

Figure 12. Sensitivity of mean summer evapotranspiration to vegetal canopy density at subwatershed U.

Table 3. Application of the VEHBAL Procedure to Sabino Watershed (Summer Rainy Season)

Subarea	k_c	$\bar{\epsilon}$	$h_{,}$, cm	$Ev[E_T]$, cm	$Ev[R_s]$, cm
L	0.55	0.18	1.70	18.67	1.90
L	0.56	0.19	1.95	19.03	1.54
L	0.57	0.20	2.29	19.38	1.19
U	0.69	1.20	2.78	26.13	1.97
U	0.70	1.25	3.14	26.49	1.61
U	0.71	1.31	3.67	26.89	1.22

2. The deterministic interface is provided by a model of surface runoff generation that should approximate many field situations, in particular, hard rock mountainous terrain where the permeability is secondary and fracture controlled.

3. A relationship between the seasonal surface runoff and precipitation was established on the basis of a first-order approximation to the relationship between their mean seasonal values.

4. In virtue of our conceptualization of the hydrologic processes occurring in hard rock mountainous areas, surface runoff equals water yield, and an analytical model of the seasonal streamflow, as measured at the base of the mountain, was derived directly from the definition of water yield. In this model the initial abstraction and the long-term effective subsurface outflow, or mountain front recharge, are viewed as unknown model parameters.

5. A numerical procedure that enables the estimation of mean seasonal evapotranspiration and surface runoff jointly with the evaporation parameter and initial abstraction was introduced. This procedure, called VEHBAL, combines the water balance equation with a relationship provided by the "vegetal equilibrium hypothesis."

The VEHBAL procedure was applied to Sabino Creek watershed in southern Arizona for the lower slopes and the tops of the mountain separately, inasmuch as the contrast in vegetation type and slope between these two major subareas should determine different soil-related hydrologic properties.

6. The output from the VEHBAL procedure exhibits a rather high sensitivity to the plant coefficient k_c, which, in the general case, is difficult to evaluate with a high degree of accuracy. The estimate of effective initial abstraction obtained here can be improved through the procedure for parameter estimation presented in paper 2. This procedure enables the incorporation of prior information about the model parameters and provides the stochastic properties of the estimators.

7. An analytical model of seasonal streamflow for the winter season that considers surface runoff generation by both rainfall and snowmelt remains to be developed in agreement with our general approach. We observe, however, that the "vegetal equilibrium hypothesis" could not be invoked in this case to obtain prior estimates of soil-related parameters because the hypothesis does not operate during the dormant season of species.

Appendix

Evapotranspiration from natural surfaces is composed of evaporation from bare soil and transpiration from vegetation. *Eagleson* [1978d] derived the expected value of seasonal evapotranspiration in terms of soil and vegetation properties, potential evapotranspiration, and the known distributions of storm depth and time between storms. He first calculated the bare soil evaporation and vegetal transpiration for an interstorm period and then averaged over the rainy season. By using an exfiltration analogy to the Philip infiltration equation and selecting an exponential distribution for time between storms and a gamma distribution for storm depth, Eagleson obtained an expression for the expected values of bare soil evaporation in the interstorm period j, Ev $[E_S]$. By eliminating those terms that include capillarity rise from the water table because of our conceptualization of the hydrologic processes in mountainous terrain, that expression is written as

$$\begin{aligned}\text{Ev}\,[E_{s_j}] = {} & \frac{\beta}{\bar{e}_p}\,\frac{\gamma[\kappa,\ \lambda h_0]}{\Gamma(\kappa)} - \left[1 - \frac{\beta h_0/\bar{e}_p}{\lambda h_0}\right]^{-\kappa} \\ & \cdot \frac{\gamma[\kappa,\ \lambda h_0 + \beta h_0/\bar{e}_p]}{\Gamma(\kappa)}\, e^{-BE} \\ & \cdot \left\{1 - \frac{\gamma[\kappa,\ \lambda h_0]}{\Gamma(\kappa)}\right\} \\ & \{1 - e^{-BE - \beta h_0/\bar{e}_p}[1 + Mk_v + (2B)^{1/2}E] \\ & + e^{CE - \beta h_0/\bar{e}_p}[Mk_v + (2C)^{1/2}E] \\ & + (2E)^{1/2} e^{-\beta h_0/\bar{e}_p}[\gamma(3/2,\ CE) - \gamma(3/2,\ BE)]\} \\ & + \left[1 - \frac{\beta h_0/\bar{e}_p}{\lambda h_0}\right]^{-\kappa} \frac{\gamma[\kappa,\ \lambda h_0 + \beta h_0/\bar{e}_p]}{\Gamma(\kappa)} \\ & \cdot \{(2E)^{1/2}[\gamma(3/2,\ CE) - \gamma(3/2,\ BE)] \\ & + e^{-CE}[Mk_v + (2C)^{1/2}E] \\ & - e^{-BE}[Mk_v + (2B)^{1/2}E]\end{aligned} \tag{A1}$$

where

$$B = \frac{1 - M}{1 - Mk_v} + \frac{M^2 k_v}{2(1 - Mk_v)^2} \tag{A2}$$

$$C = \frac{1}{2}(Mk_v)^2 \tag{A3}$$

in which

- $\bar{e}_p$ long-term average rate of potential evapotranspiration,
- M vegetation canopy density,
- k_v plant transpiration coefficient
- E evaporation parameter,
- β reciprocal of mean time between storms,
- κ parameter of gamma distribution of storm depth,
- λ parameter of gamma distribution of storm depth,
- h_0 surface retention capacity,
- $\Gamma(\ )$ gamma function,
- $\gamma(\ ,\ )$ incomplete gamma function

In turn, Eagleson expressed the expected value of vegetal transpiration in the interstorm period j, Ev $[E_{v_j}]$, as

$$\text{Ev}\,[E_{v_j}] = \frac{\bar{e}_p}{\beta}\,k_v \tag{A4}$$

where he assumed that transpiration is always at the potential rate $\bar{e}_p$ and that k_v reflects the effective area of transpiring leaf surface per unit of vegetated land surface, thus using it as an amplification factor to approximate the surface retention loss from vegetation

By weighting (A1) and (A4) according to the canopy density, the expected total interstorm evapotranspiration Ev $[E_{T_j}]$ is given by

$$\text{Ev}\,[E_{T_j}] = (1 - M)\ \text{Ev}\,[E_{s_j}] + M\ \text{Ev}\,[E_{v_j}] \tag{A5}$$

If v is the number of interstorm periods in a season, the seasonal evapotranspiration E_{T_s} is

$$E_{T_s} = \sum_{j=1}^{v} E_{T_j} \tag{A6}$$

of which the expected value is

$$\text{Ev}\,[E_{T_s}] = m_v\ \text{Ev}\,[E_{T_j}] \tag{A7}$$

where

$$m_v \equiv \text{Ev}\,[v] \tag{A8}$$

Notation

- A shortwave albedo of surface,
- $\bar{e}_p$ long-term average rate of evapotranspiration
- E evaporation parameter
- E_s soil moisture evaporation from bare soil fraction
- E_T total evapotranspiration
- E_{T_s} seasonal evapotranspiration
- E_v transpiration from vegetated fraction
- f infiltration capacity
- G long-term effective seasonal groundwater runoff (or mountain front recharge)
- G_s seasonal groundwater runoff
- h storm depth
- h_0 surface retention capacity,
- h_a space- and time-effective initial abstraction
- $\bar{h}_s$ average storm depth in a season
- H residual sensible heat flux
- i rainfall intensity,
- j counting variable for events,
- k_v plant coefficient,
- L_v latent heat of vaporization,
- m_H mean storm depth
- m_{P_s} average seasonal precipitation
- m_v mean number of storms per season,
- n_s mean length of rainy season
- M vegetation canopy density
- M_0 equilibrium vegetal canopy density
- N fractional cloud cover
- P_s seasonal precipitation,
- q_b net rate of outgoing longwave radiation,

q_i rate of insolation at surface
Q_s seasonal streamflow.
R region of integration.
R_s seasonal surface runoff.
S fractional relative humidity.
t time.
t_a time at which initial abstraction is satisfied.
t_b time between storms
t_r storm duration.
T_a atmospheric temperature
Z value of storm surface runoff.
α reciprocal of average rainstorm intensity
β reciprocal of mean time between storms.
δ reciprocal of average storm duration
γ/Δ atmospheric parameter
κ parameter of gamma distribution of storm depth
λ parameter of gamma distribution of storm depth.
ν counting variable for number of storms
ρ_e mass density of evaporating water.
$E_V[\ ]$ expected value of $[\ ]$
$\Gamma(\ )$ gamma function
$\gamma[\ ]$ incomplete gamma function
$K_0[\ ]$ Bessel function of order zero
$K_1[\ ]$ Bessel function of order one

Acknowledgments. The authors gratefully acknowledge the constructive comments and recommendations provided by P. C. D. Milly of the Geophysical Fluid Dynamics Laboratory (GFDL), Paul Hsieh of the U. S. Geological Survey, and Amado Guzman, Vijai Gupta, and Jene Michaud of the University of Arizona. Partial support was provided by the National Science Foundation under grants ECE-8610548 and BCS-8920851.

References

Adar, E., Estimation of recharge in a small southern Arizona basin by means of hydrological, hydrochemical, and environmental isotope data, Ph.D. dissertation, Dep. of Hydrol. and Water Resour., Univ. of Ariz., Tucson, 1984.

Belan, R. A., and W. G. Matlock, Groundwater recharge from a portion of the Santa Catalina Mountains, paper presented at Hydrology and Water Resources in Arizona and the Southwest, 1973 Meetings, Ariz. Sect. Am. Water Resour. Assoc. and Hydrol. Sect., Ariz. Sci. Acad., Tucson, Ariz., 1973.

Carrera, J., and S. P. Neuman, Estimation of aquifer parameters under transient and steady state conditions, 1, Maximum likelihood method incorporating prior information, *Water Resour. Res.*, 22(2), 199–210, 1986a.

Carrera, J., and S. P. Neuman, Estimation of aquifer parameters under transient and steady state conditions, 2, Uniqueness, stability, and solution algorithms, *Water Resour. Res.*, 22(2), 211–227, 1986b.

Chavez, A., S. Sorooshian, and S. N. Davis, Estimation of mountain front recharge to regional aquifers, 2, A maximum likelihood approach incorporating prior information, *Water Resour. Res.*, this issue.

Clapp, R. B., A wetting front model of soil water dynamics, Ph.D. dissertation, Dep. of Environ. Sci., Univ. of Va., Charlottesville, 1982.

Duckstein, L., M. M. Fogel, and J. L. Thames, Elevation effects on rainfall: A stochastic model, *J. Hydrol.*, *18*, 21–35, 1973.

Eagleson, P. S., *Dynamic Hydrology*, McGraw-Hill, New York, 1970.

Eagleson, P. S., Climate, soil, and the water balance: A framework for their analytical coupling, paper presented at the Tenth Annual John R. Freeman Memorial Lecture, Mass. Inst. of Technol., Cambridge, 1977.

Eagleson, P. S., Climate, soil, and vegetation, 1, Introduction to water balance dynamics, *Water Resour. Res.*, *14*(5), 705–712, 1978a.

Eagleson, P. S., Climate, soil, and vegetation, 2, The distribution of annual precipitation derived from observed storm sequences, *Water Resour. Res.*, *14*(5), 713–721, 1978b.

Eagleson, P. S., Climate, soil, and vegetation, 3, A simplified model of soil moisture movement in the liquid phase, *Water Resour. Res.*, *14*(5), 722–730, 1978c.

Eagleson, P. S., Climate, soil, and vegetation, 4, The expected value of annual evapotranspiration, *Water Resour. Res.*, *14*(5), 731–740, 1978d.

Eagleson, P. S., Climate, soil, and vegetation, 5, A derived distribution of storm surface runoff, *Water Resour. Res.*, *14*(5), 741–748, 1978e.

Eagleson, P. S., Climate, soil, and vegetation, 6, Dynamics of the annual water balance, *Water Resour. Res.*, *14*(5), 749–764, 1978f.

Eagleson, P. S., Climate, soil, and vegetation, 7, A derived distribution of annual water yield, *Water Resour. Res.*, *14*(5), 765–776, 1978g.

Eagleson, P. S., and T. E. Tellers, Ecological optimality in water-limited natural soil-vegetation systems, 2, Tests and application, *Water Resour. Res.*, *18*(2), 341–354, 1982.

Feth, J. H., Hidden recharge, *Ground Water*, *2*(4), 14–17, 1964.

Gallaher, B. M., Recharge properties of the Tucson Basin aquifer as reflected by the distribution of a stable isotope, M.S. thesis, Dep. of Hydrol. and Water Resour., Univ. of Ariz., Tucson, 1979.

Handy, R. M., and R. W. Durrenberger, Solar radiation and sunshine data for the southwestern United States, 1966–1974, report, State of Ariz. Sol. Energy Comm. and State Climatol. for Ariz., Phoenix, 1976.

Milly, P. C. D., An event-based simulation model of moisture and energy fluxes at a bare soil surface, *Water Resour. Res.*, *22*(12), 1680–1692, 1986.

Milly, P. C. D., and P. S. Eagleson, Parameterization of moisture and heat fluxes across the land surface for use in atmospheric general circulation models, *Tech. Rep. 279*, Dep. of Civ. Eng., Mass. Inst. of Technol., Cambridge, 1982.

Olson, M. C., Mountain-front recharge to the Tucson Basin from Tanque Verde Canyon, Arizona, M.S. thesis, Dep. of Hydrol. and Water Resour., Univ. of Ariz., Tucson, 1982.

Penman, H. L., Natural evaporation from open water, bare soil, and grass, *Proc. R. Soc. London A*, *193*, 120–145, 1948.

Shreve, F., The vegetation of a desert mountain range as conditioned by climatic factors, *Publ. 217*, Carnegie Inst. of Wash., Washington, D. C., 1915.

Simpson, E. S., D. Thourud, and I. Friedman, Distinguishing seasonal recharge to groundwater by deuterium analysis in southern Arizona, paper presented at World Water Balance, the Reading Symposium, Int. Assoc. of Sci. Hydrol., Reading, England, July 1970.

Tellers, T. E., and P. S. Eagleson, Estimation of effective hydrologic properties of soils from observations of vegetal density, *Rep. 258*, 126 pp., Ralph M. Parsons Lab., Dep. of Civ. Eng., Mass. Inst. of Technol., Cambridge, 1980.

Thorne, D. P., A chemical and isotopic study of groundwater flow in the Tucson Mountains, Arizona, M.S. thesis, Dep. of Hydrol. and Water Resour., Univ. of Ariz., Tucson, 1982.

Van Bavel, C. H. M., Potential evaporation: The combination concept and its experimental verification, *Water Resour. Res.*, *2*(3), 455–467, 1966.

Whittaker, R. H., S. W. Buol, W. A. Niering, and Y. H. Havens, A soil and vegetation pattern in the Santa Catalina Mountains, Arizona, *Soil Sci.*, *105*, 440–449, 1968.

Wilson, L. G., K. J. DeCook, and S. P. Neuman, Regional recharge research for southwest alluvial basins, final report, Water Resour. Res. Cent., Univ. of Ariz., Tucson, 1980.

A. Chavez, Facultad de Ingeniería, Universidad Autonoma de Chihuahua, Apartado Postal 1528 C, Chihuahua, Chih. 31160, Mexico.

S. N. Davis and S. Sorooshian, Department of Hydrology and Water Resources, University of Arizona, Tucson, AZ 85721.

(Received August 19, 1993; revised November 15, 1993; accepted November 29, 1993.)

FACULTAD DE INGENIERIA U.N.A.M.
DIVISION DE EDUCACION CONTINUA

CURSOS ABIERTOS

XII CURSO INTERNACIONAL DE CONTAMINACIÓN DE ACUÍFEROS

MODULO III: MODELOS MATEMÁTICOS EN GEOHIDROLOGIA Y CONTAMINACIÓN DE ACUIFEROS

TEMA

GROUN – WATER MODELING IN A SOUTHWESTERN ALLUVIAL BASIN

EXPOSITOR: DR. ADOLFO CHAVEZ RODRIGUEZ
PALACIO DE MINERIA
OCTUBRE DEL 2000

Ground-Water Modeling in a Southwestern Alluvial Basin

by David B. Hawkins[a] and Daniel B. Stephens[b]

ABSTRACT

A two-dimensional finite-difference computer code was used to model the ground-water flow system in an alluvial basin in southwest New Mexico. A three-step approach was used to determine the transmissivity distribution for the model. First, values of the natural logarithm of transmissivity (ln T) were interpolated from existing data using the kriging technique. This interpolation scheme also produced a map of standard deviations of the kriging errors. Second, a conventional flow net was drawn from steady-state water levels with the aid of the kriged hydraulic head distribution. Third, the approximate transmissivity map, the standard deviation map of the kriged ln T values, and the flow net were used to select the segment of each stream-tube where transmissivity was known with greatest certainty (smallest ln T kriging error). Then, transmissivities for other segments of the stream tubes were calculated from Darcy's Law. This distribution, when input to the numerical model, did not have to be altered appreciably during the calibration for a steady-state and seven-year transient period. Most of the transient calibration was accomplished by adjusting storage coefficients. Considering the uncertainty in the available pumping data, very good agreement was found between observed and predicted water levels during a four-year model verification period.

INTRODUCTION

This paper focuses on the application of a numerical ground-water flow model to part of a southwestern alluvial basin. The model study emphasizes the parameter estimation and calibration process. In particular, we discuss the application of a flow net and a stochastic interpolation scheme called kriging to determine the distribution of transmissivities to be used as input to the model. Calibration was by the trial-and-error approach.

SETTING

This study area is located in Animas Valley, Hidalgo County, New Mexico, in the southwestern corner of the State (Figure 1). The part of the basin selected for investigation is the Lower Animas Valley which lies approximately between the village of Animas and Interstate Route 10, and between the Pyramid and Peloncillo Mountains.

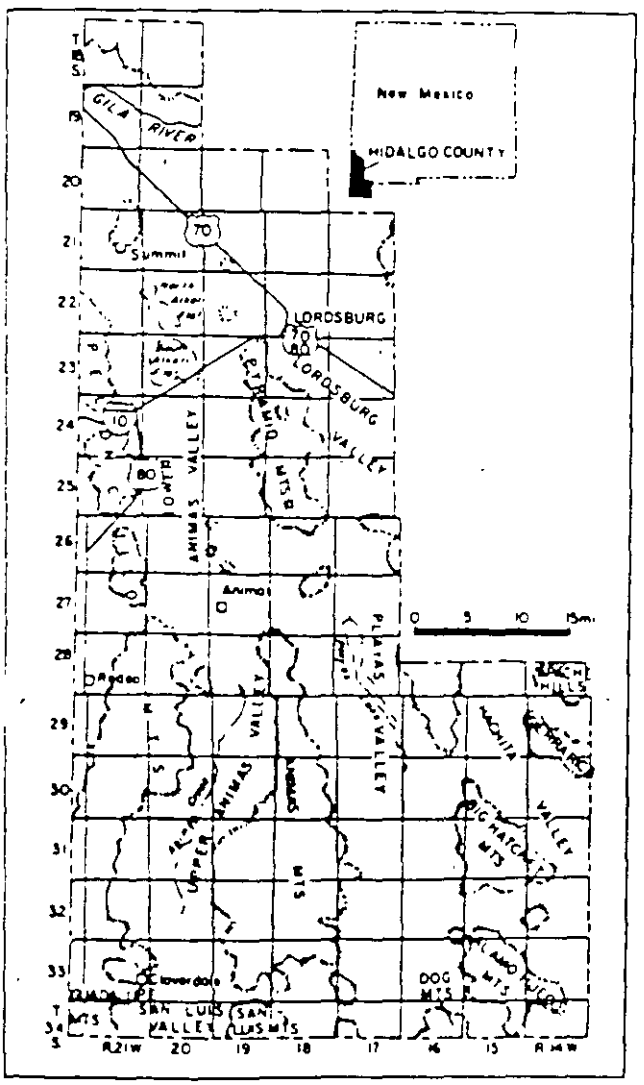

Fig. 1. Location map.

[a]Hydrologist, Hargis and Montgomery, Inc., 1735 East Lowell Road, Tucson, Arizona 85719.

[b]Assistant Professor of Hydrology, New Mexico Institute of Mining and Technology, Department of Geoscience, Socorro, New Mexico 87801.

Received February 1983, revised July 1983, accepted July 1983.

Discussion open until May 1, 1984.

The model area also encompasses most of the Lightning Dock Known Geothermal Resource Area (KRGA) which is centered around the apparently localized expression of a geothermal system in the eastern part of Lower Animas Valley.

The climate is semiarid with an average annual rainfall of about 10 inches (25.4 cm) on the valley floor and more than twice this amount in parts of the surrounding mountain areas. There is no well-defined surface drainage in the broad, flat lower portion of the valley, although occasionally surface runoff reaches playas at the north end of the valley.

The structural basin which includes Animas Valley was apparently formed by Basin-and-Range type normal faulting during the Tertiary Period. Sediments shed from the rising mountain blocks were carried by an ancestral fluvial system to a lake in the north-central portion of the valley. Sedimentary facies in the unconsolidated portion of the sequence include fluvial, deltaic, and lacustrine deposition (Fleischhauer, 1977). Depth to well-consolidated bedrock in the basin varies from less than 85 feet (25.9 m) to more than 1890 feet below land surface.

Ground water occurs under unconfined conditions in most of the valley. A perched aquifer of poorly defined areal extent is present in the southernmost part of the model area and, locally, discontinuous clay layers may define small areas where there are confined conditions. In general, ground water flows northward between north-south trending low-permeable mountain blocks from a water table divide near the International Boundary, through Animas Valley, and toward the Gila River (Reeder, 1957). A large portion of the southern part of Lower Animas Valley has been irrigated with ground water since about 1948. Subsequently, water levels have declined appreciably over large areas. Recharge directly on the Lower Animas Valley bottom lands prior to irrigation was probably negligible. Some recharge from deep percolation of irrigation probably has occurred after 1948 although based on estimated rates of consumptive use by crops and water applications, there is little excess water available for recharge (Hawkins, 1981). Recharge to the Lower Animas Valley aquifer presumably occurs along portions of the mountain fronts having well-defined drainages and alluvial fans, and also by underflow from Upper Animas Valley. Conditions in the Upper Animas Valley are more favorable for ground-water recharge than in the Lower Animas Valley. The upper valley receives more precipitation and has a well-defined surface drainage system with permeable stream courses.

MODEL SELECTION

Our general objective in this investigation was to develop a calibrated ground-water flow model which would enable us to better understand the hydrogeology of the principal aquifer near the KGRA, as a first step in simulating long-term impacts due to geothermal development. After a review of available aquifer data it was felt that a three-dimensional treatment was not warranted, and therefore a two-dimensional finite-difference method was chosen. Although a number of computer codes are available to handle this type of problem, we selected the finite-difference model formulated by Trescott, Pinder, and Larson (1976), principally because it is well documented, and widely used.

PARAMETER ESTIMATION

To predict water-level changes due to continued irrigation or geothermal resource development, the spatial distribution of transmissivity and storage coefficients must be determined. In our approach this distribution was determined from a trial-and-error model calibration process. The number of adjustments can be minimized if aquifer characteristics are reasonably well known over a large part of the model area. However, in the Animas Valley, estimates of transmissivity are limited to results of 21 specific capacity tests concentrated in the irrigated central part of the valley and one aquifer pumping test (Figure 2). Using specific capacity to estimate transmissivity (Walton, 1970), it became obvious that there were

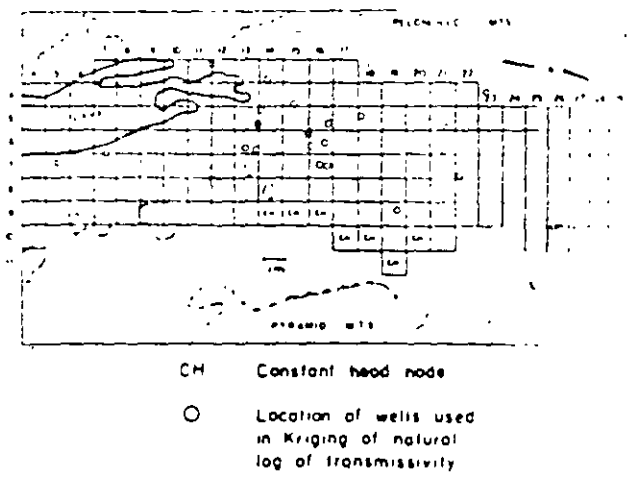

Fig. 2 Model grid and location of specific capacity and transmissivity measurements.

so field data with which to estimate transmissivity for grid blocks of the model over a large portion of the valley.

To estimate transmissivity in model grid ..cks where there are no data, a linear interpolation technique called kriging was employed (Delhomme, 1979; Gambolati and Volpi, 1979a, 1979b; and Binsariti, 1980).

A number of other interpolation schemes could have been used to estimate the transmissivity distribution. However, the kriging algorithm was chosen because it takes into account the spatial correlation structure of the existing data, and because it produces a map of the kriging error of the interpolated quantity. In order to use kriging, a semivariogram is constructed from field data. The semivariogram is a graph of the sample variance minus the autocovariance, $\gamma(h)$, versus distance between pairs of data points, h. Differences in transmissivity between any two wells may increase with increasing separation distance because of the nature of variability on the geologic materials. Thus $\gamma(h)$ often increases gradually and reaches a maximum, constant value with increasing h. The distance at which $\gamma(h)$ becomes constant, called the range, implies for example, that transmissivities ot correlated with each other over distances ing this value. If this rise is exponential, an integral scale is defined for kriging purposes as approximately one-third of the range.

The small number of aquifer test data and their localized distribution over the area of interest was considered inadequate to generate the semivariogram for kriging in T values. However, for two-dimensional phreatic aquifers, Gelhar (1976) relates the variance of the head distribution to the variance of the natural log of the transmissivity by the following equation (as rewritten by Delhomme, 1979),

$$\sigma_h = (2/\pi) \cdot \sigma_{lnT} \cdot \bar{h} \cdot I \cdot [\ln(1.15/I)]^{1/2} \qquad (1)$$

where

σ_h = standard deviation of hydraulic head (4.219 ft),

σ_{lnT} = standard deviation of natural log of transmissivity (0.7145),

I = $\beta\lambda/\bar{h}$,

β = the slope of the water table at its midpoint (0.0013),

$\bar{h}$ = mean saturated thickness at aquifer (300 ft assumed), and

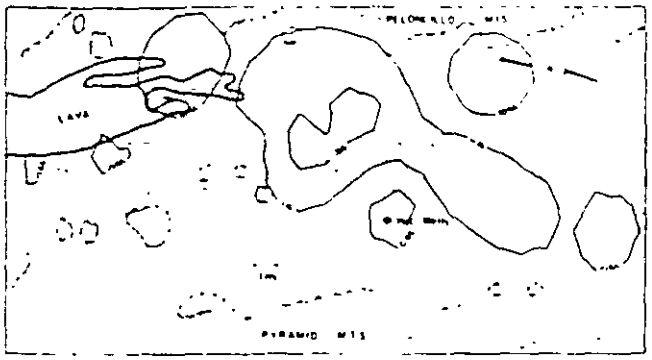

Fig. 3. Contours of ln T by kriging.

λ = integral scale of lnT process (i.e., about one-third the range of influence assuming an exponential variogram).

The range for lnT is approximately three times the integral scale, nearly two miles. Thus, our finite-difference grids of one square mile could reflect variability at this scale. Using a computer algorithm for the kriging process, contour maps of lnT and the kriging error were developed as shown in Figures 3 and 4, respectively. For details of the application of kriging to this study, refer to Hawkins (1981).

The kriged estimates of lnT in Figure 3 are independent of any information on transmissivity which can be inferred from the spacing of water-level elevation contours, although the kriged estimates of lnT are to some extent dependent on the head distribution through the head standard deviation and gradient as described above. To condition the distribution of lnT on the head distribution further, a flow net was constructed for steady-state conditions using data prior to 1948 in the irrigated

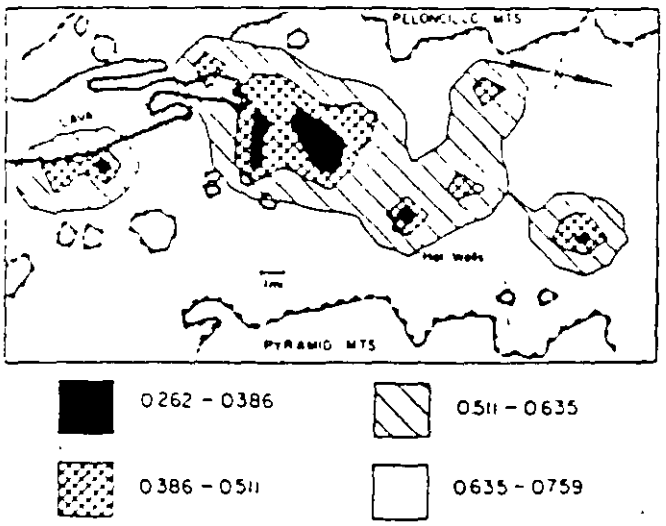

Fig 4 Kriging error in ln T.

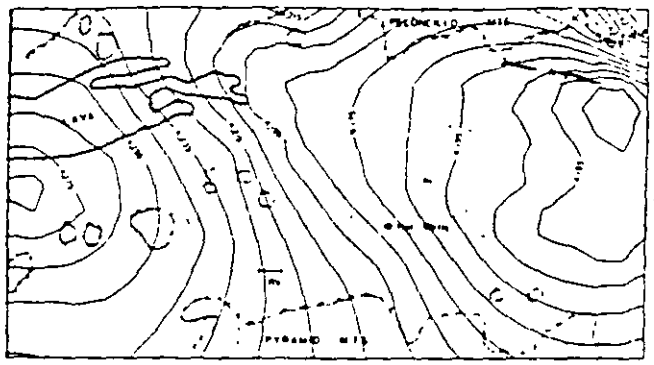

(Elevations in feet above mean sea level)

Fig. 5. Water-level elevations predicted by kriging.

areas, along with some subsequent data in areas which are relatively unaffected by irrigation pumping. The equipotential lines in the flow net were constructed by kriging 106 point measurements of steady-state hydraulic heads. In order to krige the steady-state hydraulic heads (Figure 5), the regional gradient of the head surface had to be taken into account because of a drift. The presence of drift implies that the degree of correlation between head measurements depends upon the direction and length of the separation distance vector. To remove this drift, planar surfaces were fitted to the data and then the residual head values were kriged. This method has been applied elsewhere (Sophocleous and others, 1982). Analysis of the resulting flow net revealed that the kriged values of hydraulic head were unreasonable in several peripheral portions of the basin where pre-irrigation head data were generally sparse. For example, in the southern area a ground-water mound is predicted where none should exist on the basis of hydrogeologic judgement. The same is true for the ground-water discharge area at the north end of the modeled area. As a result, the predicted water-level contour map (Figure 6) had to be modified to reflect more realistic conditions near recharge areas and impermeable boundaries (Figure 7).

To obtain the initial input estimates for transmissivity for the model grid (Figure 2), the flow net in Figure 6 was superimposed on the kriging error map of the InT process in Figure 4. The flow net interval within each streamtube which had the smallest kriging error was determined, and the corresponding average transmissivity from Figure 3 was assigned to this interval of the streamtube. Neglecting the effects of vertical recharge, the flow rate through each streamtube is constant under the assumed steady-state condition. Therefore, transmissivity for all other blocks in each of the stream-

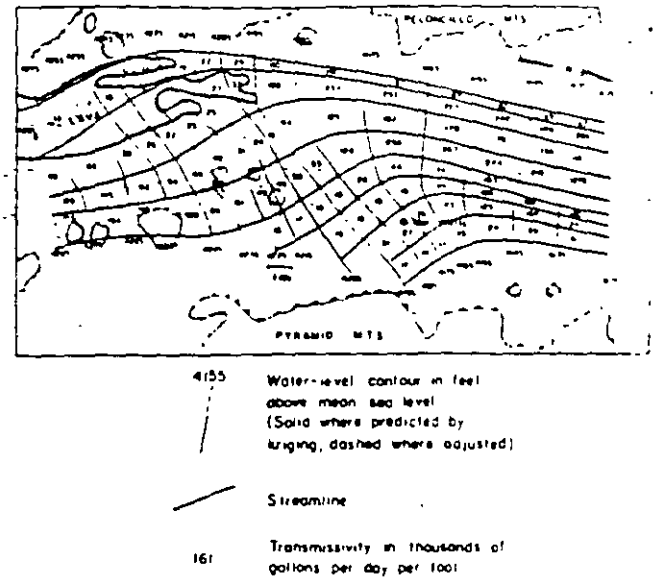

Fig. 6. Steady-state flow net.

tubes could be calculated simply from Darcy's Law. Finally, the finite-difference mesh (Figure 2) was superimposed on this transmissivity distribution and average values were assigned to each grid block by inspection (Figure 6).

The flow net analysis also aided in establishing boundary conditions for the model. For example, a constant flux rate was assigned at the southern end of the model at a reasonable distance from pumping influences. The same was done at the northern boundary, based on flow net calculations. Because of the difficulty in quantifying mountain-front recharge, the western and parts of the eastern boundaries were shifted toward the center of the basin to correspond with impermeable boundaries defined by the outer streamlines near the mountain fronts in Figure . Where the streamlines indicate mountain-front recharge, constant head boundaries were assigned, although if estimates of mountain front recharge were available, constant flux boundaries could have been assigned.

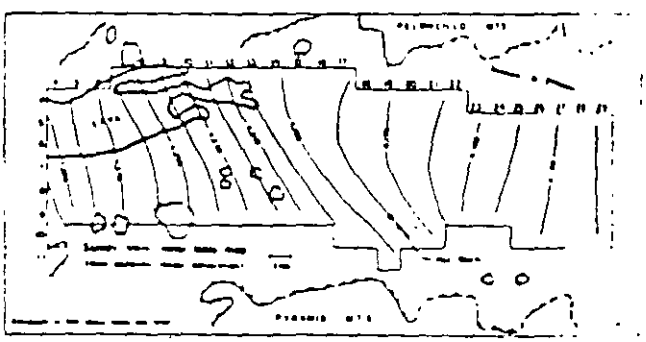

Fig. 7. Model predicted steady-state water-level elevations.

Because of the lack of information on the spatial distribution of storage coefficients, an initial estimate of 0.11 was assigned over the entire mesh. This value is based mostly on the estimate by Reeder (1957) who calculated the storage from pumping volumes and water-level decline. Storage coefficients were adjusted during calibration with transient water-level data.

Average pumping rates in irrigation wells were estimated from well discharge measurements and farmers' pumping duration records, and electrical power consumption (Reeder, 1957, 1960, 1961, 1962). Where actual discharge measurements were not available, pumpage was estimated from records of irrigated acreage in conjunction with estimates of water requirements for particular crops (Blaney and Hanson, 1965). The duration of the pumping season is normally from April through September (Reeder, 1957).

CALIBRATION RESULTS

Model calibration for steady-state conditions prior to irrigation involves adjusting only the transmissivities and boundary conditions until an acceptable agreement is reached between model predicted values and observed water-level elevations. However, the steady-state flow equation in the numerical model is actually the same as the one governing the rules used to construct the flow net. Thus, the steady-state hydraulic heads predicted by the numerical model with these initial transmissivity data should produce nearly the same heads as in the flow net. Only a few steady-state runs with minor adjustments to transmissivity were needed to produce the results shown in Figure 7. In comparison to observed water-level elevations in Figure 6, there is very good agreement in most areas. Some sources of error reflected in the model results are due mostly to small amounts of pumping in the valley which occurred prior to 1948, discretization in the flow net and numerical model to estimate transmissivity, specification of boundary conditions, and neglecting recharge on the valley floor.

The model was also calibrated for the irrigation period April 1948 to January 1955. The total pumpage estimated by Reeder was held constant during each irrigation season, although rates at some of the nodes were adjusted slightly. Boundary conditions were not altered in this step, and recharge from irrigation return flow was neglected. The transient calibration process was accomplished primarily by adjusting storage coefficients in each grid block. Transmissivity had to be adjusted in only a few blocks. The best results which could be obtained in this manner, after a minimal number of trials, are shown in Figure 8. The final maps of transmissivity and storage coefficients are shown in Figures 9 and 10, respectively. The lower values of transmissivity in the southern and eastern parts of the model and high values in the central areas are reasonably consistent with gravity survey interpretations which suggest the variations in transmissivity may be due mostly to changes in valley fill thickness (Smith, 1978, Wynn, 1981).

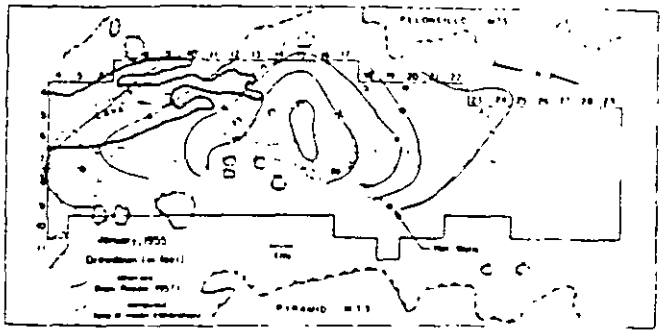

Fig. 8. Results of transient simulation.

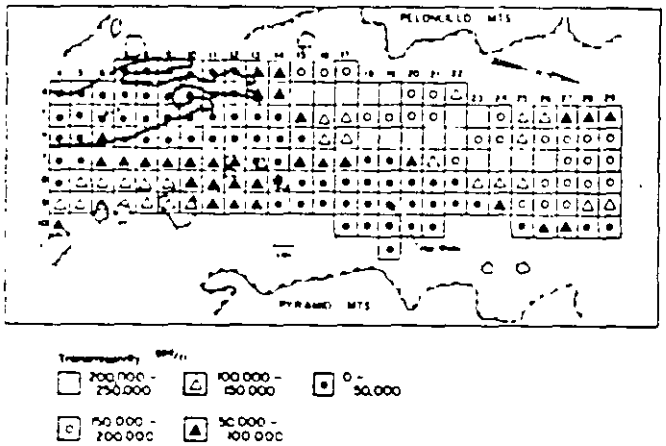

Fig. 9 Transmissivity distribution—after calibration.

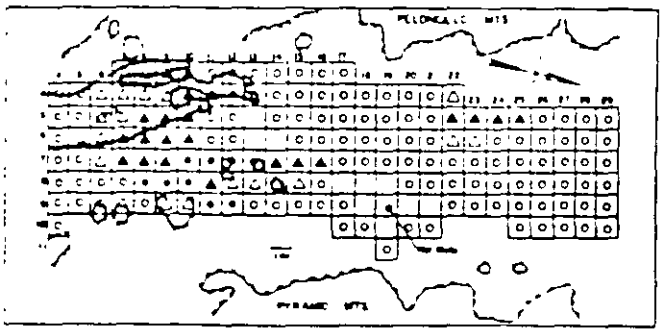

Fig. 10. Storage coefficient distribution—after calibration.

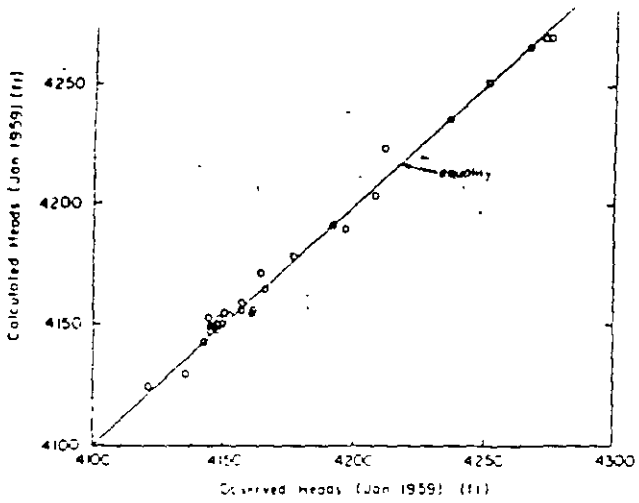

Fig 11. Comparison of predicted and observed water levels in wells, 1959

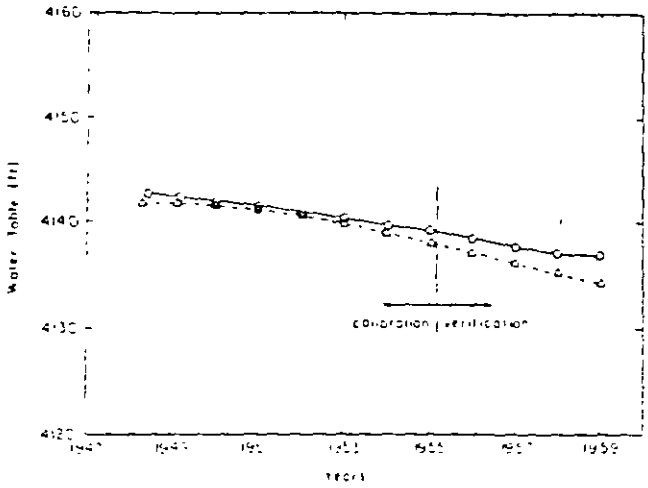

Fig. 12. Hydrograph of well in the north-central part of the model (Observed—Solid Line, Predicted—Dashed Line).

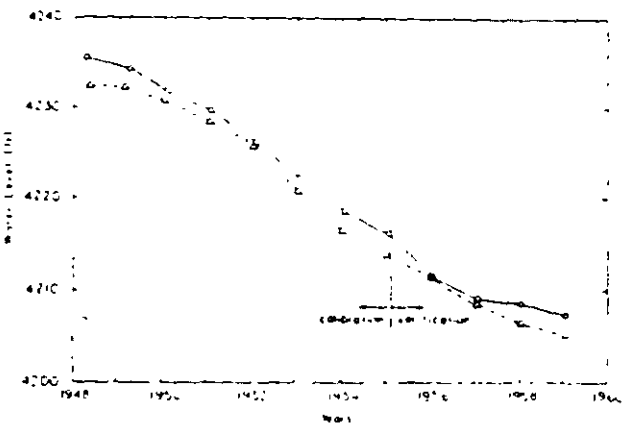

Fig 13. Hydrograph of a well just south of the heavily irrigated area (Observed—Solid Line, Predicted—Dashed Line).

Calibrating the model over a seven-year period left four years, January 1955 to January 1959, for the model verification period, because the distribution of pumpage in the valley could not be estimated with much confidence thereafter. During model verification, all aquifer coefficients were unchanged from the calibration process. Estimates of pumping rates input at each node for the four-year period were computed in the same manner as during the calibration process. The predicted water levels and observed water levels in wells for January 1959 are shown in Figure 11. The hydrographs of selected wells showing water levels in the nonpumping season from 1948 to 1959 are given in Figures 12-14. These and other results indicated that reasonably good predictions of future impacts due to ground-water development could be expected from the model, if accurate pumping-rate data are provided.

CONCLUSIONS

Using a conventional flow net in conjunction with kriging to predict the spatial distribution of transmissivity led to a minimization of computer effort to calibrate a two-dimensional, steady-state numerical model by the trial-and-error method. In retrospect, it is believed that the flow net analysis alone would have led to nearly the same results for this particular problem; however, our success may be problem-specific, inasmuch as large errors in estimating the spatial distribution of ln T from flow nets could occur where hydraulic head gradients are very low. The uncertainty prediction

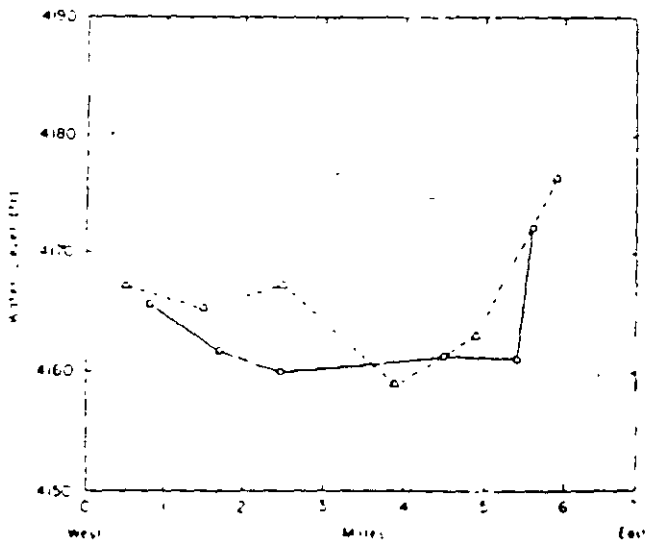

Fig 14. Water-level elevations in an east-west cross section through the pumping center in 1959 (Observed—Solid Line, Predicted—Dashed Line).

afforded by kriging could have been estimated qualitatively by examining the density and distribution of the data base. Kriging of ln T values may well prove valuable in situations where observed values are evenly distributed over the area of interest. In addition, one would have more confidence in the inferred spatial correlation structure of the data if it were much denser, in addition to being more evenly spaced. Of course, with a large number of closely-spaced, equidistant data points, the entire question of parameter estimation is somewhat moot.

A transient calibration was accomplished by trial and error for seven years of irrigation by adjusting storage coefficients, with only minor adjustments in transmissivity and pumping rate distributions.

Very good agreement was found in using the calibrated model to predict water levels during a four-year period following the calibration period. This was in spite of likely errors in total pumpage and the approximate methods used to assign pumping rates.

ACKNOWLEDGMENTS

The authors would like to thank Professors Lynn Gelhar and Allan Gutjahr for many helpful discussions. Funding for this project was provided by the U.S. Department of Energy through the New Mexico Energy Institute Low Temperature Geothermal Resource Assessment Program subcontract 14-23408-X1. Additional support was provided through the Geophysical Research Center at the New Mexico Institute of Mining and Technology.

REFERENCES

Binsariti, A. A. 1980. Statistical analyses and stochastic modeling of the Cretaro Aquifer in southern Arizona. Unpublished Ph. D. dissertation, University of Arizona. 243 pp.

Blaney, H. F. and E. G. Hanson. 1965. Consumptive use and water requirements in New Mexico. New Mexico State Engineer Technical Report 32. 82 pp.

Delhomme, J. P. 1979. Spatial variability and uncertainty in groundwater flow parameters: a geostatistical approach. Water Resources Research, v. 15, no. 2, pp. 269-280.

Fleischhauer, H. L., Jr. 1977. Quaternary geology of Lake Animas, Hidalgo County, New Mexico. New Mexico Institute of Mining and Technology, Master's Thesis. 149 pp.

Gambolati, G. and G. Volpi. 1979a. Groundwater contour mapping in Venice by stochastic interpolators, 1 theory. Water Resources Research, v. 15, no. 2, pp. 281-290.

Gambolati, G. and G. Volpi. 1979b. A conceptual deterministic analysis of the kriging technique in hydrology. Water Resources Research, v. 15, no. 3, pp. 625-629.

Gelhar, L. W. 1976. Effects of hydraulic conductivity variations on groundwater flows. Paper presented at Second International Symposium on Stochastic Hydraulics, International Association for Hydraulics Research, Lund, Sweden.

Hawkins, D. B. 1981. Geohydrology of the Lower Animas Valley, Hidalgo County, New Mexico: a computer simulation study. Unpublished Master's Degree Independent Study, New Mexico Institute of Mining and Technology.

Reeder, H. O. 1957. Groundwater in Animas Valley, Hidalgo County, New Mexico. New Mexico State Engineer Technical Report 11. 101 pp.

Reeder, H. O., ed. 1960. Ground-water levels in New Mexico, 1956. New Mexico State Engineer Technical Report 19. 251 pp.

Reeder, H. O., ed. 1961. Ground-water levels in New Mexico, 1957. New Mexico State Engineer Technical Report 22. 306 pp.

Reeder, H. O., ed. 1962. Ground-water levels in New Mexico, 1959. New Mexico State Engineer Technical Report 24. 125 pp.

Smith, Christian. 1978. Geophysics, geology and geothermal leasing status of the Lightning Dock KGRA, Animas Valley, New Mexico. New Mexico Geological Society Guidebook to the 29th Field Conference. pp. 343-348.

Sophocleous, M., J. E. Paschetto, and R. A. Olea. 1982. Ground-water network design for northwest Kansas, using the theory of regionalized variables. Ground Water, v. 20, no. 1, pp. 48-58.

Trescott, P. C., G. F. Pinder, and S. P. Larson. 1976. Finite-difference model for aquifer simulation with results of numerical experiments. Techniques of Water-Resources Investigations of the U.S. Geological Survey, Book 1, Chap. C1. 116 pp.

Walton, W. C. 1970. Groundwater Resource Evaluation. McGraw-Hill, New York. 666 pp.

Wynn, J. C. 1981. Complete Bouger gravity anomaly map of the Silver City 1° X 2° quadrangle, New Mexico-Arizona. U.S.G.S. Misc. Inv. Series, Map I-1310-A.

• • • • •

David B. Hawkins received a B.A. in Anthropology from the University of Arizona in 1975 and a B.S. in Applied Geology from Northern Arizona University in 1979. He completed an M.S. in Hydrology at New Mexico Institute of Mining and Technology in 1981. Currently employed by Hargis & Montgomery, Inc., his interests include application of geostatistical methods and contaminant transport studies.

Daniel B. Stephens obtained a B.S. in Geological Science at Pennsylvania State University in 1971, an M.S. in Hydrology at Stanford University in 1974, and a Ph.D. in Hydrology at the University of Arizona. During this period he also worked for a number of geotechnical consulting firms as a Hydrogeologist. At present, he is an Associate Professor of Hydrology at New Mexico Institute of Mining and Technology, where his research interests include mechanisms of natural ground-water recharge, seepage through the vadose zone, and hydraulic properties of mine and mill tailings.

FACULTAD DE INGENIERIA U.N.A.M.
DIVISION DE EDUCACION CONTINUA
CURSOS ABIERTOS

XII CURSO INTERNACIONAL DE CONTAMINACIÓN DE ACUÍFEROS

MODULO III: MODELOS MATEMÁTICOS EN GEOHIDROLOGIA Y CONTAMINACIÓN DE ACUIFEROS

TEMA

COMPUTER MODELS IN GROUND – WATER EXPLORATION

EXPOSITOR: DR. ADOLFO CHAVEZ RODRIGUEZ

PALACIO DE MINERIA
OCTUBRE DEL 2000

Computer Models in Ground-Water Exploration

by Irwin Remson[a], Steven M. Gorelick[b], and Julianne F. Fliegner[c]

ABSTRACT

Four case histories illustrate the various roles that digital computer simulation models can play in ground-water exploration. The case histories describe their use in evaluating aquifer parameters and characteristics, in estimating ground-water recharge, in resolving data inconsistencies, and in determining the optimal allocation of exploration funds. The models are especially useful in identifying data deficiencies and inconsistencies.

INTRODUCTION

Digital computer simulation models are employed extensively as predictive and management tools in ground-water investigations. While ultimately an aid to water planning, the computer simulation approach serves equally important functions in ground-water exploration.

The first advantage of model development is that it requires the investigator to determine and deal with data inadequacies. Second, construction of a model allows the hydrogeologist to test a conceptualized view of a complex ground-water system. Interaction with the model forces an accurate representation of system characteristics and checks assumptions regarding system functioning. Third, optimal allocation of exploration funds may be determined by incorporating the simulation model into a linear program and performing sensitivity analysis.

Four case histories are used to illustrate the various roles that such digital computer simulation models can play in ground-water exploration.

FOUR CASE HISTORIES

1. Estimating Aquifer Characteristics in the Palo Alto Baylands, California

The first case history describes the use of modeling in estimating aquifer parameters and characteristics in the Palo Alto Baylands, California. The area modeled is located on the southwestern margin of San Francisco Bay, California (Figure 1). A portion of this marsh in its natural state was the subject of a near-surface hydrogeologic investigation by Howland (1976). The study was intended to provide insight into the functioning of a tidal marsh ground-water system and to develop a ground-water model for use in marsh management.

The baylands are characterized by an intricate network of incised surface-water channels 3-5 ft (0.9 to 1.5 m) deep and 5 to 15 ft (1.5 to 4.6 m) wide. Shallow ground water is present in a 20-ft (6.1 m) thick layer of "bay mud," which consists of silty clay with lenses of sand, gravel, peat and shell fragments. Hydraulic information was obtained by installing a line of 5 to 10-ft (1.5 to 3-m) deep piezometers in the marsh deposits along

[a]Professor of Applied Earth Sciences and Geology, Stanford University, Stanford, California 94305.

[b]Research Assistant, Department of Geology, Stanford University, Stanford, California 94305.

[c]Former Graduate Student, Department of Geology, Stanford University, Stanford, California 94305.

Discussion open until March 1, 1981.

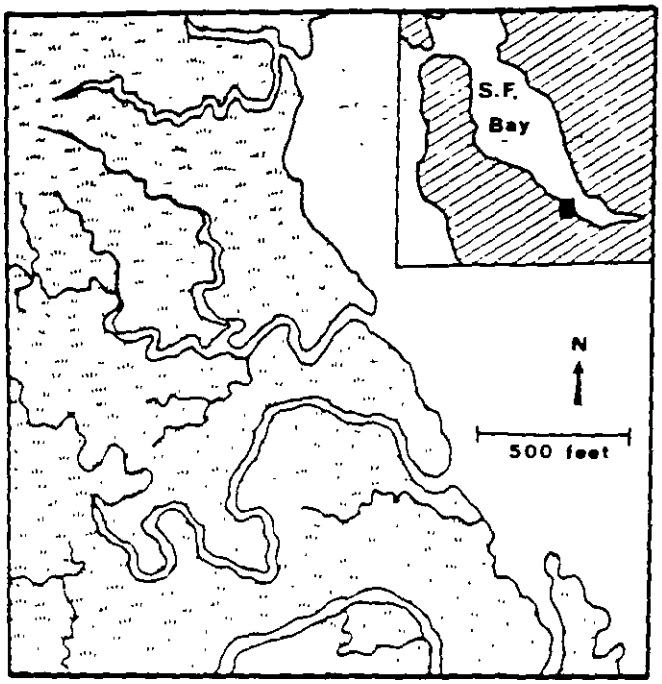

Fig 1. Surface-water channels in the Palo Alto Baylands, California.

a 30-ft (9.1-m) perpendicular to a main tidal channel. The piezometers were monitored for two days during a neap tide cycle. Water levels in the piezometers responded to the rise and fall of the channel stage

A computer model was prepared in an attempt to simulate the channel-marsh interactions as observed in the monitored wells. The hydrogeologic system was simulated as an unconfined aquifer discharging to and being recharged from the channel as the stage varied with the tide The one-dimensional finite difference model was based upon the Boussinesq equation, and was solved using a predictor-corrector technique. Expressed in nondimensional form, the model equations included two unknown parameters The first parameter corresponded to the ratio of hydraulic conductivity to storage coefficient, and the second parameter corresponded to the thickness of the permeable sediments

The hydraulic parameters were varied systematically in an attempt to simulate observed water levels. Best results were obtained using an effective thickness of 2.5 ft (0.76 m) for the permeable layer and 1,350 ft (412 m) per day for the ratio of hydraulic conductivity to storage coefficient. Assuming a typical storage coefficient range of between 0.1 and 0.3, the above ratio would indicate a large hydraulic conductivity (between 135 and 405 ft (41.2 and 123.6 m) per day) for the sediments in the permeable layer Because of this anomalous result, sampling of the uppermost 3 ft (0.91 m) of the bay mud was undertaken. It showed a dense system of root channels up to 0.2 in. (5 mm) in diameter It is likely that the large hydraulic conductivity is a result of ground-water piping along these root channels. Finally, the observed water-level fluctuations were less than the simulated water-level fluctuations at distances greater than 6 to 8 ft (1.8 m to 2.4 m) from the channel This suggested that the thickness of permeable sediments becomes less than the assumed 2.5 ft (0.8 m) at those distances. Field excavations verified that the permeable layer is indeed wedge-shaped, thinning away from the channel.

The model results alerted the investigator to the need for re-evaluation of certain field characteristics of the ground-water system. This led to a realization of the importance of piping along root channels in the channel-marsh hydrogeologic system. In fact, it is possible that a rigorous predictive model might have to consider non-Darcian flow as a result of ground-water piping. Finally, the hypothesis and subsequent field validation of the thinning of the permeable zone with distance from the channel was guided by the model results.

2. Determining Ground-Water Recharge in the San Jacinto Valley, California

The second case history describes the use of a model to estimate ground-water recharge in the San Jacinto Valley, California. Figure 2 shows the San Jacinto Valley, California (Fliegner, 1978). It is a graben that has been downfaulted along the San Jacinto fault on the northeast and the Casa Loma fault on the southwest. Bedrock rises to over 8,000 ft (2,440 m) above the valley floor in

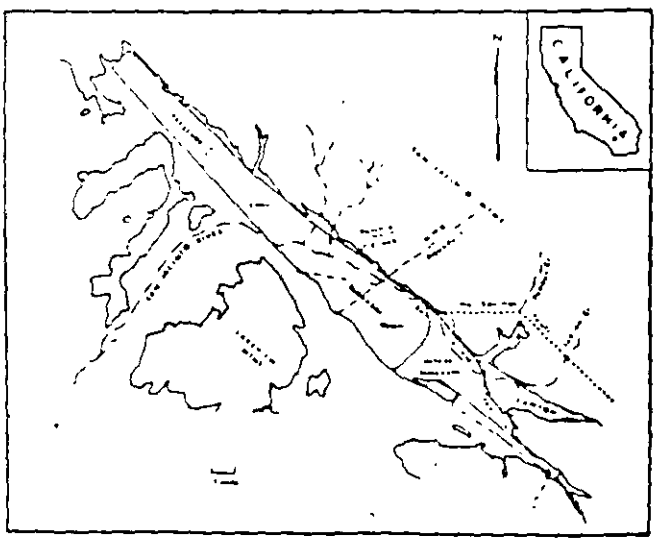

Fig. 2. Ground-water subbasins in the San Jacinto Valley.

the San Jacinto Mountain block to the northeast. Bedrock in the valley is as much as 8,000 ft (2,440 m) below the land surface. An excellent ground-water supply is found in the unconsolidated Quaternary alluvium that fills the graben to a depth of up to 2,000 ft (610 m).

At various times during its Quaternary history, the valley bottom was covered by a lake, where clay settled and formed a seemingly continuous layer over the Lower and Upper Pressure Subbasin shown in Figure 2. Fine sediments in the uppermost 150 to 200 ft (46 to 61 m) create artesian conditions. It has been the accepted view that stream infiltration and leakage to ground water do not occur in the Pressure Subbasin. Instead, all ground-water recharge was believed to occur by infiltration from streams flowing in the Intake Subbasin.

A preliminary two-dimensional finite difference model was prepared using the Illinois State Water Survey Code (Prickett and Lonnquist, 1971). It had no leakage in the Pressure Subbasin. Within a few years after the start of pumping, the simulated water levels were hundreds of feet below the historical water levels. A mass water balance was then prepared. Because the water deficiency was great and because the recharge in the Intake Subbasin was known, the model could be satisfied only if substantial leakage occurred in the Pressure Subbasin. Therefore, a revised model was prepared incorporating leakage in the Pressure Subbasin, and it successfully reproduced the historical water levels.

The partial differential equation incorporated into the digital computer code used for the San Jacinto study requires that the conservation of water mass be satisfied. The assumption of zero ground-water recharge as leakage in the Pressure Subbasin left a large deficit in the mass water balance when compared with the large ground-water discharge. The resulting excessive decline in ground-water levels was readily identified when comparisons were made with the historic water levels. Once the problem was recognized, the leakage in the Pressure Subbasin was easily determined because all other values in the water balance were known.

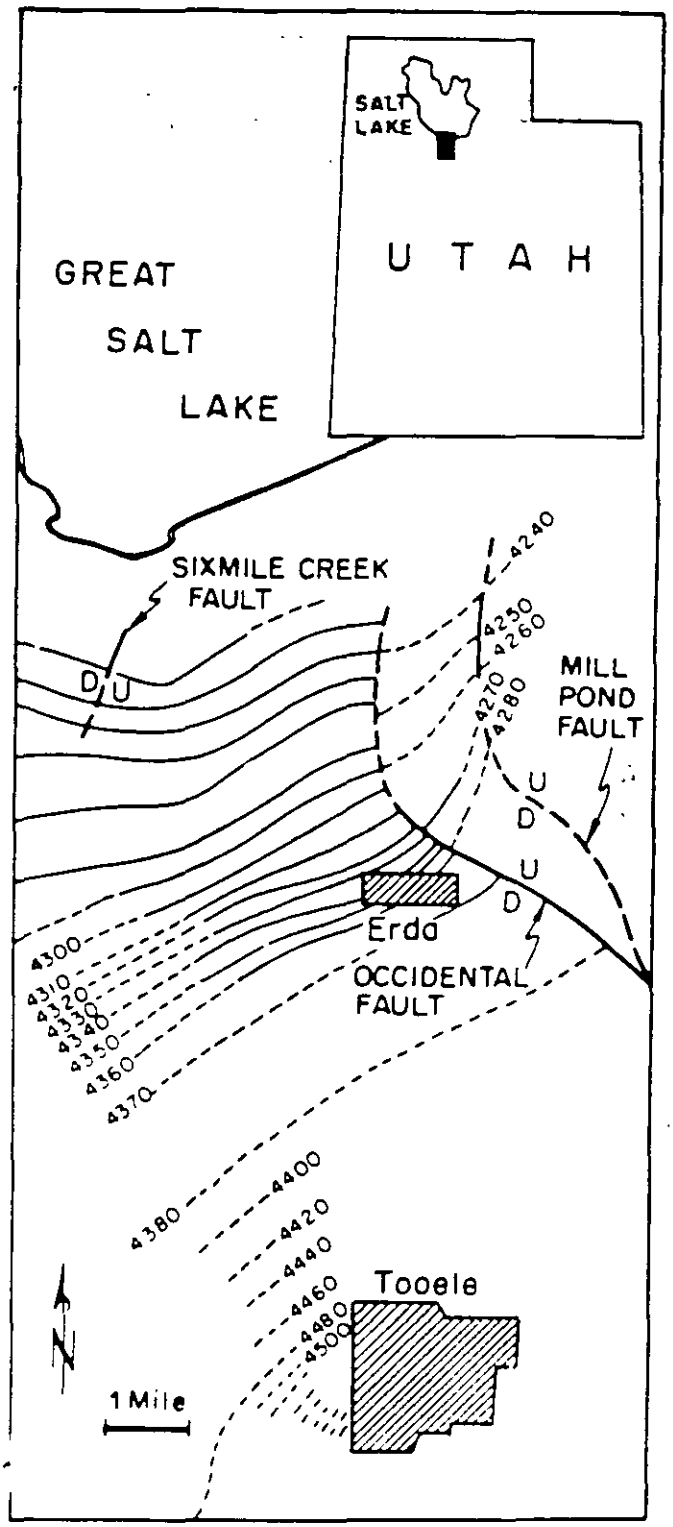

Fig. 3 Ground-water elevations in feet above mean sea level in the vicinity of Tooele, Utah (Gates, 1965).

3. Resolving Data Inconsistencies at Tooele, Utah

The third case history discusses the use of modeling to resolve data inconsistencies at Tooele, Utah. Figure 3 (Gates, 1965) shows contours based on water-level measurements in the vicinity of Tooele, Utah. The aquifer is part of a thick alluvial fan that is recharged by streams flowing out of the adjacent mountains, located mainly south of Tooele. The aquifer thickness is so great in comparison to drawdown that it could be modeled as a confined aquifer. The ground water discharges to wells, springs and Great Salt Lake in the northern part of the fan.

Preliminary analysis of the available data showed some inconsistencies. Pumping tests

indicated large transmissivities throughout. Values over 1,000,000 gpd/ft (134,000 ft²/d) (12,500 m²/d) were indicated in parts of the aquifer. On the other hand, specific capacity determinations suggested transmissivities in the neighborhood of 100,000 gpd/ft (13,000 ft²/d) (1,250 m²/day), and these are out of line with the data from pumping tests

During the preparation of a two-dimensional finite-difference ground-water model, using the Pinder and Bredehoeft Code (1968), transmissivities were determined by trial and adjustment. Because the differential equation that is solved incorporates Darcy's law, excessively low transmissivities generate ground-water gradients steeper than the historical gradient. Similarly, the use of excessively high transmissivities in the model generates ground-water gradients flatter than the historical gradients. In order to generate historical ground-water gradients, the model required transmissivities in the neighborhood of 700,000 gpd/ft (94,000 ft²/d) (8,750 m/d) in the southern part of the alluvial fan. This value was verified by a carefully controlled pumping test

The Occidental Fault (Figure 3) is said to be a semipermeable fault where it crosses the alluvial fan. Yet, the ground-water contour lines in Figure 3 meet the Occidental Fault at right angles implying that the fault is a flow line. If one prepared a computer model that incorporated leakage across the fault, the model could not generate contours orthogonal to the fault. Once again, preparation of a model in an attempt to generate historical water levels would be a safeguard against the acceptance of inconsistent data

4. Optimizing Use of Exploration Funds in Taiwan

The fourth case history discusses a management model that was used to determine the optimal allocation of exploration funds for a dewatering project in Taiwan. Aguado *et al* (1977) were concerned with two problems related to the dewatering of a drydock site in Taiwan (Figure 4). The water level in the excavation was to be maintained at a depth of 49 ft (15 m) using the smallest possible discharge. Therefore, the first problem was to determine the locations and discharges of wells that would maintain water levels at the design depth while using the smallest possible total discharge. The second problem was to identify the kinds and locations of data that affected the management decision most so that the available exploration funds could be used most

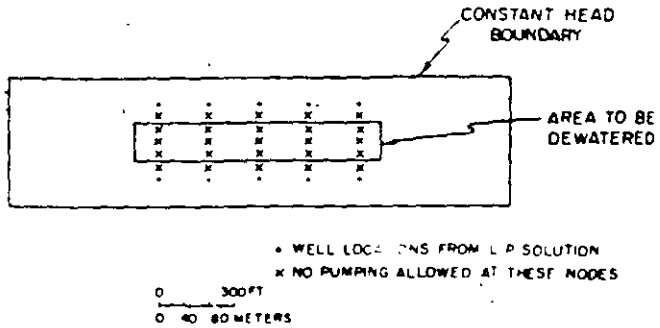

Fig. 4. Optimal pumping locations to dewater a drydock site in Taiwan using minimum discharge as determined from the linear programming model.

effectively. Our concern herein is mainly with the second problem.

The approach used by Aguado *et al* (1977) was to incorporate a finite difference ground-water simulation model into a linear program. A finite element simulation was used in an alternate formulation. The difference equations together with the boundary conditions and dewatering requirements served as constraints in the management model. The objective function to be minimized was the total pumping needed to meet the dewatering constraints while satisfying the boundary conditions and the ground-water equations in numerical form. The answer to the first problem was obtained by solving the linear program to find the locations and discharge rates of pumping wells that would minimize the objective function while meeting the constraints. It must be noted that the number and locations of discharging wells were constrained by the discretization grid. This constraint has been removed using an improved formulation that minimizes the total cost of the variable pumping charges and the fixed well installation costs (Aguado and Remson, 1980)

The solution to the second problem was obtained by subjecting the management model to sensitivity analysis to determine which system parameters affected the minimum objective value the most and in which part of the system. Both problems were solved using IBM Mathematical Programming System/360 (MPS/360)

The objective function proved most sensitive to values of hydraulic conductivity along the constant head boundaries parallel to the long sides of the excavation (Figure 4). Therefore, the exploration funds are best spent on pumping tests along these boundaries. Hydraulic conductivity of the sediments in other parts of the system had less effect. Hydraulic conductivity values within the excavation had no effect on the minimum value

of the objective function as might be expected for steady-state solution. Thus, pumping tests within the area to be excavated would contribute no useful information to the management of the system. The use of exploration funds to improve knowledge of head distributions at the boundaries was shown by the sensitivity analysis to be less productive than use of the funds to obtain hydraulic conductivity data.

CONCLUSIONS

In each of the ground-water investigations discussed, the results of model manipulation helped with the system conceptualization. Furthermore, the site dewatering example showed how sensitivity analysis of a management model could be used to optimize allocation of exploration funds. After such experiences, it has become standard procedure for us to frame problems in the context of ground-water models at the inception of a study whether or not the models are needed for purposes of prediction or management. We find that the utilization of models in identifying data inconsistencies and conceptualization errors thoroughly justifies their use.

REFERENCES

Aguado, E., and I. Remson. 1980. Groundwater management with fixed charges. ASCE, Journal to the Water Resources Planning and Management Division, July (in press).

Aguado, E., N. Sitar, and I. Remson. 1977. Sensitivity analysis in aquifer studies. Water Resources Research, v. 13, no. 4, pp. 733-737.

Fliegner, J. F. 1978. A groundwater model and the hydrogeology of the San Jacinto Valley, Riverside County, California with emphasis on the Soboba Indian Reservation. MS thesis, Stanford University, Stanford, California, 189 pp.

Gates, J. S. 1965. Re-evaluation of the groundwater resources of Tooele, Utah. Utah State Engineer. Tech. Pub. No. 12, 68 pp.

Howland, M. D. 1976. Hydrogeology of the Palo Alto Baylands, Palo Alto, California, with emphasis on the tidal marshes. MS thesis, Stanford University, Stanford, California, 138 pp.

Pinder, G. F., and J. D. Bredehoeft. 1968. Application of the digital computer for aquifer evaluation. Water Resources Research, v. 4, pp. 1069-1093.

Prickett, T. A., and C. G. Lonnquist. 1971. Selected digital computer techniques for groundwater resource evaluation. Illinois State Water Survey Bull. 55, 62 pp.

• • • •

Irwin Remson is Professor of Applied Earth Sciences and Geology and Chairman of the Department of Applied Earth Sciences at Stanford University. He holds A.B., M.A., and Ph.D. degrees from Columbia University. His publications have dealt with saturated and unsaturated flow, hydrologic modeling, and ground-water management. His latest book, Geology in Environmental Planning (with A. D. Howard) complements his academic programs in Hydrogeology and Environmental Earth Sciences.

Steven M. Gorelick is a Research Assistant in the School of Earth Sciences, Stanford University. He holds a B.A. in Environmental Science from New College, Florida and an M.S. in Hydrology from Stanford University. His doctoral research involves developing models for the management of ground-water solutes.

Julianne F. Fliegner received a B.S. from the University of Redlands, and an M.S. in Hydrogeology from Stanford University. She is currently employed as a Hydrologist in Montana with the Water Resources Division, U.S. Geological Survey.

FACULTAD DE INGENIERIA U.N.A.M.
DIVISION DE EDUCACION CONTINUA

CURSOS ABIERTOS

XII CURSO INTERNACIONAL DE CONTAMINACIÓN DE ACUÍFEROS

MODULO III: MODELOS MATEMÁTICOS EN GEOHIDROLOGIA Y CONTAMINACIÓN DE ACUIFEROS

TEMA

AUTOMATED CALIBRATION OF A CONTAMINANT TRANSPORT MODEL FOR A SHALLOW SAN AQUIFER

EXPOSITOR: DR. ADOLFO CHAVEZ RODRIGUEZ
PALACIO DE MINERIA
OCTUBRE DEL 2000

Automated Calibration of a Contaminant Transport Model for a Shallow Sand Aquifer

by K. John Holmes[a], Wen-sen Chu[b], and Denis R. Erickson[c]

ABSTRACT

This paper presents an application of an automated calibration technique for the United States Geological Survey Method of Characteristics (USGS-MOC) code. The model was applied to a shallow sand aquifer where contamination due to leakage from a solvent recycling plant was detected. Using available water-table observations, transmissivity parameters for the USGS-MOC model were calibrated by an automated parameter identification (PI) technique. Dispersivity was determined from trial-and-error simulations. For comparison purposes, the transmissivity parameters were also independently calibrated by trial and-error simulations. The study results show that, although the PI-calibrated model can produce water-table contours that are in good agreement with observations and the contaminant plumes produced by the USGS-MOC using parameters determined from the PI technique and the trial-and-error approach are not vastly different, the parameters determined by this technique are not considered to be physically plausible in all cases. The best strategy in model calibration would be to use both methods conjunctively.

INTRODUCTION

In the past two decades engineers and scientists have developed a number of mathematical models to simulate fluid flow and contaminant transport in the subsurface stratum (Anderson, 1979, Faust and Mercer, 1980, and Javandel *et al.*, 1984). In each application, these models require the input of certain parameters to characterize the flow and transport processes. To make these models effective simulation tools, parameters must be appropriately calibrated against field observations. Because the validity of the simulation depends on how well these parameters are chosen, model calibration is a critical step in field application.

There are two basic approaches to model calibration. One approach is a trial-and-error process in which certain model parameter values are carefully adjusted until the model output mimics some observed conditions as closely as possible. The outcome of this type of calibration is highly dependent on the user's experience and can vary substantially from user to user. The other approach to model calibration involves the use of a computer search algorithm that computes model parameter values by minimizing some measures of the differences between model solutions and available field observations. This procedure is known in ground-water modeling as parameter identification (PI) (Yeh, 1986). The advantages of this calibration method are that it helps to reduce the number of model calibration runs and it tends to limit the variation in calibration results by different users. Parameter identification is, however, not without its problems. The formulation for most ground-water problems has been shown to be ill-posed (Yeh, 1986), and it works well only with abundant, high-quality data (Sadeghipour and Yeh, 1984, and Chu *et al.*, 1987). Neither the trial-and-error nor the PI approach work very well for cases with limited data. The accuracy of model simulation is only as good as that of the data set and of the model calibration.

This paper reports the use of a simulation model in the investigation of contaminant movement through a shallow sand aquifer. The primary focus of the study was to examine the effects due to different calibration approaches on model simulation results. Using the same set of monitoring

[a]Interstate Commission on the Potomac River Basin, Suite 300, 6110 Executive Blvd., Rockville, Maryland 20852-3903.

[b]Department of Civil Engineering, FX-10, University of Washington, Seattle, Washington 98195.

[c]Washington State Department of Ecology, MS LU-11, Olympia, Washington 98504-6811.

Received May 1988, revised November 1988, accepted December 1988.

Discussion open until January 1, 1990.

data from the study site, the United States Geological Survey's Method of Characteristics (USGS-MOC) code (Konikow and Bredehoeft, 1978) was calibrated using both an automated parameter identification algorithm and a manual trial-and-error approach. To compare and contrast the calibration results, parameters determined by the two approaches were used in independent simulation runs to characterize the probable migration patterns of the contaminant plume at the site.

The USGS-MOC model was chosen for the study because of its excellent documentation, its widespread usage (Konikow, 1977, Warner, 1979, Bedient *et al.*, 1984, and Freeberg *et al.*, 1987; El-Kadi, 1988), and because a parameter identification algorithm for USGS-MOC called PI-MOC has already been developed (Strecker and Chu, 1986). With PI-MOC, selected parameters (transmissivity, dispersivity, etc.) in USGS-MOC can be found by a quadratic programming routine which minimizes the sum of the squared deviations between chosen observations and model output. Formulation and applications of PI-MOC have been reported by Strecker and Chu (1986) and Chu *et al.* (1987) and, for brevity, will not be repeated here.

SITE DESCRIPTION

The study site (Figure 1) has been occupied by a solvent recycling plant from 1981 to the present. The plant processed up to 1000 gallons of waste per week until 1984 when contamination of the aquifer underneath the plant was first detected. The contaminants, which seeped through the upper soil layer due to leakage from a major collection sump, consist of a variety of organic compounds including trichloroethene and toluene.

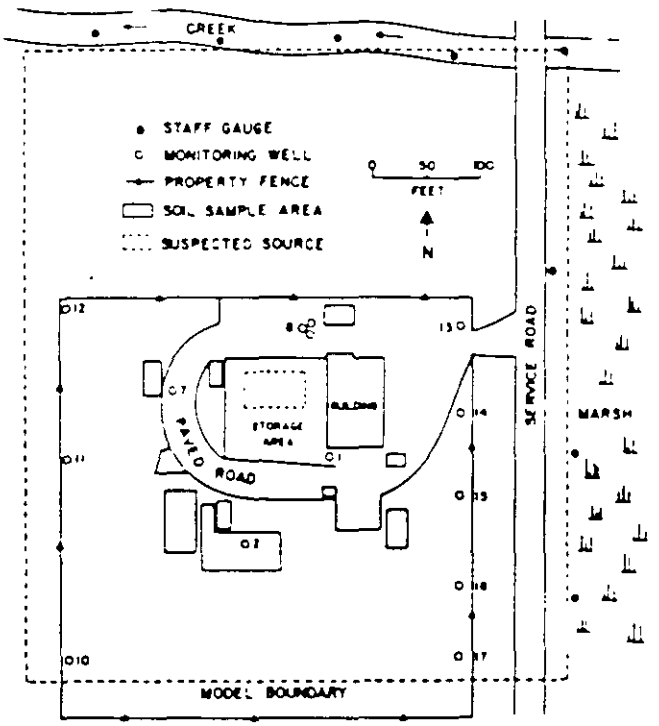

Fig. 1. Study site map.

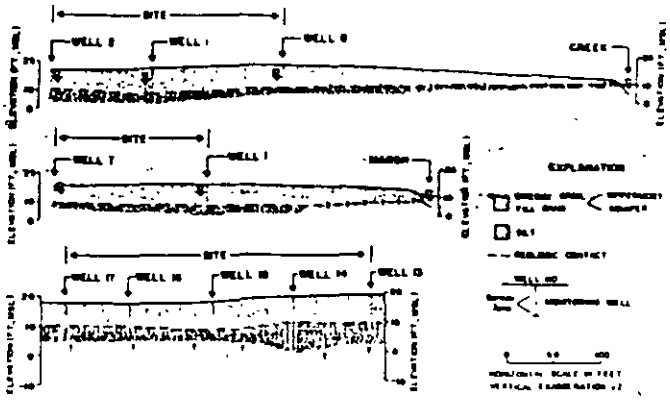

Fig. 2. Selected cross sections at the study site.

The material underlying the site and adjacent area consists of uniform, well-sorted, fine-to-medium-grained sand (dredged spoils) overlying native alluvial silt. Below these layers are Quaternary alluvium. The dredged spoils, produced from channel dredging of a nearby river, create an unconfined aquifer. Three cross sections through the site are shown in Figure 2. The sand is of fairly uniform thickness at the site and the lower silt layer is probably continuous on-site. Nearby soil borings drilled by the U.S. Army Corps of Engineers show that the silt layer extends to a depth of about 50 feet. For the model application, it is assumed that the underlying alluvial silt is comparatively impermeable and allows very little vertical movement of water into lower layers. Additional characterization of the silt layer and the underlying sediments is ongoing including the installation of monitoring wells in the underlying aquifer.

MODEL APPLICATION

Modeling of ground-water movement and contaminant transport at the study site first required the determination of some basic parameters. Parameters such as specific yield, saturated thickness, source location, and effective porosity were obtained from previous investigations done at the site, and are shown in Table 1. Except for dispersivity, these basic parameters were not adjusted during model calibration and subsequent simulation runs. The calibration of dispersivity values in the model will be reported later in this paper. Previous investigations have also estimated the

transmissivity of the sand aquifer to range from .01 to .002 ft^2/s with the most likely value of .006 ft^2/s.

The model boundaries are shown on Figure 1. General ground-water flow direction at the site has been determined through extensive monitoring and, from this earlier work, boundary conditions for modeling were inferred. Fourteen observation wells were installed in 1985 and monitored for one year. Locations of these wells are shown in Figure 1. From analysis of this field data, it was concluded that the creek and the marsh, located on the north and the east edges of the study area respectively, are hydraulically connected to the aquifer during most of the year. Monitoring data suggest that during normal conditions the creek and the marsh act as constant-head boundaries, and ground water at the site flows towards these boundaries. Since such flow pattern does not cross the southern boundary, it was treated as a no-flow boundary. Monitoring well data along the western boundary suggested that part of the boundary can be represented by constant-head nodes and the part toward the creek can be treated as a no-flow boundary.

Automated Model Calibration by PI-MOC

PI-MOC (Strecker and Chu, 1986) was used in this study for a steady-state calibration of the transmissivity values. Although PI-MOC can be used to calibrate dispersivities from contaminant concentration data (Strecker and Chu, 1986), this option was not used because of the lack of good water quality data. Instead, the dispersivity parameter was manually adjusted to give a contaminant plume shape that was consistent with field conditions.

Even with the almost homogeneous material (constant hydraulic conductivity) at the site, the input transmissivity to USGS-MOC is not constant because of the variable aquifer thickness (see Figure 2). To reflect this spatial variation, the

Table 1. Input Parameters for the Study Site

Delta X	50	feet
Delta Y	50	feet
Longitudinal dispersivity	1 100	feet
Ratio of transverse to longitudinal dispersivity	0.30	
Ratio of T_{yy} to T_{xx}	1.00	
Saturated thickness	6- 10	feet
Effective porosity	0.25	
Specific yield (transient case)	0.20	
Specific yield (steady-state case)	0.00	

CREEK

0	0	0	0	0	0	0	0	0	0	0	0	0	
0	6	6	6	6	6	6	6	6	6	6	6	0	
0	7	7	7	7	7	7	7	7	7	7	6	0	
0	8	8	8	8	8	8	8	8	8	7	6	0	
0	10	10	10	10	10	10	10	10	8	7	6	0	M
0	10	10	10	10	10	10	10	10	8	7	6	0	ARS
0	10	10	10	10	10	10	10	10	8	7	6	0	H
0	10	10	10	10	10	10	10	10	8	7	6	0	
0	10	10	10	10	10	10	10	10	8	7	6	0	
0	10	10	10	10	10	10	10	10	8	7	6	0	
0	10	10	10	10	10	10	10	10	8	7	6	0	
0	0	0	0	0	0	0	0	0	0	0	0	0	

Fig. 3. Aquifer thickness (in feet) for the modeled area (zeros denote no flow region).

aquifer was divided into a number of zones, each with a constant transmissivity. The number of zones used in this study varied from one to four. Although the selection of a zonal pattern has been shown to affect the outcome of PI calibration (Chu *et al.*, 1987), zone selection was relatively straightforward for this study site. Since the given aquifer is composed of fairly homogeneous materials, transmissivity should vary directly with aquifer thickness. Figure 3 is a map of the aquifer thickness constructed from soil samples and well log data. Different spatial patterns of transmissivity (two, three, and four zones) assumed for PI-MOC are shown in Figure 4.

PI-MOC requires the input of the number of zones, an initial estimate of zonal transmissivity values, and the numeric upper and lower bounds on transmissivity values in each zone. These upper and lower bounds were estimated from soil characteristics and pump and slug tests performed at the site in previous investigations.

Results of PI-MOC Calibration

The results from all the PI-MOC runs are summarized in Table 2. The various runs listed in Table 2 were designed to demonstrate the effects of transmissivity zonal patterns, initial parameter estimates, and parameter upper and lower bounds on the results of PI-MOC. Starting from the initial

estimates, all PI-MOC runs terminated after four iterations. The parameters found in each run at the end of the fourth iteration and the objective value of the optimization (which is the sum of squares of the differences between predicted and observed water-table elevations at all the monitoring wells and staff gauges) are given in the last two columns of Table 2.

Transmissivity was assumed constant in Run 1. The observed water-table gradient [Figure 5(a)] sharpens near the constant-head boundaries of the marsh and the creek. For an aquifer with relatively uniform soil property (constant hydraulic conductivity), this is possible only with a decreasing aquifer thickness (and therefore transmissivity) near these boundaries. Available cross sections at the site (Figure 2) also confirm such decrease in aquifer thickness. The formulation of PI-MOC apparently recognized this, and Run 1 could not find an appropriate parameter value in four iterations.

In Runs 2 and 3, the aquifer was represented by two transmissivity zones (Figure 4). With a physically plausible upper bound of .01 ft^2/s, Run 2 could not reach a convergent solution in four iterations. Relaxing this upper bound to .05 ft^2/s produced a convergent solution for transmissivity, but the values were considered too high. Earlier investigations of the site have estimated the transmissivity of the aquifer to range from .01 to .0002 ft^2/s with the most likely value as .006 ft^2/s.

The use of three transmissivity zones (Figure 4) in PI-MOC did produce a solution that was within the prescribed upper and lower bounds (see Runs 4 through 8 in Table 2). Also shown by Runs 4 through 6 are the different parameters found by PI-MOC from medium, low, and high initial parameter estimates. Run 4 with medium initial parameter estimate produced the smallest objective value (the best fit) by the optimization procedure.

Runs 7 and 8 were intended to investigate the effect of the parameter lower bound on the PI-MOC solution. Run 7 results show that relaxing the parameter lower bound does not affect the final parameter values determined by PI-MOC. Run 8 results show that tightening the lower parameter bound does affect the PI-MOC solution. Tightening the lower parameter bound acts to restrict the potential solution domain and reduces the goodness-of-fit between the predicted and observed water-table elevations as shown by the objective values of Runs 4 and 8 in Table 2.

Runs 9 through 12 assumed four zones of transmissivity for the site. Configuration of these transmissivity zones is also given in Figure 4. Runs 9 through 11 were used to study the effect of initial parameter estimates on the solution. As in the three-zone case, Run 9 with medium initial parameter estimate again produced the solution with minimum objective value. Run 12 also shows the effect of tightening the lower parameter bound.

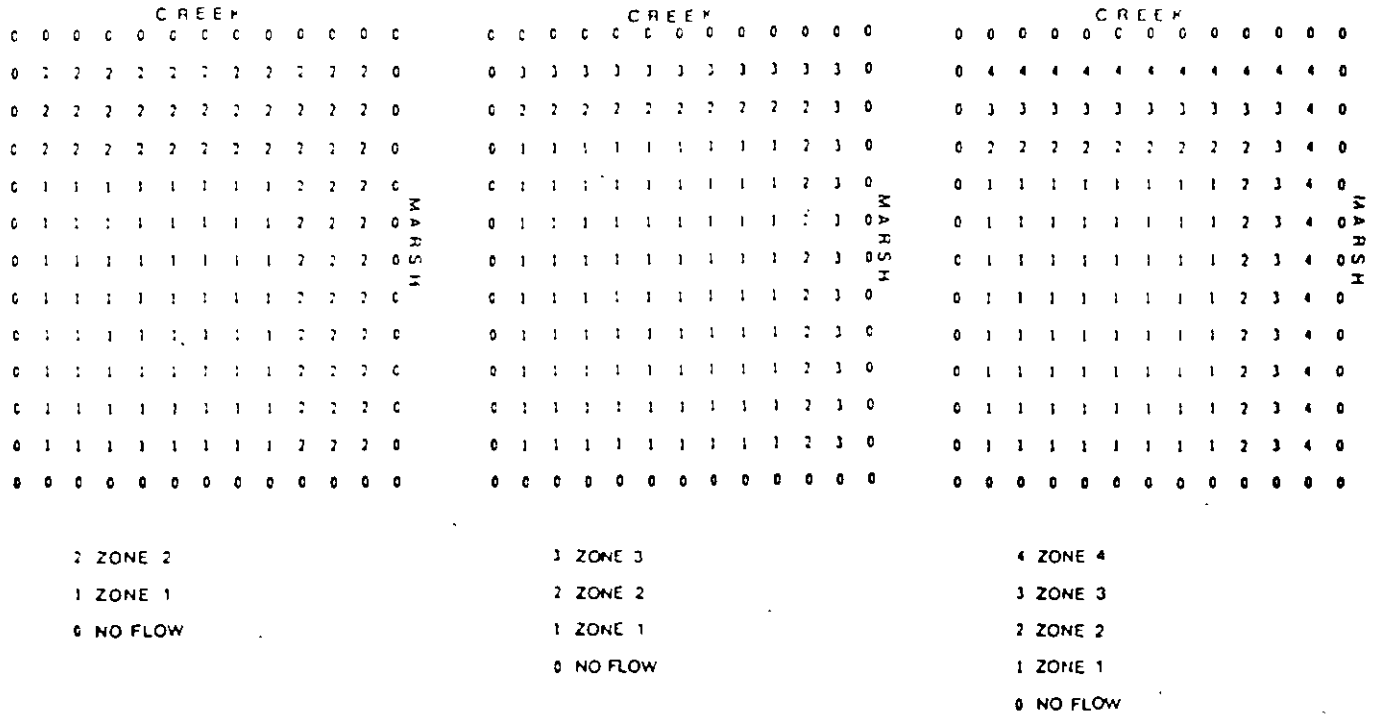

Fig. 4. Transmissivity zonal patterns investigated

the most likely value of 0.006 ft²/s based on data from the earlier investigation, model input transmissivity values were adjusted until the calculated water-table contours compared favorably with the observed water-table contours. Approximately 15 USGS-MOC runs were required for the calibration. Because of the "user intervention" during this type of calibration, the transmissivity values found follow consistently with the observed aquifer thickness data The water-table contours calculated using the transmissivities determined from the trial-and-error calibration are shown in Figure 5(c)

Dispersivity Determination

Due to the lack of monitoring data, dispersivity in USGS-MOC could not be calibrated as the transmissivity was. Instead, the proper dispersivity for the site was chosen by comparing the calculated contaminant plume with the general knowledge of the plume from field investigation. Using a continuous injection well to simulate the source of contamination (leaky storage sump) and the transmissivities determined from the trial-and-error calibration, steady-state runs of USGS-MOC were made with longitudinal dispersivity set at 1, 10, and 100 feet. The resulting contaminant plumes from these runs are compared with the observed extent of the plume (in 1984) and shown in Figure 6 The plume due to a dispersivity of 1 foot [Figure 6(c)] was so narrow that it would escape detection by most monitoring wells near the marsh which was contrary to field investigation results. The plume resulting from a dispersivity of 100 feet

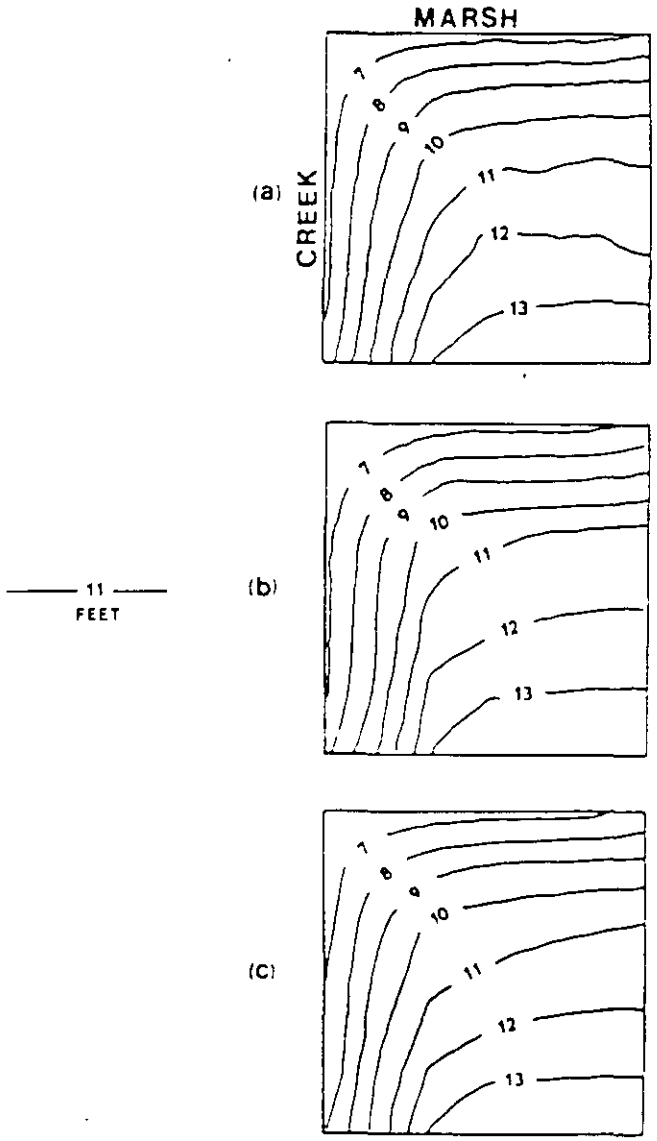

Fig. 5. (a) Observed water-table contours in 1984, (b) water-table contours calculated by USGS-MOC using transmissivity determined from PI-MOC assuming three-zone characterization, and (c) using transmissivity determined by trial-and-error calibration.

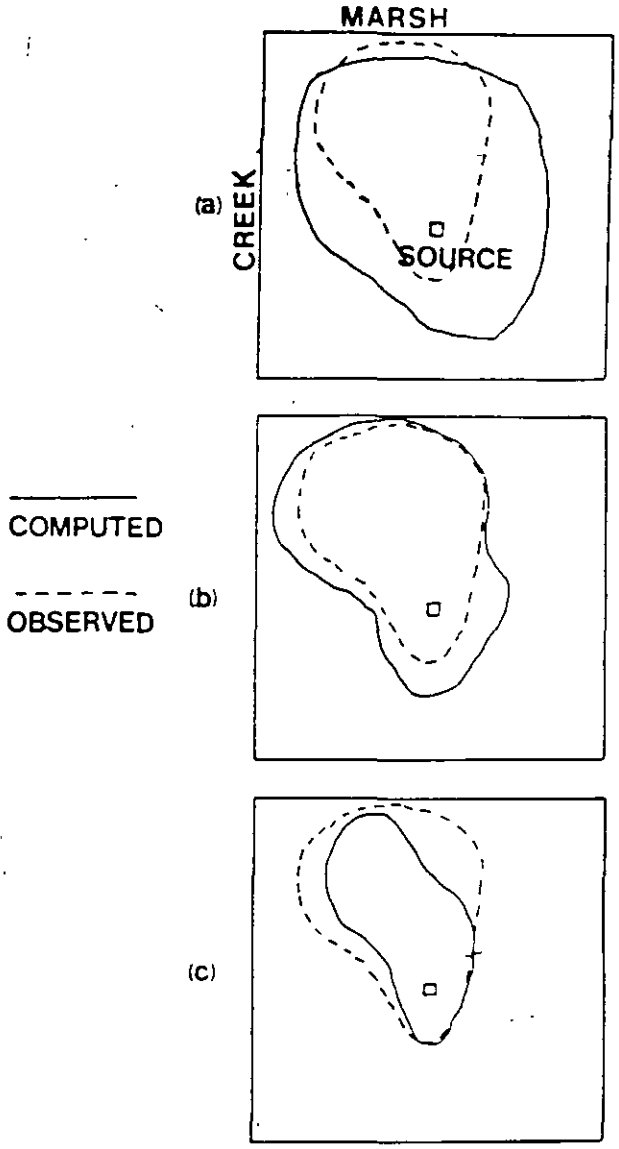

Fig. 6. (a) Simulated contaminant plume using an input longitudinal dispersivity of 100; (b) an input longitudinal dispersivity of 10; and (c) input longitudinal dispersivity of 1.

[Figure 6(a)] showed an exaggerated spread from the source which was again contrary to knowledge obtained from field investigation. The dispersivity value of 10 feet produced the most reasonable plume shape [Figure 6(b)] and was eventually adopted for further simulation.

M- -eling Plume Migration

With the chosen dispersivity of 10, USGS-MOC was used to simulate the migration of plume at the site from 1981 to 1984 during which leakage occurred. The specific yield used in these transient runs of USGS-MOC is shown in Table 1. Simulation runs were made with three-zone PI-calibrated transmissivities and with manually calibrated transmissivities.

The results from using the manually calibrated and PI-calibrated transmissivities are almost identical. The general shapes of the resulting plume are similar for all runs. The major differences are in exact contaminant concentration values. The run using PI-calibrated parameters produced slightly higher contaminant concentrations within the study area [see Figures 7(a) and 7(b)]. This is due to the presence of a low-transmissivity zone (see Run 4 in Table 2) computed by PI-MOC

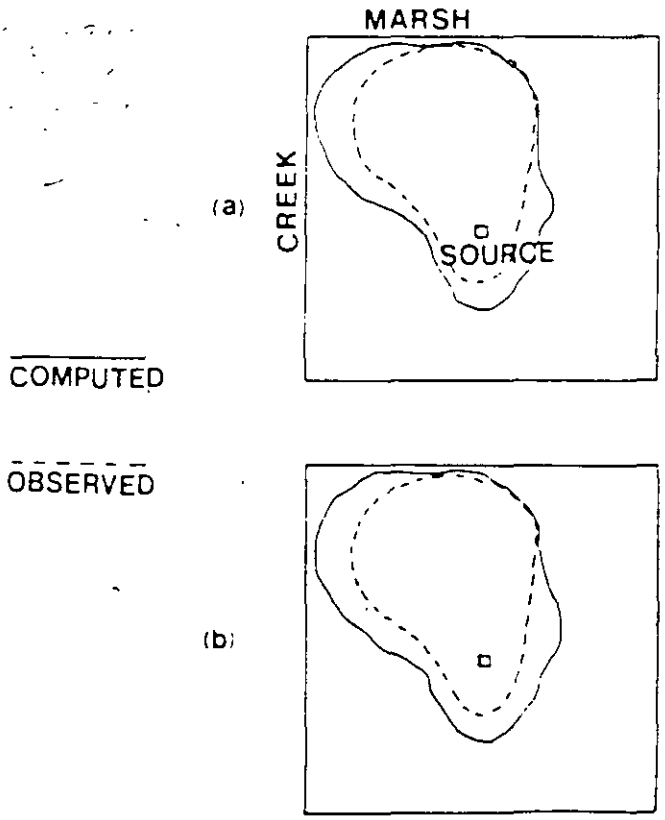

Fig. 7. (a) Simulated contaminant plume in 1984 using transmissivity determined by trial-and-error method, and (b) using transmissivity determined by PI-MOC assuming three-zone characterization (longitudinal dispersivity = 10).

that retards contaminant movement in the aquifer.

This simulation exercise once again suggests that with limited field data and parameter uncertainty, most of the current ground-water flow and transport models should be used as tools to characterize approximate extent of the contamination (plume shape), rather than to predict exact concentration values at specific locations (Chu, *et al*, 1987).

Using the contaminant concentrations at the end of the four-year simulations to represent the background condition in 1984, the model was further run, using both PI-calibrated (Runs 4 and 9) and manually calibrated transmissivity, for two more years (1984 to 1986) to characterize the behavior of the plume after the source was removed (leakage stopped in 1984). For all cases simulated, virtually all contaminants migrated out of the area within one year. This was expected since ground-water velocities across most of the modeled area were on the order of 300 feet/year.

SUMMARY

The USGS-MOC model was applied to a field problem involving aquifer contamination due to leakage of a collection sump at a solvent recycling plant. The transmissivity parameter in the model was calibrated, with available field data, by a parameter identification (PI) algorithm and by the more conventional trial-and-error method. Both calibration techniques produced calculated water-table contours that compared favorably with those observed in the field. Dispersivity was determined from simulation runs which produced the most probable shape of the contaminant plume by essentially a sensitivity analysis. No other input parameter was calibrated. The effect of the calibration technique on predicted plume migration was examined by extended simulations with the parameters determined from the two approaches.

The parameters found by the PI method in this study appeared to be sensitive to the initial estimate and the lower and upper bounds of the parameter. Although the water table calculated by USGS-MOC with PI-calibrated transmissivities compared closely with the observed data, the PI-calibrated parameter values were inconsistent with observed soil profile data. For more calibration in complex situations, a PI approach might best be used to first define certain parameter zoning patterns. The parameter values in each zone then could be fine-tuned by the trial-and-error method according to additional field data and best user judgment.

ACKNOWLEDGMENTS

The activities on which this report is based were financed in part by the Department of the Interior, U.S. Geological Survey (Grant Number G1259-05) through the Washington State Research Center (Project No. A-145-WASH) and by Washington State Department of Ecology (WDOE). We would also like to thank Will Abercrombie, Greg Laird, Kim Scattarella, and Margo Behler for their contribution to this project. The helpful comments from two anonymous reviewers are appreciated.

REFERENCES

Anderson, M. P. 1979. Using models to simulate the movement of contaminants through groundwater flow systems. Crit. Rev. Environ. Controls, v. 9, no. 2, pp. 97-156.

Bedient, P. B., A. C. Rodgers, T. C. Bouvette, M. B. Tomson, and T. H. Wang. 1984. Ground-water quality at a creosote waste site. Ground Water, v. 22, no. 3, pp. 318-329.

Chu, W-S., E. W. Strecker, and D. P. Lettenmaier. 1987. An evaluation of data requirements for groundwater contaminant transport modeling. Water Resources Res., v. 23, no. 3, pp. 408-424.

El-Kadi, A. I. 1988. Applying the USGS mass-transport model (MOC) to remedial actions by recovery wells. Ground Water, v. 26, no. 3, pp. 281-288.

Faust, C. R. and J. W. Mercer. 1980. Ground-water modeling: numerical models. Ground Water, v. 18, no. 4, pp. 395-409.

Freeberg, K. M., P. B. Bedient, and J. A. Conner. 1987. Modeling of TCE contamination and recovery in a shallow sand aquifer. Ground Water, v. 25, no. 1, pp. 70-80.

Javandel, I., C. Doughty, and C. F. Tsang. 1984. Groundwater Transport: Handbook of Mathematical Models. Water Resources Monograph 10, American Geophysical Union, Washington, DC. 228 pp.

Konikow, L. F. 1977. Modeling chloride movement in the alluvial aquifer in and adjacent to the Rocky Mountain Arsenal, Colorado. U.S. Geological Survey Open-File Report 74-342.

Konikow, L. F. and J. D. Bredehoeft. 1978. Computer model of two-dimensional solute transport and dispersion in ground water. Techniques of Water-Resources Investigations of the U.S. Geologic Survey, U.S. Geologic Survey, Reston, VA. Chapter C2.

Sadeghipour, J. and W. W-G. Yeh. 1984. Parameter identification of groundwater aquifer models: a generalized least squares approach. Water Resources Res. v. 20, no. 7, pp. 971-979.

Strecker, E. W. and W-S. Chu. 1986. Parameter identification of a ground-water contaminant transport model. Ground Water, v. 24, no. 1, pp. 56-62.

Warner, J. W. 1979. Digital-transport model study of diisopropylmethylphosphonate (DIMP) ground-water at the Rocky Mountain Arsenal, Colorado. U.S. Geological Survey, Open-File Report 79-676.

Yeh, W. W-G. 1986. Review of parameter identification procedures in groundwater hydrology: the inverse problem. Water Resources Res., v. 22, no. 2, pp. 95-108.

• • • • •

Denis R. Erickson received his B.S. degree in Geology from the University of Alaska in 1974 and his M.S. in Hydrogeology from the University of Minnesota in 1981. He has 12 years of geologic and hydrogeologic experience in the private and public sector. He is currently a Hydrogeologist with Toxics Investigation Section of the Washington State Department of Ecology. Erickson has special interest in contaminant transport modeling as applied to monitoring and corrective actions at regulated hazardous waste facilities. He is presently working on a project to help determine the influence of agricultural chemicals on ground water quality.

K. John Holmes received his B.S. degree in Geology from Indiana University in 1984 and his M.S. degree in Engineering from the University of Washington in 1987. He is currently a water resources systems engineer with the Interstate Commission on the Potomac River Basin at Rockville, Maryland. Holmes is interested in the application of computer models and expert systems for water resources systems planning and operation.

Wen-sen Chu received his B.S. degree in Agriculture from the National Chung Hsing University in Taiwan in 1973 and his M.S. and Ph.D. degrees in Water Resources Engineering from the University of California, Los Angeles in 1976 and 1979, respectively. He is currently an Associate Professor of Civil Engineering at the University of Washington. Chu's main teaching, research, and consulting interests are numerical modeling of hydrodynamics and transport in surface and ground-water systems, and water resources systems engineering.

D

FACULTAD DE INGENIERIA U.N.A.M.
DIVISION DE EDUCACION CONTINUA

CURSOS ABIERTOS

XII CURSO INTERNACIONAL DE CONTAMINACIÓN DE ACUÍFEROS

MODULO III: MODELOS MATEMÁTICOS EN GEOHIDROLOGIA Y CONTAMINACIÓN DE ACUIFEROS

TEMA

PREDICTIVE ACCURACY OF A GROUND – WATER MODEL LESSONS FROM A POSTAUDIT

EXPOSITOR: DR. ADOLFO CHAVEZ RODRIGUEZ

PALACIO DE MINERIA
OCTUBRE DEL 2000

Predictive Accuracy of a Ground-Water Model — Lessons from a Postaudit

by Leonard F. Konikow[a]

ABSTRACT

Hydrogeologic studies commonly include the development, calibration, and application of a deterministic simulation model. To help assess the value of using such models to make predictions, a postaudit was conducted on a previously studied area in the Salt River and lower Santa Cruz River basins in central Arizona. A deterministic, distributed-parameter model of the ground-water system in these alluvial basins was calibrated by Anderson (1968) using about 40 years of data (1923-64). The calibrated model was then used to predict future water-level changes during the next 10 years (1965-74). Examination of actual water-level changes in 77 wells from 1965-74 indicates a poor correlation between observed and predicted water-level changes. The differences have a mean of −7.3 ft—that is, predicted declines consistently exceeded those observed—and a standard deviation of 4.7 ft. The bias in the predicted water-level change can be accounted for by the large error in the assumed total pumpage during the prediction period. However, the spatial distribution of errors in predicted water-level change does not correlate with the spatial distribution of errors in pumpage. Consequently, the lack of precision probably is not related only to errors in assumed pumpage, but may indicate the presence of other sources of error in the model, such as the two-dimensional representation of a three-dimensional problem or the lack of consideration of land-subsidence processes. This type of postaudit is a valuable method of verifying a model, and an evaluation of predictive errors can provide an increased understanding of the system and aid in assessing the value of undertaking development of a revised model.

[a]U.S. Geological Survey, Mail Stop 431, National Center, Reston, Virginia 22092.

Received May 1985, revised August 1985, accepted September 1985.

Discussion open until September 1, 1986

INTRODUCTION

Hydrogeologic studies commonly include the use of deterministic, distributed-parameter, ground-water models to predict responses of an aquifer system to changes in stresses. The extreme example of using such models for predictions may be in the planning of high-level radioactive waste repositories, where regulators desire and require projections of ground-water flow and transport for 1,000 to 10,000 years into the future. Is there any evidence, either on the basis of a postaudit of the outcome of past predictive efforts or otherwise, that deterministic simulation models can indeed accurately predict future responses in ground-water systems? Is forecasting the only or primary motivation for applying a deterministic ground-water model, or does the modeling exercise have some other value?

The underlying philosophy of process-simulating deterministic-modeling approaches is that, given a comprehensive understanding of the processes by which stresses on a system produce subsequent responses in that system, the system's response to any set of stresses can be defined or predetermined through that understanding of the governing (or controlling) processes, even if the magnitude of the new stresses falls outside of the range of historically observed stresses. Predictions made this way assume an understanding of cause-and-effect relations. The accuracy of such deterministic forecasts thus depends, in part, upon how closely our concepts of the governing processes reflect the processes that actually control the system's behavior. But more is involved. Even if we

have an accurate conceptual model of the governing processes, and if the processes were represented accurately in a deterministic simulation model, we also need (1) a definition of the properties and boundaries of the domain over which these processes and stresses are acting; (2) the state of the system at some point in time (either past or present); and (3) an estimate (or prediction) of what the future stresses will be, which, though it is an obvious requirement, is not necessarily a trivial matter. Thus, the "model" of an aquifer system incorporates processes, specifications for parameters, and stresses.

Ground-water hydrologists are becoming increasingly aware that inadequate and insufficient data limit the reliability of traditional deterministic ground-water models. The data may be inadequate because aquifer heterogeneities occur on a scale smaller than can be defined on the basis of available data, time-dependent variables are monitored too infrequently, and measurement errors exist.

The purpose of this paper is to review the use and reliability of deterministic models for predicting future changes in ground water by examining the outcome of a past predictive effort. A model study of an area in central Arizona was selected as an example because it represents one of the first well-documented deterministic, distributed-parameter, model analyses of a ground-water system. Consequently, it was also done sufficiently long ago that a long-term (10-year) forecast period has passed. Furthermore, there are now available historical observations of the aquifer for the time for which the forecast was made. The purposes of this example are (1) to illustrate how accurate (or inaccurate) a prediction made with a supposedly well-calibrated model can be, recognizing that only limited generalizations should be drawn on the basis of a single example; (2) to try to isolate the sources of predictive error, and (3) to evaluate the importance of conducting a postaudit of model predictions.

DESCRIPTION OF STUDY AREA

The Salt River Valley and the lower Santa Cruz River basin are located near Phoenix, Arizona (see Figure 1) and are the two largest agricultural areas in Arizona. According to Anderson (1968), about 1,250 mi² (800,000 acres) are under cultivation. Because of the arid climate (rainfall averages about 8 inches per year), the agricultural economy is dependent on a reliable source of irrigation water. Since the early 1900's, the ground-water system had been developed extensively in the area. By the mid-1960's, ground water was providing approximately 80 percent (3.2 million ac-ft) of the total annual water supply. Summarizing the discussion of Anderson (1968), such withdrawals greatly exceed the rate of ground-water recharge and resulted in water-level declines of as much as 20 ft per year in some places. Maximum declines from 1923 to 1964 were about 360 ft. Because of the economic importance of ground water in this area, there was much concern that continued declines would cause significantly increased pumping costs and decreased well yields. As part of an analysis of the ground-water resources of the area, Anderson (1968) constructed and calibrated an electric-analog model of the aquifer system, partly ". . . to determine the probable future effects of continued ground-water withdrawals in central Arizona."

The hydrogeologic setting of this area is described in detail by Anderson (1968) and Davidson (1979). A summary of their descriptions follows. The central Arizona area lies in the Basin and Range lowlands water province (Figure 1). The area is characterized by broad and gently sloping valleys or basins that surround and separate steep and rugged mountains. The mountains are composed mainly of low-permeability crystalline rocks, although some sedimentary rocks are present. The valleys are underlain by thousands of feet of unconsolidated to consolidated alluvial deposits, including thick permeable sand and gravel units. In general, coarser material is found near the mountains, which border the margins of the basins, and fine-grained material is deposited in the central, deeper parts of the basins. Most ground water used in the basin is derived from the uppermost unit of the alluvium, which is a high permeable sand and gravel as much as 600 ft in thickness. Below this unit is the middle silt and clay unit, which is discontinuous, less permeable, and as much as 2,000 ft in thickness. Below that lies the more consolidated lower sand and gravel unit, which is intermediate in permeability.

The water-table configuration in 1923, prior to extensive development of the ground-water resource, is indicated in Figure 2. At that time, ground-water flow was predominantly to the west and northwest, generally paralleling the flow directions of the Santa Cruz, Gila, and Salt Rivers. Anderson (1968) considered the ground-water system to be in an approximate equilibrium condition prior to 1923. He further states, "Since the early 1920's, pumping has exceeded replenishment in central Arizona. Beginning in the early 1940's,

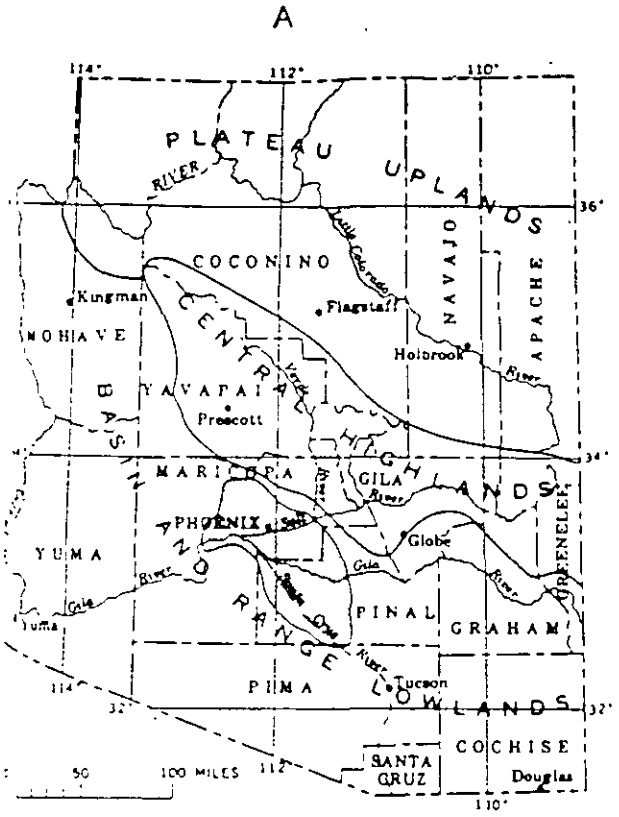

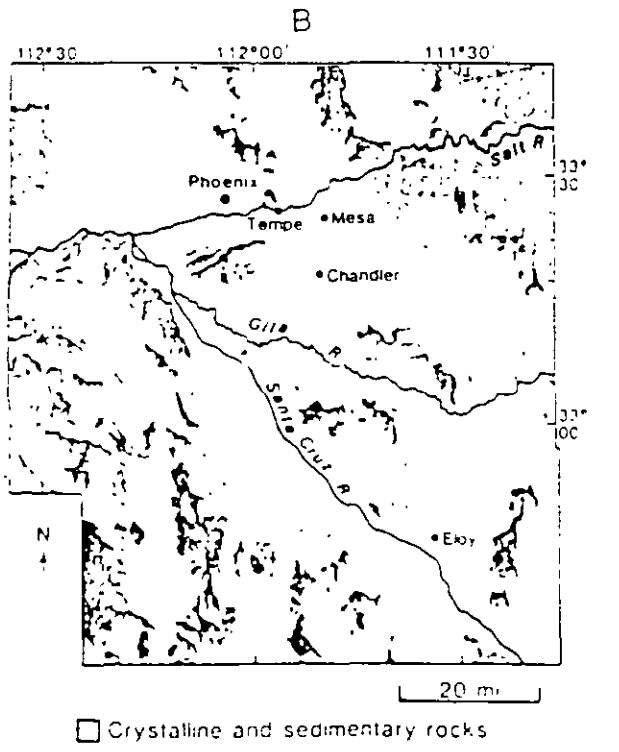

Fig 1 Location of study area in Arizona (from Anderson, 1968) (A), and main geographic and physiographic features within the study area (B).

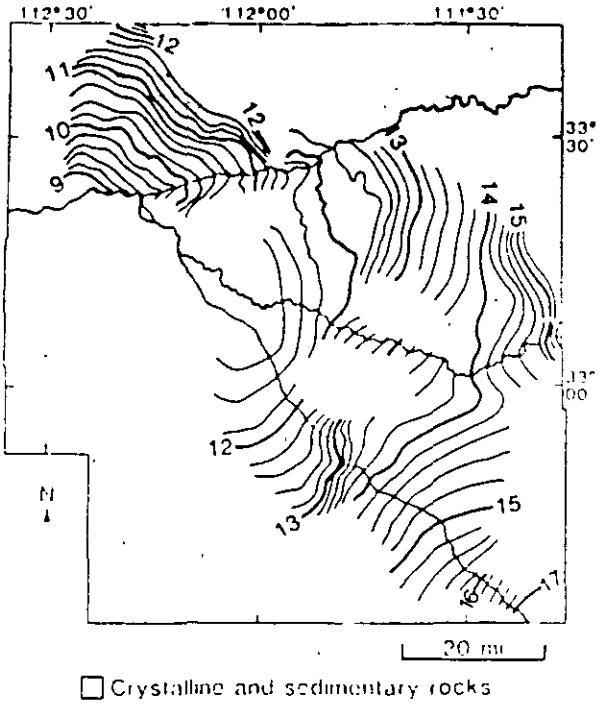

Fig. 2. Altitude of the water table, spring 1923, in central Arizona (from Anderson, 1968).

pumping was greatly accelerated and within a few years reached a rate many times greater than the rate of recharge. Water levels have declined in the entire area, and the rate of decline in some places is as much as 20 feet per year."

The annual water use in the study area during 1923-64 is shown in Figure 3. Because all the flow

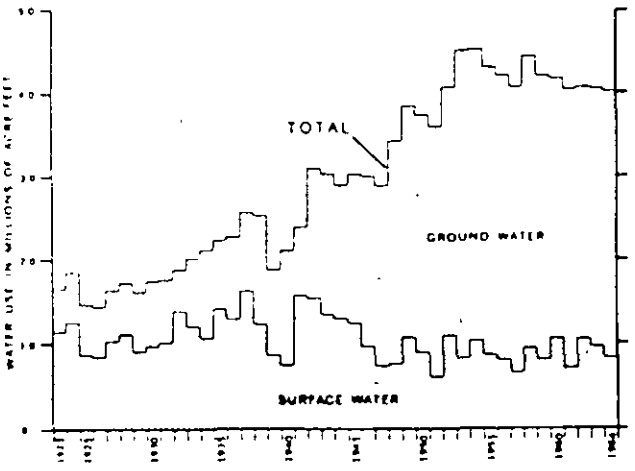

Fig. 3. Annual water use in study area, 1923-64 (from Anderson, 1968). Ground-water use is the difference between total and surface-water use.

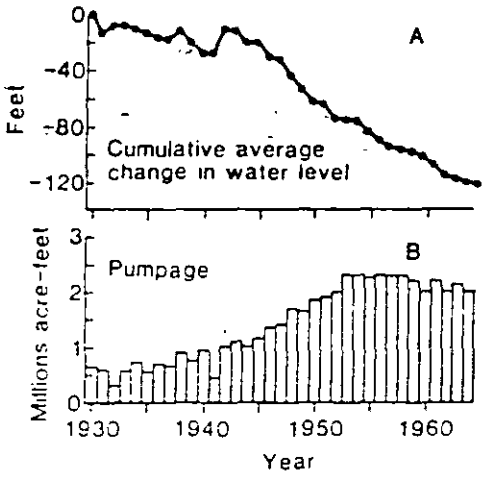

Fig. 4 Average water-level change in the Tempe-Mesa-Chandler area of the Salt River Valley (A), and annual ground-water withdrawals in the Salt River Valley (B), 1930-64 (modified from Babcock, 1970).

in the Gila and Salt Rivers, except for floodwaters, is diverted for irrigation, increasing demands for water have been met primarily by increases in ground-water withdrawals. The greatest increase in ground-water use occurred during the 1940's and early 1950's. As indicated in Figure 4 by the data for Tempe-Mesa-Chandler area in the Salt River basin, the onset of the major water-level declines generally coincides with the increased ground-water withdrawals, although changes in the rate of decline appear to be lagging behind changes in the pumpage. Anderson (1968) reports that the total volume of ground water withdrawn from this aquifer system during 1923-64 was 80 million ac-ft, and that in 1964 the pumpage was about 3.2 million ac-ft, of which approximately 2.2 million ac-ft were from the Salt River Valley and 1.0 million ac-ft were from the lower Santa Cruz basin.

By the end of 1964 these large ground-water withdrawals, far in excess of recharge, had a major impact on the aquifer system. Anderson (1968) states, "A general regional flow pattern no longer exists, and the flow is directed radially toward the center of the large cones of depression." Figure 5 shows the magnitude of the water-level declines that occurred from 1923 to 1964; the declines exceeded 300 ft in places and exceeded 100 ft in most of the study area. Thus, by 1964 the depth to the water table exceeded 300 ft in parts of the area and exceeded 100 ft in most of the study area (see Figure 6). The increased pumping lifts increased

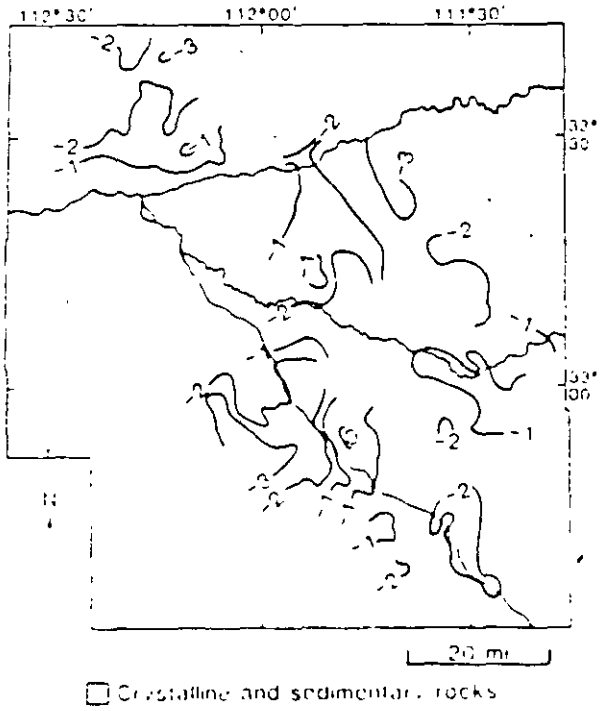

Fig. 5 Water-level declines, spring 1923 to spring 1964 (from Anderson, 1968)

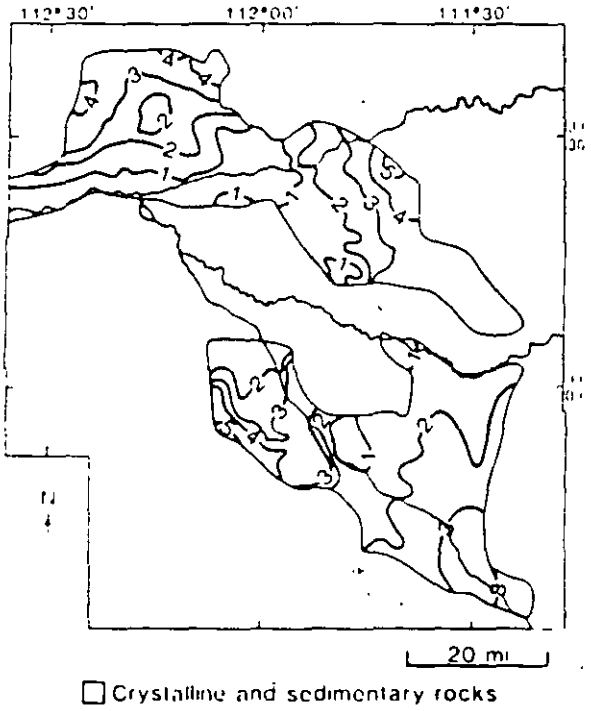

Fig. 6 Observed depth to water, spring 1964, in central Arizona (from Anderson, 1968).

the costs of withdrawing ground water, hence was of great concern to the users of ground water (mostly agricultural). Anderson (1968) further notes that another consequence of the increased pumping since 1923 is a reduction in natural discharge, including less evapotranspiration losses and less discharge to rivers, exemplified by the observation that "the Gila River no longer flows as it once did in the reach downstream from its confluence with the Salt."

MODEL CALIBRATION AND PREDICTION

Anderson (1968) used a two-dimensional electric-analog model to simulate the uppermost 1200 ft of the aquifer system. Although the technology of electric-analog models of ground-water systems has generally been superseded by numerical (digital computer) models, the principles are the same, and the results of both would be essentially identical. The analog model constitutes a deterministic, distributed-parameter, simulation model and hence provides an appropriate example for analyzing the predictive accuracy of deterministic ground-water models.

The model was based on the assumption that, prior to 1923, an equilibrium existed in the aquifer in which recharge balanced discharge. The analog model then simulates changes in hydraulic head that occur in response to changes in stresses since the assumed steady-state time. The model was calibrated by adjusting aquifer properties, stresses, and boundary conditions to reproduce observed historical changes in ground-water levels during 1923-64 (as shown in Figure 5). The model was constructed at a scale of 1 inch equals 1 mile, with nodes (resistor junctions) placed at 1-inch intervals. Values of the storage coefficient varied spatially in the model from 0.10 to 0.19. One limitation of the model is that it is a two-dimensional approximation of a three-dimensional system. Furthermore, although the transmissivity and storage coefficient are proportional to saturated thickness, a limitation of the model noted by Anderson was that values of these two aquifer properties were not corrected with time to transient changes in water levels. Also, significant land subsidence is known to be occurring within the modeled area, although this process was not explicitly represented in the model. Anderson concluded that the model was a valid representation of the actual hydrologic system for 1923-64, and states, "The close comparison of the field and model data for these periods is the basis for the assumption that the electrical-analog system can be used to predict future ground-water conditions."

Although the model is used to predict future responses, first the future stresses must also be assumed or predicted. In this case, past trends provided the basis for the simplifying assumption that the future amount and areal distribution of pumping would remain about the same as during the most recent six-year period (1958-64). Thus, the future pumpage was assumed to equal 3.2 million ac-ft per year. However, Anderson cautions that, "The amount of water pumped probably will be less because the ever-increasing pumping lifts will make pumping increasingly expensive, and economically marginal lands may be withdrawn from cultivation." He then states that this assumed continuation of the most recent pumpage patterns ". . . will cause the predicted water-level declines to be greater than are actually probable."

The model was thereby used to predict changes in water levels for 10 years into the future. The prediction is illustrated in Figure 7 as the predicted depth to water in 1974. Comparison with Figure 6 shows that the predicted depth to water in 1974 is consistently greater than the depth to water in 1964, in many places by more than 100 ft.

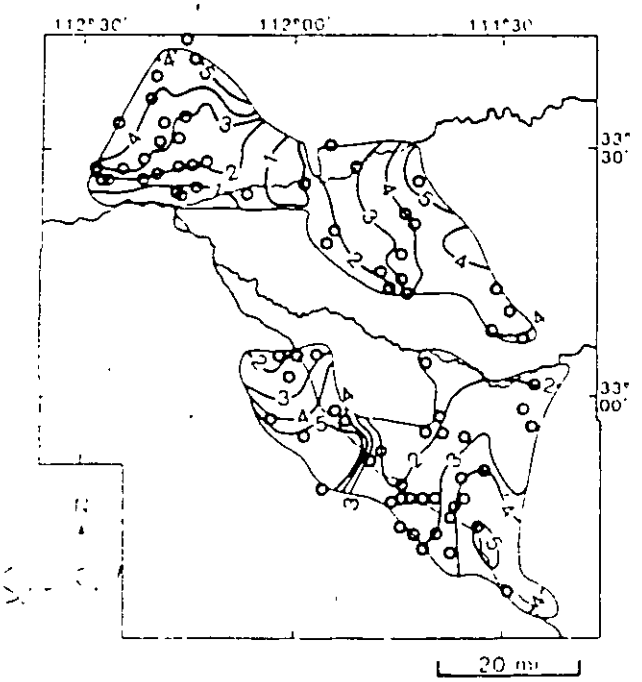

Fig. 7. Predicted depths to water in central Arizona, spring 1974 (modified from Anderson, 1968).

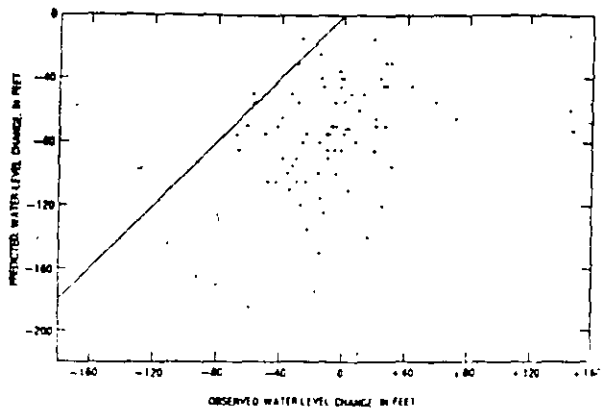

Fig 8 Relation between predicted and observed changes in water level in the Tempe-Mesa-Chandler area of the Salt River basin, Arizona, 1964-74. Solid line shows where predicted equals observed values.

ASSESSMENT OF PREDICTION

Water-level records are available for 77 wells in the study area for both 1964 and 1974, the locations of these wells are shown in Figure 7. These wells are distributed fairly uniformly throughout the basins, that is, their locations are not clustered in any single subarea or environment. A comparison of the predicted and observed changes in water level at those 77 points provides a basis for evaluating the accuracy of the model prediction. For the entire study area, the predicted water-table decline averages about 50 ft after 10 years. For the 77 available wells, the predicted 10-year decline averages about 82 ft and ranges from 15 ft to 215 ft. However, 10 years after the end of the model-calibration period, measurements of the actual change in water level in the same wells declined an average of only 9 ft, and the observed change ranged from a decline of 92 ft to a rise of 146 ft.

The relationship between the predicted and observed changes in water levels is illustrated in Figure 8. If the predictions were relatively accurate, the data should plot along (or close to) the 45° line connecting equal values of predicted and observed changes. Instead, data from all but three wells fall below that line, indicating poor accuracy and the presence of a bias in the model predictions. Also, the data show a relatively wide scatter, indicating that the model prediction is imprecise. The correlation coefficient is 0.29, although this is statistically significant at the $\alpha = .05$ level for a one-sided test, it is low and indicates a poor correlation between the predicted and observed water-level changes. It is further evidence of the relatively poor accuracy of the prediction of the future water levels in this aquifer system.

If there are any lessons to be learned from looking back at this prediction, we must try to ascertain and differentiate among the many possible sources of error. The most obvious question focuses on how much of the error can be attributed simply to errors in the assumed future stresses. In other words, if the future stresses had been estimated accurately and precisely, would the water-level changes have been predicted more closely? This question could best be answered by rerunning the model for the 1965-74 period under an imposition of the stresses that actually occurred. Unfortunately, the original analog model no longer exists and the necessary detailed data on the spatial distribution of pumpage and recharge in the entire study area for 1965-74 are not available. So we are limited to inferring and deducing as much as possible about the sources of error based on the nature and distribution of the errors and our knowledge of the hydrogeologic system.

A frequency distribution of the differences between the observed and predicted changes (that is, the residuals or errors) is presented in Figure 9. The errors are approximately normally distributed [based on the Kolmogorov D statistic (SAS Institute, 1982, p. 580), probability level, $p = 0.043$] and have a mean of −73 ft, a standard deviation of 47 ft, and range from 11 to −226 ft. Ideally, the central tendency of the error distribution should be near zero and the standard deviation should be much smaller than it is.

From Figure 8 it is clear that declines were predicted everywhere, but the changes that occurred turned out to be either much smaller

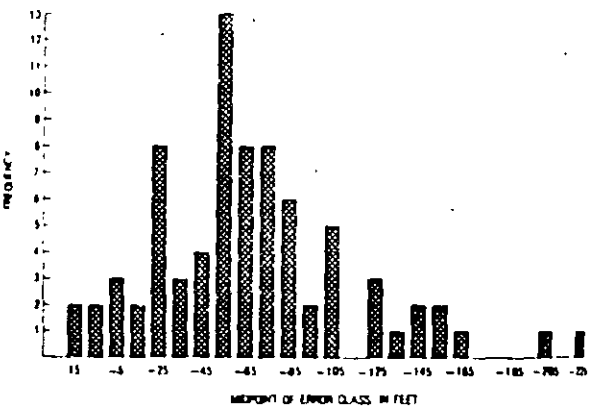

Fig. 9. Histogram showing frequency distribution of errors for the flow model of the Tempe-Mesa-Chandler area of the Salt River basin, Arizona, 1964-74.

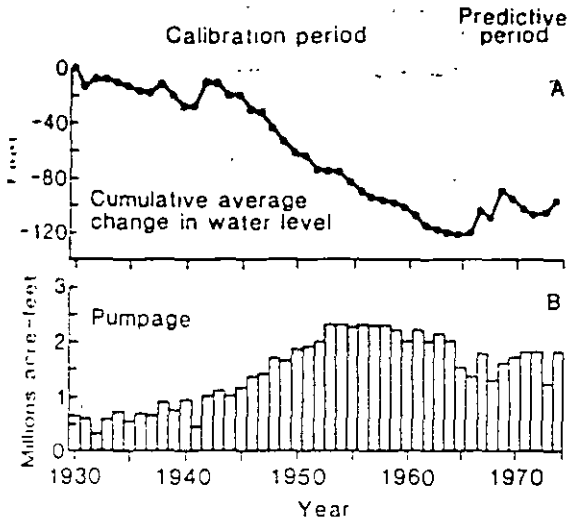

Fig. 10. Average water-level change in the Tempe-Mesa-Chandler area (A) and annual ground-water withdrawals in the Salt River Valley, Arizona (B), 1930-74 (modified from Babcock, 1970).

declines or actual rises, which is a significant deviation from previous long-term trends. This is illustrated in Figure 10, which shows the cumulative average change in water level in wells in the Tempe-Mesa-Chandler area of the Salt River Valley and estimated annual pumpage in the Salt River Valley for 1930-74, which includes most of the calibration period and, in contrast to Figure 4, all of the predictive period. A fairly uniform trend in water-level change prevailed from the early 1940's through the early 1960's, which represented the last 20 years of the model calibration period. But a marked break in this trend occurred very soon after the end of the calibration period. This break corresponds closely with the change to a regime of lesser withdrawal that prevailed since 1964, after a nearly constant and high rate of withdrawal that prevailed from 1953-64. Because the prediction was based on the assumption that stresses observed during the latter few years of the calibration period would continue unchanged, the model basically could do nothing else but extrapolate the water-level trends observed during the latter part of the calibration period.

Estimated actual withdrawals during 1965-74 averaged about 2.5 million ac-ft per year for the entire model area (T. W. Anderson, U.S. Geological Survey, written communication, 1984). The difference between the assumed and actual rates of withdrawal, 0.7 million ac-ft per year, represents an error in the predicted future withdrawals of only about 22 percent of the estimated value. Because the analog model was based on the principle of superposition of solutions and assumed a background withdrawal of 0.5 million ac-ft per year, the difference between the observed and predicted withdrawals actually imposed on the model is about 26 percent of the predicted value (T. W. Anderson, U.S. Geological Survey, written communication, 1985). Regardless, over the 10-year period, the cumulative error then becomes 7.0 million ac-ft. Over the entire modeled area of 1.1 million acres this is equivalent to 6.4 ft of water, and over the cultivated area of 0.8 million acres this is equivalent to 8.8 ft of water. Assuming that the storage coefficient (or specific yield) might be between 0.10 and 0.19, these amounts of water are equivalent to a saturated thickness in the aquifer of between 34 and 64 ft over the entire modeled area and 46 to 88 ft over the cultivated area. In assessing the range of effects of the error in 1965-74 withdrawals, we consider the cultivated area separately because most of the water-level observations, as well as withdrawals, are in these parts of the basins. Therefore, it is possible that the gross error in assumed pumpage can account for a large part of the average bias in the predicted water-level changes.

However, there still remains a relatively large spread in the error distribution shown in Figure 9, which will not be reduced by removing the bias. To help assess whether this lack of precision is also related to errors in the assumed pumpage, we would like to evaluate whether the spatial distribution of errors in assumed pumpage correlates with the spatial distribution of errors in predicted water-level change. Data on actual withdrawals by township (36 mi² area) during 1965-74 are available only for the Salt River Valley (T. W. Anderson, U.S. Geological Survey, written communication, 1984, from data prepared by M. R. Long, Arizona Department of Water Resources). Figure 11 shows the relation between the error in pumpage for 1965-74 in each township in both the upper and lower basins (that is, the eastern and western parts, respectively) of the Salt River Valley and the average error in the predicted water-level change (or drawdown) for the same township. The very low correlation between these two factors ($r = -0.086$) indicates that the relatively large spread in errors in predicted water-level change is probably not attributable, either solely or in any large part, to a variance in the accuracy of pumpage estimates. Hence, it appears that there are other sources of error in the model that have not yet been ascertained.

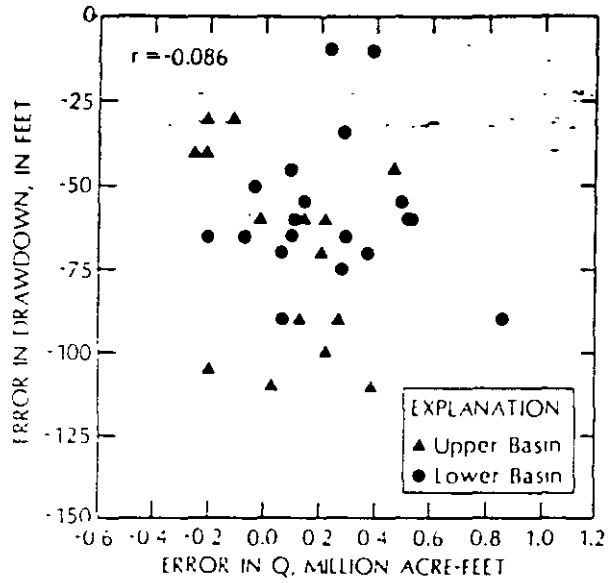

Fig. 11 Relation between the error in the predicted water-level change and the error in the estimated pumpage per township in the upper (eastern) and lower (western) basins of the Salt River Valley, central Arizona, 1965-74.

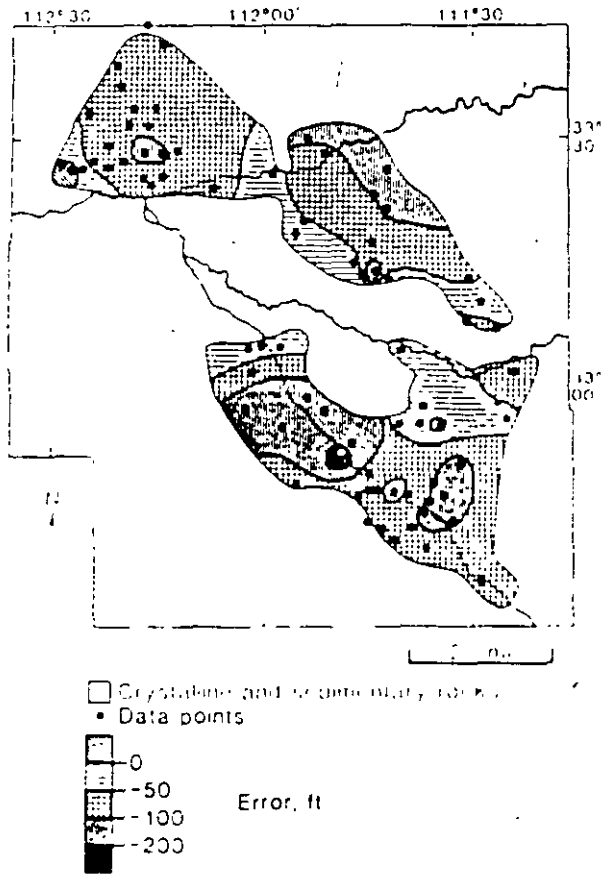

Fig 12 Map showing the spatial distribution of errors in predicted water-level change, 1965-74 in the Salt River and lower Santa Cruz River basins, Arizona.

The error in the predicted water level for 1974 was plotted on a map of the area and contoured. As shown in Figure 12, it appears that the errors are not just randomly distributed in space, but rather exhibit some persistent patterns in which the errors at nearby data points are usually close in value. However, the error pattern does not correspond closely with the pattern for any single factor for which data are available. In general, the errors seem greatest near the centers of the basins and least near their margins, but exceptions exist In the southeastern part of the modeled area, the error appears to correlate somewhat closely with depth to water and water-level decline, but elsewhere does not. For the area as a whole, the correlation coefficients for the relationships between the predicted water-level change and the observed water level in 1964 and in 1974 are 0.46 and 0.47, respectively, which are both significant at the 0.05 level for a sample size of 77 However, the correlation coefficients between the errors in predicted water-level change and the two sets (1964 and 1974) of observed water levels are only 0.14 and 0.04, which are not significant at the 0.05 level. Thus, the errors are not strongly associated with water-table elevations. Also, the absence of any important relation between the predictive error and either predicted pumpage or observed pumpage is reflected by the relatively low correlation coefficient of −0.20 for both relationships, and overlaying the transmissivity distribution map on the error map indicates no important association between these two factors

There are a number of factors that contributed to the reduction in the net withdrawals during 1965-74. Perhaps some of these could have been anticipated and their effects incorporated into the predictive analysis As noted previously, Anderson did recognize the possibility that net withdrawals would decrease, but he did not account for this in his prediction

Reexamining the history of the study area for the 1965-74 period, it is believed that the following factors contributed to lower than anticipated net withdrawals (1) Farmers in certain parts of the area ceased operations because of economic or other reasons, thereby eliminating their withdrawals for irrigation; (2) other farmers took measures, such as leveling their fields, to increase irrigation efficiency, thereby reducing their water requirements; (3) in some areas many wells were deepened to obtain water from deeper permeable zones, thereby reducing the drawdown relative to that resulting from equivalent withdrawals from

wells that penetrate less of the aquifer; (4) additional surface water was available for irrigation, reducing the dependence on ground water for supply; (5) in April 1965 an unusual flow event resulted in about 20,000 ac-ft of recharge from infiltration in the channel of the Salt River, which is otherwise normally dry (Briggs and Werho, 1966); and (6) significantly greater than average precipitation occurred in the Salt River watershed in 1972-73, and the subsequent unusually large runoff resulted in the direct recharge of about 0.5 million ac-ft of water along the river channels during 1973-74 (Babcock, 1975). Local variations in these same factors also could have contributed to the variability in the error distribution.

It is also possible that errors in the observed data could be contributing to this variability in the errors. For example, individual water-level measurements may not reflect the local static water level, perhaps due either to recent prior pumping in the observation well or to transient effects from pumps in nearby wells going on or off. These sources of error could not be accurately assessed from existing historical records. Of course, it should not be expected that long-term predictions based on long-term average stresses would predict fluctuations or short-term variations in response to short-cycle stresses (such as local transient well effects) or to unusual hydrologic conditions (such as seasonal recharge from a usually dry river channel).

Because significant land subsidence is known to be occurring in parts of this study area (Schumann, 1974, Laney and others, 1978), the possibility was considered that this process, which was not explicitly represented in the model, could account for some of the error in predicted water-level change. The land subsidence is caused by the compaction of the unconsolidated or partly consolidated sediments in the alluvial-fill basins. The compaction, in turn, is related to the compressibility of the sediments and to the decline in head in the aquifer, the latter of which is obviously induced by the major ground-water withdrawals in the area. Schumann (1974) shows the land subsidence that occurred within the study area from 1948-67. Laney and others (1978) present maps of the study area showing the extent of observed land subsidence in the lower Santa Cruz River basin from 1905 to 1977. Their data indicate that the greatest subsidence within the study area occurred in the lower Santa Cruz basin, where as much as 12.5 ft of subsidence were observed, whereas less than 5 ft of subsidence are reported for the Salt River Valley. Within the lower Santa Cruz basin, Laney and others show that most (more than 90 percent) of the subsidence occurred since 1948; as seen in Figure 10, withdrawals since 1948 were consistently greater than those prior to 1948, except for a few years during the 1965-74 predictive period. Furthermore, they show that the greatest subsidence (between 7.0 and 12.5 ft) occurred in two areas that total about 120 mi^2. The largest of these two areas is about 110 mi^2 and is located in the southwestern part of the basin near Eloy.

Hydrologically, the compaction that causes land subsidence also in effect acts as a source of water to the aquifer system. If this fluid source were not accounted for in the model, then the water produced by compaction might cause the actual drawdowns to be less than would occur otherwise, which is indeed the nature of the predictive error observed here. However, if this hypothesis were correct, we would expect to see some spatial correlation between the amount of subsidence (as shown by Shumann, 1974, and Laney and others, 1978) and the magnitude of the error (as shown in Figure 12). Comparison of these two factors shows that the maximum subsidence zone near Eloy corresponds closely with a high error (> 100 ft) zone in that same area, but that elsewhere there is no obvious association between patterns of errors and subsidence. As much as 4 ft of subsidence were observed in the Eloy area during 1965-74. As a first approximation, if we assume that 4 ft of subsidence generate 4 ft of water and if the specific yield of the aquifer in that area averages 0.15, then the subsidence may cause the water level to be 27 ft higher than it would have been otherwise. In the remainder of the study area the subsidence during 1965-74 averaged about 1 ft, which may similarly be equivalent to about 7 ft of head. These estimates are equivalent to about 20 percent of the error around Eloy and less elsewhere. Furthermore, if the compacting sediments are disseminated and distributed fairly uniformly with depth, then both land subsidence and the storage coefficient are linear functions of aquifer compressibility. Because much of the total subsidence through 1974 occurred during the model calibration period, much of its impact would have been implicitly incorporated into the model parameters during the calibration process, most likely through compensating errors in estimated aquifer properties and stresses. Then if the rate of subsidence (or ratio of rate of subsidence to rate of water-level decline) were essentially the same during the calibration period as during the

predictive period, the predictive errors resulting from not explicitly considering the subsidence process in the model would probably be negligible. Laney and others (1978) present subsidence data at various times from 1905 through 1977 along a northwest-southeast cross section that passes through Eloy. These data indicate that subsidence during the 10-year predictive period on the average represented about 33 percent of the total subsidence that occurred through 1974, although the percentage ranged from 12 to 71 percent. However, although ground-water levels declined fairly steadily during 1948-64, on the average the water level did not decline during 1965-74, yet subsidence continued at a significant or even accelerated rate, at least near Eloy. This could be explained if the compacting low-permeability sediments were restricted to just a few discrete but perhaps relatively thick layers within the total vertical profile of the alluvium. In such a case, the compaction and subsidence would be related to the compressibility of just these low-permeability sediments, rather than to an effective compressibility for the entire aquifer thickness, and the sediments within the low-permeability beds could continue to compact for years after ground-water levels had stabilized. The water produced by the compaction process would act as a delayed-yield or transient-leakage phenomena, which would cause long-term water-level declines to unit stresses to be less than they would otherwise if there were no leakage. It thus appears that, for the Eloy area, the lack of consideration of the land-subsidence process in the model contributed to the error in predicted water-level changes during 1965-74. For the rest of the modeled area, there is no evidence to indicate that this could have been a significant factor.

It also follows that such a significant lack of uniformity with depth in the properties of the sediments would imply the existence of significant variations in hydraulic conductivity and specific storage with depth. This could induce significant vertical components of flow in places, which obviously could not be represented in the two-dimensional model of Anderson, and might thus be a contributor to the predictive error. In fact, Laney (R. L. Laney, U.S. Geological Survey, written communication, 1985) states that in much of this area at least three layers of differing transmissivity would be required to adequately describe the system. For example, the uppermost and highest transmissivity layer has gradually been dewatered since the 1940's and now is saturated only in parts of the basin (R. L. Laney, U.S. Geological Survey, written communication, 1985). This implies that the effective transmissivity may have changed significantly when and where dewatering has occurred. A rigorous test of this hypothesis would require the construction of alternative two- and three-dimensional models, which is beyond the scope of this study.

This example from central Arizona illustrates the weakness of basing a prediction of aquifer responses on a single set of assumed future stresses. Because the uncertainty of the 1965-74 stresses was not assessed, we do not know whether the actual 1965-74 responses fall within some associated confidence interval; hence, we cannot make a judgment based solely on these predictive errors as to whether the model is "good" or "bad." In cases like this, it would be preferable to assess the uncertainty in estimated (or assumed) future stresses and then present the forecasts as a range of responses with associated probabilities of occurrence or confidence intervals. Because Anderson had indicated (correctly) that the assumed stresses were probably greater than would occur, the predictions can be viewed as a "worst-case" estimate. From that perspective, the model predictions are reasonably accurate.

CONCLUSIONS

There is no sure way to reliably predict the future, but, because management decisions must be made, predictions of future conditions are needed and will be made in one manner or another. To make the most reliable prediction for a given ground-water problem, all relevant information should be considered and evaluated in order to arrive at the best estimate of the future behavior of the system. Deterministic simulation models can help accomplish this quantitatively by providing a format to integrate and synthesize all available information in a manner consistent with theories describing the governing processes. Our present understanding of the many processes affecting ground water is sufficiently adequate to allow us, in theory, to forecast the behavior of a ground-water system. In practice, we are severely limited by the inadequacy of available data to describe aquifer properties and historical stresses and responses, and by an inability to predict future stresses.

Overall, extreme caution is required in making, presenting, and accepting predictions of future ground-water behavior. Partly because the confidence in estimates of future stresses decreases

with length of predictive time, and partly because historically observed system behavior may not reflect the relative dominance or strengths of different governing processes under a new set of stresses, forecasts will have greater uncertainty with increasing predictive time. The example discussed in this paper showed that calibrating a model with more than 40 years of data, in itself, did not provide a reliable basis for predicting changes in ground-water levels for a 10-year period. This example, although certainly neither exhaustive in scope nor firmly conclusive in implication, at least tends to raise serious questions concerning our ability to forecast the future state of ground-water systems. At a minimum it can be called on to question the credibility and validity of predictions of waste transport in ground water for perhaps thousands of years in areas where there may be no historical observations of flow or transport phenomena. Regardless, all ground-water predictions should be accompanied by some indication of their uncertainty; confidence intervals and explicit statements of probabilities of occurrence should be estimated.

In light of the predictive accuracy demonstrated by the model in the example presented in this paper, one might legitimately question the value of deterministic ground-water models. Although, in general, deterministic ground-water simulation models represent a valuable tool for analyzing aquifer systems and for predicting responses to specific stresses, the predictive accuracy of these models does not necessarily represent their primary value. Rather, they provide a means to quantitatively assess and assure the consistency within and between (1) concepts of the governing processes, and (2) data describing the relevant coefficients. In this manner, a model helps the investigators improve their understanding of the factors controlling ground-water flow.

An aquifer-simulation model is no more than an approximation of a complex field situation. Improvements in the approximation are always possible; thus, models should be considered as dynamic representations of nature, subject to further refinement and improvement. As new information becomes available, previous forecasts could and should be modified. Feedback from preliminary models not only helps an investigator to set improved priorities for the collection of additional data, but also helps test hypotheses concerning governing processes in order to develop improved conceptual model of the system and problem of concern. In summary, the primary value of deterministic ground-water models in many analyses is in providing a disciplined format to improve one's understanding of the aquifer system. This, in turn, should allow better management of ground-water resources of an area, regardless of the predictive accuracy of the model.

It is fairly common now for comprehensive and intensive hydrogeologic investigations to include the development, application, and calibration of a simulation model, as well as to use that model to make predictions. It is also not unusual for data collection and monitoring efforts in the study area to be curtailed after the project has ended. This will inevitably result in a future deficiency in data on actual stresses and responses during the forecast period. The uncertainty in the natural and man-imposed stresses may be so large (as in this example from Arizona) that it appears impossible to separate out the other sources of error in a postaudit. Although in the Arizona case it is possible that errors in assumed stresses can account for all predictive errors, it is more likely that errors in conceptualization and in estimated values of hydraulic parameters have also contributed. But the significance of these factors remains largely elusive. It seems reasonable to infer that the use of a more finely discretized two-dimensional model would not have improved the predictive capabilities for that aquifer system, but that a three-dimensional model or the inclusion of the land subsidence process might have helped.

It should be recognized that when model parameters have been adjusted during calibration to obtain a "best fit" to historical data, there is a bias towards extrapolating existing trends when predicting future conditions, in part because predictions of future stresses are often based on existing trends. Thus, although one advantage of deterministic models is that they represent processes and thus have cause-and-effect relationships built into them, careful attention must be paid to the accuracy with which future "causes" (stresses) can be predicted (or estimated), because that can be the major source of error in the predictions of future "effects" (system responses). Furthermore, concepts inherent in a given model (for example, two-dimensional flow and vertically-averaged parameter values, or assumed geometry and boundary conditions) may be adequate over the observed range of stresses, but may prove to be oversimplified or invalid approximations under a new and previously inexperienced type or magnitude of stresses.

The example also clearly demonstrates that if

a model is to be used for prediction, it should be periodically postaudited, or recalibrated, to incorporate new information, such as changes in imposed stresses or revisions in the assumed conceptual model. In the example, in spite of the inconclusiveness in pinpointing the exact sources of error, the postaudit pointed out the large predictive error and the major change in withdrawal trends that fortuitously occurred immediately after the end of the calibration period. The original forecasts had been extended to 1984, and subsequent to this type of postaudit, the extended prediction could have been revised to more accurately account for the change in pumping patterns and the occurrence of occasional but significant recharge events.

Thus, in general, predictions should not be made and accepted but then forgotten, plans should next focus on conducting a postaudit. Sufficient data should continue to be collected after a prediction is made so that the model can continue to be tested and evaluated as the stress history in the area continues to evolve. A postaudit offers the only true way to "verify" a model, in the sense of demonstrating its predictive accuracy for a particular field application. But more important, the evaluation of the nature and magnitude of predictive errors may itself lead to a large increase in the understanding of the system and in the value of a subsequently revised model. Revised predictions can then be made with greater reliability.

ACKNOWLEDGMENTS

Thomas W. Anderson kindly provided assistance and recent data from Arizona. William M. Alley, Richard L. Cooley, Jurate M. Landwehr, Robert L. Laney, and E. P. Patten, Jr. provided many helpful comments and suggestions during the course of this investigation. Mark A. Person assisted in data analysis.

REFERENCES CITED

Anderson, T. W. 1968. Electric analog analysis of ground-water depletion in central Arizona. U.S. Geological Survey Water-Supply Paper 1860. 21 pp.

Babcock, H. M. 1970. Annual report on ground water in Arizona, spring 1969 to spring 1970. Arizona State Land Department Water-Resources Report 43. 44 pp.

Babcock, H. M. 1975. Annual report on ground water in Arizona with special emphasis on Gila Bend Basin and McMullen Valley and the southeast part of the Harquahala Plains, spring 1973 to spring 1974. Arizona Water Commission Bull. 9. 45 pp.

Briggs, P. C. and L. L. Werho. 1966. Infiltration and recharge from the flow of April 1965 in the Salt River near Phoenix, Arizona. Arizona State Land Dept. Water-Resources Report 29. 12 pp.

Davidson, E. S. 1979. Summary appraisal of the nation's ground-water resources—lower Colorado region. U.S. Geological Survey Professional Paper 813-R. 23 pp.

Laney, R. L., R. H. Raymond, and C. C. Winikka. 1978. Maps showing water-level declines, land subsidence, and earth fissures in south-central Arizona. U.S. Geological Survey Water-Resources Investigations 78-83. 2 sheets.

SAS Institute, Inc. 1982. SAS User's Guide: Basics. Cary, North Carolina. 921 pp.

Schumann, H. H. 1974. Land subsidence and earth fissures in alluvial deposits in the Phoenix area, Arizona. U.S. Geological Survey Misc. Inv. Ser. Map I-845-H. 1 sheet.

* * * * *

Leonard F. Konikow received a B.A. in Geology in 1966 from Hofstra University. His graduate studies were at the Pennsylvania State University, where he received an M.S. and a Ph.D. in Geology in 1969 and 1973, respectively. He has worked for the Water Resources Division of the U.S. Geological Survey since 1972, and presently is a Research Hydrologist in their Reston, Virginia office.

FACULTAD DE INGENIERIA U.N.A.M.
DIVISION DE EDUCACION CONTINUA

CURSOS ABIERTOS

XII CURSO INTERNACIONAL DE CONTAMINACIÓN DE ACUÍFEROS

MODULO III: MODELOS MATEMÁTICOS EN GEOHIDROLOGIA Y CONTAMINACIÓN DE ACUIFEROS

TEMA

HOW GOOD ARE ESTIMATES OF TRANSMISSIVITY FROM SLUG TEST IN FRACTURED ROCK?

EXPOSITOR: DR. ADOLFO CHAVEZ RODRIGUEZ

PALACIO DE MINERIA
OCTUBRE DEL 2000

How Good Are Estimates of Transmissivity from Slug Tests in Fractured Rock?

by Allen M. Shapiro[a] and Paul A. Hsieh[b]

Abstract

Slug tests in fractured rock usually are interpreted with models that assume homogeneous formation properties, even though hydraulic properties of fractures can vary by many orders of magnitude over the length of boreholes. To investigate the impact of heterogeneity on the interpretation of slug tests in fractured rock, slug tests were conducted over large intervals of boreholes in crystalline rock in central New Hampshire, and interpreted using a homogeneous model. The results of the slug tests were then compared with estimates of transmissivity from fluid-injection tests conducted over shorter intervals in the same boreholes. The fluid-injection tests showed transmissivity to vary more than six orders of magnitude over the length of the boreholes; however, the sum of the transmissivities from the fluid-injection tests were within an order of magnitude of the transmissivity estimated from the slug tests. Although the two estimates of transmissivity were within an order of magnitude of each other, the water level responses during the slug tests did not exactly match the responses predicted by the homogeneous model. To investigate the effect of heterogeneity on water level responses during slug tests, a Laplace-transform solution was developed for slug tests conducted in boreholes containing multiple fractures with hydraulic properties that vary over the length of the borehole. A comparison of this solution with the homogeneous model shows no difference between the shape of water level responses in a homogeneous formation and a (layered) heterogeneous formation. Furthermore, the transmissivity estimated using a homogeneous model is within an order of magnitude of the prescribed transmissivity in the heterogeneous model. Thus, differences between responses predicted from a homogeneous model and measured water levels during slug tests can be attributed to phenomena such as nonradial flow in the vicinity of the borehole, and not heterogeneous hydraulic properties over the length of the borehole. The experimental results of this investigation show that even when conditions such as nonradial flow are present in the vicinity of the borehole, interpretations of slug tests using a homogeneous model provided order-of-magnitude estimates of transmissivity in the crystalline rock terrane under consideration.

Introduction

Slug tests are single-hole hydraulic tests used to estimate formation transmissivity, T, and storativity, S. Usually, slug tests are conducted by perturbing the water level in a well and monitoring the subsequent water-level response. Because the volume of water used to perturb hydraulic conditions in the well is small relative to the volume of fluid in the formation, slug tests stress only a small volume of the formation about a given well. Thus, slug tests cannot be used to determine large-scale formation properties or to identify heterogeneity in formation properties, which are important factors when considering fluid movement and contaminant migration in subsurface environments. Nevertheless, slug tests are regarded as a simple and efficient means of estimating T and S in the vicinity of a given well. In many formations with contaminated waters, slug tests are regarded as the only means of hydraulic characterization, because they involve limited contact with contaminated formation waters and thus, limited costs associated with cleaning equipment and disposal of contaminated waters extracted from the formation. Consequently, slug tests have been applied widely in characterizing a variety of geologic settings, including unconsolidated sediments and fractured rock.

Solutions to mathematical models of slug tests in fractured rock have been developed by several investigators. Barker and Black (1983) considered slug tests in a formation where horizontal fractures intersect a borehole and interact with regularly spaced slab-shaped rock matrices between the fractures. Dougherty and Babu (1984, 1985) solved the equations for slug tests conducted in a homogeneous dual-porosity medium, including the effects of a borehole that partially penetrates the formation. Karasaki et al. (1988) developed a range of slug test solutions that consider different combinations of flow geometries in fractures intersecting the borehole.

For the most part, the solutions discussed above have relied upon the assumption of homogeneity in formation properties, even though it is widely recognized that hydraulic properties of fractures can vary significantly over the length of boreholes. Furthermore, in many cases, the water-level responses from the slug test solutions

[a]U.S. Geological Survey, 431 National Center, Reston, Virginia 20192

[b]U.S. Geological Survey, 345 Middlefield Road, Mail Stop 496, Menlo Park, California 94025

Received August 1996, accepted January 1997.

discussed above are nonunique, meaning that different combinations of parameter values and flow geometries may lead to similar hydraulic responses in the borehole (Barker and Black 1983; Karasaki et al. 1988). Thus, it is difficult to apply the solutions discussed above to differentiate among conceptual models and uniquely identify formation properties.

Consequently, slug-test solutions developed specifically for fractured formations are not commonly applied when estimating T and S from slug tests conducted in fractured rock. Instead, models of slug tests developed for homogeneous porous media have been used, for example, the models of Hvorslev (1951), Cooper et al. (1967) and Bouwer and Rice (1976), even though the measured water levels from slug tests in fractured rock may show only a qualitative similarity to these models. Therefore, when characterizing fractured rock terranes using slug tests, where heterogeneity in fracture properties is anticipated, we must ask if estimates of T and S are reasonable if they are based on conceptual models of homogeneous porous media.

Barker and Black (1983) performed a comparison between their slug-test solution and the slug-test solution of Cooper et al. (1967). Barker and Black (1983) showed that estimates of T made using a homogeneous model were within an order of magnitude of the transmissivity of the fractures. However, their comparison was based on their conceptual model of fractured rock, which assumed homogeneous fracture properties over the length of the borehole. Harvey (1992) investigated the estimation of formation properties from slug tests simulated in three-dimensional, random hydraulic conductivity fields; however, the distribution of heterogeneity was not representative of fractures in rock terranes.

The purpose of this paper is to examine experimentally the robustness of interpreting slug tests in fractured rock with a conceptual model that assumes homogeneous porous-medium properties. Boreholes completed in crystalline rock in the Mirror Lake watershed in central New Hampshire were tested hydraulically using two methods, slug tests and fluid-injection tests using straddle-packer apparatus. The straddle-packer apparatus provid detailed estimates of transmissivity over 5 m intervals of the bo hole; whereas the slug tests were conducted over intervals in t same boreholes that ranged from 8 to 166 m in length. The tran missivity estimated from the slug tests, using the solution of Coop et al. (1967), is compared with the sum of the transmissivities est mated from the fluid-injection tests over comparable sections of t borehole to investigate the effect of assuming homogeneity whe interpreting slug tests conducted in boreholes with heterogeneou fracture properties.

This paper also examines the role of heterogeneous fractu properties on slug-test responses. A Laplace-transform solution developed to investigate slug tests conducted in boreholes havin fractures with variable T and S over the length of the borehole. B prescribing distributions for T and S, the slug-test response in a he erogeneous formation is compared with the solution of Cooper et al. (1967) to investigate the effect of assuming homogeneous fo mation properties when interpreting slug tests.

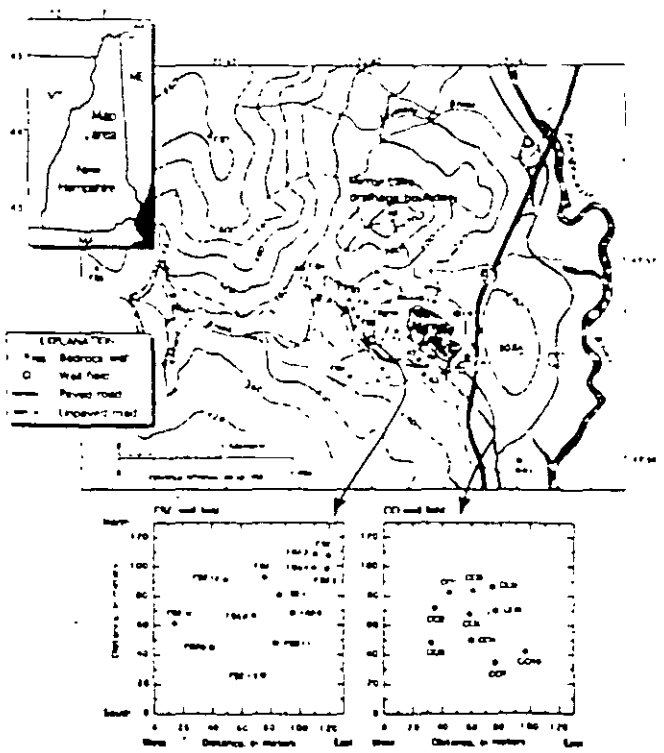

Figure 1. Map of Mirror Lake area in New Hampshire and location of bedrock boreholes.

Mirror Lake Site

The Mirror Lake watershed is at the lower end of the Hubbar Brook Valley in the southern part of the White Mountains in cen tral New Hampshire (Figure 1). The Mirror Lake watershed lie partly within the Hubbard Brook Experimental Forest, which is a ecosystem research site operated by the U.S. Forest Service. Startin in 1990, the U.S. Geological Survey installed an array of borehole in the bedrock and piezometers in the glacial drift in the Mirror La area and Hubbard Brook Valley as part of investigations to develo and evaluate field techniques and interpretive methods of charac terizing fluid movement and chemical transport in fractured roc over distances from meters to kilometers (Shapiro and Hsieh 1991 1996, Shapiro et al. 1995). The hydraulic tests and interpretation discussed in this paper are a part of the research initiative in frac tured-rock hydrogeology at the Mirror Lake site.

In the Mirror Lake area, pelitic schist, which was folded an metamorphosed to a sillimanite grade, has been extensively intrude by dikes, anastomosing fingers and pods of granite (Barton 1996). Small amounts of pegmatite and lamprophyre in the form of dike also are present in the bedrock. The distribution of rock types an fractures in road cuts and outcrops in the Mirror Lake area indicate that granite and schist are not spatially persistent over distance greater than approximately 15 m, and the spatial configuration o these rock types is highly irregular. Furthermore, the granite appear to be more densely fractured than the schist, and the fractures in th granite appear to be shorter and more nearly planar than those in th schist (Barton 1996).

Boreholes in the Mirror Lake area are cased through glacial drif and completed as open holes in the bedrock. The boreholes ar approximately 15 cm in diameter and generally are completed t depths ranging from 60 to 300 m. Figure 1 shows the location o boreholes in the Mirror Lake area at the end of 1996. The hydraulic tests described in this article were conducted in boreholes CO2, FS2 FS3, R1 and TR1.

Standard geophysical logging tools, an acoustic-televiewer log and a submersible borehole television camera were used in each borehole to determine the location and orientation of fractures borehole characteristics and rock type (Johnson 1996; Paillet 1996). Figure 2 is an interpretation of the acoustic-televiewer log conducted in a portion of borehole R1. The figure shows an opened and ori-

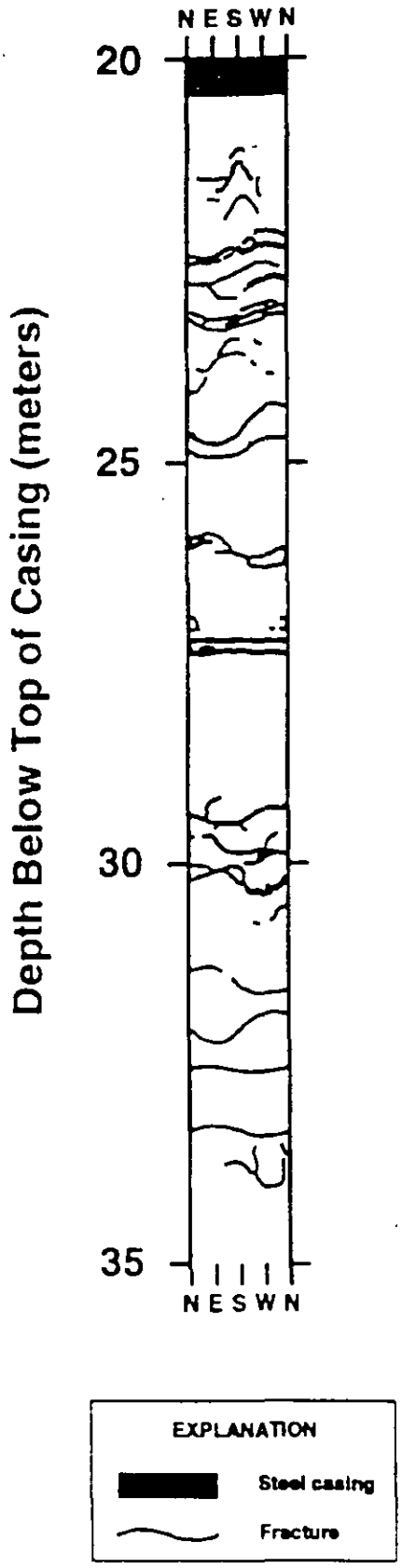

Figure 2. Distribution of fractures interpreted from acoustic-televiewer log of borehole R1 from 20 to 35 m below top of casing.

ented view of the inside of the borehole wall and the location of fractures intersecting the borehole. The fracturing in most boreholes in the Mirror Lake area is similar to that shown in Figure 2. In general, a large number of fractures intersect the boreholes, however,

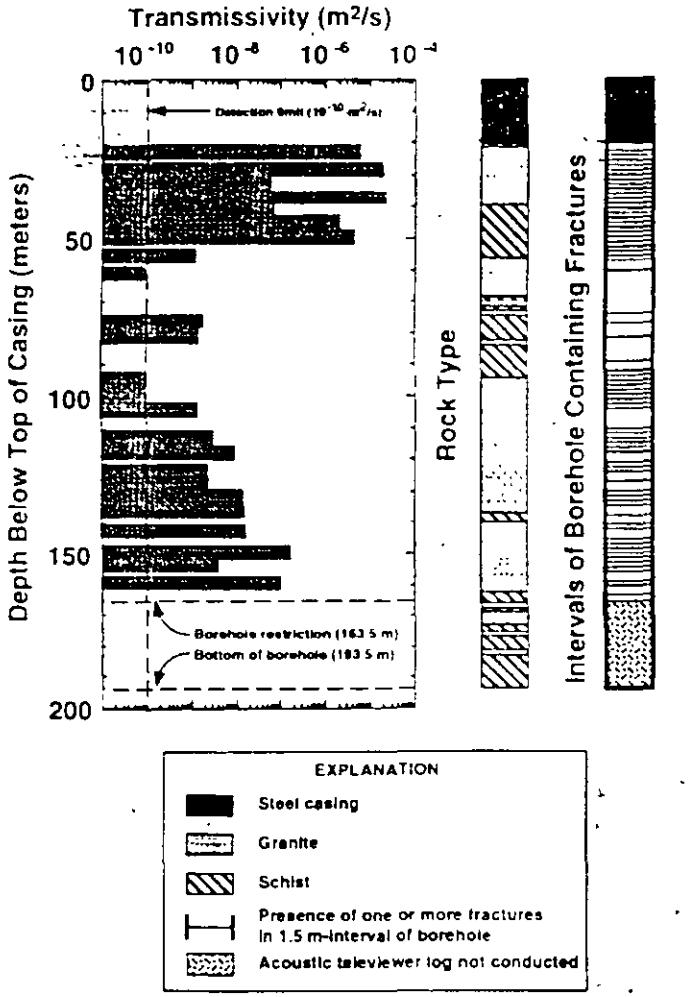

Figure 3. Distribution of transmissivity interpreted from fluid-injection tests, rock type and fractures in borehole R1.

boreholes are not uniformly fractured, and the degree of fracturing depends on the rock type (Figure 3).

Slug Tests

Slug tests were conducted in intervals of boreholes CO2, FS2, FS3, R1 and TR1. Inflatable packers were installed in these boreholes to isolate large intervals for the long-term monitoring of hydraulic heads in the bedrock (Hsieh et al. 1996). In boreholes FS2, FS3, R1 and TR1, two packers were installed in each well to isolate three intervals, while in borehole CO2, one packer was installed to isolate two intervals. The intervals ranged from 8 to more than 160 m in length (Table 1). The intervals were instrumented so that fluid pressure in each interval could be monitored from land surface by directly measuring a water level open to the atmosphere (Figure 4). The water level in the middle interval of each borehole was accessed using continuous tubing that extended through the upper packer. The water level in the lower interval in each borehole was accessed through the core pipe through the center of the packers.

Slug tests were conducted in each interval of the boreholes by adding water to the 5.08 cm diameter pipes at land surface (Figure 4). The water levels in the pipes were monitored over time using pressure transducers connected to a data logger. Manual measurements using an electric water-level sounder were made periodically as a check on the transducer readings. Water-level responses from

Table 1

Transmissivity and Storativity Estimated from Slug Tests (using solution of Cooper et al. [1967]) in Intervals of Boreholes CO2, FS2, FS3, R1, and TR1, at the Mirror Lake Site and the Sum of Transmissivities from Fluid-Injection Tests Conducted in Similar Intervals of the Same Boreholes

Well Name	Interval Top: Depth below Top of Casing m	Interval Bottom: Depth below Top of Casing m	Number of Fluid-Injection Tests over Interval	Fluid-Injection Test: Transmissivity Summed over Interval m^2/s	Slug Test: Transmissivity of Interval m^2/s	Slug Test: Storativity of Interval
CO2	8.2	32.6	4	9.4×10^{-7}	2.7×10^{-6}	1.0×10^{-9}
CO2	33.2	61.6	5	1.0×10^{-6}	1.5×10^{-5}	1.1×10^{-10}
FS2	10.5	32.7	2	1.7×10^{-9}	***	***
FS2	33.3	66.2	9	2.3×10^{-7}	7.6×10^{-5}	1.1×10^{-3}
FS2	66.8	108.9	8	3.3×10^{-7}	4.1×10^{-7}	1.1×10^{-4}
FS3	12.2	26.2	3	8.2×10^{-6}	3.4×10^{-6}	1.0×10^{-2}
FS3	26.8	59.7	3	2.5×10^{-6}	5.0×10^{-5}	1.1×10^{-2}
FS3*	60.3	226.1	11	6.2×10^{-5}	2.4×10^{-4}	1.1×10^{-8}
R1	20.6	31.3	1	2.3×10^{-5}	1.7×10^{-5}	1.0×10^{-2}
R1	31.9	64.8	9	5.0×10^{-5}	1.5×10^{-5}	1.1×10^{-10}
R1**	65.4	194.3	15	3.2×10^{-7}	5.9×10^{-7}	1.1×10^{-4}
TR1	52.8	61.1	1	1.9×10^{-7}	2.8×10^{-6}	1.0×10^{-2}
TR1	61.7	91.8	4	3.2×10^{-6}	8.0×10^{-6}	1.1×10^{-10}
TR1	92.7	191.2	11	1.5×10^{-6}	1.1×10^{-6}	1.1×10^{-5}

* Borehole FS3 restricted at 196.6 m. Fluid-injections test not conducted below 196.6 m.

** Borehole R1 restricted at 165.5 m. Fluid-injection tests not conducted below 165.5 m.

*** Response too slow to measure.

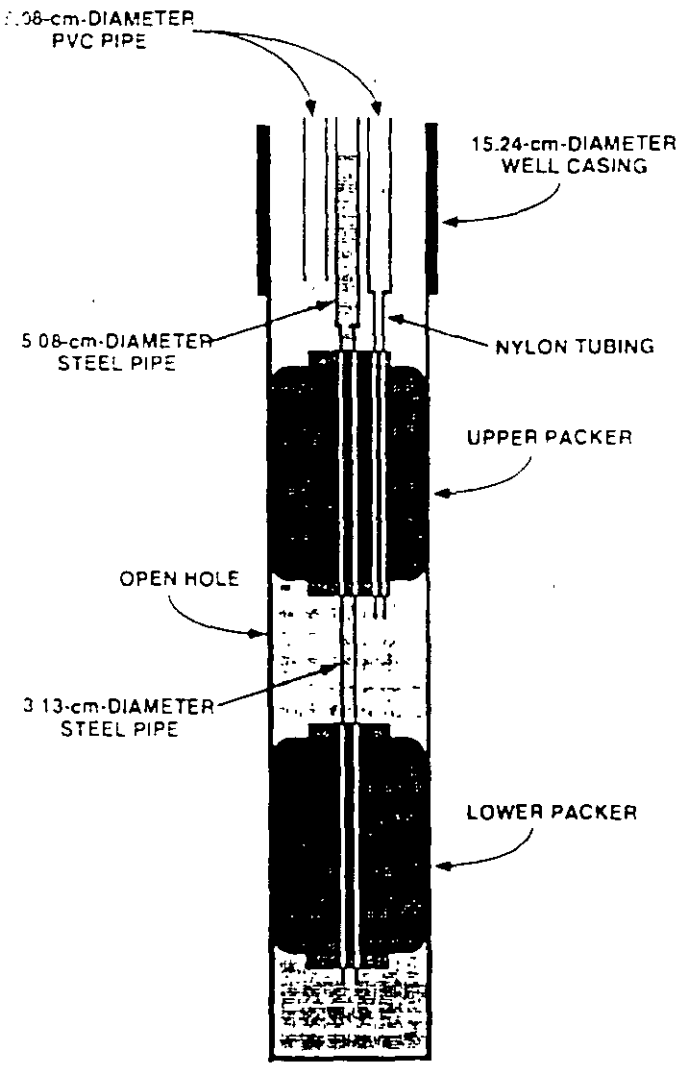

Figure 4. Instrumentation for multilevel monitoring of hydraulic head in a bedrock well.

the slug tests conducted in intervals of borehole R1 are shown in Figure 5. In Figure 5, the dimensionless water-level response in the well, $\Delta H/\Delta H_0$, is plotted as a function of time, where ΔH is the time-varying change in the water level from the initial static water level and ΔH_0 is the initial change in the water level at the onset of the slug test. The oscillatory water level recorded in the upper interval of the well is the result of water moving between the 5.08 cm diameter PVC pipe and the larger (15.24-cm) diameter well casing; in the upper interval, water was poured into the 5.08 cm diameter PVC pipe to initiate the slug test.

Transmissivity and storativity were estimated from the results of each slug test by using the solution of Cooper et al. (1967), which is based on the assumption of radially symmetric flow in a confined, homogeneous and isotropic formation, where the well fully penetrates the formation. Estimates of T and S from each slug test were made by minimizing the sum of the squared residuals between the measured dimensionless water level and the solution of Cooper et al. (1967). The minimization procedure is based on the following expression:

$$\rho(\alpha,\beta) = \sum_{i=1}^{N}\left(\frac{\Delta H(t_i)}{\Delta H_0} - \frac{\Delta H'(\beta t_i,\alpha)}{\Delta H_0}\right)^2 \qquad (1)$$

where ρ is the sum of the squared residuals, $\Delta H'$ is the change in water level as predicted by the solution of Cooper et al. (1967), ΔH is the measured change in water level from the slug test, α is the dimensionless constant defining the ratio of storage in the formation to storage in the borehole, $\alpha = r_c^2 S/r_w^2$, r_c is the radius of the borehole, r_w is the radius of the casing, t_i corresponds to times at which equivalent values of ΔH and $\Delta H'$ are achieved, N is the number of points of comparison between the slug-test data and the solution of Cooper et al. (1967), and β scales the time in the solution of Cooper et al. (1967) for comparison with the measured water levels. In this analysis, values of t_i correspond to $\Delta H/\Delta H_0$ and $\Delta H'/\Delta H_0$ equal to 0.95, 0.90, 0.85, 0.80 . . ., 0.05. In cases where the slug test was terminated prior to reaching the ambient water level in the interval, a truncated series of values for t_i was used in performing the minimization procedure. The values of α and β, which minimize

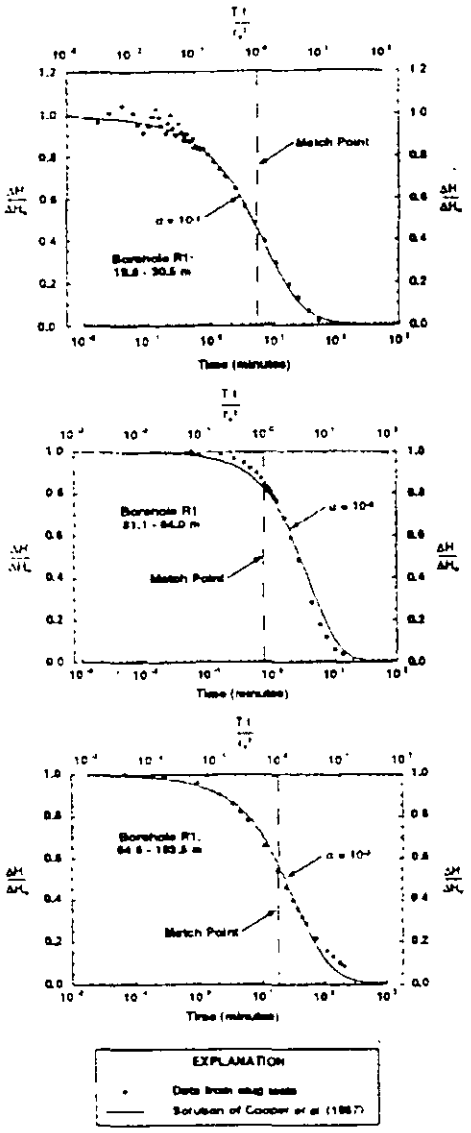

Figure 5. Water level responses for slug tests conducted in borehole R1 and the slug-test solution of Cooper et al. (1967).

the sum of the squared residuals in Equation 1, are used to estimate T and S, β is used to estimate T and α is used to estimate S (Cooper et al. 1967). In this analysis, only values of α equal to 10^{-1}, 10^{-2}, 10^{-3}, . . ,10^{-9} were considered in the minimization procedure.

Values of T and S estimated from the slug tests using the minimization procedure discussed above are given in Table 1. Figure 5 shows the fit between the slug test data and the solution of Cooper et al. (1967) for the slug tests conducted in intervals of borehole R1. In general, the results of the slug tests shown in Figure 5 resemble the shape of curves predicted by the solution of Cooper et al. (1967). However, the match between the data and the type curves is not an exact one; the differences are most pronounced at the early and late times during the tests. The solution of Cooper et al. (1967) assumes homogeneous formation properties, whereas the boreholes at the Mirror Lake site have numerous fractures with different hydraulic properties over the length of the tested intervals. In addition, fracture connectivity and individual fracture properties may create flow conditions that are not radially symmetric about the well.

The transmissivity of the tested intervals ranges over three orders of magnitude, 10^{-8} to 10^{-5} m^2/s, which is reasonable in

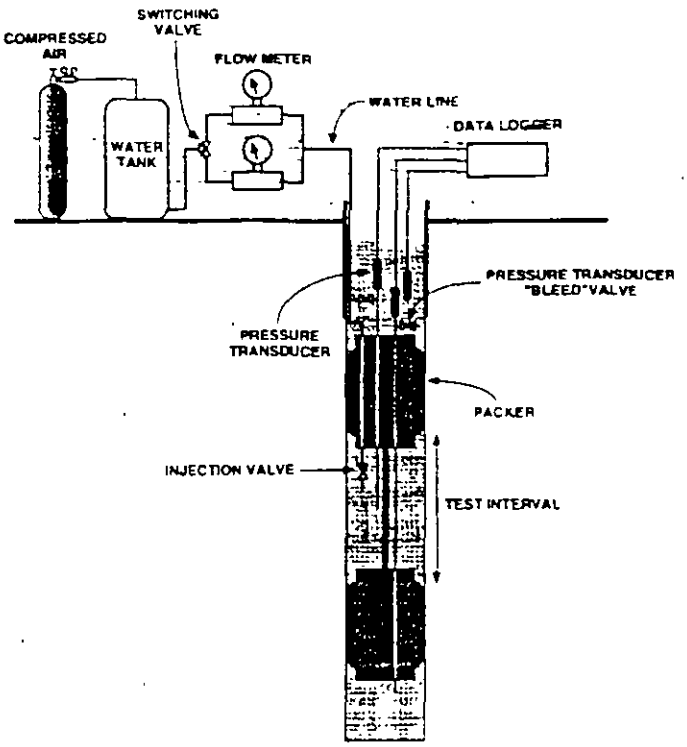

Figure 6. Instrumentation for conducting fluid-injection tests in a bedrock well.

light of the heterogeneous distribution of fractures in the granite and schist at the Mirror Lake site. The storativity estimated from the slug tests ranges from 10^{-10} to 10^{-2}, where most of the values of S are at the extremes of this range. This range of storativity probably is not physically realistic in granite and schist; however, estimates of S usually are regarded as being unreliable from single-hole tests such as slug tests. The range in the estimates of S also may indicate the assumptions implicit in the solution of Cooper et al. (1967), for example, radially symmetric flow, are not being encountered in the tested intervals.

Fluid-Injection Tests

Fluid-injection tests were conducted in all boreholes at the Mirror Lake site to provide a detailed description of the hydraulic properties in the bedrock. Fluid-injection tests were conducted using a straddle-packer apparatus, which hydraulically isolates a short interval of the borehole (Figure 6); usually, a 5 m interval was used for the fluid-injection tests. For each test, fluid was injected between the packers using a pressurized tank at land surface, while the flow rate and fluid pressure in the isolated interval were monitored. Fluid pressures above and below the isolated interval also were measured as a means of checking for fluid leaking around packers or the "short-circuiting" of fluid to the borehole through fracture connections in the rock. Fluid pressures were measured using pressure transducers, and an in-line flowmeter was used to measure the flow rate. A valve was used to switch between two flowmeters depending on the permeability of the packed-off interval. One flowmeter was calibrated between 6.75×10^{-5} and 5.09×10^{-3} liters per second (L/s), while the second flowmeter was calibrated between 2.93×10^{-3} and 1.33×10^{-1} L/s. An air-actuated, down-hole valve in the packed-off interval was used to start and stop the flow of water during the test.

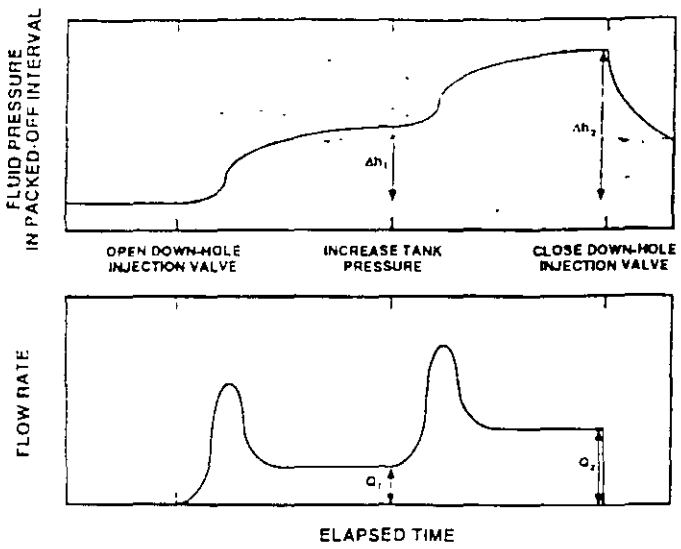

Figure 7. Typical results for fluid pressure and flow rate measured in the packed-off interval during fluid-injection tests.

Intervals for fluid-injection tests were chosen on the basis of the acoustic-televiewer survey of the borehole wall. Only those sections of the borehole that penetrated fractures were tested. Intervals that penetrated no fractures were assumed to be below the detection limit of the flowmeters in the apparatus, which is approximately 5×10^{-5} L/s.

Typical responses for the fluid pressure in the packed-off interval and the flow rate during an injection test are shown in Figure 7. At the start of the test there is an increase in both the fluid pressure and the flow rate as water pressurizes the borehole between the packers. Gradually the flow rate declines and begins to stabilize as the formation accepts fluid. The test is continued until a quasi-steady flow rate and fluid pressure are achieved (usually within 10 minutes). A second fluid injection test is conducted at a higher injection pressure (Figure 7) to test if fracture properties are a function of the injection pressure. For tests conducted in the crystalline rock of the Mirror Lake area, there was no detectable change in fracture properties over the range of injection pressures used.

Using the flow rate, Q, and the change in hydraulic head, Δh, measured in the packed-off interval at the end of the injection test, the transmissivity of the packed-off interval can be estimated using the Thiem equation (Bear 1979),

$$T = \frac{Q}{2\pi\Delta h} \ln\left(\frac{R}{r_c}\right), \qquad (2)$$

where R is the radius of influence at which there is assumed to be no change in the hydraulic head, and r_c is the radius of the borehole. For tests conducted at the Mirror Lake site, the borehole radius is 0.075 m and the radius of influence was assumed to be 3 m.

The Thiem equation is based on the assumption of steady-state, radial flow in a homogeneous, isotropic, and confined formation with no measured drawdown at a given radial distance (R) from the well. However, transient responses are exhibited in the fluid-injection tests, even at the end of the test period; thus, interpreting fluid-injection tests using a steady-state assumption is an approximation. Although transient pressure responses from the fluid-injection tests can be interpreted to estimate T, analyses that consider the variable flow rate and the compressibility of the straddle-packer apparatus usually are not warranted because other simplifying assumptions (for example, radially divergent flow) may not be appropriate. Thus, estimates of T from the Thiem equation are regarded as order-of-magnitude estimates. In general, we may anticipate that an estimate of T from Equation 2 should be lower than that obtained from an interpretation of the transient pressure responses, because a steeper hydraulic gradient is imposed by fixing the drawdown to be zero at a distance from the well, R. Also, the radius of influence is not known; however, only order-of-magnitude changes in the radius of influence will affect estimates of T.

Estimates of T from fluid-injection tests conducted in borehole R1 are shown in Figure 3. The transmissivity of the tested (fractured) intervals range from the detection limit, which is about 10^{-10}, to 10^{-4} m²/s. Flow in the untested (unfractured) intervals is assumed to be below the detection limit. The results shown in Figure 3 are typical of most boreholes in the Mirror Lake area. The transmissivity over the length of the borehole varies more than six orders of magnitude and there are only two or three highly transmissive intervals over the entire length of the borehole. Estimates of T for most intervals are two or more orders of magnitude below those for the most permeable intervals. Furthermore, estimates of T do not vary smoothly over the length of the borehole. The most permeable intervals may be adjacent to unfractured intervals or intervals with transmissivity at the detection limit.

The lower parts of boreholes FS3 and R1 were inaccessible to the straddle-packer apparatus due to restrictions in the borehole diameter. However, slug tests conducted in FS3 and R1 probably tested the entire lower interval of these boreholes, because it is unlikely that the restrictions hydraulically isolated the lower section of the borehole.

Comparison of Estimates of Transmissivity

In Table 1, the transmissivity estimated from the slug tests using the model of Cooper et al. (1967) is compared to the sum of the

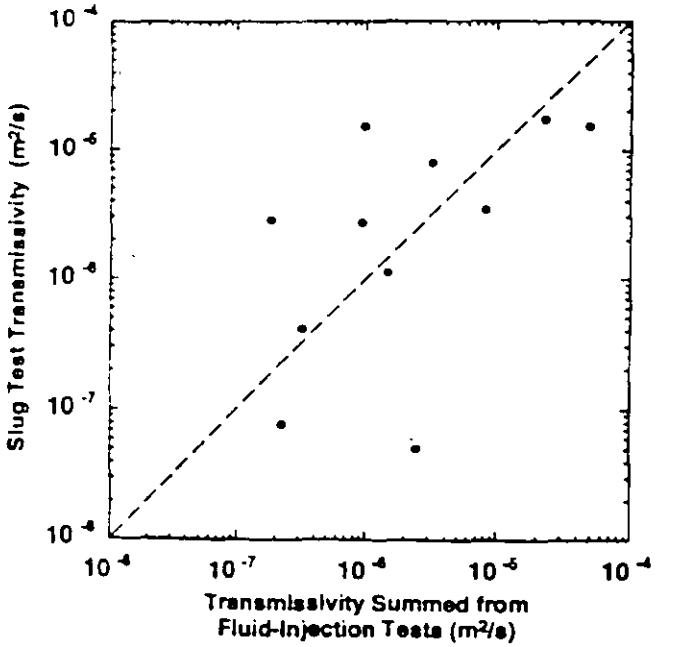

Figure 8. Transmissivity estimated from slug tests (using solution of Cooper et al. (1967)) in intervals of boreholes CO2, FS2, FS3, R1, and TR1, and the sum of transmissivities from fluid-injection tests conducted in similar intervals of the boreholes.

transmissivities estimated from fluid-injection tests conducted in the same boreholes. Figure 8 shows a plot of the results given in Table 1 where the logarithm of the two estimates of T are compared. In general, the two estimates of T for a given interval are within an order of magnitude of each other, and Figure 8 shows there is no apparent bias between the two estimates of T. However, for tests conducted in the lower intervals of boreholes FS3 and RE, the interpretation of the slug tests provided a larger estimate of T than the sum of the transmissivities from the fluid-injection tests (Table 1). This may be the result of being unable to access a portion of these intervals with the straddle-packer apparatus because of restrictions in these boreholes; thus, the sum of the transmissivities from the fluid-injection tests does not account for the transmissivity of the intervals that were inaccessible.

The fluid-injection tests provide details of the variable transmissivity over the length of the boreholes. However, the sum of the transmissivities from the fluid-injection tests is within an order of magnitude of the estimates of T interpreted from slug tests using a homogeneous porous medium model. Although the slug tests and fluid-injection tests most likely are testing a similar volume of rock about the borehole, it is unlikely that a better correlation can be achieved between the estimates of T from the two types of tests. The interpretation of the fluid-injection tests assumes a radius of influence and a steady-state flow regime, whereas a transient fluid response is assumed in the interpretation of the slug tests. Furthermore, because of the likelihood of complex fracture connectivity in the vicinity of the borehole, both tests probably are subject to nonradial flow. However, both tests may not be affected similarly by a nonradial flow regime, because the slug tests and fluid-injection tests are conducted over different lengths of the same borehole. Therefore, the difference between the estimates of T from the slug tests and fluid-injection tests should be considered within the error of the analyses. Finally, because a steady-state interpretation of the fluid-injection tests was considered, estimates of storativity from the fluid-injection test were not made. Thus information on the variability of S over the length of the borehole is not available for comparison with the estimate of S from the interpretation of the slug tests.

Heterogeneous Fracture Properties and Slug Test Responses

Although the two estimates of T discussed above are within an order of magnitude of each other, the measured water levels during the slug test do not exactly match the type curves predicted by the model of Cooper et al. (1967). It remains to be seen whether this is an artifact of the heterogeneous fracture properties over the length of the borehole or other processes such as nonradial flow in the vicinity of the borehole (Karasaki et al. 1988) or the hydraulic interaction between fractures and a porous rock matrix (Barker and Black, 1983). In this section, we investigate the effect of conducting slug tests in boreholes having heterogeneous fracture properties. The equations defining the water-level response during a slug test are solved for conditions where the borehole is intersected by numerous fractures, each with unique hydraulic properties. The fractures intersecting the borehole are assumed to respond analogously to a layered formation in which there is no hydraulic communication between fractures (Figure 9). Furthermore, each fracture is assumed to be homogeneous and isotropic, and thus, flow is radially symmetric about the borehole in each fracture.

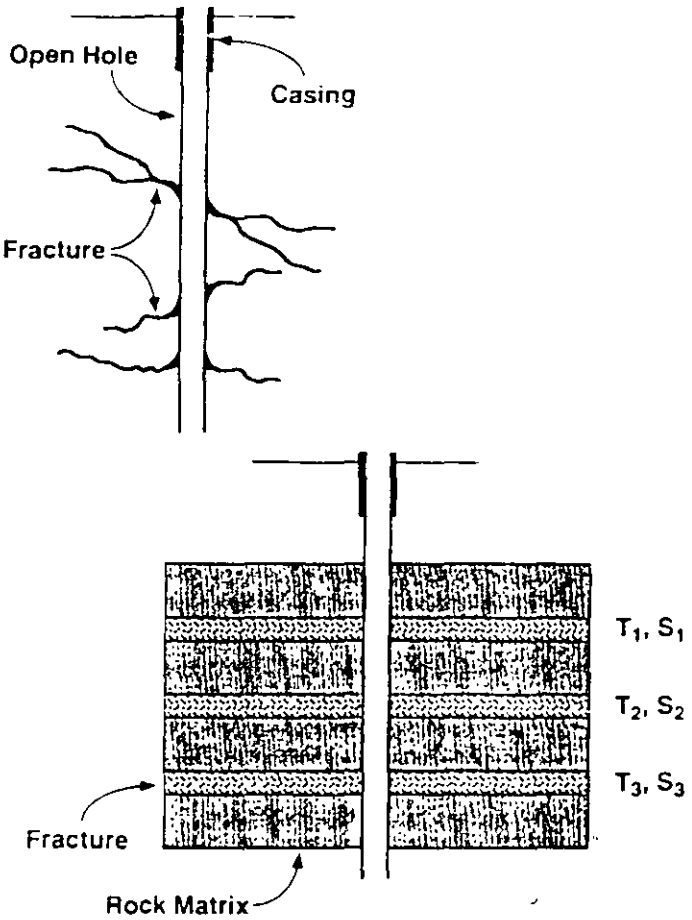

Figure 9. Conceptual model of multiple fractures intersecting a borehole as a layered aquifer where T_i and S_i are the transmissivity and storativity of individual fractures.

The conceptual model discussed above is analogous to layered formations considered in other aquifer-test interpretations (Wikramaratna 1984). Karasaki et al. (1988) also considered slug tests in boreholes that intersected two layers; here, that solution is extended to consider multiple fractures intersecting the borehole. Obviously, this conceptual model is a simplification of complex fractured rock formations; nevertheless, the results of this analysis will allow us to illustrate the effect that heterogeneous fracture properties have on water levels during slug tests, and the estimation of T and S in such formations using models that assume homogeneous porous-medium properties.

The Laplace-transform solution for the water-level response during a slug test conducted in a borehole that intersects multiple fractures is given in the Appendix. In this solution, we assume that there are a discrete number of fractures, where T_i and S_i, $i=1,2,\ldots,M$, are the transmissivity and storativity of the individual fractures intersecting the borehole, and M is the number of fractures intersecting the borehole. The effective formation transmissivity of the heterogeneous model, T_f, is assumed to be the sum of the transmissivities of the individual fractures, or

$$T_f = \sum_{i=1}^{M} T_i \qquad (3)$$

The formation storativity, however, is not readily defined from the storativities of the individual fractures. The formation storativity depends on the hydraulic diffusivity, T_i/S_i, of the individual frac-

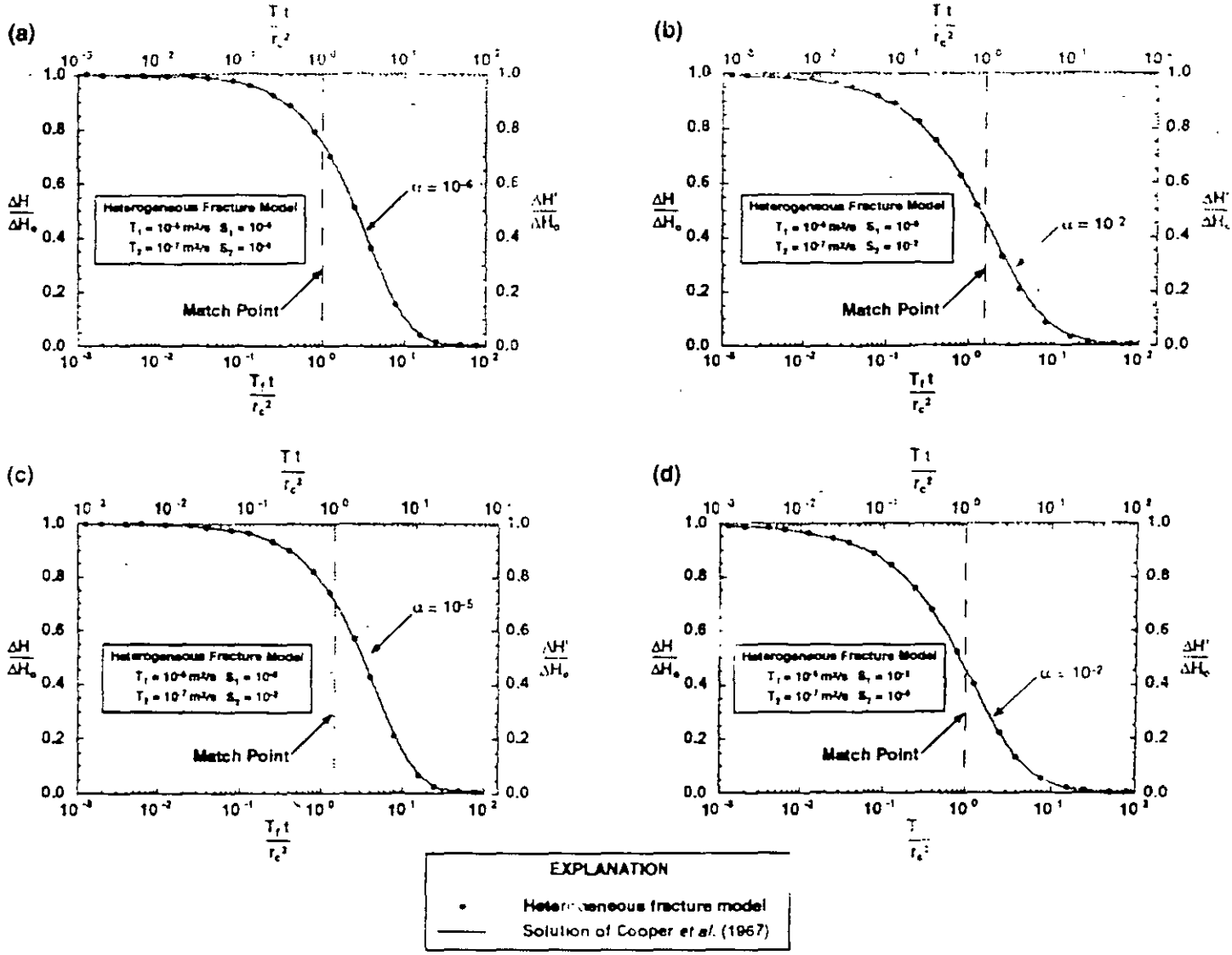

Figure 10. Four cases of slug tests in boreholes having two fractures with different transmissivity and storativity; the solution from the heterogeneous model (given in the Appendix) is compared with the slug test solution of Cooper et al. (1967).

Table 2
Transmissivity, T_f, from the Heterogeneous Model and Estimate of T from the solution of Cooper et al. (1967) for the Cases Shown in Figures 10 and 11

Example	M, Number of Fractures	$T_f = \sum_{i=1}^{M} T_i$ (m^2/s)	T, from Solution of Cooper et al. (1967) (m^2/s)	S, from Solution of Cooper et al. (1967)
Figure 10a	2	1.01×10^{-5}	1.01×10^{-5}	10^{-6}
Figure 10b	2	2.00×10^{-5}	1.29×10^{-5}	10^{-2}
Figure 10c	2	1.01×10^{-5}	0.70×10^{-5}	10^{-5}
Figure 10d	2	1.01×10^{-5}	1.01×10^{-5}	10^{-2}
Figure 11a	20	9.40×10^{-5}	9.18×10^{-5}	10^{-6}
Figure 11b	20	9.40×10^{-5}	9.62×10^{-5}	10^{-9}
Figure 11c	20	9.40×10^{-5}	6.65×10^{-5}	10^{-4}
Figure 11d	20	$\times 10^{-5}$	8.00×10^{-5}	10^{-7}

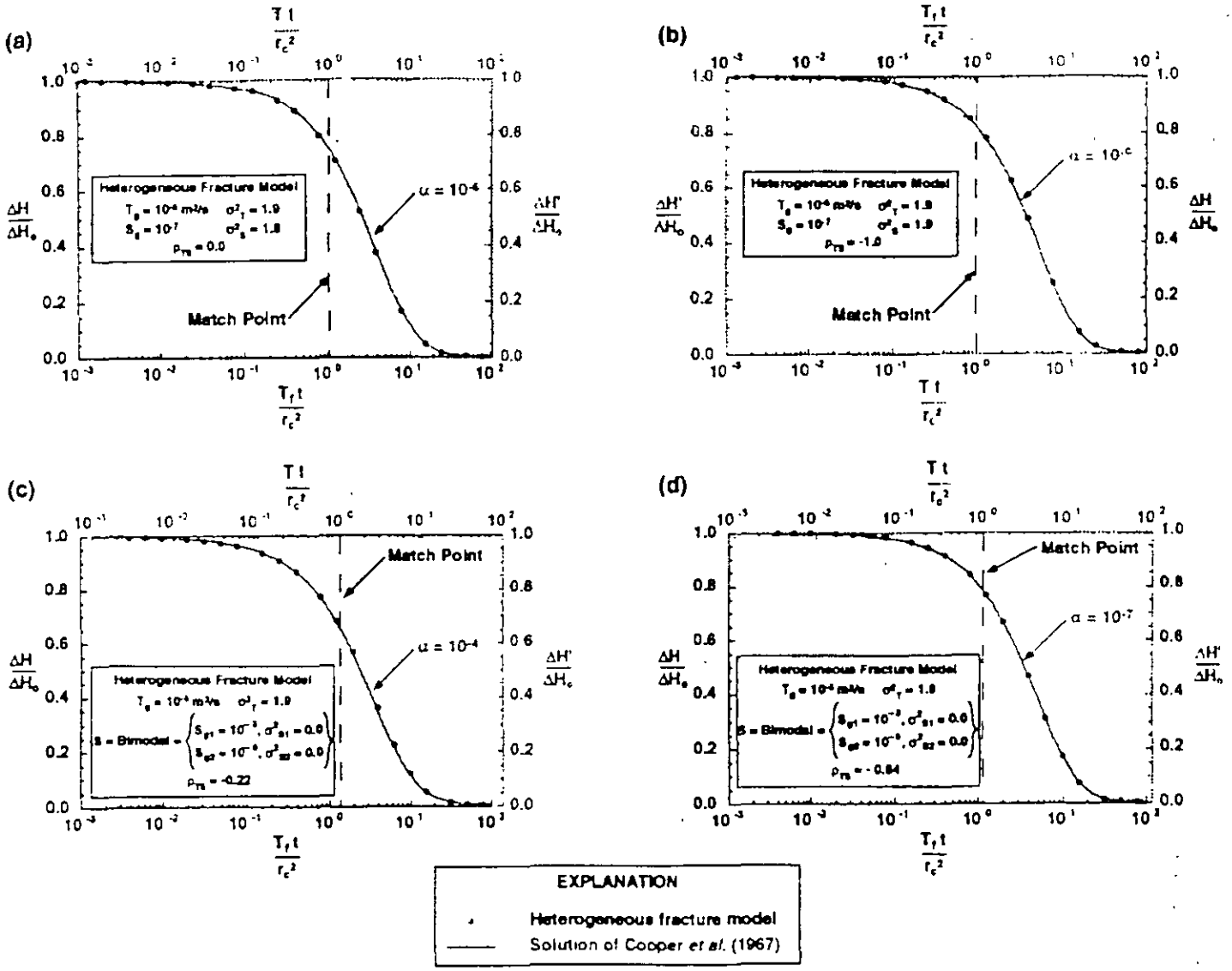

Figure 11. Four cases of slug tests in boreholes having multiple fractures with different transmissivity and storativity; the solution from the heterogeneous model (given in the Appendix) is compared with the slug test solution of Cooper et al. (1967).

tures. Only for the case in which the storativity of each fracture is the same will the formation storativity be equal to the sum of the storativities of the individual fractures.

The slug-test solution in a heterogeneous formation will be compared with the solution of Cooper et al. (1967) to illustrate the effect of heterogeneity on slug-test responses. Estimates of formation transmissivity from the solution of Cooper et al. (1967) will be denoted by T and will be made by minimizing the sum of the squared residuals between the two solutions in a manner similar to that discussed following Equation 1.

To illustrate the effect of heterogeneous fracture properties on slug-test responses, we first simulate several simple examples of a borehole intersected by two fractures only. This will be followed by more complex examples, where distributions for T_i and S_i are assumed for a number of fractures. Figure 10 shows four cases of slug tests simulated in boreholes intersected by two fractures, where the fractures have different hydraulic properties. In figure 10, extreme values of S_i are examined, for example, variability in the storativity of fractures may be dependent on the presence of fracture-fill material. In each case, the water-level response of the slug test simulated in the heterogeneous model is compared to the solution of Cooper et al. (1967). The formation transmissivity as defined by Equation 3 is compared to estimates of T using the solution of Cooper et al. (1967). The results of this comparison are given in Table 2.

From the results shown in Figure 10 and Table 2, the following conclusions are drawn. If the storativities of the fractures are equal, while the transmissivities are different, T_f is estimated correctly by the homogeneous model (Figure 10a). If, however, the transmissivities of the fractures are equal, while the storativities are different, there may be errors in estimating T_f using a homogeneous model (Figure 10b). However, the error in estimating T_f from the homogeneous model is within an order of magnitude of the calculated transmissivity from Equation 3. In cases where both the transmissivity and the storativity of the layers vary (Figures 10c and 10d), the robustness of estimating T_f using a homogeneous model depends on the storativity of the fracture with the largest transmissivity. In Figure 10c, the fracture having the largest transmissivity has the smallest storativity (i.e., a negative correlation between T and S). In this case, there is in an error in estimating T_f; however, again, the error in estimating T_f using a homogeneous model is less than an order of magnitude. In Figure 10d, the fracture with the

largest transmissivity also has the largest storativity. In this case, there is no error in estimating T_f using a homogeneous model. Furthermore, in all of these examples, the shape of the water-level responses as predicted by the heterogeneous model is similar to the shape of the response for the homogeneous model.

In Figure 11, slug-test responses in boreholes intersected by multiple fractures with varying hydraulic properties are considered. In the examples shown in Figure 11, 20 fractures are assumed to intersect the borehole. The transmissivity of the fractures is assumed to be log-normally distributed with a geometric-mean transmissivity (T_g) equal to 10^{-5} m^2/s and a variance of $\log_{10}T$ (σ^2_T) equal to 1.9. In realizations of the transmissivity, these parameters produce values of T_f that vary over six orders of magnitude or more. For the slug-test responses shown in Figure 11a and 11b, the storativity of the fractures also is assumed to be log-normally distributed with a geometric mean (S_g) equal to 10^{-7} and a variance of $\log_{10}S$ (σ^2_S) equal to 1.9. In Figure 11a, the transmissivity and storativity are assumed to be uncorrelated, $\rho_{TS}=\sigma^2_{TS}/(\sigma^2_T\ \sigma^2_S)^{1/2}=0$, where ρ_{TS} is the correlation coefficient of $\log_{10}T_f$ and $\log_{10}S_f$, and σ^2_{TS} is the covariance of $\log_{10}T_f$ and $\log_{10}S_f$. In Figure 11b, the transmissivity and storativity are assumed to be negatively correlated with $\rho_{TS}=-1$; thus, larger values of transmissivity are associated with smaller values of storativity. Negative correlation between T and S for fractures may naturally arise if fractures contain fill material; fractures with fill material may have lower permeability than unfilled fractures while also having a larger storativity than unfilled fractures. In Figures 11a and 11b, there is only a slight error in estimating the formation transmissivity when using the model of Cooper et al. (1967) (see Table 2).

In Figures 11c and 11d, 20 fractures also are assumed to intersect the borehole. The transmissivity of the fractures again is assumed to be log-normally distributed where $T_g = 10^{-5}$ m^2/s and $\sigma^2_T = 1.9$. However, in these cases the fractures are assumed to have a bimodal distribution for $\log_{10}S_f$ which is assumed to be the sum of two normal distributions where equal probability is given to each distribution. For the results shown in Figures 11c and 11d, the variance of the modes of the distributions are assumed to be zero; thus, the storativity assigned to the fractures is either 10^{-3} or 10^{-7}. Bimodal values of storativity rather than a continuous distribution of storativity could arise if some fractures are filled with the same type of geologic material while other fractures are unfilled. In Figure 11c, $\log_{10}T_f$ and $\log_{10}S_f$ have only a slight negative correlation, while in Figure 11d T_f and S_f are assumed to be more negatively correlated than the case shown in Figure 11c. The cases where S_f has discrete bimodal values produces more pronounced differences between T_f as prescribed in the heterogeneous model and the transmissivity estimated from the homogeneous model than cases where the storativity continuously varies over the range of a distribution. However, again, in Figures 11c and 11d, the error in estimating the transmissivity with the homogeneous model is less than an order of magnitude (Table 2).

As was the case for the heterogeneous model with two fractures, the cases where 20 fractures are assumed to intersect the borehole did not alter the shape of the water-level response in comparison to the homogeneous model. Thus, differences between the shape of measured water-level responses and the homogeneous model of Cooper et al. (1967) must be attributed to phenomena other than heterogeneous fracture properties. Phenomena such as nonradial flow or changing flow geometries in the vicinity of the borehole (Karasaki et al. 1988) or the hydraulic interaction between fractures and a porous rock matrix (Barker and Black 1983) are the most likely causes of differences between measured slug-test responses and the homogeneous model of Cooper et al. (1967).

Summary and Conclusions

Slug tests are used commonly to estimate transmissivity, T, and storativity, S, in the vicinity of boreholes in fractured rock terranes. However, solutions that have been derived specifically to interpret slug tests in conceptual models of fractured rock have too many parameters to obtain unique fits between predicted and measured water-level responses. Therefore, slug tests in fractured rock usually are interpreted with models that assume homogeneous formation properties, even though fracture properties may vary over the length of the borehole, or measured water-level responses may only qualitatively resemble the predicted responses of the homogeneous model. This paper investigated the impact of heterogeneous fracture properties on slug test responses and the estimation of T using an interpretive model that assumes homogeneous formation properties.

Slug tests were conducted in five boreholes in crystalline rock in central New Hampshire in intervals that ranged from 8 to more than 160 m. The slug tests were interpreted using the solution of Cooper et al. (1967), which assumes homogeneous T and S over the tested interval. Fluid-injection tests conducted over 5 m intervals in the same boreholes showed the transmissivity to vary over six orders of magnitude in the boreholes. However, the sum of the transmissivities from the fluid-injection tests were within an order of magnitude of the estimated T from the slug tests. The water-level responses of the slug tests, however, did not exactly match the predicted responses from the solution of Cooper et al. (1967).

To investigate the effect of heterogeneous fracture properties on slug-test responses, a Laplace transform solution was developed for slug tests conducted in boreholes containing multiple fractures with varying hydraulic properties over the length of the borehole. Using a homogeneous model to estimate T in boreholes having fractures with varying hydraulic properties results in errors of less than an order of magnitude. The variability in the storativity of the fractures influences the magnitude of this error. For cases where the storativities of fractures varies continuously over the range of a distribution, errors in estimating T using a homogeneous model are less than 5 percent. However, for cases where the storativities of the fractures have discrete bimodal values, errors in estimating T using a homogeneous model were shown to be as great as 30 percent for the cases considered in this paper.

Furthermore, water-level responses in slug tests conducted in boreholes with heterogeneous fracture properties over the length of the borehole have the same shape as slug-test responses in homogeneous formations. Thus, differences between measured water-level responses during slug tests and the responses predicted by the homogeneous model cannot be attributed to fracture properties that vary over the length of the borehole. Differences between the homogeneous model and measured water-level responses during slug tests are most likely the result of phenomena such as nonradial flow, the varying geometry of flow in the vicinity of the borehole, or the interaction between fractures and a porous rock matrix.

The experimental results of this investigation showed that estimates of T interpreted using a homogeneous model of slug-test responses provided order-of-magnitude estimates of T in comparison to fluid-injection tests using a straddle packer apparatus in crystalline rock in central New Hampshire. All fractured rock terranes

may not yield similar results to those given here. However, the conditions in the crystalline rock considered in this investigation are extreme because the transmissivity of fractures varies over six orders of magnitude in most boreholes and phenomena such as nonradial flow in the vicinity of the boreholes is detected. Thus, interpreting slug tests in fractured rock using a homogeneous model of formation properties may be adequate in providing order-of-magnitude estimates of transmissivity in the vicinity of the borehole in most fractured rock terranes. However, caution should be used in applying the estimates of T from slug tests, because slug tests hydraulically stress only a small volume of the formation and thus cannot be used to interpret formation heterogeneity or large-scale formation properties.

Appendix

The conceptual model of fractures intersecting a borehole given in Figure 9 is considered. There is assumed to be no cross flow between the fractures, and each fracture is assumed to be homogeneous and isotropic. Furthermore, under ambient hydraulic conditions, the hydraulic heads in the fractures are assumed to be equal and spatially uniform. Also, frictional forces along the borehole wall are assumed to be negligible. Thus, throughout the duration of the slug test, the hydraulic head in each fracture at the borehole radius is equal to the water level in the borehole. This is expressed as

$$w(t) = h_i(r = r_c, t) \qquad i = 1,2,\ldots M \qquad (A.1)$$

where w(t) is the time-varying water level in the borehole, h_i is the hydraulic head in an individual fracture denoted by the subscript i, r is the radial coordinate measured from the center of the well, r_c is the radius of the open interval of the borehole, t is time and M is the total number of fractures intersecting the borehole.

The slug test is conducted by perturbing the water level in the borehole at t = 0 and then measuring the subsequent water-level response. The equation governing the conservation of fluid volume in the borehole is

$$-\pi r_c^2 \frac{dw}{dt} + 2\pi r_c \sum_{i=1}^{M} T_i \frac{\partial h_i}{\partial r}\bigg|_{r=r_c} = 0 \qquad (A.2)$$

where r_c is the radius of the well casing and T_i is the transmissivity of an individual fracture denoted by the subscript i. Equation A.2 is subject to the initial condition

$$w(t = 0) = H_1 = h_i(r = r_c, t = 0) \qquad i = 1,2,\ldots M \qquad (A.3)$$

where H_1 is the water level in the well at the onset of the slug test.

The solution to Equations A.2 and A.3 requires a knowledge of the hydraulic responses in the individual fractures. The equation of fluid volume conservation in each fracture is written

$$\frac{\partial h_i}{\partial t} - T_i \frac{1}{r}\frac{\partial}{\partial r}\left(r \frac{\partial h_i}{\partial r}\right) = 0 \qquad i = 1,2,\ldots M \qquad (A.4)$$

where S_i the storativity of an individual fracture denoted by the subscript i. Equation A.4 is subject to the initial condition

$$h_i(r, t = 0) = H \qquad i = 1,2,\ldots M \qquad (A.5)$$

where H is the spatially uniform hydraulic head in each fracture at the onset of the slug test. Equation A.1, written for each fracture, serves as the boundary condition at the borehole for Equation A.4. The boundary condition for each fracture at a distance far from the borehole is

$$h_i(r \to \infty, t) = H \qquad i = 1,2,\ldots M \qquad (A.6)$$

For the purpose of solving the previous equations and comparing the results with the model of Cooper et al. (1967), the following dimensionless variables are considered

$$w' = \frac{H - w}{H - H_1} \qquad (A.7)$$

$$h' = \frac{H - h}{H - H_1} \qquad (A.8)$$

$$t' = \frac{T_f t}{r_c^2} \qquad (A.9)$$

$$r' = \frac{r}{r_c} \qquad (A.10)$$

where w', h', t' and r' are the dimensionless forms of w, h, t and r, respectively, and T_f is the formation transmissivity for the system of fractures,

$$T_f = \sum_{i=1}^{M} T_i \qquad (A.11)$$

Introducing the dimensionless variables into (A.1)-(A.6) yields

$$w'(t') = h_i'(r' = 1, t') \qquad i = 1,2,\ldots M \qquad (A.12)$$

$$-\frac{dw'}{dt'} + 2\sum_{i=1}^{M} \sigma_i \frac{\partial h_i'}{\partial r'}\bigg|_{r'=1} = 0 \qquad (A.13)$$

$$w'(t' = 0) = 1 = h_i'(r' = 1, t' = 0) \qquad i = 1,2,\ldots M \qquad (A.14)$$

$$\frac{\alpha_i}{\sigma_i}\frac{\partial h_i'}{\partial t'} - \frac{1}{r'}\frac{\partial}{\partial r'}\left(r' \frac{\partial h_i'}{\partial r'}\right) = 0 \qquad i = 1,2,\ldots M \qquad (A.15)$$

$$h_i'(r', t' = 0) = 0 \qquad i = 1,2,\ldots M \qquad (A.16)$$

$$h_i'(r' \to \infty, t') = 0 \qquad i = 1,2,\ldots M \qquad (A.17)$$

where the dimensionless parameters, σ_i and α_i are defined as

$$\sigma_i = \frac{T_i}{T_f} \qquad i = 1,2,\ldots M \qquad (A.18)$$

$$\alpha_i = \frac{r_c^2 S_i}{T_f} \qquad i = 1,2,\ldots M \qquad (A.19)$$

Taking the Laplace transform of (A.12)-(A.17) yields

$$\overline{w'} = \overline{h_i'}(r' = 1) \qquad i = 1,2,\ldots M \qquad (A.20)$$

$$\frac{p\alpha_i}{\sigma_i}\overline{h_i'} - \frac{1}{r'}\frac{\partial}{\partial r'}\left(r'\frac{\partial \overline{h_i'}}{\partial r'}\right) = 0 \quad i = 1,2,\ldots M \qquad (A.21)$$

$$\overline{h_i'}(r' \to \infty) = 0 \qquad i = 1,2,\ldots M \qquad (A.22)$$

$$1 - p\overline{w'} + 2\sum_{i=1}^{M}\sigma_i \left.\frac{\partial \overline{h_i'}}{\partial r'}\right|_{r'=1} = 0 \qquad (A.23)$$

where $\overline{w'}$ and $\overline{h_i'}$ are the Laplace transforms of w' and h_i', respectively, and p is the Laplace transform variable.

The solution to Equation A.21, using Equations A.20 and A.22 as boundary conditions, is

$$\overline{h_i'}(r') = \frac{\overline{w'}K_0\left(r'\sqrt{\frac{p\alpha_i}{\sigma_i}}\right)}{K_0\left(\sqrt{\frac{p\alpha_i}{\sigma_i}}\right)} \qquad i = 1, 2, \ldots M, \qquad (A.24)$$

where K_0 is the Bessel function of the second kind of order zero.

The solution for $\overline{w'}$ is obtained by introducing Equation A.24 into Equation A.23:

$$\overline{w'} = \frac{1}{p + 2\sum_{i=1}^{M}\sqrt{p\alpha_i\sigma_i}\,\frac{K_1\left(\sqrt{\frac{p\alpha_i}{\sigma_i}}\right)}{K_0\left(\sqrt{\frac{p\alpha_i}{\sigma_i}}\right)}} \qquad (A.25)$$

where K_1 is the Bessel function of the second kind of order one.

The Laplace transform solution for the distribution of the hydraulic head in each fracture is obtained by introducing Equation A.25 into Equation A.24:

$$\overline{h_i'}(r') = \frac{K_0\left(r'\sqrt{\frac{p\alpha_i}{\sigma_i}}\right)}{K_0\left(\sqrt{\frac{p\alpha_i}{\sigma_i}}\right)\left[p + 2\sum_{i=1}^{M}\sqrt{p\alpha_i\sigma_i}\,\frac{K_1\left(\sqrt{\frac{p\alpha_i}{\sigma_i}}\right)}{K_0\left(\sqrt{\frac{p\alpha_i}{\sigma_i}}\right)}\right]} \qquad i = 1,2,\ldots M \qquad (A.26)$$

The real-time solution for w' and h_i' is obtained by numerically inverting Equations A.25 and A.26, respectively (Stehfest 1970).

Acknowledgments

These investigations were conducted with the support of the Toxic Substances Hydrology and National Research Programs administered by the U.S. Geological Survey. The authors also gratefully acknowledge the logistical support provided by Mr. C. Wayne Martin of the U.S. Forest Service, who is stationed at the Hubbard Brook Experimental Forest. The Hubbard Brook Experimental Forest is operated and maintained by the Northeastern Forest Experiment Station, USDA Forest Service, Radnor, Pennsylvania.

References

Barker, J.A., and J.H. Black. 1983. Slug tests in fissured aquifers. *Water Resources Research* 19, no. 6: 1558-1564.

Barton, C. 1996. Characterizing bedrock fractures in outcrop for studies of ground-water hydrology. An example from Mirror Lake, Grafton County, New Hampshire. In U.S. Geological Survey Toxic Substances Hydrology Program—Proceedings of the Technical Meeting, Colorado Springs, Colorado, September 20-24, 1993, ed. D.W. Morganwalp and D.A. Aronson. U.S. Geological Survey Water-Resources Investigations Report 94-4015, 81-87.

Bear, J. 1979. *Hydraulics of Groundwater*. New York: McGraw-Hill.

Bouwer, H., and R.C. Rice. 1976. A slug test for determining hydraulic conductivity of unconfined aquifers with completely or partially penetrating wells. *Water Resources Research* 12, no. 3: 423-428.

Cooper, H.H. Jr., J.D. Bredehoeft, and I.S. Papadopulos. 1967. Response of a finite-diameter well to an instantaneous charge of water. *Water Resources Research* 3, no. 1: 263-269.

Dougherty, D.E., and D.K. Babu. 1984. Flow to a partially penetrating well in a double-porosity reservoir. *Water Resources Research* [illegible] no. 8: 1116-1122.

Dougherty, D.E., and D.K. Babu. 1985. Correction to "Flow to a partially penetrating well in a double-porosity reservoir." *Water Resources Research* 21, no. 2: 265.

Harvey, C.F. 1992. Interpreting parameter estimates obtained from slug tests in heterogeneous aquifers. Unpublished Master of Science Thesis, Department of Applied Earth Sciences, Stanford University.

Hsieh, P.A., R.L. Perkins, and D.O. Rosenberry. 1996. Field instrumentation for multilevel monitoring of hydraulic head in fractured bedrock at the Mirror Lake site, Grafton County, New Hampshire. In U.S. Geological Survey Toxic Substances Hydrology Program—Proceedings of the Technical Meeting, Colorado Springs, Colorado, September 20-24, 1993, ed. D.W. Morganwalp and D.A. Aronson. U.S. Geological Survey Water-Resources Investigations Report 94-4015, 137-140.

Hvorslev, M.J. 1951. Time lag and soil permeability in ground-water observations. *Bulletin No. 36. Waterways Experiment Station*. Vicksburg, Mississippi: Corps of Engineers, U.S. Army.

Johnson, C.D. 1996. Use of a borehole video camera to identify lithologies, fractures and borehole conditions in bedrock wells in the Mirror Lake area, Grafton County, New Hampshire. In U.S. Geological Survey Toxic Substances Hydrology Program—Proceedings of the Technical Meeting, Colorado Springs, Colorado, September 20-24, 1993, ed. D.W. Morganwalp and D.A. Aronson. U.S. Geological Survey Water-Resources Investigations Report 94-4015, 89-93.

Karasaki, K., J.C.S. Long, and P.A. Witherspoon. 1988. Analytical models of slug tests. *Water Resources Research* 24, no. 1: 115-126.

Pallet, E.L. 1996. Use of well logs to prepare the way for packer strings and tracer tests: Lessons from the Mirror Lake study. In U.S. Geological Survey Toxic Substances Hydrology Program—Proceedings of the Technical Meeting, Colorado Springs, Colorado, September 20-24, 1993, ed. D.W. Morganwalp and D.A. Aronson. U.S. Geological Survey Water-Resources Investigations Report 94-4015, 103-109.

Shapiro, A.M., and P.A. Hsieh. 1991. Research in fractured-rock hydrogeology: Characterizing fluid movement and chemical transport in fractured rock at the Mirror Lake drainage basin, New Hampshire. In U.S. Geological Survey Toxic Substances Hydrology Program—Proceedings of the Technical Meeting, Monterey, CA, March 11-15, 1991, ed. G.E. Mallard and D.A. Aronson, 155-161. U.S. Geological Survey Water-Resources Investigations Report 91-4034, 155-166.

Shapiro, A.M., and P.A. Hsieh. 1996. Overview of research on use of hydrologic, geophysical and chemical methods to characterize flow and chemical transport in fractured rock at the Mirror Lake site, New Hampshire. In U.S. Geological Survey Toxic Substances Hydrology Program—Proceedings of the Technical Meeting, Colorado Springs, Colorado, September 20-24, 1993, ed. D.W. Morganwalp and D.A. Aronson. U.S. Geological Survey Water-Resources Investigations Report 94-4015, 71-80.

Shapiro, A.M., P.A. Hsieh, and T.C. Winter. 1995. The Mirror Lake fractured-rock research site—A multidisciplinary research effort in characterizing ground-water flow and chemical transport in fractured rock. U.S. Geological Survey Fact Sheet FS—138-95.

Stehfest, H. 1970. Algorithm 368 numerical inversion of Laplace transforms. D-5. *Commun. ACM* 13, no. 1: 47-49.

Wikramaratna, R.S. 1984. An analytical solution for the effects of abstraction from a multi-layered confined aquifer with no cross flow. *Water Resources Research* 20, no. 8: 1067-1074.

FACULTAD DE INGENIERIA U.N.A.M.
DIVISION DE EDUCACION CONTINUA

CURSOS ABIERTOS

XII CURSO INTERNACIONAL DE CONTAMINACIÓN DE ACUÍFEROS

MODULO III: MODELOS MATEMÁTICOS EN GEOHIDROLOGIA Y CONTAMINACIÓN DE ACUIFEROS

TEMA

SCALE DEPENDENCY OF HYDRAULIC CONDUCTIVITY MEASUREMENTS

EXPOSITOR: DR. ADOLFO CHAVEZ RODRIGUEZ

PALACIO DE MINERIA
OCTUBRE DEL 2000

Scale Dependency of Hydraulic Conductivity Measurements

by Charles W. Rovey II[a] and Douglas S. Cherkauer[b]

Abstract

The hydraulic conductivity of five stratigraphic units in a carbonate aquifer has been measured with slug, pressure, and pumping tests, and with two calibrated digital models. The effective test radii range from less than one to greater than 10,000 meters. On log-log plots hydraulic conductivity increases approximately linearly with test radius to a range between 20 and 220 meters, but thereafter, it is constant with scale.

The increase in magnitude of hydraulic conductivity is similar to scaling effects reported at seven additional sites in a variety of geologic media. Moreover, the increase in magnitude correlates with an increase in variance of log-hydraulic conductivity measured at successively greater separation distances.

The rate of increase in both parameters, and particularly the range, have characteristic values for different pore systems. The larger ranges are consistently present in units with greater secondary porosity. Therefore, scaling effects provide a qualitative measure of the relative importance of secondary and primary permeability, and they can potentially be used to distinguish the dominant type of pore system.

Introduction

Considering the effort devoted to studying scale effects on dispersivity, it seems strange that hydraulic conductivity, a more fundamental parameter, has not been similarly investigated. The lack of attention is even more puzzling, given the numerous anecdotal reports, amounting to common knowledge, that lab tests consistently give hydraulic conductivities less than field tests. A compilation by Herzog and Morse (1984) remains one of the few sources where the scale of measurement was specifically recognized as a factor for these differences.

The relationship between hydraulic conductivity and scale, however, is more complex than a simple correction factor between lab and field measurements. Bredehoeft et al. (1983) compared hydraulic conductivities of a shale as measured by lab, slug, and pumping tests with that from a calibrated digital model. The long-term pumping test in an underlying sandstone had a radius of influence of approximately 10,000 m, and gave a similar value for the overlying shale as the calibrated model value. The lab tests had values approximately one thousandth that of the regional value, while small-scale field measurements, slug tests, had values approximately one tenth of the regional value. Therefore, hydraulic conductivity appears to increase with scale regardless of the method of measurement. Based on field measurements at different scales, we first quantify how hydraulic conductivity varies with test radius for five hydrostratigraphic units within a dolomite aquifer in southeast Wisconsin (Figure 1). These results are then compared with published data of hydraulic conductivity from additional sites in a variety of geologic media and with variograms of log-hydraulic conductivity distribution. The increase in hydraulic conductivity with measurement scale appears to be a general phenomenon which is correlated to an increase in the variance of its distribution.

Previous Work

The most complete report on the scale dependency of hydraulic conductivity measurements is by Bradbury and Muldoon (1990). They measured hydraulic conductivity at scales from approximately 10^{-2} to 10^{4} meters in both glacial outwash and mixed outwash-diamicton (fine-grained glacigenic) sediment. In both media regional estimation methods (pumping tests, digital models) gave hydraulic conductivities approximately three to five times greater than small-scale field measurements (slug tests) and nearly 10 times greater than lab tests (Figure 2a, b). They also noticed that scale effects vary with the nature of heterogeneity. Hydraulic conductivity of outwash sands increases with test radius at a log-log slope of 0.38, whereas the mixed outwash-diamicton increases at a greater slope, 0.92.

Bruner and Lutenegger (in press) and Keller et al. (1986) measured hydraulic conductivity in jointed, clay-rich glacial tills with lab, slug, and pumping tests (Figure 2c, d). The measurement scale is not as accurate in these cases, but using the best estimates, hydraulic conductivity increases with a slope of approximately 1.0 to a range between two and five meters on log-log graphs.

Sauter (1991) investigated a mature karstic limestone (Figure 2e). The rate of increase in hydraulic conductivity (0.66) is intermediate between the jointed tills and the porous outwash, but the most notable difference is the range in scale effect. Hydraulic conductivity increases with mea-

[a]Department of Geography, Geology and Planning, Southwest Missouri State University, 901 S. National Ave., Springfield, Missouri 65804.

[b]Department of Geosciences, University of Wisconsin-Milwaukee, Milwaukee, Wisconsin 53201

Received December 1993, revised September 1994, accepted October 1994.

surement scale to at least 3200 meters, a much greater distance than the jointed or granular media. Thus, an increase in hydraulic conductivity over many orders of magnitude in test radius appears typical of karst aquifers in contrast with shorter ranges in other media.

In summary, data available to date suggest that different geologic media have characteristic measures of scale effects (slope and range). Further, these measures may be useful in distinguishing different types of flow (i.e. granular, fracture, or conduit) in cases where it is unknown. In the remainder of this paper we test this hypothesis, first with data from a carbonate aquifer comprised of numerous stratigraphic units (Figure 3a), and then with values gathered from previously published reports.

Data Base

Hydrostratigraphy

Rovey (1990) and Rovey and Cherkauer (1994a, b) divided the carbonate aquifer of southeastern Wisconsin into nine major hydrostratigraphic units by correlating hydraulic conductivity from pressure-injection tests with stratigraphic intervals (Figure 3b). Each hydrostratigraphic unit has a regionally consistent hydraulic conductivity related to depositional environment, lithology, and mode of secondary porosity. Fine-grained (mudstone) lithologies have little macroporosity, and ground-water flow in these units is predominantly through joints. Coarse-grained units contain both intergranular porosity in grainstone facies and moldic porosity in packstone facies, produced by selective dissolution of fossil grains.

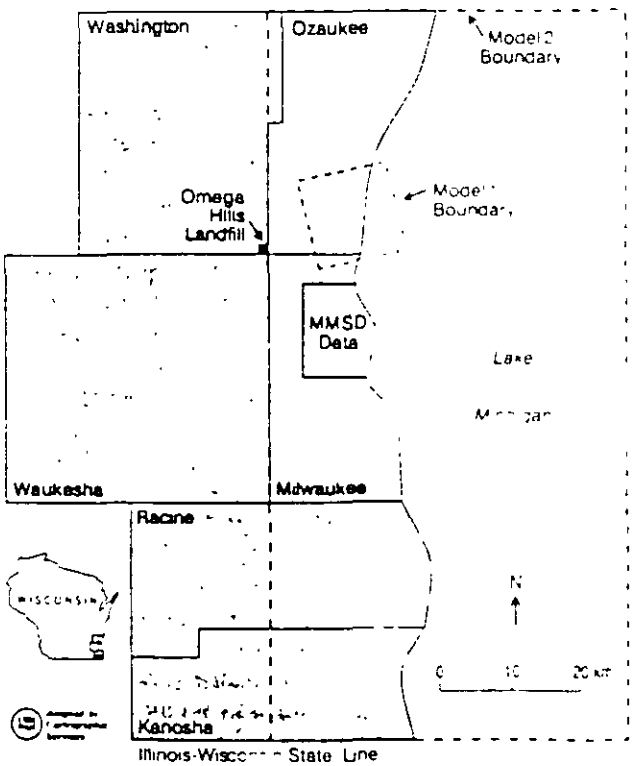

Fig. 1. Study area, southeast Wisconsin. Insets show data collection sites and digital model boundaries.

The upper 6 meters of rock (weathered zone on Figure 3b) are characterized as incipient epikarst and constitute a separate hydrostratigraphic layer. The weathered zone cuts across formation boundaries, but is developed almost exclusively in the fine-grained, joint-dominated strata which comprise the majority of the aquifer. It is the only unit with abundant nonselective dissolution features, including abundant vugs and nominal (< .5 cm) solutional widening along joints and hairline fractures. However, it has no geomorphic expression of karst such as dolines, karren, or conduits, and it also lacks hydrologic characteristics of karst such as rapid recharge, spring discharge, and erratic fluctuations in potentiometric surface and carbonate saturation.

MMSD Data

The Milwaukee Metropolitan Sewerage District (MMSD) performed numerous slug, pressure-injection, single-well, and multiwell pumping tests to develop a geotechnical database for an extensive tunneling project (MMSD, 1981; 1984a, b; 1988, Table 1). The geometric mean of hydraulic conductivity increases steadily with the scale of testing. For example, the Thiensville value increases from 2.5×10^{-4} to 10^{-3} to about 10^{-2} cm/sec as measured by slug, pressure, and pumping tests. The same general pattern holds for the other units, although pressure-injection values are not consistently greater than slug test values. Two explanations account for this minor inconsistency. The small number of slug and pressure tests within some units introduces some inaccuracy. Also, as shown later, the two test methods have overlapping ranges in test radii.

Miscellaneous Data

Rovey (1990) analyzed four additional fully penetrating multiwell pumping tests tapping the entire Silurian portion of the aquifer. Files of the Wisconsin Geological and Natural History Survey (WGNHS) also contain unpublished drawdown data from 29 single-well, fully penetrating tests throughout the study area (within the digital model-2 boundaries, Figure 1). We have collected these data and analyzed the single-well tests with the Bradbury and Rothschild (1985) specific capacity conversion program using an average storage coefficient of 5×10^{-4} from the multiwell pumping tests (Rovey, 1990). Use of a single average value is justified, because it is largely determined by the degree of confinement by the overlying glacial sediments which are fairly uniform throughout the area. Moreover, the final value is relatively insensitive to the storage coefficient value, so even large errors have little effect on calculated hydraulic conductivity.

When hydraulic conductivities calculated with this procedure can be compared to values calculated using type-curve matching or semilog analysis on observation wells monitored during the same test, the results are encouraging. The average difference in value is approximately a factor of two with no apparent bias toward an over or underestimation (Rovey, 1990). Moreover, the average bulk Silurian value from the single-well tests is virtually identical with that from multiwell tests (Table 1). Therefore, hydraulic conductivities converted from specific capacities are accepted as

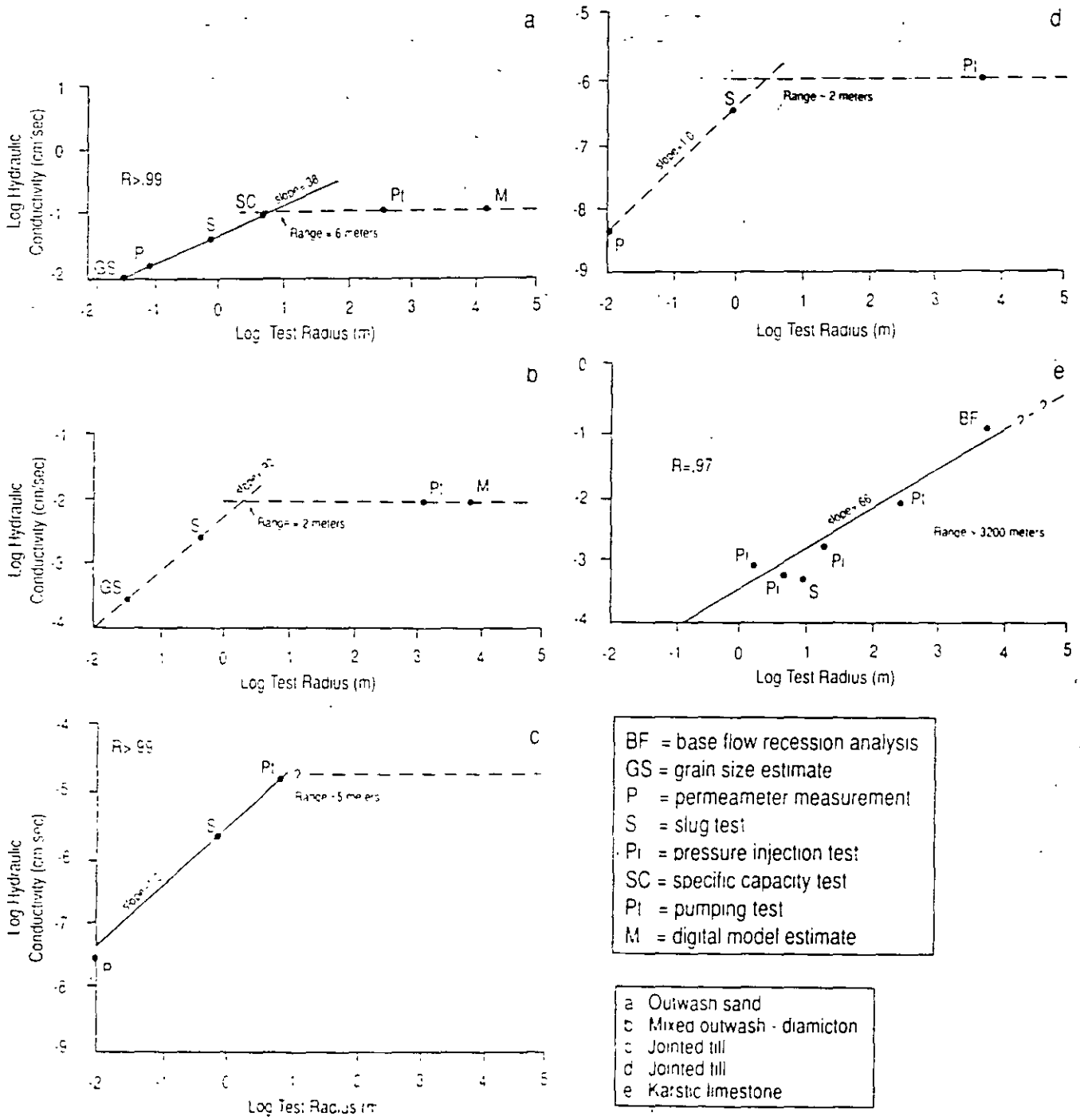

Fig. 2. Increase in hydraulic conductivity with test radius. Solid lines are linear regressions between 3 or more points; dashed lines are fit by hand. The measured range listed is the test radius beyond which hydraulic conductivity is approximately constant. a: Outwash sand. Modified from Bradbury and Muldoon (1990). Test radius is calculated using thicknesses and test intervals from Bradbury (1993). b: Mixed outwash-diamicton. Modified from Bradbury and Muldoon (1990). c: Jointed till. Modified from Bruner and Luteneggar (in press). Test radius estimate is from Bruner (1993). d: Jointed till. Calculated from data in Keller et al. (1986). The pumping test value is calculated from diffusivity and storage coefficient values measured during pumping test of an underlying sand. Test radius for the pumping test is calculated assuming hydraulic conductivity in the sand is .1 cm/sec. See text for discussion of radius of slug tests. e: Karstic limestone. Modified from Sauter (1991) using field test values only. The hydraulic conductivities shown are the midpoints of the "common range" in the original.

valid, and the term "pumping test" will hereinafter refer to both multiwell and single-well tests unless a distinction is specifically made.

Pearson (1993) also collected specific capacity values from the Wisconsin Department of Natural Resources for wells near the Omega Hills Landfill (Figure 1). Many of these wells are open to multiple strata. However, he was able to calculate hydraulic conductivities for individual strati-

graphic units, using the Bradbury and Rothschild (1985) conversion in tandem with the equation for effective hydraulic conductivity in a layered medium.

Finally, two digital flow models have been independently calibrated within the study area. Rovey (1983) simulated flow over a 110 square kilometer area using separate bulk parameters within the Silurian and Devonian portions of the aquifer. Mueller (1992) modeled the entire study area

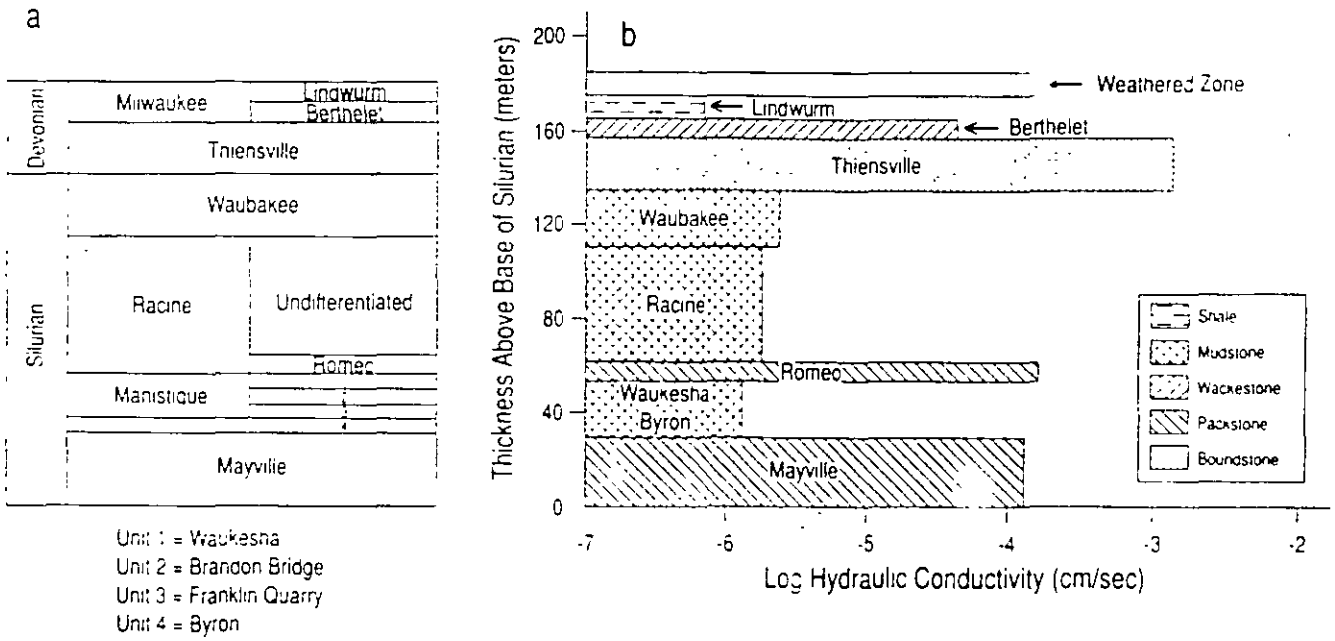

Fig. 3. Relation of hydraulic conductivity to stratigraphy, dolomite aquifer, southeastern Wisconsin (Rovey and Cherkauer, 1994a). Geometric means and number of tests are also listed in Table 1. a: Stratigraphy. Primary subdivision is at the formation level. Member subdivisions are informal, except within the Milwaukee Formation. b: Hydraulic conductivity measured by pressure-injection tests. Each bar is the average thickness of a particular unit and extends to the geometric mean hydraulic conductivity. Patterns depict the dominant texture of each unit.

Table 1. Geometric Mean Hydraulic Conductivity Grouped by Test Method and Stratigraphic Unit for the Dolomite Aquifer of Southeast Wisconsin

Stratigraphic Unit	*Slug Tests*[a] *(Hvorlsev Method)*	*Pressure-Injection Tests*[b] *(5 Min.)*	*Short-Term Single-Well Tests*[c] *(53 Min Ave)*	*Long-Term Single-Well Tests*[d] *(5 Hrs)*	*Multiwell Pumping Tests*[e] *(12-24 Hrs)*	*Digital Models*[f]
Weathered Zone	-4.7 (16)	-4.3 (37)	-3.4 (6)	-1.9 (78)		-2.0 (1)
Lindwurm	-5.8 (2)	-6.2 (5)				
Berthelet	-5.1 (2)	-4.4 (8)				
Thiensville	-3.6 (8)	-3.0 (49)	-2.1 (3)		-1.7 (2)[g]	-2.0 (1)
Waubakee	-6.1 (1)	-5.6 (50)	-4.8 (5)			-4.4 (1)
Racine	-5.7 (7)	-5.8 (129)	-4.8 (5)	-4.3 (171)		-4.4 (1)
Romeo		-3.8 (17)	-4.1 (1)			-2.7 (1)
Waukesha-Byron	-5.8 (4)	-5.9 (23)				-4.7 (1)
Mayville	-5.1 (7)	-3.9 (11)	-3.8 (3)	-3.3 (18)		-3.3 (1)
Bulk Silurian				-3.6 (21)	-3.7 (6)	-3.4 (1)
Approximate R_i (meters)[h]	1	1-10	5-20	100	100-500	30,000

(Values are the $\log_{10}$ in cm/sec. Numbers in parentheses are the number of tests in a respective unit for a given test method.)

[a] Unpublished field data from MMSD.

[b] MMSD (1981, 1984a, b). Additional values for the weathered zone are taken from MMSD (1988), changing the mean value presented in Rovey and Cherkauer (1994a) who also discuss the pressure test methods and limitations.

[c] MMSD (1984a). Specific capacity values are converted to hydraulic conductivities using the Bradbury and Rothschild (1985) conversion. Tests from the Racine and Waubakee are averaged together, because test intervals intercepted both formations.

[d] Individual unit values are from Pearson (1993). Bulk Silurian value is calculated from WGNHS well records. Both are converted to hydraulic conductivity using Bradbury and Rothschild (1985).

[e] MMSD (1984a) and Rovey (1990).

[f] Individual unit values are from Mueller (1992). Bulk Silurian value is from Rovey (1983).

[g] Actual values are given in Table 2.

Table 2. Calculated Radius of Influence Grouped by Test Method and Stratigraphic Unit, Dolomite Aquifer, Southeast Wisconsin

Stratigraphic Unit	Slug Tests	Pressure-Injection Tests	Short-Term Single-Well Tests	Long-Term Single-Well Tests	Multiwell Pumping Tests	Digital Models
Weathered Zone	-0.03	-0.08	1.2	2.4		4.8
Lindwurm	-0.05	-1.2				
Berthelet	0.02	0.58				
Thiensville	0.15	1.0	1.9		3.0	4.6
Waubakee	-0.07	-0.32	0.73			4.3
Racine	-0.04	-0.40	0.73	1.6		4.8
Romeo		0.56	0.90			4.8
Waukesha-Byron	-0.03	-0.48				4.8
Mayville	-0.02	0.52	1.3	2.0		4.8
Bulk Silurian						3.3

(Values are base 10 logs in meters. For example, the value −0.03 is the exponent in $10^{-0.03}$ which is a radius of influence of 0.93 meters.)

with a fully three-dimensional model using six layers corresponding closely to the major hydrostratigraphic units delineated by Rovey and Cherkauer (1994a, b).

Radius of Influence Calculations

Based on Table 1 and the preceding discussion, measured hydraulic conductivity depends on the scale of measurement. To quantify that dependency some length parameter must be associated with each test. Bradbury and Muldoon (1990) and Bruner and Lutenegger (in press) used test volume as the measure of scale. However, in the more numerous reports on dispersivity, travel distance, a one-dimensional measure, is routinely used. Also, established geostatistical methods of quantifying spatial variability use a one-dimensional separation distance (lag) term. Therefore, to facilitate comparison with results from mass transport studies and measures of aquifer heterogeneity, a radius of influence (R_i) is used here.

Calculating a meaningful R_i is problematic. For digital model values R_i is taken as the square root of the modeled area, or the area of the layer, if it is smaller. For consistency, the R_i for all other field tests is estimated using a form of the Cooper-Jacob distance-drawdown equation

$$R_i^2 = \frac{2.25\,Tt}{S} \qquad (1)$$

where T = transmissivity [measured hydraulic conductivity (m^2/day) multiplied by thickness of tested interval], t = time duration of test (days), and S = storage coefficient [mean value = 5×10^{-4} (dimensionless) measured from multiwell pumping tests, Rovey, 1990]. Thus, the assumption is made that any variation of storage coefficient with location or scale is negligible compared to hydraulic conductivity.

The use of the Cooper-Jacob equation is well-established for pumping tests, but the assumptions of a constant injection/withdrawal rate and local homogeneity may not be reasonable for every small-scale test. For example, the rate of inflow or outflow during a slug test decreases with time. Therefore, the effective time duration of the slug tests is taken as the basic time lag (measured from the field plots), the length of time at which recovery would be complete if the initial rate of inflow/outflow remained constant.

The use of the Cooper-Jacob equation is also not entirely consistent with the assumption of a steady state employed in calculating hydraulic conductivities during pressure testing (Cedergren, 1977). In practice, however, the necessary conditions are less restrictive and only a quasi-steady state is reached during the test, where there is no significant change in gradient or injection rate during the short (5 minute) test duration.

Where comparison is possible, calculated values of R_i are similar to those based on other methods. Bliss and Rushton (1984) simulated pressure tests for an aquifer with hydraulic conductivity averaging approximately 10^{-3} cm/sec, similar to the Thiensville pressure-injection mean (Table 1). At the midpoint of the test interval the modeled R_i was approximately 12 meters which is very close to the 10 meter R_i estimated for the Thiensville (Table 2).

The calculated values of R_i for the slug tests are approximately one meter (Table 2). Bruner (1993) estimated a slug test R_i between 0.5 and 1.0 meters by directly monitoring responses in adjacent wells during tests. Guyonnet et al. (1993) generated a series of theoretical type curves and related regression equations showing effective R_i of slug tests for combinations of dimensionless wellbore storage and dimensionless head. In a 5 cm diameter well, the dimensionless head decreases to 0.1, the typical value at the end of a slug test, by the time a measurable disturbance has propagated a distance approximately 25 times the wellbore radius. The wellbore radius is approximately 10 cm in this case, giving an approximate R_i of 2.5 m.

Therefore, based on comparisons with field measurements, models, and theory, the calculated values of R_i based on the Cooper-Jacob equation, are accurate to within a factor of two to three. This magnitude of possible error is much smaller than the range of values that were investigated (approximately five orders of magnitude, Table 2). Therefore, any errors in calculated R_i should have little effect on the overall comparison of results.

Results from Southeastern Wisconsin

Hydraulic Conductivity Magnitude

The relationship between hydraulic conductivity and scale of measurement (R_i) is plotted on log-log coordinates

(Figure 4) for units which have at least four independent methods of measurement. All plots have an initial linear increase in hydraulic conductivity, with slopes varying between 0.86 and 1.0 before hydraulic conductivity reaches a constant value.

The range over which hydraulic conductivity increases varies considerably among units. Hydraulic conductivity in the Waubakee and Racine Formations is joint-controlled and increases with R_t to approximately 20 meters. The Thiensville and Mayville Formations both contain complex pore systems. The Mayville contains both intergranular and secondary porosity as solution-enlarged molds of fossil grains. The Thiensville also contains intergranular porosity, but has horizons of nonselective dissolution beneath several minor paleo-weathering surfaces. Hydraulic conductivity increases with scale to 50 and 125 meters in the Mayville and Thiensville, respectively, coinciding with the greater degree of dissolution. The weathered zone, with the greatest degree of secondary effects, has the greatest range of hydraulic conductivity increase, 220 meters. Summarizing, the range of scale increase correlates with the degree, and possibly the type, of secondary porosity.

Explanations for Measured Scale Effects

Inspection of Table 1 and Figure 4 reveals that the measured hydraulic conductivity of a given unit increases with the scale of measurement. The increase is too uniform and too large to be coincidence. The increase also cannot be attributed to systematic differences or inaccuracy among the different measurement techniques. The ratio of values as measured by different methods varies considerably from one formation to another.

Measured hydraulic conductivity does increase with the scale of measurement. However, the factor(s) causing the correlation is not yet clear. In principle, several factors besides scale dependency could cause or contribute to the observed relationships, such as limitation of test methods, skin effects, and borehole storage effects.

The first possibility is that the small-scale tests may be incapable of measuring extremely high values. Thus the calculated means would be biased toward low values. For example, two slug tests in the Weathered Zone and one in the Thiensville recovered fully within the time required to make the first measurement. Therefore they are averaged with the remaining slug tests as "greater than" values, and the true means would be somewhat greater than those in Table 1. However, all slug tests within the remaining units had finite values. Thus, a test bias could not cause slug test means in these units to be lower than those of pumping tests.

Similarly, the upper measurable limit of the pressure-injection tests was somewhere in the range 10^{-3} to 10^{-2} cm/sec (MMSD, 1984a). Therefore, the means of some of the high conductivity units may have been underestimated, particularly the Thiensville which has numerous values within that range (MMSD, 1984a). However, this explanation is again inconsistent with results in other units. The lower measurable limit of the pressure-injection tests was 10^{-5} cm/sec, and the low conductivity units (Waubakee, Racine, Waukesha-Byron) occasionally tested at this boundary, causing their calculated means to be too high. Consequently, accuracy limitations in the pressure-injection tests cannot account for the low conductivity units lower values relative to the pumping tests. To summarize, a bias against large values among the small-scale tests cannot be a major factor contributing to the observed scale increase.

A second possibility also relates to test methodology. If the wellbore is damaged during drilling, skin effects dampen the borehole response, particularly during shorter times and at small radial distance, lowering calculated hydraulic conductivities (Streltsova, 1988). Such an effect could systematically bias the measured hydraulic conductivities of the small-scale, shorter duration tests toward lower values.

Based on available information, however, the skin effect in the wells considered here is negligible. First, none of the wells considered here were drilled with mud; hence, a significant invaded zone around the well bore would be unlikely. Second, the Silurian bulk value measured by the shorter duration single-well tests is actually slightly larger than the value from the longer duration, multiwell tests (Table 1). Third, early drawdown measurements were taken within the pumped well during two of the multiwell tests. These measurements allow calculation of the skin factor using type curve analysis (Earlougher, 1977), and in these two wells at least, the skin factor is zero. Finally, similar increases in hydraulic conductivity with measurement scale have been simulated with digital models of heterogeneous media where skin effects are absent (Rayne, 1993). Therefore, it is reasonable to conclude that skin effects are not an important factor contributing to the increase of hydraulic conductivity.

For pumping tests, borehole storage effects can lower the calculated hydraulic conductivity at early times and small radial distance, much like a positive skin factor (Tongpenyai and Raghavan, 1981). However, neither the Hvorslev method of slug test analysis nor the pressure-injection tests assume a line source/sink when calculating hydraulic conductivity. Instead these methods account for the initial volume of water in the borehole. Therefore, borehole storage effects would lower only the pumping test values, but this is inconsistent with the pumping test values, exceeding the slug and pressure test values in all cases.

As listed in Table 1, the values of the short-term single-well tests are less than values from the longer pumping tests. To determine if the difference in values could be caused by storage effects, the short-term tests were analyzed using the following equation (Driscoll, 1986)

$$t = \frac{.017\,(d_c^2 - d_p^2)}{Q/s} \qquad (2)$$

where t = time in minutes, after which borehole storage is negligible, d_c = diameter of borehole (cm), d_p = diameter of discharge pipe (cm), and Q/s = specific capacity of the well at time t in liters/minute/cm of drawdown. The short-term single-well tests were conducted in 10 cm diameter boreholes with an average duration of 53 minutes. Conservatively assuming a discharge pipe of 2.5 cm, the minimum specific capacity for negligible storage effects at 53 minutes is calculated to be .02 liters/minute/cm. This value is below the

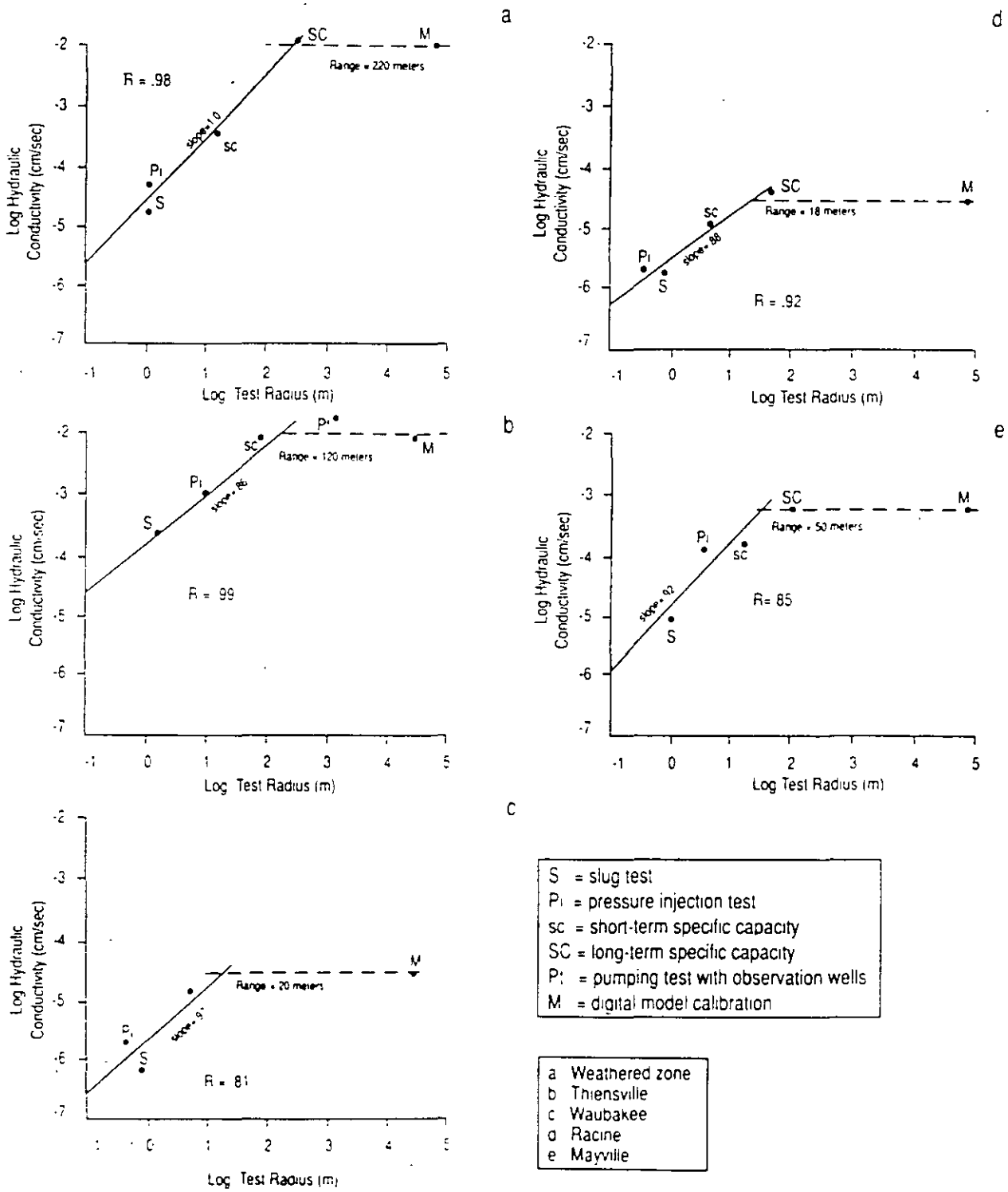

Fig. 4. Relation between measured hydraulic conductivity and effective test radius, dolomite aquifer. Hydraulic conductivities are from Table 1; test radii from Table 2. Solid lines are linear regressions between 3 or more points; dashed lines are fit by hand. The measured range listed is the test radius beyond which hydraulic conductivity is approximately constant.

measured specific capacity for the majority of tests, except those of the Waubakee/Racine. Therefore, borehole storage effects may have lowered the Racine/Waubakee value of the short-term single-well tests. However, this value of 1.6×10^{-5} cm/sec, which is admittedly low, is still much larger than the slug and pressure test values of approximately 2×10^{-6} cm/sec

In summary, the various alternatives can be used to explain the observed variability in measured hydraulic conductivity in some instances. However, for every case in which an alternative could be valid, there is at least one contradictory relationship. The one explanation which is universally consistent with the measured increase is that hydraulic conductivity increases with the scale of measure-

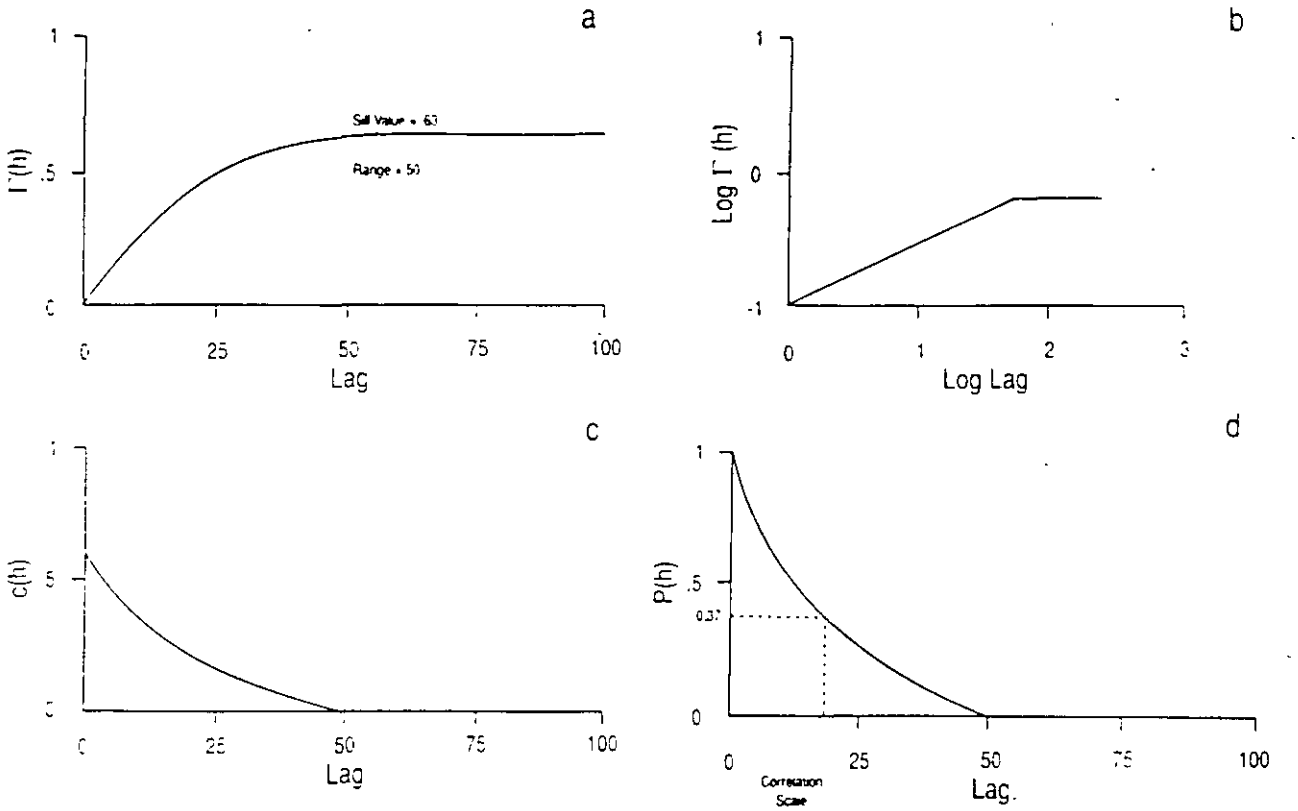

Fig. 5. Graphical measures of spatial correlation. All parameter values are arbitrary, for illustration only. a: Variogram, arithmetic scale. b: Variogram, log-log scale. c: Covariance function, arithmetic scale. d: Correlation function, arithmetic scale.

ment, much like dispersivity. At small scales hydraulic conductivity and ground-water flow tend to be uninfluenced by rare heterogeneities which raise conductivity and flow rates over a regional scale. Stated otherwise, the chances of a small-scale test encountering an extremely rare high-conductivity heterogeneity are disproportionately small relative to the degree with which that heterogeneity raises regional hydraulic conductivity.

Comparison to Scale Increase in Dispersivity

In the previous section the hypothesis was introduced that the increase in hydraulic conductivity with scale is somehow related to heterogeneity. In this section we expand this hypothesis by showing similarities with scale increases in dispersivity and variance of hydraulic conductivity.

Like hydraulic conductivity, dispersivity increases linearly on log-log plots, generally to distances between 10 and 100 meters. Thereafter, the spread in values is nearly constant and a best-fit line is approximately horizontal. The same general pattern is apparent from data or plots of dispersivity from single sites (Freyberg, 1986; Garabedian et al., 1991) and on plots with values combined from multiple sites (Gelhar et al., 1992; Neuman, 1990).

Stochastic theories dealing with dispersivity generally relate scaling effects to increases in spatial variability of hydraulic conductivity with distance (Dagan, 1982, 1984; Gelhar and Axness, 1983). They also predict that dispersivity should approach a constant value as the hydraulic conductivity becomes statistically uncorrelated at increased distances, that is, as the scale of an equivalent homogeneous medium is reached. These conclusions are reasonably consistent with results of intensive field investigations employing geostatistical methods to describe spatial variability in hydraulic conductivity (Sudicky, 1986; Freyberg, 1986; Hess et al., 1992; LeBlanc et al., 1991; Garabedian et al., 1991). Therefore, we further hypothesize that a (or the) common factor between the scale effects in dispersivity and hydraulic conductivity is variability in the hydraulic conductivity field.

Three common graphical measures of spatial variability are the semivariogram (or simply variogram), the covariance (autocovariance) function, and the correlation function (Figure 5, Isaaks and Srivastava, 1989). The functions for each respective measure are given by:

$$\Gamma(h) = 1/2E[K(z+h) - K(z)]^2 \qquad (3)$$

(equals semivariance between points at various lags)

$$C(h) = E[K(z+h) * K(z)] - E^2[K(z)] \qquad (4)$$

(equals covariance between points at various lags)

$$\rho(h) = \frac{C(h)}{C(0)} \qquad (5)$$

(equals covariance function divided by variance)

where: E[ ] denotes an average value over all paired samples at a given lag; z is a spatial coordinate location; h is a distance or lag from z; and K(z) = hydraulic conductivity measured at z. The three measures are interrelated, and the covariance function is converted to the variogram by:

$$\Gamma(h) = C(0) - C(h) \qquad (6)$$

Of these, the covariance and correlation functions are the most widely used in mass transport studies, and the usual correlation scale is defined for convenience as the distance or lag at which $\rho(h)$ declines to e^{-1} or 0.37 (Figure 5). Note, however, that this distance is shorter than that at which the covariance declines to zero (complete uncorrelation) or alternatively, the distance (range) at which the variogram reaches a constant variance (sill). This latter measure is used here because it facilitates direct comparison with the plots of hydraulic conductivity presented earlier.

Additional Site Data

Geostatistical parameters and hydraulic conductivity measurements at different scales are available, or can be calculated, for several additional systems (Figure 6). Pertinent results from an outwash sand at the Borden Site in Ontario, Canada were presented by Sudicky (1986) and Mackay et al. (1986). Variance in log hydraulic conductivity increases with scale at a low (0.24) log-log slope with a range of 10 meters (Figure 6a). Any scale increase in the magnitude of hydraulic conductivity cannot be accurately determined,

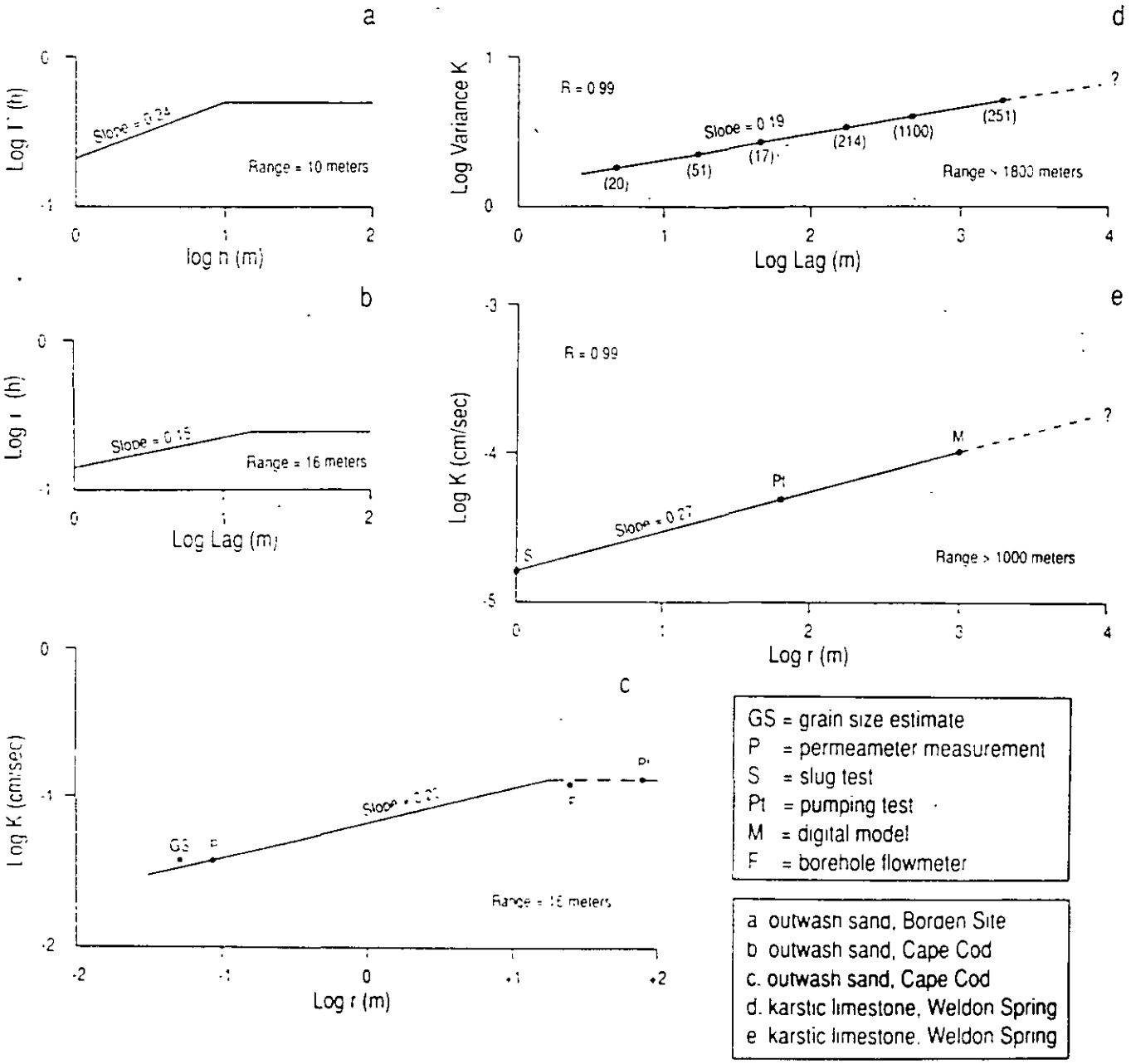

Fig. 6. Scaling effects in mean and variance of log hydraulic conductivity at other study sites. a: Glacial outwash, Borden Site. Generated from modeled correlation function, line A-A' in Sudicky (1986). b, c: Glacial outwash, Cape Cod, Massachusetts. The variogram (b) is from the modeled isotropic variogram with nugget effect using flowmeter data in Hess et al. (1992). Hydraulic conductivity plot (c) is generated from values in LeBlanc et al. (1991) and Wolf et al. (1991), assuming test durations of 1 and 12 hours for the borehole flowmeter and pumping tests. d, e: Karstic limestone, Weldon Springs, Missouri. Variogram (d) is nondirectional, generated from slug test values calculated from raw field data and surveyed locations supplied by MK-Ferguson Company, St. Charles, Missouri. Lag tolerance is .5 log units; annotated values are number of data pairs. Hydraulic conductivity plot (e) is generated using data from MK-Ferguson and Jacobs (1990) and Durham (1991). The model conductivity is the area-weighted average of values from three separate modeled zones.

but is minimal, close to zero. Mean hydraulic conductivities from grain-size analyses, permeameters, and slug tests are essentially equal.

Another glacial outwash sand was investigated at Cape Cod, Massachusetts (LeBlanc et al., 1991; Garabedian et al., 1991; Hess et al., 1992). As a qualification, there is less control on the R_i for some of these tests, but both hydraulic conductivity and its variance again have small slopes and ranges (Figures 6b and c; approximately 0.2 and 16 meters, respectively).

Data from an additional karstic limestone aquifer are also available from Weldon Spring, Missouri (Price, 1991; Carman, 1991, Durham, 1991; MK-Ferguson and Jacobs, 1990). Hydraulic conductivity was measured with slug tests, pumping tests, and a calibrated digital model. Both hydraulic conductivity and variance increase with measurement scale (Figures 6d, e); however, the slopes (0.27 and 0.19, respectively) are significantly less than the 1.0 slope typical of fractured media (Figures 2c, d). However, the most striking contrast is not the slope, but the range of the scale increase. In a second karstic carbonate aquifer the range in both hydraulic conductivity and variance exceeds the maximum scale of investigation, in this case, approximately 2000 meters.

The indefinite range in karstic aquifers contrasts sharply with finite ranges in nonkarstic carbonates and unconsolidated media (Table 3). In nonkarstic carbonates the maximum range of hydraulic conductivity is approximately 200 meters, with distances less than 50 meters typical for units with the smallest degree of dissolution. The range in variance also is finite for the nonkarstic carbonates (Figure 7). Although the variogram shape is questionable at small lags, the nonkarstic carbonates all have distinct sills, and their maximum range is approximately 200 m, similar to the maximum range in hydraulic conductivity.

In summary, the variograms are strikingly similar to the hydraulic conductivity plots of the same geologic unit. As heterogeneity increases, so does mean hydraulic conductivity, and as statistical homogeneity is reached, hydraulic conductivity becomes constant.

Summary

The hydraulic conductivities of five carbonate hydrostratigraphic units were measured over radial distances ranging from less than one to greater than 10,000 m. The observed increase in hydraulic conductivity with scale is consistent with results from a variety of geologic media, including glacial outwash, jointed clay-rich tills, and karstic limestones. The results reinforce Bradbury and Muldoon's (1990) conclusion that hydraulic conductivities based on small-scale field measurements will generally be less than regional values, even if they are based on 100 or more individual tests.

Scaling effects vary consistently with the type of geologic medium and degree of secondary porosity (Table 3). Glacial outwash, with primary porosity only, generally has the smallest rate and range of scale increase. Thus, small-scale field measurements such as slug tests will be closest to regional values, generally within a factor of three (Figures 2a, 6a, 6c). The rate of scale increase is much greater in consolidated/joint-dominated media. Slug tests in these media may underestimate regional values by factors ranging from 2 to 500, depending on the range in effects (Figures 2c, d; 6) which correlate to the degree of secondary dissolution. In mature karst aquifers hydraulic conductivity increases without apparent bound, so it may not even be possible to speak of a unique regional hydraulic conductivity.

Finally, the increase of hydraulic conductivity with

Table 3. Characteristic Values of Slope and Range for Various Geologic Media

	Glacial Outwash[a]	*Jointed Till*[b]	*Carbonates Joint-Dominated*[c]	*Carbonates Secondary Moldic Porosity*[d]	*Carbonates Incipient Dissolution Along Joints*[e]	*Carbonates Mature Karst*[f]
Range, K	7.3 (0-16) [3]	3.5 (2-5) [2]	19 (18-20) [2]	50 — [1]	170 (120-220) [2]	— (>1000, >3200) [2]
Range, Variance	13.0 (10-16) [2]	— —	<100 m [2]	— —	<200 m [2]	>1800 — [1]
Slope, K	0.19 (0-0.38) [3]	1.0 (1.0) [2]	0.92 (0.88-0.97) [2]	0.92 — [1]	(0.86-1.0) [2]	0.46 (0.27-0.66) [2]
Slope, Variance	0.20 (0.15-0.24) [2]	— —	— —	— —	— —	0.19 — [1]

(Range and slope are taken from Figures 2, 4, and 6. The first number is the arithmetic mean, that in parentheses is range of all values, that in brackets is the number of different geologic units summarized.)

[a] From Figures 2a, 6a, 6b, 6c.
[b] From Figures 2c, d.
[c] Racine and Waubakee Formations, Figures 4c, d; 7c, d.
[d] Mayville Formation, Figure 4e.
[e] Thiensville Formation and Weathered Zone, Figures 4a, b; 7a, b.
[f] Figures 2e, 6d, 6e.

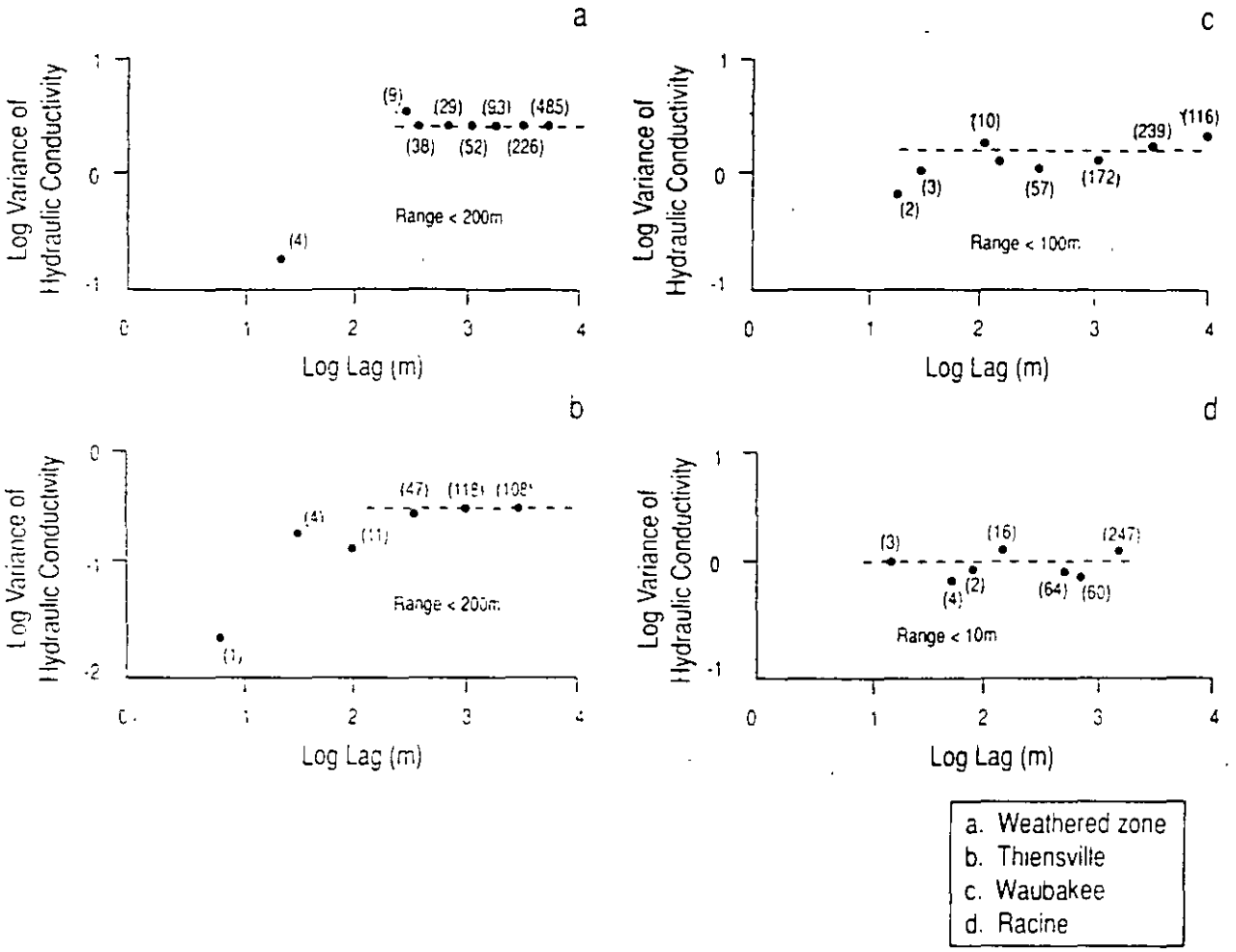

Fig. 7. Log-log variograms of log hydraulic conductivity distribution in dolomite aquifer. Variograms are nondirectional, generated from pressure test values (Table 1) using surveyed borehole locations. Annotated values are the number of data pairs at a given lag. Lag tolerance is 0.5 log units.

radius of influence in the test method is related to an increase in variance of log-hydraulic conductivity at greater lag distances between measurement points. This correlation suggests that increases in hydraulic conductivity and dispersivity are related through a common dependency on variance.

Acknowledgments

We thank Steve Fradkin of STS Inc., formerly at the Project Management Office, Milwaukee Metropolitan Sewerage District, who often went to great lengths to make various project data available. We also acknowledge the help and data supplied by Ken Bradbury of the Wisconsin Geologic and Natural History Survey, Roger Bruner of Foth and Van Dyke, Minneapolis, Minnesota, and the MK-Ferguson Company, St. Charles, Missouri. Carry McConnell of the University of Missouri-Rolla reviewed an early version of the manuscript, resulting in significant improvements. This research was funded by the University of Wisconsin Sea Grant Institute under grants from the National Sea Grant College Program, National Oceanic and Atmospheric Administration, U.S. Department of Commerce, and from the State of Wisconsin Federal Grant NA90AA-D-SG469, project R/MW-35.

References

Bliss, J. C. and K. R. Rushton. 1984. The reliability of packer tests for estimating the hydraulic conductivity of aquifers. Quarterly Journal of Engineering Geology, v. 17, pp. 81-91.

Bradbury, K. R. 1993. Personal communication. Wisconsin Geological and Natural History Survey.

Bradbury, K. R. and E. R. Rothschild. 1985. A computerized technique for estimating the hydraulic conductivity of aquifers from specific capacity data. Ground Water, v. 23, pp. 240-246.

Bradbury, K. R. and M. A. Muldoon. 1990. Hydraulic conductivity determinations in unlithified glacial and fluvial materials. In: D. M. Nielsen and A. I. Johnson (eds.), Ground Water and Vadose Zone Monitoring. ASTM STP 1053, pp. 138-151.

Bredehoeft, J. D., C. E. Neuzil, and P.C.D. Milly. 1983. Regional flow in the Dakota Aquifer: A study of the role of confining layers. U.S. Geological Survey Water-Supply Paper 2237. 45 pp.

Bruner, D. R. and A. J. Lutenegger. (In press). Measurement of saturated hydraulic conductivity in fine-grained glacial tills in Iowa. Comparison of in situ and laboratory methods. In: D. E. Daniel and S. J. Trautwein (eds.). Hydraulic Conductivity and Waste Contaminant Transport in Soils. ASTM STP 1142.

Bruner, D. R. 1993. Personal communication. Foth and Van Dyke, Minneapolis, MN.

Carman, J. 1991. Aquifer characteristics of the shallow

Burlington-Keokuk Limestone at the Weldon Spring Site. Weldon Spring Site Remedial Action Project, DOE Contract DE-AC05-86OR21548. pp. 155-201.

Cedergren, H. R. 1977. Seepage, Drainage and Flow Nets. Wiley Interscience. 534 pp.

Dagan, G. 1982. Stochastic modeling of groundwater flow by unconditional and conditional probabilities, 2. The solute transport Water Resources Research. v. 18, no. 4, pp. 835-848.

Dagan, G. 1984. Solute transport in heterogeneous porous formations. Journal of Fluid Mechanics. v. 145, pp 151-177.

Driscoll, F G 1986. Groundwater and Wells. Johnson Division, St. Paul, MN. 1089 pp.

Durnam, L 1991. Groundwater modeling at the Weldon Spring chemical plant/raffinate pits and vicinity properties. Weldon Spring Site Remedial Action Project, DOE Contract DE-AC05-86OR21548. pp 203-228.

Earlougher, R C. Jr. 1977. Advances in well test analysis. Society of Petroleum Engineers Monograph. v. 5

Freyberg, D L 1986. A natural gradient experiment on solute transport in a sand aquifer, 2. Spatial moments and the advection and dispersion of nonreactive tracers Water Resources Research v. 22, no 13, pp. 2031-2046

Garabedian, S P., D. R. LeBlanc, L W. Gelhar, and M. A. Celia. 1991. Large-scale natural gradient tracer test in sand and gravel, Cape Cod, Massachusetts, 2. Analysis of spatial moments for a nonreactive tracer Water Resources Research v 27, no 5, pp. 911-924.

Gelhar, L W., C. Welty, and K. R. Rehfeldt. 1992. A critical review of data on field-scale dispersion in aquifers. Water Resources Research v. 28, no. 7, pp 1955-1974.

Gelhar, L. W. and C L. Axness. 1983. Three dimensional stochastic analysis of macrodispersion in aquifers. Water Resources Research v 19, no 1, pp. 161-180

Guyonnet, D , S Mishra, and J McCord. 1993. Evaluating the volume of porous medium investigated during slug tests. Ground Water. v 31, no. 4, pp. 627-633.

Herzog, B. L. and W J Morse 1984. A comparison of laboratory and field determined values of hydraulic conductivity at a waste disposal site Proceedings, Seventh Annual Madison Waste Conference, Dept of Engineering Professional Development, Univ of Wisconsin-Madison, Madison, WI pp 30-52.

Hess, K. M., S H Wolf, and M A. Celia 1992. Large-scale natural gradient test in sand and gravel, Cape Cod, Massachusetts, 3 Hydraulic conductivity variability and calculated macrodispersivities. Water Resources Research v 28, no 8, pp. 2011-2027

Isaaks, E H and R M Srivastava 1989 An Introduction to Applied Geostatistics. Oxford University Press. 561 pp

Keller, C K , G Van Der Kamp, and J A. Cherry 1986 Fracture permeability and groundwater flow in clayey till near Saskatoon, Saskatchewan Canadian Geotechnical Journal v 23, pp. 229-240

LeBlanc, D R , S P Garabedian K M Hess, L. W Gelhar, R D. Quadri, D G Stollenwerk, and W W Wood 1991 Large-scale natural gradient tracer test in sand and gravel, Cape Cod, Massachusetts, 1 Experimental design and observed tracer movement. Water Resources Research v 27, no 5, pp 895-910.

Mackay, D. M., D L Freyberg, and P V Roberts 1986 A natural gradient experiment on solute transport in a sand aquifer, 1. Approach and overview of plume movement Water Resources Research, v 22, no 13, pp 2017-2029

MK-Ferguson Company and Jacobs Engineering Group. 1990 Aquifer characteristics data report for the Weldon Spring site chemical plant/raffinate pits and vicinity properties. DOE Contract No. DE-AC05-86OR21548. 111 pp.

Milwaukee Metropolitan Sewerage District (MMSD). 1981. Inline Storage Facilities Plan. v. 4, Borehole Logs.

Milwaukee Metropolitan Sewerage District (MMSD). 1984a. North Shore Interceptor Geotechnical Report. v. 3, Contract Documents.

Milwaukee Metropolitan Sewerage District (MMSD). 1984b. Cross Town Interceptor Geotechnical Report. v. 3, Contract Documents.

Milwaukee Metropolitan Sewerage District (MMSD). 1988. Kinnickinnic/Lake Michigan Tunnel System Geotechnical Report. v. 3, Contract Documents.

Mueller, S. 1992 Three-dimensional digital simulation of the ground-water contribution to Lake Michigan from the Silurian aquifer of southeastern Wisconsin. Unpublished M.S. thesis, Univ. of Wisconsin-Milwaukee. 231 pp.

Neuman, S. P. 1990. Universal scaling of hydraulic conductivities and dispersivities in geologic media. Water Resources Research. v. 26, no. 8, pp. 1749-1758.

Pearson, R. 1993. The controls on hydraulic conductivity distributions in the Silurian aquifer at Omega Hills Landfill, southeastern Wisconsin. Unpublished M.S. thesis, Univ. of Wisconsin-Milwaukee. 110 pp.

Price, P 1991. Shallow groundwater investigations at Weldon Spring, Missouri. Weldon Spring Site Remedial Action Project, DOE Contract DE-AC05-86OR21548. pp. 141-153.

Rayne, T. 1993. Variability of hydraulic conductivity in sandy till: The effects of scale and methodology. Unpublished Ph.D. dissertation, Univ. of Wisconsin-Madison. 135 pp.

Rovey, C W. II. 1990. Stratigraphy and sedimentology of Silurian and Devonian carbonates, eastern Wisconsin, with implications for ground-water flow into Lake Michigan. Unpublished Ph.D. dissertation, Univ. of Wisconsin-Milwaukee. 427 pp.

Rovey, C. W II. 1983. Computer modeling of the interaction between Lake Michigan and the dolomite aquifer at Mequon, Wisconsin. Unpublished M.S. thesis, Univ. of Wisconsin-Milwaukee. 271 pp.

Rovey, C W. II and D S. Cherkauer. 1994a. Relation between hydraulic conductivity and texture in a carbonate aquifer: Observations. Ground Water. v. 32, no. 1, pp. 53-62.

Rovey, C. W. II and D. S. Cherkauer. 1994b. Relation between hydraulic conductivity and texture in a carbonate aquifer: Regional continuity. Ground Water. v. 32, no. 2, pp. 227-238

Sauter, M 1991. Assessment of hydraulic conductivity in a karst aquifer at local and regional scale. Proceedings of Third Conference on Hydrogeology, Ecology, Monitoring and Management of Ground Water in Karst Terranes. National Ground Water Assoc pp. 39-56.

Streltsova, T D 1988 Well Testing in Heterogeneous Formations Exxon Monograph, John Wiley & Sons.

Sudicky, E. A 1986 A natural gradient experiment on solute transport in a sand aquifer: Spatial variability of hydraulic conductivity and its role in the dispersion process. Water Resources Research. v. 22, no. 13, pp. 2069-2082.

Tongpenyai, Y. and R. Raghavan. 1981. The effect of wellbore storage and skin on interference test data. Journal of Petroleum Technology. January, 1981, pp. 151-160.

Wolf, S H., M A. Celia, and K. M. Hess. 1991. Evaluation of hydraulic conductivities calculated from multiport-permeameter measurements. Ground Water. v. 29, no. 4, pp. 516-525.

FACULTAD DE INGENIERIA U.N.A.M.
DIVISION DE EDUCACION CONTINUA

CURSOS ABIERTOS

XII CURSO INTERNACIONAL DE CONTAMINACIÓN DE ACUÍFEROS

MODULO III: MODELOS MATEMÁTICOS EN GEOHIDROLOGIA Y CONTAMINACIÓN DE ACUIFEROS

TEMA

REDUCING UNCERTAINTY ASSOCIATED WITH GROUND – WATER FLOW AND TRANSPORT PREDICTIONS

EXPOSITOR: DR. ADOLFO CHAVEZ RODRIGUEZ

PALACIO DE MINERIA
OCTUBRE DEL 2000

Reducing Uncertainty Associated with Ground-Water Flow and Transport Predictions

by Eileen P. Poeter and Sean A. McKenna[a]

Abstract

Effective evaluation of ground-water flow and transport problems requires consideration of the range of possible interpretations of the subsurface given the available, disparate types of data. Geostatistical simulation (using a modified version of ISIM3D) of hydrofacies units produces many realizations that honor the available geologic data and represent the range of subsurface interpretations of unit geometry. Hydraulic observations are utilized to accept or reject the geometric configurations of hydrofacies units and to estimate ground-water flow parameters for the units (using MODFLOWP). These realizations are employed to evaluate the uncertainty of the resulting value of the response function (ground-water flow velocity and contaminant concentration) using MT3D. The process is illustrated with a synthetic data set for which the "truth" is known, and produces a striking reduction in the distribution of predicted contaminant concentrations. The same system is evaluated three times: first with only hard data, then with both hard and soft data, and finally with only the realizations that honor the hydraulic data (i.e., those accepted after parameter estimation via inverse flow modeling). Using only hard data, the mean concentration predicted for all realizations at the point of interest is nearly two orders of magnitude lower than the true value and the standard deviation of the log of concentration is two. The addition of soft data brings the mean concentration within one order of magnitude of the true value and reduces the standard deviation of the log of concentration to one. After eliminating realizations using inverse flow modeling, the mean concentration is one-third of the true value and the standard deviation of the log of concentration less than 0.5.

Introduction

A fundamental problem with interpreting the earth's subsurface is that we only sample a small fraction (typically less than one millionth) of the material we are characterizing. The challenge is to determine the character of the material between boreholes and the continuity of high (or low) hydraulic conductivity units. For example, consider a site where there are three boreholes that intersect two hydrofacies (black and white) as shown in Figure 1. If no other information is available, all six interpretations shown (and many more that are not shown) are reasonable interpretations of the subsurface. Knowing that heterogeneity is critical to the movement of contaminants (Poeter and Gaylord, 1990), each interpretation will affect ground-water flow and contaminant transport prediction in different ways. Decisions regarding remedial actions at such a site will differ depending on the actual configuration of units in the subsurface.

Usually we know more about a site than just the location of hydrofacies in boreholes, and this information can be used to rule out some, but not all, of the alternative interpretations. "Fusion" of these data (Olhoeft, 1992) reduces uncertainty associated with the interpretation. If each circle in Figure 2 represents the range of possible interpretations, then using all of the information together can significantly reduce the range of possible interpretations, thus reducing the uncertainty of the nature of ground-water flow and contaminant transport. In short, the sum of the parts is less than the whole! If the data circles do not overlap, the project team should strive to identify the shortcomings/errors in the data or determine what assumptions have been made that falsely constrain the interpretation.

It is important to work with a range of subsurface interpretations because consideration of these alternative interpretations of the subsurface will yield a range of the response function (ground-water flow and advection-dispersion equation) values (head, flow rate, and concentration). For example, assume there is a contaminated site with two alternative remediation schemes. If there is only one deterministic picture of the subsurface, and the predicted

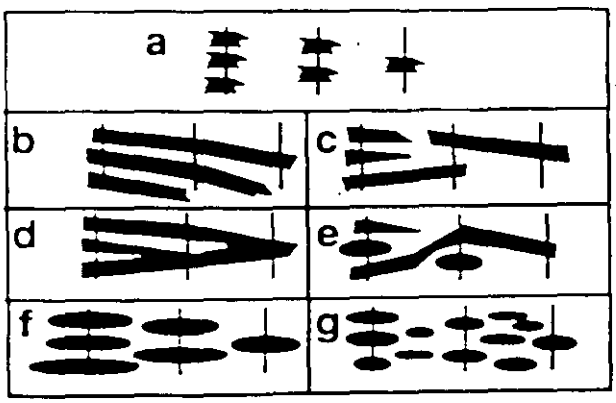

Fig. 1. Alternative subsurface interpretation. a: field knowledge of the occurrence of hydrofacies in borings; b through g: a few alternative interpretations of interwell connections.

[a]Department of Geology and Geological Engineering, Colorado School of Mines, Golden, Colorado 80401. (McKenna's current address: Sandia National Laboratories, Geohydrology Department, P.O. Box 5800, M.S. 1324, Albuquerque, New Mexico 87185-1324.)

Received August 1994, revised December 1994, accepted January 1995.

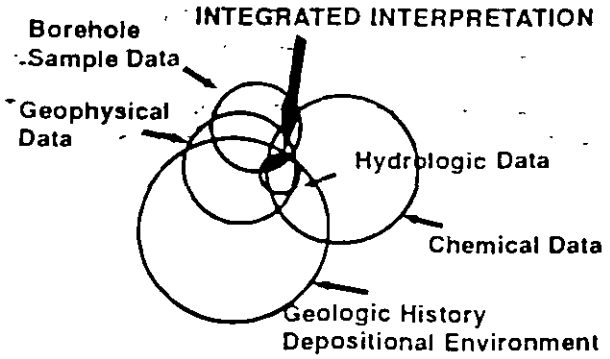

Fig. 2. Integrated interpretation constrains predictions.

concentration at the point and time of interest is 5×10^{-3} ppm for remedial alternative 1 and 5×10^{-4} ppm for remedial alternative 2, than alternative 2 appears to be the better choice. However, when the range of possible subsurface conditions is considered, it may be found that remedial alternative 2 actually has a higher probability of poor performance and the opposite selection would be made (Figure 3).

A current approach to this problem is geostatistical simulation using hard data, soft data, and spatial statistics to describe the character of the subsurface (McKenna and Poeter, 1994). Hard data are data with negligible uncertainty, such as direct measurements of hydraulic conductivity or observations of lithology. Soft data are information with nonnegligible uncertainty, such as indirect measurements gathered in a geophysical survey and expert opinion regarding geologic fabric or structure. Hard and soft data are used to develop indicator semivariograms for the hydrofacies (represented by integer indicators) and to simulate numerous realizations [using multiple indicator conditional stochastic simulations, MICSS (Gomez-Hernandez

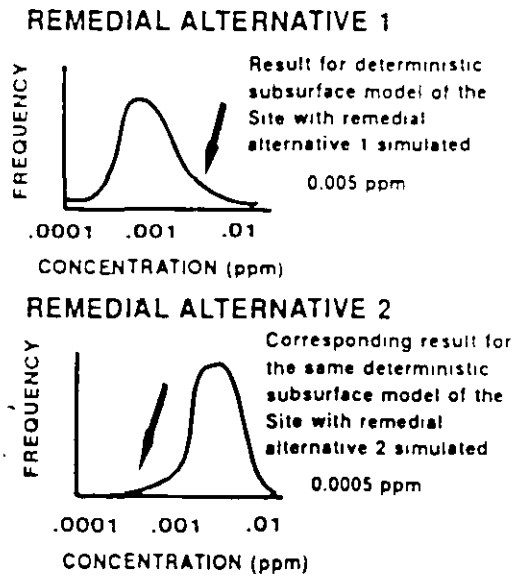

Fig. 3. Evaluation of alternative remedial actions using a range of interpretations (indicated by the frequency distribution) as opposed to one deterministic interpretaion (indicated by the arrow) of the geology may result in selection of a different remedial action.

and Srivastava, 1990)] of the hydrofacies configuration which honor the data and the statistical character of the subsurface. The hydrofacies within each realization are populated with hydraulic parameters and a forward flow and transport model is run to yield the distribution of predicted contaminant concentration over the model domain for a period of time. This process is extended through the use of inverse flow modeling which can be used to: (1) improve geologic interpretation, somewhat narrowing the distribution of predicted concentrations, and (2) eliminate realizations that do not fit the hydrologic data, significantly reducing uncertainty.

Hypothetical Problem

To facilitate demonstration of the process, a scenario requiring a decision concerning establishment of a water-supply well near a stream (Figure 4) is constructed. Alternatively, but at much greater cost, water could be supplied by pipeline. Use of water from the nearby stream is not an option due to poor water quality, which improves by infiltration through the aquifer and dilution with ground water. Knowledge of the probability distribution of concentration at the proposed well location resulting from contaminants entering the ground water from a nearby landfill will aid in the decision.

This study explores the uncertainty associated with predicted contaminant concentration calculated using three approaches and compares those uncertainties with the known concentration. Uncertainty of the geometric configuration and hydraulic conductivity of five hydrofacies are

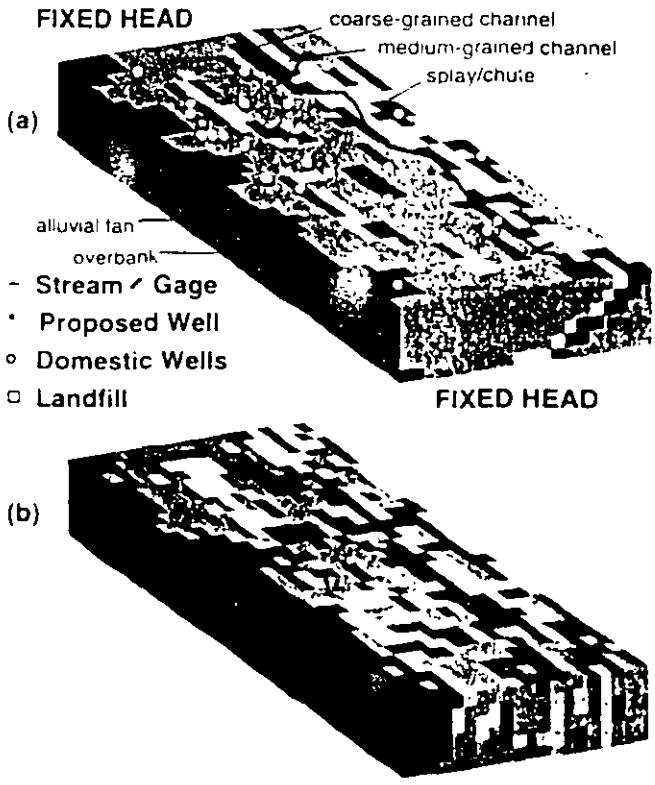

Fig. 4. Synthetic model used to illustrate uncertainty reduction procedure.

considered. The approaches include: (1) using hard geologic data from the domestic wells in MICSS to produce geologic realizations which are populated with hydraulic conductivities based on hydrofacies type and used in forward flow and transport modeling to predict the probability distribution of contaminant concentration at the proposed well location; (2) repetition of the first approach with addition of soft information regarding continuity of alluvial fan hydrofacies gained through inverse ground-water flow modeling; and (3) repetition of the second approach incorporating hydraulic data through application of inverse flow modeling. The MICSS code used is ISIM3D (Gomez-Hernandez and Srivastava, 1990) as modified by McKenna (1994)

Synthetic Setting

A synthetic data set is used to demonstrate the process because, with a synthetic data set, the true conditions are known. Reduction of uncertainty is only useful if the distribution of predicted concentration narrows on the truth. The synthetic data set represents a simplified system of fluvial hydrofacies, with a north to south hydraulic head gradient, no-flow conditions at the eastern, western, and underlying boundaries, recharge on the surface, and discharge to a stream. The model domain is 6000 m long, 2000 m wide, 60 to 80 m thick (depending on the elevation of the water table in the uppermost block), and is represented by a grid of 30 × 20 × 6 cells. A landfill and stream are located as shown in Figure 4(a).

A synthetic "true stratigraphy" is constructed consisting of six layers of geologic materials designed to mimic a generic fluvial geology. Five hydrofacies are used in the synthetic data set: (1) medium-grained alluvial fan material, (2) fine-grained overbank deposits, (3) fine to medium-grained splay/chute deposits, (4) medium-grained channel deposits, and (5) coarse-grained channel deposits [Figure 4(a)]. All of the hydrofacies have a constant value of effective porosity and lognormally distributed (but not spatially correlated) hydraulic conductivities with a standard deviation of 1/6 in natural log space (thus K varies by a factor of three within any one facies and there is no significant overlap of K's between facies). These simplified hydrofacies properties are not representative of a field situation; however, a complex hypothetical distribution is not necessary to illustrate the process presented herein. The percentage that each hydrofacies represents in the synthetic system and their hydraulic properties are presented in Table 1.

The alluvial fan hydrofacies are limited to the western edge of the alluvial valley, and are discontinuous. The main channel hydrofacies are oriented north-south and are further east in sequentially younger layers. Coarse-grained channel hydrofacies are discontinuous and occur on the outside bends of meanders. The medium-grained channel hydrofacies are more continuous. Fine to medium-grained channel hydrofacies are located along the main channels to represent splay deposits. Some medium-grained hydrofacies are located within the floodplain area to represent chute cutoff oxbow lakes. Fine to medium-grained hydrofacies of similar distribution represent neck cutoff oxbow lakes. This definition and spatial distribution of hydrofacies is a gross simplification of fluvial hydrofacies as presented by Allen (1965), Bridge and Leeder (1979), and Walker and Cant (1984).

Table 1. Facies Statistics for Synthetic Model

Facies	*Volume percent*	*Mean K** *(m/d)*	*Effective porosity*
Alluvial fan	6	50.00	0.25
erbank	61	0.05	0.08
lay/chute	11	5.00	0.15
Medium channel	15	50.00	0.25
Coarse channel	11	500.00	0.30

*All K distributions have $\sigma_{lnK} = 1/6$

A "true" steady-state flow system is obtained with heads fixed at 100 m on the northern and 90 m on the southern boundary. An average recharge of 2×10^{-4} m/d is applied to the top of the domain with three times that rate applied at the margin of the valley (where overland flow from surrounding uplands infiltrates the system), and a zero rate near the stream which is a discharge area. The 31 domestic wells [Figure 4(a)] penetrate to various depths and pump at low rates (their discharges are normally distributed with a mean of 1 m^3/d and a standard deviation of 1/6 m^3/d). A head dependent flux boundary represents the stream [Figure 4(a)]. The USGS code MODFLOWP (Hill, 1992) is utilized for the forward and inverse ground-water flow modeling. The forward simulation of the synthetic system using MODFLOW yields heads at 37 wells (31 domestic and 6 monitoring wells near the landfill) and ground-water discharge to the stream between gaging stations. Multilayer heads from MODFLOW were composited by averaging head of each layer weighted by transmissivity of the layer.

A "true" event of a breached landfill with recharge through the landfill at a dimensionless concentration $C_o = 1.0$ is simulated for a conservative contaminant with constant dispersivities of 5 m, 1.5 m, and 0.25 m in the longitudinal, transverse horizontal and vertical directions, respectively, for all hydrofacies. These dispersivities reflect advective variation at small scale within each hydrofacies, while larger scale dispersion is attained through the use of heterogeneity in the flow model. The simplification of similar small-scale dispersivity for each facies does not interfere with the illustration of the analysis process presented herein. The MT3D code is used with the MOC (Method of Characteristics) option and the fourth-order Runge-Kutta algorithm for particle tracking to simulate transport (Zheng, [illegible]). Time steps on the order of 10 days yield mass balances on the order of 1%. Forward transport modeling yields the "true" dimensionless concentration of 1.2×10^{-2} (i.e. $C/C_o = 0.0012$) at the proposed well location 50 years after the landfill began leaking. For the purpose of discussion we assume the regulatory level for this contaminant is $C/C_o = 1.0 \times 10^{-1}$.

Inverse Modeling

Performance of inverse modeling on the true stratigraphy is evaluated before exploring the possibility of using inverse modeling to eliminate some of the stratigraphic

realizations. Because we have a synthetic truth to work with, "perfect" input can be provided (i.e., exact zonations, heads, flows, and initial values for the parameters) to the inverse model, in which case the model quickly converges without substantial change of parameter values. However, stochastic simulation of parameter values within the hydrofacies is not considered here because it is not necessary in order to illustrate the uncertainty reduction process, thus the inverse model estimates only one value of K for each hydrofacies (the mean of the lognormal distribution of K is used as the starting value for the inverse run). In addition, because use data are not typically available for domestic wells, each is assigned a discharge of 1 m^3/d. Consequently, the inverse model undertakes a number of iterations attempting to match the head distribution that resulted from a system of heterogeneous K within hydrofacies to heads produced by a system in which each hydrofacies is represented as internally homogeneous. If desired, MODFLOWP can accommodate stochastic variation of K within zones.

Variance of field observations must be defined for an inverse modeling procedure. The specified variance must reflect not only measurement error but also error related to the fact that the grid block represents average head over an area while the head measured in the well represents the head over the open interval at one location. Interpolation of head between grid blocks is used to determine the head that will be compared with the measurement; however, such interpolation does not consider the flow equations, thus a variance greater than that associated with measurement error must be specified for observations. In short, the selection of accuracy and confidence interval is somewhat arbitrary in both field and synthetic studies. How reasonably the user assesses this uncertainty is reflected by the code output. For this study, true head observations are specified with 90% confidence that the measured head is within 1.2 m of the head it represents in the model. The one flow observation (groundwater seepage into the stream between gage stations) is defined with 90% confidence that the measurement is within 400 m^3/day of the true flows which are 10,500 and 15,300 m^3/d at the up and downstream stations, respectively.

Parameter Estimation

Initially, hydraulic conductivities of all five hydrofacies were independently estimated by the inverse model along with vertical anisotropy, recharge, and streambed conductance. The number of estimated parameters was eventually reduced to five for reasons given below. The data do not provide a basis for estimating K of all hydrofacies independently (perhaps due to the minimal number of wells in the alluvial fan facies); therefore, the alluvial fan and medium-grained channel deposits (hydrofacies 1 and 4) are represented by one estimate because of their hydraulic similarity. The K of overbank deposits (hydrofacies 2) and the recharge rate are correlated with a coefficient of 1.0. This is a typical situation encountered in many ground-water models but often goes unrecognized because calibration is undertaken by trial-and-error procedures; thus, correlation coefficients are not calculated. In this model, the correlation was addressed by fixing the recharge rate at the "true" value and estimating K of hydrofacies 2. The parameter estimation is insensitive to the streambed conductivity; hence, it is omitted from the estimation process. This situation is also common in ground-water modeling but typically goes unnoticed because sensitivities are not calculated for all estimated parameters. Given these adjustments, the parameter estimation is performed on 5 parameters: the vertical anisotropy of K and the K of the five hydrofacies with hydrofacies 1 and 4 grouped together. Prior information on the estimated parameters is defined as the mean of the true distribution with a standard deviation of 0.5 of the ln of K to constrain the estimates of K to reasonable values and a standard deviation of 0.2 to constrain estimates of the vertical anisotropy factor. Standard deviations on prior information can occasionally be obtained from statistical analysis of many field tests (e.g., based on numerous specific capacity tests conducted within an area); however, often the value is based on qualitative judgment and is employed as a tool to prevent the code from estimating parameters substantially different from those measured in aquifer tests or from what is deemed reasonable for a given lithology. Such decisions are typically made, but not quantified, when trial-and-error parameter estimation is undertaken.

Geostatistical Simulation and Concentration Distributions

Semivariograms are developed with hydrofacies data from the 37 wells and stochastic simulations are conducted with the semivariograms and hard data using a modified version (McKenna, 1994) of ISIM3D (Gomez-Hernandez and Srivastava, 1990) in the public domain software UNCERT (Wingle et al., 1994), resulting in 100 realizations. Flow is simulated in these configurations using "field estimates" of K equal to the "true" mean ln of K for each hydrofacies. Using MT3D, the range of concentrations at the proposed well location after 50 years of contaminant leakage is broad and the "truth" (indicated by the arrow) falls within the distribution (Figure 5A). The vertical line at the center of the gray bars indicates the mean of the concentration distribution for all of the realizations and the gray bars represent one, two, and three standard deviations. The distribution straddles the assumed regulatory level ($\log 0.001 = -3$). There is no clear case of the range of possibilities falling entirely above or below the regulatory level and the decision of whether to use a well or a pipeline is not obvious. One can only conclude that the uncertainty must be reduced. Either additional analyses or data collection must be undertaken to narrow the distribution. Given that analysis is less expensive than data collection, it is desirable to use the available data to reduce the uncertainty as much as possible. Once this is achieved, the results can be used to design further data collection if the distribution is still not narrow enough.

When inverse flow modeling (MODFLOWP) is used to estimate the hydraulic parameters of the system in each of these initial 100 realizations, the results do not produce the proper relative order of hydraulic conductivity for the hydrofacies. The relative order of hydraulic conductivity is determined from hydraulic testing of the hydrofacies in the

field and observations of the material character: coarse-grained channel deposits have the highest hydraulic conductivity, followed by medium-grained channel deposits and alluvial fan deposits, fine-grained splay/chute deposits, and overbank deposits. Parameter estimations from this initial inverse modeling consistently indicate that the hydraulic conductivity of the alluvial fan hydrofacies is lower than that of the overbank hydrofacies.

It is concluded that the simulated alluvial fan hydrofacies are too well-connected in these initial 100 realizations. As a consequence, the inverse modeling procedure is estimating a low K for the alluvial fan hydrofacies in order to fit the "measured" heads which exhibit higher gradients produced by the "true" discontinuous zones of high K. Inspection of the realizations reveals the alluvial fan hydrofacies to be either completely continuous along the left boundary of the domain or connected to the high hydraulic conductivity hydrofacies of the continuous channel hydrofacies near the centerline of the domain in all of these first 100 realizations [Figure 4(b)]

Incorporation of Expert Opinion as Soft Data

Based on this observation, soft data are added to the simulation process in the form of a decreasing probability of occurrence of alluvial fan material with distance from the surface manifestation of each alluvial fan. For each 10 feet of depth directly below the alluvial fan, probability of occurrence of alluvial fan hydrofacies is specified as 95%, 80%, 30%, 10%, and 0%. On the periphery of the fan a 95% probability of occurrence 100 feet to the east and 200 feet to the north or south is specified (distances are limited by grid spacing in the model) with a zero probability at greater distances. A 10% probability of occurrence is specified at locations underlying these peripheral zones. The same semivariograms are used with both the hard and soft data to simulate 400 realizations. Again, using MT3D, the concentration at the proposed well location after 50 years of contaminant leakage is calculated for each realization. Uncertainty is slightly reduced (Figure 5B), that is, precision is improved (note the narrower gray bars). The distribution still includes the "truth," so accuracy is maintained. However, the distribution of predicted concentrations is still broad, straddles the regulatory level, and does not provide a definitive basis for a decision.

Elimination of Realizations Using Inverse Flow Modeling

Many of the 400 realizations are eliminated using inverse flow modeling based on four criteria. The realization is eliminated if the flow model does not converge to a fairly loose tolerance (0.1 m) on heads at any point during the parameter estimation procedure (30% are eliminated by this criterion). The realization is eliminated if the flow model does not converge to a fairly loose tolerance (1% change in parameter value) on changes in parameters between iterations within the specified maximum number of 20 iterations (20 iterations is large for estimating 5 parameters) (20% eliminated). Examination indicates that realizations eliminated for lack of convergence were progressing in a direction

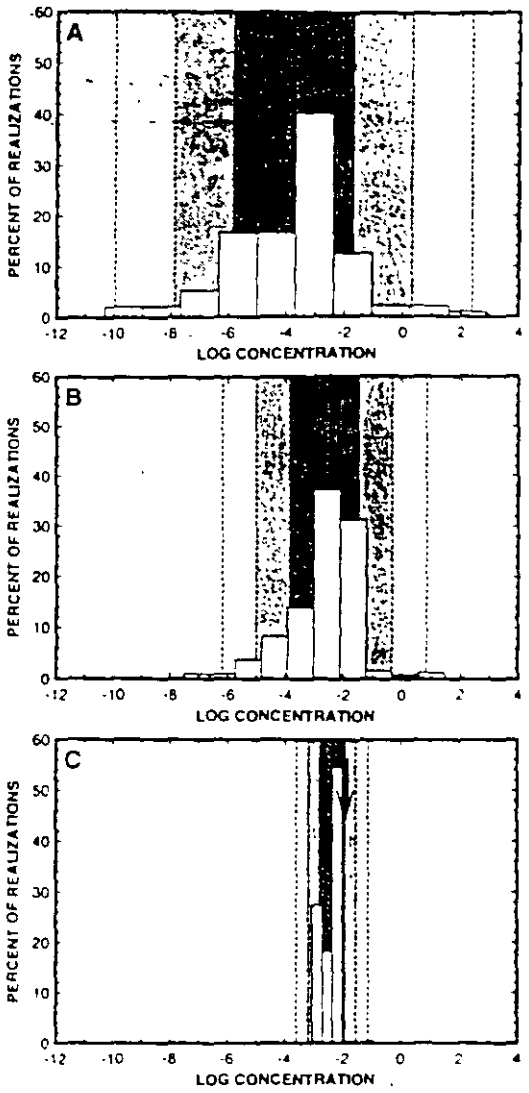

Fig. 5. Histograms of predicted concentrations at the proposed well location 50 yrs after breach of the landfill. A: based on hard data and field estimated hydraulic parameters; B: based on hard and soft geologic data and field estimated hydraulic parameters; and C: after eliminating configurations from B and estimating parameters using inverse modeling.

of unreasonable parameter values. The realization is also eliminated if the relative order of hydraulic conductivities is not as expected (7% eliminated). Examination suggests that these realizations have hydrofacies connections that are not similar to the true connectivity of hydrofacies. Finally, the realization is eliminated if the converged parameter estimation is a relatively poor fit to the field measurements (heads and stream flow) based on the value of the sum of squares of weighted residuals (40% eliminated). Sum of squares values range from approximately 180 to about 1200 for this problem. Realizations yielding values greater than 600 (half the maximum value) are eliminated; this is an arbitrary cutoff. Only 2.5% of the realizations remain after these eliminations. Contaminant transport is simulated in these realizations with MT3D using the hydraulic parameters estimated with MODFLOWP. The uncertainty is substantially reduced (Figure 5C) and the distribution mean is near the truth,

indicating that inverse flow modeling is a promising approach to incorporating hydrologic data into the simulation process to reduce uncertainty. Although the elimination criteria are subjective, we emphasize that it is preferable to eliminate many acceptable realizations in order to avoid retaining any unacceptable realizations; thus the elimination criteria should be stringent.

Summary

The problem presented herein illustrates a situation in which the use of hard data and multiple indicator conditional stochastic simulation leads to a large uncertainty. Inverse flow modeling identifies too much continuity in hydrofacies based on inappropriate estimates of relative hydraulic conductivity values for the hydrofacies. This observation is used to incorporate expert opinion on the probability of the extent of the alluvial fan hydrofacies as soft data in the simulations, resulting in some reduction of the uncertainty in contaminant concentrations. Finally, inverse modeling eliminates geologic realizations that do not yield a close fit to the hydrologic data, substantially reducing uncertainty.

Given that hydrogeologists must make decisions based on incomplete information, it is necessary that these decisions incorporate a recognition of uncertainty. Stochastic modeling of geologic uncertainty provides a means of quantitatively addressing uncertainty in the response function (advection and dispersion). As shown in Figure 2, this paper presents incorporation of disparate types of information for reduction of uncertainty. This "data fusion" forces the resulting predictions of flow and transport to be consistent with all available data. Furthermore, this work demonstrates two techniques for incorporating disparate types of data into site assessment: use of soft data in stochastic simulation of geologic units and inverse flow modeling. In this case soft data are in the form of expert opinion on geologic conditions which is identified through inconsistent results of inverse flow modeling). The same approach can be used to incorporate geophysical data (McKenna, 1994, McKenna and Poeter, 1994) and other types of expert knowledge about the site. Inverse modeling allows the incorporation of hydrologic data into uncertainty assessment through automated flow model calibration.

The first step in the demonstration of data fusion in this paper illustrates the danger of ignoring some of the available data. Using only hard data to generate stochastic geostatistical simulation yields realizations of the subsurface which are implausible. These implausible realizations are most likely the result of biased sample data and violations of the underlying geostatistical assumptions of stationarity and ergodicity. Without the incorporation of hydrologic data into the modeling process, these implausibilities might not have been identified and the resulting response function would have remained imprecise. Analyses and data collection must focus on reducing uncertainty (increasing precision) while capturing the truth in the distribution of predicted concentration (maintaining accuracy).

Acknowledgments

This work was partially supported by the U.S. Bureau of Reclamation under agreement number 1-FC-81-17500.

References

Allen, J.R.L. 1965. A review of the origin and characteristics of recent alluvial sediments. Sedimentology, v. 5, pp. 89-191.

Bridge, J. S. and M. R. Leeder. 1979. A simulation model of alluvial stratigraphy. Sedimentology, v. 26, pp. 617-644.

Gomez-Hernandez, J. J. and R. M. Srivastava. 1990. ISIM-3D: An ANSI-C three dimensional multiple indicator conditional simulation program. Computers in Geoscience, v. 16, no. 4, pp. 395-414.

Hill, M. C. 1992. A computer program (MODFLOWP) for estimating parameters of a transient, three-dimensional, ground-water flow model using nonlinear regression. USGS OFR 91-484.

McKenna, S. A. 1994. Utilization of soft data for uncertainty reduction in groundwater flow and transport modeling. Colorado School of Mines PhD dissertation T-4291.

McKenna, S. A. and E. P. Poeter. 1994. Simulating geological uncertainty with imprecise data for groundwater flow and advective transport modeling. In: Stochastic Modeling and Geostatistics: Case Histories and Practical Examples. J. Yarus and R. Chambers, eds. American Assoc. Petroleum Geologists Special Publication, Computer Applications in Geology, no. 3.

Olhoeft, G. R. 1992. Data fusion. Chapter 3 in Workshop on Non-invasive Geophysical Site Characterization. Compiled by E. Van Eeckhout and C. Calef. Los Alamos Report LA-12311-C UC-903, pp. 4-6.

Poeter, E. P. and D. R. Gaylord. 1990. Influence of aquifer heterogeneity on contaminant transport at the Hanford site. Ground Water, v. 28, no. 6, pp. 900-909.

Poeter, E. P. and S. A. McKenna. 1994. Geostatistical simulation and inverse flow modeling to reduce uncertainty associated with flow and transport predictions. Proceedings of the International Ground Water Modeling Center's 2nd conference, Fort Collins, CO.

Walker, R. G. and Douglas J. Cant. 1984. Sandy fluvial systems. In: Hydrofacies Models, 2nd ed., R. G. Walker, ed. Geoscience Canada Reprint Series 1, pp. 71-90.

Wingle, W. S. A. McKenna, and E. P. Poeter. 1994. UNCERT, A geostatistical tool for evaluating, modeling, and designing remediation facilities. Colorado School of Mines.

Zheng, C. 1991. MT3D, a Modular Three-Dimensional Transport Model User's Manual. S. S. Papadopulos & Assoc., Rockville, MD.

FACULTAD DE INGENIERIA U.N.A.M.
DIVISION DE EDUCACION CONTINUA

CURSOS ABIERTOS

XII CURSO INTERNACIONAL DE CONTAMINACIÓN DE ACUÍFEROS

MODULO III: MODELOS MATEMÁTICOS EN GEOHIDROLOGIA Y CONTAMINACIÓN DE ACUIFEROS

TEMA

A CONTROLLED EXPERIMENT IN GROUND WATER FLOW MODEL CALIBRATION

EXPOSITOR: DR. ADOLFO CHAVEZ RODRIGUEZ

PALACIO DE MINERIA
OCTUBRE DEL 2000

A Controlled Experiment in Ground Water Flow Model Calibration

by Mary C. Hill[a], Richard L. Cooley[a], and David W. Pollock[b]

Abstract

Nonlinear regression was introduced to ground water modeling in the 1970s, but has been used very little to calibrate numerical models of complicated ground water systems. Apparently, nonlinear regression is thought by many to be incapable of addressing such complex problems. With what we believe to be the most complicated synthetic test case used for such a study, this work investigates using nonlinear regression in ground water model calibration. Results of the study fall into two categories. First, the study demonstrates how systematic use of a well designed nonlinear regression method can indicate the importance of different types of data and can lead to successive improvement of models and their parameterizations. Our method differs from previous methods presented in the ground water literature in that (1) weighting is more closely related to expected data errors than is usually the case; (2) defined diagnostic statistics allow for more effective evaluation of the available data, the model, and their interaction; and (3) prior information is used more cautiously. Second, our results challenge some commonly held beliefs about model calibration. For the test case considered, we show that (1) field measured values of hydraulic conductivity are not as directly applicable to models as their use in some geostatistical methods imply; (2) a unique model does not necessarily need to be identified to obtain accurate predictions; and (3) in the absence of obvious model bias, model error was normally distributed. The complexity of the test case used implies that the methods used and conclusions drawn are likely to be powerful in practice.

Introduction

Regression has been a powerful tool for using data to test hypothesized physical relations and to calibrate models in many fields (Draper and Smith 1981; Seber and Wild 1989). Despite its introduction into the ground water literature in the 1970s (reviewed by McLaughlin and Townley 1996), regression has been used very little with numerical models of complicated ground water systems. The sparsity of data, nonlinearity of the regression, and complexity of the physical systems produce substantial difficulties. Obtaining tractable models that are sufficiently representative of the true system to yield useful results is arguably the most important problem in the field. The only options are improving the data, ignoring the nonlinearity, and(or) carefully ignoring some of the system complexity. Sparsity of data is a perpetual problem not likely to be alleviated at most field sites despite recent impressive advances in geophysical data collection and analysis (e.g., Hyndman and Gorelick 1996; Eppstein and Dougherty 1996). Methods that ignore nonlinearity are presented by, for example, Hoeksema and Kitanidis (1984) and Sun (1994, p. 182). The large changes in parameter values that occur in most nonlinear regressions of ground water problems after the first iteration, however, indicate that linearized methods are unlikely to produce satisfactory results in many circumstances. Thus, simplification related to parameterization appears to be the only potentially useful option, and is the mechanism considered in this work.

Defining a tractable but useful level of parameterization for ground water inverse problems has been an intensely sought goal, focused mostly on the representation of hydraulic conductivity or transmissivity. Suggested approaches vary considerably in complexity. The most complex parameterizations are cell- or pixel-based methods in which hydraulic conductivity or transmissivity varies from one finite-difference cell or other basic model entity to another, using prior information or regularization to stabilize the solution (for example, McLaughlin and Townley 1996; Clifton and Neuman 1982; Tikhonov and Arsenin 1977). Prior information and regularization produce similar penalty function terms in the objective function, but prior information needs to satisfy either classical or Bayesian assumptions, while regularization does not. Grid-scale parameterizations minimize user-imposed simplifications, but have the following problems: (1) heterogeneities smaller than the grid scale often are important, so use of grid-scale parameterization generally does not eliminate the scale problem; (2) more hydraulic-conductivity or transmissivity data than are available in most circumstances or often unrealistic assumptions about smoothness generally are needed; and (3) as presently developed, it is not straightforward to include knowledge about geologic structure into

[a]U.S. Geological Survey, P.O. Box 26034, MS 413, Lakewood, CO 80225. E-mail: mchill@usgs.gov (first author)

[b]U.S. Geological Survey, 12201 Sunrise Valley Dr., MS 411, Reston, VA 22092.

Received March 1997, accepted October 1997

grid-scale methods to produce: for example, constraints that can reduce the need for so many measurements of hydraulic conductivity or transmissivity.

Simpler parameterizations include zonation, interpolation, or eigenvectors of the variance-covariance matrix of grid-scale parameters (for example, Jacobson 1985; Sun and Yeh 1985; Cooley et al. 1986; RamaRao et al. 1995; Reid 1996, D'Agnese et al. 1998, in press). Stochastic methods (for example, Gelhar 1993; Yeh et al. 1995, Kitanidis 1995) also generally fall into this category, although they share some of the characterisucs of the grid-scale methods. These simpler parameterizations produce a more tractable problem, but it is not clear at what point the simplicity diminishes utility. The principle of parsimony (Box and Jenkins 1976, Parker 1994) suggests that simple models should be considered, but the perception remains that complex systems cannot be adequately represented using parsimonious models. For example, Gelhar (1993, p. 341) claims that "there is no clear evidence that [nonlinear regression] methods [using simple parameterizations] actually work under field conditions." Indeed, Beven and Binley (1992) even suggest that for some problems it may be best to abandon the concept of parameterizations simple enough to produce an optimal set of parameter values. A concept as useful as parsimony should not be given up lightly, yet there has been no conclusive evaluation of how complex parameterizations need to be to produce useful results.

This study originally had two purposes: (1) to present an approach that makes nonlinear regression methods more useful for the types of problems typical in ground water; and (2) to use a synthetic test case to evaluate the method and some general issues of model calibration. Because several articles describing and applying the approach have recently been published or are in review (Anderman et al. 1996, Barlebo et al. 1996; Poeter and Hill 1996, 1997, Hill 1998; D'Agnese et al. 1998, in press; Barlebo et al. in press), this paper will focus less on presentation of the approach and more on its evaluation using the synthetic test case. Issues of concern are whether the approach can be used as a scientific hypothesis-testing and data analysis tool that is likely to yield substantial insight into, and accurate models of, complex ground water systems, and whether problems simple enough to produce a well-posed nonlinear regression are useful in terms of model calibration and accurate predictions.

Methods and Previous Works

The synthetic test case is set in the framework of numerical ground water flow model calibration and prediction. In this work, model calibration is divided into model construction and parameter evaluation and estimation (as in, for example, Gupta and Sorooshian 1985, Sun 1994). Model construction includes: (1) Choosing appropriate mathematical and numerical methods and developing or choosing a computer program, (2) defining system discretization, representation of boundary conditions, and so on, and (3) selecting what aspects of the physical system to represent with parameters. Using this terminology, the same system characteristics may be classified differently in different applications. For example, when using zonation, defining the zones generally is classified under model construction as defined above. If the locations of the zone boundaries are represented by parameters, these would become part of the parameter evaluation and estimation (for example, Hyndman and Gorelick 1996). Given a model structure, model parameters can be evaluated for their importance under calibration and prediction conditions, and are estimated to achieve a model that in some way reproduces measured values. The resulting match is used to reevaluate model structure. Commonly, calibration is achieved using only trial and error. Problems with using trial and error alone have been discussed by many authors, including Carrera and Neuman (1986), Cooley and Naff (1990) and Hill (1992, p. 3).

Model calibration can be addressed more effectively by replacing trial and error with inverse modeling as much as possible, where inverse modeling refers to using formal optimization and stochastic methods to evaluate and estimate parameter values. In this work, inverse modeling is accomplished using nonlinear regression (Bard 1974; Cooley 1977, 1979, 1982, Sun 1994), associated advantages are discussed by, for example, Poeter and Hill (1997) and Hill (1998).

In this work, nonlinear regression is accomplished using the inverse ground water flow model MODFLOWP (Hill 1992). This model allows a wide variety of system characteristics to be calculated with defined parameters and allows for general definition of parameters so that spatially distributed quantities such as hydraulic conductivity and areal recharge can be defined using zones of constant value, interpolation methods, and some stochastic methods.

To conduct a definitive study of regression methods, it is necessary to use a complex synthetic test case in which all aspects are known. This is only possible if the synthetic test case is a numerical model. The true system in this work is a steady-state, three-dimensional numerical ground water flow model with five layers and five times smaller grid spacing than the calibrated model. The test case is characterized by aquifer heterogeneity, a confining unit, areal recharge, and ground water interaction with a lake and a stream. The turning bands stochastic method (Mantoglou and Wilson 1982), as implemented by Wilson (1989), was used to produce hydraulic-conductivity and areal-recharge distributions, and the areal extent of a confining unit. Some aspects of this test case were used by Eppstein and Dougherty (1996). Calibration is accomplished using nonlinear regression to estimate parameter values that represent aquifer and confining unit hydraulic conductivities, lakebed and streambed conductances, and areal recharge. This work is distinguished by the wide range of parameter types estimated in the regression, most studies only estimate parameters related to the hydraulic-conductivity distribution (for example, RamaRao et al. 1995). Model calibration was conducted by two of the authors of this report who knew only the information presented in the section "The Synthetic Test Case," except that they did not know the true head distribution.

As implemented, this is believed to be the most complicated test case that has been used in the evaluation of ground water inverse modeling. Other complex test cases include the following: Chu et al. (1987) estimated transmissivity and dispersivity of a two-dimensional synthetic test case. Gomez-Hernandez and Gorelick (1989) used a two-dimensional synthetic test case to investigate effective hydraulic-conductivity values, but did not investigate many of the model calibration issues studied in the present work. Poeter and McKenna (1995) present an innovative method of evaluating the hydraulic-conductivity distribution in detail using a three-dimensional test case, but do not consider other aspects of model construction or data availability.

In this report, the nonlinear regression method is presented briefly, data on the true system available for model calibration is presented, model construction and calibration using nonlinear regression are described, and the calibrated models are compared with the

true system characteristics. Predictions from the true and calibrated models are presented and compared with management criteria. Finally, the results are evaluated to determine the strengths and weaknesses of the regression and parameterization methods used.

Nonlinear Regression

This section briefly describes the regression methods used. Aspects of the approach are discussed further by Hill (1992), Anderman et al. (1996), Poeter and Hill (1997), D'Agnese et al. (1998, in press), and Barlebo et al. (in press); the most complete description is by Hill (1998). Nonlinear regression was used to find parameter values that minimize the weighted sum of squares objective function, S ($\underline{b}$), calculated as (Seber and Wild 1989, p. 27),

$$S(\underline{b}) = (\underline{y} - \underline{\hat{y}})^T \underline{\omega} (\underline{y} - \underline{\hat{y}}) \qquad (1)$$

where

$\underline{b}$ = an np × 1 vector containing values of the estimated parameters

np = the number of estimated parameters

$\underline{y}$ = an n × 1 vector of observed hydraulic heads, flows, and prior information

n = the number of observations of hydraulic head, flows, and items of prior information used in the regression

$\underline{\hat{y}}$ = an n × 1 vector of simulated (using $\underline{b}$) hydraulic heads, flows, and prior information.

$(\underline{y} - \underline{\hat{y}})$ = an n × 1 vector of residuals (observed minus simulated values)

$\underline{\omega}$ = an n × n weight matrix.

Weighted residuals are important indicators of model fit, and are calculated as $\underline{\omega}^{\frac{1}{2}} (\underline{y} - \underline{\hat{y}})$. The objective function is minimized with respect to the parameter values using a modified Gauss-Newton method.

It is desirable to estimate parameters with the smallest possible variance to achieve estimated values that are most likely to be close to the true values. To do this using Equation 1, linear theory indicates that three conditions need to be satisfied (Bard 1974, Tarantola 1987):

1. The model needs to be correct.
2. The weight matrix needs to be proportional to the inverse of the variance-covariance matrix of the measurement errors of the observed hydraulic heads, flows, and prior parameter information.
3. The measurement errors need to be random.

In addition, if Equation 1 is derived by classical Gauss-Markov arguments, the errors need not be normally distributed (Helsel and Hirsch 1992); if it is derived using maximum-likelihood arguments, normality is needed (Carrera and Neuman 1986).

Two aspects of nonlinear regression as implemented in the present work are discussed in more detail — weighting and diagnostic statistics.

eighting

To assign the weighting needed in Equation 1, it was assumed that measurement errors were uncorrelated, producing a diagonal weight matrix with nonzero elements proportional to one divided by the variance of the measurement errors. The actual lack of measurement error in the synthetically produced observation was unknown by the modelers, and weights were assigned based on expected measurement error (Cooley et al. 1986, Hill 1992, p. 48), as represented by standard deviations and coefficients of variation used to calculate the variances. Because the guidance provided by condition (2) allows room for adjustment, the weights are said to be subjectively determined. In practice, the determination of weights is always somewhat subjective except when they are automatically updated as part of the regression (Huber 1981; Barlebo et al. in press). Although useful for problems with large data sets (as in Neele et al. 1993), automatic updating can obscure the use of model fit in discovering erroneous data and model error when data sets are sparse, as is typical in ground water problems. In the approach presented in this work, weighting is not automatically adjusted. It is sometimes adjusted based on regression results after careful consideration.

The weighting procedure used in this work is a variation of common methods described by Theil (1963), Carrera and Neuman (1986), Cooley and Naff (1990) and Hill (1992), but eliminates use of the common error variance. Here, the weight matrix is assumed to equal (instead of being proportional to) the inverse of the measurement-error variance-covariance matrix and the flexibility previously assigned to the common error variance is now used to allow the calculated error variance to differ from its expected value of 1.0. The change reduces confusion for problems with more than one kind of observation — so-called coupled (Sun and Yeh 1990, Sun 1994), multiresponse (Seber and Wild 1989), or joint (Neele et al. 1993) problems. The convenience of the method results from (1) added clarity about the meaning of the weights and, therefore, the ability to compare any weighting used against expected values; and (2) the ability to use the standard error of the regression to infer possible dominance of measurement error versus model error.

Conditions 1 and 3 above are satisfied only if the weighted residuals from all types of observations and prior information appear to be statistically consistent with each other or if any statistical inconsistency can be explained by the correlation of the weighted residuals expected through the regression (Cooley and Naff 1990, p. 167-172; Hill 1992, p. 66-69). With this requirement, the method described here is consistent with methods using the common error variance.

With the weight matrix defined as being equal to the inverse of the variance-covariance matrix of the measurement errors, the objective function (Equation 1) is dimensionless. The regression standard error is commonly used to evaluate model fit, and is calculated as

$$s = \left(\frac{S(\underline{b})}{n - np} \right)^{1/2} \qquad (2)$$

and also is dimensionless. Using s directly as a measure of model fit is sometimes unsatisfactory because it cannot be used to compare models with different weighting and because it has little intuitive appeal. To obtain values that more effectively reflect model fit in this work, s is multiplied by the standard deviations or coefficients of variation used to calculate the weights for the head observations. The resulting statistic is defined here as the fitted standard deviation or the fitted coefficient of variation.

Diagnostic Statistics

During calibration, many statistics can be used to diagnose problems with the calibration and the regression in addition to the

standard error and fitted statistics described above. The statistics described here have proved to be extremely effective.

Composite scaled sensitivities and parameter correlation coefficients are used to measure the information available from the data to estimate parameters or, equivalently, to determine which parameters could likely be estimated uniquely with the available data. Composite scaled sensitivities are dimensionless quantities calculated as:

$$css_i = \left[(1/n) \sum_{j=1}^{n} \omega_{jj} \left(b_i \frac{\partial y_j}{\partial b_i} \right)^2 \right]^{1/2} \qquad (3)$$

These quantities were derived from similar statistics used by Cooley et al. (1986), and were first presented by Hill (1992). They resemble the CTB statistics derived independently by Sun and Yeh (1990). Each composite scaled sensitivity is the square root of a diagonal element of the Fisher information matrix (Rao 1973, p. 33, Carrera and Neuman 1986) scaled by the parameter value and n. The authors' experience indicates that if composite scaled sensitivities range over more than about two orders of magnitude, the regression is commonly unstable.

Correlation coefficients are calculated from the elements of the variance-covariance matrix on the parameters, which are calculated as

$$v_{ij} = s^2 \left[\left(\frac{\partial \underline{y}}{\partial \underline{b}} \, \underline{\omega} \, \frac{\partial \underline{y}}{\partial \underline{b}} \right)^{-1} \right]_{ij} \qquad (4)$$

The correlation between parameters i and j is calculated as $v_{ij}/(v_{ii}v_{jj})^{1/2}$. In general, correlations exceeding 0.95 indicate that all the parameter values may not be estimated uniquely.

One of the most obvious features of using nonlinear regression is that, for the well-posed problems developed in this work, optimal parameter values are obtained. These values and their individual 95% linear confidence intervals (Seber and Wild 1989, Hill 1994, p. 26-38) are used diagnostically in two ways. First, they are used to indicate whether unrealistic optimal parameter estimates suggest the presence of model error or not. If the model is correct and sufficient data are used and are being simulated correctly, optimized parameter values are expected to be reasonable. Unreasonable optimal parameter values often indicate problems with the model, the data, or the way the data are being related to the model. Linear confidence intervals on unrealistic optimized parameter values that include or nearly include realistic values suggest that the data are insufficient for conclusive evaluation, and the problem is less likely to be model error.

Confidence intervals on optimized parameter values are also used to indicate possible model simplifications. If the confidence intervals of two optimized recharge parameters, for example, largely overlap, it is likely that they could be represented as one recharge parameter.

The Synthetic Test Case

Synthetic Valley is an undeveloped alluvial valley surrounded by low permeability bedrock (Figure 1a). Surface water features are Blue Lake and the Straight River.

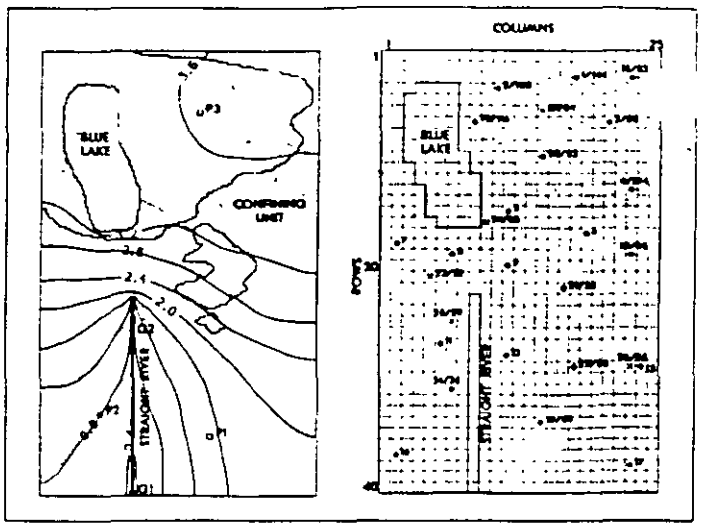

Figure 1a. (left) The 6096-m by 3810-m areal extent of the true and calibrated models used to represent Synthetic Valley, the true areal extent of Blue Lake and the confining unit, the location of stream gauges G1 and G2, the proposed locations of production wells P1, P2, and P3 (Development scenario A includes pumpage at P1 and P3; scenario B at P2 and P3), the true hydraulic heads for the water table (solid contours) and the basal part of the ground water system (dotted contours).

Figure 1b. (right) 152.4-m finite-difference grid spacing used in the calibrated models, finite-difference cells used to simulate the Straight River and Blue Lake, well numbers and locations, and, following the well numbers, hydraulic conductivities (in meters per day) measured using slug tests and, for well 27, an aquifer test. Figure 1b shows the loca' of wells available from the beginning of the study (●), wells drill field season 1 (o), wells drilled in field season 2 (x), and the well dr. in field season 3 (+).

Development Scenarios and Management Criteria

The design of the model and data collection efforts depend on the proposed development, so it is described first. Proposed development includes: (1) a 7600 m^3/d (cubic meters per day) well in the southern part of the valley at either well location P1 or P2 (Figure 1a), and (2) a 1900 m^3/d well at location P3 (Figure 1a). Development scenario A includes the pumpage at P1 and P3; development scenario B includes the pumpage at P2 and P3. Management criteria are: (1) Drawdown of the water table cannot exceed 0.6 m anywhere in the northern half of the valley; and (2) streamflow at gauge site G2 (Figure 1a) cannot be decreased by more than 20%. Because the development is characterized by constant rates of pumpage and the management criteria involve long-term effects of pumpage, predictive simulations are steady state.

Model Discretization and Boundary Conditions

The finite-difference cells used to represent Blue Lake and the Straight River in the true model are outlined in Figure 1a. The Straight River is a head-dependent boundary; Blue Lake is represented as a volume of very high hydraulic conductivity. The top of the model is simulated as a water table free-surface boundary subjected to areal recharge, which is represented as a defined flux. The four sides and the bottom of the model are no-flow boundaries. Five model layers were used in the true model.

Data

All data used for model construction and calibration are either calculated using the true system or derived from true system characteristics; they were not corrupted by added random noise. Thus, the data are more accurate than the data available for most model calibrations. This lack of what is commonly called measurement error allows for a definitive evaluation of model error, which plagues all model calibrations, but which generally cannot be characterized.

Data were collected at 17 existing wells and 10 additional wells drilled in subsequent field seasons (Figure 1b), and included drillers' logs, water table levels, and water levels at the screened intervals for all wells, and, for three wells, depth to bedrock. The valley sediments are mostly medium to coarse sands, some gravels, and a thin layer of lake clay in the north (confining unit of Figure 1a). Data from similar valleys indicate that horizontal hydraulic conductivity of the non-clay deposits ranges between 3 and 150 m/d (meters per day), which spans one and a half orders of magnitude. Remarkable vertical homogeneity displayed in the well logs was used in model calibration to justify using aquifer horizontal hydraulic conductivities that do not vary with depth, and are the same for all model layers representing aquifer material. In this way, the test case is simpler than most field sites, in which vertical inhomogeneity dominates, but the overall complexity of the test case is substantial despite this simplification.

Contour maps constructed using measured water table levels and hydraulic heads at the screened intervals are not shown in this report, but are similar to the true hydraulic-head maps shown in Figure 1a except that contours in the northeastern corner are smoother than the true contours. The true hydraulic-head maps were drawn by the authors calibrating the model until the end of the study. For all wells, water table levels are higher than the water levels at the screens. Where the confining unit occurs, the hydraulic head declines with depth by 0.031 to 0.183 m; where no confining unit occurs, it is as large as 0.03 m, but is less than 0.003 m for nine of the 13 wells.

Mean annual precipitation is 91 cm/y (centimeters per year), and there is no surface water flow into the valley. At the southern boundary, the stage in the Straight River is zero, the datum for all other elevations. The river gradient is 0.0002, so the stage at the head waters (2743 m upstream) is 0.55 m. Generally, the river ranges from 7.6 to 22.9 m wide and is 0.3 m or less deep. Gauged streamflows at G1 and G2 of Figure 1a are 25,046 and 27,30 m^3/d, respectively.

Blue Lake is a 5 m deep, sandy-bottom lake with no surface water inflow or outflow. A previous study of Blue Lake yielded the following: stage = 3.35 m, area of the lake = 1.510×10^6 m^2, lake evaporation = 69 cm/y. Because there are no surface water flows to or from Blue Lake, the difference between precipitation (91 cm/y) and evaporation from the lake (69 cm/y) recharges 910 m^3/d to the ground water system.

The ground water budget for Synthetic Valley can be expressed as $P - ET + 910\ m^3/d = 25{,}046\ m^3/d$, where P is precipitation, ET is evapotranspiration from the land surface, 910 m^3/d is the net flow from the lake, and the right-hand side equals the measured flow at G1. Thus, $P - ET = 24{,}136\ m^3/d$, which is equivalent to 0.00111 m/d, or 40 cm/y over Synthetic Valley minus the area of Blue Lake.

The long-term effect of local ground water pumpage on Blue Lake will be a decline in lake level. It will not be an increase in the net flow from the lake to the ground water system because Blue Lake is a closed lake with no surface water inflow or outflow, and precipitation on and evaporation from the lake surface generally are not affected by the lake-level changes.

Model Calibration

Calibration progressed through the development of seven models named CAL0 (the initial model), CAL0-G1 (tests the importance of the G1 flow measurement), CAL0+PR (tests using prior information to make one of the CAL0 estimated parameter values more reasonable), CAL1 (constructed after field season 1), CAL2 (constructed after field season 2), CAL3 (constructed after field season 3), and NO LAKE (tests the importance of representing the lake). The data available for the CAL0 models consisted of the data for wells 1 through 17, as described above, streamflows at G1 and G2, of which G2 and G1 minus G2 are used in the regression, and the net loss from the lake. Additional data were collected during the three field seasons.

Model parameters were defined to calculate the model characteristics listed in Table 1. All defined parameters were estimated by nonlinear regression, except as noted in Table 1.

Model Discretization and Boundary Conditions

The areal finite-difference grid and the cells used to represent Blue Lake and the Straight River in the calibrated models are shown in Figure 1b; the lake and river were head-dependent boundaries. To avoid adding nonlinearity that would promote longer, more unstable regression runs, during calibration the top layer of all calibrated models was represented as confined instead of unconfined. Resulting inaccuracies were found to be negligible for these steady-state models. The sides and bottom of the models were no-flow boundaries. Vertical discretization is shown in Figure 2. In the north, the bottom of layer 1 coincides with the bottom of the lake; the bottom of layer 2 coincides with the top of the clay confining unit (which is simulated as vertical leakance between layers 2 and 3). In the south, the bottom of layer 1 is deep enough to ensure that no cells go dry; the bottom of layer 2 was placed about 15 m lower for all models except CAL0, in which layer 3 is absent and layer 2 extends to the bottom of the model. The bottom of the model was derived from bedrock elevations measured at wells 1, 5, and 27 and some geophysical data.

Calibration Results

Some of the questions posed and answered at major steps of the calibration are presented in Table 2 to display the hypothesis-testing framework and to demonstrate how nonlinear regression and the diagnostic statistics were used. There were no problems with uniqueness in any of the regressions — optimal parameter values were readily identified for each model and parameter correlation was low; the largest correlation of 0.95 was calculated for CAL0-G1, and even then starting the regression at several sets of initial values indicated that the optimal parameter values were unique. Using the diagnostic statistics to evaluate the importance of different parameters to the predictions, as suggested by Hill (1998), might have been useful, but was not considered in this study.

The hydraulic conductivity distribution of the CAL0 models is defined using the zones shown in Figure 3a, which produced the best overall results of the many zone configurations considered. Interpolations based on linear triangular finite elements are used to define the hydraulic conductivity distributions of the other models; Figure 3b shows the finite elements used for CAL0. For the interpolations, most of the estimated values were at nodes of the finite-

Table 1
Parameters of the Calibrated Models

[Parameter labels: KRB*, the conductance of the streambed at the head-waters of the Smargit River; K_1^*, K_2^*, and K_3^*, zonal horizontal hydraulic-conductivity values (Figure 3a); KRB_1, KRB_2, and KRB_3, zonal streambed-conductance values (Figure 7); KLB, leakance (vertical hydraulic conductivity divided by thickness) of the lakebed; RCH, areal recharge rate; KV, leakance of the confining unit (Figure 4); ANIV, vertical anisotropy of aquifer material; w/prior, parameters had prior information.]

	Model Characteristic Calculated Using the Parameter					
Model	Streambed Conductance	Horizontal Hydraulic Conductivity	Lakebed Conductance	Areal Recharge	Confining Unit Leakance	Vertical Anisotropy
CAL0 CAL0-G1 CAL0+PR	KRB*	K_1^* K_2^* K_3^*	KLB	RCH	[1]KV	[1]ANIV
CAL1	KRB_1 KRB_2 KRB_3	[2]12 w/prior	do	do	KV	do
CAL2	do	[2]16 w/prior [3]+3	do	do	do	do
CAL3	do	do	[4]none	do	do	do
NO LAKE	do	do	[4]none	do	do	do

[1]Not estimated by nonlinear regression because of insensitivity, as indicated by small composite scaled sensitivities.

[2]The parameter labels are K*, where * is a well number from Figure 1b. These parameters are used in the interpolation scheme shown in Figure 3b with prior information used in the regression equal to the slug-test value shown in Figure 1b, for example, for well 1, it is 144 m/d.

[3]The parameter labels are K*, where * identifies location A, B, or C of Figure 3b. These parameters have no prior information.

[4]For CAL3 and NO LAKE, KLB is calculated as the hydraulic conductivity of the underlying cell, divided by the product of ANIV and the vertical distance to the center of the underlying cell (6.9 m in all models). No separate KLB parameter was defined.

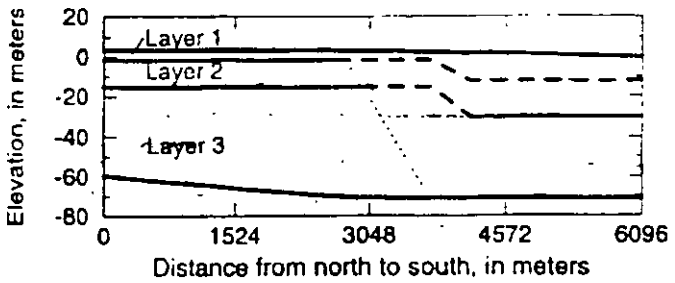

Figure 2. North-south cross-section showing the layers used in the calibrated models, including divisions used in all models (—), top is the water table; divisions used for all CAL0 models (···); and divisions used for all models except the CAL0 models (---). For any model, all north-south cross-sections are the same.

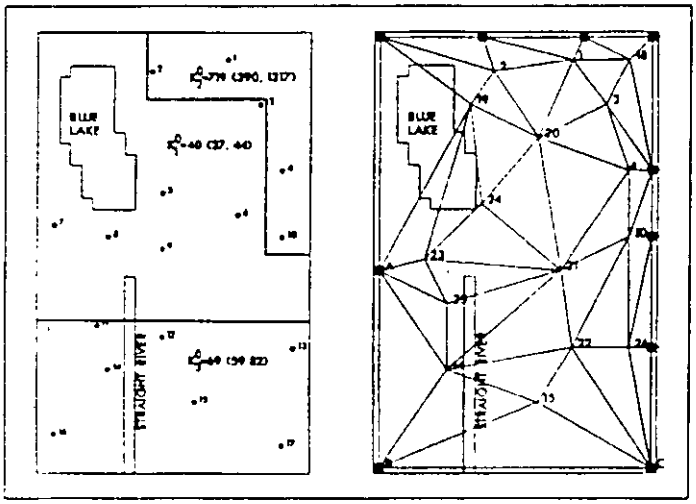

Figure 3a. (left) Zones used to parameterize the horizontal hydraulic-conductivity distribution for all model layers for the CAL0 models, with the wells used to construct the zones, the parameter labels of Table 1, and the estimated values and the 95% linear individual confidence intervals, in meters per day.

Figure 3b. (right) Triangular finite elements are used to parameterize the horizontal hydraulic-conductivity distribution for all model layers for the CAL3 model. The hydraulic conductivity is changed by the regression at the numbered apexes of the triangles (the numbers are well numbers) and at the squares labeled A, B, and C.

element grid located where slug tests had been conducted. The slug-test values are used as prior information for these parameters with weights on the prior information just large enough (or, equivalently, coefficients of variation just small enough) to achieve convergence of the regression. The final coefficients of variation are about 20%, which is somewhat smaller than the 30% that would be consistent with the authors' prior beliefs about the accuracy of the prior information. Thus, this application needs to be regarded as a regularization procedure instead of Bayesian prior (Backus 1988).

The weights used for observations in the regression were calculated using the standard deviations and coefficients of variation of the measurement errors in hydraulic heads and flows, respectively, shown in Table 3, which were based on typical measurement error for these data types. The covariance between flows G2 and G1-G2 (Hill 1992, p. 43), was not included in the weighting, but its omission is not expected to significantly affect the results. The statistics used to calculate the weights were modified within reasonable limits during calibration to achieve statistically consistent weighted residuals. The standard errors, s, in Table 3 are all less than 1.0, indicating that the model fit is better than would be consistent with the assigned weighting. This produces the small fitted statistics of Table 3 and Figure 5, and is because, unbeknownst to the modelers, the data have no noise added to them.

Graphs of weighted residuals against weighted simulated values for CAL0 and CAL3 are shown in Figure 6. Graphs for CAL0-G1 and CAL0+PR were similar to the CAL0 graph; graphs for the other models were similar to the CAL3 graph. For CAL0 (Figure 6a), six out of the seven weighted residuals between weighted simulated values of 15 and 30 are positive, suggesting they may be nonrandom. For CAL3, there is no indication of model bias related to the head and flow data, but estimated parameter values tend to be slightly smaller, on average, than the measured slug-test values, as indicated by predominantly positive weighted residuals.

Observed streamflow gains and those simulated using the CAL0 and CAL3 models are shown in Figure 7. For the CAL0 simulations, there were streamflow gain observations at G2 and between G1 and G2; for the CAL3 simulations there were streamflow gain observations every 152.4 m. In general, streamflows are matched within 150 m^3/d. The 910 m^3/d lake budget, which is smaller than any of the per cell streamflow gains, was matched within 2% by all models.

Table 2
Short Description of Results from the Calibrated Models

Model Label: Number of Regression Data and Parameters	Questions Addressed	Answers Derived from Regression Results for the Listed Model *:Conclusion contradicts the true model. Confidence intervals are 95%, linear intervals. Diagnostic statistics are *italicized*.
CAL0 34 heads 3 flows 6 parameters	1. What are the basic relations between the parameters and the head and flow data? 2. Can zones of constant hydraulic conductivity be used to produce a good model? 3. Does the areal recharge vary spatially? 4. Does streambed hydraulic conductivity vary spatially? 5. Does the confining unit extend all the way under the lake?	1. Head data alone: most ***correlation coefficients*** are 1.0, indicating that all parameters except ANIV are completely correlated. Adding lake budget data reduces correlation slightly. Adding the G2 and (G1-G2) flow data reduces correlation substantially, but ***composite scaled sensitivities*** suggest that these data are insufficient to estimate KV and ANIV. 2. No. The zones shown in Figure 3a produced a good fit to heads and flows (Figures 5 and 7), but K_2^0 (719 m/d) ***exceeds the expected maximum*** (152 m/d), and its ***confidence interval*** (390,1317) excludes reasonable values. This indicates that the model is significantly biased. 3. No. Estimated recharge rates applied to distinct zones fell within each others' ***confidence intervals***, indicating that one areal recharge rate was sufficient. 4. Yes(*). The best ***model fit*** to the data resulted when the simulated streambed hydraulic conductivity was increased by a factor of three from the head waters to the southern end. 5. No(*, see 2b for CAL3). Having the confining unit extend under the lake such that it covered both the dotted and striped areas of Figure 4a resulted in poor ***model fit***
CAL0-G1 34 heads 2 flows 6 parameters	1. Does model accuracy depend on the unusual situation found in CAL0, in which 100% of the flow exiting the system was measured at G1?	1. Yes. Omitting the G1 flow, only 11% of the flow exiting the system (the G2 flow) is included in the regression. The G2 flow was matched closely because it alone reduced what would otherwise be extreme ***correlation*** of the estimated parameters. Overall ***model fit*** was closer than for CAL0 (see s, Table 3, Figure 5), but CAL0-G1 predictions were less accurate than CAL0 predictions (Figure 10).
CAL0+PR 34 heads 3 flows 1 prior 6 parameters	1. Can prior information be used to make K_2^0 more reasonable? 2. Does this produce a more accurate model?	1. Yes. Imposing a prior information value of 122 m/d, with a confidence interval of (74;200) (equivalent to a standard deviation of 0.25 for the log-transformed prior), resulted in a high, but more reasonable, estimate of 273 m/d, with a confidence interval of (177;421). 2. No. CAL0+PR predictions are less accurate than CAL0 predictions (Figure 10).
CAL1 44 heads 19 flows 12 prior 18 parameters	1. Can the slug-test data be used to realistically represent spatial heterogeneity of the hydraulic conductivity? 2. Is it most likely that the spatial variation of flow into the Straight River is caused by variations in streambed hydraulic conductance or subsurface hydraulic conductivity?	1. Yes. The slug-test data were used as prior information to estimate a smoothly varying hydraulic conductivity field (Figure 9c). This distribution appears to represent the true distribution with sufficient accuracy in that all ***estimated parameter values*** are reasonable and ***weighted residuals*** are generally random. 2. (*) The ***model fit*** the measured flows into the Straight River more closely using the streambed conductances of Table 1 than by variations in subsurface hydraulic conductivity represented with four finite element nodes along the Straight River. It is likely that variations of either hydraulic property cause similar variations in the measured and predicted heads and flows. The streambed hydraulic conductivity is actually constant.
CAL2 52 heads 19 flows 16 prior 25 parameters	1. Do the data provide enough information to estimate the hydraulic conductivity at any of the boundary nodes?	1. Yes. ***Composite scaled sensitivities*** indicated that hydraulic-conductivity parameters probably could be estimated by the regression at boundary points A, B, and C (Figure 3b) and the resulting regression was, indeed, successful. No new prior information was used.
CAL3 54 heads 19 flows 16 prior 24 parameters	1. How do values from the aquifer test at well P3 (Figure 1a) in field season 3 compare to simulated values? 2. Evaluate two assumptions used so far: a. The leakance of the lakebed is constant over the area of the lake. b. The confining unit does not extend westward under the lake.	1. The ***simulated and aquifer-test horizontal hydraulic conductivities were comparable;*** aquifer-test derived vertical leakance of the confining unit of 0.00337/d was ***significantly lower than the optimized value*** (outside the ***confidence interval*** of Figure 8b), indicating possible model error. 2a. As an alternative consistent with available data, the separate lakebed was omitted from the model so that water flowing to and from the lake simply flowed through the aquifer material beneath the lake. This produced a similar ***model fit***, and was used in the final CAL3 model. 2b. With the lakebed represented as in 2a, good model fit was achieved with the confining unit extending under the lake (Figure 4b). This was used in the final CAL3 model.
NO LAKE 54 heads 18 flows 16 prior 24 parameters	1. Is including the lake in this simulation important given the predictive quantities of interest?	1. No. When the lake was omitted from the simulation, estimated parameter values were adjusted by the regression so that results were similar to CAL3. The estimated value of K19, the hydraulic conductivity parameter closest to the center of the lake, was unrealistically high, but its ***confidence interval*** included realistic values (Figure 8d).

Selected estimated parameter values and their 95% linear, individual confidence intervals are shown in Figure 8. These figures show how the estimated values and their precision changed for the different models. Notice that parameters with prior information (Figure 8d) never have confidence intervals greater than the confidence interval on the prior information (also noted by Carrera and Neuman 1986). Also, confidence intervals on hydraulic-conductivity values without prior information tend to increase as the estimated value increases, which is consistent with the smaller sensitivities commonly calculated for larger hydraulic conductivities.

The results presented in Table 2 demonstrate a number of situations that are likely to be common in practice. In CAL0, correlation coefficients and composite scaled sensitivities are used to detect data that provide insufficient or marginally sufficient information for the estimation of two of the defined parameters. The CAL0-G1 model demonstrates that with one outflow measurement including only 11% of the flow leaving the system, correlations are as high as 0.95, but a better-fitting model results (the standard error of the regression was less than for the CAL0 model, Table 3). The better fit apparently resulted from there only being one correlation-reducing observation (the G2 flow); the simulated and observed G2 flow were nearly identical, which is typical of single correlation-reducing observations. The consequence is that any error in a single correlation-reducing observation or in the way it is simulated will be directly transmitted to the estimated parameters, so that such an observation can act like an influential outlier on the regression. As discussed below, less accurate predictions were obtained with CAL0-G1 than with CAL0.

CAL0+PR shows prior information being used in a way that diminishes model accuracy, while CAL1 through CAL3 show prior information being used in a way that improves model accuracy. Thus, for this problem, using prior information to force optimal parameter values to be realistic reduced model accuracy, using prior information to include complexity not directly supportable by the other data improved model accuracy.

Table 3

Statistics for Weighting and of the Final Models

[s, standard error of the regression (Equation 2); a value of 1.0 indicates that the model, on average, fits the hydraulic head, streamflow gain, and lake loss data as closely as is consistent with the statistics used to calculate the weights; smaller values indicate a better fit; R_K^2, correlation coefficient for the weighted residuals and expected normal values, with values ranging from 0.0 to 1.0; values close to 1.0 indicate that the weighted residuals are independent, random, and normally distributed.]

Statistic	Model						
	CAL0	CAL0-G1	CAL0+PR	CAL1	CAL2	CAL3	NO LAKE
Statistics used to calculate the weights for the observations:							
Preliminary standard deviation for heads (m)	0.10	0.10	0.10	0.10	0.10	0.10	0.10
Preliminary coefficient of variation for							
Streamflow gains	0.063	0.063	0.063	0.12	0.17	0.17	0.17
Lake loss	0.13	0.13	0.13	0.23	0.33	0.33	0.33
Statistics of the final models:							
s	0.78	0.60	0.99	0.60	0.45	0.33	0.42
$^1R_K^2$	0.960	0.939	0.879	0.962	0.980	0.981	0.976
	(0.943)	(0.943)	(0.943)	(0.969)	(0.972)	(0.972)	(0.972)
Fitted statistics of the final models (s times the statistic used to calculate the weights)							
Fitted standard deviation for heads (m)	0.078	0.060	0.099	0.066	0.045	0.033	0.042
Fitted coefficient of variation for							
Streamflow gains	0.049	0.038	0.063	0.070	0.075	0.055	0.070
Lake loss	0.099	0.076	0.12	0.14	0.15	0.11	0.14

$^1R_K^2$ evaluated for the observations and the prior information. Critical values are in parentheses; if the residuals are independent and normally distributed, then there is only a 5% chance that R_K^2 is less than this value.

Comparison with the True Hydrogeology

The true system has a 30.4-m grid spacing, compared to the 152.4-m spacing used in the calibrated models, and has five model layers instead of two or three. The area of Blue Lake and the location of the Straight River are the same in the true and calibrated models. The side no-flow boundaries are the same in all models. In the true model, the elevation of the impermeable bottom of the ground water flow system was not as smooth as in the calibrated models (Figure 2), and varied from about −46 m on the east to about −91 m on the west.

The confining unit in the final calibrated models (Figure 4b) extends over more of the modeled area than the true confining unit (Figure 1a) because (1) the confining unit present at well 21 was assumed erroneously to be continuous with the larger confining unit to the north, and (2) none of the available data indicates that the confining unit is actually absent along the northeastern model boundary. Neural network analysis of the confining unit data (Risso 1993) correctly represented the break in the southern part of the confining unit, but did not resolve the second problem. No simulations were done with the neural network results as part of the present study.

True parameter values are plotted with the optimized parameter values and their confidence intervals in Figure 8. The true recharge rate plotted in Figure 8a is the average of a stochastically generated distribution with a small variance (5%), so that the true recharge is essentially constant, as concluded in the calibration. Only the CAL0-G1 and CAL0+PR models excluded the true value from the confidence interval. This reflects the importance of the G1 flow in the accurate estimation of recharge and the ability of prior information inappropriately applied to one parameter to affect other estimated parameters. For the vertical leakance of the confining unit (Figure 8b), the confidence intervals only include values that are greater than the actual values. This probably results from the excessive areal extent of the confining unit in the calibrated models discussed previously.

The value of hydraulic conductance of the streambed used in the true model is 244 m^2/d per meter of stream along the length of the Straight River instead of being variable, as simulated in all calibrated models. For all simulations, Figure 8c shows that the smallest estimated conductances are simulated for KRB_1 in the northern reach of the river, where the true underlying hydraulic conductivity is less than the calibrated value (Figure 9; see Figure 1a for stream location). The analysis in Appendix A indicates that little grid-size effect would be expected.

The lakebed was represented in the true system as in CAL3 and NO LAKE, so that there was no distinct lakebed. There is, therefore, no true value of lakebed leakance to compare with the estimates and their confidence intervals, and these values are not presented in this report.

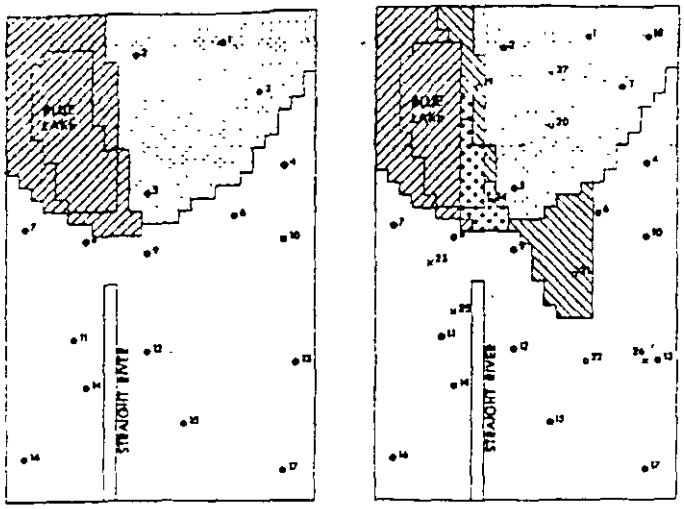

Figure 4a. (left) The simulated extent of the confining unit in the CAL0 calibration. Simulations included a confining unit covering both the dotted and striped areas; in the final CAL0 model the confining unit extended only over the dotted area.

Figure 4b. (right) The simulated extent of the confining unit in the CAL3 and NO LAKE models, with the areas added for the CAL1(///), CAL2 (♦), and CAL3(\\\) models. The locations of wells available at the beginning of the study (●), drilled in field season 1 (o), drilled in field season 2 (x), and the well drilled in field season 3 (+) are shown.

Vertical anisotropy equals 10 in most of the true system instead of 2.5, as used in the final calibrated models; the inaccurate estimate is consistent with the small composite scaled sensitivities of this parameter.

Aquifer horizontal hydraulic conductivity for the true system is shown in Figure 9a and is essentially vertically homogeneous, as assumed in model calibration. The calibrated hydraulic-conductivity distribution for the CAL0 model, with its three zones of constant value, is shown in Figure 3a. It is clear why zonation could not successfully represent this true hydraulic conductivity distribution. The triangular finite-element grid used for interpolation for the CAL3 model is shown in Figure 3b; the same grid is used for the NO LAKE model, and the grid used for the CAL1 and CAL2 models is similar but has fewer nodes.

The calibrated hydraulic-conductivity distribution for model CAL3 is shown in Figure 9b. Most of the major highs and lows of the true hydraulic conductivity are represented. Processes that depend on the smaller scale variations of hydraulic conductivity, such as flow into the Straight River, can only be simulated well if other aspects of the model can make up for the overly smooth estimated hydraulic-conductivity distribution. As mentioned before, low estimated streambed conductance at the headwaters of the Straight River probably making up for the hydraulic conductivity being too high.

The hydraulic heads simulated using CAL3 are not shown, but are nearly identical to the true hydraulic heads (Figure 1a) except in the northeastern corner, where the confining unit was simulated differently and the CAL3 hydraulic-head contours are smoother.

Comparison with the True Predictions

The simulated predictions relevant to management criteria 1 and 2 are (1) the maximum drawdown anywhere in the northern part of the study area (not supposed to exceed 0.6 m), and (2) the percent change in streamflow at gauging station G2 (not supposed to exceed 20%), calculated as 100 times the simulated change divided by 2730 m^3/d, the observed flow under unstressed conditions. As described previously, development scenario A includes pumpage at P1 and P3, scenario B includes pumpage at P2 and P3. Blue Lake is a closed lake so that pumpage was expected to affect the lake level. This was simulated for each prediction by reducing the lake level so that the contribution to the ground water system was the same with pumpage as it had been without pumpage. In the true system, this was accomplished by assigning the lake cells very large hydraulic conductivities.

Figure 10 shows that prediction accuracy for the best-fitting CAL2, CAL3, and NO LAKE models is extremely good; the CAL0-G1 model had the least accurate predictions.

The maximum drawdown may be located anywhere in the northern part of the model. The true maximum drawdown is located along the eastern boundary for scenario A, and along the northern boundary for scenario B. For the three CAL0 models, in which the vertical leakance of the confining unit is very small, the maximum simulated drawdown for both the A and B development scenarios is located along the eastern model boundary at or near row 5, column 25 (Figure 1b). For the other calibrated models, it was simulated at or adjacent to proposed well location P3 (Figure 1a).

From a management perspective, the predictions made by the different models are similar. For development scenario A, all models indicate that management criteria 1 and 2 would be violated, which is correct. For development scenario B, the predictions for the maximum drawdown are close to the management criterion (which is correct), with the greatest discrepancy simulated by the CAL0-G1 model; the predictions for the percent streamflow change are closer to the management criterion for the CAL1, CAL2, CAL3, and NO LAKE models than truly occurs, and the CAL0, CAL0-G1, and CAL0+PR predictions exceed the management criterion more than truly occurs.

The less accurate predictions of the CAL0+PR model relative to the CAL0 model show that, in this circumstance, when the linear confidence interval on the unrealistic parameter value included no reasonable values, the model with more accurate predictions was

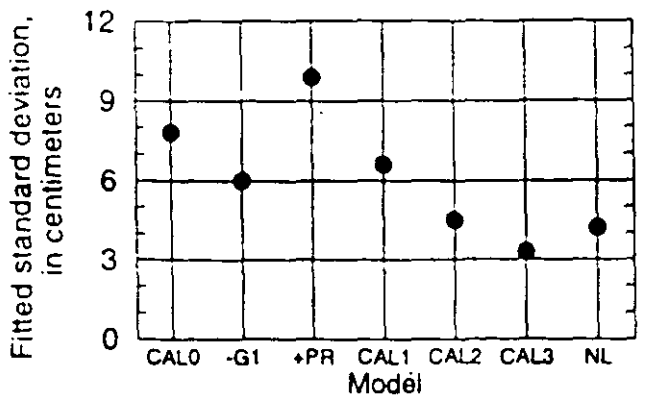

Figure 5. Fitted standard deviations of hydraulic heads for the final models. (NL is the NO LAKE model)

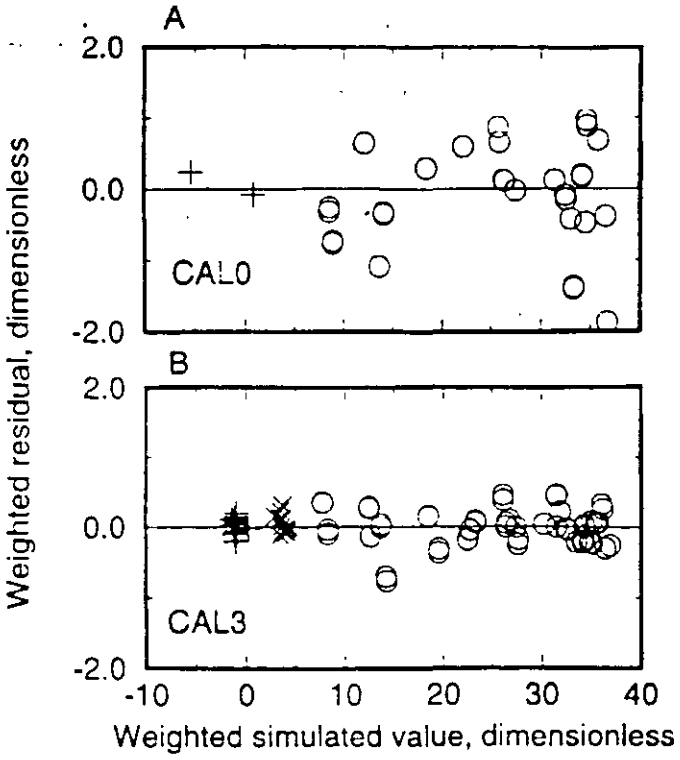

Figure 6. Weighted residuals versus weighted simulated values for the (a) CAL0 and (b) CAL3 models, for hydraulic heads (o), flows (+), and prior information from slug tests (x). In (a), one out of range flow at (-102, -1.2) is not shown.

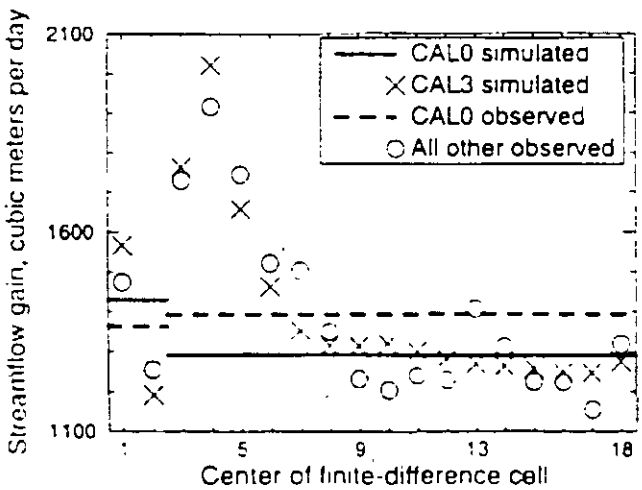

Figure 7. Measured and simulated streamflow gains along the Straight River for the CAL0 and CAL3 models. Values are per finite-difference cell, and finite-difference cell 1 is at the upstream end of the river. For the CAL3 model, parameter KRB_1 applies to cells 1 and 2, KRB_2 applies to cell 3, and KRB_3 applies to cells 4 through 18. Gauge G1 is located between cells 2 and 3. Gauge G2 is located at the downstream end of cell 18.

the model that fit the data better, even though one of the estimated parameter values was unreasonable. This is consistent with Troutman's (1983, p. 801) results for rainfall-runoff modeling, and suggests that when an unreasonable value is well supported by observation data (as indicated by large composite scaled sensitivities and a confidence interval that excludes reasonable parameter values), use of prior information often is not a productive mechanism with which to resolve the problem. More accurate predictions were obtained in this study with a more complex parameterization; prior information was used to achieve a stable regression with the additional parameters.

The results show that, for this problem, the most obvious indicator of a model likely to produce inaccurate predictions was an unreasonable estimated parameter value. In addition, weighted residuals were slightly nonrandom for the less accurate models. Models with a closer fit to the data (Figure 5 and s of Table 1) generally, but not always, produced more accurate predictions.

The predictions shown in Figure 10 are, of course, uncertain, which could be important to their use for management decisions. Analysis of measures of prediction uncertainty is beyond the scope of this report.

Discussion

The power of this work comes from the test case being complex enough to test how the methods are likely to work in actual application. Thus, test case realism is the first issue discussed in this section. Subsequent sections focus on three issues crucial to the use of calibrated models to evaluate ground water systems: Model nonuniqueness and its practical consequences, appropriate representation of small- and large-scale heterogeneities of the hydraulic-conductivity distribution, and the effect of model error.

Test Case Realism

The test case is more realistically complex than any other test case used for this purpose in that (1) the flow system is fully three-dimensional and has commonly encountered types of boundary conditions, (2) the areal hydraulic-conductivity distribution, areal recharge, and areal extent of the confining unit are reasonably complicated, except as noted below; and (3) the problem is posed in terms of a management problem. The test case, however, is simpler than most field problems in that (1) the hydraulic conductivity of the aquifer material did not vary with depth much, a condition rarely, if ever, encountered in natural environments (the flow system, however, was still three-dimensional because of the boundary conditions and the presence of a confining unit); (2) both the true and calibrated systems were truly at steady state, thus avoiding transient effects; (3) the location and impermeability of the lateral and bottom boundaries were better known than in most field problems, and (4) the range of hydraulic conductivities was somewhat narrower than in many field problems.

The regression data used to calibrate the seven models developed in this work were hydraulic heads, lake seepage, streamflow gains, and hydraulic-conductivity values produced by slug tests, all of which were derived from the synthetic test case. The data were generally typical of the type of data available in most field studies, except as follows: (1) The "observed" values of hydraulic head and flow were derived directly from the true models, with no random errors added, (2) the hydraulic-head data were more evenly distributed in space than commonly occurs; (3) the streamflow-gain measurements included 100% of the outflow from the system (except for the CAL0-G1 model) and, for some of the models, were of higher resolution (every 152.4 m) than streamflow gains generally can be determined from measured streamflows given common measurement errors, and (4) the slug-test data were equal to the hydraulic conductivity of a 30.6-m square finite-difference cell,

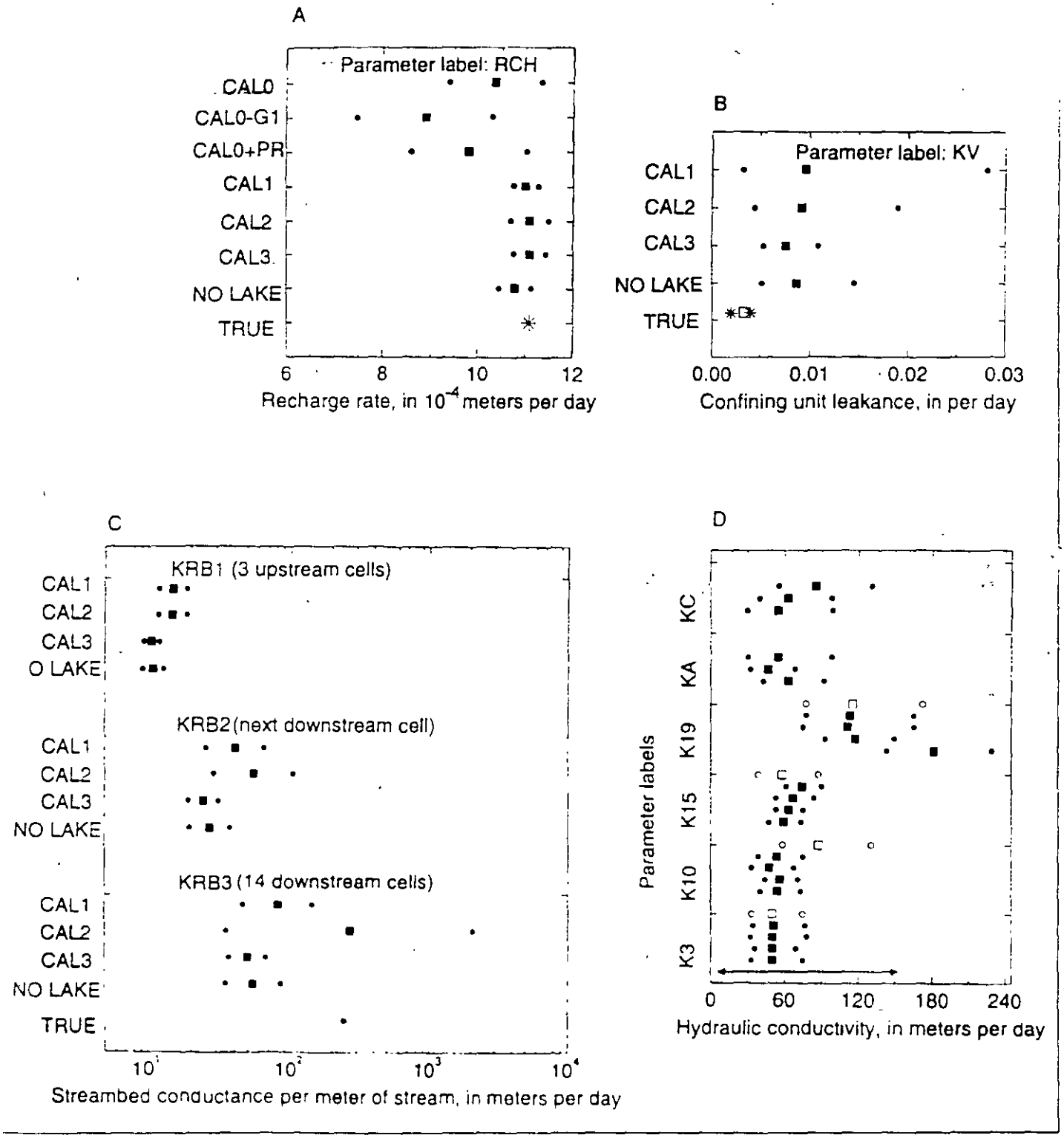

Figure 8. (a–d). Estimated values of selected parameters used to calculate the following model characteristics: (a) recharge rate; (b) vertical leakance of the confining unit, (c) streambed conductance; and (d) horizontal hydraulic conductivity. The graphs show the estimated values (■); their 95% linear, individual confidence intervals (●); true values (*) or, in (Figure 8b), the range of true values (between the *s). Figure 8d includes measured values (□), for measured values used as prior information in the regression (Figure 8d), the 95% linear, individual confidence intervals (o), calculated using the statistics specified for the prior information in the regression; the expected range of values is plotted using a line with arrows. Prior information, if used, is plotted as the first row for each parameter; subsequent rows are results from the CAL1, CAL2, CAL3, and NO LAKE models. See Table 1 for definition of parameter labels.

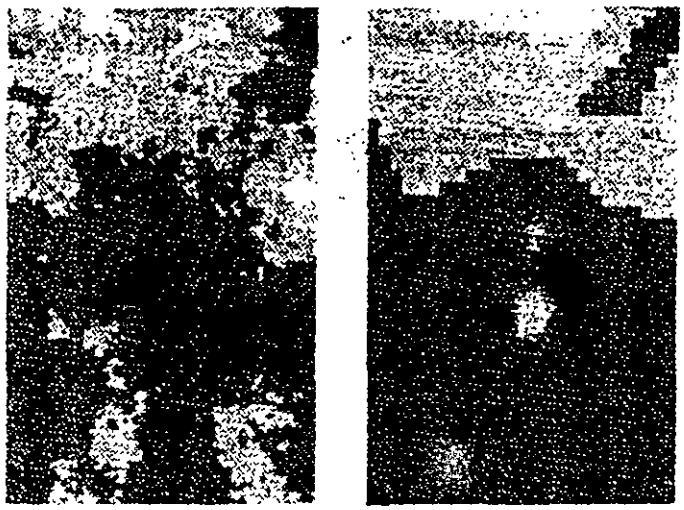

Figure 9a. (left) Map showing the true hydraulic-conductivity distribution.

Figure 9b. (right) Map showing the optimized distribution of hydraulic conductivity for model CAL3.

Gray shade	Hydraulic conductivity, in m/d
(darkest)	0-36
	36-72
	72-108
	108-144
(lightest)	144-180 [occurs only in one cell of (A)]

which is a larger amount of material than slug tests usually sample. Repeating some of the regressions using noisy data would be an important contribution, but this was considered to be beyond the scope of this report.

Despite the simplifications, the test case appears to have been complex enough to serve the objectives of this work.

Model Uniqueness and Its Practical Consequences

Given the advantages inherent in the synthetic test case, one might have expected to find one model that was clearly the best and thus be able to avoid the problem of nonuniqueness normally found in ground water flow problems. Nonetheless, nonuniqueness proved to be a problem. Models CAL2, CAL3, and NO LAKE yielded a remarkably similar quality of calibration (Table 3, Figure 5) and prediction (Figure 10), despite different assumptions regarding the hydraulic-conductivity distribution, areal extent of the confining unit, vertical anisotropy, and representation of the lakebed and the lake. Even CAL1, for which the calibration was not as good, produced accurate predictions. This is important because it indicates that the lack of uniqueness pervasive in ground water models does not necessarily indicate that the models produce inaccurate predictions and, therefore, are useless. Instead of uniqueness, prediction accuracy appears to depend on the type and accuracy of the available data and the calibration methodology. Basically, if the calibration is sufficiently constrained, different calibrated models are likely to produce results of similar accuracy.

Appropriate Representation of Small- and Large-Scale Heterogeneity

Representing the hydraulic-conductivity field using three zones in the CAL0 models had the advantage of allowing a clear evaluation of the relation between the data and the parameters. In this test case, use of head data alone or in combination with the lake-budget data resulted in extremely correlated parameters, which would have prohibited estimation of individual parameter values. Such an evaluation generally is not possible with more complex parameterizations in which some parameters are not estimated and(or) prior information is used, because both affect the statistics used to identify parameter correlation.

Representing the hydraulic-conductivity field using three zones had the disadvantage of being too unrealistic in this test case, as indicated by one unrealistic hydraulic-conductivity value estimated by the regression, somewhat nonrandom weighted residuals, and inaccurate predictions.

Representing the hydraulic-conductivity field using a simple interpolation method based on linear triangular finite elements produced good fitting models capable of accurate predictions of drawdown and changes in streamflow gain. Use of other interpolation methods could have some advantages, for example, kriging allows the distance of influence of each interpolation point to be easily adjusted. We do not expect that using another interpolation method would significantly change the results, but this was not tested in the present study because such a good fit was achieved with the simpler methods. Methods that allow smaller scale variation, such as grid-scale parameterizations, also were not tested for the same reason.

Using the slug-test data as prior information on estimated parameters located at interpolation points of the finite-element grid allowed the regression to adjust the estimated parameter values so that the simulated hydraulic conductivities were more representative of the hydraulic conductivities at the larger scale. This is in contrast to the pilot-points method (Marsily et al. 1984; Certes and Marsily 1991; RamaRao et al. 1995), in which the hydraulic conductivity at the slug-test measurement points would have been set (or nearly set) to the slug-test value and parameters located at additional points would be estimated. It is also in contrast to other geostatistical methods (Kitanidis 1995; Yeh et al. 1995), in which the point values are used with little or no change and the majority of the effort is spent modeling the variogram. Estimated values differed from prior estimates by as much as 57%, and 26% for the best-fitting model and it is thought that much of the difference is related to scale. Certes and Marsily (1991) suggest that the scale effect can be neglected, but that didn't appear to be the case in the present study.

Accurate predictions were obtained despite the lack of pumping in calibration conditions, and its presence in prediction conditions. Although changes in the flow field can change effective values of hydraulic conductivity, this problem did not appear to be significant in the present test case.

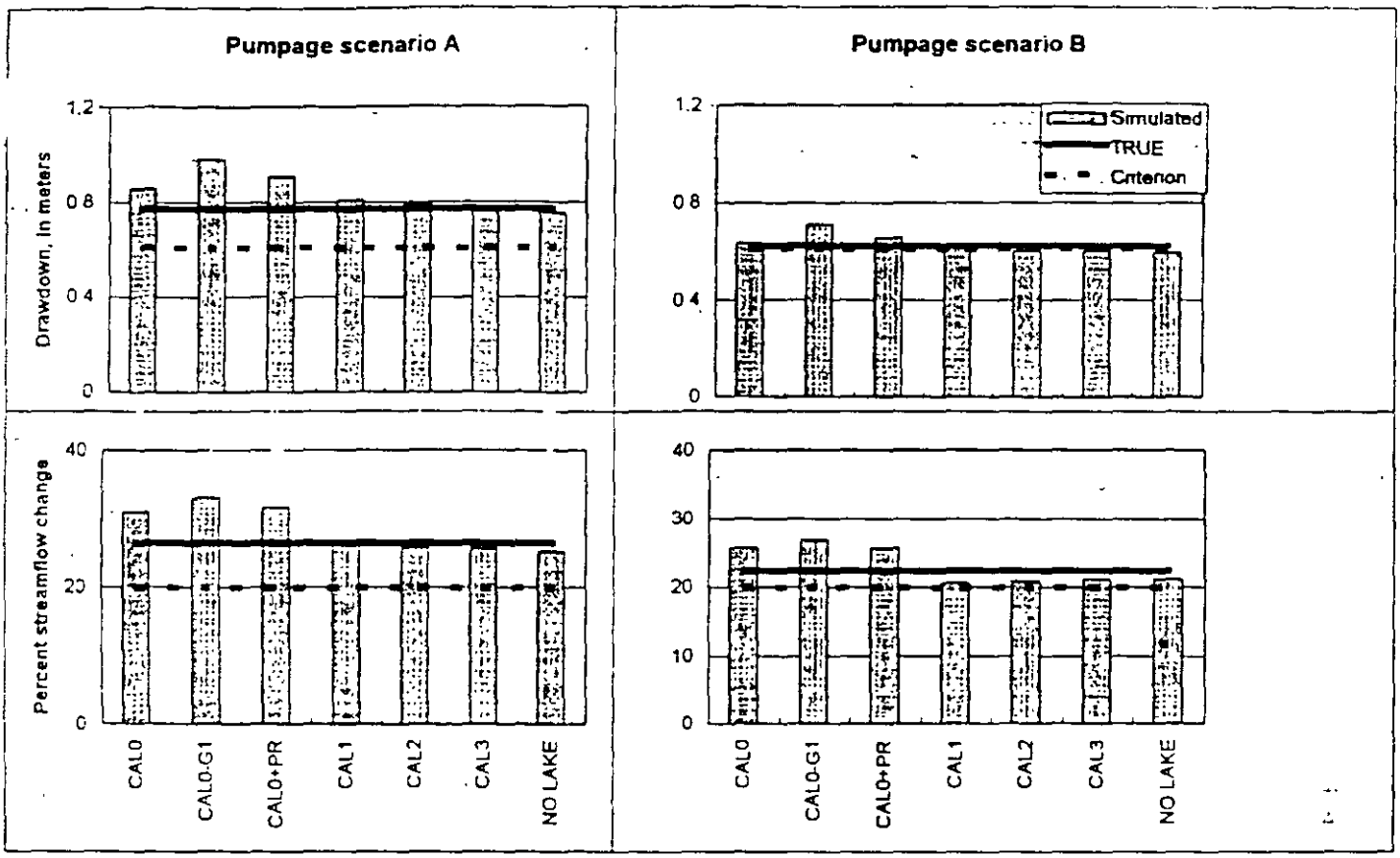

re 10. Graphs showing predictions for pumping scenarios A and B calculated using the calibrated and true models and the relevant management criteria.

Effects of Model Errors

In this test case, residuals result from model error because no random measurement errors were introduced into the simulated data. This provides a unique opportunity to investigate model error.

The R_x^2 values of Table 3 indicate that all sets of weighted residuals are, or are nearly, independent and normally distributed, and spatial plots of weighted residuals (not shown) generally revealed no spatial trends. Two aspects of this are important. The most basic is that the weighted residuals appear to be random. Randomness of residuals in regression analysis usually is thought to result from measurement errors (Draper and Smith 1981, p. 22-24). A possible explanation for the apparent randomness of the residuals in this synthetic test case is that each residual is the result of model errors from several sources, such as errors in parameterization, boundary conditions, and other aspects of model construction. Weighted residuals that are in effect random suggest that weighted true errors are also effectively random. This is significant because if true, it suggests that certain types of model error might be accommodated by standard regression assumptions that require that the true errors be random (Seber and Wild 1989, p. 573; White 1981). In addition, the assumption of random true errors is required to assure asymptotic consistency and normality of estimated parameter values (Seber and Wild 1989, p. 563-572). This work indicates that presence of model error may not violate these requirements as the estimated parameter values, weighted residuals, or other measures indicate model bias.

In addition to being random, the weighted residuals were normally distributed. As with randomness, the normality of the weighted residuals is often thought to be a result of measurement error, which was not present in this synthetic problem. The normality of the weighted residuals suggests that despite the pervasive presence of model error in numerical ground water flow models, the assumption of normality often may be valid. This would result if a process similar to that described by the classical central limit theorem (Draper and Smith 1981, p. 24) were operating, and means that the formulation of Tarantola (1987, p. 58) would be valid. By the central limit theorem, contributions of error from multiple independent sources result in random, normally distributed values, regardless of the probability distribution of each of the individual errors. As stated above, indication of model bias, such as nonrandom weighted residuals or unrealistic optimal parameter values, could indicate that a limited number of errors are dominating so that the central limit theorem would not apply.

Conclusions

In this test case, properly used nonlinear regression either produced effective, though nonunique, calibrated models capable of accurately predicting two quantities important to resource management, or provided clear evidence of model or data inadequacy. The conclusions listed here relate both to effective use of the nonlinear regression methods (conclusions 1–4) and to challenging some common practices and commonly held beliefs in model calibration (conclusions 5–7).

1. The method of determining the weights for the weighted least-squares objective function tested in this study was used to correctly detect much smaller measurement error than would normally occur.

2. The most conclusive indicator of model bias was unrealistic optimal parameter estimates that also had confidence intervals that excluded reasonable values. Nonrandom weighted residuals were a less conclusive indicator of model bias in the present study, but this may not always be the case, especially when models are more biased than those considered here.
3. Including prior information in the regression diminished model accuracy when used to force optimal parameter values to be reasonable, but improved model accuracy when used to represent the hydraulic-conductivity distribution with more complexity than was supportable with the head and flow observations alone. Excluding all prior information initially allowed for clear evaluation of the contributions of different types of data.
4. The importance of flow data was clearly demonstrated in this study. This is important because few field studies have measurements representing all of the flow leaving the system, so that problems of completely correlated parameters and the effects of a single correlation-reducing observation, as documented for the CAL0-G1 model, are probably common. These problems can be clearly characterized and understood by first representing ground water systems very simply, and building complexity as warranted by the data and modeling objectives.
5. The results of this study indicate that, given present technology, hydraulic-conductivity values measured in the field often are not as directly applicable to a numerical model of the system as would be consistent with how these data are sometimes used in model calibration. Two aspects of the controlled experiment presented in this paper support this conclusion.
   (a) In four of the models, the hydraulic-conductivity distribution was adequately represented (as evidenced by accurate simulated predictions) by an interpolation scheme in which values that were held constant were limited to the model boundaries, while nearly all values within the modeled area were estimated. Unusually accurate slug-test values were used as prior information in the regression; corresponding estimated aquifer hydraulic-conductivities differed from the slug-test values by as much as 57%, suggesting that direct imposition of the slug-test values, as is done in some geostatistical methods, would probably produce a less accurate model. This situation largely reflects problems of scale. Here, the numerical grid spacing was five times larger than in the true system; in field applications the scale problem is likely to be more severe.
   (b) Streambed hydraulic-conductance estimates were affected by underlying subsurface heterogeneities that were not well represented by the simulated aquifer hydraulic-conductivity distribution. If field work had determined that the streambed conductance was constant along the river (which it was) and this had been imposed, the calibrated models probably would have produced less accurate predictions. This situation does not represent a scale problem as much as error in representing one part of the system affecting the parameters representing another part of the system.
6. For three of the calibrated models, the fit to the regression data was nearly equally good and there was no evidence of model bias. This lack of uniqueness is probably unavoidable in complex ground water problems, but the results of this work indicate that such nonuniqueness is not necessarily a debilitating problem. In the synthetic test case, all three models produced similar accurate predictions, probably because the data used in model construction and in the regression sufficiently constrained the solutions.
7. Weighted residuals (observed minus simulated hydraulic heads, flows, and prior information) resulting from the regression were, in general, random and normally distributed, which is surprising because no errors had been added to the synthetically generated observations. Thus, all error was model error. It is generally thought that if model error dominates measurement error, the regression results are invalid, but the results of this work imply that the dominance of model error does not necessarily produce an inaccurate model if there is no obvious indication of model bias.

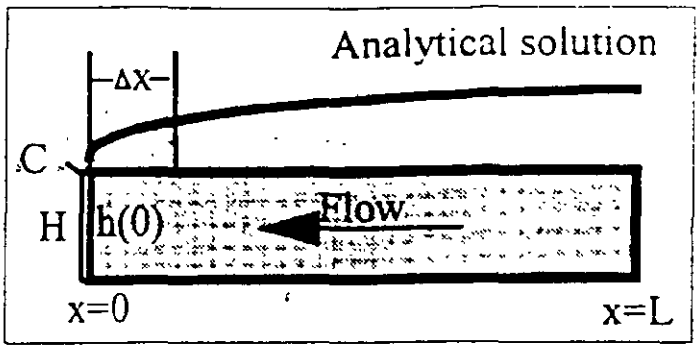

Figure A1. Simple system of ground water flow toward a fully penetrating stream with a streambed of different hydraulic properties. C is the conductance of the streambed for the analytical problem. h(0) is the hydraulic head on the aquifer side of the streambed for the analytical problem.

Taken with conclusion 2, conclusion 5 produces a dilemma, because unrealistic optimal parameter values (as determined by comparing optimal and measured values) are said to indicate a less accurate model, but parameter values cannot be expected to equal measured values because parameter values are accommodating model error. A useful resolution is derived by noting that if model error is so large that best fit parameter values are far from measured values, the resulting model is likely to produce less accurate predictions than a model for which the best parameter values are close to measured values. Thus, models with more realistic best-fit parameter values are more likely to be accurate.

Conclusions 4 and 6 suggest that improved accuracy of ground water models is likely to be attained by using available data more effectively and by designing methods to collect new kinds of data, perhaps using regression methods as a guide.

Appendix A

Effects of Grid Size on Simulated Streambed Conductance

This appendix evaluates the effects of grid size on the simulated streambed conductance using a simple one-dimensional analytical equation. The results are expected to approximate the effects related to the three-dimensional system considered in this study.

Flow to a stream with a streambed having conductance C, through a homogeneous ground water system of hydraulic conductivity K, given a constant recharge rate of W, can be idealized as shown in Figure A1, where h(0) is the hydraulic head on the

ground water system side of the streambed. Using the variables shown in Figure A1, recharge rate W, and constant layer thickness , the analytical solution for hydraulic head is

$$h(x) = \frac{W}{Kb}\left(Lx - \frac{x^2}{2}\right) + h(0)$$

When a finite-difference grid is imposed, a linear gradient is enforced between finite-difference cell centers, over distance Δx in Figure A1. Note that the system can be approximated this way, regardless of whether the stream abuts the grid on the side, as in Figure A1, or on the top, as in most models. Farther from the stream, it is assumed that the finite-difference grid closely simulates the analytical head solution. Thus, the following equations apply:

$$h(x) = \frac{W}{Kb}\left(Lx - \frac{x^2}{2}\right) + h(0) \qquad x \geq \Delta x \qquad (A1)$$

$$h_{\Delta x}(x) = \frac{W(L - \Delta x/2)}{Kb}x + h(0) \qquad 0 < x < \Delta x \qquad (A2)$$

Subscript Δx indicates that the quantity is related to the linear gradient imposed near the stream. The flow through the finite-difference cell next to the stream is evaluated midway between cell centers, so equals $W(L - \Delta x/2)$. The condition of head continuity at $x = \Delta x$ was used to determine the constant of integration as $h(0)$ in Equation A2.

Flow through the streambed at $x \geq 0$ can be described using Darcy's law as,

for the analytical system,

$$WL = C(h(0) - H), \text{ or } h(0) = H + \frac{WL}{C} \qquad (A3)$$

for the discretized system,

$$WL = C_{\Delta x}(h_{\Delta x}(0) - H), \text{ or } h_{\Delta x}(0) = H + \frac{WL}{C_{\Delta x}} \qquad (A4)$$

where, C and $C_{\Delta x}$ are the streambed conductances of the analytical and discretized solutions, respectively, and $h(0)$ and $h_{\Delta x}(0)$ are the hydraulic heads on the aquifer side of the streambed applicable to the analytical and discretized solutions, respectively. Flow out of the model is considered to be positive to coordinate with Equation (A1). Substituting Equations A3 and A4 into Equation A2 evaluated at $x = 0$ shows that $C_{\Delta x} = C$. Solve Equation A2 for $x = 0$ to yield $h_{\Delta x}(0) = h(0)$. Thus, grid size does not affect the variables related to simulation of the river.

This analysis does not completely represent the dynamics of flow to a stream in a three-dimensional, heterogeneous system. The results, however, indicate that grid effects are not likely to be important in the calibration of streambed conductance in the present work.

References

Anderman, E.R., M.C. Hill, and E.P. Poeter. 1996. Two-dimensional advective transport in ground water flow parameter estimation. *Ground Water* 34, no. 6: 1001-1009.

Backus, G.E. 1988. Bayesian inference in geomagnetism. *Geophysical Journal*, 92, 125-142.

Bard, J. 1974. *Nonlinear Parameter Estimation*. New York: Academic Press.

Barlebo, H.C., M.C. Hill, and D. Rosbjerg. 1996. Identification of ground-water parameters at Columbus, Mississippi, using three-dimensional inverse flow and transport model. In Proceedings of the 1996 Model CARE Conference, Golden Colorado, September, ed. K. Kovar and P. van der Heidje.

Barlebo, H.C., M.C. Hill, D. Rosbjerg, and K.H. Jensen. In press. On concentration data and dimensionality in groundwater models. *Nordic Hydrology*.

Beven, K., and A. Binley. 1992. The future of distributed models. Model calibration and uncertainty prediction. *Hydrological Processes* 6, 279-298.

Box, G.E.P., and G.M. Jenkins. 1976. *Time Series Analysis: Forecasting and Control*. 2nd ed. San Francisco: Holden-Day.

Carrera, J., and S.P. Neuman. 1986. Estimation of aquifer parameters under transient and steady-state conditions. *Water Resources Research* 22, no. 2, 199-242.

Certes, C., and de Marsily. 1991. Application of the pilot point method to the identification of aquifer transmissivities. *Advances in Water Resources* 14, no. 5: 284-300.

Chu, Wen-sen, E.W. Strecker, and D.P. Lettenmaier. 1987. An evaluation of data requirements for groundwater contaminant transport modeling. *Water Resources Research* 23, no. 3: 408-424.

Clifton, P.M., and S.P. Neuman. 1982. Effects of kriging and inverse modeling on conditional simulation of the Avra Valley aquifer in southern Arizona. *Water Resources Research* 18, no. 4: 1215-1234.

Cooley, R.L. 1977. A method of estimating parameters and assessing reliability for models of steady-state ground water flow, 1. Theory and numerical properties. *Water Resources Research* 13, no. 2: 318-324.

Cooley, R.L. 1979. A method of estimating parameters and assessing reliability for models of steady-state ground water flow, 2. Application of statistical analysis. *Water Resources Research* 135 no. 3: 603-617.

Cooley, R.L. 1982. Incorporation of prior information on parameters into nonlinear regression groundwater flow models—1. Theory. *Water Resources Research* 18, no. 4: 965-976.

Cooley, R.L., L.F., Konikow, and R.L. Naff. 1986. Nonlinear regression groundwater flow modeling of a deep regional aquifer system. *Water Resources Research* 22, no. 13. 1759-1778.

Cooley, R.L., and R.L. Naff. 1990. Regression modeling of ground-water flow. U.S. Geological Survey Techniques of Water-Resources Investigations, Book 3, Chapter B4.

D'Agnese, F.A., C.C. Faunt, M.C. Hill, and A.K. Turner. In press. Death Valley regional ground water flow model calibration using optimal parameter estimation methods and geoscientific information systems. Advances in Water Resources.

D'Agnese, F.A., C.C. Faunt, A.K. Turner, and M.C. Hill. 1998. Hydrogeologic evaluation and numerical simulation of the Death Valley Regional ground water flow system, Nevada and California. U.S. Geological Survey Water-Resources Investigation Report 96-4300. 124 p.

Draper, N.R., and H. Smith. 1981. *Applied Regression Analysis*. 2nd ed. New York: John Wiley and Sons.

Eppstein, M.J., and D.E. Dougherty. 1996. Simultaneous estimation of transmissivity values and zonation. *Water Resources Research* 32, no. 11: 3321-3336.

Gelhar, L.W. 1993. *Stochastic Subsurface Hydrology*. Englewood Cliffs, New Jersey: Prentice-Hall.

Gomez-Hernandez, J.J., and S.M. Gorelick. 1989. Effective groundwater model parameter values: Influence of spatial variability of hydraulic conductivity, leakance, and recharge. *Water Resources Research* 25, no. 3: 405-419.

Gupta, V.K., and S. Sorooshian. 1985. The relationship between data and the precision of parameter estimates of hydrologic models. *Journal of Hydrology* 81: 57-77.

Helsel, D.R., and R.M. Hirsch. 1992. *Statistical Methods in Water Resources*. New York: Elsevier.

Hill, M.C. 1992. A computer program (MODFLOWP) for estimating parameters of a transient, three-dimensional, ground water flow model using nonlinear regression. U.S. Geological Survey Open-File Report 91-484.

Hill, M.C. 1994. Five computer programs for testing weighted residuals and calculating linear confidence and predictions intervals on results from the ground water parameter-estimation computer program MODFLOWP. U.S. Geological Survey Open-File Report 93-481.

Hill, M.C. 1998. Methods and guidelines for effective model calibration, with application to UCODE, a computer code for universal inverse modeling. U.S Geological Survey Water-Resources Investigations Report 98-4005.

Hocksema, R.J., and P.K. Kitanidis. 1984. An application of the geostatistical approach to the inverse problem in two-dimensional groundwater modeling. *Water Resources Research* 20, no. 7: 1003-1020.

Huber, P.J. 1981. *Robust Statistics*. New York: John Wiley and Sons.

Hyndman, D.W., and S.M. Gorelick. 1996. Estimating lithologic and transport properties in three dimensions using seismic and tracer data: The Kesterton aquifer. *Water Resources Research* 32, no. 9: 2659-2670.

Jacobson, E.A. 1985. A Statistical Parameter Estimation Method Using Singular Value Decomposition with Application to Avra Valley Aquifer in Southern Arizona. Ph.D. diss., University of Arizona, Department of Hydrology and Water Resources.

Kitanidis, P.K. 1995. Quasi-linear geostatistical theory for inversing. *Water Resources Research* 31, no. 10: 2411-2419.

Mantoglou, A., and J.L. Wilson. 1982. The turning bands method for simulation of random fields using line generation by a spectral method. *Water Resources Research* 18, no. 5: 1379-1394.

Marsily, G. de, G. Lavedon, M. Boucher, and G. Fasinino. 1984. Interpretation of inference tests in a well field using geostatistical techniques to fit the permeability distribution in a reservoir model. In *Geostatistics for natural resources characterization*, vol. 122, ed. G. Verly, M. David, A.G. Journel, and A. Marechal, 831-849. New York: NATO ASI Series C.

McLaughlin, D., and L.R. Townle. 1996. A reassessment of the groundwater inverse problem. *Water Resources Research* 32, no. 5: 1131-1161.

Neele, F., J. VanDecar, and R. Snieder. 1993. The use of P-wave amplitude data in a joint inversion with travel times for upper mantle velocity structure. *Journal of Geophysical Research* 98, no. B7: 12,033-12,054.

Parker, R.L. 1994. *Geophysical Inverse Theory*. Princeton, New Jersey: Princeton University Press.

Poeter, E.R., and M.C. Hill. 1996. Unrealistic parameter estimates in inverse modeling: A problem or a benefit for model calibrations? In Proceedings of the ModelCARE Conference, Golden Colorado, ed. K. Kovar and P. van der Heide. IAHS Publ. no. 237: 227-285.

Poeter, E.P., and M.C. Hill. 1997. Inverse modeling: A necessary next step in groundwater modeling. *Ground Water* 35, no. 2: 250-260.

Poeter, E.R., and S.A. McKenna. 1995. Reducing uncertainty associated with ground water flow and transport predictions. *Ground Water* 33, no. 6: 899-904.

RamaRao, B.S., M.A. LaVenue, G. de Marsily, and M.G. Marietta. 1995. Pilot point methodology for automated calibration of an ensemble of conditionally simulated transmissivity fields. 1. Theory and computational experiments. *Water Resources Research* 31, no. 3: 475-493.

Reid, L.B. 1996. A functional inverse approach for three-dimensional characterization of subsurface contamination. Ph.D. diss., Department of Civil Engineering, Massachusetts Institute of Technology.

Risso, D. 1993. Written communication. University of Vermont, Burlington, Vermont.

Roa, C.R. 1973. *Linear Statistical Inference and Its Applications*. 2nd ed. New York: John Wiley.

Seber, G.A.F., and C.J. Wild. 1989. *Nonlinear Regression*. New York: Wiley.

Sun, N-Z. 1994. *Inverse Problems in Groundwater Flow and Transport*. Boston: Kluwer Academic Publishers.

Sun, N-Z., and W.W.-G. Yeh. 1985. Identification of parameter structure in groundwater inverse problem. *Water Resources Research* 21, no. 6: 869-883.

Sun, N-Z, and W. W.-G. Yeh. 1990. Coupled inverse problems in groundwater modeling. *Water Resources Research* 26, no. 10: 2507-2540.

Tarantola, A. 1987. *Inverse Problem Theory*. New York: Elsevier.

Theil, H. 1963. On the use of incomplete prior information in regression analysis. *American Statistical Association Journal* 58, no. 302: 401-414.

Tikhonov, A.N., and V.Y. Arsenin. 1977. *Solutions of Ill-Posed Problems*. New York: Winston and Sons.

Troutman, B.M. 1983. Runoff prediction errors and bias in parameter estimation induced by spatial variability of precipitation. *Water Resources Research* 19, no. 3: 791-810.

White, H. 1981. Consequences and detection of misspecified nonlinear regression models. *Journal of the American Statistical Association* 76: 419-433.

Wilson, J. 1989. Written communication. New Mexico Institute of Technology, Socorro, New Mexico.

Yeh, T.-C. J., A.L. Gutjahr, and M. Jin. 1995. An iterative cokriging-like technique for ground water flow modeling. *Ground Water* 33, no. 1: 33-41.

FACULTAD DE INGENIERIA U.N.A.M.
DIVISION DE EDUCACION CONTINUA

CURSOS ABIERTOS

XII CURSO INTERNACIONAL DE CONTAMINACIÓN DE ACUÍFEROS

MODULO III: MODELOS MATEMÁTICOS EN GEOHIDROLOGIA Y CONTAMINACIÓN DE ACUIFEROS

TEMA

A DIGITAL MODEL OF THE VILLA DE REYES AQUIFER, MEXICO

EXPOSITOR: DR. ADOLFO CHAVEZ RODRIGUEZ

PALACIO DE MINERIA
OCTUBRE DEL 2000

A DIGITAL MODEL OF THE VILLA DE REYES AQUIFER, MEXICO

A. Chávez*, N. Mobayed, E. García,
J. Ríos, M. Hernández, y S. Flores
Comisión Federal de Electricidad, México
* also at Universidad Autónoma de Chihuahua

ABSTRACT. A two-layer finite-difference groundwater flow model of the Villa de Reyes aquifer, in central México, was constructed by using the computer code MODFLOW. The aquifer system is composed by an upper layer of alluvial sediments and a lower layer of fractured volcanic rock. The digital model is intended to simulate hydraulic response toward diverse hydrologic stresses. Of special interest is the effect of a remarkable upward recharge emerging in a localized zone of the aquifer from a deep regional fault system. The model was calibrated by trial and error over the two-year period of 1986-1987, and tested over the year 1988. A sensitivity analysis was performed, revealing in particular a very high response of lower-layer computed heads to variations in deep recharge.

INTRODUCTION

Prior to 1986, the Villa de Reyes aquifer, in central México, supplied water for only agricultural and domestic uses through wells tapping the alluvial fill of the basin. This groundwater development exceeded the rate of aquifer recharge and caused an average water-level decline of about 1.5 m/year. In 1986, deep wells owned by the national power generation company (CFE) tapping the underlying fractured volcanic rock began to operate, adding an extra stress on the system that caused a piezometric-level decline of 3.0 m/year in the lower volcanics and increased to 2.0 m/year the water-level decline in the upper alluvium.

This aquifer condition prompted the construction of a groundwater flow model that could assist in planning future exploitation. This model represents the first stage in the development of an aquifer management model intended to be used more directly to design optimal pumping schemes.

HYDROGEOLOGY OF THE VILLA DE REYES BASIN

The Villa de Reyes basin, in the semiarid zone of central México, extends between the lines of latitude 21°40′ and 21°60′ N and the lines of longitude 100°60′ and 101°00′ W, and the modeling area occupies about 115 km^2 in the valley. The mean annual precipitation is 430 mm, with a potential evaporation slightly over 2 000 mm.

The valley is of tectonic origen and limited by the Sierra San Miguelito to the northwest and the Sierra Santa María to the southeast. The structural depression has been filled by volcanic material of over 700 m in thickness, composed mainly of welded tuff and rhyolite which have developed secondary permeability by fracturing. Alluvial fill of an average thickness of 150 m overlies the fractured volcanics. This alluvial material is composed of pyroclastics intermixed with gravel, sand and silt and its permeability is moderate.

The regional groundwater flow occurs in the preferential direction SW-NE parallel to the mountain ranges. In the alluvium, groundwater is in phreatic conditions. Well cuttings revealed no impervious or semipervious layer separating the alluvium from the fractured volcanics throughout the study area. However, the vertical hydraulic conductivity between the alluvium and the fractured volcanics is low enough in the central and southwest portion of the area to maintain a distinct hydraulic response between the layers. An upconing in the piezometric surface of the lower volcanics, due to deep upward recharge, is not observed in the upper alluvium. In the northest portion of the area the discrepancy between the upper and lower hydraulic heads is much less.

Minor local recharge is provided from a small surface reservoir located just outside the north corner of the modeling area. At depth, in the zone of CFE wells 7, 9 and 21, occurs an important upward recharge identified by a remarkable upconing of the piezometric surface and by structural studies that determined the existence of a deep regional fault system conveying water from outside the zone.

Areal recharge was regarded to be negligible because of the relatively low precipitation, the high potential evapotranspiration, and the depth of the water table (over 40 m). Recharge from irrigation return flow was also assumed not significant because crop fields occupy a relatively small portion of the area and farmers are not believed to apply enough water to offset moisture deficits.

Pumping in the modeling area was in 1986, 1987 and 1988 performed by 27 irrigation and domestic wells that tap the alluvium and discharged an average of 20 100 m^3/day, and by 17 deep CFE wells tapping the fractured volcanics that entered gradually into operation starting in 1986, and jointly discharged 11 500, 29 700, and 29 100 m^3/day in 1986, 1987 and 1988, respectively.

MODEL CONSTRUCTION

A two-layer finite-difference groundwater flow model for the Villa de Reyes aquifer was constructed by using the computer code MODFLOW developed by McDonald & Harbaugh (1984). The upper layer of the model stands for the alluvial fill and the lower layer for the fractured volcanic rock.

A variable grid pattern was used for the model. Along the SW-NE direction, cell width varied from 500 to 1 300 m, whereas along the NW-SE direction it varied from 500 to 1 000 m. Smaller cells were used for the zones where the most accurate results are required, i.e., where most pumping occurs (CFE wells) and where the hydraulic gradient is larger (in the center and southwest portion of the modeling region).

The following parameters were entered in the model at each cell in the upper layer: the elevation of the initial water level (January, 1986), the horizontal hydraulic conductivity, the specific yield, the altitude of the bottom for the layer (alluvium-volcanic rock contact). As for the lower layer, the parameters entered were: the elevation of the initial piezometric level, the transmissivity, the storage coefficient, the altitude of the top for the layer (alluvium-volcanic rock contact as before). Furthermore, the vertical conductance between the layers, and for the appropriate cell: pumpage, deep upward recharge, and inflow or outflow along the model boundaries.

The horizontal hydraulic conductivity in the upper layer was calculated on the basis of saturated thickness and transmissivities obtained from seven pumping tests carried out in the zone where hydraulic connection between the layers is almost null. The calculated hydraulic conductivities ranged from 0.55 to 3.55 m/day, and their geometric mean (1.63 m/day) was entered to all the cells in the layer. The specific yield was initially given a value of 0.10 for the whole layer by considering the composition of the alluvial fill. The elevation of the bottom of the layer was approximated at each cell from geologic cross sections.

For the lower layer, transmissivity was obtained from pumping tests at two deep CFE wells that tap only the volcanic rock and using other deep wells for observation. A transmissivity of 800 m^2/day was obtained for the zone of well 7 where hydraulic connection with the alluvium is negligible. For the test performed at well 2 a correction was introduced in order to account for the contribution from the alluvium, resulting in a estimate of 200 m^2/day. Transmissivities were assigned to the rest of the lower-layer cells on the basis of those two values and attending primarily to the intensity of the horizontal hydraulic gradients in the layer. A storage coefficient of 0.0005 was obtained from the pumping test at well 7 and this value was assigned initially to the whole layer.

The vertical conductance between the layers is a function of the thickness and the vertical hydraulic conductivity of the individual layers. Because the lack of data about most of these quantities arbitrary initial estimates were entered in the model guided only by the difference in hydraulic head between neighboring cells in the vertical direction, i.e., the lowest values were selected for the zone to the east of the power plant where the differences between the water levels in the alluvium and the piezometric levels in the volcanic rock are the largest, and the highest values were assigned over the northeast portion of the modeling region where heads are about the same.

Pumpage was entered into the model by obtaining the average discharge of all wells in a cell for each of the years considered. Irrigation and domestic wells tap the alluvium and their discharge was roughly estimated by indirect methods, whereas CFE wells have accurate pumping records. Deep upward recharge was entered at the six lower-layer cells (4-6, 5-5, 5-6, 5-7, 6-5, 6-6) where it is known to occur. Lateral inflow was introduced mainly in the south corner cells and lateral outflow mainly in the east corner cells. Most of the cells along the northwest (Sierra de San Miguelito) and southeast (Sierra de Santa María) boundaries were assumed to be impermeable with no recharge. Cells at northern corner receive some lateral inflow originated at a small surface reservoir.

Model Calibration and Testing

The Villa de Reyes aquifer has been long subject to overdraft and the water-level records do not extend back long enough to identify a steady-state condition. Prior to 1986 only irrigation and domestic wells tapping the alluvium

were pumping. In that year 10 CFE wells tapping the lower volcanics entered into operation, and seven more did in 1987.

The model was calibrated by trial-and-error over the transient period of 1986 and 1987, and the agreement of observed and computed water-level declines for both model layers is shown in Figs 1 and 2. The discharges of the CFE wells were not adjusted because their measuring is known to be very reliable.

The parameters estimated through the calibration process are as follows: For the upper layer, the initial horizontal hydraulic conductivity (1.63 m/day) and the altitude of the bottom of the layer mantained their original estimates, whereas the specific yield was adjusted to 0.08. For the lower layer, the estimated transmissivity exhibits a minimum of 200 m^2/day in the central part of the area and a maximum of 2 000 m^2/day near the northeast boundary. The storage coefficient maintained its original value of 0.0005. The vertical conductance resulted to be negligible, about 2 x 10^{-7} day^{-1}, in and around cells 2-8, 3-8, 4-8, and 5-8, and a maximum of about 2 x 10^{-3} day^{-1} in the east corner of the area.

The components of the ground-water balance as determined by the calibration process are as follows: lateral inflow, lateral outflow, and deep upward recharge were 3 800, 20 400, and 26 700 m^3/day in 1986, and 3 800, 19 200, and 26 700 in 1987, respectively. Pumping rates were 31 600 and 49 800 m^3/day in 1986 and 1987, respectively.

To test model reliability the one-year period starting in January 1988 was used, and the results can be appreciated in Figs 3 and 4. In this verification stage, minor adjustments on some parameters were made whenever they also produced a better agreement between observed and computed head declines for the period used in calibration.

Sensitivity Analysis

A sensitivity analysis was performed to gain insight into the reliability of the parameter estimates. This analysis was done considering the same year used for verification.

One parameter of particular interest is the deep upward recharge because its magnitude was totally unknown initially, and after calibration it turn out to be a very contributing component of the water balance. Deep upward recharge was varied +/- 20 % about its estimate, observing that model response to these variations was very high in

the lower layer (over +/- 5 m in most of it) and virtually null in the zone of the upper layer above the cells where recharge occurs. This effect is explained by the negligible hydraulic connection between layers in that zone.

Then, the storage coefficient of the lower layer was varied one order of magnitude about its estimate, obtaining almost no change in response at 0.00005 and a relatively moderate variation at 0.005 (about 1 m for the layer). Here we notice that the latter value is about the maximum the elastic storage coefficient can hold. Lateral groundwater inflow into the lower layer was also tested for sensitivity, finding that its effect is not significant except for the cells located at or near the inflow boundary. Furthermore, we recall at this point that the discharge of the deep CFE wells is accurately measured and no test on it is required.

These facts and results reveal that possible compensatory effects from the above parameters on deep upward recharge are minimal, and considering the very high sensitivity of computed heads to this recharge, we conclude that its estimate is reliable.

Finally, the specific yield of the alluvium was varied about its estimate of 0.08, testing for 0.06 and 0.10, and observing a rather high sensitivity to the change in both directions, which reveals that the existing large water-level declines properly activate this parameter.

REFERENCE

McDonald, M.G. & Harbaugh, A.W. (1984) A modular three-dimensional finite-difference ground-water flow model. U.S. Geological Survey, Reston, Virginia, 528 pp.

VILLA DE REYES AQUIFER

MODEL CALIBRATION

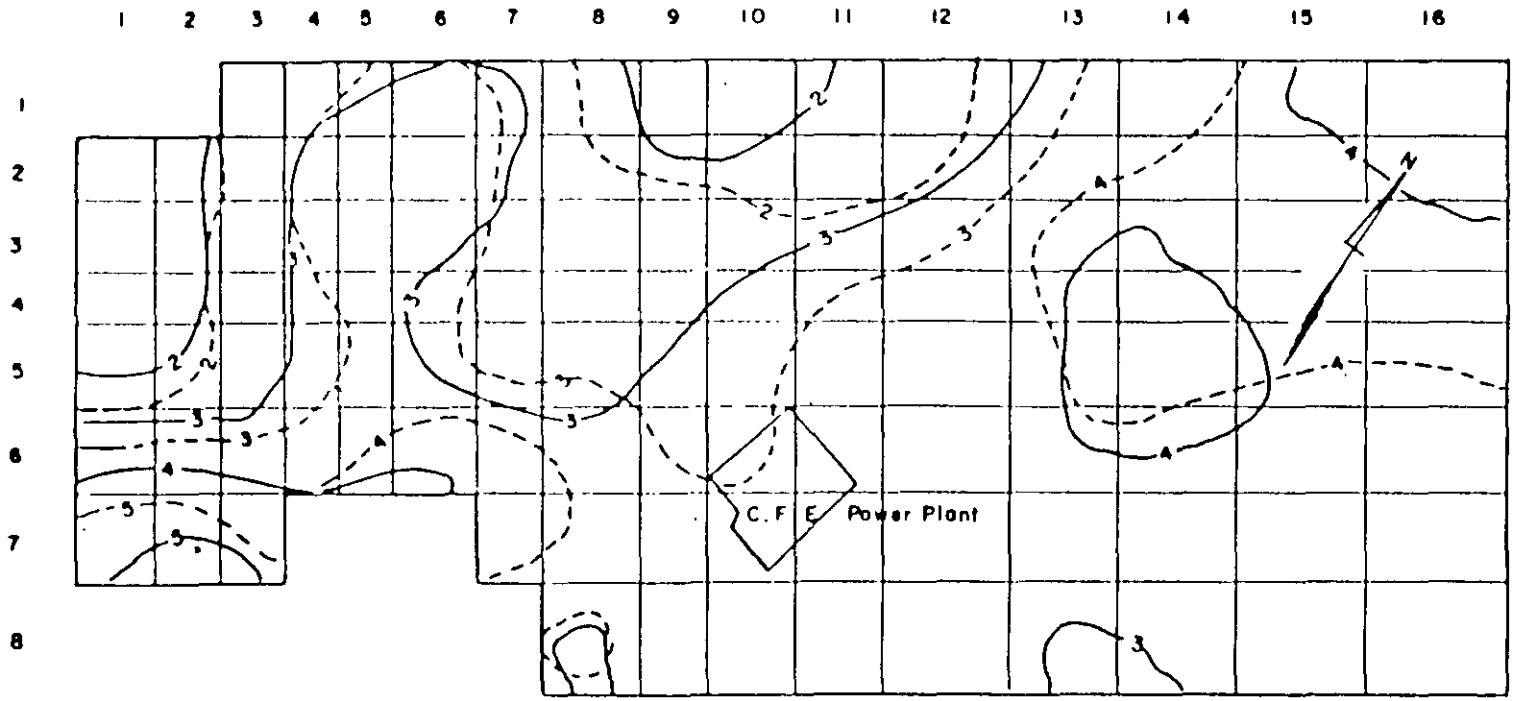

UPPER LAYER. DECLINE IN WATER LEVELS FOR 1986-88 (Meters)

——— OBSERVED
– – – – COMPUTED

0 5 10 15 20 25
KILOMETERS

Figure 1

VILLA DE REYES AQUIFER

MODEL CA[illegible]RATION

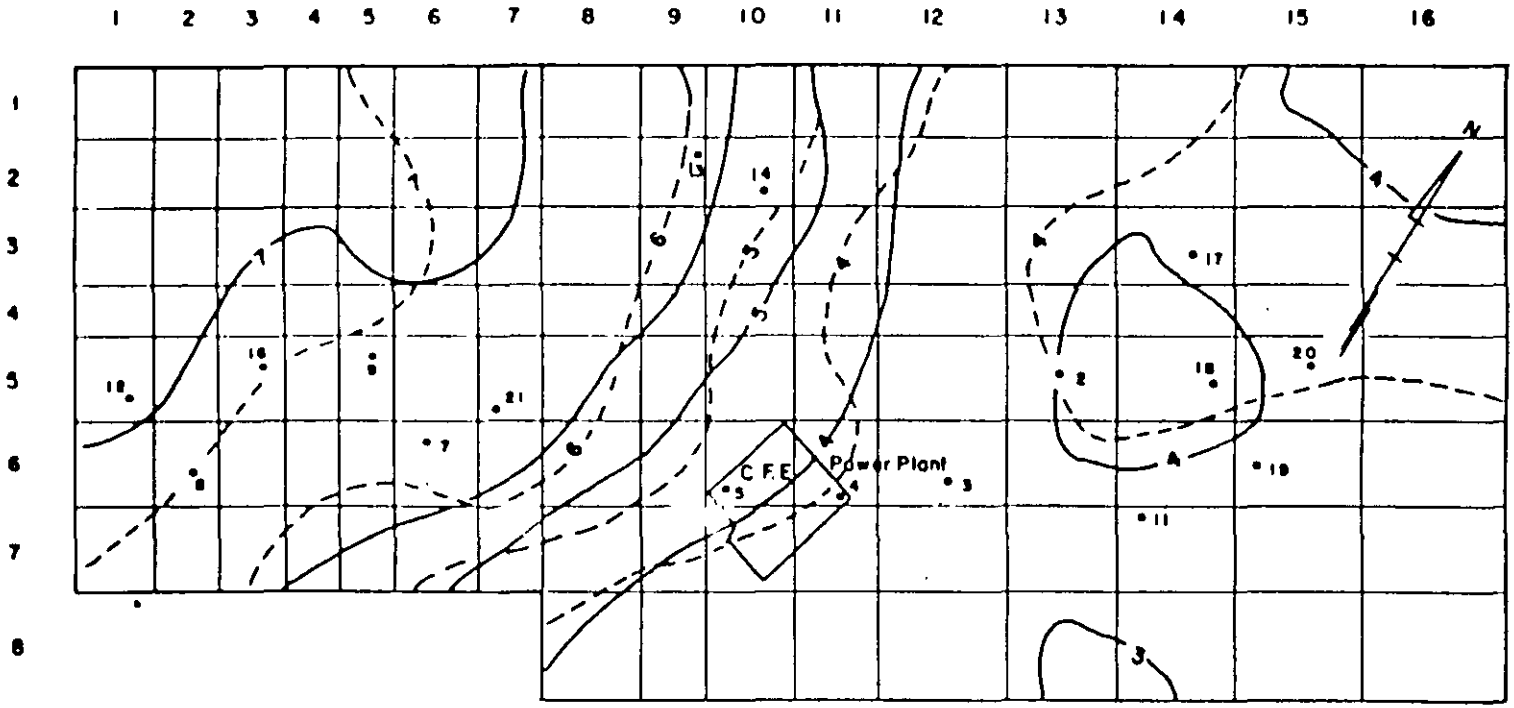

LOWER LAYER. DECLINE IN PIEZOMETRIC LEVELS FOR 1986-88 (Meters)

OBSERVED
COMPUTED
CFE DEEP WELLS

0 5 10 15 20 25
KILOMETERS

Figure 2

VILLA DE REYES AQUIFER

MODEL TESTING

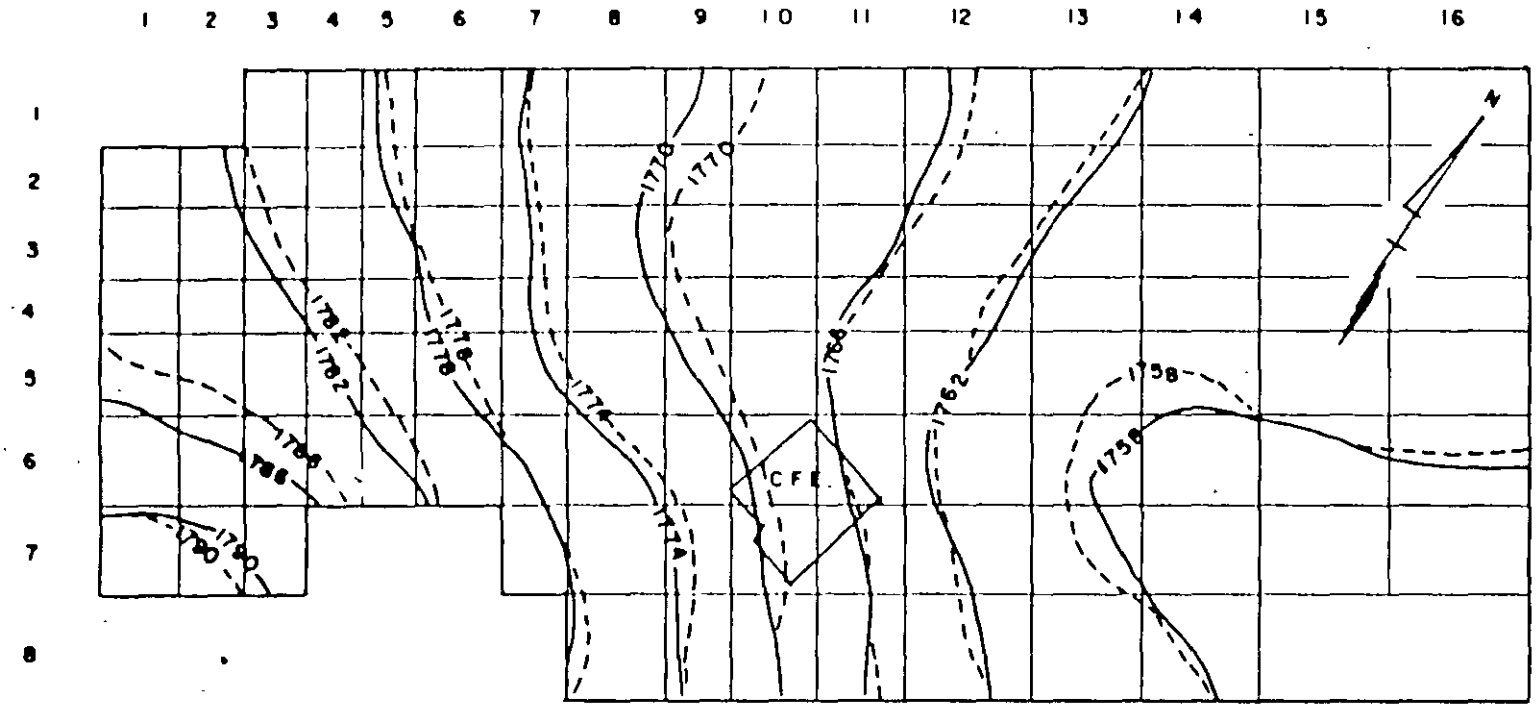

UPPER LAYER. WATER LEVEL CONTOURS IN JANUARY 1989 (Meters, msl)

——— OBSERVED

– – – – – COMPUTED

0 5 10 15 20 25
KILOMETERS

Figure 3

VILLA DE REYES AQUIFER

MODEL TESTING

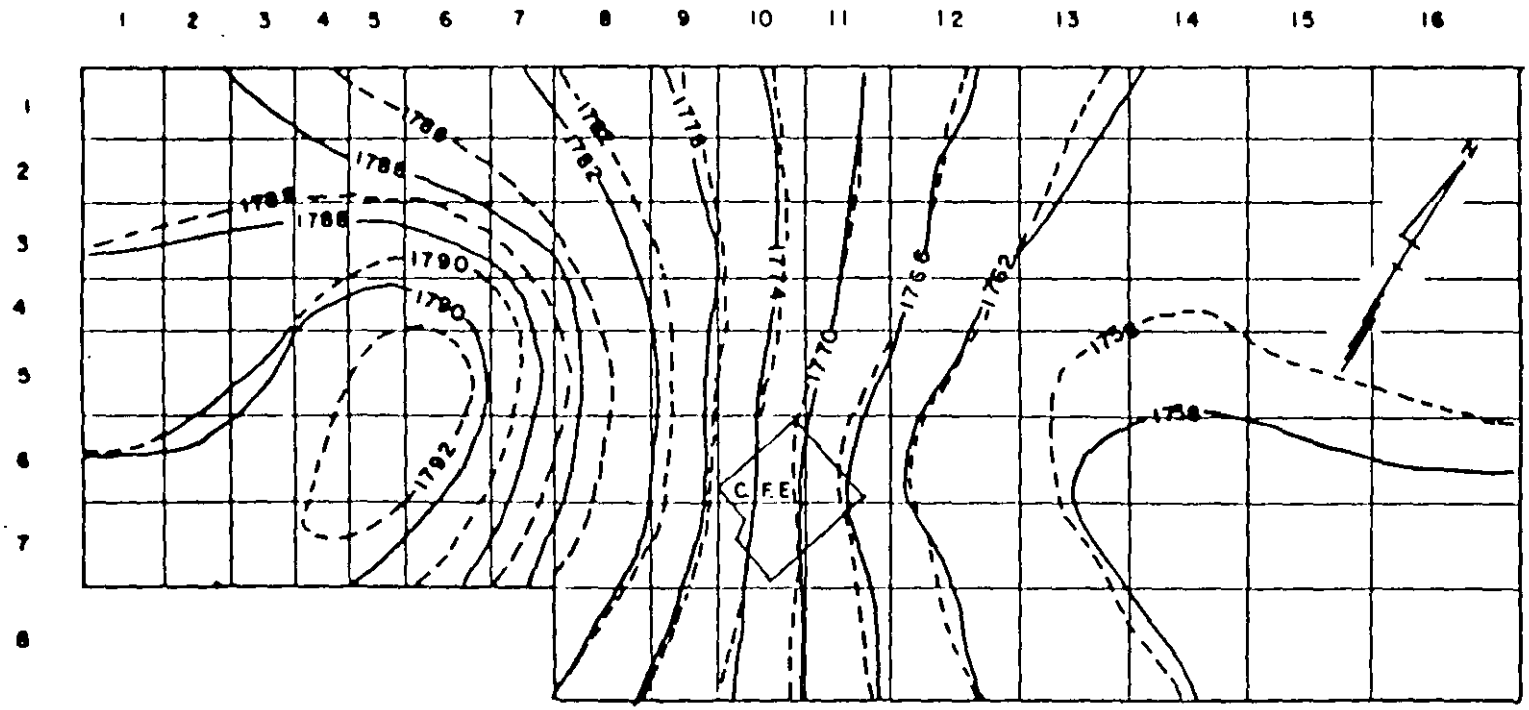

LOWER LAYER. PIEZOMETRIC CONTOURS IN JANUARY 1989 (Meters, msl)

0 .5 1.0 1.5 2.0 2.5
KILOMETERS

——— OBSERVED
– – – – COMPUTED

Figure 4

FACULTAD DE INGENIERIA U.N.A.M.
DIVISION DE EDUCACION CONTINUA

CURSOS ABIERTOS

XII CURSO INTERNACIONAL DE CONTAMINACIÓN DE ACUÍFEROS

MODULO III: MODELOS MATEMÁTICOS EN GEOHIDROLOGIA Y CONTAMINACIÓN DE ACUIFEROS

TEMA

MODEL CALIBRATION WITH MULTIPLE TARGETS: A CASE STUDY

EXPOSITOR: DR. ADOLFO CHAVEZ RODRIGUEZ

PALACIO DE MINERIA
OCTUBRE DEL 2000

Model Calibration with Multiple Targets: A Case Study

by Kangjoo Kim[a], Mary P. Anderson[b], and Carl J. Bowser[b]

Abstract

Multiple calibration targets were used to calibrate a two-dimensional finite-difference model of a ground water lake system. The calibration targets included (1) steady-state head data, (2) transient head data, (3) head gradients, and (4) flowpath information. Because calibration was sensitive to the ratio of horizontal to vertical hydraulic conductivity, four models, each with different assumptions about anisotropy, were developed. All four models produced acceptable calibration to either heads or flowpath, but only one model was well calibrated to all targets. In that model, stratification of the upper aquifer was represented by introducing several dipping layers of low permeability. This allowed the use of a small ratio of horizontal to vertical anisotropy for individual layers but produced a large effective anisotropy for the upper aquifer as a whole.

Introduction

Achieving a unique calibration is an important goal in most modeling studies, but methods of identifying the best calibration are still under development (e.g., Poeter and Hill 1997). It is generally recognized, however, that both heads and fluxes should be used as calibration targets (e.g., Anderson and Woessner 1992). Additionally, some investigators have used vertical head gradients (Thomas et al. 1989), velocities (Duffield et al. 1990), and information on solute distribution (Krabbenhoft et al. 1990, Medina et al. 1990, Kauffmann et al. 1990) to help narrow the search for a unique set of calibration parameters. In this study, four different types of calibration targets were used to calibrate a flow model: steady-state heads, transient heads, head gradients, and flowpath information. The calibration was sensitive to the ratio of horizontal to vertical hydraulic conductivity of the upper aquifer. Calibration with multiple targets led us to identify a way of representing this anisotropy that allowed the model to match all four of the calibration targets. In the final calibrated model, stratification in the upper aquifer was simulated by inserting layers of low conductivity to represent the dipping bedding planes. This set of layers is at an angle to the horizontal axis of the grid so that the direction of anisotropy is preserved in the model.

The study area is the isthmus between Crystal Lake and Big Muskellunge Lake, which are two of seven lakes in NSF's (National Science Foundation) Long Term Ecological Research (LTER) Program in northern Wisconsin (Figure 1). This LTER site has been the subject of numerous ecological and hydrologic studies since the 1920s (e.g., Juday et al. 1935; Frey 1963). Precipitation averages 80 cm per year and annual average ground water recharge is 26 cm. Crystal Lake is a small, topographically isolated lake with a surface area of 3.6×10^5 m^2 and no surface inlets or outlets. About 90% of the inflow is from precipitation (Kenoyer and Anderson 1989; Hurley et al. 1985). Its average and maximum depths are 10 and 20 m, respectively. Big Muskellunge Lake is situated about 130 m north and downgradient of Crystal Lake. It has no surface inlets, but occasionally loses water through a small outlet at the northeastern end. The water levels of these lakes fluctuate in a similar mode maintaining a head difference of about 1.2 m (Anderson and Cheng 1993). Four well nests with a total of 28 piezometers were installed in a vertical plane oriented in the direction of ground water flow (Kenoyer 1986); an additional multilevel well was installed in 1993 (Figure 2a).

Precambrian bedrock is covered by 40 to 60 m of Pleistocene glacial outwash (Okwueze 1983), which makes up the surficial aquifer. There are two silt layers with thicknesses up to 1 m (Kenoyer and Bowser 1992a). The upper silt layer dips about 7 degrees toward Crystal Lake. Persistent steep vertical head gradients across this layer suggest that it is continuous and acts as a confining unit. The lower silt layer is likely to be discontinuous since only one silt layer was encountered when constructing the multilevel well and no notable head changes are observed across the layer (Figure 2b). Hydraulic conductivity from slug tests ranges from 0.17 to 17.3 m/day for sandy sediments and from 8.6×10^{-5} to 3.5×10^{-3} m/day for silt layers (Kenoyer 1986).

Ground water in the isthmus is recharged in part by seepage from Crystal Lake and in part by precipitation on the upland between the two lakes. Ground water flows through the isthmus from Crystal Lake toward Big Muskellunge Lake. A ground water mound forms between the lakes during spring snowmelt in response to ground water recharge (Anderson and Cheng 1993). The mound gradually dissipates during the summer when ground water recharge is low. These transient effects cause enhanced dispersion in this system (Kim et al. 1999).

[a]Now with the Department of Environmental Engineering, Kunsan National University, Korea; revisions are solely the responsibility of Anderson and Bowser.

[b]Department of Geology and Geophysics, University of Wisconsin-Madison, 1215 W. Dayton St., Madison, WI 53706.

Received March 1997, accepted September 1998.

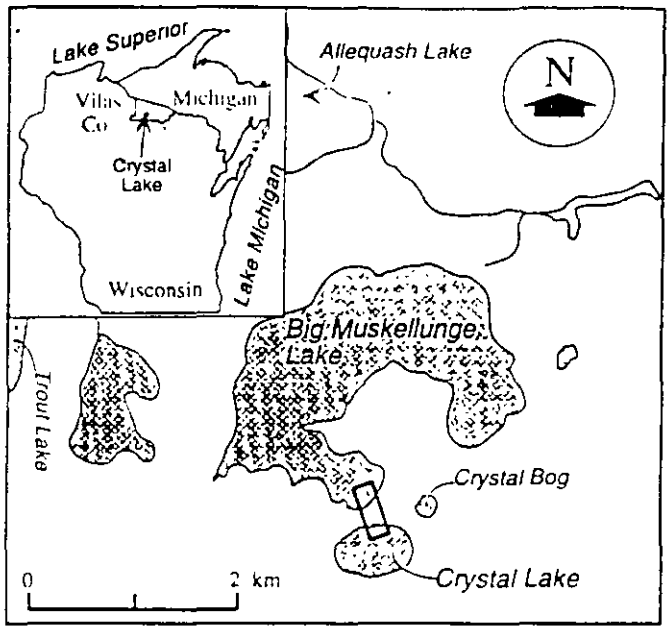

Figure 1. Location of the study area in northern Wisconsin. The study area is the isthmus between Crystal Lake and Big Muskellunge Lake shown in the rectangular block.

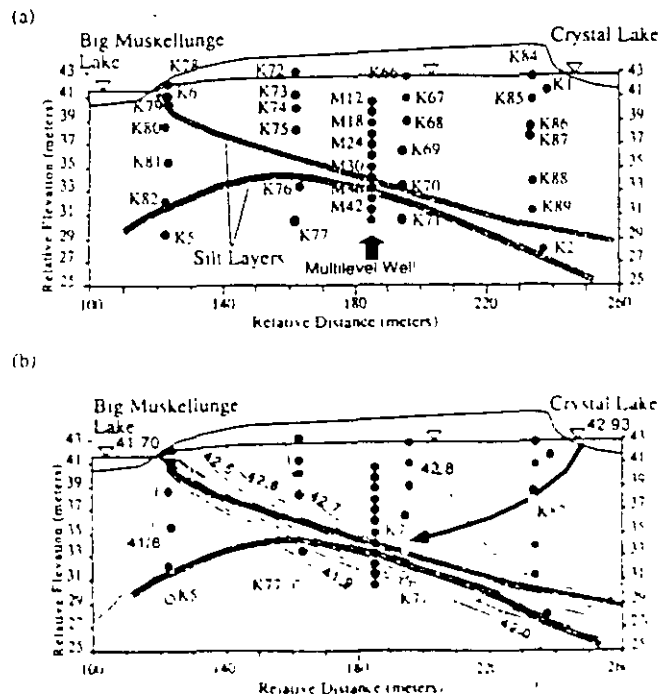

Figure 2. (a) Location of wells and silt layers in the isthmus. Piezometers labeled 'K' were installed during 1981–1982. Those labeled 'M' were installed in 1993 for this study. (b) Equipotential lines based on head measurements taken on August 25, 1993, by Schindler (1994). The upper portion of the flowpath determined by Kim (1996) based on oxygen isotope measurements is also shown. The labeled piezometers were used in travel time calculations reported in Table 4.

Kenoyer and Bowser (1992a) delineated a flowpath in the upper aquifer using a flow net analysis and postulated geochemical reactions along this path (Kenoyer and Bowser 1992b). Krabbenhoft et al. (1992) and Bullen et al. (1996) identified a

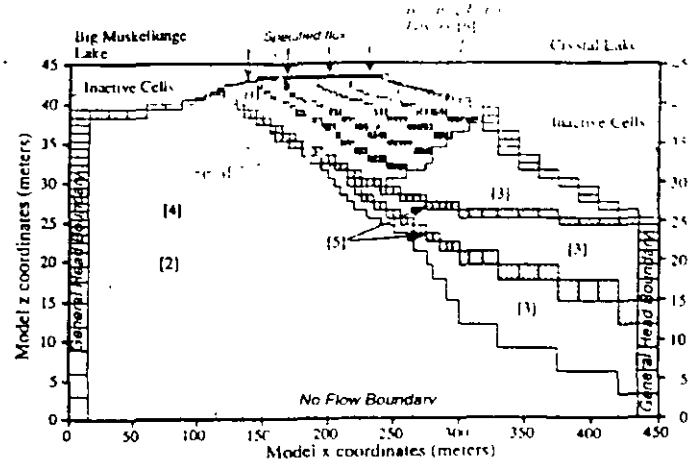

Figure 3. Model grid. The numbers in brackets designate conductivity zones. Inner tic marks represent grid spacings and the open circles represent well points.

flowpath through the upper aquifer using oxygen isotope measurements. Kim (1996) used an independent set of oxygen isotope measurements collected at a later period, including data from the multilevel well installed subsequent to the work by Bullen et al. (1996), to delineate a flowpath through the upper aquifer. The upper portion of Kim's flowpath, which coincides with the path identified by Krabbenhoft et al. (1992) and Bullen et al. (1996), is shown in Figure 2b. Subsequent analyses have raised some uncertainty about the lower portion of the path, which is the subject of ongoing work.

Model Design

The problem domain is a profile 450 m long and 45 m deep that encompasses the area from near the center of Crystal Lake to 100 m offshore of Big Muskellunge Lake (Figure 3). The three-dimensional finite-difference code MODFLOW (McDonald and Harbaugh 1988) with the BCF2 block centered flow package (McDonald et al. 1991) was used to simulate the system. In profile view, the model has 58 columns and 40 rows (layers). The nodal spacing varies from 5 to 15 m in the horizontal direction and 0.2 to 3 m in the vertical direction. Smaller horizontal nodal spacing was used in the area of interest, namely beneath the isthmus. The upper 10 layers are 0.2 to 0.5 m thick in order to simulate the gently sloping lake bottoms.

Both lakes were simulated as specified head boundaries using the general head boundary (GHB) package so that temporal changes in lake levels could be input easily. The lake bottom sediments were simulated by setting conductances of the GHB cells, where conductance is equal to the hydraulic conductivity of the sediment times the area of the cell in contact with the lake divided by the thickness of the sediment.

Side boundaries were also simulated using the GHB package to allow easy input of the temporal fluctuation of these boundary heads. In order to reproduce the observed flow pattern beneath Crystal Lake, head values 5 cm less than lake level were assigned to all the general head boundary cells below the lake and a low conductivity zone (zone 3 in Figure 3) was introduced in the upper part of the aquifer near the right-hand-side boundary. Along the left boundary of the model, heads were assumed to be the same as in

Table 1
Hydraulic Conductivity (K) Values Measured by Kenoyer (1986) from Slug Tests
(Locations of piezometers are shown in Figure 2a.)

Upper Sand	K (m/day)	Lower Sand	K (m/day)	Silt Layers	K (m/day)
K1	12.1	K2[a]	0.17	K83[b]	8.6E-05
K86	8.6	K5	3.5	K76	5.2E-04
K87	13.0	K71	3.0	K70[a]	3.5E-03
K88	17.3	K77	0.26		
K89	13.0	K80	1.3		
K67	6.9	K81	2.6		
K68	4.3	K82[a]	0.09		
K69	7.8				
K73	9.5				
K74	7.8				
K75	7.8				
Mean	9.8	Mean	2.1	Mean	3.0E-04

[a]Wells with screens located in both sand and silt were excluded from the mean.
[b]Well K83 is not shown in Figure 2a because it was lost sometime after its construction. It was originally located between K5 and K82.

Big Muskellunge Lake. A no-flow boundary was used along the bottom of the system to represent relatively crystalline bedrock. The upper boundary was simulated as a specified flux boundary using the recharge package.

Parameters and Lake Levels

Six hydraulic conductivity zones were defined as shown in Figure 3. Zones 1 through 3 represent sand layers while zones 4 and 5 represent silt layers. Zone 6 represents the bedding plane layers in the upper sand aquifer that were introduced in one set of simulations. The hydraulic conductivity values in these zones were estimated from slug test results (Table 1). Kenoyer (1988) estimated the anisotropy ratio (K_x/K_z) to be 3.5 to 7.8 from small scale tracer tests that covered only about one meter. Since anisotropy ratio is known to be scale-dependent, a range of anisotropy values was tested in our model.

Lakebed sediments for Crystal Lake were zero to 0.3 m thick depending on lake depth and those for Big Muskellunge Lake were uniformly 0.2 m thick. These values are consistent with field observations. Hydraulic conductivity of lakebed sediments for both lakes was assumed to be 0.04 m/day, or the same as the silt in zone 4.

Effective porosity of the sandy sediment, estimated from the average of laboratory measurements of three samples, was 0.35 (Kim 1996). The effective porosity of the silt layers was assumed to be 0.3. Both steady-state and transient models were developed. The transient model required values of storativity and average monthly recharge rates. Values for storage coefficient and specific yield were tested during calibration and final values of 10^{-4} for storage coefficient and 0.27 for specific yield were selected for all units.

Recharge rates were calculated using Thornthwaite's method (Thornthwaite and Mather 1955, de Marsily 1986) and also considering the melting rate of snow as suggested by Barten (1988). The calculated annual recharge rate ranges from 17.1 to 41.7 cm and averages 26.2 cm/yr. Monthly recharge ranges from zero to 21.2 cm in the period of record (1984 to 1993). Average monthly rates for 1993 are shown in Figure 4.

Lake levels, which were used to specify boundary conditions, were taken from the LTER database (LTER 1995). During the period 1984 to 1993, lake levels ranged from 42.4 to 43.4 m for Crystal Lake and 41.2 to 42.5 m for Big Muskellunge Lake, relative to an arbitrary datum. Data were averaged for each month and missing data points were estimated either from the closest available point or from Buffalo Lake, located 14 km to the south.

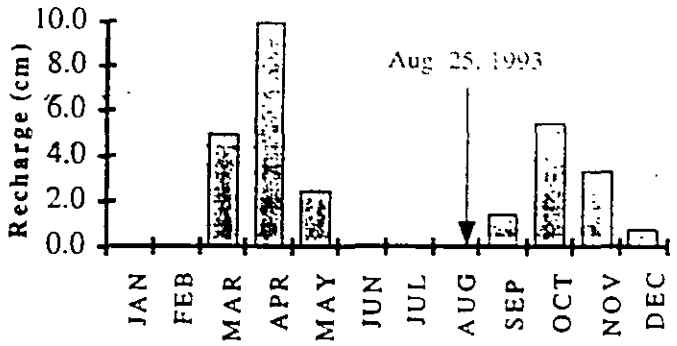

Figure 4. Calculated monthly recharge for 1993. Heads used in the quasi steady-state calibration were measured on August 25, 1993 (Schindler 1994), after a relatively long period of negligible recharge.

Calibration Strategy

Two steady-state simulations and one transient simulation were performed for each trial set of calibration parameters. In the first steady-state simulation, heads were calibrated to measurements made in late summer (August 25, 1993) when recharge is negligible due to evapotranspiration (Figure 4) and the system is in quasi steady state. In these simulations, recharge was equal to zero and lake levels were set at 42.93 m for Crystal Lake and 41.70 m for Big Muskellunge Lake, which were the recorded levels on that date. We performed transient simulations for the period 1984 to 1993 and input average monthly recharge rates. The calibration was checked against observed heads on August 25, 1993, and compared to heads measured in five wells during the period 1984 to 1993 (Figure 5). In the quasi steady-state and transient simulations, observed head differences between selected adjacent well points were also used as calibration targets. The use of spatial differences in heads allows for calibration to gradients as well as point head data. A total of eight well pairs (K1-K73, K1-K89, K89-K2, K70-K71, K71-K5, K75-K76, K75-K80, and K5-K80) was selected (Figure 2a).

Calibration to the observed flowpath shown in Figure 2b was performed in a second steady-state simulation using an average yearly recharge rate (26.2 cm/yr) and average lake levels (42.9 m for Crystal Lake and 41.8 m for Big Muskellunge Lake). While the observed flowpath is the result of long-term transients in the flow system, Reilly and Pollock (1996), among others, demonstrated that fluctuations in recharge do not appreciatively affect the overall flowpaths calculated by models that assume average steady-state conditions. Therefore, we used a model with average steady-state recharge and lake levels to produce a steady-state velocity distribution, which was input to the particle tracking code, PATH3D (Zheng 1989). Backward particle tracking was used to delineate a ground water flowpath from well K5 (Figure 2b) and to estimate travel times from Crystal Lake.

During calibration we discovered that the model was sensitive to the ratio of horizontal to vertical hydraulic conductivity. It is well

Table 2
Parameter Values Used in Models 1 through 4 and Field Estimates by Kenoyer (1986)

		Kenoyer (1986)	Model 1	Model 2	Model 3	Model 4
Hydraulic Conductivity	Upper sand (1)	9.8	2.0	2.0	2.0	8.0
	Lower sand (2)	2.1	2.0	2.0	2.0	2.0
	Lower sand (3)	—	0.7	0.7	0.7	0.7
	Silt (4)	—	0.04	0.04	0.04	0.04
	Silt (5)	0.003	0.004	0.004	0.004	0.004
	Bedding plane layers (6)	—	—	—	—	0.3
Porosity	Sand	0.3	0.35	0.35	0.35	0.35
	Silt	—	0.3	0.3	0.3	0.3
Anisotropy ratio (K_x/K_z)		3.5–7.8	5	10	20	5

Numbers in parentheses ( ) indicate conductivity zones shown in Figure 3

known that a heterogeneous system consisting of a sequence of horizontal isotropic layers can be represented for hydraulic purposes by an equivalent system that is homogeneous but anisotropic (e.g., Freeze and Cherry 1979). When geologic units dip from the horizontal, the coordinate axes should be aligned colinear with the principal directions of the hydraulic conductivity tensor. In most applications, however, the dip of the units is small and the units are represented as horizontal for purposes of modeling (e.g., Phillips 1987). When this is done, the orientation of anisotropy within the dipping units is not preserved. We developed four sets of model parameters to test the effect of anisotropy.

Parameters used for each of the four models are summarized in Table 2. All of the parameter values except for anisotropy ratio are the same for models 1, 2, and 3. The anisotropy ratio ranges from five in models 1 and 4 to 20 in model 3. In model 4, additional layers were inserted parallel to the upper silt layer to represent bedding plane layers in the upper sand aquifer (zone 6 in Figure 3) and thereby capture the appropriate angle of anisotropy. The upper silt layer dips slightly toward Crystal Lake, suggesting that stratification of the upper sandy sediments is parallel to this layer. Thus, we assumed that the bedding planes that cause anisotropy in the sandy aquifer are tilted approximately 7 degrees to the horizontal axis of the grid. Models 1, 2, and 3 do not incorporate the effects of the angle of stratification of the sand unit because the components of the conductivity tensor are assumed to be colinear with the principal coordinate axes, which are horizontal and vertical. The bedding plane layers (zone 6 in model 4, however, effectively simulate the correct orientation of anisotropy of the upper sand unit as a whole. In the low-permeability bedding plane layers, hydraulic conductivity is equal to 0.3 m/day, while in the rest of the unit hydraulic conductivity equals 8 m/day, which is closer to the average of field values (9.8 m/day; Table 1) than the value of 2 m/day used in models 1, 2, and 3 (Table 2). All the hydraulic conductivity zones in model 4 have an anisotropy ratio of five, which is in the range of values estimated from small scale tracer tests (Table 2). The anisotropy ratio of the upper sand unit taken as a whole, however, is greater than five.

Results

The root mean squared (RMS) error in heads and the ratio of observed to simulated head differences between well pairs were calculated. Model 1, with an anisotropy ratio of five, does not calibrate well to heads, with RMS errors of 9.6 cm for the quasi steady-state calibration and 7.8 cm for the transient calibration (Table 3). Because of the poor calibration to heads, model 1 is rejected even though the calibration to the observed flowpath is relatively good (Figure 6b).

Among models 1, 2, and 3, model 3, which has a relatively high anisotropy ratio of 20, is best calibrated to heads (Table 3). The RMS error is only 3.7 cm for the quasi steady-state simulation and all of the head difference ratios are relatively close to one except between K1 and K89 (Figure 6a). The simulated flowpath, however, is different from the observed flowpath (Figure 6b). Model 2 similarly

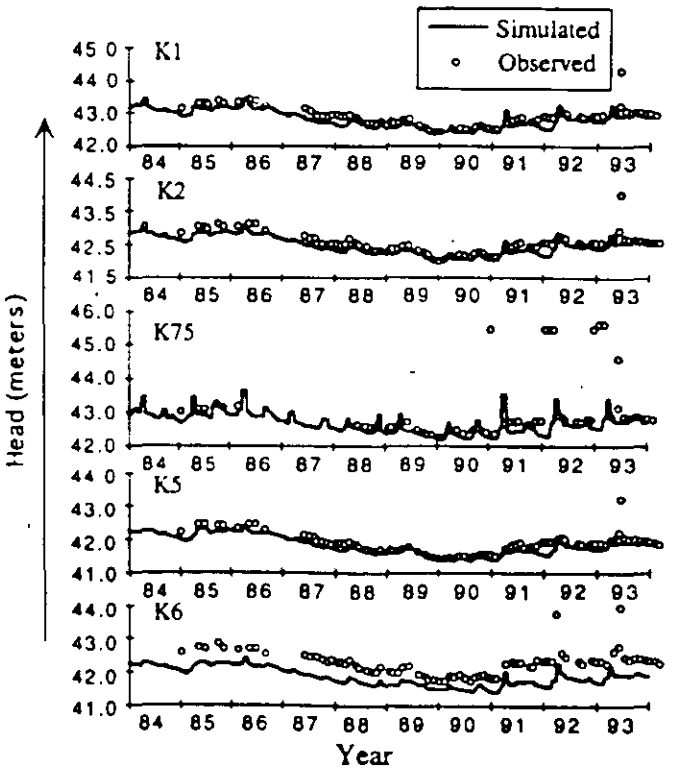

Figure 5. Comparisons of simulated to observed heads in five wells. Observed heads are from the LTER database (LTER 1995). Simulated heads are from model 4.

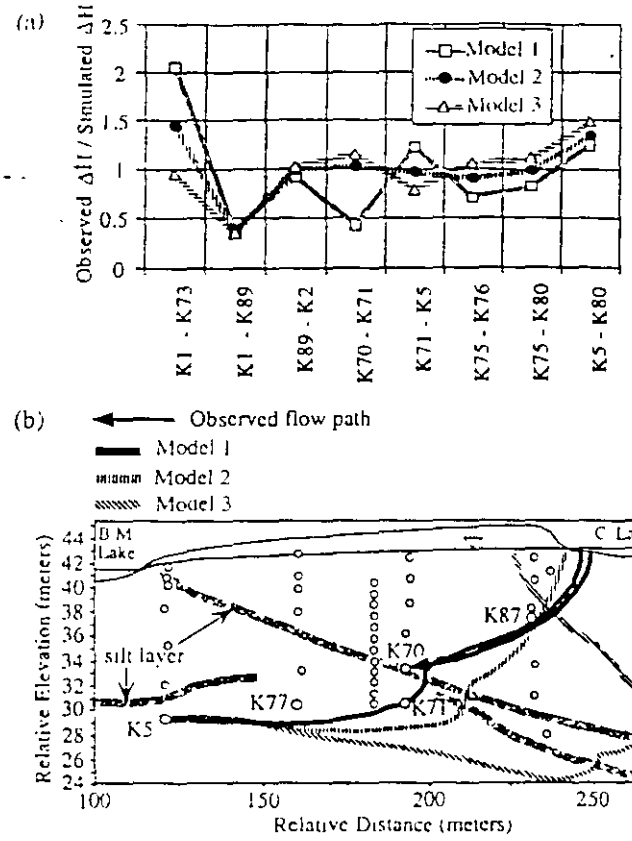

Figure 6. (a) Ratios of observed to simulated head differences (ΔH) between selected well pairs for models 1, 2, and 3 for the quasi steady-state simulation for which zero recharge and lake levels measured on August 25, 1993, were assumed. (b) Simulated flowpaths for average steady-state models 1, 2, and 3. Average recharge rate (26.2 cm/yr) and average lake levels (42.9 m for Crystal Lake and 41.8 m for Big Muskellunge Lake) were assumed.

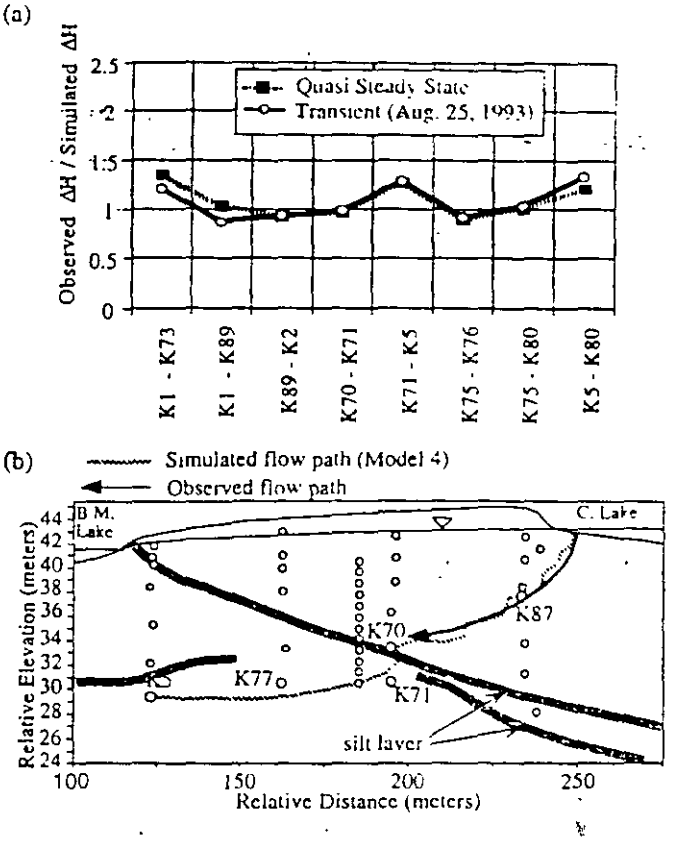

Figure 7. (a) Ratios of observed to simulated head differences (ΔH) between selected well pairs for quasi steady-state and transient runs of model 4. Zero recharge and the lake levels on August 25, 1993, were assumed for the steady-state simulation. The transient results are for August 25, 1993, in a simulation that used average monthly recharge rates and lake levels for the period 1984-1993. (b) Simulated flowpath for average steady-state model 4. Average recharge rate (26.2 cm/yr) and average lake levels (42.9 m for Crystal Lake and 41.8 m for Big Muskellunge Lake) were assumed.

Table 3
Root Mean Square (RMS) Errors in Heads

	Simulation	RMS Error (cm)
Model 1	Transient*	7.8
	Quasi steady state	9.6
Model 2	Transient*	3.1
	Quasi steady state	4.2
Model 3	Quasi steady state	3.7
Model 4	Transient*	3.5
	Quasi steady state	3.2

*Results for August 25, 1993; a transient calibration was not performed using model 3.

Table 4
Travel Times in Years from Crystal Lake to Selected Piezometers
(Wells shown in the table are located close to the simulated flowpath calculated by model 4 [Figure 7b]. Estimates by Bullen et al. (1996) were based on tritium analyses.)

	K87	K70	K71	K77	K5
Model 1	3.2	11.2	12.5	17.1	24.1
Model 2	—	—	—	—	40.7
Model 3	—	—	—	—	97.8
Model 4	2.9	10.2	12.2	16.6	23.6
Bullen et al. (1996)	1.3	7.0	--	15[a]	30[b]

[a]Measurement for K76; see Figure 2a for location.
[b]Reported measurement is the average for K82 and K5; see Figure 2a for location of K82.

produced a flowpath that deviates from the observed. Hence, both models 2 and 3 are rejected.

Comparison of the flowpaths in Figure 6b shows that as the anisotropy ratio is decreased (from 20 in model 3 to five in model 1), the simulated flowpath approaches the observed. When the anisotropy ratio is five (model 1) the flowpath is nearly the same as the observed. In model 4, where the anisotropy ratio is also equal to five, the overall calibration is much improved relative to models 1, 2, and 3. The RMS errors are 3.2 cm for the quasi steady-state simulation and 3.5 cm for the transient calibration (Table 3). Moreover, the ratios of head differences between points are close to one (Figure 7a) and the simulated flowpath is close to the observed (Figure 7b). Comparison between simulated and measured heads during the period 1984 to 1993 is also good (Figure 5), allowing for the fact that observed head peaks due to rain storm events are not captured by the model because the stress period used in the simulation was one month. Scatter plots of simulated vs. observed heads (Figure 8) also indicate a good calibration.

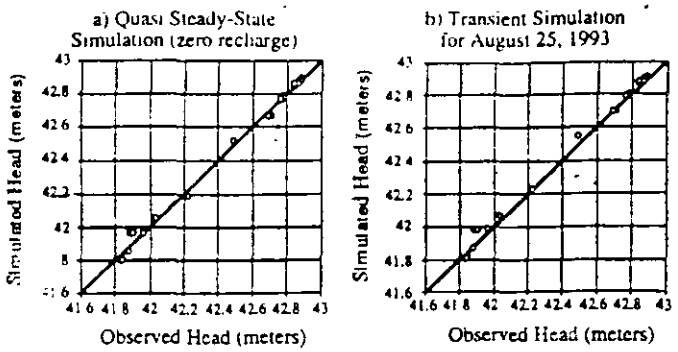

Figure 8. Scatter plots of simulated vs. observed heads for model 4 for: (a) quasi steady-state model; (b) transient model.

The transient calibrated model (model 4) was used to simulate enhanced dispersion of an oxygen isotope plume from Crystal Lake (Kim et al. 1999). Enhanced dispersion is caused by transience in the flow field as a result of fluctuations in recharge and lake levels. Kim et al. (1999) found that the dipping bedding plane layers in model 4 were essential to simulate the observed spreading of the plume, providing additional evidence in support of model 4.

Travel Times

Travel times (Table 4) were estimated from the average steady-state models using the PATH3D particle tracking code (Zheng 1989). Particles were back-tracked from each of the wells listed in Table 4. These wells are located along the flowpath delineated by model 4 (Figure 7b). The results from model 4 show that it takes nearly 24 years for a particle from Crystal Lake to reach well K5. Travel times reported by Bullen et al. (1996) from tritium analyses (Table 4) indicate that the travel time to K5 as calculated by model 4 is too low by at least six years. Ongoing work in collaboration with the U.S. Geological Survey District Office in Middleton, Wisconsin, which is aimed at delineating the lower portion of the observed flowpath shown in Figure may help resolve this discrepancy and lead to further refinement of the flow model.

Models 1 and 4, which match the observed flowpath, give similar travel times from Crystal Lake to K5 (Table 4) because of their similar flowpaths and similar overall head gradients and conductivity values along the flowpath. Models 2 and 3 give travel times that are too long. As expected, travel times are sensitive to path lengths and path lengths are dependent on the anisotropy ratio (Figures 6b and 7b).

Summary and Conclusions

Multiple calibration targets—namely, steady-state and transient heads, head gradients, and flowpath information—were used to calibrate a two-dimensional finite-difference model. Four sets of parameter values (Table 2) were tested during the calibration. Overall model calibration was much improved when local anisotropy caused by stratification of the upper sand unit was simulated directly with dipping layers of lower permeability (model 4). Travel times from Crystal Lake to well K5 were calculated from results of each of the four models with the aid of a particle tracking code. Travel times to well K5 (Table 4) range from 24 years (models 1 and 4) to 98 years (model 3) and are dependent on the length of the flowpath, which is sensitive to the anisotropy ratio (Figures 6b and 7b).

Our results indicate that calibration with multiple targets, especially using flowpath information, is helpful in identifying the best calibration among a set of possible calibrations. Without flowpath information, models 2 or 3, which gave acceptable RMS errors in heads (Table 3), might have been accepted as valid. Neither of these models, however, was able to reproduce the flowpath delineated from field data (Figure 6b) or the observed dispersion of an oxygen isotope plume (Kim et al. 1999). Obtaining a good calibration to heads required a large anisotropy ratio in the upper sand aquifer, as in models 2 and 3. In model 4, we simulated anisotropy in the upper sand aquifer directly by inserting dipping layers of low permeability. The improved calibration provided by model 4 indicates that such bedding plane layers effectively simulate the overall anisotropy and also preserve the angle of anisotropy observed in the field.

Acknowledgments

This study was supported by the NSF-LTER program (LTER-DEB #9011660) and NSAF-EAR (#9304811). We thank Daniel Feinstein, David Krabbenhoft, and Randy Hunt, all with the U.S. Geological Survey, for helpful discussions and John Schindler for field assistance. This paper benefited from comments by three reviewers, especially those by Bruce Hensel.

References

Anderson, M.P., and W.W. Woessner. 1992. *Applied Groundwater Modeling. Simulation of Flow and Advective Transport*. San Diego, California: Academic Press.

Anderson, M.P., and X. Cheng. 1993. Long and short term transience in a groundwater/lake system in Wisconsin, U.S.A. *Journal of Hydrology* 145, no. 1-2, 1–18.

Barten, P.K. 1988. Modeling streamflow from headwater catchments in the northern lake states. Ph.D. diss., Dept. of Forest Resources, University of Minnesota, Minneapolis.

Bullen, T.D., K.P. Krabbenhoft, and C. Kendall. 1996. Kinetic and mineralogic controls on the evolution of groundwater chemistry and $^{87}Sr/^{86}Sr$ in a sandy silicate aquifer, northern Wisconsin, U.S.A. *Geochimica et Cosmochimica Acta* 60, no. 10, 1807–1821.

de Marsily, G. 1986. *Quantitative Hydrogeology*. Orlando, Florida: Academic Press.

Duffield, G.M., D.R. Buss, and D.E. Stephenson. 1990. Velocity prediction errors related to flow model calibration uncertainty. In *Calibration and Reliability in Groundwater Modeling*, ed. K. Kovar, 159–170. IAHS Publ. v. 195. Wallingford, Oxfordshire, UK: IAHS.

Freeze, R.A., and J. Cherry. 1979. *Groundwater*. Englewood Cliffs, New Jersey: Prentice-Hall.

Frey, D.G. 1963. *Limnology in North America*. Madison, Wisconsin: University of Wisconsin Press.

Hurley, J.P., D.E. Anderson, G.J. Kenoyer, and C.J. Bowser. 1985. Groundwater as a silica source for diatom production in a precipitation-dominated lake. *Science* 227, no. 4694, 1576–1578.

Juday, C.E., E.A. Birge, and V.W. Meloche. 1935. Mineral contents of the lake waters of northeastern Wisconsin. *Transactions of the Wisconsin Academy of Science and Arts Letters* 29: 223–275.

Kauffmann, C., W. Kinzelbach, and J.J. Fried. 1990. Simultaneous calibration of flow and transport models and optimization of remediation measures. In *Calibration and Reliability in Groundwater Modeling*, ed. K. Kovar, 159-170. IAHS Publ. v. 195. Wallingford, Oxfordshire, UK: IAHS.

Kenoyer, G.J. 1986. Groundwater/lake dynamics and chemical evolution on a sandy silicate aquifer in northern Wisconsin. Ph.D. diss., Department of Geology and Geophysics, University of Wisconsin-Madison.

Kenoyer, G.J. 1988. Tracer test analysis of anisotropy in hydraulic conductivity of granular aquifers. *Ground Water Monitoring Review* 8, no. 3: 67–70.

Kenoyer, G.J., and M.P. Anderson. 1989. Groundwater's dynamic role in regulating acidity and chemistry in a precipitation dominated lake. *Journal of Hydrology* 109: 287–306.

Kenoyer, G.J., and C.J. Bowser. 1992a. Groundwater chemical evolution in a sandy silicate aquifer in northern Wisconsin, 1. Patterns and rates of change. *Water Resources Research* 28, no. 2: 579–589.

Kenoyer, G.J., and C.J. Bowser. 1992b. Groundwater chemical evolution in a sandy silicate aquifer in northern Wisconsin, 2. Reaction modeling. *Water Resources Research* 28, no. 2: 591–600.

Kim, K. 1996. A geochemical and flow modeling study on groundwater in a sandy, silicate aquifer, northern Wisconsin, U.S.A. Ph.D. diss., Department of Geology and Geophysics, University of Wisconsin-Madison.

Kim, K., M.P. Anderson, and C.J. Bowser. 1999. Enhanced dispersion in groundwater caused by temporal changes in recharge rate and lake levels. In review for *Water Resources Research*.

Krabbenhoft, D.P. 1998. Personal communication.

Krabbenhoft, D.P., M.P. Anderson, and C.J. Bowser. 1990. Estimating groundwater exchange with lakes, 2. Calibration of a three-dimensional, solute transport model to a stable isotope plume. *Water Resources Research* 26, no. 10: 2455-2462.

Krabbenhoft, D.P., T.D. Bullen, and C. Kendall. 1992. Isotopic indicators of groundwater flow paths in a northern Wisconsin aquifer. *EOS* 73, no. 43: 190.

LTER (Long Term Ecological Research) – North Temperate Lakes of Wisconsin. 1995. LTER program, NSF, J.J. Magnuson, Center for Limnology, University of Wisconsin-Madison. http://limnosun.limnology.wisc.edu/lataca.html#ground

McDonald, M.G., and A.W. Harbaugh. 1988. A modular three-dimensional finite-difference ground-water flow model. USGS Techniques of Water-Resources Investigations Report 06-A1.

McDonald, M.G., A.W. Harbaugh, B.R. Orr, and D.J. Ackerman. 1991. A method of converting no-flow cells to variable-head cells for the U.S. Geological Survey modular finite-difference ground-water flow model. USGS Open File Rep. 91-536.

Medina, A.J. Carrera, and G. Galarza. 1990. Inverse modeling of coupled flow and solute transport problems. In *Calibration and Reliability in Groundwater Modeling*, ed. K. Kovar, 185–194. IAHS Publ. v. 195. Wallingford, Oxfordshire, UK. 14HS.

Okwueze, E. 1983. Geophysical investigation of the bedrock and the groundwater–lake flow system in the Trout Lake region of Vilas County, northern Wisconsin. Ph.D. diss., Department of Geology and Geophysics, University of Wisconsin-Madison.

Phillips, S.W. 1987. Hydrogeology, degradation of ground-water quality, and simulation of infiltration from the Delaware River into the Potomac aquifers, northern Delaware. USGS Water Resources Investigation Report 87-4185.

Poeter, E.P., and M.C. Hill. 1997. Inverse models, A necessary next step in ground-water modeling. *Ground Water* 35, no. 2: 250–260.

Reilly, T.E., and D.W. Pollock. 1996. Sources of water to wells for transient cyclic systems. *Ground Water* 34, no. 6: 979–988.

Schindler, J.E. 1994. Groundwater flow and carbon transport in a sandy silicate aquifer. B.S. honors thesis, Department of Geology and Geophysics, University of Wisconsin-Madison.

Thomas, J.M., S.M. Carlton, and L.B. Hines. 1989. Ground-water hydrology and simulated effects of development in Smith Creek valley, a hydrologically closed basin in Lander County, Nevada. USGS Professional Paper 1409-E.

Thornthwaite, C.W., and J.R. Mather. 1955. *The Water Balance*. Publication 8. Centerton, New Jersey: Laboratory of Climatology.

Zheng, C. 1989. PATH3D. Rockville, Maryland: S.S. Papadopulos & Associates.

FACULTAD DE INGENIERIA U.N.A.M.
DIVISION DE EDUCACION CONTINUA
CURSOS ABIERTOS

XII CURSO INTERNACIONAL DE CONTAMINACIÓN DE ACUÍFEROS

MODULO III: MODELOS MATEMÁTICOS EN GEOHIDROLOGIA Y CONTAMINACIÓN DE ACUIFEROS

TEMA

CHARACTERIZING THREE – DIMENSIONAL HYDRAULIC CONDUCTIVITY DISTRIBUTIONS USING QUALITATIVE AND QUATITATIVE GEOLOGIC BOREHOLE DATA: APPLICATION TO A FIELD SITE

EXPOSITOR: DR. ADOLFO CHAVEZ RODRIGUEZ
PALACIO DE MINERIA
OCTUBRE DEL 2000

Characterizing Three-Dimensional Hydraulic Conductivity Distributions Using Qualitative and Quantitative Geologic Borehole Data: Application to a Field Site

by Zhihui Zhang[a] and Mark L. Brusseau[a,b]

Abstract

The focus of this paper is the characterization of three-dimensional hydraulic conductivity distributions using qualitative and quantitative geologic borehole data. We illustrate an approach that entails a three-step procedure, where lithologic information reported in the borehole logs is first classified into texture classes. Representative hydraulic conductivity values are then calculated for each texture class using a correlation relating measured lithologic and hydraulic data from core samples. The generalized kernel estimator method, which can take full advantage of the characteristics of borehole log data and is applicable to statistically nonstationary systems, is used thereafter to generate the three-dimensional distributions of hydraulic conductivity. An application using borehole data from a trichloroethene (TCE)-contaminated Superfund site in Tucson, Arizona, is presented and used to test the proposed methodology. The simulated hydraulic conductivity distributions appear reasonable and the simulated permeability distributions for several cross sections agree well with the hydrogeologic cross-sectional maps. The use of mean permeability indicators for differentiating zones of high and low permeability is also investigated.

Introduction

Hydraulic properties of aquifers vary spatially as a result of the complex geologic processes through which they are formed and altered. Spatial variability of the hydraulic properties leads to spatially variable pore water velocities, which can significantly influence contaminant transport in the subsurface. Numerous investigators have commented on the importance of incorporating heterogeneity into studies of ground water flow and contaminant transport (e.g., Matheron and de Marsily 1980; Gelhar and Axness 1983; Guven et al. 1986; Brusseau 1994). Characterizing the spatial distribution of hydraulic conductivity is critical to the accurate representation of flow and transport. Unfortunately, complete, three-dimensional information about hydraulic conductivity is not readily available at the field scale. Therefore, the spatial distributions are estimated using whatever limited data are available (e.g., geologic borehole logs, pumping test data, and geophysical logs).

At most sites, the primary sources of information for subsurface hydraulic properties are geologic borehole logs and pumping tests. Pumping tests produce values that are averaged over a relatively large vertical and areal extent and are, therefore, of limited use for characterizing the spatial variability of hydraulic conductivity. As discussed by Ali and Lall (1996), existing pumping-test methodologies alone are inappropriate for the identification of subsurface heterogeneities because they focus on the estimation of large-scale average hydraulic parameters, and the aquifer response to pumping is damped and smoothed over the discontinuities in the hydraulic conductivity. However, pumping test data are useful for calibrating three-dimensional hydraulic conductivity distributions obtained using other approaches.

Borehole log data, which are generally available for any site, can provide local stratigraphic information of a three-dimensional nature. However, borehole logs are usually qualitative, providing information on texture rather than hydraulic conductivity. Several methods based on correlations between hydraulic conductivity and texture are available to transform the qualitative information obtained from borehole logs into representative hydraulic conductivity data. For example, Uma et al. (1989) presented a new statistical grain-size method for evaluating the hydraulic conductivity of granular aquifers. The equation is of the form $K = Cd_{10}^2$ (cm/sec), which is similar to the well-known Kozeny-Carman equation (Carman 1937). However, in this case, the coefficient C, which is normally taken as a constant, is found to be a variable that depends on the nature of the geologic environment. It was established that C = 6.0 for unconsolidated and poorly cemented sandy materials; C = 3.8 for moderately consolidated/cemented rocks; and C = 2.0 for fairly well compacted and cemented rocks. It was reported that the estimates obtained from this method compared favorably with those determined from pumping test methods. Several other examples are also available (Masch and Denny 1966; Mishra et al. 1989; Temples and Waddell 1996).

[a]Department of Soil, Water, and Environmental Science, The University of Arizona, Tucson, AZ 85721. E-mail: zhihui@u.arizona.edu
[b]Department of Hydrology and Water Resources, The University of Arizona, Tucson, AZ 85721. E-mail: brusseau@ag.arizona.edu
Received March 1997, accepted December 1997

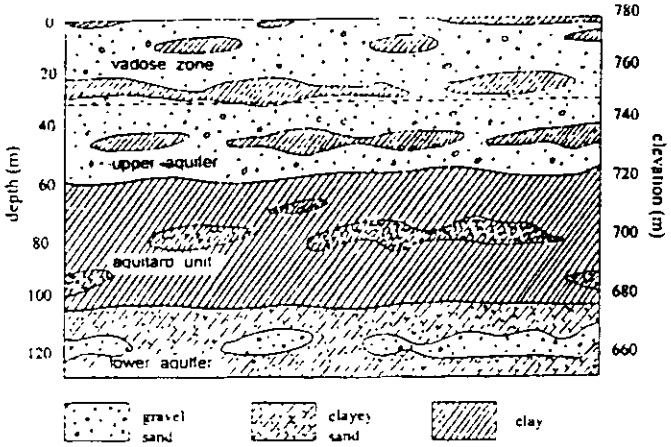

Figure 1. A schematic vertical profile of geological conditions at the site.

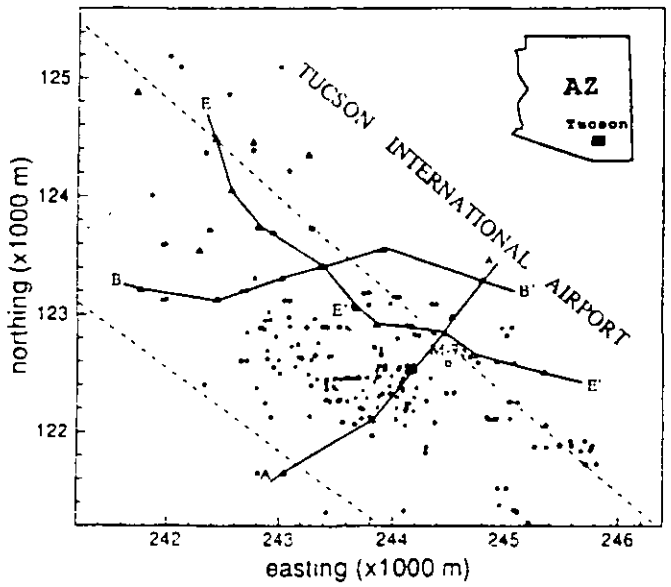

Figure 2. Borehole locations and hydrogeological cross sections at the site.

- Shallow well
- Medium well
- Deep well
- Recharge well

As noted, borehole logs and pumping tests are the primary sources of information for subsurface hydraulic properties. The magnitude and distribution of hydraulic conductivity at a given borehole location can be derived by combining the information in borehole logs with hydraulic conductivity values measured for core samples. If the data are sufficient, three-dimensional distributions of hydraulic conductivity can be generated using an appropriate stochastic interpolation method. In this paper, such an approach will be applied to a Superfund site in Tucson, Arizona, to characterize hydraulic conductivity distributions using qualitative and quantitative geologic borehole data.

Field Site

The aquifer system at the site is comprised of alluvial formations that are heterogeneous in the vertical and horizontal directions. The system can be divided into four regional hydrogeologic units from top to bottom as shown in Figure 1 (Hargis and Montgomery Inc. 1982): (1) an unsaturated zone extending to the water table, located at 34 to 40 m below land surface (BLS); (2) an upper

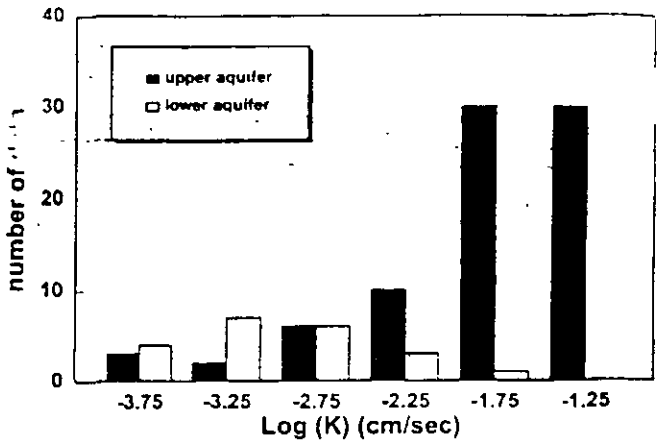

Figure 3. Hydraulic conductivity distribution determined from pumping test data.

aquifer extending 61 to 67 m BLS; (3) an aquitard unit extending to about 107 m BLS; and (4) a lower aquifer. The upper aquifer, in which a trichloroethene (TCE) plume resides, consists of gravelly sand with some clayey sand and sandy clay. Its saturated thickness ranges from less than 15 m to more than 23 m. The lower aquifer is composed of lenses of sand and gravel interspersed within clayey sand and sandy clay. The aquitard unit is comprised of a thick layer of clayey sediments. In the unsaturated zone, a 6 to 12 m thick laterally extensive clay or sandy clay unit, located at 23 to 26 m BLS, overlies the upper aquifer. This unit is largely discontinuous and, while it confines the upper aquifer at some locations, ground wa occurs primarily under unconfined conditions in the upper aqu Ground water is under confined conditions in the lower aquifer. Potentiometric head in the lower aquifer is 18 to 37 m lower than the water level in the upper aquifer (Mock et al. 1985).

Figure 2 shows the location of the 200 geological boreholes within the site boundaries. Most of the boreholes (144) were completed in the upper aquifer, and are about 61 m deep. Some of the boreholes (89) were completed in the vadose zone, and are about 30 m deep. The remaining boreholes (17) penetrate into the lower aquifer and are about 122 m deep. Each borehole log contains the borehole name, the depth intervals, material descriptions, and the corresponding United Soil Classification System (USCS) formation codes. About 85% of the boreholes are located between the two dashed lines, an area for which more accurate simulations are expected. Also shown in the figure are three geological cross sections that will be used to help evaluate the simulated distributions.

Pumping tests were conducted in about 80 wells in the upper aquifer. The hydraulic conductivity values determined from these tests range between 1.1×10^{-4} and 9.5×10^{-2} cm/sec, with a mean value of 2.8×10^{-2} cm/sec. Eighty-five percent of these values are within $[3.0 \times 10^{-3}, 9.0 \times 10^{-2}]$ cm/sec (Figure 3). For the lower aquifer, the hydraulic conductivity values span a range of 1.1×10^{-4} to 1.1×10^{-2} cm/sec, with a mean value of 2.2×10^{-3} cm/sec. It is clear from Figure 3 that, at most locations, the permeabilities in the upper aquifer are higher than those in the lower aquifer.

Approach

The approach for characterizing three-dimensional hydraulic conductivity distributions using qualitative and quantitative geologic borehole data at the site consists of several steps. First, the lithological information contained in the borehole logs are classified into

Table 1
USCS Formation Codes, Particle Weight Percentages, Representative Hydraulic Conductivities, and Permeability Indicators

USCS Code	Particle Weight Percentage (%) Clay	Silt	Sand	Gravel	$\log_{10}K$ (cm/sec)	Permeability Indicator
GW	5	5	20	70	−4.157	
GP	5	5	15	75	−4.106	
GM	5	15	15	65	−4.827	
GC	15	5	15	65	−4.819	1
SW	5	5	75	15	−4.191	
SP	5	5	70	20	−4.267	
SM	5	15	65	15	−4.814	
SC	15	5	65	15	−4.806	
ML	10	70	10	10	−5.749	
MH	15	70	10	5	−5.843	
CL	70	15	10	5	−8.476	0
CH	75	15	5	5	−8.784	

G, gravel; S, sand; M, silt; C, clay; W, well graded (i.e., poorly sorted); P, poorly graded; L, low plasticity; H, high plasticity.

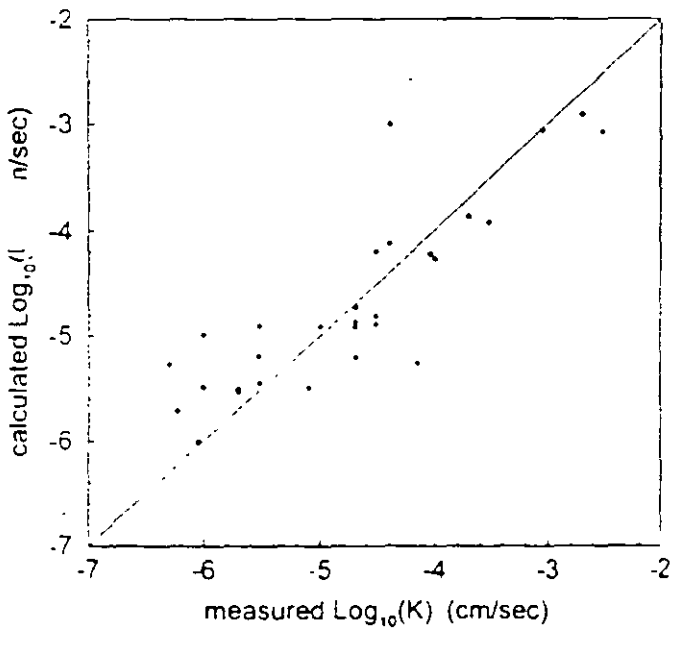

Figure 4. Calculated (using Equation 1) vs. measured hydraulic conductivity for core samples (correlation coefficient $r^2 = 0.87$).

12 representative texture classes, with each class assigned a USCS code representing a certain particle-size distribution (Soil Classification Handbook 1986). Second, a quantitative relationship between hydraulic conductivity and texture is developed using data obtained from cores collected from the field site. Third, the generalized kernel estimator method is used to generate three-dimensional hydraulic conductivity distributions using the transformed borehole log data. The estimated hydraulic conductivity value at each point is formed as a local weighted average of the available transformed hydraulic conductivity values that lie within an averaging interval of the point.

As discussed previously, abundant borehole log data are available for the site. However, the borehole log data provide only a qualitative description of the formation materials within certain intervals of a core and its formation code, which is based on the USCS system. No direct information on the particle-size distributions is available. This problem is circumvented by grouping the lithologic characterizations into 12 representative classes (Table 1), with each class being assigned a certain weight percentage of clay, silt, sand, and gravel according to the USCS formation code definitions (Soil Classification Handbook 1986). Various numbers of classes were evaluated and 12 classes were found to be optimal. Using less than 12 texture classes provides insufficient characterization, whereas it becomes difficult to distinguish among larger numbers of classes. Once the formation descriptions have been transformed, an equation relating hydraulic conductivity to texture can be applied to the 12 classes to calculate their respective logarithmic hydraulic conductivities.

Table 2
Summary of Lithologic and Hydraulic Data from Core M-73

Sample Number	Depth BLS (m)	Particle Weight Percentage (%) Clay	Silt	Sand	Gravel	K (cm/sec)
R3	36.9	18	31	49	2	1.0e-6
S3	37.2	12	40	48	0	2.0e-5
T3	37.8	9	22	69	0	3.0e-5
U3	38.4	9	15	64	12	1.0e-6
V3	39.0	20	42	37	0	2.0e-5
W3	39.6	31	53	16	0	9.0e-7
X3	40.5	22	64	14	0	2.0e-6
Y3	41.1	13	57	30	0	2.0e-5
Z3	41.8	23	56	21	0	2.0e-6
A4T	42.1	16	33	51	0	2.0e-5
A4U	42.2	25	37	38	0	8.0e-6
A4M	42.4	13	19	60	8	7.0e-5
A4L	42.5	16	16	63	5	3.0e-6
B4T	42.7	14	12	67	6	1.0e-5
B4U	42.8	14	11	69	6	3.0e-5
B4M	43.0	2	6	29	63	4.0e-5
B4L	43.1	3	5	53	39	9.0e-5
C4	43.3	2	0	66	32	4.0e-5
D4U	43.9	3	0	54	43	9.0e-4
D4L	44.1	3	0	82	15	2.0e-3
E4	44.2	2	3	41	54	2.0e-4
F4	44.8	3	4	29	62	3.0e-4
G4U	46.0	5	7	77	11	1.0e-4
G4M	46.3	3	0	60	37	3.0e-3
G4L	46.5	4	15	39	42	3.0e-6
H4U	46.6	12	32	41	15	6.0e-7
H4L	46.7	12	37	46	5	3.0e-6
I4	46.9	17	30	52	1	5.0e-7
J4	47.5	14	37	49	0	3.0e-5

The hydraulic conductivity–texture correlation equation was obtained using particle-size distributions and saturated hydraulic conductivities measured for 30 samples obtained from a core collected within the upper aquifer at the site. A summary of the measured data is given in Table 2. The following nonlinear regression equation was obtained for these data:

$$\log_{10} K = 1.854 - 9.640\times10^{-2}*(CL\%) - 5.936\times10^{-1}*(SL\%)^{0.5} - 3.478\times10^{-2}*(SD\%) - 4.196\times10^{-1}*(GV\%)^{0.5} \quad (1)$$

where $\log_{10} K$ is the common logarithm of hydraulic conductivity in cm/sec, CL%, SL%, SD%, and GV% are weight percentages of clay, silt, sand, and gravel, respectively. The other factors that may affect the magnitude of hydraulic conductivity, such as porosity and bulk density, are not explicitly shown in the equation, but are implicitly incorporated because they are also related to texture.

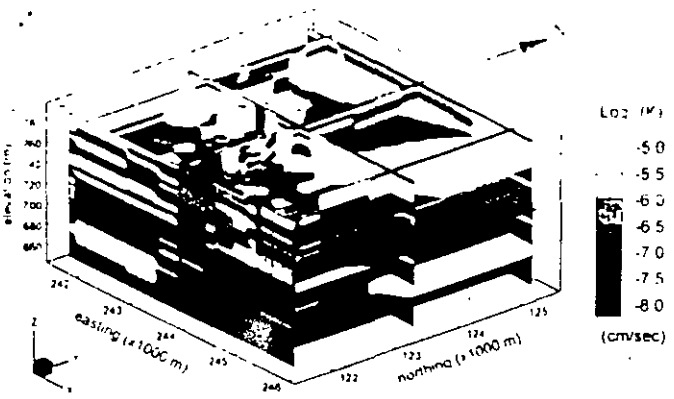

Figure 5. Simulated three-dimensional distribution of hydraulic conductivity in the domain.

A scatter graph of calculated versus measured hydraulic conductivity values indicates that Equation 1 provides reasonable estimates of hydraulic conductivity. Close inspection of Figure 4, however, reveals trends in the residuals. For most of the low-permeability ($\log_{10} K < -5$ cm/sec) samples, the calculated values are greater than the measured. Conversely, for most of the high permeability ($\log_{10} K > -5$ cm/sec) samples, the calculated values are smaller than the measured. This may be caused by the nonuniform distribution of the samples, i.e., the majority of the samples fall into the high-permeability range. Equation 1 is considered applicable to the other borehole logs based on the similarity of depositional environments.

The generalized kernel estimator method is applied to estimate the distribution of hydraulic conductivity values for the site (4877 × 4572 × 152 m^3), using a 87 m × 81 m × 3 m grid. This method is a modification of the original kernel estimator method presented by Ali and Lall (1996), which was developed for stochastic subsurface characterization based on kernel function estimation using borehole log information. Parameter calculation at each estimation point is formed as a local weighted average of observed parameter values that lie within an averaging interval of the point. Using a kernel function, observations closer to the point are weighted higher, whereas those further away are weighted less. The averaging strategy is designed to accommodate the special attributes of the borehole data (i.e., continuity in the vertical direction and sparsity in the horizontal). This method takes full advantage of the spatial characteristics of the borehole log data and no assumption of statistical stationarity is made in its development.

There are two major differences between the modified method and the original kernel estimator method (Zhang and Brusseau 1996). First, unlike the original method, which can only take binary input data, the modified method can accept any parameter value. Second, the data can be classified into any number of categories for the modified method, compared to the binary classification used in the original method. With these two new features, the generalized kernel estimator method can be used to generate three-dimensional distributions of hydraulic conductivity using borehole log data.

Results and Discussion

The simulated three-dimensional distribution of hydraulic conductivity is shown in Figure 5, which is useful for visualizing the strata in the system and their variations in space. A large degree of heterogeneity can be observed for this alluvial aquifer system. There is a distinct layer of high permeability (indicated by light shading) located between 720 m and 750 m to 760 m above MSL. This zone corresponds to the upper aquifer. Some discontinuous low-permeability lenses (indicated by dark shades) are embedded within this

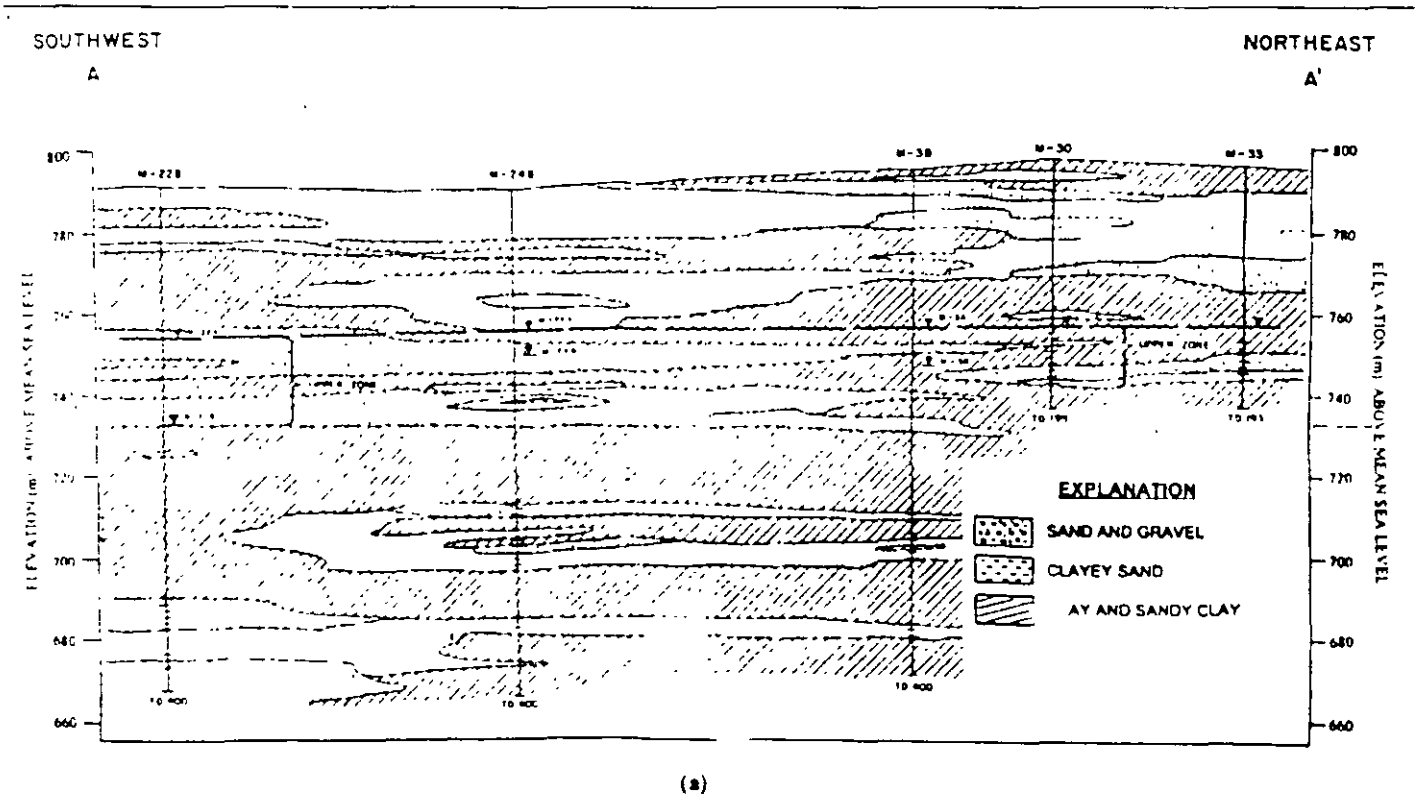

(a)

Figure 6a. Comparison of the simulated hydraulic conductivity distribution and the hydrogeological map along section A-A' shown in Figure 2. (a) Hydrogeological map.

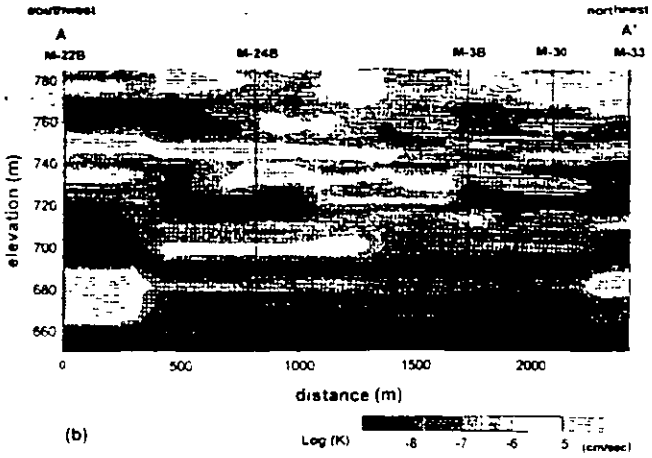

Figure 6b. Comparison of the simulated hydraulic conductivity distribution and the hydrogeological map along section A-A′ shown in Figure 2. (b) Simulated distribution.

layer. A thick layer of low permeability can be observed between 680 m and 720 m to 730 m above MSL. This corresponds to the aquitard unit separating the upper and the lower aquifers. The results at the northeast side and southwest corner of the domain should be viewed with caution because there are insufficient borehole logs in these areas (Figure 2) to obtain reliable information.

To examine if the simulated three-dimensional spatial distribution of hydraulic conductivity is an accurate representation of the site, distributions along three cross sections A-A′, B-B′, and E-E′ (Figures 6b, 7b, 8c, and 8d) are compared to the corresponding hydrogeological cross-sectional maps developed by Hargis and Associates Inc. (1985) (Figures 6a, 7a, 8a, and 8b). The locations of the three cross sections are shown in Figure 2. The three maps were made based on the hydrogeologists' interpretation of the borehole log data and their understanding of the geological and hydrogeological conditions at the site. Examination of Figures 6 to 8 reveals that the simulated cross-sectional hydraulic conductivity distributions compare favorably with the corresponding hydrogeological cross-sectional maps.

Inspection of Figures 6 to 8 reveals high-permeability material at a certain depth for one location and low-permeability material at the same depth for another location. It is difficult to discriminate geologic layers in such a complex heterogeneous subsurface system. However, layer differentiation is required during the design of a remediation system, is necessary for conceptualization of layered models, and is useful for vertical domain-discretization for mathematical modeling. For example, it is not good practice to locate an element across different layers because the hydraulic property in the element is supposed to be constant in a numerical model.

The correspondence among the USCS formation code, particle weight percentages, representative hydraulic conductivities, and permeability indicators for the 12 classes of materials are presented in Table 1. Hydraulic conductivities range from 10^{-5} to 10^{-4} cm/sec for high-permeability material (i.e., sand and gravel), are about 10^{-6} cm/sec for silt, and about $10^{-8.5}$ cm/sec for clay. A threshold value of $\log_{10} K = -5.0$ cm/sec can be used to separate the 12 classes of materials into two categories: those with $\log_{10} K > -5.0$ cm/sec (high permeability, indicator = 1) and those with $\log_{10} K < -5.0$ cm/sec (low permeability, indicator = 0). The permeability indicators developed in this manner can be used to quantitatively discriminate geologic layers. This binary data classification scheme is consistent with one of the schemes presented by Johnson and Dreiss (1989), which is based on interpretations of the USCS system for the binary classification of borehole data into high and low hydraulic conductivity regions.

The indicator method is applied to the subdomain (bounded by dashed lines) shown in Figure 2. Simulated hydraulic conductivities are considered more reliable within the subdomain because of the greater density of borehole logs. The value of the permeability indicator (either 0 or 1) at each grid point in the subdomain is assigned according to the estimated hydraulic conductivity value at the point using the threshold of log10 K = -5.0 cm/sec. The indicators for all the points at a specific elevation are then analyzed to

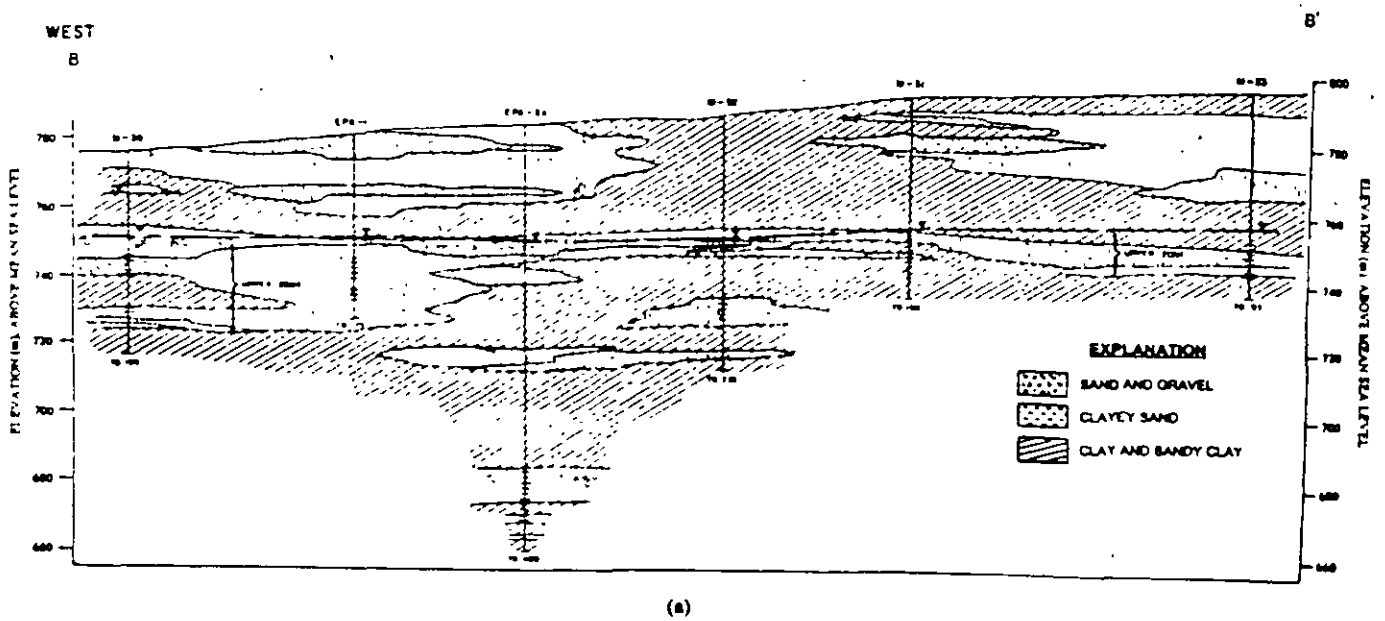

Figure 7a. Comparison of the simulated hydraulic conductivity distribution and the hydrogeological map along section B-B′ shown in Figure 2. (a) Hydrogeological map.

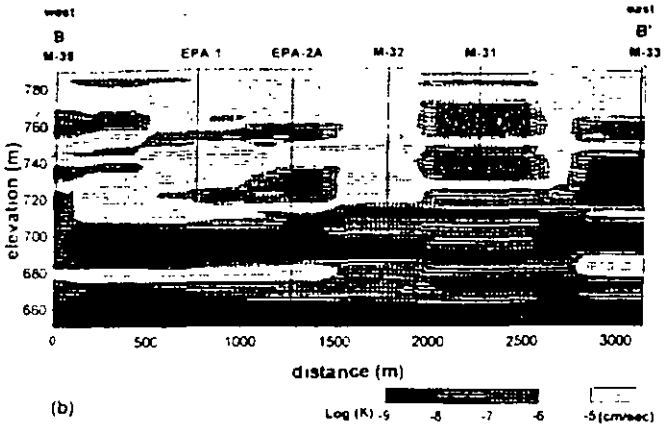

Figure 7b. Comparison of the simulated hydraulic conductivity distribution and the hydrogeological map along section B-B' shown in Figure 2. (b) Simulated distribution.

determine their mean and standard deviation. The variation of the mean permeability indicator, and the corresponding deviations, with elevation are shown in Figure 9. A large mean indicator indicates that generally high-permeability materials are dominant at this elevation, and vice versa. A deviation smaller than the mean indicator indicates a less heterogenous zone at the elevation, whereas a larger deviation indicates a more heterogeneous zone.

Figure 9 clearly shows several geologic layers at the site: vadose zone, upper aquifer, aquitard unit, and lower aquifer. The vadose zone and the aquitard unit appear to be more heterogeneous than the upper and lower aquifers. Interestingly, two relatively permeable layers separated by one less permeable layer are shown within the upper aquifer. They correspond to the upper and lower zones of the upper aquifer, and the local confining layer between them (Figure 1). The permeability of the upper zone is shown to be higher than that of the lower zone. These results are consistent with the available hydrogeologic cross sections and pumping test data.

As shown previously, the aquifer system at the site consists of several geologic layers. However, it is clear through the previous discussion that each layer is not uniform in composition. For example, gravel, sand, and clayey sand are dominant in the upper aquifer, in which lenses of clay and sandy clay are imbedded. High-permeability layers may merge, become thinner, or even disappear at some locations. These layers control the migration of the TCE plume. Conversely, the low-permeability lenses provide retention domains for TCE and, therefore, are likely to become long-term sources of contamination during the operation of the remediation systems. In Figure 9, a low-permeability layer can be observed between the vadose zone and the upper aquifer. Such a layer could shield the aquifer from contaminants introduced on the land surface or into the vadose zone. However, examination of Figures 6 to 8 reveals the presence of "windows" of high-permeability within this layer. These preferential pathways may have been partially responsible for the development of the ground water plume.

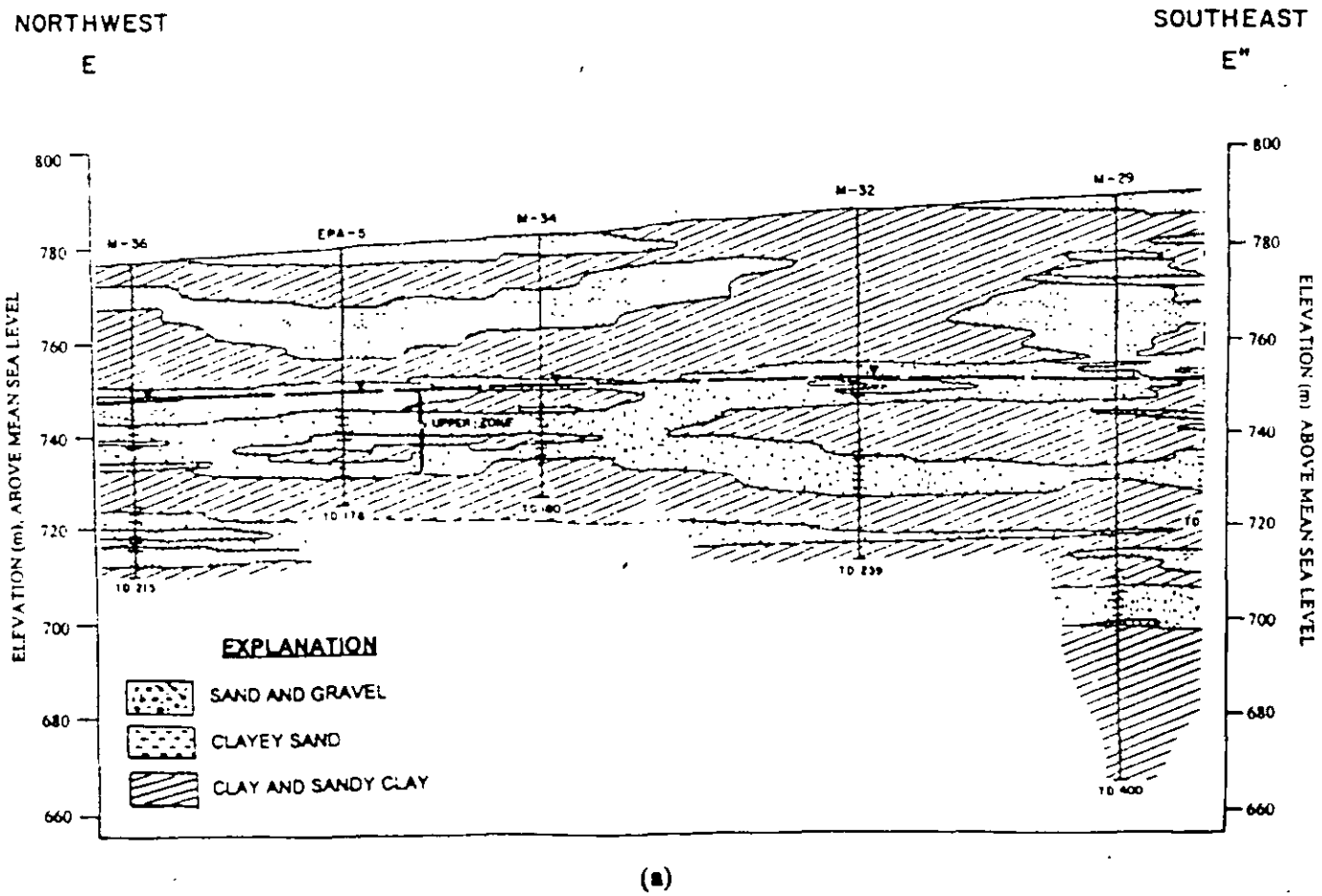

Figure 8a. Comparison of the simulated hydraulic conductivity distribution and the hydrogeological map along section E-E' shown in Figure 2. (a) Hydrogeological map.

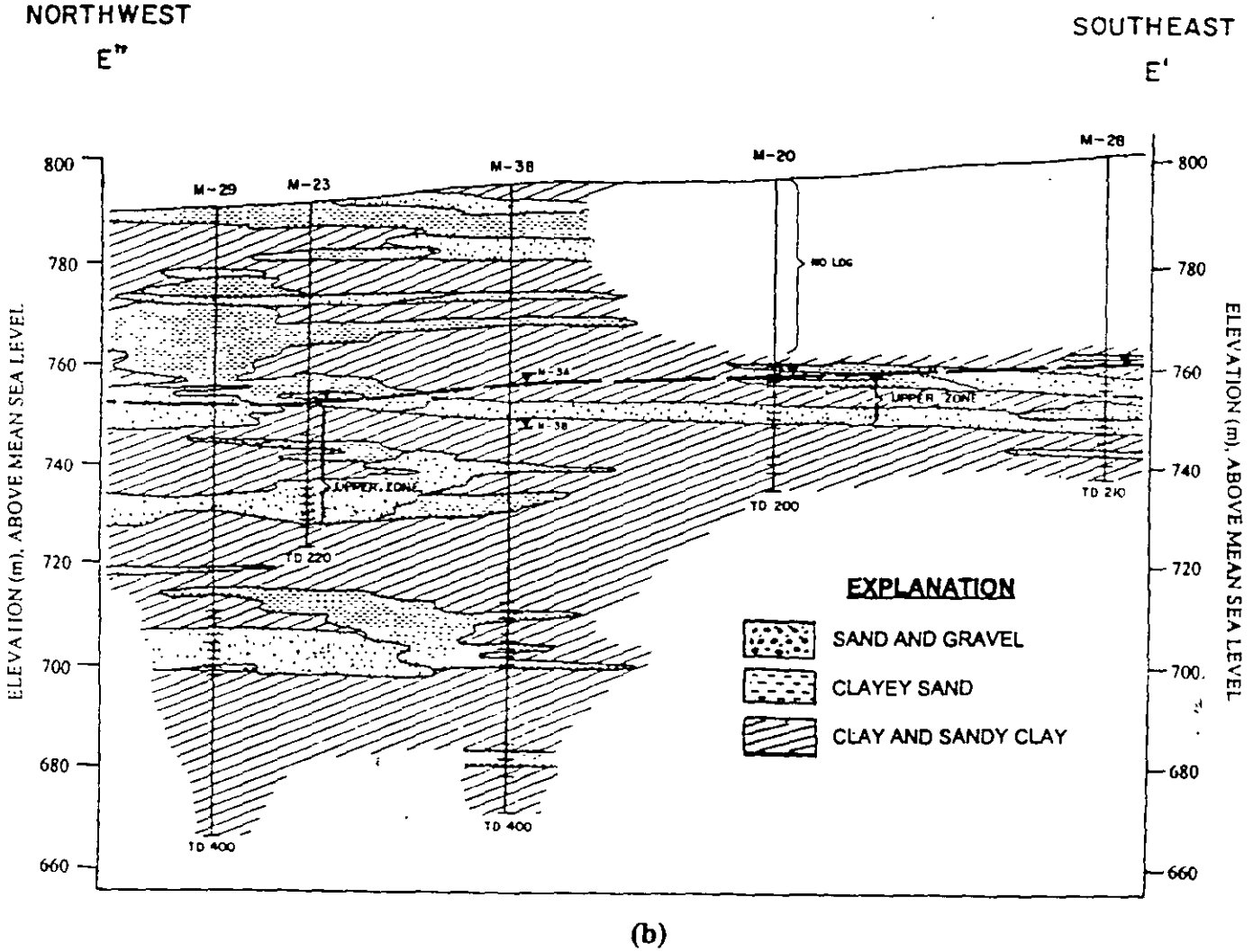

(b)

Figure 8b. Comparison of the simulated hydraulic conductivity distribution and the hydrogeological map along section E-E' shown in Figure 2. (b) Hydrogeological map.

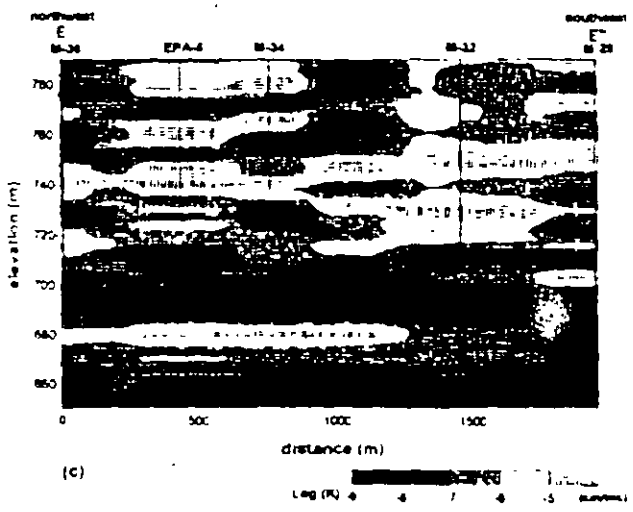

Figure 8c. Comparison of the simulated hydraulic conductivity distribution and the hydrogeological map along section E-E' shown in Figure 2. (c) Simulated distribution.

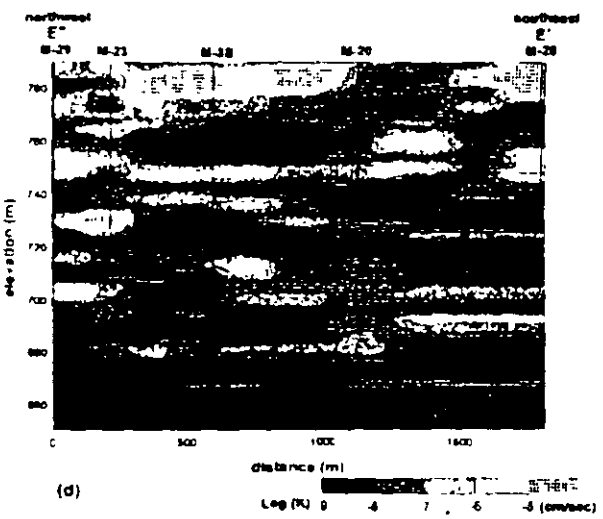

Figure 8d. Comparison of the simulated hydraulic conductivity distribution and the hydrogeological map along section E-E' shown in Figure 2. (d) Simulated distribution.

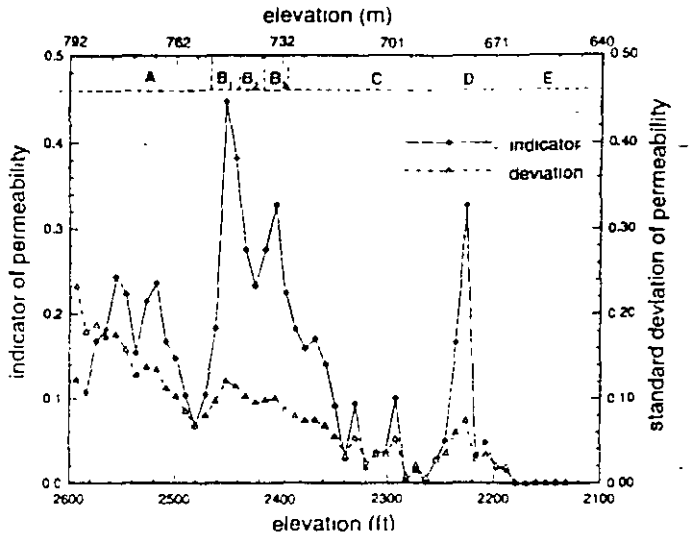

Figure 9. Mean permeability indicator and standard deviation vs. elevation. A: vadose zone; B_1: upper zone in the upper aquifer; B_2: confining layer in the upper aquifer; B_3: lower zone in the upper aquifer; C: aquitard unit; D: lower aquifer; E: unknown (no data available).

Conclusions

Geological borehole log data and pumping test data are the primary sources of information for subsurface hydraulic properties. For sites where pumping test data are scarce, the borehole logs are the only basis for site characterization and for model calibration. Typically, however, they are not used fully because of their qualitative nature and their uncertainty in the interpretation of hydraulic properties. For example, borehole log data may be used for model conceptualization, but they are not directly incorporated into numerical models.

An approach for generating three-dimensional hydraulic conductivity distributions using qualitative and quantitative borehole log data was illustrated in this paper. Several steps are involved in this approach. Lithologic information reported in the borehole logs is first classified into texture classes. Representative hydraulic conductivity values are then calculated for each texture class using a correlation relating measured lithologic and hydraulic data from core samples. The generalized kernel estimator method is used thereafter to generate the three-dimensional distributions of hydraulic conductivity.

Classification systems other than the USCS can be used in the first step, such as the ASTM (American Society for Testing and Materials) system, which is quite similar to USCS. Twelve texture classes appear to be sufficient for differentiating formation materials for a sedimentary system. Difficulty in assigning particle weight percentages to each texture class may arise if more classes are used. In deriving the relationship between hydraulic conductivity and texture from core sample measurements in the second step, it is desirable that core samples be taken from various boreholes and at different depths to decrease the uncertainty of the correlation equation. It is preferable to use different correlation equations for different areas in the domain if sufficient data are available for each area. The generalized kernel estimator method, rather than kriging, is used to generate hydraulic conductivity distributions because the kernel estimator method is specifically designed to accommodate the special attributes of borehole log data, and because it is applicable to statistically nonstationary systems.

Application of the approach to a field site in Tucson appeared to produce satisfactory results. For example, the hydraulic conductivity distributions generated for the three cross sections within the study area matched the corresponding hydrogeological cross section maps. The concept of the mean permeability indicator was used to quantitatively differentiate geologic layers in this complex heterogeneous subsurface system. These approaches should prove useful for planning remediation activities and for developing mathematical models at this and other sites.

Acknowledgments

This research was supported, in part, by a project funded by the U.S. Air Force. The assistance of Dr. Kathryn Kilroy and Martin L. Barackman is greatly appreciated.

References

Ali, A.I., and U. Lall. 1996. A kernel estimator for stochastic subsurface characterization. *Ground Water* 34, no. 4: 647-658.

Brusseau, M.L. 1994. Transport of reactive contaminants in heterogeneous porous media. *Reviews of Geophysics* 32, no. 3: 285-313.

Carman, P.C. 1937. Fluid flow through a granular bed. *Trans. Inst. Chem. Eng* (London) 15: 150-156.

Gelhar, L.W., and C.L. Axness. 1983. Three-dimensional stochastic analysis of macrodispersion in aquifers. *Water Resour. Res.* 19, no. 1: 161-180.

Geotechnical Branch Division of Research and Laboratory Services. 1986. *Soil Classification Hand Book*. Denver, Colorado: Geotechnical Branch Division of Research and Laboratory Services.

Guven, O., F.J. Molz, and J.G. Melville. 1986. Comment on "An advection-diffusion concept for solute transport in heterogeneous unconsolidated geological deposits" by Gelhar et al. *Water Resour. Res.* 22, no. 1: 89-91.

Hargis and Associates Inc. 1985. Design of Reclamation Wellfield, U.S. Air Force Plant No. 44. Tucson, Arizona: Hargis and Associates.

Hargis and Montgomery Inc. 1982. Investigation of subsurface conditions in the vicinity of abandoned waste disposal sites, Hughes Aircraft Company Manufacturing Facility, vol. 1. Tucson, Arizona: Hargis and Montgomery Inc.

Johnson, N.M., and S.J. Dreiss. 1989. Hydrostratigraphic interpretation using indicator geostatistics. *Water Resour. Res.* 25, no. 12: 2501-2510.

Masch, F.D., and K.J. Denny. 1966. Grain size distribution and its effect on the permeability of unconsolidated sands. *Water Resour. Res.* 2, no. 4: 665-677.

Matheron, G., and G. de Marsily. 1980. Is transport in porous media always diffusive? A counterexample. *Water Resour. Res.* 16, no. 5: 901-917.

Mishra, S., J.C. Parker, and N. Singhal. 1989. Estimation of soil hydraulic properties and their uncertainty from particle size distribution data. *Journal of Hydrol.* 108, no. 1-4: 1-18.

Mock, P.A., B.C. Travers, and C.F. Williams. 1985. Results of the Tucson Airport Area Remedial Investigation, Phase I, vol. 1. Tucson, Arizona: Arizona Dept. of Water Resources.

Temples, T.J., and M.G. Waddell. 1996. Application of petroleum geophysical well logging and sampling techniques for evaluating aquifer characteristics. *Ground Water* 34, no. 3: 523-531.

Uma, K.O., B.C.E. Egboka, and K.M. Onuaha. 1989. New statistical grain-size method for evaluating the hydraulic conductivity of sandy aquifers. *Journal of Hydrol.* 108, no. 1-4: 343-366.

Zhang, Z., and M.L. Brusseau. 1996. Quantitative characterization of subsurface heterogeneity using a generalized kernel-estimator method. Appendix I in *Advanced characterization study to improve the efficiency of pump-and-treat operations at a Superfund site: An integrated field, laboratory, and modeling approach*. UA/Hughes/USAF Project, Tucson, Arizona.

FACULTAD DE INGENIERIA U.N.A.M.
DIVISION DE EDUCACION CONTINUA

CURSOS ABIERTOS

XII CURSO INTERNACIONAL DE CONTAMINACIÓN DE ACUÍFEROS

MODULO III: MODELOS MATEMÁTICOS EN GEOHIDROLOGIA Y CONTAMINACIÓN DE ACUIFEROS

TEMA

MODELING SEA – WATER INTRUSION WITH OPEN BOUNDARY CONDITIONS

EXPOSITOR: DR. ADOLFO CHAVEZ RODRIGUEZ

PALACIO DE MINERIA
OCTUBRE DEL 2000

Modeling Sea-Water Intrusion with Open Boundary Conditions

by Francisco Padilla and Javier Cruz-Sanjulián[a]

Abstract

The present study concerns the application of a new numerical approach to describe the fresh-water/sea-water relationships in coastal aquifers. Essentially, a solution to the partial differential equation governing the regional motion of a phreatic surface and the resulting interface between fresh water and salt water is analyzed by a Galerkin finite-element formulation. A single-phase steady numerical model was applied to approximate, with simple triangular elements, the regional behavior of a coastal aquifer under appropriate sinks, sources, Neumann, outflow face, and open boundary conditions. On the one hand, outflow open boundaries at the coastline were not treated with other classical boundary conditions (Dirichlet or the outflow face approach), but instead with a formal numerical approach for open boundaries inspired in this particular case by the Dupuit approximation of horizontal outflow at the boundary. The solution to this numerical model, together with the Ghyben-Herzberg principle, allows the correct simulation of fresh-water heads and the position of the salt-water interface for a steeply sloping coast. Although the solutions were precise and do not present classical numerical oscillations, this approach requires a previous solution with Dirichlet boundary conditions at the coastline in order to find a good convergence of the solution algorithm. On the other hand, the same precise results were obtained with a more restrictive open boundary condition, similar in a way to the outlow face approach, which required less computer time, did not need a prior numerical solution and could be extended to different coastline conditions. The steady-state problem was solved for different hypothetical coastal aquifers and fresh-water usage through three types of numerical tests. Calculated fresh-water heads, interface positions and discharges show very precise results throughout the domain and especially at the coastline when compared to analytical, experimental, and numerically correct solutions. Therefore, interface positions, fresh-water heads, and discharges originating from the steady regional behavior of coastal aquifers can be precisely predicted by numerical modeling when open boundaries towards the sea are properly treated for the likely conditions of the coastline.

Introduction

Coastal aquifers are major sources of drinking water and agricultural irrigation in many countries. Nevertheless, sea-water intrusion into such aquifers is of great concern when assessing total amounts of available fresh water. Salt and fresh waters are miscible fluids. The salt concentration varies in a transition zone between fresh and salt ground waters. When fresh-water discharge across the coastline is relatively important, the zone of transition can be quite narrow in comparison with the overall thickness of the aquifer. For the sake of computational simplicity, this zone is usually considered as a sharp interface. In the case of aquifers of large horizontal extent, compared to their thickness, it may be assumed that the variations of the ground-water head in a vertical direction are so small that they can be ignored. Although this approach is far from being rigorous, it seems to provide satisfactory results when modeling the horizontal flow of fresh water by two-dimensional models of coastal aquifers with sea-water intrusion (Bear and Verruijt, 1987).

Several types of horizontal numerical models with a sharp interface approximation for coastal aquifers have been developed during recent years (Shamir and Dagan, 1971; Pinder and Page, 1977, Wilson and Sa da Costa, 1982; Verruijt, 1987; Ledoux et al., 1990; Essaid, 1990a and b; Huyakorn et al., 1996). These models consider two equations for the simultaneous flow of fresh water and salt water with a sharp interface between both liquids assumed to be immiscible. It is customary to solve the two sets of equations for transient problems involving an initially known interface or sea-water heads, and inflow or outflow amounts of salt water at the coastline. Both these types of data are difficult to measure in the field. The same goes for the need to know the thickness of the seepage face and the total and local discharges of fresh water from the coastal aquifer at the edge of the sea. These discharges are also very difficult to establish along the coastline of a two-dimensional aquifer whose fresh water flows horizontally. Therefore, the water table is often imposed at the coastline to sea level (Dirichlet boundary conditions) or the boundary is prescribed by a flux condition based for instance on

[a]Instituto del Agua, Universidad de Granada, Rector López Argueta s/n, 18071 Granada, Spain

Received April 1996, revised October 1996, accepted November 1996

head dependent leakance functions (Essaid, 1990b) or on analytical solutions like the more extended outflow face approach (Bear and Dagan, 1964; Huyakorn et al., 1996). It results in the well known limitations of the calculated depths of the fresh-water/salt-water interface near the coastline. These limitations are a direct consequence of using prescribed fresh-water heads or flux conditions at the coastline based on analytical solutions which do not always properly consider actual coastal aquifers with different types of coastlines, fresh-water recharges, and usages

In this paper, a steady two-dimensional vertically averaged finite-element model, based on the assumption of horizontal fresh-water flow, is essentially developed for unconfined coastal aquifers. The Ghyben-Herzberg principle was used to estimate the position of the sharp fresh-water/salt-water interface for the present single-phase numerical approach. Instead of other numerical models, outflow open boundaries at the coastline were treated with the help of recently developed open boundary conditions (Padilla et al., 1990; Padilla et al., in press).

On the one hand, the present open boundary conditions for sea-water intrusion problems were inspired from the Dupuit approximation of horizontal outflow at a coastline with a very steep coast. This allows the numerical model to consider in the solution procedure the fresh-water discharges and seepage conditions of this type of coastline. Numerical tests show that fresh-water heads and steady interface depths, as evaluated by the Ghyben-Herzberg principle, are correctly and precisely calculated by the model in the aquifer and in proximity to the coastline. Nevertheless, the solution algorithm GMRS employed did not prove very efficient in solving an elliptic problem of this type for the recently developed open boundary conditions

On the other hand, a much more efficient flux type boundary condition was found, showing identical results to the open boundary condition based on the Dupuit assumption, which was successfully applied and extended to several characteristics of the coastline For three different numerical tests, comparison of the results of application of this and other flux type boundary conditions with analytical, experimental, and numerically correct solutions shows only advantages in applying the latest numerical approach for this type of open boundary

Theoretical Model

Flow in phreatic coastal aquifers that have a large horizontal extent, compared to their thickness, may be assumed to have variations in the ground-water head in a vertical direction so small that they can be ignored. This assumption leads to the two-dimensional averaged equation of fresh-water flow in a horizontal plane. Additionally, by considering salt water in equilibrium with sea level and the existence of a sharp fresh-water/salt-water interface below a less dense fresh water, the two-dimensional equation (1) governing the motion of the phreatic surface in a coastal aquifer can be written as follows (Shamir and Dagan, 1971):

$$n_f \frac{\partial h}{\partial t} - n_s \frac{\partial s}{\partial t} = \frac{\partial}{\partial x}\left(K_{xx}(h-s)\frac{\partial h}{\partial x}\right) + \frac{\partial}{\partial x}\left(K_{xy}(h-s)\frac{\partial h}{\partial y}\right) + \frac{\partial}{\partial y}\left(K_{yx}(h-s)\frac{\partial h}{\partial x}\right) + \frac{\partial}{\partial y}\left(K_{yy}(h-s)\frac{\partial h}{\partial y}\right) + Q \qquad (1)$$

where, taking as reference the sea level (Figure 1), h is the fresh-water head (positive above sea level); s is the level of the salt-water interface (negative below sea level); n_f and n_s are the effective porosities for the movement of the phreatic surface and the interface, respectively; Q is the net source (positive) or sink (negative) from the surface of the aquifer in volumetric flow of water per surface unit; and K_{ij} is the hydraulic permeability tensor in the fresh-water zone.

For unconfined coastal aquifers, the Ghyben-Herzberg principle approximates the position of the salt-water interface in equilibrium with the sea-water level by the following relationship:

$$s = -\frac{\rho_f}{\rho_s - \rho_f} h \quad \text{if} \quad (s = -Gh) > p$$
$$s = p \quad \text{if} \quad (s = -Gh) \le p \qquad (2)$$

where $G = [\rho_f/(\rho_s - \rho_f)]$, ρ_f and ρ_s are the densities of fresh and salt waters, respectively; and p is the height of the impervious substratum of the aquifer (below or above sea level, corresponding to negative or positive values, respectively). In the case of phreatic coastal aquifers, the governing partial differential equation can be obtained by substituting (2) in (1) as follows:

$$(n_f + n_s G)\frac{\partial h}{\partial t} = \frac{\partial}{\partial x}\left(K_{xx}(h-s)\frac{\partial h}{\partial x}\right) + \frac{\partial}{\partial x}\left(K_{xy}(h-s)\frac{\partial h}{\partial y}\right) + \frac{\partial}{\partial y}\left(K_{yx}(h-s)\frac{\partial h}{\partial x}\right) + \frac{\partial}{\partial y}\left(K_{yy}(h-s)\frac{\partial h}{\partial y}\right) + Q \quad \text{if} \quad (s = -Gh) > p \qquad (3)$$

$$n_f \frac{\partial h}{\partial t} = \frac{\partial}{\partial x}\left(K_{xx}(h-p)\frac{\partial h}{\partial x}\right) + \frac{\partial}{\partial x}\left(K_{xy}(h-p)\frac{\partial h}{\partial y}\right) + \frac{\partial}{\partial y}\left(K_{yx}(h-p)\frac{\partial h}{\partial x}\right) + \frac{\partial}{\partial y}\left(K_{yy}(h-p)\frac{\partial h}{\partial y}\right) + Q \quad \text{if} \quad (s = -Gh) < p \qquad (4)$$

Thus, the mathematical model is represented by equation (3) when sea-water intrusion interacts vertically with fresh water, and by equation (4) otherwise, that is, when only fresh groundwater flow is vertically averaged. In other words, the position of the toe of the interface determines the domain of applicability of

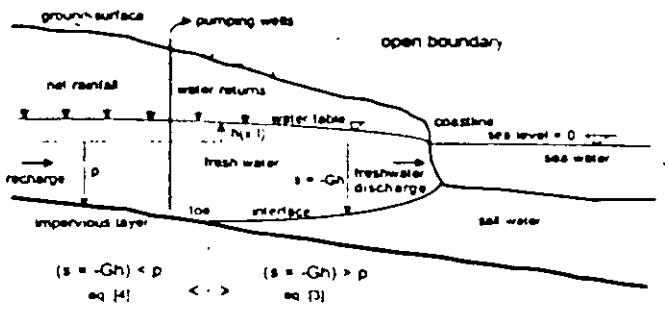

Fig. 1. Vertical schematic section of a phreatic coastal aquifer.

equation (4) where only fresh water can be vertically found, and of equation (3) where vertically there is both fresh water and salt water.

It is important to note that the above basic equations correspond to a classical regional model of sea-water intrusion in equilibrium with the sea-water regional level (Bear and Verruijt, 1987). What will not be classical are the boundary conditions that will be used to solve them numerically.

Boundary Conditions for Sea-Water Intrusion

When solving steady-state problems, several types of boundary conditions are possible on the boundaries $\Gamma = \Gamma_1 + \Gamma_2 + \Gamma_3 + \Gamma_4$ of the whole domain Ω. The proper choice of the type of boundary conditions must also take into account the type of problem in order to optimize the convergence, stability, and accuracy of the solution.

Prescribed Solutions (Dirichlet Boundary Condition)

Fresh-water heads can be imposed on the boundaries Γ_1, or even within the flow domain Ω, when these boundaries represent a continuous source of surface water (lakes, permanently flowing rivers, etc.).

$$h(x, y) = h_1 \qquad \text{on } \Gamma_1 \text{ or on parts of } \Omega \qquad (5)$$

Often the Dirichlet boundary condition is also prescribed on outflow open boundaries, like on the coastline of some sea-water intrusion models. This has considerable inconveniences (Bear and Verruijt, 1987). First, it prevents the Ghyben-Herzberg principle from correctly calculating the depths of the salt-water interface at equilibrium in the proximity of the coastline. Second, fresh-water discharges need to be known along the coastline—a very rare and almost impossible task—to allow the prescription of the sea level somewhere else off the coastline. Third, two transient partial differential equations—one for fresh water and another for salt water—need to be solved in order to give the main responsibility of the position of the interface to the unsteady movement of the salt water into the phreatic aquifer (Essaid, 1990a and b). In this last case, the classical model requires a knowledge of salt-water flux and initial salt-water heads along the coastline which are very unusual field data.

Prescribed Flux (Neumann Boundary Condition)

The flux of water can normally be prescribed on inflow boundaries Γ_2 with recharge of fresh water, that is, where entries of water coming from neighboring watersheds are well-known.

$$-\left(K_{xx}(h - s)\,\frac{\partial h}{\partial x}\right) n_x - \left(K_{yy}(h - s)\,\frac{\partial h}{\partial y}\right) n_y = q_2$$

$$\ldots \text{on } \Gamma_2 \qquad (6)$$

where: q_2 is the prescribed flux of fresh water, and (n_x, n_y) are the direction cosines of the normal pointing outwards to the boundary Γ_2. The natural condition is given for impermeable boundaries by the homogeneous version of equation (6), $q_2 = 0$. Neumann conditions can be applied to outflow boundaries when steady or transient ground-water discharges are known along the boundaries; however, these discharges are in fact rarely known.

Dirichlet boundary conditions (imposed fresh-water heads) must not substitute inflow or outflow boundaries unless the boundary represents a penetrating and continuous source of fresh water. Otherwise, the model is not correctly applied. In particular, outflow boundaries are better represented by outflow face or open boundary conditions as defined here below.

Prescribed Gradient or Head-Dependent Flux (Outflow Face Boundary Condition)

This head-dependent flux type boundary condition can take different forms, depending often on experience, numerical approximations, or analytical solutions for the hypothetical hydrogeological characteristics of the coast. The forms that this type of boundary condition take can change depending on the assumptions, but in general, the ground at the coast is considered to have a gentle slope and the gradient of the fresh-water head is prescribed indirectly.

A leaky, head-dependent boundary condition can be used to represent coastline boundaries (Essaid, 1990b) with the form

$$\text{flux} = \text{leakance}\,(h_3 - h) \qquad \text{on } \Gamma_3 \qquad (7)$$

The leakance term, as used by Essaid (1990a and b), does not have a very clear physical meaning as a boundary condition. For application purposes, the leakance is fixed together with the head value h_3 at the coastline. Thus, as the calculated head h in the aquifer changes, the flux across the boundary changes.

In another approach, it is assumed that the fresh-water discharges into the sea are determined by an analytical expression such as that used by Huyakorn et al. (1996) and derived by Bear and Dagan (1964).

$$-\left(K_{xx}(h - s)\,\frac{\partial h}{\partial x}\right) n_x - \left(K_{yy}(h - s)\,\frac{\partial h}{\partial y}\right) n_y =$$

$$-(K_{xx}h)\,n_x - (K_{yy}h)\,n_y \qquad \text{on } \Gamma_3 \qquad (8)$$

This equation is not very dissimilar to expression (7) and works numerically in an analogous way. The outflow face boundary condition is still rigorous for a nonlinear elliptic equation of this type, in the sense that the calculated head-dependent flux at the boundary is sufficient for the numerical model to converge towards the solution sought, thus evaluating the thickness of the seepage face for the correct fresh-water discharge at the coastline. Nevertheless, this outflow face approach has the obvious limitation of using a very specific solution (analytical or with a prescribed gradient), to assess the discharge at a coastline, as an extensive solution to actual aquifers with different coastal characteristics, fresh-water recharges, and water management.

Nonprescribed Flux (Open Boundary Condition)

In order to establish the feasibility of the so-called open boundary conditions (Padilla et al., 1990; Padilla et al., in press, Bear, 1972), it can be assumed that at permeable outflow open boundaries (Γ_4), the flux within the domain needs to be equal to the flux outside it. The latter can be described, for a steeply sloping coast, by the Dupuit approximation which considers horizontal flow and the interface position as also being horizontal in the proximity of the coastline

$$-\left(K_{xx}(h - s)\,\frac{\partial h}{\partial x}\right) n_x - \left(K_{yy}(h - s)\,\frac{\partial h}{\partial y}\right) n_y =$$

$$-K_{xx}(h - s)\left(\frac{\partial (h - s)}{\partial x}\right) n_x - \left(K_{yy}(h - s)\,\frac{\partial (h - s)}{\partial y}\right) n_y$$

$$\ldots \text{on } \Gamma_4 \qquad (9)$$

Nevertheless, a linear treatment of open boundary conditions is necessary in order to numerically find the correct solutions resulting from the ground-water discharges at the coastline as a consequence of the simulated conditions. For sea-water intrusion problems, the resulting open boundary condition becomes:

$$-\left(K_{xx}(h-s)\,\frac{\partial h}{\partial x}\right)n_x-\left(K_{yy}(h-s)\,\frac{\partial h}{\partial y}\right)n_y=$$

$$-\left(\frac{1}{2}\,K_{xx}\,\frac{\partial(h-s)^2}{\partial x}\right)n_x-\left(\frac{1}{2}\,K_{yy}\,\frac{\partial(h-s)^2}{\partial y}\right)n_y$$

$$\ldots\ \text{on}\ \Gamma_4 \qquad (10)$$

This kind of boundary condition is far from being rigorous and it can be totally monitored if treated linearly by the numerical resolution procedure and it is formally incorporated into the formulation and into the numerical solution schemes related to the finite-element method. This means that when the slope at the coast is quite steep, as in this particular case, the coastline can be treated with this kind of open boundary condition, and thus the fresh-water discharges and heads become part of the solution of the numerical model. Calculated fresh-water heads along and in the proximity of the coastline do not need to be the same as the sea-water level, and as a result, the thickness of the seepage face is determined. Hence, for example, a salt-water interface deeper than the sea-water level could occur at this coastline, as calculated by the Ghyben-Herzberg principle of equilibrium, as a consequence of calculated positive fresh-water heads resulting from the application of the numerical model when positive ground-water balances or discharges take place in the aquifer.

In order to avoid part of the above inconveniences encountered when modeling regional sea-water intrusion, neither initial salt-water heads, nor fresh-water and salt-water heads and flux need to be prescribed at this coastline. Instead, this kind of open boundary condition can be applied for a steeply sloping coast in numerical models describing sea-water intrusion in coastal aquifers

Finite-Element Approximation and Solution Strategy

For the steady-state problems treated in this particular research, a standard weighted residual approach with Galerkin type weighting functions is used to determine approximate solutions to equations (3) or (4) under the appropriate boundary conditions. In the finite-element method, the computational domain and the unknowns are represented on an irregular grid composed of a finite number of subdomains of simple geometrical shape, called the finite elements

More details of the involved finite-element formulation and how open boundary conditions are dealt with can be found in Padilla et al. (1990 and in press). It is worth noting that in order to formally incorporate open boundary conditions, all the elements of the domain having at least one node at the boundary will contribute to the term of the equation accounting for open boundaries in the finite-element formulation. Former research (Padilla et al., in press) showed that the application of open boundary conditions to linear hyperbolic and parabolic advection-diffusion flows in two dimensions, were much more stable and precise than when using the suggested Dirichlet boundary condition for tested analytical cases. Nevertheless, when solving essentially parabolic problems, the need for an increase in the required boundary conditions (Lapidus and Pinder, 1982) means that care must be taken to avoid sources of error such as excessively large elements and mesh anisotropy near the boundaries. In general, parabolic systems with open boundary conditions will be more strongly influenced by the above-mentioned sources of error.

In order to improve computing efficiency, we selected a linear element fulfilling the minimal global and local continuity requirement, the triangular first-order Lagrange element with three nodes (T3). This element permits analytical integration of the terms of the elementary weak form and suppresses the loop over the quadrature points, leading to a more efficient and better vectorization of the computer code (Secretan, 1991; Pickens et al., 1979). When considering point sources and sinks, the surface affected by the water injected or abstracted depends on the type of element used in the numerical discretization. In the case of linear triangular elements, this surface is equal to 1/3 of the surface of the elements connected to the nodes where the sources and sinks are prescribed.

The algorithm of the solution for the numerical system of equations is the generalized minimal residual GMRES (Saad and Schultz, 1986). This iterative method has been applied successfully to nonlinear systems (Brown, 1987). It does not need computation and storage of the global matrix, and therefore it is very suitable for mesh refinement.

Numerical Simulations

Conditions of Simulation

Some theoretical implications of the proposed conditions of simulation are worth noting. The present numerical applications consider simulation conditions for the steady-state version of equations (3) or (4), depending on the presence of sea-water intrusion in the simulated aquifer. The relevant equation would be in every case nonlinear and mainly elliptic (Lapidus and Pinder, 1982). Nevertheless, a strong nonlinearity is associated with equation (3) which governs the fresh-water movement associated with sea-water intrusion.

As we have already mentioned, there are three types of appropriate boundary conditions at the edge of the sea for the considered numerical simulations of an actual phreatic coastal aquifer. Neumann boundary conditions for inflow boundaries when fresh-water flux of recharge coming from neighboring watersheds is well-known, outflow face boundary conditions for coasts with fairly gentle slopes, and open boundary conditions for coasts with steep slopes. Other external sources and sinks of fresh water could be infiltration from net rainfall and irrigation returns, as well as abstractions from pumping wells. When using these types of boundary conditions as well as sources and sinks of fresh water, the total water balance in the aquifer will correspond to the total fresh-water discharge of the aquifer. This fresh-water discharge will be distributed along the coastline if the model correctly simulates the ground-water processes.

It is important to note that elliptic partial differential equations require more rigorous boundary conditions than hyperbolic and parabolic ones. Moreover, the present quasilinear problem enhances the difficulties associated with the application of open boundary conditions on outflow boundaries (Padilla et al., 1990 and in press). Therefore, for this type of problem, special care must be taken when using the numerically soft open boundary condition on the coastline, instead of others numerically more severe like the Dirichlet or the flux type boundary

conditions. This is because very deformed or anisotropic meshes, as well as excessively large elements at the relevant boundary, are particularly likely to add to the existing numerical errors.

Another result of these difficulties was that the considered simulations did not have a unique solution for different initial conditions used in the iterative algorithm of the solution of the steady-state elliptic problem. Instead, the simulations needed to be executed in two steps. The first step calculates the solution for Dirichlet boundary conditions imposed at the sea level on the coastline. The second step takes the solution of the first step as the initial condition for the iterative algorithm of solution of a different numerical model where open boundary conditions are used at the coastline instead. Results proved to be satisfactory for the correct fresh-water discharges at the coastline of the phreatic aquifer. All this can be verified by the numerical tests which are described below.

Steady Sea-Water Intrusion in a Rectangular Phreatic Aquifer with Precipitation

To verify the precision and stability of this formal finite-element approach for open boundaries in regional sea-water intrusion problems, a simple numerical test has been conceived. The aim of this test is to find out whether the present numerical approach is correct for assessing fresh-water discharges at the coastline and, as a direct consequence, to correctly predict sea-water intrusion and the regional behavior of coastal phreatic aquifers.

The present numerical test consists of a coastal aquifer 2 km long and 1 km wide. The aquifer is surrounded by impervious boundaries except at the left-hand side (1 km long) where the coastline is at sea level. An impervious substratum under the aquifer is 20 meters below sea level. The saturated medium has an effective porosity of 20% and a hydraulic conductivity of 0.0045 m/s. Simulation conditions consider that fresh water comes only from net precipitation, 2 hm^3/year (2×10^6 m^3/year or 3.17×10^{-8} $m^3/m^2 \cdot s$), which is homogeneously distributed over the surface of the phreatic aquifer. Obviously, as regards a steady-state solution, the fresh-water discharge at the edge of the sea is known for a coast which slopes steeply. This discharge (6.342×10^{-5} $m^3/m \cdot s$) can be distributed homogeneously along the coastline, 1 km long, and will correspond to the same total amount of net precipitation over the surface of the aquifer (2×10^6 m^3/year). With regard to the spatial finite-element discretization of the aquifer, a symmetric mesh of simple triangular elements has been conceived (Figure 2). Refinement of the mesh is enhanced at the coastline in order to allow the model to precisely calculate ground-water discharges. The fresh water from net rainfall was introduced as a recharge by unit of surface at the interior nodes of the spatially discretized aquifer.

Three different types of boundary conditions were considered at the coastline in order to verify the feasibility and the precision attained by the present numerical approach. The first boundary condition considered the generally recommended prescribed solution (Dirichlet boundary condition) at sea level (taken at 0 meters). The second boundary condition used a prescribed flux of water (Neumann boundary condition) corresponding to the total amount of the discharge known for this particular case. The third simulation condition treated the open boundary of the coastline with the above defined open boundary condition. Comparison of the results from these three types of simulations would obviously show the main differences between, first, the classical modeling approach where the model fails to predict correct ground-water heads and discharges in proximity to the coastline; second, the numerically correct solution where the amounts of the discharge are well-known, as in this particular test for a steep coast; and third, the solution obtained when using open boundary conditions at this coastline for the normal cases where the discharges of fresh water are not known but can formally become part of the numerical solution.

The classical and first modeling approach (with Dirichlet boundary conditions) fails to predict correct ground-water heads and discharges at the coastline for steady conditions. In fact, this kind of solution is by definition not correct when modeling regional and horizontal ground-water flow. The computed fresh-water discharges are zero at the coastline because of the prescribed fresh-water heads at sea level and consequently no thickness available for fresh-water discharges can be justified following the Ghyben-Herzberg principle of equilibrium along the coastline. Obviously, the total water discharge along the coastline needs to be equal to the fresh-water balance, if known beforehand.

A numerically correct solution (second approach) is when the local discharges along the coastline are prescribed as boundary conditions of the Neumann type because they could be known a priori. This second approach is only possible here due to the conceived characteristics of the present numerical test (net rainfall over a rectangular aquifer surrounded by impermeable boundaries excepting at the steeply sloping coast).

Model results for open boundary conditions (third approach) are theoretically considered the best because neither fresh-water heads nor discharges need to be prescribed along the coastline for the model to calculate them precisely as part of the

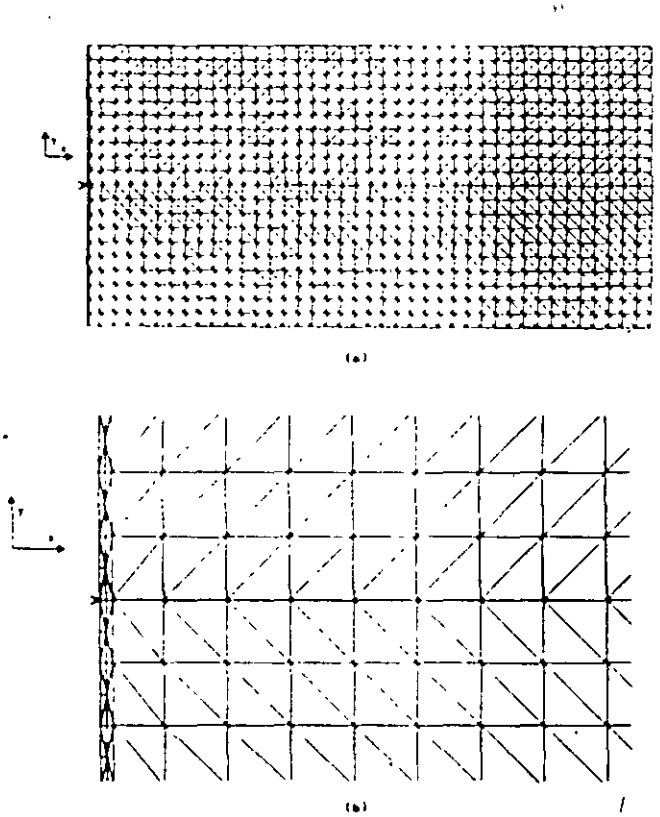

Fig. 2. Spatial finite-element discretization of a rectangular coastal aquifer 2 km long and 1 km wide (a). Detail of discretization in the proximity of the coastline (b).

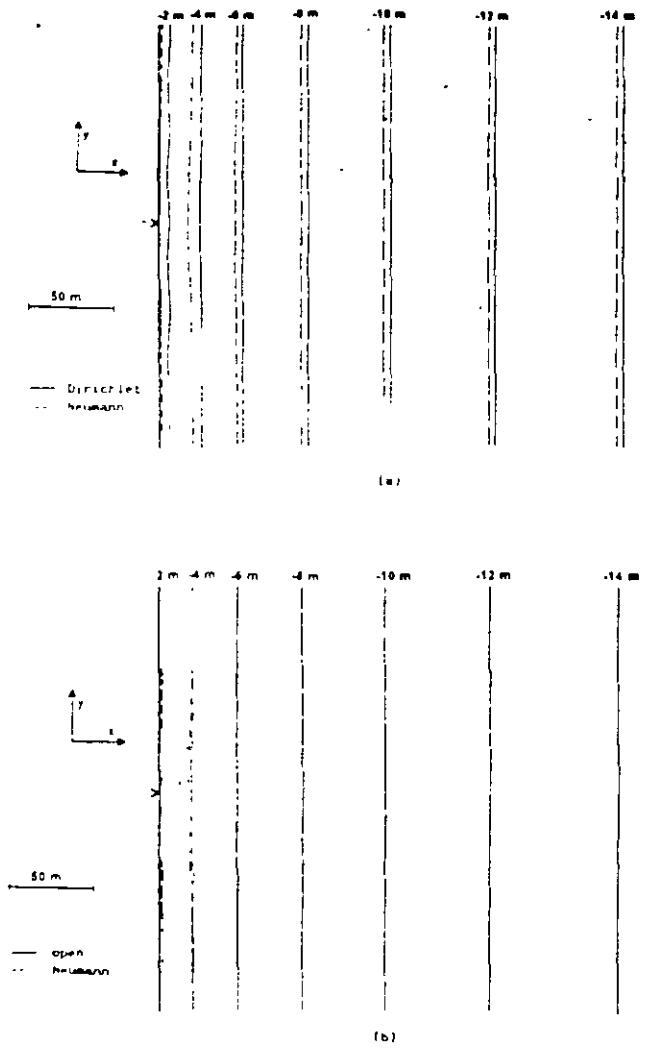

Fig. 3. (a) Map near the coast of steady-state sea-water intrusion in a rectangular phreatic aquifer for a net precipitation rate of 2 hm^3/year. Interface position for Neumann and Dirichlet boundary conditions at the coastline. (b) Map near the coast of steady-state sea-water intrusion in a rectangular phreatic aquifer for a net precipitation rate of 2 hm^3/year. Interface position for Neumann and open boundary conditions at the coastline

numerical solution. Obviously, a satisfactory comparison between the results of the second and third approaches, as well as between the previously known fresh-water balance and the total discharge, calculated from local discharges by the third approach, would verify its validity and the precision reached by the adequate treatment as an open boundary of a steeply sloping coast.

Figure 3 shows the map of fresh-water/salt-water interface positions near the coast as calculated by the model in relation to sea level for the three selected types of boundary conditions. Figure 4 shows a cross-sectional view of the above-mentioned simulated results as compared to the corresponding analytical solution of Strack (1976) for horizontal flow. Significant differences can be observed between the solutions calculated when applying Dirichlet boundary conditions and the solutions of the numerically correct approach when the boundary condition takes into account the known discharge (Neumann boundary condition). A comparison of the results clearly shows that an excellent precision is obtained when using open boundary conditions on open boundaries at a steeply sloping coast in sea-water intrusion numerical models. It is also important to note that for the present spatial discretization, results obtained when using open boundary conditions are numerically more stable than those obtained when using Neumann boundary conditions, especially in the proximity of the coastline (oscillations are present in the numerical results when applying Neumann boundary conditions). In this respect, all the numerical simulations, when applying open boundary conditions, gave a total error of less than 0.01% for the total fresh-water discharge at the coastline.

Nevertheless, this kind of problem requires a prior solution with Dirichlet boundary conditions at the coastline to be used as an initial solution for the iterative algorithm solving the problem with open boundary conditions at the coastline. This procedure permits the iterative method to attain convergence towards the correct numerical solution. To sum up, we need to solve the problem twice in two different steps, the first with Dirichlet and the second with open boundary conditions at the coastline. The computer time for the second numerical solution to converge is variable and depends on each case but, in general, it is longer than for the first.

When verifying whether the outflow face boundary condition was suitable to simulate precisely the above-mentioned numerical test, identical results to those found when using open boundary conditions were obtained with a more rigorous boundary condition of the flux type defined by the head-dependent equation (8) multiplied by a factor of ¼. These results are very encouraging because the convergence of the numerical algorithm is greatly improved, and there is no longer a need for a previous simulation with Dirichlet boundary conditions before applying open boundary conditions at a steeply sloping coast. Further justification concerning this ¼ factor on the head-dependent equation (8) for its use as a new outflow face boundary condition for this particular problem will be subject to the two other numerical tests and the concluding remarks.

Steady Sea-Water Intrusion in a Rectangular Phreatic Aquifer with a Pumping Well

This numerical test deals with sea-water intrusion in a rectangular unconfined aquifer with a pumping well near the coastline. This test case is identical to that used by Huyakorn et al. (1996) to verify the outflow face boundary condition on their

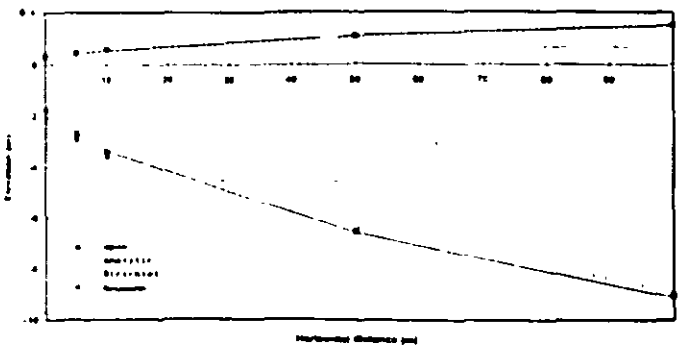

Fig. 4. Cross-sectional view near the coast of steady-state sea-water intrusion in a rectangular phreatic aquifer for a net precipitation rate of 2 hm^3/year. Fresh-water heads and interface positions for analytical solutions as well as numerical results for Neumann, Dirichlet, and open boundary conditions at the coastline.

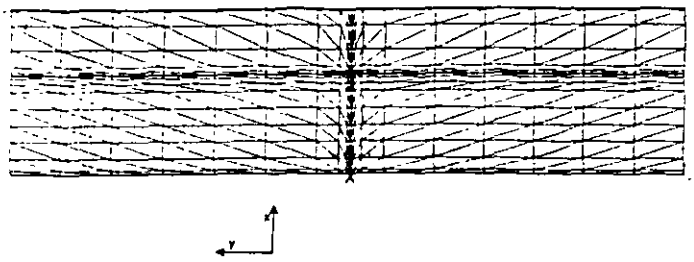

Fig. 5. Nonuniform grid discretization of a rectangular coastal aquifer 4 km of coastline and 1 km inland for a pumping well at 0.6 km from the coast.

sharp interface finite-element model. Upconing of underlying salt water occurs when the well withdraws part of the fresh-water recharge. Strack (1976) derived a two-dimensional analytical solution which was based on the assumption of horizontal flow and an areally semi-infinite aquifer. We have rigorously followed Huyakorn's guidelines concerning the application of this numerical test and used the same parameters and main conditions of simulation. In this respect, a nonuniform triangular grid was used on a rectangular aquifer with 4 km of coastline and 1 km wide. The following parameters were used in verifying the numerical model

Inland fresh-water recharge	1 m^2/d (at $x = 1000$ m, -2000 m $\leq y \leq 2000$ m)
Well pumping rate	400 m^3/d
Well location	($x = 600$ m, $y = 0$ m)
Hydraulic conductivity	70 m/d
Depth from sea level to aquifer base	20 m

The nonuniform grid for the whole domain, consisting of 399 nodes (21 rows by 19 columns), has an identical node density and similar pattern of discretization to the symmetric upper half plane of Huyakorn's application (see Figure 5). The only difference is that we used a finer element near the coast in order to properly consider open boundary conditions at the coastline. Constant fresh-water influx was specified at the inland boundary ($x = 1000$ m). Other boundaries were considered impermeable. Steady simulated profiles of the water table and the interface along the x axis are illustrated in Figure 6 together with the analytical solution.

It must be noted that in order to make the comparisons, the analytical and calculated fresh-water heads must be identical at the edge of the sea (this value being a constant in the analytical solution of Strack). The main difference from the results of the Huyakorn's model, which employs the outflow face boundary condition for a gently sloping coast, lies in the thickness of the seepage face at the edge of the sea. Even though the present simulations are more correct for very steep coasts, we find the comparison of results excellent. This is mainly because, first, solutions are very precise and nonoscillatory when applying the Galerkin finite-element method; second, a very coarse grid was used, and third, there was no need for mesh refinement and streamline upwind or upstream weighting methods in order to avoid numerical oscillations or to improve the precision of results as in Huyakorn's model. At the same time, we found that by using the outflow face boundary condition [head-dependent flux equation (8)] in our present spatial discretization, which only has a column of smaller elements near the coast, nonoscillatory solutions can be simulated (Figure 7). For this reason, we found no justification for using smearing methods and mesh refinement to improve the results of the Galerkin finite-element approach (Huyakorn et al., 1996). Thus, accurate results and nonoscillatory solutions can be found with a head-dependent flux boundary condition if a smaller element is employed in the proximity of the coastline. What is not quite sure is whether the outflow face boundary condition, as expressed by equation (8), is suitable to represent precisely actual seepage faces and interface positions at the edge of the sea and in the proximity of the coastline. The following experiment and numerical test will help us to clarify this uncertainty.

Steady Sea-Water Intrusion for a Hele-Shaw Experiment

In order to establish the possibilities of predicting seepage faces near a coast in which sea-water intrusion problems exist, two Hele-Shaw experiments (Bear and Dagan, 1964) were selected for simulation with the present steady-state numerical approach. These experiments were analyzed in the past by other

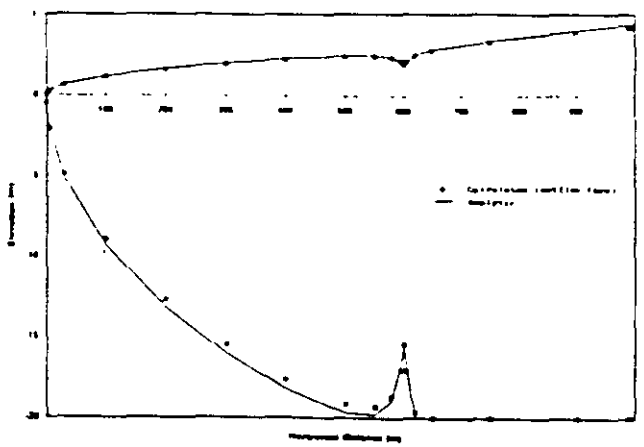

Fig. 6. Steady-state profiles of the interface and water table simulated for a coastal unconfined aquifer with a pumping well. Analytical and calculated results for open boundary conditions at the coastline.

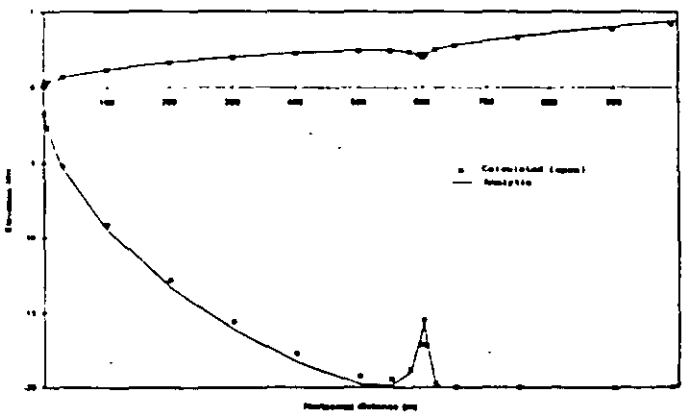

Fig. 7. Steady-state profiles of the interface and water table simulated for a coastal unconfined aquifer with a pumping well. Analytical and calculated results for outflow face boundary conditions at the coastline.

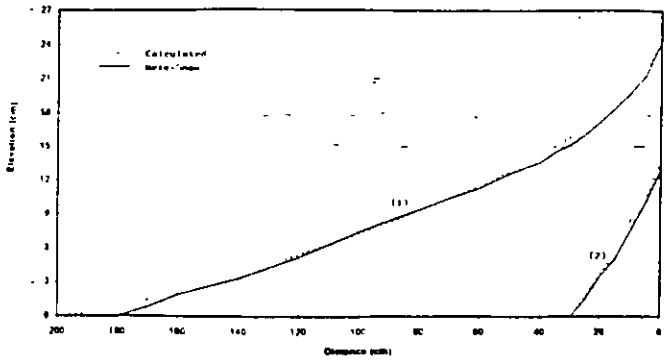

Fig. 8. Hele-Shaw experimental observations and simulated results of the steady-state interface position for fresh-water specific discharges of (1) 3.9 cm^2/s, and (2) 19.1 cm^2/s.

numerical models (Shamir and Dagan, 1971; Essaid, 1990a and b).

For this purpose, we have chosen two steady conditions of the Hele-Shaw experiments realized by Bear and Dagan (1964). The experiments were made for a profile of a hypothetically confined layer (27 cm thick and 200 cm long) covered up to the edge of the outflow boundary by an impermeable and horizontal bed located at the salt-water level and near a coast assumed to be almost horizontal. In these two experiments, the fresh-water/salt-water interface attains fixed positions, respectively, which are maintained by two different constant fresh-water discharges (3.9 cm^2/s and 19.1 cm^2/s). The pertinent data for the present steady numerical simulations are.

Thickness of the saturated layer	27 cm
Hydraulic conductivity	0.69 m/s
Salt-water density	1.029 gr/cm^3

Shamir and Dagan (1971) failed to predict steady-state experimental solutions presumably using a boundary condition similar to the head-dependent equation (8) as suggested in their research. Thus, they used the steady experimental values of the interface positions as initial conditions to improve their transient simulations. The calculated interface positions showed important discrepancies with the experimental observations. Concerning the steady-state simulations of Essaid (1990a and b), a head-dependent boundary condition such as that defined by the expression (7) was used for a high leakance value (3.3 s^{-1}) and a zero head in the overlying aquifer. With this nonjustifiable and adjustable boundary condition, their results are acceptable for the observed positions of the first experiment, but not for the second. Essaid also recognizes the difficulties encountered in realistically representing the seepage boundary condition at the outflow face.

As a consequence of the results of our research, open boundary conditions are not adequate for correctly modeling the seepage face of these experiments. Instead we used an outflow face boundary condition as the one defined by the head-dependent equation (8), suitable for gently sloping coastlines, multiplied in this case by a factor of $(1/2)^{1/2}$. Figure 8 illustrates experimental and simulated steady interface positions corresponding to the two selected Hele-Shaw experiments. It should be noted that the experimental observations are taken graphically from the illustrations of the experiments published by Shamir and Dagan (1971). We find that the factor $(1/2)^{1/2}$ multiplying the head-dependent equation (8) explains both experimental observations quite well.

We found justification for this factor $(1/2)^{1/2}$ after assuming that fresh water will obviously remain immiscible with salt water outside the outflow boundary too. Thus, if a parabolic Dupuit approximation of horizontal flow is made between the outflow boundary and the distance (L) where the fresh-water table will be zero outside the boundary, the averaged fresh-water thickness ($G\bar{h}$) outside the boundary can be written as follows:

$$G\bar{h} = G[h^2 - (h^2 - h_L^2)(x/L)]^{1/2} =$$

$$G[h^2 - (h^2 - 0)(1/2)]^{1/2} = Gh(1/2)^{1/2}$$

where h is the fresh-water head at the outflow open boundary.

Thus, this type of boundary condition for the unconfined aquifer can be defined in the x direction by

$$q_x = -\left(K_{xx} G\bar{h} \frac{\partial h}{\partial x}\right) n_x = -\left(K_{xx} Gh(1/2)^{1/2} \cdot \frac{h - h_L}{L}\right) n_x = -\left(K_{xx} Gh(1/2)^{1/2} \frac{h}{L}\right) n_x$$

which after assuming that Gh = L (Bear and Verruijt, 1987),

$$q_x = -[(1/2)^{1/2} K_{xx} h]\, n_x$$

The above development probably explains the good results obtained when using this last expression as a head-dependent outflow face boundary condition when simulating the conditions of equilibrium of the two Hele-Shaw experiments.

Concluding Remarks

The present numerical approach to describe regional sea-water intrusion problems in phreatic aquifers is mainly based on the development and application of open boundary conditions for steeply sloping or subvertical coasts. The nonlinear problem can be treated linearly for this type of coast after considering that the Dupuit approximation is appropriate in its proximity, where the position of the interface becomes horizontal and equal to its position on the boundary, as calculated by the numerical model for the correct fresh-water discharges into the sea. Two numerical tests, one with precipitation and another with a pumping well near the coast, show very stable and precise results throughout the domain and especially in the proximity of the coastline when compared to analytical and numerically correct solutions. Thus, fresh-water heads as well as the position of the fresh-water/salt-water interface at equilibrium, as predicted by the Ghyben-Herzberg principle, can be precisely calculated in order to obtain correct fresh-water discharges along subvertical or very steep coasts. Nevertheless, open boundary conditions are very loose conditions in solving nonlinear elliptic problems. As a consequence, the present numerical approach required a prior solution with Dirichlet boundary conditions at sea level to be used as an initial solution to the iterative algorithm solving the steady problem with open boundary conditions at the coastline. The computer time of convergence of the second numerical solution is variable and often longer than the first numerical solution.

A more rigorous outflow face boundary condition was found that gives identical results to those obtained when using open boundary conditions. This outflow boundary condition was obtained when using a factor of ½ on a head-dependent

equation (8) defined as an analytical solution for subhorizontal or gently sloping coasts. These results are very encouraging because the convergence of the numerical algorithm is greatly improved and there is no longer any need to realize a previous simulation with Dirichlet boundary conditions before applying open boundary conditions at steep coasts. Moreover, this factor (¼) could represent the transition from horizontal to vertical coasts. An expression for the transition between both types of coasts would be very useful as a boundary condition in numerical modeling. The factor (¼) was found after deriving some expressions for the transition between these two types of coasts or types of outflow boundaries; nevertheless, we have no definitive numerical, analytical, and experimental verifications so far. This is the object of our ongoing research.

Correct numerical results concerning the two Hele-Shaw experiments on a steady interface for constant fresh-water discharges showed a factor of $(1/2)^{1/2}$ which multiplied the outflow face boundary condition defined by the head-dependent equation (8). In this respect, we have derived a justification that seems to us to be adequate. Nevertheless, transient numerical simulations for these same experiments would be of great interest in order to verify whether the described outflow face boundary condition can improve the transient solutions of recent two-phase numerical models for actual sea-water intrusion problems.

Acknowledgments

This study has been prepared with partial financial support of the CICYT Science and Technology Inter-Ministerial Commission, Spain (AMB94-0611 Project).

References

Bear, J. 1972. Dynamics of Fluids in Porous Media. American Elsevier, New York.

Bear, J. and G. Dagan. 1964. Moving interface in coastal aquifers. J. Hydraul. Div. Am. Soc. Civ. Eng. v. 99, No. HY4, pp. 193-215.

Bear, J. and A. Verruijt. 1987. Modeling Groundwater Flow and Pollution. Reidel, Dordrecht.

Brown, P. N. 1987. A local convergence theory for combined inexact-Newton/finite-difference projection methods. SIAM J. Numer. Anal. v. 24, pp. 410-434.

Essaid, H. I. 1990a. A multilayered sharp interface model of coupled freshwater and saltwater flow in coastal systems: Model development and application. Water Resources Research. v. 26, no. 7, pp. 1431-1454.

Essaid, H. I. 1990b. The computer model Sharp, a quasi-three-dimensional finite difference model to simulate freshwater and saltwater flow in layered coastal aquifer systems. U.S. Geological Survey, Water-Resources Investigations Report 90-4130.

Huyakorn, P. S., Y. S. Wu, and N. S. Park. 1996. Multiphase approach to the numerical solution of a sharp interface saltwater intrusion problem. Water Resources Research. v. 32, no. 1, pp. 93-102.

Lapidus, L. and G. Pinder. 1982. Numerical Solution of Partial Differential Equations in Science and Engineering. Wiley & Sons, New York.

Ledoux, E., S. Sauvagnac, and A. Rivera. 1990. A compatible single-phase/two-phase numerical model: 1. Modeling the transient salt-water/fresh-water interface motion. Ground Water. v. 28, no. 1, pp. 79-87.

Padilla, F., M. Leclerc, and J.-P. Villeneuve. 1990. A formal finite element approach for open boundaries in transport and diffusion groundwater problems. Int. J. Numerical Methods in Fluids. v. 11, pp. 287-301.

Padilla, F., Y. Secretan, and M. Leclerc. (in press.) On open boundaries in the finite element approximation of two-dimensional advection-diffusion flows. Int. J. Numerical Methods in Engineering.

Pickens, J. F., R. W. Gillham, and D. R. Cameron. 1979. Finite element analysis of the transport of water and solutes in tile-drained soils. J. Hydrology. v. 40, pp. 243-264.

Pinder, G. F. and R. H. Page. 1977. Finite element simulation of salt water intrusion on the South Fork of Long Island. In: W. G. Gray, G. F. Pinder, and C. A. Brebbia (editors): Finite Elements in Water Resources. Pentech Press, London. v. 2, pp. 51-69.

Saad, Y. and M. Schultz. 1986. GMRES: A generalized minimal residual algorithm for solving non symmetric linear systems. SIAM J. Sci. Stat. Comput. v. 7, pp. 856-869.

Secretan, Y. F. 1991. Contribution à la résolution des équations de Navier-Stokes compressibles par la méthode de éléments finis adaptatifs: développement d'un élement simple. Thèse de doctorat présentée à l'Ecole Polytechnique Fédérale de Zurich, Suisse. Thèse EPFZ No. 9528.

Shamir, U. and G. Dagan. 1971. Motion of the seawater interface in coastal aquifers: A numerical solution. Water Resources Research. v. 7, no. 3, pp. 644-657.

Strack, O. D. L. 1976. A single-potential solution for regional interface problems in coastal aquifers. Water Resources Research. v. 12, no. 6, pp. 1165-1174.

Verruijt, A. 1987. A finite element model for interface problems in groundwater flow. In: B. Schrefler and R. W. Lewis (editors), Microcomputers in Engineering Applications. John Wiley, New York, pp. 251-271.

Wilson, J. L. and A. Sa da Costa. 1982. Finite element simulation of a saltwater-freshwater interface with interface toe tracking. Water Resources Research. v. 18, pp. 1078-1080.

FACULTAD DE INGENIERIA U.N.A.M.
DIVISION DE EDUCACION CONTINUA

CURSOS ABIERTOS

XII CURSO INTERNACIONAL DE CONTAMINACIÓN DE ACUÍFEROS

MODULO III: MODELOS MATEMÁTICOS EN GEOHIDROLOGIA Y CONTAMINACIÓN DE ACUIFEROS

TEMA

EFFECTIVE PARAMETER OPTIMIZATION OF GROUND – WATER MODEL CALIBRATION

EXPOSITOR: DR. ADOLFO CHAVEZ RODRIGUEZ
PALACIO DE MINERIA
OCTUBRE DEL 2000

Effective Parameter Optimization for Ground-Water Model Calibration

by T. N. Olsthoorn[a]

Abstract

This paper shows that the Levenberg-Marquardt method, modified to limit the parameter update steps to within a specified range, effectively optimizes a set of parameters in a ground-water model. In doing so it performs better than more complicated conjugate gradient algorithms.

The method has been applied to the synthetic ground-water problem of Carrera and Neuman (1986b), which has been used previously to test calibration method performance. The descent of the error criterion and the simultaneous approach of the parameters to their optimum values are smooth, both with perfect and erroneous head observation data.

It is shown that least-squares optimization can be done effectively in a simple manner and that it can be easily integrated with practical ground-water modeling. No changes have to be made to the model code. This ease of implementation is emphasized by the fact that all modeling presented here was done using an ordinary spreadsheet program on a PC.

Introduction

Model calibration is one of the most intriguing problems of modern model-based ground-water hydrology. It is considered difficult, and consequently much literature exists on the subject [see for instance the reviews of Yeh (1986) and Carrera (1988)] The theoretical development has culminated in three sound and extensive papers by Carrera and Neuman (1986a, b, c).

However, because of its complexity, most practitioners still rely on "trial and error" methods throughout the world. Though such methods exploit the insight of the hydrologist, they are neither exhaustive nor reproducible. A sound and comprehensible method that is also easy to implement may help to more systematically and reproducibly optimize ground-water models. Development of such a method is the goal of this paper.

The problem of optimal parameterization of a model, i.e. which parameters to choose and how many, is an important problem by itself, but is not discussed here For this aspect, the user should refer to excellent papers by Yeh and Yoon, 1981; Sun and Yeh, 1985; and Carrera and Neuman, 1986a, b, c. Here we concentrate on the core of calibration, i.e. the optimization of model parameters by minimization of some error criterion, and that in an effective and simple manner

To prove its effectiveness the sample synthetic model first used by Carrera and Neuman (1986c) to show their calibration performance is recalculated and compared.

The algorithm is outlined and described, as is its implementation in daily modeling practice. The method is implemented without changes to existing ground-water models.

Optimization Methodology

In this paper the theoretical background of ground-water model parameter optimization is taken for granted, because it has been profoundly developed by Carrera and Neuman (1986a). From it, we simply conclude that the various theoretical approaches, such as Bayesian or maximum-likelihood, all lead to a problem formulation in a least-squares fashion (e.g., Peck et al., 1988). We will therefore focus on this least-squares problem which is the minimization of a squared, and possibly weighted, error vector.

Without loss of generality, we focus on ground-water heads and a stationary flow situation. The deviations (errors) f_j are in general the weighted difference between the calculated head $\hat{h}_j$ and the measured head h_j at each observation well j:

$$f_j = \sqrt{\omega_j}\,(\hat{h}_j - h_j) \qquad j \in \{1 \ldots m\}$$

Here ω_j is the user-specified weight. (The root disappears in the error criterion defined below.) Choosing weights is not discussed in this paper. The hydrologist has to find his/her own rationale according to the studied ground-water system and the distribution and quality of the available observa-

[a]Amsterdam Water Supply, Vogelenzangseweg 21, 2114 BA Vogelenzang, The Netherlands.

Received August 1993, revised April 1994, accepted April 1994.

tions. In the examples presented here, all weights are taken equal to 1.

Let us define the error criterion F to be minimized as follows:

$$F = \underline{f}^T \underline{f} = \sum_{j=1}^{m} \omega_j (\hat{h}_j - h_j)^2$$

A single underscore denotes a vector, a double underscore a two-dimensional matrix. The superscript T denotes the transpose of a vector or a matrix.

The error criterion F depends on the n model parameters to be optimized. They are contained in the parameter vector $\underline{p}$. Parameters may include anything influencing the heads at observation points.

To arrive at a valid solution the problem must be regularized; the number of parameters must be limited and be substantially fewer than the number of observations (Yeh and Yoon, 1981; Sun and Yeh, 1985).

An effective step to further regularize an optimization problem is to work with the logarithm of physical parameters to be optimized (conductivities and transmissivities). The parameters are thus guaranteed to remain positive during the iterative calibration process. Furthermore, it makes changes to different parameters comparable, as a fixed change made to logarithmic parameter values is equivalent to a certain relative change of the actual parameters, irrespective of their magnitude

Because neither the error criterion F, nor the heads $\underline{h}$ vary linearly with the parameters $\underline{p}$ (e.g., Carrera and Neuman, 1986b), a Taylor expansion may be used as an approximation of the gradient of vector $\underline{g}$ of F within the (log)-neighborhood $\underline{\delta p}$ of the current (log)-parameter vector $\underline{p}$:

$$\underline{g}(\underline{p} + \underline{\delta p}) = \underline{g}(\underline{p}) + \underline{\underline{H}}(\underline{p}) \cdot (\underline{\delta p}) + O(\| \underline{\delta p} \|)$$

$\underline{\underline{H}}$ is the $(n \times n)$-Hessian matrix, the second derivative of F at $\underline{p}$. Ignoring the higher order terms, denoted by $O(..)$, and choosing a $\underline{\delta p}$ such that the resulting approximate gradient vanishes, we obtain

$$\underline{\underline{H}}(\underline{p}) \cdot (\underline{\delta p}) = -\underline{g}(\underline{p})$$

which is the standard multidimensional Newton-Raphson relation to find the minimum of a function, in this case of F. This equation can be solved for $\underline{\delta p}$ if $\underline{\underline{H}}(\underline{p})$ and $\underline{g}(\underline{p})$ are given and if $\underline{\underline{H}}(\underline{p})$ is nonsingular. The updated parameter vector then becomes $(\underline{p} + \underline{\delta p})$

Because in least-squares minimization the function F has the special form $\underline{f}^T \underline{f}$, it can be differentiated to obtain expressions for the gradient $\underline{g}$ and the Hessian matrix $\underline{\underline{H}}$ (see, for instance, Jennings and McKeown, 1992)

$$\underline{g} = 2 \underline{\underline{J}}^T \underline{f}$$

$$\underline{\underline{H}} = 2(\underline{\underline{J}}^T \underline{\underline{J}} + \underline{\underline{B}})$$

where $\underline{\underline{J}}$ is the Jacobian $(m \times n)$-matrix (see list of symbols), and $\underline{\underline{B}}$ is the f_j-weighted sum of the m second-order derivative matrices of the deviations f_j (see list of symbols and Jennings and McKeown, 1992, p. 336). $\underline{\underline{B}}$ represents the nonlinearity of the Newton-Raphson equations:

$$(\underline{\underline{J}}^T \underline{\underline{J}} + \underline{\underline{B}}) \cdot (\underline{\delta p}) = -\underline{\underline{J}}^T \underline{f}$$

Note that the first matrix in $\underline{\underline{H}}$, $\underline{\underline{J}}^T \underline{\underline{J}}$ is positive (semi)-definite because of its form. This is generally not the case for second matrix in $\underline{\underline{H}}$, $\underline{\underline{B}}$. But $\underline{\underline{B}}$ becomes zero when the calculated heads match the observed heads exactly, i.e., when $f_j = 0$ for all j. $\underline{\underline{B}}$ is therefore normally neglected, yielding the standard Gauss-Newton relation.

Neglecting $\underline{\underline{B}}$ implies that when the parameters are far from their optimum or when the model is incapable of matching the observations closely enough, $(\underline{\underline{J}}^T \underline{\underline{J}})$ is only a crude approximation of the Hessian matrix $\underline{\underline{H}}$ and may yield incorrect parameter updates if applied in an unconstrained manner.

III-Conditioning and Parameter Updates

The unconstrained Gauss-Newton parameter update formula

$$\underline{\delta p} = -(\underline{\underline{J}}^T \underline{\underline{J}})^{-1} \underline{\underline{J}}^T \underline{f}$$

demands nonsingularity of the matrix $\underline{\underline{J}}^T \underline{\underline{J}}$. This is difficult if not impossible to guarantee under practical circumstances.

An effective method to deal with this kind of problem stems from Levenberg and Marquardt (e.g., Jennings and McKeown, 1992). They add a positive definite diagonal matrix $\mu \underline{\underline{I}}$ to $\underline{\underline{J}}^T \underline{\underline{J}}$ to obtain:

$$\underline{\delta p} = -(\underline{\underline{J}}^T \underline{\underline{J}} + \mu \underline{\underline{I}})^{-1} \underline{\underline{J}}^T \underline{f}$$

where $\underline{\underline{I}}$ is the $(n \times n)$-identity matrix, and μ is a scalar > 0.

$\underline{\underline{J}}^T \underline{\underline{J}}$ is positive semidefinite due to its form. Hence its eigenvalues λ are subjected to $\lambda_{max} \geq \lambda_i \geq \lambda_{min} \geq 0$. By adding the matrix $\mu \underline{\underline{I}}$ to $\underline{\underline{J}}^T \underline{\underline{J}}$ its condition number, i.e. $\lambda_{max}/\lambda_{min}$, changes to $(\lambda_{max} + \mu)/(\lambda_{min} + \mu)$. For $\mu > 0$ this guarantees all the new eigenvalues to be positive and so prevents nonsingularity. It further shifts the condition number towards unity and so improves the solution process.

The larger μ is chosen, the larger $\mu \underline{\underline{I}}$ becomes relative to $\underline{\underline{J}}^T \underline{\underline{J}}$. $\underline{\delta p}$ will then become smaller and smaller, while at the same time pointing more and more into the direction of steepest descent. Hence any positive value of μ results in a step $\underline{\delta p}$ valued between zero and that resulting from unconstrained Gauss-Newton updating and pointing into a direction between that of the steepest descent and that dictated by the unconstrained Gauss-Newton formula.

A neat and robust descending minimization is obtained by limiting the parameter vector change $\underline{\delta p}$ at each step to within a certain trust hypersphere (with radius Δ, around the current parameter vector), each time Gauss-Newton suggests parameter update steps beyond it. From the above it follows that this can be done by increasing μ as needed. At the same time, the farther the Gauss-Newton calculated parameter vector update is beyond the hypersphere, and hence the more the actual step size $\underline{\delta p}$ is limited by increasing

μ, the more it will point into the direction of the steepest gradient.

Jennings and McKeown (1992, p. 344) state that this method has as a disadvantage that the Gauss-Newton equation has to be solved for several μ-values during each iteration. However, this is of no importance for the calibration of ground-water models, where the computational work to solve the Gauss-Newton equation is almost negligible compared to that of a single model run. This is due to the usually small dimensionality of the parameter vector, typically in the order of 5 to 50, as compared to that of the ground-water model, for which tens of thousands of equations may have to be solved simultaneously. Moreover, μ varies only gradually from iteration to iteration (see algorithm), so that in practice only about two such matrix inversions are needed per parameter vector update.

The LMS Algorithm and Its Implementation

We abbreviate the algorithm to "LMS" (Levenberg-Marquardt with limited step size). It is described below and outlined in Figure 1.

The algorithm first takes user-specified values of ϵ, Δ, μ, and *StopStep*.

- ϵ is the relative change to which each parameter is subjected in order to calculate the Jacobian (see below). It should be small as it measures the sensitivity of F at the current parameter vector. Five percent was applied here, but because logarithmic parameters are used, $\epsilon = \log(1.05)$.
- Δ is the radius of the trust hypersphere, the maximum stepsize for the parameter update vector $\underline{\delta p}$ in any iteration. It should not be too large, while too small a value would needlessly slow down the convergence. We choose 50% of its current length. Because of the logarithmic parameters $\Delta = \log(1.5)$.
- *StopStep* is the parameter vector update stepsize $|\underline{\delta p}|$, used as a criterion to stop the algorithm. We choose *StopStep* = 0.0001.
- μ is the multiplication factor of the identity matrix in $\underline{\underline{J}}^T\underline{\underline{J}} + \mu\underline{\underline{I}}$. Any small value will be good, because the algorithm adjusts it continuously in the inner loop. Once a proper value is found, it changes only slightly from one iteration to the next.

The above values work well for the examples in this paper as for the big MODFLOW ground-water model in use by the Amsterdam Water Supply.

The algorithm is given in mathematical terms in order to keep it as clear and compact as possible. It has an outer and an inner loop. The outer loop defines the iterations; the inner loop only limits the parameter vector update $\underline{\delta p}$. The outer loop first calculates the Jacobian $\underline{\underline{J}}$ and the gradient of the error criterion $\underline{g}$. The inner loop then calculates the parameter update vector $\underline{\delta p}$. While the outer loop decreases μ at each iteration in order to shift the algorithm towards a pure Gauss-Newton algorithm, the inner loop increases μ until the length of the update vector is less than the radius of the trust hypersphere Δ. The outer loop then obtains the update vector $\underline{\delta p}$ from the inner loop and uses it to compute the new parameter vector $\underline{p} + \underline{\delta p}$. If the length of the parameter update $\underline{\delta p}$ is less than the value *StopStep*, used as convergence criterion, the final solution is obtained. Otherwise a next iteration step is carried out.

Calculation of the Jacobian

The Jacobian can be computed in several ways. Because it is not the focus of this paper, the most simple method is adopted here. (For more advanced methods see, for instance, Carrera and Neuman, 1986b; Sykes, 1985; and Sun and Yeh, 1985.)

The Jacobian, as computed here in the outer loop, requires n + 1 runs of the ground-water model, n being the number of parameters to be optimized. The first run is done with the current parameter vector. In the other n runs the value ϵ is added to each parameter in turn. Each time the ground-water model is run to compute the heads at the observation points. This yields n + 1 vectors, each with m calculated heads.

From these vectors the measured heads are subtracted. These deviations are then multiplied by user specified weights, $\sqrt{\omega}$, if weights are used at all. This way n + 1 deviation vectors $\underline{f}_i = (\sqrt{\omega})^T(\underline{h}_i - \underline{h})$ are obtained; $i = 0 \ldots n$. The index i denotes the perturbated parameter. $i = 0$ denotes the current, unperturbated parameter vector.

The Jacobian, the m × n-matrix that describes the sensitivity of the error criterion F towards parameter alterations, is now calculated, column by column, from:

$$\underline{J}_i = \partial\underline{f}/\partial p_i = (\underline{f}_i - \underline{f}_0)/\epsilon \qquad i = 1 \ldots n$$

with ϵ the size of the parameter alteration (the same for all log-transformed parameters).

Implementation

Ease of implementation is demonstrated by the fact that all the calculations for this paper, including the finite-

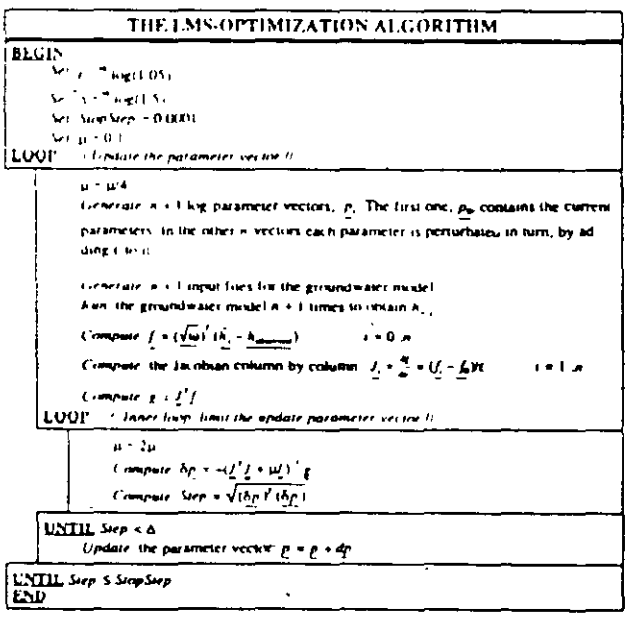

Fig. 1. The LMS algorithm (see description in text).

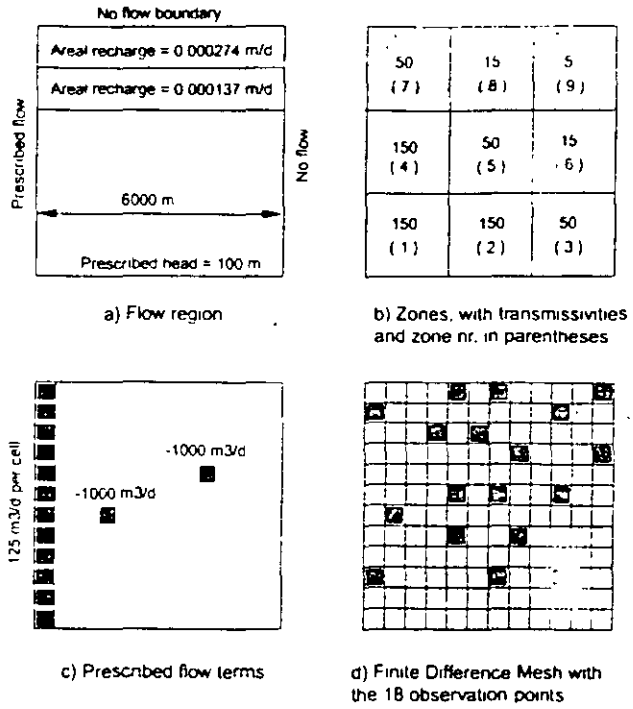

Fig. 2. Synthetic model according to Carrera and Neuman (1986) as used in this paper.

difference model itself (e.g., Olsthoorn, 1985), were implemented in an ordinary Lotus 1-2-3 spreadsheet program on a PC.

For more complicated models, a spreadsheet may be used to implement just the optimization algorithm and work in conjunction with a separate ground-water model. The 80×80 matrix capacities of Lotus 1-2-3, for example, limit the Jacobian to this size, allowing a maximum of 80 observations and theoretically 80 parameters to be optimized simultaneously.

For the 37,000 cell MODFLOW implemented groundwater model of the Amsterdam dune area, the mathematical matrix package MATLAB is used to implement the optimization algorithm. The algorithm given in Figure 1 translates on an almost one to one basis into MATLAB and is just as compact.

Optimization of model parameters in MATLAB, in conjunction with a model such as MODFLOW, works as follows:

- In each iteration MATLAB generates the $n + 1$ parameter vectors needed to compute the Jacobian. It writes these to a file and starts a FORTRAN program.
- This FORTRAN program reads these parameter vectors and generates a new input file for MODFLOW, one parameter vector at a time. For each vector it runs MODFLOW. Each time after MODFLOW has finished it collects the heads at the observation points from the MODFLOW output and writes these to a file. Finally $n + 1$ vectors with calculated heads at observation points are thus obtained.
- MATLAB then regains control. It reads the calculated heads and uses them to compute the Jacobian matrix and the parameter update vector.
- As long as convergence has not been achieved, MATLAB calculates new parameter vectors, and repeats the described loop.

Effectiveness of the Method

The effectiveness of the LMS method will be compared with the approach of Carrera and Neuman (1986b, c) who applied several conjugate gradient methods (see Table 1) to minimize the error criterion F for the synthetic example shown in Figure 2. The goal of the optimization is to find simultaneously the transmissivities of the nine shown zones, starting from different initial values, for the stationary case and assuming all flow data known. First we assume the available head data of the 18 observation points to be exact (i.e., equal to the heads at the observation points calculated by the model with the "true" transmissivity values, see Figure 2).

Table 1 compares the performance of our simple LMS algorithm with that of the various conjugate gradient algorithms used by Carrera and Neuman (1986b), in simultaneously calibrating the nine zonal transmissivities of the given problem. It shows that the LMS method converges in all cases and with fewer iterations.

Figure 3 shows the course of the error criterion and that of five of the nine transmissivities during our optimization runs. In all cases the error criterion, expressed as $\sqrt{F}$, is reduced to about 0.0001 m in a smooth manner. Furthermore, the final transmissivities are independent of the initial values and were equal to the "true" values within at least two decimals. [Note that the course of the error criterion in Figure 2 can be directly compared with Figures 9 and 10 on page 221 in Carrera and Neuman (1986b)].

Important is the behavior of the algorithm in the more practical case, where heads are corrupted with error. Carrera and Neuman (1986c, p. 230) present the calculated transmissivities for the same initial values but with Gaussian error with a standard deviation of $\sigma = 1$ m added to the true head values. The same exercise was carried out here; its results are given in Table 2.

Table 2 shows that negligible differences exist between the final transmissivities found for the various initial values,

Table 1. The Number of Iterations Required to Simultaneously Optimize the Nine Zonal Transmissivities in Figure 2

Method	*Ts = 1*	*Ts = 10*	*Ts = 100*	*Ts = 200*
F	>39	86	Failed	>80
B	>60	53	Failed	Failed
P	Failed	Failed	Failed	Failed
F-B	59	51	51	>39
LMS	55	31	32	41

Four optimization runs were made using uniform, but different initial transmissivities [Ts(m^2/d)], "Failed" means that no convergence down to the error criterion occurred within 100 iterations. The upper four rows have been copied from Carrera and Neuman (1986b, p. 220). The last row shows the results of the LMS algorithm used here. F = Fletcher-Reeves; B = Broydon; P = Fletcher-Powell; F-B = joint F and B. LMS = Levenberg-Marquardt + limited step length.

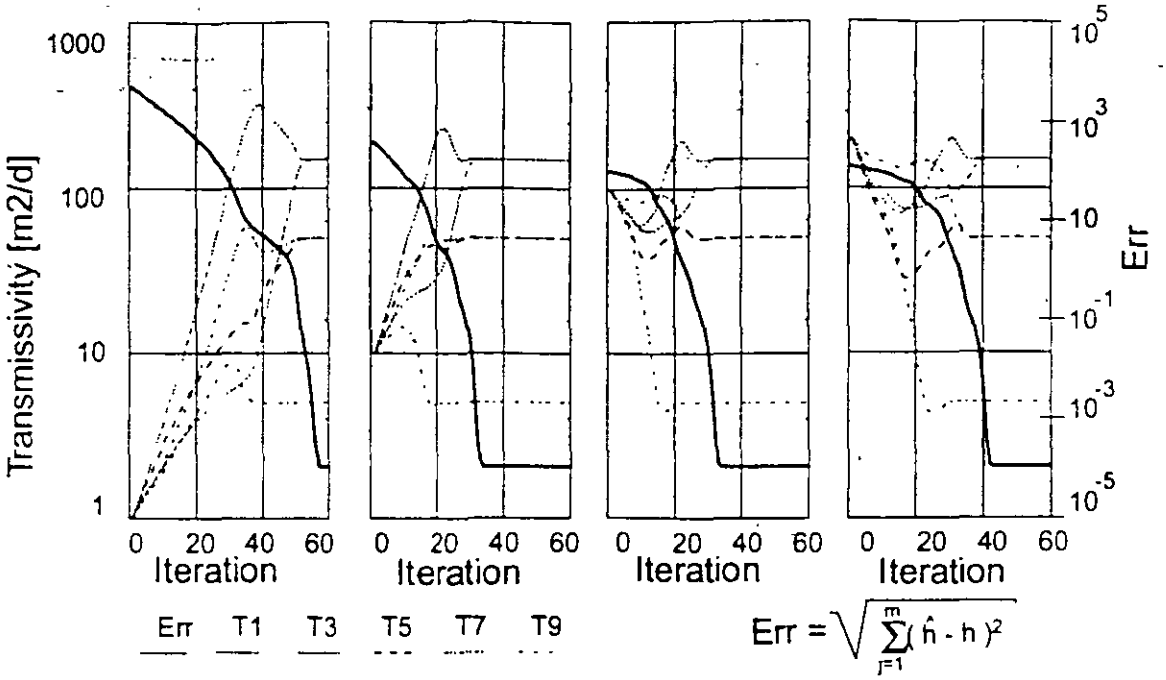

Fig. 3. Course of the error criterion and the indicated transmissivities during optimization of the model in Figure 2 by the LMS algorithm, starting from four different uniform initial transmissivities.

as was the case with Carrera and Neuman (1986c). The differences between the results of Carrera and Neuman (last column in Table 2) and the LMS algorithm used here, are attributed to different errors at the individual observation points. The individual errors used by Carrera and Neuman (1986c) are unknown to us, just the overall standard deviation of the 18 observation points is the same, i.e., Gaussian with $\sigma = 1$ m. From this we conclude that the LMS has effectively the same results as Carrera and Neuman, but it does so in less iterations.

Figure 4 shows the behavior of the LMS algorithm during the optimization of the nine transmissivities with uniform initial transmissivities of 100 m^2/d and a Gaussian error with $\sigma = 1$ m (see column 5 of Table 2). Clearly, about 30 iterations were needed. The figure further shows the size of the parameter update vector. In accordance with the algorithm, its value is limited to the user-set maximum of $|dp| \leq \log(1.5) = 0.176$. When the optimum is approached, this stepsize is reduced automatically by the algorithm (Figure 1).

Figure 5 shows the performance of the algorithm in the case that areal recharge is optimized together with the nine transmissivities. This is one parameter more than Carrera and Neuman (1986) calibrated. Perfect observations have been used to prove the retrieval of the original values. Initial values for all transmissivities are 100 m^2/d. Carrera and Neuman (1986c) used two areal recharge values in their model: 0.274 and 0.137 times 0.001 m/d (see Figure 2a). We used as start values 0.274 and 0.137 times x, where x = 0.0015 m/d and optimized x (with optimal value 0.001) together with the nine transmissivities. Figure 5 shows that the 10 parameters are optimized within about 30 iterations.

Table 2. Optimized Transmissivities When the 18 Head Values Have a Gaussian Error with Standard Deviation $\sigma = 1$ m, Using the LMS Optimization Algorithm and Uniform Initial Transmissivities [Ts (m^2/d)]

Zone	*True T*	*Ts = 1*	*Ts = 10*	*Ts = 100*	*Ts = 200*	*Ts = 100*
1	150	104	104	104	109	148
2	150	288	288	288	288	177
3	50	39.1	39.1	41	39.1	19.3
4	150	170	170	170	170	154
5	50	50.2	50.2	50.2	50.2	50.3
6	15	17.3	17.3	17.3	17.3	16.6
7	50	45.9	48.2	45.9	45.9	53.3
8	15	15.5	15.5	15.5	15.5	15.0
9	5	4.9	4.9	4.9	4.9	4.9
Carrera	—	71	54	57	90	57
LMS	—	55	32	30	40	—

The last column shows the results of Carrera and Neuman, 1986c, p. 230. The difference with our results is due to different errors at individual observation points

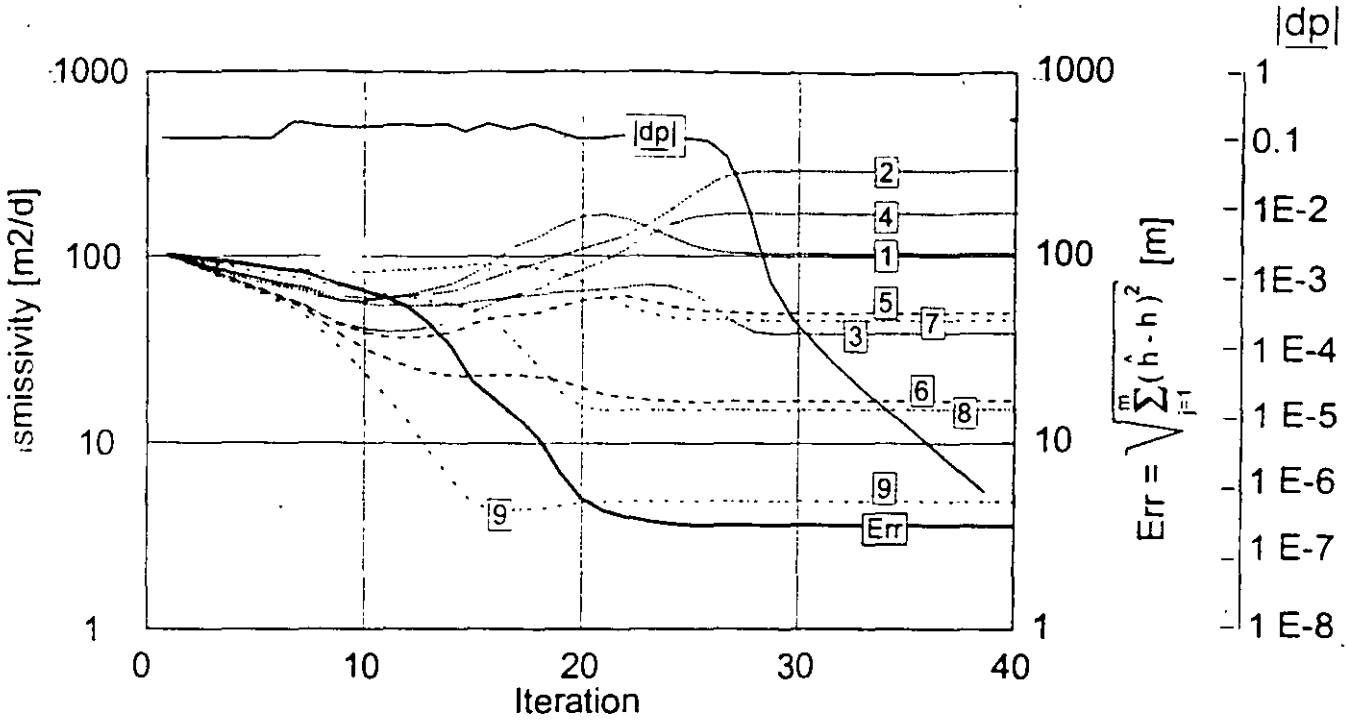

Fig. 4. Course of the error criterion and the nine simultaneously optimized zonal transmissivities (Figure 1, Table 2), starting with uniform initial values (100 m^2/d) and with measurements corrupted with a Gaussian error of $\sigma = 1$ m. Also shown is the limited log-parameter vector step size $|\underline{\delta p}|$ that is limited by the LMS algorithm.

Conclusions

The goal of this paper is the development of a sound, comprehensible, and easily implementable method to enable systematic parameter optimization in daily groundwater practice. This paper puts forward the Levenberg-Marquardt algorithm augmented by a preset limitation of the length of the parameter update vector (LMS).

The synthetic problem first used by Carrera and Neuman (1986a, b, c) has been applied to compare the method with existing optimization algorithms. The LMS method was shown to behave smoothly, reproducibly, and to perform computationally better than more sophisticated conjugate gradient approaches used by, among others, Carrera and Neuman (1986). The method is easy to implement because it is simple and no changes are made to existing model codes. It is independent of the (groundwater) model, and may be used in other disciplines as well.

It is hoped that practitioners are encouraged to make more use of parameter optimization for ground-water model calibration, instead of just relying on trial and error methods.

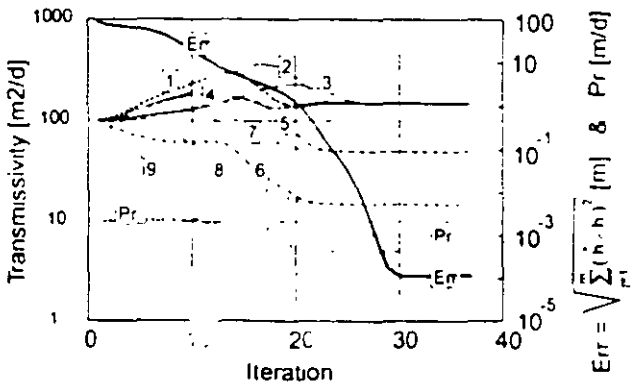

Fig. 5. Simultaneous optimization of nine transmissivities together with precipitation, denoted by Pr (= areal recharge in Figure 2a). Uniform initial transmissivities of 100 m^2/d are used. Precipitation is expressed as x times the numbers 0.274 and 0.137 shown in Figure 2a. The factor x is optimized, its initial value is 0.0015 m/d, its optimal value 0.001 m/d.

List of Symbols

$\{\}^T$	T as superscript means transpose of vector or matrix.
$\underline{\{\}}, \underline{\underline{\{\}}}$	Single underscore denotes vector, double underscore, matrix.
i	Parameter index, $\{1, \ldots, n\}$.
j	Observation well index, $\{1, \ldots, m\}$.
n	Number of parameters.
m	Number of observation wells.
$\hat{h}_j$, h_j	Computed head, measured head.
f_j	Deviation at observation point $f_j = \sqrt{\omega_j}(\hat{h}_j - h_j)$.
ω_j	Weight, in this paper $\omega_j = 1$, $j \in \{1, \ldots, m\}$.
F	Error criterion:

$$\underline{f}^T \underline{f} = \sum_{j=1}^{m} f_j^2 = \sum_{j=1}^{m} \{\omega_j (\hat{h}_j - h_j)^2\}.$$

$\underline{p}, \underline{\delta p}$ ($n \times 1$) — (log)-parameter vector and its update from one iteration to the next.

ϵ Preset, log-parameter perturbation to calculate gradient $\underline{g}$ of F numerically and compute the Jacobian.

Δ Maximum size of log parameter update $\underline{\delta p}$ in any iteration.

$\underline{\underline{J}}, \underline{\underline{J}}^T$ ($m \times n$)-Jacobian matrix and its ($n \times m$)-transpose:

$$\underline{\underline{J}} = \begin{bmatrix} \frac{\partial f_1}{\partial p_1} & \cdots & \frac{\partial f_1}{\partial p_i} & \cdots & \frac{\partial f_1}{\partial p_n} \\ \cdots & \cdots & \cdots & \cdots & \cdots \\ \frac{\partial f_j}{\partial p_1} & \cdots & \frac{\partial f_j}{\partial p_i} & \cdots & \frac{\partial f_j}{\partial p_n} \\ \cdots & \cdots & \cdots & \cdots & \cdots \\ \frac{\partial f_m}{\partial p_1} & \cdots & \frac{\partial f_m}{\partial p_i} & \cdots & \frac{\partial f_m}{\partial p_n} \end{bmatrix}$$

$\underline{g}$ ($n \times 1$)-gradient of F, with elements $[(\partial F)/(\partial p_i)]$.

$\underline{\underline{H}}$ ($n \times n$)-Hessian matrix of F, with elements $[(\partial^2 F)/(\partial p_k \partial p_l)]$.

$\underline{\underline{I}}$ ($n \times n$)-identity matrix.

μ Levenberg-Marquardt coefficient, scalar > 0.

$\underline{\underline{B}}$ $\sum_{j=1}^{m} f_j V^2 f_j$, where $V^2 f_j$ is the ($n \times n$)-matrix whose coefficients are $[(\partial^2 f_j)/(\partial p_k \partial p_l)]$, $k, l \in 1, \ldots n$. So $\underline{\underline{B}}$ is the sum of m ($n \times n$)-matrices, of which the j-th represents the second derivative of the deviation f_j with respect to the parameters, weighted by the deviation f_j itself.

References

Carrera, J. and S. P. Neuman. 1986a. Estimation of aquifer parameters under transient and steady state conditions: 1. Maximum likelihood method incorporating prior information. Wat. Res. Res. v. 22, no. 2, pp 199-210.

Carrera, J. and S. P. Neuman. 1986b. Estimation of aquifer parameters under transient and steady state conditions. 2. Uniqueness, stability and solution algorithms. Wat. Res. Res. v. 22, no. 2, pp. 211-227.

Carrera, J. and S. P. Neuman. 1986c. Estimation of aquifer parameters under transient and steady state conditions: 3. Application of synthetic and field data. Wat. Res. Res. v. 22, no. 2, pp. 228-242.

Carrera, J. 1988. State of the art of the inverse problem applied to the flow and solute transport equations. In: Custodio, E. et al. (eds.), Groundwater Flow and Quality Modelling. D. Reidel Publ. Company. pp. 549-583.

Jennings, A. and J. J. McKeown. 1992. Matrix Computation. John Wiley and Sons, Chichester. ISBN 0-471-93527-1.

Olsthoorn, T. N. 1985. The power of the electronic worksheet. Modeling without special programs. Ground Water. v. 23, no. 3, pp. 381-390.

Peck, A. et al. 1988. Consequences of Spatial Variability in Aquifer Properties and Data Limitations for Groundwater Modelling Practice. IAHS Publ 175, IAHS Press, Wallingford, UK. ISBN 0-947571-61-2.

Sun, N. Z. and W. W. Yeh. 1985. Identification of parameter structure in groundwater inverse problem. Wat. Res. Res. v. 21, no. 6, pp. 869-883.

Sykes, J. F. 1985. Sensitivity analysis for steady state groundwater flow using adjoint operators. Wat. Res. Res. v. 21, no. 3, pp. 359-371.

Yeh, W. W. and Y.S. Yoon. 1981. Aquifer parameter identification with optimum dimension in parameterization. Wat. Res. Res. v. 17, no. 3, pp. 664-672.

Yeh, W. W. 1986. Review of parameter identification procedures in groundwater hydrology: The inverse problem. Wat. Res. Res. v. 22, no. 2, pp. 95-108.

FACULTAD DE INGENIERIA U.N.A.M.
DIVISION DE EDUCACION CONTINUA

CURSOS ABIERTOS

XII CURSO INTERNACIONAL DE CONTAMINACIÓN DE ACUÍFEROS

MODULO III: MODELOS MATEMÁTICOS EN GEOHIDROLOGIA Y CONTAMINACIÓN DE ACUIFEROS

TEMA

MODELING A COMPLEX MULTI – AQUIFER SYSTEM: THE WATERLOO MORAINE

EXPOSITOR: DR. ADOLFO CHAVEZ RODRIGUEZ
PALACIO DE MINERIA
OCTUBRE DEL 2000

Modeling a Complex Multi-Aquifer System: The Waterloo Moraine

by P.J. Martin[a,b] and E.O. Frind[a]

Abstract

The Regional Municipality of Waterloo in Ontario, Canada (population 250,000) depends on ground water for most of its water supply. The ground water is extracted from the Waterloo Moraine, an extensive and complex glacial aquifer system extending over a 400 km^2 area. A methodology is being developed to inventory the ground water resource, to define its susceptibility to contamination, and to create the basis for optimal management and protection strategies. A key component of this methodology is a three-dimensional conceptual hydrogeologic model based on the geologic characteristics of the multiple-aquifer Moraine system. The steps in the development of the model include screening of the large database, interpretation and interpolation of the data to define the variable hydrostatigraphy and to generate consistent hydraulic conductivity functions, and model calibration. The numerical basis is a fully three-dimensional finite element model that provides flexibility and adaptability in representing the natural boundaries, the highly irregular stratigraphy, and the numerous wellfields. The model has the capability to automatically find the location of the water table consistent with given recharge and pumping conditions, and to direct recharge from low-permeability areas to higher-permeability areas. Capture zones generated by the model are found to be highly sensitive with respect to the geologic structure, in particular the presence or absence of windows in the aquitard units. Professional judgment is found to be an essential component of the modeling process.

Introduction

The Regional Municipality of Waterloo, comprising the cities of Kitchener, Waterloo, and Cambridge, Ontario, with an urban population of about 250,000, derives about 90% of its water supply from ground water. The water is extracted from a complex multi-aquifer system of glacial origin, the Waterloo Moraine, which extends over approximately 400 km^2. Although the Moraine has historically provided a plentiful supply of excellent water with little need for coordinated exploration, the dramatic growth of the region in recent decades has provided a motivation for obtaining, as a basis for sustainable use, a sound understanding of this vital resource, its capacity, and its susceptibility to contamination.

Therefore, the region is conducting an extensive research program to inventory the ground water resource and to delineate wellhead protection areas. From earlier studies of the numerous individual wellfields within the Moraine, it was clear that a key component of the program must be a conceptual geologic model of the entire complex system. The model would integrate the extensive but fragmented database, represent the connection between the many components of the system, and provide a link between the wellfields and the corresponding recharge areas. Because future wellhead protection zones will lie for the most part within urban and suburban areas, reliability is essential.

This paper describes the methodology used to develop the Waterloo Moraine model and to overcome the challenges raised by the extraordinary complexity of the glacial aquifer system. It also discusses some of the key characteristics of the system revealed by the model, including the controlling influence of the model structure on the capture zone predictions. The same methodology is currently also being applied in the study of other aquifer systems in Ontario.

Review of Aquifer Modeling Literature

Aquifer modeling has experienced an explosive growth within the last two decades. We will briefly review some recent literature relevant to flow and capture zone modeling of complex three-dimensional ground water flow systems, focusing on three key aspects that arise in this context: (1) the importance of the geologic structure, (2) parameter estimation and model calibration; and (3) techniques for the delineation of three-dimensional capture zones.

The importance of the geologic structure is convincingly demonstrated in a classic paper by Fogg (1986), who describes ground water flow in a complex sandstone aquifer consisting of many discontinuous bodies of sands, silts, and clays. He found that flow is not so much controlled by the hydraulic conductivity of the more permeable units, but by their continuity and interconnectedness, particularly in the vertical direction. He concludes that geological insight and interpretation are crucially important, and that indeed a conceptual model of the system based only on hydraulic data (for example, by contouring transmissivity data from pumping tests) would have been incorrect and misleading. He also noted

[a]Department of Earth Sciences, University of Waterloo, Waterloo, Ontario, Canada N2L 3G1. E-mail: frind@uwaterloo.ca

[b]Now at Waterloo Hydrogeologic Inc. E-mail: pmartin@flowpath.com

Received May 1996, accepted December 1997

that for complex aquifer systems the three-dimensional representation is important since the vertical interconnectedness would be lost in a two-dimensional model. He further found calibration with respect to heads in a three-dimensional model to be difficult since heads are not necessarily sensitive to the degree of hydraulic connection. Looking at the same problem from a different angle, Anderson (1989) points out the use of hydrogeologic facies models to delineate large-scale trends in heterogeneity and to provide input into ground water flow and transport models.

The subject of parameter estimation (also known as inverse modeling) and model calibration has been explored by numerous authors. Poeter and Hill (1997) give an overview of the state of the art and summarize the requirements and benefits of the approach. The inherent difficulty of inverse modeling is brought out by, among others, Poeter and Hill (1996) in a generic study involving a heterogeneous aquifer, which showed that optimizing the hydraulic parameters can lead to unrealistic results, but that these can be used to advantage to develop a better conceptual model. A similar approach was used by d'Agnese et al. (1996) in calibrating a three-layer regional model, the authors concluded that the problem of nonuniqueness is never completely eliminated, but that substantial constraints can be developed on the basis of the geologic framework. The same conclusion was reached by Olsthoorn and Kamps (1996) who used an automatic inverse routine to calibrate a large-scale three-dimensional finite difference aquifer model, and found that the most important role of the inverse model was to allow the identification of unrealistic parameters. Optimal calibration was also applied to a regional quasi-three-dimensional finite element model by Leijnse and Pastoors (1996), the approach was successful because the number of parameters to be optimized was restricted to about 10, resulting in a severely simplified conceptual model. In an insightful paper, Young et al (1996) describe the development of a three-dimensional aquifer model for a complex aquifer system containing a TCE plume, finding that an earlier application of an automatic inverse technique had produced misleading results, even though the calculated error was low. In the same vein as Fogg (1986), these authors stress the importance of a realistic three-dimensional conceptual model based on geologic judgment, making a convincing case for the selection of a finite element model to allow accurate representation of thin deformed layers. A finite element model along with trial-and-error calibration was also used by Mergia and Kelly (1994) in modeling a regional aquifer system.

There is also an extensive body of literature on the topic of well capture zone delineation techniques, but interest in three dimensions has arisen only recently. Comprehensive overviews of two-dimensional and three-dimensional analytical solutions for steady-state capture zones in homogeneous aquifer systems are given by Kinzelbach et al. (1992) and Schafer (1996). For more complex systems, the standard method is by tracking particles upgradient from a well to the water table, thus defining the area on the ground surface that contributes the recharge to the well. The semianalytical method developed by Pollock (1988) for rectangular grids is widely used for this purpose. Kinzelbach et al. (1992) point out that for complex aquifer-aquitard systems, the zone that contributes the recharge and the zone that should be protected from contamination are not necessarily the same, the latter possibly being larger if the risk of spills of dense nonaqueous liquids is included. Uncertainties in the definition of the aquifer structure can have a major effect on the capture zone prediction, as explained by Kinzelbach et al. (1996), who recommend the stochastic approach for generating capture

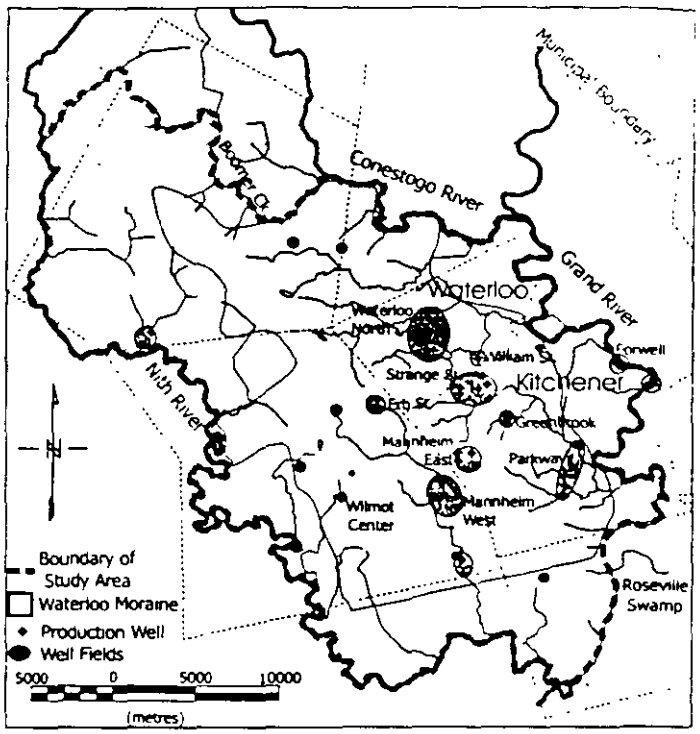

Figure 1. Modeling study area.

zones in cases of scarce data, but stress the need for the deterministic identification of large-scale features. An alternative approach to the generation of well capture zones is the method by Wilson and Liu (1995), who obtain a probabilistic well capture zone by solving the advective-dispersive transport equation in the upstream direction from the well.

From this review, it is evident that a three-dimensional conceptual model based on the geologic structure is essential for a valid definition of the flow field, and hence for creating a credible basis for delineating well capture zones. Although optimal calibration techniques presented in the recent literature are promising, constraints still exist in the number of variables that can be realistically handled. In real-world applications, optimal calibration appears to have been used mainly as a tool to supplement geologic and hydrogeologic judgment, rather than an automated technique for generating hydrogeologic parameters. With respect to three-dimensional capture zone delineation, suitable numerical techniques have been developed, but as yet there is no clear way to overcome uncertainties in the aquifer structure which can control capture zones.

Geology and Hydrogeology of the Waterloo Moraine: Previous Studies

The study area (Figure 1) of approximately 750 km^2 encompasses the Waterloo Moraine and surrounding areas, and includes the cities of Waterloo and Kitchener as well as portions of neighboring townships. The Moraine, located on the eastern rim of the Michigan basin, was mapped by Karrow et al. (1990). The study area is drained by the Grand River and its tributaries, the Nith and Conestogo Rivers. The topography is characteristic of a moraine, with an undulating surface and isolated swampy areas and ponds where the water table intersects the ground surface. The geology of the Moraine is a quaternary kame and kettle complex formed by interlobate glacial activity during the late Wisconsin stage. The glacial overburden consists of a variety of materials including

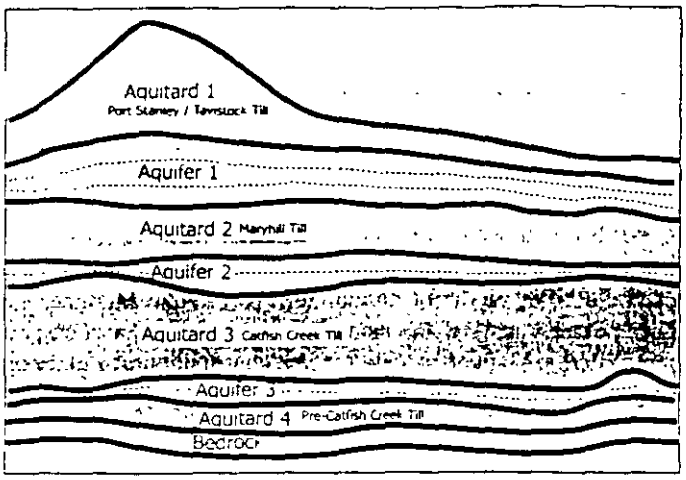

Figure 2. Hydrostratigraphic layering scheme.

clay, interbedded tills, fine sand, sandy gravel, and coarse gravel, and ranges in thickness from 30 to > 100 m. A detailed description of the glacial geology is given by Chapman and Putnam (1984), and Karrow (1993). The climate is semihumid with an average annual precipitation of 780 to 1000 mm (Karrow 1987).

The stratigraphy is complex with a heterogeneous distribution of hydraulic conductivity. Despite this heterogeneity, three relatively continuous till units, the Port Stanley/Tavistock, Maryhill, and Catfish Creek tills have been identified throughout the Moraine (Karrow 1993). The youngest of these, the Port Stanley/Tavistock till, is found near the surface overlying large portions of the upper aquifer. The next youngest, the Maryhill till, is a clay-rich, low-permeability unit lying beneath the upper aquifer. In many areas, this unit acts as an infiltration and contamination barrier for the underlying aquifers; however, windows of high-conductivity material have been observed or inferred in recent studies. The Catfish Creek till, lying below the Maryhill till, is a dense, stony silt till containing portions that act as an aquifer (Karrow 1993; Petrie 1985). Because of this variability, it has appeared to be discontinuous at a local scale. A fourth discontinuous till unit, named the Pre-Catfish Creek till, is found locally overlying the bedrock. The hydrostratigraphic relationships are shown schematically in Figure 2.

Glaciofluvial sand and gravel deposits located between the major till units form the major aquifers in the system. The upper aquifer (Aquifer 1), thought to be reworked Maryhill till, is the most extensive and regionally continuous unit, it is also the most productive source of water. The two lower aquifers (Aquifers 2 and 3), which often are found as pockets of discontinuous sand and gravel, are productive locally. The underlying bedrock consists of the Salina Formation, a Silurian dolomitic limestone in the western portion of the region, or the Guelph Formation, a Silurian limestone in the eastern portion of the region (Karrow 1987, 1993). The bedrock has been observed to be fractured in the top few meters (Terraqua 1995), and is also thought to act as a relatively continuous aquifer which provides a hydraulic connection between discrete pockets of the lower confined aquifer.

The abundant and high-quality water resource provided by the Moraine has been used since the late 1800s. As a result of this abundance, an understanding of the capacity of the resource was not important until the industrial boom of the 1960s. Serious exploration then commenced to define the resource and to provide a basis for expanding use. One of the first comprehensive studies was conducted by Dixon (1973), who conceptualized the quaternary deposits

Table 1
Wellfields and Pumping Rates

Name	Wells	Aquifer(s)	Pumping Rate (m^3/s)	Percent of Total
Mannheim West	4	1	.163	16.83
Mannheim East	7	1	.141	14.56
Parkway	5	3	.129	13.32
Greenbrook	7	2 and 3	.126	12.96
Wilmot Center	2	1	.092	9.50
Erb St.	3	1	.079	8.12
William St	4	2 and Bedrock	.078	8.09
Strange St.	4	1 and 2	.007	7.17
Forwell	7	3 and Bedrock	.034	3.47
Baden	2	1	.025	2.60
Waterloo North	2	1	.024	2.48
New Dundee	2	1	.002	0.25
Heidelberg	2	3	.002	0.21
Wellesley	3	3	.002	0.20
St. Clements	2	1	.0012	0.12
Roseville	1	3	0008	0.08
St. Agatha	1	1	.0002	0.016
Total			.970	

into the three aquifer groups (lower, middle, upper), separated by three partly discontinuous till units (Figure 2), a grouping that is still accepted today, although the details have changed. This early work also included the first attempt to model the entire aquifer system, using a two-dimensional finite element model. Important contributions to the understanding of Moraine hydrostratigraphy were made by Rudolph (1985), Farvolden et al. (1987); Rudolph and Farvolden (1989); Woeller and Farvolden (1989); Paloschi (1993); and Terraqua (1995), the latter providing comprehensive large-scale stratigraphic interpretations throughout the core and flanks of the Waterloo Moraine. These studies generally confirmed Dixon's (1973) characterization of the Moraine stratigraphy as a three-aquifer, three-aquitard system, with relatively continuous aquifers and evidence of lateral connections between wellfields. Local wellfields within the Moraine have been studied in detail in the past, particularly the Greenbrook wellfield (e.g., Farvolden and Weitzman 1980; Woeller 1982, Rudolph 1985; Beland 1977; and Lotimer 1985), using field methods as well as a variety of models including a quasi-three-dimensional model and a two-dimensional radially symmetric model.

The wellfields supplying the water for the cities of Kitchener and Waterloo extract water from all three of the Moraine aquifers, while the rural communities surrounding the cities are supplied mostly from the shallow aquifer. Wellfields, pumping rates, and pumped aquifers are listed in Table 1. The most important wellfields, including Mannheim East/West with 31% of production, Parkway with 13%, Greenbrook with 13% (identified in Figure 1), and others, are located within the cities of Kitchener and Waterloo or just beyond their boundaries. Most of these wellfields consist of several wells, and some tap two aquifers.

Recharge to the Moraine system is believed to enter mainly through sand hills along the core area of the Moraine, with estimated average recharge rates between 15 and 25 cm/yr. For the Maryhill till on the flanks of the moraine, leakage rates have been found to be 6 to 8 cm/year on the basis of tritium profiles through the till (Russell 1993). Under these conditions, even a 10 m thick till unit

would result in recharge travel times of at least 125 years. However, municipal production wells screened in the lower aquifer throughout the flanks of the Moraine show elevated tritium levels (Terraqua 1995), suggesting post-1953 recharge. Chloride originating from road salting activities, which became significant only in the 1950s, provides further evidence of young water in the lower aquifer. This young water is believed to be recharged by way of windows in the aquitards, fractures within the till fabric, or both.

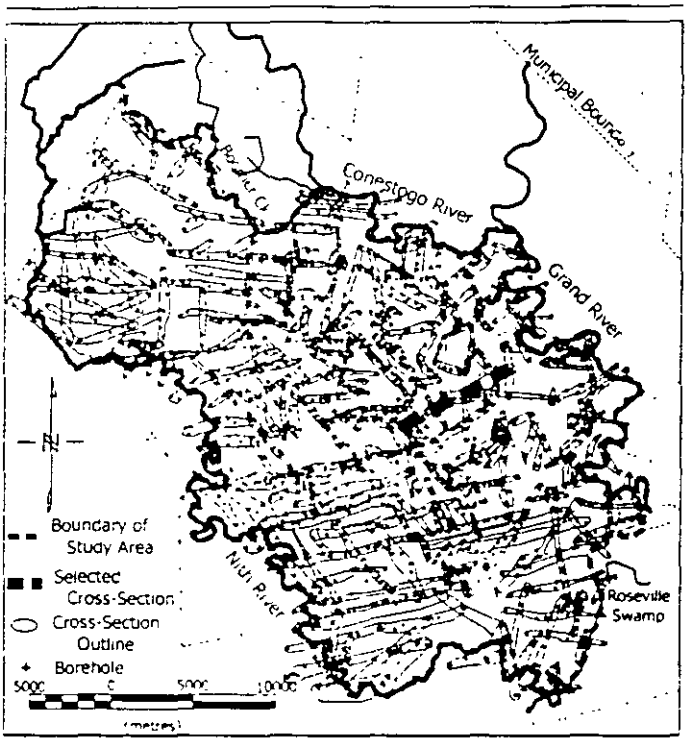

Figure 3. Location of selected boreholes and hydrostratigraphic cross sections.

A frequent problem encountered in early modeling studies of local wellfields was the definition of valid boundary conditions in a highly heterogeneous multiaquifer system hosting many wellfields in close proximity. This provided the impetus for the development of regional models. The first step in this direction was the work of Rudolph and Sudicky (1990), who developed a quasi-three-dimensional subregional model encompassing the main wellfields, followed by Fitzpatrick (1993), who modeled the aquifer system within the urban area of Kitchener-Waterloo. Martin (1994) developed a detailed model of the northern part of the Moraine, the Laurel Creek watershed; this model became the precursor of the present Waterloo Moraine model. A recent contribution was made by Callow (1996), who studied options to optimize production in the Greenbrook wellfield using three-dimensional modeling with both MODFLOW (McDonald and Harbaugh 1988) and WATFLOW (Molson et al. 1995). Callow extracted his boundary conditions from the regional Moraine model.

One of the key conclusions of previous hydrogeologic studies is that the ground water flow system appears to be at steady state. Dixon (1973), Woeller (1982), Lotimer (1985), and Rudolph (1985) all found portions of the ground water flow system to be at steady state, or to quickly reach steady state when stressed. Woeller and Farvolden (1989) concluded that the flow system is in equilibrium throughout the entire region. This observation is also consistent with the recharge of young water to the lower aquifer.

Development of the Conceptual Model

On the basis of present knowledge of the Waterloo Moraine, as well as the literature (particularly Fogg 1986), it is clear that in order to have credibility, the conceptual model must be three-dimensional and incorporate as much of the geologic structure as is available. If the objective were to investigate aquifer yield, where the quantity of interest is the total water reaching a well, without regard of its origin, a simpler model (such as a quasi-three-dimensional model) might be considered. On the other hand, when

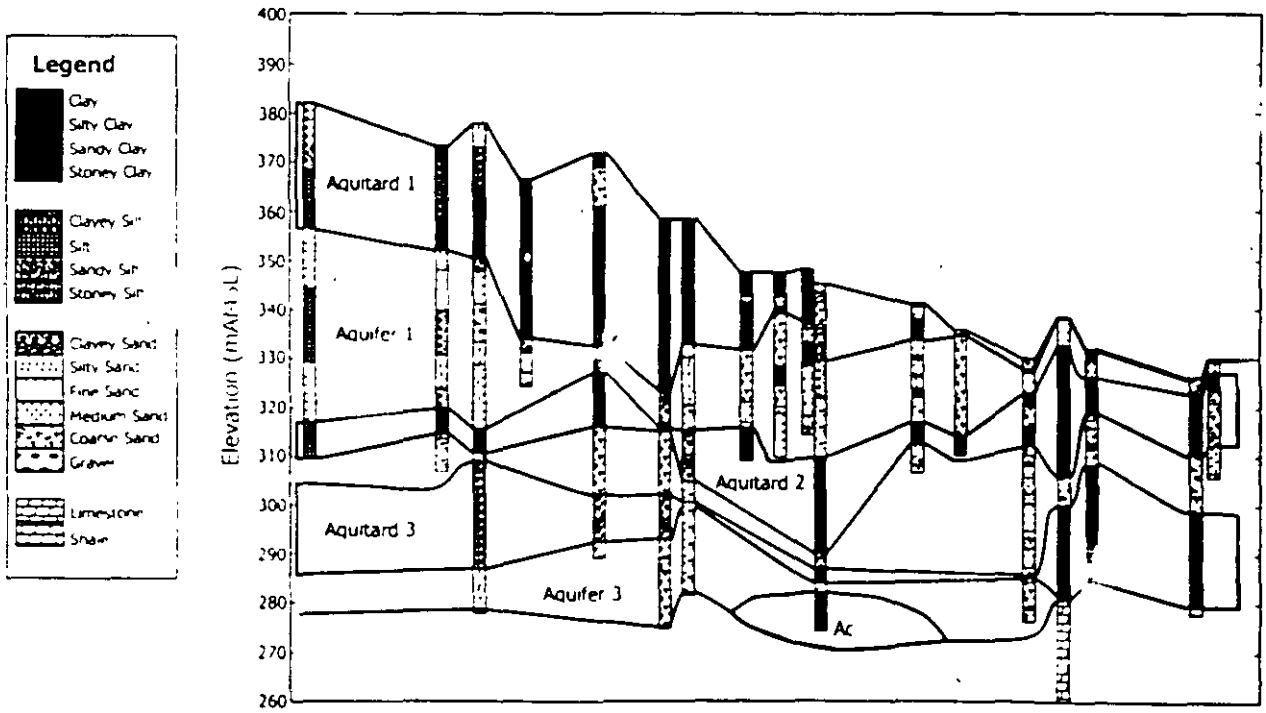

Figure 4. Typical hydrostratigraphic cross section (for location see Figure 3).

Table 2
Standardized Lithologic Categories and Hydraulic Conductivities

Material Number	Lithologic Unit	Hydraulic Conductivity (m/s) From Literature*	From Field Measurements	Final Calibrated K_h	Final Calibrated K_v
2	Clay	$10^{-9} - 10^{-12}$	$2\times10^{-9} - 3\times10^{-11}$	1×10^{-11}	1×10^{-12}
3	Silty clay	$10^{-9} - 10^{-11}$	-	1×10^{-10}	1×10^{-11}
4	Sandy clay	$10^{-7} - 10^{-10}$	-	1×10^{-8}	1×10^{-9}
5	Gravelly clay	$10^{-7} - 10^{-9}$	$1\times10^{-7} - 1\times10^{-10}$	5×10^{-8}	5×10^{-9}
6	Clayey silt	$10^{-7} - 10^{-9}$	$3\times10^{-7} - 2\times10^{-8}$	1×10^{-9}	1×10^{-10}
7	Silt	$10^{-5} - 10^{-9}$	$1\times10^{-6} - 1\times10^{-10}$	5×10^{-8}	5×10^{-9}
8	Sandy silt	$10^{-6} - 10^{-8}$	$4\times10^{-7} - 2\times10^{-9}$	5×10^{-7}	5×10^{-8}
9	Gravelly silt	$10^{-5} - 10^{-7}$	$1\times10^{-6} - 1\times10^{-7}$	1×10^{-6}	1×10^{-7}
10	Clayey sand	$10^{-5} - 10^{-7}$	-	5×10^{-5}	5×10^{-6}
11	Silty sand	$10^{-3} - 10^{-5}$	$1\times10^{-6} - 1\times10^{-6}$	5×10^{-4}	5×10^{-5}
12	Fine sand	$10^{-4} - 10^{-6}$	$2\times10^{-4} - 3\times10^{-6}$	1×10^{-3}	1×10^{-4}
13	Medium sand	$10^{-2} - 10^{-6}$	$4\times10^{-4} - 4\times10^{-6}$	5×10^{-3}	1×10^{-3}
14	Coarse sand	$10^{-2} - 10^{-4}$	$5\times10^{-3} - 2\times10^{-6}$	1×10^{-2}	5×10^{-3}
15	Gravel	$10^{0} - 10^{-3}$	$2\times10^{-3} - 4\times10^{-4}$	5×10^{-2}	1×10^{-2}
16	Limestone bedrock	$10^{-2} - 10^{-9}$	-	1×10^{-4}	1×10^{-4}
17	Shale bedrock	$10^{-6} - 10^{-13}$	-	1×10^{-8}	1×10^{-8}
99	Unknown	-	-	1×10^{-4}	1×10^{-5}

*Freeze and Cherry 1979

the key objective is the definition of capture zones, and when the origin of the water reaching a well is important, a fully three-dimensional representation is essential. The following is a brief outline of the procedure used for transforming the extensive base of raw data into a self-consistent three-dimensional conceptual model.

The Province of Ontario requires by law that all drilling logs be filed with the Ministry of the Environment; as a result, more than 4500 borehole logs exist for the study area. These data include logs prepared by well drillers, professional hydrogeologists, and researchers. Because of the uneven quality and reliability of the data from these various sources, screening and data quality controls were essential in the development of the database. Of the original set of borehole logs, 2044 were selected as reliable after screening and adjustment. Groups of these were linked into 317 local-scale cross sections (Figure 3) to allow continuous interpretation of the stratigraphy. Figure 4 is a typical cross section (see Figure 3 for location) showing the hydrostratigraphic interpretation of the borehole data. Considerable hydrogeologic judgement was necessary to produce meaningful, representative cross sections and eliminate or correct erroneous borehole logs. The lithologies of each hole were then grouped into 17 categories as defined by Martin (1994), and representative hydraulic conductivity values for each category were identified from the literature (Freeze and Cherry 1979) as well as from previous pumping and slug test results in the wellfield areas. These values are shown in Table 2, which also shows the final calibrated values.

The methodology for development of the conceptual model is schematically illustrated in Figure 5. The cross-sectional analysis resulted in a number of stratigraphic units represented by stratigraphic segments for each borehole, with each segment containing several lithologic units. For each of the defined hydrostratigraphic segments, horizontal and vertical hydraulic conductivity values, K_h and K_v, were calculated as the arithmetic and harmonic mean values, respectively, of the hydraulic conductivities of the individual lithologic units contained in each segment. This process resulted in spot observations of the elevations of the surfaces delineating the aquifer hydrostratigraphic units, along with estimates of the anisotropic hydraulic conductivities of these units. To obtain laterally continuous elevations and hydraulic conductivities throughout the domain, the spot elevations and conductivities were interpolated areally using universal kriging (Davis 1986; Journel and Huijbregts 1978). Kriging assumes that the variable in question is normally distributed throughout the domain and provides estimates of the most probable value, as well as the variance, of the variable at any specified point for a given distribution of known or measured neighboring values. The procedure allows for a deterministic component and a random component, both of which are needed for the description of geologic deposits. Since the natural log hydraulic conductivity of geologic deposits is usually considered to be normally distributed (Sudicky 1986; Boman et al. 1995), the hydraulic conductivity distributions K_h and K_v were interpolated in terms of their natural logarithmic values. The kriging, using a routine contained in the finite element preprocessor GRID BUILDER (McLaren 1995), provided sets of hydrostratigraphic surfaces and hydraulic conductivities defining the various units in the conceptual model. Martin (1994) gives a full description of the procedure. Variances of the kriged variables between the observation points are also obtained; these are not used in the present version of the model.

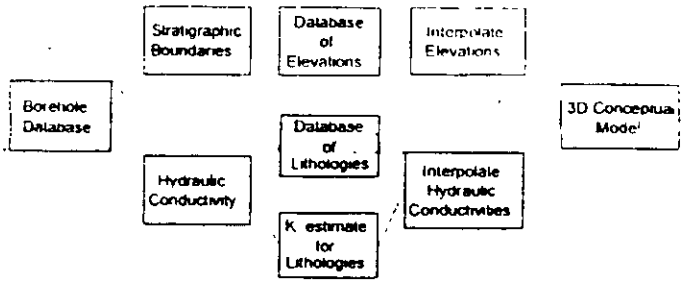

Figure 5. Methodology for conceptual model development.

The Ground Water Flow Model

The numerical model chosen for this study, WATFLOW, is a well-proven three-dimensional finite element ground water flow code developed at the University of Waterloo (Molson et al. 1992, 1995). It is based on the general three-dimensional form of the governing differential equation for transient saturated ground water flow in heterogeneous anisotropic media (Bear 1979), and it uses triangular prismatic finite elements which allow the grid to be deformed to fit irregular or sloping stratigraphy and variable layer thicknesses, and which allow efficient grid refinement in critical areas such as wellfields. The finite element grid is generated automatically in the two-dimensional plane using the preprocessor GRID BUILDER (McLaren 1995), and projected in the vertical to form a three-dimensional grid. The model allows the usual Dirichlet (specified head) and Neuman (specified flux) boundary conditions. The top boundary of the saturated model domain is the water table, which can be represented either in terms of specified head or specified recharge; in the latter case, the location of the water table is determined iteratively by satisfying the criterion of zero pressure head at the water table. The interflow mechanism that would occur if the water table is located in a low-permeability layer is approximated

by means of a thin recharge spreading layer that conducts recharge from low-K areas to higher-K areas able to accept the recharge without causing excessive mounding. Well screens are represented by one-dimensional line elements (Sudicky et al. 1995). Streams are represented as specified head boundaries in the unit that is intersected by the stream. For mass balance calculations, the inflow/outflow fluxes at these stream boundaries are obtained directly from the partitioned global finite element matrix equation. Since the model is fully three-dimensional, leaky aquitard or river bottom boundary conditions are automatically represented.

The matrix equations are solved for nodal heads using an efficient preconditioned conjugate-gradient matrix solver with a block-line-relaxation procedure designed to efficiently manage high horizontal-to-vertical aspect ratios (Braess and König 1995). From the nodal heads, elemental velocity components are calculated in the standard way by means of the Darcy equation. WATFLOW contains a post-processing particle tracking routine, WTC-TRAC, which is used to delineate well capture zones. This routine uses the element-wise constant velocity vectors calculated on the basis of the Darcy equation, and advectively tracks swarms of particles backward from a well, in the upgradient direction, through the three-dimensional velocity vector field. The particles can either be tracked for a specified length of time to generate a specific isochrone, or tracked until a recharge boundary is reached.

WATFLOW was compared to MODFLOW (McDonald and Harbaugh 1988) by Callow (1996), who applied both models to a subregion of the Waterloo Moraine, the highly complex Greenbrook wellfield which contains multiple wells. In both models, the top boundary was specified in terms of recharge, and the grid was refined in the vicinity of the wells. MODFLOW required a total of about 870,000 cells (of which about 15,000 were inactive) over 17 layers, giving a 10-m discretization near the wells, while WATFLOW used about 118,000 nodes for the same number of layers, achieving a discretization of 0.5 to 1 m near the wells. Callow encountered a number of problems in using MODFLOW, the most serious one being a difficulty to converge to a stable solution due to some cells oscillating between draining and rewetting conditions while iterating to locate the water table corresponding to a given recharge. He also reported large amounts of unrealistic water table mounding in low-permeability zones. According to Callow, difficulties also arose due to the large variations in layer thicknesses and large contrasts in the permeability of the layers (up to seven orders of magnitude). None of these problems occurred with WATFLOW, which handles large permeability contrasts, irregular stratigraphy, and thickness variations efficiently, eliminates the mounding problem by means of the recharge spreading layer, and has a moving water table boundary. Execution times for MODFLOW ranged from hours to days on an IBM 6000/560 machine, while those for WATFLOW averaged about 20 minutes on the same machine. Both models use a preconditioned conjugate gradient solver, but the WATFLOW solver is optimized for large permeability contrasts. In terms of set-up time, Callow reports an expenditure of three months for MODFLOW, while only two days were needed to produce the first successful run with WATFLOW. Based on Callow's experience, MODFLOW was not considered to be appropriate for the Waterloo Moraine study.

Model Architecture and Calibration

The boundaries of the model domain follow natural features such as rivers, creeks, and swamps, including the Nith River in the west and the Grand and Conestogo Rivers in the east, which form ground water divides for the overburden aquifers (Figure 1). In many locations, these rivers have cut through much of the overburden (particularly Aquifer 1), and in the southeast corner of the study area, the Grand River is in direct hydraulic connection with the bedrock. The northern boundary was located mostly along tributary streams (one being Boomer Creek), while the southeastern boundary was placed at the Roseville Swamp, a natural ground water discharge location. Vertically, the hydrostratigraphy is divided into 12 layers as shown in Figure 2 (three for Aquifer 1, two for each of Aquifers 2 and 3, and one for each of the other units). This vertical discretization was considered to be the minimum for an adequate three-dimensional representation on the regional scale under steady-state conditions (future subregional models will use a finer vertical discretization). In addition, the recharge spreading layer, which reroutes recharge from low-K zones in the surficial layer to higher-K zones, is draped over the entire model. The finite element grid in the horizontal plane, generated automatically, has elements ranging from ≈10 m at the wells to a maximum of 500 m in more remote areas (Figure 6). The vertical projection of the planar grid onto the 14 layer interfaces resulted in a total of about 116,000 nodes and 210,000 prismatic elements (Figure 7). The boundary condition over the top surface is the recharge flux, except at stream or open-water boundaries where a constant-head boundary condition is specified. Initially, the top surface of the model is located at the ground surface; during execution this surface is moved automatically to the water table that is consistent with the given recharge. The lower aquifers have lateral no-flow boundaries on the assumption that they discharge to the overlying streams. The bottom boundary is the impermeable bedrock. Since all layers are continuous, aquitard windows are represented as high-conductivity zones and aquifer discontinuities as low-conductivity zones in the respective units. The anisotropic hydraulic conductivity varies element-by-element within each layer. The elemental porosity was estimated on the basis of the horizontal hydraulic conductivity value using the method of

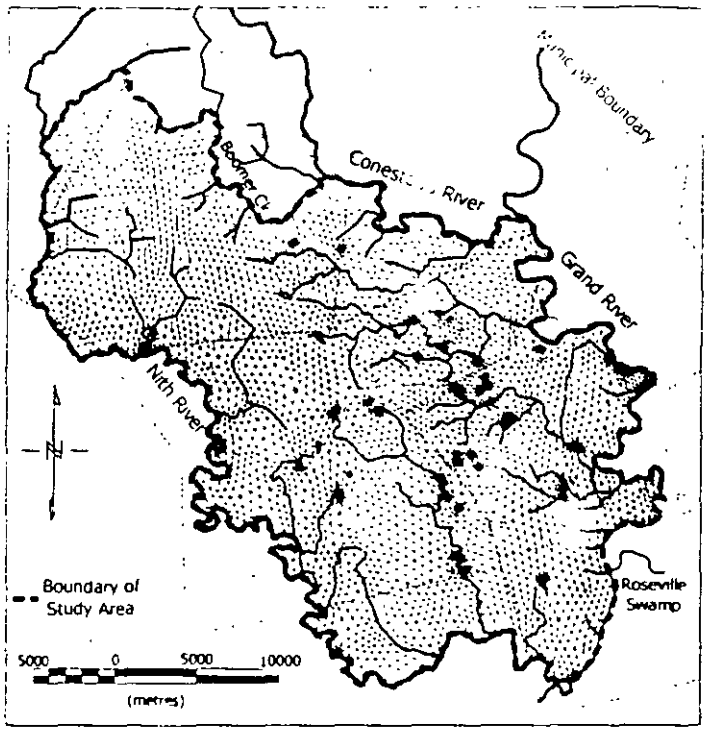

Figure 6. Finite element grid in horizontal plane.

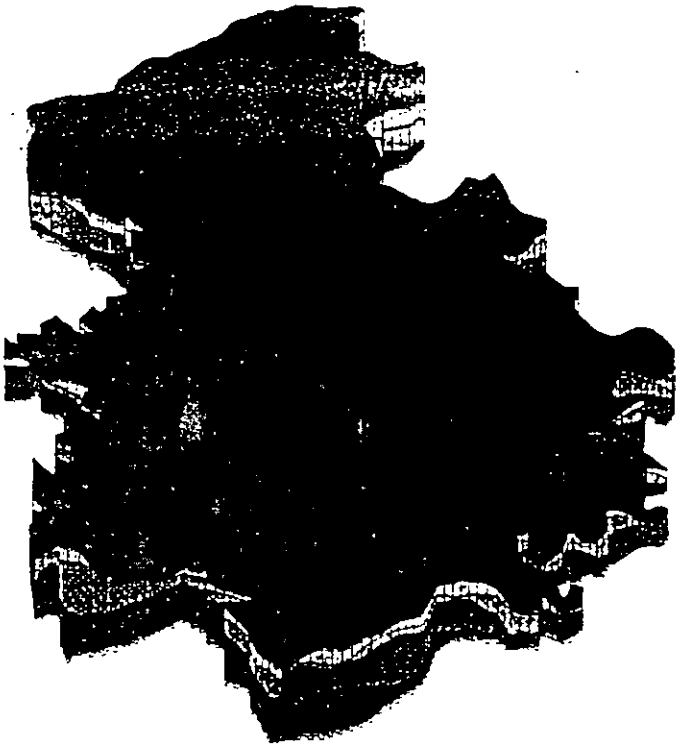

Figure 7. Three-dimensional view of finite element grid (initial condition).

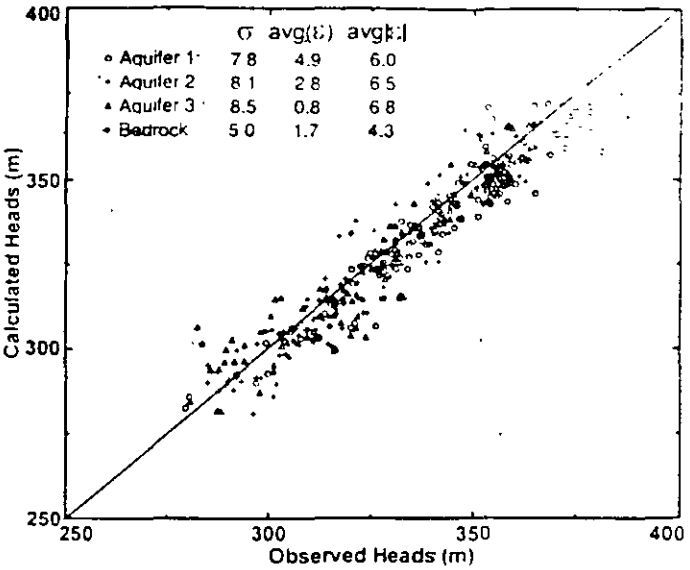

Figure 8. Assessment of model calibration (σ = standard deviation, avg(ε) = average error, avg|ε| = average absolute value of error).

Domenico and Schwartz (1990). The model is designed so that sub-domains of particular interest, such as areas surrounding wellfields, can be easily extracted along with their boundary conditions.

Steady-state flow conditions are assumed for the regional model on the basis of field observations (Lohmer 1985; Woelier and Farvolden 1989). We do not rule out the possibility that aquitards may be under transient conditions locally, this option will be pursued at a later stage. Because of the heterogeneity of the system, as well as geochemical evidence, it would appear that the aquifers are recharged predominantly by flow through high-permeability windows, while leakage through low-permeability material plays a lesser role. Under this mechanism, the steady-state assumption is reasonable.

For calibration under steady-state conditions, a total of 398 monitoring wells were identified where measured heads can be considered sufficiently accurate and representative of present pumping conditions. The majority of these wells are screened in the upper two aquifers. Since heads alone are not sufficient for a unique calibration under steady-state conditions (K-values can be multiplied by any constant to give the same head distribution), estimated net average recharge rates were also included in the calibration, while pumping rates at wellfields provided fixed constraints. Stream baseflows, where available, were reserved for use in subsequent water balance calculations to help validate the model. The calibration was done by trial and error because the number of variables would be too large for automatic calibration using existing tools. Also, the geologic and hydrogeologic structure had already been well developed, making calibration a relatively straightforward task and allowing for adjustments to be based on judgment in weighing the credibility of the various data types. Selective adjustments were applied to the hydraulic conductivity values in strategic locations, where needed, to improve the match between simulated and observed heads. For the most part, the calibrated hydraulic conductivity values are within one order of magnitude of observed field values, but in portions of some till aquitard units, the hydraulic conductivity had to be lowered by one to two orders of magnitude to decrease the interaction between the aquifer units. The recharge was varied from 18 cm/year along the flanks to 22 cm/year in the core area of the Moraine, and to a high of 31 cm/year in the immediate vicinity of the Mannheim sand hills, giving an area-weighted average of 20 cm/year, or 22% of the total average precipitation of about 90 cm/year, which is within the 15 to 25 cm/year range.

The final calibrated values of horizontal and vertical hydraulic conductivity for the various lithologic categories are shown in Table 2, and an assessment of the calibration showing simulated versus observed heads is given in Figure 8. The head residuals are uniformly distributed over the system. Some of the residual scatter seen in the plot can be explained by the uncertainty in the elevation of the measurement points (borehole elevations and observed head values), data that are not representative of existing water levels, and local-scale heterogeneities below the level of discretization. Uncertainty in elevations is estimated to be approximately 5 m, the contour interval of the topographic maps used to estimate borehole elevations, this source of error can only be eliminated by accurately surveying all borehole elevations. The calibration will be refined in the next stage of the study focused on individual wellfields.

As an example of the heterogeneity of the system, Figure 9 shows the calibrated hydraulic conductivity fields of Aquitard 1 and Aquifer 1 (K_h for aquifer, K_v for aquitard). The aquifer plot also shows the wells ending in this unit. Because the aquitard contains high-conductivity zones (windows) which act as part of an aquifer, while the aquifer contains low-conductivity zones which locally act as an aquitard, the range of hydraulic conductivity is similar for all units, and the same range of grayscale was used for both plots. Aquifer 1 is the thickest and most consistent aquifer, with continuous high-conductivity zones throughout the central portion; it supplies about 60% of the total production. Aquitard 1 provides protection to Aquifer 1 over most of the area through its extensive low-K_v zones; it also allows recharge through windows that appear as high-K_v zones. For example, the large high-K_v zone in the south third of Aquitard 1 is a window through which the zone of Aquifer 1 containing the Mannheim West wellfield is exposed.

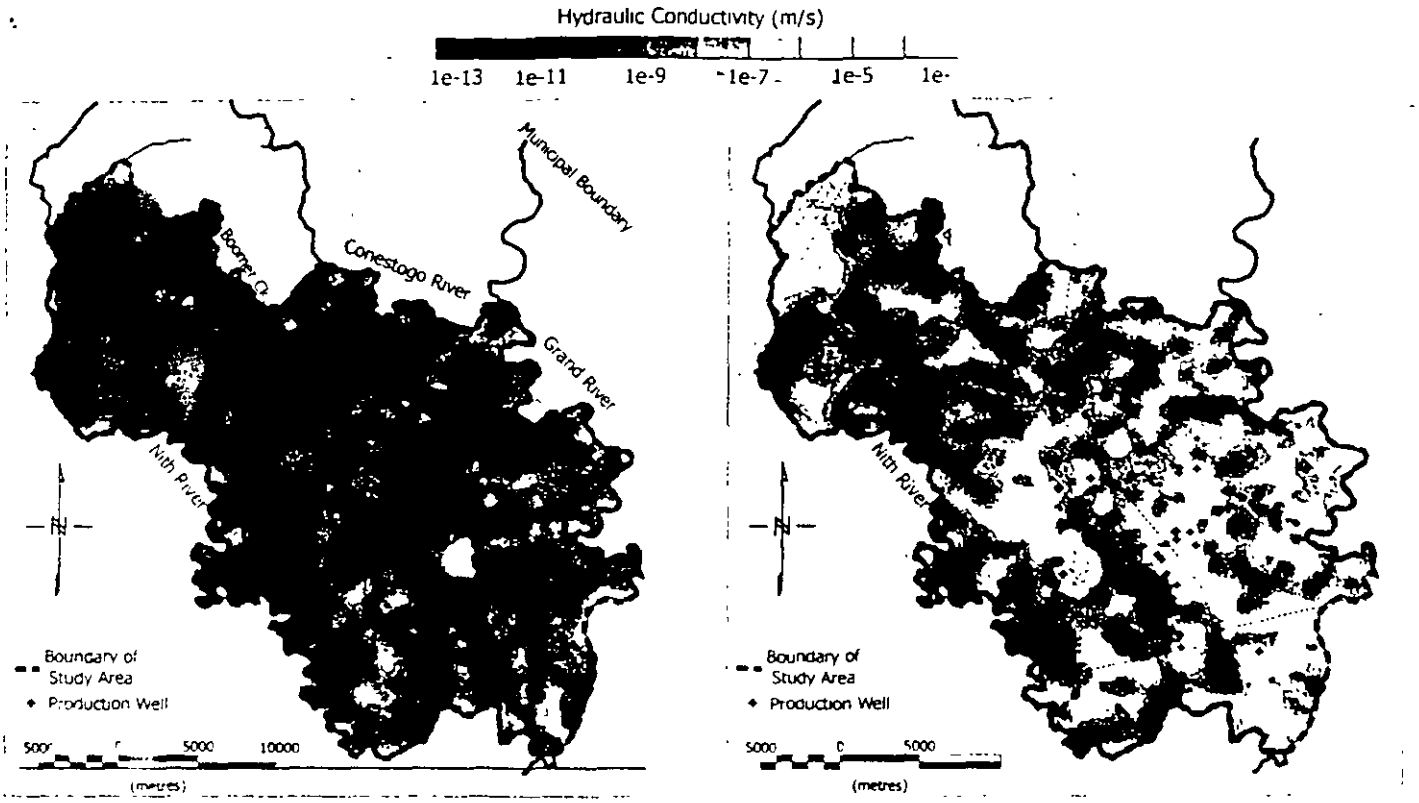

Figure 9. Calibrated hydraulic conductivity distributions for Aquitard 1 and Aquifer 1.

Table 3
Water Balance at Nith and Grand River Boundaries

Stream	Observed Base Flow (m^3/s)	Simulated Base Flow (m^3/s)	% Error
Nith River	1.56	1.51	-3.2%
Grand River	3.40	3.52	+3.5%

The remaining aquifer/aquitards (not shown) show similar heterogeneity patterns. Aquifer 2, which supplies about 20% of production, is thinner than Aquifer 1 but also has continuous zones of high conductivity. It is protected by Aquitard 2, the Maryhill Till (Figure 2), which is a fairly continuous till sheet with a few windows. Aquifer 3, the thinnest of the three aquifers, supplies about 5% of total production. Aquitard 3, the Catfish Creek Till which overlies Aquifer 3, is less continuous and has some large windows, particularly in the area of the Parkway wellfield, allowing recharge to Aquifer 3. Aquitard 4 is a rather thin discontinuous till sheet which locally separates Aquifer 3 from the bedrock aquifer. The latter supplies about 5% of total production.

Water Balance and Water Budget

Streamflows at a small number of locations within the study area are measured regularly by Water Survey Canada and the Grand River Conservation Authority. Base flows extracted from these data, and used in water balance calculations, provide the only independent data available for model validation at this time. (Eventually selected local models to be developed in the near future will be validated against environmental tracer data.) From the streamflow records, base flow contributions were estimated from summer low-flow conditions. In the case of the Nith River, a boundary stream with two gauging stations conveniently located on the model boundary, upstream flows were subtracted from downstream flows and the difference divided by two (assuming one-half of the base flow is derived from the study area) to obtain the base flow contribution from the western half of the Moraine. A similar procedure was used for the Grand River, which forms part of the eastern boundary but has gauging stations located some distance outside the model boundaries, requiring interpolation to obtain base flow contributions consistent with the model boundaries. Corresponding simulated base flows were determined by integrating the model discharge/recharge along the appropriate portion of the stream boundaries. The observed and simulated baseflows for these two streams are given in Table 3. The mass balance errors (simulated − observed)/observed) of −3.2% and +3.5%, respectively, are well within the margin of error associated with the data. Mass balances were also calculated for several smaller streams within the study area for which base flow data were available; the errors here were about ±20%. The larger error is mainly due to the scale of the regional model being too large to allow adequate grid refinement in the vicinity of these streams (this aspect will be addressed in future smaller-scale subregion simulations). The arithmetic sum of all the mass balance errors (recognizing the signs) is nearly zero. Thus, the model can be considered validated with respect to mass balance.

To put the base flow values into context, we may also consider the other contributions to the total water budget. On the basis of the net average recharge of 20 cm/year, the amount of water recharged directly to the ground water system over the 745 km^2 study area is approximately 1.49×10^8 m^3/year. An additional 0.57×10^8 m^3/year recharges the ground water system through influent streams, as an indirect form of recharge, giving a total of 2.06×10^8 m^3/year that

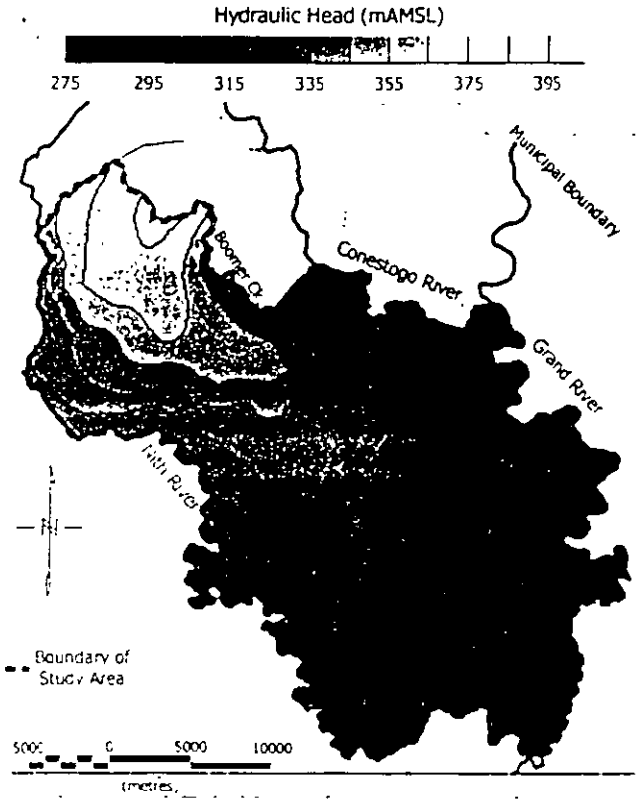

Figure 10. Hydraulic head distribution at the water table under steady-state pumping.

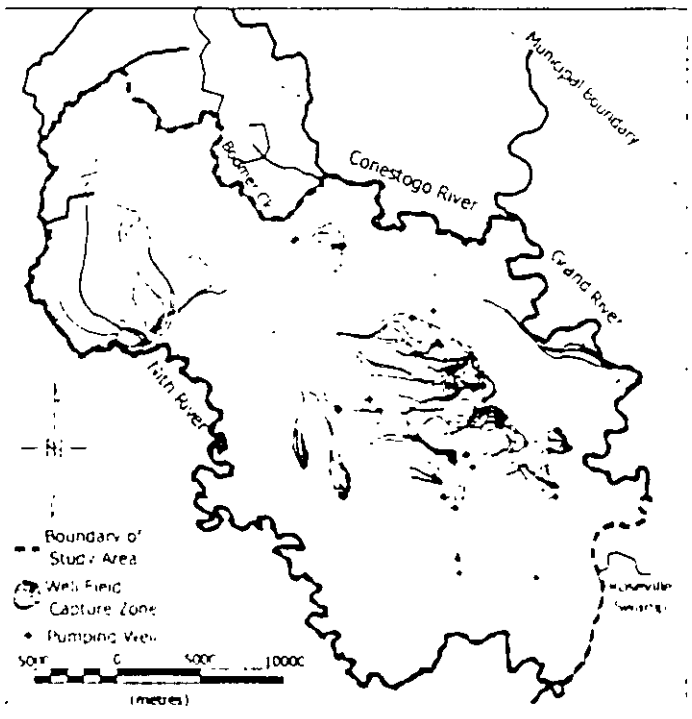

Figure 11. Horizontal-plane projection of flowpaths and estimated surface capture zones.

recharges the ground water system. The average extraction rate from all wellfields (Table 1) is 0.97 m^3/s or 0.31×10^8 m^3/year, equivalent to about 15% of the total recharge. This leaves a net difference of approximately 1.75×10^8 m^3/year, or 85% of the total recharge, to leave the study area as stream base flow. Of this total, the Nith River carries about 27% and the Grand, with its tributary the Conestogo, carries the remainder. This calculation does not consider storm flows. The total amount of water entering the river system from the study area consists of the ground water discharge, the storm runoff from the 745 km^2 land surface, and the returned treated waste water, which accounts for a large part of the water extracted by pumping. On balance, most of the water that would enter the rivers under natural conditions also enters under pumping conditions. Thus, the effect of the ground water extraction on the river system is small, although local streams within the study area can be affected significantly. It should be noted that budget contributions other than ground water are external to the model and are provided only to put the ground water component into context.

Flow and Capture Zone Simulation

Figure 10 shows the hydraulic head distribution at the water table, produced by the calibrated model under steady pumping conditions using the pumping rates shown in Table 1. As expected, ground water flow is generally from northwest to southeast along the core of the Moraine, and toward the Nith and Grand Rivers. Some impact on the water table due to pumping is noticeable at the Mannheim West, Erb St., William St., and Waterloo North wellfields (compare Figures 10 and 1), but on the whole the impacts are subdued because the pumped aquifers for the most part are covered by aquitards. The hydraulic head distributions in the aquifers themselves (not shown) follow a similar regional trend but are much more irregular due to heterogeneities. The execution of the fully three-dimensional model with about 116,000 nodal points, running in steady-state mode, required about 30 minutes on a Pentium-200 PC.

The particle tracking routine WTC-TRAC was applied to generate estimates of the steady-state surface capture zones for all wellfields in the Moraine area. Horizontal-plane projections of the three-dimensional flowpaths, with the areas encompassed by these flowpaths shaded, are shown in Figure 11. The major part of the eastern flank of the Waterloo Moraine, within the city boundaries of Waterloo and Kitchener, is covered by these potential protection zones. For some wellfields, the actual recharge zones may be smaller than the zones encompassed by the flowpaths; however, the protection zone for a well should comprise the complete projection of the three-dimensional flowpaths onto the ground surface to account for the possibility that dense liquids could penetrate from the ground surface to reach lower-lying flowpaths (Kinzelbach et al. 1992). The particle travel times from the wells to the water table range from <1 year for locally recharged water to >100 years for water recharged within the core area of the Moraine. The shorter travel times are consistent with observations of young (post-1953) water which may have reached the aquifers through windows, while the longer travel times suggest that leakage through low-conductivity layers may also play a significant role. These capture zones estimates, obtained with the coarse regional grid, will be refined in the near future, using more detailed local three-dimensional models of the individual wellfields. If pumping rates change, the capture zones will change accordingly.

In order to demonstrate the sensitivity of the flowpaths (and hence the capture zones) with respect to the geologic structure, we consider the Greenbrook area which is known to be geologically complex. Figure 12 is an enlargement of the area upgradient of the Greenbrook wellfield, showing a plot of vertical hydraulic conductivity of Aquitard 2, and a cross section through the system placed approximately along the upgradient direction. This wellfield has wells screened in Aquifers 2 and 3. We select a well ending in

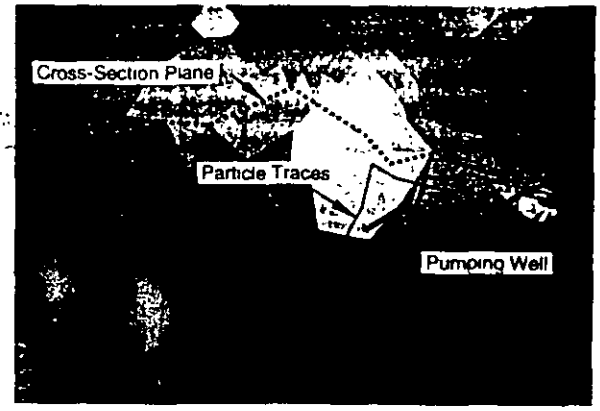

Plan view of Aquitard 2

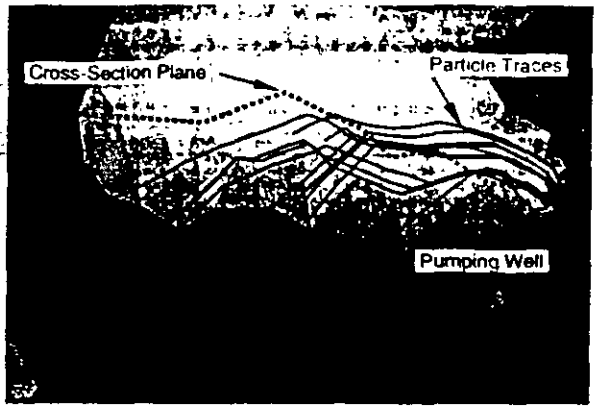

Plan view of Aquitard 2 with Kv averaged upgradient of well

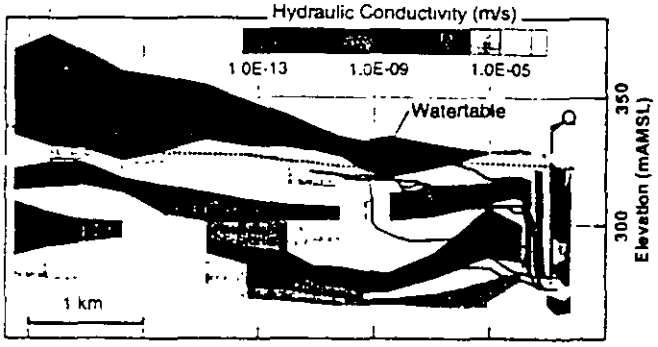

Vertical Cross-Section

Figure 12. Sensitivity of flowpaths, Greenbrook wellfield: Plan view showing Aquitard 2 hydraulic conductivity distribution (K_v); and vertical cross section upgradient of well.

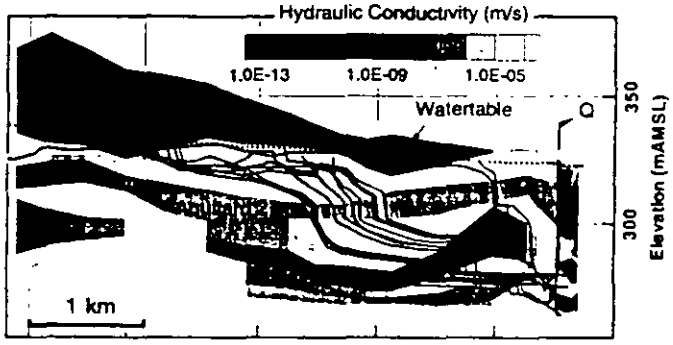

Vertical Cross-Section

Figure 14. Sensitivity of flowpaths, Greenbrook wellfield: Plan view showing Aquitard 2 with averaged hydraulic conductivity distribution (K_v); and cross section upgradient of well.

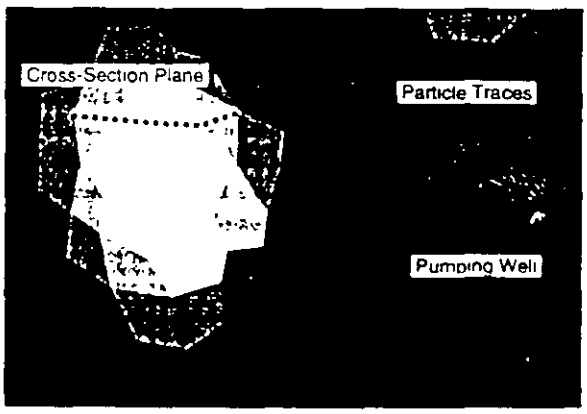

Plan view of Aquitard 3 with window near well closed

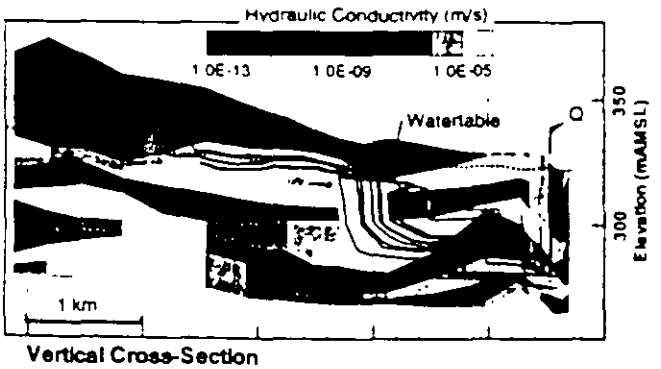

Vertical Cross-Section

Figure 13. Sensitivity of flowpaths, Greenbrook wellfield: Plan view showing Aquitard 3 hydraulic conductivity distribution (K_v) with window near pumping well closed; and vertical cross section upgradient of well.

Aquifer 3 to demonstrate the development of the capture zone. Particles are inserted around the well screen and tracked in the upgradient direction until they intersect the water table. The cross section shows the three-dimensional particle tracks projected onto the plane of the cross section, while the plan view shows a projection of the particle tracks onto the plane of Aquitard 2. The intersection points of the particle tracks with the water table generally lie off the cross section. The figure illustrates a typical recharge condition where recharge to the well has a local component which captures water infiltrating near the well, and a regional component, which captures water from farther afield. The local component reaches the well directly through windows near the well in both Aquitards 2 and 3, while the regional component passes through Aquifer 1 and through relatively high-K zones in Aquitard 2. A number of pathlines have travel times of <10 years, with the shortest travel times (closest to the well) being <1 year. The particle tracks in Aquifer 2 are generally east-west; upon reaching Aquifer 1, the direction changes abruptly to northeast-southwest.

We now close the small window in Aquitard 3 just west of the well by decreasing the aquitard hydraulic conductivity to approximately that of the surrounding aquitard material (Figure 13). This represents the condition that would arise if the information indicating the existence of the window (a single borehole log) had not been available. The water table changes only slightly as a result of this change; the model was therefore not recalibrated. The change has caused the local recharge component at the well to vanish. Particles now pass through the relatively high-conductivity zone in Aquitard 3 over a wider area, and then through a window in Aquitard 2. The surface capture zone based on these flowpaths is about 1.5 km longer

than that obtained with the window present, and the zone contributing the recharge is now physically separated from the well itself.

Next, we change the variable vertical hydraulic conductivity in Aquitard 2, upgradient of the well, to an average value of 10^{-7} m/s, which is representative of the area (Figure 14). This change could represent an attempt to simplify the model by using average conductivity values. Although the window in Aquitard 3 has been restored, the change has again caused the local recharge component to vanish, and recharge is now drawn from a larger area. Particles pass through the relatively high-K_v zone in Aquitard 3 upgradient of the well, and then through the thinnest part of Aquitard 2 on their way to the water table. The surface capture zone now becomes spread out and is much larger than before.

These results, although obtained with a coarse grid, illustrate the high sensitivity of the capture zones with respect to the geologic structure. Aquitard windows have a controlling influence on the capture zone delineations, and even small but strategically placed windows can cause large changes in the capture zones. Also, these windows tend to focus the capture zones, and conversely, an absence of windows will cause the capture zones to spread out. While the effect of windows on the capture zones is profound, the effect on the water table is small. The reason for this behavior is obvious from consideration of the mathematics: particle tracks are based on velocities which are determined by differentiation of heads; the differentiation magnifies small changes in the heads to give large changes in the capture zones.

This confirms the statement made previously that the geologic structure must be determined as accurately as possible in order to obtain credible capture zones. Using the best available data, sources of uncertainty residing in the geologic structure should be explored by means of scenario and sensitivity analyses of the type shown here. The effect of smaller-scale heterogeneities could be explored either by superimposing a stochastic component onto the deterministic hydraulic conductivity distribution of an individual unit, or by using the method of Wilson and Liu (1995), which is based on solving the transport equation for capture probability.

Conclusions

This work is a major milestone in the evolution of the understanding of the complex Waterloo Moraine system. The three-dimensional conceptual model contains all the information available in the extensive database; it represents a credible structure of the complex system, and it provides a useful starting point for the development of management and protection strategies for the resource. The methodology for conceptual model development, including database screening, stratigraphic and lithologic interpretation/interpolation, model calibration, sensitivity analyses and capture zone delineation, is extensive but necessary. The exercise of geologic and hydrogeologic judgement is an essential component of this methodology. The model provides a basic understanding of the complex flow system, the interactions between the various units, and the recharge mechanism of the system. Further refinements are necessary to more definitively delineate capture zones.

The results demonstrate that the geologic structure has a controlling influence on the capture zone delineations. Windows in the confining aquitards near wells can redirect flow paths and can therefore substantially change the capture zone delineations. The presence or absence of windows is therefore a major source of uncertainty. The effect of this uncertainty can be explored, but not eliminated, by sensitivity analyses investigating a range of judiciously selected scenarios.

The next stage of the overall study, which will extend over the next few years, calls for the development of detailed capture zone models for the local wellfields, with calibration/validation against environmental tracer data. The regional Moraine model provides the basic structure as well as the boundary conditions for these local-scale three-dimensional models. Further work will include the development of optimal calibration techniques and of criteria for the optimal location of new data points. The methodology is currently being applied to other glacial aquifer systems in southern Ontario where ground water resources are being threatened by urbanization.

Acknowledgments

We wish to dedicate this paper to the memory of Robert N. Farvolden, the founder of the ground water research group at the University of Waterloo, and the driving force behind the Waterloo Moraine study. Dr. Farvolden's enthusiasm, initiative, and leadership motivated generations of students and researchers alike, and his genuine caring personality and human concern touched the lives of many. Farvolden's vision in seeing the importance of ground water to human welfare all over the world remains a major impetus to the advancement of the understanding of ground water systems. His pioneering thought will always be an inspiration to us.

We thank R. Blackport of Terraqua Investigations Ltd., J. Robinson of the Regional Municipality of Waterloo, D. Boyd of the Grand River Conservation Authority, and N. Guiguer of Waterloo Hydrogeologic for important contributions in the form of data and insight into the complexities of the Moraine aquifer system. We also thank D. Rudolph, E. Sudicky, J. Cherry, I. Callow, J. Beckers, J. Molson, and R. McLaren, our colleagues at the University of Waterloo, for helpful discussions on all aspects of this research. We gratefully acknowledge the financial support of the Waterloo Centre for Groundwater Research and the Regional Municipality of Waterloo, without whose help the project could not have been done. The development of the methodology and the initial application of the model to the North Waterloo aquifer study (Martin 1994) was funded by an NSERC operating grant to E.O. Frind, while ongoing work is being supported by an NSERC Strategic Project Grant focused on the development of methodologies for the protection of ground water resources in complex glacial aquifer systems in Canada.

References

Anderson, M.P. 1989. Hydrogeologic facies models to delineate large-scale spatial trends in glacial and glaciofluvial sediments. *Geolog. Soc. of America Bulletin* 101, 501-511.

Bear, J. 1979. *Hydraulics of Groundwater*. New York: McGraw-Hill.

Beland, A. 1977. Management of the Greenbrook Well Field. M.Sc. project, Dept. of Earth Sciences, University of Waterloo, Waterloo, Ontario, Canada.

Boman, G.K., F.J. Molz, and O. Güven. 1995. An evaluation of interpolation methodologies for generating three-dimensional hydraulic property distributions form measured data. *Ground Water* 33, no. 2, 247-258.

Braess, D., and Ch. Konig. 1995. A Fast Conjugate-Gradient Algorithm for Three-Dimensional Groundwater Flow Problems. Report, Faculty of Mathematics. Bochum, Germany: Ruhr-Universtät Bochum.

Callow, I. 1996. Opumizing aquifer production for multiple well field conditions in Kitchener, Ont. M.Sc. thesis, Dept. of Earth Sciences, University of Waterloo, Waterloo, Ontario, Canada.

Chapman, L.J., and D.F. Putnam. 1984. *The Physiography of Southern Ontario*. 3rd ed., Special Volume 2. Toronto, Ontario, Canada: Ontario Geological Survey.

D'Agnese, F.A., C.C. Faunt, M.C. Hill, and A.K. Turner. 1996. Death Valley regional ground water flow model calibration using optimal parameter estimation methods and geoscientific information systems. In *Calibration and Reliability in Groundwater Modelling*. Proceedings of ModelCARE '96 Conference, ed. K. Kovar and P. van der Heijde, 41. Wallingford, Oxfordshire, United Kingdom: IAHS Press.

Davis, J.C. 1986. *Statistics and Data Analysis in Geology*. 2nd ed. New York: John Wiley & Sons.

Dixon, V.R. 1973. Kitchener-Waterloo ground water evaluation. International Water Supply. Unpublished Report to the Regional Municipality of Waterloo, Ontario, Canada.

Domenico, P.A., and F.W. Schwartz. 1990. *Physical and Chemical Hydrogeology*. New York: John Wiley & Sons.

Farvolden, R.N., J.P. Greenhouse, P.F. Karrow, P.E. Pehme, and L.C. Ross. 1987. Subsurface quaternary stratigraphy of the Kitchener-Waterloo area using borehole geophysics. Open File Rep. 5623. Toronto, Ontario, Canada: Ontario Geological Survey.

Farvolden, R.N., and M.J. Weitzman. 1980. Greenbrook Well Field Study (Report). Department of Earth Sciences, University of Waterloo, Waterloo, Ontario, Canada.

Fitzpatrick, [illegible]. 1993. Groundwater flow and contamination at Kitchener-Waterloo, Ontario. M.A.Sc. thesis, Dept. of Civil Engineering, University of Waterloo, Waterloo, Ontario, Canada.

Fogg, G.E. 1986. Groundwater flow and sand body interconnectedness in a thick, multiple-aquifer system. *Water Resour. Res.* 22, no. 5: 679-694.

Freeze, R.A., and J.A. Cherry. 1979. *Groundwater*. Englewood Cliffs, New Jersey: Prentice-Hall.

Journel, A.G., and Ch.J. Huijbregts. 1978. *Mining Geostatistics*. New York: Academic Press.

Karrow, P.F. 1987. Quaternary geology of the Hamilton-Cambridge area, Southern Ontario. Report 255. Ontario, Canada: Ontario Geological Survey.

Karrow, P.F. 1993. Quaternary geology, Stratford-Conestoga area, Southern Ontario. Report 283. Ontario, Canada: Ontario Geological Survey.

Karrow, P.F., B.G. Warner, C.J. Ellis, and J.D. MacDonald. 1990. What's beneath our feet in Waterloo Region. Publ. #1. Quaternary Sciences Institute, Waterloo, Ontario, Canada: University of Waterloo.

Kinzelbach, W., M. Marburger, and W.-H. Chiang. 1992. Determination of groundwater catchment areas in two and three spatial dimensions. *J. Hydrol.* 34, 221-246.

Kinzelbach, W., S. Vassolo, and G.-M. Li. 1996. Determination of capture zones of wells by Monte Carlo simulation. In *Calibration and Reliability in Groundwater Modelling*. Proceedings of ModelCARE '96 Conference, ed. K. Kovar and P. van der Heijde, 543. Wallingford, Oxfordshire, United Kingdom: IAHS Press.

Leijnse, A., and M.J.H. Pasto[illegible] 1996. Calibration of the RIVM large-scale ground water flow [illegible]odel (LGM) for The Netherlands. In *Calibration and Reliability in Groundwater Modelling*. Proceedings of ModelCARE '96 Conference, ed. K. Kovar and P. van der Heijde, 147. Wallingford, Oxfordshire, United Kingdom: IAHS Press.

Lotimer, R.A. 1985. Groundwater flow in a multiple aquifer system at Kitchener, Ontario. M.Sc. project, University of Waterloo, Waterloo, Ontario, Canada.

Martin, P.J. 1994. Modeling of the North Waterloo multi-aquifer system. M.Sc. thesis, Dept. of Earth Sciences, University of Waterloo, Waterloo, Ontario, Canada.

McDonald, M.G., and A.W. Harbaugh. 1988. A modular, three-dimensional finite-difference ground water flow model. USGS TWRI, Book 6, Ch. A1.

McLaren, R.G. 1995. GRID BUILDER 4.0: A Generator for 2D Triangular Finite Element Grids and Grid Properties, User's Guide. Waterloo, Ontario, Canada: Waterloo Centre for Groundwater Research, University of Waterloo.

Mergia, G., and W.E. Kelly. 1994. Modeling groundwater remediation in the High Plains Aquifer. *Ground Water* 32, no. 1: 129-138.

Molson, J.W., P.J. Martin, and E.O. Frind. 1995. WATFLOW Version 1.0: A Three-Dimensional Groundwater Flow Model, User's Guide. Waterloo, Ontario, Canada: Waterloo Centre for Groundwater Research.

Molson, J.W., E.O. Frind, and C.D. Palmer. 1992. Thermal energy storage in an unconfined aquifer: 2. Model development, validation, and application. *Water Resour. Res.* 28, no. 10: 2857-2867.

Olsthoorn, T.N., and P.T.W.J. Kamps. 1996. Ground water model calibration for the Amsterdam Water Supply dune area. In *Calibration and Reliability in Groundwater Modelling*. Proceedings of ModelCARE '96 Conference, ed. K. Kovar and P. van der Heijde, 105. Wallingford, Oxfordshire, United Kingdom: IAHS Press.

Paloschi, G.V. 1993. Subsurface stratigraphy of the Waterloo Moraine. M.Sc. thesis, Dept. of Earth Sciences, University of Waterloo, Waterloo, Ontario, Canada.

Petrie, J.M. 1985. Field response of a clay till in a layered aquifer system at Waterloo, Ontario. M.Sc. project, Dept. of Earth Sciences, University of Waterloo, Waterloo, Ontario, Canada.

Poeter, E.P., and M.C. Hill. 1997. Inverse models: A necessary next step in ground-water modeling. *Ground Water* 35, no. 2: 250-260.

Poeter, E.P., and M.C. Hill. 1996. Unrealistic parameter estimates in inverse modeling: A problem or a benefit for model calibration? In *Calibration and Reliability in Groundwater Modelling*. Proceedings of ModelCARE '96 Conference, ed. K. Kovar and P. van der Heijde, 277. Wallingford, Oxfordshire, United Kingdom: IAHS Press.

Pollock, D.W. 1988. Semianalytical computation of pathlines for finite-difference models. *Ground Water* 26, no. 6: 743-750.

Rudolph, D.L. 1985. A quasi three-dimensional finite element model for steady-state analysis of multiaquifer systems: B. Application to the Greenbrook Well Field, Kitchener, Ontario. M.Sc. thesis, Dept. of Earth Sciences, University of Waterloo, Waterloo, Ontario, Canada.

Rudolph, D.L., and R.N. Farvolden. 1989. Numerical analysis of regional groundwater flow in a complex multi-aquifer system in Kitchener, Ontario. Waterloo, Ontario, Canada: Waterloo Centre for Groundwater Research.

Rudolph, D.L., and E.A. Sudicky. 1990. Simulation of groundwater flow in complex multiaquifer systems: Performance of a quasi-3D technique in the steady-state case. *Candn. Geotechnical J.* 27, no. 5: 590-600.

Russell, B.R. 1993. Nitrate persistence in slightly permeable sediments in Southern Ontario. M.Sc. thesis, Dept. of Earth Sciences, University of Waterloo, Waterloo, Ontario, Canada.

Schafer, D.C. 1996. Determining 3D capture zones in homogeneous, anisotropic aquifers. *Ground Water* 34, no. 4: 628-639.

Sudicky, E.A. 1986. A natural gradient experiment on solute transport in a sand aquifer: Spatial variability of hydraulic conductivity and its role in the dispersion process. *Water Resour. Res.* 22, no. 13: 2069-2082.

Sudicky, E.A., A.J.A. Unger, and S. Lacombe. 1995. A noniterative technique for the direct implementation of well bore boundary conditions in three-dimensional heterogeneous formations. *Water Resour. Res.* 31, no. 2: 411-415.

Terraqua Investigations Ltd. 1995. Study of the hydrogeology of the Waterloo Moraine. Unpublished report to the Regional Municipality of Waterloo, Ontario, Canada.

Wilson, J.L., and J. Liu. 1995. Backward tracking to find the source of the pollution. In *Waste-Management. From Risk to Reduction* (Ch. 10), ed. R. Bahda. Albuquerque, New Mexico: ECM Press.

Woeller, R.M. 1982. Greenbrook Well Field management study 1981-1982. M.Sc. project, Dept. of Earth Sciences, University of Waterloo, Waterloo, Ontario, Canada.

Woeller, R.M., and R.N. Farvolden. 1989. The past, present and future of groundwater development in the tri-cities of Kitchener, Waterloo and Cambridge, Ontario, Canada. In Proceedings of the NWWA Focus Conference on Eastern Regional Groundwater Issues, Kitchener, Ontario. Dublin, Ohio: NWWA.

Young, S.C., N.J. Williams, B.T. Hurst, and D.H. Barton. 1996. Incorporation of sedimentological data into a groundwater model at Portsmouth, Ohio. In *Calibration and Reliability in Groundwater Modelling*. Proceedings of ModelCARE '96 Conference, ed. K. Kovar and P. van der Heijde, 491. Wallingford, Oxfordshire, United Kingdom: IAHS Press.

FACULTAD DE INGENIERIA U.N.A.M.
DIVISION DE EDUCACION CONTINUA

CURSOS ABIERTOS

XII CURSO INTERNACIONAL DE CONTAMINACIÓN DE ACUÍFEROS

MODULO III: MODELOS MATEMÁTICOS EN GEOHIDROLOGIA Y CONTAMINACIÓN DE ACUIFEROS

TEMA

ASSINGNMENT OF BOUNDARY CONDITIONS IN EMBEDDED GROUND WATER FLOW MODELS

EXPOSITOR: DR. ADOLFO CHAVEZ RODRIGUEZ

PALACIO DE MINERIA
OCTUBRE DEL 2000

Assignment of Boundary Conditions in Embedded Ground Water Flow Models

by S.A. Leake[a], Peter W. Lawson[b], Michael R. Lilly[c,d], and David V. Claar[c]

Abstract

Many small-scale ground water models are too small to incorporate distant aquifer boundaries. If a larger-scale model exists for the area of interest, flow and head values can be specified for boundaries in the smaller-scale model using values from the larger-scale model. Flow components along rows and columns of a large-scale block-centered finite-difference model can be interpolated to compute horizontal flow across any segment of a perimeter of a small-scale model. Head at cell centers of the larger-scale model can be interpolated to compute head at points on a model perimeter. Simple linear interpolation is proposed for horizontal interpolation of horizontal-flow components. Bilinear interpolation is proposed for horizontal interpolation of head values. The methods of interpolation provided satisfactory boundary conditions in tests using models of hypothetical aquifers.

Introduction

Some ground water models are focused on relatively small parts of large aquifer systems. Such detailed studies are common for analysis of wellfields, investigations of contaminant transport, and delineation of recharge areas for pumping wells. Model boundaries should, if possible, coincide with hydrologic aquifer boundaries, however, accurate simulation of physical hydrologic boundaries often is not possible for small-scale studies because distances to the boundaries are large in relation to the dimensions of the small-scale model. Previous investigators (Townley and Wilson 1980, Buxton and Reilly 1986; Miller and Voss 1987, Ward et al. 1987) have used larger-scale ground water flow models to define specified flow and specified head boundary conditions for smaller-scale models. This process is referred to as "telescopic mesh refinement" because it can be applied successively to smaller models with each larger model providing boundary conditions for the next smaller embedded model.

This paper evaluates methods that can be used to interpolate smaller-scale model-boundary flows and heads from large-scale block-centered finite-difference models such as MODFLOW (McDonald and Harbaugh 1988). Smaller-scale models may use finite-difference or finite-element methods and have perimeters that are not necessarily coincident with cell walls or cell centers of the larger-scale model. The scope of this analysis includes horizontal interpolation of horizontal-flow components and head. Methods presented in this analysis have been successfully used in the past for problems such as particle tracking and are modified here for the application of computing boundary conditions for smaller-scale models.

Methods

Specified-Flow Boundaries

This analysis presents a general method of computing horizontal flow across any line segment within the domain of a finite-difference model. With this method, specified flows can be determined for smaller-scale model grids that are not orthogonal to larger-scale model grids. For this discussion, an arbitrary horizontal line segment in a model domain is denoted as l, the x axis is parallel to rows, and the y axis is parallel to columns of a finite-difference grid (Figure 1). Only interpolation of flow components from steady-state solutions will be considered; however, the same method could be applied to transient models by interpolating flow components for each time step.

MODFLOW computes flow across all faces of finite-difference cells. Particle tracking and solute transport programs such as MODPATH (Pollock 1994) and MOC3D (Konikow et al. 1996) use linear interpolation of cell wall flow terms to compute ground water velocity anywhere in the model domain. Linear interpolation represents velocities in the x and y directions, V_x and V_y, respectively, as $V_x = f(x)$ and $V_y = f(y)$. According to Goode (1990), this approach is consistent with basic assumptions in the block-centered finite-difference modeling approach. Simple linear interpolation of flow components is used in this analysis to compute horizontal flow at any point in the model domain. Bilinear interpolation of flow components was not tested; however, Goode (1990) discusses the merits of bilinear interpolation of velocity.

[a]U.S. Geological Survey, Tucson, AZ 85719.
[b]CH2M Hill, Redding, CA 96001
[c]U.S. Geological Survey, Fairbanks, AK 99775-5170
[d]Now at Arctic Region Supercomputing Center, Fairbanks, AK 99775
Received July 1997, accepted November 1997

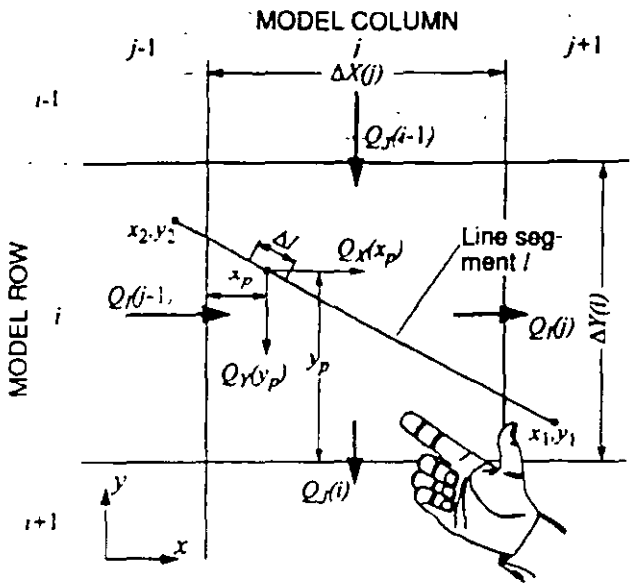

Figure 1. Variables used in development of method to compute flow across line segment l and convention for right-hand rule.

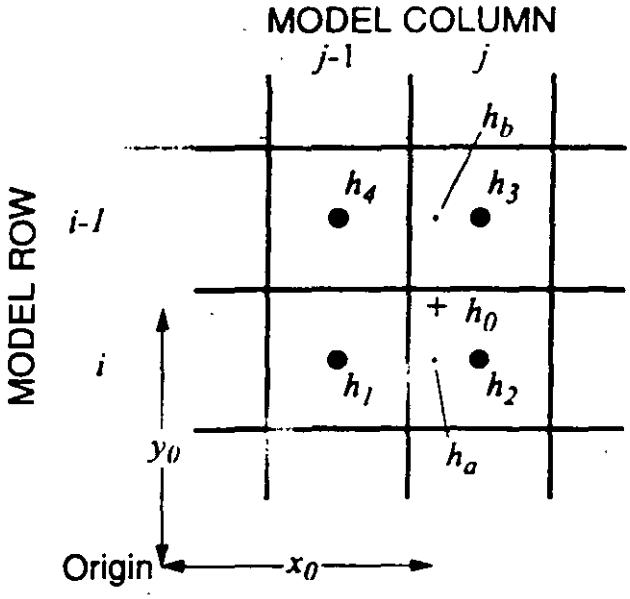

Figure 2. Variables used in bilinear interpolation of head.

Values of cell wall flow for an individual cell in model row i and column j are denoted here as $Q_j(j-1)$ and $Q_j(j)$ for flow along rows and as $Q_j(i)$ and $Q_j(i-1)$ for flow along columns (Figure 1). These quantities are positive if water is moving in the directions of arrows crossing cell walls in Figure 1. This analysis uses a right-hand rule in which flow crossing a line segment is positive in the direction of the extended thumb with the right hand positioned as shown in Figure 1.

To compute horizontal flow across line segment l, divide l into n equal subsegments of length Δl, compute flow components in the x and y directions at the center of each subsegment, and sum the flow components for all subsegments to compute flow for the entire length of l. For subsegment p in cell i,j, components of flow Q_X and Q_Y can be computed as

$$Q_X(x_p) = -\left[\frac{Q_j(j-1) + \frac{x_p}{\Delta X(j)}[Q_j(j) - Q_j(j-1)]}{\Delta Y(i)}\right]\Delta y$$

$$Q_Y(y_p) = -\left[\frac{Q_j(i) + \frac{y_p}{\Delta Y(i)}[Q_j(i-1) - Q_j(i)]}{\Delta X(j)}\right]\Delta x$$

where $\Delta x = (x_2 - x_1)/n$, $\Delta y = (y_2 - y_1)/n$, and other variables are defined in Figure 1. The component of flow normal to l is the sum of Q_X and Q_Y for all n subsections. This result is correct for both isotropic cases (hydraulic conductivity or transmissivity along rows and columns are equal) and anisotropic cases.

Values for n can be selected by trial and error. As n is increased, computed flow across a segment will no longer change significantly with further increases in n. For segments that are contained within a few model cells, values of n in the range of 1 to 5 are appropriate. For segments that span many model cells, values of n in the hundreds may be required.

Specified-Head Boundaries

For this analysis, bilinear interpolation is used to compute head anywhere in the model domain. Bilinear interpolation results in a continuous function, $h_0 = f(x_0, y_0)$, over the domain. The method was chosen because it works well for most model-generated head surfaces, which commonly are smoothly varying. Also, the simplicity of the method makes it easier to apply than higher-order interpolation methods. In areas where adjacent pairs of cells have large differences in horizontal hydraulic conductance, the slope of the water level surface will change at the cell boundary. For these cases, a method that incorporates the hydraulic properties might be better than bilinear interpolation.

For finite-difference models, bilinear interpolation is a simple procedure to interpolate head h_0 at coordinates x_0, y_0 (Figure 2). First, find the group of four cell centers that surround x_0, y_0 with head values denoted as h_1, h_2, h_3, and h_4. Use linear interpolation in the x or row direction to determine head value, h_a, between h_1 and h_2, and to determine head value, h_b, between h_4 and h_3. Finally, use linear interpolation in the y or column direction to calculate h_0 from h_a and h_b.

Application in Single-Layer Model

A two-dimensional model of a hypothetical aquifer system was constructed to test methods of extracting flow and head values (Figure 3). The rectangular flow domain is 10,000 m and 12,000 m in the x and y dimensions, respectively, and is subdivided with an irregular grid of 15 rows and 13 columns. Head in row 1, column 1, is set at a constant 500 m and head in row 15, column 1, is set at 0 m. With a transmissivity of 5000 m^2/d (along rows and columns) and a recharge rate of 5.5555×10^{-3} m/d, the steady-state head distribution computed by MODFLOW is two-dimensional and nonsymmetrical (Figure 3). Inflow from the upgradient constant-head cell is 496,220 m^3/d, and outflow to the downgradient constant-head cell is 1,151,800 m^3/d.

The procedure for computing flow across line segments was first tested using segments 1-2, 3-4, 4-5, and 5-3. The area upgradient from segment 1-2 is 5.8×10^7 m^2 (not including the area of

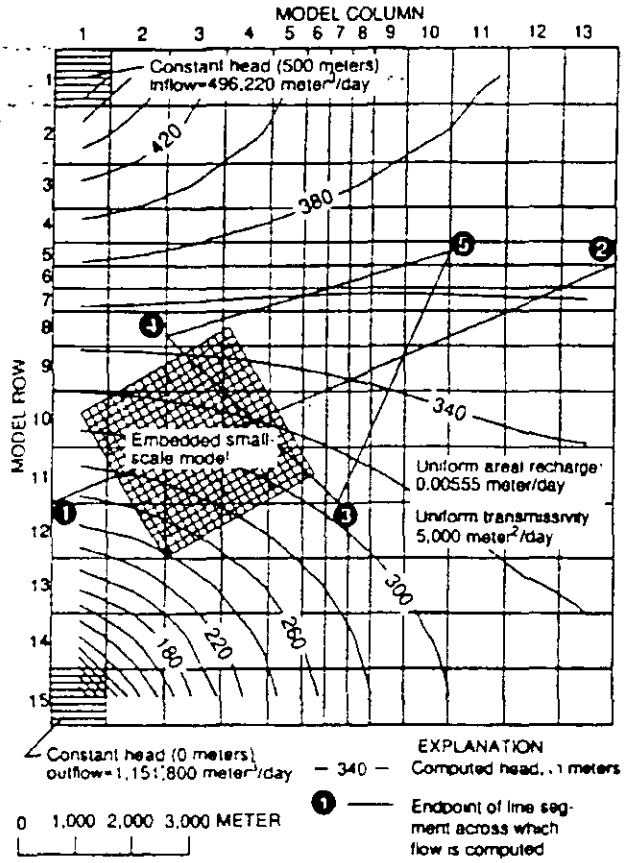

Figure 3. Model of hypothetical aquifer used to test methods.

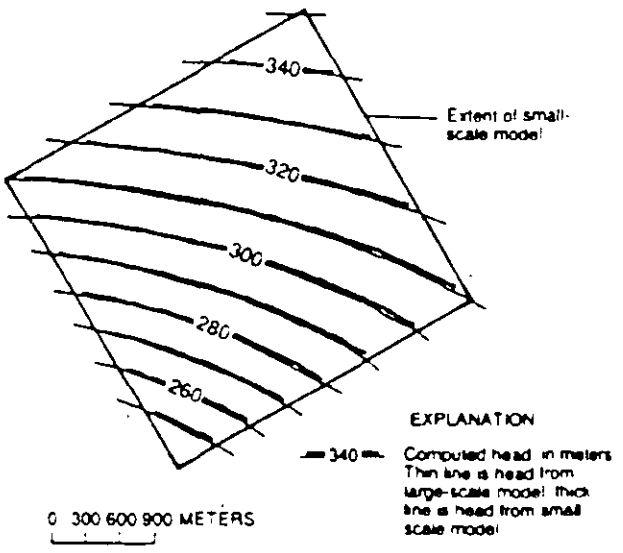

Figure 4. Computed head from large- and small-scale models in area of embedded model.

ie constant-head cell) and the total recharge on this area is 322,219 m^3/d. That recharge plus 496,220 m^3/d of inflow from the constant-head cell is the total of 818,439 m^3/d that crosses segment 1-2. Using 500 subsegments, the total computed flow across segment 1-2 is 818,468 m^3/d, which is within 0.004% of the true value. Segments 3-4, 4-5, and 5-3 define a triangle with an area of 9×10^6 m^2. Areal recharge of 5.5555×10^{-3} m/d to this area results in a volumetric rate of 50,000 m^3/d. Because flow is steady, the net flow across all three sides must be −50,000 m^3/d, using the sign convention that flow out of the region is negative. Using the method previously described with 400 subsegments results in flows of −383,071; 375,385; and −42,222 m^3/d, respectively, for the three sides of the triangle. Summing these values results in a net flow of −49,908 m^3/d, which is within 0.2% of the correct value of −50,000 m^3/d. In a separate test with transmissivity varying from 500 to 25,000 m^2/d in and around the triangle, the net flow across the sides is −50,186 m^2/d. This result shows the method also works with heterogeneous properties.

For another test of the methods, the smaller-scale embedded model shown in Figure 3 was constructed using 20 rows and 20 columns of 150-m square cells and grid lines at a 30-degree angle from grid lines in the larger model. Boundary-flow values were specified around the entire perimeter, except at the cell shaded black where a head value of 240.86 m was specified. That value was calculated by bilinear interpolation of surrounding head values in the larger model. Flows across the outside edges of all other boundary cells of the smaller-scale model were calculated using the procedure presented in this paper. Following edge segments around the region in a clockwise direction results in the proper sign convention of sources and sinks for MODFLOW. The transmissivity along rows and columns was set at 5000 m^2/d and recharge was set at 5.5555×10^{-3} m/d. Note that MODFLOW could not have been used for the embedded model with a 30-degree rotation angle if the system was anisotropic. Computed head values in the embedded model are nearly the same as calculated by the larger model (Figure 4). For specified-flow boundary cells, a measure of error is the difference between the computed head in the embedded model and interpolated head from the regional model at corresponding locations. For specified-head boundary cells, a measure of error is the difference between computed specified-head outflow and interpolated flow in the regional model crossing edges of the specified-head boundary cells. For this analysis, the mean absolute error in head at 75 specified-flow boundary cells is 0.44 m and the maximum absolute error is 1.07 m. The maximum error is 1% of the total head variation in the embedded model. At the specified-head cell, computed outflow in the embedded model is 37,586 m^3/d and interpolated flow across its two outer segments is 37,878 m^3/d, resulting in an absolute difference of 292 m^3/d.

Application in Multilayer Model

A three-dimensional ground water flow model was constructed by Reilly and Pollock (1993) to study areas contributing recharge to pumping wells in a hypothetical shallow stream-aquifer system. Their model was used as the basis for a larger-scale model in which a smaller-scale finite-element model is embedded. The larger-scale model will be called the MODFLOW model. The overall geometry of the MODFLOW model is the same as was used by Reilly and Pollock (1993), but dimensions and elevations have been scaled by a factor of 3.28 so that the original values in feet are interpreted for this study to be in meters. Also, other model parameters have been changed. The MODFLOW model has 54 rows and 69 columns of 125-m square cells in the horizontal directions. Six model layers with approximate thicknesses of 25 m each are used to simulate steady-state flow in the aquifer. The upper layer (layer 1) includes a river with stage varying from 154.8 m in column 1 to 150.9 m in column 69 and with a river bed conductance of 15,000

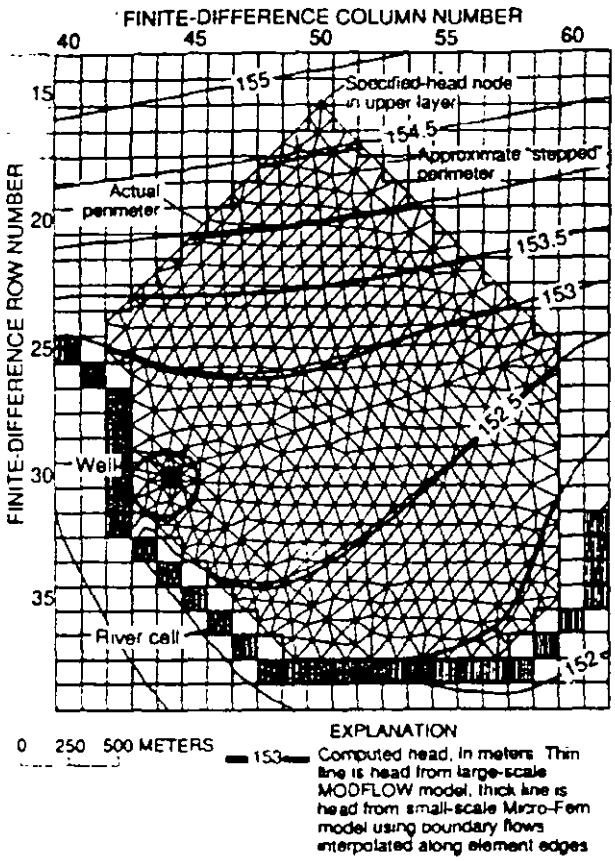

Figure 5. Finite-element model embedded in finite-difference model. Perimeter finite-element nodes in all layers are specified-flow except for the specified-head node in upper layer.

m^2/d for each river cell. A uniform areal recharge of 0.0015 m/d is applied to the surface of layer 1, and an additional inflow of 125 m^3/d is specified in layer 1 to each cell in rows 1 and 54. A well in layer 1, row 30, column 44, pumps 5000 m^3/d. Layer 1 is simulated with a head-dependent saturated thickness using a base elevation of 125 m. In the lower five layers, saturated thickness is not head dependent. The model has two zones of hydraulic properties—zone 1 includes rows 1 through 24, columns 1 through 69, and layers 1 through 6; zone 2 includes rows 25 through 54, columns 1 through 69, and layers 1 through 6. In zone 1, hydraulic conductivity in layer 1 is 20 m/d, transmissivity in layers 2 through 6 is 500 m^2/d and vertical leakance between all layers is 0.2 d^{-1}. In zone 2, hydraulic conductivity in layer 1 is 50 m/d, transmissivity in layers 2 through 6 is 1250 m^2/d, and vertical leakance between all layers is 0.5 d^{-1}.

To test the methods described in this paper, an embedded finite-element model was constructed using the finite-element model program Micro-Fem (Hemker and Nijsten 1996). This model will be called the Micro-Fem model. The Micro-Fem model includes layering, recharge, pumping, and aquifer properties that are equivalent to the MODFLOW model. A total of 607 nodes are included in each layer (Figure 5). Perimeter nodes are coincident with centers of MODFLOW cell walls, thereby allowing lateral boundary flows to be specified either along an approximate stepped perimeter using MODFLOW cell wall flow terms or along the actual perimeter using the interpolation methods described here. Sizes of the triangular element edges are as large as 125 m on the perimeter and as small as 10 m around the well.

Table 1
Water Budgets for MODFLOW Simulation for Areas Within Approximate and Actual Perimeters of Small-Scale Model
[Values are in cubic meters per day]

Flow component	Approximate Perimeter[1]	Actual Perimeter[2]
Inflow		
Horizontal flow, layers 1-6	15,191	13,349
Recharge	6539	6527
Total Inflow	21,730	19,876
Outflow		
Horizontal flow, layers 1-6	16,730	14,875
Pumping	5000	5000
Total Outflow	21,730	19,875
Imbalance (inflow-outflow)	0	1

[1]Flow values are from MODFLOW cell wall flows.
[2]Flow values are interpolated using methods in this paper.

Before constructing the Micro-Fem model, water budgets were calculated for subregions in the MODFLOW model defined by the approximate stepped perimeter and the actual perimeter of the Micro-Fem model. The budget for the approximate perimeter was calculated using MODFLOW cell wall terms with appropriate adjustments of signs to denote inflow or outflow. The budget for the actual perimeter was calculated using horizontal-flow interpolation methods described earlier. Budgets using both methods balance nearly perfectly (Table 1). Horizontal inflow and outflow components for the approximate perimeter, however, are more than 10% higher than for the actual perimeter. The totals are higher because summing cell wall inflows and outflows separately does not cancel out flow terms to get a net flow for boundary reaches where adjacent sets of cell wall flow terms (along rows and columns) alternate between inflow and outflow. For example, suppose that the component of flow normal to a diagonal boundary segment is 100 m^3/d crossing into a region. Suppose also that 150 m^3/d crosses an approximate stepped boundary into the region along model rows and 50 m^3/d crosses the stepped boundary out of the region along model columns. The difference is the correct value of 100 m^3/d for the actual segment, however, including 150 m^3/d as an inflow term and 50 m^3/d as an outflow term in an overall budget for a region results in values of total inflow and total outflow that are too high.

For the Micro-Fem model, boundary conditions were assigned from the MODFLOW model as follows: (1) at the specified-head node in layer 1 shown in Figure 5, head was computed using bilinear interpolation of head at the centers of surrounding MODFLOW cells; and (2) at all other perimeter nodes in all layers, a simulation was made in which flow was computed for each element edge between adjacent perimeter nodes using horizontal-flow interpolation techniques described earlier. For each edge, half of the crossing flow was assigned to nodes on the endpoints. Another simulation was made in which horizontal inflow was taken from MODFLOW cell wall flow terms across the approximate perimeter.

Computed head from the Micro-Fem model using interpolated perimeter flows is nearly the same as head computed by MODFLOW (Figure 5). For 79 variable-head nodes on the perimeter of the Micro-Fem model, the average absolute difference between computed head and interpolated MODFLOW-computed head is 2.6 cm and the maximum absolute difference is 6.4 cm. The

computed inflow at the specified-head cell is 33 m^3/d and the inflow interpolated from MODFLOW cell wall flow terms is n^3/d. Computed head from the Micro-Fem model using the MODFLOW cell wall flows also is nearly the same as head computed by MODFLOW. The average absolute difference between computed head at the perimeter nodes and interpolated MODFLOW-computed head is 2.9 cm and the maximum absolute difference is 8.4 cm. The computed inflow at the specified-head cell is 55 m^3/d. For this problem, either method of computing lateral flow is acceptable for the small-scale model. Use of flows across the actual perimeter may be preferable for many models, however, because the small-scale model does not have to be constructed with perimeter nodes on MODFLOW cell walls.

Conclusions

Interpolation methods allow calculation of flow and head values for boundary conditions in smaller-scale ground water flow models embedded in larger block-centered finite-difference flow models. For models of hypothetical aquifer systems, the methods allowed calculation of boundary conditions for grids that were not aligned with larger-scale model grids. Results from each small-scale model were nearly the same as results in the corresponding subregion of the larger model. The ability to extract flow and head values from any location within a larger-scale model allows greater flexibility in design of smaller-scale models.

Acknowledgments

This work was supported by the St. Johns River Water Management District, Florida; the Fairbanks International Airport, Alaska, the University of Alaska Fairbanks; the U.S. Army Alaska; and the U.S. Army Corps of Engineers, Alaska District.

References

Buxton, H., and T.E. Reilly. 1986. A technique for analysis of ground-water systems at regional and subregional scales applied to Long Island, New York. U.S. Geological Survey Water-Supply Paper 2310, 129-142.

Goode, D.J. 1990. Particle velocity interpolation in block-centered finite difference groundwater flow models. *Water Resources Research* 26, no. 5: 925-940.

Hemker, C.J., and G.J. Nijsten. 1996. Groundwater flow modeling using Micro-Fem: Version 3. Amsterdam, The Netherlands., Hemker Geohydroloog.

Konikow, L.F., D.J. Goode, and G.Z. Hornberger. 1996. A three-dimensional method-of-characteristics solute-transport model (MOC3D). U.S. Geological Survey Water-Resources Investigations Report 96-4267.

McDonald, M G., and A.W. Harbaugh. 1988. A modular three-dimensional finite-difference ground-water flow model. Techniques of Water Resources Investigations of the U.S. Geological Survey, Book 6, Ch. A1.

Miller, R.T., and C.I Voss. 1987. Finite-difference grid for a doublet well in an anisotropic aquifer. *Ground Water* 24, no 4: 490-496.

Pollock, D W. 1994. User's guide for MODPATH/MODPATH-PLOT, version 3 A particle-tracking program for MODFLOW, the U.S. Geological Survey finite-difference ground-water flow model. U.S. Geological Survey Open-File Report 94-464

Reilly, T.E., and D.W. Pollock. 1993. Factors affecting areas contributing recharge to wells in shallow aquifers. U.S. Geological Survey Water-Supply Paper 2412.

Townley, L.R., and J.L. Wilson 1980. Description of and user's manual for a finite element aquifer flow model AQUIFEM-1 Massachusetts Institute of Technology Ralph M. Parsons Laboratory Technology Adaptation Program Report 79-3, Cambridge, Massachusetts.

Ward, D.S., D.R. Buss, J.W. Mercer, and S.S. Hughes. 1987. Evaluation of a groundwater corrective action at the Chem-Dyne hazardous waste site using a telescope mesh refinement modeling approach. *Water Resources Research* 23, no 4: 603-617.

FACULTAD DE INGENIERIA U.N.A.M.
DIVISION DE EDUCACION CONTINUA

CURSOS ABIERTOS

XII CURSO INTERNACIONAL DE CONTAMINACIÓN DE ACUÍFEROS

MODULO III: MODELOS MATEMÁTICOS EN GEOHIDROLOGIA Y CONTAMINACIÓN DE ACUIFEROS

TEMA

DEVELOPMENT OF A PRELIMINARY GROUND WATER FLOW MODEL FOR WATER RESOURCES MANAGEMENT IN THE PINGTUNG PLAIN, TAIWAN

EXPOSITOR: DR. ADOLFO CHAVEZ RODRIGUEZ

PALACIO DE MINERIA
OCTUBRE DEL 2000

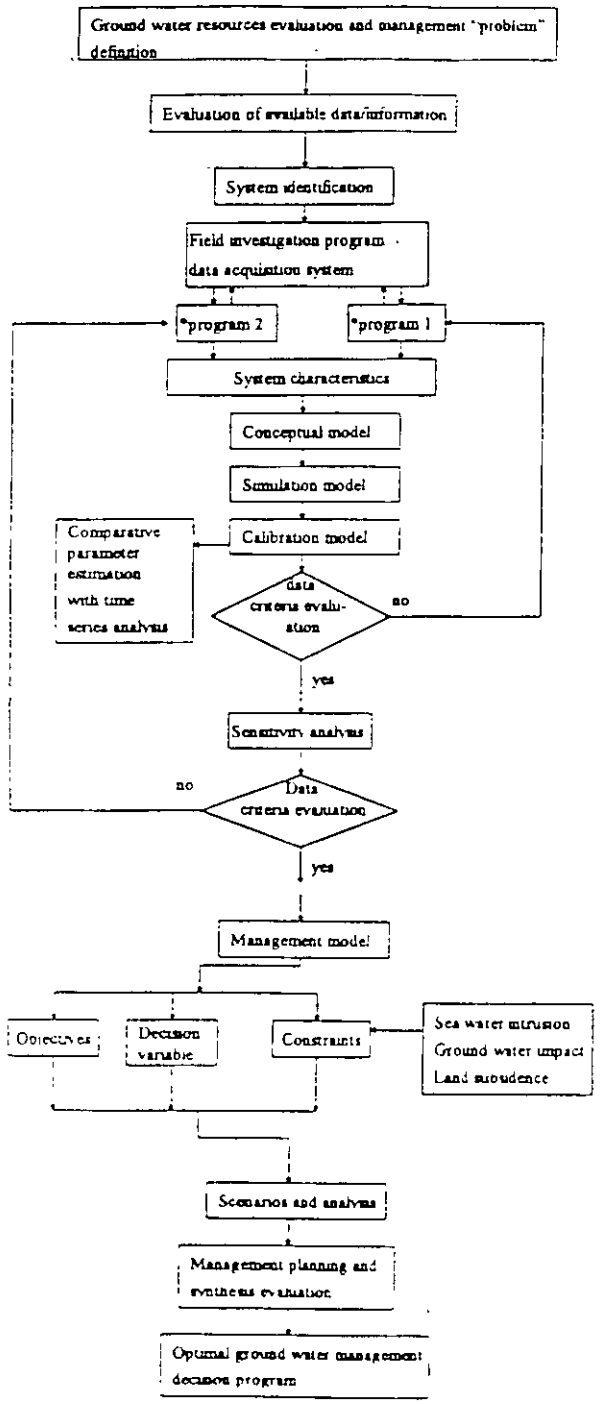

Figure 1. Flow diagram for a ground water resources evaluation and management study in Pingtung Plain (modified from Summers 1984).

involved. With well-recorded data on ground water levels, precipitation and river discharge, comparative estimation of parameters (e.g., infiltration coefficients) using time series analysis is also presented. A project is being executed which applies geostatistical methods to design a future ground water monitoring network.

The fifth phase involves a sensitivity analysis; this may recognize that the calibrated model does not represent a unique match of the calibration target. The dominant parameters will be identified in this phase. A separate project, already executed, is a ground

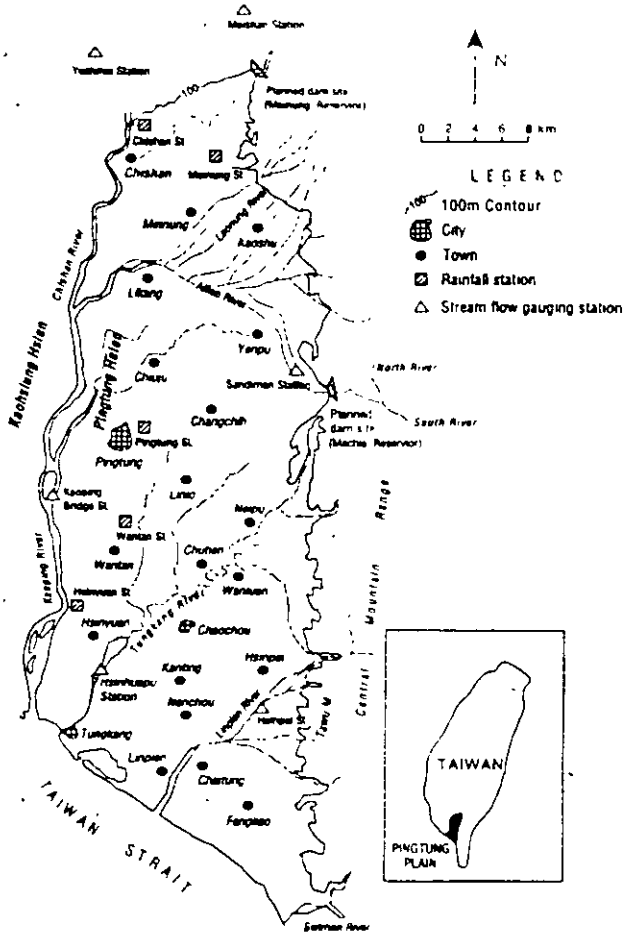

Figure 2. Location map of Pingtung Plain.

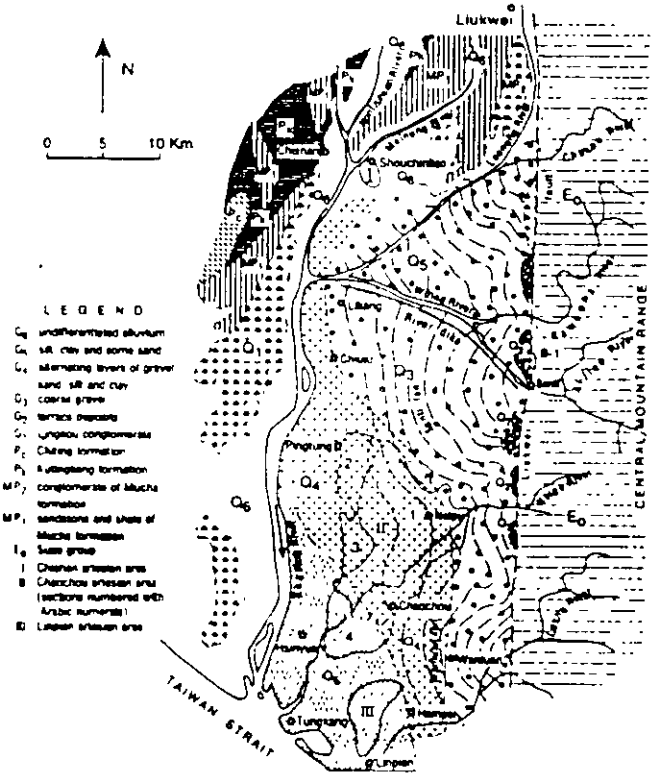

Figure 3. Geological map of the Pingtung Region (after Hsu 1961).

water recharge evaluation study of the Pingtung Plain, aimed at recognizing and quantifying the dominant recharge components.

Prediction is to quantify the response of the system to future events. The prediction model is run with calibrated values for parameters and stresses, except for those stresses (water and environmental protection requirements) that are expected to change in the future. Estimates and analysis of the future stresses are needed in order to perform the different exploitation simulation scenarios of the management model, such that an optimal ground water management program is determined via management planning and synthesis evaluation.

The main objectives of this preliminary ground water model can be summarized as:

1. To evaluate ground water occurrence, aquifer characteristics, ground water recharge and ground water exploitation.
2. To prepare an inventory of the ground water situation in the study area in order to identify the problems due to human activities.
3. To establish a conceptual model of ground water behavior.
4. To develop a transient, numerical groundwater model.
5. To provide decision-makers with a tool to evaluate and predict the influence of various water-use scenarios on the environment. This results will give a framework for future research on a practical DSS (Decision Support System) for ground water management in the Pingtung Plain.

Physiographic Description

Geomorphology

The Pingtung Plain is located in the southwestern part of Taiwan. It includes most of Pingtung Hsien and some of Kaohsiung Hsien, and covers an area of 1210 km². It is bounded in the north by low hills, by foothills lying along the right bank of the Kaoping River in the west, by the Central Mountain Range in the east and by the Taiwan Strait to the south. It is rectangular in shape, 22 km wide in an east-west direction and 55 km long in the north-south direction. Being surrounded by hills in the north, west and east, this plain may be considered in a broad sense as a valley. The topography of the Pingtung area may be classified into four categories: (1) The Pingtung Valley, (2) The Eastern Mountain Region, (3) The Northern Mountain Region, and (4) The Region of the Western Foothills.

Geology

The subsurface geology of Pingtung Plain and its adjacent area has been explored by examining outcrops and interpreting the logs of test holes and existing wells. Rock formations related to ground water occurrence in the area are indicated in Figure 3. A brief description of the consolidated rocks and unconsolidated deposits found in the area is presented as follows. The mountainous regions surrounding the Pingtung Plain consist of rocks of Tertiary age which can be subdivided into the Suao Group, the Mucha, the Kutingkeng, and the Chiting Formations. The unconsolidated sediments underlying Pingtung Plain are of Quaternary age and are the main aquifer of the ground water province in the plain. With respect to their character, they may be divided into the Linkou conglomerate, an older alluvium and a recent alluvium which may be divided into three categories: a zone of coarse gravel, a zone of alternating gravel and sand, and a zone of fine sediments.

Climate

The climate of Pingtung Plain is sub-tropical in accordance with its position just south of the tropic of Cancer. Rainfall is

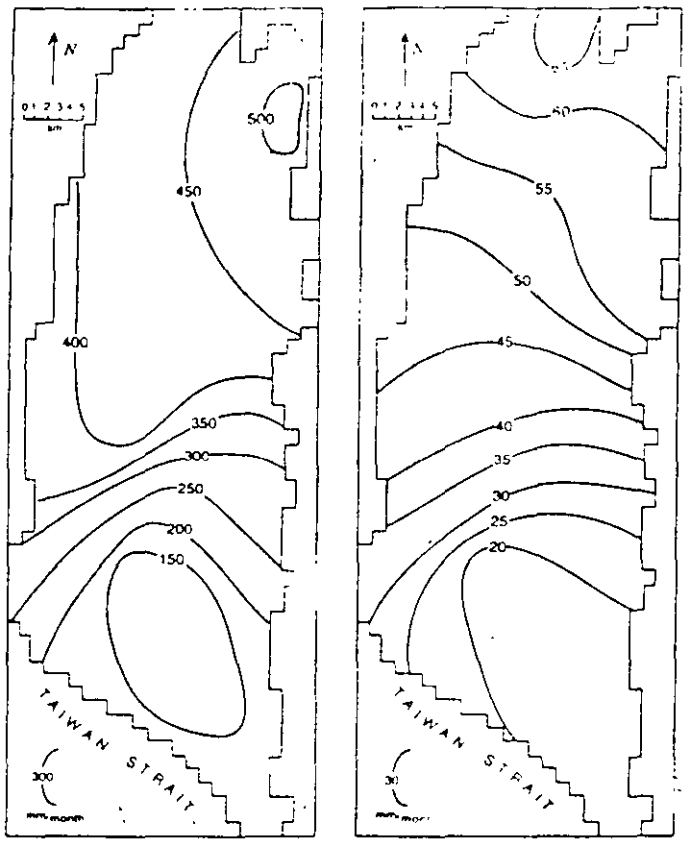

Figure 4a. (left) Average monthly rainfall during the wet season (May–September) and (b) Average monthly rainfall during the dry season (October–April).

alternately affected by typhoons in summer and monsoons in winter. During the summer, typhoons and thunderstorms occur regularly, producing most of the rainfall, while during the winter the monsoons cause a dry season. The rainy season lasts from May to September. Precipitation in the remaining seven months amounts to only about 10 percent of the total, there is usually less than 1 mm rain per month in the dry season.

Total precipitation for the month with highest rainfall at Pingtung Meteo station was 927 mm in August 1988; the lowest monthly precipitation was zero in November 1989 at the same location. The average annual precipitation was 2118 mm (period of record 1951–1990). Spatial and monthly precipitation distributions are shown in Figures 4a and b and a comparison between precipitation and ground water level is shown in Figure 5. The latter diagram shows a seasonal fluctuation in the order of 10 m, indicating a phreatic storativity of approximately 5–10 percent.

Average annual temperature in Pingtung is 24° C, with the highest monthly mean value in July (28° C) and the lowest in January (19° C).

Open water (pan) evaporation observations have been made at six hydrometric stations over a period of 10 years (1981–1990). Average annual pan evaporation is about 1200 mm.

Water Resources Systems

The Pingtung Plain mainly comprises flat areas of the Kaoping, Tungkang and Linpien River catchments as well as several small streams; the three main rivers finally flow into Taiwan Strait. The plain covers an area of 1210 km², about 30 percent of the total for the Pingtung catchments (4070 km²). Since the only source of ground water supplied to the plain comes either directly or indirectly from

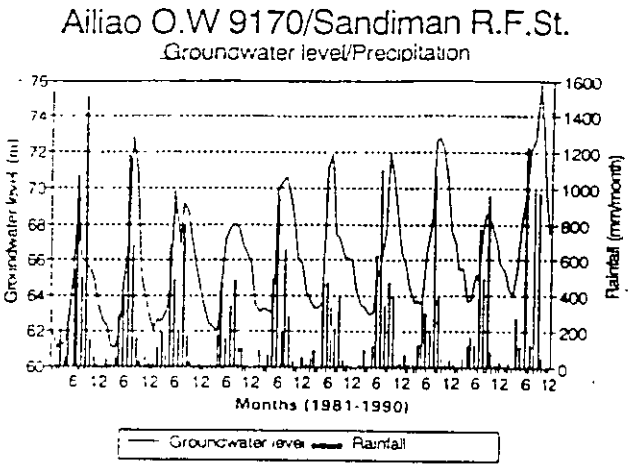

Figure 5. Comparison of monthly precipitation and ground water levels (1981–1990).

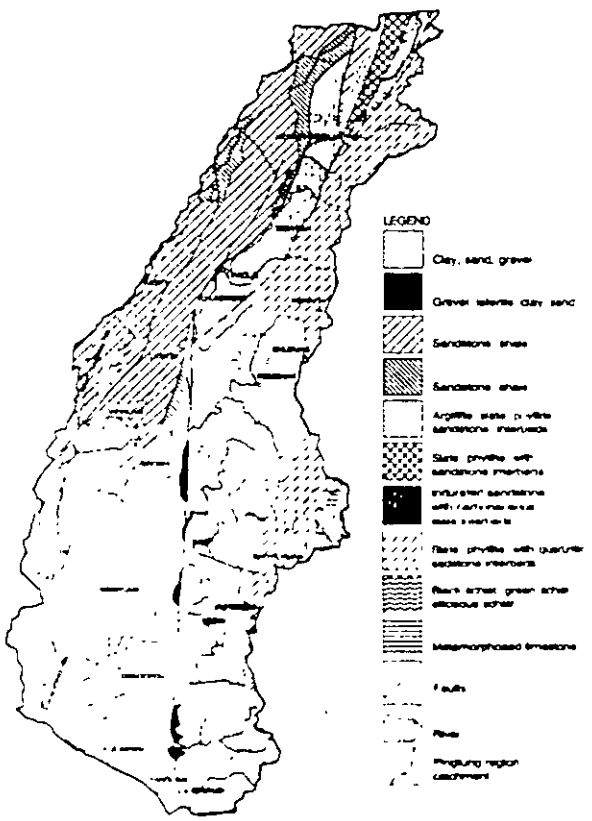

Figure 6. Surface water resource system in the Pingtung Plain.

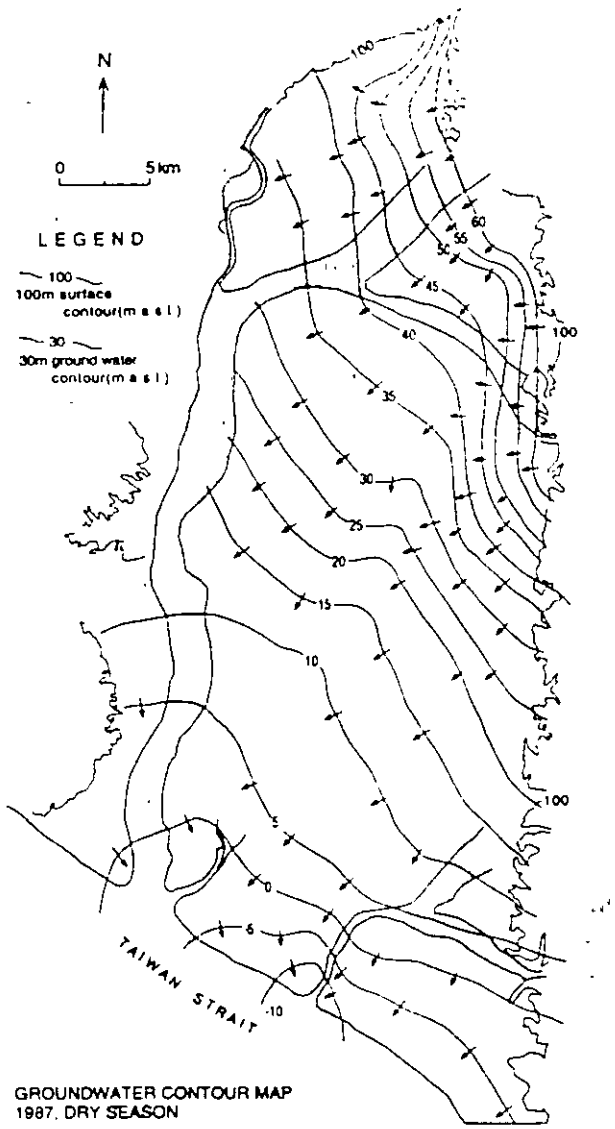

Figure 7. Ground water contour map (after TPWCB 1989).

rainfall in the catchment, rainfall characteristics are the main controlling factor for water resource availability in the plain (Figure 6).

The Kaoping River, with a catchment area of some 3257 km² and a length of 171 km, is the second longest river in Taiwan. At the Kaoping meteorological station (Kaoping Bridge) average annual discharge for the period 1981–1990 was 74×10^8 m³/year; the highest discharge was 38×10^8 m³/month in September 1990 and the lowest 0.27×10^8 m³/month in February 1984. Rainfall occurs mainly in the period May to September; precipitation for these five months totals about 90 percent of the 2517 mm average for the year. A dam is planned in the upstream recharge area, which will have a significant impact on the ground-water regime in the whole plain. This

Table 1
Hydrological Components of the Pingtung Plain Catchment

	Catchment Area (km^2)	Discharge (10^8 m^3/year)	Rainfall (mm/year)	Runoff Coefficient Percent
Kaoping River	3257	74	2517	90
Tungkang River	472	9.2	2066	94
Linpien River	343	8.5	3156	79

factor will need to be taken into consideration during the proposed integrated surface- and ground water management study.

The Tungkang River is located southeast of the Kaoping River and north of the Linpien River. It is the most important surface resource for domestic water supply and industrial use in the neighboring city. It has a catchment area of about 472 km^2 and is 44 km in length. The highest discharge was 11.5 × 10^8 m^3/month in July 1972 and the lowest was 0.3 × 10^8 m^3/month in June 1980. Average annual discharge for the Tungkang River (Hsinhuapu Station) is 9.2 × 10^9 m^3/year (1968–1990). Mean annual rainfall at the flow measuring site is 2066 mm, that for the upstream, midstream and downstream areas are 2493, 2006 and 1700 mm respectively.

The Linpien River is located in the south of the study region and has a catchment area of about 343 km^2. Average annual discharge for the Linpien River (Hsinpei Station) is 8.5 × 10^8 m^3/year (1972–1982). The maximum discharge was 13.4 × 10^8 m^3/month in August 1972, the minimum was 2.6 × 10^8 m^3/month in June 1980. Annual rainfall is about 3156 mm; the highest monthly rainfall of 1125 mm occurred in June 1977 and the lowest was 0.4 mm in March 1980. The above information is summarized for easy reference in Table 1.

Ground Water System

The Pingtung Plain is surrounded to the east and north by mountainous areas and to the west by foothills. These mountainous regions comprise rocks of Eocene-Oligocene age and form a thick sequence of black slate intercalated with beds of coarse or fine-grained quartzose sandstone. The porosity of the slate is very low and hence only local joints and cleavages are available for water storage. Most of the precipitation becomes surface runoff, flowing into the streams and thus across the plain.

The unconsolidated sediments underlying the Pingtung Plain are of Quaternary age and form the main aquifer for ground water in the plain area. In general, ground water is derived principally from direct precipitation onto the plain and partly from local influent, as inferred from the river seepage. The ground water contour map is shown in Figure 7, and surface water resource system diagram is shown in Figure 6. The recharge derives mainly from direct infiltration through unconsolidated deposits along the foothill belts to the north and east and from infiltration of rivers in the upper part of the plain. Ground water generally moves westward to the Kaoping and Tungkang rivers and southwestward to the sea.

Conceptual Model of the Ground Water System

Schematization of the Aquifer Systems

An important tool used to characterize the aquifer are hydrogeological profiles. From cross-section (Figure 8), located as shown on Figure 7, the aquifer system can be classified into three zones by the characteristics of typical alluvial structure. The proximal-fan consists of coarse gravel with poorly sorted pebbles, cobbles and boulders. This zone is considered as the upper unconfined aquifer

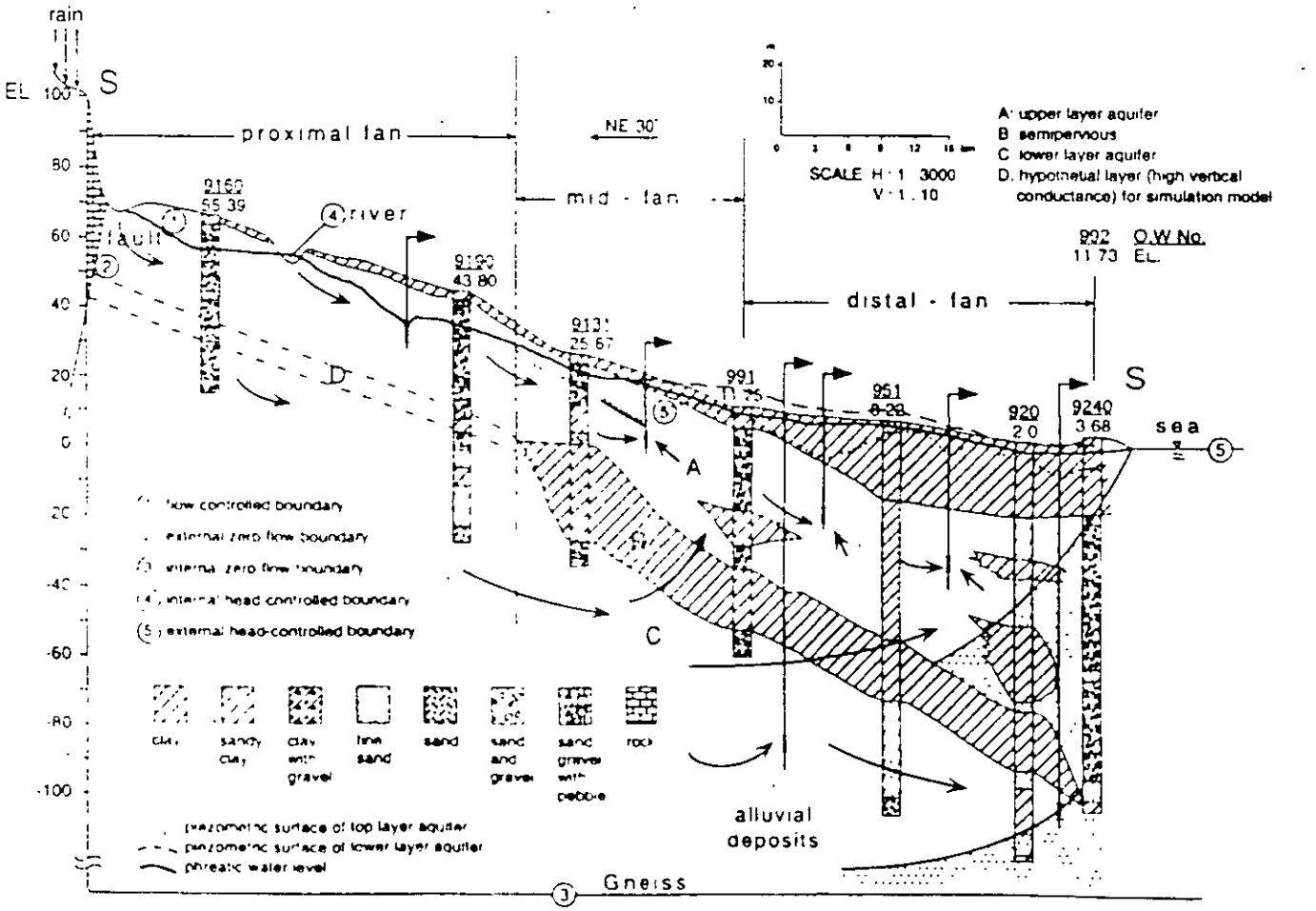

Figure 8. Schematic section for the hydrogeological conceptual model.

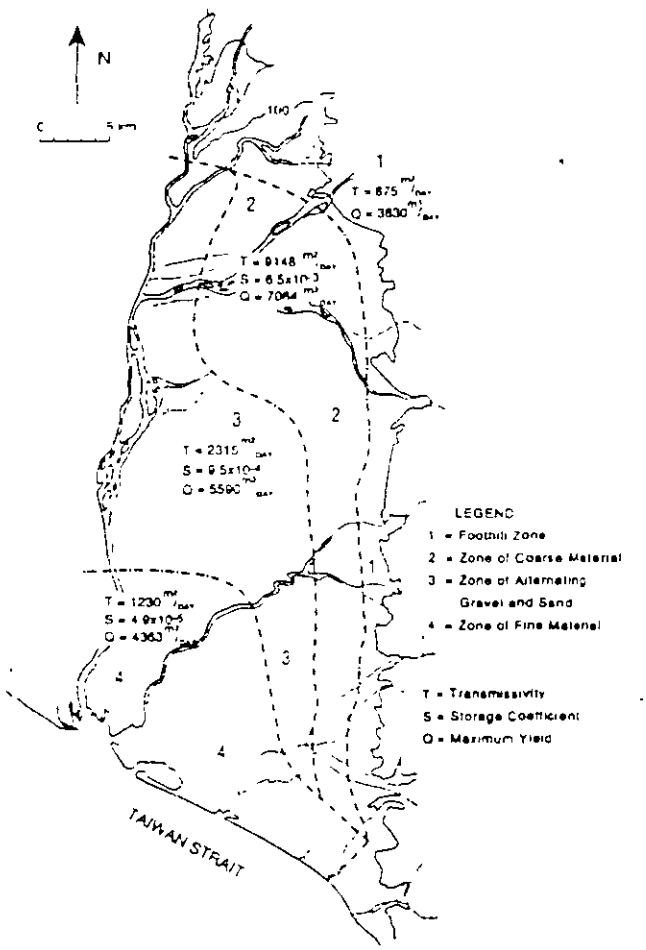

Figure 9. Map showing the properties of water-bearing materials in the Pingtung Plain (after TPGDB 1961).

The mid-fan is composed of moderate size pebbles with thin layers of sand and clay. The distal-fan is mainly an accumulation of clay silt and black sand. From the mid-fan to distal-fan an intercalation of clay with a thickness of 10-20 m occurs. The main semi-confining clay layer (aquitard) forms the geological boundary between the upper and lower aquifers.

The ground water basin in the study area, its cross-section (Figure 8), can be schematically subdivided into three hydrogeological layers that coincide with the well field inventory by the defined depths 10-30 m, 30-60 m, and below 60 m (Ting 1992). The upper layer, the thickness which varies from 10-60 m, is assumed to be an unconfined aquifer, i.e., the transmissivity varies with saturated thickness. The aquifer of the fluvial deposits in the foothills consists of coarse sand and gravel decreasing in size to sand in a downstream direction with a thickness in excess of 220 m (the lower boundary of the basin has not yet been reached by drilling but extends to a depth of at least 150 m below sea level). The middle layer, assumed to be semipervious, is a geological formation which has a very low transmissivity compared to the aquifer, with a thickness of about 20 m of clay and sandy clay. Since this layer does not exist in the proximal-fan, high vertical conductance values are assumed. The lower layer is assumed to be unconfined in the upper reaches of the area and confined from the mid-fan, the storage coefficient may thus alternate between confined and unconfined values. The aquifers are recharged directly by rainfall, by the rivers and by subsurface inflow from the northern upstream part of the fluvial-fan. The study area is hydraulically bounded in the south by the sea (Taiwan Strait).

Aquifer Characteristics

The magnitude and spatial distribution of aquifer characteristics need to be specified. Depending on the type of aquifer, these characteristics are: hydraulic conductivity, K, or transmissivity, T; storage coefficient, S; specific yield, μ and vertical conductance, Vc. As a result of analyses made of the samples from test holes and existing well logs, the Pingtung Plain is initially divided into four subzones with respect to the identified geological formations (Figure 9).

Boundary Conditions

Ground water flow in the main aquifer layers is governed by conditions at the boundaries of the regional system. In this aquifer study three types of boundary conditions are defined: the specified head boundary, specified flux boundary and the head-dependent flux boundary. For present study the multilayered aquifer system has, for practical purposes, been modeled as a two-layered aquifer system: an upper phreatic aquifer and a lower semiconfined aquifer, separated from the upper aquifer by a discontinuous semiconfining layer. In the lower plain, the upper unconfined aquifer becomes confined by surficial clay layers.

Hydrological Stress

There are three types of hydrological stresses which need to be considered for simulation of ground water flow in the plain. These are areal recharge, evapotranspiration, and abstraction.

Numerical Modeling of Ground Water Flow

Model Structure

The computer model MODFLOW is widely applied in hydrogeological practice for simulating ground water flow. This is a modular three-dimensional finite difference ground water flow model (McDonald and Harbaugh 1988) which simulates transient/steady ground water flow in a complicated ground water basin with various natural hydrological processes and/or artificial activities. It has been used for multiaquifer-oriented modeling; for example, to simulate the response of aquifer systems to ground water resource development scenarios. It can also be used for full three-dimensional modeling. In addition to the determination of ground water head distribution in space and time, MODFLOW can calculate flow fluxes across cell boundaries. In this study MODFLOW was applied for the reasons mentioned above and, moreover, because the program (1) is well documented and in public domain code, and (2) the program has been divided into a main program and a series of independent subroutines called modules. The modules have, in turn, been grouped into packages. For example, the Recharge option simulates the effect of rainfall and the soil infiltration recharge coefficient, the River package simulates the effect of a river, etc. This feature makes the use of the model very flexible. The last reason is that future studies may readily couple the program with MODMAN (GeoTrans Inc., Sterling, Virginia) and GIS for optimal ground water management.

Discretization

Based on data availability and hydrogeological conditions, in the case studied here the two aquifer system was divided into 23 columns and 63 rows for simulating ground water flow, grid spacing in both the x and y directions was 1000 m and the grid cells total 1449 (Figure 10). Again based on data availability and the dynamic behavior of ground water level, a month is chosen as the period

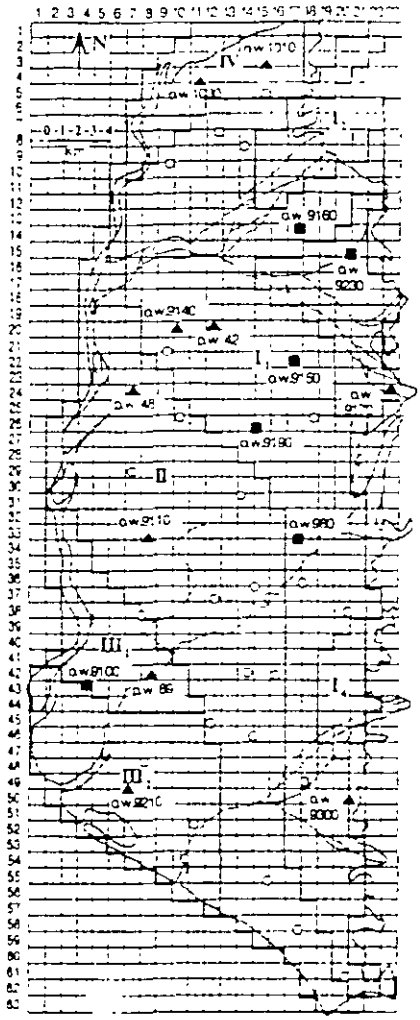

Figure 10 Finite difference grid indicating observation wells and subregion divisions.

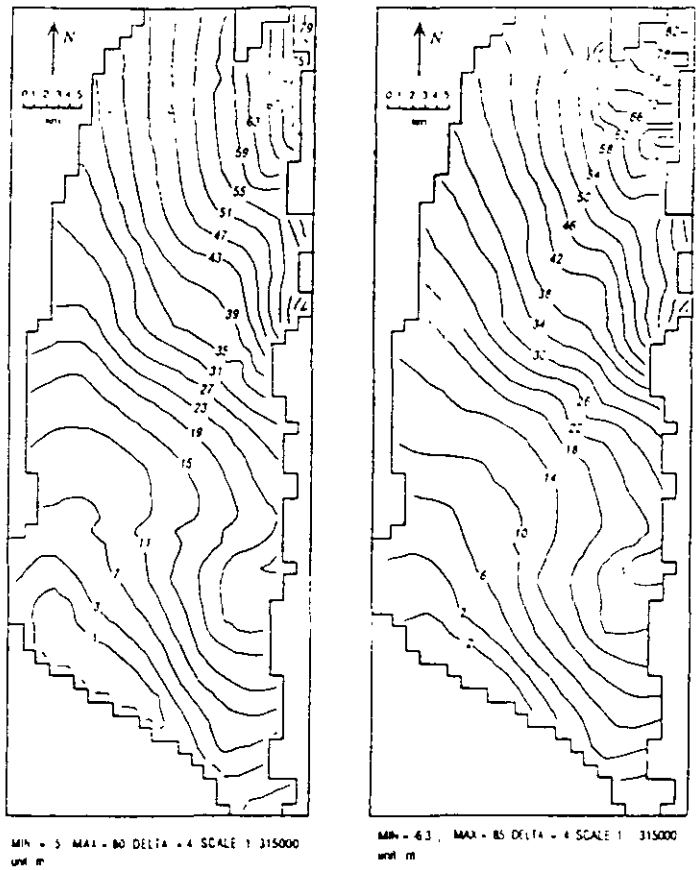

Figure 11a. (left) Contour map of the initial ground water level for layer 1 (December 1987) and (b) Contour map of the initial ground water level for layer 2 (December 1987).

within which all hydrological stresses are assumed constant. Each stress period is divided into two time steps with respect to the timing of calculated and measured ground water level.

Initial Conditions and Historical Ground Water Levels

For reasons of data availability, 1988 was chosen to calibrate the model. To start the calculations one must know the initial ground water head throughout the basin. For this purpose contour maps of ground water levels for the two aquifers have been derived (Figure 11), based on measurements from observation wells and river water levels.

Because of inadequate water table records for the shallow aquifer in the Pingtung monitoring network, measurements at several local pumping wells are also used (Figure 10) for interpolation and plotting. The number of observation wells was greater for the deep aquifer than for the shallow aquifer and the measurement series is also longer. Initial ground water levels for the two aquifers are estimated for all cells from the contour maps.

Model Inputs

The model inputs include hydrogeological parameters, areal recharge, evapotranspiration, abstraction, river influence and boundary conditions. Each of these hydrological phenomena is simulated in MODFLOW by a separate package.

Hydrogeological Parameters

Phreatic Storage Factor, μ, is a characteristic property of the upper aquifer. Based on previous studies (TPGDB 1961) four subregions have been created and initial μ values specified. With the aim being to test the conceptual model, which has already been divided into two aquifers (upper layer and lower layer), eight subregions (I_1,I_2,I_3,I_4,II_1,III_1,III_2,IV), were introduced. The initiating values were taken from previous studies (TPGDB 1961; WRPC 1982, and Tsao 1991) in which four subregions were also considered (Figure 9). These values are thus assumed to be appropriate for preliminary calibration purposes.

Transmissivity, T, for a confined aquifer of thickness b is defined as T = k × b, where K is the hydraulic conductivity, in an unconfined aquifer transmissivity is not as well defined but can still be approximated. However, in the latter case b is the saturated aquifer thickness. In the Pingtung Plain two aquifers are distinguished from the conceptual model. The transmissivities of each layer are therefore estimated individually from the thickness of the aquifer and the hydraulic conductivity. For the upper unconfined aquifer b is taken as the initial saturated thickness. In general, to reflect both the sedimentary situation with respect to the alluvial aquifer for the model area and previous pumping tests in the plain (WRPC 1989), the T values decrease in a downstream direction.

Elastic Storage Coefficient, S. The storage coefficient for a saturated confined aquifer of thickness b can be defined as the volume of water that an aquifer releases from storage per unit surface area of aquifer per unit decline in the component of hydraulic head normal to that surface. In the study area these values decrease

from mid-fan to distal-fan because of a reduction in pore size and increasing confinement. The subregions for storativity are the same as those derived for transmissivity; initial values have been taken from the same above studies (TPGDB 1961, Ting 1992, and Tsao 1991) and are shown in Figure 9.

Vertical conductance, V_c, for a semi-confining layer is defined as k'/b', where k' and b' are respectively vertical hydraulic conductivity and thickness of the semi-pervious layer. Five subregions for V_c are used in the study; the initial values assessed from hydrogeological characteristics are shown Figure 8. Since the proximal-fan is a thick, unconfined aquifer extending to the mid-fan area, the semi-pervious horizon does not exist in the former. A higher value is therefore assumed, so that it represents a physical discontinuity in the model.

Interaction with Rivers

Rivers and streams either contribute to ground water or drain water from it, depending on the head gradient between the river and ground water system. The purpose of the River package (RIV) is to simulate the effects of flow between surface water features and ground water systems. To do this, a river or stream is divided into reaches so that each is completely confined by a single cell. Stream-aquifer seepage is simulated for each reach within the model cell that contains that reach.

River surface and bed elevations and river (stream) bed conductance are contained in this package. River water elevations are calculated for each month using stream discharges and river cross section (Ting 1992); several points have been interpolated. Water surface elevations for the Linpein River were based on the 1972–1982 recorded data. River bed conductance was derived from hydrogeological properties and was subjected to calibration procedures. To complete the process of calculations the RIV1.EXE program was developed for easier manipulation of the data file.

Areal Recharge

The Recharge package (REC) is designed to simulate areal distributed recharge to the ground water flow system. Most commonly, areal recharge is from direct precipitation infiltration, i.e. $R = \alpha \times P$, where R is areal recharge, α is the infiltration recharge coefficient and P is precipitation. It was known from a previous water resources study that annual recharge on the plain is approximately 30 percent of annual precipitation (TPGDB 1961). Due to the distributed character of the TPCDB study, this figure is initially used for comparative purposes and to test the robustness of the model. Because of the different soil properties, geological characteristics, vegetation, rainfall intensity and phreatic water table, etc., varying values may be derived for each of the different subregions. In the present study six subregions are distinguished based on the above mentioned study. In brief, therefore, recharge is first estimated by the TPGDB method, this is then used to calibrate the model and results finally checked against those from the water budget method.

The maximum effective stress for the package is the precipitation amount in each subregional area as obtained by the Thiessen polygon method. Areal abstraction was uniformly distributed within each individual polygon. The infiltration recharge coefficient is an approximate value and is based on the above stated 30 percent of precipitation, this percentage is then distributed in each polygon, though it may be changed during the calibration process the REC1.EXE program has been developed for easy calibration. Anderson and Woessner (1992) have stated that a universally applicable method for estimating ground water recharge has yet to be devised. Given these uncertainties, the model estimates of ground water recharge have been carefully cross-checked against independent results from the water budgeting and chloride mass balance methods (Ting and Overmars 1995). A further estimate of the infiltration recharge coefficient was derived by time series analysis, as presented in Ting (1993, 1996).

Abstraction

The Well package is designed to simulate the inflow or outflow through recharging or pumping wells. Wells are handled in the package by specifying the location of each well and its rate, Q. Negative values of Q are used to indicate well discharge, while positive Q indicates a recharge well.

The package does not accommodate wells which are open to more than one layer of the model. However, a well of this type can be represented as a group of single-layer wells, each open to one of the layers and having an individual Q term specified for each stress period. If this approach is used the discharge from the multilayer well must be divided among the group of single-layer wells, proportional to the layer transmissivities.

More than 20 thousand private abstraction wells and hundreds of pumping stations are situated in the plain (WRPC 1989). Based on the conceptual model described above and the well field inventory, the shallow wells are defined, precipitation minus abstraction is calculated and translated to the recharge package. The residual abstraction amounts are assigned to 99 well cells (a model limitation) representing the well fields used for aquaculture. Each designated well cell represents total pumpage from the actual wells in that cell. The program WELL1.EXE was also developed.

Evapotranspiration

The Evapotranspiration package (ET) simulates the effects of plant transpiration via capillary rise from the saturated zone, i.e., directly from the water table. Evapotranspiration from the unsaturated zone is included in the recharge component. ET subregions are the same as for REC. In this package the maximum rate of evapotranspiration, surface elevation and the extinction depth need to be defined. This model component represents only a minor part of the evapotranspiration in the phreatic area where the water table is close to the surface. A linear relationship between E_t and E_0 is assumed, depending on the ground water depth, with E_t tending to zero for ground water depths approaching 4.5 m.

Surface elevation is derived from the elevation of well locations. From this, a surface elevation contour map is plotted and an extinction depth of 4.5 meters based on soil properties is assumed. With the aim to allow easy manipulation of the data file, the ETR1.EXE program was also developed for this package.

Boundary Conditions

Head-Dependent Flux Boundary. The General-head boundary (GHB) package is used to simulate interactions between the Kaoping River and the upper aquifer. The data required are the same as for the River package, i.e., river surface and bed elevations and river bed conductance. Similarly, the program GHB1.EXE was developed for easy data use. Because of the lack of information on the Kaoping River bed conductance, values were derived from the hydrogeological properties used for the Atliao River. River bed conductance is therefore subject to calibration.

Specified Head Boundary. Because the area adjoins the Taiwan Strait and part of the tidal river, the relevant boundary cells were assigned constant heads for the phreatic aquifer. In the upper con-

fined aquifer in the lower area, with artesian characteristics, a constant head boundary is represented by the ground water table.

Lateral Inflow Boundary. A flux through some of the cells in the foothills was assumed to flow downwards to the plain. These cell values were initially declared as having zero flux before calibration.

Due to the complex input formats and revised factors for the ETR, REC, WEL, RIV and GHB packages in the present study, five input file programs were developed for these packages; it is easy to adjust the factors during calibration. The final data file was hence imported to a newly developed processing program (Chiang and Kinzelbach 1992), called PM, for MODFLOW simulation.

Model Calibration

The model must first be calibrated before it can be used to generate water head forecasts, that is, model parameters are adjusted until the simulation is consistent with the analyst's understanding of the ground water system and all available data. Computed values of head should closely match those measured at selected points (observation wells) in the aquifer (Figure 10). This means that a set of historical data is used to compare with the generated water heads derived by simulation. Analysis of the difference between measured and computed heads gives an indication as to where adjustment of output parameters may be necessary in order to minimize this difference.

In most hydrogeological settings, such as in the area of this study, it is inappropriate to assume steady-state conditions because of large seasonal fluctuations in water levels, steady-state data may also not be available (Anderson and Woessner 1992). There are basically two methods of model calibration: trial-and-error adjustment of parameters and automated parameter optimization.

In the present study the calibrated period is January to December 1988, during which large seasonal fluctuations in water level occur. Transient calibration and trial-and-error procedures are used.

Calibration Procedures

In trial-and-error calibration (Figure 12) initial parameter values are assigned to each cell. Computed and measured values of head are compared and model parameters adjusted to improve the fit.

The following input parameters have received particular attention during the initial calibration:

- Phreatic storage factor
- Transmissivity (layers 1 and 2)
- Vertical conductance (between upper and lower clay)
- Elastic storage coefficient
- Infiltration recharge coefficient
- Factor for potential ET
- Hydraulic conductance of river interconnections
- Conductance between the external source and cell

It will be clear that with optimization using eight parameters the physical meaning of the model is limited.

The accepted generalities of transient calibration are: (1) To first change the input parameters for those nodal areas where the largest deviations occur; (2) To change one type of input parameter in each run, and (3) To determine whether any change of input parameter in one nodal area will have positive or negative effects in other nodal areas.

In the present study 10 shallow and 31 deep wells (Figure 10) were selected as the fitting wells after consideration of their data availability and distribution in each region. The program FIT (Zhou 1991b) is used to select computed values of head from the simulation model output at locations for which observed values were available and to calculate their differences. These differences give the error values (positive or negative) which needs to be minimized during the process of calibration.

With the objective to gain a better insight to the trend of these differences, the error values were contoured for the two aquifers separately. Positive values indicate that the measured heads were greater than those computed. To increase the computed heads in this subregion, either the transmissivity was decreased or the infiltration recharge coefficient was increased or reduced and lateral inflow from the foothills was increased. The negative error values were treated conversely.

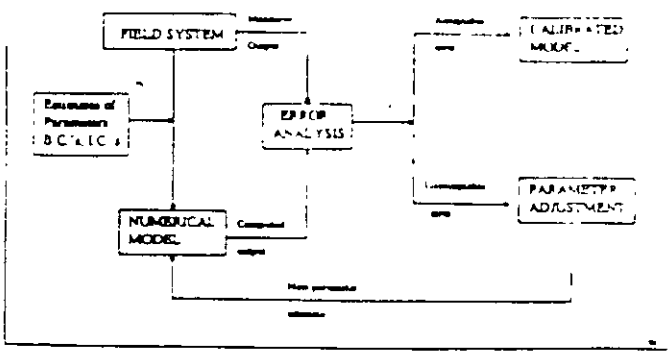

Figure 12. Trial-and-error calibration procedure (after Anderson and Woessner 1992).

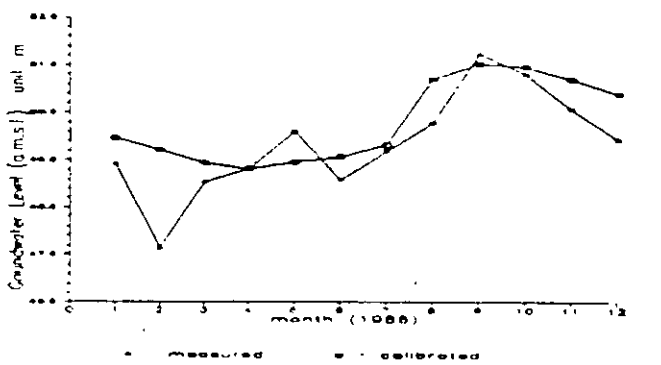

Figure 13a. Calibrated versus historical ground water level (O.W.1010).

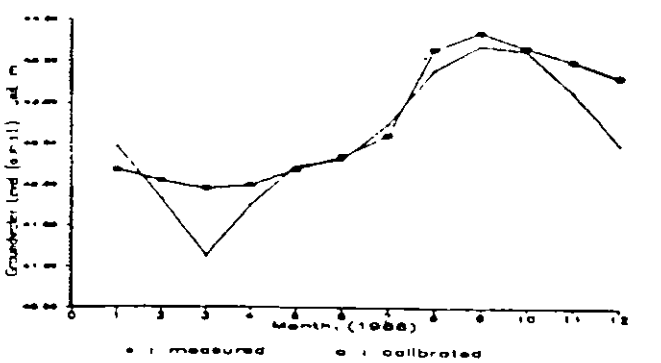

Figure 13b. Calibrated versus historical ground water level (O.W.1030).

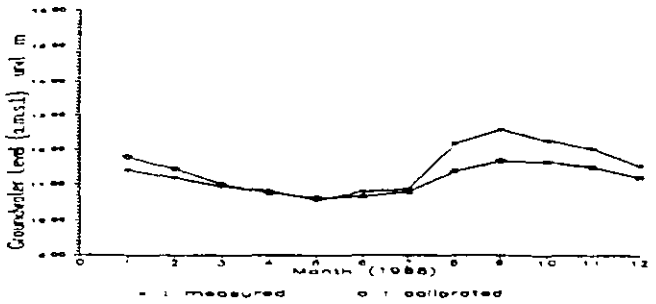

Figure 13c. Calibrated versus historical ground water level (O.W.9110).

Figure 13d. Calibrated versus historical ground water level (O.W.9140).

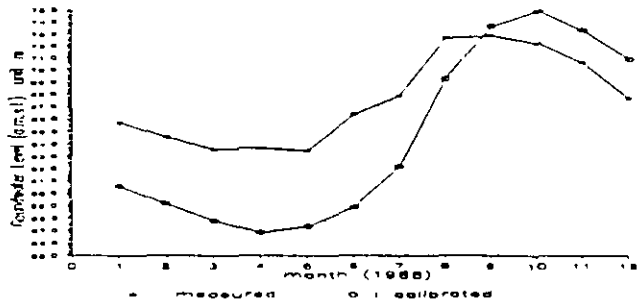

Figure 13e. Calibrated versus historical ground water level (O.W.9170).

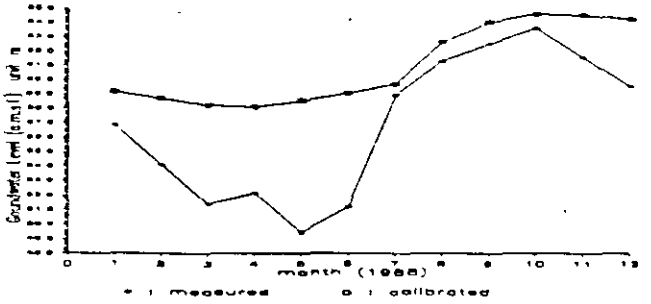

Figure 13f. Calibrated versus historical ground water level (O.W.9230).

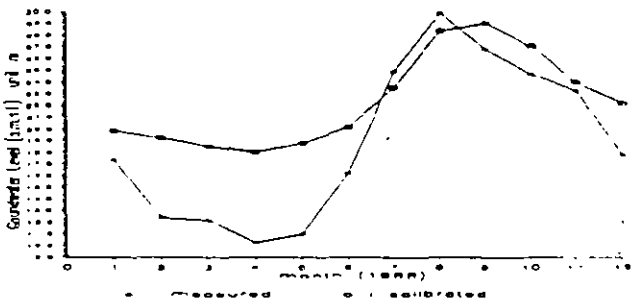

Figure 13g. Calibrated versus historical ground water level (O.W.9300).

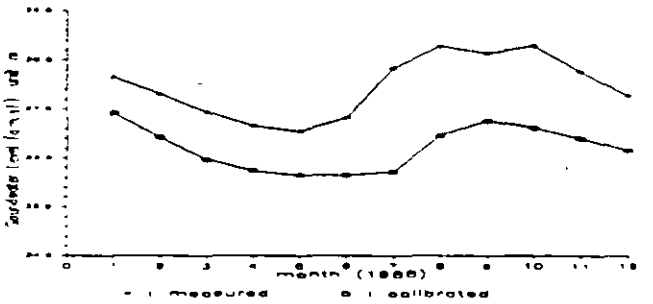

Figure 13h. Calibrated versus historical ground water level (P.W.42).

Figure 13i. Calibrated versus historical ground water level (P.W.48).

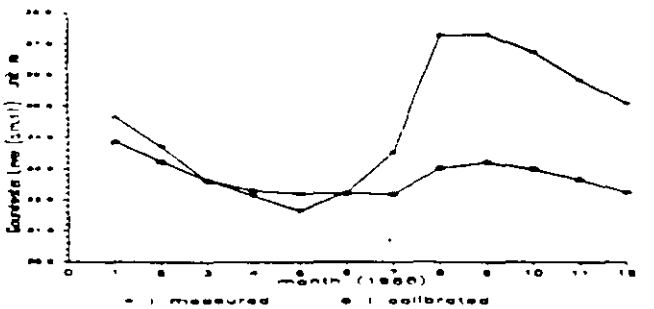

Figure 13j. Calibrated versus historical ground water level (O.W.9190).

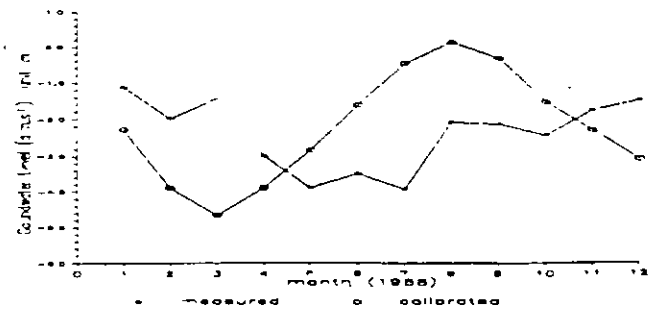

Figure 13k. Calibrated versus historical ground water level (O.W.9210).

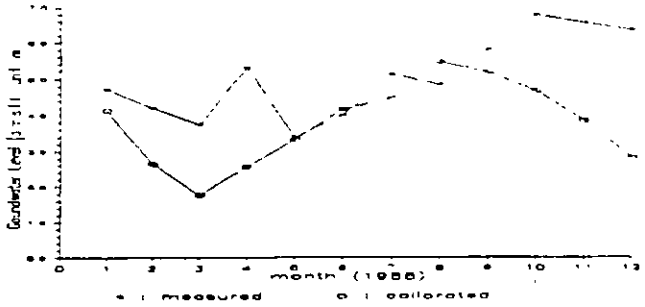

Figure 13l. Calibrated versus historical ground water level (P.W.89).

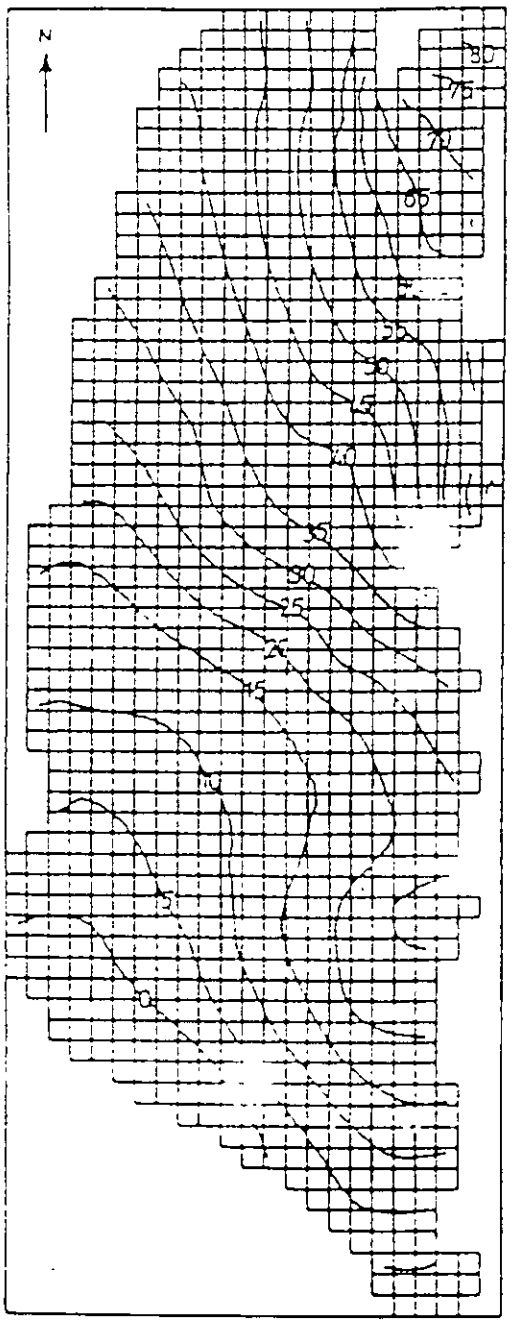

Figure 14a. Contour map of the initial ground water level for layer 1 (December 1987).

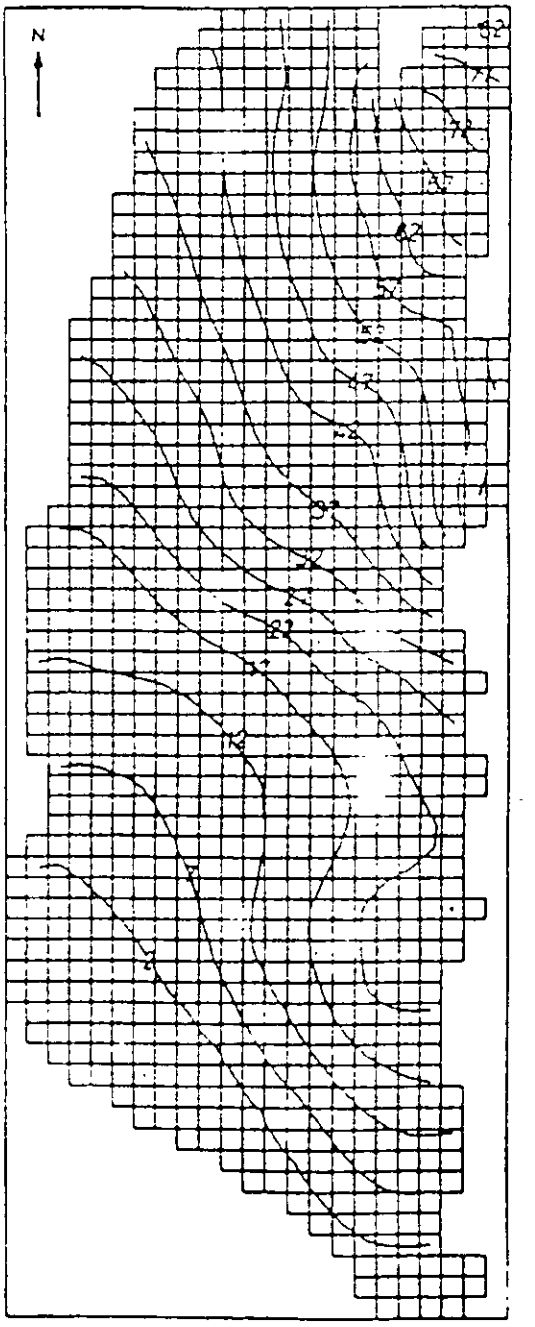

Figure 14b. Contour map of the initial ground water level for layer 2 (December 1987).

Table 2
Results of Parameter Calibration

Parameter Subregion	Phreatic Storativity μ	Transmissivity T_1 (m^2/D)	Vertical Cond. K_v (m/D)	Elastic Storativity S	Transmissivity T_2 (m^2/D)
I_1	0.11	1440	1.1	0.075	2000
I_2	0.12	3000	1.1	0.10	3500
I_3	0.12	2200	1.1	0.10	1700
I_4	0.12	2200	1.1	0.10	3000
II	0.085	1000	0.01	0.0004	1600
III_1	0.0041	200	0.004	0.00004	1500
III_2	0.0011	200	0.001	0.00001	1000
IV	0.10	600	0.05	0.00075	1500

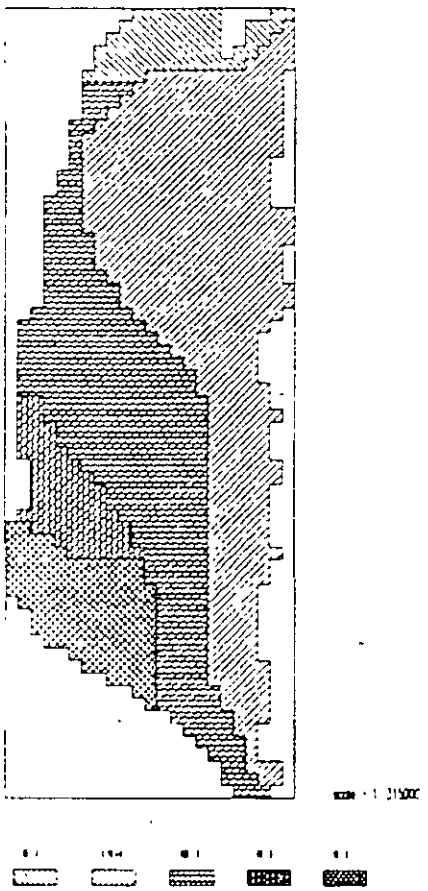

Figure 15c. Sub-regional Transmissivities (T_2).

Results

Calibrated Vs. Historical Water Levels

Most of the calibration fits were reasonable given the only marginally adequate data from this reconnaissance study. For the selected observation wells O.W 1010, 1030, 9110, 9140, 9170, 9190, 9210, 9230, 9300 and P.W 42, 48, 89 (Figures 13a to 13b) the differences between calibrated and measured values were within 2 m. However, results for wells 9170, 9230 and 9300 located in the foothills (for locations see Figure 10), show that differences exceed m. This situation reflects the large seasonal fluctuations in water levels affected by high transmissivity and areal recharge.

Water Level Contours

After calculating the water levels, contour maps for both aquifer 1 and 2 were plotted using the SURFER package. The

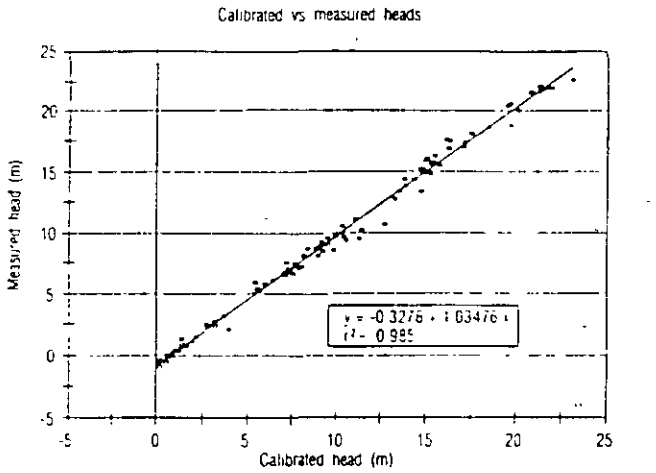

Figure 16. Scatter plot and linear regression analysis of measured heads against calibrated heads.

contour maps are shown in Figures 14a and b, which indicate that the trend in ground water movement was along the artificially induced (pumping stress) slope in a northeast to southwest direction.

Calibrated Parameters

Results from the parameter calibration are presented in Table 2 and Figures 15a to 15c. The global mean error is −0.102 m and global mean absolute error is 0.579 m. The global root mean squared root is 0.465 m, while the global mean relative error is less than 2 percent. A scatterplot and a regression analysis of the measured head against the calibrated heads is given in Figure 16, which can be recognized a reasonable fit between these two data sets.

Water Budget Components from Simulation Results

Results for water budget components derived from the calibrated model are presented in Table 3.

Overexploitation is evident, since about 99 percent of the total ground water recharge is consumed by well extraction. This alarming figure emphasizes the need for a sound ground water management policy.

Sensitivity Analysis

The development of a mathematical model for multiple aquifer systems is a difficult task in that such systems are complex. Interpretation of field and laboratory data used in the regional ground water flow model also requires considerable professional judgement. A sensitivity analysis is thus an essential step in all mod-

Figure 15a. Sub-regional Phreatic Storage Factor (μ_s).

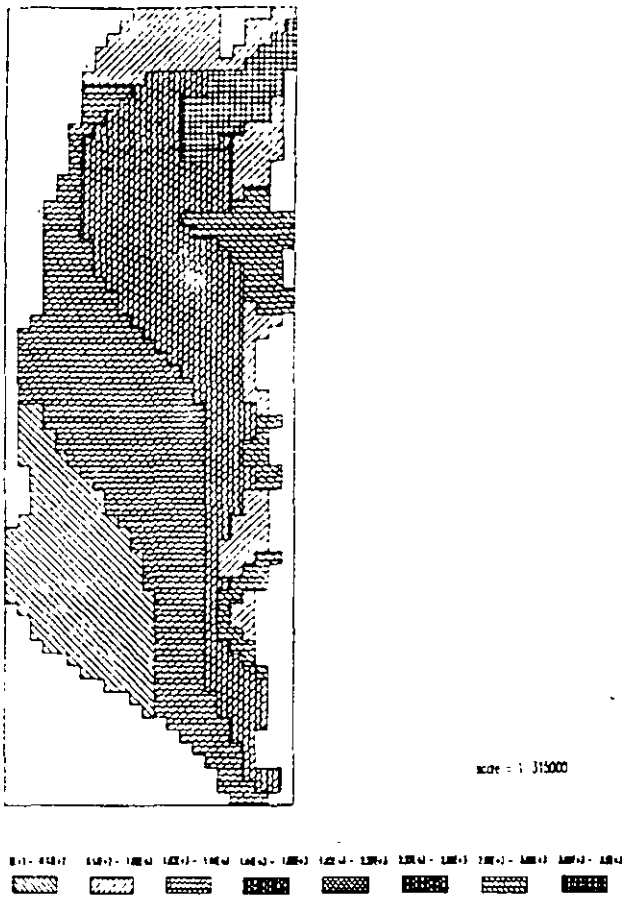

Figure 15b. Sub-regional Transmissivities (T_f).

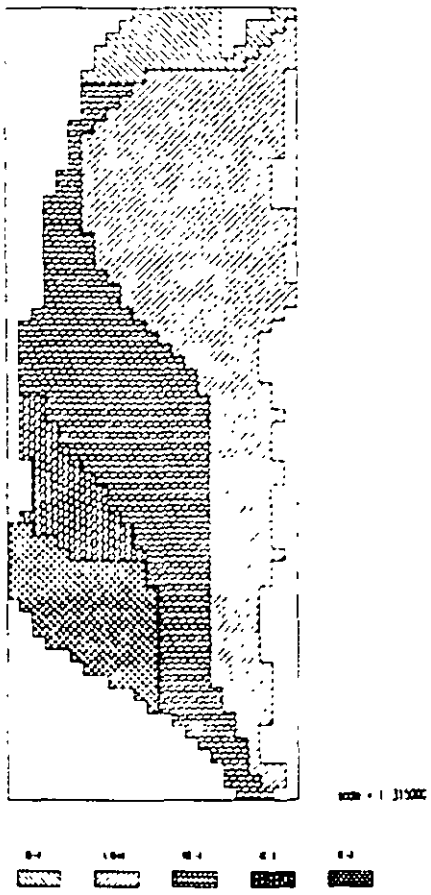

Figure 15c. Sub-regional Vertical Conductance (V_c).

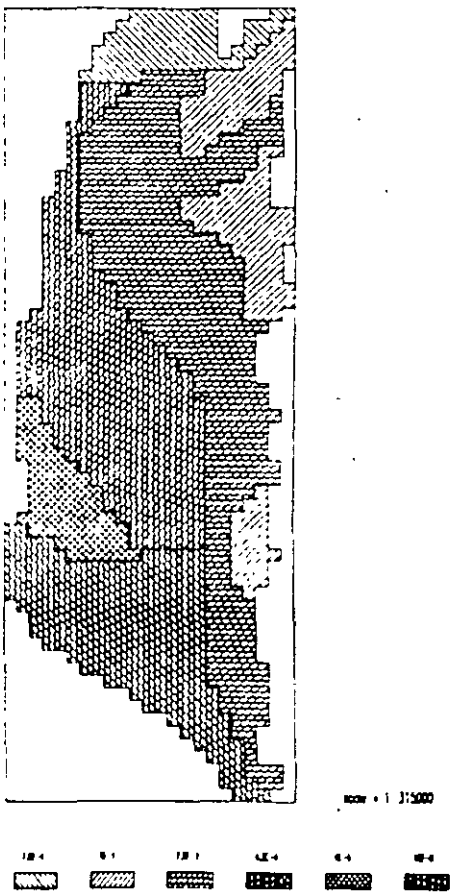

Figure 15d. Sub-regional Elastic Storage Factors (S).

cific yield, transmissivity, storage coefficient and vertical conductance, plus the natural stress processes of infiltration recharge coefficient and the factor for evapotranspiration.

A 50 percent increase/decrease for the above calibrated values are initially assigned in order to assess how sensitive different parts of the aquifer are to deviations from the designated values when parameters are changed drastically. The subsequent stage is to compare the simulated and historical ground water elevations.

Results

Sensitivity of Parameters

There are five major parameters to analyze with respect to sensitivity: phreatic storage factor μ, transmissivities T_1 and T_2, storage coefficient S and vertical conductance V_c. These values are distributed within the eight subregional areas I_1, I_2, I_3, I_4, II, III_1, III_2, IV, as indicated in Figure 10.

Phreatic Storage Factor: The 50 percent increase/decrease in μ caused large changes in hydraulic head over most of the area (Figure 17a), notably in subregion IV. This is the area with the lowest ground water table in the phreatic aquifer and hence the marked change may be due to a higher specific yield in the distal phreatic zone. In general, μ is the most sensitive of all the parameters in the unsaturated zone for this study. Its value is not only affected by climate, but is also influenced by the sediment and soil properties, irrigation and ground water depth. It is thus one of the important components of ground water recharge which should be emphasized during future investigations.

Transmissivity: A similar exercise was carried out with an increase/decrease in the calibrated values for transmissivity within both aquifers. Its value is found to be less sensitive than for phreatic storativity. Subregion $I_{1,2,3,4}$ is the most sensitive in this respect, since T1 and T2 are of greater magnitude than found for other subregions (Figures 17b and 17c).

Elastic Storage Coefficient: Figure 17d suggests that the system barely reacts to large changes in storativity. The reason for this may be that the coefficients are smaller in comparison with other parameters involved in the water balance, and that the seasonal variations in water budget mainly affect the phreatic layer.

Vertical Conductance: Large changes give the same small differences as found for the storage coefficient, though the changes are more significant in cells close to the rivers. The results are further influenced by the difference between river surface elevation and that for the water table. If the difference is smaller, then the sensitivity is also less. Figure 17e presents a general overview of the analysis.

In summary, the most sensitive parameters are the phreatic storage factor, transmissivities T1 and T2, and the storage coefficient. Being a small component, vertical conductance is the least sensitive parameter in any subregion.

Sensitivity of Hydrogeological Stresses

Sensitivity of Areal Recharge and Discharge: The infiltration recharge coefficient, which is related to direct precipitation, is the most sensitive of all stress factors over the total area; this coefficient should, in fact, be considered together with the storage factor. The component ET (evapotranspiration) is found to be less sensitive than the infiltration recharge coefficient, dependent of course on whether its influence reaches the water table in the considered subregion. The effect is considerable in areas with a shallow water table. Lateral inflow naturally has more influence in areas near the recharging rivers; for example, O.W.9300, 9170, 9230 and 1010. This means

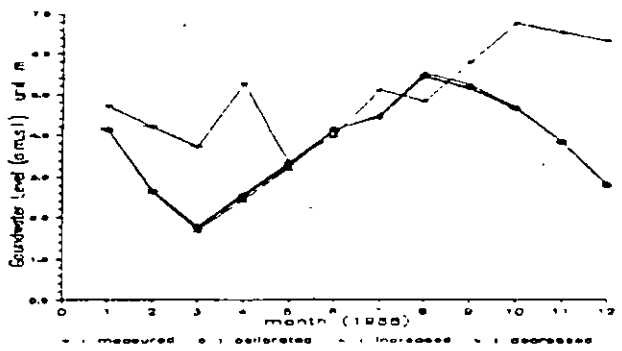

Figure 17e. Vertical Conductance (V_c) for well P.W.89.

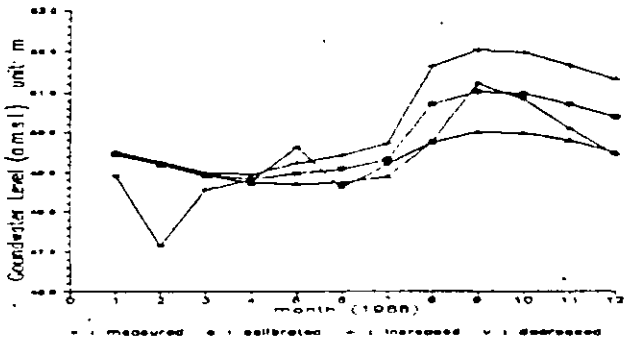

Figure 17f. Infiltration Recharge Coefficient (α) for well O.W.1010.

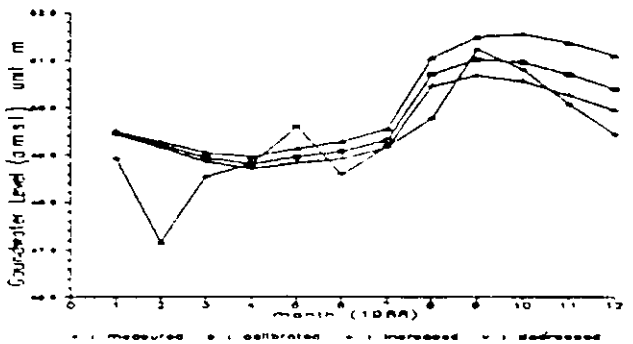

Figure 17g. Value of factor for ET (β) for well O.W.1010.

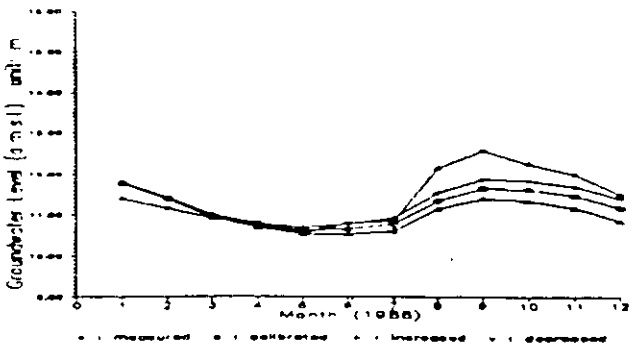

Figure 17h. River leakage for well O.W.9110.

Table 3 1988 Ground Water Balance for Pingtung Plain (10^6 m^3)		
Lateral inflow from mountains	335[1]	280 mm
Inflow from river leakage	73	60 mm
Recharge from rainfall and irrigation	542	450 mm[2]
Total inflow	950	790 mm
River drainage	16	13 mm
Evapotranspiration from water table	57	50 mm
Well abstraction	943	790 mm
Total outflow	1016	850 mm
Storage change	−66	55 mm

[1] Surface water irrigation recharge is not explicitly included by the model. However, [1] and [5] probably include part of this component through the calibration which would explain the rather high values.
[2] This value is for the whole of the Pingtung Plain. If the phreatic area is only 50 percent then the recharge in that area will be approximately 900 mm. This seems rather high but could also include recharge from surface water irrigation (not explicitly introduced by the model).

eling applications where calibration model differences are caused by uncertainties in estimating the aquifer parameters. This is particularly so when many of the parameters have been optimized by the calibration. Different sets of data may in fact produce identical results.

First estimated hydrogeological parameters in Pingtung Plain were determined for the assumed total thickness of the basin and need also to be specified for the individual aquifers. Therefore, for example, the conductivity K was calculated by dividing T by the thickness of each aquifer. River bed conductance cell values for the various reaches were inferred from the relevant geological characteristics in each cell. Areal recharge rate was initially assumed to be 36 percent of the average annual precipitation for the total area. Actual evapotranspiration from the water table in the phreatic area was calculated in the model using an estimated factor, f, times measured evaporation from a free water surface; the depth of zero evapotranspiration flux was assumed to be 4.5 m. Between the surface and 4.5 m, a linear relationship between E_a and E_p is used with f depending on water table depth. This is not very accurate, but only applies to small areas where the water table in the phreatic area is close to the surface. The component accounts for only approximately 5 percent of total evapotranspiration. The location of aquifer boundaries at the border of the mountain range are also required in order to specify the size and shape of the problem domain. In the present study, the effects of the above uncertainties and model assumptions with respect to aquifer boundaries, recharge processes and estimated parameters, hydrological stress, etc., indicate that the derived results need to be carefully evaluated by sensitivity analysis.

The main objectives of such an analysis in the present effort are (1) to gain better insight to the influence of the various hydrogeological parameters and hydrological stresses within the aquifer systems on ground water head, and (2) to determine the most sensible parameter values for further work.

Procedures

It is first necessary to review all the assumed and estimated values for the study area: the hydrogeological characteristics of spe-

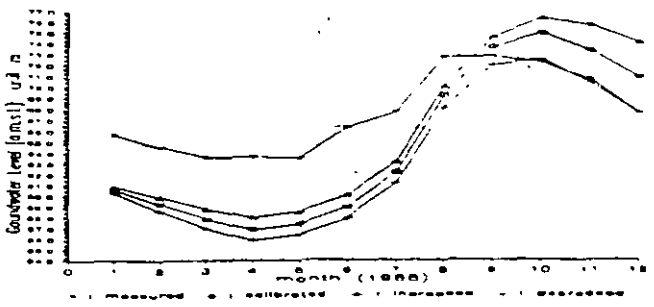

Figure 17a. Transmissivity (T_1) for well O.W.9170.

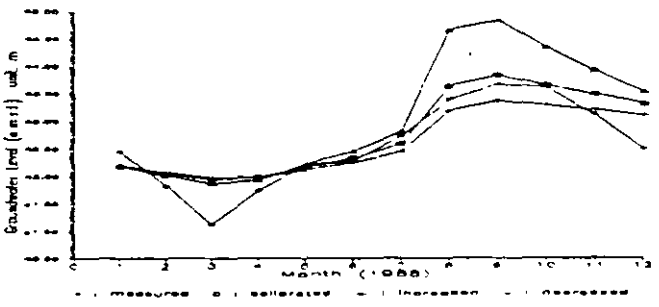

Figure 17b. Phreatic Storage Coefficient (μ) for well O.W.1030.

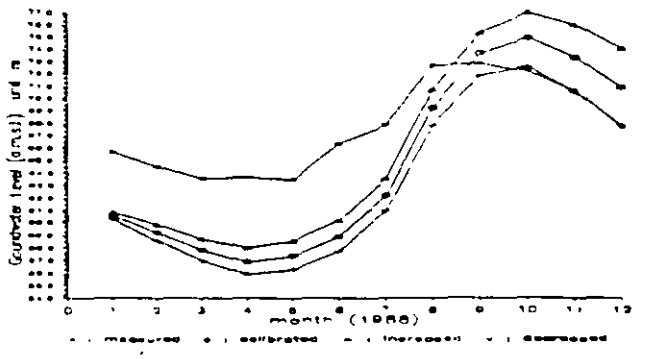

Figure 17c. Transmissivity (T_2) for well O.W. [illegible]0.

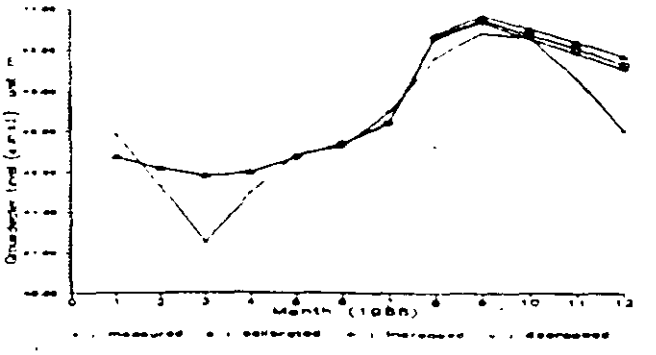

Figure 17d. Storage Coefficient (S) for well O.W.1030.

that lateral inflow is the principal process involved in ground water recharge along the foothills. The overall results are illustrated in Figures 17f and 17g.

Sensitivity to River Leakage The influence of river bed conductance can be compared with that for aquifer hydraulic conductivity. O W 9140, 9110 and 1010 have a slight sensitivity to GHB stream conductance, being located closer to the Kaoping River than the other wells. There are no suitable observation wells along the river to confirm this, but any cell near a river can be chosen to check the sensitivity of this factor (Figure 17h), values are found to be in the same order of magnitude as those for vertical conductance.

Discussion

Model Structure

The present study assumes two time steps and 1449 identically sized cells were specified. It is of course desirable to use small cell spacing and time steps so that the numerical representation better approximates the partial differential equation. However, ground water table levels were only measured once a month, which is obviously insufficient to sample the considerable seasonal fluctuations in the area. Sampling frequency should thus be reassessed for future research, especially in the foothills recharge area (Ting 1993). Cell grid size should also be reduced for the coastal aquifers in order to produce the detail required for calculating the effects of local land subsidence and sea water intrusion.

Initial conditions relate to the distribution of heads in the domain at the beginning of simulation. In this respect the ground water level series were less adequate for the upper aquifer in the study area than for the corresponding lower aquifer values, the calibration procedure thus took considerable time in order to match the observed and computed hydrographs. Boundary conditions are commonly selected to achieve a dynamic average steady-state calibration, which is then used as the initial condition for transient simulation. During the initial calibration, observation wells located at the edge of the foothills showed abnormal fluctuations. The reason is believed to be due to the importance of one of the external stresses. Lateral inflow from the upstream area into the plain was considered first, and the effects from the specified flux boundary cells were translated to the hypothetically relevant recharge well cells. The flux translated as expected and the result better fit the historical heads. It is thus implicit that boundary conditions are also uncertainties when modeling.

Higher and lower parameters were assumed for each package. Since the real physical boundaries were not yet defined by the BAS package, discretization of the model domain was based on the conceptual model. Specifying initial and boundary conditions and the discretization of time have been discussed above. For the BCF package, the previous four subregional areas were expanded to eight. The RIV and GHB packages concerning stream bed conductance lacked experimental data. However, they indicated that experiments on infiltration from the river should be the thrust of further research. Infiltration recharge coefficients and values for the model ET factor are important stress parameters. Because of a lack of experimental data for these, a ground water recharge evaluation study for the Pingtung Plain has been carried out (Ting and Overmars 1995) in order to establish an adequate information base for development of a more precise water resources management model of the area.

Model Calibration

During the transient calibration phase the model was calibrated to water levels observed in the period January to December 1988. In the initial run the calibration process was mainly focused on hydrogeological parameters; lateral inflow derived from upstream to recharge the aquifer along the foothills in the eastern part of the plain was not yet taken into consideration. Although the results fitted reasonably well, it was obvious that the parameter input values were too high compared with previous exploration results (TPWDB 1961) and exceed the range of actual hydrogeological characteristics. Further, from the computed water balance it was seen that lateral inflow to the plain from the northeast contributes approximately 30 percent of total input (Table 3). The parameters, especially transmissivity, were thus decreased for some locations. In addition, hydrological stresses such as the infiltration recharge coefficient in the recharge package were also amended; the coefficient was initially suppressed to note the effect on computed heads. A previous study on the plain showed that ground water recharge for the total area is approximately 36 percent of annual precipitation (TPWDB 1961). The question thus remains whether the infiltration recharge coefficient should be 36 percent for each subregion. Ground water recharge is influenced by different soil properties, the geological characteristics, vegetation, rainfall intensity and depth to the phreatic water table, etc. The infiltration recharge coefficient with respect to specific yield or phreatic storativity, μ, for each subregion was thus obtained by application of time series analysis (Ting 1996). Although the values of α and μ both have uncertainties, this procedure at least reduces the range of estimates in the calibration work. In general, the calibration exercise resulted in a better understanding with respect to the hydraulic behaviour of the aquifer system and improved information concerning its physical properties.

A trial-and-error calibration may produce non-unique solutions, and is also influenced by the modeler's expertise and preferences when different combinations of parameters yield essentially the same head distribution. Further research is thus required using automated inverse modeling by either a direct or an indirect approach, followed by careful calibration evaluation and monitoring. The objective of quantified calibration is to minimize the average error by the so-called calibration criterion. Three ways of expressing the average difference between simulated and measured heads are commonly used: mean error, mean absolute error and standard deviation (Anderson and Woessner 1992). In addition, an error map is able to indicate where aquifer parameter adjustment is required or changes to the assumed hydrological stress are needed. However, if fewer measured data are available, with interpolations between distant observation wells, this may give misleading results for parameter calibration. For example, at present there are only six observation wells available in the phreatic aquifer for the whole domain, in such a situation it is better to compare the individual corresponding values from the lower aquifer.

Sensitivity Analysis

Sensitivity analysis is typically performed by changing one parameter value at a time in the study area. From this analysis, the infiltration recharge coefficient for ground water recharge was shown to be the most sensitive parameter. The reason for this is the fact that direct precipitation infiltration to ground water is the main water balance component. Both the infiltration recharge coefficient (α) and phreatic storage factor (μ) are uncertain parameters, their values significantly affecting the amount of ground water

recharge. Comparative estimation by time series analysis was also performed (Ting 1996). From this it can be seen that for the proximal alluvial fan, for example, at well O-W 9160 the infiltration recharge coefficient, α, is about 0.57-0.85. It would seem from the study that satisfactory results could be obtained if at least one of the coefficients were better defined. It is therefore concluded that specific values are required before real-time modeling is contemplated. This demands additional field experiments.

Conclusions and Recommendations

The following general conclusions and recommendations are drawn from this ongoing research program to date:

This study was initiated to improve knowledge of the hydrogeological situation in the Pingtung Plain in order to make efficient management of the water resources possible.

Previous studies on the use of ground water resources in the Pingtung Plain have been developed on an ad hoc basis and few data were available. This research was therefore based on a simple conceptual model, with many aquifer properties such as the phreatic storage factor, transmissivity, storage coefficient and river conductance having to be estimated. The initial results have proved encouraging, however, and have confirmed that the need for integrated management of both surface and ground water is urgent. The data base has been significantly enhanced, though there is still a need for more complete information to improve and verify the initial model and calibration. To this end, available data on hydrogeology should be organized and located within one authority and additional field experiments should be carried out to better specify the important hydrological parameters.

The present calibration exercise and sensitivity analyses have given better insight to the hydraulic behaviour of the aquifer system and have improved the state of knowledge relating to its physical properties. The sensitivity analyses also clearly show that the infiltration recharge coefficient is a dominant hydrological stress component, ground water recharge research is thus an important issue for the Pingtung Plain.

The numerical model MODFLOW was used to simulate ground water flow, though required considerable calibration effort in order to arrive at realistic hydrogeological parameters and stresses. The calibrated recharge figures match rather well with results from the water budget calculations. To facilitate further work, a comprehensive computer data base should be established (e.g. at the Water Resources Department) for the storage and processing of observation data and for construction of a redesigned ground water monitoring system. The standard of observation wells and the observations themselves should be inspected regularly.

Acknowledgment

Support of the study was received from the National Science Council and National Pingtung Polytechnic Institute for the first author on his doctoral research program. This support is gratefully acknowledged.

References

Anderson, M.P. and W. W. Woessner. 1992. *Applied ground water modeling - simulation of flow and advective transport*. Calif: Academic Press, Inc.

Chiang, W.H. and W. Kinzelbach. 1992. *Processing MODFLOW*. Kassel University, Germany: Dept. of Civil Engineering.

Hsu, T.L. 1961. The artesian water system beneath the Pingtung Valley southern Taiwan. In *Proceedings of the Geological Society of China*, no. 4: 73-81.

McDonald, M.G. and A. W. Harbaugh. 1988. A modular three-dimensional finite-difference ground water flow model. U.S. Geological Survey Open File Report 83-875, Book 6.

Simmers, I. 1984. A systematic problem-oriented approach to hydrological data regionalisation. *Journal of Hydrology* 73: 71-87.

Taiwan Provincial Groundwater Development Bureau (TPGDB). 1961. Investigation report on ground water resources of the Pingtung Plain. Taichung, Taiwan: Taiwan Provincial Groundwater Development Bureau.

Taiwan Provincial Water Conservancy Bureau (TPWCB). 1989. Study on the improvement of the groundwater monitoring system in Taiwan-Pingtung Plain. Taichung, Taiwan: Taiwan Provincial Water Conservancy Bureau.

Ting, C.S. 1992. Application of a groundwater model in the dispute among water users in the Pingtung Coastal Plain, Taiwan. In Proceedings of international workshop on ground water and environment, 332-345, Beijing, China.

Ting, C.S. 1993. Groundwater resources evaluation and management studies for the Pingtung Plain, Taiwan, PhD Program Series Report, Amsterdam: Free University.

Ting, C.S. and M. Overmars. 1995. Groundwater Recharge in Pingtung Plain, South Taiwan. Pingtung, Taiwan: National Pingtung Polytechnic Institute.

Ting, C.S. 1996. Estimation of Groundwater Recharge Rate by Application of Time Series Analysis in the Pingtung Plain, Taiwan. In Proceedings of 7th IAHR International Symposium of Stochastic Hydraulics, 485-490, Mackay, Old Australia, Australia.

Tsao, M.J. 1991. A Study of the Local Effective Groundwater Resources Usage and Pollution Prevention. M.Sc. thesis, National Chung Hsing University, Taichung, Taiwan, ROC (in Chinese).

Water Resources Planning Commission (WRPC), Ministry of Economic Affairs, ROC. 1982. Groundwater resources investigation on Pingtung Plain, September, Taipei, Taiwan: Water Resources Planning Commission, Ministry of Economic Affairs, Republic of China.

Water Resources Planning Commission (WRPC), Ministry of Economic Affairs, ROC. 1989. An investigation on a groundwater basin impacted by Machia Reservoir, December. Taipei, Taiwan: Water Resources Planning Commission, Ministry of Economic Affairs, Republic of China.

Zhou, Y. 1991a. KALMOD, A stochastic-deterministic model for simulating groundwater flow with kalman filtering, Part A, Methodology.

Zhou, Y. 1991b. KALMOD, A stochastic-deterministic model for simulating groundwater flow with kalman filtering, Part B, User's Manual. Delft, The Netherlands: IHE, International Institute for Hydraulic and Environmental Engineering.

FACULTAD DE INGENIERIA U.N.A.M.
DIVISION DE EDUCACION CONTINUA

CURSOS ABIERTOS

XII CURSO INTERNACIONAL DE CONTAMINACIÓN DE ACUÍFEROS

MODULO III: MODELOS MATEMÁTICOS EN GEOHIDROLOGIA Y CONTAMINACIÓN DE ACUIFEROS

TEMA

RELATIONSHIP BETWEEN PUMPING – TEST AND SLUG – TEST PARAMETERS: SCALE EFFECT OR ARTIFACT?

EXPOSITOR: DR. ADOLFO CHAVEZ RODRIGUEZ
PALACIO DE MINERIA
OCTUBRE DEL 2000

Relationship Between Pumping-Test and Slug-Test Parameters: Scale Effect or Artifact?

by James J. Butler Jr.[a], and John M. Healey[a]

Abstract

In most field investigations, information about hydraulic conductivity (K) is obtained through pumping or slug tests. A considerable body of data has been amassed that indicates that the K estimate from a pumping test is, on average, considerably larger than the estimate obtained from a series of slug tests in the same formation. Although these data could be interpreted as indicating a natural underlying scale dependence in K, an alternate explanation is that the slug-test K is artificially low as a result of incomplete well development and, to a much lesser extent, failure to account for vertical anisotropy. Incomplete well development will often result in only the most permeable zones being cleared of drilling debris, with much of the screened interval remaining undeveloped. More cursory development can leave a low-K skin along the entire screened interval. Failure to recognize such conditions can result in a K estimate from a slug test that is much lower than the average K of the formation in the vicinity of the well. By contrast, neither a skin nor vertical anisotropy will have a significant impact on K estimates from pumping tests when semi-log analyses and/or observation wells are used. However, a reasonable estimate of aquifer thickness is required to convert the transmissivity calculated from a pumping test into an average K for the aquifer. Prior to invoking a natural scale dependence to explain the results of different types of hydraulic tests, head data should be closely examined and serious consideration given to alternate explanations.

Introduction

Pumping and slug tests are the primary means by which hydrogeologists obtain in situ estimates of the transmissive properties of a formation (Kruseman and de Ridder 1990, Butler 1997). Since the duration of most pumping tests is on the order of hours to days, the formation volume that is affected by the average pumping test is considerably larger than that affected by a slug test. Given the different formation volumes involved, it is not surprising that these tests can yield different parameter estimates when performed at the same well. In many geologic settings, one might expect that the average value obtained from a program of slug tests would converge on the estimate obtained from a large-scale pumping test as the number and spatial coverage of the slug tests increased. However, a large body of field data indicates that the hydraulic conductivity (K) estimate obtained from a series of slug tests is, on average, considerably lower than that obtained from pumping tests in the same formation (e.g., Bradbury and Muldoon 1990, Rayne 1995, Rovey and Cherkauer 1995). Recently, Rovey and Cherkauer (1995), among others, have interpreted these data as indicating a natural underlying scale dependence in K. Their basic hypothesis is that a pumping test is strongly affected by infrequent-in-space channels (conduits) of relatively high K, while a slug test rarely samples such "extremely rare" heterogeneities.

In this paper we examine the relationship between pumping-test and slug-test parameters in an attempt to offer another explanation for this widely observed difference. We show that it is difficult to theoretically substantiate the infrequent-conduit hypothesis. Instead, we propose that the difference is primarily a function of incomplete well development and, to a lesser degree, uncertainty concerning aquifer thickness and vertical anisotropy. Both hypothetical examples and field data are used to support our explanation. We want to emphasize that the primary purpose of this paper is not to dispute the existence of a natural underlying scale dependence in hydraulic conductivity. Rather, the purpose is to demonstrate how head data from hydraulic tests can be used to ascertain whether an observed scale dependence is a product of natural processes or an artifact of human activity and analysis methodology.

Examination of the Infrequent-Conduit Hypothesis

Butler and Liu (1991, 1993) developed a series of semianalytical solutions to investigate the effects of lateral heterogeneities on pumping-induced drawdown in idealized non-uniform formations. These same solutions can be used to assess the influence of infrequent high-K conduits on parameter estimates obtained from pumping tests. Figures 1a and 1b show two simple models of lateral heterogeneities in which a high-K zone (an infinite strip in Figure 1a and a circular disk in Figure 1b—labeled K_1 in both plots) is embedded in a uniform matrix of lower K (labeled K_2 in both plots). Although clearly idealized, these configurations enable considerable insight to be gained concerning pumping-induced drawdown in heterogeneous formations in which the major element of heterogeneity is a discrete zone of much higher K than the surrounding medium.

Figure 2 displays the dependence of pumping-induced drawdown on the magnitude of the contrast between the conductivity of

[a]Kansas Geological Survey, 1930 Constant Ave., Campus West, University of Kansas, Lawrence, Kansas 66047

Received May 1996, accepted July 1997

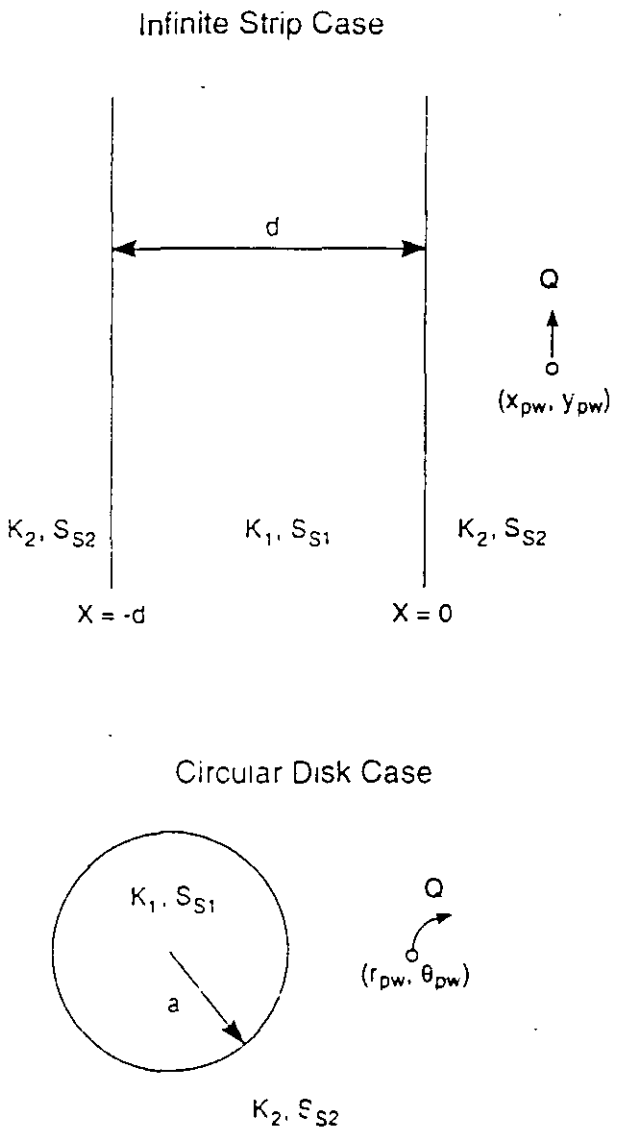

Figure 1. (a) Configuration consisting of an infinite strip (width=d) embedded in an otherwise uniform formation (pumping well located at x_{pw}, y_{pw}); (b) Configuration consisting of a circular disk (radius=a) embedded in an otherwise uniform formation (pumping well located at r_{pw}, θ_{pw}; origin at center of disk).

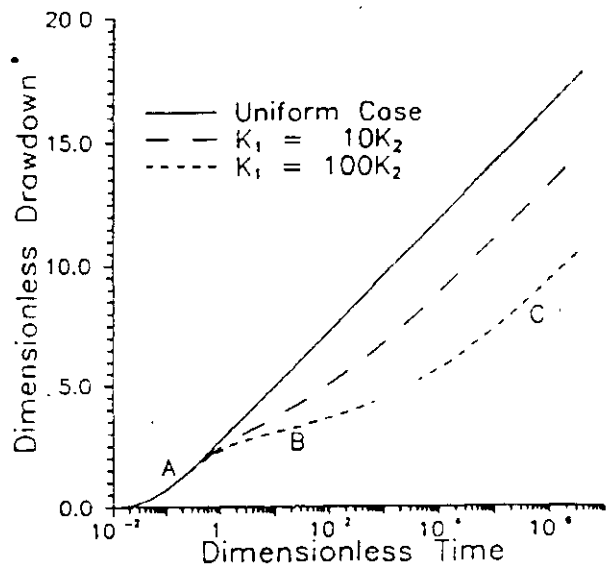

Figure 2. Dimensionless drawdown ($4\pi K_2 bs/Q$, where b is formation thickness and s is actual drawdown) versus the log of dimensionless time ($4K_2 t/S_{s2}d^2$) plot for the case of a pumping well located a very short distance from the strip ($x_{pw} = 0.5d$, $y_{pw} = 0.0$; specific storage of the strip and formation assumed equal; observation well located between pumping well and strip at position (0.3d, 0.0); intervals A, B, and C defined in text).

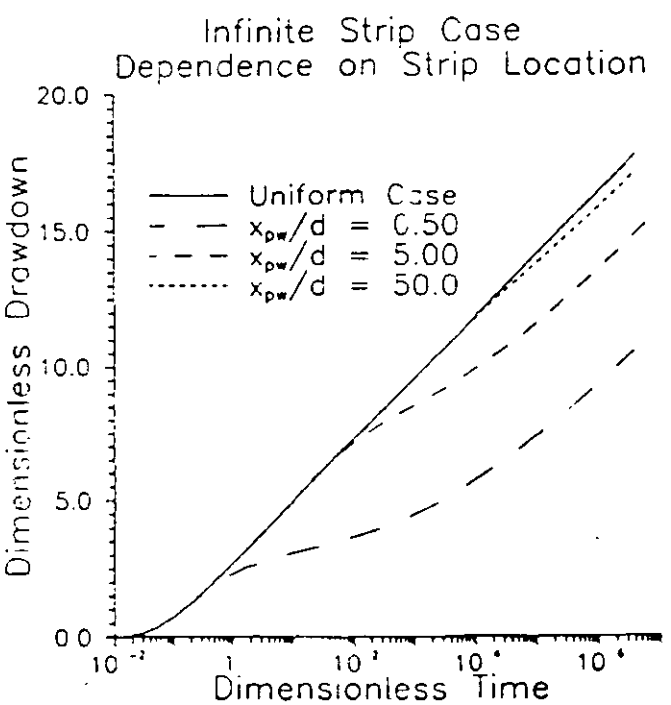

Figure 3. Dimensionless drawdown versus the log of dimensionless time plot as a function of the distance between the pumping well and the strip ($K_1 = 100K_2$; specific storage of the strip and formation assumed equal; observation well located between pumping well and strip at position ($x_{pw} = 0.2d$, 0.0)).

the strip (K_1) and that of the matrix (K_2) for the case of a pumping well located a very short distance (0.5d) from the strip of Figure 1a. Note that there are three segments marked on the drawdown curve for the case of $K_1 = 100K_2$. Segment A reflects radial flow before the front of the cone of depression passes through the right-hand boundary of the strip; a Cooper-Jacob semi-log analysis (Cooper and Jacob 1946, Kruseman and de Ridder 1990) of this interval will yield the K of the matrix. Segment B reflects conditions as the front of the cone of depression passes through the strip. If a straight line can be identified for this period, a Cooper-Jacob analysis will yield a hydraulic conductivity that is an arithmetic average of the strip and matrix K (Streltsova 1988). Segment C reflects the large-time behavior of the system. A Cooper-Jacob analysis of this segment will yield a K equal to that of the matrix, since the changes in drawdown at large times are independent of the properties of the strip (Butler and Liu 1991). It is important to emphasize that only during the time interval denoted as Segment B are changes in drawdown a function of the properties of the strip.

Figure 3 shows how the relationships of Figure 2 depend on distance from the strip. Clearly, the influence of the strip diminishes quickly as its distance from the pumping well increases. At large normalized distances, the strip-induced deviation from the semi-log straight line of the uniform case will essentially be negligible. In

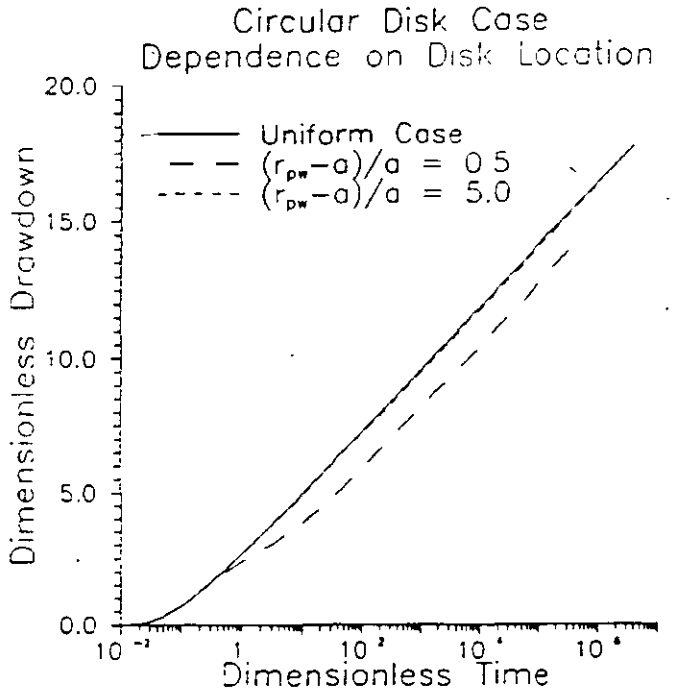

Figure 4. Dimensionless drawdown ($4\pi K_z bs/Q$) versus the log of dimensionless time ($4K_z t/S_{ss}a^2$) plot as a function of the distance between the pumping well and the disk ($K_1 = 100K_2$; specific storage of the disk and formation assumed equal; observation well located on ray connecting pumping well and disk at radial position $r_{pw} = 0.2a$).

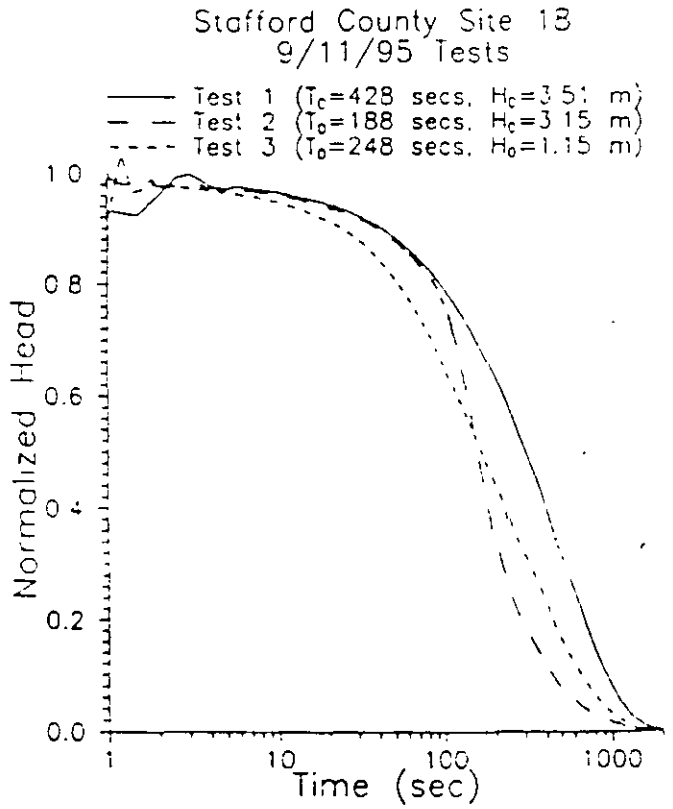

Figure 5. Normalized head ($H(t)/H_0$, where $H(t)$ is measured deviation from static and H_0 is magnitude of the initial displacement) versus log time plot of a series of slug tests performed at well 1 of monitoring site 18 in Stafford County, Kansas.

practice, if the strip is much further than a normalized distance of five from the pumping well, the moderate- to large-time deviation produced by the strip would undoubtedly be considered a boundary effect, and the K estimate would be obtained from the earlier-time linear data segment. From these results, it is difficult to see how an infrequent high-K conduit (e.g., a buried stream channel in a finer-grained matrix, a zone of intense fracturing in an otherwise sparsely fractured formation, an igneous dike intruding a less-permeable country rock, etc.) would have a significant effect on parameter estimates in the general case.

Figures 2 and 3 display results for the case of a high-K strip of infinite length. If the high-K zone is of finite extent, its influence can be considerably less. Figure 4 displays results analogous to Figure 3 for the circular disk configuration shown in Figure 1b. In this case, if the circular disk is more than a few radii (a) away from the pumping well, its influence is insignificant. As shown by Butler and Liu (1993), a Cooper-Jacob analysis of the large-time drawdown will again yield the K of the matrix. Thus, a relatively equi-dimensional high-K zone of limited extent will have virtually no impact on pumping-test K estimates unless it is large and close to the pumping and observation wells.

The conclusion of this simple analysis is that, in general, infrequent zones of relatively high K will have little impact on pumping-induced drawdown. If such a zone does play a significant role in a particular pumping test, that situation should be clearly revealed on a semi-log plot of the drawdown data. If pumping-induced drawdown display the ideal behavior predicted by the homogeneous-aquifer models of the well-hydraulics literature (e.g., Cooper and Jacob 1946; Hantush 1964), then one can be very confident that the resulting K estimate is not significantly affected by a zone of anomalous properties. Based on this analysis, one would expect that the hydraulic conductivity estimate obtained from a series of slug tests would, on average, be quite close to the estimate obtained from a large-scale pumping test in formations in which the major elements of heterogeneity are infrequent zones of relatively high conductivity. Thus, the infrequent-conduit hypothesis does not appear to be a convincing explanation for the widely observed difference between pumping-test and slug-test parameters.

An Alternative Hypothesis

An alternative to the infrequent-conduit hypothesis is that hydraulic conductivity estimates obtained from slug tests are artificially low as a result of incomplete well development and a failure to account for vertical anisotropy, both of which have relatively little influence on K estimates obtained from pumping tests. In this section, each of the elements of this alternate hypothesis are briefly described and a numerical example is presented to demonstrate the major points of the discussion. A field investigation is described in the following section to provide further support for this hypothesis.

Incomplete Well Development

Incomplete well development is the failure to remove the majority of drilling-related debris (e.g., remnant drilling fluids, fine material created/mobilized by the drilling process, etc.) and/or products of human-induced biochemical action from the near-well portions of the formation. Since slug tests are extremely sensitive to near-well conditions (e.g., Moench and Hsieh 1985), incomplete well development can result in slug-test estimates that are more reflective of the altered (lower permeability), near-well material (well

skin) than the formation itself. Based on a large number of slug tests performed by Kansas Geological Survey (KGS) personnel, incomplete development appears to be an extremely common situation. Examples drawn from recent KGS investigations can be used to illustrate the type of conditions that are often found in the field.

Figure 5 displays normalized head data from a series of slug tests performed on the same day at a site in Stafford County, Kansas. In all three tests, the slug-induced disturbance produced a flow of water out of the well (into the formation). The data from these tests can be compared using T_0, the basic time lag (i.e., the time at which a normalized head of 0.37 is obtained [Hvorslev 1951]), which is inversely proportional to the hydraulic conductivity estimate. In this series of tests, T_0, and thus the estimated K, varied by a factor of 2.3. This large variation in estimated K between tests performed consecutively on the same day is an example of what Butler et al. (1996) term an "evolving" or "dynamic" skin. Apparently, fine material is mobilized by the slug-induced disturbance and moves in a manner that produces large changes in hydraulic conductivity estimates between tests. The tests shown in Figure 5 were done after the well had been extensively developed in late 1994. A slug test performed at this same well shortly after installation (approximately 14 years earlier) and after relatively little development yielded a T_0 estimate of over 20,000 seconds. This dramatic difference in T_0 (188 versus over 20,000) is a graphic illustration of the critical need for proper well development prior to the performance of slug tests. Although the well development in late 1994 significantly improved conditions at the well, the dynamic-skin effects observed in the tests shown on Figure 5 indicate that still further development activities would be beneficial. This was verified by a later test at this same well that had a T_0 value of less than 88 seconds.

The sensitivity of slug-test responses to near-well conditions can be further demonstrated with data from a monitoring well in Trego County, Kansas. In the series of slug tests performed at this well, a subset of which are presented in Figure 6, T_0 varied by close to two orders of magnitude. The tests labeled "in" were configured so that the slug-induced disturbance produced a flow of water into the well, while the test labeled "out" was configured so that the disturbance produced a flow of water out of the well (into the formation). The differences seen among the tests labeled "in" were again considered to be an example of a dynamic skin. The differences between the tests labeled "in" and the test labeled "out" were attributed to the buildup of a bacterial/oxyhydroxide "mat," which is thought to consist of iron and manganese bacteria, associated byproducts, and oxyhydroxide deposits. This mat, which is most likely building up on the well screen, essentially acts as a check valve; flow toward the well pushes the mat into the well, while flow out of the well pushes it into the screen and the gravel pack. The result is that flow into the well is much less impacted by the buildup than flow in the opposite direction. A somewhat similar situation could also be produced by a buildup at the interface between the gravel pack and the formation. However, an amorphous black material, thought to consist primarily of iron and manganese oxyhydroxide deposits (Whittemore 1995), was repeatedly found in bailers that were lowered to the bottom of the well, so the well screen is considered the most likely location for the buildup.

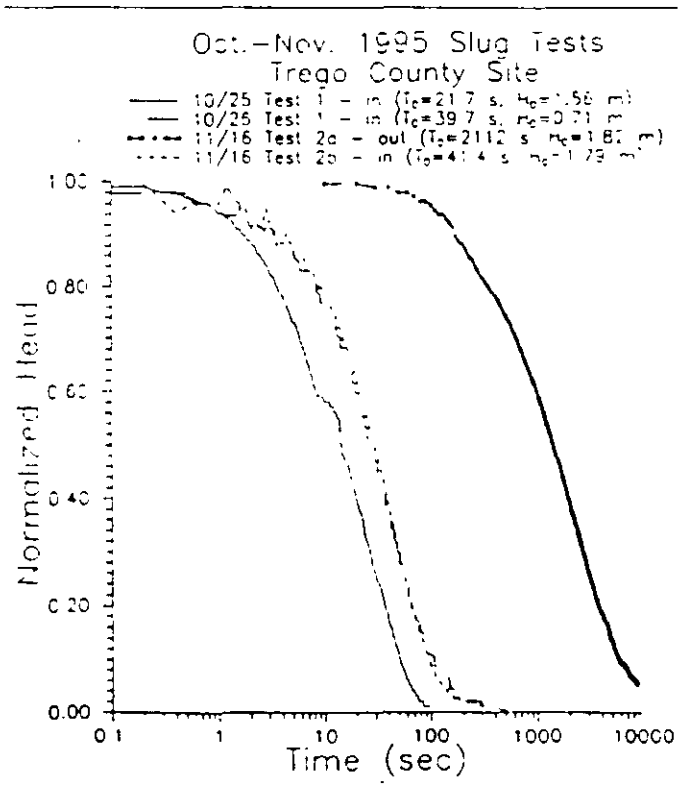

Figure 6. Normalized head versus log time plot of a series of slug tests performed during October and November 1995 in a monitoring well in Trego County, Kansas.

These field examples clearly show that slug-test estimates may be heavily influenced by altered, near-well conditions. Based on our experience, unless special care is taken in well installation and development, the conditions illustrated in these examples may well be the norm, and not the exception. It is therefore critical that the design, performance, and analysis of slug tests be directed at the identification of such conditions. Butler et al. (1996) and Butler (1997) propose approaches to help assess the presence of a low-K skin using slug tests. Butler (1997) emphasizes that hydraulic conductivity estimates obtained with the Hvorslev (1951) or Bouwer and Rice (1976) methods will be particularly vulnerable to the effects of a low-K well skin. Although previous discussion implies that close agreement between T_0 values from repeat slug tests would be a demonstration of a properly developed well, such agreement does not ensure that test responses are unaffected by a low-K skin. Thus, the preliminary screening approach described by Butler (1997) should be used in all cases to assess the adequacy of well development prior to formal analysis.

Vertical Anisotropy

Uncertainty about vertical anisotropy (K_v<K_h, where K_v and K_h are the vertical and horizontal components of hydraulic conductivity, respectively) can also introduce error into slug-test estimates. Hyder et al. (1994) and Hyder and Butler (1995) show that failure to account for the presence of vertical anisotropy can lead to an under-prediction in K that may be as large as a factor of three. Although Butler et al. (1993) and Butler (1997) demonstrate a rapid screening approach to assess if significant vertical anisotropy (K_v << K_h) is present, quantification of that anisotropy will not be possible using single-well slug tests. Based on our experience, however, vertical anisotropy does not commonly appear to be an important control on slug-test responses. It is most likely to be significant in strongly stratified systems with frequent low-K layers.

Impact on Estimates From Pumping Tests

Hydraulic conductivity estimates from pumping tests, in contrast to those from slug tests, are not heavily impacted by near-well conditions or vertical anisotropy. As explained by Butler (1990),

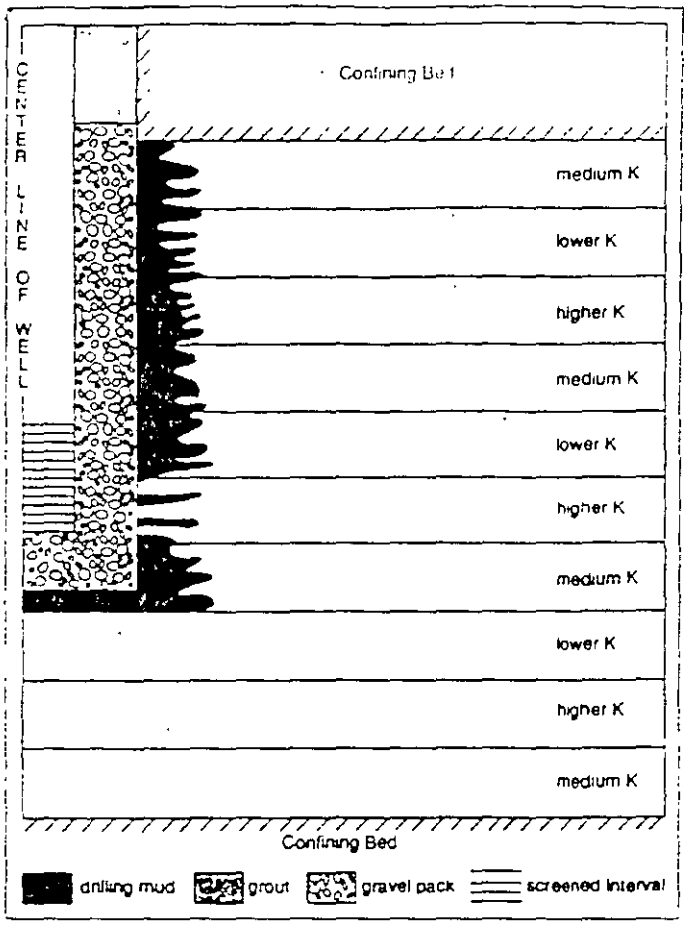

Figure 7. Cross sectional view of hypothetical layered aquifer (well and aquifer parameters defined in Table 1; figure not to scale).

Table 1
Parameter Set for Numerical Demonstration

Higher K	=	15 m/d
Medium K	=	5 m/d
Lower K	=	1 m/d
Low-K skin	=	0.1 m/d
Low-K skin for partially blocked zone	=	1.5 m/d
Gravel-pack K	=	200 m/d
Specific storage (all layers of equal S_s)	=	2.0×10^{-5} m^{-1}
Total aquifer thickness		10 m
Layer thickness (all layers of equal thickness)	=	1 m
Screen length	=	2 m
Gravel pack length	=	7 m
Distance from top of aquifer to top of screen	=	4 m
Radius of well casing	=	0.05 m
Radius of well screen	=	0.05 m
Radius of gravel pack	=	0.11 m
Radius of mud-invaded zone	=	0.20 m

pumping-test drawdown can be analyzed with the Cooper-Jacob semi-log method to remove the effects of near-well conditions from K estimates. This semi-log method will also remove the effects of vertical anisotropy if the pumping well only partially penetrates the aquifer (Kruseman and de Ridder 1990). If an observation well at some distance from the pumping well is used, low-K skin(s) at the pumping and/or observation well, as well as vertical

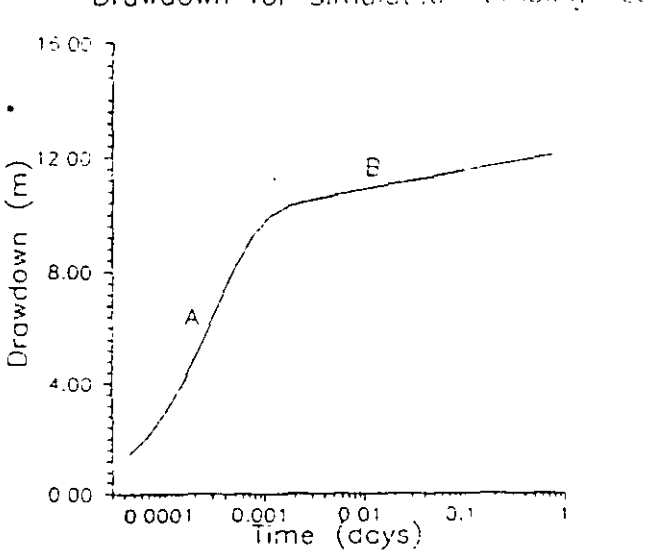

Figure 8a. Plot of drawdown at the discharge well versus log of tim for the pumping test simulated in the layered aquifer of Figure (well and aquifer parameters defined in Table 1; Q = 272.6 m³/d duration of pumping = 24 hr; intervals A and B defined in text).

anisotropy, will have a very limited impact on parameter estimates, regardless of the method employed to analyze the drawdown data (Hantush 1964; Butler 1990). Thus, since most large-scale pumping tests utilize drawdown from observation wells and/or are analyzed with the Cooper-Jacob semi-log method, K estimates from pumping tests are generally not affected by near-well conditions or vertical anisotropy.

Numerical Demonstration

A hypothetical example can be used to illustrate many of the points of the preceding discussion. A cylindrical-coordinate, three-dimensional, finite-difference model developed at the Kansas Geological Survey for the analysis of hydraulic tests (Butler et al. 1994) was used to simulate pumping and slug tests in the configuration shown in Figure 7. This particular configuration was chosen to demonstrate the influence of incomplete well development, layering-induced anisotropy, and partial penetration on test estimates. The model parameters used in this example are given in Table 1. As shown in Figure 7, the low-K skin completely blocks all but the "higher K" layer opposite the well screen, which is assumed to be only partially blocked (designated as "partially blocked zone" in Table 1). This would be the expected situation unless a very concerted effort was made to develop discrete intervals along the well screen (Campbell and Lehr 1973; Kill 1990).

Figures 8a and 8b display the drawdown and recovery, respectively, from the discharge well for a 24-hour, constant-rate pumping test simulated in this hypothetical layered system. The large head change in the interval marked A on both plots is a product of wellbore storage, the low-K skin, the layering, and the partially penetrating nature of the well (partial penetration is exacerbated here by the low-K skin). The rate of head change in the interval marked B on both plots is much less and is the result of the full thickness of the aquifer contributing to flow to the well. A Cooper-Jacob semi-log analysis of this interval on Figure 8a yielded a transmissivity estimate of 80.3 m²/day, while an analysis of this interval on Figure 8b using the standard superposition-based approach (Kruseman and

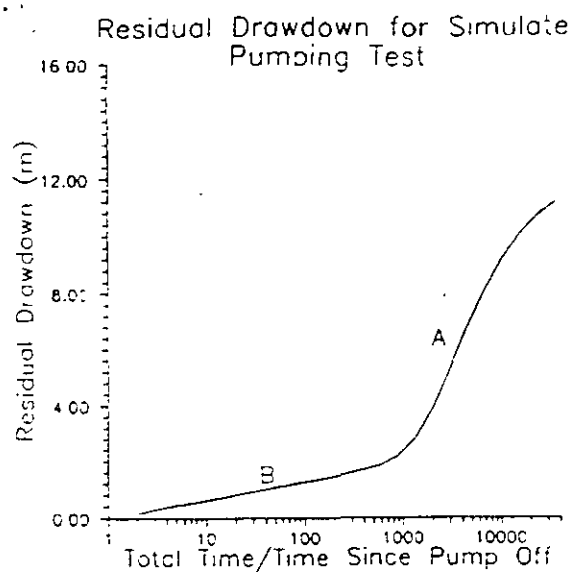

Figure 8b. Plot of residual drawdown at the discharge well versus the log of the ratio of the total time since pumping began over the time since pump was cut off for the pumping test simulated in the layered aquifer of Figure 7 (well and aquifer parameters defined in Table 1; Q = 272.6 m^3/d; duration of pumping = 24 hr; intervals A and B defined in text)

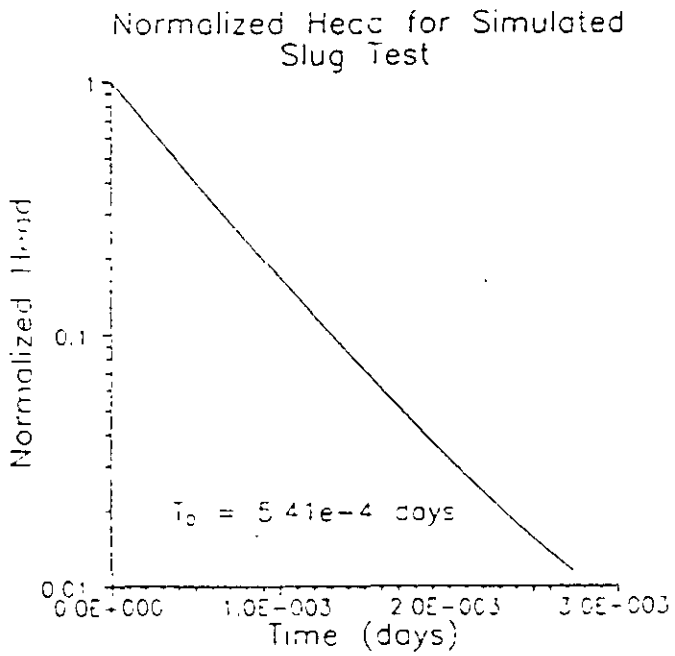

Figure 9. Log normalized head versus time plot of the slug test simulated in the layered aquifer of Figure 7 (well and aquifer parameters defined in Table 1)

de Ridder 1990) yielded a transmissivity estimate of 78.8 m^2/day. Both estimates are very close to the actual model transmissivity of 80.0 m^2/day. These results demonstrate that the full thickness of the aquifer must be used to convert a transmissivity estimate from a pumping test into an average K for the aquifer, regardless of whether the pumping well fully or partially penetrates the unit.

Figure 9 displays the results of a slug test simulated in the same configuration. Following standard practices, the Hvorslev method (shape factor is that for case 8 of Hvorslev 1951) was used to analyze the simulated responses. As is often the case with slug tests, there was considerable uncertainty about what quantity to employ

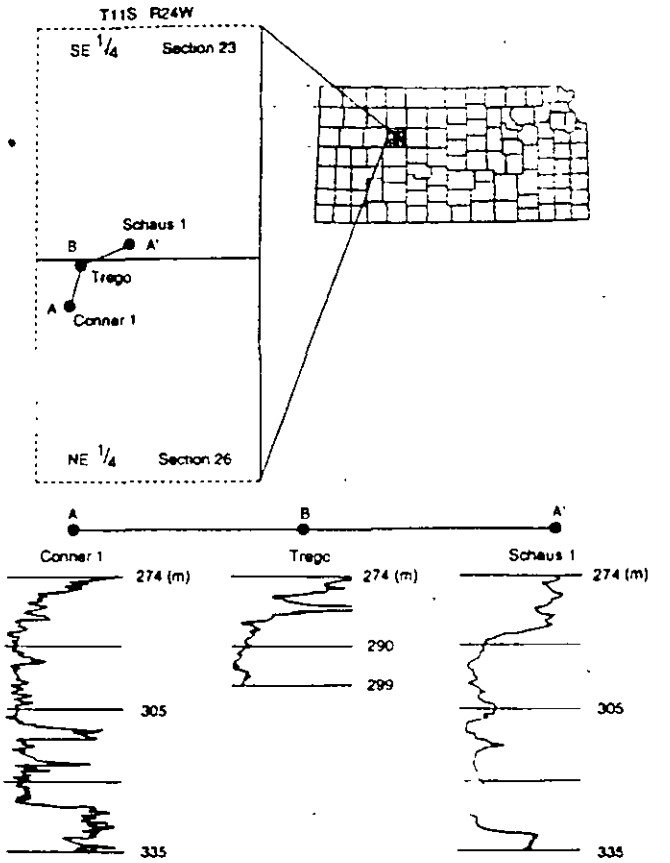

Figure 10. (a) Location map for the Trego County monitoring well (labeled Trego) and two nearby petroleum wells; (b) Natural gamma logs for Trego County monitoring well and two nearby petroleum wells (scale is in depth (m) below land surface (lsf); Schaus 1 has higher ( ) elevation than other wells; depth to water approx. 131 m below lsf; nominal screened interval is 290.2–294.8 m below lsf; gravel pack interval is 279–300 m below lsf; quarter sections are approximately 402 m on a side).

for the effective screen length. If the nominal screen length is used, the resulting K estimate (3.3 m/d) is considerably less than the average value obtained from the pumping test as well as the average value of the layers adjacent to the screen (8.0 m/d in both cases). One might be tempted to follow the common practice of using the length of the gravel pack for the effective screen length, because the gravel pack is considerably more permeable than the formation. This, however, would produce a much lower K estimate (1.4 m/d). If one could somehow recognize that virtually all of the flow is moving into the aquifer via the "higher K" layer opposite the well screen, then an effective screen length of one meter would be used. Although the resulting K (5.1 m/d) is larger than the previous estimates, it is still much less than the K for that layer (15 m/d) because of the effect of the incomplete well development and layering-induced anisotropy. Unfortunately, as shown in this example, commonly met field conditions can result in a slug test only being able to provide a rough estimate of the transmissive properties of the formation in the vicinity of the well screen. Note that if a "higher K" layer had not intersected the screened interval in this example, the K estimate from the slug test could have been considerably lower. Thus, this example must be considered a rather conservative demonstration of what might be found in actual applications.

The general conclusion of this hypothetical example is that pumping tests can yield reasonable estimates of the average hydraulic conductivity of an aquifer, even in the presence of mud-invaded zones, partial penetration, and layering-induced anisotropy, as long as the full thickness of the aquifer is used to convert the transmissivity estimate into an average hydraulic conductivity for the system. However, slug tests (at least as conventionally performed by hydrogeologists) should not be expected to yield estimates of the same quality. Under conditions similar to those considered here, hydraulic-conductivity estimates obtained from pumping tests will virtually always be considerably larger than those obtained from slug tests.

In the preceding example, mud invasion was assumed responsible for the alteration of the near-well portions of the formation. Although mud invasion is probably the worst-case scenario, it is important to emphasize that most drilling technologies will create considerable quantities of drilling debris (e.g., fine materials) that can produce a situation very similar to that shown in Figure 7 (Aller et al. 1989). Thus, in virtually all situations, unremoved drilling debris will undoubtedly have an effect similar to that shown here. Biochemical action, inappropriate sizing of the gravel pack, etc. will only further worsen this effect.

Field Example

In May 1994, a KGS monitoring well was drilled into a sand body in the Dakota Formation in Trego County, Kansas (Figure 10). In July 1994, a 21.5-hour, constant-rate (Q = 53 gpm = 290 m^3/d) pumping test was performed using this well as both the pumping and observation well (Butler and Healey 1995). Recovery data were employed to estimate transmissivity using the standard superposition-based approach (Kruseman and de Ridder 1990). Figure 11a displays the complete record of recovery data, while Figure 11b is a closeup of the interval of analysis. Note that the similarities between Figure 11a and Figure 8b can be interpreted as indicating that well-bore storage, partial penetration, and possibly, a low-K skin are important controls on drawdown at this well. Figure 11b shows that the data display the large-time linear relationship that would be predicted from theory. An analysis of this linear segment produced a transmissivity estimate of 594 m^2/day.

Because the purpose of this test was to obtain an estimate of the average hydraulic conductivity of the Dakota sand, the transmissivity calculated from the recovery data needed to be converted into an average K for the sand body. In order to make this conversion, the thickness of the sand unit had to be estimated. Figure 10b shows natural gamma logs from the monitoring well (labeled "Trego") and two nearby petroleum wells. Note that the Trego well was installed in the upper portion of the Dakota sands, so it is impossible to estimate sand thickness from this well alone. The logs from these three wells indicate the presence of discontinuous shale lenses in the Dakota sands. If the major shale lens near 710 m in the Conner 1 log is used as the lower boundary of the sand unit, an average conductivity estimate of 21.6 m/d is obtained. This value would certainly be on the high end of hydraulic conductivity estimates obtained for the Dakota sands in Kansas (Macfarlane et al. 1990). If the approximate thickness of the total sand interval for both the Conner 1 and Schaus 1 logs is used (44 m), a more reasonable estimate of 13.5 m/d is obtained. One might be tempted to use the length of the screened interval or the gravel pack for the aquifer thickness. If the nominal screen length of 4.57 m is employed for the sand thickness, an average hydraulic conductivity of 130 m/d is obtained, an estimate that could be considered near the bounds of physical plausibility for the semi-consolidated Dakota sand. An estimate based on the length of the gravel pack (21 m) would also produce a value (28.2 m/d) that would be considered quite high for the Dakota sand.

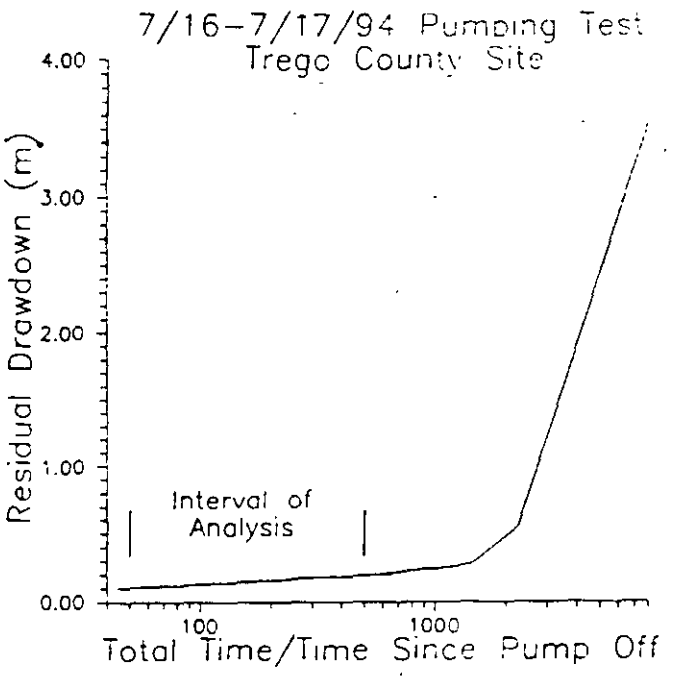

Figure 11a. Plots of residual drawdown for entire period of data collection versus the log of the ratio of the total time since pumping began over the time since pump was cut off for July 1994 pumping test at monitoring well in Trego County, Kansas (Q = 290 m^3/d; duration of pumping = 21.5 hr; measurements obtained with an electric tape).

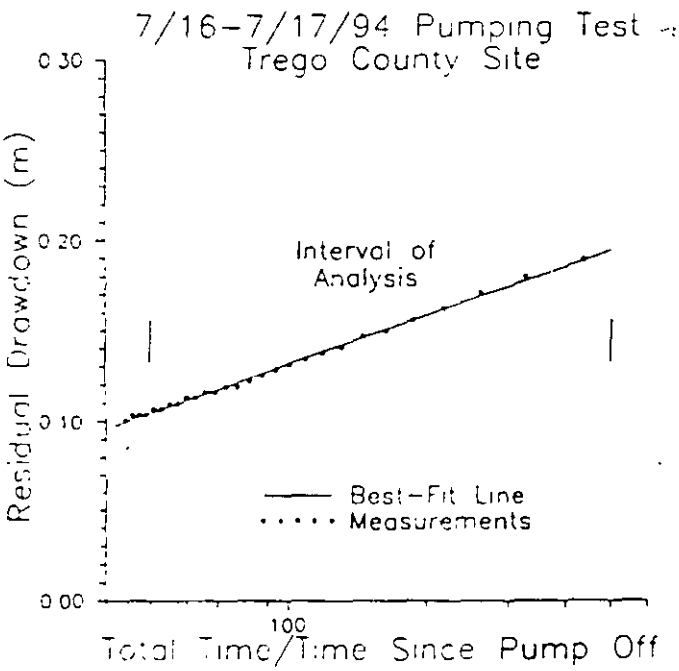

Figure 11b. Plot of residual drawdown and the best-fit straight line for the interval used in the recovery analysis (Q = 290 m^3/d; duration of pumping = 21.5 hr; measurements obtained with an electric tape).

The above analysis shows that the estimate for the average hydraulic conductivity of the Dakota sand can vary over a considerable range depending on what value is assigned for sand thick-

ness. In this particular case, the apparent discontinuous nature of the shale lenses, in conjunction with the simulation results of the previous section, suggest that a K of around 14 m/d is probably the most reasonable estimate for the average hydraulic conductivity of the Dakota sand. Because this estimate was obtained using the total thickness of the sand interval, it clearly is very near the lower bound for the sand-body K.

Butler and Healey (1995) describe the series of slug tests performed at this well. Figure 6 shows a subset of the tests from this series. The test labeled 10/25 Test 1, the first slug test at this well, was the most rapid test of the series (all other slug tests performed at this well had T_0 values greater than 30 seconds). If data from this test are analyzed with the Hvorslev method (case 8 of Hvorslev 1951), the nominal screen length is used for the effective screen length, and isotropic conditions are assumed, a K estimate of 6.7 m/d is obtained. Because we suspect that slug tests at this well are being affected by a dynamic skin and the buildup of a bacterial/oxyhydroxide mat, and that the effective screen length is less than the nominal screen length for the reasons illustrated in Figure 7, the estimate obtained from this test must be considered a lower bound for the average K of the interval opposite the screen.

Although the lower bounds for the pumping-test and slug-test K estimates only differ by a factor of two, the results of the Trego County field tests demonstrate just how easily a much larger difference between pumping-test and slug-test estimates can be obtained. If tests had only been performed in the configuration labeled "out" on Figure 6, the slug-test estimate would have underpredicted the formation K by over two orders of magnitude. Even when the configuration labeled "in" on Figure 6 was used, all tests after the first yielded K estimates that were two-thirds or less of that determined from the first test (10/25 test 1). Additionally, if the length of the gravel pack or that of the screened interval was used to convert the transmissivity estimate from the recovery analysis to an average conductivity for the sand body, the pumping-test K estimate would have been a factor of two to a factor of ten larger than the value employed here. Clearly, incomplete well development, in conjunction with uncertainty regarding aquifer thickness, plays a very important role in producing the commonly observed difference between pumping-test and slug-test parameters.

Conclusions

Field data from many different sources have shown that the hydraulic-conductivity estimate obtained from a pumping test is considerably larger than the average conductivity estimate obtained from a program of slug tests performed in the same formation. The primary purpose of this paper was to evaluate possible explanations for this widely observed difference. The results of this evaluation can be summarized as follows.

1. Infrequent in-space zones of relatively high hydraulic conductivity will, in general, have a very limited impact on parameter estimates obtained from pumping tests. Thus, it is difficult to explain the difference between pumping-test and slug-test parameters on the basis of the existence of infrequent high-K conduits.
2. If infrequent-in-space zones of relatively high hydraulic conductivity do have a significant impact on the drawdown from a particular pumping test, this should be clearly revealed on a semi-log drawdown versus time plot. If pumping-induced drawdown displays the ideal behavior predicted by the homogeneous-aquifer models of the well-hydraulics literature, then one can be very confident that the resulting K estimate is not significantly affected by a zone of anomalous properties.
3. Slug tests are extremely sensitive to altered, near-well conditions. Low-K skins can produce slug-test estimates that may be orders of magnitude lower than the average hydraulic conductivity of the formation in the vicinity of the well screen. Estimates from pumping tests, however, will be unaffected by low-K skins if the Cooper-Jacob semi-log method and/or observation wells at a distance from the pumping well are used.
4. Failure to account for vertical anisotropy in the analysis of slug-test data can lead to an underestimation of hydraulic conductivity of up to a factor of three. Estimates from pumping tests, however, will be unaffected by vertical anisotropy if the Cooper-Jacob semi-log method and/or observation wells at a distance from the pumping well are used.
5. The full thickness of the aquifer will contribute flow to the discharge well in a pumping test, regardless of whether that well fully or partially penetrates the unit. Thus, a reasonable estimate of the aquifer thickness is required to convert the transmissivity calculated from a pumping test into an average K for the aquifer. Error can be introduced in this conversion as a result of uncertainty about the actual aquifer thickness.
6. The effective screen length, which is required for the analysis of a slug test, may be difficult to estimate in practice. Use of the nominal screen length or the length of the gravel pack may introduce considerable error into the slug-test K estimate if the well has not been thoroughly developed. Uncertainty about this quantity will have no effect on K estimates from pumping tests if the Cooper-Jacob semi-log method and/or observation wells at a distance from the pumping well are used.

The overall conclusion of this work is that the commonly observed difference between pumping-test and slug-test parameters is much more likely to be an artifact introduced by effects related to well installation and development than to be a product of a natural underlying scale dependence in hydraulic conductivity. Further efforts to assess this relationship should therefore focus on identifying and removing the effects of drilling-induced disturbances from slug-test estimates. The use of appropriate procedures for well development (e.g., Campbell and Lehr 1973; Aller et al. 1989, Kill 1990) in wells in which slug tests are to be performed cannot be over-emphasized. Estimates obtained from slug tests in wells that have undergone limited development will, at best, be quite rough estimates of the average K of the formation in the vicinity of the well. In almost all cases, these estimates will considerably underpredict the average hydraulic conductivity of the medium.

Finally, it is important to stress that, other than demonstrating the inappropriateness of the infrequent-conduit hypothesis, this work does not reach any conclusions about the possibility of a natural underlying scale dependence in hydraulic conductivity. Although a theoretical analysis by Neuman (1994) casts doubt on the existence of an underlying scale dependence in the vertically averaged K of an aquifer, further field and theoretical investigations are needed. If parameter estimates from slug tests and pumping tests are to be used in these investigations, the performance and analysis of these tests must be done quite carefully. Clearly, the rigorous evaluation of possible scaling relationships can only be done when both types of hydraulic tests are providing representative estimates of the transmissive nature of the medium.

Acknowledgments

We would like to thank John Fio, Michael Campbell, and one anonymous reviewer for providing comments that significantly improved the final version of this manuscript.

References

Aller, L., T.W. Bennett, G. Hackett, R.J. Petty, J.H. Lehr, H. Sedoris, D.M. Nielsen, and J.E. Denne. 1989. *Handbook of suggested practices for the design and installation of ground-water monitoring wells*. Dublin, Ohio: National Water Well Association.

Bouwer, H., and R.C. Rice. 1976. A slug test for determining hydraulic conductivity of unconfined aquifers with completely or partially penetrating wells. *Water Resour. Res.* 12, no. 3: 423-428.

Bradbury, K.R., and M.A. Muldoon. 1990. Hydraulic conductivity determinations in unlithified glacial and fluvial materials. In *Ground Water and Vadose Monitoring*, ed. D.M. Nielsen and A.I. Johnson, 138-151. ASTM STP 1053. Philadelphia: American Soc. for Testing and Materials.

Butler, J.J., Jr. 1990. The role of pumping tests in site characterization: Some theoretical considerations. *Ground Water* 28, no. 3: 394-402.

Butler, J.J. Jr. 1997. *The design, performance, and analysis of slug tests*. Boca Raton: Lewis Publishers.

Butler, J.J. Jr., and J.M. Healey. 1995. Analysis of 1994-95 hydraulic tests at Trego County monitoring site. Kansas Geological Survey Open-File Rept. 95-66. Lawrence, Kansas: KGS.

Butler, J.J. Jr., and W.Z. Liu. 1991. Pumping tests in nonuniform aquifers: The linear strip case. *Jour. of Hydrology* 128: 69-99.

Butler, J.J. Jr., and W.Z. Liu. 1993. Pumping tests in nonuniform aquifers: The radially asymmetric case. *Water Resour. Res.* 29, no. 2: 259-269.

Butler, J.J. Jr., W.Z. Liu, and D.P. Young. 1993. Analysis of October 1993 slug tests in Stafford, Pratt, and Reno counties, south-central Kansas. Kansas Geological Survey Open-File Rept. 93-52. Lawrence, Kansas: KGS.

Butler, J.J. Jr., C.D. McElwee, and W.Z. Liu. 1996. Improving the quality of parameter estimates obtained from slug tests. *Ground Water* 34, no. 3: 480-490.

Butler, J.J. Jr., G.C. Bohling, Z. Hyder, and C.D. McElwee. 1994. The use of slug tests to describe vertical variations in hydraulic conductivity. *Jour. of Hydrology* 156: 137-162.

Campbell, M.D., and J.H. Lehr. 1973. *Water well technology*. New York: McGraw-Hill.

Cooper, H.H. Jr., and C.E. Jacob. 1946. A generalized graphical method for evaluating formation constants and summarizing well-field history. *EOS Trans.* AGU 27, no. 4: 526-534.

Hantush, M.S. 1964. Hydraulics of wells. In *Advances in Hydroscience*, vol. 1, ed. V.T. Chow, 281-432. New York: Academic Press.

Hvorslev, M.J. 1951. Time lag and soil permeability in ground-water observations. Bulletin no. 36. Waterways Exper. Sta., Corps of Engrs., U.S. Army.

Hyder, Z., J.J. Butler Jr., C.D. McElwee, and W.Z. Liu. 1994. Slug tests in partially penetrating wells. *Water Resour. Res.* 30, no. 11: 2945-2957.

Hyder, Z., and J.J. Butler Jr. 1995. Slug tests in unconfined formations: An assessment of the Bouwer and Rice technique. *Ground Water* 33, no. 1: 16-22.

Kill, D.L. 1990. Monitoring well development — Why and how. In *Ground Water and Vadose Monitoring*, ed. D.M. Nielsen and A.I. Johnson, 82-90. ASTM STP 1053. Philadelphia: American Soc. for Testing and Materials.

Kruseman, G.P., and N.A. de Ridder. 1990. Analysis and evaluation of pumping test data. ILRI publication 47. The Netherlands: ILRI.

Macfarlane, P.A., D.O. Whittemore, M.A. Townsend, J.H. Doveton, V.J. Hamilton, W.G. Coyle III, A. Wade, G.L. Macpherson, and R.D. Black. 1990. The Dakota Aquifer Program. Annual report, FY89. Kansas Geological Survey Open-File Rept. 90-27. Lawrence, Kansas: KGS.

Moench, A.F., and P.A. Hsieh. 1985. Analysis of slug test data in a well with finite-thickness skin. In Memoirs of the 17th Int. Cong. on the Hydrogeology of Rocks of Low Permeability, vol. 17, 17-29.

Neuman, S.P. 1994. Generalized scaling of permeabilities: Validation and effect of support scale. *Geophysical Research Letters* 21, no. 5: 349-352.

Rayne, R.W. 1993. Variability of hydraulic conductivity in sandy till: The effects of scale and method. Ph.D. diss., Department of Geology and Geophysics, Univ. of Wisc. at Madison, Madison, Wisconsin.

Rovey, C.W. II, and D.S. Cherkauer. 1995. Scale dependency of hydraulic conductivity measurements. *Ground Water* 33, no. 5: 769-780.

Streltsova, T.D. 1988. *Well testing in heterogeneous formations*. New York: John Wiley and Sons.

Whittemore. 1995. Interview by author, November 1995, Lawrence, Kansas.

FACULTAD DE INGENIERIA U.N.A.M.
DIVISION DE EDUCACION CONTINUA
CURSOS ABIERTOS

XII CURSO INTERNACIONAL DE CONTAMINACIÓN DE ACUÍFEROS

MODULO III: MODELOS MATEMÁTICOS EN GEOHIDROLOGIA Y CONTAMINACIÓN DE ACUIFEROS

TEMA

ON THE STRATEGY OF ESTIMATING REGIONAL – SCALE TRANSMISSIVITY FIELDS

EXPOSITOR: DR. ADOLFO CHAVEZ RODRIGUEZ

PALACIO DE MINERIA
OCTUBRE DEL 2000

On the Strategy of Estimating Regional-Scale Transmissivity Fields

by Steen Christensen[a]

Abstract

A case study of a leaky fluvioglacial aquifer concentrates on methods of estimating the zonated $\log_{10}$-transmissivities of a regional-scale ground-water model covering 450 km^2. Mainly three estimation methods are discussed: (a) kriging based on local measurements and predictions, (b) hydrologic inversion (i.e., nonlinear regression) based on head data, and (c) hydrologic inversion based on head data and on prior estimates from kriging. (a) Due to the shortage of data which is usual in heterogeneous aquifers, the present study questions the practical value of forming zonal kriging estimates from local data whenever estimates are to be used as an input to ground-water models. In some parts of the homogeneous aquifers local data are sufficient to make such estimates. (b) In this study zonal hydrogeological parameters can be estimated by inversion based on head data. However, inaccuracies in head data may seriously damage the reliability of estimated parameters and, as a consequence, the ground-water model. (c) Using zonal kriging estimates as prior information in the regression reduces the width of the confidence intervals of the parameters with prior information by up to 75%. The study indicates, however, that using prior information in the estimation of the hydrologic model parameters only minimally reduces the uncertainty of the predicted hydraulic heads.

For this specific case, the results suggest that in order to parameterize and identify the parameters of the ground-water model one should concentrate on qualitative mapping of the hydrogeology, on sampling accurate head data and on subsequent estimation of the zonal parameters by inversion (or manual calibration).

Introduction

The most basic parameter field of regional-scale ground-water flow models is the transmissivity field. In practice, due to the lack of data, the transmissivity field of such models has to be simplified, e.g. by assuming constant transmissivity within distinct zones of tens or hundreds of square kilometers. In the present paper, the mean transmissivity of such a zone or domain is termed a zonal transmissivity, whereas the transmissivity in the vicinity of a well is termed a local transmissivity. The zonal transmissivity can be estimated in various ways, such as analysis of long duration pumping tests with multiwell observations within the zone, estimation of the zonal mean from local transmissivities, or hydrologic inversion.

The transmissivity can be estimated by pumping test analysis i.e., from a long-duration test for zonal transmissivity, and from a short-duration test for local transmissivity. Unfortunately, these tests are rarely used because they are laborious and expensive. It is thus attractive to supplement such estimates with transmissivity predictions made from correlated parameters (termed "predictors") which are obtainable in great numbers at low cost. For instance, the prediction of transmissivity from the specific capacity of wells has been common practice for decades (e.g., Theis et al., 1963; Dellhommie, 1974). However, Christensen (1995a) shows that the quality of the prediction varies strongly from aquifer to aquifer.

In most situations, the transmissivities estimated from pumping tests or predicted from well data are local transmissivities. To estimate the zonal transmissivity from local transmissivities one can use kriging (Journel and Huijbregts, 1978). This gives an unbiased estimate with minimum variance from a linear combination of the local transmissivities. Clifton and Neuman (1982), among others, used this method to estimate zonal transmissivities of a ground-water model.

Due to the development of inverse procedures it is possible to estimate the hydrogeological parameters of ground-water models from observations of hydraulic head, etc., for instance by nonlinear regression (e.g., Neuman and Yakowitz, 1979; and Cooley and Naff, 1990). It follows that in order to achieve objective estimates by inversion it is desirable to weight the head measurements individually in terms of their reliability. This reliability depends on possible errors in the measured heads as well as on the small-scale variance of the true heads (see below). A few case studies published in the literature have demonstrated that the parameters of large-scale ground-water flow models can be estimated by inversion, e.g., Cooley et al. (1986) and Clifton and Neuman (1982).

A hydrogeologist who is modeling regional-scale ground-water flow can thus select various data sampling strategies to estimate the zonal transmissivities. For instance, one can concentrate on long-duration pumping tests, which may be very expensive. One can use zonal estimation based on local predictions, but this may also be expensive or inaccurate. One can use hydrologic inversion based primarily on hydraulic head measurements, and these measurements can be obtained by methods ranging from inexpensive and inaccurate to expensive and accurate. Finally, one can combine all of these strategies. The hydrogeologist naturally wants to use the strategy that gives the best result, i.e., that minimizes the uncertainties, within the given economical restrictions. Which strategy is the best will depend on the actual hydrogeological conditions, so we need quantitative experience of the estimation potential of various sampling strategies under specified conditions.

[a]Department of Earth Sciences, Aarhus University, Denmark
Received May 1995, revised January 1996, accepted March 1996

This study presents a specific case study of the potential of three alternative methods of estimating zonal transmissivities (or, rather, zonal $\log_{10}$-transmissivities which are more appropriate, Neuman, 1980), namely: (A) estimation based on direct measurements; (B) estimation by hydrologic inversion, and (C) estimation by combining these methods. The paper goes on to discuss the best data sampling strategy for estimating the zonal transmissivities of the aquifer studied.

The study of the aquifer was conducted, firstly because the hydrogeology is typical for large parts of Northern Europe and some parts of North America, and secondly because the density of data in this area is relatively large. It is therefore expected that the conclusions can be transferred to areas of similar hydrogeology.

Hydrogeology and Problem Formulation

The studied aquifer is located in the western part of the Danish island of Zealand (Figure 1). Earlier detailed studies of the hydrogeology and hydrology in the area formed the basis for the hydrological model of Christensen (1994a) which covers an area of 450 km^2 (Figure 1). The present study is partly based on this work and partly on more recent supplementary data on geology and transmissivity.

The semiconfined aquifer is in a layer of Quaternary fluvioglacial deposits which is overlain by semipermeable glacial till and underlain by impervious Tertiary clay (Christensen, 1994a). In the northeastern, central, and southern-central parts of the area, the fluvioglacial sand and gravel are 10-30 meters thick and form a regional, rather homogeneous, aquifer with transmissivities between 10^{-3} and 10^{-2} m^2/s. In the remaining areas the fluvioglacial layer is heterogeneous with transmissivities between 10^{-5} and 10^{-2} m^2/s, and the transmissivity varies within short distances (Christensen, 1994a). In areas around Slagelse and Høng the fluvioglacial deposits are absent and substantial portions of Tertiary clay are mixed into the till. Lithological information from wells shows that the thickness of the till layer varies between 10 and 80 meters and the vertical hydraulic conductivity is about $8 \cdot 10^{-9}$ m/s (Christensen, 1994a).

A phreatic aquifer is found in the more permeable upper zone of the till. The water table is located a few meters below ground level and the flow is dominated by near-surface horizontal flow towards the streams. However, there is significant vertical flow in the till and this is of major importance to the overall water balance of both the till and the underlying fluvioglacial aquifer. In high-lying areas, the water table in the till is higher than the hydraulic head in the fluvioglacial aquifer and leakage is downward, whereas it is upward in areas with low elevations such as stream valleys and coastal areas. The simulations of Christensen (1994a) show that 46 mm/y leaks to the fluvioglacial aquifer in the recharge areas. Just under half of this recharge, 20 mm/y, is withdrawn from the aquifer for consumption and irrigation purposes, while most of the remainder discharges back to the phreatic aquifer (24 mm/y). Only 2 mm/y leaks to the sea (Christensen, 1994a).

Based partly on pumping test analyses (Figure 1) and partly on geological information, the fluvioglacial aquifer was divided into the transmissivity zones shown in Figure 2. This zonation differs slightly from that used in Christensen (1994a) because additional data were used. Zones 10 to 17 represent the homogeneous part of the aquifer, zones 1 to 5 and 6 to 7 represent areas where the aquifer is heterogeneous, and zones 8 and 9 represent

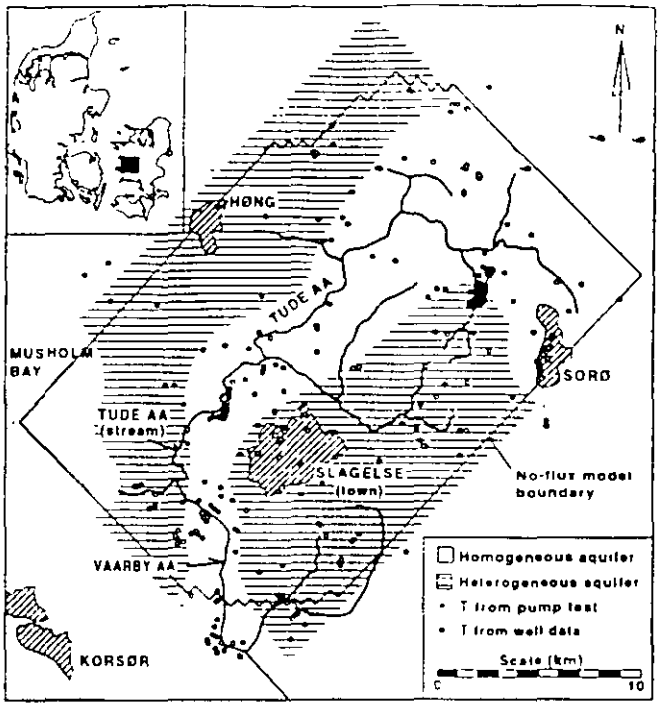

Fig. 1. Location of the field area.

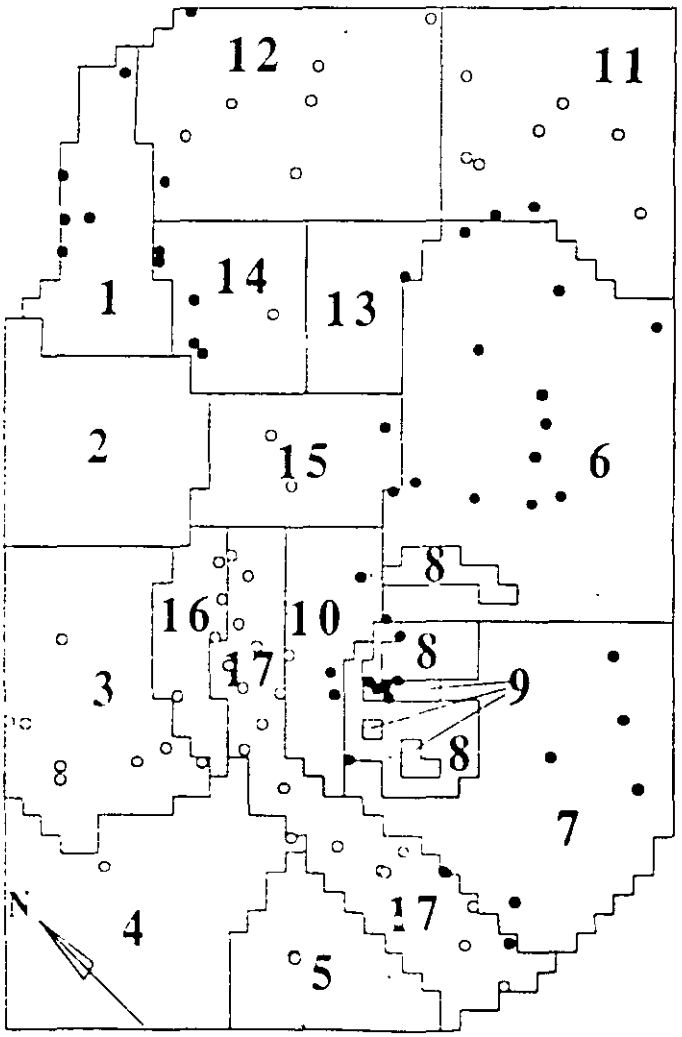

Fig. 2. Head measurement locations. The well symbols refer to the measured head variances in Table 3.

Table 1. Methods Used to Estimate Zonal Log_{10}-Transmissivity

Case	*Estimation method*
(A)	From local-scale pumping tests (averaging by kriging).
(B1)	Inversion based on accurate head measurements
(B2)	Inversion based on inaccurate head measurements
(C)	Inversion based on accurate head measurements and prior information from (A)

Table 2. Available Data on Log_{10}-Transmissivity (Y) and Hydraulic Head

Zone	*No. of local Y-estimates*	*No. of local Y-predictions*	*No. of head measurements*
1	1	4	5
2	1	1	0
3	4	0	8
4	0	1	2
5	3	10	2
6	3	21	13
7	11	10	8
8	0	0	0
9	0	8	8
10	2	5	4
11	6	20	9
12	6	8	8
13	0	2	1
14	4	2	6
15	2	3	3
16	2	2	4
17	18	25	19
utside model area	27	17	
Total	90	139	100

the extremely heterogeneous Slagelse area with local sand layers (zone 9) surrounded by till (zone 8). The following paragraphs consider how well each of the methods listed in Table 1 can be used to estimate the log_{10}-transmissivity of these zones. The data used for estimation are summarized in Table 2 as well as in Figures 1 and 2.

Estimation from Local-Scale Pumping Tests

Constant-rate pumping tests were carried out in 63 wells within the study area and in 27 wells just outside the area (Figure 1). The test durations ranged from half an hour to several days. Jacob's straight-line method was applied to estimate transmissivities from the test results. The lines were fitted to the first linear part of the drawdown curves (typically after 10 minutes) that are not affected by well bore storage, partial penetration or distant boundary conditions (Kruseman and de Ridder, 1990). For all the tested wells, the estimated transmissivity represents the local aquifer transmissivity within (at least) a few hundred meters from the well.

Specific capacity and lithology data were available for 229 wells within and just outside the studied area (Figure 1). Ninety of these wells were pump-tested.

Christensen (1995a; 1995b) compared specific capacities, lithology and pump-test derived transmissivities using regression, and showed that using specific capacity gives fair predictions of log_{10}-transmissivity in the heterogeneous parts of the aquifer, whereas specific capacity and lithology should be used jointly to predict log_{10}-transmissivity in the homogeneous part of the aquifer (Christensen, 1995b). The prediction models only explained about 60% (heterogeneous) and 40% (homogeneous) of the observed variance, and the latter transmissivity predictions were obviously biased. Therefore, the present study does not use predicted log_{10}-transmissivities in the homogeneous part of the aquifer. In the heterogeneous areas specific capacity was used to predict the local-scale log_{10}-transmissivity at wells without pump tests.

In case (A), kriging (Journel and Huijbregts, 1978) was used to estimate the zonal log_{10}-transmissivity from the local-scale values. For this purpose two semivariograms of log_{10}-transmissivity were estimated: one for the homogeneous part of the aquifer and one for the heterogeneous parts (Figure 1). Each variogram was estimated from local log_{10}-transmissivities, determined exclusively from pumping test analyses (i.e., at the sites marked with solid circles in Figure 1), using the method of Samper and Neuman (1989). The estimated semivariograms are shown with their experimental counterparts in Figure 3. The reader is referred to Christensen (1994b) for further information on the actual estimation of the semivariograms.

The zonal estimators were formed by combining local kriging estimates (Journel and Huijbregts, 1978, pp. 320-324; see Christensen, 1995c, for specific details). Each local estimate represents a 500 × 500 m^2 subarea of the aquifer, which compares roughly to the area influenced by the pump tests. Zonal estimation was only carried out for six zones (6, 7, 12, 14, 16, and 17) within which there was (subjectively and optimistically judged) an adequate number of local transmissivity estimates or predictions. The six zonal estimates and their approximate 95% confidence intervals (estimate ± two standard errors) are shown in Figure 4. The estimated values are within the expected ranges. The uncertainty of the zonal estimates are mainly due to covariance between the local kriging estimates that form the zonal estimates (cf. Journel and Huijbregts, 1978, eq. V.19). The covariance term has the greatest influence on the uncertainty of the estimates of the heterogenous zones 6 and 7, which therefore have the widest intervals. This indicates that the number and location of data within these zones may be inadequate for making proper kriging estimates.

Table 3. Estimated Variances of Measured Heads [m^2] (Standard Deviation in Parenthesis)

Set of head measurements	*Well symbol in Figure 2* ○	●
(B1)	1.0 (1.0)	4.3 (2.1)
(B2)	5.0 (2.2)	7.7 (2.8)

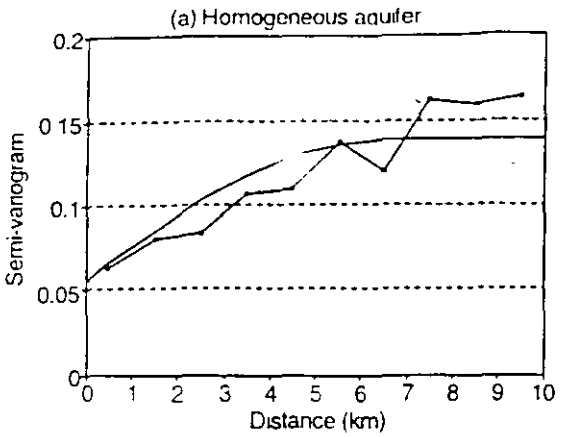

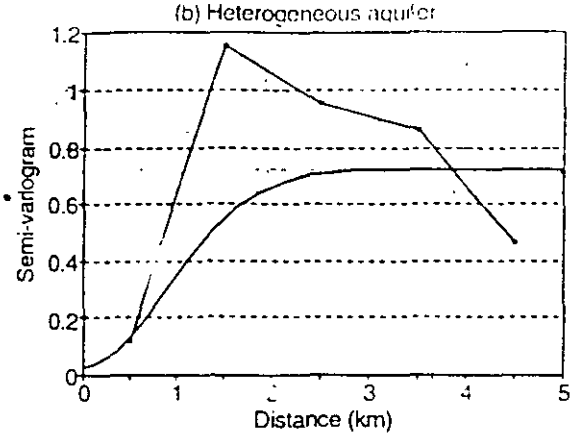

Fig. 3. Semivariograms for $\log_{10}$-transmissivity.

Hydrologic Inversion by Nonlinear Regression

Suppose that some of the hydrogeological parameters in a ground-water model are considered to be model parameters that have to be estimated from measurements of hydraulic head. The model parameters then can be estimated by minimizing the least-squares criterion (e.g., Neuman and Yakowitz, 1979; Cooley and Naff, 1990, or Hill, 1992)

$$S(\mathbf{b}) = [\mathbf{h}^* - \hat{\mathbf{h}}(\mathbf{b})]^T \mathbf{V}_h^{-1} [\mathbf{h}^* - \hat{\mathbf{h}}(\mathbf{b})] + [\mathbf{b}^* - \mathbf{b}]^T \mathbf{V}_b^{-1} [\mathbf{b}^* - \mathbf{b}] \quad (1)$$

where $\mathbf{b}$ is the vector of model parameters to be estimated; $\mathbf{h}^*$ is the vector of measured hydraulic heads, $\hat{\mathbf{h}}(\mathbf{b})$ is the corresponding vector of predicted (modeled) heads at the measured wells using the parameters $\mathbf{b}$; $\mathbf{V}_h$ is the covariance matrix of the assumed Gaussian distributed uncorrelated true errors in head residuals, $\mathbf{h}^* - \hat{\mathbf{h}}(\mathbf{b})$, $\mathbf{b}^*$ is the vector of prior estimates of the parameters, and $\mathbf{V}_b$ is the covariance matrix of the true errors of $\mathbf{b}^*$. In this study a modified version of the USGS program MODFLOWP (Hill, 1992) was used for the minimization of equation (1). The modified version allows for a full weight matrix on the prior information, as is needed because the prior are correlated (see previous section).

The weighting of head data and the choice of model parameters must always be considered when using nonlinear regression to estimate ground-water model parameters. The considerations made in the present study are briefly discussed in the following.

Weighting Hydraulic-Head Data

The head residuals, $\mathbf{h}^* - \hat{\mathbf{h}}(\mathbf{b})$, are functions of the errors of measured heads, $\mathbf{h}^*$, and of the errors of the modeled heads, $\hat{\mathbf{h}}(\mathbf{b})$.

Errors in $\mathbf{h}^*$ are normally caused by inaccuracies in the measurement equipment or by reading errors. In practice there is a further source of errors, namely errors due to inaccurate or wrong interpretations of what has actually been measured. A wrong interpretation will, for instance, arise if a measured head is assumed to be in the investigated aquifer but actually represents the head in another hydrogeological unit. An inaccurate interpretation will, for instance, arise if the heads measured in a number of wells are assumed to represent a quasi-stationary situation but were actually taken during a period with systematic changes in head. Such inaccurate or wrong assumptions are common.

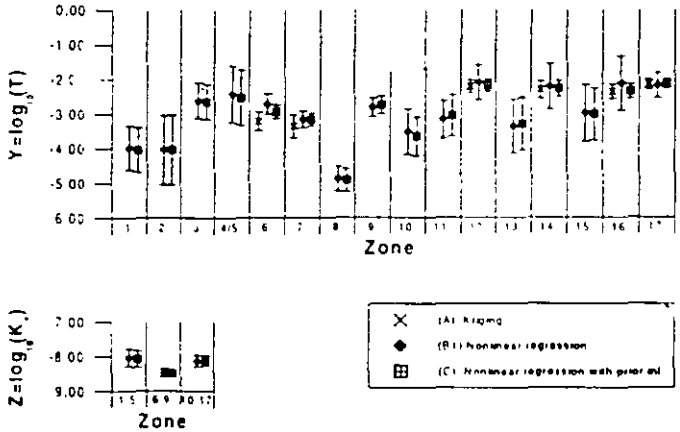

Fig. 4. Estimated parameters and 95% confidence intervals.

Errors in the modeled heads, $\hat{\mathbf{h}}(\mathbf{b})$, arise (1) from the fact that the solved flow equation provides at best only an approximate description of true aquifer behavior; (2) from the numerical discretization of the flow equation; and (3) from the discretization of the hydrogeology (Neuman and Yakowitz, 1979; and Peck et al., 1988). A type (1) error will arise if flow is assumed to be horizontal, whereas the true flow is three-dimensional. The three-dimensionality will be reflected by the measurements if the measured wells screen different parts of the aquifer. Type (2) errors can be reduced by choosing a suitable numerical discretization. Type (3) errors arise from the scarcity of field data so that important hydrogeological properties may not even be recognized or, if such properties are recognized, field observations are only sufficient to estimate a limited number of model parameters. One therefore has to concentrate on the estimation of a relatively small number of key parameters, for instance by using parameter zonation. The first and third kinds of model errors are common in practice and the consequence is that the model can only predict the large-scale variations ("the drift") of the ground-water head/flow field, but not the small-scale variabilities.

We thus have to accept that the ground-water model is at best a model of the drift of the true head field, and that the variance of $\mathbf{h}^*$ from the drift (from now on termed the measured head variance) is the sum of the variance of $\mathbf{h}^*$ mentioned above and the small-scale variance of the true head field.

3

Objective weighting of the head residuals, $\mathbf{h}^* - \hat{\mathbf{h}}(\mathbf{b})$, in equation (1) requires that $\mathbf{V}_h$ contains the measured head variances. For the following cases such variances were estimated by Christensen (1995d) through analysis of residuals between an estimated drift and the measured heads. The analysis showed that the measured head variance differs between two types of subareas: it is relatively small in the homogeneous part of the aquifer and in the coastal areas; but larger in the heterogeneous parts of the aquifer (Figure 2).

Two sets of hydraulic-head data from the 100 wells within the model area (Figure 2) are used in the following:

(B1) Accurate measurements, where the depth to the water table of wells was measured by electric sounding during November 1988 and the wells were levelled. The typical measurement error of head is therefore within a few centimeters.

(B2) Rough measurements from the well database of the Geological Survey of Denmark and Greenland (GEUS).

For the latter set of measurements the depth to the water table was measured by the drilling contractor at the time the well was drilled. As the wells within the model area were constructed over a period of decades the heads have varied considerably during the measurement period (see hydrograph in Christensen, 1994a). The ground level reference of (B2) was estimated from 1:25000 maps with a 2.5 m topographical contour interval. The precision of the contours is within 0.5 m. With the additional uncertainty from unprecise positioning of the well on the map, the typical error of the ground level reference will be one to two meters. The typical error of the measured heads of (B2) is thus expected to be several meters.

The estimated measured head variances are listed in Table 3. The variance increases with the heterogeneity of the aquifer as well as with the measurement uncertainty. The estimated variances of the accurately measured (B1) heads is one to two orders of magnitude larger than the expected measurement variance from above. This is mainly due to small-scale variance of the true heads (horizontally as well as vertically).

Model Parameters

A number of hydrogeological parameters must be known or estimated in order to model the steady ground-water flow in the studied leaky aquifer. In the present study the aquifer transmissivity and the vertical conductivity of the confining layer were estimated by nonlinear regression, whereas the thickness of the confining layer, the head of the overlying aquifer, and the withdrawal rates from the aquifer were assumed to be known. The latter parameters were taken from the previous work of Christensen (1994a), who estimated the confining layer thickness from lithological data, modeled the hydraulic heads of the overlying aquifer, and estimated the withdrawal rates from data on the annual withdrawals. The model boundary (Figure 1) and the model grid are identical to those in Christensen (1994a).

The zonation of transmissivities and the available head measurements are shown in Figure 2 and described above. Figure 2 and Table 2 show that data are scarce in zones 2, 4, and 13 and rather scarce in zone 5. Further, the seaward ground-water flow through zones 4 and 5 is small (Christensen, 1994a) and the hydraulic gradients within these zones are also small. These circumstances are consistent with the discovery that the estimation of $\log_{10}$-transmissivity by nonlinear regression is very uncertain in these four zones. To stabilize the estimation, prior information from the lithology observed when drilling was used for these $\log_{10}$-transmissivities in the minimization criterion equation (1): for zone 2 the prior estimate is -4.0 with a standard error of 0.5; for zones 4, 5, and 13 the prior estimate is -3.0 with a standard error of 0.5. The prior information from lithology was assumed to be uncorrelated. Further, estimation showed that the $\log_{10}$-transmissivities of zones 4 and 5 could be combined into one parameter. These priors, based on lithology, was used in the three cases B1, B2, and C.

The distribution of vertical hydraulic conductivities of the confining layer was divided into three regions: (1) a region containing the transmissivity zones 1 to 5 (Figure 2); (2) a region containing the transmissivity zones 6 to 9, and (3) a region containing the transmissivity zones 10 to 17. Using alternative conductivity regions in the regression showed that fewer regions led to a poorer model fit to data, whereas more than three did not improve the fit. Using as many as six conductivity regions led to significant parameter correlations.

We thus end up with 19 model parameters to be estimated by regression, namely 16 zonal $\log_{10}$-transmissivities (Y_1, Y_2, Y_3, $Y_{4/5}$, Y_6, . . . Y_{17}) and 3 regional $\log_{10}$-conductivities (Z_{1-5}, Z_{6-9}, and Z_{10-17}).

Results

For **case (B1)**, only measurements in head data set B1 are used. The estimated parameters and their approximate 95% confidence intervals (estimate ± two standard errors) are shown in Figure 4 (e.g., Cooley and Naff, 1990, equations 5.4-13 for the calculation of standard error). The weighted residuals are normally distributed with a variance of 1.09 (−), and they do not indicate any bias.

The estimated $\log_{10}$-transmissivities are generally within the expected ranges even though the estimate of Y_6 lies slightly outside the confidence interval for the corresponding estimate found by kriging (Figure 4). The width of the confidence intervals for Y_6, Y_7, Y_8, Y_9, and Y_{17} is between half and one, whereas it is between one and two for the remaining $\log_{10}$-transmissivities. The largest confidence intervals occur in zones within which the head observations are scarce (e.g. zones 2 and 13) and (or) the head gradients are small (e.g. zones 1, 3, 4/5, and 15). In the homogeneous part of the aquifer, the confidence intervals are large for the estimates in zones with small head gradients. Contrary to this, the intervals are small for estimates in the eastern heterogeneous part of the aquifer where head gradients are significant.

Comparing the confidence intervals of the regression estimates to those of the kriging estimates (Figure 4) shows that they are similar for Y_6 and for Y_7, i.e. in the heterogeneous part of the aquifer, whereas the regression intervals are three to four times wider than the kriging ones for Y_{12}, Y_{14}, Y_{16}, and Y_{17} in the homogeneous part of the aquifer.

The estimated $\log_{10}$-conductivities of the confining till layer (Figure 4) correspond quite well to Christensen (1994a), who found an average value of -8.10 for the model area as a whole. However, according to the present study the value is somewhat lower (-8.46) for Z_{6-9}. The confidence intervals of the estimated $\log_{10}$-conductivities are all quite narrow compared to those of the $\log_{10}$-transmissivities.

The predicted heads and the corresponding approximate standard errors (calculated as given by Cooley and Naff, 1990, equations 5.7-8) are contoured in Figure 5. This figure shows that the standard error of predicted heads is less than 1 m in the

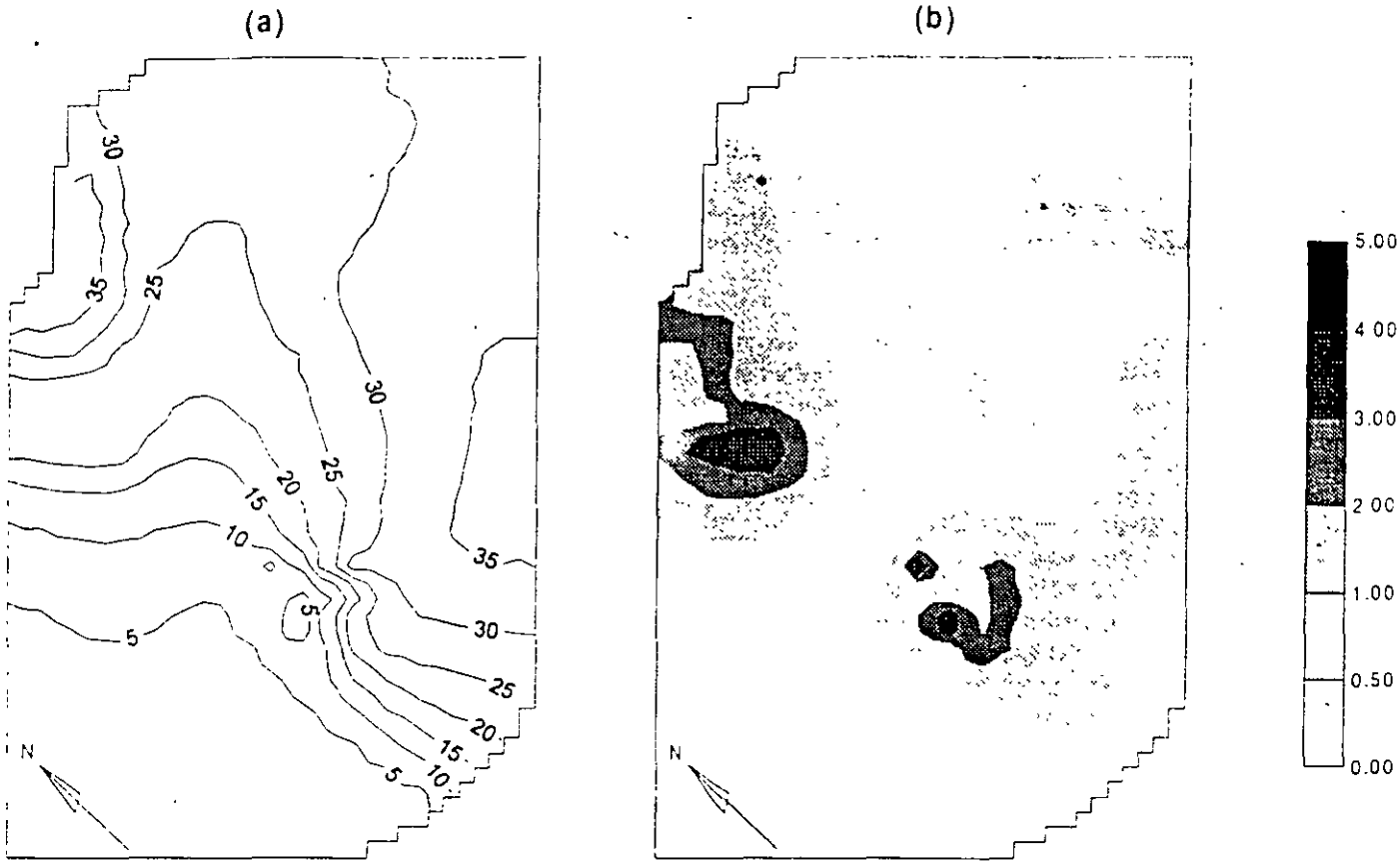

Fig. 5. (a) Predicted heads [m], and (b) standard error of predicted heads [m] in case (B1).

homogeneous part of the aquifer, and generally less than 2 m in the heterogeneous part. It is notable, however, that the error is up to 5 m within zone 2 due to the great sensitivity of the head to the local parameters, which have large variances. Further, the standard error is 2 to 5 m around well fields in the heterogeneous zones at Slagelse, where the stress of flow is large. A result of this is that the predicted head is very sensitive to the estimated local parameters, especially the conductivity of the confining layer. A similar observation was made and explained by Cooley (1993).

In case (B2), the inaccurate head data set (B2) is used. If case (B2) is compared to case (B1), then one can see from Figure 6 that the estimated log-transmissivities change significantly (i.e. by more than two standard errors of the case B1 estimates) in three areas: around Slagelse (zones 8 and 9), in the northeastern area (zone 11), and in the area of zones 3, 16, and 17.

In case (B2), there is practically no difference between the estimated Y_8 and Y_9 log-transmissivities, which is inconsistent with the geological information in this area. The unrealistic estimates result from the fact that the inaccurate head observations in the Slagelse area do not show the actual dramatic local variations in head.

Both the estimated mean of Y_{12} and its standard error are large, which is because the heads observed in case (B2) within and adjacent to zone 12 vary randomly and show no distinct flow direction. The estimated mean of Y_{11} is very small because the observed heads within this zone (by coincidence) show a steep gradient. Due to the low estimated transmissivity of zone 11, the estimate of the adjacent Y_{13} is larger. The standard error of Y_{13} is smaller than in the previous cases because some of the heads observed within zones 6, 11, and 12 are more sensitive to this parameter than in the previous cases.

The estimated mean of Y_3 is very small, and Y_{16} is also reduced, because the observed head gradients in these zones are larger in case (B2) than in case (B1). To compensate for the reduced estimate of Y_{16}, the estimated mean of Y_{17} increases in case (B2).

Figure 6 shows that Z_{10-17} has increased significantly from case (B1) to case (B2). This is probably because the observed heads within these zones on average are 0.3 m larger in the latter case than in the former, which tends to reduce the predicted leakage. An increase of Z_{10-17} will balance this tendency.

Due to the large data uncertainty it is not surprising that case (B2) has wide confidence intervals (Figure 6). Most of the

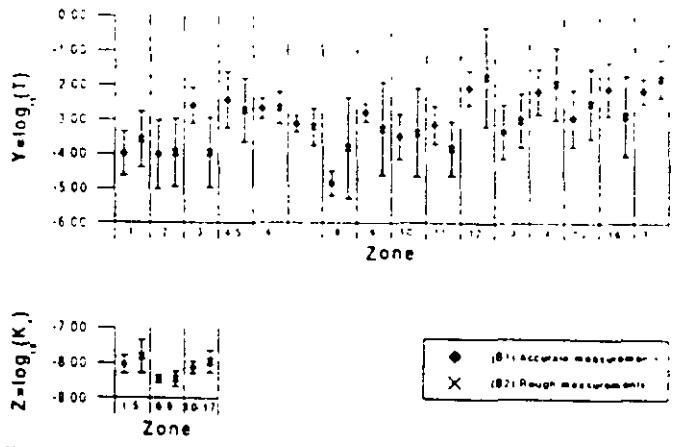

Fig. 6. Estimated parameters and 95% confidence intervals.

estimated log-transmissivities have very wide intervals, whereas the intervals for the log-conductivities are still quite narrow. Therefore, in outline, the estimated transmissivities are very uncertain while the vertical conductivities of the confining layer seem to be well-determined

Figure 7 shows a map of the predicted heads in case (B2). A comparison with the head predictions in case (B1), Figure 5, shows that the heads differ significantly within three areas: firstly, the predicted heads in case (B2) have increased by up to 10 m in zones 2 and 3; secondly, the heads around Slagelse have changed by up to 5 m and the local variations are less dramatic than in case (B1); and thirdly, the predicted heads in zone 11 have increased as well as decreased locally by up to 3 m. This is due to the mentioned changes in the estimated transmissivities of these areas.

Figure 7 also shows that the standard error of predicted head in case (B2) in general has increased by 0.3 to 1.0 m compared to case (B1), Figure 5. This increase is due to the general increase of the model parameter variances. The error is, however, reduced by up to 1 m within zone 2, and by up to 2 m within the Slagelse area.

Christensen (1995d) also used a set of head measurements of moderate accuracy to estimate the studied model parameters These heads were measured almost simultaneously in wells whose ground level was estimated from 1:25000 maps. In this case some of the estimated parameters change by up to two standard errors compared to case (B1), and the confidence interval increases for all the parameters. The consequence is that the standard error of the predicted heads generally increase by 0.1 to 0.5 m compared to case (B1), but the local increase may be up to 1 m.

Inversion with Prior Information from Pumping Tests

If prior information on $\log_{10}$-transmissivity is available from pumping tests, this information can be used in the minimization criterion, equation (1). In this study such information was available (see above) for Y_6, Y_7, Y_{12}, Y_{14}, Y_{16}, and Y_{17}. These parameters were estimated by kriging of local-scale transmissivities evaluated from pumping test data. The kriging covariance between these estimates was calculated from Christensen (1995c) equation (12), which is similar to the zonal variance equation (V.19) in Journel and Huijbregts (1978). In the regression, these covariances were contained in V_b of equation (1)

The regression in case (C) was thus based on the prior information from pumping tests and on the set of accurately measured heads from above (case B1). Residual analysis indicates that the weighted residuals are normally distributed with a variance of 1.11 (−), which is similar to the previous case (B1). The predicted heads of the two cases generally differ by less than 0.1 meters. However, in a part of zone 6, at the model boundary, the head of case (C) is up to 1.5 m higher than the head of case (B1). No doubt this is due to the decreased estimate of Y_6. Head measurements are sparse in this area, yet it might indicate a weak bias either in the flow model or in the kriging estimate of Y_6.

Figure 4 shows that no parameter estimates deviate significantly from those that were estimated without prior information from kriging. The confidence intervals are narrower in the zones

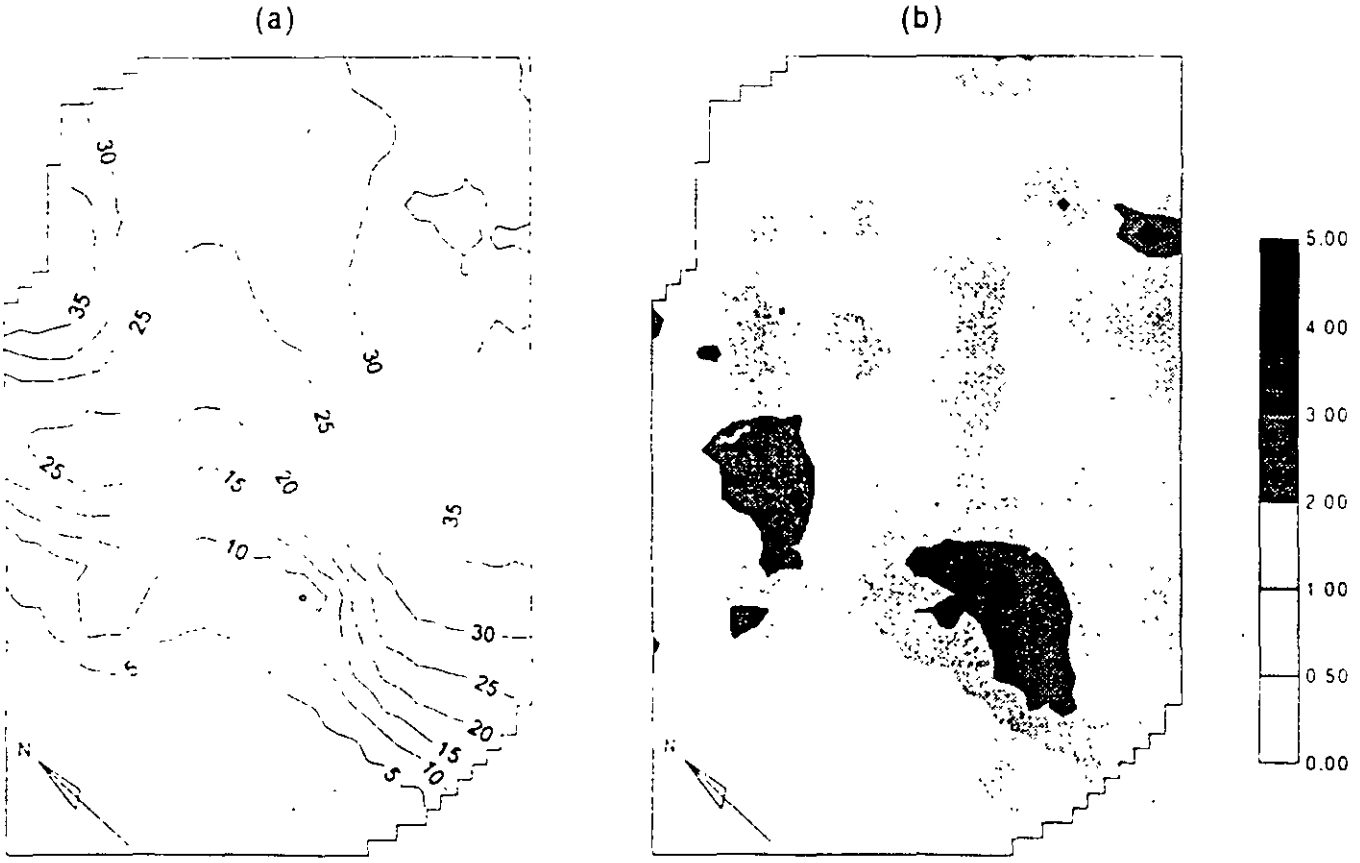

Fig. 7 (a) Predicted heads [m], and (b) standard error of predicted heads [m] in case (B2).

where kriging estimates were used, especially for Y_{12}, Y_{14}, Y_{16}, and Y_{17}. For these estimates the interval width is about the same as for the kriging estimates. On the whole the width of the confidence intervals is unchanged for parameters where no prior information is used.

Figure 8 shows the reduction of the standard error of predicted heads from case (B1) to case (C) due to the introduction of prior zonal estimates based on pumping tests. The standard error is reduced by less than 0.1 meter within most of the area, and the reduction only exceeds 0.2 m in a few small areas. The largest reductions occur in zones where the $\log_{10}$-transmissivity estimation variance is significantly reduced through the use of prior estimates. The generally small standard error reductions may seem surprising when compared to the reduction of some of the estimation variances. However, the significant reductions of estimation variance occur in the high-transmissive zones, and the predicted heads are relatively insensitive to these transmissivities

Discussion and Conclusions

The zonal $\log_{10}$-transmissivity can be estimated (1) by analysis of long-duration pumping tests with multiwell observations, (2) by combining (averaging) local $\log_{10}$-transmissivity estimates; (3) by hydrologic inversion based on head data, or (4) by hydrologic inversion based on head data and on prior information from pumping tests

(1) The zonal $\log_{10}$-transmissivity can only be estimated by analysis of long-duration pumping tests within confined and semiconfined aquifers It is laborious and expensive and the testing causes inconvenience to other ground-water developers. In practice such tests are therefore only carried out at a few selected sites

Fig. 8. Reduction in standard error of predicted hydraulic heads [m], from using prior information in the nonlinear regression.

(2) Forming zonal estimates by combining local estimates requires closely spaced local data from the entire zone This fact makes it attractive to supplement accurately estimated local $\log_{10}$-transmissivities with predictions made from specific capacity and lithology, both of which are obtainable at low cost However, for the prediction model to produce unbiased predictions requires quite a lot of accurate transmissivity data for estimating the parameters of the prediction model. That is, good predictions can only be made in areas where one already has considerable knowledge of the transmissivity field. Further, the studies of Christensen (1995a; 1995b) indicate that in some situations it is difficult (or practically impossible?) to use well data as predictors when the transmissivity only varies within one to two orders of magnitude.

In the present paper the zonal estimates were formed by combining local kriging estimates. It is important to note that if kriging is used, $\log_{10}$-transmissivity data, preferably from pumping test analyses, are required to estimate the semivariogram. In the present case this is fulfilled for the homogeneous parts of the aquifer, whereas it is questionable whether there are adequate data for the heterogeneous parts (compare for instance the theoretical and the experimental semivariograms of Figure 3b)

In a heterogeneous zone, within which the $\log_{10}$-transmissivity is characterized by a large variance and a small correlation scale, a large amount of data is needed to estimate the semivariogram and to produce a zonal unbiased estimate from kriging Unfortunately, it is often difficult to get such data in heterogeneous areas, because wells are scarce (see for instance, Figure 1). Further, if the $\log_{10}$-transmissivity variance is large then the zonal variance may still be comparable to, or even larger than, the corresponding variance of an estimate made by hydrologic inversion from head data. In the present study, the inversion estimate (in case B1) of $\log_{10}$-transmissivity within such heterogeneous zones was better than the zonal kriging estimate, and the width of the confidence interval of the inversion estimate was only reduced moderately by using the kriging estimates as prior information. Even though the data are too scarce to draw firm conclusions, the present study leads one to doubt the practical value of forming zonal kriging estimates from local data in heterogeneous aquifers if the estimates are to be used as an input for ground-water models

In homogeneous zones, where the $\log_{10}$-transmissivity variance is small and the correlation scale is large, it is possible to sample the data to estimate the semivariogram and to form unbiased zonal estimates In the present case study the confidence intervals of the zonal kriging estimates of the homogeneous zones were three or four times narrower than the intervals of the corresponding estimates made by hydrologic inversion.

(3) The zonal hydrogeological parameters can be estimated directly from observations of hydraulic head by nonlinear regression. If the purpose of zonal $\log_{10}$-transmissivity estimation is to produce input for a hydrologic model then inversion is an attractive estimation method. The present case study of a leaky aquifer demonstrates, however, that inaccuracies in the head data may seriously damage the reliability of the estimated parameters and, as a consequence, of the ground-water model

Using accurate head data (case B1), the estimated zonal parameters (16 $\log_{10}$-transmissivities and 3 $\log_{10}$-conductivities of the confining layer) were within the expected ranges, whereas the corresponding confidence intervals were both smaller and larger than the intervals of the zonal estimates produced by

kriging (mentioned above). The standard error of predicted heads is generally between 0.2 and 2 m.

The estimated transmissivities are very uncertain when rough head measurements are used (case B2). The estimated transmissivity within three subareas differs significantly from case (B1) and some of these estimates are inconsistent with the documented hydrogeology. Further, the estimated conductivity of the semiconfining layer increases significantly within large subareas. The consequence of using rough instead of accurate measurements is thus that the predicted heads deviate strongly from those of case (B1) and that the standard error of the predicted heads generally increases by 0.3 to 1 m.

(4) When zonal kriging estimates were used in the inversion as prior information on 6 out of 16 $\log_{10}$-transmissivities, then the width of the confidence intervals of the parameters with prior information was reduced by up to 75%. The present study and the study of Clifton and Neuman (1982) both indicate, however, that using prior information in the estimation of the hydrologic model parameters hardly reduces the uncertainty of the predicted hydraulic heads. For instance, in the present case the use of prior information reduced the standard error of predicted head by less than 0.1 m within most of the area, and the reduction only exceeds 0.2 m in a few small areas.

For this specific case the results suggest that, given the high costs of sampling the necessary local $\log_{10}$-transmissivity data and of forming the zonal estimates, one should concentrate on qualitative mapping of the hydrogeology, on sampling accurate head data and on subsequent estimation of the zonal parameters by inversion (or manual calibration). Long-duration pumping tests at a few key locations may be used to verify the estimated hydrologic model, or at a later stage of the investigation, to reduce model uncertainties. Whether or not these site-specific conclusions can be extended to other field sites may depend upon the economic considerations and the degree of heterogeneity of the aquifer under consideration.

Acknowledgments

This study was funded by the Aarhus University Research Foundation and by the Danish Environmental Research Programme 1992-1996. I wish to thank Keld Rømer Rasmussen and Michael Sørensen for useful discussions during the preparation of the paper and Conrad Aun-Robinson for improving the English text. Mary C. Hill is thanked for her review of the revised version of the paper.

References

Christensen, S. 1994a. Hydrological model for the Lade aa catchment. Nordic Hydrology, v. 25, no. 3, pp. 145-166.

Christensen, S. 1994b. A case study of the estimation of the log-transmissivity semi-variogram by cross-validation error minimization. Internal Research Report, Dept. of Earth Sciences, Aarhus Univ., Aarhus. 37 pp.

Christensen, S. 1995a. Prediction of log-transmissivity—1. Using specific capacity. Nordic Hydrology, v. 26, no. 1, pp. 1-20.

Christensen, S. 1995b. Prediction of log-transmissivity—2. Using lithology and specific capacity. Nordic Hydrology, v. 26, no. 1, pp. 21-36.

Christensen, S. 1995c. On the strategy of estimating the transmissivity field of a regional-scale groundwater model. Internal Research Report, Dept. of Earth Sciences, Aarhus Univ., Aarhus. 37 pp.

Christensen, S. 1995d. Calibration data accuracy in a regional-scale groundwater model. Internal Research Report, Dept. of Earth Sciences, Aarhus Univ., Aarhus. 29 pp.

Clifton, P. M. and S. P. Neuman. 1982. Effects of kriging and inverse modelling on conditional simulation of the Avra valley aquifer in southern Arizona. Water Resources Research, v. 18, no. 4, pp. 1215-1234.

Cooley, R. L. 1993. Exact Scheffé-type confidence intervals for output from groundwater flow models—1. Use of hydrologic information. Water Resources Research, v. 29, no. 1, pp. 17-33.

Cooley, R. L., L. F. Konikow, and R. L. Naff. 1986. Non-linear regression groundwater flow modelling of a deep regional aquifer system. Water Resources Research, v. 22, no. 13, pp. 1759-1778.

Cooley, R. L. and R. L. Naff. 1990. Regression modelling of groundwater flow. U.S. Geological Survey Techniques of Water-Resources Investigations, book 3, ch. B4, 232 pp.

Delhomme, J. P. 1974. La cartographie d'une grandeur physique a partir de donnees de differentes qualites. International Association of Hydrogeologists, Memoires, v. 10, no. 1, pp. 185-194.

Hill, M. 1992. A computer program (MODFLOWP) for estimating parameters of a transient, three-dimensional ground-water flow model using nonlinear regression. USGS, Open-File Report 91-484, 358 pp.

Journel, A. G. and C. Huijbregts. 1978. Mining Geostatistics. Academic Press, New York. 600 pp.

Kruseman, G. P. and N. A. de Ridder. 1990. Analysis and evaluation of pumping test data (2nd ed.). Int. Inst. for Land Reclamation and Improvement, Waageningen, The Netherlands. Publ. 47, 377 pp.

Neuman, S. P. 1980. A statistical approach to the inverse problem of aquifer hydrogeology—3. Improved solution method and added perspective. Water Resources Research, v. 16, no. 2, pp. 331-346.

Neuman, S. P. and S. Yakowitz. 1979. A statistical approach to the inverse problem of aquifer hydrogeology—1. Theory. Water Resources Research, v. 15, no. 4, pp. 845-860.

Peck, A., S. Gorelick, G. de Marsily, S. Foster, and V. Kovalevsky. 1988. Consequences of spatial variability in aquifer properties and data limitations for groundwater modelling practice. IAHS Publ. no. 175, Wallingford. 272 pp.

Samper, F. J. and S. P. Neuman. 1989. Estimation of spatial structures by adjoint state maximum likelihood cross validation—1. Theory. Water Resources Reserach, v. 25, no. 3, pp. 351-362.

Theis, C. V., R. H. Brown, and R. R. Meyer. 1963. Estimating the transmissibility of aquifers from the specific capacity of wells. Methods of determining permeability, transmissibility and drawdown. USGS Water Supply Paper 1536-I, pp. 331-341.

FACULTAD DE INGENIERIA U.N.A.M.
DIVISION DE EDUCACION CONTINUA

CURSOS ABIERTOS

XII CURSO INTERNACIONAL DE CONTAMINACIÓN DE ACUÍFEROS

MODULO III: MODELOS MATEMÁTICOS EN GEOHIDROLOGIA Y CONTAMINACIÓN DE ACUIFEROS

TEMA

SIMULATION OF REGIONAL FLOW AND SALINITY INTRUSION IN AN INTEGRATED STREAM – AQUIFER SYSTEM IN COASTAL REGION: SOUTHWESTREGION OF BANGLADESH

EXPOSITOR: DR. ADOLFO CHAVEZ RODRIGUEZ

PALACIO DE MINERIA
OCTUBRE DEL 2000

Simulation of Regional Flow and Salinity Intrusion in an Integrated Stream-Aquifer System in Coastal Region: Southwest Region of Bangladesh

by N. Nobi and A. Das Gupta[a]

Abstract

A numerical model for simulation of the regional flow and salt-water intrustion in an integrated stream-aquifer system in coastal regions is developed, considering the dynamic interaction between the streams and the aquifer. The stream-aquifer model comprised of a two-dimensional depth-average finite-element model of the aquifer system and a quasi-steady node and reach model of the river network. The applicability of the model was demonstrated, through simulation of the spatial and temporal distributions of flow and salinity in the estuaries and in the underlying aquifer of the Southwest Region of Bangladesh. The important management aspects of water transfer and additional pumping and their effects on the system were evaluated. The interactions between the streams and the aquifer significantly influenced the flow and salt-water intrusion in the aquifer and the river network. An increased abstraction of ground water in the area caused a significant increase in the estuarine salinity. The salinity intrusion in the estuaries of the area, except in the southwest corner, could be reduced significantly by diverting the available water from the Ganges through the boundary river Gorai.

Introduction

The goal of water resources planning and management is to meet the water demand of different uses in a most effective manner. One of the pressing environmental problems in the management of water resources is to ensure adequate water supply of acceptable quality. As the development of all the possible sources progress with time, it becomes important to utilize all the sources in an integrated manner. The simulation models alone or in conjunction with the optimization techniques (by embedding or externally producing the system responses) are widely used to analyze the optimal development and management problems of the water resources systems.

A typical coastal stream-aquifer system consists of a complex river network hydraulically connected with the underlying composite aquifer system (mixed confined and unconfined conditions) (Figure 1). Both surface and ground water play an important role in meeting the domestic, industrial, and agricultural water demand. Depending on the hydrological conditions, the stream-aquifer interaction plays a significant role in planning and management of water sources in these systems. The aquifer and the river network are heterogeneous in character, and the system inputs like rainfall, runoff, recharge, and the water demands also vary spatially and temporally. Both systems are bounded by the sea along the coast causing salt-water intrusion. Water resources management in such a system requires prediction of the combined effects of flow from the upstream and tides generated along the coast on the surface- and ground-water systems.

Simulation models for independent processes such as flow and solute transport in aquifer systems and in river networks, salt-water intrusion, and stream-aquifer interaction have been developed. However, the simulation of the regional flow and solute transport in a hydraulically connected stream-aquifer system has received very little attention. Reilly and Goodman (1985) reviewed the historical advancement in the quantitative analysis of sea-water intrusion in aquifers. Numerical models are based on the approximation of the transition zone between fresh water and salt water as a sharp interface (Volker and Rushton, 1982, Ledoux et al., 1990; Essaid, 1990), as well as on the concept of a dispersed transition zone (Segol et al., 1975, Huyakorn et al., 1987, Voss and Souza, 1987). The areal distribution of water

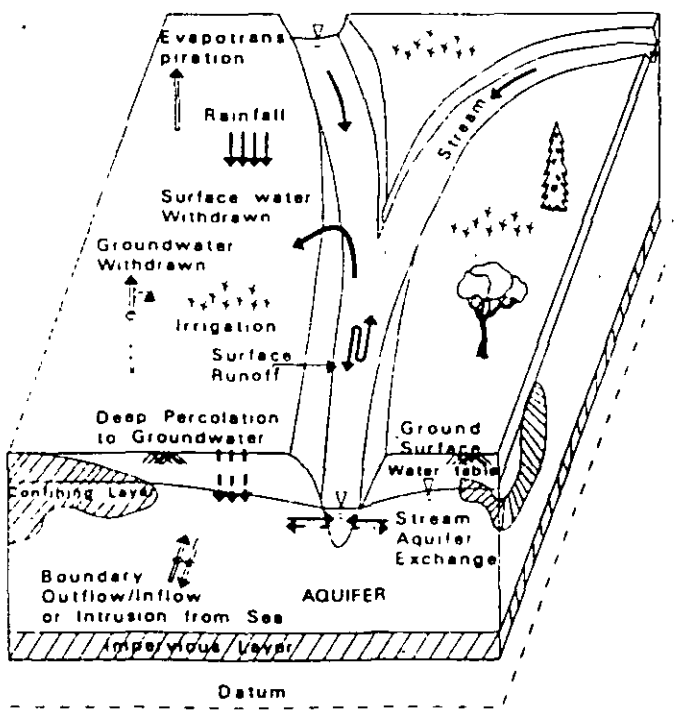

Fig. 1. A typical integrated stream-aquifer system in coastal region.

[a]Water Engineering and Management Program, School of Civil Engineering, Asian Institute of Technology, P.O. Box 4, Klong Luang 12120, Thailand

Received November 1995, revised August 1996, accepted September 1996.

withdrawal and recharge and their influences on the areal salt distribution are the key issues for management of coastal aquifers (Andersen et al., 1988). From the practical point of view a regional analysis dealing with an areal two-dimensional dispersive model would be adequate for management purpose (Ledoux et al., 1990). Numerical models have also been developed for simulation of instantaneous fluctuating flow and solute transport in a river network (Shen, 1979, Suppataratarn, 1990; Choi and Molians, 1993) However, due to the inherent computational complexity of the available hydrodynamic models, especially when associated with the management modeling, it is necessary to develop a simplified river network model to couple with the optimization algorithm.

This paper, therefore, deals with the development of a simulation model for the regional flow and solute transport in a coastal stream-aquifer system. This model can be used for the analysis of management problems with the conjunctive use of surface and ground water as well as for the control of salt-water intrusion. The model comprised of a two-dimensional depth-average finite-element model of the aquifer system and a quasi-steady node and reach model for the mean flow and salt transport in the river network. The models of the aquifer system and the river network are coupled, through the dynamic exchange of flow and salt between the aquifer and the rivers, and are solved iteratively. The developed model is applied to simulate the areal distributions of flow and salinity in the river network and the underlying aquifer system of the Southwest Region of Bangladesh. Important management aspects of the water resources development of the region are analyzed. The simplified forms of the model, particularly for the river network (for mean flow and solute concentrations rather than the instantaneous fluctuations) are used with the objective that the model can be coupled with a nonlinear optimization technique to obtain the optimal water resources development policies for the system (Nobi, 1994)

The Study Area

The study area covers 16,195 km^2 in the Southwest Region of Bangladesh as shown in Figure 2. The area is bounded by the river Ganges in the north, river Gorai-Modumati-Baleswar in the east, the Bay of Bengal in the south, and by the international border between Bangladesh and India in the west. The water resources in the area consist of a complex river network which is hydraulically connected to the underlying alluvial aquifer system. In the wet season when the rivers are in high stage, the river system recharges the aquifer and in the dry season as the river stage declines, water flows from the aquifer to the rivers as seepage flow. The available data for analysis correspond to 41 ground-water level observation wells, 13 ground-water quality monitoring stations, 6 river gauging stations, 5 river flow measuring stations, and 15 river water quality monitoring stations (Figure 2)

The study area is in a humid climate with an annual rainfall ranging from 1500 to 2100 mm; about 90% of the annual rainfall occurring in the wet season (May-Sept.). Input to the aquifer system occurs mainly as natural recharge from rainfall and irrigation. Except for the boundary river Gorai-Modumati-Baleswar along the east boundary of the area, all other rivers of the system originate within the region. Inputs to the river system are the internal runoff, seepage flow, and inflow from outside through the off-take of the river Gorai, Madanpur Beel route (MB route), and Sarupkathi (Figure 2). The land slope of the region is from north to south. Following topography, the flow in the aquifer and the rivers is towards the Bay of Bengal in the south.

Along the coast, salt water from the Bay of Bengal intrudes into the aquifer and the river system and degrades the water quality. The total dissolved solid (TDS) concentration in ground water varies from 0.1 ppt (parts per thousand or g/l) in the north of the area to 1.7 ppt in the south (along the coast) of the area. About 60% of the area has the TDS concentration more than 0.5 ppt. The TDS concentration in the river fluctuates seasonally depending on the amount of fresh-water flow. During the dry season the extent of 1 ppt concentration is about 120 km from the coast.

Hydrogeology

The hydrogeological system of the southwest region has been investigated by the Ground Water Hydrology Circle (GWHC) of Bangladesh Water Development Board (BWDB), through shallow and deep holes and pump tests at different locations. Altogether 41 hydrogeological sections (bore logs) and 33 pump test records were available from GWHC. The subsurface formation consists of a top silt layer (2-40 m thick) followed by a mixed fine and medium sand layer (20-100 m thick) lying on a relatively coarser layer of medium and coarse sand (30-140 m thick). This coarser layer is underlain by a fine sand and clay layer. Information for deeper strata below the bed of the lower coarser layer are very limited. Within these depth ranges, layers of clay, silt, and very fine sands are also observed in some bore logs. Most of the shallow wells pump from the upper fine and medium sand layer, while the deep wells are in the lower coarser layer. Both the upper (mixed fine and medium sand) and the lower (medium to coarse sand) water-bearing layers are hydraulically connected

In this study the system has been conceptualized as a composite aquifer lying on an impervious layer. The representative thickness of the conceptualized composite aquifer at a location depends on the thickness of the finer and coarser layers. The hydraulic conductivity and specific yield values for the aquifer were available from pump test reports. The aquifer thickness varies from 180 m in the north to 60 m in the south of the area. The maximum thickness of the top silt layer is about 40 m in the middle, and the minimum thickness is about 1 m in the north of the area. The hydraulic conductivity and specific yield values vary from 70 to 180 m/d and from 0.001 to 0.2, respectively. The regional distributions of the thickness of the aquifer layers and aquifer parameters are estimated through block kriging of the available data.

Methodology

Combined Stream-Aquifer Model

The hydraulic connection and exchange of flow between streams and aquifer significantly influenced the distribution of flow and solute concentration in the river and the aquifer systems. The river and the aquifer systems were therefore analyzed interactively. The rate of flow exchange between the stream and the aquifer was considered dependent linearly on the head difference between the aquifer and the stream (Herbert, 1970; Morel-Seytoux, 1975; Morel-Seytoux and Daly, 1975; Besbes et al., 1978)

$$Q_w = Cr\,\Delta h' \qquad (1)$$

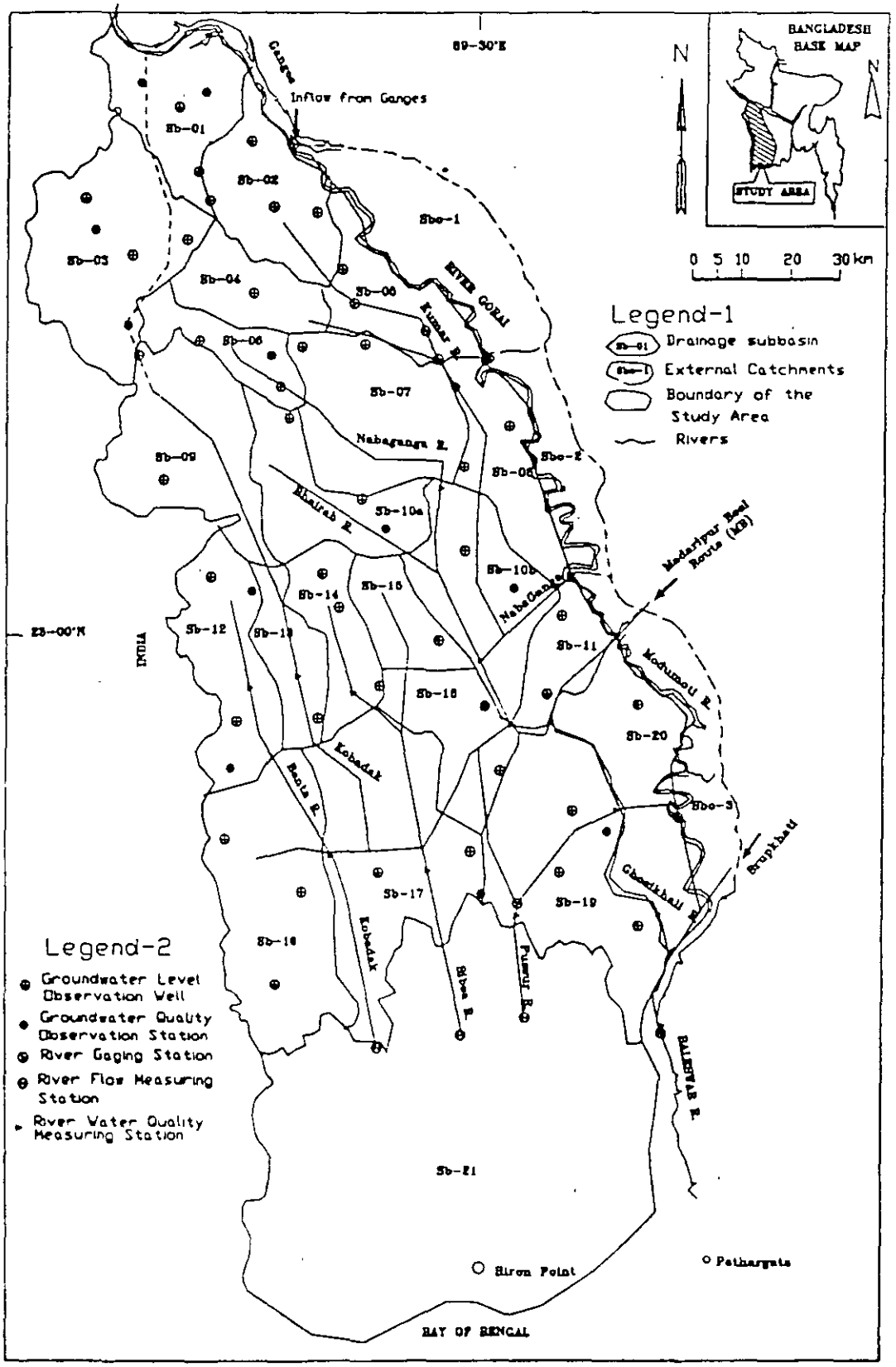

Fig. 2. Study area, conceptual river network, and location of observation stations.

where Q_{ig} is the exchange flow from stream to aquifer; $\Delta h' = (h - H)$ is the head difference between the stream head (h) and the aquifer head (H) in the vicinity of the stream; and Cr is designated as the stream reach transmissivity which depends on the stream bed characteristics and the shape of the stream cross section. Cr was expressed in a simplified form as $Cr = K_r L_r$; where K_r is defined as the conductivity or leakage factor of the reach, and L_r is the length of the stream reach. Only the advective transport of solute by the exchange flow (i.e., $Q_{ig}\dot{C}_{ig}$) was considered as the solute exchange between the stream and the

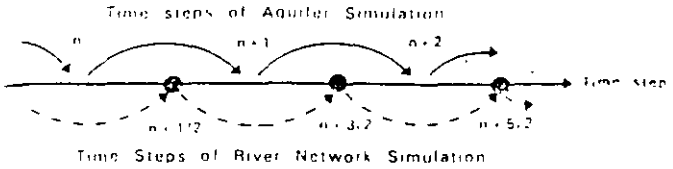

Fig. 3. Staggered time scheme for solution of the combined stream-aquifer model.

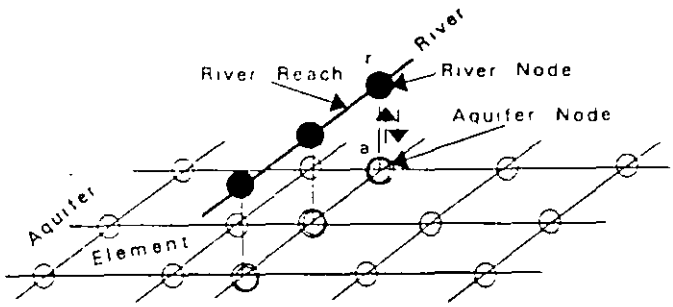

Fig. 4. Definition sketch of discretization of the integrated stream-aquifer system.

aquifer. Q_{ra} stands for the exchange flow between the river and the aquifer while C_{ra} represents the concentration of stream-aquifer flow exchange described as the concentration in the system (river or aquifer) from which water is flowing to the other.

The flow and solute transport in the aquifer system (mixed confined and unconfined condition) was described by a depth-average two-dimensional finite-element model. For the river network, a quasi-steady node and reach model was used to simulate the flow and solute transport. The exchange of flow and solute between the two systems was incorporated through nodal inflows or withdrawals in the aquifer model and the river network model. The governing equations for these models are provided in the Appendix. Since the interaction between the aquifer and the river system was dynamic depending on the state (head) of both systems, the aquifer model and the river network model were interdependent.

The flow and solute transport model for the two systems along with the interaction between the systems constituted the combined stream-aquifer model. To avoid the computational effort for simultaneous solution (iterative) of the nonlinear aquifer model and the river network model, a staggered scheme was employed to solve the models alternatively with a lag of half time step (Figure 3). The river network and the aquifer system were discretized integratedly with an aquifer node (a) corresponding to each of the river nodes (r) (Figure 4). At n^{th} time step the exchange flow was approximated in the aquifer model as $Q^n_{ra} = K_r L_r[h^{n-1/2}_a - (H^{n-1}_r + H^n_r)/2]$; where the subscript a denotes aquifer node corresponding to the river node r. The exchange flows (Q_{ra} at different nodes) computed at n^{th} time step were used as known values in the river network simulation at $(n + 1, 2)$ time step.

Conceptual System and Associated Data

The aquifer system was discretized into 586 elements with 653 nodes (Figure 5). A variable element size (4.5-7.5 km) was used with finer discretization near the coast. For the regional simulation, the complex river system of the area was conceptualized with a simplified network of total length 1528 km (Figures 2 and 5). In this conceptualization river courses in close proximity of one another were lumped together and small creeks and channels were ignored. The river network was discretized into 173 reaches (reach length varies from 5 to 20 km as shown in Figure 5) with 170 river nodes, each of which corresponded to an aquifer node for the computation of river-aquifer interaction.

The cross-sectional data of most of the reaches (water area, hydraulic radius, channel width at different elevations) were available from the South-West Area Water Resource Management Project (SWAWRMP) of Bangladesh Government. Cross sections of the intermediate reaches, for which no data were available, were estimated by linear interpolation of upstream and downstream sectional properties (Traver and Miller, 1993). For efficient computation, the cross-sectional area and hydraulic radius of the river sections were approximated by parabolic relation of the form $p = a(H - c)^b$; where p stands for the cross-sectional area or hydraulic radius; H is the water elevation; c is the lowest bed elevation at that section, and a and b are constants (different for different reaches). The parabolic relation for all cross sections had a correlation coefficient (R^2 value) ranging between 0.84 and 0.99. The water surface area and the volume for individual river node were also computed from the cross sections of the connecting reaches and were approximated with the parabolic expression.

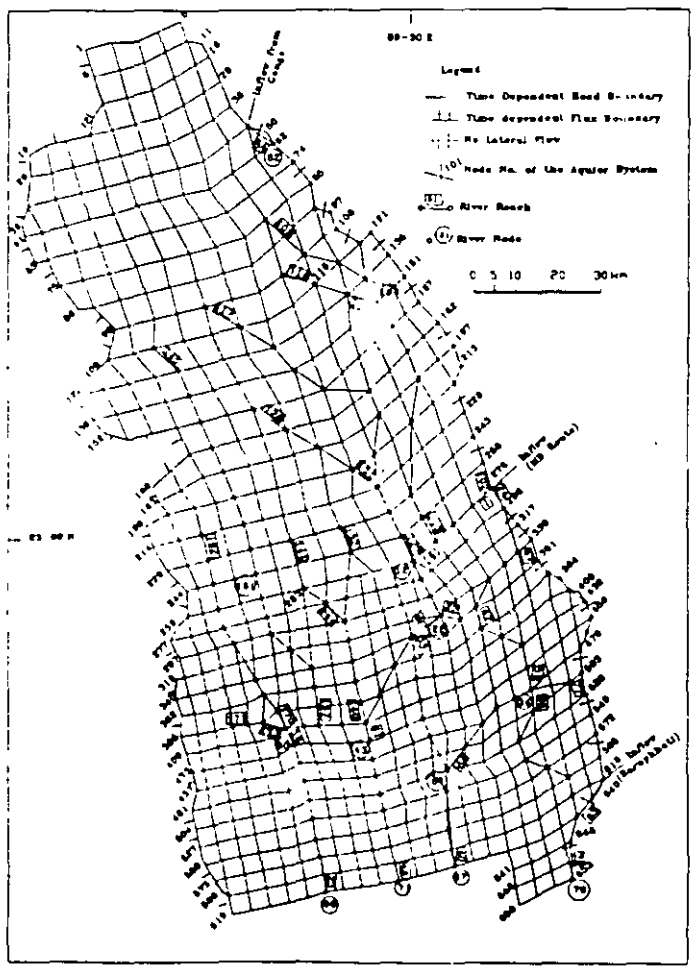

Fig. 5. Discretization of aquifer flow domain, river network, and boundary of the conceptual stream-aquifer system.

Boundary System and Conditions

The aquifer system and the river network were hydraulically connected to the Bay of Bengal in the south. The model boundary was extended in the south to establish a sea boundary (Figure 5). A time dependent head and solute concentration (TDS) were defined along the southern boundary for both the aquifer and the river system. Boundary values were specified as the monthly water level and TDS concentration at Pathargata and monthly TDS concentration at Hironpoint (stations indicated in Figure 2). The monthly inflows through the offtake of the Gorai, MB route, and Sarupkathi were used as time dependent flux boundary for the river system.

The aquifer was bounded by the river Ganges to the north. A time dependent head boundary condition, specified by the water levels of the river Ganges, was defined for the aquifer along the Ganges. Along the eastern boundary of the system the observed water levels of the Gorai-Modumati-Baleswar and the ground-water levels in the vicinity of the river indicated that the rivers and aquifer were hydraulically connected. No lateral flux across the aquifer boundary was assumed along the Gorai-Modumati-Baleswar rivers. The western boundary of the model was along the international boundary of Bangladesh and India. The information of the aquifer system beyond the western boundary was not available. The observed ground-water levels along the western boundary varied from 1.0 to 14.0 m with an average annual fluctuation of $\pm$ 0.75 to 2.0 m. A significant flow varying spatially and temporally was expected across this boundary (as reflected by the simulation results, with a total average inflow of -11.2 m^3/s and an average annual fluctuation of $\pm$ 18.9 m^3/s). As such, a time dependent flux condition would be appropriate for the western boundary. However, the boundary fluxes were not known. The system was, therefore, calibrated with the estimated water levels (obtained by kriging on observations) as time dependent head boundary values along the western edge. The average monthly boundary flows (1985-1990), for each western boundary node, obtained from simulation with known boundary levels were considered as known time dependent flux conditions along the western boundary for prediction of system behavior in response to future development scenarios.

Inputs and Stresses

The monthly runoff and natural recharge of individual drainage subbasins (Figure 2) for the period 1985-1990 were available from the water balance study of SWAWRMP (1992) and were assumed uniformly distributed over the subbasins. The monthly withdrawals of surface water for individual subbasin area were estimated based on irrigation-water requirements. The monthly ground-water abstraction (total of agricultural, industrial, and domestic) of individual subbasins for the period 1985-1990 were available (SWAWRMP, 1992). Depending on the thickness of the top silt layer, 10 to 20 percent of the irrigation water was considered as irrigation recharge to the aquifer. The TDS concentration in the surface runoff was considered zero, and a TDS concentration of 0.1 ppt was considered for the boundary inflows to the river system (as measured at Kamarkhali, node 92). The salinity of the soil of the southern part was relatively high which might be attributable to the capillary rise of the saline ground water (SWAWRMP, 1993). The recharge water leached the top soil and the solute concentration of the recharge water was considered ranging from 0.1 to 0.5 ppt varying uniformly from the north to the south of the area.

Results

Calibration

The model calibration consisted of adjustment of the model parameters until the model acceptably reproduced the observed sequences of ground-water levels and concentrations, and river levels, flows, and concentrations. The adjustable parameters of the stream-aquifer model were hydraulic conductivity, specific yield, and dispersion parameter of the aquifer system; roughness coefficient (Manning's n), longitudinal dispersion parameter, and tidal velocity of the river network; and leakage factor of the stream-aquifer interaction.

Continuous sequences of inputs, stresses (e.g. surface runoff, recharge, and surface- and ground-water abstractions), boundary values for a given period along with the observed sequences of water level, flow, and salinity were needed for the calibration of the model. A long sequence (1965-1990) of runoff, recharge, and boundary values were available (SWAWRMP, 1992). However, the water abstraction data and observation records were available for a short period (1985-1990). A simulation period from October 1985 to September 1990 (with 60 time steps of one month each) was therefore considered for calibration of models. The observed water levels and solute concentrations of September 1985 (kriged over the whole domain) were used as the intial conditions.

The ground-water levels showed a uniform seasonal fluctuation (range 2 to 5 m), reaching a minimum level in the dry months (March-April) and recovering with recharge, to a maximum level at the end of the wet season (Figure 6). The spatial distribution of simulated ground-water levels in the area during April 1988 matched satisfactorily with the observed distributions (Figure 7). The overall root mean square error (RMSE) of the ground-water level calibration was 0.64 m with a 90% confidence

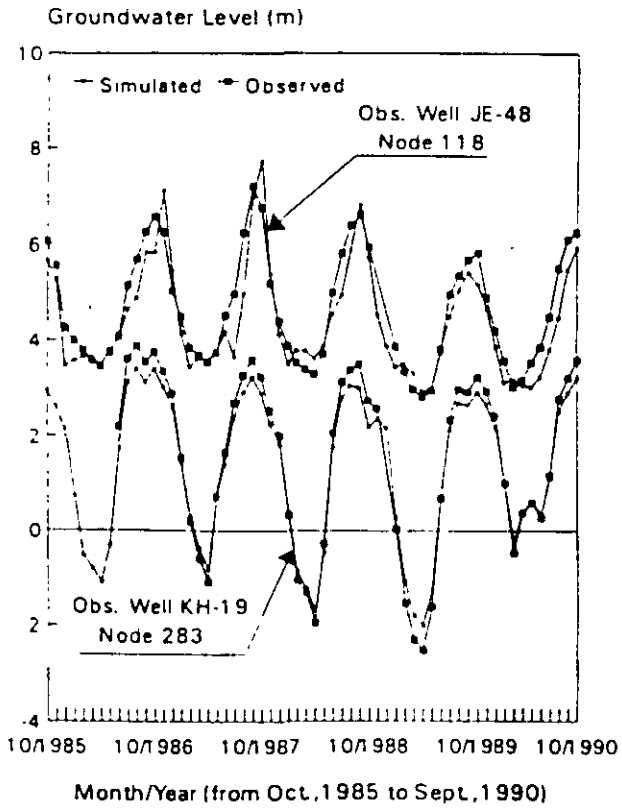

Fig. 6. Comparison of the simulated and the historical ground-water hydrographs for selected locations.

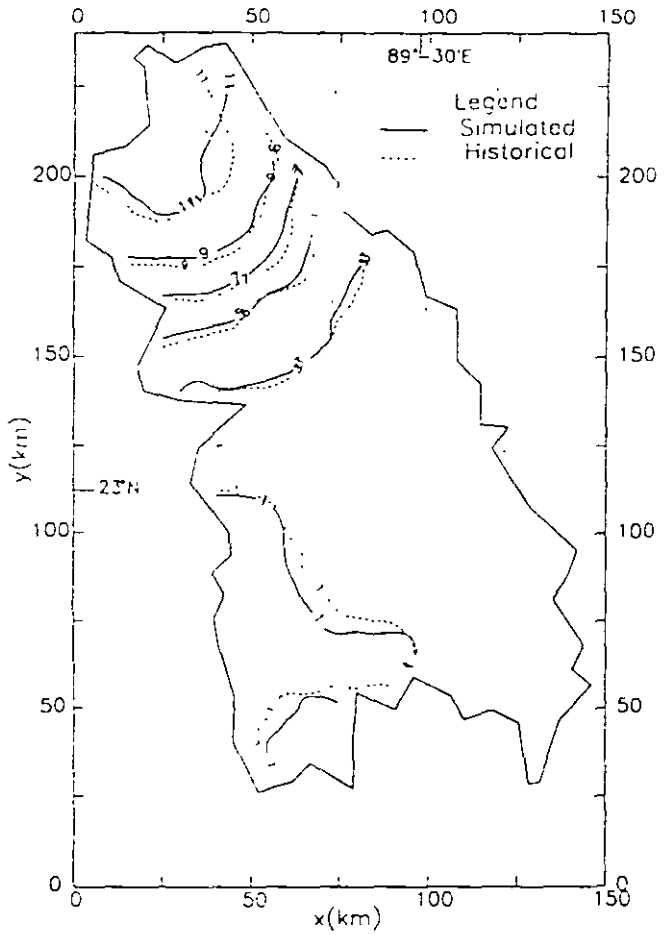

Fig. 7. Simulated ground-water levels compared with observed levels in April 1988 (levels in m above mean sea level).

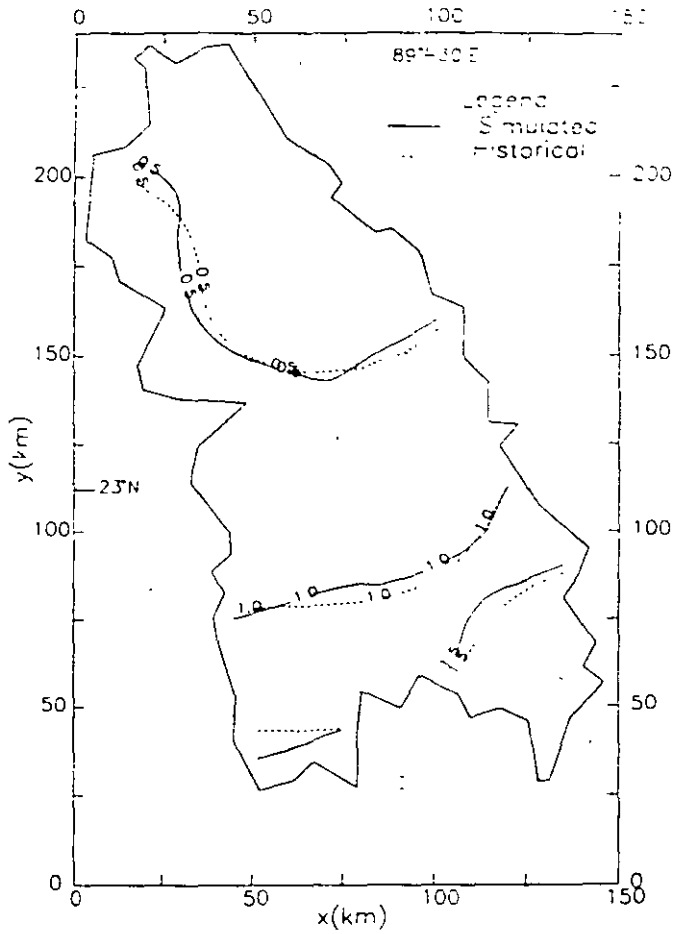

Fig. 8. Simulated and observed solute concentration (in ppt) in ground water during April, 1990.

interval of ± 1.05 m. The calibration error was relatively high with RMSE of 1.46 m and a 90% confidence interval of 2.46 m at node 46 (KT-38); however, the error was localized. In the absence of observed time series of TDS concentration, the simulated distributions of TDS concentration in aquifer were compared with observed values during April 1990 and a good agreement was found (Figure 8). No observation station was available within 20 km of the coast to properly calibrate the model for salt-water intrusion.

There was a very good agreement between the observed and the simulated river levels and flow hydrographs (Figures 9 and 10). The RMSE and 90% confidence interval of the overall river level calibration were 0.35 m and ± 0.58 m, respectively. The overall RMSE of river flow calibration was 137.63 m^3/s, however, higher errors were associated with high flows, and relative error was quite less. The model simulated the distribution of flow in the river network adequately. Discrepancies between the observed and the simulated results of the monthly average TDS concentrations in river water were not significant (Figure 11). The overall RMSE of TDS calibration was 0.95 ppt. The calibration errors were slightly high for some locations. However, the estimation of monthly average values from the observed monthly maximum records (available) might involve uncertainties.

The calibrated hydraulic conductivity of the aquifer ranged from 70 m/d in the south of the area to 180 m/d in the north. The specific yield varied from 0.001 to 0.18. The calibrated channel roughness coefficient (Manning's n) was in the range 0.02 to 0.039. Since there was no field measurement for stream-aquifer

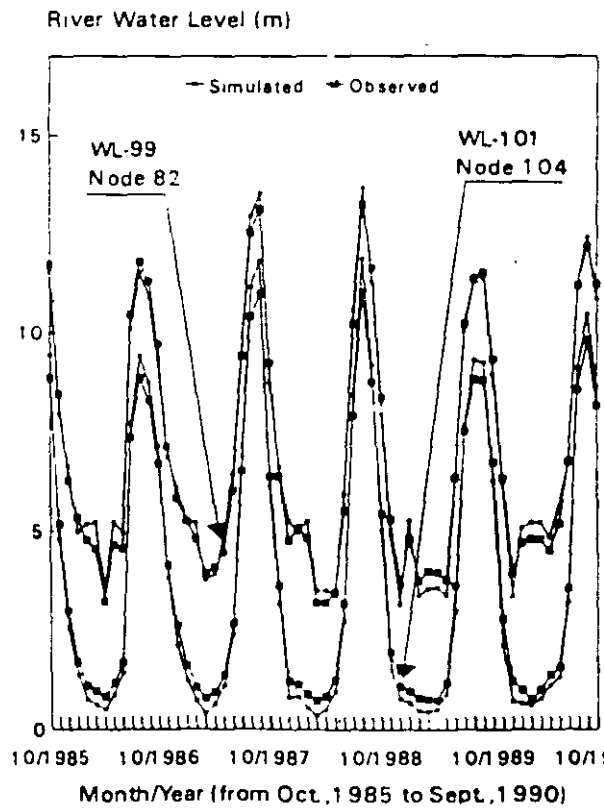

Fig. 9. Comparison of the simulated and the historical river level hydrographs at selected stations.

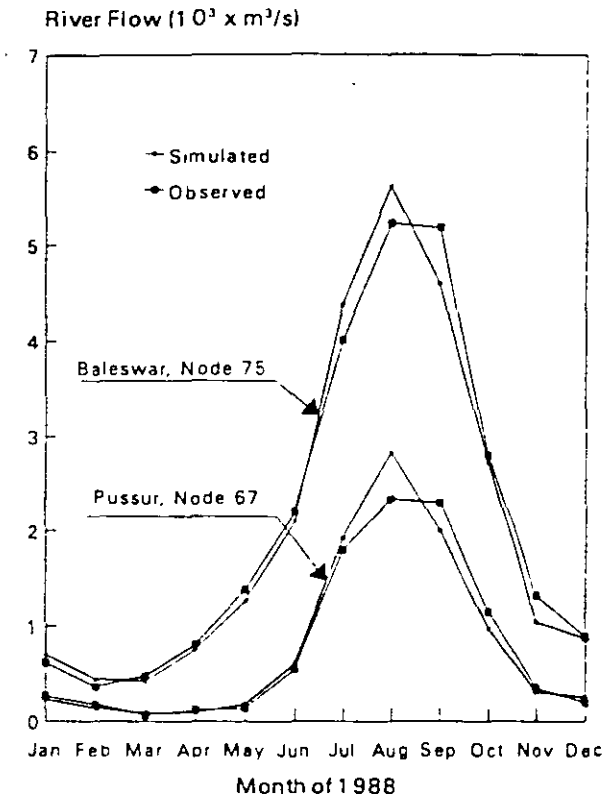

Fig. 10. Comparison of the simulated and the historical river flow hydrographs at selected stations.

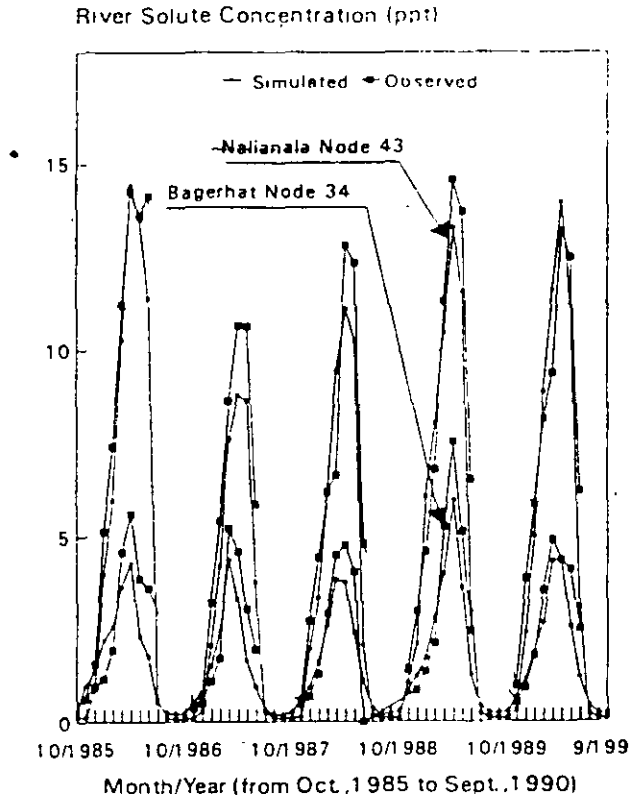

Fig. 11. Simulated monthly average solute concentrations (in ppt) in river water compared with observed values at different locations.

leakage factor, initially the leakage factor was estimated as 10% of the hydraulic conductivity of the underneath aquifer. The calibrated leakage factor ranged from 0.5 to 10 m/d; rather a high value because of accounting for leakage from the numerous small creeks and rivers which were ignored in the conceptual river network of the regional model. The tidal velocity of different reaches were estimated from the tidal volume (volume of water flow through a river section over a half tidal cycle due to tide only) of different reaches (SWAWRMP, 1992). The tidal velocities were tuned with other parameters to adjust the model results (river TDS concentration) with the observed records. The tidal velocity of the river highly influenced the solute concentration of rivers. Field measurements of effective porosity, and dispersion parameters of aquifer and rivers were not available. For the aquifer system, an effective porosity of 0.2 with longitudinal and lateral dispersivity as 350 m and 100 m respectively, were adopted for a satisfactory model response. The longitudinal dispersivity of rivers was taken as 8 m.

Sensitivity Analysis

The effects of changes in model parameter values and boundary values on simulated results were evaluated through a sensitivity analysis. For selected observation stations, these results with respect to defined base conditions are provided in Table 1. A 0.5 m change in water level along the western boundary resulted in a change of 0.05 m in water level at a distance of 5 to 15 km from the boundary. The observation well JE-48 (node 118) (Figure 6) was close to the eastern boundary and the well KG-19 (node 283) was 6 nodes (35 km) away from the western boundary. Water levels at these wells were not significantly influenced by the western boundary condition and represented the system's performance.

The changes in K value, stream-aquifer leakage factor, and Manning's n affected the exchange flow between aquifer and streams. Also, changes in tidal velocity affected the river salinity. However, the extent of variability with respect to base conditions was not significant. The ground-water velocities in the regional model were comparatively low, and the model was found to be less sensitive to the dispersion parameter of the aquifer. For the ranges of parameter values considered, the model response was found to be stable.

Discussion

Stream-Aquifer Interaction

The stream-aquifer exchange flow and the flow across the boundaries of the aquifer of the system were simulated for the period 1985 to 1990 (Figures 12 and 13). The stream-aquifer interaction in the system was quite significant. In fact in the dry season there was no surface runoff, and the dry season flow of the internal rivers was mainly the seepage flow from the aquifer. The stream-aquifer exchange flow of the system fluctuated seasonally. In the wet season, when the river stage was high, water flow was from the river to the aquifer. In the dry season as the river level dropped below the ground-water levels, the flow condition was reversed (from aquifer to river). The rate of flow exchange was highest immediately after the wet season as the river level dropped quickly and after that the rate of exchange flow reduced gradually as the river and the ground-water levels became closer.

Evaluation of Management Aspects

The water resources management in the area mainly involved optimal allocation of surface water and ground water (to maximize the benefits) as well as controlling the salt-water

Table 1. Results of Sensitivity Analysis

Items	Base condition	Change western boundary ground-water (GW) level by +0.5 m	Change western boundary ground-water (GW) level by -0.5 m	Change storativity / specific yield by +20%	Change storativity / specific yield by -20%	Change hydraulic conductivity by +20%	Change hydraulic conductivity by -20%	Change stream-aquifer leakage factor by +20%	Change stream-aquifer leakage factor by -20%	Change Manning's n by +20%	Change Manning's n by -20%	Change max. velocity by +20%	Change max. velocity by -20%
		Changes with respect to base condition											
GW level[1] at node 118 (m)	5.93	0	0	-0.1	0.12	-0.02	0.02	-0.08	0.1	0.57	-0.6	0	0
GW level[1] at node 283 (m)	2.64	0.01	-0.01	-0.08	0.11	0	0	-0.04	0.05	0.22	-0.22	0	0
Average GW level[1] in the system (m)	4.63	0.09	-0.1	-0.13	0.16	-0.1	0.13	-0.02	0.02	0.15	-0.17	0	0
GW salinity[1] at node 118 (ppt)	0.304	0	0	0	0	0	0	0	0.001	0	0.001	0	0
GW salinity[1] at node 283 (ppt)	0.829	-0.001	0.001	-0.005	0.013	0	0	0.001	-0.001	-0.006	0.005	0.003	-0.003
Max. river level[2] at node 82 (m)	13.66	0	0	-0.01	0	0	0	-0.01	0	1.08	-1.18	0	0
Max river flow[2] at node 75 (m^3/s)	5621.7	0	-0.2	-8.2	9.7	-1.8	1.4	-5	6.2	68.2	-97.1	0	-0
Max. river salinity[2] at node 43 (ppt)	14	0	-0.01	-0.04	0.05	-0.01	0	0.02	-0.04	-0.01	-0.05	0.21	-0.31
Average total boundary inflow[3] (m^3/s)	-27	3.319	-3.251	-0.069	0.075	-0.264	0.555	0.475	-0.632	-0.562	0.55	0	0
Average total exchange flow[4] (m^3/s)	-11	-1.739	1.729	-0.313	0.136	-1.774	2.446	-0.949	1.32	2.922	-3.029	0	0

[1] At the end of simulation period (Sept. 1985 to Aug. 1990)
[2] Maximum over the simulation period (Sept. 1985 to Aug. 1990)
[3] Average over the simulation period (Sept. 1985 to Aug. 1990).
[4] Average over the simulation period (Sept. 1985 to Aug. 1990) and flow from river to aquifer.

intrusion in the estuaries and aquifer (SWAWRMP, 1993). The level of salinity in the estuaries was quite high and it was desirable to reduce the salinity intrusion. At the same time the irrigation abstractions in the area were much less than that required for full agricultural development (Nobi, 1994). It was therefore, preferable to abstract more water for irrigation, if the resource was available so there was a scope of diverting water from the Ganges through the river Gorai (Figure 2) to control the salinity intrusion in the estuaries (SWAWRMP, 1993; Nobi, 1994). To find the effect of additional flow in the river network and an increased abstraction of ground water from the aquifer, the calibrated model was further applied to simulate (for the period 1985-1990) two conditions (a) with an additional flow of 250 m^3/s (during dry months Jan.-May) through the Gorai, and (b) with a 30% increased ground-water abstraction. With the increased ground-water abstraction, as the ground-water level declined, the stream-aquifer exchange flow (from aquifer to river) reduced significantly (Figure 13). Consequently, the salinity in the river estuaries increased (Figure 14). The existing

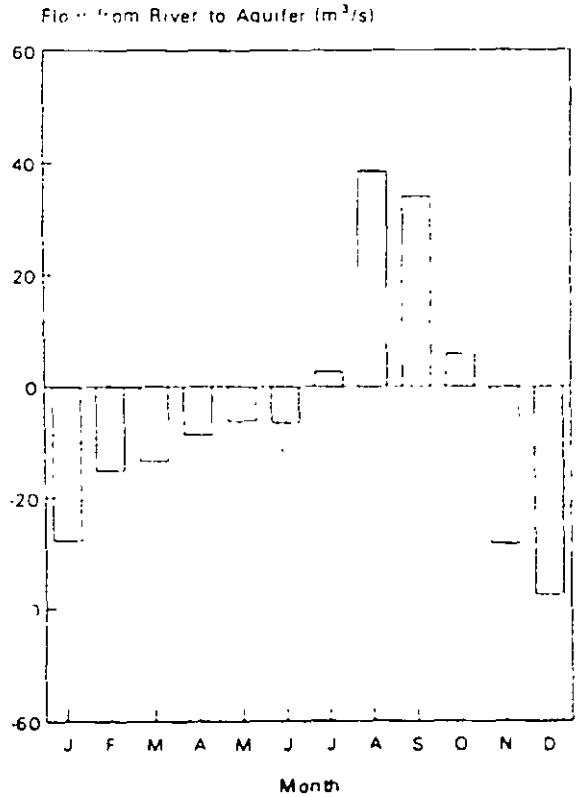

Fig. 12. Mean monthly exchange of flow between river and aquifer at node 81-99.

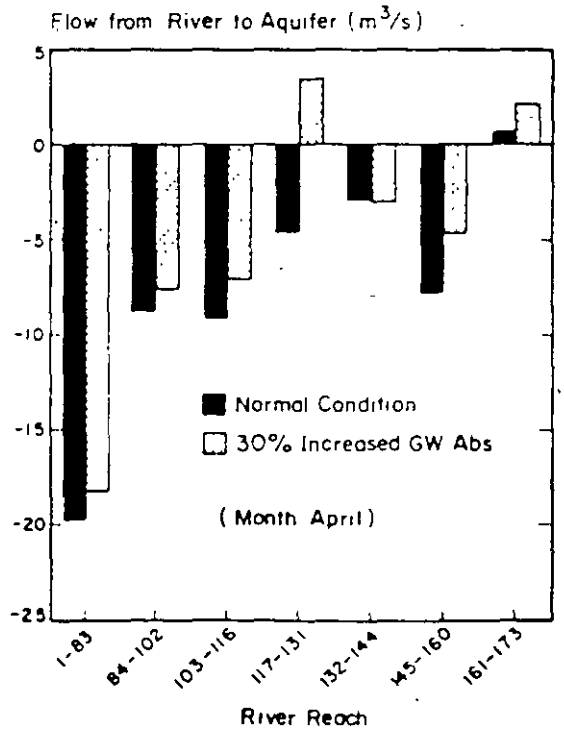

Fig. 13. Changes in flow exchange for different conditions.

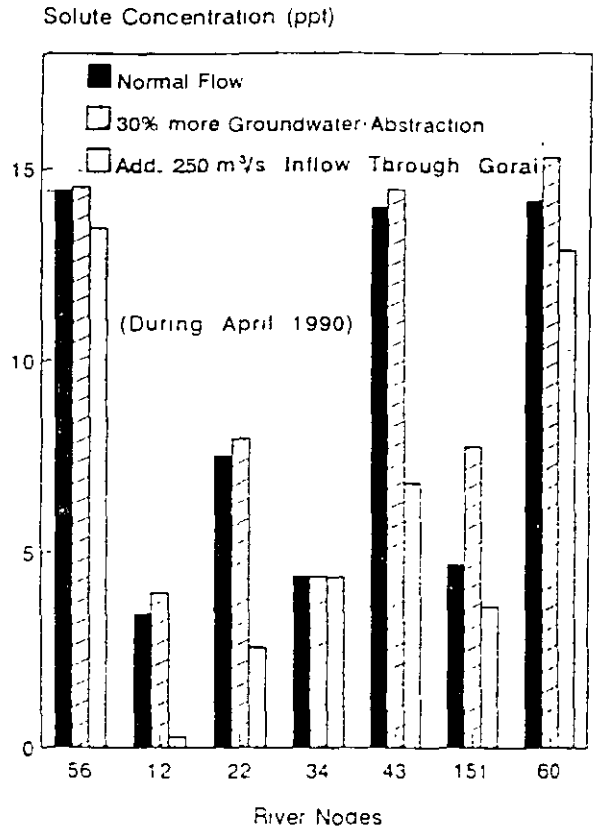

Fig. 14. Changes in river salinity for different conditions.

abstraction of ground water in the southern part (near the coast) of the region was very low, and a 30% increase in the abstraction of ground water, therefore, did not change the regional distribution of TDS concentration in ground water significantly. However, an increased abstraction near the coast induced salinity intrusion.

An additional flow of 250 m^3/s through the Gorai significantly reduced the salinity in estuaries (Figure 14), as additional flow flushed salinity towards the sea. In the dry season, 90% of the flow of Gorai passed through the rivers Pussur and Sibsa, and the additional flow therefore significantly reduced the salinity in the Pussur and Sibsa estuaries (in the middle of the southern boundary, Figure 2). The effect of additional flow was comparatively much less on the Kobadhak estuary (node 60 in the southwest corner, Figure 14) and Goshikhali (node 34, in the southeast corner). It was not feasible to control the salinity intrusion in the Kobadhak estuary by an additional flow through Gorai. However, the effect of increased abstraction was relatively higher on the Kobadhak estuaries. Thus, the salinity in the estuaries could be controlled up to a certain extent in certain sections by diverting additional flow from the Ganges through the river Gorai. The effects of additional flow through Gorai, and the increased ground-water withdrawal on the regional distribution of salinity in the estuaries are shown in Figure 15.

Conclusions

Conjunctive use of surface and ground water in coastal stream-aquifer systems is one of the most significant strategies for optimal development of water resources maintaining the salinity intrusion level within the desirable limit. This requires an assessment of flow and saline-water intrusion in the river network as well as in the aquifer system under dynamic conditions. The models presented herein to simulate the regional flow and the extent of salinity intrusion are comprised of a two-dimensional depth-average finite-element model for a composite aquifer system and a quasi-steady node and reach model for the mean flow and solute transport in a coastal river network. The aquifer model and the river network model are coupled and solved interactively to account for the dynamic exchange of flow and solute transport between the streams and the aquifer system.

Simulation of the areal distribution of flow and salinity in the river network and in the underlying aquifer system of the Southwest Region of Bangladesh during the period 1985-1990, through proper calibration of model parameters, demonstrated the practical applicability of the modeling approach. The dynamic interaction between the rivers and the aquifer system significantly influenced the flow and the salinity intrusion in both systems. An increase in ground-water abstraction resulted in a reduction of stream-aquifer exchange flow (from aquifer to river) and a consequent increase in salinity level in rivers. However, with the diversion of additional flow through the Gorai, the salinity intrusion in the area could be controlled to a significant extent. The extent of ground-water use in the southern part of the region was very low, and a marginal increase in ground-water abstraction or river flow did not change appreciably the regional distribution of TDS concentration in ground water. The simulation models, thus developed, provide a useful tool for assessment of any water management scheme prior to implementation.

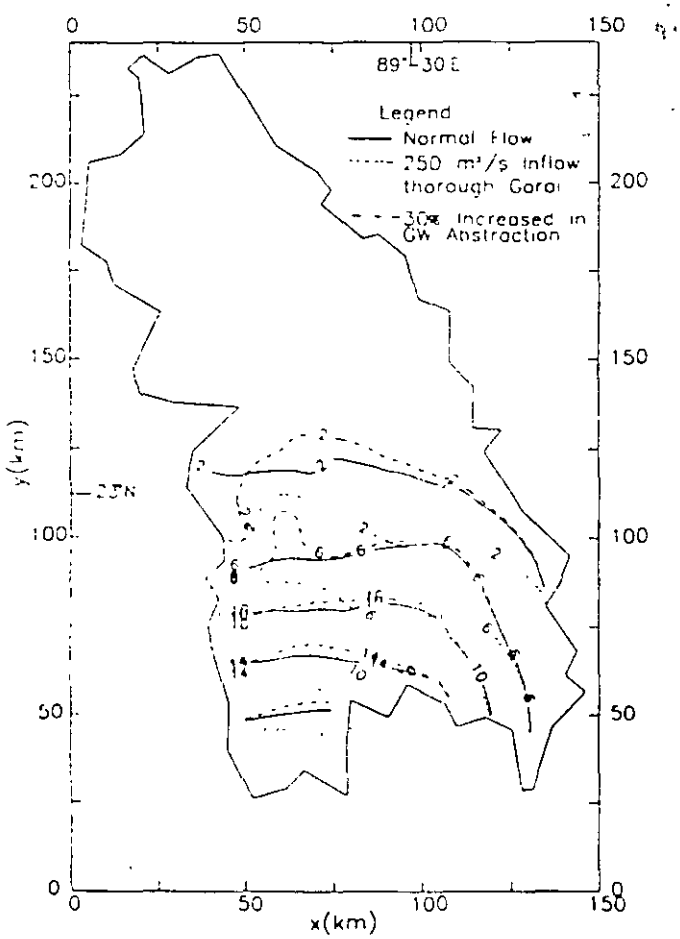

Fig. 15. Regional distribution of solute concentration (in ppt) in rivers for different flow conditions during April, 1990.

Acknowledgment

The study reported herein is a part of the research work conducted by the first author for the degree of Doctor of Engineering at the Asian Institute of Technology (AIT), Bangkok, Thailand. The authors gratefully acknowledge the financial support provided by AIT for carrying out this study.

The data required for this study were collected from various organizations of Bangladesh Government and other related consultant's offices. The authors sincerely acknowledge the help rendered by various officials of Ground Water Hydrology Circle (GWHC) and Surface Water Hydrology Circle (SWHC) of Bangladesh Water Development Board (BWDB), Master Plan Organization (MPO), South-West Area Water Resources Management Project (SWAWRMP), and Surface Water Modeling Center (SWMC) for giving access to their data base and for providing relevant data and information to carry out the study.

Appendix: Mathematical Model

Aquifer System

By combining the momentum equation with the mass balance of the fluid per unit horizontal area of the aquifer, the equation for the depth-average flow is described as

$$S_s \frac{\partial H}{\partial t} - \nabla(BK\nabla H) = Q_p \qquad (A.1)$$

where $H(x, y, t)$ is the total energy head above datum (L), B is the saturated thickness of flow (L); constant for confined condition and approximated as $(H - Z)$ for unconfined condition, $Z(x, y)$ being the elevation of the aquifer bottom above the datum (L), $K(x, y)$ is the hydraulic conductivity (L/T); $Q_p(x, y, t)$ is the fluid injected (−ve for withdrawal) per unit area of the aquifer (L^3/L^2T); $S_s(x, y)$ is the specific yield for unconfined condition and storativity for confined condition; and t is the time (T). The fluid velocity, $v(x, y, t)$ is defined as $-K\nabla H/\epsilon$ (L/T), in which $\epsilon(x, y)$ is the porosity.

The solute mass balance per unit area of the aquifer in conjunction with the fluid mass balance is given by (Voss and Souza, 1987; Nobi, 1994)

$$\epsilon B \frac{\partial C_\epsilon}{\partial t} + \epsilon Bv\nabla C_\epsilon - \nabla[\epsilon BD\nabla C_\epsilon] = Q_p(C_\epsilon^* - C_\epsilon) \qquad (A.2)$$

where $C_\epsilon(x, y, t)$ is the solute concentration (M_s/M), $C_\epsilon^*(x, y, t)$ is the concentration of the solute in source or sink (M_s/M), $D(x, y, t)$ is the dispersion coefficient tensor, defined for isotropic porous media in two dimensions as (Scheidegger, 1961)

$$D = \begin{vmatrix} D_{xx} & D_{xy} \\ D_{yx} & D_{yy} \end{vmatrix} \qquad (A.3)$$

with $$D_{xx} = \frac{1}{|v|}(\alpha_L v_x^2 + \alpha_T v_y^2) + D_m;$$

$$D_{yy} = \frac{1}{|v|}(\alpha_T v_x^2 + \alpha_L v_y^2) + D_m,$$

$$D_{xy} = D_{yx} = \frac{1}{|v|}(\alpha_L - \alpha_T)\, v_x v_y, \quad \text{and} \quad |v| = (v_x^2 + v_y^2)^{1/2}$$

where D_m is the molecular diffusion coefficient of the solute (L^2/T); $\alpha_L(x, y)$ is the longitudinal dispersivity (L), $\alpha_T(x, y)$ is the transverse dispersivity (L); $v_x(x, y, t)$ is the x component of the velocity v (L/T); and $v_y(x, y, t)$ is the y component of the velocity v (L/T).

The Galerkin weighted residual finite-element technique is used to generate approximating equations for the ground-water flow and solute transport equations. For detail formulation, reference can be made to Voss and Souza (1987) and Nobi (1994).

River Network

For the regional-water management in an integrated stream-aquifer system, the mean flow, mean water levels, and the average salinity (daily, weekly, or monthly) in the river networks are important rather than the instantaneous fluctuations of flow, water levels, and salinity. This implies that the physical behavior of the surface-water system in the hydraulically connected stream-aquifer system is represented by a simplified network model for mean flow and salt transport.

The hydrodynamic characteristics of a river network can be described by the following equations

$$\frac{\partial A}{\partial t} + \frac{\partial Q}{\partial x} - Q_l = 0 \text{ (continuity)} \qquad (A.4)$$

$$\frac{\partial Q}{\partial t} + \frac{\partial}{\partial x}\left(\alpha \frac{Q^2}{A}\right) + gA\frac{\partial h}{\partial x} = -\frac{gn^2 Q|Q|}{AR^{4/3}} \text{ (momentum)} \qquad (A.5)$$

where A is the water area (L^2); Q is the river discharge (L^3/T); Q_l is the lateral inflow (L^3/T); n is the Manning roughness coefficient; R is the hydraulic radius (L); and h is the hydraulic head in the river (L).

Considering a quasi-steady-state condition, the average salinity over a tidal period or a multiple of it, can be described by a time average one-dimensional dispersion equation (Ippen, 1966)

$$\frac{\partial C_s}{\partial t} + U_f \frac{\partial C_s}{\partial x} = \frac{\partial}{\partial x}\left(D_s \frac{\partial C_s}{\partial x}\right) \qquad (A.6)$$

where $U_f(x, t)$ is the fresh-water velocity (L/T); $C_s(x, t)$ is the average salinity (or solute concentration) in the river water (M_s/M), and D_s is the dispersion coefficient (L^2/T).

In the modeling process, the river network is conceptualized as a number of river reaches by nodes. All lateral inflows or outflows (runoff, withdrawal, flow exchange with aquifer, diversion from external sources) from the network are considered only at the nodes, and the flow in an individual reach is assumed to be quasi-steady and density independent. The fluid mass balance (A.4) for an individual node is expressed as

$$AN_i \frac{\Delta h_i}{\Delta t} = \sum_{r \in NR_i} Q_{ri} - Q_{si} - Q_{ai} + Q_{li} \qquad (A.7)$$

where h_i is the water surface elevation above datum at node i (L); AN_i is the nodal area of node i (L^2); Q_{ri} is the inflow to the node i from node r (L^3/T); NR_i is the set containing nodes that are connected to node i; Q_{si} is the water withdrawal from node i (L^3/T), Q_{ai} is the exchange flow between the river and the aquifer at node i (L^3/T); Q_{li} is the inflow (boundary flow, runoff, diversion from external sources, etc.) to node i (L^3/T).

With the assumption of a quasi-steady flow, the momentum equation for an individual reach is reduced to Manning's equation as

$$Q_n = w_n(h_r - h_i)/|h_r - h_i|^{1/2} \qquad (A.8)$$

where subscript ri stands for the average value of the associated parameters of the reach between node r and i; $w_n = A_n R_n^{2/3}/n_n L_n^{0.5}$ is the reach factor; and L_n is the length of the reach ri. By incorporating the boundary conditions and expressing the temporal derivatives by an implicit finite-difference approximation, the resulting nonlinear system of equations is solved iteratively, employing the Newton-Raphson method with the empirical relaxation scheme as in the aquifer model. Parameters of the river cross sections (such as area, hydraulic radius, top width, etc.) are approximated in terms of water depths with parabolic expressions for efficient computation (Nobi, 1994).

In the conceptual river network, salt concentration is assumed to be uniform throughout an individual node (i.e., well-mixed condition). The solute mass balance (A.6) for an individual node is described as

$$V_i \frac{\Delta C_{ii}}{\Delta t} = \sum_{r \in NR} Q_n \hat{C}_{ni} + A_n D_n \frac{C_{ni} - C_{ii}}{L_n} - Q_{ii} C_{ii} - Q_{si} \hat{C}_{si} + Q_{li} C_{li} \qquad (A.9)$$

where V_i is the volume of water in node i (L^3); A_n is the average water area of reach ri (L^2); D_n is the dispersion coefficient of reach ri (L^2/T), $\hat{C}_{ni}$ is the concentration of advective flux described as the concentration of the upstream node of the reach (i.e., the node from which water is flowing) (M_s/M), $\hat{C}_{si}$ is the concentration of stream-aquifer flow exchange described as the concentration in the system (river or aquifer) from which water is flowing to the other (M_s/M), and C_{li} is the concentration of the lateral inflowing water (M_s/M).

The dispersion process associated in a coastal river network is conceptualized as the combined effect of three different processes, viz., (1) molecular diffusion, (2) longitudinal dispersion due to fresh-water flow, and (3) tidal dispersion or mixing due to tidal fluctuations. Thus the overall dispersion coefficient for the time-average dispersion model is defined as

$$D_n = D_m + D_{Ln} + D_{Tn} \qquad (A.10)$$

where D_m is the molecular diffusion coefficient (L^2/T), D_{Ln} is the longitudinal dispersion coefficient for reach ri $= \alpha |U_{fn}|$ (L^2/T), in which U_{fn} is the fresh-water velocity in reach ri, and α is the longitudinal dispersivity; and D_{Tn} is the tidal dispersion coefficient for reach ri (L^2/T). Within the tidal zone, tidal mixing is the main dispersion process. The tidal mixing is accounted in the time-average dispersion equation (A.9) by incorporating the net advective transport of tidal fluctuations as $[A_n(C_n - C_{ii})(v_{Tn} - U_{fn})/2]_n$ in the dispersion coefficient, where v_{Tn} is the average tidal velocity over half tidal cycle in reach ri (L/T). The tidal advective transport results from the difference of transport during one-half of the tidal cycle from the downstream node of a reach to the upstream and the transport from the upstream node to the downstream during another half of the tidal cycle. Thus the tidal dispersion coefficient is described as $D_{Tn} = L_n(v_{Tn} - U_{fn})/2 \geq 0$.

By approximating the temporal derivative with an implicit finite-difference scheme and incorporating the specified concentration boundary condition in (A.9), the resulting linear system of equations are solved by the Gaussian elimination method, at every time step after the solution of the flow model.

References

Andersen, P. F., J. W. Mercer, and H. O. White, Jr. 1988. Numerical modeling of salt-water intrusion at Hallandale, Florida. Ground Water, v. 26, no. 5, pp. 619-630.

Besbes, M., J. P. Delhomme, and G. de Marsily. 1978. Estimating recharge from ephemeral streams in arid regions: A case study at Kairouan, Tunisia. Water Resources Research, v. 14, no. 4, pp. 281-290.

Choi, G. W. and A. Molians. 1993. Simultaneous solution algorithm for channel network modeling. Water Resources Research, v. 29, no. 2, pp. 321-328.

Essaid, H. I. 1990. A multilayered sharp interface model of coupled freshwater and saltwater flow in coastal systems: Model development and application. Water Resources Research, v. 26, no. 7, pp. 1431-1454.

Herbert, R. 1970. Modeling partially penetrating rivers on aquifer models. Ground Water, v. 8, no. 2, pp. 29-36.

Huyakorn, P. S., P. F. Andersen, J. W. Mercer, and H. O. White, Jr. 1987. Saltwater intrusion in aquifers: Development and testing of a three-dimensional finite element model. Water Resources Research, v. 23, no. 2, pp. 293-312.

Ippen, A. T. 1966. Estuary and Coastline Hydrodynamics. McGraw Hill Book Co., New York, pp. 578-585.

Ledoux, E., S. Souvagnac, and A. Rivera. 1990. A compatible single-phase/two-phase numerical model, 1. Modeling the transient salt-water/fresh-water interface motion. Ground Water, v. 28, no. 1, pp. 79-87.

Morel-Seytoux, H. J. 1975. A combined model of water table and river stage evolution. Water Resources Research, v. 11, no. 6, pp. 968-972.

Morel-Seytoux, H. J. and C. J. Daly. 1975. A discrete kernel generator for stream-aquifer studies. Water Resources Research, v. 11, no. 2, pp. 253-260.

Nobi, N. 1994. Groundwater quality management in an integrated surface-ground water system: Southwest region of Bangladesh. D. Engg. dissertation, Asian Institute of Technology, Bangkok.

Reilly, T. E. and A. S. Goodman. 1985. Quantitative analysis of saltwater-freshwater relationships in groundwater systems—A historical perspective. Journal of Hydrology, v. 80, pp. 125-160.

Scheidegger, A. E. 1961. General theory of dispersion in porous media. Journal of Geophysical Research, v. 66, no. 10, pp. 3273-3278.

Segol, G., G. F. Pinder, and W. G. Gray. 1975. A Galerkin-finite element technique for calculating the transient position of the saltwater front. Water Resources Research, v. 11, no. 2, pp. 343-347.

Shen, S. H. 1979. Modeling of Rivers. Willy-Interscience, New York.

South West Area Water Resources Management Project (SWAWRMP). 1992. Interim Report. Ministry of Irrigation, Water Development and Flood Control, Government of Bangladesh, v. I-III.

SWAWRMP. 1993. Final Report. Ministry of Irrigation, Water Development and Flood Control, Government of Bangladesh, v. I-XI.

Suppataratarn, P. 1990. Modeling of river networks. D. Engg. dissertation, Asian Institute of Technology, Bangkok.

Traver, R. G. and A. C. Miller. 1993. Open channel interpolation of cross-sectional properties. Water Resources Bulletin, v. 29, no. 5, pp. 767-776.

Volker, R. E. and K. R. Rushton. 1982. An assessment of the importance of some parameters for sea water intrusion in aquifers and a comparison of dispersive and sharp-interface modeling approaches. Journal of Hydrology, v. 56, pp. 239-250.

Voss, C. I. and W. R. Souza. 1987. Variable density flow and solute transport simulation of regional aquifers containing a narrow freshwater-saltwater transition zone. Water Resources Research, v. 23, no. 10, pp. 1851-1866.

FACULTAD DE INGENIERIA U.N.A.M.
DIVISION DE EDUCACION CONTINUA

CURSOS ABIERTOS

XII CURSO INTERNACIONAL DE CONTAMINACIÓN DE ACUÍFEROS

MODULO III: MODELOS MATEMÁTICOS EN GEOHIDROLOGIA Y CONTAMINACIÓN DE ACUIFEROS

TEMA

EFFICIENT AND RESPONSIBLE USE OF PRIOR INFORMATION IN INVERSE METHODS

EXPOSITOR: DR. ADOLFO CHAVEZ RODRIGUEZ
PALACIO DE MINERIA
OCTUBRE DEL 2000

Efficient and Responsible Use of Prior Information in Inverse Methods

by Richard Weiss[a] and Leslie Smith[a]

Abstract

Prior information on parameters such as hydraulic conductivity or ground water recharge rates is often used to stabilize the inverse problem in parameter estimation. A cautious use of prior information is advisable, however, because it may be biased or unrepresentative of the model parameters and/or it may not significantly stabilize the parameter estimates. Procedures are given: (1) to identify the model parameters for which prior information may best stabilize the parameter set; and (2) to identify the model parameters for which errors in the prior information lead to the smallest possible errors in the final set of parameter estimates. The first case is referred to as the efficient use of prior information; the second case is referred to as the responsible use of prior information. The procedures are based on an analysis of the model parameter space using response surfaces, multiparameter confidence regions, and eigenspace analysis. The guidelines lead to the selection of prior information on those parameters whose axes are most closely aligned with the longest axis of the parameter confidence region. Simple synthetic examples are used to explain the concepts. The advantages gained in screening the model parameters to identify those parameters for which prior information will be most efficient and responsible in determining the final values of the parameter estimates are demonstrated in the calibration of a ground water flow and solute transport model for the San Juan Basin, New Mexico.

Introduction

The inverse problem in ground water hydrology is the basis for formalized parameter estimation, but it is generally ill-posed (Yakowitz and Duckstein 1980). Three major issues result from the ill-posed nature of the inverse problem: uniqueness, identifiability, and stability (e.g., Carrera and Neuman 1986a, McLaughlin and Townley 1996). A solution to the inverse problem is unique if the set of estimated parameters is the only set which satisfies the conditions to be a solution (Tarantola and Valette 1982). A model parameter is non-identifiable if the model output is not sensitive to that parameter (Chavent 1979). For instance, in a one-dimensional model with prescribed head boundaries, the hydraulic conductivity is non-identifiable using only hydraulic head data. When all model parameters, including those describing the boundary conditions, are estimated using only hydraulic head data, the set of model parameters is non-identifiable (e.g., Cooley and Naff 1990). As a consequence, it is common practice to estimate only a subset of the model parameters, usually the internal model parameters such as hydraulic conductivity or recharge. Parameter instability occurs when small errors in the data lead to large errors in the estimated parameters. Because errors in the data are unavoidable, large errors in estimated parameters are common in unstable problems. Unstable parameter sets also lead to large uncertainties in the values of the estimated parameters.

Independent information on the estimated parameters (called prior information) has been recognized as valuable in stabilizing the inverse problem (e.g., Cooley 1982). A cautious use of prior information is advisable, however, for two reasons. First, prior information may not significantly stabilize the parameter estimates. There is little advantage to be gained in obtaining prior information about a parameter that will not be effective in stabilizing the model parameter set. We define the efficient use of prior information as the identification of those parameters for which prior information will stabilize the parameter set to the greatest possible extent. Second, the prior information may be unrepresentative or biased with respect to the model parameter values. Prior information influences not only the final estimates of those parameters with prior information, but also the estimates for the other model parameters. Small errors in prior information may lead to greatly magnified errors in the final estimates for other model parameters. The responsible use of prior information is defined in terms of the identification of how errors in the prior information will influence the final parameter estimates. The most responsible parameters for prior information are those parameters for which errors in the prior information have the least influence on the final parameter estimates. Note that no moral connotation is attached to the use of the term responsible, rather it simply reflects a prudent decision based on prior information.

Several factors may cause the prior information to be biased or in error with respect to the model parameter values. First, prior information is often obtained at a scale that is different from the scale that applies to a zone in the simulation model, which can create a

[a]Department of Earth and Ocean Sciences, Geological Engineering Program, University of British Columbia, Vancouver, B.C., Canada

Received January 1997, accepted September 1997

consistent bias in the prior information relative to the values that apply at the model scale (e.g., Beckie 1996). Second, prior information is sometimes extrapolated from measurements taken outside the modeled region, and may not represent parameter values within the model domain. Third, prior information may be obtained in regions that are not representative of the entire unit. In low-permeability units, hydraulic conductivity measurements are often obtained in higher permeability lenses within those units. If the prior information is obtained from tests near the outcrop of a hydrogeological unit, it may not represent the parameter values for the same unit at depth.

Procedures are given in this paper to identify those parameters for which prior information will most efficiently stabilize the parameter set, and to identify those parameters for which errors in the prior information lead to the smallest possible errors in the final parameter estimates. Simple two-parameter examples are used to demonstrate the concepts, which are then applied to a multiparameter problem. Finally, these concepts are used in the calibration of a ground water flow model of the San Juan Basin in New Mexico.

Concepts of Parameter Space Analysis

In this work the inverse problem is solved using a nonlinear regression approach and a modified Gauss-Newton method, following Cooley and Naff (1990) and Hill (1992). The nonlinear regression approach minimizes an objective function S(b) to estimate the parameters b, with the resulting parameter estimates defined as $\hat{b}$. For a parameter estimation problem using hydraulic head and prior information on model parameters, the objective function is

$$S(b) = (Y - f(b))^T V_h^{-1} (Y - f(b)) + (b_p - b)^T V_p^{-1} (b_p - b) \qquad (1)$$

where the model is represented by the relationship f(b) and Y is the set of hydraulic head measurements (i = 1,n). Matrix V_h defines the covariances among the hydraulic head data. Vector b_p represents the prior information on model parameters, and matrix V_p defines the covariances among the prior information.

The parameter space for a model is the p-dimensional space that contains all possible combinations of parameter values, where p is the number of model parameters. Each model parameter is represented by an axis in parameter space. Values of the objective function S(b) can be mapped into the parameter space, and these values define a p-dimensional surface called the response surface (or the objective function surface). The global minimum in this response surface defines the set of the parameter estimates $\hat{b}$. When only two model parameters are estimated, a map of the response surface can be constructed and visualized using a contour plot (e.g., Poeter and Hill 1997).

Parameter space analysis is a valuable tool in understanding and calibrating simulation models. This technique has been used to understand parameter estimation issues in rainfall-runoff models (Sorooshian and Dracup 1980, Sorooshian and Arfi 1982; Kuczera 1983, Sorooshian and Gupta 1983; Sorooshian and Gupta 1985; Gupta and Sorooshian 1985), to show that log-transformation of hydraulic conductivity generally results in better-conditioned parameter estimates for ground water models (Carrera and Neuman 1986a), and to evaluate the influence of two data types on parameter estimates in unsaturated flow experiments (Toorman et al. 1992). In this paper we demonstrate how an analysis of the parameter space can be used to guide the efficient and responsible use of prior information.

By the likelihood ratio method, contours of the response surface represent boundaries of the confidence region for the parameter estimates (Ratkowsky 1984). For large n, and under the assumptions that the uncertainties in the data are normally distributed, known and included in V_h and V_p, and that model error is negligible, an approximate $(1-\alpha)$ 100% confidence region for the parameter set is given by:

$$\frac{S(b) - S(\hat{b})}{s^2} \le pF_\alpha(p, n-p) \qquad (2)$$

where F(p,n-p) denotes an F distribution with p and (n-p) degrees of freedom (Dunn and Clark 1974), and $s^2 = \frac{S(\hat{b})}{n-p}$.

If the response surface is plotted using values of $(S(b)-S(\hat{b}))/s^2$, contours of the response surface represent confidence regions. Figure 1 illustrates a response surface and confidence regions for a two-parameter system. The parameter axes b_1 and b_2 are scaled by their estimated values, so that the parameter space represents the relative uncertainties in the parameter estimates, and not just differences in parameter values. Scaling parameter space is equivalent to comparing coefficients of variation rather than comparing parameter values. Because of the scaling, the point in parameter space

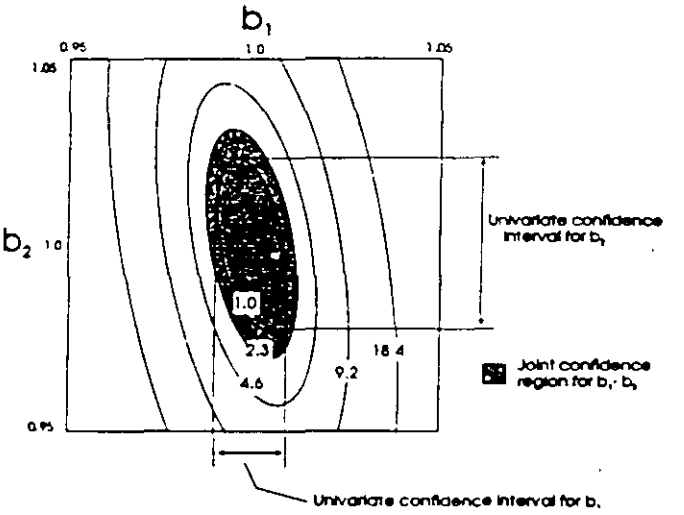

Figure 1. Response surface, univariate confidence interval and joint confidence region for parameters b_1 and b_2.

at b_1=1.0, b_2=1.0 represents the parameter estimates. For large n, a univariate confidence interval on either b_1 or b_2 at one standard deviation (68.6% confidence level) is calculated from the 1.0 contour. The joint confidence region for both parameters at a 68.6% confidence level is given by the 2.3 contour.

The confidence region defined by the response surface reflects the true nonlinearity of model parameters. It is often convenient to work with a linearized approximation to this nonlinear confidence region. The linearized confidence region can be defined as:

$$(b - \hat{b})^T \hat{X}^T V^{-1} \hat{X} (b - \hat{b}) \le ps^2 F_\alpha(p, n-p) \qquad (3)$$

where $\hat{X}$ is the sensitivity matrix evaluated at the parameter estimates. The elements of $\hat{X}$ are $\frac{\partial [f(b)]_i}{\partial \hat{b}_j}$, where $f(\hat{b})_i$ is the model estimate of the ith data value and $\hat{b}_j$ is the jth parameter estimate. The

atrix V^{-1} is the inverse of the total covariance matrix. The boundv of the linearized confidence region given by Equation 3 forms ellipsoid in parameter space centered on $\hat{b}$.

The ellipsoid in p-dimensional space is difficult to visualize. s more convenient to calculate its major axes. The length and oritation of these axes can be calculated from the approximate ssian matrix $(\hat{X}^T V^{-1} \hat{X})$ using singular value decomposition VD) to obtain the eigenvalues and eigenvectors. The square root the inverse of the eigenvalues are the lengths (L) of the axes of ellipsoid. The associated eigenvectors are unit vectors (U) fining the orientation of the axes of the ellipsoid with respect to parameter axes. The boundary of this ellipsoid is calculated to incide with the 1.0 contour of the response surface. The total coefient of variation for each parameter, CV_i, can be calculated m the axes of the confidence ellipsoid as.

$$CV_i = \sqrt{\Sigma_{j=1,p}(U_{ji}L_j)^2} \qquad i = 1,p \qquad (4)$$

Conceptually, the projections of each axis of the confidence ion j in the direction of the parameter i are squared and summed e total CV is the square root of this sum. The information needed calculate the major axes of the ellipsoid can be determined from a routinely available from the common nonlinear regression les used in inverse modeling.

The ratio of the length of the longest axis to the shortest axis the confidence region is termed the condition number (CN) for parameter estimates (Sorooshian and Gupta 1985). The CN is easure of the stability of the parameter estimates. As the paramension increases, CN will increase, so no absolute scale can ssigned to the magnitude of CN.

ficient and Responsible Use of Prior Information

Parameter space analysis can be used to develop guidelines for iciently and responsibly stabilizing the inverse problem using prior ormation. A simple two-dimensional, steady-state flow model is d to illustrate the concepts. The synthetic flow system is 6 km 6 km, and contains two transmissivity zones, one zone of anced recharge, and two constant head boundary zones (Figure The remaining model boundaries are no-flow boundaries. teen observation points are used. Observed values of hydraulic d are simulated by running a forward simulation using the true ameter values and calculating the data values at the sampling ations. Random Gaussian errors with a standard deviation of 1 m added to these values to generate the observed data values. Five ameters describe the flow system: two transmissivity zones (T_1 T_2), one recharge zone (R), and two specified head zones (H_1 H_2). For ease in presenting response surfaces, only two parateis will be estimated at one time. The other three parameters are ed at their true values.

Figure 3 shows the response surface for estimating parameters and R. The response surface is plotted as $(S(b)-S(\hat{b}))/s^2$, so the conrs represent the height of the response surface above the minim. Because the parameter space is scaled by the parameter ues, the parameter estimates are at the point $T_1 = 1.0$, $R = 1.0$ parameter space. The response surface contains a long, narrow ley. The axis of this valley is oriented such that it makes a ch smaller angle with respect to the R parameter axis than the parameter axis.

The confidence ellipse is a linearized picture of the response face and can be characterized by its major axes, calculated

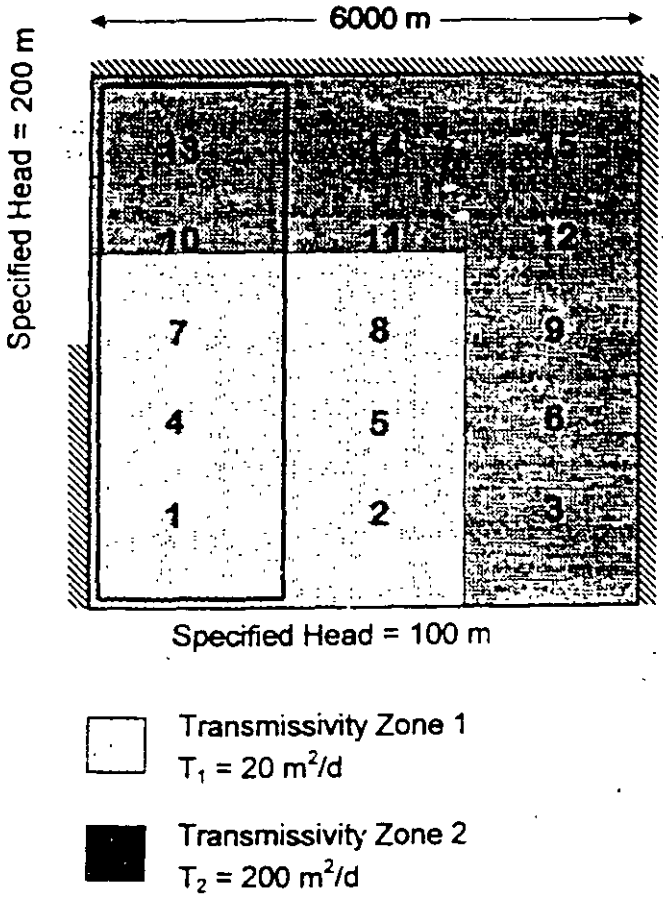

Figure 2. Synthetic flow system used for simple examples. The numbers identify measurement locations.

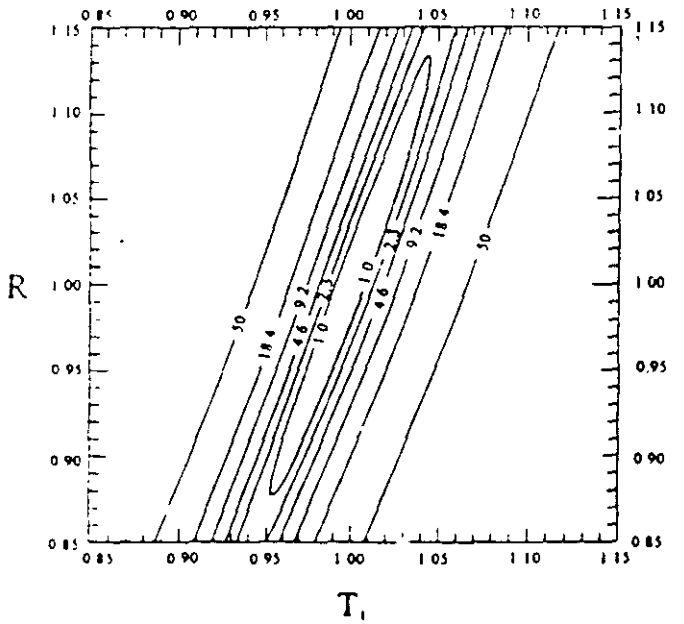

Figure 3. Response surface for T_1 – R parameter set using hydraulic head data.

Table 1
Axes of Confidence Ellipse for T_1–R Parameter Set

Unit Vectors	U_1	U_2
T_1 axis	−0.94	−0.32
R axis	0.32	0.94
Lengths of Axes	$L_1 = 0.0077$	$L_2 = 0.129$

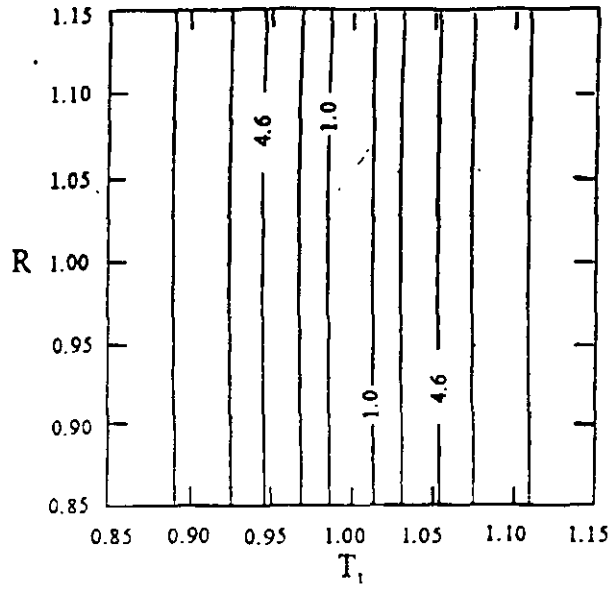

(a) Prior information on T_1 only

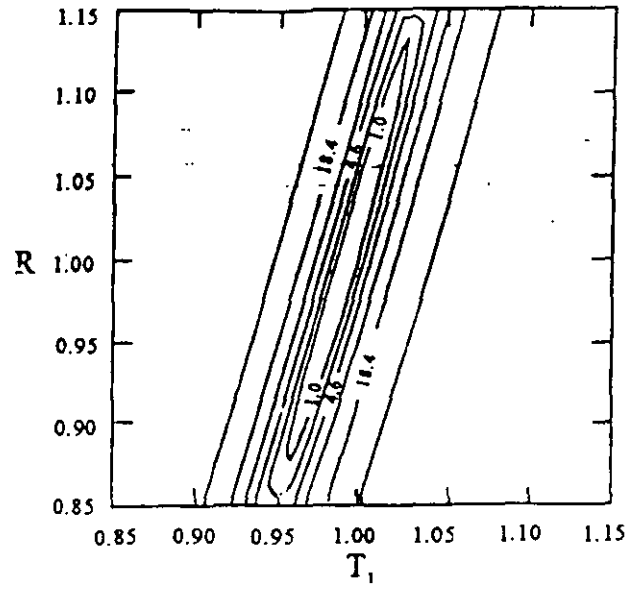

(b) Head and prior information on T_1

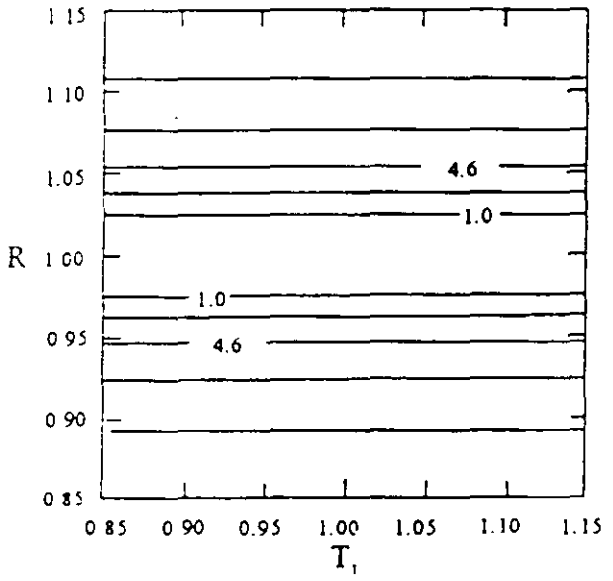

(c) Prior information on R only

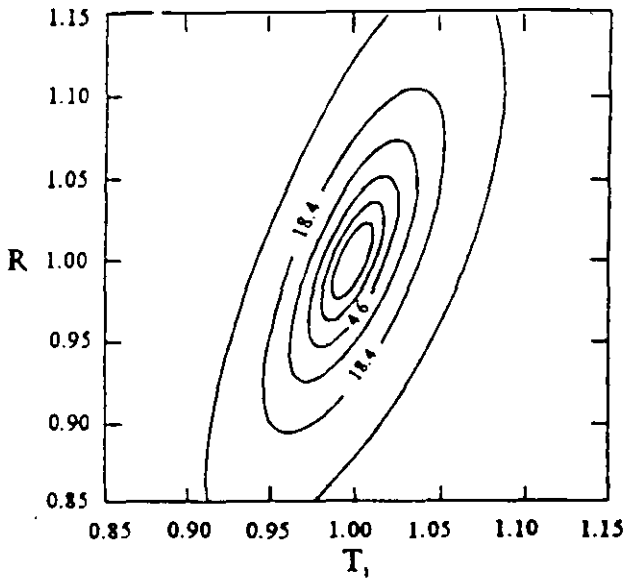

(d) Head and prior information on R

Figure 4. Response surface for T_1 – R parameter set for (a) prior information on T_1 only; (b) hydraulic head and prior information on T_1; (c) prior information on R only; (d) hydraulic head and prior information on R.

from SVD decomposition of the scaled Hessian matrix at the parameter estimates. Table 1 gives the axes of the confidence ellipse for this parameter set. L_1 and L_2 are the lengths of the two axes, and U_1 and U_2 are the unit vectors defining the orientation of the axes. The CN for this parameter set is 16.8, indicating that axis 2 is about 17 times longer than axis 1. Both the response surface and the axes of the confidence ellipse indicate that along the direction of axis 2 the response surface is relatively flat. Axis 2 is the major contributor to the uncertainty in both parameters. If the length of axis 2 can be reduced, then the uncertainty in both parameter estimates would be decreased, and the stability of the parameter set can be increased.

Efficient Use of Prior Information

In order to stabilize this parameter set, prior information is used to alter the topology of the response surface. Figure 4a illustrates the response surface for prior information on parameter T_1 only, where the scaled prior value equals 1.0 with an uncertainty of 2%. The total response surface for hydraulic head and prior information on T_1 is shown in Figure 4b. The size of the confidence region is similar to that using hydraulic head data only. Prior information on T_1 does not reduce the size of the confidence region or increase the stability of the parameter estimates significantly. Figure 4c illustrates the response surface for prior information on parameter R only, where the scaled prior value equals 1.0 with an uncertainty of 2%. The total response surface for hydraulic head and prior information on R is shown in Figure 4d. The size of the confidence region is significantly reduced, and the parameter set is more stable than using hydraulic head data only. Prior information on R is more efficient because it reduces the size of the confidence region the most for a given quality of prior information. Prior information on the para-

meter whose axis is most closely aligned with the valley in the response surface is the most efficient parameter to stabilize the solution.

This graphical approach can be formalized using the axes of the confidence region. Prior information on the parameter with the largest element of the longest axis of the confidence region reduces the uncertainty of the remaining parameter estimates most efficiently. The parameter with the largest element of the longest axis of the confidence region is the parameter whose axis is most closely aligned with the longest axis of the confidence region. From Table 1, axis 2 is the longest axis, and parameter R has the largest element of that axis (0.94).

Consequences of Errors in Prior Information

If errors exist in the prior information, these errors influence the estimates of the remaining parameters. The consequences of errors in prior information can be illustrated using the two parameter set T_1-R introduced above. When prior information is used only on parameter T_1, and the prior estimate of T_1 is 5% greater than its true value, the resulting parameter estimate for R is 13% greater than its true value. A small error in the prior estimate of T_1 results in a significantly larger error in the estimate of R. Conversely, when prior information is used only on parameter R, and the prior estimate of R is 5% greater than its true value, the resulting parameter estimate for T_1 is only 2% greater than its true value. Errors in the prior estimate of T_1 result in poorer parameter estimates than similar errors in the prior estimate of R.

To characterize this behavior, an error ratio is defined as the ratio of the scaled error in the estimated parameter value to the scaled error in the prior parameter value. Errors in the prior value of T_1 lead to error ratios of 2.5 for R, meaning that the errors in the estimates of R are nearly 2.5 times larger than the original error in the prior value of T_1. Errors in the prior value of R lead to error ratios of 0.4 for T_1, meaning that the errors in the estimates of T_1 are only 0.4 times as large as the original error in the prior value of T_1.

The effect of errors in the prior parameter values is shown graphically in Figure 5. The parameter estimates resulting from a 5% error in the prior parameter value are plotted in the scaled $T_1 - R$ parameter space, along with the response surface. The true parameter values plot at $T_1 = 1.0$, $R = 1.0$. A 5% error in the prior value of T_1 leads to parameter estimates that plot much further from the true parameter values than the parameter estimates resulting from a 5% error in R. Figure 5 illustrates that the parameter estimates resulting from errors in the prior information plot along the bottom of the valley in the response surface. This valley in the response surface is also the trace of the longest axis of the confidence region. The orientation of the valley in the response surface defines how errors in the prior information translate into errors in the estimated parameters. Prior information on parameters whose axes are closely aligned with the longest axis of the confidence region result in relatively small error ratios. Prior information on parameters whose axes are oriented nearly perpendicular to the longest axis of the confidence region result in relatively large error ratios. Incorporating prior information on parameters which lead to small error ratios is a responsible method of using prior information.

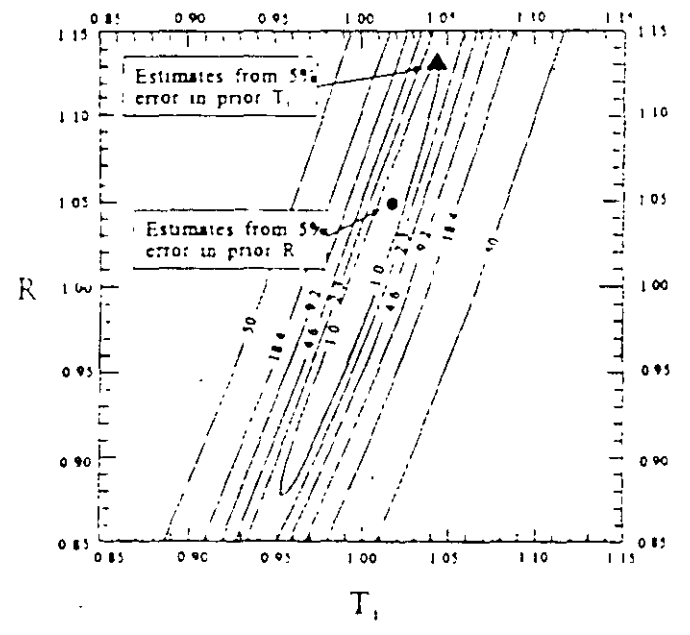

Figure 5. Location of parameter estimates for T_1 and R in parameter space, showing consequences of 5% errors in prior parameter estimates.

The error ratio is directly related to the shape and orientation of the parameter confidence region. For a nonlinear parameter confidence region, the error ratio changes with the magnitude of error in the prior parameter value. For relatively small errors, or nearly linear confidence regions, a linearized approximation can be used. The error ratio can be constructed graphically from the confidence region, or it can be calculated from the axes of the linearized parameter confidence ellipse (Weiss 1994). The error ratio is

$$ER_{i,j} = \frac{\sum_{k=1,p}\left[U_{i,k}U_{j,k}L_k^2\right]}{CV_j^2} \qquad (5)$$

where $ER_{i,j}$ is the linearized error ratio for an error in the ith estimated parameter, given an error in the jth parameter with prior information. CV_j is the total coefficient of variation for the parameter with prior information, defined in Equation 4.

Error Ratios for Prior Information with Uncertainty

The linearized error ratio defined in Equation 5 is based on prior information without uncertainty. In terms of the error ratio, the main difference between using prior information with uncertainty and prior information without uncertainty lies in how close the final parameter estimate is to the prior estimate. Two factors determine how close the final estimate will be to the prior estimate. (1) the assigned uncertainty in the prior information; and (2) the shape of the response surface before prior information is included. If the uncertainty assigned to the prior estimate is small, there is a large penalty in moving away from this prior estimate, and the final estimate will be close to the prior estimate. If the response surface using only hydraulic head data reflects a poorly-conditioned problem, the final estimate will be close to the prior estimate. A poorly-conditioned parameter set is characterized by a valley with a flat bottom. The prior information, even if it has a large uncertainty, will produce a definite minimum in the valley at the value of prior estimate. The final estimate will be very close to the prior estimate. If the response surface using only hydraulic head data is well conditioned, the minimum defined by the hydraulic head data will have a large influence on the final parameter estimates, regardless of the uncertainty in the prior information.

When prior information is assigned for more than one parameter, the relationship between the prior and final estimate is more

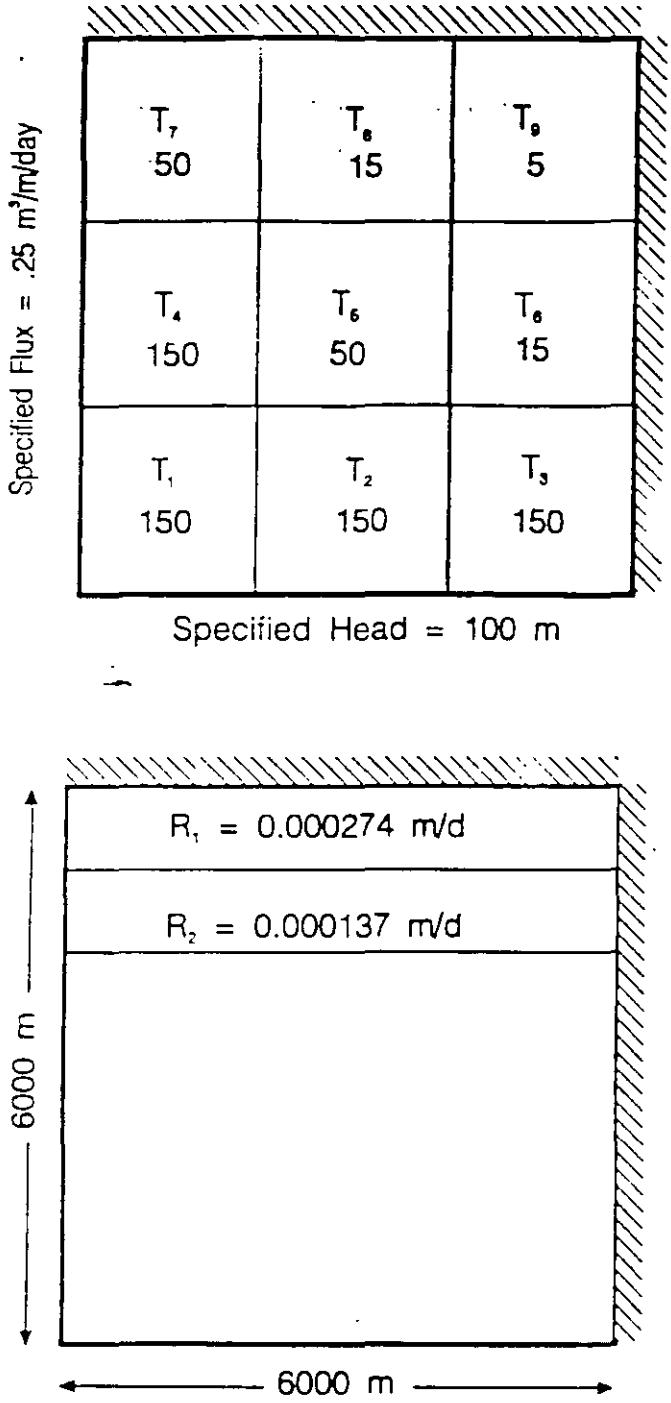

Figure 6. Multiparameter synthetic flow system adapted from Carrera and Neuman (1986b). The upper plot shows the transmissivity zones (m²/day), the lower plot the recharge zones.

complicated. In addition to the factors described above, the final estimates also depend on the relationship between the orientation of the data response surface and the location of the minimum and shape of the response surface using prior inform... These relationships are too complicated to form any specific conclusions. In general, we find that for an inverse problem that is ill-conditioned before adding prior information, one or more of the final parameter estimates will be strongly constrained by its prior estimate. If the final estimate is in error, it will introduce errors in the final parameter estimates of the other parameters. Thus, for an ill-conditioned or non-identifiable inverse problem, the final parameter estimates will be close to the prior estimates, regardless of the assigned uncertainty in the prior estimates. The error ratio method will be valid for determining the effects of errors in the prior information. For a well-conditioned problem, the final estimates may not be close to the prior estimates, and the error ratios may be less than those calculated from the linearized error ratios.

Throughout the above analysis, linear approximations to the confidence regions are used to calculate the linearized error ratios. In several examples not presented in this paper, indications of non-linearity are apparent. Lines in parameter space reflecting the trace of the longest axis of the confidence region are curved, and error ratios are not always constant, as they would be in a linear system. Because the analysis is based on the orientation of the parameter confidence region, the linear approximations are generally robust. The true error ratios may differ from the linearized error ratios, but the conclusions based on the linearized error ratios are still valid. The parameters that result in the smallest error ratios will generally be the same even if the non-linearity were taken into account.

Use of Prior Information for a Multiparameter Meter System

To demonstrate the application of these guidelines for the use of prior information in a more complex problem, a synthetic example taken from Carrera and Neuman (1986b) is considered (Figure 6). The data consist of 18 hydraulic head measurements with uncertainties of 1 m (see Carrera and Neuman 1986b for the locations of the measurement points). The parameters to be estimated include nine transmissivity zones, two recharge zones, one specified flux boundary and one specified head boundary. Without prior information, this inverse problem is non-identifiable if all the model parameters are estimated.

Identification of Efficient and Responsible Parameters for Prior Information

Before including prior information to stabilize this problem, the shape and orientation of the parameter confidence region should be understood. The axes of the parameter confidence region are given in Table 2, which are then used to calculate the linearized error ratio matrix (Table 3). The longest axis of the confidence region is axis 13, which is 75 times longer than any other axis. The valley in the multidimensional response surface is oriented in the direction of this axis, and is very long and flat, leading to high correlations between any parameters that contribute to this axis. Examining the unit vector that corresponds to axis 13, all parameters except H (the specified head boundary) have a contribution in the direction of axis 13. The axes of parameters F, R_1 and R_2 are most closely aligned with axis 13. The axis of parameter T_9 has the largest component in the direction of axis 13 of all the transmissivity parameters. Axis 13 contributes nearly all the uncertainty to every parameter except H. If axis 13 could be shortened, the uncertainty in all parameters except H would be reduced.

The linearized error ratio matrix (Table 3) shows that errors in parameters R_1, R_2, and F lead to small error ratios for the other parameters. Errors in the transmissivity zones lead to larger error ratios for the other parameters, with T_9 leading to the smallest error ratios among the transmissivity parameters. Errors in the hydraulic head boundary value lead to the largest error ratios.

Three groups of parameters are apparent from the parameter space information. The hydraulic head boundary value can be

Table 2
Axes of Parameter Confidence Region for Multiparameter Problem

Axis Lengths	0.002	0.008	0.010	0.022	0.025	0.027	0.038	0.056	0.083	0.20	0.22	0.3	22.3
Unit Vectors	U_1	U_2	U_3	U_4	U_5	U_6	U_7	U_8	U_9	U_{10}	U_{11}	U_{12}	U_{13}
T_1	−0.30	0 08	−0.24	0.18	−0.08	0.68	−0.44	0.22	−0.06	0.28	0.09	−0.01	0.10
T_2	−0.12	0.03	0.00	0.01	−0.02	0.15	−0.02	0.15	0.83	−0.49	−0.05	0.02	0.11
T_3	−0 06	−0.01	0.08	−0.10	0.06	−0.13	0.09	−0.18	0.50	0.79	−0.04	0.19	0.10
T_4	−0.20	−0.07	−0.54	−0.02	0.10	0.10	0.10	−0.77	0.00	−0.15	0 03	−0.04	0.10
T_5	−0.13	−0.14	−0.09	−0.32	−0.07	0.39	0.77	0.26	−0.12	0.03	−0.06	0.10	0.14
T_6	−0.11	−0 24	0.17	−0.70	0.45	0.05	−0 37	0.00	−0.09	−0.09	−0.08	0.06	0.22
T_7	−0 15	−0.06	−0 66	0.04	0.25	−0.48	−0.02	0 48	0.00	0.05	0.05	0 05	0.13
T_8	−0 11	−0.35	−0.08	−0.24	−0.81	−0.21	−0.21	−0 02	−0.04	−0.03	−0.02	0.19	0.22
T_9	−0 10	−0 66	0.24	0.54	0.23	0.02	0 04	−0.03	−0.06	−0.05	0.00	0.28	0.30
R_1	0.20	0.50	0 02	0.02	0.02	0.00	−0.02	−0.05	−0.13	−0.13	0.11	0.64	0.50
R_2	0 07	0.12	0.00	0.11	−0.04	−0.04	−0 02	0 00	−0.06	0.05	−0 76	−0.38	0.49
H	0 86	−0.29	−0.31	−0.06	0.01	0.24	−0 09	0.03	0.12	0.06	0 00	0.01	0.00
F	0.07	−0 01	0.13	−0.04	−0.04	−0.06	0.07	0.00	0.03	0.04	0.63	−0.53	0 53

Table 3
Error Ratio Matrix for Synthetic Multiparameter System

Estimated Parameters	Specified Parameters												
	T_1	T_2	T_3	T_4	T_5	T_6	T_7	T_8	T_9	R_1	R_2	H	F
T_1	1.00	0 95	0 88	1.04	0 72	0 47	0.78	0.47	0.33	0.21	0.22	40.2	0.22
T_2	1 05	1 00	0.92	1.09	0 76	0 49	0.82	0.50	0.33	0.22	0.23	39.8	0.23
T_3	1 14	1.08	1 00	1.18	0.82	0.53	0.89	0.54	0.32	0.24	0.25	39.8	0.25
T_4	0 96	0.92	0 85	1.00	0.70	0.45	0.75	0.46	0.32	0.20	0.21	40.0	0.21
T_5	1 39	1.32	1.22	1 44	1.00	0.65	1.08	0.66	0.41	0.30	0.30	49.2	0.30
T_6	2.13	2.03	1.87	2.21	1.54	1.00	1.66	1.01	0.59	0.46	0.46	70.1	0.46
T_7	1.28	1.22	1.13	1.33	0.93	0 60	1.00	0.61	0 41	0.27	0.28	49.2	0.28
T_8	2.11	2.01	1.86	2.19	1.52	0 99	1.65	1.00	0.59	0.45	0.46	70.2	0 46
T_9	3 03	3 04	3 11	3 12	2 43	1 69	2 44	1.68	1.00	0 62	0 64	101.	0 57
R_1	4 61	4.39	4 06	4 79	3 33	2 16	3 60	2.19	1.63	1.00	1 00	124.	1.00
R_2	4 61	4 39	4 06	4 79	3.33	2.16	3.60	2.19	1.62	1 00	1.00	124.	1.00
H	0 00	0 00	0 00	0 00	0 00	0 00	0 00	0 00	0.00	0.00	0.00	1.00	0.00
F	4 61	4 39	4.06	4.79	3.33	2.16	3.60	2.19	1.74	1.00	1.00	125.	1.00

Table 4
Parameter Estimation Results Using Prior Information on Selected Parameters
(Parameters with large components of L_{max} are more closely aligned with the longest axis of the confidence region. The condition number represents the stability of the confidence region, and the average CV represents the uncertainty of the parameter estimates.)

	Full Parameter Set	Prior T_1	Prior T_5	Prior T_9	Prior R_1	Prior F	Prior H
Component of L_{max}	N/A	0.10	0.14	0 30	0.50	0.53	0 00
Condition Number	9900.0	1181.9	973 6	413.2	274.0	295 0	8944.0
Average CV	5 51	0 63	0.51	0 24	0.17	0 19	5 49

identified quite well using hydraulic head data only. Prior information on parameter H will not reduce the ill-conditioning of the parameter set significantly. However, errors in the prior information for H would cause very large errors in the other parameter estimates. Prior information for parameter H would be a poor choice, because it is not necessary, provides no advantage in identifying the other parameter estimates, and leads to large error ratios. The flux boundary value and the recharge parameters all have large components of the unit vector associated with the long axis of the confidence region. These three parameters also have the smallest error ratios. Any of these three parameters are good choices for prior information because they efficiently reduce the ill-conditioning of the parameter set while reducing the influence of any errors in the prior information. The transmissivity parameters have smaller but still significant components of the unit vector associated with the longest axis of the confidence region. Prior information for any of these parameters will reduce the ill-conditioning of the parameter set significantly, but at the expense of potentially magnifying any errors in the prior values of the parameters. These results need to be checked against the actual modeled results

Comparison with Modeled Results

We first examine the issue of which parameters most efficiently stabilize the inverse problem. Table 4 gives the CN and average CV of the parameter estimates when using prior information on the given parameters, where prior information is included for one parameter at a time with an uncertainty in the prior information of ±25% of the prior value The component of the longest axis for each parameter is also listed. Prior information on R_1 and F results in the most stable parameter estimates with the lowest uncertainties of any parameters. Of the transmissivity parameters, prior information on T_6 results in the best parameter estimates Prior information on those parameters with the largest elements of the unit vector associated with the longest axis of the confidence region are most effective in stabilizing the parameter set and reducing the average CV

To determine the responsible parameters for use of prior information, error ratios can be calculated. Prior information is included for one parameter at a time, where the prior value is 25% greater than the true value. Table 5 gives the calculated error ratios. Because the data contain errors, the calculated error ratios are not exactly the same as the linearized error ratios from Table 3. However, the calculated error ratios do follow the trend of the linearized error ratios estimated from the parameter space. For instance, when T_1 is specified, the error ratios for T_1 through T_5 are near one, T_6 through T_8 are between one and two, T_9 is above two, and the recharge and flux parameters are much higher. The calculated error ratios for prior information on recharge and flux parameters are much lower than the error ratios for prior information on transmissivities. No error ratios for H are calculated, because the parameter set is so ill-conditioned when using only prior information on H that parameter estimates could not be reliably estimated.

Because the parameter set is ill-conditioned without prior information, the final estimates do not depend on the uncertainty assigned to the prior information. Even if the prior information is assigned an uncertainty of 100%, the final estimates are identical to those using prior information without uncertainty. Table 5 is unchanged for any reasonable uncertainty in the prior information.

If prior information is provided for more than one parameter, the situation becomes more complicated. The relationship between the location of the prior estimates in parameter space, the relative uncertainties of the prior estimates, and the location of the valley in parameter space determine the final parameter estimates For instance, when prior information on F, R_1 and R_2 is provided, and all three prior estimates are 25% greater than their true value, the final parameter estimate for R_1 and R_2 are approximately 15% greater than their true values, and the final estimate for F is approximately 35% greater than its true value. In another example, when the prior estimate of F is 25% less than its true value, and the prior estimates of R_1 and R_2 are 25% greater than their true values, then all three final estimates are within 5% of the true parameter values. The errors in the prior estimates are averaged, and the final estimates do not reflect the errors in the prior estimates.

Efficient/Responsible Prior Information vs. Uncertain Prior Information

In order to stabilize this problem, the parameters F, R_1 and R_2 were found to be the most efficient and responsible parameters to select for prior information. Practically, these three parameters may be the most difficult to measure in order to obtain the prior information. It is difficult to estimate the value of a flux boundary

Table 5
Calculated Error Ratios Due to 25% Error in the Prior Parameter Estimate

	Error Ratio Due to Error in Prior Parameter Estimate					
Parameters	Prior T_1	Prior T_5	Prior T_9	Prior T_6	Prior R_1	Prior F
T_1	1.00	0 89	0 56	0.34	0.19	–0 02
T_2	0 37	0 66	0.33	0.11	–0.04	–0.24
T_3	0.63	0 49	0.16	–0.07	–0.21	–0.42
T_4	0 92	–0.10	0 68	0.46	0.31	0.10
T_5	0 93	2 42	0 57	0.28	0.10	–0.17
T_6	1 46	1.59	0.97	0.57	0.27	–0.10
T_7	1 23	1 26	0 84	0.55	0 37	0.10
T_8	1 49	1 61	1.00	0.57	0.27	–0.07
T_9	2 52	2 71	1 67	0.97	0.53	–0.11
R_1	7 11	8 00	3 93	2.01	1 00	–0.16
R_2	6 54	7.50	3 56	1.72	0.76	–0.35
H	–0 05	–0 07	–0 07	–0.07	–0.07	–0.07
F	11 70	11 61	6 30	3.81	2.50	1.00

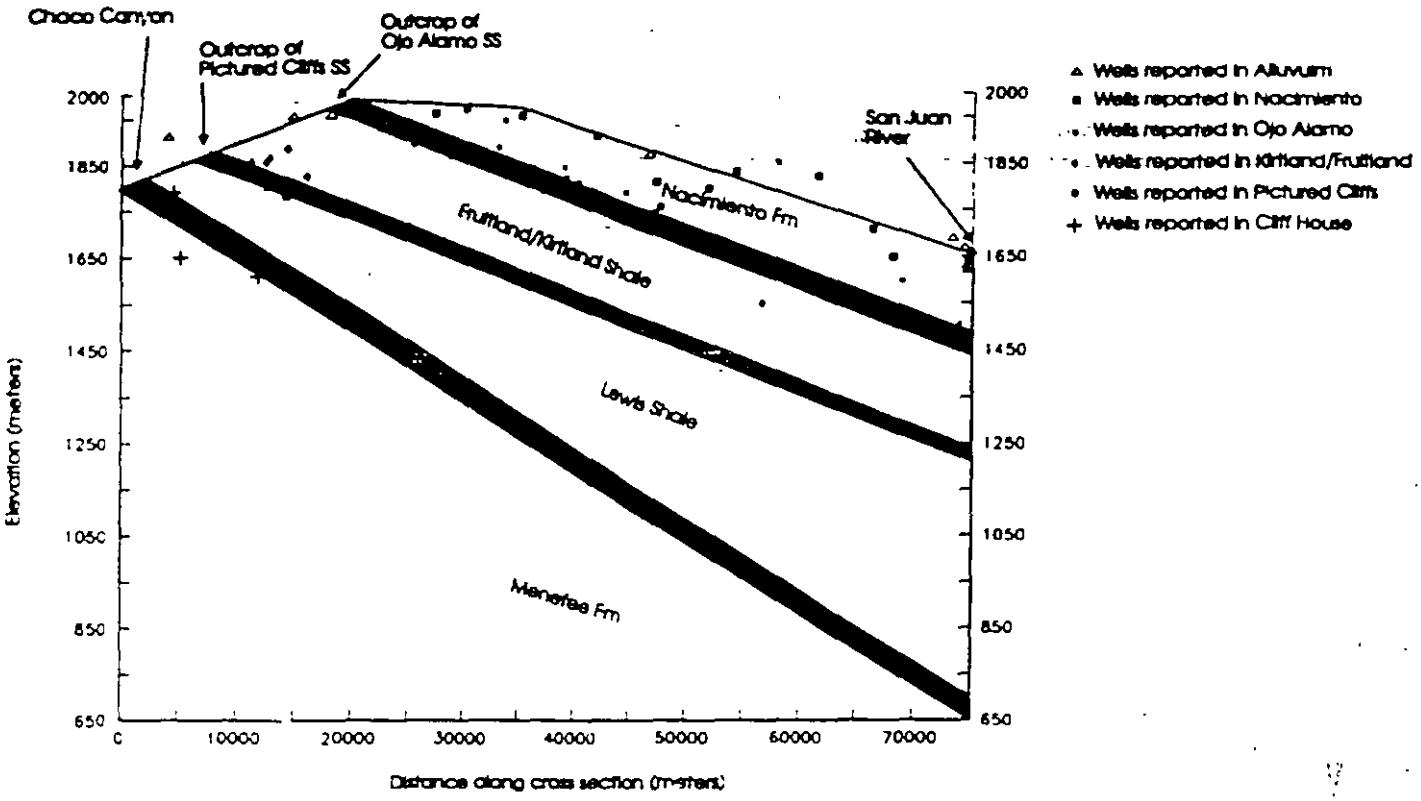

Figure 7. Generalized north-south cross section of the San Juan Basin, showing the location of the midpoint of screened interval for wells in the hydraulic head data set.

pendent of the model. Recharge is also a difficult parameter to timate without the use of the model unless a detailed field measurement program is implemented. However, errors in the prior estimates of these parameters translate into relatively small errors in the estimates of transmissivity parameters. Prior estimates on these three parameters, even if they are in error or have large uncertainties, may be better for parameter estimation than prior information on the transmissivity parameters. A systematic underestimation of prior estimates on transmissivity parameters may lead to large errors in the estimation of the recharge and flux parameters.

Should prior information on parameters be used if it is highly uncertain or has the potential for significant errors? Three factors need to be considered: the conditioning of the parameter set without prior information; the error ratio of the parameters with prior information; and the distribution of the prior information. If the parameter set is ill-conditioned without the prior information, then the prior information will constrain the model parameter estimates. However, if the error ratio is large for the parameters with prior information, then errors in the prior values may lead to large errors in the estimated values of the other parameters. Should the prior information have the potential to systematically over or underestimate the true parameter values, then the prior information may lead to errors in parameter estimates. If the prior information is randomly distributed about the true value of the parameter estimate, then the prior information might not lead to significant errors in the final parameter estimates. Unfortunately, the assumption that prior information is randomly distributed about the true parameter value is rarely fulfilled in practice. In this synthetic system, the full parameter set is well-conditioned without prior information. Parameters R_1, R_2 and F lead to small error ratios, but these are difficult parameters to measure independent of the model. The transmissivity parameters lead to larger error ratios, but are easier to measure in the field. However, it is common for prior information on transmissivity to be significantly biased, because of scaling differences between the measurement of transmissivity in the field and the model transmissivity. One solution to this dilemma is to provide prior information on parameter T_9. This parameter leads to the smallest error ratios of any of the transmissivity parameters. Errors in this parameter value will not be magnified as much as errors in any of the other transmissivity parameters.

Application to Calibrating a Model for the San Juan Basin

This section describes the application of parameter space methods for calibrating a regional ground water flow model for the San Juan Basin, New Mexico. The data available include hydraulic head data, ^{14}C data, and prior information on parameter values. A cross-sectional ground water flow and solute transport model in the west-central portion of the basin is constructed. A joint inversion scheme is used to include information from the ^{14}C measurements in the estimation of the parameters for the ground water flow model (Weiss and Smith 1997). Only selected results are presented in this paper; a complete description of the model and application are contained in Weiss (1994). Phillips et al. (1989) constructed a quasi-3D model of ground water flow in the upper permeable units within the San Juan Basin, using a manual calibration procedure to infer transmissivity values and vertical conductance using hydraulic head measurements and estimates of ground water residence time based on ^{14}C data.

Model Construction

The San Juan Basin is a large asymmetric structural depression (77000 km^2) in northwestern New Mexico and southwestern Colorado. Figure 7 is a schematic cross section of the upper

Cretaceous and Tertiary units along the section that we model. Six hydrogeological units are included in the model; the Cliff House Sandstone, the Lewis Shale, the Pictured Cliffs Sandstone, the Kirtland/Fruitland Shale, the Ojo Alamo Sandstone, and the Nacimiento Formation. The location and thickness of all units were obtained from well data. The model extends from Chaco Canyon in the south to the San Juan River in the north, approximately 75 km along the center of R10W.

The flow system is assumed to be at steady state. A finite element mesh is aligned with the regional slope of the hydrogeological units. The upper boundary of the model coincides with the elevation of the water table, and is represented as a specified hydraulic head boundary using four specified head nodes. The value of the hydraulic head at each of these nodes is esumated, and the hydraulic head along the rest of the boundary is interpolated linearly between these nodes. During model calibration, the upper boundary elevations change and the finite element grid can adjust to reflect these changes. The lower boundary is represented by a no-flow boundary at the Menefee Formation. The northern and southern boundaries are both no-flow boundaries, representing ground water divides.

Hydraulic head data, taken from Phillips et al. (1989), indicates recharge along the outcrops and discharge to the San Juan River. Fifty-six wells with hydraulic head data located in the area between R9W and R11W from Chaco Canyon to the San Juan River are used in the cross-sectional model. Figure 7 shows the midpoint of the screened interval for all wells in the hydraulic head data set. The head data are assigned uncertainties which depend in part on the length of screened interval and the distance from the well to the line of section.

The ^{14}C data are obtained from Phillips et al. (1989) and Stute (1995). Carbon-14 samples have been collected in 18 wells in the Ojo Alamo and Nacimiento Formations. The uncertainty assigned to the ^{14}C data is based on the magnitude of the ^{14}C concentration and the distance of the well from the line of cross-section. The ^{14}C concentrations are assumed to be at steady state. An initial concentration of 85 pmc (Vogel 1967) is used at the water table in the region where downward flow from the water table occurs. A horizontal dispersivity of 300 m (Phillips et al.1989) is assumed. These parameter values are uncertain, and the consequences of incorrectly specifying the parameters controlling the concentration distribution are examined below.

Direct information on hydraulic conductivities is taken from Stone et al. (1983) and the model of Phillips and Tansey (1984). This direct information can be used as either prior information on parameter values or initial parameter estimates for model calibration purposes. The efficient and responsible use of the prior information is investigated.

Model Calibration Strategy

The flow model described above contains 10 parameters that need to be estimated, four hydraulic head boundary parameters (the hydraulic head at each of the four nodes that define the upper surface of the model), and six hydraulic conductivity parameters, one for each layer in the model. The hydraulic conductivities are denoted Cliff House Sandstone (K_{ch}), Lewis Shale (K_l), Pictured Cliffs Sandstone (K_{pc}), Kirtland/Fruitland Shale (K_k), Ojo Alamo Sandstone (K_o), and the Nacimiento Formation (K_n). The anisotropy for each hydraulic conductivity zone is assigned a value of 100, and subsequently the effect of errors in the specified value of anisotropy on the parameter estimates is determined.

Table 6
Parameter Estimates and Uncertainties for 10 Parameter and 6 Parameter Inversions for San Juan Basin Cross Section Model

	10 Parameter Inversion		6 Parameter Inversion	
Parameter	Estimate	Standard Error	Estimate	Standard Error
K_{ch}	1.1	4.5	1.1	N/A
K_l	1.39e-03	4.7	1.39e-03	N/A
K_{pc}	7.00e-01	5.2	7.00e-01	N/A
K_k	1.57e-03	0.26	1.57e-03	N/A
K_o	5.67	0.18	5.36	0.073
K_n	1.78e-01	0.14	0.234	0.066
H_1	1804.0	29.0	1812.0	21.0
H_2	1972.0	15.0	1975.0	9.4
H_3	1956.0	7.9	1969.0	6.0
H_4	1678.0	11.0	1677.0	11.0

Two stages of model calibration results are presented. In the first stage, all 10 model parameters are estimated. The parameter space for the joint data set is examined to determine how to use prior information to efficiently and responsibly stabilize the parameter set. It is shown that prior information on the hydraulic conductivity of the lower layers of the model stabilizes the parameter space, and leads to small error ratios for the remaining parameters. In the second stage, prior information is used to specify the parameter values for the lower model layers, and the remaining parameters are estimated. The effects of possible errors in the anisotropy ratio, ^{14}C source strength, and dispersivity are analyzed using the parameter space during the second stage of parameter estimation.

Identification of Efficient and Responsible Parameters for Prior Information

Table 6 summarizes the parameter estimates and uncertainties for model inversions based on the joint hydraulic head and ^{14}C data sets, without incorporating prior information on hydraulic conductivity. The hydraulic conductivity parameters are presented in units of m/yr. Since the inversion was performed using log-transformed hydraulic conductuvities, the standard errors reported are for log-transformed hydraulic conductivities. A standard error of one implies an uncertainty in the parameter estimate of one order of magnitude. The hydraulic head boundary parameters and their standard errors are both in units of meters, and are not transformed. The parameters K_{ch}, K_l and K_{pc} all have standard errors near five orders of magnitude. The parameters K_k, K_o and K_n all have standard errors of between 0.1 and 0.3. The hydraulic head parameters have standard errors between 7 and 30 m.

Table 7 lists the axes of the confidence region for the final parameter estimates using the joint data set. The CN of the parameter space is approximately 43,000, meaning the longest axis is 43,000 times as long as the shortest axis. Axes 9 and 10 are the longest axes of the confidence region. Both have significant components from the parameter axes K_{ch} and K_{pc}, but small components from the other parameter axes. The third longest axis, axis 8, is nearly parallel to parameter axes K_l. The fourth and fifth longest axes, axes 7 and 6, have their largest components from parameter axes K_o and K_n. The

Table 7
Axes of Confidence Region for Parameter Estimates Based on Joint Data Set for San Juan Basin Cross Section Model

Axis Lengths	2.6e-03	4.3e-03	6.2e-03	1.2e-02	4.4e-02	1.6e-01	2.1e-01	2.9e-01	1.1e+02	1.3e+01
Parameters	U_1	U_2	U_3	U_4	U_5	U_6	U_7	U_8	U_9	U_{10}
K_{ch}	0.00	0.00	0.00	0.00	0.00	0.00	0.00	0.00	-0.97	0.25
K_l	0.00	-0.01	0.00	-0.04	0.14	-0.01	0.08	-0.99	0.01	0.06
K_{pc}	0.00	0.00	0.00	0.00	0.01	0.00	0.01	-0.06	-0.25	-0.97
K_k	-0.01	-0.10	0.01	-0.11	0.97	0.10	0.05	0.14	0.00	0.00
K_o	-0.01	0.00	0.00	0.00	-0.10	0.47	0.87	0.05	0.00	0.00
K_n	0.01	-0.01	-0.01	0.00	-0.05	0.88	-0.48	-0.05	0.00	0.00
H_1	0.01	0.02	-0.03	-0.99	-0.12	-0.01	-0.01	0.02	0.00	0.00
H_2	0.18	0.97	-0.13	0.01	0.10	0.01	0.01	0.00	0.00	0.00
H_3	0.95	-0.14	0.27	0.00	-0.01	-0.01	0.01	0.00	0.00	0.00
H_4	0.25	-0.18	-0.95	0.02	0.00	-0.01	0.01	0.00	0.00	0.00

Table 8
Error Ratio Matrix for Parameter Estimates Based on Joint Data Set for San Juan Basin Cross Section Model

Estimated Parameters	Parameters with Prior Information									
	K_{ch}	K_l	K_{pc}	K_k	K_o	K_n	H_1	H_2	H_3	H_4
	1.0	-58.0	3.3	-700.	6.4	10	2600	-280	-680	1400
	-0.01	1.0	-0.04	9.4	-0.04	0.00	-35.0	3.8	9.1	-19.
K_{pc}	0.26	-15.0	1.0	-180.	6.0	3.80	670	-72.	-174	367
K_k	0.00	0.03	0.00	1.0	0.00	0.00	-1.3	0.14	0.35	-0.73
K_o	0.00	0.00	0.00	-0.01	1.0	0.00	0.03	0.00	-0.01	0.01
K_n	0.00	0.00	0.00	0.00	0.00	1.0	0.00	0.00	0.00	0.00
H_1	0.00	0.00	0.00	-0.04	0.00	0.00	1.0	-0.02	-0.04	0.09
H_2	0.00	0.00	0.00	0.00	0.00	0.00	0.00	1.0	0.00	0.00
H_3	0.00	0.00	0.00	0.00	0.00	0.00	0.00	0.00	1.0	0.00
H_4	0.00	0.00	0.00	0.00	0.00	0.00	0.01	0.00	0.00	1.0

error ratio matrix (Table 8) shows the smallest error ratios result from prior information on K_{ch}, while the second smallest error ratios result from prior information on K_{pc}. Prior information on any of the parameters K_{ch}, K_{pc}, K_l, or K_k result in very small error ratios for the remaining parameters. Errors in any other parameters lead to very large error ratios for the parameters K_{ch}, K_{pc}, and K_l. Since these parameters have large uncertainties, the errors due to the error ratio must be within the parameter uncertainties. However, prior information on the parameters K_{ch}, K_{pc}, and K_l are the most responsible because they lead to the smallest error ratios.

Three groups of parameters can be defined based on the parameter space. The first group contains parameters K_{ch}, K_{pc}, K_l and K_k. Prior information on K_{ch} is the most efficient in reducing the overall parameter uncertainty, and leads to the smallest linearized error ratios. Prior information on any of the parameters in this group will reduce the uncertainty for all the parameters in the group. The second group contains the parameters K_o and K_n. Prior information on these parameters will not reduce the uncertainty of any of the parameters in the first group. Prior information on K_o or K_n will mainly reduce the uncertainty in these two parameters. The third group contains the hydraulic head parameters. Prior information on the hydraulic head parameters will not reduce the uncertainty in any of the hydraulic conductivity parameters significantly. The linearized error ratios show that the hydraulic head parameters are not the more responsible parameters for prior information.

Based on the above analysis, it is efficient and responsible to use prior information to define the parameter values for the lower four hydraulic conductivity parameters, K_{ch}, K_l, K_{pc} and K_k. In the second stage of model calibration, these four parameters are specified using the estimates developed from the 10-parameter inversion (which are very close to their prior values), and only six model parameters are estimated. The model parameters estimated are the two hydraulic conductivity parameters, Ko and Kn, and the four hydraulic head parameters. The resulting parameter estimates and uncertainties are given in Table 6. For the two hydraulic conductivity parameters, K_o and K_n, the parameter uncertainties have decreased significantly from the 10-parameter inversion, with a standard error of the log-transformed hydraulic conductivity of less than

Table 9
Error Ratio Matrix for Transport Parameters Using Parameter Space Based on Joint Data Set for San Juan Basin Cross Section Model

Estimated Parameters	Specified Transport Parameters						
	P_o	P_n	c_{init}	α_L	α_T	An_o	An_n
K_o	0.55	0.52	–3.6	–9.0	–0.30	–0.01	0.61
K_n	–0.79	–0.71	3.3	11.5	0.86	0.01	–1.4
H_1	0.00	0.00	–0.01	0.02	0.00	0.00	0.00
H_2	0.00	0.00	0.01	–0.01	0.00	0.00	0.00
H_3	0.00	0.00	0.00	0.00	0.00	0.00	0.01
H_4	0.00	0.00	–0.02	0.00	0.01	0.00	0.01

0.1. The uncertainties in the hydraulic head parameters have decreased only slightly. This slight decrease is expected, since the hydraulic head parameters are nearly uncorrelated with the hydraulic conductivity parameters. The CN for the parameter space is approximately 93, a reduction of nearly three orders of magnitude from the 10-parameter inversion.

Effect of Errors in Other Parameters

In calibrating the above model, many parameters were not estimated. These parameters include the effective porosity in each unit, the anisotropy for each unit, the initial concentration for ^{14}C at the water table, and the longitudinal and transverse dispersivities (α_L, α_T). These parameters were assigned a specified value. It is important to determine whether errors in the specified values of these parameters influence the estimated parameters significantly. The linearized error ratio matrix can be used to determine how potential errors in these specified values influence the estimated parameters.

The error ratio matrix is shown in Table 9. The parameters P_o and P_n are the effective porosity of the Ojo Alamo and Nacimiento respectively, and An_o and An_n describe the anisotropy of the Ojo Alamo and Nacimiento. The parameters with significant error ratios are the hydraulic conductivity parameters as a result of errors in c_{init}, α_L, and An_n. Errors in specifying the boundary ^{14}C concentration may be magnified over three times when estimating the hydraulic conductivity parameters. Errors in α_L lead to largest error ratios for K_o and K_n, while errors in α_T lead to small error ratios for K_n and K_o. The estimates of the hydraulic conductivity parameters are sensitive to errors in the estimate of α_L. This sensitivity can cause difficulty, since prior information on α_L is difficult to obtain. The parameter estimates are insensitive to errors in the anisotropy of K_o, but more sensitive to the anisotropy of K_n. These error ratios are consistent, because in the Ojo Alamo, the flow direction is dominantly along the dip of the unit, and therefore not very sensitive to the anisotropy of K_o. In the Nacimiento, there is a small component of vertical flow, and the anisotropy of the unit does affect the flow field. Based on these linearized error ratios, estimating both c_{init} and α_L along with the flow parameters for this model would be more responsible than simply using prior information on these transport parameters. Using prior information for the other transport parameters is responsible, since the linearized error ratios are small.

Based on the above error ratio analysis, parameter estimation for the flow system was performed for eight parameters: the six flow parameters and c_{init} and α_L. For c_{init}, the final parameter estimate is 79.5 pmc. For α_L, the final parameter estimate is 350 m. Both of these parameter estimates are close to their prior values, so the estimates for the flow parameters are similar to the parameter estimates using prior information on c_{init} and α_L. The linearized error ratios show the potential for large errors when using prior information on c_{init} and α_L, but these prior estimates are close to the estimates using the calibration data, so it is probable that no large errors occur.

Concluding Comments

Parameter estimation problems are often not identifiable or unstable using only hydraulic head data. Prior information on some of the parameters may be used to stabilize the parameter set for the purpose of parameter estimation. Guidelines have been developed and demonstrated for efficient and responsible use of prior information in parameter estimation. The most efficient parameters for prior information are those with the largest element of the unit vector (eigenvector) associated with the longest axis of the parameter confidence region. The most responsible parameters for prior information are those that lead to the smallest error ratios. The linearized error ratios can be calculated from the axes of the parameter confidence region. Those parameters that are the most efficient are often the most responsible. Both guidelines lead to selecting parameters whose axes are closely aligned with the longest axis of the parameter confidence region.

Parameter space analysis was applied to synthetic and field examples with good results. The parameters for which prior information most efficiently and responsibly stabilized the parameter set were correctly identified using the parameter space analysis. The linearized error ratios followed the pattern observed in the true error ratios. Parameter space analysis may lead to selecting parameters about which reliable prior information is difficult to obtain. The modeler must make a judgment regarding the reliability of the prior information against the potential effects of errors in the prior estimate. Parameter space analysis gives the modeler a tool to judge the potential effects of errors and uncertainties in the prior estimates. The error ratio analysis is also valuable for judging the potential effects of errors in specified model parameters.

Acknowledgments

This research was supported by grants from the Natural Sciences and Engineering Research Council of Canada. We thank Martin Shute for use of his unpublished ^{14}C data from the San Juan Basin, and Richard Cooley for his review comments.

Author's Note

Rich Weiss died in a kayaking accident on the White Salmon River in June 1997, several weeks before the reviews of this manuscript were received. While obtaining his doctoral degree at the University of British Columbia, he was also a member of the U.S. Olympic Whitewater Slalom team. A professor could not hope to have a finer graduate student than Rich. He is sadly missed.

References

Beckie, R. 1996. Measurement scale, network sampling scale, and ground water model parameters. *Water Resources Research* 32, no. 1: 65-76.

Carrera, J., and S.P. Neuman. 1986a. Estimation of aquifer parameters under transient and steady state conditions. 2. Uniqueness, stability, and solution algorithms. *Water Resources Research* 22, no. 2: 211-227.

Carrera, J., and S.P. Neuman. 1986b. Estimation of aquifer parameters under transient and steady state conditions. 3. Application to synthetic and field data. *Water Resources Research* 22, no. 2: 228-242.

Chavent, G. 1979. About the stability of the optimal control solution of inverse problems. In *Inverse and Improperly Posed Problems*, ed. G. Anger, 45-58. Berlin, Akademie-Verlag.

Cooley, R.L. 1982. Incorporation of prior information on parameters into non linear regression ground water flow models. 1. Theory. *Water Resources Research* 18, no. 4: 965-976.

Cooley, R.L., and R.L. Naff. 1990. Regression modeling of groundwater flow. U.S. Geological Survey Technical Water Resources Investigations, Book 3, Ch. 34. Washington, D.C.: USGS.

Dunn, O.J., and V. Clark. 1974. *Applied Statistics: Analysis of Variance and Regression*. New York: John Wiley and Sons.

Gupta, V.K., and S. Sorooshian. 1985. The relationship between data and the precision of parameter estimates of hydrologic models. *J. Hydrology* 81, no. 1-2: 57-77.

Hill, M.C. 1992. A computer program (MODFLOWP) for estimating parameters of a transient, three dimensional ground-water flow model using nonlinear regression. USGS Open-File Report 91-484. Denver, Colorado: USGS.

Kuczera, G. 1983. Improved parameter inference in catchment models. 2. Combining different types of hydrologic data and testing their compatability. *Water Resources Research* 19, no. 5: 1163-1172.

McLaughlin, D., and L. Townley. 1996. A reassessment of the ground water inverse problem. *Water Resources Research* 32, no. 2: 1131-1161.

Phillips, F.M., M.K. Tansey, L.A. Peeters, S. Cheng, and A. Long. 1989. An isotopic investigation of ground water in the central San Juan basin, New Mexico: Carbon-14 dating as a basis for numerical flow modeling. *Water Resources Research* 25, no. 10: 2259-2273.

Phillips, F.M., and M.K. Tansey. 1984. An integrated isotopic/physical approach to a numerical model of ground water flow in the San Juan Basin. Report 197. Las Cruces, New Mexico: New Mexico Water Resources Research Institute.

Poeter, E.P., and M.C. Hill. 1997. Inverse models: A necessary next step in ground-water modeling. *Ground Water* 35, no. 2: 250-260.

Ratkowsky, D.A. 1984. *Nonlinear Regression Modeling*. New York: Marcel Dekker.

Sorooshian, S., and F. Arfi. 1982. Response surface sensitivity analysis methods for post calibration studies. *Water Resources Research* 18, no. 5: 1531-1538.

Sorooshian, S., and J. Dracup. 1980. Stochastic parameter estimation procedures for hydrologic rainfall-runoff models: Correlated and heteroscedastic error cases. *Water Resources Research* 16, no. 20: 430-442.

Sorooshian, S., and V.K. Gupta. 1983. Automatic calibration of conceptual rainfall-runoff model parameters: The question of parameter observability and uniqueness. *Water Resources Research* 19, no. 1: 260-268.

Sorooshian, S., and V.K. Gupta. 1985. The analysis of structural identifiability. Theory and application to conceptual rainfall-runoff models. *Water Resources Research* 21, no. 4: 487-495.

Stone, W.J., F.P. Lyford, P.F. Frenzel, N.H. Mizell, and E.T. Padgett. 1983. Hydrogeology and water resources of the San Juan Basin, New Mexico. Mineral Resources Report 6. N.M. Bureau Mines Mineral Resources.

Stute, M.J., J.F. Clark, P. Schlosser, W.S. Broecker, and G. Bonani. 1995. A high altitude continental paleotemperature record derived from noble gases dissolved in groundwater from the San Juan Basin, New Mexico. *Quaternary Research* 43, 209-220.

Tarantola, A., and B. Valette. 1982. Generalized nonlinear inverse problems using the least squares criterion. *Rev. Geophys.* 20, no. 2: 219-232.

Toorman, A.F., P.J. Wierenga, and R.G. Hills. 1992. Parameter estimation of hydraulic properties from one step outflow data. *Water Resources Research* 28, no. 11: 3021-3028.

Weiss, R. 1994. Efficient and responsible use of prior information and joint parameter estimation for estimating parameters of groundwater flow models. Ph.D. diss., Dept. of Earth and Ocean Sciences, University of British Columbia, Canada.

Weiss, R., and L. Smith. 1997. Parameter space methods in joint parameter estimation for ground water flow models. *Water Resources Research*, in press.

Yakowitz, S., and L. Duckstein. 1980. Instability in aquifer identification. Theory and case studies. *Water Resources Research* 16, no. 6: 1045-1064.

Vogel, J.C. 1967. Investigation of ground water flow with radiocarbon. In *Isotopes in Hydrology*, 235-237. Vienna: International Atomic Energy Agency.

FACULTAD DE INGENIERIA U.N.A.M.
DIVISION DE EDUCACION CONTINUA

CURSOS ABIERTOS

XII CURSO INTERNACIONAL DE CONTAMINACIÓN DE ACUÍFEROS

MODULO III: MODELOS MATEMÁTICOS EN GEOHIDROLOGIA Y CONTAMINACIÓN DE ACUIFEROS

TEMA

SIMULACIÓN DE ACUIFEROS

EXPOSITOR: M. EN C. LUIS ERNESTO LESSER CARRILLO

PALACIO DE MINERIA
OCTUBRE DEL 2000

SIMULACION DE ACUIFEROS

- LA SIMULACION DE UN SISTEMA ACUIFERO CONSISTE EN LA CONSTRUCCION Y OPERACION DE UN MODELO CUYO COMPORTAMIENTO SE APROXIMA AL DEL ACUIFERO REAL .

- EL USO DEL MODELO TIENE TRES OBJETIVOS PRINCIPALES :

  (1) ENTENDIMIENTO

  (2) PREDICCION

  (3) CONTROL

MODELO DE SIMULACION

- EL TERMINO MODELO SE REFIERE A:

  (1) LA TEORIA QUE DESCRIBE AL PROCESO BAJO CONSIDERACION;
  (2) EL CODIGO DE COMPUTADORA QUE SE USA PARA SIMULAR EL PROCESO;
  (3) LA APLICACION DEL CODIGO A UN CASO PRACTICO ESPECIFICO.

- SE PUEDEN APLICAR CRITERIOS DE EJECUCION PARA LOS TRES CASOS.

M O D E L O S

- FISICOS
- ANALOGICOS ELECTRICOS
- MATEMATICOS
  - DETERMINISTICOS
  - ESTOCASTICOS
  - COMBINADOS

MODELOS MATEMATICOS

- CONSISTE EN
  - ECUACION (ES) DIFERENCIAL (ES) PARCIAL (ES)
  - CONDICIONES INICIALES
  - CONDICIONES DE CONTORNO
- SE BASA EN
  - CONSERVACION DE LA MASA
  - CONSERVACION DEL IMPULSO

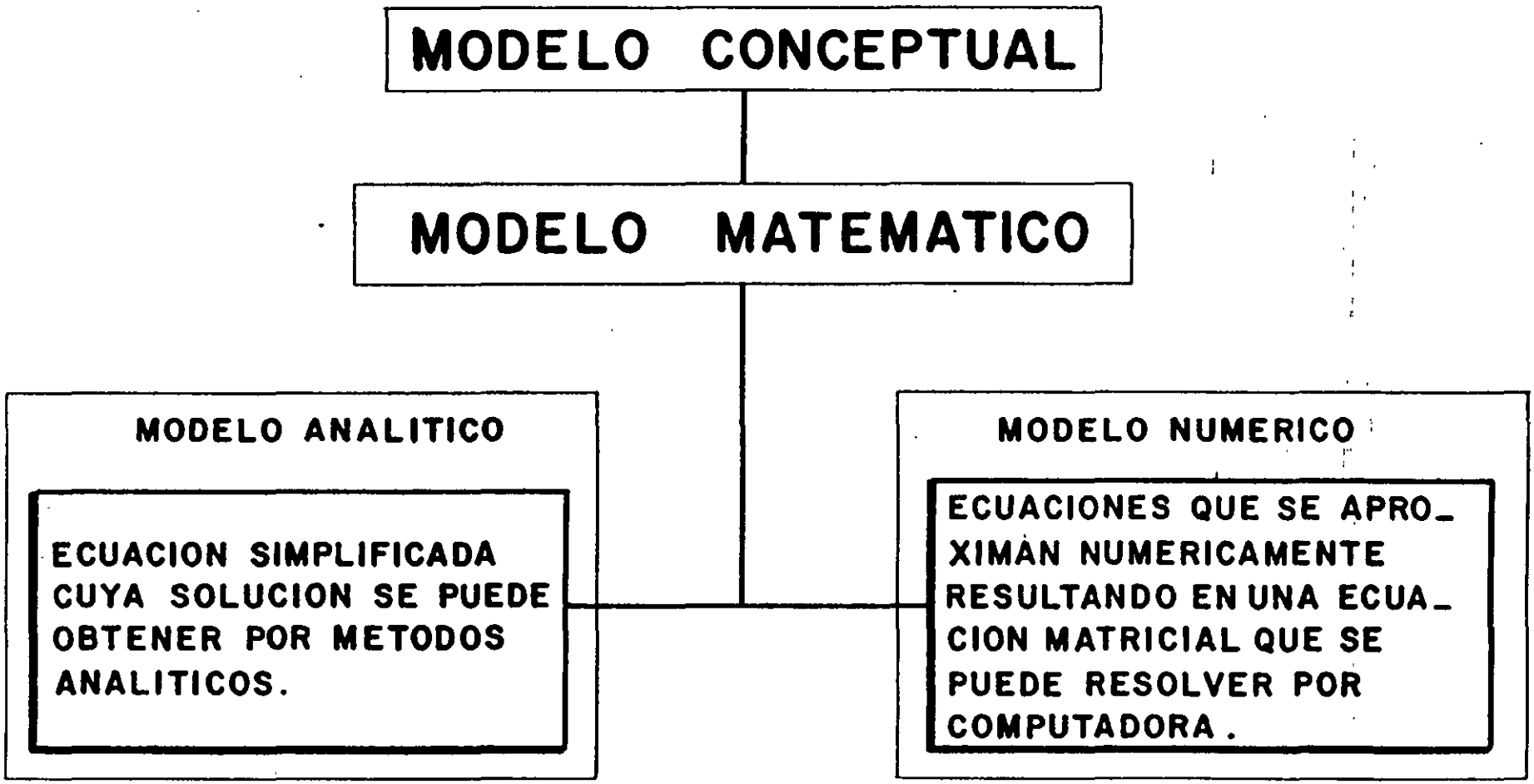
MODELO CONCEPTUAL
MODELO MATEMATICO
MODELO ANALITICO
ECUACION SIMPLIFICADA CUYA SOLUCION SE PUEDE OBTENER POR METODOS ANALITICOS.
MODELO NUMERICO
ECUACIONES QUE SE APRO_ XIMAN NUMERICAMENTE RESULTANDO EN UNA ECUA_ CION MATRICIAL QUE SE PUEDE RESOLVER POR COMPUTADORA .

METODOS NUMERICOS

- OFRECEN VENTAJAS PARA
  - AMBIENTES GEOLOGICOS COMPLEJOS
    - HETEROGENEIDAD
    - ANISOTROPIA
  - CONTORNOS IRREGULARES
  - PROCESOS NO LINEALES
  - PROCESOS ACOPLADOS

AREA TO BE MODELED

FINITE DIFFERENCE GRID

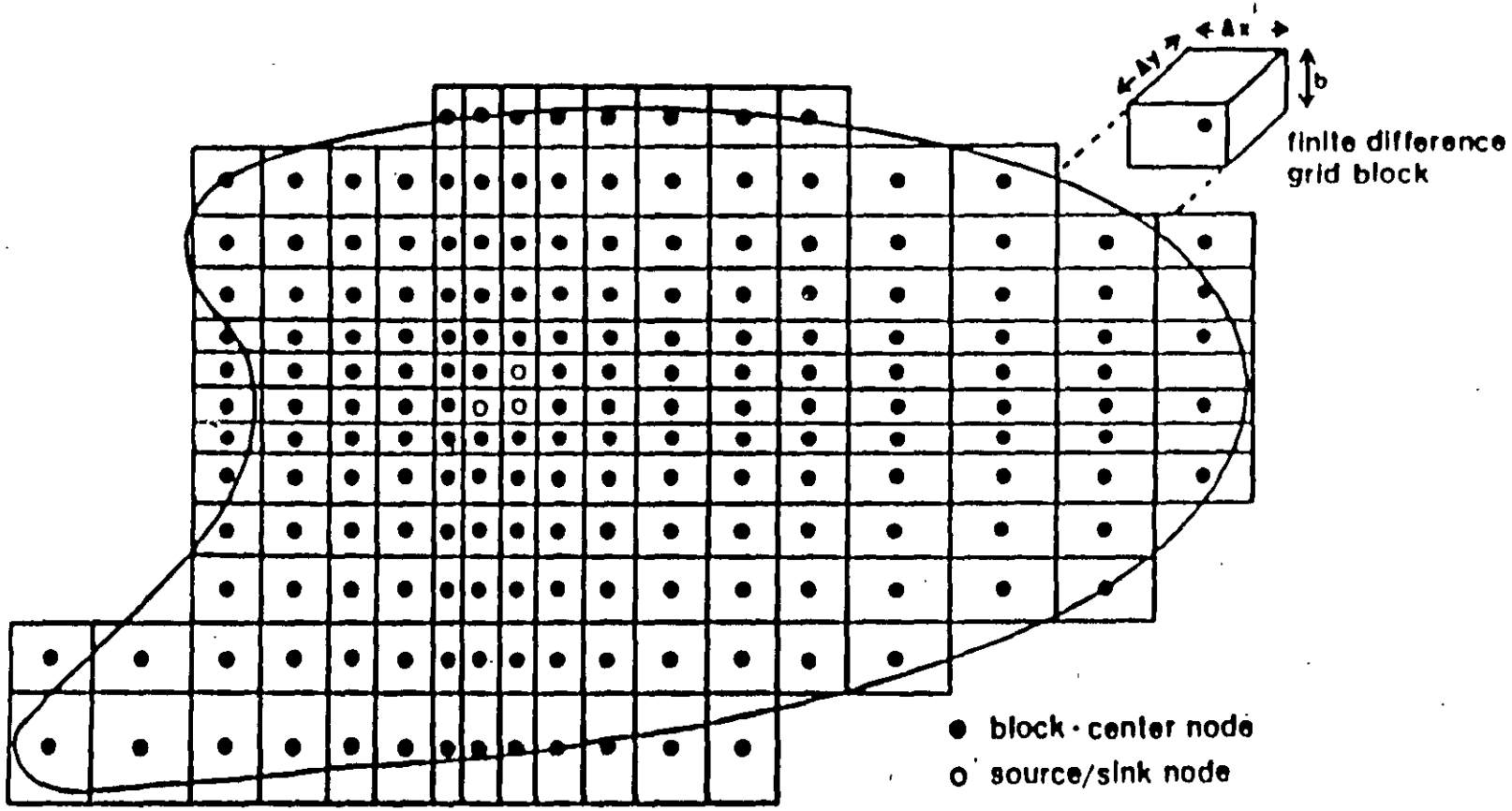

FINITE ELEMENT MESH

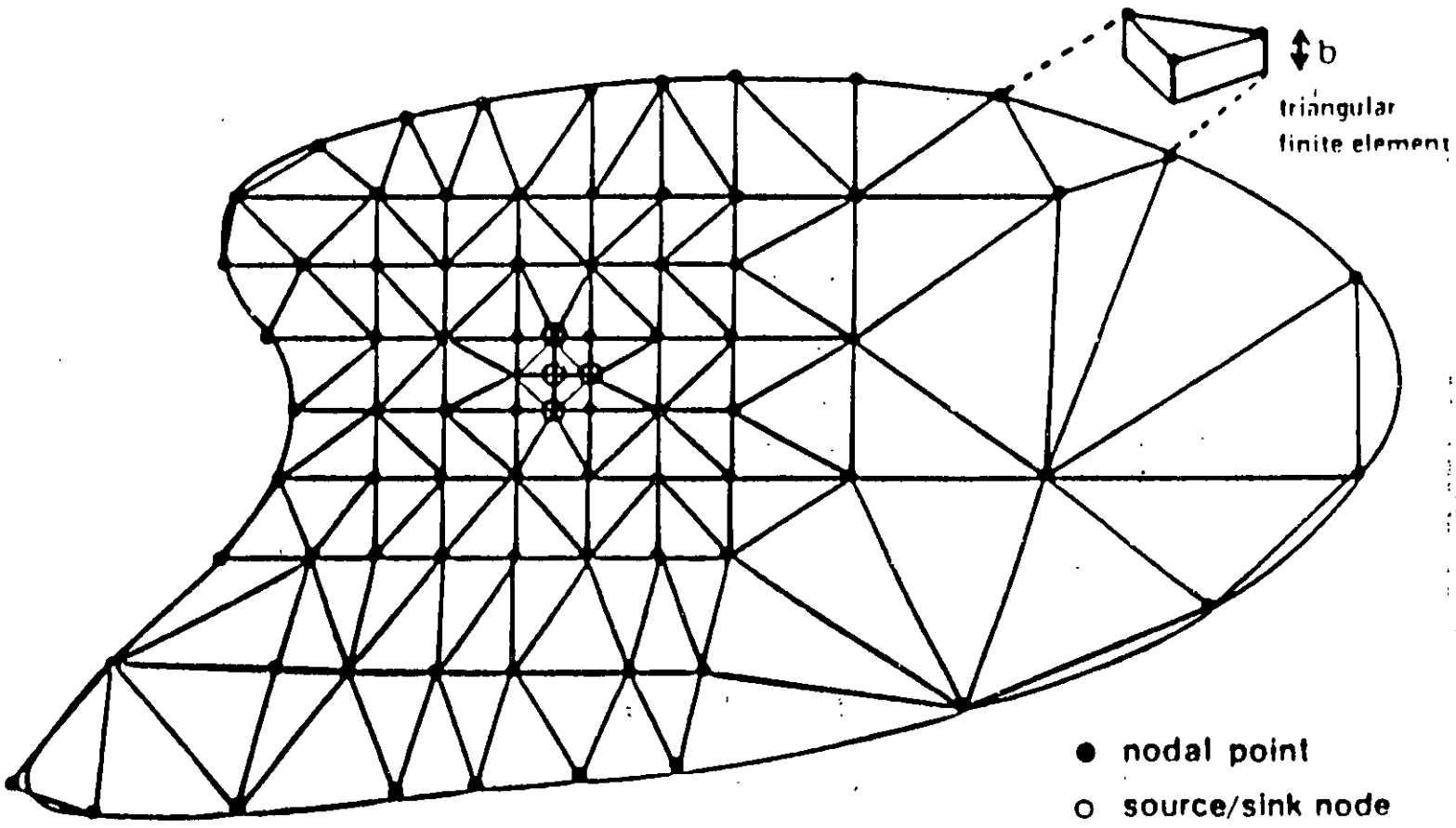

PROPOSITO DE LA MODELACION

- ENTENDIMIENTO DEL SISTEMA Y DE LOS PROCESOS.
  - INVESTIGACIONES DEL AREA
  - CONDICIONES PASADAS
- PREDICCION
  - CONDICIONES FUTURAS
  - ANALISIS DE DISEÑOS CORRECTIVOS
  - ANALISIS PARA CRITERIOS DE REGLAMENTACION
- CONTROL
  - IMPLEMENTACION DE PROGRAMAS DE APROVECHAMIENTO O CORRECTIVOS
  - OPCIONES DE OPERACION
  - EXPLOTACION OPTIMA

IDENTIFICACION DEL MODELO

- A LA DETERMINACION DEL MODELO TEORICO CORRECTO SE LE CONOCE COMO IDENTIFICACION DEL MODELO.

- DADA UNA CLASE DE MODELOS Y UN PROCESO, EL PROBLEMA DE IDENTIFICACION CONSISTE EN DETERMINAR EL MEJOR MODELO EN ALGUN SENTIDO MEDIANTE OBSERVACIONES DE ENTRADA-SALIDA DEL PROCESO.

- LA SELECCION DEL "MODELO MAS VERDADERO" ES UNA TAREA SUBJETIVA QUE DEBE REALIZAR EL MODELADOR.

SELECCION DEL CODIGO

- UNA VEZ QUE LA TEORIA SE IDENTIFICA, SE PROCEDE A LA SELECCION DEL CODIGO.

- EL CODIGO DE COMPUTADORA (PROGRAMA) ES UN CONJUNTO DE INSTRUCCIONES DISEÑADAS PARA RESOLVER EL MODELO TEORICO. LA MAYORIA DE LOS INDICES DE EJECUCION SE HAN DESARROLLADO PARA LOS CODIGOS DE COMPUTADORA, A LO QUE SE LLAMA VALIDACION DEL MODELO.

- LA VALIDACION ES UN PROCESO DE PRUEBA APLICADO AL CODIGO DE COMPUTADORA, DONDE LOS OBJETIVOS SON :

  (1) VERIFICAR LA EXACTITUD DEL ALGORITMO COMPUTACIONAL EMPLEADO PARA RESOLVER LAS ECUACIONES QUE DESCRIBEN EL FENOMENO.

  (2) ASEGURAR QUE EL CODIGO DE COMPUTADORA SEA COMPLETAMENTE OPERACIONAL.

SELECCION DEL CODIGO (CONTINUA)

- SE DICE QUE UN CODIGO DE COMPUTADORA ESTA 'VALIDADO' SI SE HAN EFECTUADO LAS PRUEBAS SUFICIENTES PARA DEMOSTRAR QUE REPRESENTA CON EXACTITUD AL MODELO TEORICO.

- LAS PRUEBAS PUEDEN CONSISTIR EN :

  (1) COMPARACION CON SOLUCIONES ANALITICAS.

  (2) COMPARACION CON OTROS CODIGOS

FLUJO DEL AGUA SUBTERRANEA

MARCO FISICO

- PLANO HIDROGEOLOGICO MOSTRANDO LA EXTENSION, CONTORNOS, Y CONDICIONES DE CONTORNO DE TODOS LOS ACUIFEROS
- PLANO TOPOGRAFICO MOSTRANDO LOS CUERPOS DE AGUA SUPERFICIALES
- PLANOS DE CONFIGURACION DE LA SUPERFICIE FREATICA, DEL BASAMENTO, Y DEL ESPESOR SATURADO
- PLANO DE TRANSMISIVIDAD MOSTRANDO EL ACUIFERO Y SUS CONTORNOS
- PLANO DE CONDUCTIVIDAD HIDRAULICA Y ALMACENAMIENTO ESPECIFICO DE LA CAPA CONFINANTE
- PLANO DE VARIACION DEL COEFICIENTE DE ALMACENAMIENTO EN EL ACUIFERO
- CONEXION HIDRAULICA ENTRE EL ACUIFERO Y LOS CUERPOS DE AGUA SUPERFICIALES

FLUJO DE AGUA SUBTERRANEA (CONT)

ESFUERZOS SOBRE EL SISTEMA

- TIPO Y EXTENSION DE LAS AREAS DE RECARGA (AREAS IRRIGADAS, CUERPOS DE AGUA SUPERFICIALES, POZOS DE RECARGA, ETC.
- BOMBEO DE AGUA SUBTERRANEA (DISTRIBUIDO EN TIEMPO Y ESPACIO)
- GASTO EN CAUCES SUPERFICIALES (DISTRIBUIDO EN TIEMPO Y ESPACIO)
- PRECIPITACION
- EVAPOTRANSPIRACION

OTROS FACTORES

- CONDICIONES ECONOMICAS
- ASPECTOS LEGALES
- USO DEL SUELO

APLICACION DEL MODELO

- LA APLICACION DEL MODELO TIENE TRES ETAPAS PRINCIPALES :
  (1) CONCEPTUALIZACION DEL SISTEMA
  (2) CALIBRACION DEL MODELO
  (3) PREDICCION

- LA MAYORIA DE LAS APLICACIONES INCLUYEN A LAS TRES ETAPAS, AUNQUE CON DIFERENTES GRADOS DE ESFUERZO.

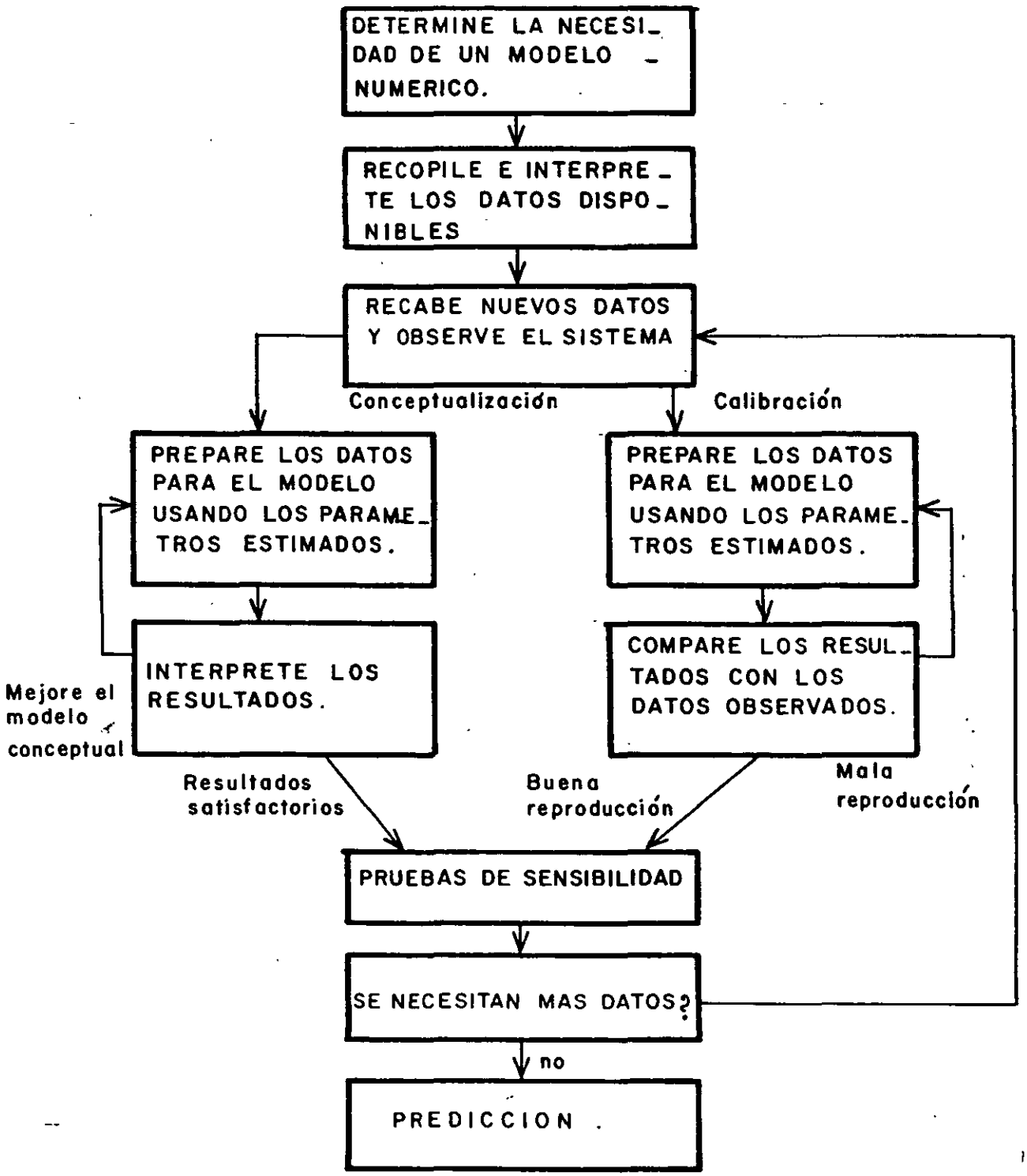
DETERMINE LA NECESIDAD DE UN MODELO NUMERICO.
RECOPILE E INTERPRETE LOS DATOS DISPONIBLES
RECABE NUEVOS DATOS Y OBSERVE EL SISTEMA
Conceptualización
Calibración
PREPARE LOS DATOS PARA EL MODELO USANDO LOS PARAMETROS ESTIMADOS.
PREPARE LOS DATOS PARA EL MODELO USANDO LOS PARAMETROS ESTIMADOS.
INTERPRETE LOS RESULTADOS.
Mejore el modelo conceptual
COMPARE LOS RESULTADOS CON LOS DATOS OBSERVADOS.
Resultados satisfactorios
Buena reproducción
Mala reproducción
PRUEBAS DE SENSIBILIDAD
SE NECESITAN MAS DATOS?
no
PREDICCION .

APLICACION DEL MODELO (CONT.)

- LA CONCEPTUALIZACION DEL SISTEMA INCLUYE LA ORGANIZACION DE LA INFORMACION SOBRE EL SISTEMA ACUIFERO DENTRO DE UN MARCO INTERNAMENTE CONSISTENTE. LA CONCEPTUALIZACION INCLUYE LOS FACTORES QUE CONTROLAN AL SISTEMA DE FLUJO TALES COMO GEOMETRIA Y ESTRATIGRAFIA, CONDICIONES INICIALES Y DE CONTORNO, Y PARAMETROS IDROLOGICOS.

- LA CONCEPTUALIZACION DEL SISTEMA ES UNA TAREA SUBJETIVA Y NO SE DISPONE EN GENERAL DE INDICES CUANTITATIVOS DE CORRECCION.

APLICACION DEL MODELO (CONT.)

- LA REPRODUCCION HISTORICA O CALIBRACION DEL MODELO SE EMPLEA PARA REFINAR LAS ESTIMACIONES DE LOS PARAMETROS HIDROLOGICOS Y CONDICIONES DE CONTORNO MEDIANTE LA COMPARACION DE LOS RESULTADOS CON LOS DATOS OBSERVADOS.

- LA CALIBRACION SE PUEDE EFECTUAR POR ENSAYO Y ERROR O POR REGRESION AUTOMATICA. PARA AMBOS, EL ANALISIS DE SENSIBILIDAD ES PARTE DEL PROCESO DE AJUSTE.

- EL GRADO DE AJUSTE ENTRE LAS VARIABLES CALCULADAS (P.E. CARGAS HIDRAULICAS) Y LOS VALORES MEDIDOS PERMITE JUZGAR EL PROCESO DE CALIBRACION.

APLICACION DEL MODELO (CONT.)

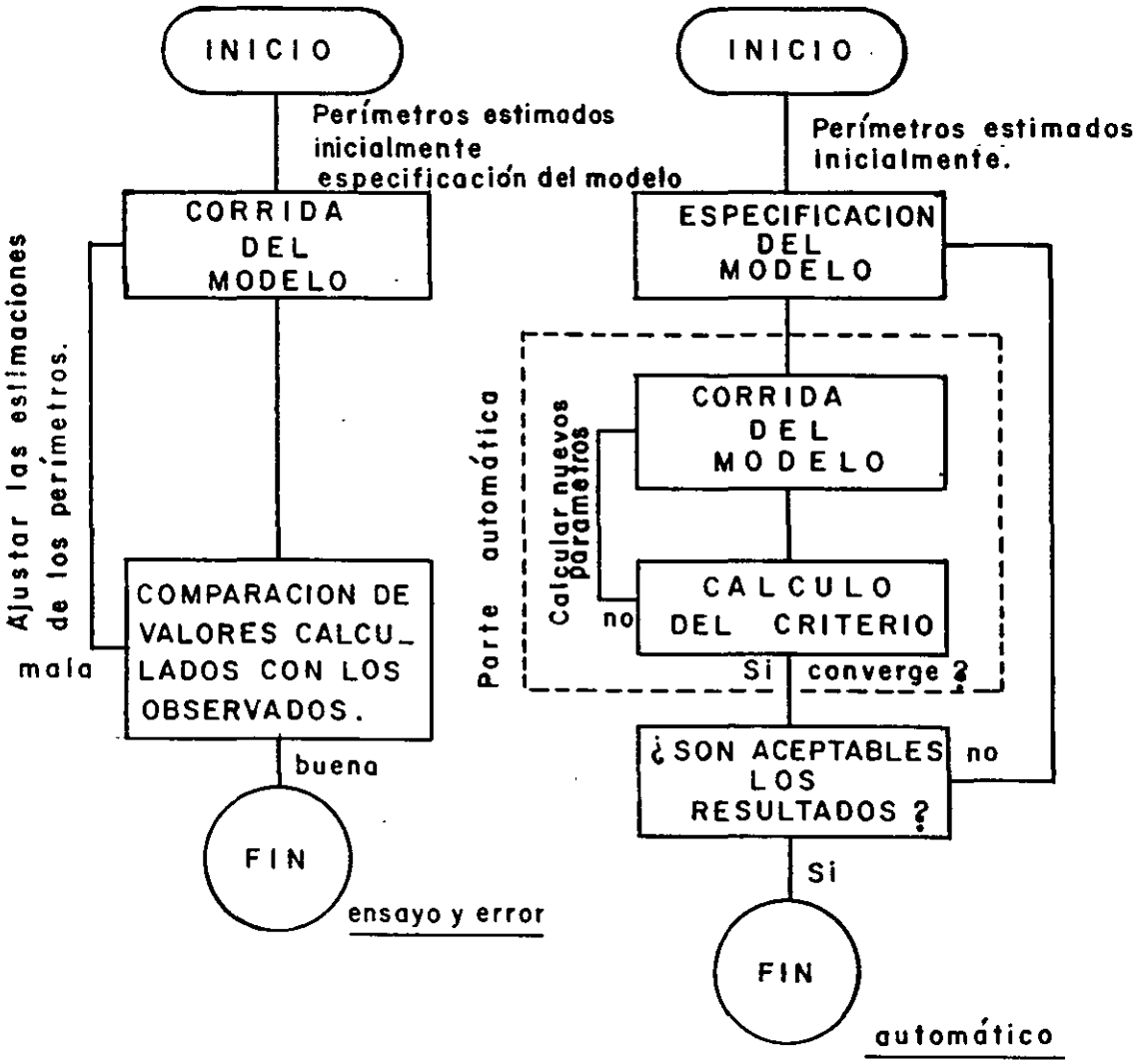

PROCEDIMIENTOS PARA CALIBRACION DEL MODELO MEDIANTE ENSAYO Y ERROR Y AJUSTE AUTOMA_ TICO.

APLICACIÓN DEL MODELO (CONT)

- **LA PREDICCION ES POR LO GENERAL LA PARTE FINAL Y LA MAS CORTA DE LA APLICACIÓN DE UN MODELO**

- **LAS PREDICCIONES SE BASAN EN LOS RESULTADOS DEL MODELO QUE UTILIZAN LA MEJOR ESTIMACIÓN DE LOS PARÁMETROS DEL SISTEMA OBTENIDA POR CALIBRACIÓN Y CON ELLAS SE PRONOSTICAN LOS EFECTOS DE UN CAMBIO EN EL SISTEMA.**

USO ERRONEO DEL MODELO

- LA MAYORIA DE LOS ERRORES DE MODELACION OCURREN EN LA APLICACION DEL MODELO; ENTRE LOS EJEMPLOS MAS COMUNES DE MAL USO SE TIENEN :

  (1) SOBREMODELACION – HACER EL MODELO MAS COMPLEJO QUE LO PERMITIDO POR LOS DATOS, O QUE LO REQUERIDO POR LOS OBJETIVOS;

  (2) CONCEPTUALIZACION INCORRECTA — BASAR EL MODELO EN UNA CARACTERIZACION POBRE O INCOMPLETA DEL ACUIFERO;

  (3) SELECCION INCORRECTA DEL MODELO — SELECCIONAR UN MODELO SIN ENTENDER BIEN SUS LIMITACIONES;

  (4) CONDICIONES DE CONTORNO Y/O PARAMETROS DEL MODELO INCORRECTOS

  (5) PREDICCION INAPROPIADA — PRONOSTICAR BAJO CONDICIONES MUY DIFERENTES A LAS EMPLEADAS EN LA CALIBRACION;

USO ERRONEO DEL MODELO (CONT.)

(6) MALA INTERPRETACION —— INTER_ PRETACION HIDROLOGICA POBRE DE LOS RESULTADOS CALCULADOS.

(7) APROXIMACION NUMERICA BURDA (IMPORTANCIA DEL BALANCE DE MASAS)

(8) ERRORES NO DETECTADOS EN EL CODIGO NUMERICO (IMPORTANCIA DE LA VALIDACION).

INTRODUCCION AL MODELO MODULAR DE FLUJO DE AGUA SUBTERRANEA DEL U.S.G.S.

VENTAJAS

- Las modificaciones se limitan a paquetes individuales .
- Los paquetes se pueden incluir o quitar sin dificultad .
- Corre en varios tipos de máquinas sin modificación.
- Modelo en 1, 2 ó 3 dimensiones .
- Relativamente fácil de entender .
- Muchas opciones.
- Los formatos se pueden especificar por el usuario.
- Calcula el flujo entre celda y celda.
- Completamente documentado.

VARIAS OPCIONES PARA :

- Condiciones de flujo de agua subterranea.
- Términos fuente.
- Métodos de solución numérica.
- Entrada y salida de datos.
- Condiciones de contorno.
- Datos dependientes del tiempo.

CONDICIONES DE FLUJO DE AGUA SUBTERRANEA

- Problemas en 1, 2 ó 3 dimensiones.
- Condiciones artesianas.
- Condiciones freáticas.
- Condiciones parcialmente convertibles de artesianas a freáticas y viceversa.
- Condiciones totalmente convertibles de artesianas a freáticas y viceversa.

TERMINOS FUENTE

- POZOS DE BOMBEO O INYECCION.
- DRENES.
- INTERACCION CON RIOS.
- EVAPOTRANSPIRACION.
- RECARGA DISTRIBUIDA.
- FUENTES O SUMIDEROS EXTERNOS.

METODOS NUMERICOS DE SOLUCION

- Procedimiento altamente implícito (SIP).
- Sobrerrelajación sucesiva por secciones verticales. (SSOR).

ENTRADA

- Grupos de datos separados se pueden manejar en archivos de datos distintos.
- Formatos especificados por el usuario.
- Sólo las opciones seleccionadas entran al modelo.

SALIDA

- Cargas hidráulicas.
- Abatimientos.
- Balance de masas.
- Datos de iteración.
- Datos de tiempo.
- Cálculos de flujo celda a celda.
- Opción de archivos en binario.
- Selección de salidas para impresión .

CONDICIONES DE CONTORNO

- Carga prescrita .
- Flujo prescrito .
- Flujo nulo .
- Flujo dependiente de la carga .

REQUERIMIENTO DE DATOS

- Datos sobre la malla de diferencias finitas.
- Periodos de esfuerzo e intervalos de tiempo.
- Parámetros del método de resolución.
- Opciones .
- Parámetros hidráulicos .
- Condiciones de contorno.
- Términos fuente — sumidero .

PAQUETE BASICO

- Tamano del modelo .
- Contornos.
- Longitud de los intervalos de tiempo.
- Condiciones iniciales .
- Salida .
- Opciones (Paquetes utilizados)

REQUERIDO

Assignment of Major Options to Elements
in the IUNIT Array

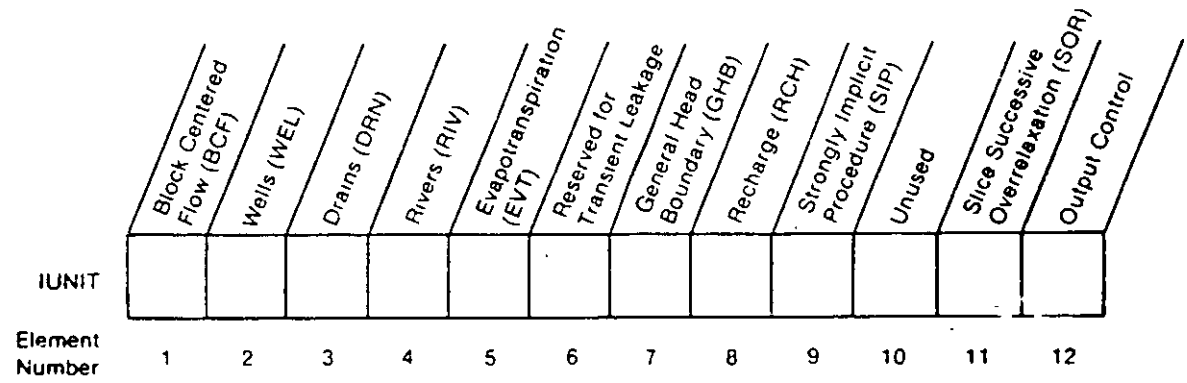

Sample IUNIT Input Record

	Element Number											
	1	2	3	4	5	6	7	8	9	10	11	12
IUNIT	13	41	0	0	81	0	0	0	26	0	0	17

1	BCF	Input Is on Unit 13
2	WEL	Input Is on Unit 41
3	DRN	Is Inactive
4	RIV	Is Inactive
5	EVT	Input Is on Unit 81
7	GHB	Is Inactive
8	RCH	Is Inactive
9	SIP	Input Is on Unit 26
11	SOR	Is Inactive
12	Output Control	Input Is on Unit 17

34

Figure 17.—Specification of major options using the IUNIT array.

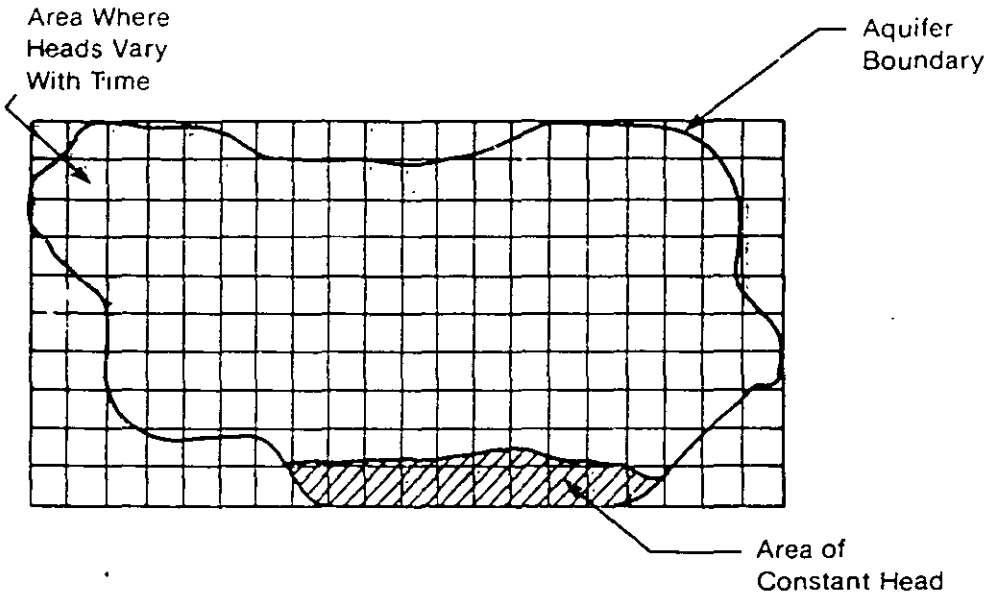

0	1	1	1	1	1	0	0	0	0	0	0	0	1	1	1	1	1	0	0
1	1	1	1	1	1	1	1	1	1	1	1	1	1	1	1	1	1	1	0
1	1	1	1	1	1	1	1	1	1	1	1	1	1	1	1	1	1	1	0
0	1	1	1	1	1	1	1	1	1	1	1	1	1	1	1	1	1	1	0
0	0	1	1	1	1	1	1	1	1	1	1	1	1	1	1	1	1	1	0
0	0	1	1	1	1	1	1	1	1	1	1	1	1	1	1	1	1	1	1
0	0	1	1	1	1	1	1	1	1	1	1	1	1	1	1	1	1	1	1
0	0	1	1	1	1	1	1	1	1	1	1	1	1	1	1	1	1	1	0
0	0	0	0	0	0	1	1	1	1	1	1	1	1	1	1	1	1	0	0
0	0	0	0	0	0	0	-1	-1	-1	-1	-1	-1	-1	-1	-1	-1	0	0	0

IBOUND Codes

< 0 Constant Head
= 0 No Flow
> 0 Variable Head

35

Figure 19 —Example of the boundary array (IBOUND) for a single layer.

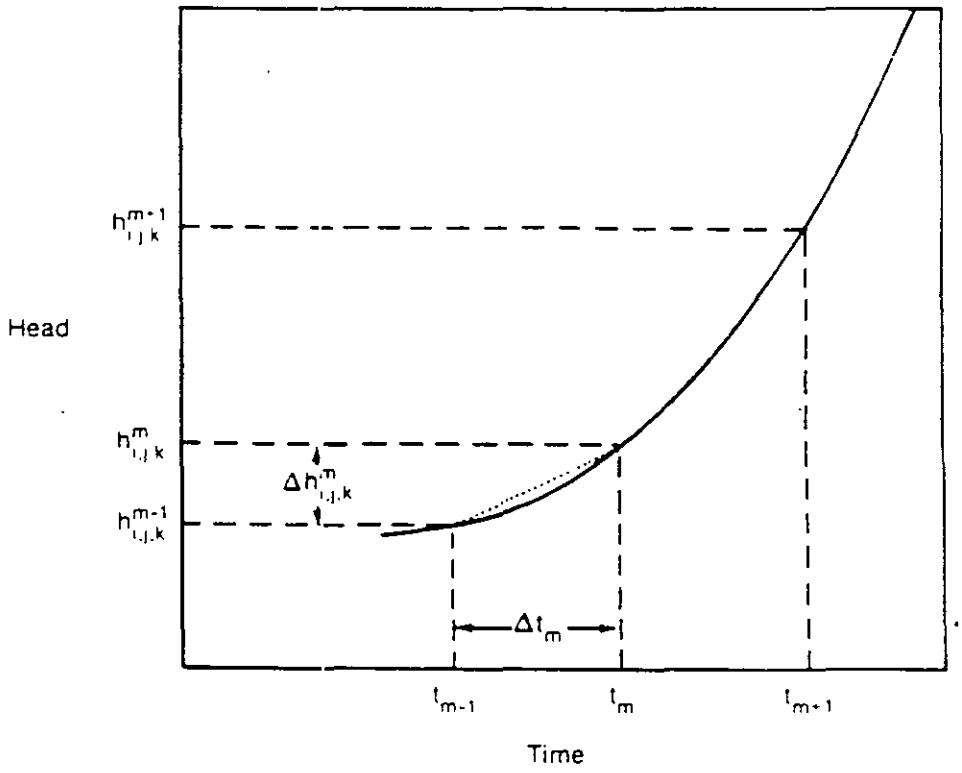

Explanation

t_m	time at end of time step m
$h^{m}_{i,j,k}$	head at node i,j,k at time t_m
.....	Backward difference approximation to slope of hydrograph at time t_m

Figure 6.—Hydrograph for cell i,j,k.

PAQUETE DE FLUJO CENTRADO EN LA CELDA

- Lee los parámetros de acuífero .
- Define los tipos de capas .
- Calcula los coeficientes de las ecuaciones de diferencias finitas .

REQUERIDO

RESUMEN DE CONDICIONES DE FLUJO DE AGUA SUBTERRANEA Y DATOS REQUERIDOS

CONDICION DE FLUJO	Tipo de Capa	DESCRIPCION	REQUERIMIENTO DE DATOS						
			S	Sy	T	K	BASE	TECHO	VCONT
Artesiano	0	Estrictamente confinado	tr	no	si	no	no	no	cd
Freático	1	Estrictamente libre (sólo la capa superior)	no	tr	no	si	si	no	cd
Parcialmente Convertible	2	T constante (acuífero grueso) conversión S – Sy	tr	tr	si	no	no	si	cd
Totalmente Convertible	3	Conversión T – K Conversión S – Sy	tr	tr	no	si	si	si	cd

X = Parámetro utilizado

no = Parámetro no utilizado

tr = Parámetro utilizado en simulaciones en transitorio

cd = Parámetro utilizado si existe una capa debajo

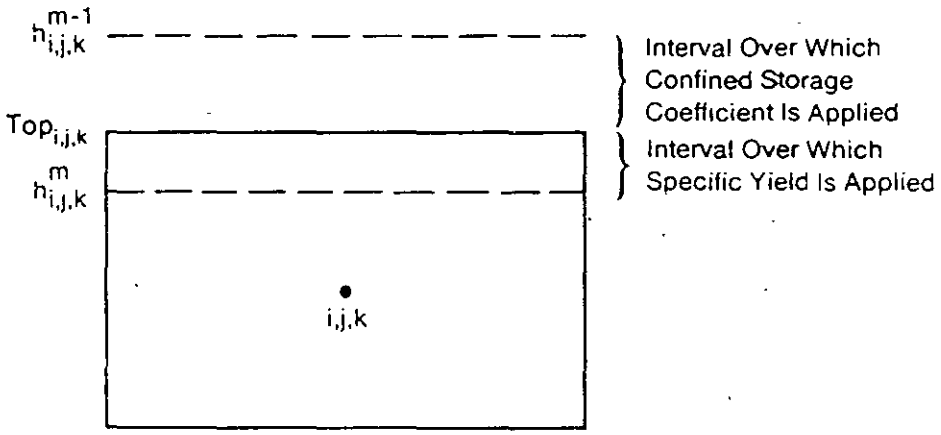

Figure 30.—A model cell which uses two storage factors during one iteration.

PAQUETE DE POZOS

- Lee datos de pozos.
- Añade términos de pozo a las ecuaciones de diferencias finitas.

- Condición de flujo prescrito.
- Pozo en el centro de la celda.
- Conceptualmente solo un pozo por celda.

  ∴ en la formulación las descargas se concentran.

PAQUETE DE RECARGA

- Lee los datos de recarga .
- Multiplica la taza de recarga por el area de la celda.

  $L / T * L^2 = L^3 / T$

- Añade términos de recarga a las ecuaciones de diferencias finitas.
- Condición de flujo prescrito .

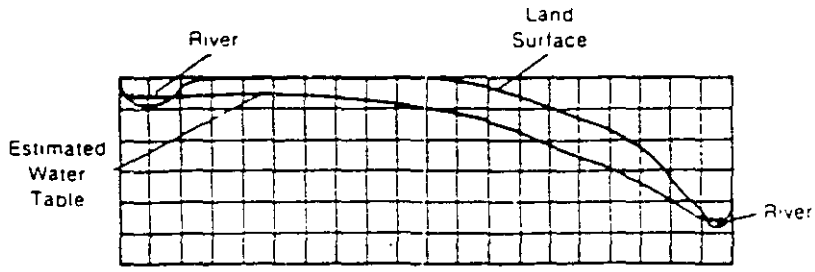

Vertical Cross-Section Showing Field
Situation With Finite Difference Grid Superimposed

a

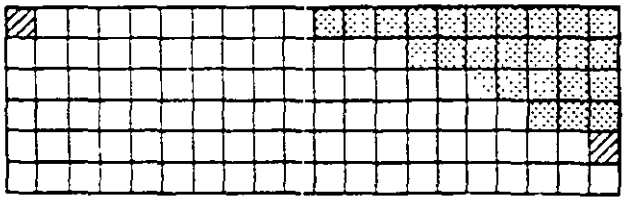

Variable Head

Constant Head

Inactive

Status of Cells at End of Simulation

b

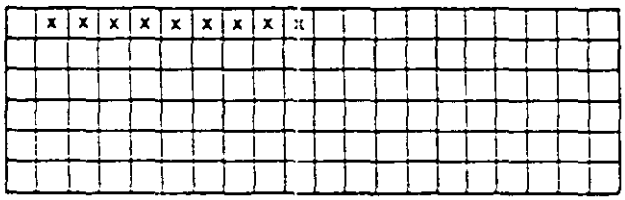

Cell Which Receives Recharge

Cells Which Receive Recharge Under Option 1

c

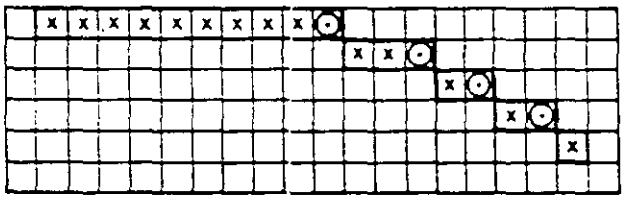

Cell Which Receives Recharge

Inactive Cell Specified by User to Receive Recharge

Heavy Line Encloses Cells User Thought Would Receive Recharge Based on Estimated Water Table

Cells Which Receive Recharge Under Option 2

d

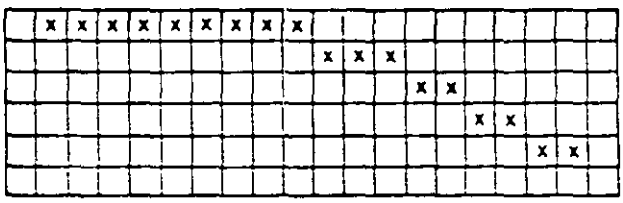

Cell Which Receives Recharge

Cells Which Receive Recharge Under Option 3

e

Figure 38.—Hypothetical problem showing which cells receive recharge under the three options available in the Recharge Package.

PAQUETE DE RIOS

- Lee datos de río .
- Calcula los términos de filtración .
- Añade términos a las ecuaciones de diferencias finitas .

- Condición de flujo dependiente de la carga.
- Flujo vertical solamente .
- El río es una fuente infiníta .

$$Q_{RIV} = \boxed{\frac{KLW}{M}} \quad (H_{RIV} - H_{AQ})$$

conductancia

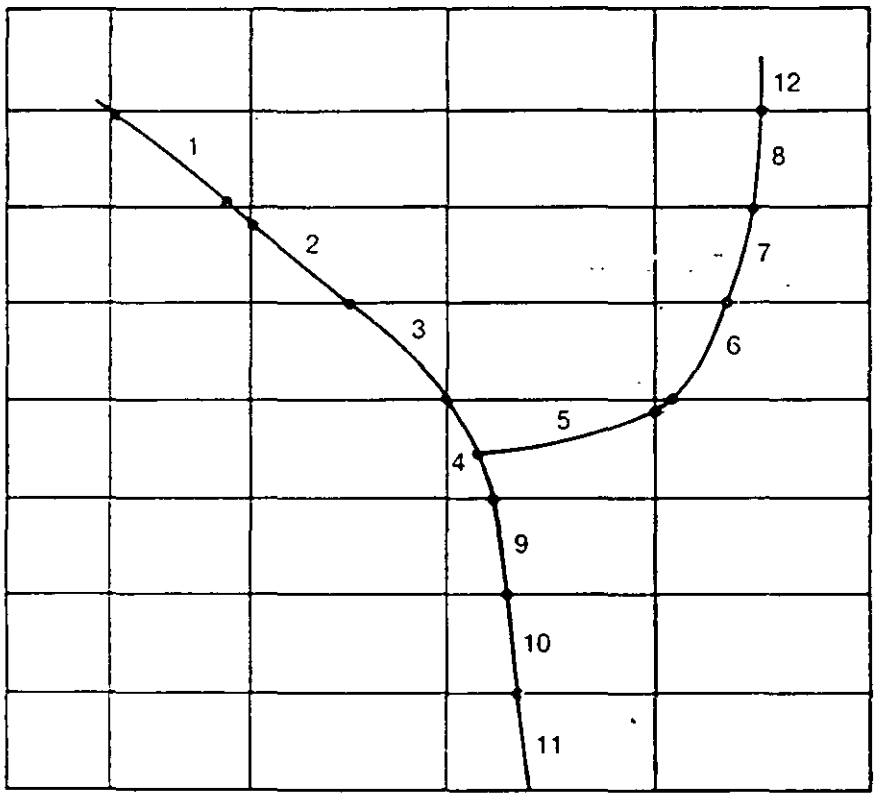

Figure 32.—Discretization of a stream into reaches. Some small reaches are ignored.

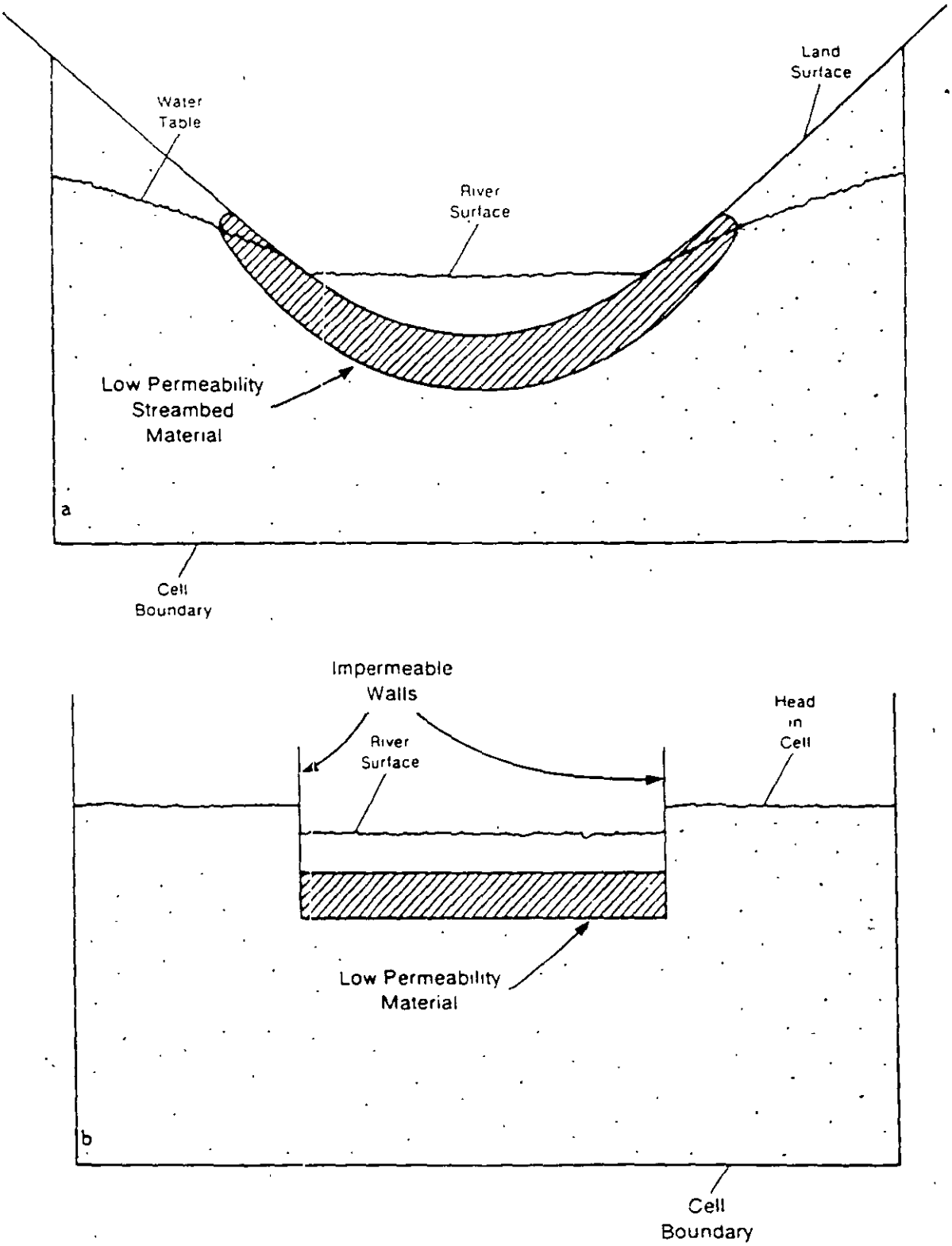

Figure 33.—(a) Cross section of an aquifer containing a stream and (b) Conceptual representation of stream-aquifer interconnection in simulation.

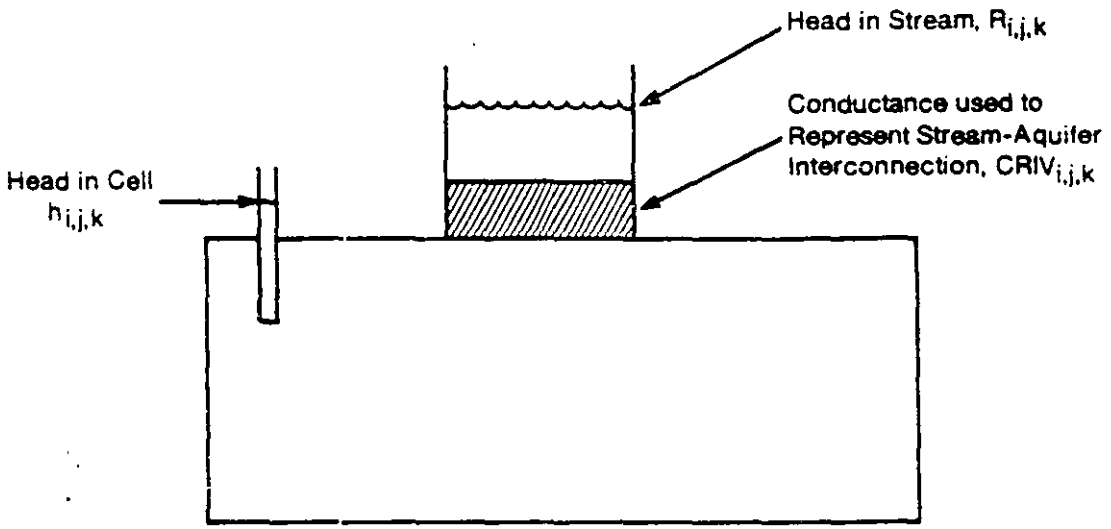

Figure 5.—Conceptual representation of leakage through a riverbed into a cell.

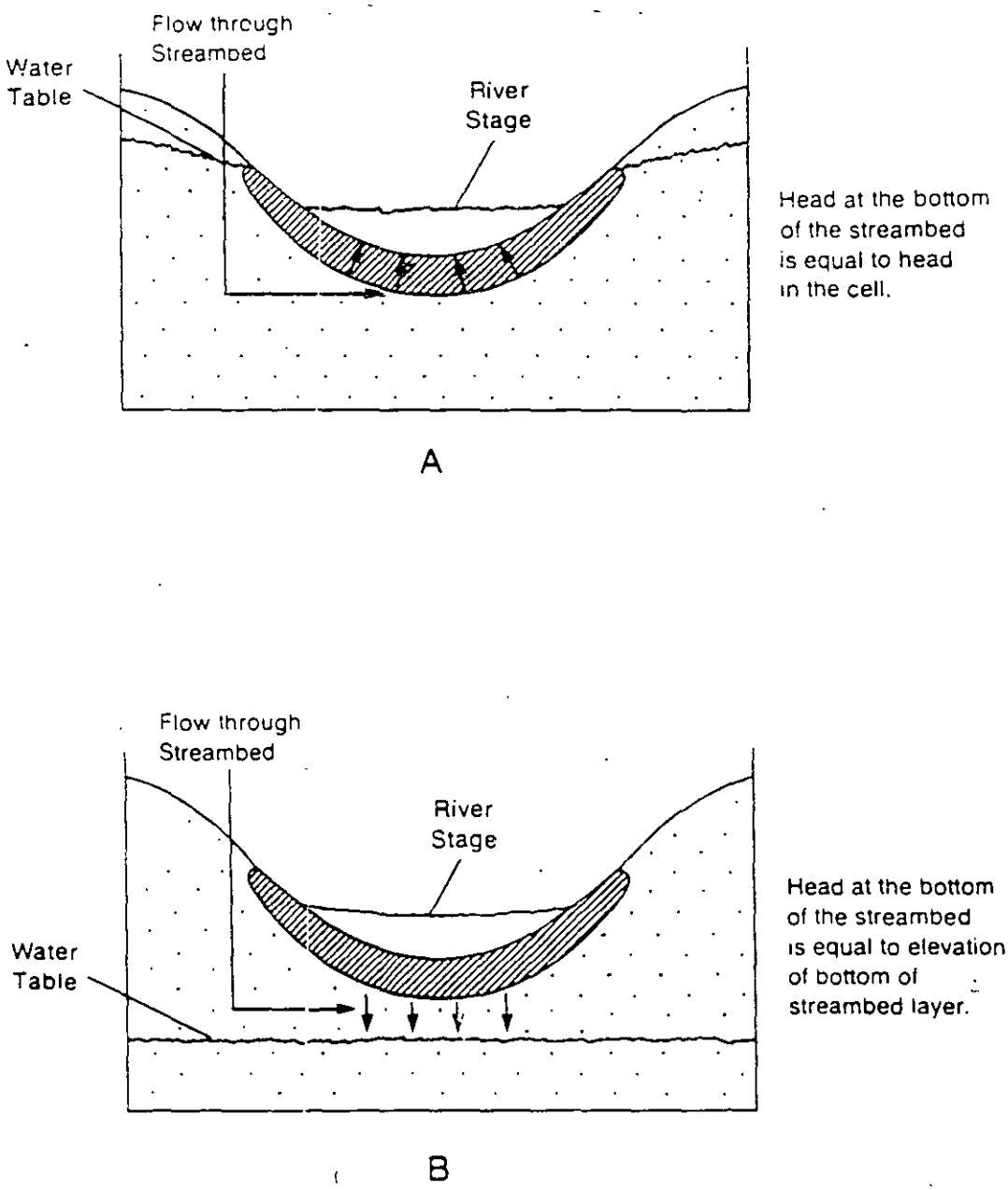

Figure 35.—Cross sections showing the relation between head at the bottom of the streambed layer and head in the cell. Head in the cell is equal to the water-table elevation.

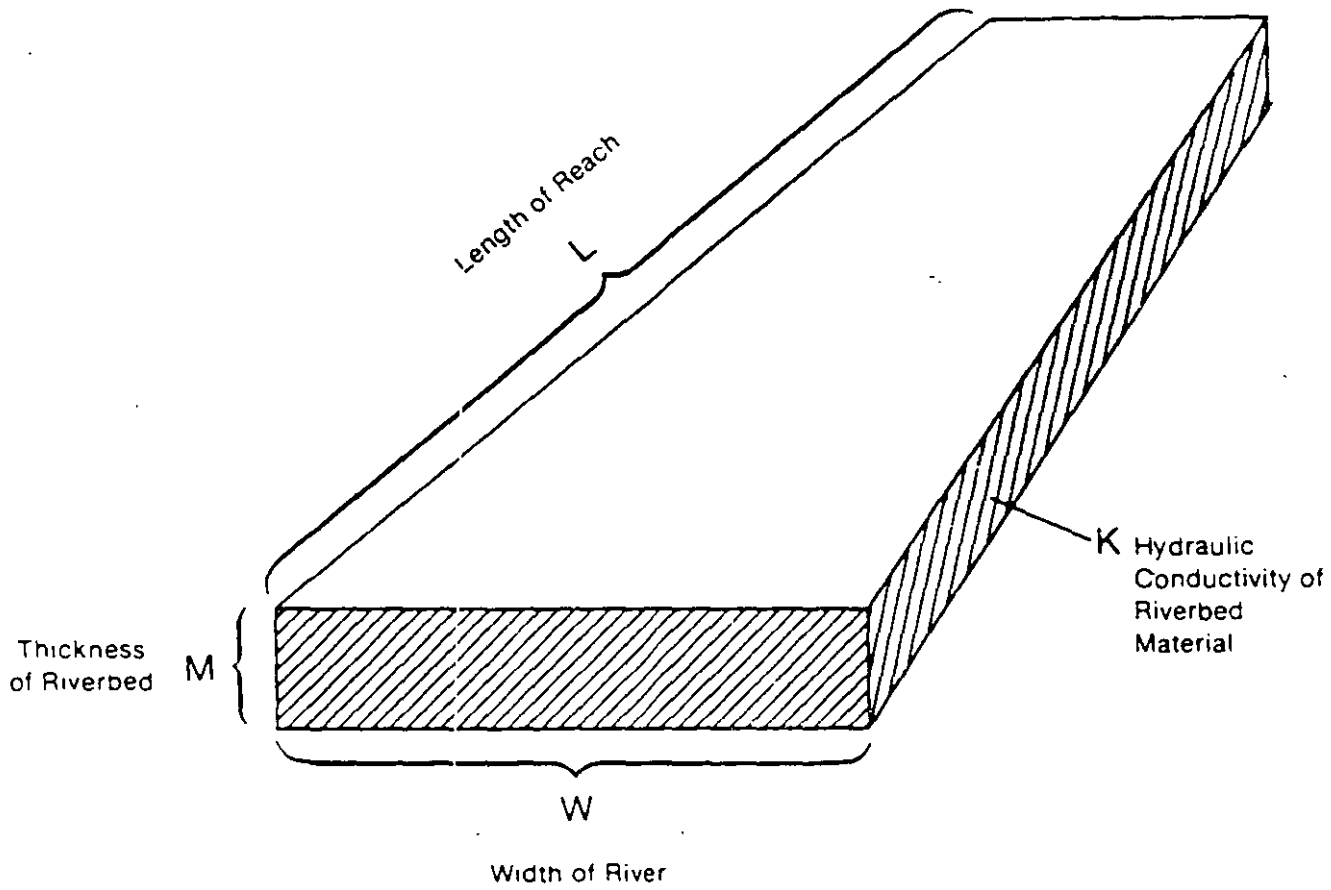

Figure 34.--Idealization of streambed conductance in an individual cell.

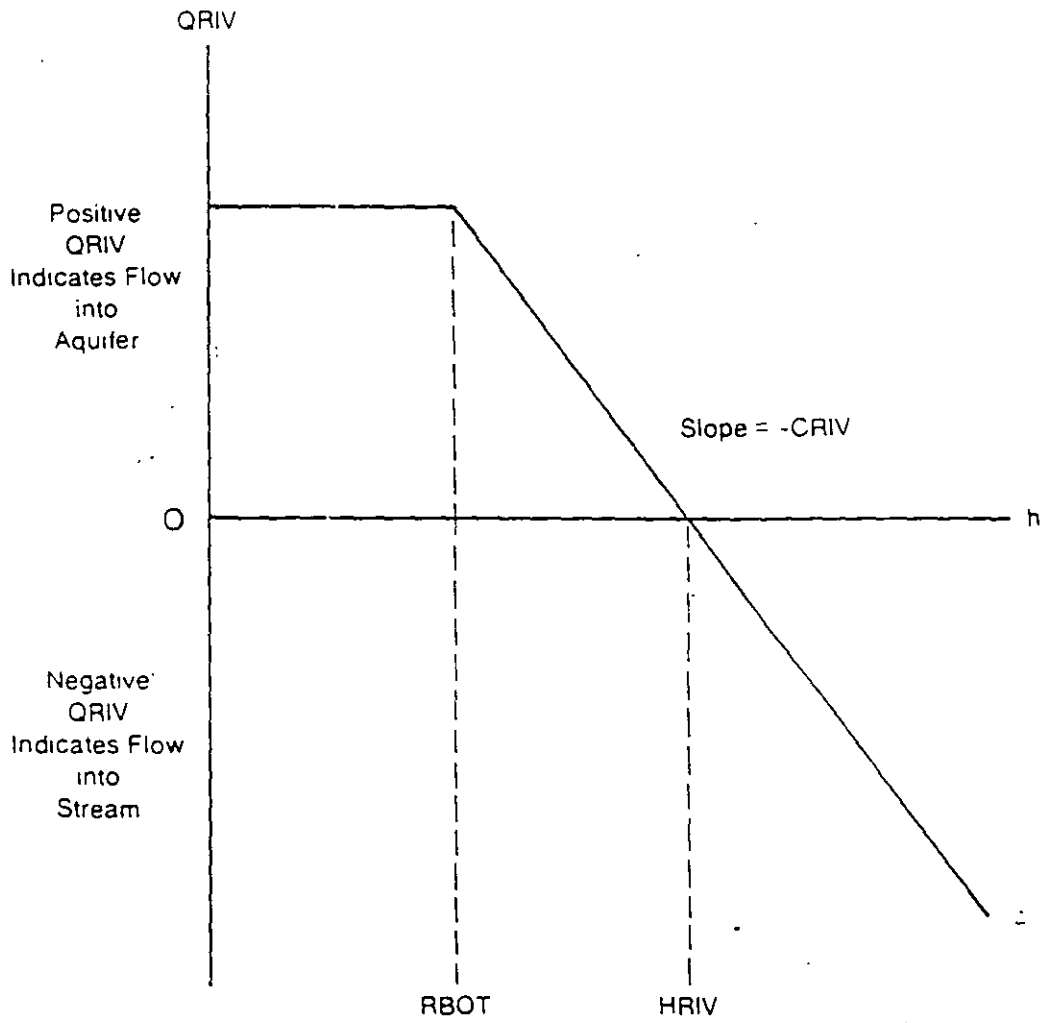

Figure 36.—Plot of flow, QRIV, from a stream into a cell as a function of head, h, in the cell where RBOT is the elevation of the bottom of the streambed and HRIV is the head in the stream.

PAQUETE DE DRENES

- Lee datos de drenes.
- Calcula la filtración del dren.
- Añade términos a las ecuaciones de diferencias finitas.
- Condición de flujo dependiente de la carga.
- Elevación del dren = carga en el dren.
- Flujo al dren proporcional a la diferencia de carga.
- Factor de proporcionalidad = conductancia L^2/T
- Flujo al dren solamente.

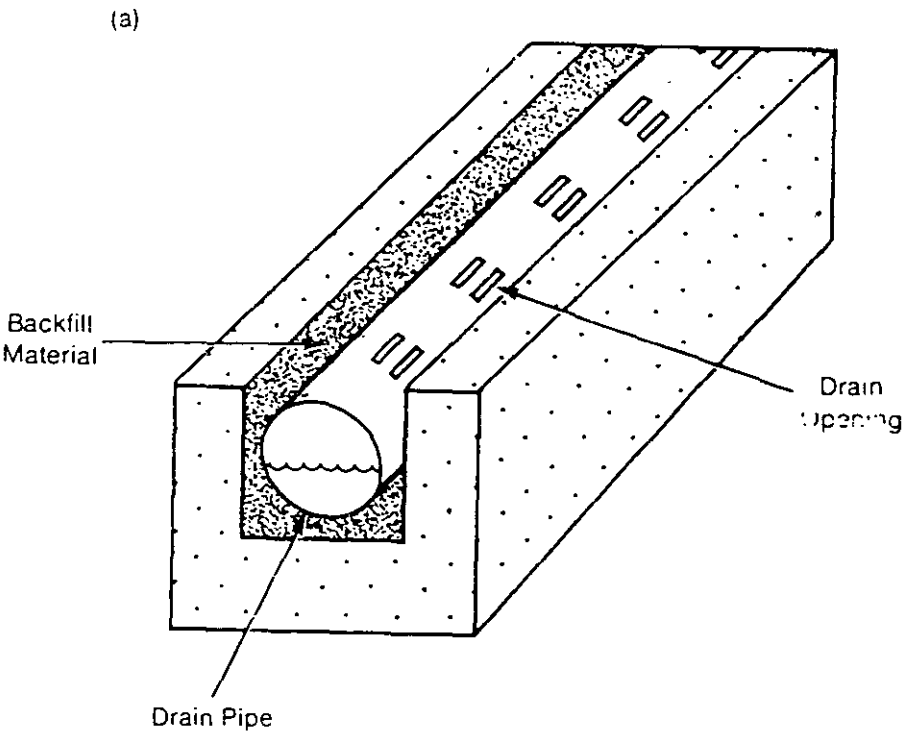

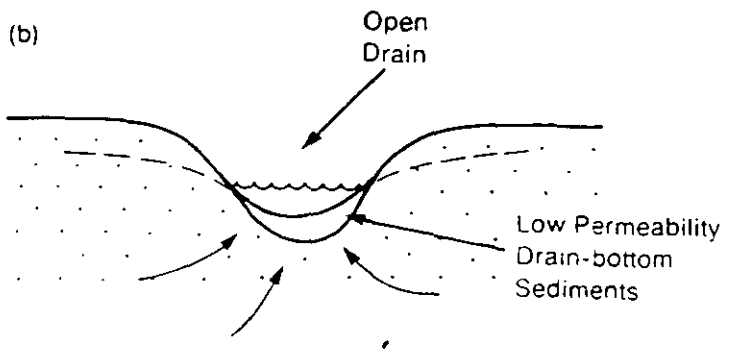

Figure 40 —Factors affecting head loss immediately around a drain (a) buried drain pipe in backfilled ditch and (b) open drain

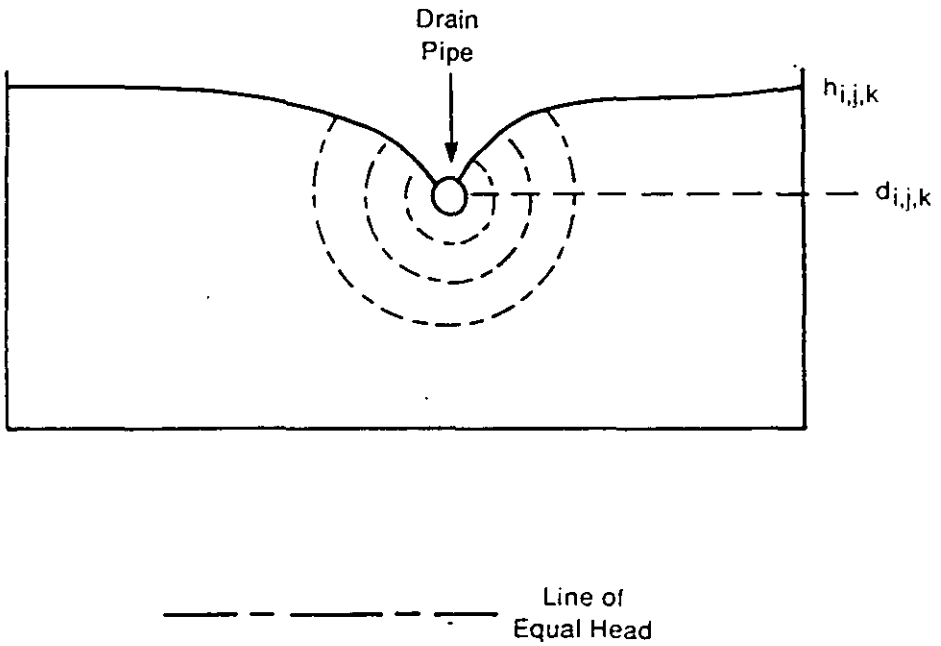

Figure 39.—Cross section through cell i,j,k illustrating head loss in convergent flow into drain.

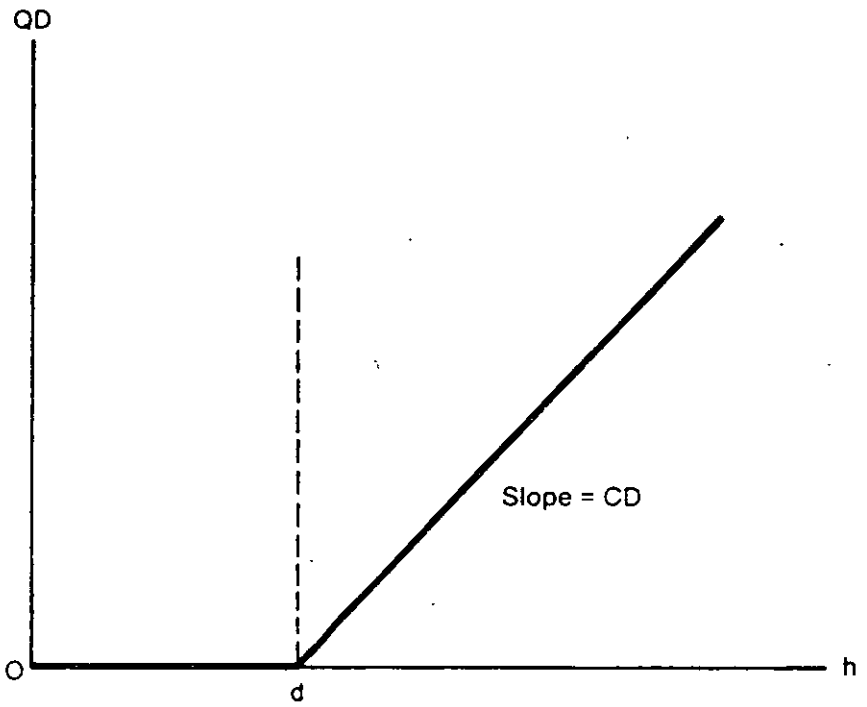

Figure 41.—Plot of flow, QD, into a drain as a function of head, h, in a cell where the elevation of the drain is d and the conductance is CD.

PAQUETE DE EVAPOTRANS_ PIRACION .

- Lee datos de ET
- Calcula la tasa de ET
- Añade términos a las ecuaciones de diferencias finitas.
- Condición de flujo dependiente de la carga.
- Función lineal .
- Q = 0 si h < elevación especificada .
- $Q = ET_{max} \dfrac{h - \text{elevación especificada}}{\text{profundidad de extinción}}$
- Q = ETmax , para h < superficie .

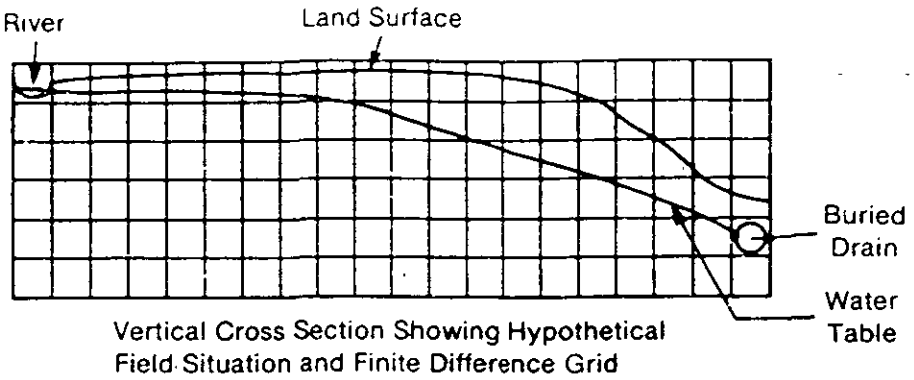

Vertical Cross Section Showing Hypothetical Field Situation and Finite Difference Grid

a

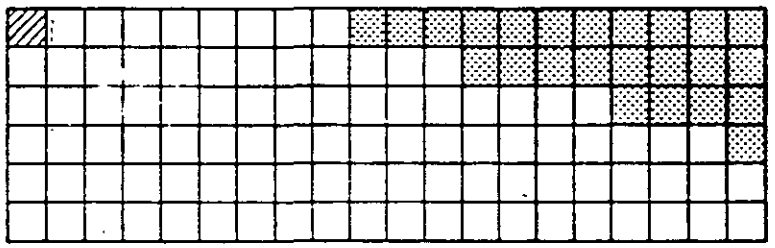

Variable Head Cell

Constant Head Cell

Inactive Cell

Status of Cells at End of Simulated Period

b

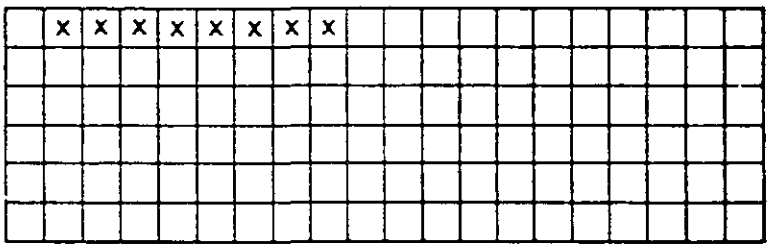

Cell from Which ET Is Abstracted

Cells from Which ET Is Abstracted Under Option 1

c

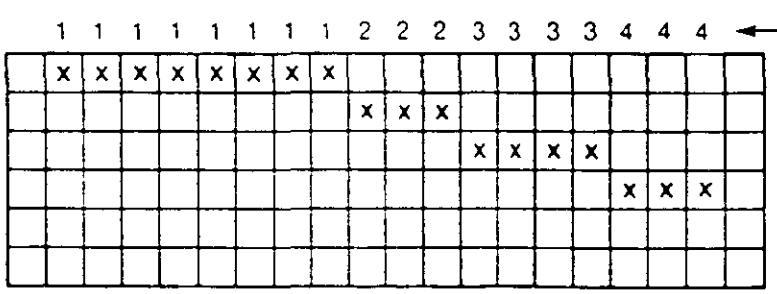

Layer Indicators Specified in the IEVT Array

Cell from Which ET Is Abstracted

Cells from Which ET Is Abstracted Under Option 2

d

Figure 43.—Hypothetical problem showing cells from which ET will be abstracted under the two options available in the ET Package.

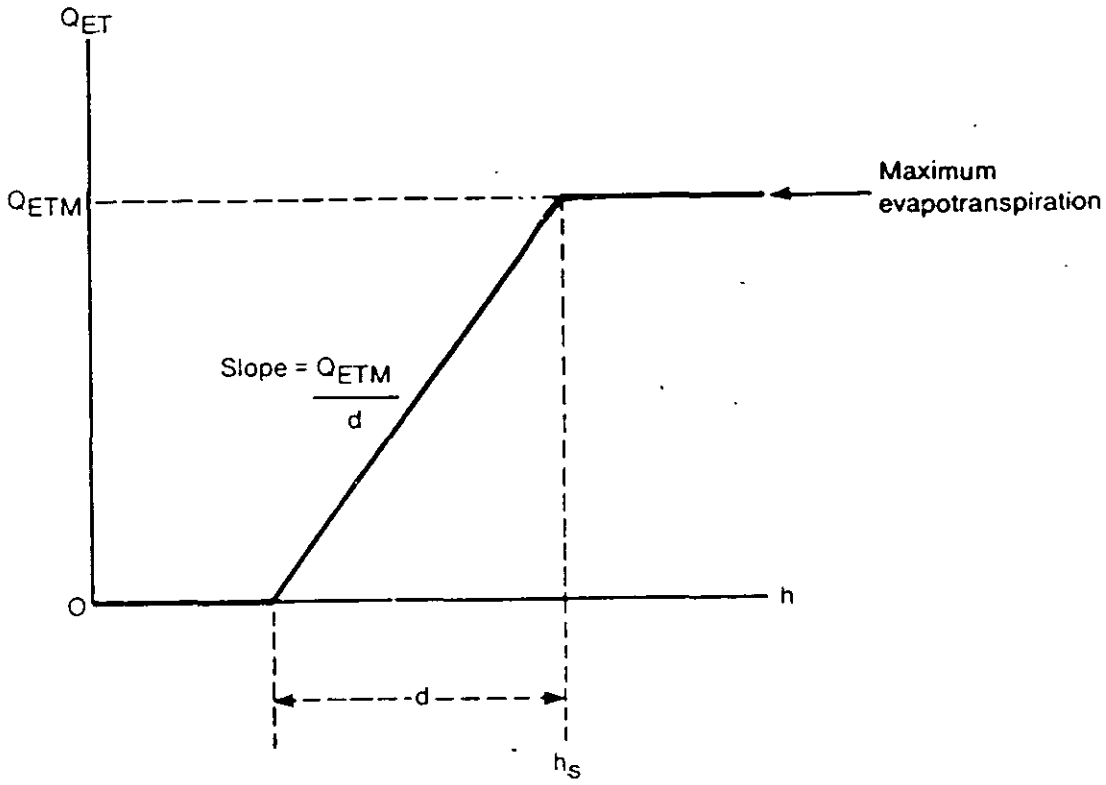

Figure 42.—Plot of volumetric evapotranspiration, Q_{ET}, as a function of head, h, in a cell where d is the cutoff depth and h_s is the ET surface elevation.

PAQUETE DE CONTORNO GENERAL DE CARGA (GHB)

- Lee datos de contorno general de carga.
- Calcula los flujos .
- Añade términos a las ecuaciones de diferencias finitas.

- Condición de flujo dependiente de la carga .
- Función lineal .
- Similar al dren pero flujo puede ser + ó —

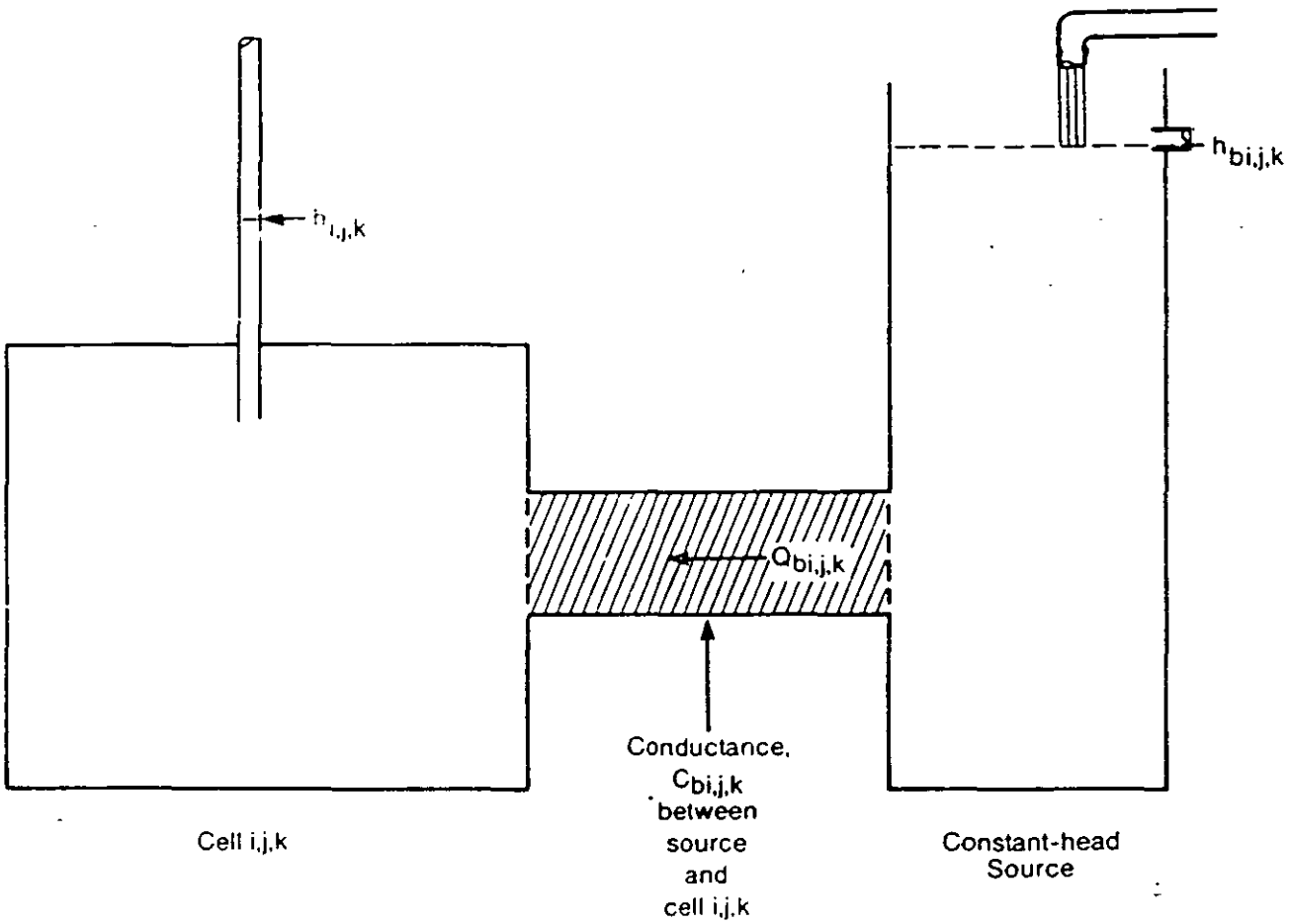

Figure 44.—Schematic diagram illustrating principle of general-head boundary package.

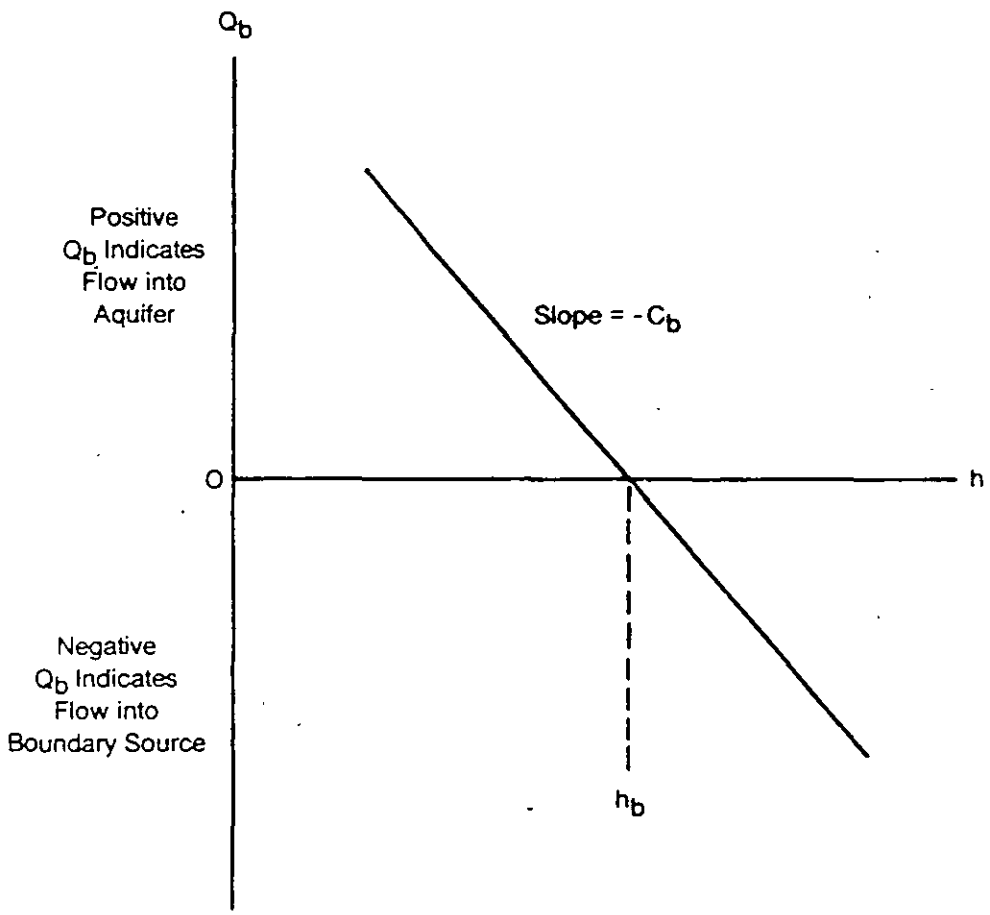

Figure 45.—Plot of flow, Q_b, from a general-head boundary source into a cell as a function of head, h, in the cell where h_b is the source head.

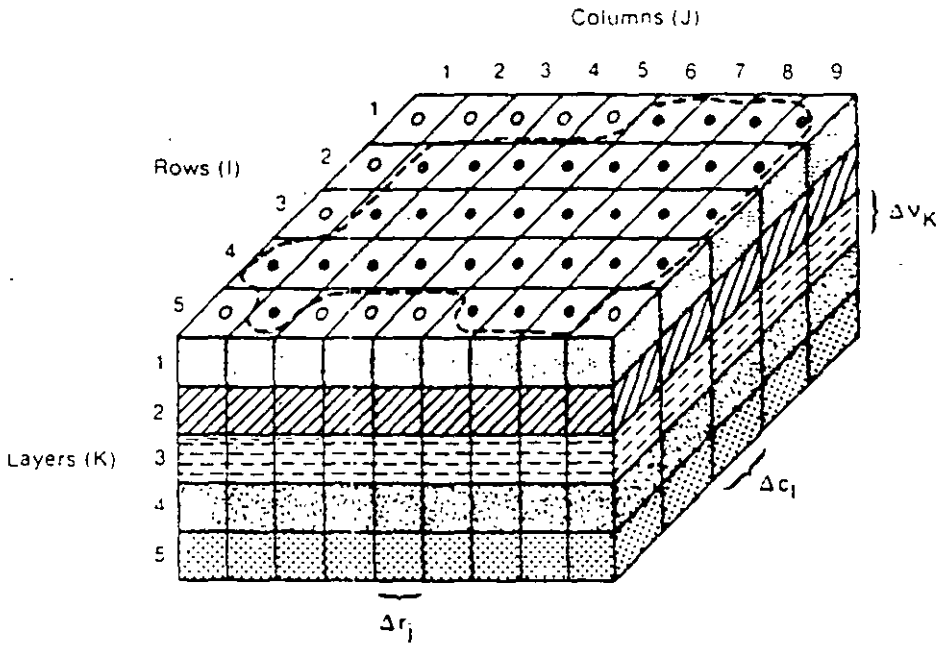

Explanation

---- Aquifer Boundary

• Active Cell

0 Inactive Cell

Δr_J Dimension of Cell Along the Row Direction. Subscript (J) Indicates the Number of the Column

Δc_I Dimension of Cell Along the Column Direction. Subscript (I) Indicates the Number of the Row

Δv_K Dimension of the Cell Along the Vertical Direction. Subscript (K) Indicates the Number of the Layer

Figure 1.—A discretized hypothetical aquifer system.

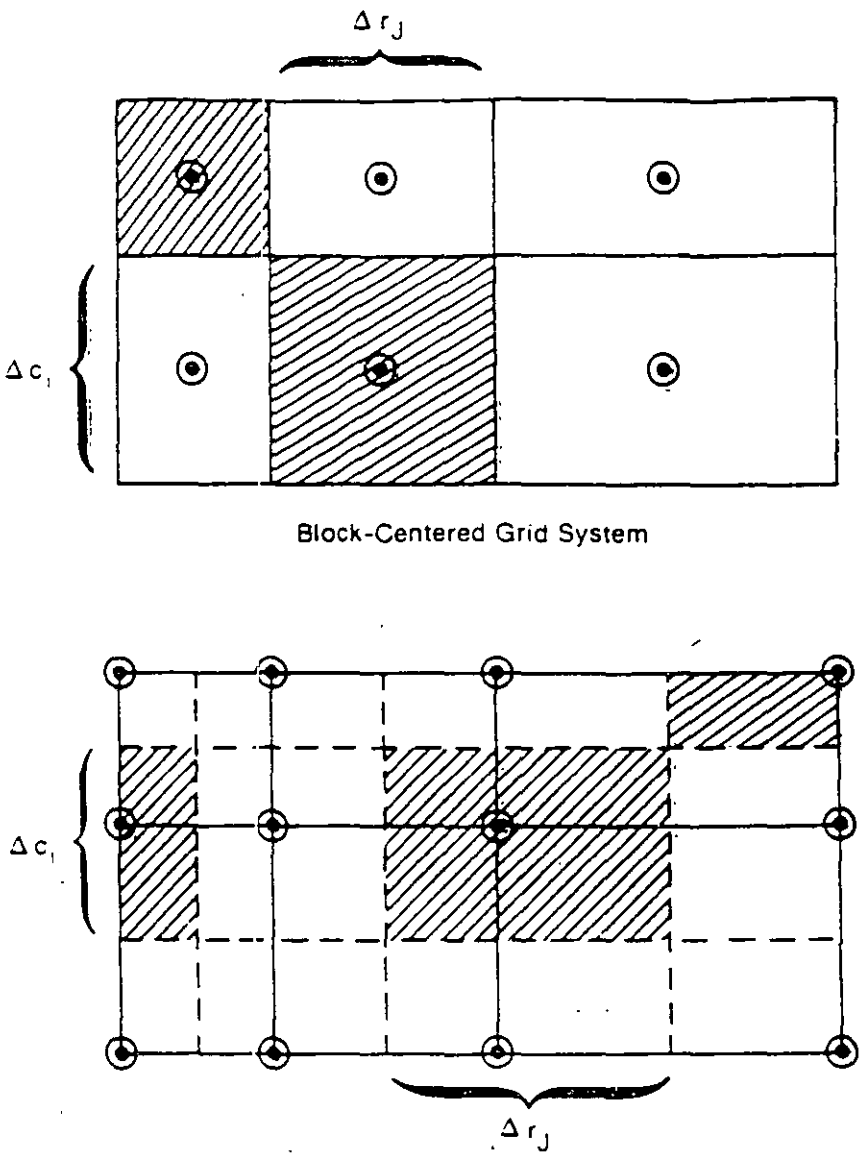

Figure 2.—Grids showing the difference between block-centered and point-centered grids.

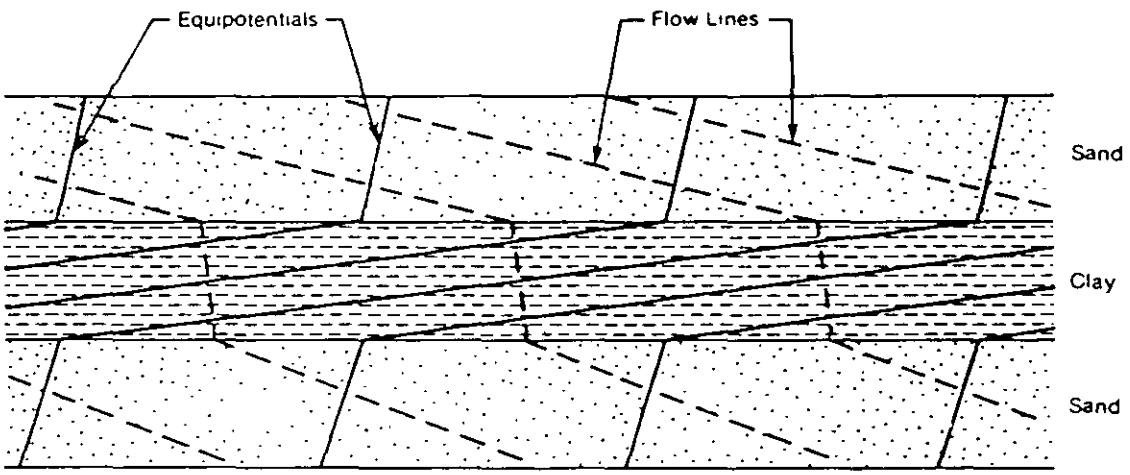

Figure 10.—Possible pattern of flow in a cross section consisting of two high conductivity units separated by a low conductivity unit.

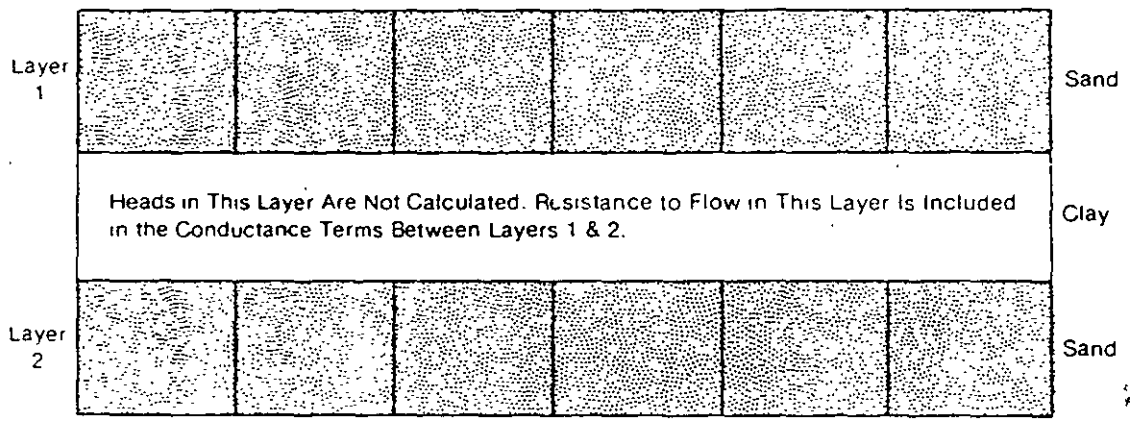

Figure 12 —A cross section in which a low conductivity unit is represented by the conductance between model layers.

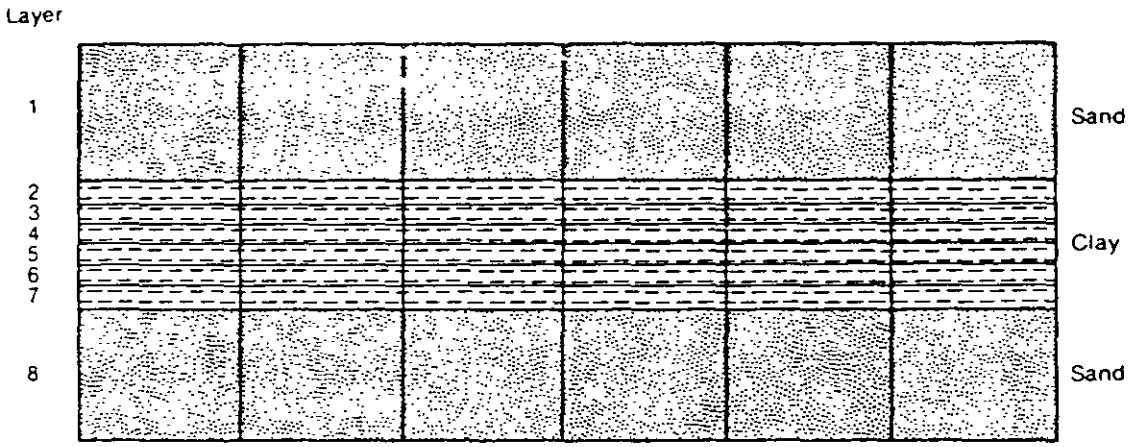

Figure 11.—A cross section in which a low conductivity unit is represented by six model layers.

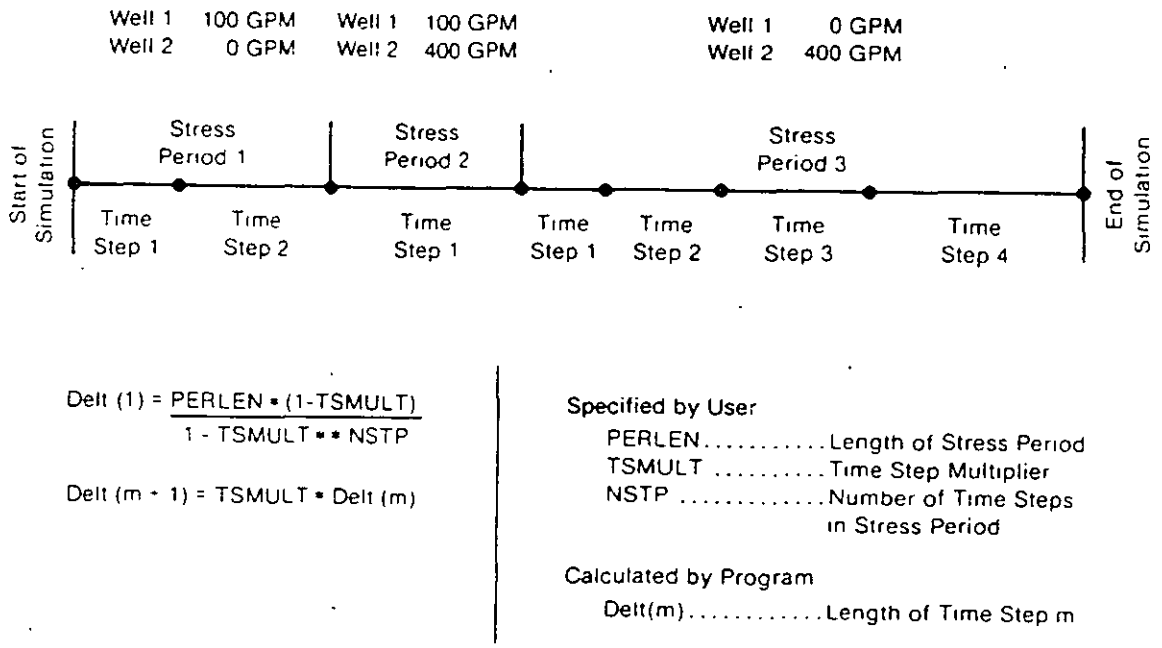

$$Delt(1) = \frac{PERLEN * (1-TSMULT)}{1 - TSMULT^{**} NSTP}$$

$$Delt(m+1) = TSMULT * Delt(m)$$

Specified by User

PERLEN.....Length of Stress Period
TSMULT .....Time Step Multiplier
NSTP .....Number of Time Steps in Stress Period

Calculated by Program

Delt(m).....Length of Time Step m

Figure 21.—Division of simulation time into stress periods and time steps.

```
          VOLUMETRIC BUDGET FOR ENTIRE MODEL AT END OF TIME STEP  1 IN STRESS PERIOD  1
          ------------------------------------------------------------------------------

CUMULATIVE VOLUMES      L**3                        RATES FOR THIS TIME STEP      L**3/T
------------------                                  ------------------------

      IN:                                                 IN:
      ---                                                 ---
        STORAGE =     .0                                    STORAGE =     .0
  CONSTANT HEAD =     .0                              CONSTANT HEAD =     .0
          WELLS =     .0                                      WELLS =     .0
         DRAINS =     .0                                     DRAINS =     .0
       RECHARGE =     .13608E+08                           RECHARGE =     157.50
       TOTAL IN =     .13608E+08                           TOTAL IN =     157.50
     OUT:                                                OUT:
     ----                                                ----
        STORAGE =     .0                                    STORAGE =     .0
  CONSTANT HEAD =     .43265E+07                      CONSTANT HEAD =     50.075
          WELLS =     .64800E+07                              WELLS =     75.000
         DRAINS =     .28010E+07                             DRAINS =     32.419
       RECHARGE =     .0                                   RECHARGE =     .0
      TOTAL OUT =     .13607E+08                          TOTAL OUT =     157.49
       IN - OUT =     303.00                               IN - OUT =     .34943E-02
PERCENT DISCREPANCY =                 0.00          PERCENT DISCREPANCY =                 0.00
```

Figure 22.--Sample overall volumetric water budget.

PROTOCOLO DE MODELACION

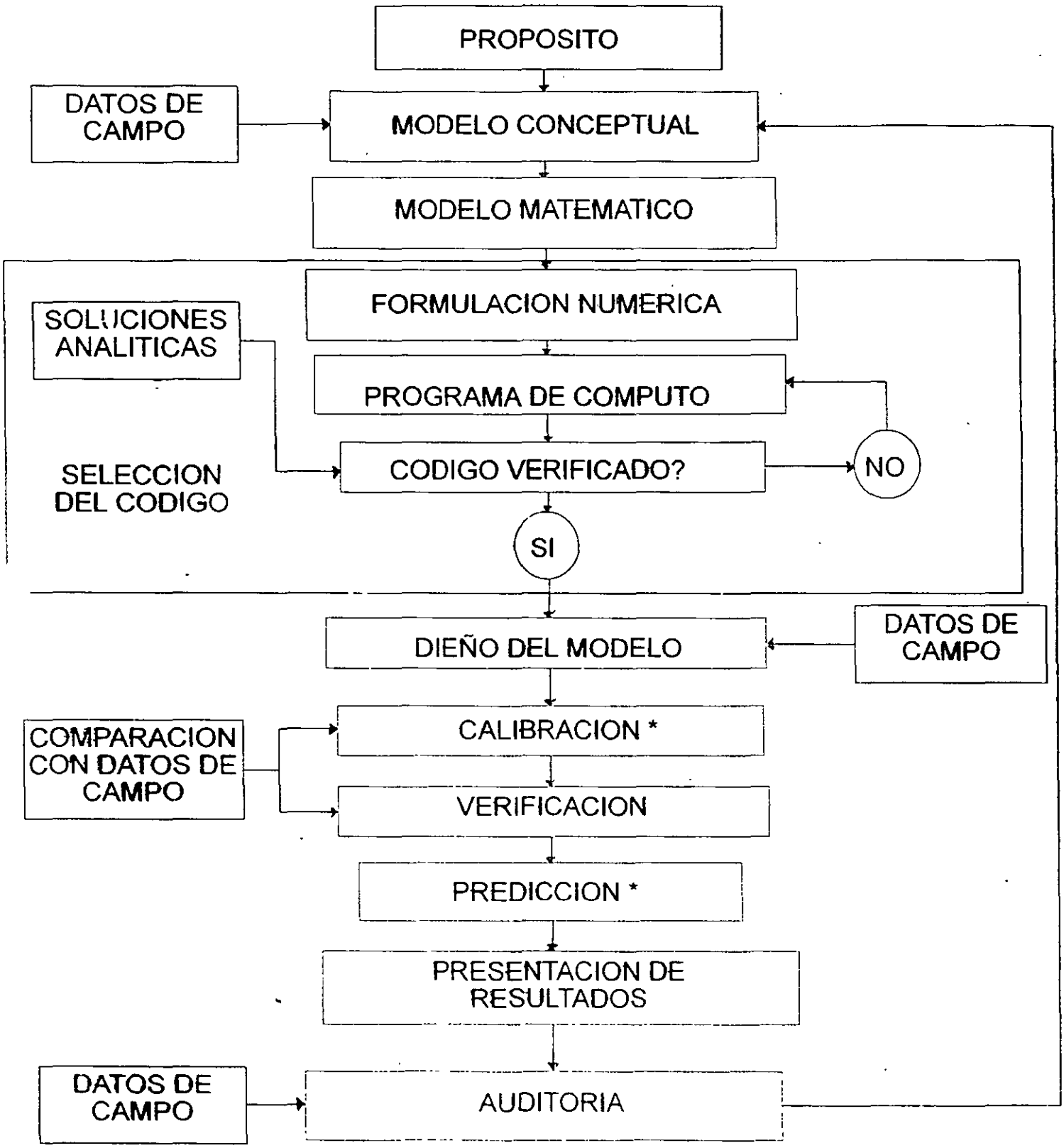

* INCLUYE ANALISIS DE SENSIBILIDAD

PROTOCOLO DE MODELACION

1. ESTABLECER EL PROPOSITO DEL MODELO.

* EL MODELO SERA CONSTRUIDO PARA PREDICCION, INTERPRETACION O ANALISIS GENERICO?

* QUE SE APRENDERA DEL MODELO?, A QUE INTERROGANTES RESPONDERA EL MODELO?

* ES EL MODELO LA MEJOR MANERA DE OBTENER RESPUESTA A NUESTRA INTERROGANTES?

* PUEDE UN MODELO ANALITICO PROPORCIONAR LA RESPUESTA O SE TIENE QUE CONSTRUIR UN MODELO NUMERICO?

DETERMINAR LA ECUACION GOBERNANTE

SELECCIONAR EL CODIGO DE COMPUTADORA

TIPOS DE MODELOS EN TERMINOS DE SU APLICACION

* **PREDICTIVO:** SE USA PARA PREDECIR EL FUTURO. REQUIERE CALIBRACION.

* **INTERPRETATIVO:** SE USA PARA ORGANIZAR Y SINTETIZAR LOS DATOS DE CAMPO, Y PARA ENTENDER MEJOR LA DINAMICA DE UN SISTEMA DE FLUJO. NO NECESARIAMENTE REQUIERE CALIBRACION.

* **GENERICO:** SE USA PARA ANALIZAR EL FLUJO EN SISTEMAS HIDROGEOLOGICOS HIPOTETICOS. PUEDEN SER UTILES PARA FINES DE NORMATIVIDAD DE UNA REGION ESPECIFICA. NO NECESARIAMENTE REQUIERE CALIBRACION.

2. DESARROLLO DE UN MODELO CONCEPTUAL DEL SISTEMA.

* IDENTIFICACION DE LAS UNIDADES HIDROESTRATIGRAFICAS Y LAS FRONTERAS DEL SISTEMA.

* ORGANIZACION DE LOS DATOS DE CAMPO. BALANCE HIDRICO, PARAMETROS DE ACUIFERO, ESFUERZOS HIDROLOGICOS.

* VISITA AL SITIO. INFLUENCIA POSITIVA SOBRE LAS DECISIONES SUBJETIVAS QUE SE TOMARAN DURANTE LA CONSTRUCCION DEL MODELO.

3. SELECCION DE LA ECUACION GOBERNANTE Y DE UN CODIGO DE COMPUTADORA.

* LA ECUACION GOBERNANTE DEBE DESCRIBIR CON PRECISION LOS PROCESOS FISICOS ACTUANTES EN EL SISTEMA. SE VERIFICA APLICANDO EL MODELO A VARIOS SITIOS ESPECIFICOS.

* LA VERIFICACION DEL CODIGO SE REFIERE A LA COMPARACION DE LA SOLUCION NUMERICA CON UNA O MAS SOLUCIONES ANALITICAS O CON OTRAS SOLUCIONES NUMERICAS.

* LA VERIFICACION DEL CODIGO ASEGURA QUE EL PROGRAMA DE COMPUTADORA RESUELVA CON PRECISION LAS ECUACIONES QUE CONSTITUYEN EL MODELO MATEMATICO.

4. DISEÑO DEL MODELO

EL MODELO CONCEPTUAL SE ACOMODA EN UNA FORMA ADECUADA PARA LA MODELACION.

INCLUYE:

* DISEÑO DE LA MALLA.

* SELECCION DE PERIODOS DE ESFUERZO.

* ESPECIFICACION DE CONDICIONES INICIALES Y DE FRONTERA.

* ESTIMACION PREVIA DE PARAMETROS DE ACUIFERO Y ESFUERZOS HIDROLOGICOS.

5. CALIBRACION

* SU PROPOSITO ES ESTABLECER QUE EL MODELO PUEDA REPRODUCIR LAS CARGAS Y LOS FLUJOS MEDIDOS EN CAMPO.

* SE OBTIENE UN CONJUNTO DE VALORES PARA LOS PARAMETROS DE ACUIFERO Y LOS ESFUERZOS HIDROLOGICOS QUE APROXIMA LAS CARGAS Y FLUJOS DE CAMPO.

* SE PUEDE EFECTUAR POR ENSAYOS Y ERROR O MEDIANTE CODIGOS AUTOMATIZADOS DE ESTIMACION DE PARAMETROS.

6. ANALISIS DE SENSIBILIDAD EN CALIBRACION

* EL MODELO CALIBRADO ESTA INFLUENCIADO POR LA "INCERTIDUMBRE" QUE SE DERIVA DE LA IMPOSIBILIDAD DE DEFINIR CON EXACTITUD LA DISTRIBUCION ESPACIAL (Y TEMPORAL) DE LOS VALORES DE LOS PARAMETROS, ESFUERZOS, Y CONDICIONES DE FRONTERA.

* SU PROPOSITO ES ESTABLECER EL EFECTO DE ESTA INCERTIDUMBRE SOBRE EL MODELO CALIBRADO.

7. VERIFICACION DEL MODELO

* SU PROPOSITO ES EL DE INCREMENTAR LA CONFIANZA EN EL MODELO, UTILIZANDO EL CONJUNTO DE VALORES CALIBRADOS DE LOS PARAMETROS Y DE LOS ESFUERZOS PARA REPRODUCIR UN SEGUNDO CONJUNTO DE DATOS DE CAMPO.

8. PREDICCION

* CUANTIFICA LA RESPUESTA DEL SISTEMA HACIA EVENTOS FUTUROS.

* SE CORRE EL MODELO CON VALORES CALIBRADOS DE LOS PARAMETROS Y LOS ESFUERZOS, CON EXCEPCION DE AQUELLOS QUE SE ESPERA QUE CAMBIEN EN EL FUTURO.

* LA INCERTIDUMBRE EN LA PREDICCION SE DERIVA DE LA INCERTIDUMBRE EN EL MODELO CALIBRADO Y DE LA IMPOSIBILIDAD DE ESTIMAR CON PRECISION LA OCURRENCIA Y MAGNITUD DE ESFUERZOS FUTUROS.

9. ANALISIS DE SENSIBILIDAD EN PREDICCION

* CUANTIFICA EL EFECTO DE LA INCERTIDUMBRE DE LOS VALORES DE LOS PARAMETROS SOBRE LA PREDICCION.

* SE SIMULAN LOS AMBITOS DE VARIACION DE ESFUERZOS FUTUROS ESTIMADOS PARA EXAMINAR SU IMPACTO EN LA PREDICCION.

10. PRESENTACION DE RESULTADOS

* LA PRESENTACION CLARA DEL DISEÑO DEL MODELO Y DE LOS RESULTADOS ES ESENCIAL PARA UNA COMUNICACION EFECTIVA DEL ESFUERZO DE MODELACION.

11. AUDITORIA

* LA AUDITORIA SE EFECTUA DESPUES DE VARIOS AÑOS DE CONCLUIDO EL ESTUDIO DE MODELACION.

* SE RECABAN NUEVOS DATOS DE CAMPO PARA DETERMINAR SI LA PREDICCION FUE CORRECTA. SI ASI LO ES, EL MODELO ESTA "VALIDADO" PARA EL SITIO ESPECIFICO DE APLICACION.

12. REDISEÑO DEL MODELO

LA AUDITORIA, POR LO GENERAL, APORTARA NUEVOS ELEMENTOS SOBRE EL COMPORTAMIENTO DEL SISTEMA, QUE PUEDEN LLEVAR A CAMBIOS EN EL MODELO CONCEPTUAL O EN LOS PARAMETROS DEL MODELO.

ENFOQUES CONCEPTUALES

ENFOQUE DE ACUIFERO:

* SE BASA EN EL CONCEPTO DE ACUIFEROS CONFINADOS Y LIBRES.

* SUPONE FLUJO HORIZONTAL EN ACUIFEROS Y FLUJO VERTICAL DE ACUITARDOS

* LA CONDUCTIVIDAD HIDRAULICA SE INTEGRA EN LA VERTICAL PARA OBTENER TRASMISIVIDAD.

* SE USA PARA SIMULAR FLUJO BIDIMENSIONAL DEN PLANTA Y FLUJO CUASI-TRIDIMENSIONAL.

* LAS CARGAS HIDRAULICAS SE CALCULAN EN LOS ACUIFEROS, PERO NO EN LOS ACUITARDOS.

* SE INCORPORA EL ESPESOR Y LA CONDUCTIVIDAD HIDRAULICA DE LOS ACUITARDOS PARA CONECTAR LOS ACUIFEROS.

ENFOQUE DE ACUIFERO

ECUACION GOBERNANTE:

$$\frac{\delta}{\delta x}\left[Tx\ \frac{\delta h}{\delta x}\right] + \frac{\delta}{\delta y}\left[Ty\ \frac{\delta h}{\delta y}\right] = S\ \frac{\delta h}{\delta t} - R + L$$

DONDE:

h: CARGA HIDRAULICA, [m]

T: TRASMISIVIDAD, [m²/día]

S: COEFICIENTE DE ALMACENAMIENTO, [---]

R: RECARGA (+) O DESCARGA (-) , [m/día]

L: GOTEO VERTICAL, [m/día], DADO POR:

$$L = -K'_z\ \frac{h_s - h}{b'}$$

DONDE:

K'_s: CONDUCTIVIDAD HIDRAULICA DE ACUITARDO, [m /día]

b': ESPESOR DEL ACUITARDO, [m]

h_s: CARGA HIDRAULICA DE LA FUENTE AL OTRO LADO DEL ACUIFERO, [m]

ENFOQUE DE ACUIFERO

SI EL ACUIFERO ES LIBRE:

* SE UTILIZAN LAS HIPOTESIS DE DUPUIT.

* $T_x=K_xH$ y $T_y=K_yh$, DONDE **K** ES CONDUCTIVIDAD HIDRAULICA Y **h** EL ESPESOR SATURADO DEL ACUIFERO.

* **S** ES EL RENDIMIENTO ESPECIFICO.

* **L** ES CERO, A MENOS QUE HAYA UNA FUENTE SUBYACIENDO AL ACUIFERO.

ENFOQUE DE SISTEMA DE FLUJO

* NO ES IMPORTANTE IDENTIFICAR LOS ACUIFEROS Y LOS ACUITARDOS "PER SE", SINO CONSTRUIR LA DISTRIBUCION TRIDIMENSIONAL DE LAS CARGAS, LAS CONDUCTIVIDADES HIDRAULICAS Y LAS PROPIEDADES DE ALMACENAMIENTO.

* SE INCORPORAN LAS COMPONENTES HORIZONTALES Y VERTICALES DE FLUJO A TRAVES DE TODO EL SISTEMA.

* APTO PARA MODELOS BIDIMENSIONALES EN PERFIL Y PARA MODELOS TRIDIMENSIONALES.

ENFOQUE DE SISTEMA DE FLUJO

ECUACION GOBERNANTE:

$$\frac{\delta}{\delta x}\left[Kx\ \frac{\delta h}{\delta x}\right] + \frac{\delta}{\delta y}\left[Ky\ \frac{\delta h}{\delta y}\right] + \frac{\delta}{\delta x}\left[Kz\ \frac{\delta h}{\delta z}\right] = Ss\ \frac{\delta h}{\delta t} - R^*$$

DONDE:

K: CONDUCTIVIDAD HIDRAULICA, [m /día]

Ss: ALMACENAMIENTO ESPECIFICO, [1/m]

R*: VOLUMEN DE INGRESO (+) O EGRESO (-) POR UNIDAD DE VOLUMEN Y UNIDAD DE TIEMPO, [1/día]

FINITE DIFFERENCE METHOD

The governing partial differential equation is

$$\frac{\partial}{\partial x}\left(T_x \frac{\partial h}{\partial x}\right) + \frac{\partial}{\partial y}\left(T_y \frac{\partial h}{\partial y}\right) = S \frac{\partial h}{\partial t}$$

The finite difference equivalent of this equation is derived by writing a mass balance expression for the rectangle $\Delta x \Delta y$ shown in Fig. 17:

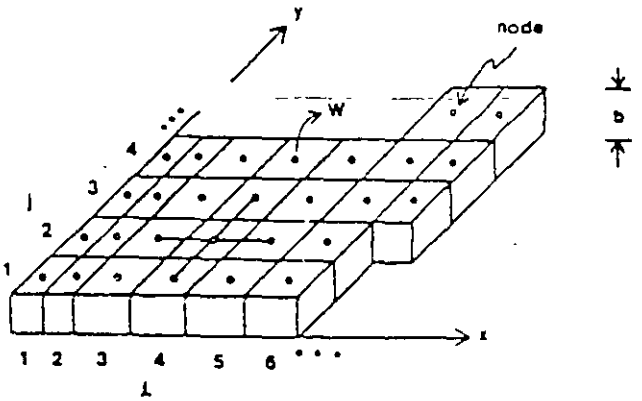

Fig. 17a. Finite-difference grid, showing typical node connections (modified after Freeze and Cherry, 1979).

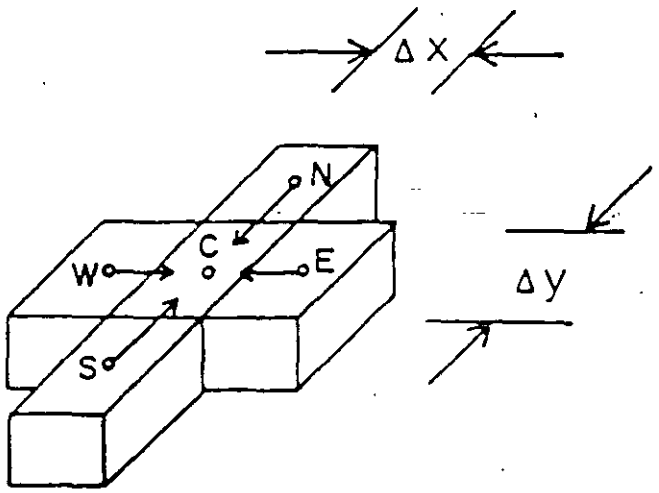

Fig. 17b. Water balance over a typical finite-difference block (modified after Freeze and Cherry, 1979).

$$T_y \frac{h_N - h_C}{\Delta y}\Delta x + T_y \frac{h_S - h_C}{\Delta y}\Delta x + T_x \frac{h_E - h_C}{\Delta x}\Delta y + T_x \frac{h_W - h_C}{\Delta x}\Delta y = S \frac{h_C^{k+1} - h_C^{k}}{\Delta t}\Delta x \Delta y$$

Net Inflow Rate = Net Accumulation Rate

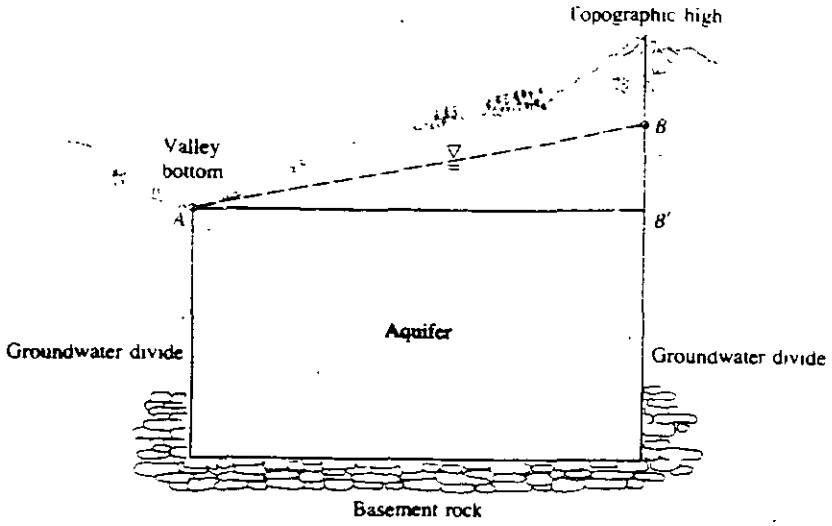

Figure 1.6
Schematic representation of the boundaries of a two-dimensional regional groundwater flow system.

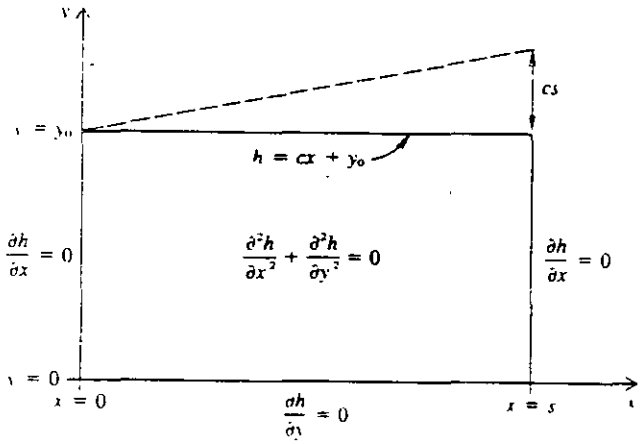

Figure 1.7
Mathematical model of the regional groundwater flow system shown in Figure 1.6

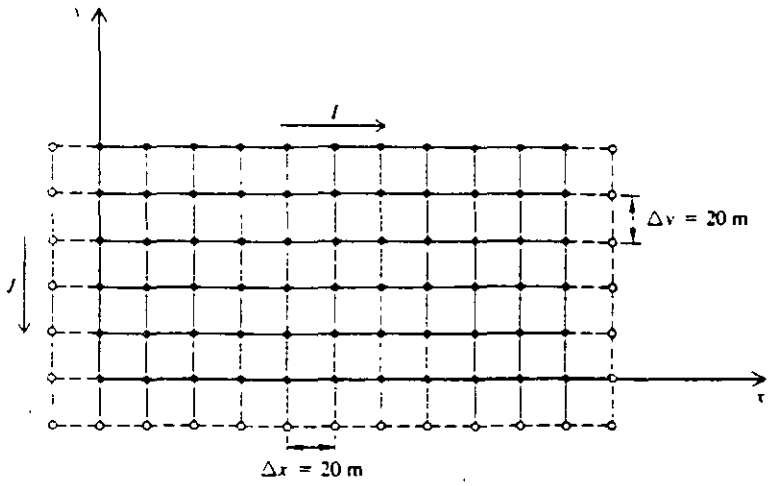

Figure 2.9
Finite difference grid for computer model of the regional groundwater flow example. Solid circles represent the problem domain of Figure 1.7. Open circles represent fictitious nodes used to specify no-flow boundary conditions. The fictitious node at the upper left-hand corner of the diagram represents $I = 1, J = 1$

Figure 2.10
Computer program for regional flow example using Gauss–Seidel iteration

```
1.      C   REGIONAL FLOW SYSTEM EXAMPLE
2.          DIMENSION H(13,7)
3.      C   INITIALIZE ALL H(I,J) VALUES TO BE 100.
4.          DO 5 J=1,7
5.          DO 5 I=1,13
6.          H(I,J) = 100.
7.      5   CONTINUE
8.      C   WATER TABLE BOUNDARY
9.          DX=20.
10.         DO 10 I=2,12
11.         H(I,1) = 0.02*DX*(I-2)+100.
12.     10  CONTINUE
13.     C   KEEP TRACK OF NUMBER OF ITERATIONS AND OF LARGEST ERROR
14.     C   NO-FLOW BOUNDARIES NEED TO BE RESET WITHIN EACH ITERATION LOOP
15.         NUMIT = 0
16.     35  AMAX = 0.
17.         NUMIT = NUMIT + 1
18.     C   LEFT AND RIGHT NO-FLOW BOUNDARIES
19.         DO 20 J=1,7
20.         H(1,J) = H(3,J)
21.         H(13,J) = H(11,J)
22.     20  CONTINUE
```

```
23.     C   BOTTOM NO-FLOW BOUNDARY
24.         DO 30 I=2,12
25.         H(I,7) = H(I,5)
26.     30  CONTINUE
27.     C   SWEEP INTERIOR POINTS WITH 5-POINT OPERATOR
28.         DO 40 J=2,6
29.         DO 40 I=2,12
30.         OLDVAL = H(I,J)
31.         H(I,J) = (H(I-1,J) + H(I+1,J) + H(I,J-1) + H(I,J+1))/4.
32.         ERR = ABS(H(I,J) - OLDVAL)
33.         IF(ERR.GT.AMAX) AMAX=ERR
34.     40  CONTINUE
35.     C   DO ANOTHER ITERATION IF LARGEST ERROR AFFECTS 3RD DECIMAL PLACE
36.         IF(AMAX.GT.0.001) GO TO 35
37.     C   WE ARE DONE.
38.         PRINT 50,NUMIT,((H(I,J),I=2,12),J=1,6)
39.     50  FORMAT(///1X,'NUMBER OF ITERATIONS IS',I4,///6(11F8.2///))
40.         STOP
41.         END
```

Figure 2.11
Output for regional flow example from the computer program in Figure 2.10. Output consists of values of head for nodes represented by solid circles in Figure 2.9; head values for fictitious nodes are not printed. Equipotential lines and flow paths can be drawn over the output.

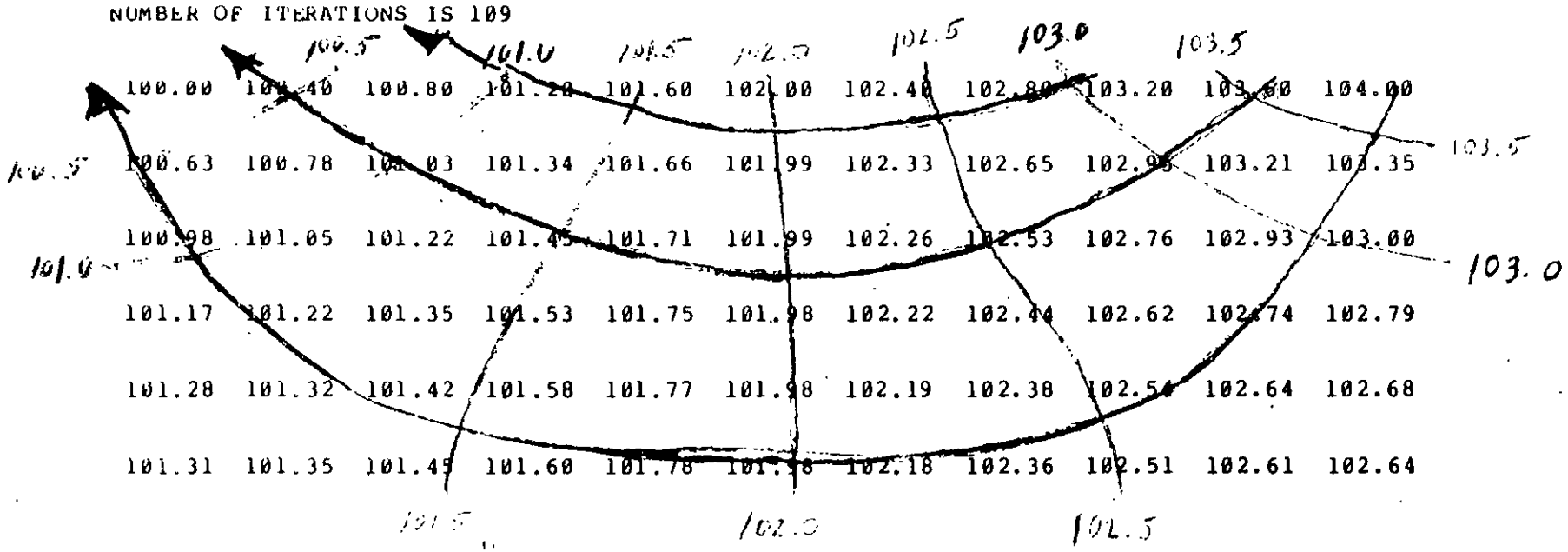

```
NUMBER OF ITERATIONS IS 109

100.00  100.40  100.80  101.20  101.60  102.00  102.40  102.80  103.20  103.60  104.00
100.63  100.78  101.03  101.34  101.66  101.99  102.33  102.65  102.93  103.21  103.35
100.98  101.05  101.22  101.45  101.71  101.99  102.26  102.53  102.76  102.93  103.00
101.17  101.22  101.35  101.53  101.75  101.98  102.22  102.44  102.62  102.74  102.79
101.28  101.32  101.42  101.58  101.77  101.98  102.19  102.38  102.54  102.64  102.68
101.31  101.35  101.45  101.60  101.78  101.98  102.18  102.36  102.51  102.61  102.64
```

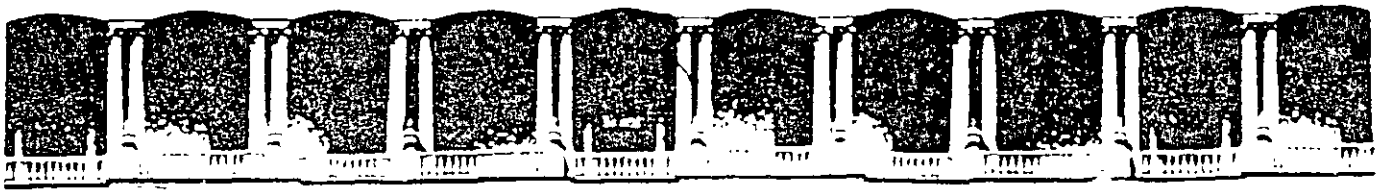

FACULTAD DE INGENIERIA U.N.A.M.
DIVISION DE EDUCACION CONTINUA
CURSOS ABIERTOS

XII CURSO INTERNACIONAL DE CONTAMINACIÓN DE ACUÍFEROS

MODULO III: MODELOS MATEMÁTICOS EN GEOHIDROLOGIA Y CONTAMINACIÓN DE ACUIFEROS

TEMA

AQUACHEN VER3.7

EXPOSITOR: M. EN C. LUIS ERNESTO LESSER CARRILLO
PALACIO DE MINERIA
OCTUBRE DEL 2000

M. en C. Luis E. Lesser
Octubre 2000

AquaChem Ver.3.7

AquaChem es un programa de visualización gráfica de resultados geoquímicos. AquaChem también cuenta con ina interace para correr el programa de especiación PHREEQC. Este programa calcula indices de saturación y modela la disolución/precipitación de minerales en agua.

Varios programas de saturación y especiación, incluyendo PHREEQC y WATEQF4 son de dominio público y pueden ser obtenidos sin costo alguno del web de la USGS (http://water.usgs.gov/).

Ejercicio 1:

🖱🖱 en el ícono de AquaChem

🖱 cancel (en la venatna que aparece).

🖱 File (del menú superior)

🖱 New

llame al nuevo trabajo: Ejercicio 1

y 🖱 en Save

En la ventana que aparece seleccionar la opción superior "Copy an existing data base template", y 🖱 en el ícono derecho que tiene los puntos suspensivos. Dar un 🖱 en el archivo DEMO.MSK

🖱 Open

🖱 OK

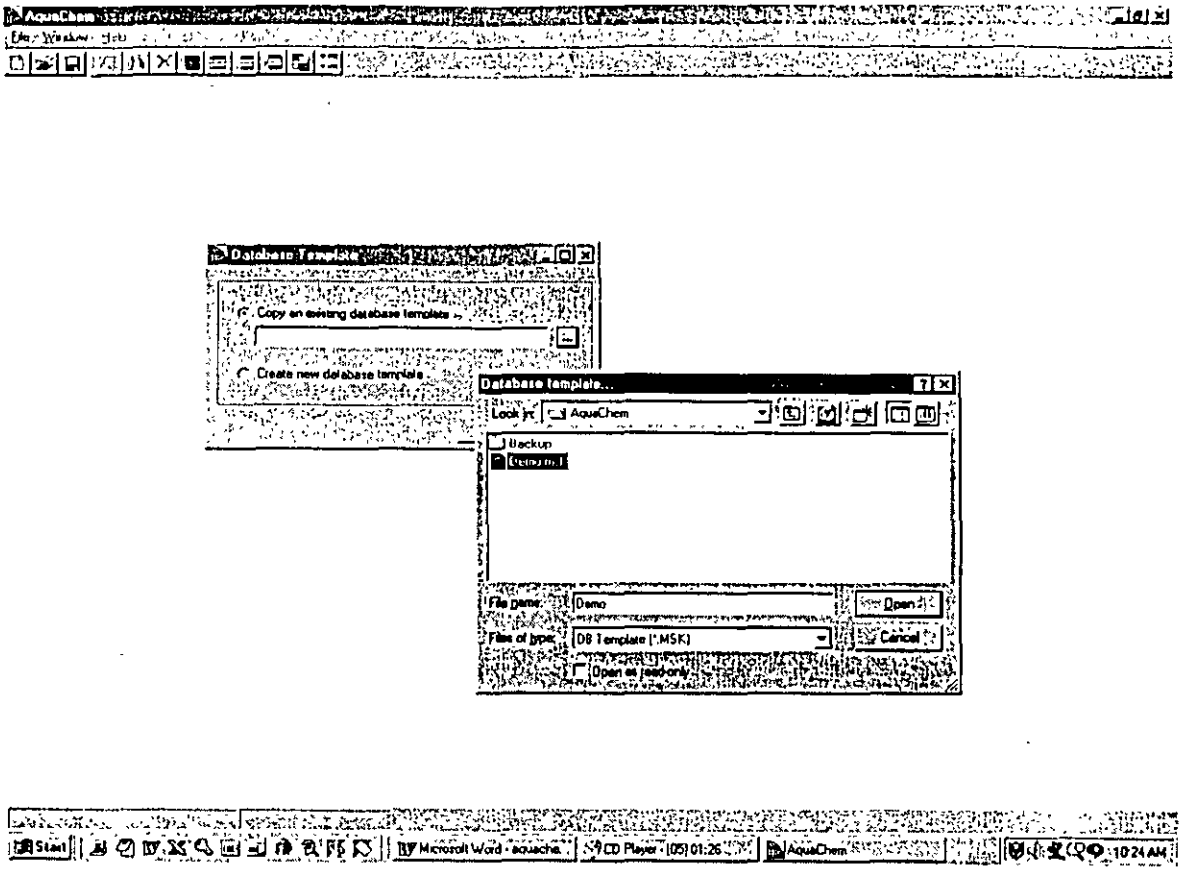

- Records (del menú superior)
- New

Llenar la tabla que aparece con la información que aparece en la siguiente página:

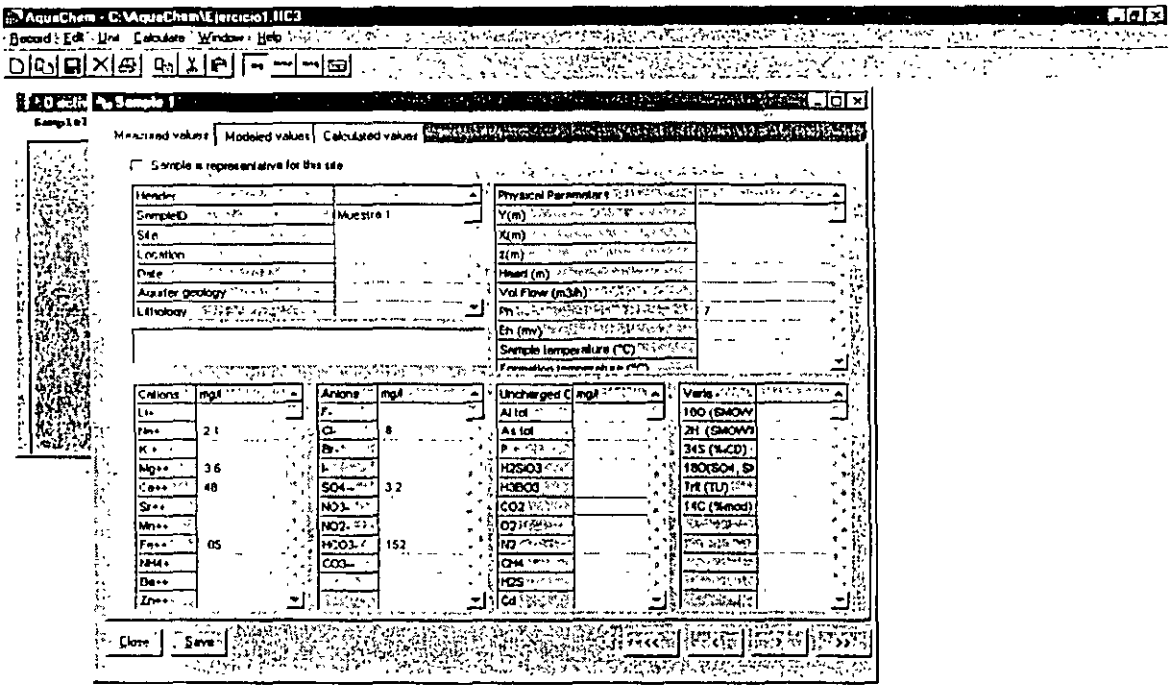

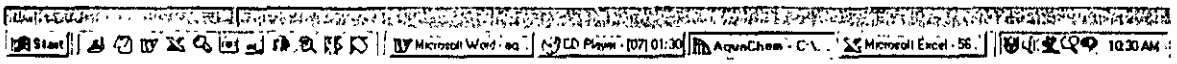

- SAVE (muy importante)
- Close

En la pantalla azul se verá el nombre de la muestra que se acaba de almacenar, y el tipo de agua (cálcica-bicarbonatada).

De la misma manera capture las muestras que aparecen en la siguiente tabla. Note que no es necesario cerrar la tabla (Close) entre muestras, pero se debe de salvar cada muestra (SAVE).

Muestra #	Ca^{+2} mg/L	Mg^{+2} mg/L	Na^{+} mg/L	K^{+} mg/L	HCO_3^{-} mg/L	SO_4^{-2} mg/L	Cl^{-} mg/L	NO_3^{-} mg/L	Fe mg/L	pH
1	48	3.6	2.1		152	3.2	8		0.05	7
2	144	55	29		622	60	53	0.3		7.4
3	182	93	258		157	132	538	5		7.1
4	40	22	0.4	1.2	213	4.9	2	4.8	0.24	6.5
5	140	43	21		241	215	38	4.1	0.01	6.8
6	3	7.4	359	2.4	950	1.6	71	0.2	0.15	6.8
7	12	50	150	8	456	58	17	1.9	0.4	7.2
8	120	115	413	4	355	73	1200	4	0.01	7.8

Debe de notarse que estos datos están en mg/L. Tambien se pueden dar los datos en mmol/L o mEq/L, solo hay que seleccionar el ícono correspondiente. Para una muestra a la que ya se lan dado los datos, al escoger otras unidades se transformarán los datos a las unidades seleccionadas.

Para ver las diferentes representaciones gráficas:

- Graphics (del menú superior)
- New

aparecerán las distintas opciones gráficas con que AquaChem cuenta, incluso las que por falta de datos no puedan representarse. Las gráficas mas comunes en hidrogeología son: Piper, Stiff y Schoeller.

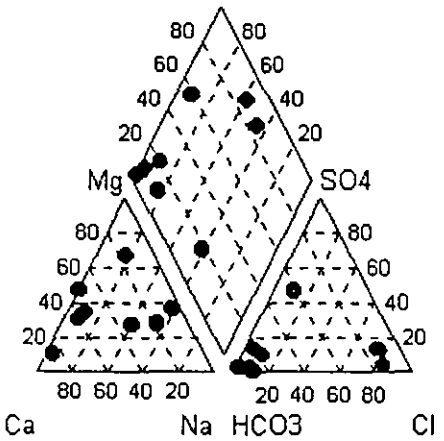

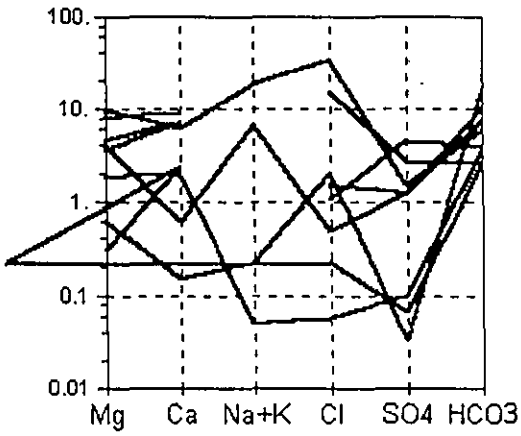

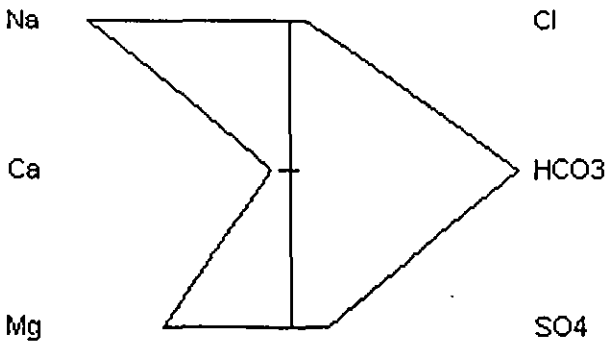

Antes de ver cada gráfica aparece una ventana como la siguiente en el caso de la gráfica de Piper:

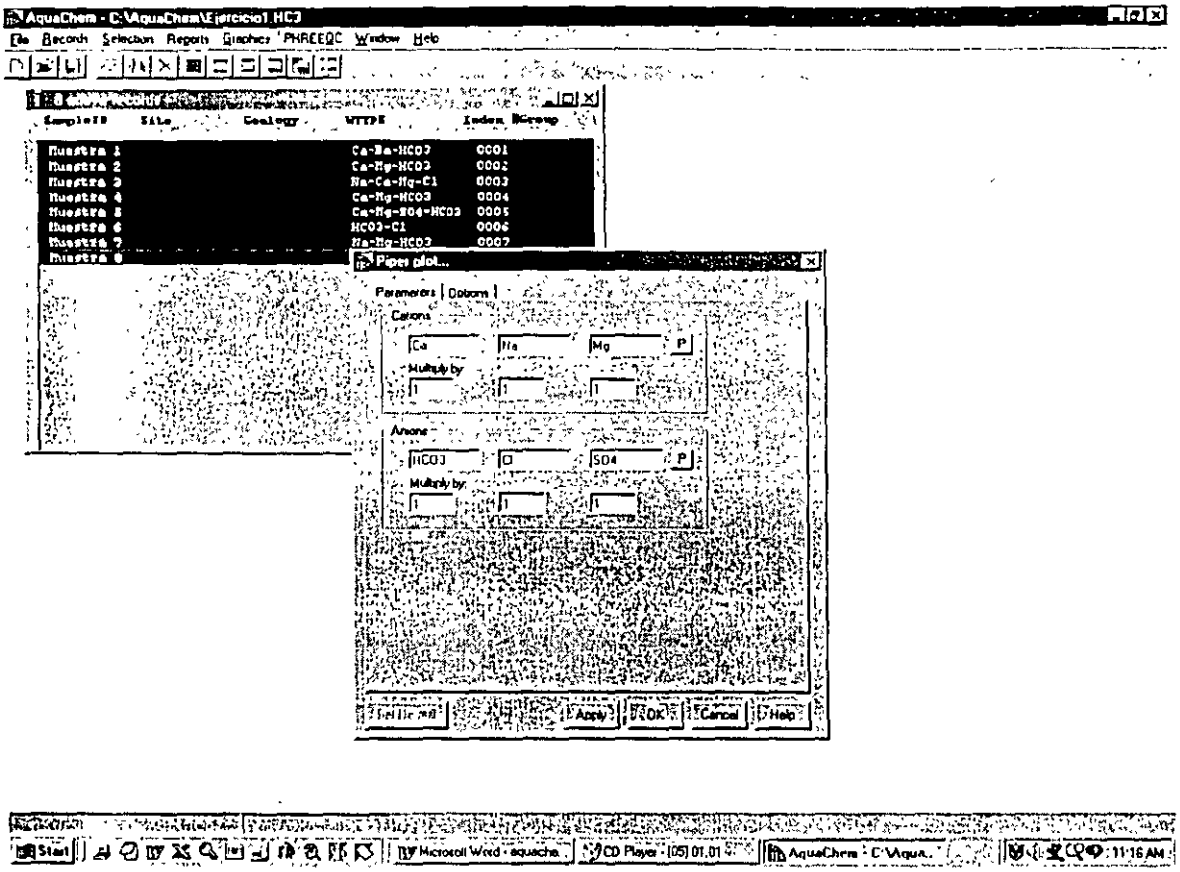

En estas ventanas se puede modificar, si se desean, los parámetros de cada gráfica, o los factores relativos para representarlos. Por lo general estas gráficas tienen por default los parámetros y valores mas comunmente usados.

OK

para ver la gráfica, o

Apply

si se hicieron cambios.

Para seleccionar una sola muestra en la muestra, y aparecera en un color azul marino. Para visualizar varias gráficas se pueden seleccionar varias muestras se puede utilizar <Shift> y en 2 muestras distintas, todas las muestras entre esas 2 serán seleccionadas. También se puede utilizar <CTRL> y en varias muestras distintas, todas las muestras en que se serán seleccionadas.

Para distinguir las muestras podemas asingnarles distintos simbolos:

🖱 en cualquier muestra de la ventana "active records"

🖱 *derecho* en la muestra

🖱 assign to symbol

escoger algun número/símbolo dando un 🖱

🖱 assign

🖱 close

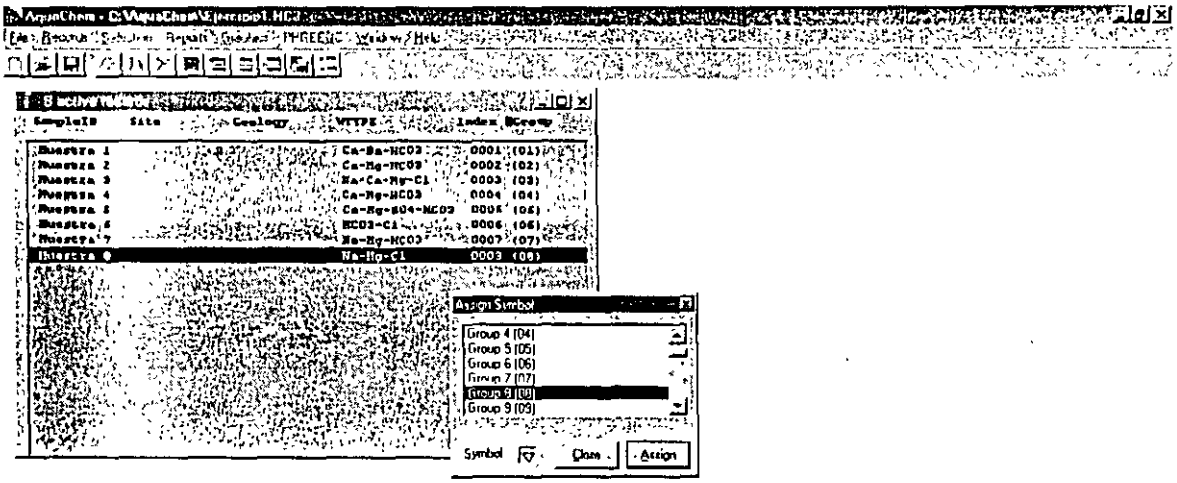

Hacer lo mismo con cada muestra y vuelva a ver el gráfico de Piper o el Ternary.

Para agregar una leyenda:

🖱 Graphics (del menú superior)

🖱 New

🖱 Piper

en la ventana 🖱 en la pestaña de "options".

Seleccionar "legend" haciendo un 🖱 en el recuadro

OK

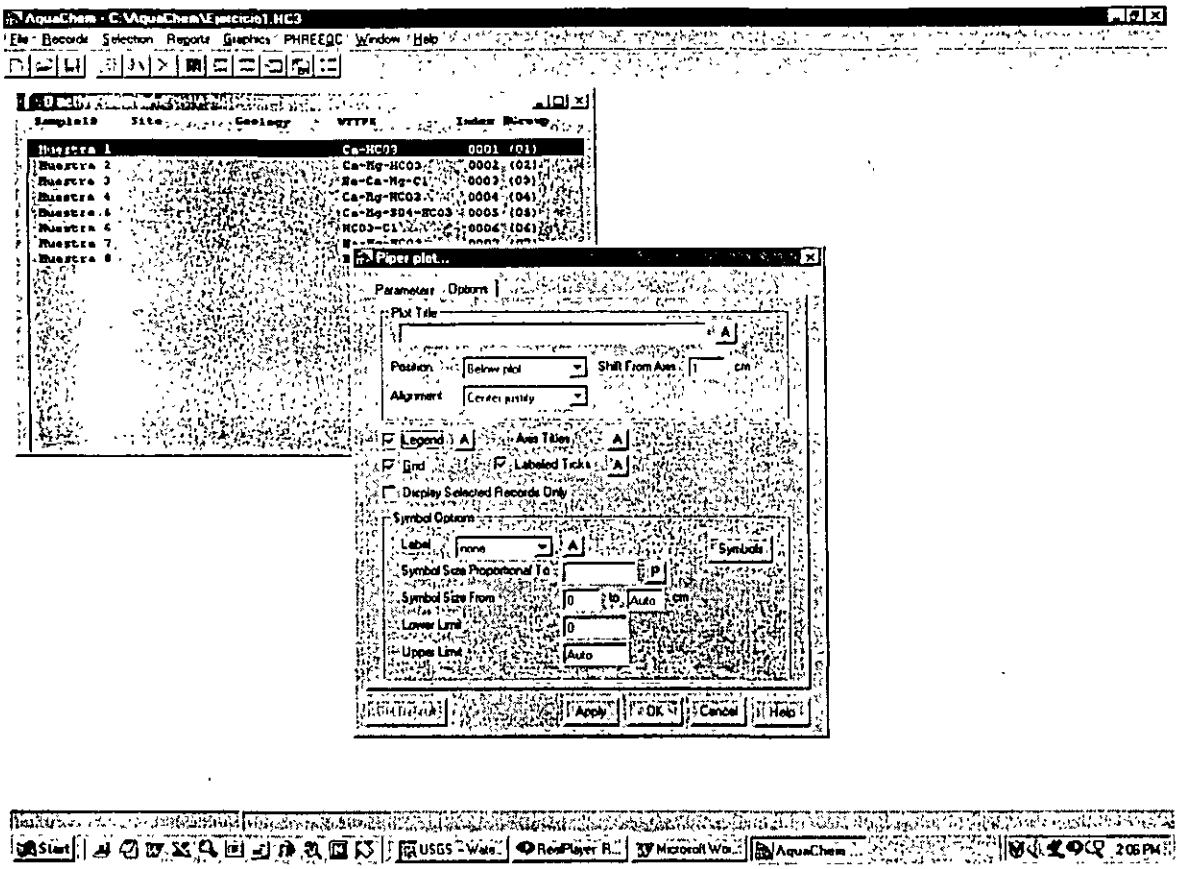

Nótese que se pueden asignar varias muestras al mismo grupo, si el propósito es separar 2 tipos de muestras

Para cambiar el tipo de línea para otros diagramas como el de Schoeller:

Graphics (del menú superior)

Define simbol or line

en la pestaña "conecting line"

aqui se pueden modificar los tipos de linea.

Haciendo uso de estas opciones, se pueden modificar las gráficas para darles el terminado deseado.

Para copiar las gráficas en reportes:

Edit (del menú superior)

Copy graph

Al hacer eso la gráfica se guarda en memoria. Si se abre Word, se puede pegar utilizando el comando 'Paste'.

Otros resultados que nos da este programa se pueden obtener:

Reports (del menú superior)

General

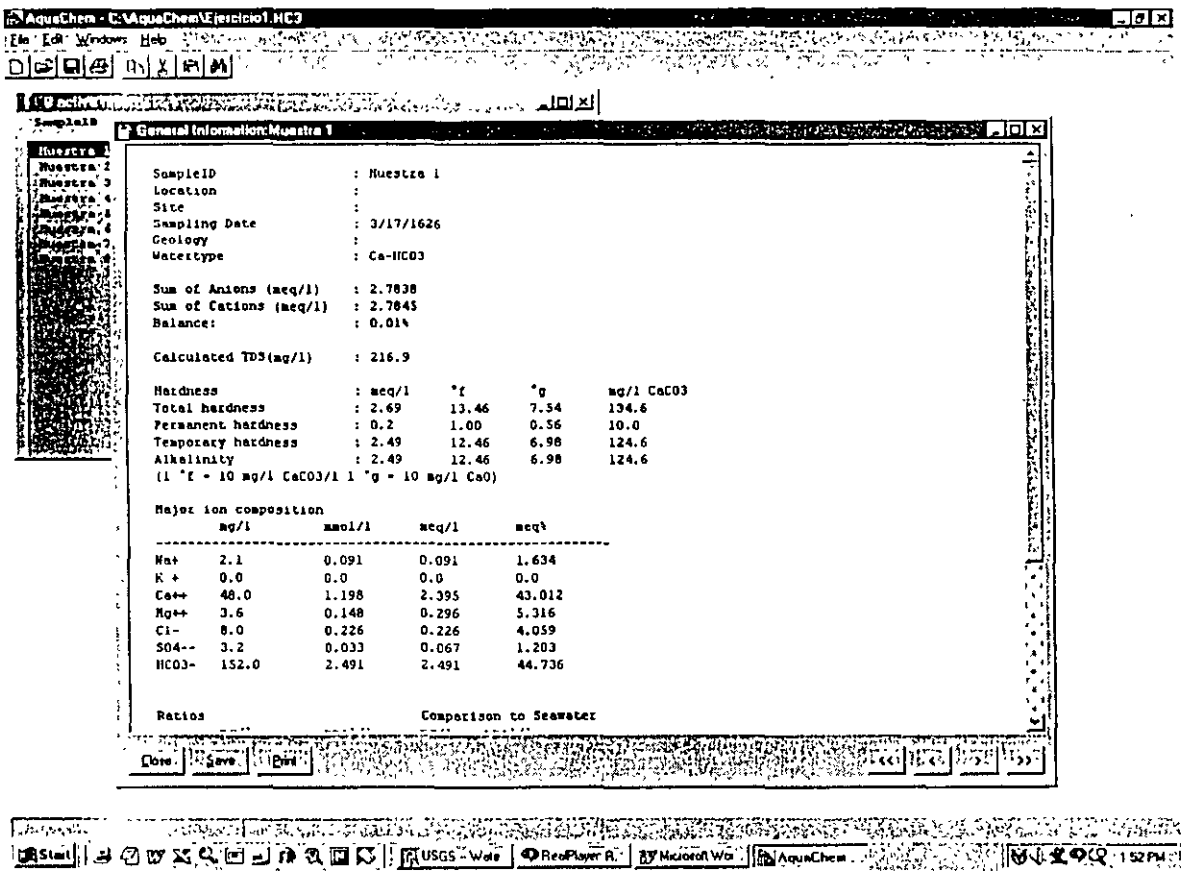

Aparece una ventana que da información general de las muestras. Incluyendo:

- un balance de cargas, por lo general este balance debe de ser menor de 5%
- Calculo de sólidos totales disueltos, dureza y alcalinidad
- Se da un resumen de los datos geoquímicos en distintas unidades

Resultados de otras muestras pueden obtenerse presionando los íconos [<] y [>]

Comparación de la calidad del agua con estándares de la World Health Organization (WHO) se puede obtener:

- Reports (del menú superior)
- Drinking Water Regulations

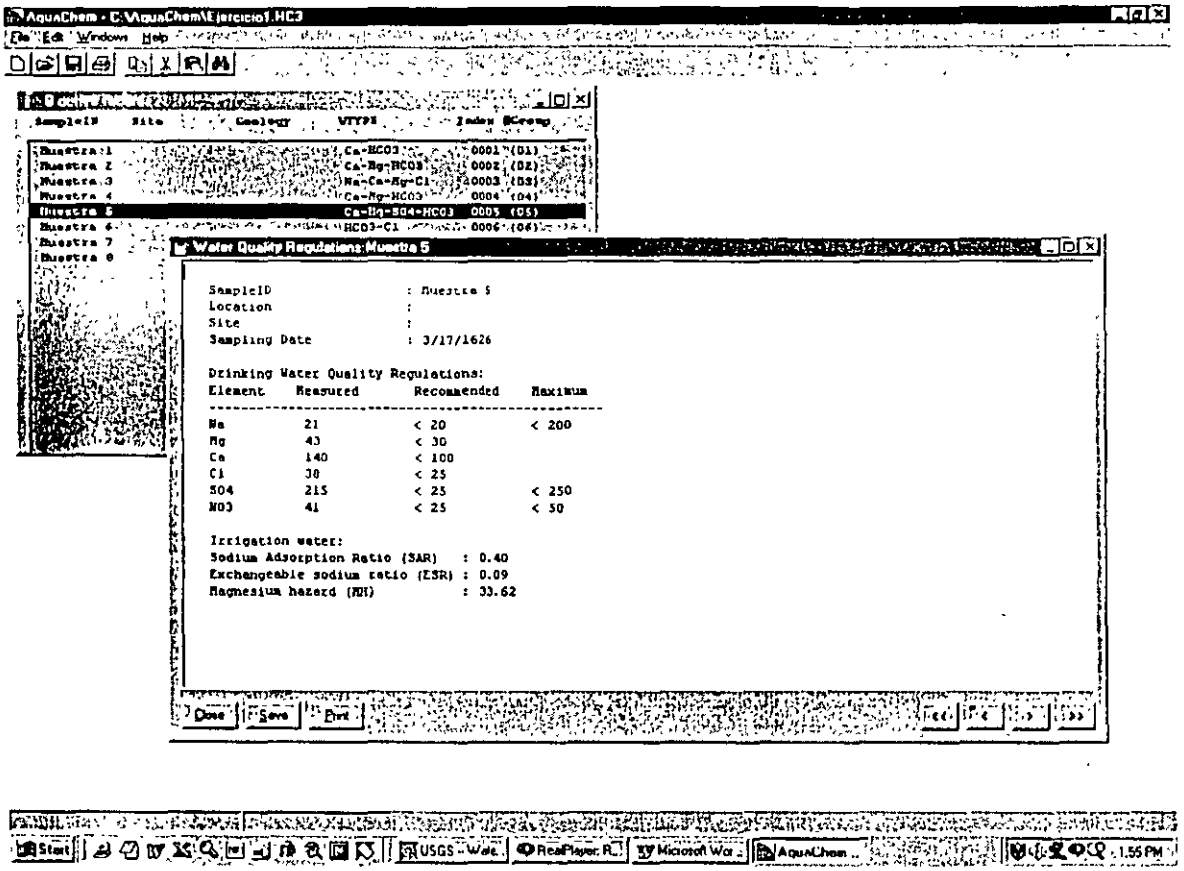

Esta tabla resalta únicamente los parámetros que estan fuera del rango sugerido por la (WHO).

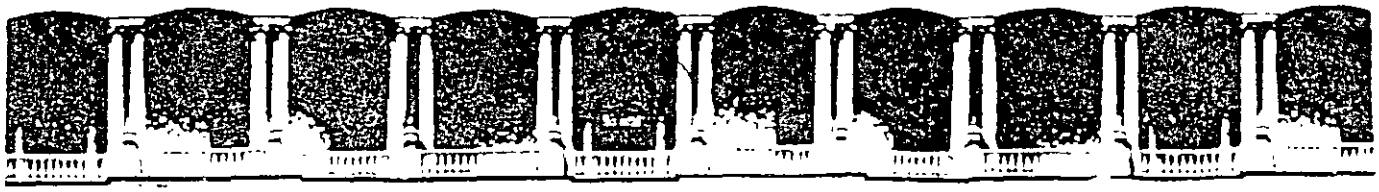

FACULTAD DE INGENIERIA U.N.A.M.
DIVISION DE EDUCACION CONTINUA
CURSOS ABIERTOS

XII CURSO INTERNACIONAL DE CONTAMINACIÓN DE ACUÍFEROS

MODULO III: MODELOS MATEMÁTICOS EN GEOHIDROLOGIA Y CONTAMINACIÓN DE ACUIFEROS

TEMA

EJERCICIO DE AQUIFERTEST VER3.0

EXPOSITOR: M. EN C. LUIS ERNESTO LESSER CARRILLO
PALACIO DE MINERIA
OCTUBRE DEL 2000

EJERCICIO DE AQUIFERTEST VER.3.0

EJERCICIO 1: Planeando una prueba de bombeo

Esta versión de Aquitest permite, además de interpretar los resultados provenientes de pruebas de bombeo. el planear la prueba antes de salir al campo. Esta capacidad de aquitest permite obtener sugerencias para los valores de caudal óptimo. la distancia óptima entre el pozo bombeado y los pozos de observación. Este ejercicio esta diseñado para aprender a obtener cual es el caudal necesario para la prueba de bombeo.

El proposito de este ejercicio es estimar el caudal necesario para producir una abatimiento minimo (2mm=0.002m) en un pozo de observación que está a 10 metros del pozo de bombeo, en los primeros 2 minùtos de la prueba de bombeo.

1. CREAR UN NUEVA BASE DE DATOS

- en el icono de Aquifer Test 3.0
- File (del menú superior)
- Create database...

En la ventana que aparece accesar el directorio **Exercises** y nombrar al archivo Ejercicio1, y en Save. Una venatan aparecera confirmando que la base de datos ha sido creada.

- OK

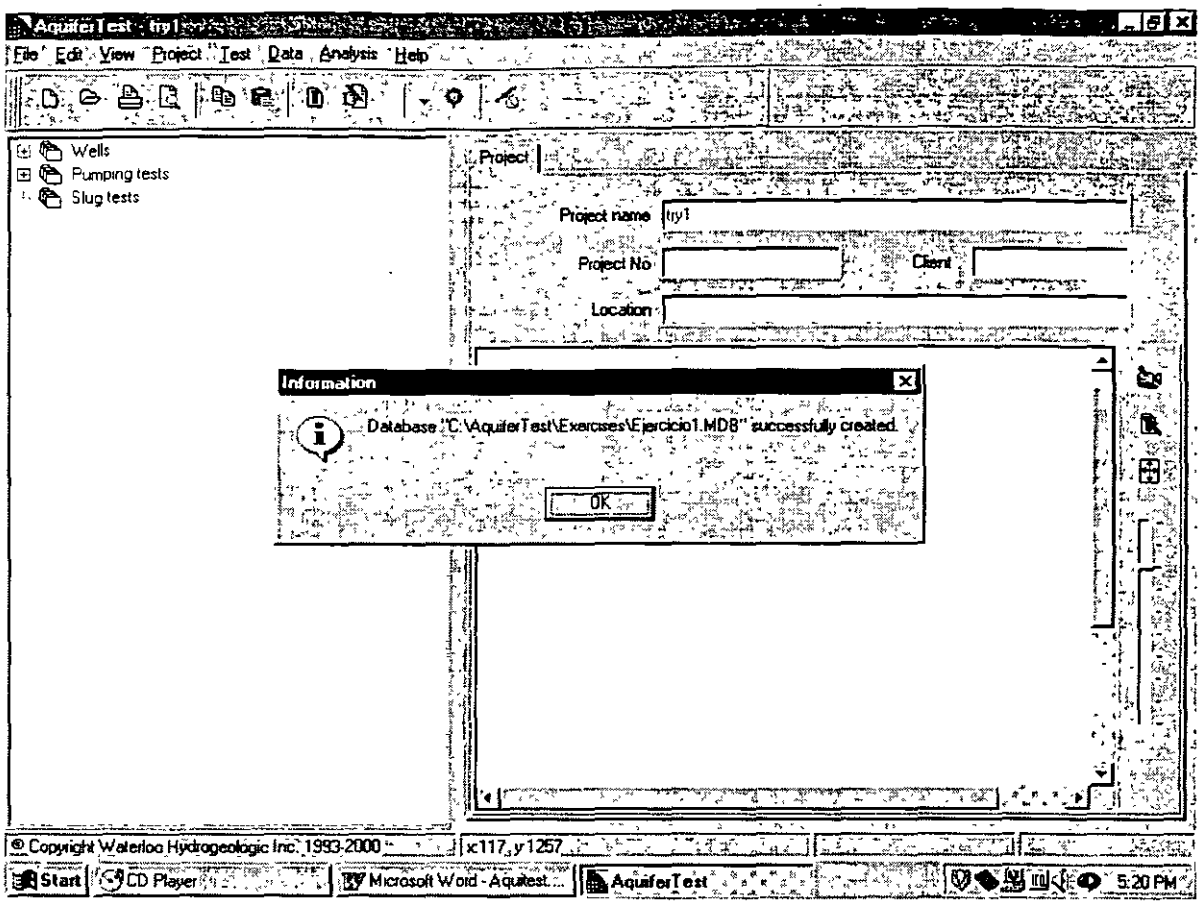

- File (del menú superior)
- Open project
- en el icono para abrir proyectos en la parte superior de la ventana

Seleccionar Ejercicio1 (el archivo que acaba de ser creado) y en Open

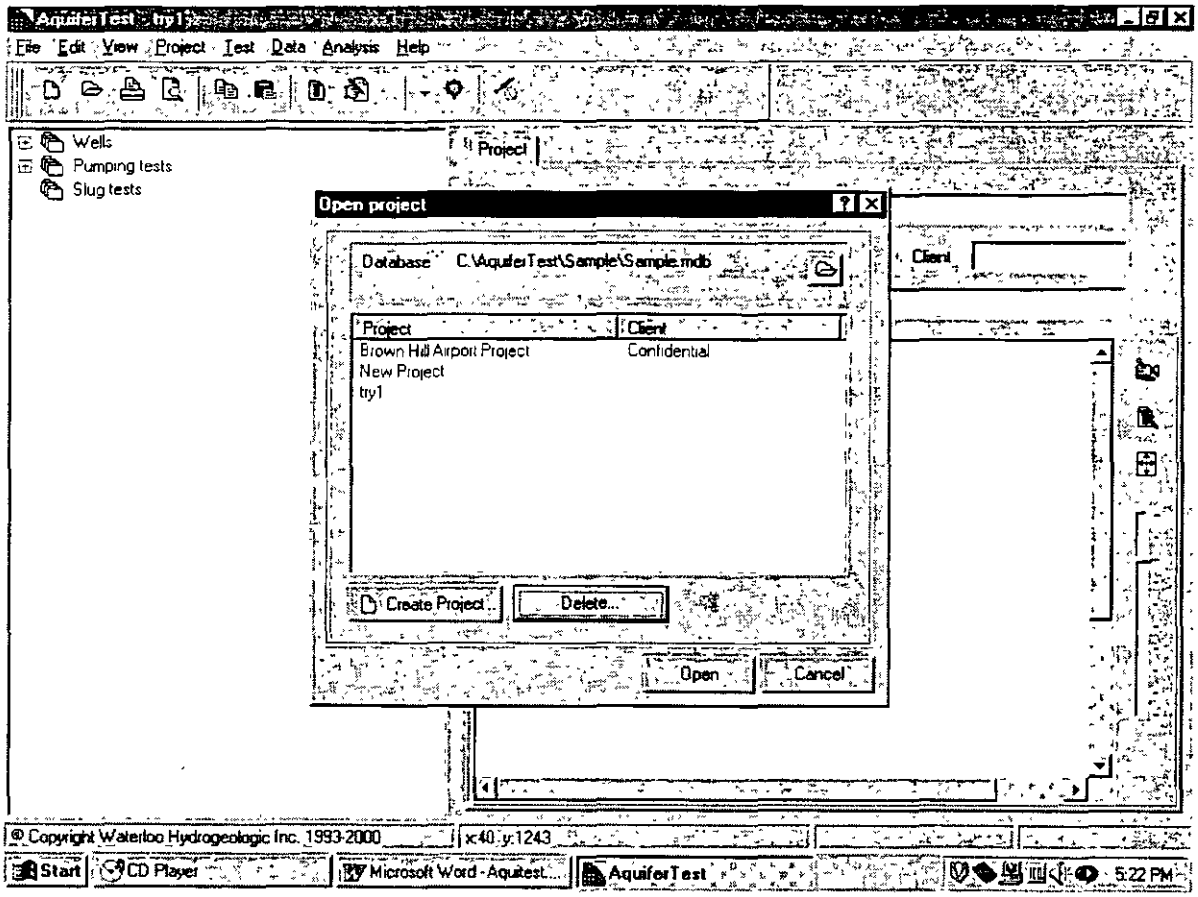

2. CREAR UN NUEVO PROYECTO

En la ventana que aparece, seleccionar

Create project

En el **project name** escriba: Planeacion prueba de bombeo y en OK

En la ventana anterior que aun seguira abierta, en **open**

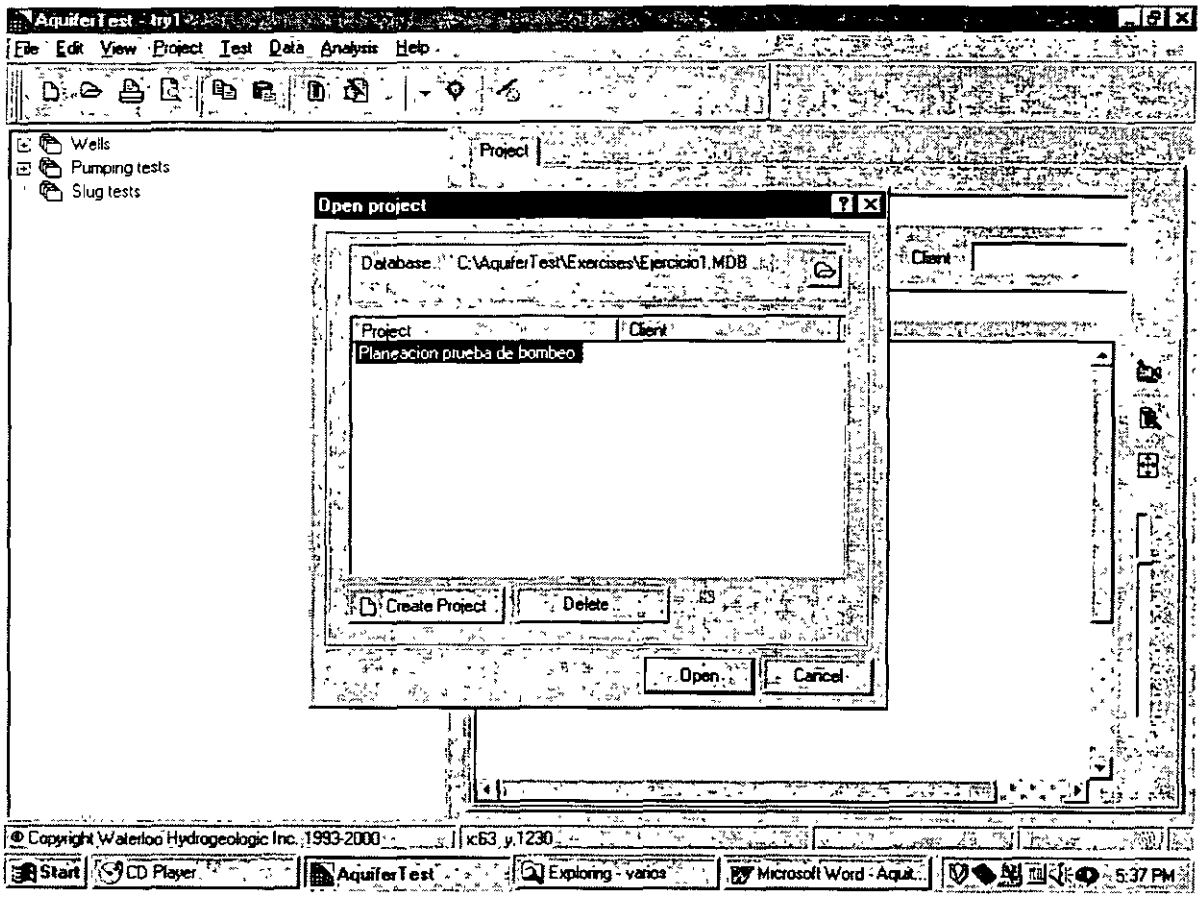

3. SELECCIÓN DEL SISTEMA DE UNIDADES PARA EL PROYECTO

- Project (del menú superior)
- Units...

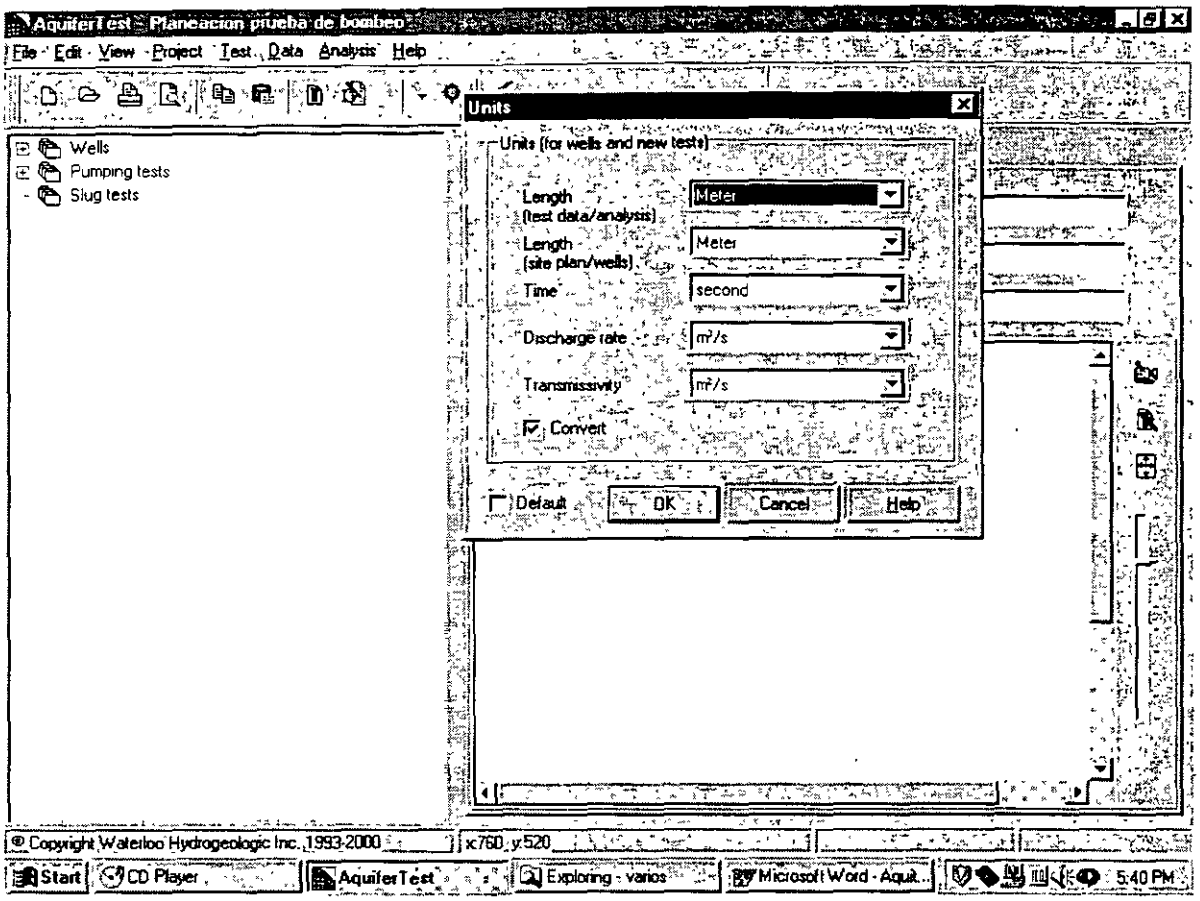

OK

3. CREAR UN NUEVO ANÁLISIS

En cualquier lugar del panel izquierdo (donde se encuentra el menú expandido) hacer un *derecho.* De la venatana que aparece escoger:

Expand all (para expander las opciones)

Analysis (cambiará de color)

derecho en Create Analysis

En las opciones que aparecen a la derecha escoger **Time vesrus Dradown plot** con un y aparecerá una figura como la que aparece en la siguiente página.

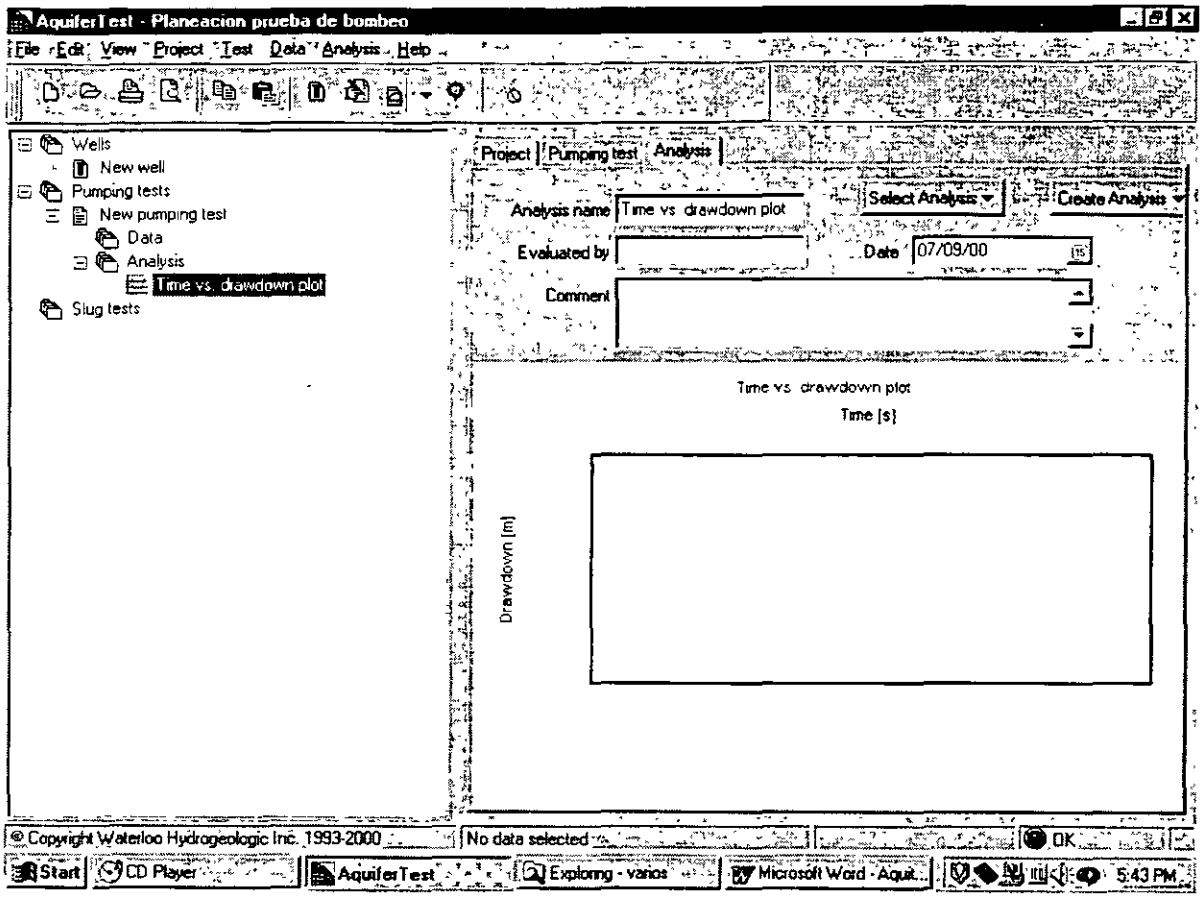

- Analysis (**del menú superior)**
- Method
- Predicted (Theis) (al final de la lista)

Por default, Aquifer Test mostrará una gráfica de abatimiento con tiempo a una distancia de 10 metros del pozo de bombeo.

Nótese que no se a introducido al modelo ningún tipo de infromacion de abatimiento respecto al tiempo para ver esta gráfica. Aquifer test crea una serie de datos "sintéticos" que corresponde al abatimiento característico por Theis.

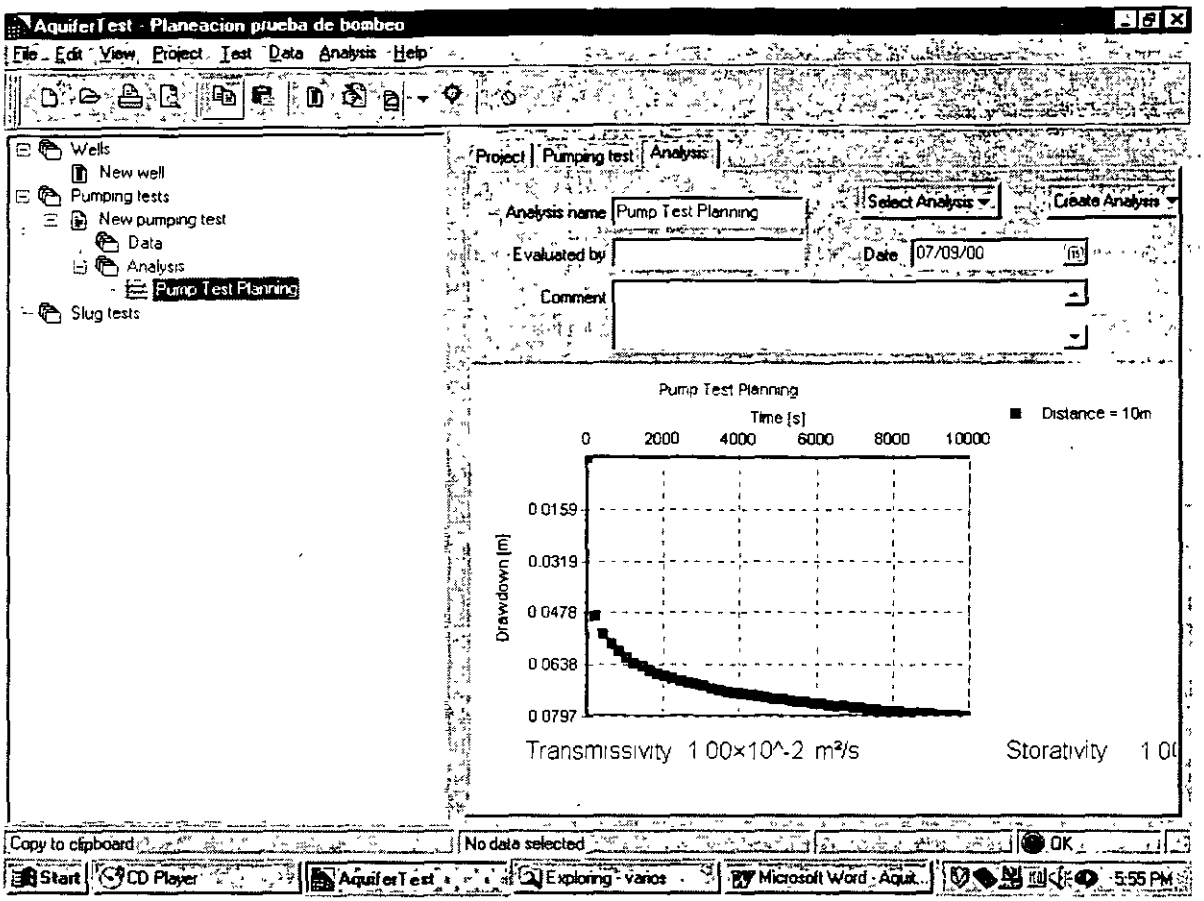

5. CAMBIANDO LAS CARACTERISTICAS DEL ANALISIS

Las caracteristicas para la predicción de Theis observada en la última figura pueden ser editados para permitir hacer una evaluación de los efectos que pueden resultar en la planación de una prueba de bombeo.

- *derecho* en cualquier lugar de la gráfica
- settings

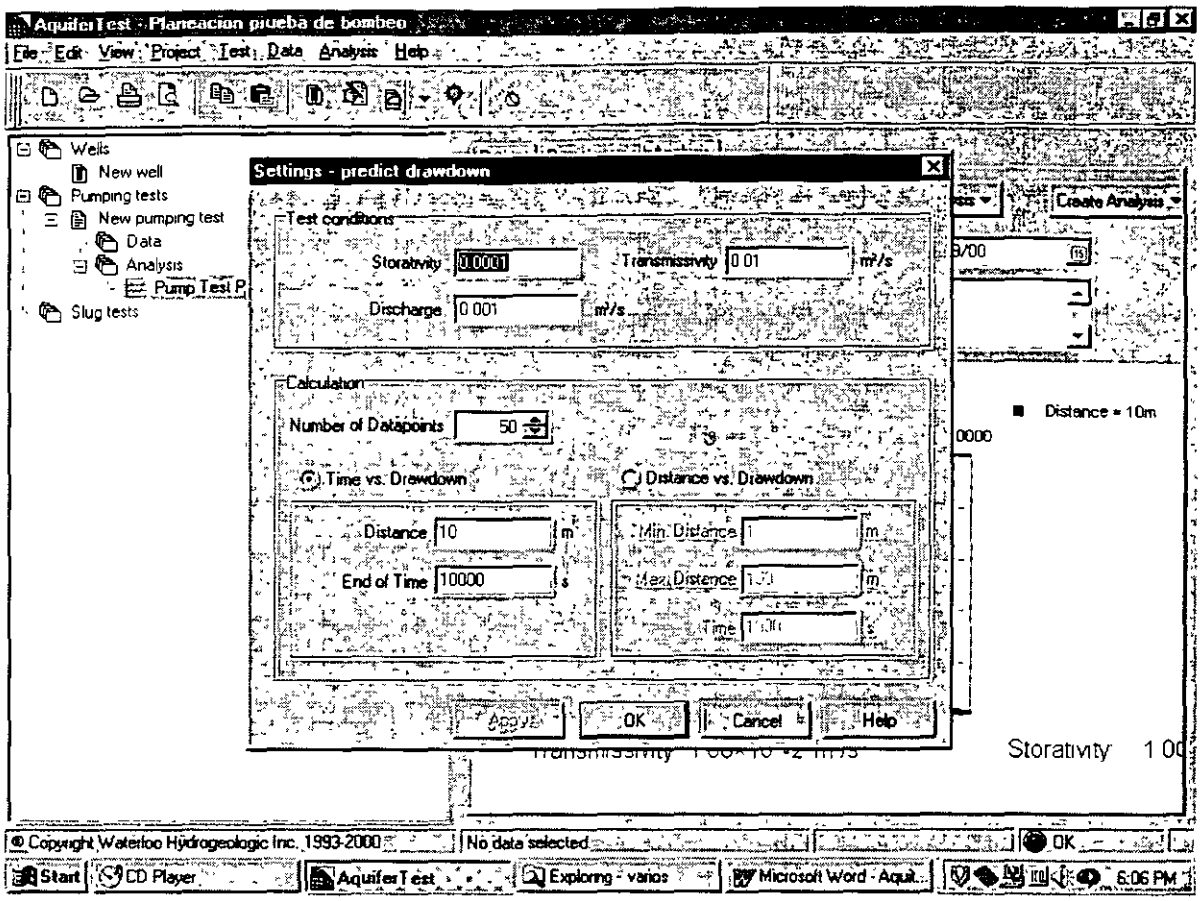

Nótese que en "Test Conditions" se requieren valores de almacenamiento, transmisibilidad y caudal. Con información acerca del sitio de estudio se puede estimar el orden de la transmisibilidad y el almacenamiento. Con estos valores estimados, se puede entonces varir el caudal hasta que se obtenga el abatimiento deseado a la distancia establecida.

En "Calculation" se define el número de puntos a ser calculados en la gráfica. Tambien se puede escoger entre estudiar la gráfica de abatimiento vs. Tiempo, o abatimiento vs. Distancia. Estas opciones permiten variar la distancia de los pozos de observación y el tiempo de la prueba de bombeo para ajustarlas a las condiciones reales del sitio.

Por ejemplo, en la mayoría de los casos se utilizan como pozos de monitoreo, pozos ya existentes en el sitio de estudio. Un pozo de monitoreo puede estar a 25 metros del pozo de bombeo y no a 10 metros como lo sugiere el modelo. Se puede sustituir el valor de 10

metros por el de 25 metros. y posteriormente se podrá observar el abatimiento esperado a una distancia de 25 metros del pozo de bombeo.

Asegúrese de que en ""Settings" se ha seleccionado tiempo vs. Abatimiento (Time versus drawdon).

En "Test Conditions" cambie la siguiente infromación:
Storativity: 0.0001
Transmissivity: 0.01 m^2/s (basado en $K=10^{-3}$ m/s; b= 10 m)
Discharge: 0.001 m^3/s (1 lps)

En "Calculation":
Distance: 10 m (al pozo de observación)
End of time: 300 seg (5 min)
OK
Debe de aparecer una gráfica como la siguiente:

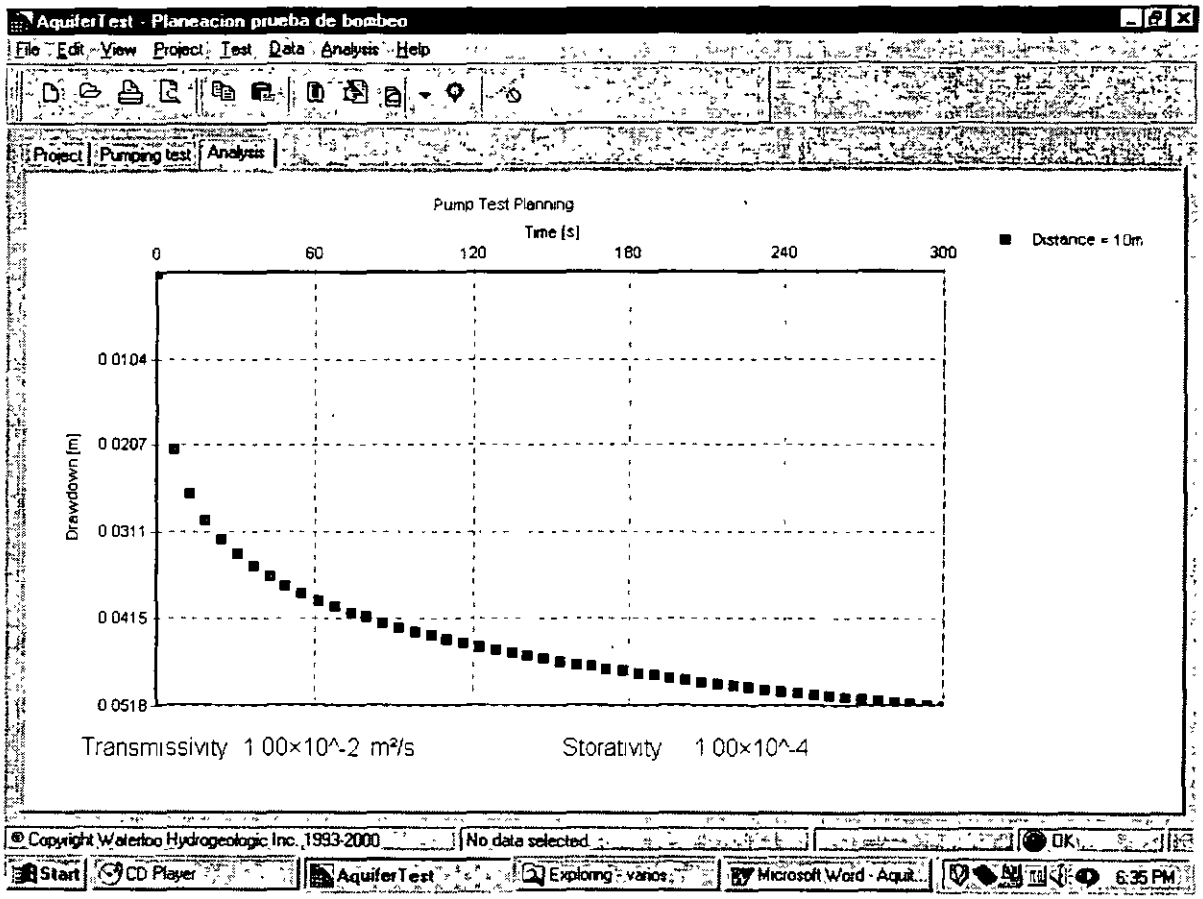

Para agrandar la gráfica se presiona CTRL-E, para regresar al modo normal se vuelve a presionar CTRL-E.

Deacuardo con esta gráfica, un caudal de 0.001 m^3/s, producirá un abatimiento de aproximadamente 4.3 cm a los 2 minutos del inicio de la prueba, en el pozo de observación localizado a 10 metros de distancia. De esta manera, se satisface con este caudal el criterio que nos habiamos propuesto al principio del ejercicio.

Analizemos ahora otra pregunta: que tan lejos llegará el cono de depresión despues de 2 dias de bombeo? Esto nos indicará si podemos llegar a tener interferencia con otros pozos de bombeo cercanos.

Nuevamente haga *derecho* en cualquier lugar de la gráfica y seleccione

Settings

En "Calculation" ☞ Distance vs. Drawdown

Min. Distance: 1 (metros)

Max. Distance: 50 (metros)

Time: 172800 (segundos = 2 dias)

☞ OK

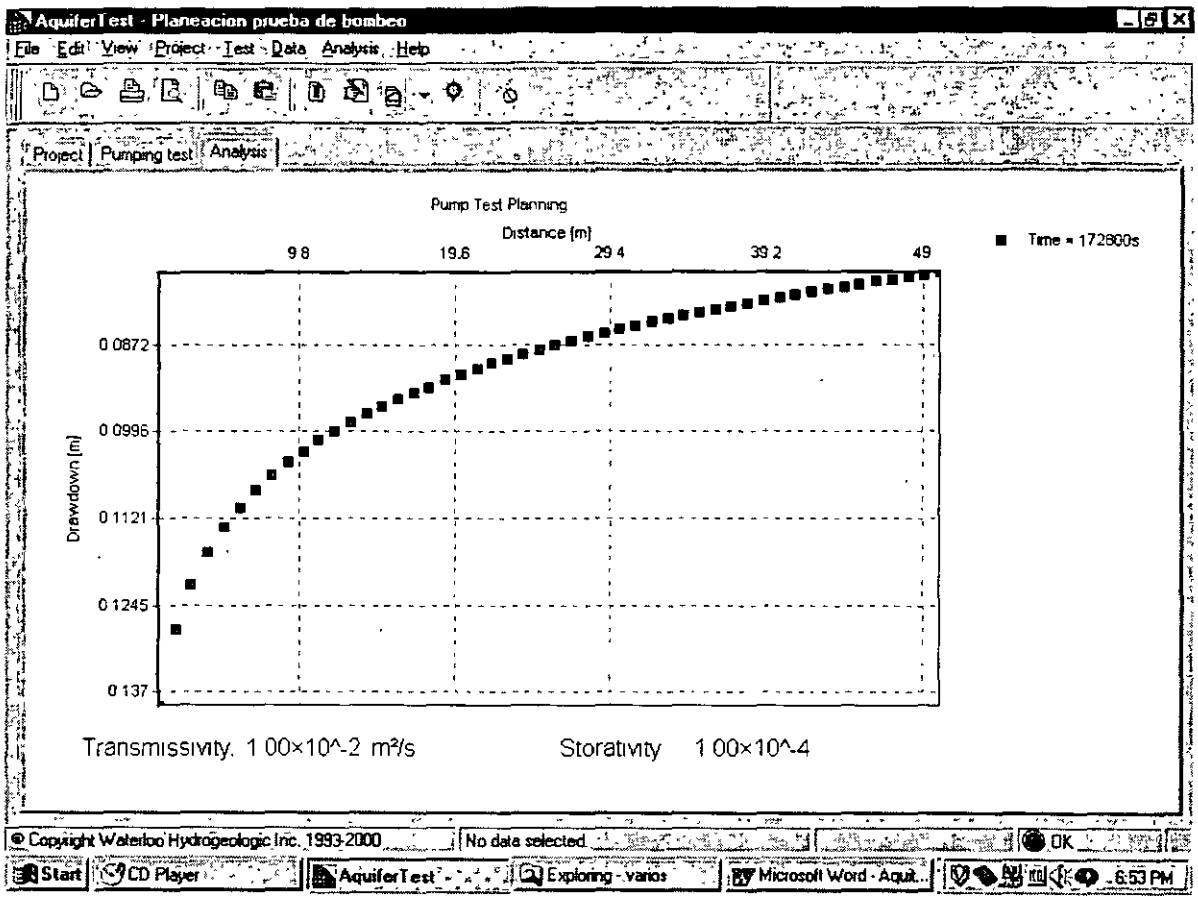

En la figura se puede apreciar la extension del cono de abatimiento de nuestro pozo de bombeo. Como se puede observar.la prueba de bombeo produce muy pequeños efectos a una distancia mayor de 50 metros, si en este radio no existen pozos de bombeo, no existirá entonces ningun problema de interferencia.

Tecleando CTRL-E regresa a la imagen de la gráfica en pequeño.

Final del Ejercicio 1

EJERCICIO DE AQUIFERTEST VER.3.0

EJERCICIO 2: Analisis de una prueba de bombeo en acuífero confinado – Theis analisis

1. CREAR NUEVO PROYECTO

- en el icono de Aquifer Test 3.0
- File (del menú superior)
- New Project...

En el **project name** escriba: Ejercicio 2: Analisis de Theis, y DESELECCIONAR la opciones de **Well** y **Pumping test**. Estas opciones las añadiremos mas

- OK

2. SELECCIÓN DEL SISTEMA DE UNIDADES PARA EL PROYECTO

- Project (del menú superior)
- Units... (asegurese que son las mismas unidades que el ejercicio anterior)
- OK

3. CREAR NUEVOS POZOS

- Wells (del menú izquierdo)
- *derecho* Wells
- New Well (del menu que aparece)

Nombrar al pozo PW-1 (Well name)

- OK

aparecera la siguiente pantalla:

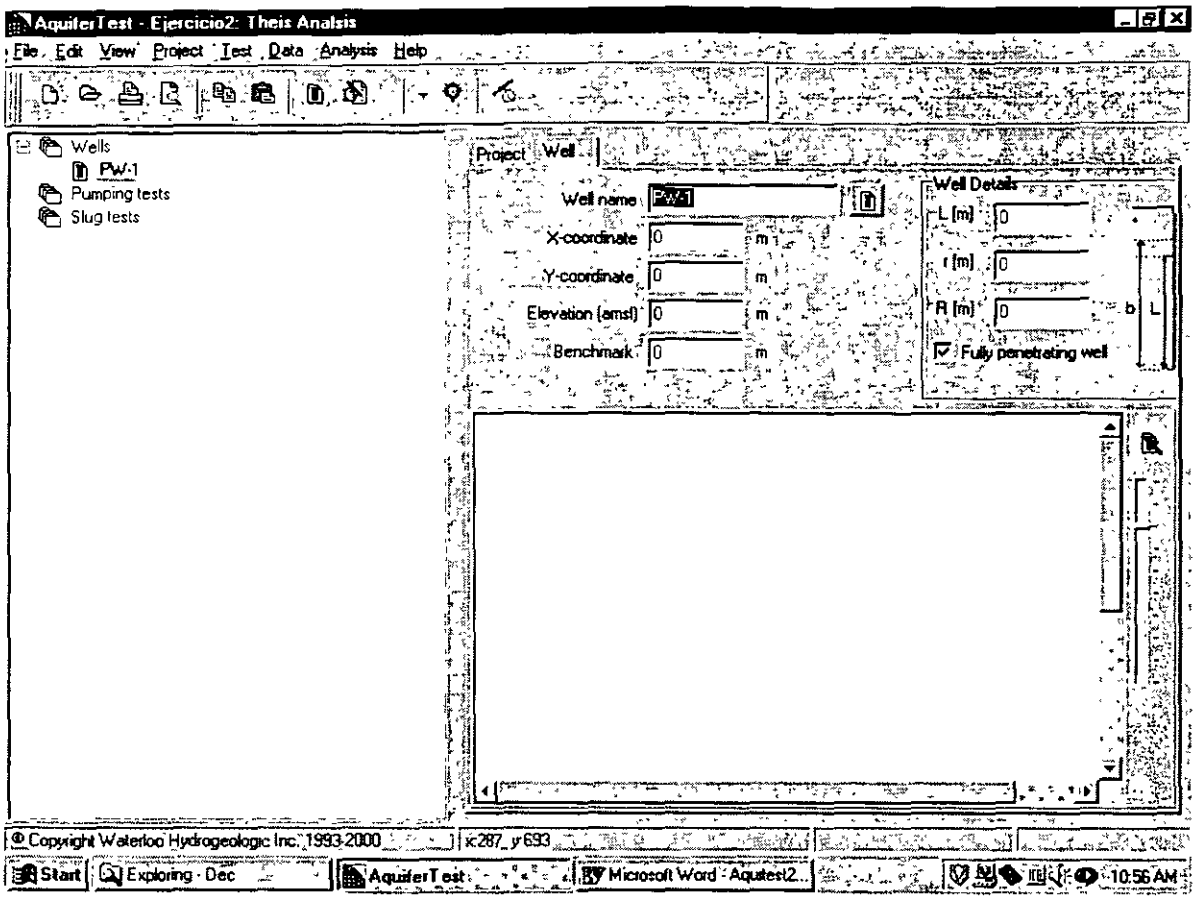

Nuevamente

- Wells (del menú izquierdo)
- *derecho* Wells
- New Well (del menu que aparece)

Nombrar al pozo OW-3a (Well name)

- OK

agregar en:

X coordinate: 12 (metres)

(El pozo PW-1 sera el pozo de bombeo, y el OW-3a el pozo de observación)

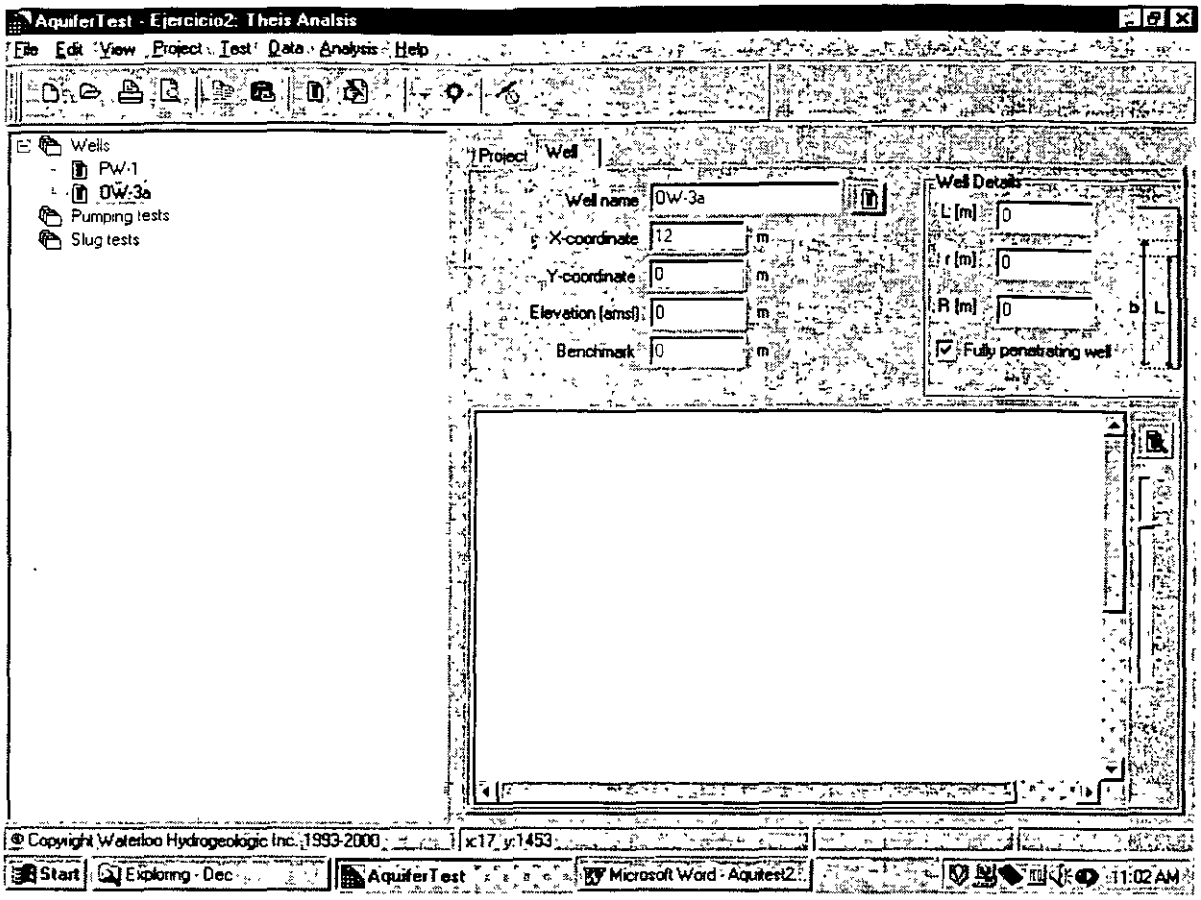

4. CREAR UNA PRUEBA DE BOMBEO

- Test (del menú superior)
- Create pumping test...

En el nombre de la prueba (name) escribir: Prueba de Bombeo – Theis

- PW-1
- OK

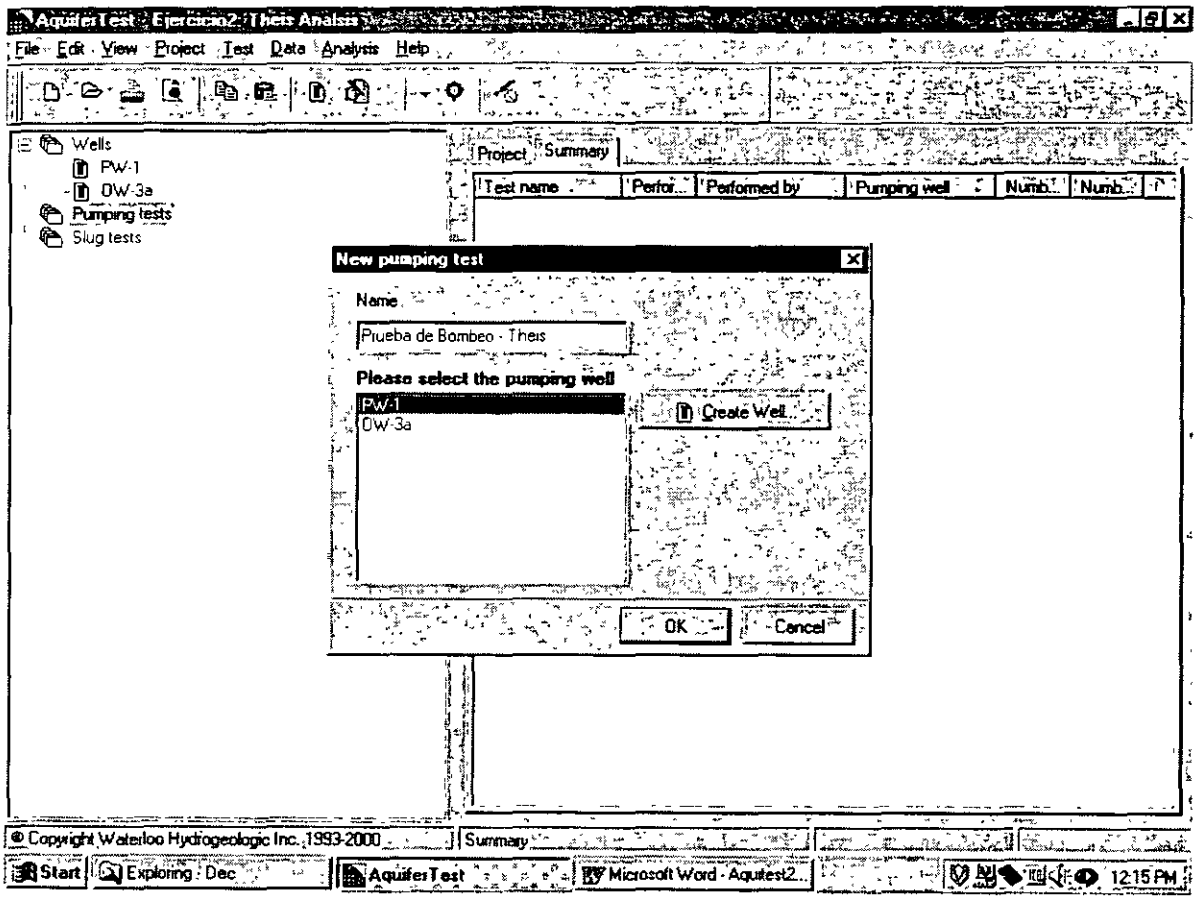

Llene la forma con la siguiente información:

Pumping Test name: Prueba de Bombeo – Theis (ya debe de estar automáticamente)

Perfomed by: <Escriba su nombre>

Date: <Escriba la fecha de la prueba de bombeo>

Time: <Escriba la hora de inicio de la prueba de bombeo>

Pumping well: Asegurese de que el pozo PW-1 esté seleccionado

Discharge rate: seleccione **constant, 1.5 m^3/s**

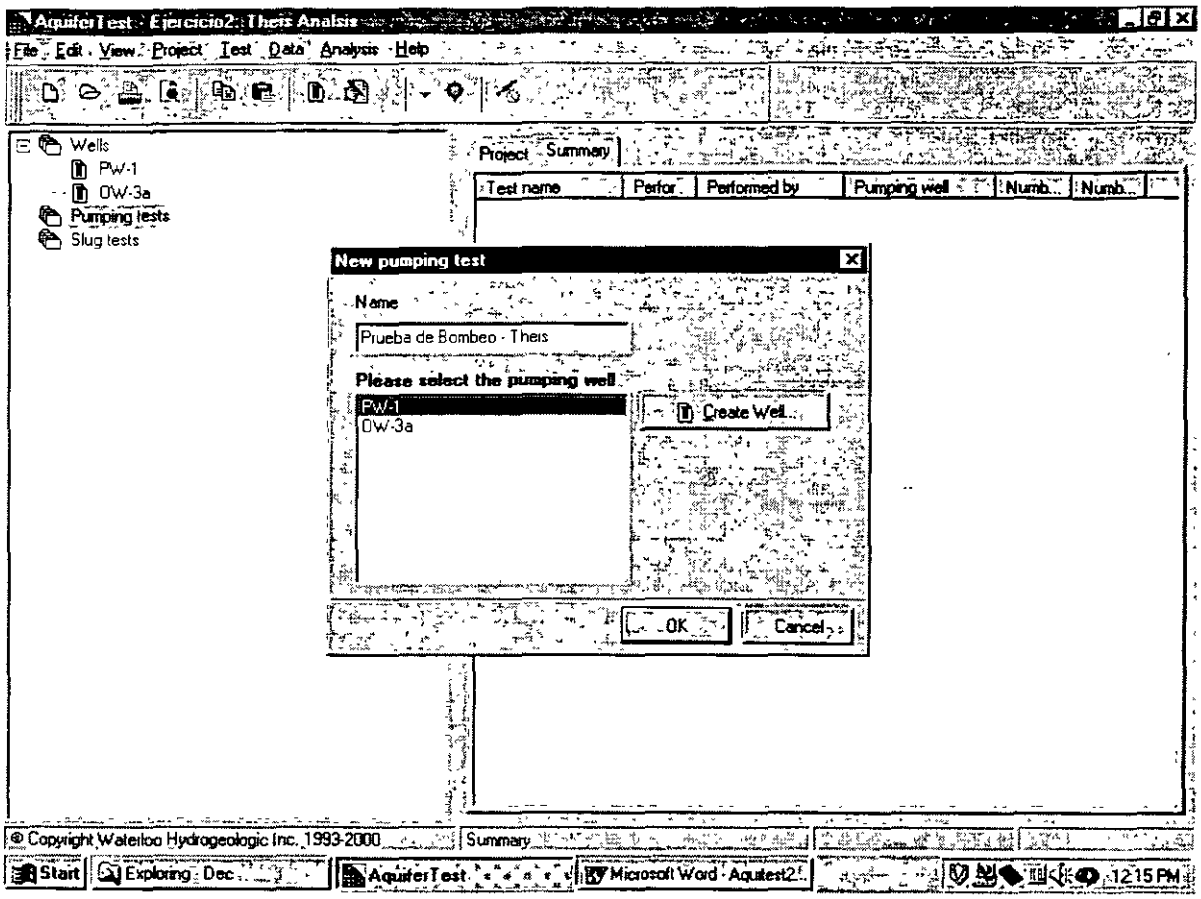

5. CREAR UN NUEVO GRUPO DE DATOS

- Prueba de Bombeo – Theis (menú izquierdo)
- data
- *derecho* data
- Create Datalist... (del menú que aparece)
- OW-3a (en el cuadro inferior, create data)
- OK

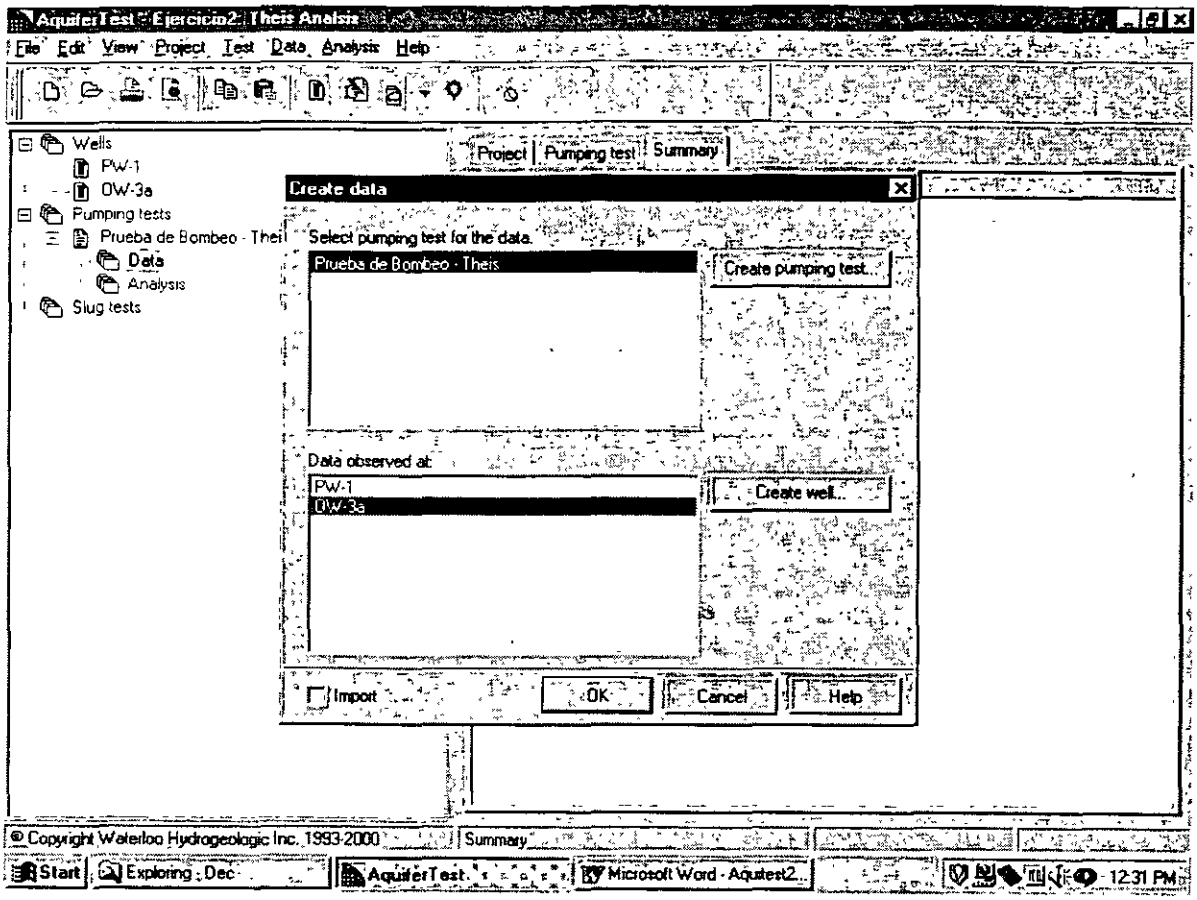

Llenar con la información que aparece en la siguiente figura. Se puede utilizar <enter> para pasar al siguiente espacio de información.

Nótese que estos valores son profundidades al nivel estático, que es el valor que generalmente se obtiene en campo en las pruebas de bombeo.

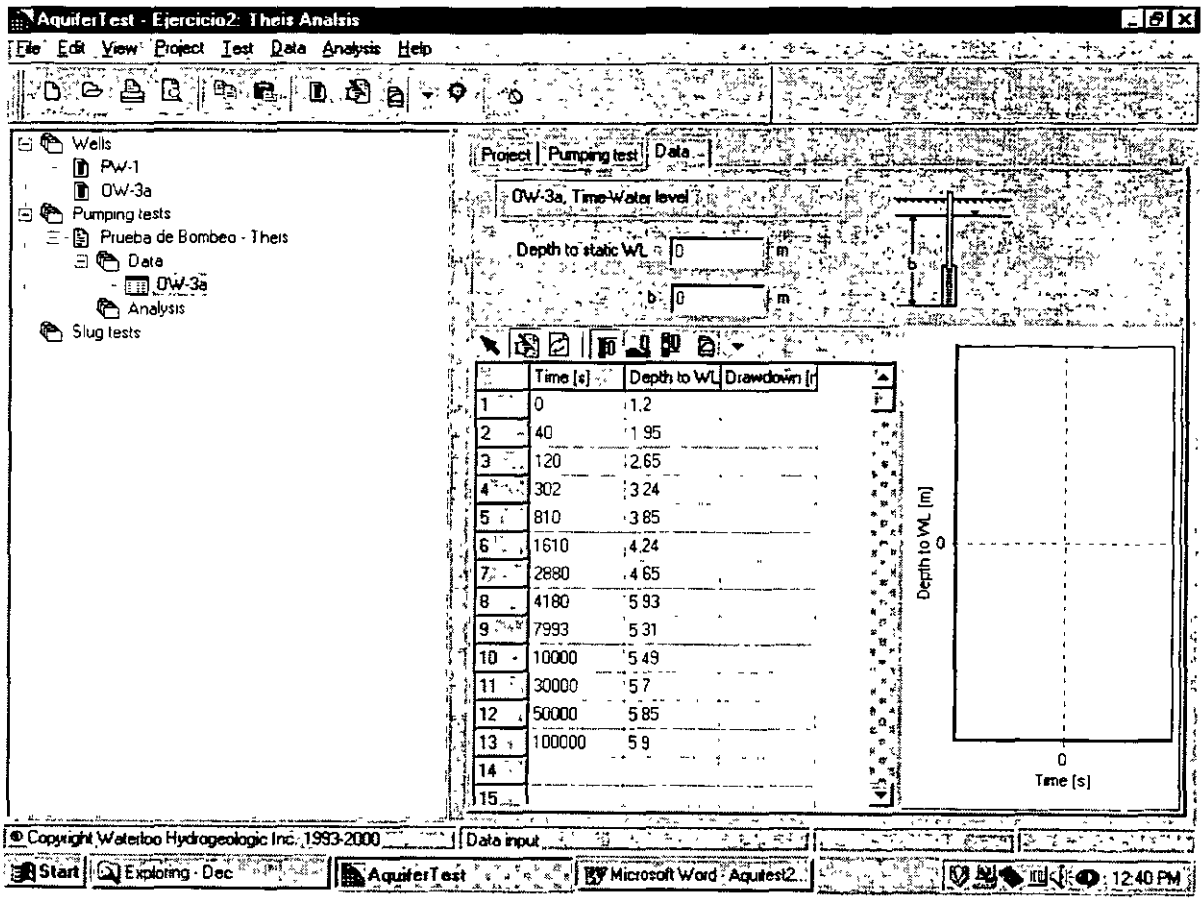

- *derecho* en cualquier lugar de la tabla
- Refresh graph (hasta abajo del menú que aparece)

La siguiente gráfica aparecerá

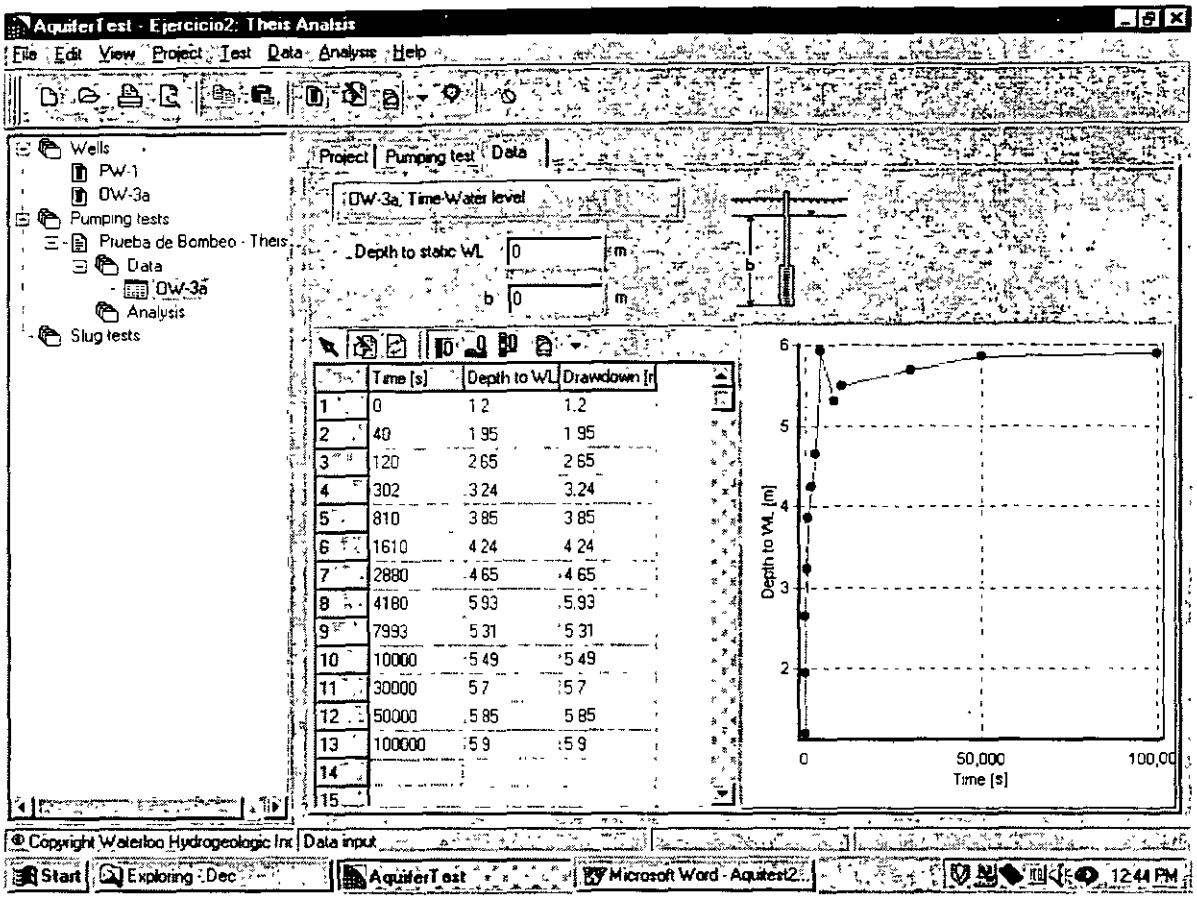

Esto también se puede hacer presionando la tecla F5, o el ícono de **Refresh graph** que está arriba de la tabla. Busque cual es el ícono moviendo el mouse por los diferentes íconos en la parte superior de la gráfica y leyendo le función que aparece, *sin presionar el mouse.*

También, para poder apreciar la gráfica mejor, se puede colocar el el mouse entre el menú izquierdo y la porción de los datos y mover la separación cuando el símbolo del mouse se convierta en ⇔. Asímismo se puede ampliar el tamaño de la gráfica con respecto a la tabla con el mismo procedimiento.

6. MODIFICANDO UN GRUPO DE DATOS

Un valor en la gráfica parece estar mal, de los íconos que estan arriba de la tabla, 🖱 en la flecha **(select measurement values).**

En la tabla de valores, 🖱 en el valor con tiempo de 4180 segundos.

🖱 *derecho* en el valor.

Delete (del menú que aperece).

La gráfica se modificará automáticamente.

Ahora agregaremos el nivel estático al inicio de la prueba de bombeo. En **Depth to Static WL** escriba 1.2 (metros).

Nuevamente haga un **refresh graph** con el ícono o con F5, y obtendrá una figura como la siguiente. Nótese, que los abatimientos han sido correguidos tomando en cuenta el nuevo nivel estático.

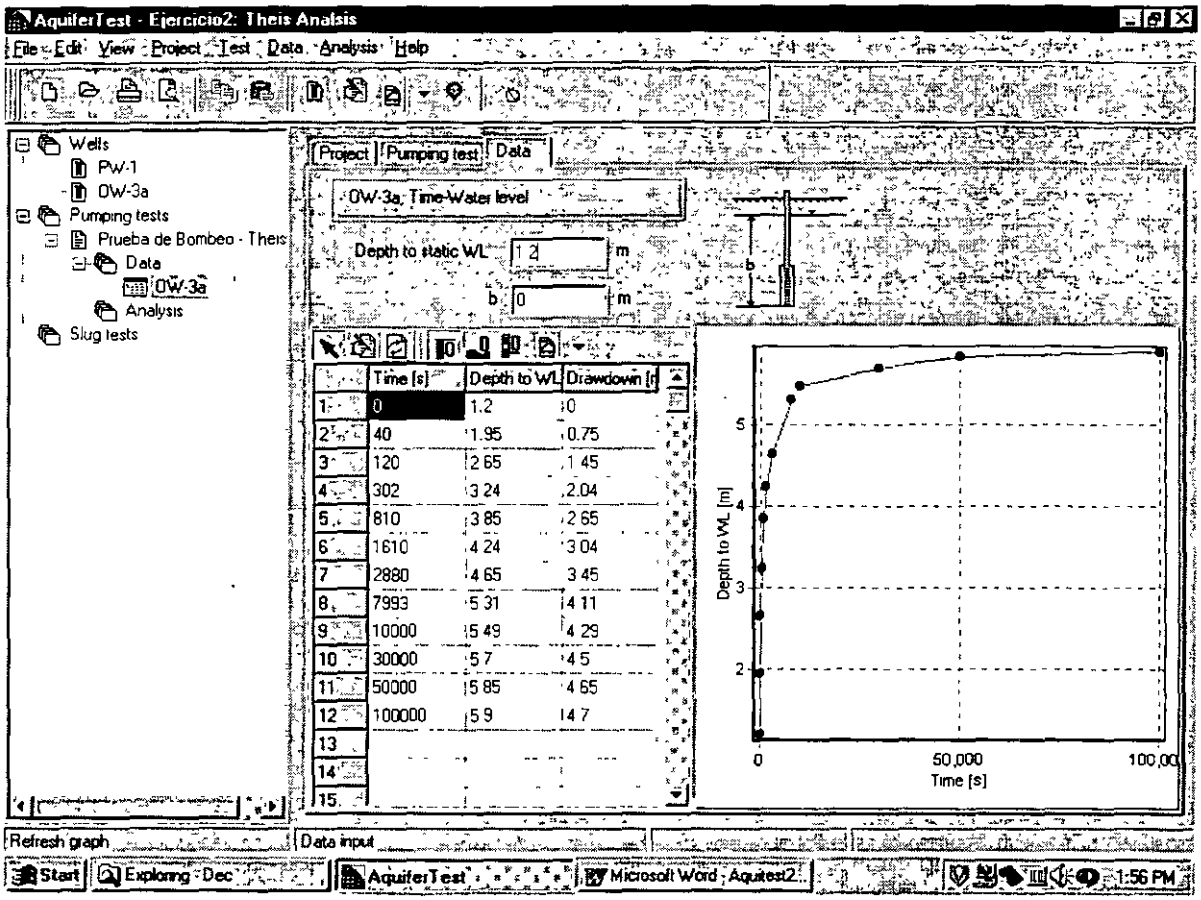

7. CREAR UN NUEVO ANALISIS

En el menú izquierdo, dentro de Prueba de bombeo – Theis, seleccionar:

analysis

derecho en analysis

en Create Analysis, en Theis

aparecera la siguiente gráfica:

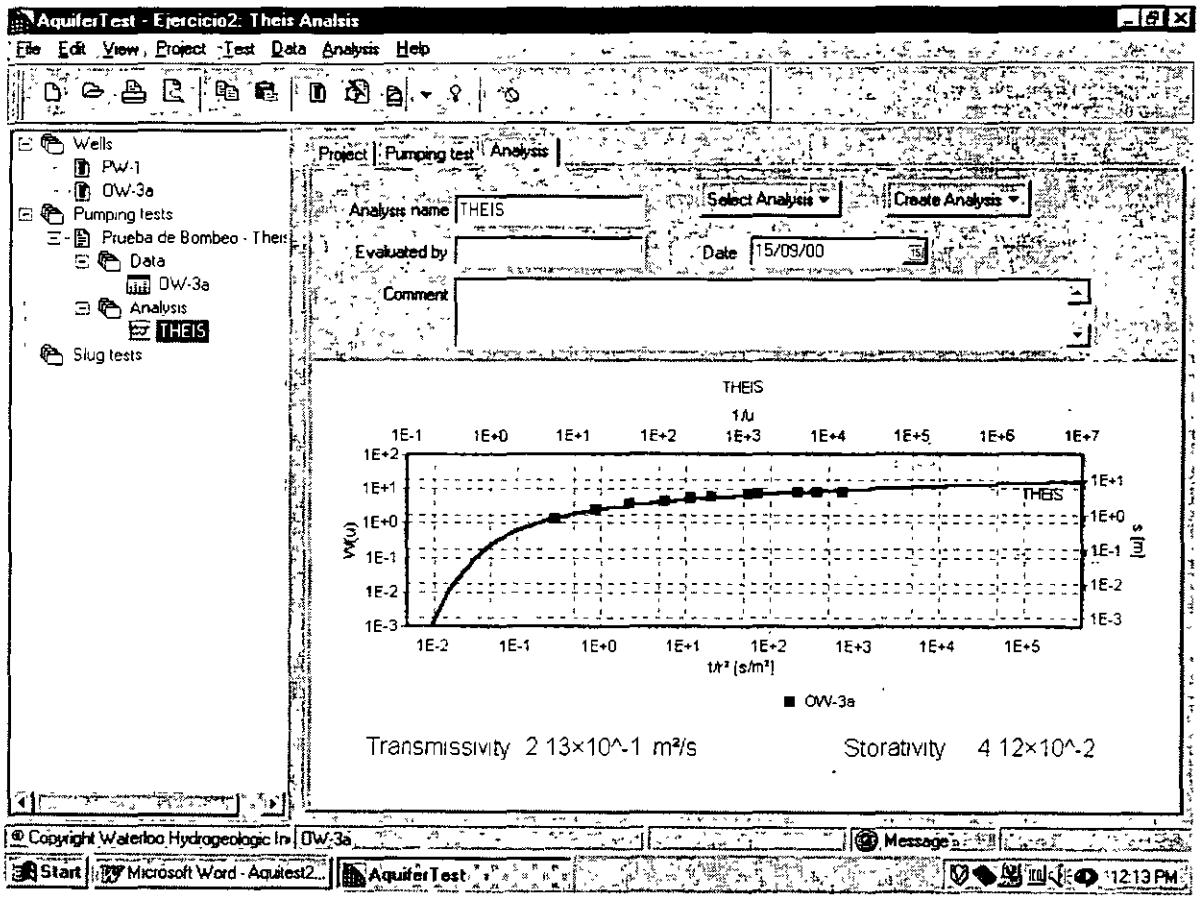

Nótese que la leyenda aparece del lado dercho, para que aparezca en la parte de abajo haga un 🖱 *derecho* en cualquier lugar de la gráfica, 🖱 properties del menú que aparece y en Legend, seleccionar Bottom , y 🖱 OK.

Nótese también en la parte inferior aparece la palabra "message"
🖱 en el círculo verde, y 🖱 en details:

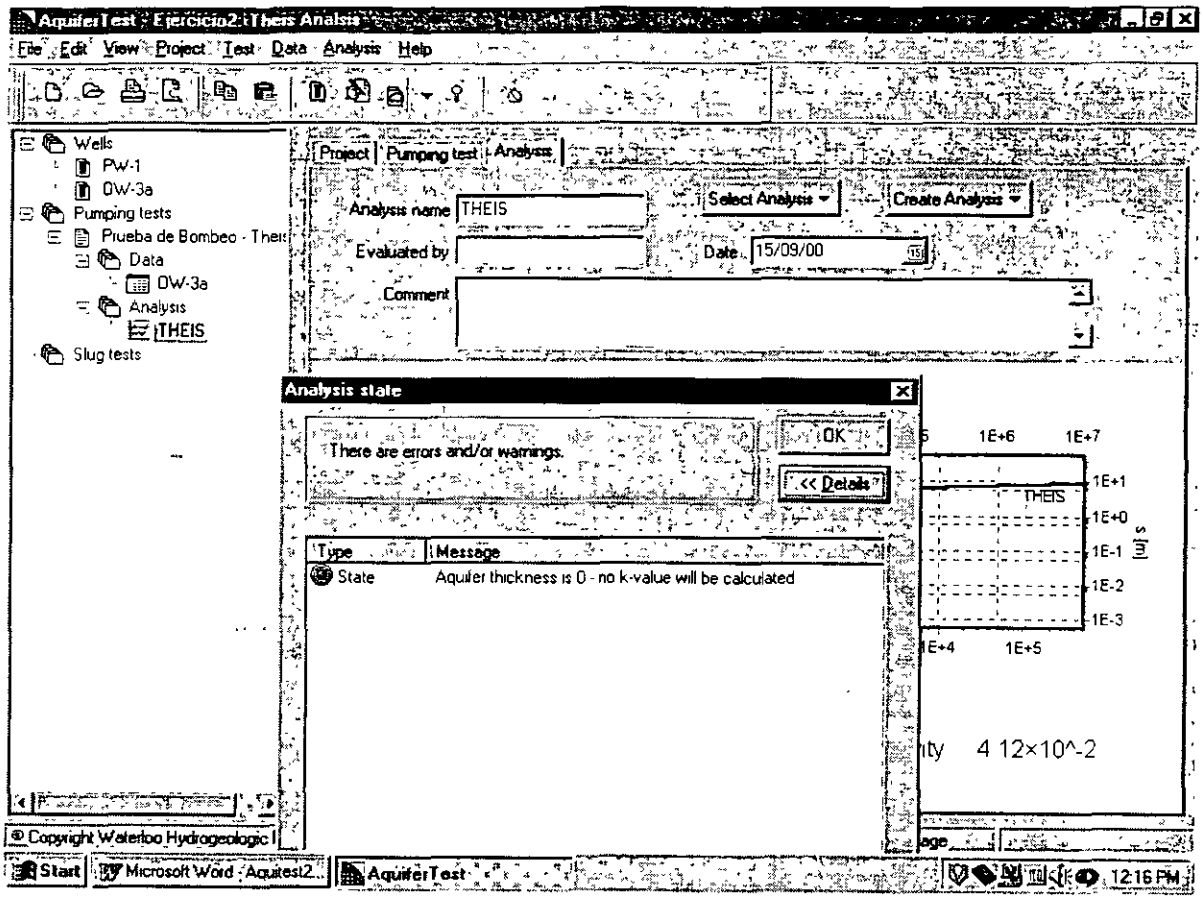

Este mensaje nos informa que no hemos dado un espesor del acuífero y por lo tamto no se calcula la conductividad hidráulica (K) sino únicamente la transmissibilidad (T).

Recuérdese que K=T/b, donde b es el espesor del acuífero.

OK

En las pestañas en la porción superior derecha de la pantalla seleccionar: en Pumping test. En Saturated aquifer thickness, escribir: 5.

Regresar a la sección de resultados dando un en la pestaña de Analysis. Esta vez verá calculada una conductividad hidráulica (approx. 4.3 $x10^{-2}$ m/s), como se ve en la siguiente gráfica:

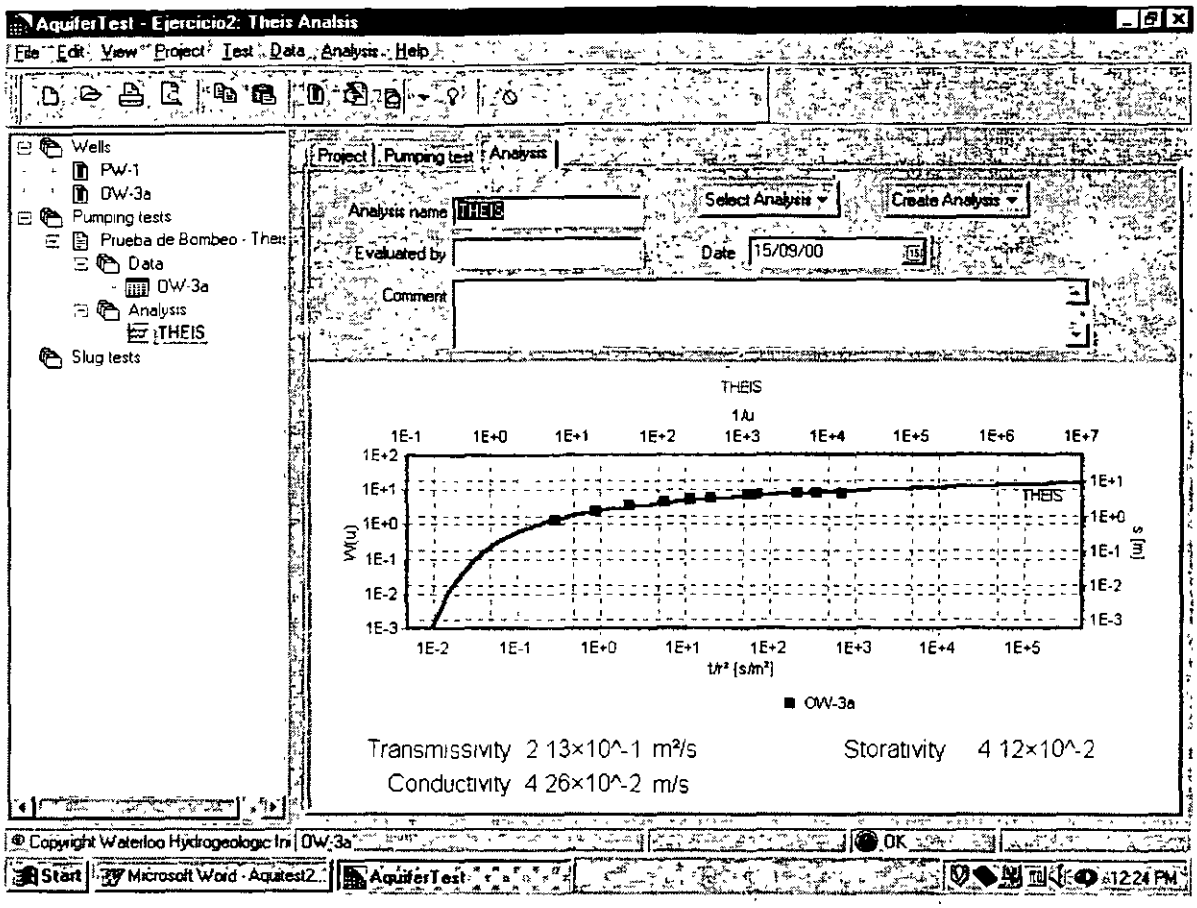

Nótese que ahora en la sección de mensajes dice: OK. Existen 4 mensajes que Aquifer Test puede dar:

Error (color rojo)

Warning (color amarillo)

Message (color verde)

O.K. (color verde fuerte)

Por los general los errores son producidos por falta de información en algún menú.

La gráfica puede agrandarse con <CTRL-E> o por medio del menú superior:

- View
- Enlarge graph

y de la misma manera se puede regresar a la pantalla normal.

Aquifer test produce una estimación de la mejor curva de Theis para los datos basado en un método de cuadrados mínimos (least squares fit).

Los resultados obtenidos deben ser aprosimadamente:

Transmisibilidad (transmissivity): $2.13x10^{-1}m^2/s$

Coeficiente de almacenamiento (Storativity): $4.12x10^{-2}$

Conductividad hidráulica (Hydraulic conductivity): $4.26x10^{-2}m/s$

8. ZOOM

Para hacer un zoom dentro de la gráfica se requiere pocicionar el mouse en la esquina superior izquierda del area en que se quiera el zoom, y *sin soltar el botón* colocarse en la esquina inferior derecha de la que se quiere hacer el zoom.

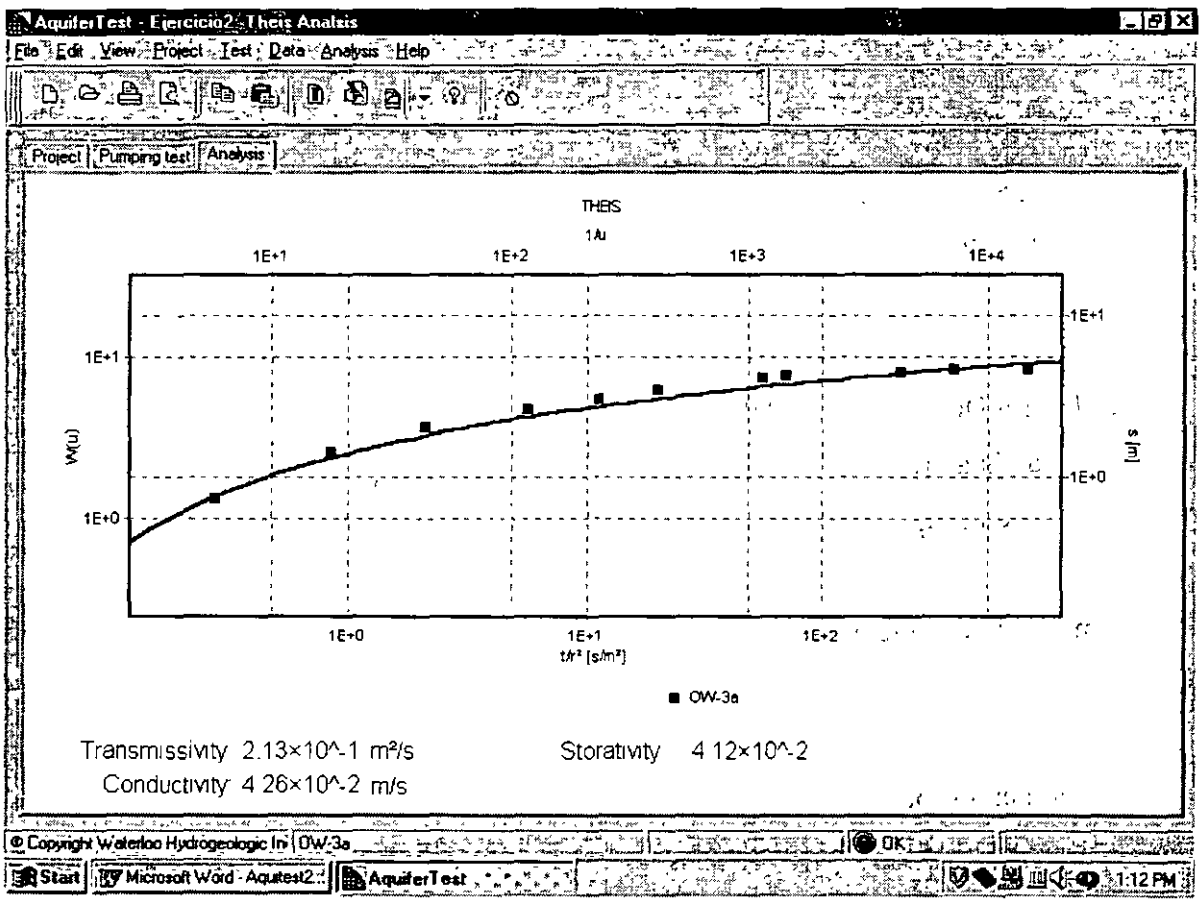

Para ver nuevamente todos los datos hacer en cualquier lugar de la gráfica, y *sin soltar el botón* moverlo tratando de hacer un recuadro hacia arriba y a la izquierda, al soltarlo, se mostrarán nuevamente la gráfica completa.

9. AJUSTE DE DATOS "A MANO"

Por lo general es necesario ajustar los datos a la curva de Theis "a mano" tomando en cuenta el juicio profesional. Ya sea por que problemas durante la prueba de bombeo hacen más o menos válida cierta porción de los datos, o por que sencillamente, la calibración automática no parece ser la mejor para los datos obtenidos.

Los datos se pueden mover de arriba abajo y derecha a izquierda utilizando las flechas del teclado. Nótese que al mover la gráfica a la izquierda o dercha, únicamente se modifica el coeficiente de almacenamiento.

Presione <CTRL-E> para regresar a una vista normal.

10. OTROS ANALISIS

Aquifer test pérmite visualisar otro tipo de soluciones fácilmente.

Select analysis

Aquí aparecen otros métodos de interpretación de pruebas de bombeo. Intente algún otro método y analise los resultados.

10. IMPRIMIENDO DESDE AQUIFER TEST

Pare tener una vista previa antes de imprimir de esta prueba de bombeo

File (en el menú superior)

Print preview

O simplemente en el ícono de vista previa.

Para imprimir:

File (en el menú superior)

Print

O simplemente en el ícono de impresión